BEILSTEIN JOURNAL OF ORGANIC CHEMISTRY

Organo-fluorine chemistry V

Edited by David O'Hagan

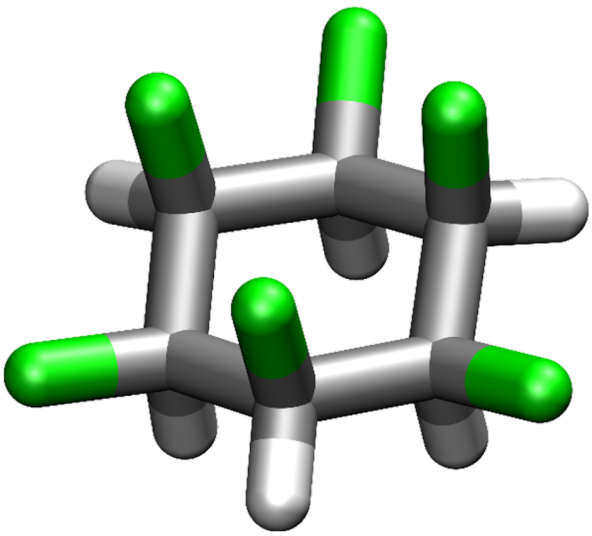

Generated on 08 April 2026, 14:43

Imprint

Beilstein Journal of Organic Chemistry
www.bjoc.org
ISSN 1860-5397
Email: journals-support@beilstein-institut.de

The *Beilstein Journal of Organic Chemistry* is published by the Beilstein-Institut zur Förderung der Chemischen Wissenschaften.

Beilstein-Institut zur Förderung der Chemischen Wissenschaften
Trakehner Straße 7–9
60487 Frankfurt am Main
Germany
www.beilstein-institut.de

The copyright to this document as a whole, which is published in the *Beilstein Journal of Organic Chemistry*, is held by the Beilstein-Institut zur Förderung der Chemischen Wissenschaften. The copyright to the individual articles in this document is held by the respective authors, subject to a Creative Commons Attribution license.

The cover image is copyright 2021 David O'Hagan under the terms of the Creative Commons Attribution License (https://creativecommons.org/licenses/by/4.0); licensee Beilstein-Institut.

BEILSTEIN JOURNAL OF ORGANIC CHEMISTRY

Organo-fluorine chemistry V

David O'Hagan

Editorial

Open Access

Address:
School of Chemistry, Biomedical Sciences Research Complex, University of St Andrews, North Haugh, St Andrews, Fife KY16 9ST, United Kingdom

Email:
David O'Hagan - do1@st-andrews.ac.uk

Keywords:
Organo-fluorine chemistry

Beilstein J. Org. Chem. **2021,** *17,* 737–738.
https://doi.org/10.3762/bjoc.17.63

Received: 26 February 2021
Accepted: 11 March 2021
Published: 17 March 2021

This article is part of the thematic issue "Organo-fluorine chemistry V".

Guest Editor: D. O'Hagan

© 2021 O'Hagan; licensee Beilstein-Institut.
License and terms: see end of document.

This is the fifth thematic issue on organo-fluorine chemistry in the *Beilstein Journal of Organic Chemistry* that I have had the pleasure to edit, and these themed issues have gone progressively from strength to strength ever since the first was assembled in 2008. In this issue 45 papers are collected, a record for a thematic issue in the Journal, and there is no doubt that the *Beilstein Journal of Organic Chemistry* has become a settled home for papers in contemporary organo-fluorine chemistry. Authors have presented their recent findings or, in some cases, reviewed important areas, from bioactives to materials, and collectively the papers highlight the vibrancy and range of activity associated with this theme. Organo-fluorine chemistry merits our attention as an important discipline within contemporary organic chemistry contributing in a unique way to innovation and performance in the development of functional molecules.

This issue will be historically memorable as all of the manuscripts were submitted through the covid-19 virus lockdown period which impacted universities and research laboratories across the world. As Guest Editor I am indebted to all of the authors for maintaining their commitment to contribute through what was a particularly difficult and unusual period of professional life.

I thank the referees who gave of their time, and also the outstanding level of professionalism of the Editorial and Production Team at the *Beilstein Journal of Organic Chemistry* for their continuous attention to detail and the quality of the final published copy. The papers appear as contributions to the Journal in the normal sense, but they are also conveniently collected here as a single document.

David O'Hagan

St Andrews, Scotland, February 2021

ORCID® iDs

David O'Hagan - https://orcid.org/0000-0002-0510-5552

License and Terms

This is an Open Access article under the terms of the Creative Commons Attribution License (https://creativecommons.org/licenses/by/4.0). Please note that the reuse, redistribution and reproduction in particular requires that the author(s) and source are credited and that individual graphics may be subject to special legal provisions.

The license is subject to the *Beilstein Journal of Organic Chemistry* terms and conditions: (https://www.beilstein-journals.org/bjoc/terms)

The definitive version of this article is the electronic one which can be found at: https://doi.org/10.3762/bjoc.17.63

BEILSTEIN JOURNAL OF ORGANIC CHEMISTRY

Asymmetric synthesis of CF_2-functionalized aziridines by combined strong Brønsted acid catalysis

Xing-Fa Tan[1,2], Fa-Guang Zhang[*1,2] and Jun-An Ma[*1,2]

Full Research Paper

Open Access

Address:
[1]Department of Chemistry, Tianjin Key Laboratory of Molecular Optoelectronic Sciences, and Tianjin Collaborative Innovation Centre of Chemical Science & Engineering, Tianjin University, Tianjin 300072, China and [2]Joint School of NUS & TJU, International Campus of Tianjin University, Fuzhou 350207, China

Email:
Fa-Guang Zhang[*] - zhangfg1987@tju.edu.cn; Jun-An Ma[*] - majun_an68@tju.edu.cn

* Corresponding author

Keywords:
aziridines; chiral disulfonimides; difluoromethyl compounds; fluorinated diazo reagents; strong Brønsted acids

Beilstein J. Org. Chem. **2020,** *16,* 638–644.
doi:10.3762/bjoc.16.60

Received: 17 February 2020
Accepted: 27 March 2020
Published: 07 April 2020

This article is part of the thematic issue "Organo-fluorine chemistry V".

Guest Editor: D. O'Hagan

© 2020 Tan et al.; licensee Beilstein-Institut.
License and terms: see end of document.

Abstract

A diastereo- and enantioselective approach to access chiral CF_2-functionalized aziridines from difluorodiazoethyl phenyl sulfone ($PhSO_2CF_2CHN_2$) and in situ-formed aldimines is described. This multicomponent reaction is enabled by a combined strong Brønsted acid catalytic platform consisting of a chiral disulfonimide and 2-carboxyphenylboronic acid. The optical purity of the obtained CF_2-substituted aziridines could be further improved by a practical dissolution–filtration procedure.

Introduction

Chiral aziridines are prevalently found in natural products and artificially made bioactive molecules, thus receiving significant attention in the past decades [1-6]. Among them, the introduction of fluorine or fluoroalkyl groups into three-membered N-heterocycles has emerged as an attractive direction due to the unique fluorine effect in pharmaceuticals and biology [7-11]. In this context, it is not surprising that the syntheses of trifluoromethylaziridines have been pursued from versatile precursors [12-25]. However, catalytic asymmetric approaches to chiral CF_3-functionalized aziridines have only been reported by Cahard in 2012, who utilized trifluorodiazoethane (CF_3CHN_2) as the nucleophile to react with aldimines catalyzed by chiral phosphoric acid (Scheme 1a) [26]. In comparison, there is a significant dearth of available synthetic approaches to CF_2-functionalized aziridines, particularly in a stereocontrolled manner. Indeed, a handful of reported methods document the employment of difluoromethylimines, difluoromethyl phenyl sulfone, and difluoromethyl vinyl sulfonium salts as the fluorinating partner en route to various CF_2-substituted aziridines [27-31], and a general protocol to chiral CF_2-aziridines remains an unsolved challenge. Thus, herein we report a diastereo- and enantioselective aza-Darzens reaction between in situ-generated

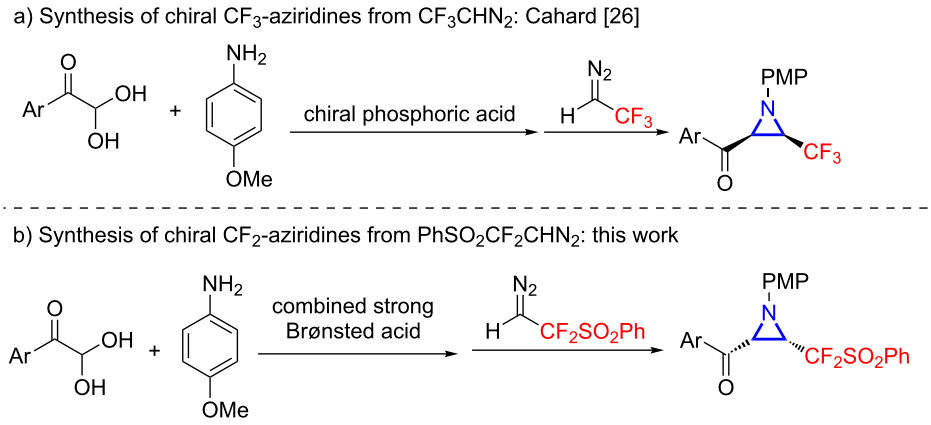

Scheme 1: Preparation of chiral aziridines from fluorinated diazo reagents.

aldimines and our recently developed difluorodiazo reagent $PhSO_2CF_2CHN_2$ acting as the difluorinated nucleophile [32-35], providing access to a variety of chiral CF_2-fuctionalized aziridines under mild conditions (Scheme 1b). The key to this multicomponent transformation hinges upon the discovery of a combined strong Brønsted acid system comprised of a chiral disulfonimide and 2-carboxyphenylboronic acid.

Results and Discussion

We commenced the desired one-pot transformation by conducting the model reaction between phenylglyoxal monohydrate (**1a**), 4-methoxyaniline (**2a**), and $PhSO_2CF_2CHN_2$ (**3**, Ps-DFA). Initial screenings were focused on the evaluation of various chiral phosphoric acids that have proven effective in similar aza-Darzens reactions of diazo esters and trifluorodiazoethane [36-39]. Unfortunately, these endeavors resulted in either no conversion or no enantioselectivity at all. As arylboronic acids have been harnessed to enhance the Brønsted acidity in asymmetric organocatalysis in combination with chiral diols or chiral aminoalcohols [40-44], we envisioned that the simultaneous use of arylboronic acids and chiral Brønsted acids may bring about a complementary catalytic platform. Encouragingly, the targeted CF_2-functionalized aziridine **4a** was obtained in up to 51% ee and high diastereoselectivity, albeit in a low yield (Table 1, entries 1 and 2). The difficulty in further improving the conversions might be ascribed to the limited Brønsted acidity of chiral phosphoric acids. Bearing this in mind, we then turned our attention to chiral disulfonimides developed by List, which have been established as a unique type of stronger Brønsted acids [45]. Putting it into practice, a range of BINOL-derived disulfonimides was used as the chiral additive in combination with 2-carboxyphenylboronic acid (**COOH-BA**) in the

Table 1: Representative screening results of the asymmetric aziridination reaction of $PhSO_2CF_2CHN_2$.[a]

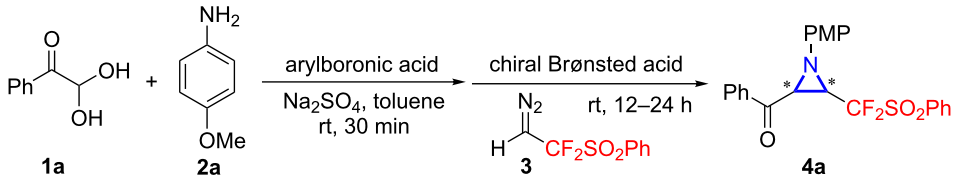

entry	arylboronic acid (mol %)	chiral Brønsted acid (mol %)	yield of **4a** (%)[b]	ee (%) of **4a** and dr of crude mixture[c]
1	**COOH-BA** (8)	**CPA-1** (5)	24	51, 13:1
2	**COOH-BA** (8)	**CPA-2** (5)	28	25, 11:1
3	**COOH-BA** (8)	**CDSI-1** (5)	21	41, 19:1
4	**COOH-BA** (8)	**CDSI-2** (5)	50	41, 9:1
5[d]	**COOH-BA** (8)	**CDSI-3** (5)	16	60, 5:1
6[d]	**COOH-BA** (8)	**CDSI-4** (5)	64	73, 13:1
7	**COOH-BA** (8)	**CDSI-5** (5)	34	33, 10:1

Table 1: Representative screening results of the asymmetric aziridination reaction of $PhSO_2CF_2CHN_2$.[a] (continued)

8	**COOH-BA** (8)	**CDSI-6** (5)	47	52, 9:1
9	**OH-BA** (8)	**CDSI-4** (5)	63	68, 28:1
10[d]	**SO_3H-BA** (8)	**CDSI-4** (5)	62	66, 16:1
11[d]	**NO_2-BA** (8)	**CDSI-4** (5)	45	62, 16:1
12	**CF_3-COOH-BA** (8)	**CDSI-4** (5)	81	67, 8:1
13[e]	**COOH-BA** (8)	**CDSI-4** (5)	60	47, 5:1
14[f]	**COOH-BA** (8)	**CDSI-4** (5)	trace	n.d.
15[d]	**COOH-BA** (8)	**CDSI-4** (10)	65	70, 12:1
16[d]	–	**CDSI-4** (5)	10	60, >20:1

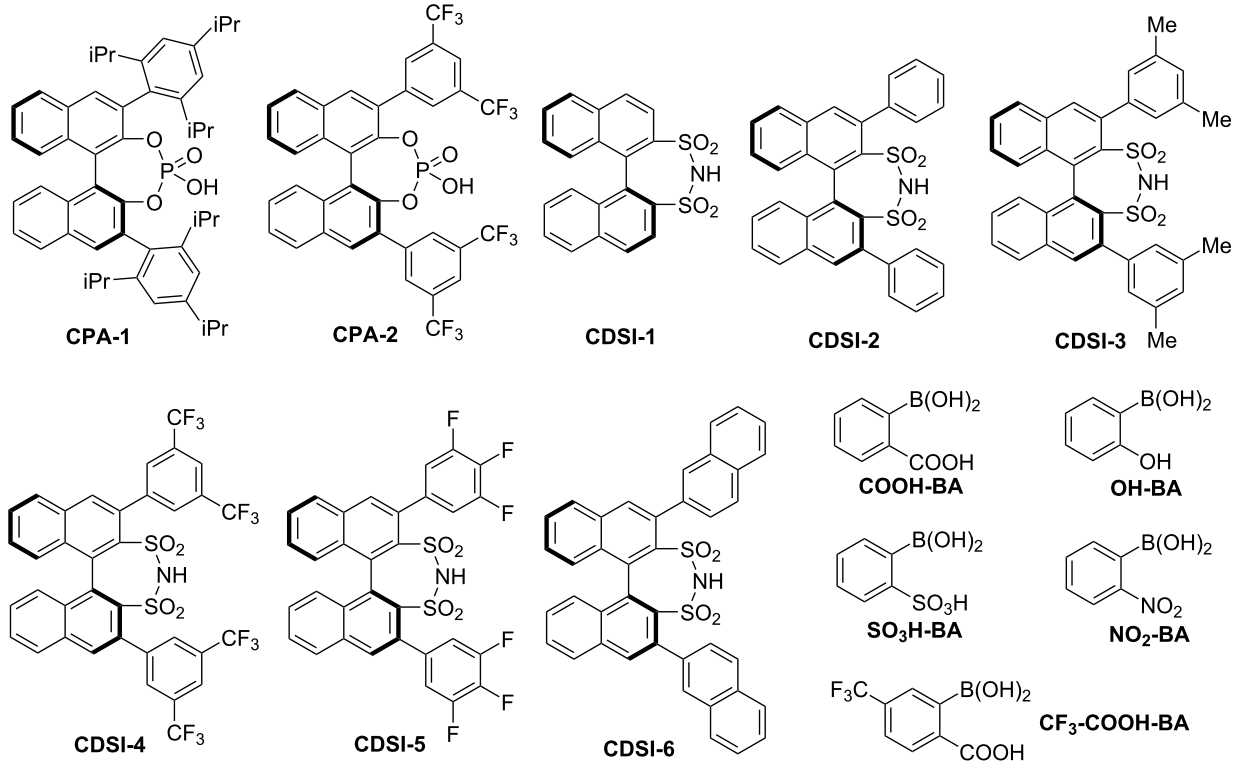

[a]General reaction conditions: **1a** (8 mg, 0.05 mmol, 1.0 equiv), **2a** (7 mg, 0.055 mmol), arylboronic acid (0.004 mmol), and Na_2SO_4 (40 mg) was stirred in toluene (1 mL) at rt for 30 min, then the chiral Brønsted acid (0.0025 mmol) and **3** (18 mg, 0.075 mmol) were added and the mixture was reacted at rt for 12 hours unless otherwise noted; [b]yield of isolated product **4a** was given for entries labelled with d; hexafluorobenzene was used as an internal standard to determine the yield in other cases; [c]ee of **4a** was determined by chiral HPLC analysis, and the dr of the crude reaction mixture was probed by ^{19}F NMR analysis; [d]0.3 mmol scale of reaction was conducted: **1a** (46 mg, 0.3 mmol, 1.0 equiv), **2a** (41 mg, 0.33 mmol), arylboronic acid (0.024 mmol), and Na_2SO_4 (200 mg) was stirred in toluene (2 mL) at rt for 30 min, then the chiral Brønsted acid (0.015 mmol) and **3** (105 mg, 0.45 mmol) were added and the mixture was reacted at rt for 12–24 hours; [e]CH_2Cl_2 was used as the solvent; [f]reaction was operated at 0 °C.

model reaction (Table 1, entries 3–8). We were pleased to find that **CDSI-4** gave the most promising result in terms of both yield and enantioselectivity (64% isolated yield with 73% ee, Table 1, entry 6). An examination on various arylboronic acids, solvent, temperature, and catalyst loadings resulted in no obvious improvement (Table 1, entries 9–15). Among them, the highest yield of **4a** was observed (81%, Table 1, entry 12), albeit with slightly reduced ee value. This enhancement in catalytic activity could be attributed to the increased Brønsted acidity when the strong electron-withdrawing trifluoromethyl group was placed on the benzene ring of the arylboronic acid. Removing the boronic acid from the reaction system leads to a dramatic decrease in both yield and enantiocontrol (Table 1, entry 16).

The challenge to further improve the enantioselectivity promoted us to search for other practical solutions. Considering the poor solubility of **4a** in organic solvents, a dissolution–filtration process with isopropanol was found to be workable for increasing the final ee value. This simple procedure could afford **4a** with excellent enantiopurity as a single diastereoisomer (>99% ee, >50:1 dr, Scheme 2). By the aid of the

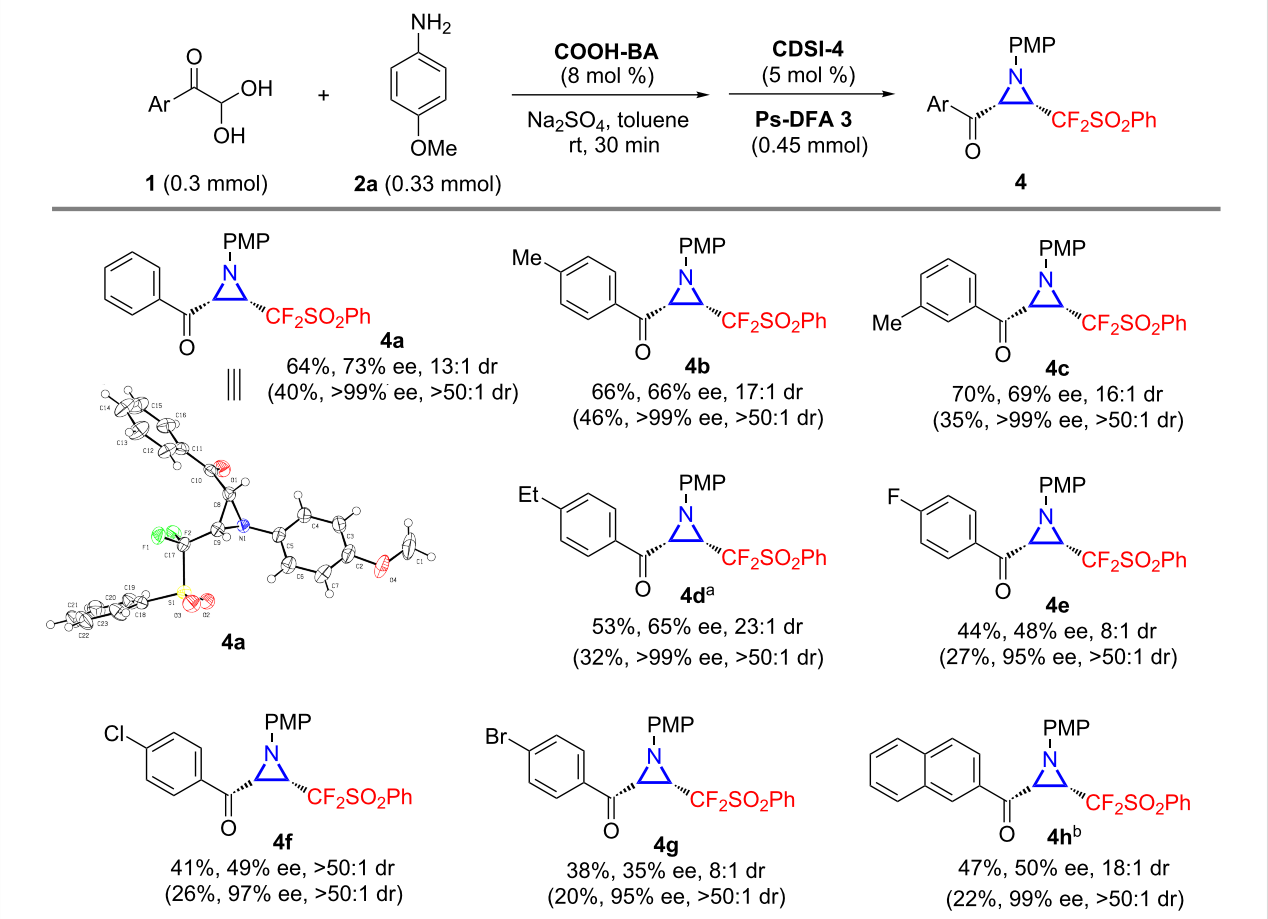

Scheme 2: Substrate scope of chiral CF_2-substituted aziridines from $PhSO_2CF_2CHN_2$. General reaction conditions: Aryl glyoxal monohydrate (**1**, 0.3 mmol), **2a** (41 mg, 0.33 mmol), **COOH-BA** (4 mg, 0.024 mmol), and Na_2SO_4 (200 mg) were stirred in toluene (2 mL) at rt for 30 min, then **CDSI-4** (12 mg, 0.015 mmol) and Ps-DFA **3** (105 mg, 0.45 mmol) were added and the mixture was reacted at rt for 24 hours unless otherwise annotated. The yields are those of isolated products, and the dr was determined by ^{19}F NMR analysis of the crude mixture. The results in parentheses are those of isolated products after the dissolution–filtration process: The corresponding CF_2-functionalized aziridine **4** was dissolved in isopropanol (0.05–0.2 mL/mg) with the help of ultrasound, followed by filtration, and the obtained solution was concentrated to give **4** with increased ee and dr values. [a]0.006 mmol of **COOH-BA** was employed. [b]The reaction was operated at 45 °C for 24 h.

developed one-pot aza-Darzens reaction and dissolution–filtration operation, a series of optically-pure CF_2-aziridines **4b–h** were furnished in moderate overall yields with uniformly excellent ee and dr values, including alkyl or halogen-substituted phenyl and 2-naphthyl ketones (Scheme 2). Unfortunately, phenylglyoxal monohydrates bearing strong electron-withdrawing groups were not compatible with the current conditions. X-ray analysis of aziridine **4a** confirmed the absolute configuration of the chiral centers, pointing at a *cis*-aziridination process [46].

Scaled-up experiments with model substrate **1a** also proved to be feasible, delivering the chiral CF_2-aziridine **4a** with comparable results (Scheme 3a). The 4-methoxyphenyl group of **4a** was cleaved smoothly with ceric ammonium nitrate, giving the free aziridine **5a** in 81% yield while maintaining the ee value. The reduction of the carbonyl moiety with either $NaBH_4$ or $LiAlH_4$ produced hydroxy-substituted CF_2-functionalized aziridine **5b** in excellent yield with exclusive diastereoselectivity [47]. Furthermore, the ring-opening of **4a** under acidic conditions underwent well and gave rise to CF_2-functionalized α-chloro-β-amino ketone **5c** in 89% yield with >99% ee and >50:1 dr (confirmed by X-ray spectroscopy) [46].

Conclusion

In summary, an array of chiral CF_2-functionalized aziridines was constructed from in situ-formed aldimines and difluorodiazoetyl phenyl sulfone under mild conditions by a combined strong Brønsted acid system consisting of chiral disulfonimide and 2-carboxyphenylboronic acid. The optical purity of the obtained CF_2-substituted aziridines could be further improved by a practical dissolution–filtration procedure. Substrate expansion and mechanistic investigation are underway and will be reported in due course.

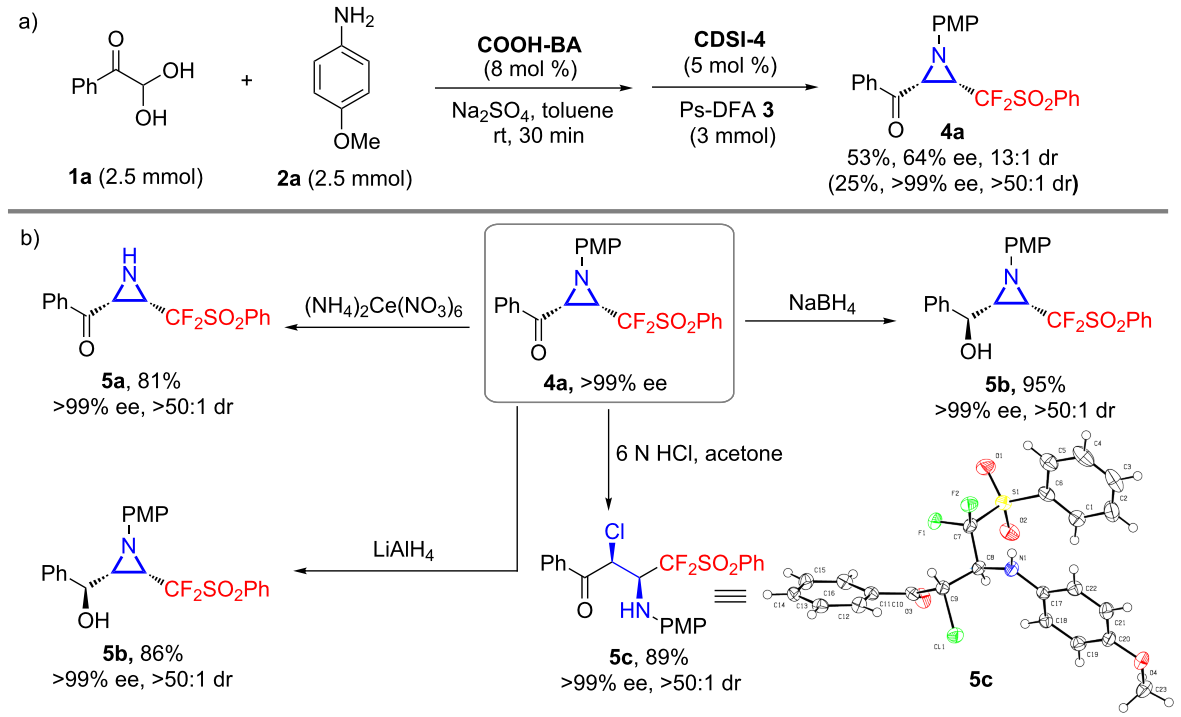

Scheme 3: Scale-up experiment to **4a** and further synthetic transformations.

Experimental

General procedure for the preparation of chiral CF_2-functionalized aziridines 4: To a 25 mL Schlenk tube equipped with a stirring bar were added 2,2-dihydroxy-1-arylethan-1-one (**1**, 0.3 mmol, 1 equiv), 4-methoxyaniline (**2a**, 40.6 mg, 0.33 mmol), 2-boronobenzoic acid (**COOH-BA**, 3.98 mg, 0.024 mmol), anhydrous Na_2SO_4 (200 mg) and toluene (1 mL) at room temperature under an argon atmosphere. After reacting for 30 minutes at room temperature, ((2-diazo-1,1-difluoroethyl)sulfonyl)benzene (Ps-DFA **3**, 104.5 mg, 77.4 uL, 0.45 mmol) was added with a micro syringe and **CDSI-4** (12.3 mg, 0.015 mmol) in toluene (1 mL) was added dropwise. The reaction was allowed to stir for 24 hours at room temperature under an argon atmosphere until the consumption of substrates was completed (as monitored by TLC). The reaction mixture was quenched with saturated aq $NaHCO_3$ and extracted with ethyl acetate three times. The combined organic layer was washed with water and brine, and then dried over anhydrous Na_2SO_4, filtered and evaporated under vacuum. The residue was purified by neutral alumina column chromatography (eluting with dichloromethane/petroleum ether) to give CF_2-substituted aziridine **4**. The enantiomeric excess was determined by chiral HPLC analysis. See Supporting Information File 1 for the dissolution–filtration procedure for each compound.

Supporting Information

Supporting Information File 1

Experimental procedures, compound characterization, NMR spectra of all new compounds, and HPLC traces.
[https://www.beilstein-journals.org/bjoc/content/supplementary/1860-5397-16-60-S1.pdf]

Supporting Information File 2

X-ray data for compound **4a**.
[https://www.beilstein-journals.org/bjoc/content/supplementary/1860-5397-16-60-S2.cif]

Supporting Information File 3

X-ray data for compound **5c**.
[https://www.beilstein-journals.org/bjoc/content/supplementary/1860-5397-16-60-S3.cif]

Funding

This work was supported by the National Key Research and Development Program of China (2019YFA0905100), National Natural Science Foundation of China (Nos. 21772142, 21901181, and 21961142015), and Tianjin Municipal Science & Technology Commission (19JCQNJC04700).

ORCID® iDs

Fa-Guang Zhang - https://orcid.org/0000-0002-0251-0456

Preprint

A non-peer-reviewed version of this article has been previously published as a preprint doi:10.3762/bxiv.2020.20.v1

References

1. Tanner, D. *Angew. Chem., Int. Ed. Engl.* **1994,** *33,* 599–619. doi:10.1002/anie.199405991
2. Sweeney, J. B. *Chem. Soc. Rev.* **2002,** *31,* 247–258. doi:10.1039/b006015l
3. Singh, G. S.; D'hooghe, M.; De Kimpe, N. *Chem. Rev.* **2007,** *107,* 2080–2135. doi:10.1021/cr0680033
4. Sweeney, J. *Eur. J. Org. Chem.* **2009,** 4911–4919. doi:10.1002/ejoc.200900211
5. Stanković, S.; D'hooghe, M.; Catak, S.; Eum, H.; Waroquier, M.; Van Speybroeck, V.; De Kimpe, N.; Ha, H.-J. *Chem. Soc. Rev.* **2012,** *41,* 643–665. doi:10.1039/c1cs15140a
6. de los Santos, J. M.; Ochoa de Retana, A. M.; Martínez de Marigorta, E.; Vicario, J.; Palacios, F. *ChemCatChem* **2018,** *10,* 5092–5114. doi:10.1002/cctc.201801026
7. Muller, K.; Faeh, C.; Diederich, F. *Science* **2007,** *317,* 1881–1886. doi:10.1126/science.1131943
8. Ma, J.-A.; Cahard, D. *Chem. Rev.* **2008,** *108,* PR1–PR43. doi:10.1021/cr800221v
9. Nie, J.; Guo, H.-C.; Cahard, D.; Ma, J.-A. *Chem. Rev.* **2011,** *111,* 455–529. doi:10.1021/cr100166a
10. Meanwell, N. A. *J. Med. Chem.* **2018,** *61,* 5822–5880. doi:10.1021/acs.jmedchem.7b01788
11. Rong, J.; Ni, C.; Hu, J. *Asian J. Org. Chem.* **2017,** *6,* 139–152. doi:10.1002/ajoc.201600509
12. Meyer, F. *Chem. Commun.* **2016,** *52,* 3077–3094. doi:10.1039/c5cc09414c
13. Dolfen, J.; De Kimpe, N.; D'hooghe, M. *Synlett* **2016,** *27,* 1486–1510. doi:10.1055/s-0035-1561379
14. Katagiri, T.; Ihara, H.; Takahashi, M.; Kashino, S.; Furuhashi, K.; Uneyama, K. *Tetrahedron: Asymmetry* **1997,** *8,* 2933–2937. doi:10.1016/s0957-4166(97)00320-0
15. Colantoni, D.; Fioravanti, S.; Pellacani, L.; Tardella, P. A. *Org. Lett.* **2004,** *6,* 197–200. doi:10.1021/ol0361554
16. Maeda, R.; Ooyama, K.; Anno, R.; Shiosaki, M.; Azema, T.; Hanamoto, T. *Org. Lett.* **2010,** *12,* 2548–2550. doi:10.1021/ol100768s
17. Künzi, S. A.; Morandi, B.; Carreira, E. M. *Org. Lett.* **2012,** *14,* 1900–1901. doi:10.1021/ol300539e
18. Yang, Y.; Huang, Y.; Qing, F.-L. *Tetrahedron Lett.* **2013,** *54,* 3826–3830. doi:10.1016/j.tetlet.2013.05.048
19. Dolfen, J.; Kenis, S.; Van Hecke, K.; De Kimpe, N.; D'hooghe, M. *Chem. – Eur. J.* **2014,** *20,* 10650–10653. doi:10.1002/chem.201304759
20. Wang, F.; Zhu, N.; Chen, P.; Ye, J.; Liu, G. *Angew. Chem., Int. Ed.* **2015,** *54,* 9356–9360. doi:10.1002/anie.201503412
21. Duan, Y.; Zhou, B.; Lin, J.-H.; Xiao, J.-C. *Chem. Commun.* **2015,** *51,* 13127–13130. doi:10.1039/c5cc04991a
22. Huang, Y.-J.; Qiao, B.; Zhang, F.-G.; Ma, J.-A. *Tetrahedron* **2018,** *74,* 3791–3796. doi:10.1016/j.tet.2018.05.033
23. Mészáros, Á.; Székely, A.; Stirling, A.; Novák, Z. *Angew. Chem., Int. Ed.* **2018,** *57,* 6643–6647. doi:10.1002/anie.201802347
24. Thi, H. D.; Thuy, G. L. N.; Catak, S.; Van Speybroeck, V.; Nguyen, T. V.; D'hooghe, M. *Synthesis* **2018,** *50,* 1439–1456. doi:10.1055/s-0036-1591537
25. Wu, K.; Zhou, C.-Y.; Che, C.-M. *Org. Lett.* **2019,** *21,* 85–89. doi:10.1021/acs.orglett.8b03514
26. Chai, Z.; Bouillon, J.-P.; Cahard, D. *Chem. Commun.* **2012,** *48,* 9471–9473. doi:10.1039/c2cc35246j
27. Mae, M.; Matsuura, M.; Amii, H.; Uneyama, K. *Tetrahedron Lett.* **2002,** *43,* 2069–2072. doi:10.1016/s0040-4039(02)00205-8
28. Palacios, F.; Ochoa de Retana, A. M.; Alonso, J. M. *J. Org. Chem.* **2006,** *71,* 6141–6148. doi:10.1021/jo060865g
29. Liu, J.; Hu, J. *Chem. – Eur. J.* **2010,** *16,* 11443–11454. doi:10.1002/chem.201000893
30. Kurosato, F.; Ishikawa, T.; Yamada, Y.; Hanamoto, T. *Synlett* **2015,** *26,* 1827–1830. doi:10.1055/s-0034-1381008
31. Zhang, W.; Wang, X.; Zhu, B.; Zhu, D.; Han, J.; Wzorek, A.; Sato, A.; Soloshonok, V. A.; Zhou, J.; Pan, Y. *Adv. Synth. Catal.* **2017,** *359,* 4267–4273. doi:10.1002/adsc.201701066
32. Zeng, J.-L.; Chen, Z.; Zhang, F.-G.; Ma, J.-A. *Org. Lett.* **2018,** *20,* 4562–4565. doi:10.1021/acs.orglett.8b01854
33. Peng, X.; Xiao, M.-Y.; Zeng, J.-L.; Zhang, F.-G.; Ma, J.-A. *Org. Lett.* **2019,** *21,* 4808–4811. doi:10.1021/acs.orglett.9b01697
34. Zeng, J.-L.; Zhang, Y.; Zheng, M.-M.; Zhang, Z.-Q.; Xue, X.-S.; Zhang, F.-G.; Ma, J.-A. *Org. Lett.* **2019,** *21,* 8244–8249. doi:10.1021/acs.orglett.9b02989
35. Zhang, Z.-Q.; Zheng, M.-M.; Xue, X.-S.; Marek, I.; Zhang, F.-G.; Ma, J.-A. *Angew. Chem., Int. Ed.* **2019,** *58,* 18191–18196. doi:10.1002/anie.201911701
36. Zhang, Y.; Wang, J. *Chem. Commun.* **2009,** 5350–5361. doi:10.1039/b908378b
37. Zhang, Y.; Lu, Z.; Wulff, W. D. *Synlett* **2009,** 2715–2739. doi:10.1055/s-0029-1217979
38. Pellissier, H. *Adv. Synth. Catal.* **2014,** *356,* 1899–1935. doi:10.1002/adsc.201400312
39. Liu, Y. *Curr. Org. Chem.* **2016,** *20,* 19–28. doi:10.2174/1385272819666150810225618
40. Yamamoto, H.; Futatsugi, K. *Angew. Chem., Int. Ed.* **2005,** *44,* 1924–1942. doi:10.1002/anie.200460394
41. Dimitrijević, E.; Taylor, M. S. *ACS Catal.* **2013,** *3,* 945–962. doi:10.1021/cs4000848
42. Hashimoto, T.; Gálvez, A. O.; Maruoka, K. *J. Am. Chem. Soc.* **2013,** *135,* 17667–17670. doi:10.1021/ja407764u
43. Huang, B.; He, Y.; Levin, M. D.; Coelho, J. A. S.; Bergman, R. G.; Toste, F. D. *Adv. Synth. Catal.* **2020,** *362,* 295–301. doi:10.1002/adsc.201900816
44. Zhang, Q.-X.; Li, Y.; Wang, J.; Yang, C.; Liu, C.-J.; Li, X.; Cheng, J.-P. *Angew. Chem., Int. Ed.* **2020,** *59,* 4550–4556. doi:10.1002/anie.201915226
45. James, T.; van Gemmeren, M.; List, B. *Chem. Rev.* **2015,** *115,* 9388–9409. doi:10.1021/acs.chemrev.5b00128
46. CCDC 1983642 (**4a**) and 1983643 (**5c**) contain the supplementary crystallographic data. The crystallographic data can be obtained free of charge via http://www.ccdc.cam.ac.uk/data_request/cif. It should be mentioned that the stereochemistry of 3-CF_2-aziridines in this reaction (2*R*,3*S*) are opposite to that of 3-CF_3-aziridines (2*S*,3*R*) in Cahard's report ([26]). We hypothesized that the enantiodetermining step in our reaction might be controlled through an in situ formed chiral boronate complex from chiral disulfonimide and 2-carboxyphenylboronic acid. Further efforts to improve the level of stereoselectivity and detailed mechanistic elucidation are still undergoing in our lab.

47. The stereochemistry of compound **5b** was determined based on the ^{1}H NMR, ^{19}F NMR, and 2D NOE analysis. In the 2D NOE spectrum, the correlation between HO (4.83 ppm) and HC–N (2.7 ppm) was observed, whereas no correlation between HC–O (3.7 ppm) and HC–CF_2 (3.02 ppm) was found.

License and Terms

This is an Open Access article under the terms of the Creative Commons Attribution License (http://creativecommons.org/licenses/by/4.0). Please note that the reuse, redistribution and reproduction in particular requires that the authors and source are credited.

The license is subject to the *Beilstein Journal of Organic Chemistry* terms and conditions: (https://www.beilstein-journals.org/bjoc)

The definitive version of this article is the electronic one which can be found at: doi:10.3762/bjoc.16.60

BEILSTEIN JOURNAL OF ORGANIC CHEMISTRY

Cascade trifluoromethylthiolation and cyclization of *N*-[(3-aryl)propioloyl]indoles

Ming-Xi Bi[1], Shuai Liu[1], Yangen Huang[1], Xiu-Hua Xu[*2] and Feng-Ling Qing[*1,2]

Letter

Open Access

Address:
[1]Key Laboratory of Science and Technology of Eco-Textiles, Ministry of Education, College of Chemistry, Chemical Engineering and Biotechnology, Donghua University, 2999 North Renmin Lu, Shanghai 201620, China and [2]Key Laboratory of Organofluorine Chemistry, Center for Excellence in Molecular Synthesis, Shanghai Institute of Organic Chemistry, University of Chinese Academy of Science, Chinese Academy of Science, 345 Lingling Lu, Shanghai 200032, China

Email:
Xiu-Hua Xu[*] - xuxiuhua@sioc.ac.cn; Feng-Ling Qing[*] - flq@mail.sioc.ac.cn

* Corresponding author

Keywords:
cyclization; indole derivatives; oxidation; radical reaction; trifluoromethylthiolation

Beilstein J. Org. Chem. **2020,** *16,* 657–662.
doi:10.3762/bjoc.16.62

Received: 20 January 2020
Accepted: 24 March 2020
Published: 08 April 2020

This article is part of the thematic issue "Organo-fluorine chemistry V".

Guest Editor: D. O'Hagan

© 2020 Bi et al.; licensee Beilstein-Institut.
License and terms: see end of document.

Abstract

A cascade oxidative trifluoromethylthiolation and cyclization of *N*-[(3-aryl)propioloyl]indoles with $AgSCF_3$ is described. This protocol allows for the synthesis of novel bis(trifluoromethylthiolated) or trifluoromethylthiolated pyrrolo[1,2-*a*]indol-3-ones in moderate to good yields. Mechanistic investigations indicated that radical processes were probably involved in these transformations.

Introduction

The trifluoromethylthio (SCF_3) group could significantly improve the lipophilicity of organic molecules as shown by its high Hansch constant (π = 1.44 for SCF_3, 0.88 for CF_3, and 0.61 for SMe) [1] that helps permeation across biological membranes. Furthermore, the strong electron-withdrawing properties of the SCF_3 group (Hammett constants: σ_p = 0.50, σ_m = 0.40) [2] with respect to metabolic stability have attracted considerable interest in pharmaceutical and agrochemical industries [3-5]. Traditional methods to access these compounds mainly include halogen–fluorine exchange of halomethyl sulfides and trifluoromethylation of sulfur-containing compounds [6-8]. Over the last decade, tremendous efforts have been triggered to develop methods for the direct incorporation of the SCF_3 group into organic compounds [9-16], such as alkynes, alkenes, arenes, and alkanes. Despite these impressive advances, there is a continued strong demand for new methods

that enable the efficient synthesis of SCF_3-containing compounds, especially those featuring medicinally promising scaffolds.

Pyrrolo[1,2-*a*]indol-3-ones are prevalent scaffolds that widely exist in many bioactive compounds and natural products [17-20]. Representative examples of biologically active pyrrolo[1,2-*a*]indol-3-one derivatives are shown in Figure 1. Recently, the development of efficient methods for the synthesis of pyrrolo[1,2-*a*]indol-3-one derivatives has attracted considerable attention. For instance, Song [21] and Liang [22] reported the one-pot synthesis of novel phosphorylated and sulfonylated pyrrolo[1,2-*a*]indol-3-ones from *N*-[(3-phenyl)propioloyl]indole and *N*-propargylindoles, respectively. Inspired by these elegant results, we became interested in the preparation of SCF_3-substituted pyrrolo[1,2-*a*]indol-3-ones, which might be potentially useful in medicinal chemistry.

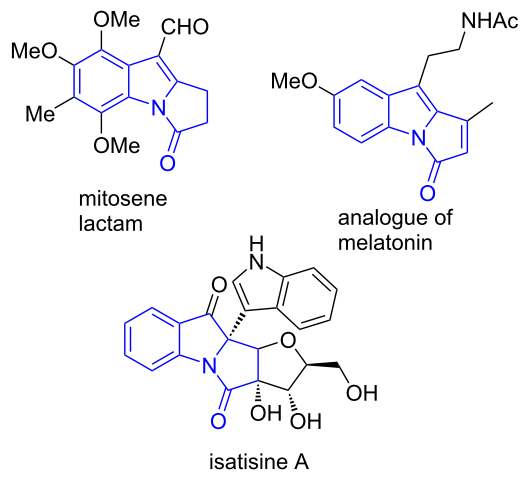

Figure 1: Representative examples of biologically active pyrrolo[1,2-*a*]indol-3-one derivatives.

Radical cascade reactions constitute highly efficient strategies for the construction of compounds with structural diversity and complexity. In 2014, Wang reported the first radical cascade trifluoromethylthiolation and cyclization of activated alkenes (Scheme 1a) [23]. Afterward, Nevado [24], Hopkinson and Glorius [25], Dagousset and Magnier [26], as well as Fu [27] applied this strategy in the synthesis of a series of CH_2SCF_3-substituted heterocycles. For the construction of SCF_3-substituted cyclic compounds, normally proper alkynes are chosen as the substrates for cascade reactions [28-32]. In 2015, Wang developed an oxidative radical cyclization of aryl alkynoate esters with $AgSCF_3$ for the synthesis of trifluoromethylthiolated coumarins (Scheme 1b) [28]. In 2016, Liu exploited the tandem trifluoromethylthiolation/cyclization of *N*-arylpropiolamides to construct the SCF_3-substituted spiro[4,5]trienones (Scheme 1c) [29]. In the same year, Zhang and Chen disclosed the transformation of arylpropynones to SCF_3-substituted indenones through the tandem trifluoromethylthiolation/cyclization processes (Scheme 1d) [30]. As part of our continuing research interest in radical trifluoromethylthiolation reactions [33-38], herein we disclose a cascade trifluoromethylthiolation and cyclization of *N*-[(3-aryl)propioloyl]indoles to access SCF_3-substituted pyrrolo[1,2-*a*]indol-3-ones (Scheme 1e).

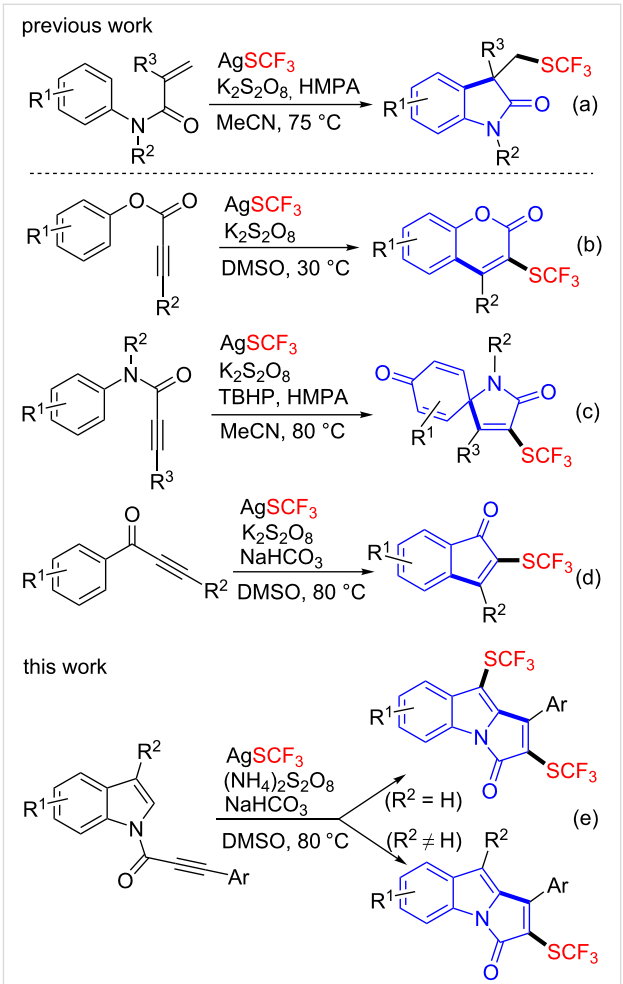

Scheme 1: Radical cascade trifluoromethylthiolation and cyclization reactions.

Results and Discussion

On the outset, 1-(1*H*-indol-1-yl)-3-phenylprop-2-yn-1-one (**1a**) was chosen as the model substrate for optimization of the reaction conditions (Table 1). To our surprise, the reaction of **1a** and $AgSCF_3$ in the presence of $K_2S_2O_8$ and $KHCO_3$ in DMSO at 80 °C gave bis(trifluoromethylthiolated) product **2a** in 28% yield (Table 1, entry 1). Only trace of mono(trifluoromethylthiolated) product was detected, and most of the substrate **1a** was not converted. To the best of our knowledge, the combination of bis(trifluoromethylthiolation) [36,39-41] and cascade cycli-

Table 1: Optimization of the reaction conditions[a].

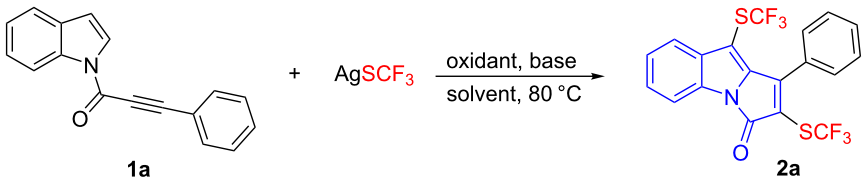

entry	oxidant	base	solvent	yield (%)[b]
1	$K_2S_2O_8$	$KHCO_3$	DMSO	28
2[c]	$K_2S_2O_8$	$KHCO_3$	DMSO	52
3[c]	$Na_2S_2O_8$	$KHCO_3$	DMSO	55
4[c]	$(NH_4)_2S_2O_8$	$KHCO_3$	DMSO	58
5[c]	$(NH_4)_2S_2O_8$	K_2CO_3	DMSO	40
6[c]	$(NH_4)_2S_2O_8$	$NaHCO_3$	DMSO	72
7[c]	$(NH_4)_2S_2O_8$	DBU	DMSO	34
8[c]	$(NH_4)_2S_2O_8$	$NaHCO_3$	MeCN	8
9[c]	$(NH_4)_2S_2O_8$	$NaHCO_3$	DMF	trace
10[d]	$(NH_4)_2S_2O_8$	$NaHCO_3$	DMSO	80

[a]Reaction conditions: **1a** (0.1 mmol), $AgSCF_3$ (0.15 mmol), oxidant (0.2 mmol), base (0.15 mmol), solvent (2.0 mL), 80 °C, 12 h. [b]Yield was determined by ^{19}F NMR using trifluorotoluene as an internal standard. [c]$AgSCF_3$ (0.3 mmol), oxidant (0.3 mmol). [d]$AgSCF_3$ (0.3 mmol), oxidant (0.3 mmol), base (0.1 mmol).

zation reactions has not been reported before. Thus, the amounts of $AgSCF_3$ and $K_2S_2O_8$ were increased to deliver **2a** in 52% yield (Table 1, entry 2). Other oxidants including $Na_2S_2O_8$ and $(NH_4)_2S_2O_8$ afforded **2a** in slightly higher yields, respectively (Table 1, entries 3 and 4). Switching $KHCO_3$ to $NaHCO_3$ could enhance the yield (Table 1, entry 6), whereas K_2CO_3 and DBU reduced the reaction efficiency (Table 1, entries 5 and 7). Subsequent evaluation of solvents revealed that MeCN and DMF were inferior to DMSO (Table 1, entries 8 and 9). Gratifyingly, the yield was improved to 80% by reducing the amount of base to 1.0 equivalent (Table 1, entry 10).

With the optimized reaction conditions in hand, we then set out to explore the substrate scope of *N*-[(3-aryl)propioloyl]indoles (Scheme 2). First, we explored the effect of the substitution on the indole ring. Both electron-donating and withdrawing groups at different positions of the indole ring produced the bis(trifluoromethylthiolated) products **2a–o** in moderate to good yields. A wide range of functionalities such as alkyl, alkoxy, nitro, nitrile, ester, aldehyde, fluoro, chloro, and bromo were well-tolerated and compatible under the mild reaction conditions. Substrate **1p** containing a methyl substituent on the phenyl ring could also participate in the reaction and furnish the desired product in moderate yield. However, attempts to prepare the substrates bearing an alkyl or electron-deficient aryl substituent on the alkynone were not successful. The structure of product **2a** was unambiguously identified by single-crystal X-ray analysis.

When the *N*-[(3-aryl)propioloyl]indole substrates (**3a–d**) with different substituents at the 3-position of the indole ring were subjected to the standard conditions, the cascade trifluoromethylthiolation and cyclization occurred to yield trifluoromethylthiolated pyrrolo[1,2-*a*]indol-3-ones (**4a–d**) in moderate yields (Scheme 3). The functionalities including alkyl, aryl, nitrile, and acyl were also well tolerated in this reaction.

In order to gain insight into the reaction mechanism, the radical scavenger 2,2,6,6-tetramethylpiperidin-1-oxyl (TEMPO) was added to the standard reactions of **1a** and **3b**, respectively. The desired product **2a** was not formed and only trace of **4b** was detected (see the Supporting Information File 1), which suggested that the radical process was probably involved in these transformations. Notably, no TEMPO-trapped product was detected by ^{19}F NMR spectra of the crude reaction mixtures. On the basis of these results and literature studies [21,23,42-47], a plausible reaction mechanism was proposed in Scheme 4. First, oxidation of $AgSCF_3$ by $(NH_4)_2S_2O_8$ generates $Ag^{II}SCF_3$, which could be further transformed to the CF_3S radical or CF_3SSCF_3 [23,36]. Then, the addition of a CF_3S radical to the alkyne function of substrates **1** or **3** afforded intermediate **A**. Subsequently, cyclization of intermediate **A**, followed by oxidation with $(NH_4)_2S_2O_8$, gave intermediate **C** [21,42-47]. Finally, deprotonation of intermediate **C** ($R^2 \neq H$) with $NaHCO_3$ delivered the aromatized product **4**. In the case of intermediate **C** ($R^2 = H$), intermediate **D** was probably formed, and further

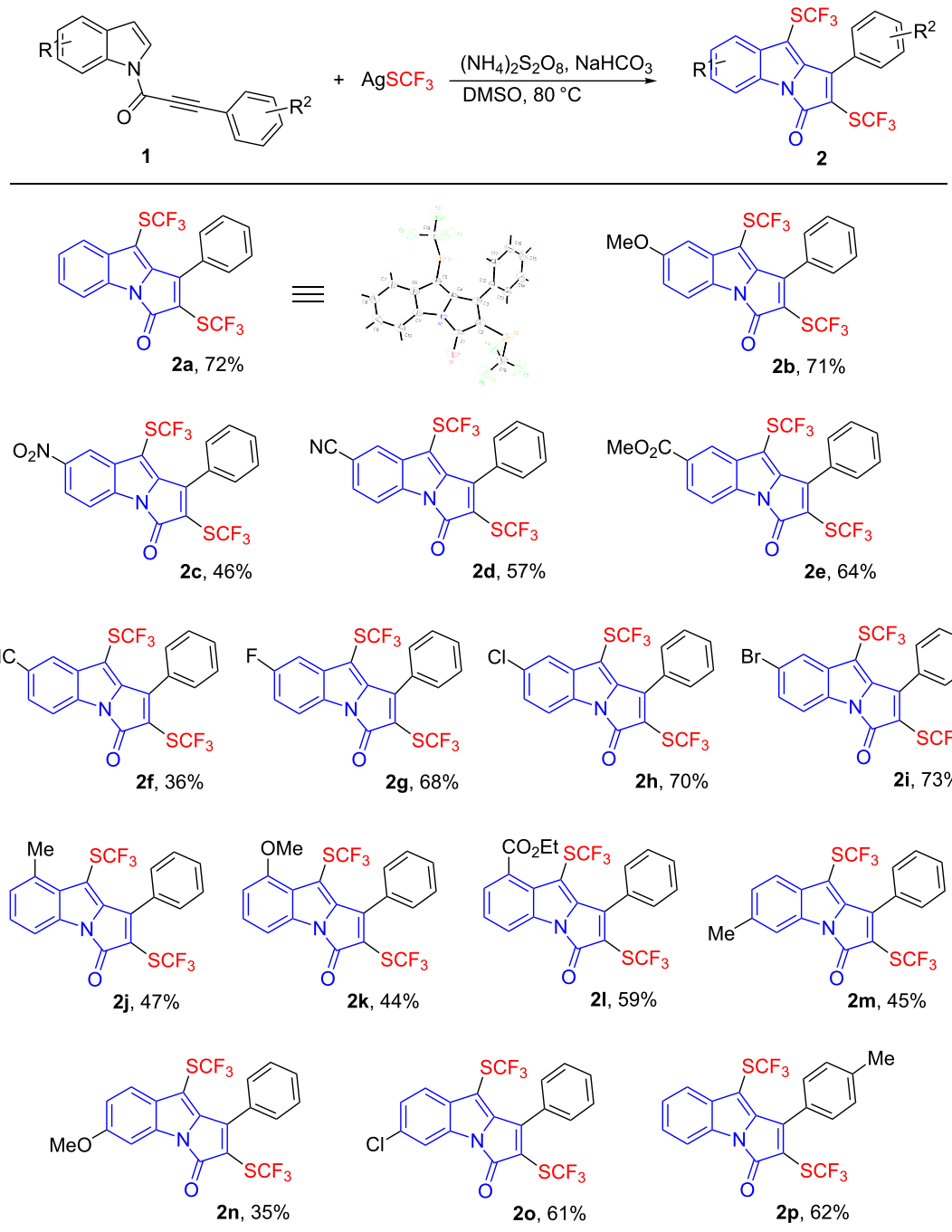

Scheme 2: Cascade bis(trifluoromethylthiolation) and cyclization of *N*-[(3-aryl)propioloyl]indoles **1**. Reaction conditions: **1** (0.25 mmol), $AgSCF_3$ (0.75 mmol), $(NH_4)_2S_2O_8$ (0.75 mmol), $NaHCO_3$ (0.25 mmol), DMSO (5.0 mL), 80 °C, 12 h, isolated yields.

underwent electrophilic trifluoromethylthiolation with CF_3SSCF_3 [48,49] to furnish the bis(trifluoromethylthiolated) product **2**.

Conclusion

We have reported the cascade trifluoromethylthiolation and cyclization reactions for the preparation of novel and potentially useful SCF_3-containing pyrrolo[1,2-*a*]indol-3-ones. Oxidative trifluoromethylthiolation of *N*-[(3-aryl)propioloyl]indoles without substituent at the 3-position of the indole ring with $AgSCF_3$ afforded the bis(trifluoromethylthiolated) products in moderate to good yields, whereas the substrates with a substituent at the 3-position of the indole ring were converted to the mono(trifluoromethylthiolated) products in moderate yields.

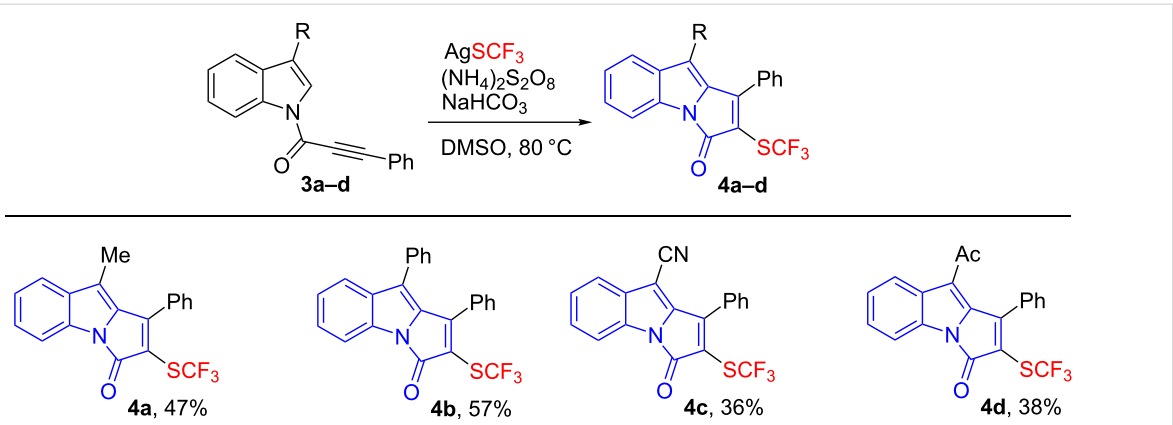

Scheme 3: Cascade trifluoromethylthiolation and cyclization of *N*-[(3-aryl)propioloyl]indoles **3**. Reaction conditions: **3** (0.25 mmol), $AgSCF_3$ (0.75 mmol), $(NH_4)_2S_2O_8$ (0.75 mmol), $NaHCO_3$ (0.25 mmol), DMSO (5.0 mL), 80 °C, 12 h, isolated yields.

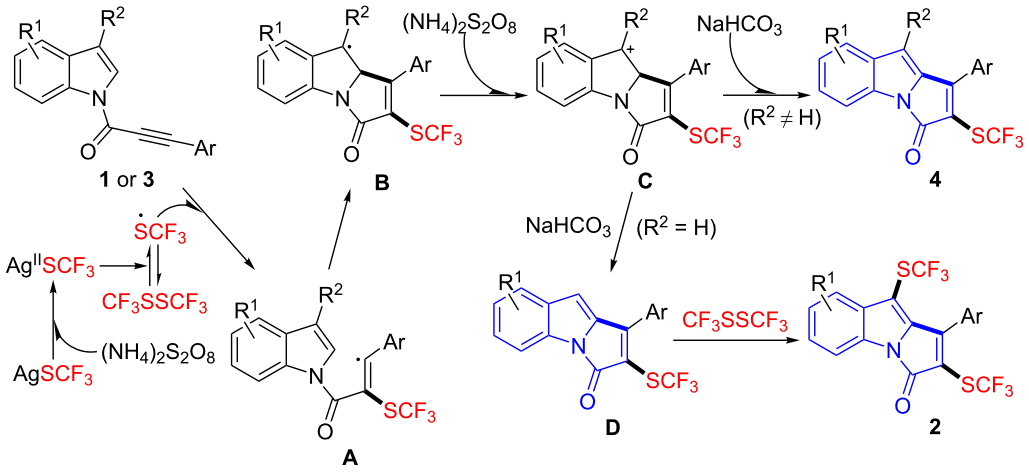

Scheme 4: Proposed reaction mechanism.

Further studies on applying radical cascade reactions to the construction of fluorine-containing heterocyclic scaffolds are in progress in our laboratory.

Supporting Information

Supporting Information File 1

Experimental procedures, spectroscopic and X-ray data (CCDC 1968129 for compound **2a**) and copies of NMR spectra.
[https://www.beilstein-journals.org/bjoc/content/supplementary/1860-5397-16-62-S1.pdf]

Funding

National Natural Science Foundation of China (21991121, 21421002), the Strategic Priority Research Program of the Chinese Academy of Sciences (XDB20000000), and Youth Innovation Promotion Association CAS (No. 2016234) are greatly acknowledged for funding this work.

ORCID® iDs

Xiu-Hua Xu - https://orcid.org/0000-0002-0759-2286

References

1. Hansch, C.; Leo, A.; Unger, S. H.; Kim, K. H.; Nikaitani, D.; Lien, E. J. *J. Med. Chem.* **1973,** *16,* 1207–1216. doi:10.1021/jm00269a003
2. Hansch, C.; Leo, A.; Taft, R. W. *Chem. Rev.* **1991,** *91,* 165–195. doi:10.1021/cr00002a004
3. Purser, S.; Moore, P. R.; Swallow, S.; Gouverneur, V. *Chem. Soc. Rev.* **2008,** *37,* 320–330. doi:10.1039/b610213c
4. Wang, J.; Sánchez-Roselló, M.; Aceña, J. L.; del Pozo, C.; Sorochinsky, A. E.; Fustero, S.; Soloshonok, V. A.; Liu, H. *Chem. Rev.* **2014,** *114,* 2432–2506. doi:10.1021/cr4002879
5. Meanwell, N. A. *J. Med. Chem.* **2018,** *61,* 5822–5880. doi:10.1021/acs.jmedchem.7b01788
6. Leroux, F.; Jeschke, P.; Schlosser, M. *Chem. Rev.* **2005,** *105,* 827–856. doi:10.1021/cr040075b

7. Boiko, V. N. *Beilstein J. Org. Chem.* **2010,** *6,* 880–921. doi:10.3762/bjoc.6.88
8. Manteau, B.; Pazenok, S.; Vors, J.-P.; Leroux, F. R. *J. Fluorine Chem.* **2010,** *131,* 140–158. doi:10.1016/j.jfluchem.2009.09.009
9. Chu, L.; Qing, F.-L. *Acc. Chem. Res.* **2014,** *47,* 1513–1522. doi:10.1021/ar4003202
10. Toulgoat, F.; Alazet, S.; Billard, T. *Eur. J. Org. Chem.* **2014,** 2415–2428. doi:10.1002/ejoc.201301857
11. Shao, X.; Xu, C.; Lu, L.; Shen, Q. *Acc. Chem. Res.* **2015,** *48,* 1227–1236. doi:10.1021/acs.accounts.5b00047
12. Xu, X.-H.; Matsuzaki, K.; Shibata, N. *Chem. Rev.* **2015,** *115,* 731–764. doi:10.1021/cr500193b
13. Chachignon, H.; Cahard, D. *Chin. J. Chem.* **2016,** *34,* 445–454. doi:10.1002/cjoc.201500890
14. Barata-Vallejo, S.; Bonesi, S.; Postigo, A. *Org. Biomol. Chem.* **2016,** *14,* 7150–7182. doi:10.1039/c6ob00763e
15. Zheng, H.; Huang, Y.; Weng, Z. *Tetrahedron Lett.* **2016,** *57,* 1397–1409. doi:10.1016/j.tetlet.2016.02.073
16. Hardy, M. A.; Chachignon, H.; Cahard, D. *Asian J. Org. Chem.* **2019,** *8,* 591–609. doi:10.1002/ajoc.201900004
17. Toyota, M.; Ihara, M. *Nat. Prod. Rep.* **1998,** *15,* 327–340. doi:10.1039/a815327y
18. Elmegeed, G. A.; Baiuomy, A. R.; Abdel-Salam, O. M. E. *Eur. J. Med. Chem.* **2007,** *42,* 1285–1292. doi:10.1016/j.ejmech.2007.01.027
19. Liu, J.-F.; Jiang, Z.-Y.; Wang, R.-R.; Zheng, Y.-T.; Chen, J.-J.; Zhang, X.-M.; Ma, Y.-B. *Org. Lett.* **2007,** *9,* 4127–4129. doi:10.1021/ol701540y
20. Bass, P. D.; Gubler, D. A.; Judd, T. C.; Williams, R. M. *Chem. Rev.* **2013,** *113,* 6816–6863. doi:10.1021/cr3001059
21. Xu, J.; Yu, X.; Song, Q. *Org. Lett.* **2017,** *19,* 980–983. doi:10.1021/acs.orglett.6b03713
22. Zhu, X.-Y.; Han, Y.-P.; Li, M.; Li, X.-S.; Liang, Y.-M. *Adv. Synth. Catal.* **2018,** *360,* 3460–3465. doi:10.1002/adsc.201800414
23. Yin, F.; Wang, X.-S. *Org. Lett.* **2014,** *16,* 1128–1131. doi:10.1021/ol403739w
24. Fuentes, N.; Kong, W.; Fernández-Sánchez, L.; Merino, E.; Nevado, C. *J. Am. Chem. Soc.* **2015,** *137,* 964–973. doi:10.1021/ja5115858
25. Honeker, R.; Garza-Sanchez, R. A.; Hopkinson, M. N.; Glorius, F. *Chem. – Eur. J.* **2016,** *22,* 4395–4399. doi:10.1002/chem.201600190
26. Dagousset, G.; Simon, C.; Anselmi, E.; Tuccio, B.; Billard, T.; Magnier, E. *Chem. – Eur. J.* **2017,** *23,* 4282–4286. doi:10.1002/chem.201700734
27. Zhu, M.; Fu, W.; Guo, W.; Tian, Y.; Wang, Z.; Ji, B. *Org. Biomol. Chem.* **2019,** *17,* 3374–3380. doi:10.1039/c9ob00342h
28. Zeng, Y.-F.; Tan, D.-H.; Chen, Y.; Lv, W.-X.; Liu, X.-G.; Li, Q.; Wang, H. *Org. Chem. Front.* **2015,** *2,* 1511–1515. doi:10.1039/c5qo00271k
29. Jin, D.-P.; Gao, P.; Chen, D.-Q.; Chen, S.; Wang, J.; Liu, X.-Y.; Liang, Y.-M. *Org. Lett.* **2016,** *18,* 3486–3489. doi:10.1021/acs.orglett.6b01702
30. Song, Y.-K.; Qian, P.-C.; Chen, F.; Deng, C.-L.; Zhang, X.-G. *Tetrahedron* **2016,** *72,* 7589–7593. doi:10.1016/j.tet.2016.10.013
31. Qiu, Y.-F.; Zhu, X.-Y.; Li, Y.-X.; He, Y.-T.; Yang, F.; Wang, J.; Hua, H.-L.; Zheng, L.; Wang, L.-C.; Liu, X.-Y.; Liang, Y.-M. *Org. Lett.* **2015,** *17,* 3694–3697. doi:10.1021/acs.orglett.5b01657
32. Qiu, Y.-F.; Niu, Y.-J.; Wei, X.; Cao, B.-Q.; Wang, X.-C.; Quan, Z.-J. *J. Org. Chem.* **2019,** *84,* 4165–4178. doi:10.1021/acs.joc.9b00181
33. Zhang, K.; Liu, J.-B.; Qing, F.-L. *Chem. Commun.* **2014,** *50,* 14157–14160. doi:10.1039/c4cc07062c
34. Pan, S.; Huang, Y.; Qing, F.-L. *Chem. – Asian J.* **2016,** *11,* 2854–2858. doi:10.1002/asia.201601098
35. Li, H.; Liu, S.; Huang, Y.; Xu, X.-H.; Qing, F.-L. *Chem. Commun.* **2017,** *53,* 10136–10139. doi:10.1039/c7cc06232j
36. Pan, S.; Li, H.; Huang, Y.; Xu, X.-H.; Qing, F.-L. *Org. Lett.* **2017,** *19,* 3247–3250. doi:10.1021/acs.orglett.7b01366
37. Pan, S.; Huang, Y.; Xu, X.-H.; Qing, F.-L. *Org. Lett.* **2017,** *19,* 4624–4627. doi:10.1021/acs.orglett.7b02249
38. Ouyang, Y.; Xu, X.-H.; Qing, F.-L. *Angew. Chem., Int. Ed.* **2019,** *58,* 18508–18512. doi:10.1002/anie.201911323
39. Tlili, A.; Alazet, S.; Glenadel, Q.; Billard, T. *Chem. – Eur. J.* **2016,** *22,* 10230–10234. doi:10.1002/chem.201601338
40. Mesgar, M.; Daugulis, O. *Org. Lett.* **2017,** *19,* 4247–4250. doi:10.1021/acs.orglett.7b01901
41. Liu, Y.-L.; Qing, F.-L.; Xu, X.-H. *Eur. J. Org. Chem.* **2020,** 1015–1018. doi:10.1002/ejoc.201901836
42. Zhang, H.; Li, W.; Zhu, C. *J. Org. Chem.* **2017,** *82,* 2199–2204. doi:10.1021/acs.joc.6b02673
43. Zhu, X.-Y.; Li, M.; Han, Y.-P.; Chen, S.; Li, X.-S.; Liang, Y.-M. *J. Org. Chem.* **2017,** *82,* 8761–8768. doi:10.1021/acs.joc.7b01497
44. Zhang, P.; Gao, Y.; Chen, S.; Tang, G.; Zhao, Y. *Org. Chem. Front.* **2017,** *4,* 1350–1353. doi:10.1039/c7qo00167c
45. Chen, H.; Liu, M.; Qiu, G.; Wu, J. *Adv. Synth. Catal.* **2019,** *361,* 146–150. doi:10.1002/adsc.201801038
46. Sun, K.; Chen, X.-L.; Zhang, Y.-L.; Li, K.; Huang, X.-Q.; Peng, Y.-Y.; Qu, L.-B.; Yu, B. *Chem. Commun.* **2019,** *55,* 12615–12618. doi:10.1039/c9cc06924k
47. Gharpure, S. J.; Shelke, Y. G. *Org. Lett.* **2017,** *19,* 5022–5025. doi:10.1021/acs.orglett.7b02005
48. Ma, L.; Cheng, X.-F.; Li, Y.; Wang, X.-S. *Tetrahedron Lett.* **2016,** *57,* 2972–2975. doi:10.1016/j.tetlet.2016.05.086
49. Chachignon, H.; Maeno, M.; Kondo, H.; Shibata, N.; Cahard, D. *Org. Lett.* **2016,** *18,* 2467–2470. doi:10.1021/acs.orglett.6b01026

License and Terms

This is an Open Access article under the terms of the Creative Commons Attribution License (http://creativecommons.org/licenses/by/4.0). Please note that the reuse, redistribution and reproduction in particular requires that the authors and source are credited.

The license is subject to the *Beilstein Journal of Organic Chemistry* terms and conditions: (https://www.beilstein-journals.org/bjoc)

The definitive version of this article is the electronic one which can be found at: doi:10.3762/bjoc.16.62

BEILSTEIN JOURNAL OF ORGANIC CHEMISTRY

Synthesis of organic liquid crystals containing selectively fluorinated cyclopropanes

Zeguo Fang[*1], Nawaf Al-Maharik[1,2], Peer Kirsch[3], Matthias Bremer[3], Alexandra M. Z. Slawin[*1] and David O'Hagan[*1]

Full Research Paper

Open Access

Address:
[1]School of Chemistry, Biomedical Sciences Research Complex, University of St Andrews, North Haugh, St Andrews, Fife KY16 9ST, United Kingdom, [2]Department of Chemistry, Faculty of Science, An Najah National University, Nablus, Palestine and [3]Merck KGaA, Liquid Crystal R&D Chemistry, Frankfurter Str. 250, 64293 Darmstadt, Germany

Email:
Zeguo Fang[*] - zf20@st-andrews.ac.uk; Alexandra M. Z. Slawin[*] - amzs@st-andrews.ac.uk; David O'Hagan[*] - do1@st-andrews.ac.uk

* Corresponding author

Keywords:
dielectric anisotropy; difluorocarbene; organic liquid crystals; selectively fluorinated cyclopropanes

Beilstein J. Org. Chem. **2020,** *16,* 674–680.
doi:10.3762/bjoc.16.65

Received: 08 February 2020
Accepted: 03 April 2020
Published: 14 April 2020

This article is part of the thematic issue "Organo-fluorine chemistry V".

Associate Editor: P. J. Skabara

© 2020 Fang et al.; licensee Beilstein-Institut.
License and terms: see end of document.

Abstract

This paper describes the synthesis of a series of organic liquid crystals (LCs) containing selectively fluorinated cyclopropanes at their termini. The syntheses used difluorocarbene additions to olefin precursors, an approach which proved straightforward such that these liquid crystal candidates could be efficiently prepared. Their physical and thermodynamic properties were evaluated and depending on individual structures, they either displayed positive or negative dielectric anisotropy. The study gives some guidance into effective structure–property relationships for the design of LCs containing selectively fluorinated cyclopropane motifs.

Introduction

Display materials associated with modern electronic devices such as personal mobile phones and TV sets, have changed dramatically in the past decades as liquid crystal display (LCD) technology has evolved [1,2]. A key challenge is to make suitable liquid crystalline (LC) materials that satisfy the requirements for different LCD technologies. For the traditional twisted nematic (TN) LCD technology, devices require liquid crystals with display positive dielectric anisotropy by which the molecular dipole moment is oriented parallel to the long axis of the molecule, while for the current vertical alignment (VA) LCD technology, liquid crystals with negative dielectric anisotropy are required [3]. Fluorine, as the most electronegative atom, forms stable bonds to carbon and can thus induce polarity. It is also attractive as a design feature due to the low polarizability of the C–F bond relative to other polar substituents such as nitrile and ester groups, and this reduces intermo-

lecular interactions leading to lower viscosities and thus increased life time reliability [4,5]. A significant effort has been devoted to the development of liquid crystals with either positive or negative dielectric anisotropy by introducing the C–F bond or the dipole of a CF_2 group either parallel or perpendicular to the long molecular axis. For example, in the area of negative liquid crystalline materials, Kirsch et al. have reported the synthesis of bicyclohexane and bis(cyclohexyl)ethane liquid crystals which contain axial fluorine substituents (Figure 1, **1** and **2**), however, due to the propensity for HF elimination from these molecules over time, these liquid crystals have not been adopted as commercial products [6,7]. 2,3-Difluoroaryl motifs such as **3** have proven to be a successful class of negative dielectric anisotropic liquid crystals and the more rigid 1,1,6,7-tetrafluoroindane **4** led to an enhanced polarity and improved negative dielectric anisotropy character [8]. Other liquid crystals of this class are the recently reported fluorinated cyclohexane **5** and 1,1,2,2-tetrafluorocyclohexane **6** [9,10], but the complexity of their synthesis has limited their development as practical materials.

As a consequence, it continues to be a research objective to introduce polar substituents in a manner that can influence the nature of the dielectric anisotropy of the resultant material. In this context we explore the cyclopropane motif containing fluorine atoms. Selectively fluorinated cyclopropanes have been widely used in pharmaceutical research [11], however, the introduction of fluorinated cyclopropanes into liquid crystal scaffolds has not received much attention. Haufe et al. [12], reported enantiomerically pure fluorinated diphenylcyclopropane carboxylates as potential chiral dopants to induce a cholesteric phase, but this was not extended to the exploration of positive or negative dielectrics. Recently, we reported the efficient synthesis of α,β,β-trifluorocyclopropanes **7** (Figure 2) through difluorocarbene addition to alpha-fluorostyrenes [13]. This used the extraordinary useful method for the generation of difluorocarbene from the Ruppert–Prakash ($TMSCF_3$) reagent [14]. DFT analysis suggests the lowest energy conformer of aryl α,β,β-trifluorocyclopropane **7** orients the C–F bond perpendicular to the aryl ring. So, if the α,β,β-trifluorocyclopropane motif were introduced into an appropriate LC scaffold, it could reasonably induce negative dielectric anisotropy if the dipole associated with the cyclopropane remains oriented perpendicular to the molecular axis. Based on this idea, we report the design and synthesis of cyclopropanes **8** and **9** with an objective to assess their LC properties. Cyclopropane **8** with a single CF_2 group offered a control to assess the influence of the alpha-fluorine atom in cyclopropane **9** containing three fluorines. In order to extend the study to explore other selectively fluorinated cyclopropane motifs we set out to prepare liquid crystal candidates **10** and isomers **11a** and **11b**. Ether **10** should have significant rotational freedom due to rotation around the ether bonds and will be compared with isomers **11a** and **11b** which are much more conformationally constrained (Figure 2).

Therefore, the aim of the study was to prepare these target liquid crystals and evaluate their properties relative to each other, to establish if there were any obvious structure–activity relationships to emerge for the design of positive or negative dielectric materials. Also the fixed spiro CF_2-containing cyclo-

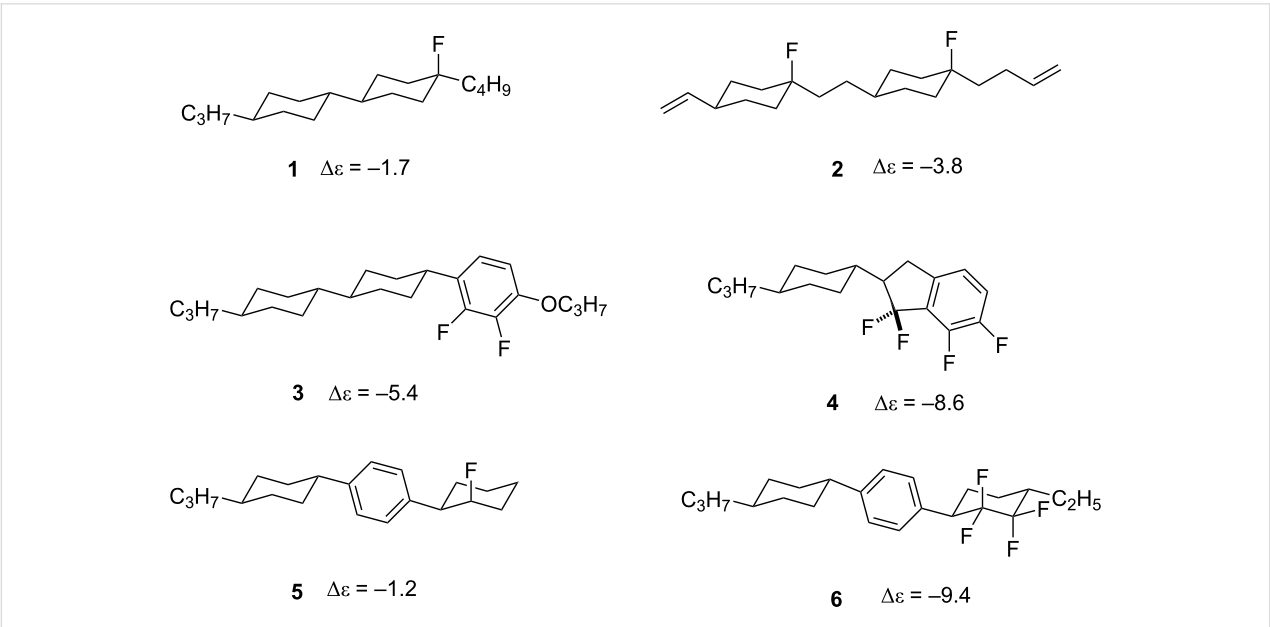

Figure 1: Examples of liquid crystal candidates with negative values for dielectric anisotropy (Δε) [6-10].

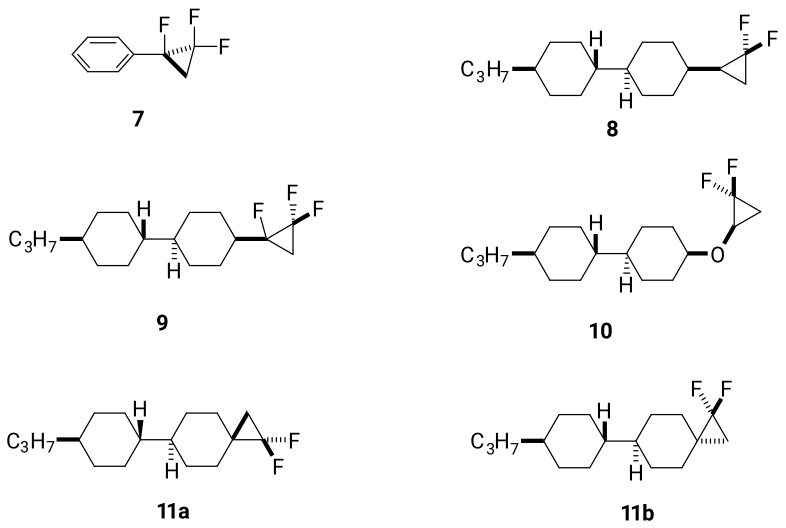

Figure 2: Synthetic candidate LC targets **8–11**.

propanes **11a** and **11b** became targets to assess the impact of a configurationally rigid bicyclic motif. It is relatively obvious that for each of these isomers the CF_2 dipole in each cyclopropane is orientated either along the molecular axis (for **11a**) or perpendicular to the molecular axis (for **11b**), and these were anticipated at the outset to give positive and negative dielectric anisotropy values, respectively.

Results and Discussion

Synthesis of liquid crystal candidates 8–11

The synthesis of cyclopropane **8** started from olefin **12** (supplied by Merck KGaA, Darmstadt), as illustrated in Scheme 1. Difluorocyclopropane **8** can be directly prepared through a [2 + 1] carbene cycloaddition reaction. Thus, treatment of **12** with trimethyl(trifluoromethyl)silane ($TMSCF_3$) and sodium iodide under refluxing conditions [13,14] gave the corresponding product **8** in one step and a 55% yield.

The synthesis of trifluorocyclopropane **9** is shown in Scheme 2. Compound **9** was prepared through bromofluorination of **12**, followed by base-induced HBr elimination [15], and then difluorocarbene addition to generate **9**. The starting olefin **12** was exposed to an excess of *N*-bromosuccinimide (NBS) and HF·Py to generate **13a** and **13b** as a mixture of regioisomers in a ratio of 4:1. There was no requirement to separate these isomers at this stage. Subsequent addition of potassium *tert*-butoxide into a mixture of **13a** and **13b** in dichloromethane (DCM) resulted in an efficient elimination to generate vinyl fluoride **14** as a major product. Vinyl fluoride **14** was purified by column chromatography in a 42% yield over the two steps. Finally, difluorocarbenene ($:CF_2$) addition using the $TMSCF_3$/NaI protocol was used to generate the target product **9** in 46% yield.

The preparation of cyclopropyl ether **10** was accomplished as illustrated in Scheme 3. Reduction of cyclohexanone **15** with $NaBH_4$ gave cyclohexanol **16** in a ratio of 2:1. The major *trans* product **16a** was purified as a single entity by column chromatography and was isolated in 45% yield. Vinyl ether **17** could be efficiently prepared using the methodology developed by Bosch [16]. Accordingly, treatment of **16a** with butyl vinyl ether, bathophenanthroline (BPhen) and Et_3N, using palladium(II) trifluoroacetate as a catalyst, gave vinyl ether **17** in 62% yield in a single step. Finally, difluorocarbene-mediated difluorocyclopropanation generated **10** in 50% yield.

The synthesis of the diastereoisomers of spiro LC candidates **11a** and **11b** also started from ketone **15** as illustrated in Scheme 4**.** Treatment of ketone **15** with methylenetriphenyl-

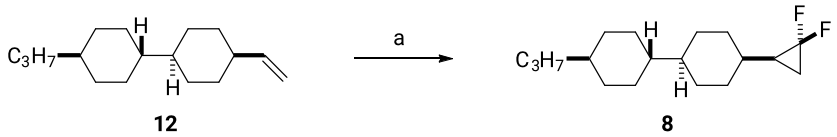

Scheme 1: Synthesis of **8**. Reagents and conditions: a) $TMSCF_3$, NaI, THF, reflux, 55% [13,14].

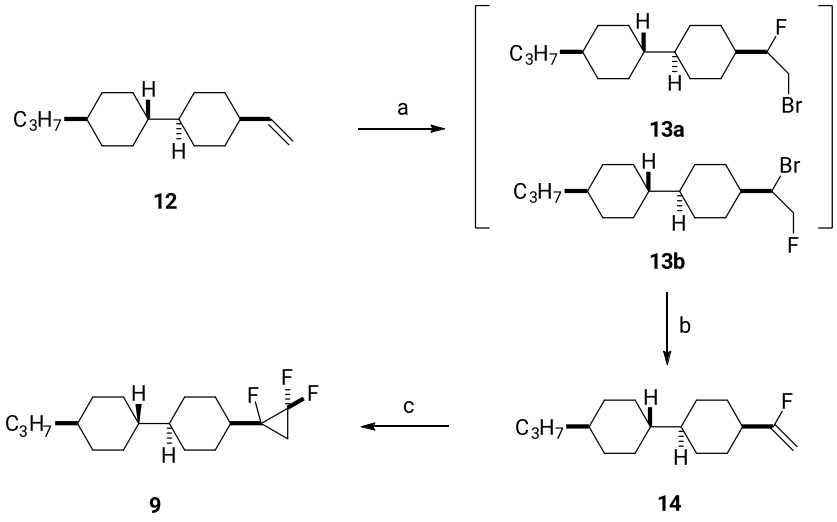

Scheme 2: Synthesis of **9**. Reagents and conditions: a) NBS, HF·Py, DCM; b) *t*-BuOK, DCM, 42% in two steps [15]; c) $TMSCF_3$, NaI, THF, reflux, 46%.

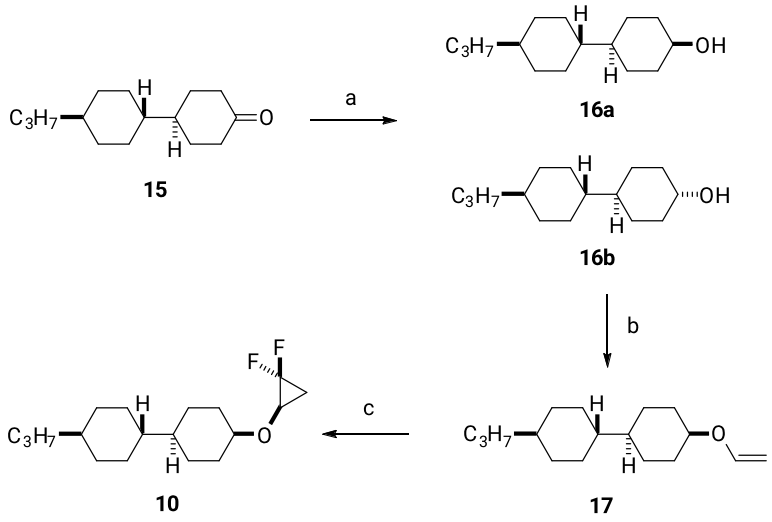

Scheme 3: Synthesis of compound **10**. Reagents and conditions: a) $NaBH_4$, MeOH, rt, 45%; b) $C_4H_9OCH{=}CH_2$, $Pd(TFA)_2$, BPhen, Et_3N, 75 °C, 62% [16]; c) $TMSCF_3$, NaI, THF, reflux, 50%.

phosphine which was generated in situ from methyltriphenylphosphonium bromide (PPh_3CH_3Br), generated *exo*-methylene cyclohexane **18** in a very straightforward manner, and the product could be isolated by chromatography in 72% yield [17]. This olefin was then subject to a difluorocarbene cyclopropanation using $TMSCF_3$ and NaI, and this generated both isomers, **11a** and **11b**, in a ratio of 5:1, respectively. After three recrystallizations, the major isomer **11a** could be isolated as a single stereoisomer. It proved impossible to isolate a sample of isomer **11b** without a significant and dominant contamination with **11a**. Thus, it was with some frustration that we were unable to prepare a suitable sample, both in quantity and purity, of isomer **11b** for subsequent analysis. Stereoisomer **11a** was a crystalline solid and a suitable crystal was subject to X-ray structure analysis and the structure is shown in Scheme 4. In this way the stereochemistry of **11a** and **11b** could be confirmed unambiguously.

Evaluation of liquid crystal candidates **8–11a**

With the four difluorocyclopropanes **8**–**11a** in hand, our attention focused on an experimental evaluation of their thermodynamic and physical properties, such as birefringence (Δn) and dielectric anisotropy ($\Delta\varepsilon$). DSC and POM analysis (Table 1) indicated that only compounds **8** and **9** exhibited smectic phases.

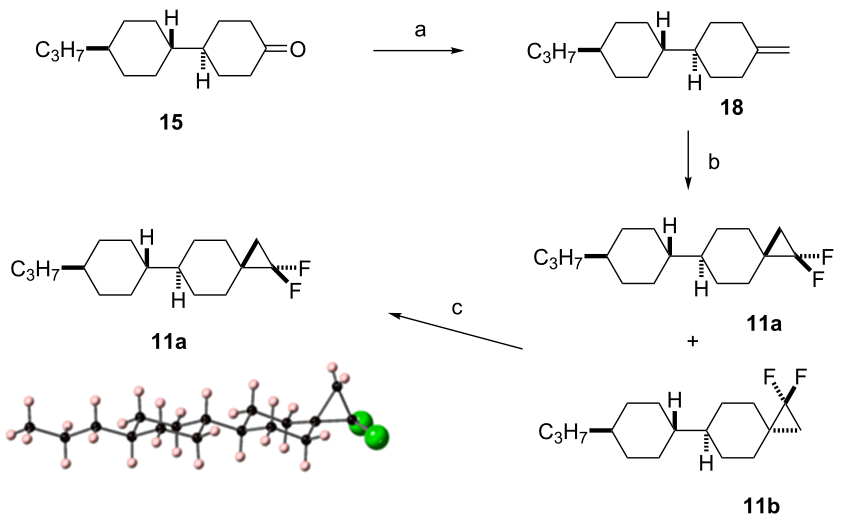

Scheme 4: Synthesis of compounds **11**. Reagents and conditions: a) PPh_3CH_3Br, *t*-BuOK, diethyl ether, 0 °C to rt, 72% [17]; b) $TMSCF_3$, NaI, THF, reflux; c) recrystallization, 27%.

The smectic phase of LC **8** was maintained over a broad temperature range (54–84 °C), whereas that for **10** and **11a** only showed a melting point and these compounds did not display any obvious liquid crystallinity (Table 1). Therefore, any development of these latter materials would require extended core structures to enhance their LC potential.

Table 1: Phase transition temperatures of compounds **8**–**11**.

	Phase transfer temperature [°C]
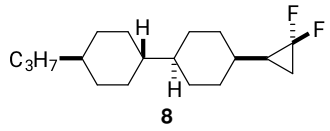 **8**	C 54 S_mB 84 I
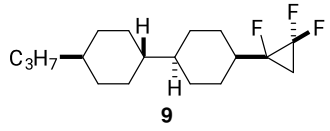 **9**	Tg –70 S_mB 82 I[a]
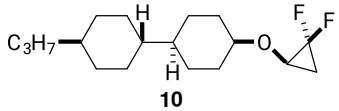 **10**	C35 I[a]
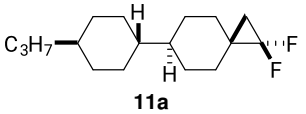 **11a**	C 42 I

[a]Decomposition (C = crystalline, S_mB = smectic B, I = isotropic, Tg = glass transition temperature).

The birefringence Δ*n* (Table 2) for compounds **8**–**11a** was measured (Abbe refractometer). In all cases the Δ*n* values were low, which is entirely consistent with their core aliphatic structures, unlike materials with aromatic rings. The differences for Δ*n* for **8**, **9** and **10**, were found to be small, whereas the spirocyclopropane **11a** had a significantly, decreased Δ*n*.

Table 2: Physical properties of compounds **8**–**11**.

Compound	Δ*n*	Δε
8[a]	0.056	–0.5
9[b]	0.055	–0.2
10[b]	0.063	1.3
11a[a]	0.036	4.8
11a[c]	0.054	4.3
11b[c]	0.051	–1.1

[a]Δ*n* were extrapolated from a 10 wt % solution in liquid crystal mixture Merck ZLI-4792. Δε were extrapolated from a 10 wt % solution in liquid crystal mixture Merck Merck ZLI-2857. [b]Δ*n* were extrapolated from a 5 wt % solution in liquid crystal mixture Merck ZLI-4792. Δε were extrapolated from a 10 wt % solution in liquid crystal mixture Merck Merck ZLI-2857. [c]Calculated data only at AM1//B3LYP/6-31G(d) level [18].

As discussed, either positive or negative dielectric anisotropy is an important parameter related to the driving voltage of LC displays and in order to reduce energy consumption, good materials should induce a large value for dielectric anisotropy. Compounds **8** and **9** were found to exhibit the expected negative Δε values, however, the overall polarity is low (**8** = −0.5, **9** = −0.2). This is presumably due to the ability of the C–C bond attached to cyclopropane to rotate, and thus the compound will adopt conformations with low overall molecular polarities. A comparison of the Δε for **8** and **9** illustrates that incorporation of the third alpha-fluorine lowers the overall Δε value. This is presum-

ably due to a resulting decrease in the overall molecular dipole moment ($\mu_\perp$) along the minor axis. When an ether was used as the linkage in compound **10**, the compound becomes more flexible and, perhaps surprisingly, the overall Δε parameter became more positive. Clearly the effect of introducing a C–O bond renders this molecule dissimilar from the others in this series. However, changing the core aliphatic structure to the more rigid spiro structure **11a**, brought about a dramatic enhancement of the molecular dipole moment ($\mu_\parallel$), resulting in a much more positive and increased parameter value (Δε = 4.8). This experimental value was close to the predicted calculated value (Δε = 4.3) as shown in Table 2. It is clear that there is an advantage in a rigid structure for imparting a maximum polarity. As stated above, we were unable to obtain a stereochemically pure sample of diastereoisomer **11b**, free from **11a**, however, theory indicates that **11b** should display negative dielectric anisotropy, although the magnitude of the parameter was relatively low (Δε = −1.1). Thus the two isomers constitute two different classes of LC materials, entirely as a consequence of stereochemistry.

The best compound of this series is **11a** and it was of interest to get some insight into its conformational flexibility. Thus, a conformational analysis of **11a** (and **11b**) was conducted computationally (ωB97X-D/6-311+G(2d,p)//ωB97X-D/6-31G(d) + ZPE level (see Supporting Information File 1)). There are many potential low energy conformations arising from alkyl side chain C–C bond rotations which would not be anticipated to change the overall properties significantly, however, we were interested in assessing the energy required for the bispirocyclohexane ring to adopt an axial rather than the lower energy equatorial arrangement. For **11a**, the lowest energy conformer found was a rotamer around the central C–C bond linking the cyclohexane rings, but an essentially isoenergetic conformer is that found in the X-ray crystal structure. The first conformers where the terminal bispirocyclohexane ring lies axial are significantly higher in energy (ΔG = +1.25 kcal/mol^{-1} and ΔG = +1.19 kcal/mol^{-1}) than the equatorial conformers as illustrated in Figure 3. Notably for both the axial and equatorial conformers, the orientation of the CF_2 group, and therefore its dipole, remains perpendicular to the long molecular axis (requirement for +ve dielectric). A similar result was obtained for stereoisomer **11b** (see Supporting Information File 1) again with the first axial conformer at ΔG = +1.14 kcal/mol^{-1} above the ground state equatorial conformer. In this case the orientation of the CF_2 group, and therefore the dipole, remains perpendicular to the long molecular axis (requirement for −ve dielectric) for both the axial and equatorial conformers. This analysis, and that of the X-ray structure, suggests that the equatorial conformers will dominate in condensed phases, and that the overall molecular dipoles will not be compromised by minor contributions of axial conformers.

Conclusion

In conclusion, a series of candidate liquid crystals **8–11a** with difluorocyclopropane motifs at their termini were prepared in a straightforward manner. In all cases the cyclopropane was introduced by difluorocarbene addition to an olefin, the difluorocar-

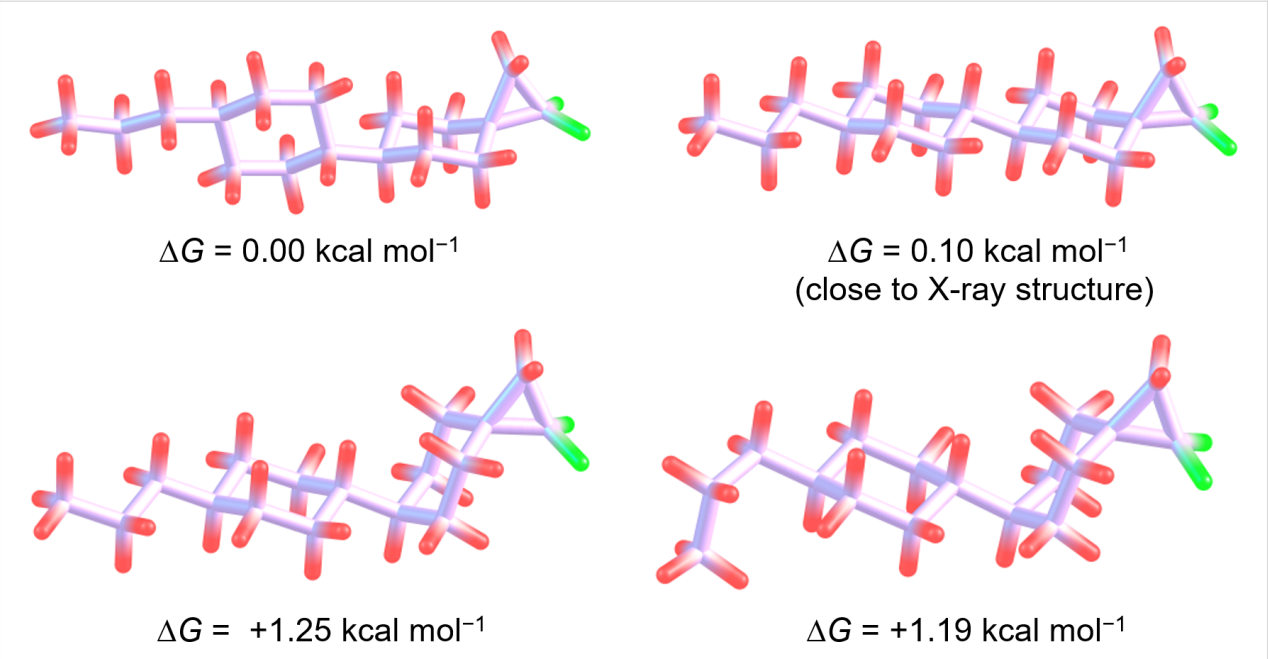

Figure 3: Theory study exploring the relative energies for different conformers of **11a**.

bene being generated from $TMSCF_3$/NaI. An evaluation of the physical properties of LC candidates **8**–**11a** revealed that LC's **8** and **9** exhibited smectic phases with low levels of negative dielectric anisotropy. The relatively high positive dielectric anisotropy of compound **11a** indicates that the configurational constrained motif is required to increase the magnitude of the Δε parameter. Although it proved challenging to isolate a stereochemically clean sample of isomer **11b** for experimental evaluation, theory predicts that it will have a modest negative dielectric value, indicating the importance of stereochemistry in dictating the class of LC material. We conclude too that the overall performance of prototype LCs **11a** and **11b** should not be compromised by conformational flexibility. Although none of the compounds prepared here met all of the criteria for commercial development, the study gives an insight into the potential for this novel difluorocyclopropane motif in liquid crystal design and development.

Supporting Information

Supporting Information File 1

Experimental protocols and NMR spectra.
[https://www.beilstein-journals.org/bjoc/content/supplementary/1860-5397-16-65-S1.pdf]

Supporting Information File 2

Crystallographic information file of compound **11a**.
[https://www.beilstein-journals.org/bjoc/content/supplementary/1860-5397-16-65-S2.cif]

Acknowledgements

The EPSRC Mass Spectroscopy Service at Swansea is acknowledged for analysis.

Funding

We thank the Chinese Scholarship Council for a studentship (ZF).

ORCID® iDs

Nawaf Al-Maharik - https://orcid.org/0000-0002-7014-6190
Peer Kirsch - https://orcid.org/0000-0002-9024-7933
Alexandra M. Z. Slawin - https://orcid.org/0000-0002-9527-6418
David O'Hagan - https://orcid.org/0000-0002-0510-5552

References

1. Kirsch, P. *Modern Fluoroorganic Chemistry,* 2nd ed.; Wiley-VCH: Weinheim, Germany, 2013. doi:10.1002/9783527651351
2. Kirsch, P.; Bremer, M. *Angew. Chem., Int. Ed.* **2000,** *39,* 4216–4235. doi:10.1002/1521-3773(20001201)39:23<4216::aid-anie4216>3.0.co;2-k
3. Hird, M. *Chem. Soc. Rev.* **2007,** *36,* 2070–2095. doi:10.1039/b610738a
4. O'Hagan, D. *Chem. Soc. Rev.* **2008,** *37,* 308–319. doi:10.1039/b711844a
5. Bremer, M.; Kirsch, P.; Klasen-Memmer, M.; Tarumi, K. *Angew. Chem., Int. Ed.* **2013,** *52,* 8880–8896. doi:10.1002/anie.201300903
6. Kirsch, P.; Tarumi, K. *Angew. Chem., Int. Ed.* **1998,** *37,* 484–489. doi:10.1002/(sici)1521-3773(19980302)37:4<484::aid-anie484>3.0.co;2-6
7. Kirsch, P.; Heckmeier, M.; Tarumi, K. *Liq. Cryst.* **1999,** *26,* 449–452. doi:10.1080/026782999205236
8. Bremer, M.; Lietzau, L. *New J. Chem.* **2005,** *29,* 72–74. doi:10.1039/b414312d
9. Al-Maharik, N.; Kirsch, P.; Slawin, A. M. Z.; Cordes, D. B.; O'Hagan, D. *Org. Biomol. Chem.* **2016,** *14,* 9974–9980. doi:10.1039/c6ob01986b
10. Yamada, S.; Hashishita, S.; Konishi, H.; Nishi, Y.; Kubota, T.; Asai, T.; Ishihara, T.; Konno, T. *J. Fluorine Chem.* **2017,** *200,* 47–58. doi:10.1016/j.jfluchem.2017.05.013
11. Fang, Z.; Cordes, D. B.; Slawin, A. M. Z.; O'Hagan, D. *Chem. Commun.* **2019,** *55,* 10539–10542. doi:10.1039/c9cc05749h
12. Hruschka, S.; Fröhlich, R.; Kirsch, P.; Haufe, G. *Eur. J. Org. Chem.* **2007,** 141–148. doi:10.1002/ejoc.200600579
13. Thomson, C. J.; Zhang, Q.; Al-Maharik, N.; Bühl, M.; Cordes, D. B.; Slawin, A. M. Z.; O'Hagan, D. *Chem. Commun.* **2018,** *54,* 8415–8418. doi:10.1039/c8cc04964e
14. Wang, F.; Luo, T.; Hu, J.; Wang, Y.; Krishnan, H. S.; Jog, P. V.; Ganesh, S. K.; Prakash, G. K. S.; Olah, G. A. *Angew. Chem., Int. Ed.* **2011,** *50,* 7153–7157. doi:10.1002/anie.201101691
15. Meyer, O. G. J.; Fröhlich, R.; Haufe, G. *Synthesis* **2000,** 1479–1490. doi:10.1055/s-2000-7103
16. Bosch, M.; Schlaf, M. *J. Org. Chem.* **2003,** *68,* 5225–5227. doi:10.1021/jo034376h
17. Conner, M. L.; Brown, M. K. *J. Org. Chem.* **2016,** *81,* 8050–8060. doi:10.1021/acs.joc.6b01446
18. Dewar, M. J. S.; Zoebisch, E. G.; Healy, E. F.; Stewart, J. J. P. *J. Am. Chem. Soc.* **1985,** *107,* 3902–3909. doi:10.1021/ja00299a024

License and Terms

This is an Open Access article under the terms of the Creative Commons Attribution License (http://creativecommons.org/licenses/by/4.0). Please note that the reuse, redistribution and reproduction in particular requires that the authors and source are credited.

The license is subject to the *Beilstein Journal of Organic Chemistry* terms and conditions: (https://www.beilstein-journals.org/bjoc)

The definitive version of this article is the electronic one which can be found at:
doi:10.3762/bjoc.16.65

BEILSTEIN JOURNAL OF ORGANIC CHEMISTRY

Efficient synthesis of dipeptide analogues of α-fluorinated β-aminophosphonates

Marcin Kaźmierczak*[1,2] and Henryk Koroniak[1]

Full Research Paper

Open Access

Address:
[1]Faculty of Chemistry, Adam Mickiewicz University in Poznań, Uniwersytetu Poznańskiego 8, 61-614 Poznań, Poland and [2]Centre for Advanced Technologies, Adam Mickiewicz University in Poznań, Uniwersytetu Poznańskiego 10, 61-614 Poznań, Poland

Email:
Marcin Kaźmierczak* - marcin.kazmierczak@amu.edu.pl

* Corresponding author

Keywords:
dipeptide analogues; fluorinated aminophosphonates; fluorine; nucleophilic fluorination; phosphorus

Beilstein J. Org. Chem. **2020,** *16,* 756–762.
doi:10.3762/bjoc.16.69

Received: 14 February 2020
Accepted: 02 April 2020
Published: 16 April 2020

This article is part of the thematic issue "Organo-fluorine chemistry V".

Guest Editor: D. O'Hagan

© 2020 Kaźmierczak and Koroniak; licensee Beilstein-Institut.
License and terms: see end of document.

Abstract

Herein, we present an efficient synthesis of dipeptide analogues of α-fluorinated β-aminophosphonates. Each step of the synthesis was optimized to provide excellent yields. Moreover, the absolute configuration of the obtained compounds was determined by X-ray analysis, which proved the stereochemistry that was proposed based on NMR studies.

Introduction

The chemistry of fluorinated aminophosphonates is constantly being developed, mainly due to their wide spectra of applications. What is more, they are valuable targets for biomedical investigations. Due to the strong interest in this type of compounds, several marvelous reviews about the synthesis and application of fluorinated aminophosphonates have been published in recent years [1-3]. To the best of our knowledge, among the many applications of fluorinated aminophosphonates and aminophosphonic acid derivatives, they exhibit antiviral [4,5], antibacterial [6] and antifungal [7] activities. Moreover, α-fluorinated phosphonates can be considered as hydrolytically stable mimics of naturally occurring phosphates [8]. Due to the fact that enzyme binding may depend on the C–F stereochemistry, the synthesis of such compounds with a specific configuration is very important [9-11]. α-Fluorinated phosphonates can be prepared by many different protocols [12-16].

Nucleophilic fluorination is one of the fundamental reactions in organic chemistry in the field of the synthesis of building blocks with a potential biological activity. To date, scientists have developed many nucleophilic fluorinating reagents [17-19]. Among others, we can distinguish a family of such chemicals having in their structure a sulfonyl fluoride system. For example 2-pyridinesulfonyl fluoride (PyFluor, **1**) [20,21] or perfluorobutanesulfonyl fluoride (PBSF, **2**) [22,23] (Figure 1). On

the other hand, Hu just recently presented a novel deoxyfluorination reagent with a similar structure to **1** and **2**, containing a sulfonimidoyl instead of sulfonyl group. 4-Chloro-*N*-tosylbenzene-1-sulfonimidoyl fluoride (SulfoxFluor, **3**, Figure 1) may be an interesting alternative to **1** or **2**. It is not commercially available yet, however, it can be obtained from inexpensive materials [24].

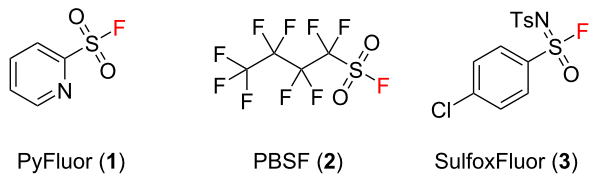

Figure 1: Chemical structure of PyFluor, PBSF and SulfoxFluor.

Very often small organic molecules containing a fluorine atom are transformed into biologically active compounds. As an example, we can consider peptide bond formation between an amine and a carboxylic acid. This transformation is a very important reaction in organic synthesis and therefore, many coupling reagents are available on the market [25-29].

Our previous studies have shown that the regioselectivity of the nucleophilic fluorination of amino alcohols can be controlled depending on the fluorinating reagent used [30,31]. This work presents the optimization of nucleophilic fluorination conditions. What is more, we discuss the effect of the base used on the regioselectivity of the fluorination reaction. The absolute configuration of the obtained compounds was determined and confirmed by X-ray analysis. Furthermore, we present the use of α-fluorinated β-aminophosphonates as building blocks in the synthesis of their dipeptide analogues. In addition, we show the results of the use of several coupling reagents in the synthesis of amide bonds.

Results and Discussion

Our goal was to increase the efficiency of the synthesis of α-fluorinated β-aminophosphonate dipeptide analogues **15**. In the first stage, we optimized Pudovik's reaction (Scheme 1) [32].

In our previous studies, the Pudovik reaction worked with satisfactory yield and diastereoselectivity [30]. Unfortunately, we were not able to isolate the pure *anti*-isomer in every case. The latest research shows that this reaction can successfully be carried out under milder conditions, without any solvent and in the presence of a weak base [33]. After testing many modifications, it turned out that the use of triethylamine (1 equiv) as a base, and without a solvent, gave the best results with aldehydes **4** (1 equiv) and diethyl phosphite (1 equiv). These conditions not only increased the diastereoselectivity of the Pudovik reaction, but also improved its yield drastically (Table 1). The implementation of this allowed us to obtain the *anti*-isomer (1*R*,2*S*) in very good yields.

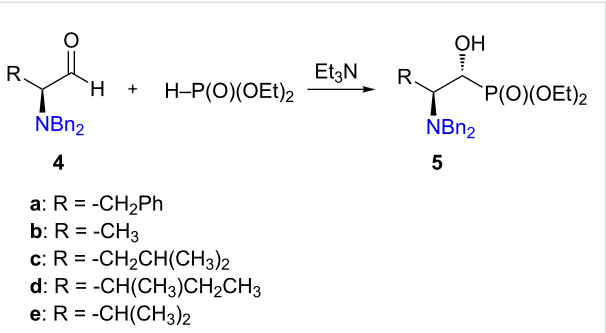

Scheme 1: Synthesis of **5**.

Table 1: Optimization of reaction conditions.

entry	product	*anti*/*syn*[a]	*anti*/*syn*[b]	yield[c]
1	**5a**	91:9	99:1	86%
2	**5b**	86:14	99:1	71%
3	**5c**	90:10	99:1	75%
4	**5d**	92:8	99:1	88%
5	**5e**	90:10	99:1	79%

[a]Crude reaction mixture ratio based on ^{31}P NMR. [b]Ratio after isolation based on ^{31}P NMR. [c]Yield of the amino alcohol **5** after isolation.

There are not many literature examples of the regioselective fluorination of amino alcohols using by PyFluor (**1**) or PBSF (**2**). In general, the fluorination reactions with these reagents require the use of a base as an activator [20]. Doyle demonstrated the combination between PyFluor or PBSF and bases such as 1,8-diazabicyclo[5.4.0]undec-7-ene (DBU, **6**), 7-methyl-1,5,7-triazabicyclo[4.4.0]dec-5-ene (MTBD, **7**), 2-*tert*-butyl-1,1,3,3-tetramethylguanidine (BTMG) **8**, *tert*-butylimino-tri(pyrrolidino)phosphorane (BTPP, **9**, Figure 2) [21]. We screened the alcohols **5** against sulfonyl fluoride reagents **1** and **2** and a combination of selected bases **6–9** (Scheme 2). All reactions during the optimization step were carried out on a 0.1 mmol scale under an argon atmosphere while the reaction medium was toluene.

In the first stage of the optimization three representative amino alcohols were chosen. Each bearing a different group in the side chain: an aromatic (**5a**), a small (**5b**) and a large aliphatic substituent (**5c**). Unfortunately, under the tested conditions, we did not observe a complete regioselectivity of the fluorination reac-

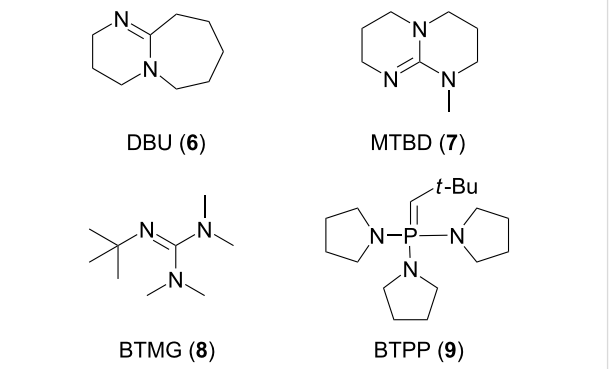

Figure 2: Chemical structure bases.

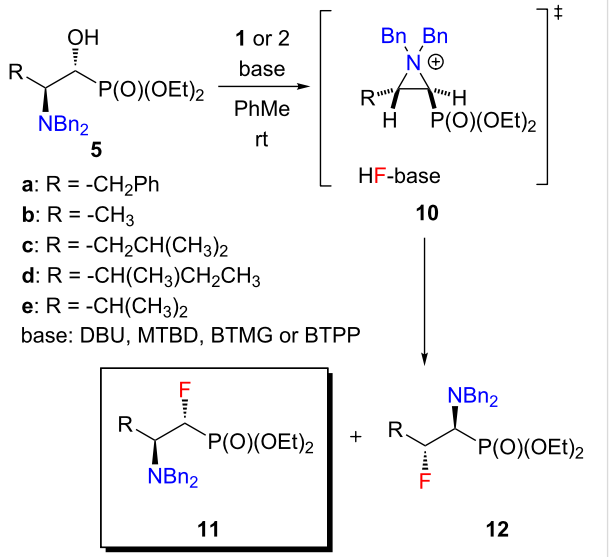

Scheme 2: Synthesis of **11**.

tion. Nevertheless, in each case, the use of PyFluor as a nucleophilic fluorinating reagent and MTBD as an activator improved the regioselectivity of this reaction, as well as, the yield of the α-isomer **11** (best results are shown in Table 2, for all tested conditions see Table S1 in Supporting Information File 1). In our experience, there was no significant correlation between steric bulkiness of the base (from DBU to BTPP) used, and the yield of α-isomer **11** formation. It is worth mentioning that application of PBSF gives slightly worse results in each case. We assume it is associated with a much greater reactivity of this reagent in relation to PyFluor.

The mechanism of the PyFluor-mediated deoxyfluorination of the α-hydroxy-β-aminophosphonates **5** was previously proposed. Based on spectroscopic studies (^{19}F,^{1}H-HOESY, ^{1}H,^{1}H-NOESY, as well as *J*-couplings) a relative configuration of *N*,*N*-dibenzyl-protected α-fluoro-β-aminophosphonates **11** was

Table 2: Optimization of reaction conditions.

entry	product	reagent	base	**11**/**12** ratio[a]	yield[b]
1	**11a**	PyFluor	MTBD	73:27	61%
2	**11b**	PyFluor	MTBD	60:40	47%
3	**11c**	PyFluor	MTBD	87:13	70%
4	**11d**	PyFluor	MTBD	68:32	59%
5	**11e**	PyFluor	MTBD	82:18	69%

[a]Crude reaction mixture ratio based on ^{31}P NMR and ^{19}F NMR; [b]Yield of α-fluorides **11** after isolation.

established as (1*R*,2*S*), but we failed to crystallize these compounds [31]. That is why the removal of the benzyl protecting group from fluorides **11** and the transfer of the free amines **13** into the salts **14** was applied. The salts **14** could be then crystallized and subjected to X-ray studies.

A standard *N*–debenzylation protocol was employed to remove the benzyl protecting group. The hydrogenolysis reaction was catalyzed by palladium on carbon (Pd/C), and was carried out in trifluoroethanol (TFE) as a solvent [34,35]. The free amines **13** were converted into stable oxalate salts **14** with quantitative yields. The precipitation reactions proceeded in the presence of 1 equiv of oxalic acid in diethyl ether (Scheme 3) [36]. Unlike amines **13**, salts **14** are very stable and can be stored for months at room temperature.

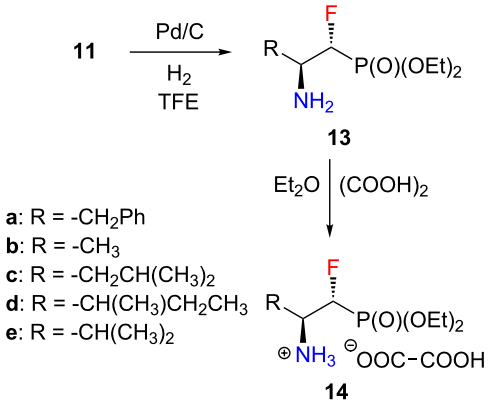

Scheme 3: Synthesis of **13** and **14**.

What is more, we attempted to crystallize at least one derivative to confirm the absolute stereochemistry of the obtained compounds. In order to obtain a single crystal suitable for X-ray diffraction studies, various crystallization techniques were tested [37,38]. Crystallization of derivative **14c** from D_2O brought the expected results. The analysis confirmed the structure of the resulting compound **14c**. The absolute configuration of **14c** is consistent with the stereochemistry we proposed based

on NMR studies. The crystals of **14c** contained the (1*R*,2*S*)-diastereoisomer (Figure 3). The correct absolute configuration was determined on the basis of Flack and Parson's parameters, as well as of slightly better R factors for the correct model.

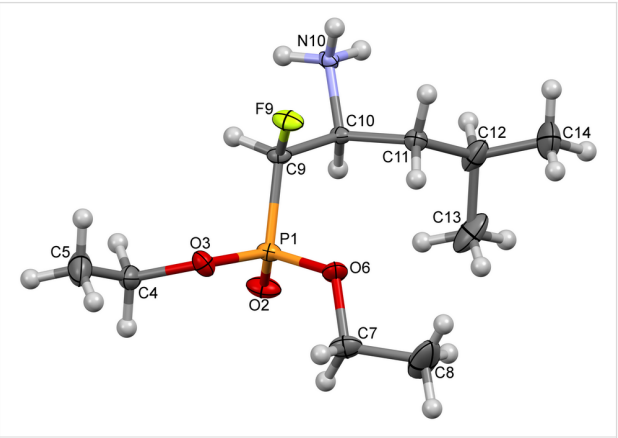

Figure 3: Molecular structure of compound (1*R*,2*S*)-**14c** (ORTEP image).

Moreover, amines **13** were used as substrates in the formation of peptide bonds with *N*-Boc-phenylalanine (Boc-Phe-OH, Scheme 4). For this purpose we examined several coupling reagents available on the market. We chose amine **13a** as a model substrate. In each case, the amine–acid coupling reaction proceeded with good to excellent yields (Table 3). At the beginning a mixture of *N*,*N*′-dicyclohexylcarbodiimide (DCC) [39] and 1-hydroxybenzotriazole (HOBt) [40] was used. The reaction took place "only" in good yield (63%). Crude products required very careful purification due to the byproduct formed during the reaction – *N*,*N*′-dicyclohexylurea (DCU), which is insoluble in the solvents used in the synthesis (CH_2Cl_2, DMF). Replacing DCC with *N*-(3-dimethylaminopropyl)-*N*′-ethylcarbodiimide hydrochloride (EDCI) [41] significantly increased the reaction yield (86%). What is more, the reaction byproduct is water-soluble and easy to remove by extraction. Nevertheless, HOBt was still used as an additive. This reagent has recently been reported to exhibit explosive properties [42]. Fortunately, stable 1-hydroxybenzotriazole substitutes are available on the market, and can be used in the reaction of peptide bond formation [43]. One of them is OxymaPure [44] which was successfully employed as a replacement for HOBt. Using EDCI/OxymaPure conditions, an even greater yield of the product formation (88%) was observed, however, the reaction still required a long reation time. Finally, COMU [45] as a coupling reagent was applied. The model reaction took place with a yield of 92% after just two hours. COMU allowed to obtain the dipeptide analogue **15a** not only with an excellent yield, but also in a very short time. Under these conditions, the remaining amines **13** were reacted, to receive a series of dipeptide analogues of α-fluorinated β-aminophosphonates **15**.

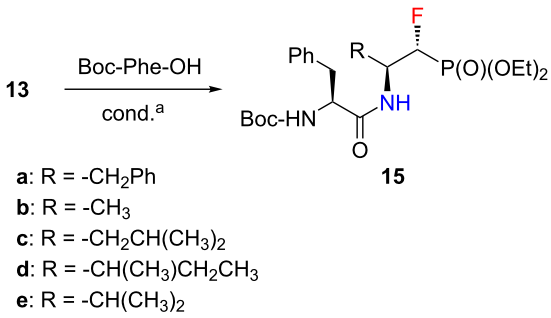

Scheme 4: Synthesis of **15**.
[a]Conditions are given in the Experimental section.

Conclusion

In summary, an efficient approach to the synthesis of dipeptide analogues of α-fluorinated β-aminophosphonates **15** was presented. These compounds were prepared in a four-step sequence starting from *N*,*N*-dibenzylamino aldehydes **5**. Each step of the synthesis has been optimized to provide very good yields (Pudovik, deoxyfluorination and amine–acid coupling reac-

Table 3: Optimization of reaction conditions.

entry	product	reagent	additive	base	time	yield[a]
1	15a	DCC	HOBt	Et_3N	24 h	63%
2	15a	EDCI	HOBt	Et_3N	18 h	86%
3	15a	EDCI	OxymaPure	DIPEA	18 h	88%
4	15a	COMU	–	DIPEA	2 h	92%
5	15b	COMU	–	DIPEA	3 h	91%
6	15c	COMU	–	DIPEA	3 h	94%
7	15d	COMU	–	DIPEA	3 h	92%
8	15e	COMU	–	DIPEA	3 h	92%

[a]Yield of dipeptide analogues **15** after isolation.

tions). Furthermore, the absolute configuration of the obtained compounds has been confirmed by X-ray analysis, which is consistent with the stereochemistry proposed based on NMR studies. Dipeptide analogues of α-fluorinated β-aminophosphonates **15** presented in this publication, after deprotection of the amine function appear to be attractive compounds with potential biological activity.

Experimental

General methods

^{1}H NMR, ^{13}C NMR, ^{19}F NMR and ^{31}P NMR spectra were obtained on a Bruker ASCEND 400 (400 MHz) and a Bruker ASCEND 600 (600 MHz) spectrometer. All 2D spectra were recorded on a Bruker ASCEND 600 (600 MHz) spectrometer. ^{1}H NMR chemical shifts were expressed in parts per million downfield from tetramethylsilane (TMS) as an internal standard (δ = 0) in $CDCl_3$ or CD_3CN. ^{13}C NMR chemical shifts were expressed in parts per million downfield from $CDCl_3$ (δ = 77.0) or CD_3CN (δ = 1.39) as internal standards. ^{19}F NMR chemical shifts were expressed in parts per million upfield from $CFCl_3$ as an internal standard (δ = 0) in $CDCl_3$ or CD_3CN. ^{31}P NMR Chemical shifts were expressed in parts per million in $CDCl_3$ or CD_3CN. High-resolution mass spectra were recorded by electron spray (ESIMS) techniques using a QToF Impact HD Bruker spectrometer. Reagent grade chemicals were used. Solvents were dried with CaH_2 (CH_2Cl_2), NaH (Et_2O), P_2O_5 (PhMe), and distilled under argon atmosphere. All moisture sensitive reactions were carried out under an argon atmosphere using ovendried glassware. TLC was performed on Merck Kieselgel 60-F254 with EtOAc/hexane and MeOH/$CHCl_3$ as developing systems, and products were detected by inspection under UV light (254 nm) and with a solution of potassium permanganate. Merck Kieselgel 60 (0.063–0.200 μm), Merck Kieselgel 60 (0.040–0.063 μm), and Merck Kieselgel 60 (0.015–0.004 μm), were used for column chromatography.

X-ray diffraction data for **14c** were collected at 100(1) K by the ω-scan technique on Rigaku four-circle Xcalibur diffractometer (Eos detector) with graphite-monochromatized Mo Kα radiation (λ = 0.71073 Å). The data were corrected for Lorentz-polarization and absorption effects [46]. Accurate unit cell parameters were determined by a least-squares fit of 4300 reflections of highest intensity, chosen from the whole experiment. The structure was solved with SHELXT and refined with the full-matrix least-squares procedure on F2 by SHELXL [47]. All non-hydrogen atoms were refined anisotropically, hydrogen atoms were placed in the calculated positions and refined as 'riding model' with the isotropic displacement parameters set at 1.2 (1.5 for methyl and hydroxy groups) times the U_{eq} value for appropriate non-hydrogen atom. As the crystals were obtained from D_2O solution, this solvent was used for final model (although, no difference between refinements with H_2O and D_2O could be found). The correct absolute configuration was determined on the basis of Flack and Parson's parameters, as well as of slightly better R factors for the correct model. The crystallographic data for the structural analysis has been deposited with the Cambridge Crystallographic Data Centre, CCDC No. 1977323 (**14c**). Copies of this information may be obtained free of charge from http://www.ccdc.cam.ac.uk.

Procedure for the synthesis of amino alcohols **5**

TEA (1,0 equiv) was added under an argon atmosphere to a mixture of a stirred solution of diethyl phosphite (1,0 equiv) and the appropriate aldehyde **4** (1,0 equiv). The reaction mixture was stirred at room temperature overnight, diluted with 20 mL of water and extracted with ethyl acetate (3 × 15 mL). The organic layers were washed with $NaCl_{sat.}$, dried over $MgSO_4$ or Na_2SO_4, filtrated and concentrated under reduced pressure. The crude products were isolated using column chromatography (chloroform → chloroform/methanol 100:0.5 v/v). The NMR spectroscopic data for amino alcohols **5** were in good agreement with our previous research [30,31,48].

Procedure for the synthesis of fluorides **11**

PyFluor (1,2 equiv) or PBSF (1,2 equiv) and base (2 equiv) were added under an argon atmosphere to a stirred solution of amino alcohol **5** (1mmol) in 2,5 mL PhMe, under an argon atmosphere. The reaction mixture was stirred at room temperature until completion of the reaction monitored by TLC (3–18 h). The reaction mixture was then diluted with 20 mL of water and extracted with ethyl acetate (3 × 15 mL). The organic layers were dried over $MgSO_4$ or Na_2SO_4, filtrated and concentrated under reduced pressure. The crude products were isolated using column chromatography (*n*-hexane/ethyl acetate 90:10, v/v → *n*-hexane/ethyl acetate 60:40, v/v). The NMR spectroscopic data for fluorides **11** were in good agreement with our previous research [31].

Procedure for the synthesis of amines **13**

The amines **13** were prepared in a similar manner as described in [35]. Fluoride **11** (1 equiv) was dissolved in 5 mL of TFE and then 10% Pd/C (20% v/v) was added. The solution was stirred under an atmosphere of hydrogen at room temperature for 3 days. After this time the catalyst was filtered off (Celite), the solvent was evaporated and the crude product was purified using flash chromatography (chloroform/methanol 100:0, v/v chloroform/methanol → 50:0.5 v/v).

Procedure for the synthesis of oxalates **14**

The oxalates **14** were prepared in a similar manner as described in [35]. A solution of amine **13** (1 equiv) was dissolved in an-

hydrous diethyl ether and was added dropwise to a vigorously stirred solution of oxalic acid (1 equiv) in diethyl ether under an argon atmosphere. The mixture was left overnight in a freezer. The next day, the precipitate was filtered off to give a white solid.

Procedure for the synthesis of dipeptide analogues **15**

DCC/HOBt conditions: The analogue **15a** was prepared in a similar manner as described in [35]. To a cooled (0 °C) solution of amine **13** (1.05 equiv) in methylene chloride a solution of a Boc-Phe-OH (1 equiv), HOBt (1.25 equiv) in a 3:7 CH_2Cl_2/DMF solution and DCC (1.25 equiv) under an argon atmosphere were added. Stirring was continued at this temperature for 30 min and then the solution was stirred for 24 h at room temperature. The DCU was filtered off, and the filtrate was washed with cold solutions of 1 M NaOH, water, 1 M citric acid, water, 1 M $NaHCO_3$, and water. The organic extract was dried over anhydrous $MgSO_4$. The drying agent was filtered off and the solvent was evaporated. The crude product was purified by flash chromatography (*n*-hexane/ethyl acetate 60:40 → 50:50).

EDCI/HOBt conditions: To a cooled (0 °C) solution of amine **13** (1.05 equiv) in DMF, Boc-Phe-OH (1 equiv), TEA (1 equiv), HOBt (1.3 equiv) and EDCI (1.25 equiv) were added. Stirring was continued at this temperature for 30 min and then the solution was stirred for 18 h at room temperature. The reaction mixture was then diluted with 20 mL of ethyl acetate and washed with $NaHCO_{3sat}$, 1 M HCl, and $NaCl_{sat}$. The organic layer was dried over $MgSO_4$ or Na_2SO_4, filtrated and concentrated under reduced pressure. The crude product was purified by flash chromatography (*n*-hexane/ethyl acetate 60:40 → 50:50).

EDCI/OxymaPure conditions: Boc-Phe-OH (1 equiv), OxymaPure (1.1 equiv), and EDCI (1.1 equiv) were mixed in DMF at 0 °C under an argon atmosphere. The reaction mixture was stirred for 5 min at 0 °C to preactivate the acid and generate the active ester, and then DIPEA (1 equiv) followed by amine **13** (1 equiv) were added. Stirring was continued at this temperature for 30 min and then the solution was stirred for 18 h at room temperature. The reaction mixture was then diluted with 20 mL of ethyl acetate and washed with $NaHCO_{3sat}$, 1 M HCl, and $NaCl_{sat}$. The organic layer was dried over $MgSO_4$ or Na_2SO_4, filtrated and concentrated under reduced pressure. The crude product was purified by flash chromatography (*n*-hexane/ethyl acetate 60:40 → 50:50).

COMU conditions: COMU (1 equiv) was added at 0 °C to a mixture of Boc-Phe-OH (1 equiv) and DIPEA (2 equiv) in DMF under an argon atmosphere. The reaction mixture was activated for 5 min, followed by the addition of amine **13** (1 equiv) in DMF. Stirring was continued at this temperature for 30 min and then the solution was stirred for 2–3 h at room temperature (monitored by ^{31}P or ^{19}F NMR). The reaction mixture was then diluted with 20 mL of ethyl acetate and washed with $NaHCO_{3sat}$, 1 M HCl, and $NaCl_{sat}$. The organic layer was dried over $MgSO_4$ or Na_2SO_4, filtrated and concentrated under reduced pressure. The crude product was purified by flash chromatography (*n*-hexane/ethyl acetate 60:40 → 50:50).

Supporting Information

Supporting Information File 1

Optimization of reaction conditions data, characterization data, copies of NMR spectra for compounds **13–15**, single crystal X-ray data for compound **14c**.
[https://www.beilstein-journals.org/bjoc/content/supplementary/1860-5397-16-69-S1.pdf]

Supporting Information File 2

CIF file of **14c**.
[https://www.beilstein-journals.org/bjoc/content/supplementary/1860-5397-16-69-S2.cif]

Acknowledgements

Marcin Kaźmierczak and Henryk Koroniak would like to thank Prof. Maciej Kubicki for X-ray diffraction analysis.

Funding

Marcin Kaźmierczak would like to thank the National Science Centre for financial support under grant 2018/02/X/ST5/02867 (MINIATURA 2).

ORCID® iDs

Marcin Kaźmierczak - https://orcid.org/0000-0003-0199-9197
Henryk Koroniak - https://orcid.org/0000-0002-4067-8508

References

1. Romanenko, V. D.; Kukhar, V. P. *Chem. Rev.* **2006,** *106,* 3868–3935. doi:10.1021/cr051000q
2. Turcheniuk, K. V.; Kukhar, V. P.; Röschenthaler, G.-V.; Aceña, J. L.; Soloshonok, V. A.; Sorochinsky, A. E. *RSC Adv.* **2013,** *3,* 6693–6716. doi:10.1039/c3ra22891f
3. Cytlak, T.; Kaźmierczak, M.; Skibińska, M.; Koroniak, H. *Phosphorus, Sulfur Silicon Relat. Elem.* **2017,** *192,* 602–620. doi:10.1080/10426507.2017.1287706
4. Song, B.-A.; Wu, Y.-L.; Yang, S.; Hu, D.-Y.; He, X.-Q.; Jin, L.-H. *Molecules* **2003,** *8,* 186–192. doi:10.3390/80100186
5. Rao, X.; Song, Z.; He, L. *Heteroat. Chem.* **2008,** *19,* 512–516. doi:10.1002/hc.20471

6. Herczegh, P.; Buxton, T. B.; McPherson, J. C.; Kovács-Kulyassa, Á.; Brewer, P. D.; Sztaricskai, F.; Stroebel, G. G.; Plowman, K. M.; Farcasiu, D.; Hartmann, J. F. *J. Med. Chem.* **2002,** *45,* 2338–2341. doi:10.1021/jm0105326
7. Yang, S.; Gao, X.-W.; Diao, C.-L.; Song, B.-A.; Jin, L.-H.; Xu, G.-F.; Zhang, G.-P.; Wang, W.; Hu, D.-Y.; Xue, W.; Zhou, X.; Lu, P. *Chin. J. Chem.* **2006,** *24,* 1581–1588. doi:10.1002/cjoc.200690296
8. Berkowitz, D. B.; Bose, M. *J. Fluorine Chem.* **2001,** *112,* 13–33. doi:10.1016/s0022-1139(01)00478-x
9. Berkowitz, D. B.; Bose, M.; Pfannenstiel, T. J.; Doukov, T. *J. Org. Chem.* **2000,** *65,* 4498–4508. doi:10.1021/jo000220v
10. Nieschalk, J.; Batsanov, A. S.; O'Hagan, D.; Howard, J. *Tetrahedron* **1996,** *52,* 165–176. doi:10.1016/0040-4020(95)00890-k
11. Nieschalk, J.; O'Hagan, D. *J. Chem. Soc., Chem. Commun.* **1995,** 719–720. doi:10.1039/c39950000719
12. Tarasenko, K. V.; Romanenko, V. D.; Sorochinsky, A. E. *J. Fluorine Chem.* **2018,** *211,* 124–128. doi:10.1016/j.jfluchem.2018.04.014
13. Berkowitz, D. B.; Bose, M.; Asher, N. G. *Org. Lett.* **2001,** *3,* 2009–2012. doi:10.1021/ol015983z
14. McKenna, C. E.; Shen, P.-D. *J. Org. Chem.* **1981,** *46,* 4573–4576. doi:10.1021/jo00335a053
15. Blackburn, G. M.; Kent, D. E. *J. Chem. Soc., Chem. Commun.* **1981,** 511–513. doi:10.1039/c39810000511
16. Blackburn, G. M.; England, D. A.; Kolkmann, F. *J. Chem. Soc., Chem. Commun.* **1981,** 930–932. doi:10.1039/c39810000930
17. Ni, C.; Hu, M.; Hu, J. *Chem. Rev.* **2015,** *115,* 765–825. doi:10.1021/cr5002386
18. Champagne, P. A.; Desroches, J.; Hamel, J.-D.; Vandamme, M.; Paquin, J.-F. *Chem. Rev.* **2015,** *115,* 9073–9174. doi:10.1021/cr500706a
19. Hu, W.-L.; Hu, X.-G.; Hunter, L. *Synthesis* **2017,** *49,* 4917–4930. doi:10.1055/s-0036-1590881
20. Nielsen, M. K.; Ugaz, C. R.; Li, W.; Doyle, A. G. *J. Am. Chem. Soc.* **2015,** *137,* 9571–9574. doi:10.1021/jacs.5b06307
21. Nielsen, M. K.; Ahneman, D. T.; Riera, O.; Doyle, A. G. *J. Am. Chem. Soc.* **2018,** *140,* 5004–5008. doi:10.1021/jacs.8b01523
22. Bennua-Skalmowski, B.; Vorbrüggen, H. *Tetrahedron Lett.* **1995,** *36,* 2611–2614. doi:10.1016/0040-4039(95)00355-g
23. Vorbrüggen, H. *Synthesis* **2008,** 1165–1174. doi:10.1055/s-2008-1067006
24. Guo, J.; Kuang, C.; Rong, J.; Li, L.; Ni, C.; Hu, J. *Chem. – Eur. J.* **2019,** *25,* 7259–7264. doi:10.1002/chem.201901176
25. Montalbetti, C. A. G. N.; Falque, V. *Tetrahedron* **2005,** *61,* 10827–10852. doi:10.1016/j.tet.2005.08.031
26. Valeur, E.; Bradley, M. *Chem. Soc. Rev.* **2009,** *38,* 606–631. doi:10.1039/b701677h
27. Pattabiraman, V. R.; Bode, J. W. *Nature* **2011,** *480,* 471–479. doi:10.1038/nature10702
28. El-Faham, A.; Albericio, F. *Chem. Rev.* **2011,** *111,* 6557–6602. doi:10.1021/cr100048w
29. Albericio, F.; El-Faham, A. *Org. Process Res. Dev.* **2018,** *22,* 760–772. doi:10.1021/acs.oprd.8b00159
30. Kaźmierczak, M.; Koroniak, H. *J. Fluorine Chem.* **2012,** *139,* 23–27. doi:10.1016/j.jfluchem.2012.03.016
31. Kaźmierczak, M.; Kubicki, M.; Koroniak, H. *Eur. J. Org. Chem.* **2018,** 3844–3852. doi:10.1002/ejoc.201800631
32. Pudovik, A. N.; Konovalova, I. V. *Synthesis* **1979,** 81–96. doi:10.1055/s-1979-28566
33. Rádai, Z.; Keglevich, G. *Molecules* **2018,** *23,* 1493. doi:10.3390/molecules23061493
34. Bailey, P. D.; Beard, M. A.; Dang, H. P. T.; Phillips, T. R.; Price, R. A.; Whittaker, J. H. *Tetrahedron Lett.* **2008,** *49,* 2150–2153. doi:10.1016/j.tetlet.2008.01.104
35. Kaźmierczak, M.; Kubicki, M.; Koroniak, H. *J. Fluorine Chem.* **2014,** *167,* 128–134. doi:10.1016/j.jfluchem.2014.06.008
36. Kafarski, P.; Lejczak, B. *Synthesis* **1988,** 307–310. doi:10.1055/s-1988-27550
37. Vaidhyanathan, R.; Natarajan, S.; Rao, C. N. R. *J. Mol. Struct.* **2002,** *608,* 123–133. doi:10.1016/s0022-2860(01)00944-9
38. Spingler, B.; Schnidrig, S.; Todorova, T.; Wild, F. *CrystEngComm* **2012,** *14,* 751–757. doi:10.1039/c1ce05624g
39. Sheehan, J. C.; Hess, G. P. *J. Am. Chem. Soc.* **1955,** *77,* 1067–1068. doi:10.1021/ja01609a099
40. König, W.; Geiger, R. *Chem. Ber.* **1970,** *103,* 788–798. doi:10.1002/cber.19701030319
41. Sheehan, J.; Cruickshank, P.; Boshart, G. *J. Org. Chem.* **1961,** *26,* 2525–2528. doi:10.1021/jo01351a600
42. Wehrstedt, K. D.; Wandrey, P. A.; Heitkamp, D. *J. Hazard. Mater.* **2005,** *126,* 1–7. doi:10.1016/j.jhazmat.2005.05.044
43. Jad, Y. E.; Khattab, S. N.; de la Torre, B. G.; Govender, T.; Kruger, H. G.; El-Faham, A.; Albericio, F. *Eur. J. Org. Chem.* **2015,** 3116–3120. doi:10.1002/ejoc.201500142
44. Subirós-Funosas, R.; Prohens, R.; Barbas, R.; El-Faham, A.; Albericio, F. *Chem. – Eur. J.* **2009,** *15,* 9394–9403. doi:10.1002/chem.200900614
45. El-Faham, A.; Funosas, R. S.; Prohens, R.; Albericio, F. *Chem. – Eur. J.* **2009,** *15,* 9404–9416. doi:10.1002/chem.200900615
46. *CrysAlis PRO,* version 1.171.38.41; Rigaku Oxford Diffraction, 2015.
47. Sheldrick, G. M. *Acta Crystallogr., Sect. A: Found. Crystallogr.* **2008,** *64,* 112–122. doi:10.1107/s0108767307043930
48. Kaźmierczak, M.; Kubicki, M.; Koroniak, H. *Phosphorus, Sulfur Silicon Relat. Elem.* **2016,** *191,* 459–468. doi:10.1080/10426507.2015.1091832

License and Terms

This is an Open Access article under the terms of the Creative Commons Attribution License (http://creativecommons.org/licenses/by/4.0). Please note that the reuse, redistribution and reproduction in particular requires that the authors and source are credited.

The license is subject to the *Beilstein Journal of Organic Chemistry* terms and conditions: (https://www.beilstein-journals.org/bjoc)

The definitive version of this article is the electronic one which can be found at:
doi:10.3762/bjoc.16.69

BEILSTEIN JOURNAL OF ORGANIC CHEMISTRY

Reaction of indoles with aromatic fluoromethyl ketones: an efficient synthesis of trifluoromethyl(indolyl)phenylmethanols using K_2CO_3/*n*-Bu_4PBr in water

Thanigaimalai Pillaiyar*[1], Masoud Sedaghati[1] and Gregor Schnakenburg[2]

Full Research Paper

Open Access

Address:
[1]PharmaCenter Bonn, Pharmaceutical Institute, Department of Pharmaceutical and Medicinal Chemistry, University of Bonn, An der Immenburg 4, D-53121 Bonn, Germany and [2]Institute of Inorganic Chemistry, University of Bonn, Gerhard-Domagk-Str. 1, D-53121 Bonn, Germany

Email:
Thanigaimalai Pillaiyar* - thanigai@uni-bonn.de

* Corresponding author

Keywords:
C–C-bond formation; C3-funtionalization of indole; diindolylmethane; Friedel–Crafts reaction; indole; indole-3-carbinol; large-scale synthesis; recyclability

Beilstein J. Org. Chem. **2020,** *16,* 778–790.
doi:10.3762/bjoc.16.71

Received: 12 February 2020
Accepted: 02 April 2020
Published: 20 April 2020

This article is part of the thematic issue "Organo-fluorine chemistry V".

Guest Editor: D. O'Hagan

© 2020 Pillaiyar et al.; licensee Beilstein-Institut.
License and terms: see end of document.

Abstract

A new, mild and efficient protocol for the synthesis of trifluoromethyl(indolyl)phenylmethanols by the reaction of indoles with a variety of aromatic fluoromethyl ketones in the presence of K_2CO_3 (15 mol %) and *n*-Bu_4PBr (15 mol %) in water. The desired products were obtained in good to excellent yields without requiring a column chromatographic purification. The reusability of the catalytic system and large-scale synthesis of indolyl(phenyl)methanols, which would further transform into biological active indole-derived compounds, are further advantages of this protocol.

Introduction

(1*H*-Indol-3-yl)methanols have emerged as versatile pre-electrophiles for C–C functionalization at the position 3 of indoles [1-4]. Friedel–Crafts alkylation of (1*H*-indol-3-yl)methanols with indoles has proven to be a powerful strategy for the preparation of biologically important 3,3′-diindolylmethanes (DIMs) [5-14]. Additionally, (1*H*-indol-3-yl)methanols have been used as key precursors for the construction of complex indole derivatives that would be useful in pharmaceuticals as drugs and agrochemicals [2-14]. The simple (1*H*-indol-3-yl)methanol, a breakdown product of glucobrassicin, which can be found in cruciferous vegetables [15], has a wide range of biomedical applications as an anticancer [16], antioxidant, and antiatherogenic agent [17].

Organofluorine compounds have attracted much attention due to their potential biological applications in medicinal and agricultural sciences. Introducing fluoro groups into organic molecules can dramatically influence their physiochemical and bio-

logical properties in comparison with non-fluorinated analogs [18] (see compounds **I** and **II** in Figure 1). Many pharmaceuticals and agrochemicals developed in recent decades have either a fluorine atom or a trifluoromethyl group [19-22]. Given this, the development of a method for the incorporation of fluorine or trifluoromethyl group into organic molecules perhaps remains a current challenge in organic chemistry methodology. For example, trifluoromethyl-substituted (1*H*-indol-3-yl)methanol derivatives were reported for their promising anti-HIV inhibitory activities [23], see for example compounds **III** and **IV** (Figure 1). However, these compounds were synthesized from multiple synthetic routes with the involvement of air sensitive conditions.

Trifluoromethyl-substituted (1*H*-indol-3-yl)methanol derivatives can be synthesized by Friedel–Crafts hydroxyalkylation reactions of indoles with trifluoromethyl ketones in the presence of either Lewis/Bronsted acid catalysts. Bandini et al. reported the trifluoromethyl hydroxyalkylation of indoles catalyzed by an organic base 2-*tert*-butyl-1,1,3,3-tetramethylguanidine (TMG), also known as Barton's base, in excellent yields (Figure 2A) [24]. Recently, Liu and co-workers reported this reaction in the presence of cesium carbonate in acetonitrile (Figure 2B) [25]. Dinuclear zinc [26], cinchonidine catalysts, and solvent-free conditions [27] have been also utilized for this reaction. The base-catalyzed reaction has a benefit because it may avoid the formation of diindolylmethane and biindoles as byproducts [28].

Although these methods were useful, they have limitations and drawbacks, which are the use of organic solvents [24], difficulties in recyclability of the catalyst [24,25], multiple reaction steps involving air sensitive/unhydrous conditions [23], generation of a large volume of waste liquids for the compound separation and column chromatographic purification [24,25], and moderate substrate scope of the reaction. Thus, finding an alternative method with broad substrate scope, functional group tolerance, and simple purification technique is highly desired.

In our continuous effort of synthesizing indole derivatives [29-31], herein, we report an efficient synthesis of multiple halogen-substituted (1*H*-indol-3-yl)methanol derivatives in the presence of potassium carbonate and tetrabutylphophonium bromide, which mediate the reaction in water through the formation of the interface between organic and aqueous phases. The advantageous of this reaction include high yields, no column chromatography, broad substrate scope, multiscale synthesis, and recyclable of the catalyst (Figure 2C).

Results and Discussion

The optimization studies were carried out with model substrates 5-methoxyindole (**1a**, 3.4 mmol) and 2,2,2-trifluoroacetophenone (**2a**, 3.70 mmol) in water (5 mL, see Table 1 for results). Using water as a solvent has the advantage that the formed product **3a** would not be soluble, which makes the purification easier through a simple filtration. In a first attempt, the reaction did not initiate at all without any base or catalyst (Table 1, entry 1). Next, we investigated the reaction in the presence of 20 mol % of base such as NaOH (Table 1, entry 2) or KOH (Table 1, entry 3). However, no product was formed (Table 1, entries 2 and 3), and it was observerd that reactant **2a** separated from the aqueous phase. This makes us add quaternary salts into the reaction, which could make the interface between organic and aqueous phase. Very interestingly, the combination of 20 mol % of tetrabutylammonium bromide (TBAB) and NaOH (20 mol %) yielded the desired product, 2,2,2-

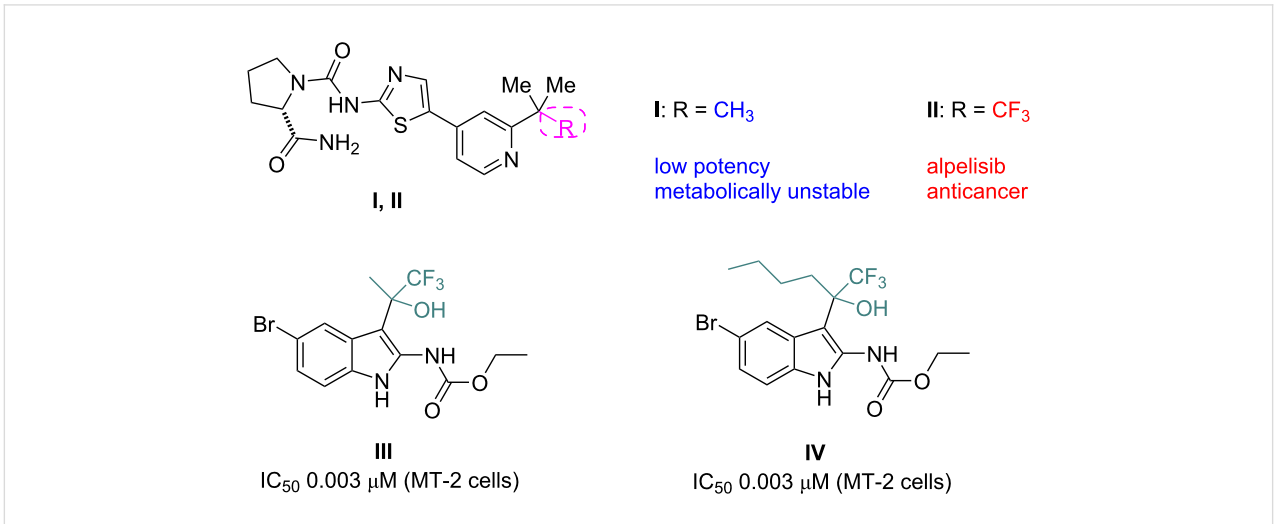

Figure 1: Structures of trifluoromethylated compounds and their biological activities.

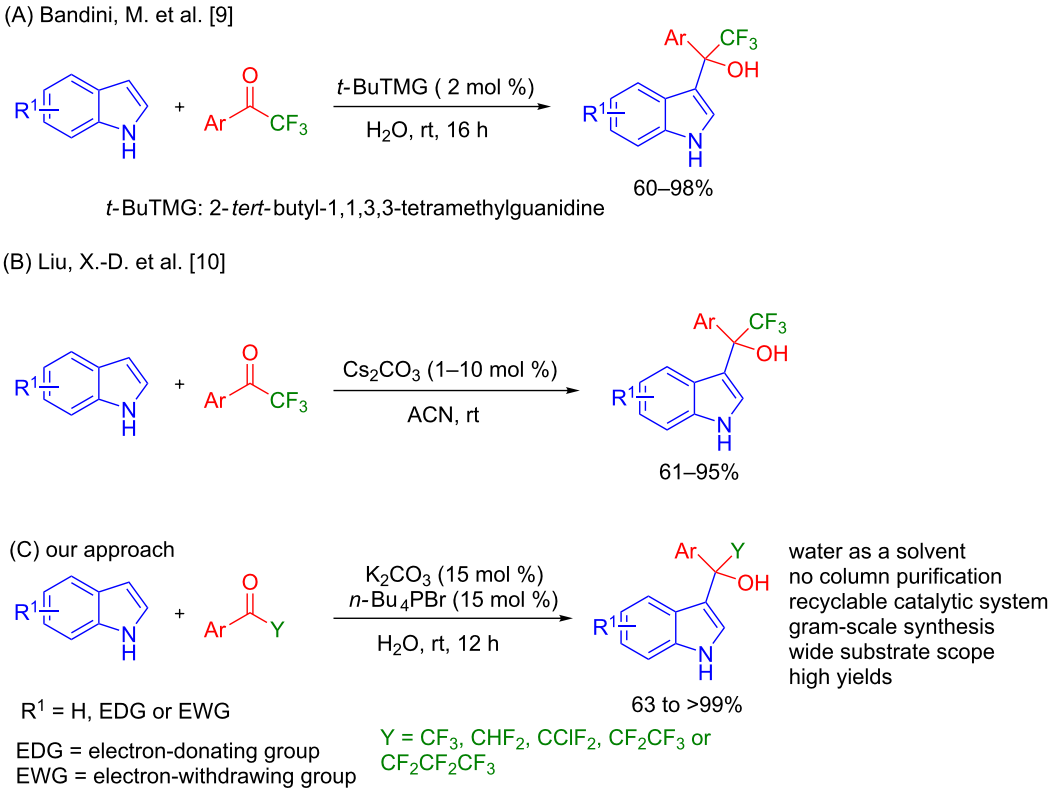

Figure 2: Synthetic approaches toward hydroxyalkylation of indole.

Table 1: Optimization of reaction conditions for the preparation of 2,2,2-trifluoro-1-(1*H*-indol-3-yl)ethan-1-ol (**3a**).[a]

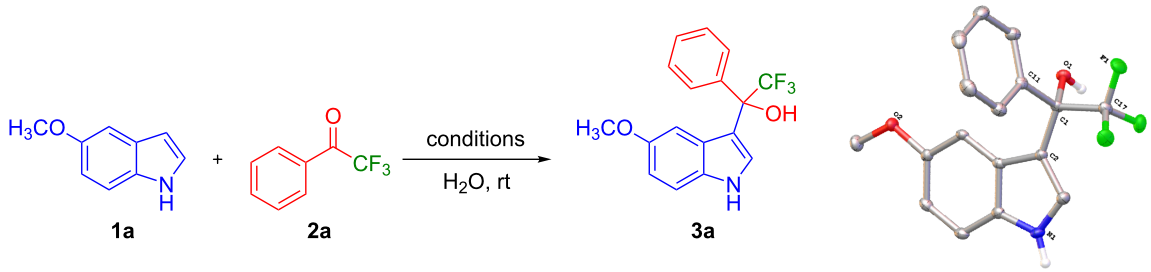

Entry	Base (mol %)	Catalyst (mol %)	Time (h)	Yield (%)[b]
1	–	–	24	0
2	NaOH (20)	–	24	0
3	KOH (20)	–	24	0
4	NaOH (20)	TBAB (20)	15	93
5	NaOH (20)	TBPB (20)	15	96
6	–	TBPB (20)	24	0
7	KOH (20)	TBPB (20)	15	91
8	K_2CO_3 (20)	TBPB (20)	12	97
9	CS_2CO_3 (20)	TBPB (20)	15	81
10	K_3PO_4 (20)	TBPB (20)	15	89
11	K_2HPO_4 (20)	TBPB (20)	15	70
12	$Na_5P_3O_{10}$ (20)	TBPB (20)	15	76

Table 1: Optimization of reaction conditions for the preparation of 2,2,2-trifluoro-1-(1*H*-indol-3-yl)ethan-1-ol (**3a**).[a] (continued)

13	K_2CO_3 (20)	TBAC (20)	15	72
14	K_2CO_3 (20)	TBAF (20)	15	61
15	**K_2CO_3 (15)**	**TBPB (15)**	**12**	**>99 (94)**[c]
16	K_2CO_3 (10)	TBPB (10)	18	90
17	K_2CO_3 (5)	TBPB (5)	24	69

[a]Reaction conditions: **1a** (500 mg, 3.4 mmol) and **2a** (524 µL, 3.70 mmol) were used in H_2O (5 mL) at room temperature. [b]Isolated yields. [c]Obtained yield in tap water.

trifluoro-1-(1*H*-indol-3-yl)ethan-1-ol (**3a**) in 93% yield (Table 1, entry 4). The product **3a** was isolated by filtration and confirmed by NMR and X-ray crystallography analysis (CCDC-1973322, see Supporting Information File 1 for detailed crystallographic data). It is noteworthy to mention that the formation of the product was even increased in the presence of tetrabutylphosphonium bromide (TBPB) to 96% (Table 1, entry 5). On the other hand, the reaction did not initiate only with TBPB (Table 1, entry 6). It indicates that quaternary salts mediate the reaction in the presence of a base through the formation of the interface between the organic and aqueous phase.

As a next step, different bases were investigated by using TBPB. In the presence of KOH and the Cs_2CO_3, the formation of the product was reduced to 91% (Table 1, entry 7) and 81% (Table 1, entry 9), respectively, while it was increased to 97% (Table 1, entry 8) in the presence of K_2CO_3. The reaction in the presence of tripotassium phosphate base (Table 1, entry 10; 89%), dipotassium phosphate base (Table 1, entry 11; 70%) or sodium triphosphate (Table 1, entry 12; 76%) did not improve the yield. These results suggest that K_2CO_3 is the best catalyst for the reaction among the bases investigated.

To find the best catalytic system, other quaternary salts were invested in the reaction. When tetrabutylammonium chloride (TBAC) or tetrabutylammonium fluoride (TBAF) was employed in the presence of K_2CO_3, the formation of the product was reduced to 72% (Table 1, entry 13) and 61% (Table 1, entry 14), respectively. These results suggest that the combination of K_2CO_3/TBPB could be the best catalytic system for this reaction.

Next, the amount of catalytic system K_2CO_3/TBPB was reduced from 20 mol % to 15 mol % to see if there any change in the yield. As indicated in Table 1, entry 15, the product **3a** was isolated in >99%. However, further reduction to 10 mol % or 5 mol % slowed the reaction rate, and only 90% (Table 1, entry 16) or 69% (Table 1, entry 17) of **3a** was isolated. These results suggest that the combination of K_2CO_3 (15 mol %)/*n*-Bu_4PBr (15 mol %) is a suitable and efficient catalytic system for this reaction.

Having the optimized conditions in hand, the substrate scope of the reaction was explored. At first, different trifluoromethyl ketones were investigated, and the results are summarized in Table 2. Trifluoroacetophenones having a halogen substituent at the *para*-position of the phenyl ring such as *p*-F (**2b**), *p*-Cl (**2c**), and *p*-Br (**2d**) provided the corresponding trifluoro-1-(1*H*-indol-3-yl)ethan-1-ols **3b**, **3c**, and **3d** in 97, 92 and 89% yields, respectively. Similarly, trifluoroacetophenones having a *p*-methyl (**2e**) and *p*-methoxy (**2f**) group at the phenyl ring resulted in **3e**, and **3f** with excellent yields of 98 and 93%, respectively. These results suggest that the electronic properties of the substituent on the phenyl ring of the trifluoroacetophenones did not significantly influence the yield of the reaction.

The trifluoromethyl ketones having electron-rich heteroaromatics such as 2-(trifluoroacetyl)furan (**2g**) and 2-(trifluoroacetyl)thiophene (**2h**) gave the desired products **3g** (97%) and **3h** (98%) in excellent yields.

Next, the role of fluorine in the reactants was explored by subjecting the reaction of 2,2-difluoro-1-phenylethan-1-one (**2i**) with **1a**. The desired product **3i** was obtained in 63% yield. However, no product was formed when the reaction was carried out with 2-fluoro-1-phenylethan-1-one (**2j**) or acetophenone (**2k**). The reason could be due to either reducing the electrophilicity of the ketone or the presence of enolizable protons in α-position to the keto group in basic medium. Supporting this hypothesis, the reaction of **1a** with 1,1,1-trifluoro-3-phenyl-2-propanone (**2l**), which has a 3-methylene group also did not proceed at all.

The scope of ketones was further extended with mixed halogen-substituted, pentafluoro or heptafluoro ketones such as 2-chloro-2,2-difluoro-1-phenylethan-1-one (**2m**), 2,2,3,3,3-pentafluoro-1-phenylpropan-1-one (**2n**) and 2,2,3,3,4,4,4-heptafluoro-1-phenylbutan-1-one (**2o**). All these reactions provided the corresponding products (**3m**: 94%, **3n**: 93%, **3o**: 90%) in excellent yields.

Next, the scope of substituted indoles was studied with trifluoromethyl ketone **2a**, and the results are shown in Table 3. In

Table 2: Substrate scope of the reaction with ketones.[a]

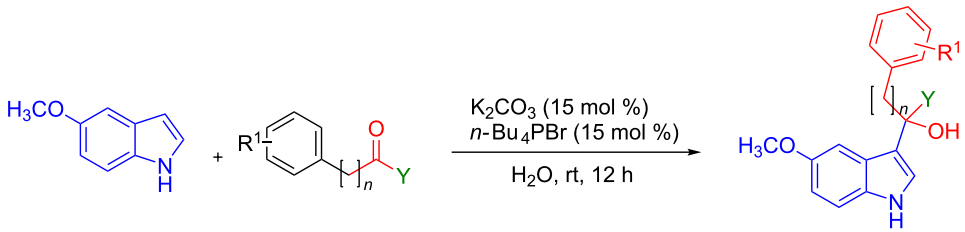

1a

2a–o
n = 1 or 0
Y = CF_3, CHF_2, CH_2F, $CClF_2$, CH_3, CF_2CF_3 or $CF_2CF_2CF_3$

3a–i,m–o
n = 0
Y = CF_3, CHF_2, $CClF_2$, CF_2CF_3 or $CF_2CF_2CF_3$

Ketones	Multihalogen-substituted hydroxylakylated indoles	Mp (°C)	Purity (%)[b]	Yield (%)[c]
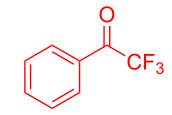 **2a**	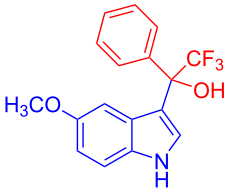 **3a** [24]	135–136 (135)[d] [24]	99	>99% (98)[e] [24]
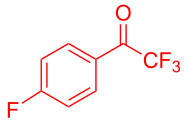 **2b**	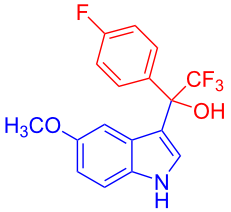 **3b**	115–116	98	97%
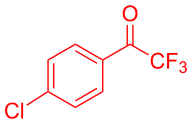 **2c**	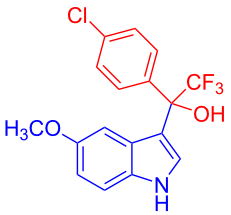 **3c**	153–154	99	92
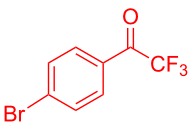 **2d**	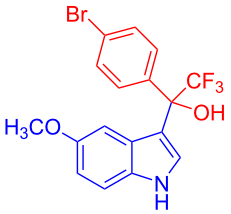 **3d**	172–173	97	89
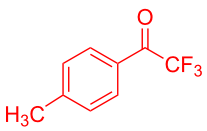 **2e**	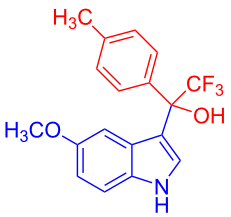 **3e**	130–131	99	98

Table 2: Substrate scope of the reaction with ketones.[a] (continued)

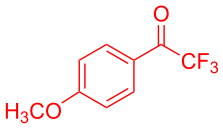 **2f**	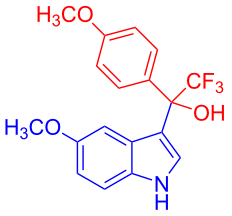 **3f**	151–152	98	93
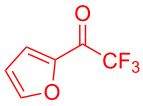 **2g**	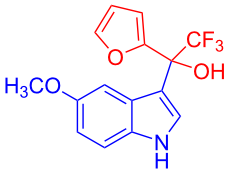 **3g**	158–159	99	97
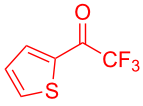 **2h**	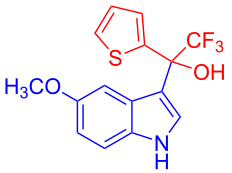 **3h**	148–149	97	98
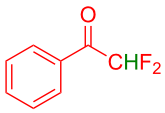 **2i**	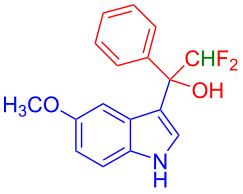 **3i**	185–186	96	63
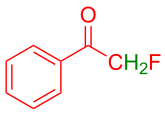 **2j**	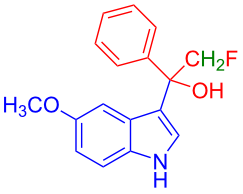 **3j**	–	–	0
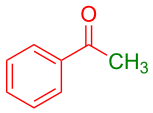 **2k**	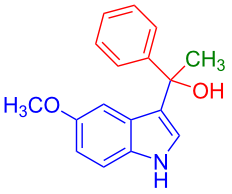 **3k**	–	–	0
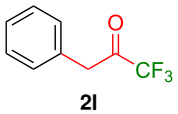 **2l**	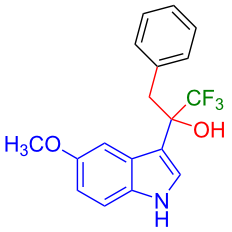 **3l**	–	–	0

Table 2: Substrate scope of the reaction with ketones.[a] (continued)

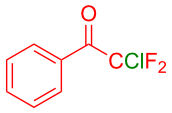 **2m**	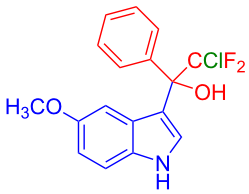 **3m**	158–159	98	94
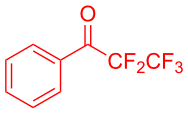 **2n**	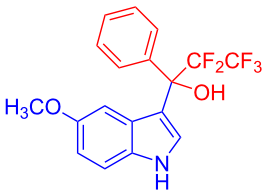 **3n**	168–169	97	93
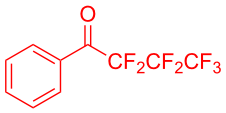 **2o**	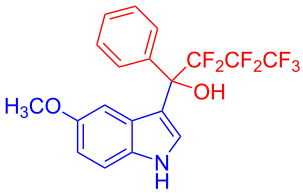 **3o**	161–163	97	90

[a]Reaction conditions: **1** (3.4 mmol) and **2** (3.75 mmol) in water (5 mL). [b]Purity was determined by HPLC coupled to a UV diode array detector (DAD) at 220–400 nm. [c]Isolated yields. [d]Reported melting points. [e]Reported yields.

Table 3: Substrate scope of the reaction with indoles.[a]

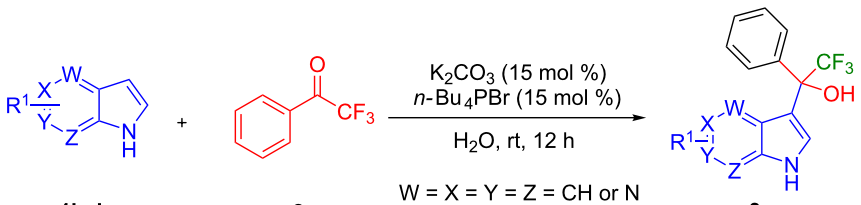

1b–j **2a** **3p–x**

Indoles	Trifluoromethly substituted hydroxylakylated indoles	Mp (°C)	Purity (%)[b]	Yield (%)[c]
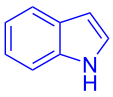 **1b**	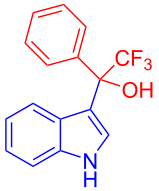 **3p**	122–124 (75)[d] [25]	98	96 (95)[e] [25]
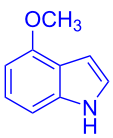 **1c**	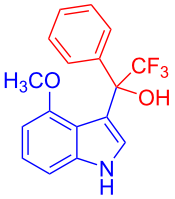 **3q**	160–161	99	79

Table 3: Substrate scope of the reaction with indoles.[a] (continued)

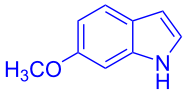 **1d**	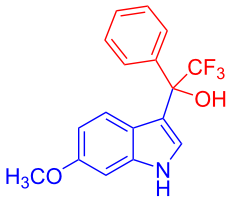 **3r**	192–193	97	90
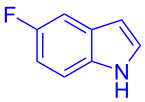 **1e**	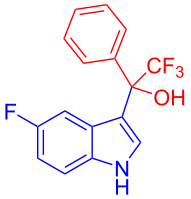 **3s**	112–113	99	94 (98)[e] [24]
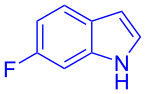 **1f**	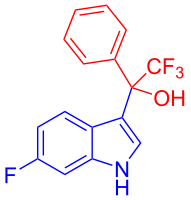 **3t**	90–91 (90)[d] [24]	99	96 (98)[e] [24]
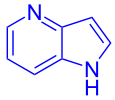 **1g**	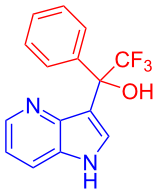 **3u**	165–166	98	91
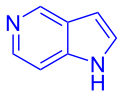 **1h**	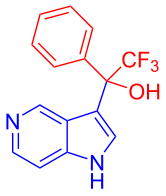 **3v**	227–228	97	92
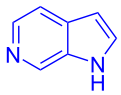 **1i**	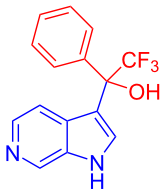 **3w**	239–240	99	97
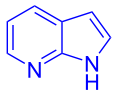 **1j**	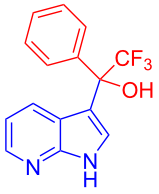 **3x**	185–186 185[d] [24]	97	90 86[e] [24]

[a]Reaction conditions: **1** (3.4 mmol) and **2** (3.75 mmol) in water (5 mL). [b]Purity was determined by HPLC coupled to a UV diode array detector (DAD) at 220–400 nm. [c]Isolated yields. [d]Reported melting points. [e]Reported yields.

the case of a simple indole (**1b**), the corresponding product **3p** was isolated in 96% yield. Indoles bearing electron-donating groups (i.e., methoxy, **1c**,**d**) and electron-withdrawing groups (i.e., F, **1e**,**f**) at different positions of indoles were well tolerated and delivered the desired fluorinated indol-3-yl-1-phenylethanols (**3q**–**t**) in excellent yields in the range from 79–96%. The reaction of **3a** with different azaindoles (4-. 5-, 6-, and 7-azaindoles, **1g**–**j**) provided the corresponding products in the range from 91–97% yield (**3u**–**x**).

We applied the developed protocol to reactions of other heterocyclic systems such as indazole (**4**), benzimidazole (**5**), carbazole (**6**), benzofuran (**7**), and benzothiophene (**8**) with ketone **2a** (Figure 3). However, no desired products are formed.

As a next step, this protocol is employed in the large-scale preparation of 2,2,2-trifluoro-1-(1*H*-indol-3-yl)-1-phenylethan-1-ols. We performed gram-scale reactions of 5-methoxyindole (**1a**, 6.8 mmol) with 2,2,2-trifluoroacetophenone (**2a**, 7.5 mmol) or of indole (**1b**, 8.5 mmol) with **2a** (9.4 mmol, Scheme 1). In both reactions, the desired products are achieved in excellent yields (**3a**: 2.14 g, 98%; **3b**: 2.39 g, 96%).

The recyclability of the catalytic system *n*-Bu_4PBr/K_2CO_3 of this protocol was investigated in the preparation of **3a** using **1a** (3.40 mmol), **2a** (3.70 mmol), K_2CO_3 (0.5 mmol) and *n*-Bu_4PBr (0.5 mmol) in distilled water (5 mL) at room temperature for 12 h (Figure 4). The product **3a** was filtered after completion of the reaction. The resulting filtrate was recovered, washed with ethyl acetate to remove any organic impurities, and reused for the next cycle. This procedure was followed for each cycle. Interestingly, the catalytic system was efficient to produce the product **3a** in excellent to good yields up to 4 cycles (99–84%). In the fifth cycle, the yield of **3a** was reduced to 67%. This could be due to the dilution of the catalytic system in each cycle.

3-Indolylmethanols are versatile pre-electrophiles for C–C functionalization at the 3-position of indoles. Particularly, the Friedel–Crafts alkylation of 3-indolylmethanols with indoles has become a useful method for the preparation of 3,3'-, and 3,6'-DIMs, which are known to possess a wide variety of biological activities, including anti-inflammatory, and anticancer effects. Therefore, we decided to synthesize DIMs from **3a**, which reacted with indole (**1b**) or 2-phenylindole (**1k**) in the presence of $Ga(OTf)_3$ in ACN at room temperature or at 80 °C as reported by Y. Ling et al. [32]. As indicated in Scheme 2, the desired unsymmetrical 3,3'-DIM (**9**: 81%) and 3,6'-DIM (**10**: 77%) with quaternary center were afforded in good yields. Besides, the protocol reported by S. Sasaki et al. [33] was also employed for the synthesis of 3,3'-DIMs in good yield, see for example product **11** (80%, Scheme 2).

Next, a plausible mechanism for the preparation of multihalogen-alkylated 1-(1*H*-indol-3-yl)-1-phenylethan-1-ols is proposed as indicated in Scheme 3. Based on the literature [34], this reaction initiates by the formation of *n*-$Bu_4P^+KCO_3^-$ salt (**A**) from the interaction of *n*-Bu4PBr and K_2CO_3. Intermediate **A** makes a hydrogen bond interaction with the NH of the 5-methoxyindole (**1a**) and form the adduct **B**. This interaction assists **1a** reacting with an electrophilic ketone (**2a**) to form the intermediate **D** via C–C bond formation (**C**). Re-aromatization of **D** generates **E**, which then protonates to form the desired product **3a** by excluding **A** for the next catalytic cycle.

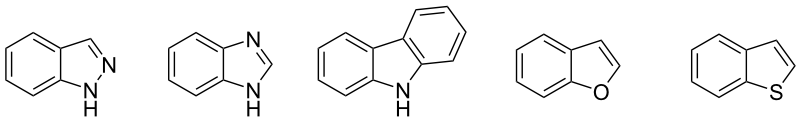

Figure 3: Structures of heterocycles that did not react with ketone **2a**.

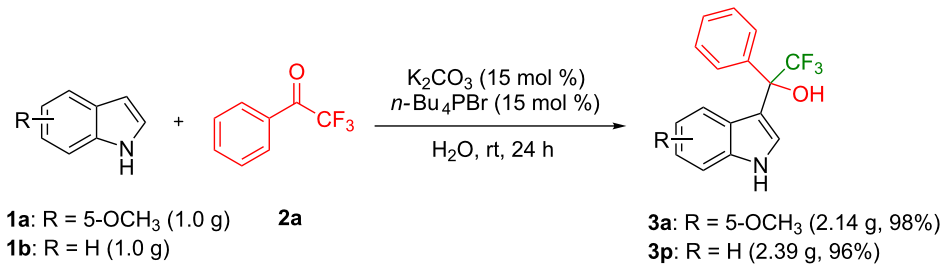

Scheme 1: Gram-scale synthesis of 2,2,2-trifluoro-1-(1*H*-indol-3-yl)-1-phenylethan-1-ols (**3a** and **3p**).

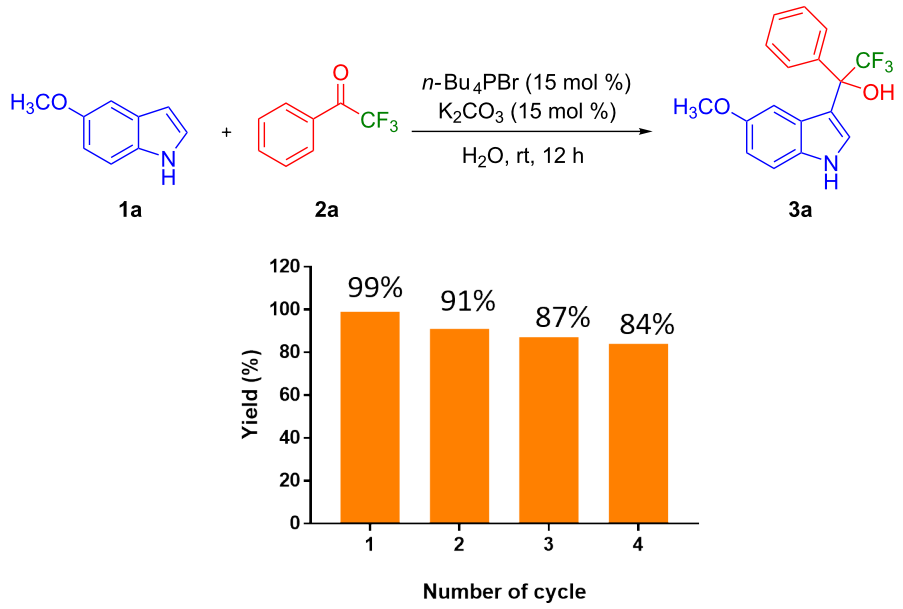

Figure 4: Recyclability of the catalytic system *n*-Bu_4PBr/K_2CO_3 for the preparation of 2,2,2-trifluoro-1-(5-methoxy-1*H*-indol-3-yl)-1-phenylethan-1-ol (**3a**).

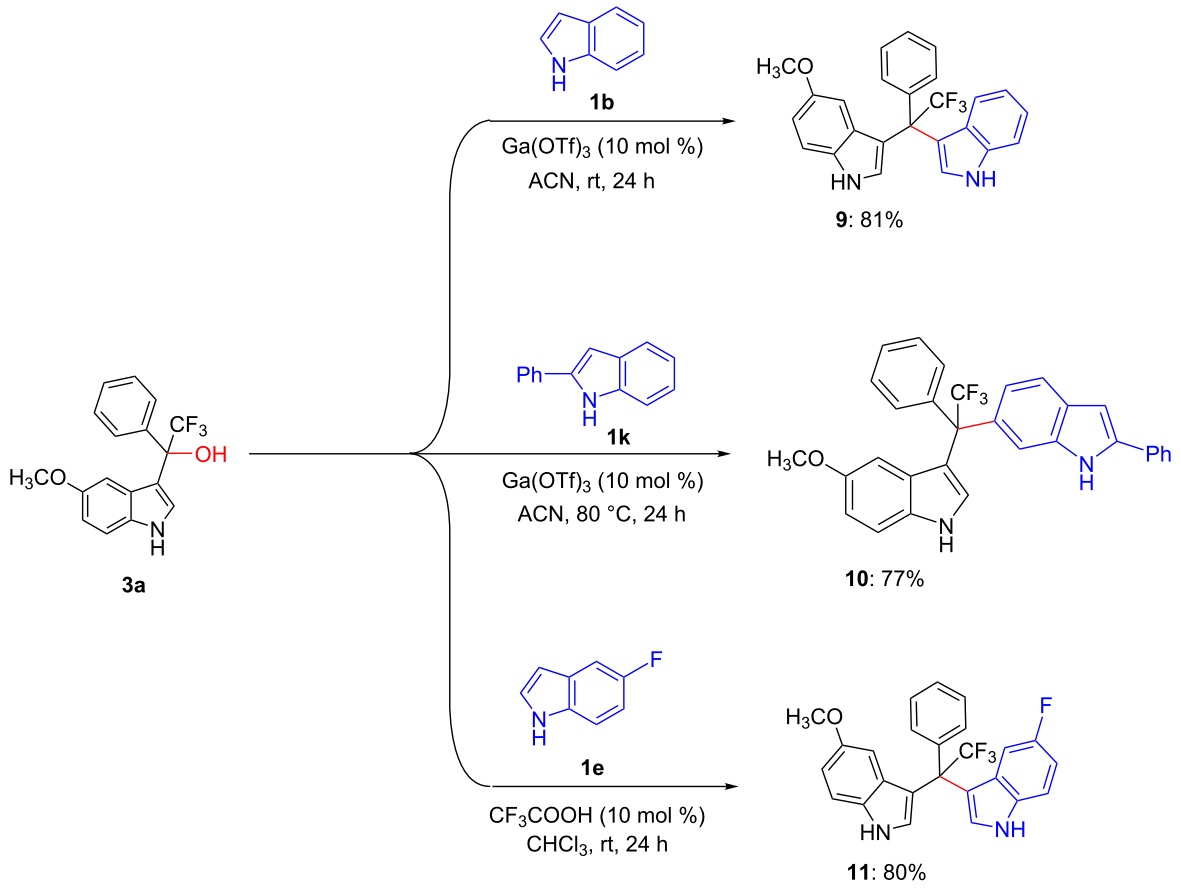

Scheme 2: Synthesis of trifluoromethylated unsymmetrical 3,3'- and 3,6'-DIMs (**9–11**).

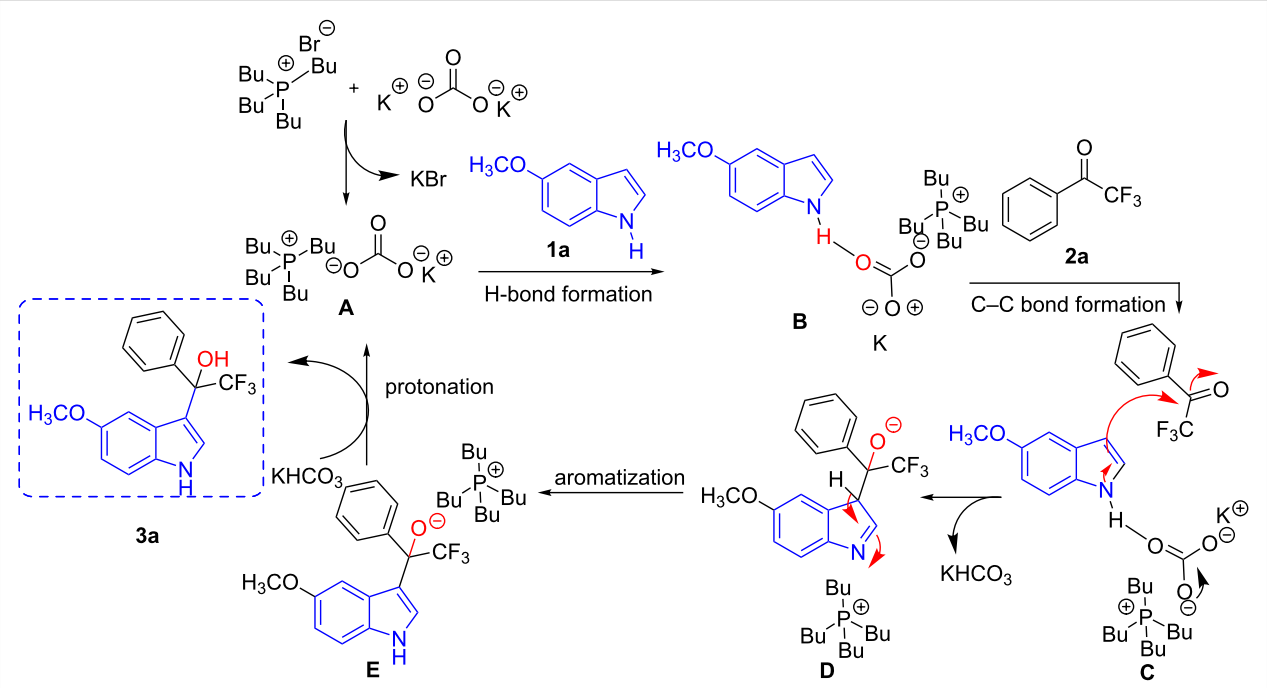

Scheme 3: Proposed mechanism for the preparation of **3a** as an example.

Further, to prove this hypothesis the following control experiments were performed. The reaction of 1-methylindole (**1l**) with **2a** failed to provide the product (Scheme 4). It suggests that the indole having a free NH-functionality is important to interact with the base, thereby initiating the reaction. To find the importance of electrophilicity of ketones, different enolizable and nonenolizable ketones were screened with the reaction of 5-methoxyindole (**1a**). The enolizable ketones **2j–l** failed to provide the products (see Table 2). Similarly, nonenolizable ketones **2p** and **2q** (Scheme 4) failed to provide the products. This

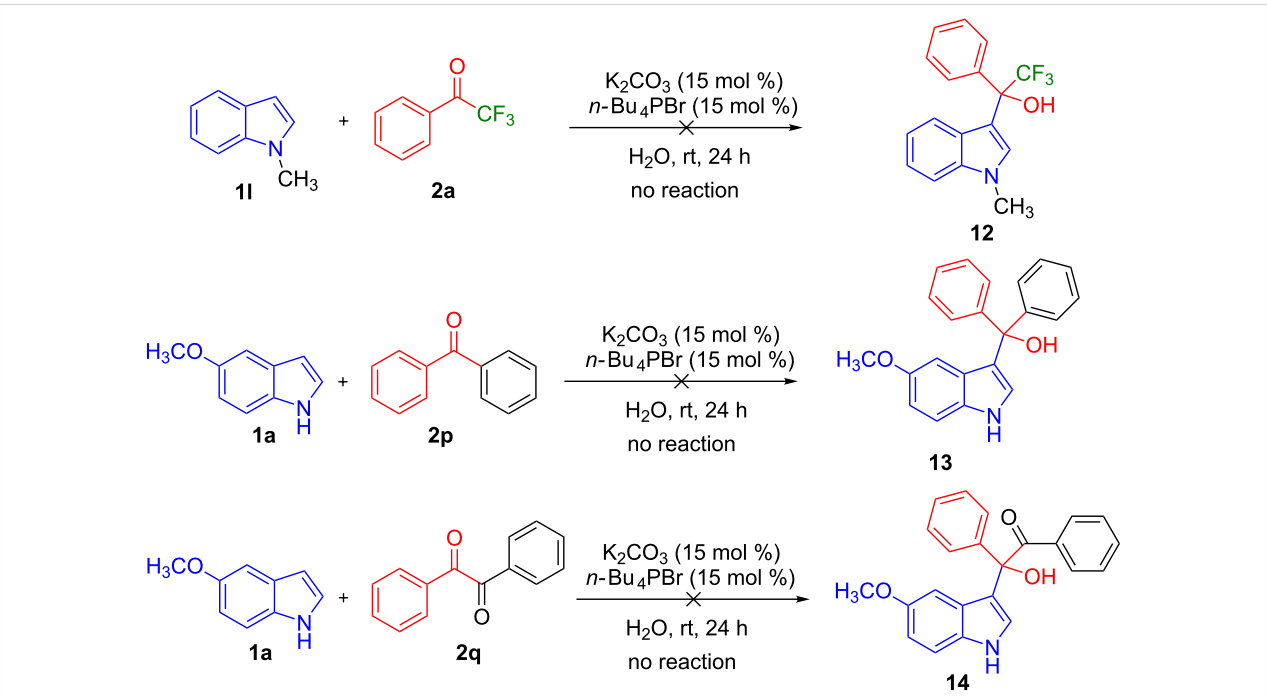

Scheme 4: Control experiments.

observation suggests that the multihalogen-substitution enhanced the electrophilicity of the ketone for the Friedel–Crafts hydroxyalkylation reaction of indole.

Conclusion

In conclusion, we have developed an efficient and practical protocol for the preparation of trifluoromethyl(indolyl)phenylmethanols, which are of significant interest serving as pre-electrophiles for C–C functionalization at the 3-position of indoles. Particularly, the Friedel–Crafts alkylation of 3-indolylmethanols with indoles has become a useful method for the preparation of 3,3'-, and 3,6'-DIMs, which are known to possess a wide variety of biological activities, including anti-inflammatory, and anticancer effects. Additionally, trifluoromethyl(indolyl)phenylmethanols itselft have various biological properties including anti-HIV activity. The developed new synthetic protocol for the preparation of trifluoromethyl(indolyl)phenylmethanols is operationally simple and provided products in high yields without requiring silica gel column chromatography. The reaction has a broad substrate scope and proceeds with high regioselectivity. The recovery and reusability of the catalytic system and large-scale synthesis of products, which would further transform into biologically active indole-derived compounds, are further advantages of this protocol.

Supporting Information

Materials and methods and detailed synthetic procedures and spectroscopic data of all compounds. Figure S1: ORTEP-type plot of the molecular structure of **3a**, Figures S2–S25: NMR spectra, Tables S1–S3: Crystal data and structure refinement for compound **3a**.

Supporting Information File 1

Experimental and analytical data.
[https://www.beilstein-journals.org/bjoc/content/supplementary/1860-5397-16-71-S1.pdf]

Acknowledgements

G.S. thanks Prof. Dr. A. C. Filippou and Prof. Dr. D. Menche for providing the X-ray infrastructure.

Funding

T.P. is grateful to the Alexander von Humboldt (AvH) foundation and to Bayer Pharma for a postdoctoral fellowship.

ORCID® iDs

Thanigaimalai Pillaiyar - https://orcid.org/0000-0001-5575-8896
Masoud Sedaghati - https://orcid.org/0000-0003-0762-2569

Preprint

A non-peer-reviewed version of this article has been previously published as a preprint doi:10.3762/bxiv.2020.17.v1

References

1. Mei, G.-J.; Shi, F. *J. Org. Chem.* **2017,** *82,* 7695–7707. doi:10.1021/acs.joc.7b01458
2. Li, X.; Tan, W.; Gong, Y.-X.; Shi, F. *J. Org. Chem.* **2015,** *80,* 1841–1848. doi:10.1021/jo502782b
3. Tan, W.; Du, B.-X.; Li, X.; Zhu, X.; Shi, F.; Tu, S.-J. *J. Org. Chem.* **2014,** *79,* 4635–4643. doi:10.1021/jo500644v
4. Liu, Y.; Zhang, H.-H.; Zhang, Y.-C.; Jiang, Y.; Shi, F.; Tu, S.-J. *Chem. Commun.* **2014,** *50,* 12054–12057. doi:10.1039/c4cc02056a
5. He, Y.-Y.; Sun, X.-X.; Li, G.-H.; Mei, G.-J.; Shi, F. *J. Org. Chem.* **2017,** *82,* 2462–2471. doi:10.1021/acs.joc.6b02850
6. Inamdar, S. M.; Gonnade, R. G.; Patil, N. T. *Org. Biomol. Chem.* **2017,** *15,* 863–869. doi:10.1039/c6ob02595a
7. Xiao, J.; Wen, H.; Wang, L.; Xu, L.; Hao, Z.; Shao, C.-L.; Wang, C.-Y. *Green Chem.* **2016,** *18,* 1032–1037. doi:10.1039/c5gc01838b
8. Suárez, A.; Martínez, F.; Sanz, R. *Org. Biomol. Chem.* **2016,** *14,* 11212–11219. doi:10.1039/c6ob02125e
9. Wen, H.; Wang, L.; Xu, L.; Hao, Z.; Shao, C.-L.; Wang, C.-Y.; Xiao, J. *Adv. Synth. Catal.* **2015,** *357,* 4023–4030. doi:10.1002/adsc.201500500
10. Pillaiyar, T.; Gorska, E.; Schnakenburg, G.; Müller, C. E. *J. Org. Chem.* **2018,** *83,* 9902–9913. doi:10.1021/acs.joc.8b01349
11. Deb, M. L.; Das, C.; Deka, B.; Saikia, P. J.; Baruah, P. K. *Synlett* **2016,** *27,* 2788–2794. doi:10.1055/s-0036-1588887
12. Jadhav, S. D.; Singh, A. *J. Org. Chem.* **2016,** *81,* 522–531. doi:10.1021/acs.joc.5b02383
13. Lancianesi, S.; Palmieri, A.; Petrini, M. *Adv. Synth. Catal.* **2012,** *354,* 3539–3544. doi:10.1002/adsc.201200632
14. Sun, F.-L.; Zheng, X.-J.; Gu, Q.; He, Q.-L.; You, S.-L. *Eur. J. Org. Chem.* **2010,** 47–50. doi:10.1002/ejoc.200901164
15. Sarubin-Fragakis, A.; Thomson, C. *The Health Professional's Guide to Popular Dietary Supplements;* American Dietetic Association, 2007; p 312.
16. Park, N. I.; Kim, J. K.; Park, W. T.; Cho, J. W.; Lim, Y. P.; Park, S. U. *Mol. Biol. Rep.* **2011,** *38,* 4947–4953. doi:10.1007/s11033-010-0638-5
17. Okulicz, M.; Hertig, I.; Chichłowska, J. *Czech J. Anim. Sci.* **2009,** *54,* 182–189. doi:10.17221/1745-cjas
18. Sarver, P. J.; Bacauanu, V.; Schultz, D. M.; DiRocco, D. A.; Lam, Y.-h.; Sherer, E. C.; MacMillan, D. W. C. *Nat. Chem.* **2020**. doi:10.1038/s41557-020-0436-1
19. Reddy, V. P. *Organofluorine compounds in biology and medicine;* Elsevier: Amsterdam, Netherlands, 2015. doi:10.1016/b978-0-444-53748-5.00001-0
20. Kirsch, P. *Modern fluoroorganic chemistry: Synthesis, reactivity, applications,* 2nd ed.; Wiley-VCH: Weinheim, Germany, 2013. doi:10.1002/9783527651351
21. Uneyama, K., Ed. *Organofluorine Chemistry;* Blackwell Publishing: Oxford, United Kingdom, 2006. doi:10.1002/9780470988589
22. O'Hagan, D. *J. Fluorine Chem.* **2010,** *131,* 1071–1081. doi:10.1016/j.jfluchem.2010.03.003
23. Jiang, H.-X.; Zhuang, D.-M.; Huang, Y.; Cao, X.-X.; Yao, J.-H.; Li, J.-Y.; Wang, J.-Y.; Zhang, C.; Jiang, B. *Org. Biomol. Chem.* **2014,** *12,* 3446–3458. doi:10.1039/c3ob42186d
24. Bandini, M.; Sinisi, R. *Org. Lett.* **2009,** *11,* 2093–2096. doi:10.1021/ol9005079

25. Liu, X.-D.; Wang, Y.; Ma, H.-Y.; Xing, C.-H.; Yuan, Y.; Lu, L. *Tetrahedron* **2017,** *73,* 2283–2289. doi:10.1016/j.tet.2017.03.012
26. Hua, Y.-Z.; Chen, J.-W.; Yang, H.; Wang, M.-C. *J. Org. Chem.* **2018,** *83,* 1160–1166. doi:10.1021/acs.joc.7b02599
27. Safrygin, A. V.; Irgashev, R. A.; Barabanov, M. A.; Sosnovskikh, V. Y. *Tetrahedron* **2016,** *72,* 227–233. doi:10.1016/j.tet.2015.11.037
28. Wang, Y.; Yuan, Y.; Xing, C.-H.; Lu, L. *Tetrahedron Lett.* **2014,** *55,* 1045–1048. doi:10.1016/j.tetlet.2013.12.078
29. Pillaiyar, T.; Köse, M.; Sylvester, K.; Weighardt, H.; Thimm, D.; Borges, G.; Förster, I.; von Kügelgen, I.; Müller, C. E. *J. Med. Chem.* **2017,** *60,* 3636–3655. doi:10.1021/acs.jmedchem.6b01593
30. Pillaiyar, T.; Dawood, M.; Irum, H.; Müller, C. E. *ARKIVOC* **2018,** No. iii, 1–19. doi:10.24820/ark.5550190.p010.259
31. Pillaiyar, T.; Uzair, M.; Ullah, S.; Schnakenburg, G.; Müller, C. E. *Adv. Synth. Catal.* **2019,** *361,* 4286–4293. doi:10.1002/adsc.201900688
32. Ling, Y.; An, D.; Zhou, Y.; Rao, W. *Org. Lett.* **2019,** *21,* 3396–3401. doi:10.1021/acs.orglett.9b01135
33. Sasaki, S.; Ikekame, Y.; Tanayama, M.; Yamauchi, T.; Higashiyama, K. *Synlett* **2012,** *23,* 2699–2703. doi:10.1055/s-0032-1317485
34. Muthukumar, A.; Sekar, G. *J. Org. Chem.* **2018,** *83,* 8827–8839. doi:10.1021/acs.joc.8b00844

License and Terms

This is an Open Access article under the terms of the Creative Commons Attribution License (http://creativecommons.org/licenses/by/4.0). Please note that the reuse, redistribution and reproduction in particular requires that the authors and source are credited.

The license is subject to the *Beilstein Journal of Organic Chemistry* terms and conditions: (https://www.beilstein-journals.org/bjoc)

The definitive version of this article is the electronic one which can be found at: doi:10.3762/bjoc.16.71

BEILSTEIN JOURNAL OF ORGANIC CHEMISTRY

Fluorinated phenylalanines: synthesis and pharmaceutical applications

Laila F. Awad* and Mohammed Salah Ayoup

Review

Open Access

Address:
Chemistry Department, Faculty of Science, Alexandria University, P.O. Box 426, Alexandria, 21321, Egypt

Email:
Laila F. Awad* - laila.fathy@yahoo.com; Mohammed Salah Ayoup - mohammedsalahayoup@gmail.com

* Corresponding author

Keywords:
α-fluorophenylalanine; β- and β,β-difluorophenylalanine; fluorinated phenylalanines; PET; pharmaceuticals application

Beilstein J. Org. Chem. **2020,** *16,* 1022–1050.
doi:10.3762/bjoc.16.91

Received: 25 February 2020
Accepted: 27 April 2020
Published: 15 May 2020

This article is part of the thematic issue "Organo-fluorine chemistry V".

Guest Editor: D. O'Hagan

© 2020 Awad and Ayoup; licensee Beilstein-Institut.
License and terms: see end of document.

Abstract

Recent advances in the chemistry of peptides containing fluorinated phenylalanines (Phe) represents a hot topic in drug research over the last few decades. D- or L-fluorinated phenylalanines have had considerable industrial and pharmaceutical applications and they have been expanded also to play an important role as potential enzyme inhibitors as well as therapeutic agents and topography imaging of tumor ecosystems using PET. Incorporation of fluorinated aromatic amino acids into proteins increases their catabolic stability especially in therapeutic proteins and peptide-based vaccines. This review seeks to summarize the different synthetic approaches in the literature to prepare D- or L-fluorinated phenylalanines and their pharmaceutical applications with a focus on published synthetic methods that introduce fluorine into the phenyl, the β-carbon or the α-carbon of D-or L-phenylalanines.

Introduction

Major efforts have been focused on the synthesis of fluorinated organic molecules particularly for drug development. The replacement of hydrogen by fluorine has been used in the development to improve the biophysical and chemical properties of bioactives. Such tuning in properties arises from the small size of fluorine, the next in size to hydrogen. However, the high electronegativity of the fluorine leads to low polarizability and a strong covalent bond to carbon [1-4]. Therefore, the introduction of fluorine into phenylalanine (Phe) can modulate the acidity, basicity, hydrophobicity, geometry, conformation, reactivity, and moreover the bioavailability of the analogue [1]. Fluorinated amino acids (FAAs) have considerable industrial and pharmaceutical potential [2]. Also, they have played an important role as enzyme inhibitors as well as therapeutic agents [3,4]. Moreover, they modulate the properties of peptides and proteins [5-7], influencing aspects such as protein folding, protein–protein interactions, ribosomal translation, lipophilicity, acidity/basicity, optimal pH, stability, thermal stability, and therapeutic properties [8-10]. This extends to metabolic properties of membrane permeability and reactivity [11-14]. The

effect of peptide structure and stability has been found to depend on the position and number of fluorine atoms within the amino acid chains [15-17]. Incorporation of fluorinated aromatic amino acids into proteins can increase their shelf life, especially in therapeutic proteins and peptide-based vaccines [18]. Enhanced catabolic stability [6] can arise from the role of particular aromatic amino acids in membrane–protein interactions [19]. Furthermore, fluorinated aromatic amino acids can alter enzymatic activity as a result of enhanced protein stability [5]. Also fluorinated aromatic amino acids can destabilize II-cation interactions whereas their increased hydrophobicity enhances binding affinity [19]. Moreover, the incorporation of fluorinated amino acids into proteins provides the opportunity for probing structure (by NMR techniques) including protein–protein and protein–ligand interactions and consequently metabolic processes [20,21].

Fluorinated phenylalanines (FPhe) have been incorporated into various proteins and enzymes [22-25] with advantageous biophysical, chemical, and biological properties, and their effect on the stability and activity of peptides in therapeutic vaccines and enzymes has been studied [19,26-33].

In this review we provide an overview for the various syntheses of FPhes and analogues. Five different categories of FPhe are represented and are classified **I**–**V** according to the position of the fluorine(s) (Figure 1).

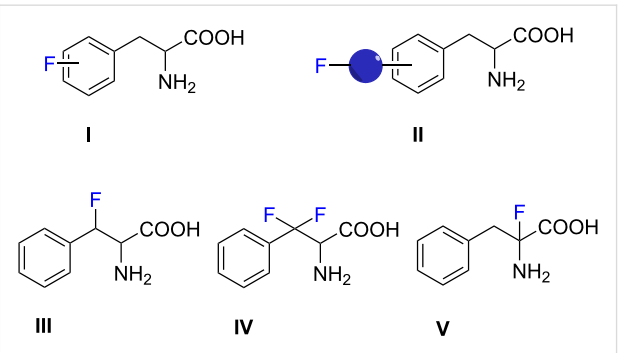

Figure 1: Categories **I**–**V** of fluorinated phenylalanines.

Review

1. Synthesis of fluorinated phenylalanine of type **I** and **II**

Direct attachment of the fluorine atom to the aryl ring of Phe or fluorinated groups directly attached to a spacer extending from the aryl ring constitute types **I** and **II** (Figure 1), accordingly we reported herein different methods for their synthesis.

1.1. Negishi cross coupling of aryl halide and organozinc compounds

Jackson and co-workers reported the synthesis of a range of phenylalanine derivatives via Negishi cross-coupling reactions of aryl halides and Zn homoenolates of the protected (*R*)-iodoalanine **2**. The reaction was activated using Pd(0) as a catalyst.

A palladium-catalyzed cross-coupling reaction between an organozinc iodide and aryl halides offers a convenient method for the direct preparation of protected fluorinated Phe analogues **3**. Thus, cross coupling of the protected iodoalanine **2** with 4-fluorobromobenzene (**1a**) or 2- and 4-fluoroiodobenzene (**1b** and **1c**), respectively, was accomplished using the reported coupling conditions in Scheme 1 to give the *N*-Boc-protected 2- or 4-fluoro-L-phenylalanine esters **3a**,**b** [34,35].

On the other hand, attempted cross-coupling of fluoroiodobenzenes **1b** and **1c** with iodoalanine **2** at room temperature using $Pd_2(dba)_3$ (2.5 mol %) and SPhos (5.0 mol %) provided excellent yields of (*S*)-phenylalanines **3a** (70% yield) and **3b** (80% yield), respectively. Such an efficiency improvement testifies to the suitability of SPhos as a ligand for these coupling reactions, rather than the less-reactive organozinc reagents [36] (Scheme 1). Decreasing the molar ratio of $Pd_2(dba)_3$/SPhos to 0.25:0.5 mol % provided a lower yield of **3a** (21%), whereas **3b** showed only a slight decrease in yield (77%).

The two-inseparable *para*/*meta* isomers of all-*cis*-2,3,5,6-tetrafluorocyclohexylphenyliodide **4** and **5** were subjected to Jackson's methodology for the synthesis of the appropriate

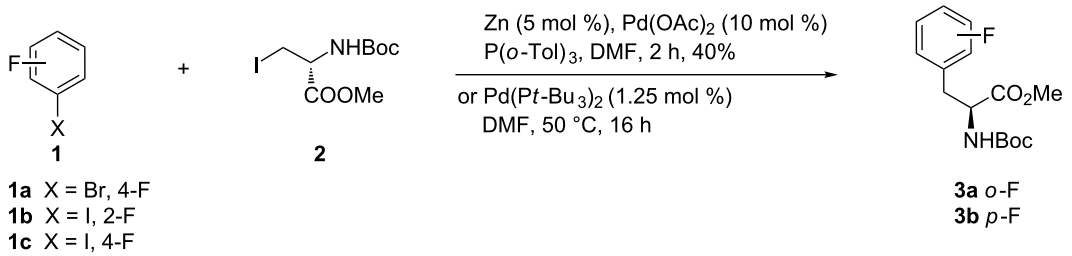

Scheme 1: Synthesis of fluorinated phenylalanines via Jackson's method.

amino acid products. Thus, the coupling of the zinc homoenolate of (*R*)-iodoalanine **2** with a mixture of **4** and **5** in the presence of $Pd(dba)_3$ and SPhos resulted in an excellent conversion to the fully protected amino acid isomers **6** and **7**, which were readily separated from each other by chromatography. Deprotection of isomers **6** and **7** gave the individual free amino acids *p*-(*S*)-**8** and *m*-(*S*)-**9** [37,38] (Scheme 2).

Coupling of one molar equivalent of neopentyl sulfonate ester **10a** or trichloroethyl ester **10b** with two molar equivalents of the zincate of Fmoc-3-iodo-L-alanine methyl ester **11**, to form the protected L-4-[sulfono(difluoromethyl)]phenylalanines **12a** and **12b**, was carried out using 5 mol % $(PPh_3)_2PdCl_2$ and 10 mol % DIBAL in THF/DMAC 1:1 at 65–70 °C for 6 h. Partial deprotection by alkaline hydrolysis of **12a** and **12b** afforded L-4-[sulfono(difluoromethyl)]phenylalanine derivatives **13a** and **13b**, respectively [39] (Scheme 3).

1.2. Alkylations of fluorinated aryl halides with a chiral auxiliary

Alternatively, the coupling of the bis(dimethoxybenzyl)-protected sulfonamide **14**, instead of the esters **10a** and **10b** with zincate **11** using a variety of catalysts and different reaction conditions, was unsuccessful. However, coupling of 4-[bis(dimethoxybenzyl)difluoromethyl]benzyl bromide (**14**) with the lithium enolate of William`s lactone **15** gave the pro-

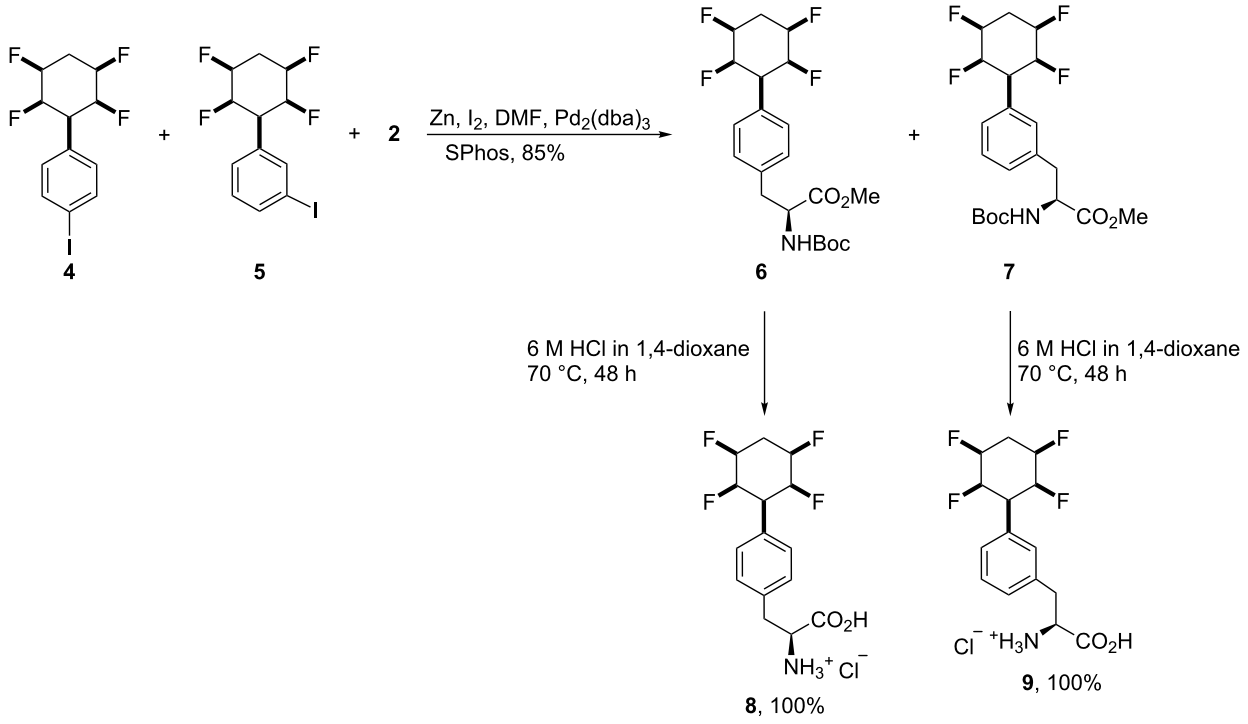

Scheme 2: Synthesis of all-*cis*-tetrafluorocyclohexylphenylalanines.

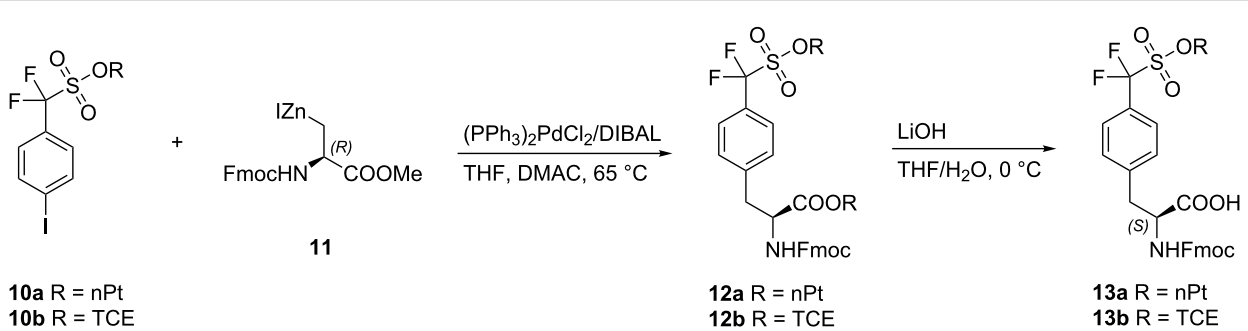

Scheme 3: Synthesis of L-4-[sulfono(difluoromethyl)]phenylalanine (nPt: neopentyl, TCE: trichloroethyl).

tected amino acid **16** in 80% yield. The desired protected amino acid **17** was readily obtained after reduction of **16** using $PdCl_2$ as a catalyst, followed by treating the product with Fmoc-OSu in dioxane/aq Na_2CO_3 (99%, two steps) [40] as illustrated in Scheme 4.

The reaction of aminomalonate **18** with fluorinated benzyl bromides **19a–c** afforded the corresponding aralkyl diesters **20a–c**. Partial hydrolysis followed by decarboxylation gave the *N*-benzyloxycarbonyl DL-amino acid esters **22a–c**, which upon enzymatic hydrolysis of the ester group using the subtilisin-type Carlsberg enzyme led to D-amino acid esters **23a–c** and the corresponding Cbz-protected *p*, *m*-fluoro-, or pentafluoro-L-phenylalanine derivatives **24a**–**c**, respectively [41] (Scheme 5).

The stereoselective benzylation of (*S*)-imidazolidinone ((*S*)-Boc-BMI) **25** with tetrafluorobenzyl bromides **26a**,**b** afforded the benzylated imidazolidinones **27a**,**b**. The acidic hydrolysis of **27a**,**b** with simultaneous deprotection to release the free amines gave amides **28a**,**b**. Treatment of the latter with aqueous potassium hydroxide finally afforded (*S*)-2-amino-3-(2,3,4,5-tetrafluorophenyl)propionic acid (**29a**) and (*S*)-2-amino-3-(2,3,5,6-tetrafluorophenyl)propionic acid (**29b**) [42] (Scheme 6).

Alternatively, phenylalanines **29a**,**b** were also synthesized by alkylation of **26a**,**b** with the chiral auxiliary **31**, which was obtained by reaction of the cyclic dipeptide **30** with triethyloxonium tetrafluoroborate. The alkylation reaction of **26a**,**b** was carried out with *n*-BuLi in THF at −78 °C to give **32a**,**b**. Acid hydrolysis of the alkylated product **32a**,**b** afforded the ethyl

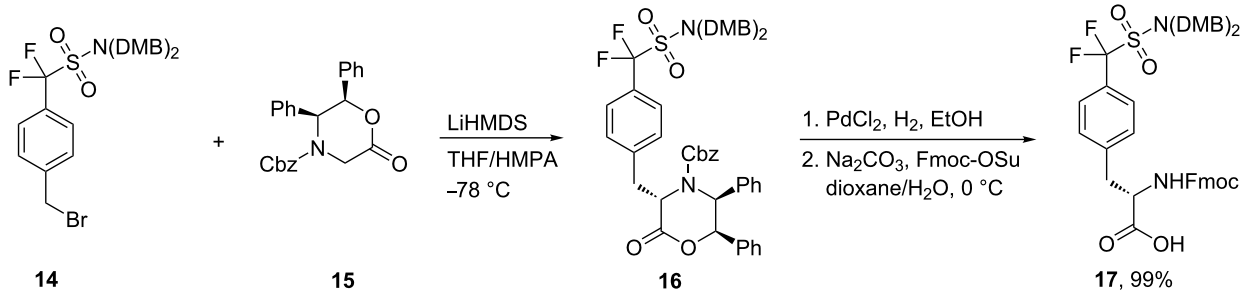

Scheme 4: Synthesis of L-4-[sulfono(difluoromethyl)]phenylalanine derivatives **17**.

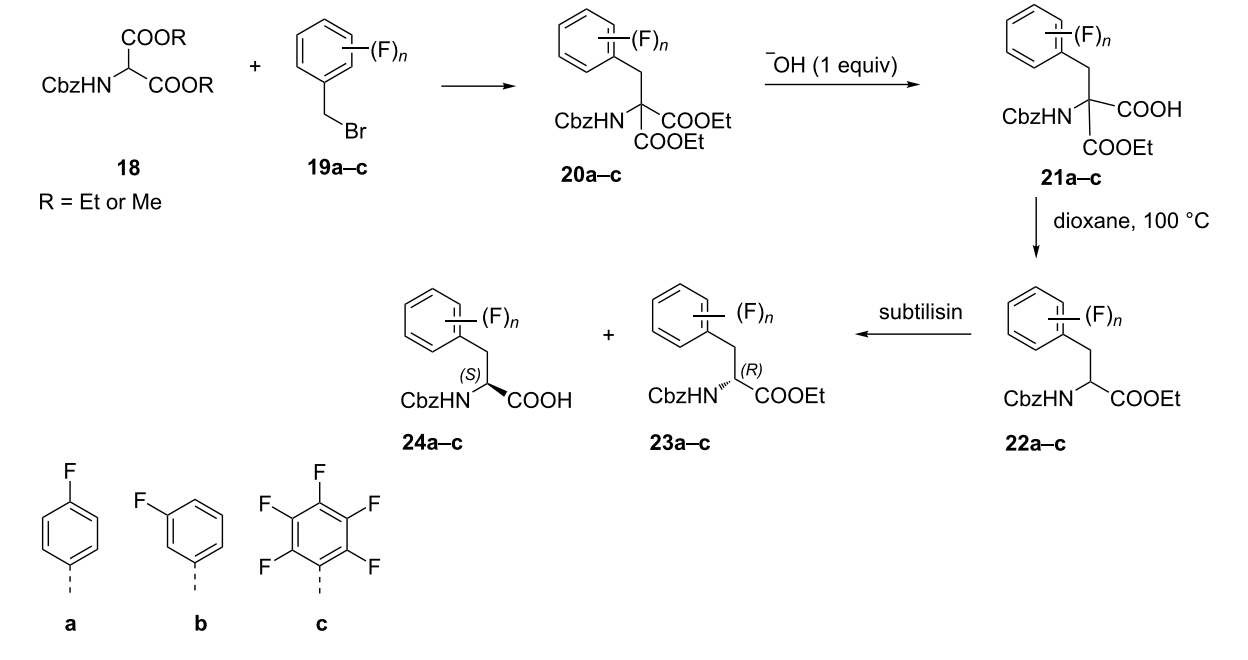

Scheme 5: Synthesis of fluorinated Phe analogues from Cbz-protected aminomalonates.

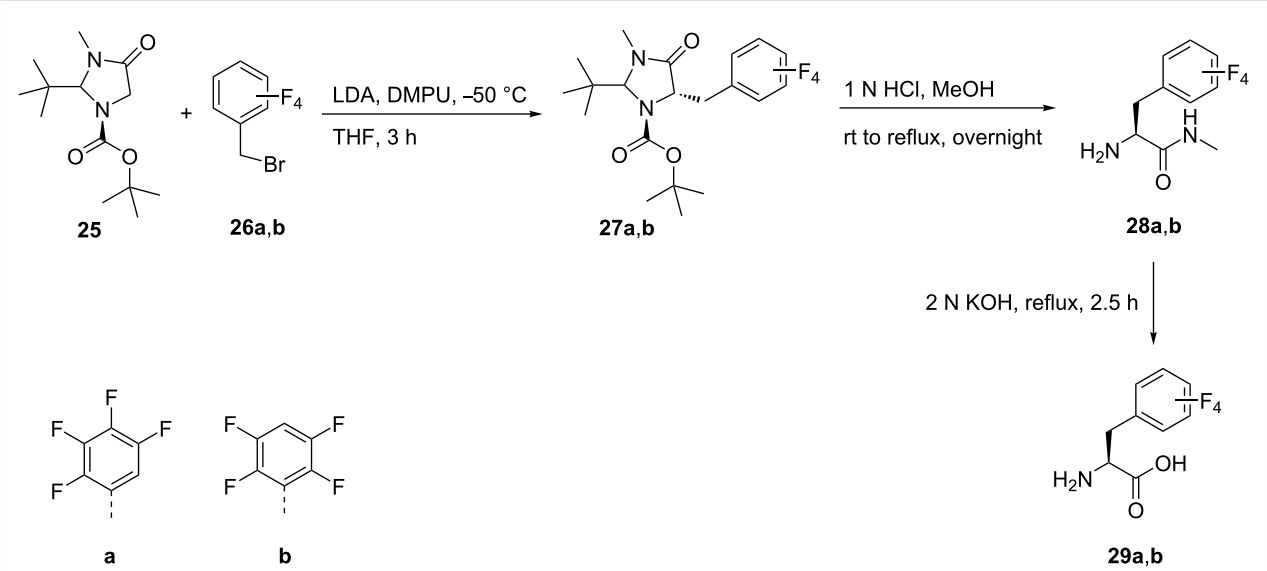

Scheme 6: Synthesis of tetrafluorophenylalanine analogues via the 3-methyl-4-imidazolidinone auxiliary **25**.

esters of tetrafluorophenylalanine **33a**,**b**, which by alkaline hydrolysis afforded the tetrafluoro derivatives **29a** and **29b**, respectively [43] (Scheme 7).

The syntheses of (*R*)-**38a** and (*R*)-**38b** were carried out by alkylation of the Schöllkopf reagent ((2*S*)-(+)-2,5-dihydro-3,6-dimethoxy-2-isopropylpyrazine, **34**) with the corresponding fluorinated benzyl bromides **35a**,**b** via intermediates **36a**,**b**. The alkylation products were then hydrolyzed to generate the amino acid esters which were directly Boc protected to give the *N*-Boc-protected amino acid methyl esters **37a**,**b**. Finally, ester hydrolysis afforded the useful Boc-(*R*)-amino acids **38a**,**b** [44] (Scheme 8).

A one-pot double alkylation of the chiral auxiliary **39** with benzyl iodides **40a**,**b** gave *cis*-dialkyl derivatives **41a**,**b** in 70–72% yield. The subsequent removal of the auxiliary followed by treatment with Fmoc-OSu gave the *N*-protected 2-fluoro- and 2,6-difluorophenylalanine derivatives **42a**,**b** in quantitative yields [45] (Scheme 9).

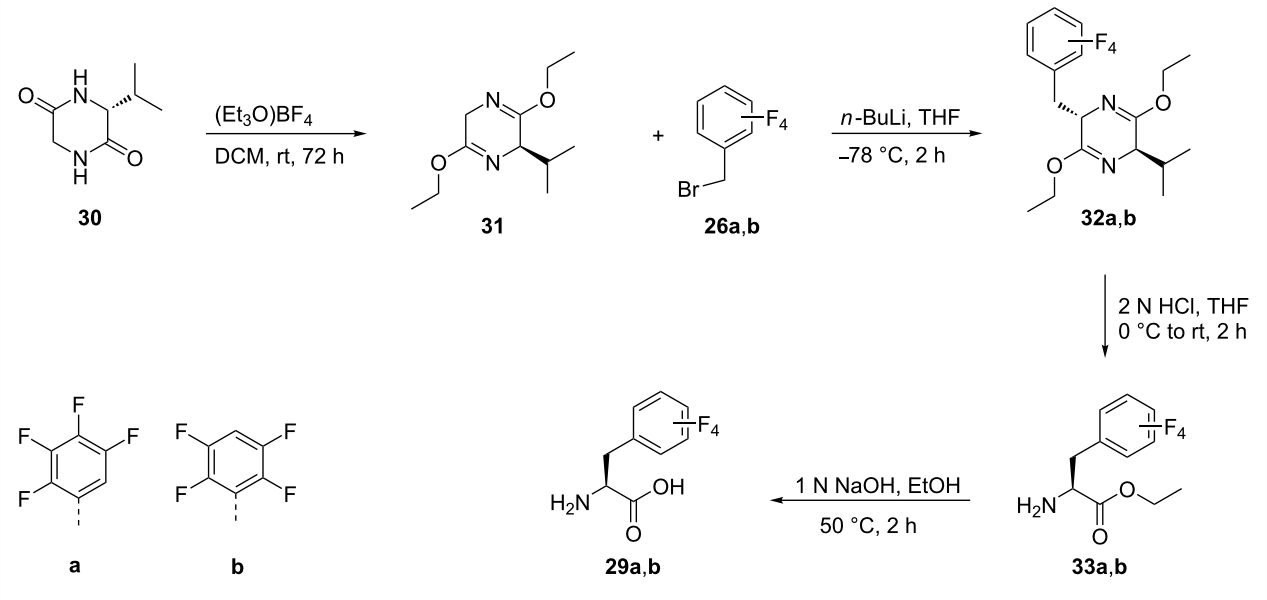

Scheme 7: Synthesis of tetrafluoro-Phe derivatives via chiral auxiliary **31**.

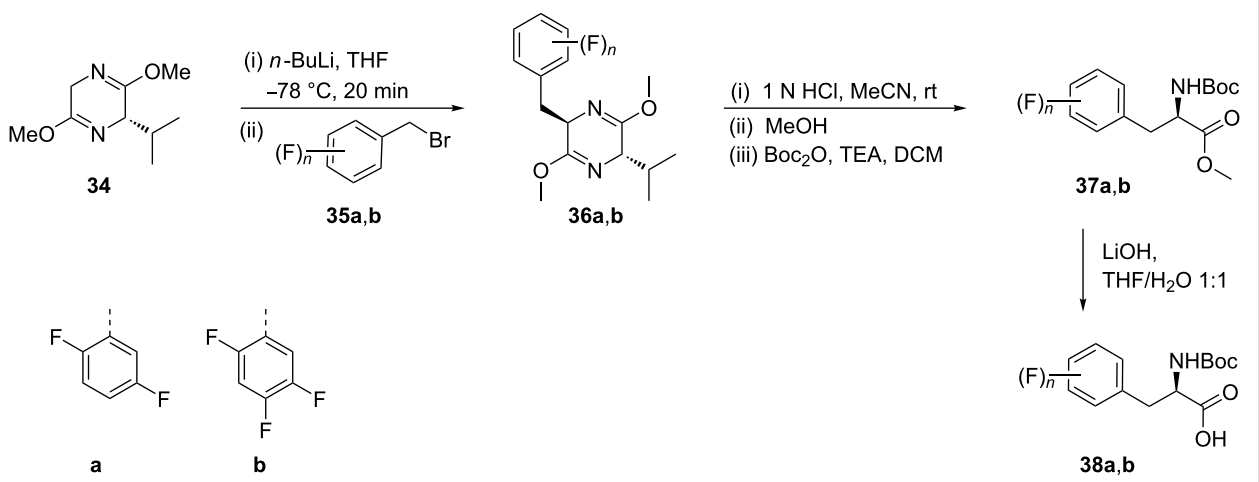

Scheme 8: Synthesis of 2,5-difluoro-Phe and 2,4,5-trifluoro-Phe via Schöllkopf reagent **34**.

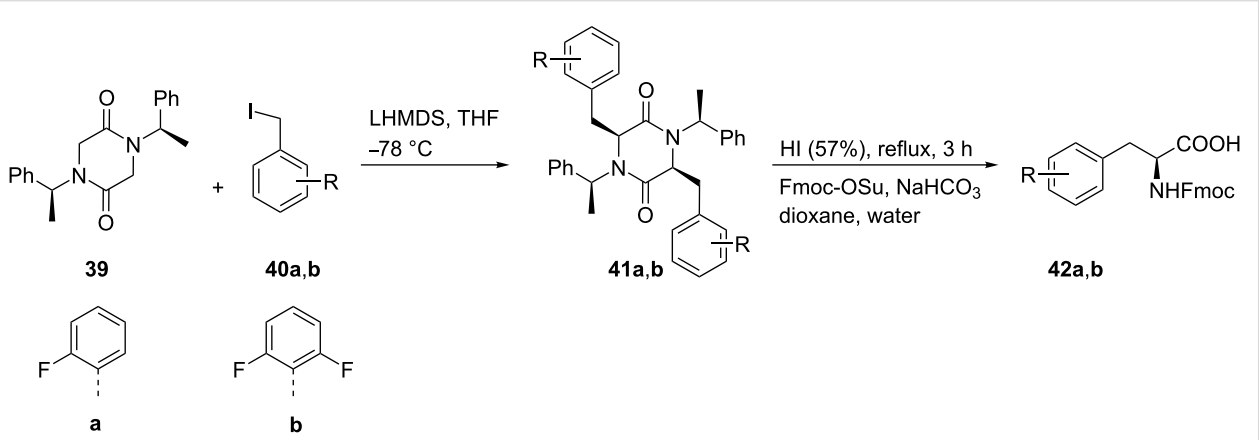

Scheme 9: Synthesis of 2-fluoro- and 2,6-difluoro Fmoc-Phe derivatives starting from chiral auxiliary **39**.

The radiolabeled 2-[^{18}F]-fluoro-L-phenylalanine **46** was synthesized as a promising radiopharmaceutical agent for molecular imaging by positron emission tomography (PET). The three-step synthesis of **46** started from [^{18}F]-fluoride exchange in **43** to generate **44**. The isotope exchange was explored by using [^{18}F]-TBA in DMF at 130 °C for 10 min to give [^{18}F]-**44**. Decarbonylation of **44** was achieved by treatment with $Rh(PPh_3)_3Cl$ to afford **45** and the subsequent removal of protecting groups gave **46**. Conventional reactions yielded the desired product 2-[^{18}F]FPhe **46** in 43% yield, whereas under microwave irradiation a 34% yield was obtained. Under the optimized conditions, the enantiomeric purity was reported to be ≥94% ee [46] (Scheme 10).

1.3. Photooxidative cyanation of fluorinated benzylamine

A convenient, protecting group-free, and semicontinuous process was reported for the synthesis of racemic fluorinated phenylalanine·HCl starting from benzylamines **47a–c**. Thus, a singlet oxygen-driven photooxidative cyanation of amines **47a–c** using tetraphenylporphyrin (Tpp), followed by an acid-mediated hydrolysis of the intermediate fluorinated α-amino nitrile **48a** with 30% HCl aq/acetic acid, gave the 4-fluorophenylalanine·HCl **49a** in a good overall yield (67%) [47] (Scheme 11).

1.4. Hydrolysis of Erlenmeyer's azalactone

A multistep Erlenmeyer azalactone synthesis was reported as an important method for the synthesis of fluorinated α-amino acids **53a–h**. Thus, a three-component condensation of a series of fluorinated benzaldehydes **50a–h**, *N*-acetyl- or *N*-benzoylglycine **51a** or **51b**, respectively, and an excess of acetic anhydride in the presence of sodium acetate afforded the oxazolones **52a–h**. The subsequent reductive ring cleavage of **52a–h** without isolation, was carried out with red phosphorus in hydroiodic acid to give the fluorinated phenyl-

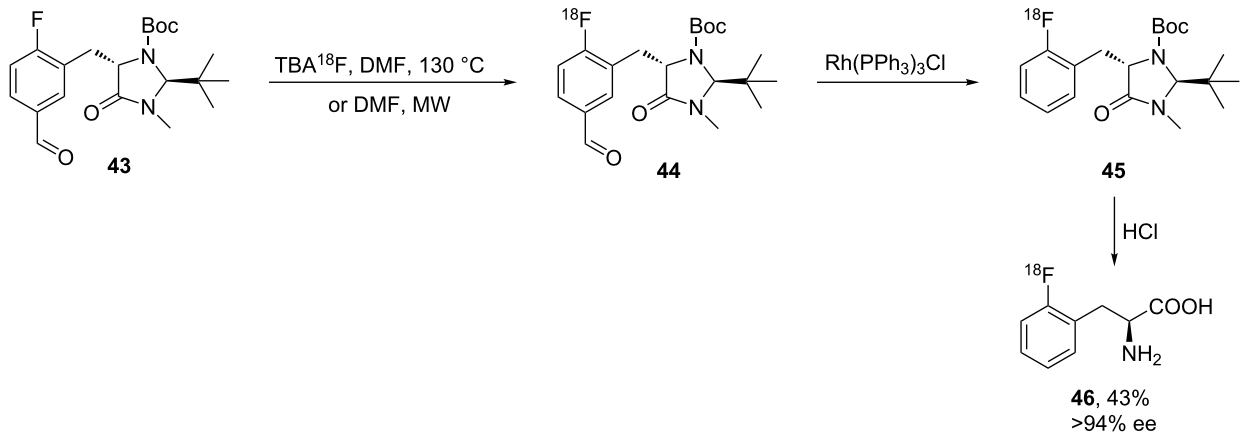

Scheme 10: Synthesis of 2-[^{18}F]FPhe via chiral auxiliary **43**.

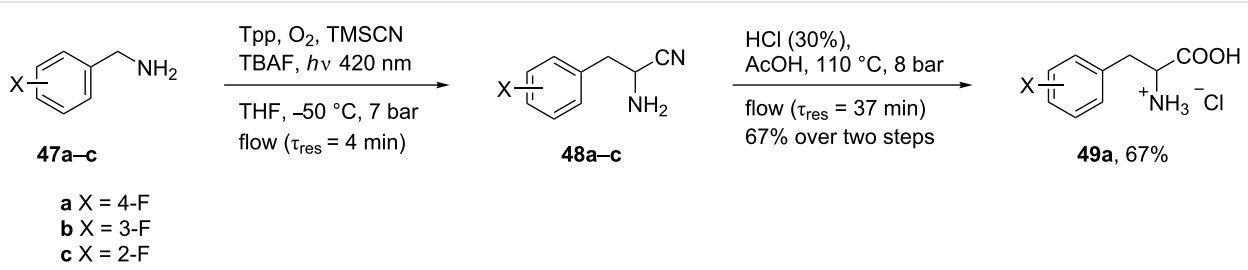

Scheme 11: Synthesis of FPhe **49a** via photooxidative cyanation.

alanine analogues **53a–h**. Alternatively, a two-step sequence to generate amino acids **53a–h** was attempted by first hydrolysis of **52a–h** to form acids **54a–h** which then were reduced with P/HI to the desired products **53a–h** [48]. The free amino acid **53i** was prepared by the same protocol [49] (Scheme 12).

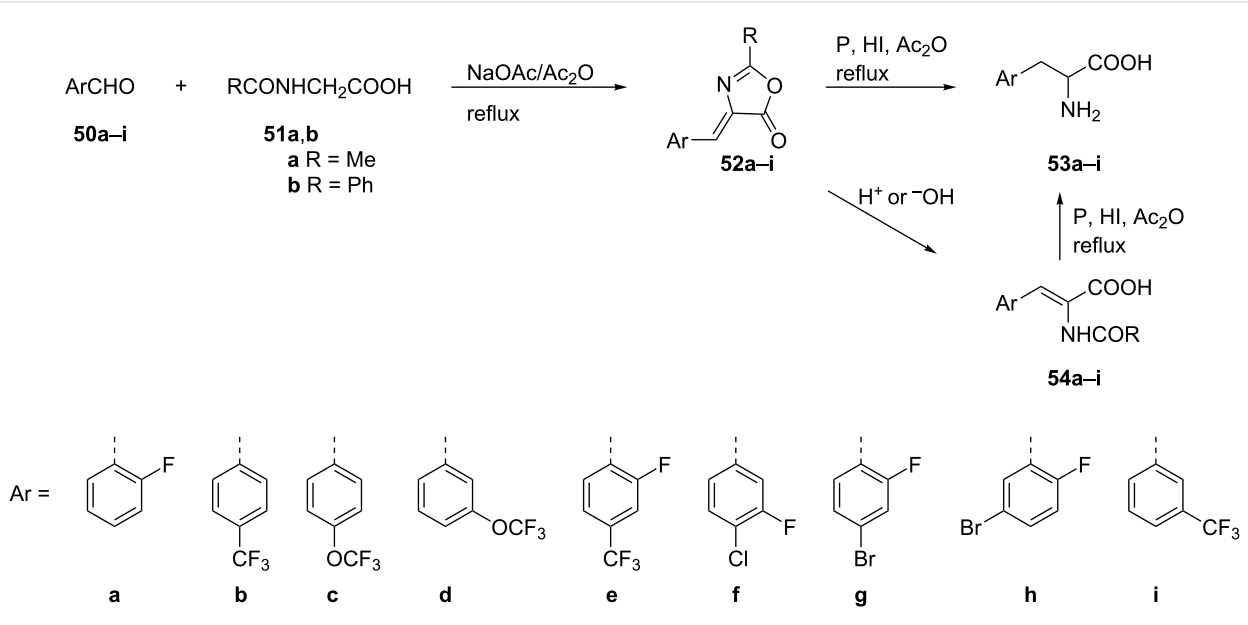

Scheme 12: Synthesis of FPhe derivatives via Erlenmeyer azalactone synthesis.

2,5-Difluorophenylalanines with either *R* or *S* configuration were synthesized also via the Erlenmeyer azalactone method. The synthesis started with the multicomponent reaction of aldehyde **55**, acetylglycine **51a** and acetic anhydride to give the azalactone **56**. The subsequent basic hydrolysis of **56** gave **57** that, on catalytic hydrogenation, afforded racemic difluorinated Phe **58**. The isomers were separated by selective hydrolysis using a protease from *Bacillius sp* to generate the (*S*)-*N*-acetyl acid **59** with >99.5% ee and the corresponding (*R*)-*N*-acetyl ester **60** with >99.5% ee [50] (Scheme 13).

The synthesis of 3-bromo-4-fluoro-(*S*)-Phe (**65**) was carried out by reacting 3-bromo-4-fluorobenzaldehyde (**61**) and *N*-acetylglycine (**51a**) to provide intermediate **63** in high yield and without purification. Then, the transition-metal-catalyzed asymmetric hydrogenation of the α-amidocinnamic acid **63** using the less frequently used ferrocene-based ligand Me-BoPhoz led to the *N*-acetyl-L-phenylalanine derivative **64** with complete conversion and with 94% ee. The desired enantiomer (*S*)-**65** was obtained as a single isomer (>99% ee) after selective enzymatic hydrolysis of **64** using an acylase under mild conditions (pH 8.0, 40 °C, 4 d, with $CoCl_2$ as co-factor) [51] (Scheme 14).

1.5. Direct radiofluorination of L-phenylalanine

The direct radiofluorination of L-phenylalanine (**66**) with either $[^{18}F]F_2$ or [^{18}F]AcOF in trifluoroacetic acid (TFA) afforded the three isomeric *o*, *m*, and *p*-fluoro-L-phenylalanines **46**, **67**, and **68**, in ratio 72.5:13.9:13.6, respectively. In this reaction, [^{18}F]AcOF showed a higher regioselectivity and less side product formation compared with $[^{18}F]F_2$ [52] (Scheme 15).

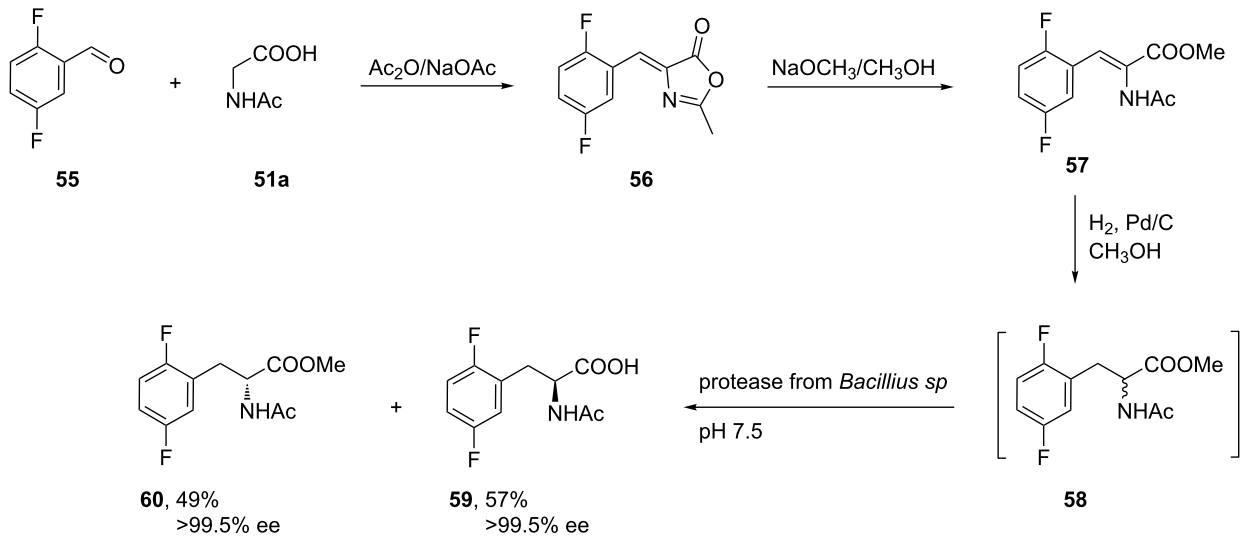

Scheme 13: Synthesis of (*R*)- and (*S*)-2,5-difluoro Phe via the azalactone method.

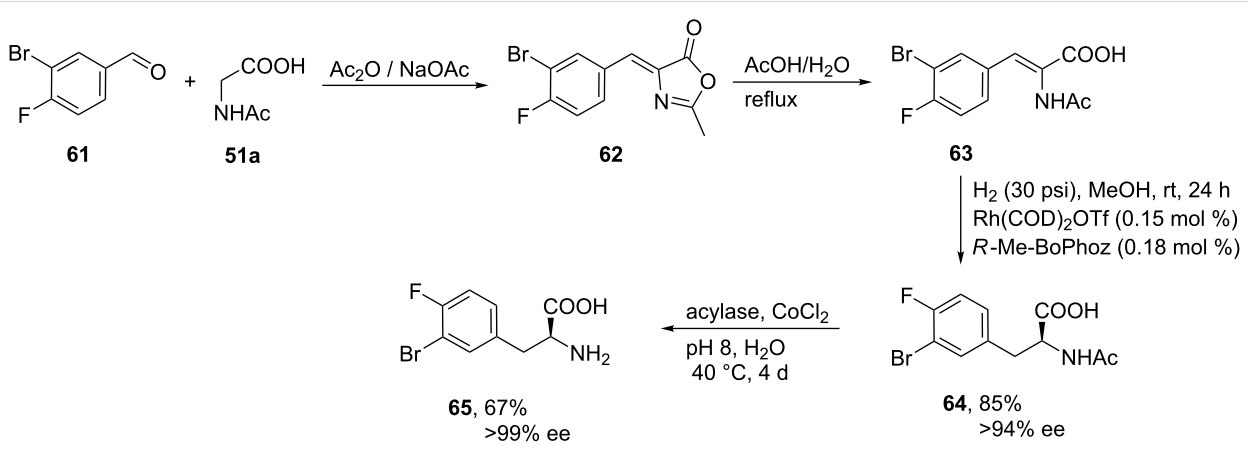

Scheme 14: Synthesis of 3-bromo-4-fluoro-(*S*)-Phe (**65**).

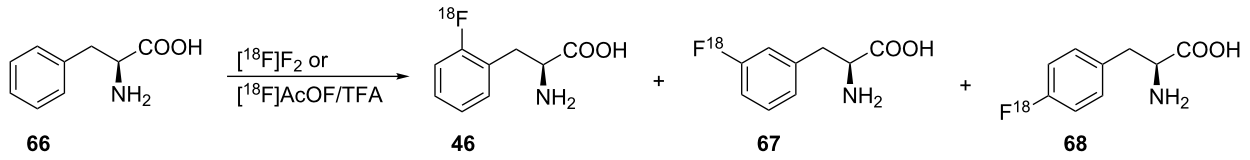

Scheme 15: Synthesis of [^{18}F]FPhe via radiofluorination of phenylalanine with [^{18}F]F_2 or [^{18}F]AcOF.

The radiolabeled compound, 4-borono-2-[^{18}F]fluoro-L-phenylalanine (**70**) was prepared by direct fluorination of 4-borono-L-phenylalanine (BPA, **69**) with [^{18}F]AcOF or [^{18}F]F_2. The reaction was followed by a HPLC separation using a Delta-Pak Cl8 cartridge 0.1% acetic acid as the mobile phase at a flow rate of 10 mL/min. The product was isolated in radiochemical yields of 25–35% and with a radiochemical purity of more than 99%. The ^{18}F-labeling of 4-borono-D,L-phenylalanine (BPA) provided a potential tool for cancer treatment by boron neutron capture therapy [53] (Scheme 16).

The syntheses of a variety of clinically relevant radiotracers including protected 4-[^{18}F]fluorophenylalanines **72a**,**b** [54] were achieved by a copper-mediated nucleophilic radiofluorination of arylstannanes **71a**,**b** with [^{18}F]KF (Scheme 17).

1.6. Alkylation of benzophenone imine of glycine ester

Pentafluoro-L-phenylalanine (**77a**) and 2,4-ditrifluoromethyl-L-phenylalanine (**77b**) were synthesized through alkylation of the benzophenone imine of glycine ester **73**, with perfluorinated benzylbromide **19c** or 2,4-bis(trifluoromethyl)benzyl bromide (**74**) in the presence of 2,7-bis[*O*(9)-allylhydrocinchonidinium-*N*-methyl]naphthalene dibromide, to afford the fluorinated phenylalanine imines **75a**,**b** with ees < 98%. The products were hydrolyzed and deprotected in a two-step protocol to afford the desired products **77a**,**b** [55] (Scheme 18).

Interestingly substitution of Phe by either **77b** or **77a** in the proteasome inhibitors bortezomib or epoxymicin, led to an increase in the efficiency as anticancer proteasome inhibitors. The fluorinated amino acids **77a** and **77b** were used mainly for two reasons, i.e., the ready availability and hydrophobicity [55].

Further, (*S*)-pentafluorophenylalanine (Pff, **77a**) was used to stabilize proteins for potential applications in various protein-based biotechnologies. To improve protein stability, natural hydrocarbon amino acids were replaced with Pff **77a**. The effect of enhanced protein stability upon this replacement is referred as to 'fluoro-stabilization effect' [56].

1.7. Knoevenagel condensation of methyl isocyanoacetate

Three isomers of fluorinated phenylalanines **53a**,**b** and **81** were synthesized by Knoevenagel condensation of methyl isocyanoacetate (**79**) and the corresponding fluorinated benzaldehyde derivatives **50a**,**b**, and *m*-fluorobenzaldehyde (**78**) as electrophiles in the presence of catalytic amounts of Cu(I) and base. The cinnamate derivatives **80a–c** obtained were hydrogenated either under homogeneous or heterogeneous conditions fol-

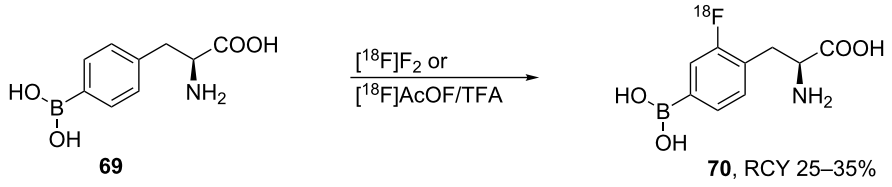

Scheme 16: Synthesis of 4-borono-2-[^{18}F]FPhe.

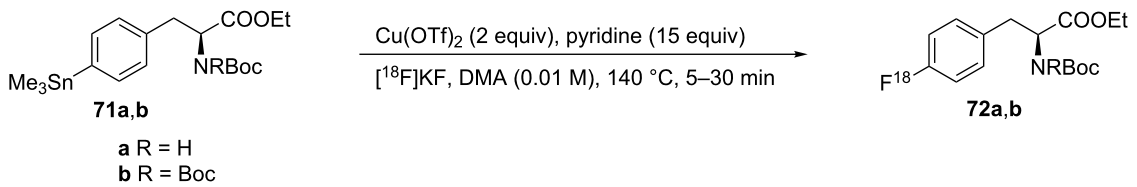

Scheme 17: Synthesis of protected 4-[^{18}F]FPhe via arylstannane derivatives.

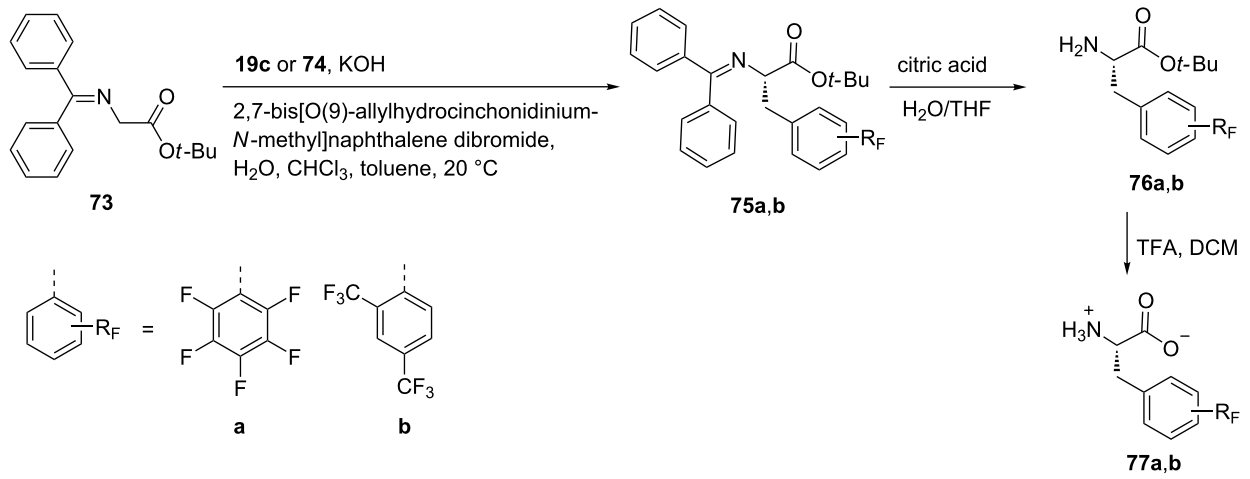

Scheme 18: Synthesis of FPhe derivatives via intermediate imine formation.

lowed by deprotection of both the amide and the ester moieties to give the racemic fluorinated phenylalanines **53a**,**b**, or *m*-fluorophenylalanine (**81**) with good yields [57] (Scheme 19).

1.8. Coupling of *N*-hydroxytetrachlorophthalimide esters with boronic acids

4-(2-Fluoroethyl)-L-phenylalanine and 3-(2-fluoroethyl)-L-phenylalanine (**88a**,**b**), respectively, were synthesized starting from partially protected L- or D-aspartic acid derivatives **82** which were activated as the *N*-hydroxytetrachlorophthalimide esters **83**. The treatment of the esters **83** with boronic acids **84a**,**b** afforded the substituted phenylalanine derivatives **85a**,**b**, respectively [58]. Deprotection of the hydroxy group was achieved by treatment with TBAF in THF to give **86a**,**b**. Finally, fluorination of the alcohols **86a**,**b** with DAST followed by deprotection gave the targeted compounds **88a**,**b** (Scheme 20).

Cross-coupling reactions with boronic acids were found to be successful only for the synthesis of *para* and *meta*-derivatives. Several attempts were made to prepare the *ortho*-substituted derivatives **93** and **95**. The synthesis of D,L-**93** or L-**95** was achieved by vinylation of the protected D,L-*N*-Boc-2-bromophenylalanine (**89**) using a Stille coupling reaction to give the *o*-vinyl derivative **90** as key intermediate. A hydroboration reaction of compound **90** afforded the primary alcohol **91**, which was directly fluorinated and deprotected to give the free amino acids **93** (D and L). Alternatively, alcohol **91** was activated by tosylation to give **94** as a precursor for radiofluorination that was achieved to give 2-[^{18}F]FELP L-**95** using [^{18}F]-fluoride complexed with Kryptofix®/K^+ followed by deprotection with HCl and purification. This product emerged as promising new PET tracer for brain tumor imaging [58] (Scheme 21).

1.9. Alkylation and hydrolysis of Ni(II) or Zn(II) complexes

The synthesis of a series of fluorinated phenylalanines was achieved by transamination reactions between (*R*) or (*S*)-(15-aminomethyl-14-hydroxy-5,5-dimethyl-2,8-dithia[9](2,5)pyr-

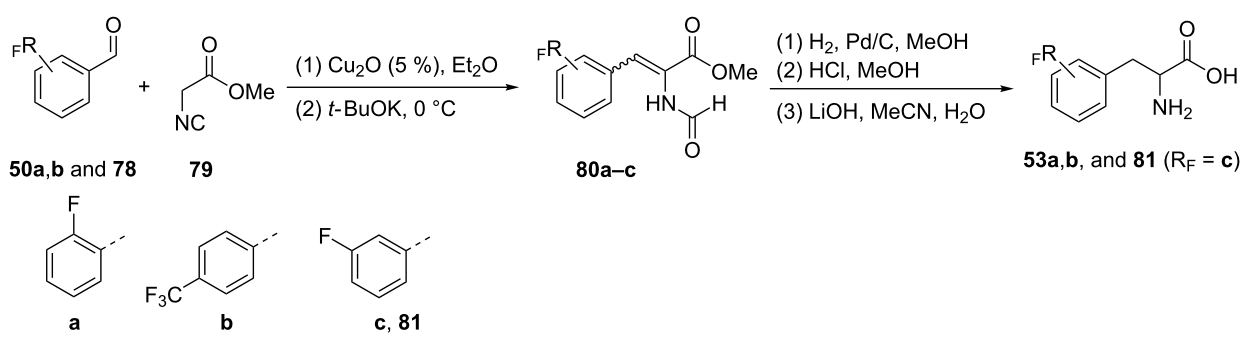

Scheme 19: Synthesis of FPhe derivatives via Knoevenagel condensation.

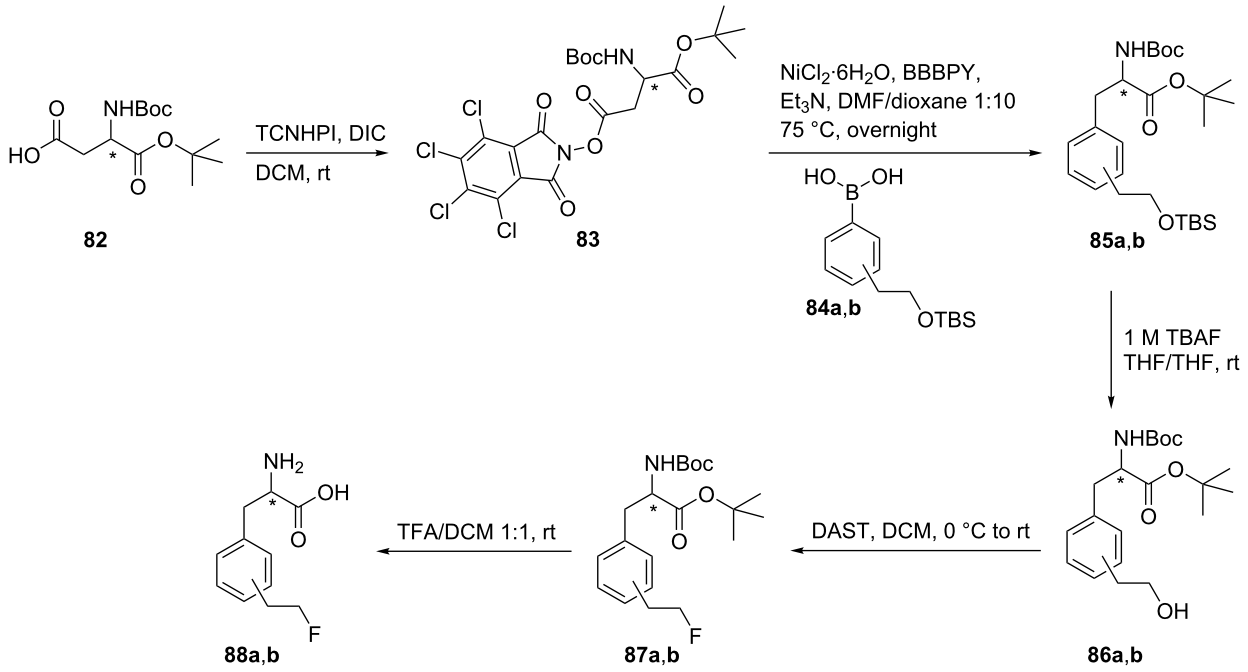

Scheme 20: Synthesis of FPhe derivatives **88a**,**b** from aspartic acid derivatives.

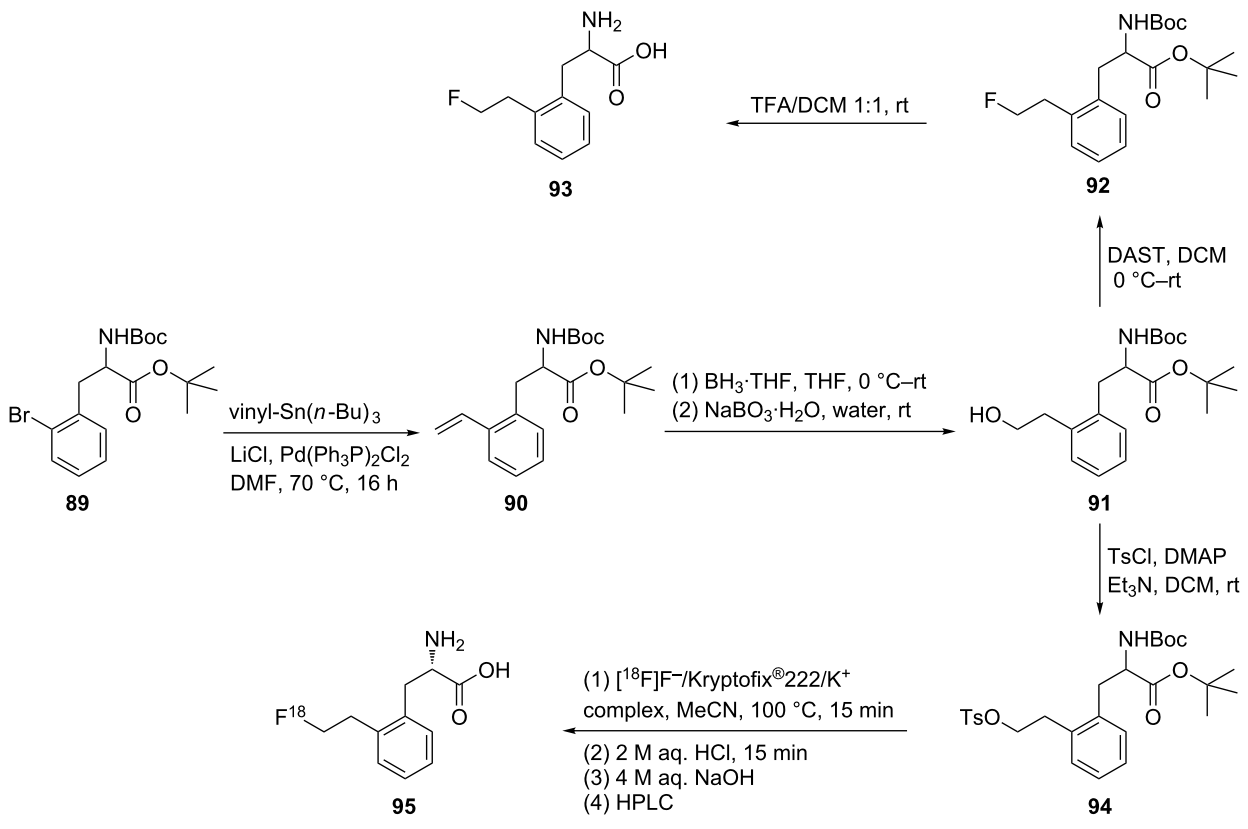

Scheme 21: Synthesis of 2-(2-fluoroethyl)phenylalanine derivatives **93** and **95**.

idinophanes) **96** and the sodium salt of *o*, *m*, or *p*-fluoro or (trifluoromethyl)phenylpyruvic acids **97a–f**. The reaction was carried out in presence of 0.5 equiv of zinc(II) acetate in the presence of NaOMe. The initially formed complexes **98a–f** underwent isomerization to **99a–f**. Acid hydrolysis then gave the FPhe derivatives **53a**,**b**, **53i**, **81**, and **101c**,**d** with modest enantiomeric excesses (33–66% ee) and in moderate yields [59] (Scheme 22).

A convenient preparative method for the synthesis of enantiomerically pure *o*-, *m*-, and *p*- or pentafluorinated phenylalanines **53a**, **81**, **101c**, and **107** was carried out by the alkylation of glycine. The Ni(II) complex **104** was obtained through the reaction of **102** with glycine (**103**) and $Ni(NO_3)_2$. The subsequent alkylation of complex **104** with fluorine-containing benzyl chlorides **105a–d** followed by hydrolysis with HCl afforded enantiomerically enriched (<90% ee) (*S*)-fluorinated phenylalanine derivatives **53a**, **81**, **101c**, and **107** [60,61] (Scheme 23).

Following the previous method, the chiral auxiliary **108** was readily cleaved under mild acidic conditions to afford the hydrochloride salt of 3,4,5-trifluoro-Phe **109** in 86% yield and 95% ee, indicating very low racemization [62] (Scheme 24).

1.10. PAM enzymatic catalytic amination of (*E*)-cinnamic acid

The enzyme phenylalanine aminomutase (PAM) from *Taxus chinensis* catalyzes the stereoselective isomerization of α-phenylalanine to β-phenyalanine **111a–c**. Mechanistic studies showed that (*E*)-cinnamic acid is an intermediate in this transformation [63]. Accordingly, addition of ammonia to *o*, *m*, or *p*-fluoro-(*E*)-cinnamic acids **110a–c** catalyzed by PAM afforded (*R*)-fluoro-β-phenylalanines **111a–c** and *o*, *m*, and *p*-(*S*)-fluorophenylalanines **53a**, **81**, **101c**, respectively, with excellent enantioselectivities (**<**99% ee) (Scheme 25).

1.11. From enamine intermediates

The synthesis (*R*)-2,5-difluorophenylalanine derivative **115** was carried out by coupling the commercially available aldehyde **55** and *N*-Boc phosphonate glycinate **112** to generate the enamino ester intermediate **113**. The asymmetric hydrogenation of this enamine afforded the *N*-Boc-protected (*R*)-2,5-difluorophenylalanine ester **114** with >99% ee. A following alkaline hydrolysis of the ester **114** gave *N*-Boc-(*R*)-2,5-difluorophenylalanine **115** (Scheme 26) [50].

After compiling the above synthetic methods, a number of conclusions can be drawn regarding the synthesis of FPhe ana-

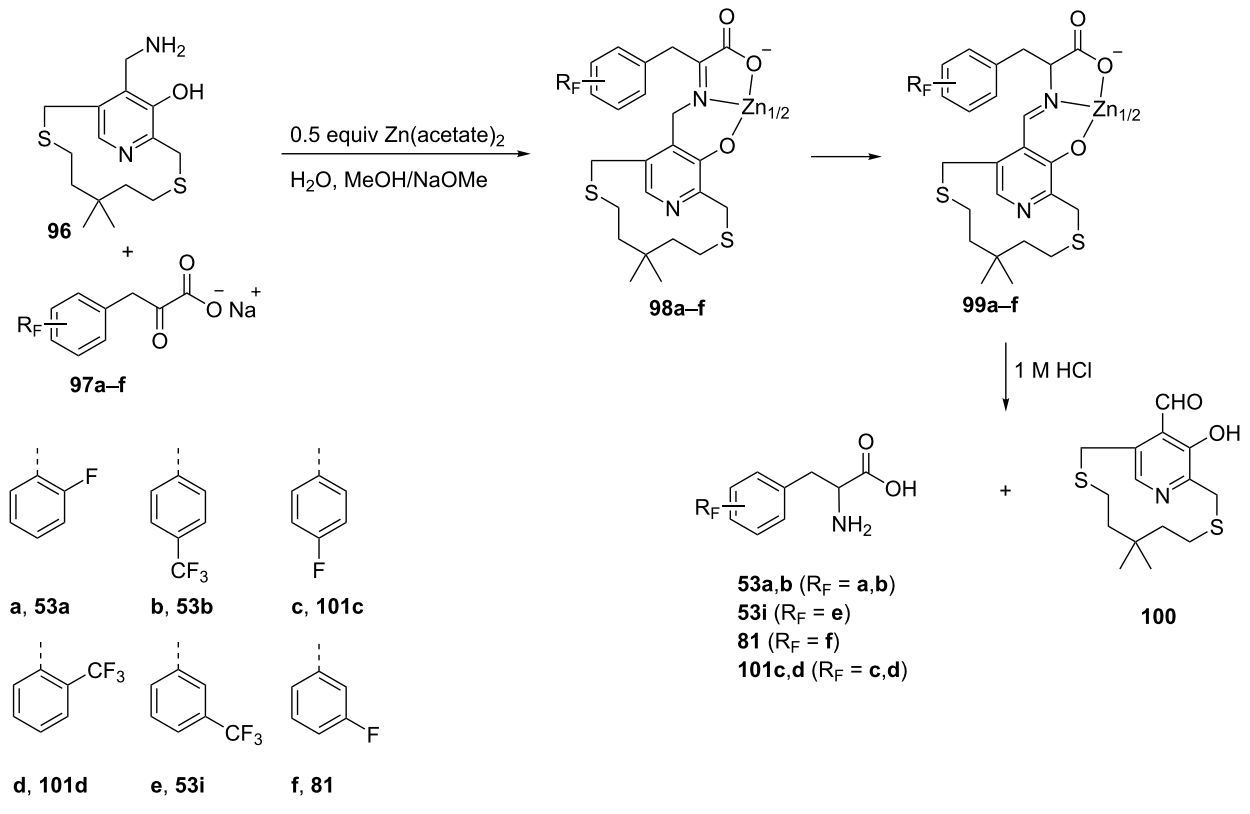

Scheme 22: Synthesis of FPhe derivatives via Zn^{2+} complexes.

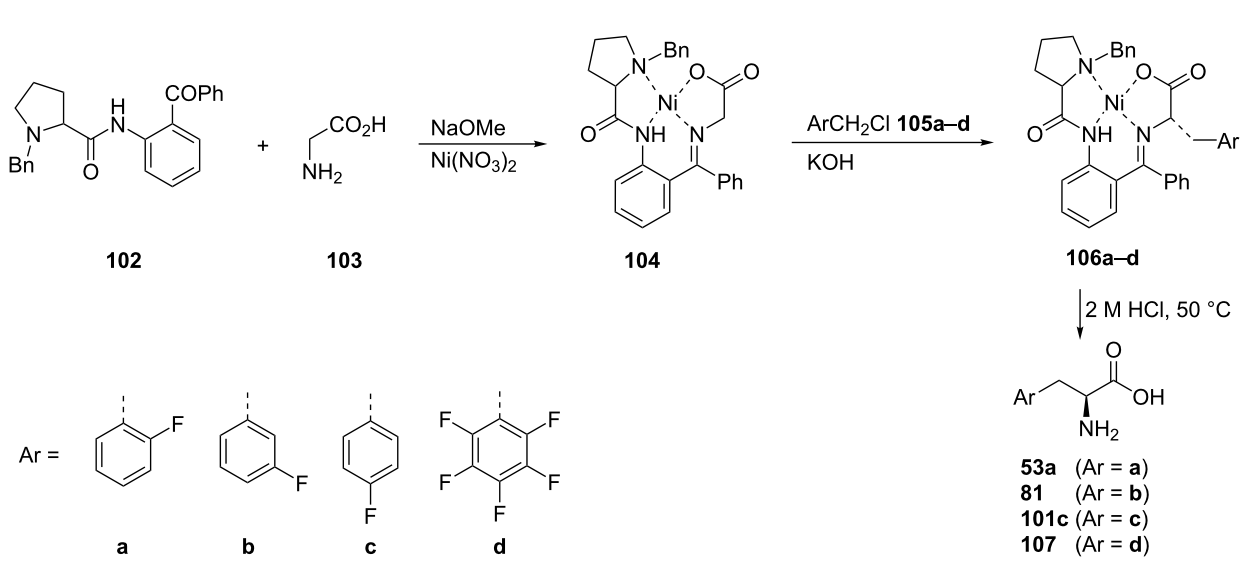

Scheme 23: Synthesis of FPhe derivatives via Ni^{2+} complexes.

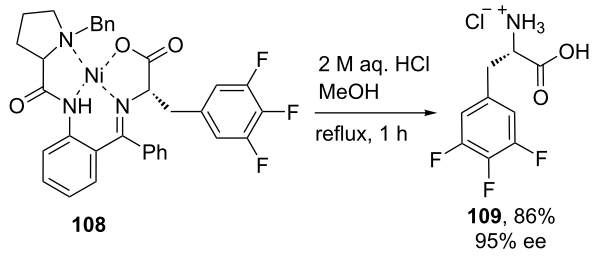

Scheme 24: Synthesis of 3,4,5-trifluorophenylalanine hydrochloride (**109**).

logues of type **I** and **II**. The most convenient method involved a Negishi cross coupling of an aryl halide and the Zn homoenolate of the protected (*R*)-iodoalanine **2** using a Pd(0) catalyst. This method provided a versatile range of fluorinated phenylalanine products with high enantioselectivities and in acceptable yields.

2. Synthesis of β-fluorophenylalanines of type **III**

2.1. Fluorination of protected (1*R*,2*R*)-2-amino-L-phenylpropane-1,3-diol

Recently, Okuda et al. reported the synthesis of (3*R*)-3-fluoro-L-phenylalanine (**121**) from (1*R*,2*R*)-2-amino-L-phenylpropane-1,3-diol (**116**). Thus, Boc-protection of the amine group in **116** followed by the protection of the primary hydroxy group (Alloc) gave alcohol **117** in good yield. The fluorination of **117** was achieved by treatment with DAST to form **118**. Then, selective removal of the Alloc protecting group using $Pd(PPh_3)_4$, was followed by oxidation of the resulting Boc-protected amino alcohol **119** to give the *N*-Boc-protected acid **120** in good yield. Finally, removal of the Boc group then generated the free amino acid (3*R*)-3-fluoro-L-phenylalanine (**121**) [64] (Scheme 27). Okuda's group used **121** in the synthesis of a nucleoside that could be used to assess the transition state of a ribosome-catalyzed peptide-bond formation [64].

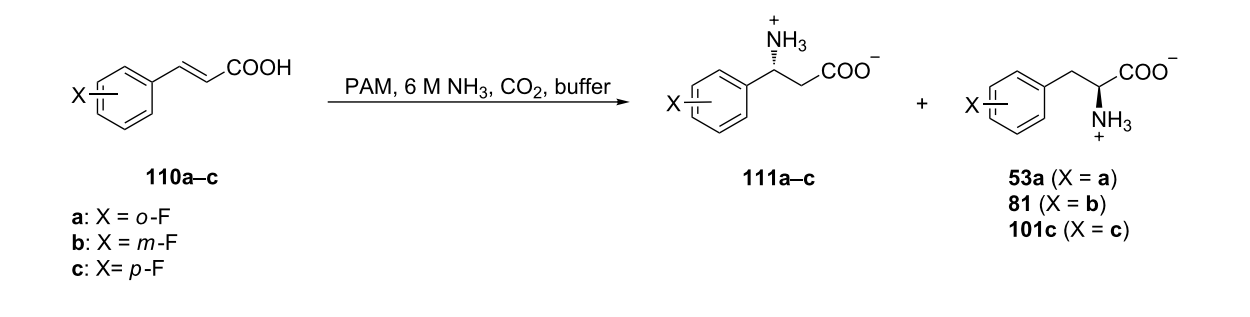

Scheme 25: Synthesis of FPhe derivatives via phenylalanine aminomutase (PAM).

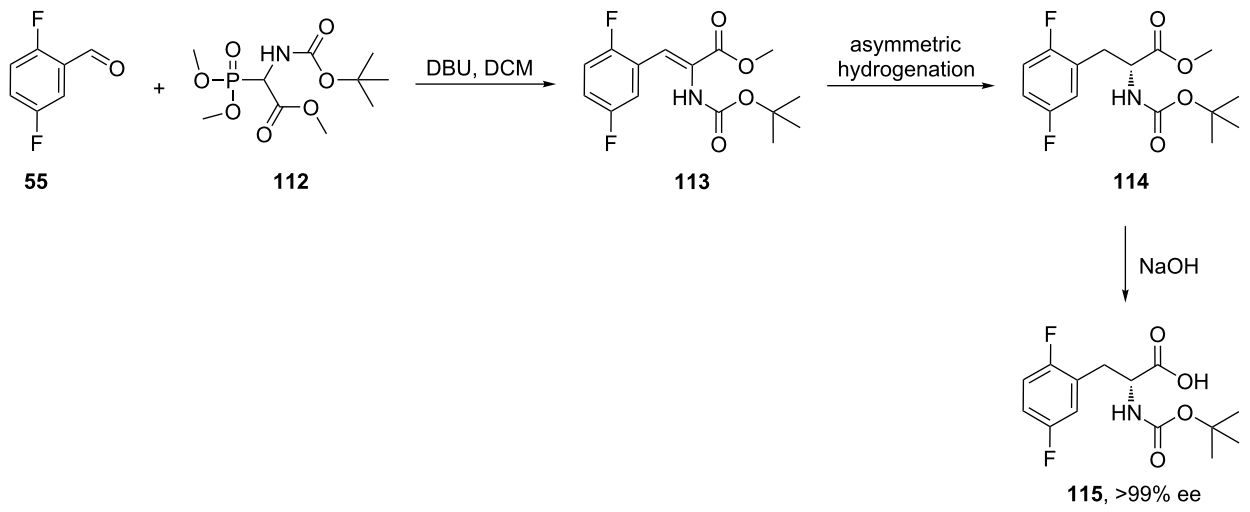

Scheme 26: Synthesis of (*R*)-2,5-difluorophenylalanine **115**.

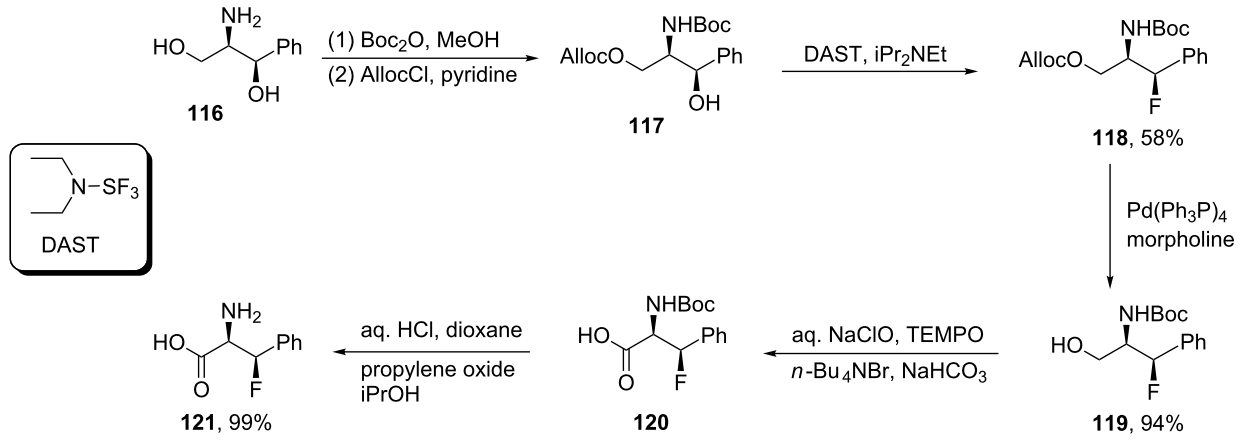

Scheme 27: Synthesis of β-fluorophenylalanine via 2-amino-1,3-diol derivatives.

2.2. Stereoselective benzylic fluorination of *N*-(2-phenylacetyl)oxazolidin-2-one using NFSI

Treatment of oxazolidinone **122** with *N*-fluorobenzenesulfonimide (NFSI) in the presence of NaHMDS afforded the fluorinated oxazolidinone derivative **123**. The reductive removal of the chiral auxiliary with $LiBH_4$ resulted in alcohol **124** which was oxidized by Dess–Martin periodinane to give (*S*)-(−)-2-fluoro-2-phenylacetaldehyde (**125**). This aldehyde is prone to racemization and decomposition and therefore was directly converted to the arylidene derivative **127**, by treatment with *p*-toluenesulfinamide (**126**). Then, reaction of **127** (1.0 mmol) with 1.5/1.0 equiv of diethylaluminum cyanide (Et_2AlCN)/iPrOH at −78 °C in THF gave nitrile **128**. Deprotection of the latter, followed by hydrolysis of the nitrile group afforded *syn*-(2*S*,3*S*)-(+)-3-fluorophenylalanine (**129**) [65] (Scheme 28) .

2.3. Multistep synthesis from ethyl trifluoropyruvate hemiketal

The reaction of ethyl trifluoropyruvate hemiketal **130** with thionyl chloride in pyridine afforded the chlorinated derivative **131**, which upon treatment with zinc powder in DMF, afforded the dihalogenated olefin **132**. The substitution of one fluorine atom in **132** with a tributylstannyl group to give **133** was accomplished by the reaction with $(Bu_3Sn)_2CuLi$ in THF at −78 °C. The reaction took place following an addition–elimination mechanism. Then, coupling of **133** with iodobenzene in the presence of $Pd(PPh_3)_4$ and CuI as the co-catalyst afforded ethyl (*E*)-3-phenyl-3-fluoro-2-methoxypropenoate (**134**) which was converted into the corresponding α-ketoacid **135** by treatment with trimethylsilyl iodide. Finally, the reaction of **135** with aqueous ammonia followed by reduction with sodium borohy-

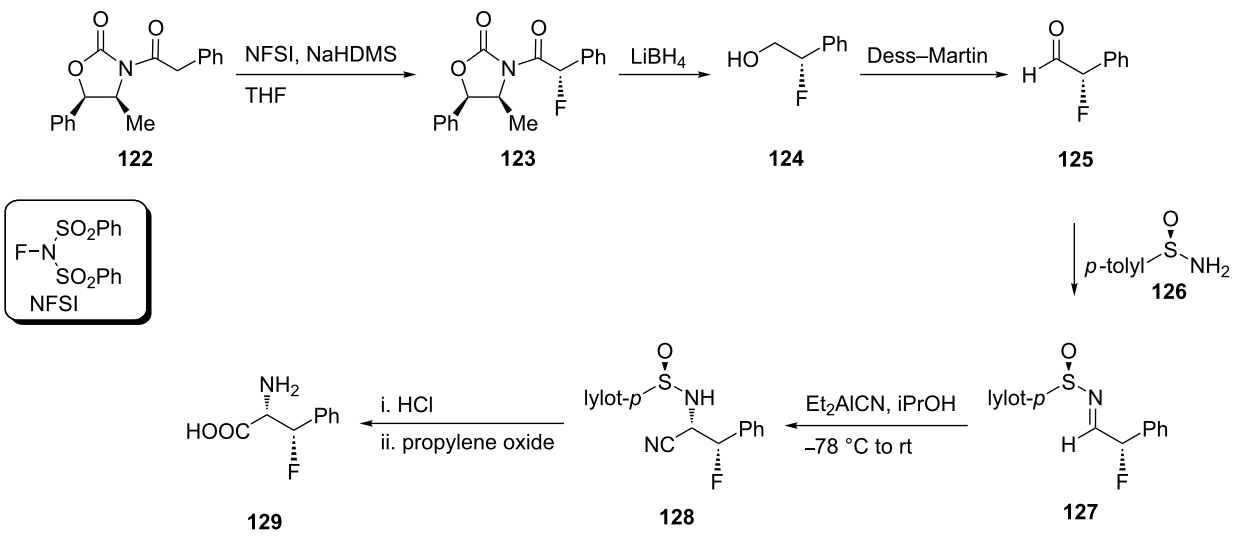

Scheme 28: Synthesis of β-fluorophenylalanine derivatives via the oxazolidinone chiral auxiliary **122**.

dride gave the racemic *erythro*-β-fluorophenylalanine **136** in 40% yield [66] (Scheme 29).

2.4. Fluorodehydroxylation of β-hydroxyphenylalanine

Alternatively, Kollonitach et al. prepared racemic 3-fluorophenylalanine (**136**) through the fluorodehydroxylation of 3-hydroxyphenylalanine (**137**) using sulfur tetrafluoride (SF_4) in HF [67] (Scheme 30).

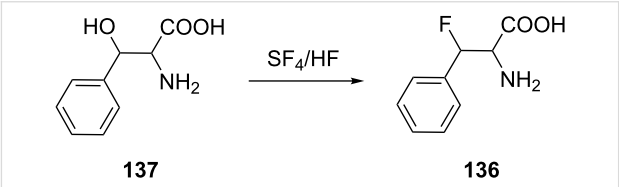

Scheme 30: Synthesis of β-fluorophenylalanine (**136**) via fluorination of β-hydroxyphenylalanine (**137**).

2.5. Ring opening of aziridine derivatives by HF/Py

The ring opening reaction of aziridines **138a**,**b** by treatment with hydrogen fluoride in pyridine afforded 3-fluorophenylalanine esters **139a,b**. The subsequent enzymatic hydrolysis of esters **139a**,**b** gave the *threo*-isomer **136** in an enantiomerically pure form [68,69] (Scheme 31).

On the other hand, Wade et al. reported that ester **138b** (R = iPr) afforded the isopropyl 3-fluorophenylalaninate (**139b**) as

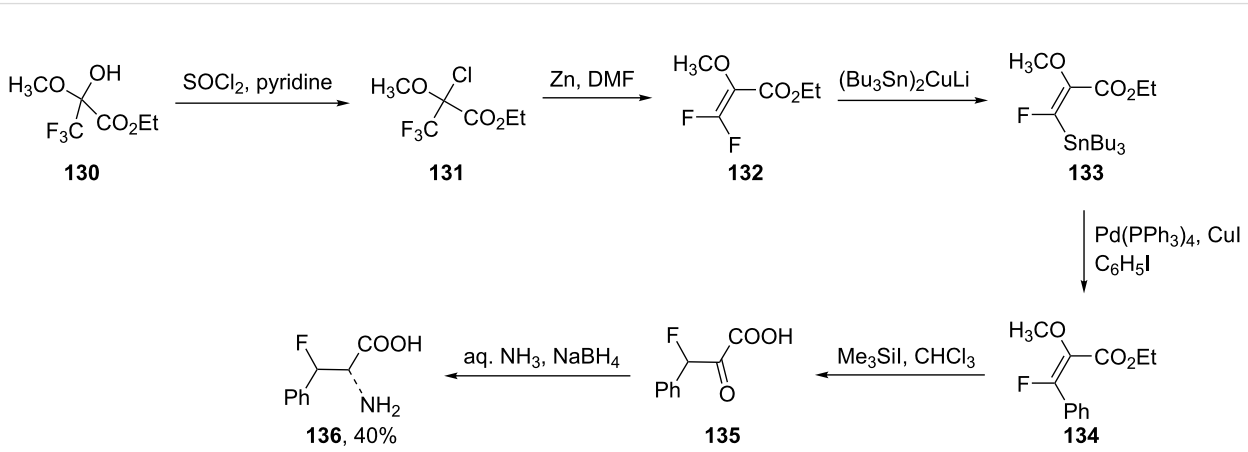

Scheme 29: Synthesis of β-fluorophenylalanine from pyruvate hemiketal **130**.

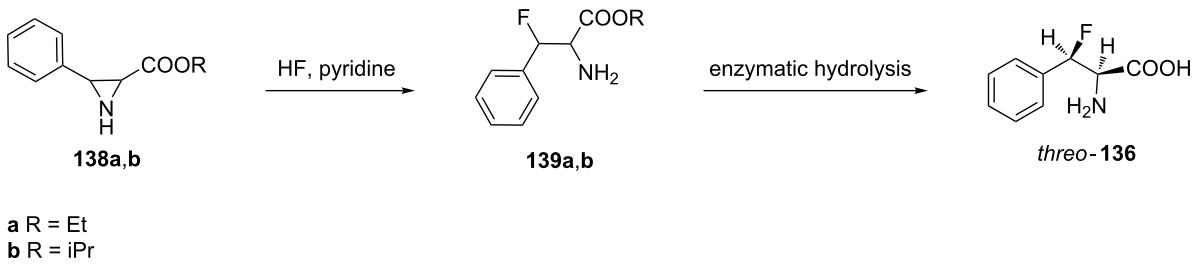

138a,b 139a,b *threo*-136

a R = Et
b R = iPr

Scheme 31: Synthesis of β-fluorophenylalanine from aziridine derivatives.

racemate in 45–50% yield [70] under similar reaction conditions (Scheme 31).

2.6. Fluorination and reductive amination of phenylpyruvate

A direct fluorination of the ester derivatives of phenylpyruvic acids **140a**,**b** with F_2 followed by hydrolysis of the resulting fluoropyruvates in 50% isopropanol in the presence of $NaHCO_3$ gave 3-fluoro-3-phenylpyruvate **141** in 40–50% yields [68]. The direct reductive amination gave a partially racemized mixture of *threo* and *erythro*-**136** with the *erythro* stereoisomer **136** as the major product (Scheme 32).

The reductive amination of 3-fluoro-3-phenylpyruvic acid (**144**) obtained by the fluorodehydroxylation of the enol form of ethyl 3-phenylpyruvate **142**, using DAST instead of SF_4 followed by hydrolysis, produced both *threo* and *erythro*-diastereomers of **136** [68] (Scheme 33).

2.7. Photocatalyzed benzylic fluorination of *N*-phthalimido phenylalanine

The photocatalyzed benzylic fluorination of phthalimide-protected phenylalanine methyl ester **145**, using the photosensitizer 1,2,4,5-tetracyanobenzene (TCB), and Selectfluor in acetonitrile was carried out using a pen lamp (λ_{max} = 302 nm). By

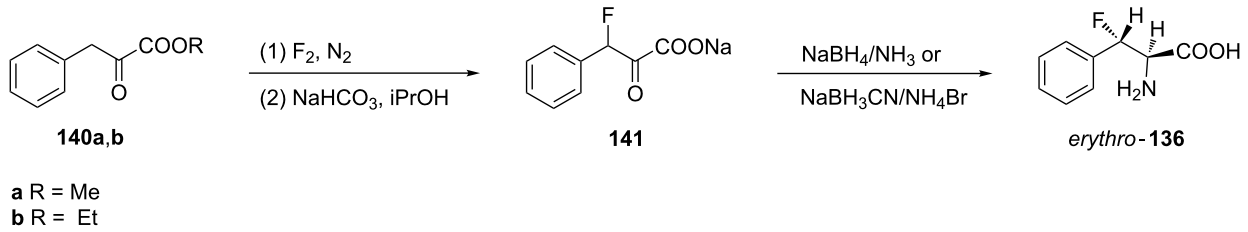

140a,b 141 *erythro*-136

a R = Me
b R = Et

Scheme 32: Synthesis of β-fluorophenylalanine **136** via direct fluorination of pyruvate esters.

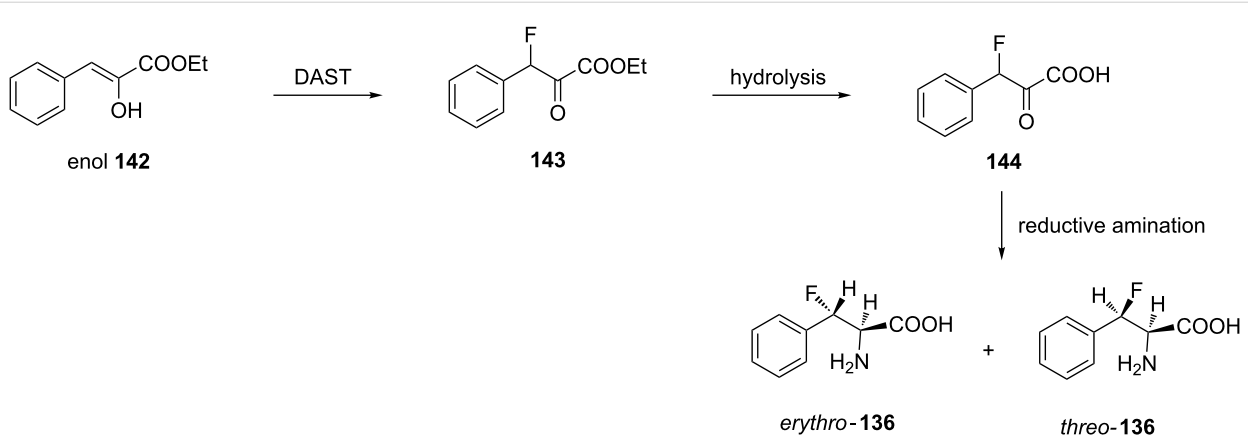

enol **142** **143** **144**

erythro-**136** *threo*-**136**

Scheme 33: Synthesis of β-fluorophenylalanine via fluorination of ethyl 3-phenylpyruvate enol using DAST.

this route, the β-fluoro derivative **146** was obtained in 62% yield as racemic mixture [71] (Scheme 34). Recently, Egami and coworker also synthesized compound **146** in 43% yield (dr = 1:1) via the fluorination of **145**, however without TCB as photosensitizer, but instead using an LED light source (365 nm) and Selectfluor in MeCN [72].

Alternatively, a visible light (14 Watt CFL) mediated benzylic fluorination of a series of *N*- and *C*-terminally protected phenylalanines **147** using Selectfluor and dibenzosuberenone in acetonitrile, afforded the β-fluorophenylalanine derivatives **148** in variable yields with partial racemization. Phthalimido and trifluoroacetyl *N*-terminal protecting groups (R^1 = Phth or TFA) and unprotected *C*-terminal derivatives (R^2 = H) provided the most efficient outcomes (80 and 67% yield, respectively). An *N*-acetyl group was also suitable as protecting group for the reaction providing the desired product with 57% yield. Also, methyl and ethyl esters as *C*-terminal protecting groups in combination with phthalimino as the *N*-terminal protecting group, were both successfully explored. However, when the trifluoroacetyl amide was used as a substrate the methyl ester performed better than the ethyl ester (74% versus 60% yield). However, *N*-protecting groups such as Boc, Fmoc, and Cbz were not compatible with the fluorination (0–10% yield). Moreover, when *tert*-butyl, trityl, and adamantyl protecting groups were installed for *C*-terminal protection additional fluorination, decomposition, and consequently low yields of the β-fluorinated derivatives **148** were observed [73] (Scheme 35).

2.8. Fluorination of aziridinium derivatives

The *N*,*N*-dibenzylated 3-fluorophenylalanine derivative **151** was prepared with excellent diastereoisomeric ratio (dr > 99:1) from α-hydroxy-β-amino ester **142**. In this case, XtalFluor-E was used to activate the OH group in the substrate and displaced by neighboring amino-group participation creating an aziridinium intermediate **150**. The latter then was opened stereo- and regioselectively by fluoride to give **151** in good yield and high diastereoisomeric purity (Scheme 36). The subsequent deprotection of **151** had to be achieved with BrO_3^-, because hydrogenolysis resulted in defluorination [74].

Alternatively, a series of substituted *anti*-β-fluorophenylalanine derivatives **154a–d** was obtained from the corresponding enantiopure α-hydroxy-β-aminophenylalanine esters [75,76] **152a–d** using XtalFluor-E. The reaction also included an aziridinium ion rearrangement as the key step. Deprotection of the resultant β-fluoro-α-amino acid esters **153a–d** afforded the corresponding enantiopure *anti*-β-fluorophenylalanines **154a–d** in good yield and high diastereoisomeric purities [74] (Scheme 37).

The deoxyfluorination of the enantiopure α-hydroxy-β-amino ester **152a** or α-amino-β-hydroxyphenylalanine ester **155** [74-

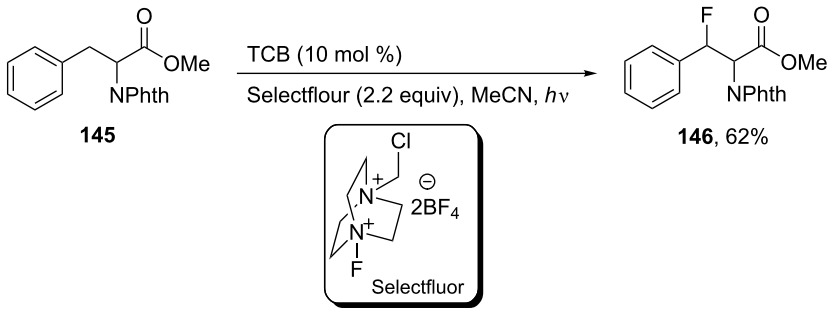

Scheme 34: Synthesis of β-fluorophenylalanine derivatives using photosensitizer TCB.

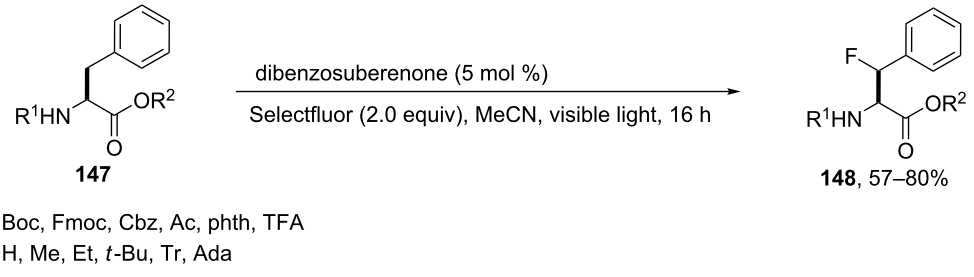

Scheme 35: Synthesis of β-fluorophenylalanine derivatives using Selectfluor and dibenzosuberenone.

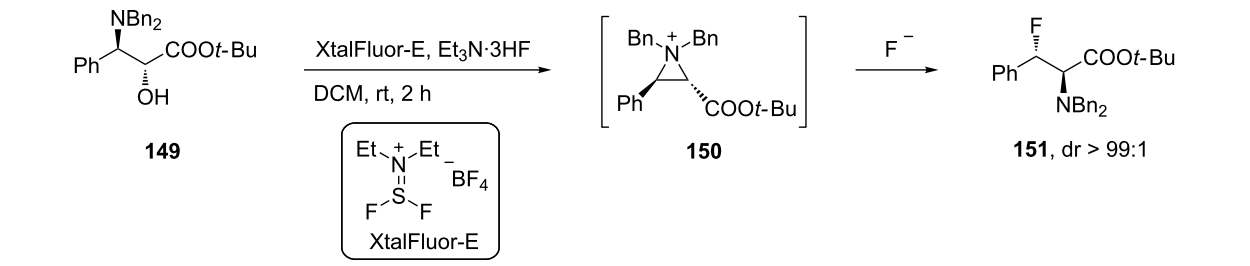

Scheme 36: Synthesis of protected β-fluorophenylalanine via aziridinium intermediate **150**.

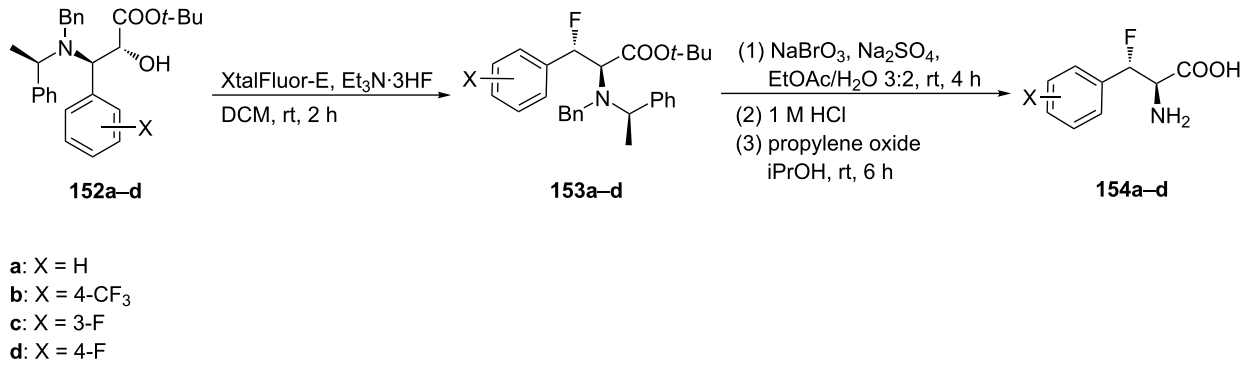

Scheme 37: Synthesis of β-fluorophenylalanine derivatives via fluorination of α-hydroxy-β-aminophenylalanine derivatives **152**.

76] under the same conditions proceeded via aziridinium ion **156** and generated β-fluoro-α-amino ester **153a** in good yield and high diastereoisomeric purity (dr > 99:1) (Scheme 38).

2.9. Direct fluorination of β-methylene C(sp^3)–H

The direct fluorination of β-methylene C(sp^3)–H bonds of Phe derivatives **157a–v** having installed the bidentate auxiliary, 2-(pyridine-2-yl)isopropylamine (PIP-amine) **158**, was attempted using Selectfluor in the presence of $Pd(OAc)_2$ as a catalyst. The corresponding β-fluoro derivatives **159a–v** were obtained with high stereoselectivity using DCM and iPrCN as co-solvent (30:1 v/v). Interestingly reducing the $Pd(OAc)_2$ concentration from 10 mol % to 6 mol % led to an improved yield of 73% for **159a**, **159g**, and **159t**. Selectfluor was found superi-

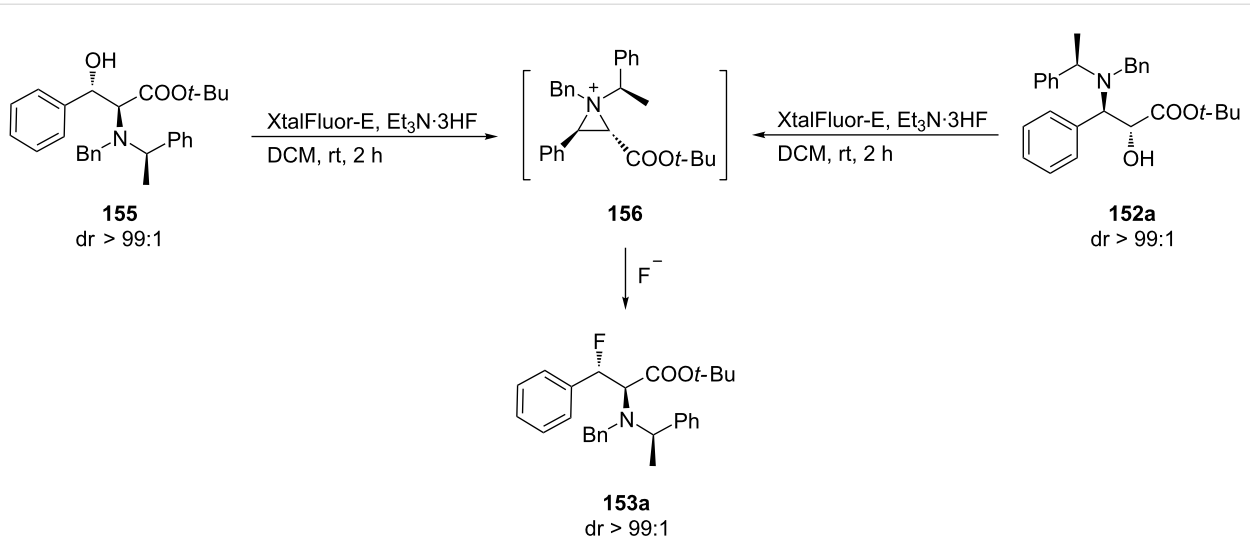

Scheme 38: Synthesis of β-fluorophenylalanine derivatives from α- or β-hydroxy esters **152a** and **155**.

or to other fluorination reagents such as fluoropyridinium tetrafluoroborate, 2,4,6-trimethylfluoropyridinium tetrafluoroborate, or NFSI. The fluorination process was explored with a broad range of substituted Phe derivatives. The removal of the PIP auxiliary group without affecting the newly introduced fluorine atom was attempted by a two-step, one-pot protocol involving an in situ esterification of a highly electrophilic pyridinium triflate intermediate [77] and afforded the *anti*-β-fluoro-α-amino acid methyl ester **160a** in 52% yield and with 98.8% ee (Scheme 39).

On the other hand, when the quinoline-based ligand **162** was used, it was shown to promote the palladium-catalyzed direct electrophilic fluorination of β-methylene C(sp^3)–H bonds. Thus, fluorinations of L-phenylalanine 4-trifluoromethylphenylamides **161a–l** carrying a range of functional groups such as fluoro, chloro, bromo, methoxy, acetyl, cyano, nitro, and trifluoromethyl, were well-tolerated and afforded the corresponding *anti*-β-fluoro-α-amino acids **163a–l** in moderate to excellent yields [78] (Scheme 40).

3. Synthesis of β,β-difluorophenylalanine derivatives of type **IV** via 2-phenyl-2,2-difluoroacetaldehyde derivatives

2-Phenyl- and 2-(4-fluorophenyl)-2,2-difluoroacetaldehyde **164a** and **164b** proved to be key starting points for the synthesis of β,β-difluorophenylalanine analogs **168a**,**b**. The conversion of **164a**,**b** into their respective cyanohydrins **165a**,**b** followed by acid hydrolysis with gaseous HCl in ethanol afforded the α-hydroxy esters **166a**,**b**. Dess–Martin oxidation [79,80] of the latter, followed by hydrolysis of the ester gave keto acids **167a**,**b**. Finally, the reductive amination of **167a**,**b** with 25% aqueous ammonia and $NaBH_4$ afforded the racemic β,β-difluorophenylalanine derivatives **168a**,**b** in 67% yield [81] (Scheme 41).

An alternative approach to the difluorinated compound **168a** was achieved by the condensation of **164a** with (*S*)-1-phenylethylamine (**169**), to give the imine **170**. Heating of imine **170** with TMSCN in the presence of zinc iodide [82] generated the nitrile **171** as a 1:1 mixture of diastereoisomers which was

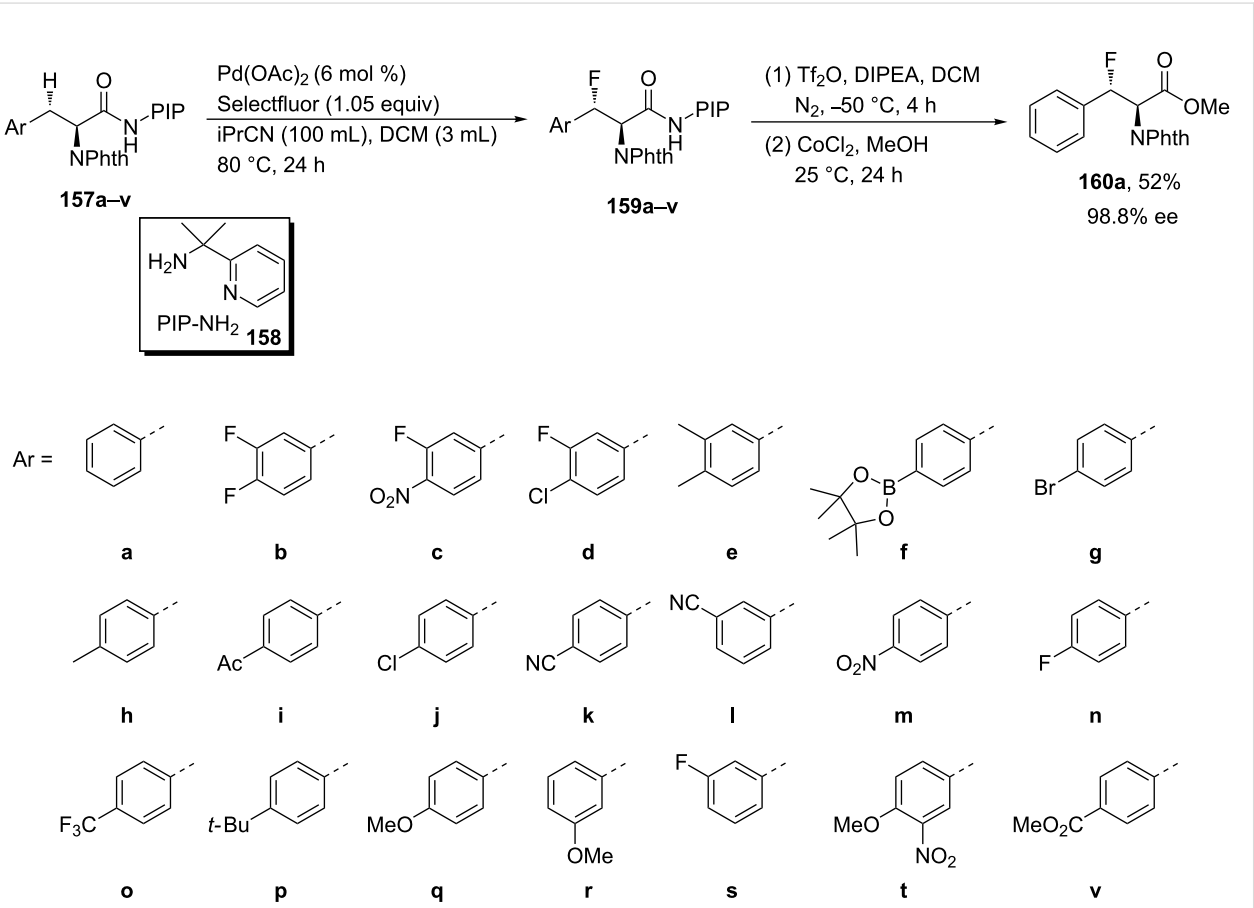

Scheme 39: Synthesis of a series of β-fluoro-Phe derivatives via Pd-catalyzed direct fluorination of β-methylene C(sp^3)–H bonds in Phe substrates functionalized with the PIP auxiliary group.

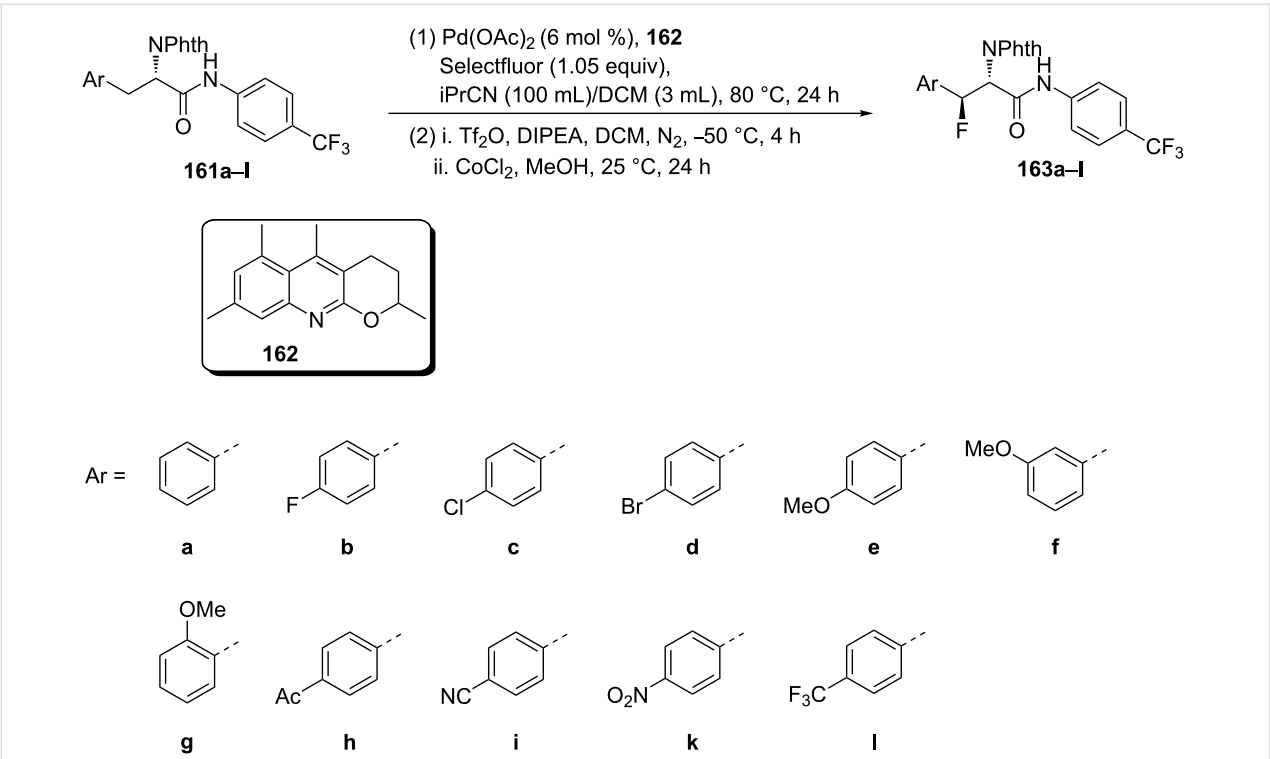

Scheme 40: Synthesis of series of β-fluorinated Phe derivatives using quinoline-based ligand **162** in the Pd-catalyzed direct fluorination of β-methylene C(sp^3)–H bonds.

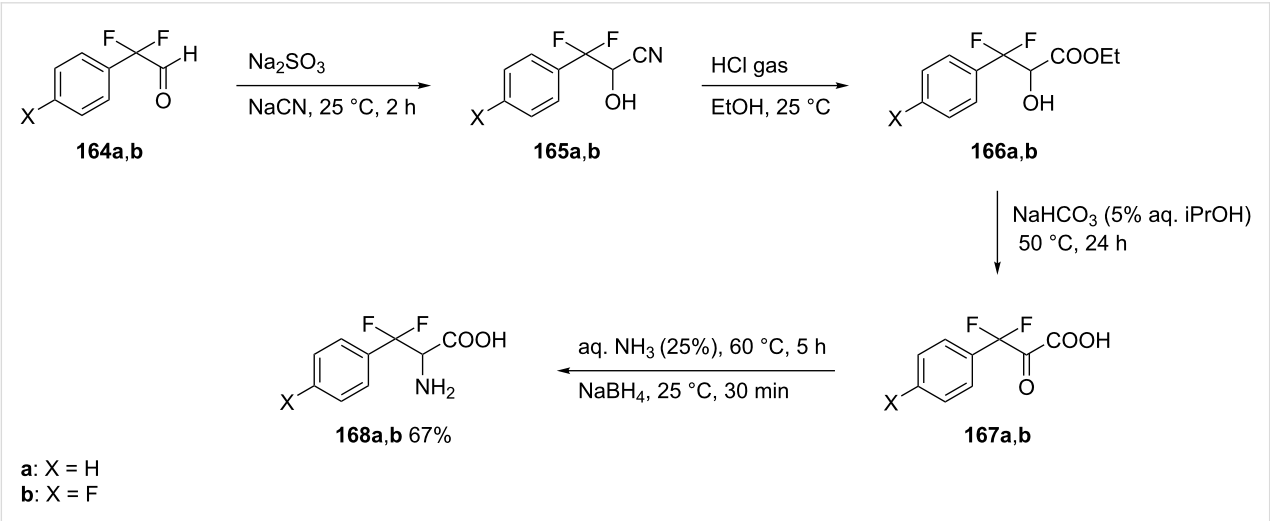

Scheme 41: Synthesis of β,β-difluorophenylalanine derivatives from 2,2-difluoroacetaldehyde derivatives **164a**,**b**.

immediately hydrolyzed to provide the racemic carboxamide **172**. The subsequent removal of the chiral auxiliary by catalytic hydrogenation then afforded the carboxamide **173**. Finally, an acid-mediated hydrolysis of the carboxamide **173** to generate the free amino acids L- or D-**168a**, was carried out with aqueous H_2SO_4. However, the acid hydrolysis step was accompanied with extensive racemization [81,83] (Scheme 42).

4. Synthesis of α-fluorophenylalanine of type V via α-fluorination of Phe derivatives

The successful α-fluorination of phenylalanine derivative **174** carrying a picolinamide auxiliary to give **176** was carried out using Selectfluor as the fluorination reagent. The direct α-C(sp^3)–H fluorination of the starting compound **174** was catalyzed by $Cu(OAc)_2$ with (*R*)-3-hydroxyquinuclidine ligand **175**.

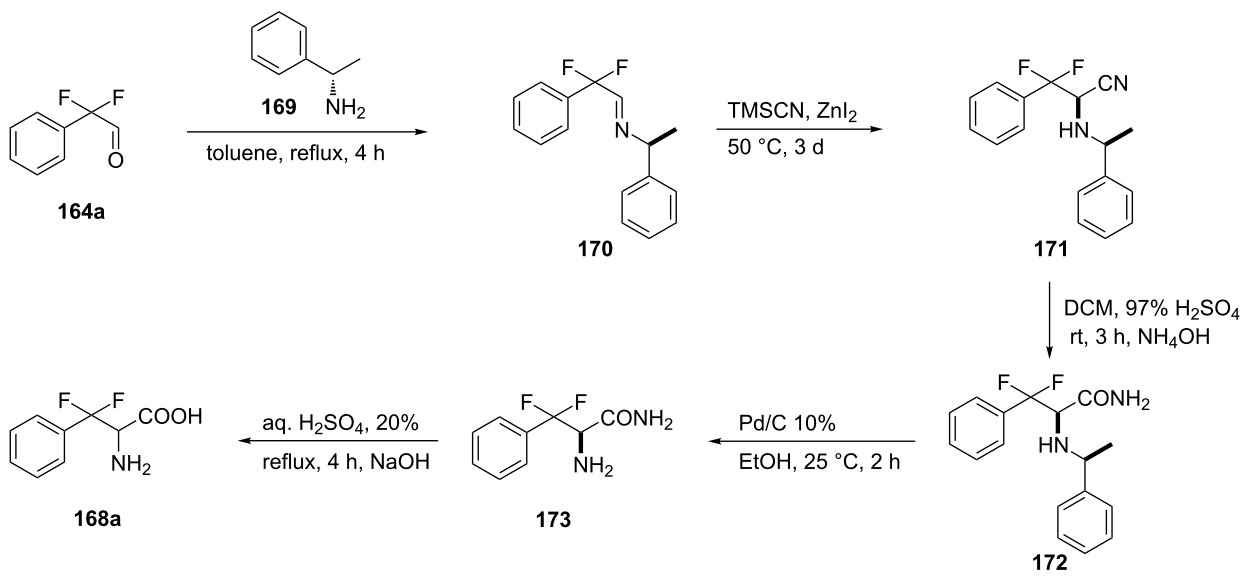

Scheme 42: Synthesis of β,β-difluorophenylalanine derivatives via an imine chiral auxiliary.

Comparative studies demonstrated that using ligand **175** rather than other ligands gave higher yields and no β-elimination products. The effective removal of the auxiliary using triflic anhydride with LiOH as nucleophile, gave product **177a** in good yield. Alternative nucleophiles such as EtOH or methyl esters of amino acids, in the presence of catalytic amounts of $CoCl_2$, afforded product **177b** or fluorinated Phe dipeptides [84] **177c–g** as racemic mixtures (Scheme 43).

5. Pharmaceutical applications of fluorinated phenylalanine derivatives

Peptides and proteins containing FPhe are important tools to identify enzyme–substrate complexes, mechanisms of protein aggregation, and modifying the chemical and thermal stabilities of proteins. The properties of protein were preserved, when low levels of fluorine are incorporated into the constituent amino acids, and were comparable with that of the original proteins.

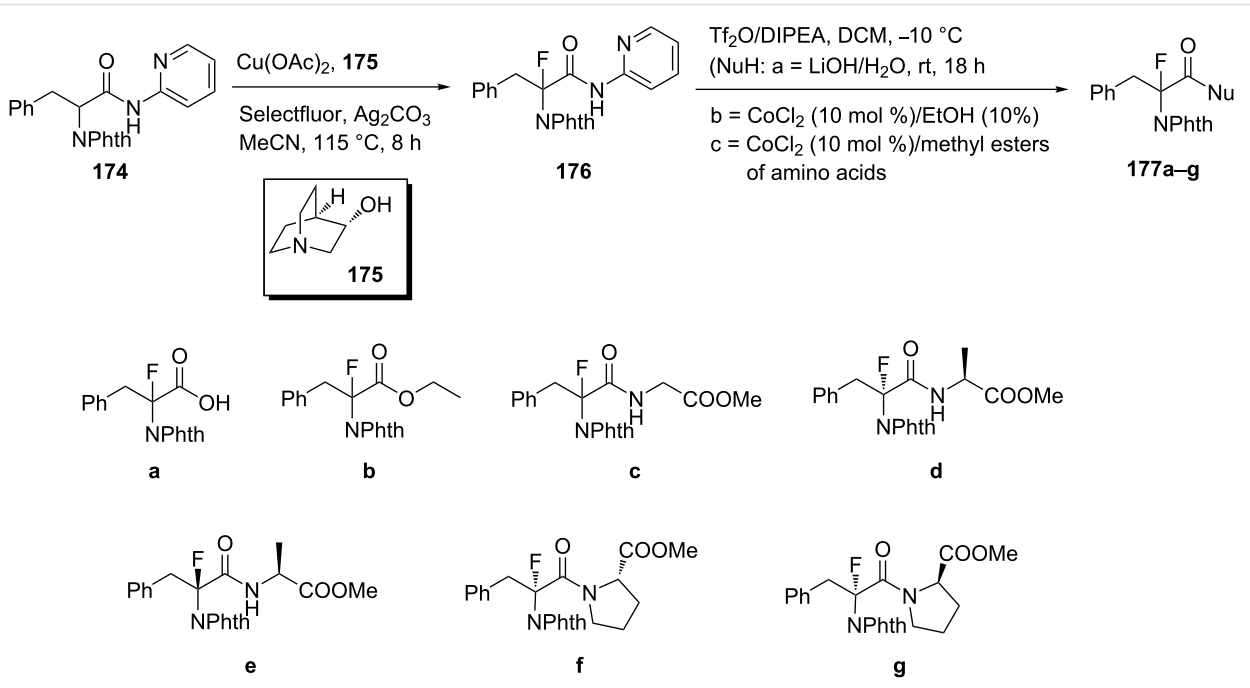

Scheme 43: Synthesis of α-fluorophenylalanine derivatives via direct fluorination of protected Phe **174**.

Helpfully, fluorine incorporation may favorably adjust protein function including improved stability and substrate selectivity.

5.1. Applications of FPhe derivatives in positron emission tomography (PET)

The molecular imaging technique positron emission tomography (PET) provides information on tumor metabolism, which allows for a more accurate diagnostic and therapy response in neuro-oncology, compared to, for example, magnetic resonance imaging (MRI). PET is particularly well-suited to differentiate neoplastic tissue from non-specific changes induced by chemotherapy treatments [85]. PET is particularly used for the early detection of tumors and metastases, and is an established tool for the diagnosis, staging, and the treatment planning of various malignancies. The selective imaging of tumors using PET exploits radiotracers that target aberrant cellular metabolism or increased protein expression [86,87]. Here, the ^{18}F isotope is particularly useful for the preparation of radiotracers to be used in PET due to its relatively long half-life (109 min). In this section we highlight two selected ^{18}FPhe derivatives which are used for PET tumor detection. 4-Borono-2-[^{18}F]fluoro-D,L-phenylalanine ([^{18}F]FBPA, **70**), is a fluorinated derivative of the parent compound designed for boron neutron capture therapy (BNCT) [53,88-92]. This compound was used for PET imaging of melanoma in animal models.

The low affinity of **178** for the L-type amino acid transporter1 (LAT1), however, limited the use of this compound as PET radiotracer for brain tumor imaging [93-96]. Therefore, for further analysis and comparison with **178** (performed in vitro), as the most promising candidate 2-[^{18}F]-2-fluoroethyl-L-phenylalanine (2-[^{18}F]FELP, **95**) was selected. In a F98 glioblastoma rat model, 2-[^{18}F]FELP exhibited improved in vitro characteristics over [^{18}F]FET **178**, especially in view of the affinity and specificity for system L [58]. Accordingly, 2-[^{18}F]FELP **95** emerged as a promising PET radiotracer for brain tumor imaging [97-101] (Figure 2).

5.2. Incorporation of FPhe for the synthesis of fluorinated drugs

5.2.1. Melflufen, an anticancer drug: 4-Fluoro-L-phenylalanine ester is required for the synthesis of melflufen (**179**), an anticancer drug currently being in clinical trials for the treatment of relapsed and refractory multiple myeloma (RRMM) [102,103]. Melflufen is a next generation form of the more historical drug, melphalan **180** (Figure 3).

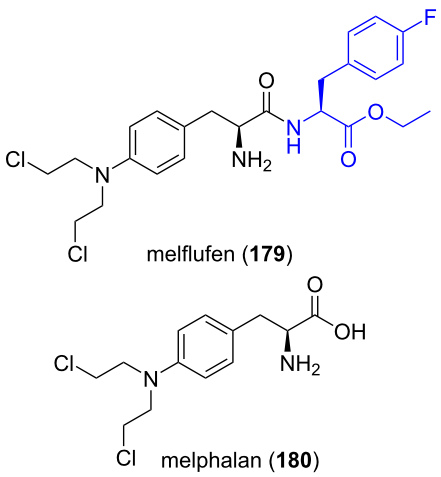

Figure 3: Structures of melfufen (**179**) and melphalan (**180**) anticancer drugs.

5.2.2. Gastrazole (JB95008), a CCK2 receptor antagonist: 2-Fluoro-L-phenylalanine derivatives are required for the synthesis of gastrazole (JB95008, **181**), a potent and highly selective cholecystokinin-2 (CCK2) receptor antagonist, originally developed at the James Black Foundation [104-109]. Roberts et al. demonstrated its inhibitory activity of gastrin-stimulated growth of pancreatic cancer both in vitro and in vivo studies [110] (Figure 4).

5.2.3. Dual CCK1/CCK2 receptor antagonists: Johnson & Johnson identified compound **182** as a dual CCK1/CCK2 receptor antagonist with desirable pharmacologic properties [51,111-113] (Figure 5). As can be seen from the structure of **182**, 3-bromo-4-fluoro-L-phenylalanine (**65**) is required for the synthesis.

5.2.4. Antidiabetes drugs, sitagliptin: (*R*)-2,4,5-Trifluorophenylalanine **38b** is a constituent of sitagliptin (**183**, Figure 6). Sitagliptin is used to decrease the level of blood sugar

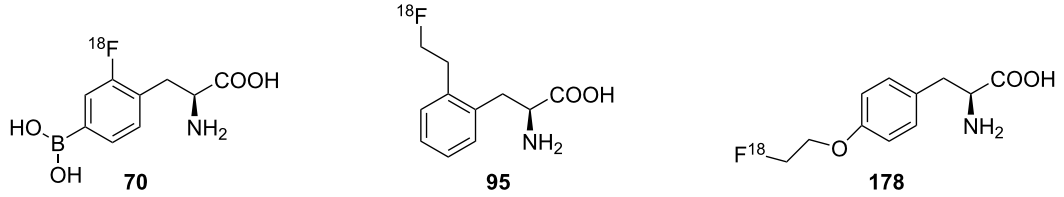

Figure 2: Structures of PET radiotracers of ^{18}FPhe derivatives.

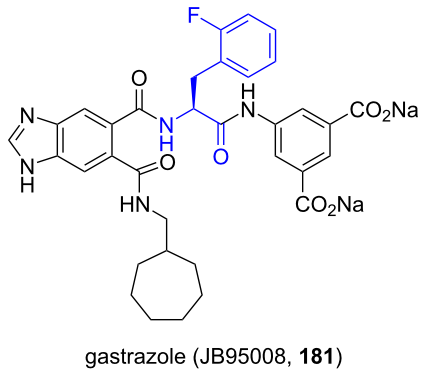

gastrazole (JB95008, **181**)

Figure 4: Structure of gastrazole (JB95008, **181**), a CCK2 receptor antagonist.

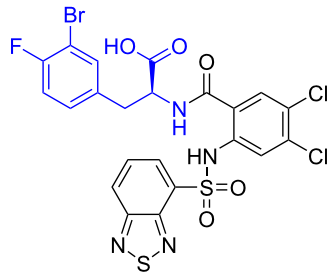

182

Figure 5: Dual CCK1/CCK2 antagonist **182**.

in patients with type 2 diabetes and belongs to the dipeptidyl peptidase-4 (DPP-4) class of inhibitors [114,115]. This enzyme breaks down the incretins GLP-1 and GIP, gastrointestinal hormones released in response to a meal. By preventing the breakdown of GLP-1 and GIP, they are able to increase the secretion of insulin by the pancreas that modulates blood sugar level when it is high. Sitagliptin was granted FDA approval in October, 2006 [116].

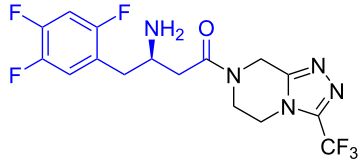

sitagliptin (**183**)

Figure 6: Structure of sitagliptin (**183**), an antidiabetic drug.

Retagliptin phosphate: Retagliptin phosphate (**184**) is under investigation as a DPP-4 inhibitor for treating type-2 diabetes. It is an analogue of sitagliptin which was developed for the same application [109,117], but compound **184** appears to have an improved activity [118]. Retagliptin showed efficacy in clinical trials and is now entering phase III studies. (*R*)-2,4,5-Trifluorophenylalanine **38b** is used as a building block in the synthesis of compound **184** [119,120] (Figure 7).

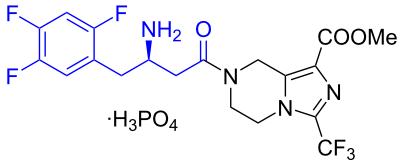

retagliptin (**184**)

Figure 7: Structure of retaglpitin (**184**) and antidiabetic drug.

Evogliptin: (*R*)-2,4,5-Trifluorophenylalanine **38b** is required for the synthesis of evogliptin (**185**, Figure 8), an antidiabetic drug in the dipeptidyl peptidase-4 (DPP-4) inhibitor or "gliptin" class of drugs. The South Korean pharmaceutical company Dong-A ST developed evogliptin (**185**) and it is currently approved for use in South Korea [121-123].

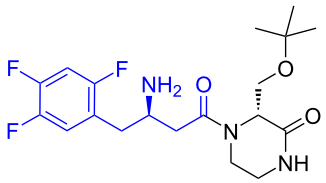

evogliptin (**185**)

Figure 8: Structure of evogliptin (**185**), an antidiabetic drug.

LY2497282: Eli Lilly identified LY2497282 (**186**) as a potent and selective DPP-4 inhibitor, also for the treatment of type II diabetes. The inhibition of GLP-1 degradation by dipeptidyl peptidase IV (DPP-4) has emerged as a promising approach for treatment. (*R*)-2,5-Difluorophenylalanine is a required building block for the synthesis of LY2497282 [50,124] (Figure 9).

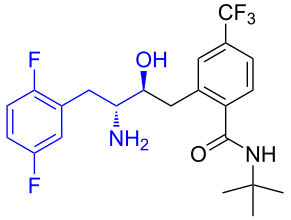

186

Figure 9: Structure of LY2497282 (**186**) a DPP-4 inhibitor for the treatment of type II diabetes.

5.2.5. Ulimorelin: Ulimorelin (**187**) is a small cyclic peptide containing D-4-FPhe. Ulimorelin acts as a selective agonist of the ghrelin/growth hormone secretagogue receptor (GHSR-1A), which is currently being developed by Tranzyme Pharma (code name TZP-101) as a first-in-class treatment for both, postoperative ileus (POI) and diabetic gastroparesis. POI describes a deceleration or arrest in intestinal motility following surgery [109,125-127] (Figure 10).

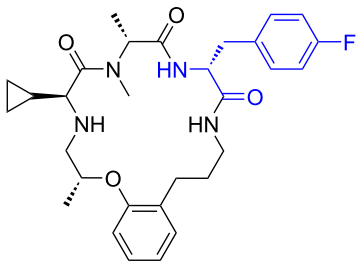

ulimorelin (**187**)

Figure 10: Structure of ulimorelin (**187**).

5.2.6. The glucagon-like peptide-1 receptor (GLP1R): 3'-Fluorophenylalanine is a key motif in the structure of the glucagon-like peptide-1 receptor (GLP1R, **188**, Figure 11). GLP1R is a receptor protein found on beta cells of the pancreas and on neurons of the brain. It is participating in the modulation of blood sugar levels by increasing insulin secretion. Consequently, GLP1R plays a key role in the development of drugs to treat diabetes mellitus [128-130].

5.2.7. Sodium channel blockers (benzazepinone Nav1.7 blocker): Sodium channel blockers are used in the treatment of neuropathic pain. This is a chronic, debilitating condition that results from injury of the peripheral or central nervous system and can be triggered by a variety of events or conditions, including diabetes, shingles and chemotherapy [131]. Merck reported [132] the discovery of a structurally novel class of benzazepinone hNav1.7 voltage-gated sodium channel blockers containing 2-trifluoromethoxy-L-phenylalanine derivative **189** and 3-L-FPhe **190** (Figure 12) [133]. Compounds **189** and **190** were investigated as potential drugs for the treatment of neuropathic pain because they inhibited action potential firing. It was suggested, based on genetic studies, that a selective Nav1.7 inhibition, will produce robust inhibition of pain without significant side effects [134,135].

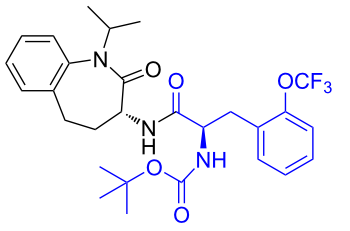

benzazepinone $Na_v1.7$ blocker **189**

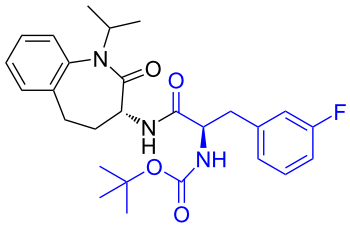

benzazepinone $Na_v1.7$ blocker **190**

Figure 12: Structures of Nav1.7 blockers **189** and **190**.

Conclusion

In view of the increased significance of FAAs in the development of bioactive compounds, considerable efforts were dedicated to the development of efficient synthetic protocols to FAAs. Among them, a range of fluorinated phenylalanines emerged, that have enhanced the biophysical, chemical and biological properties of bioactives. Accordingly, synthetic approaches to five distinct classes of fluorinated analogues were reviewed here. Synthetic protocols and strategies varied according to the position of the fluorine substituent. Also included were ^{18}FPhe derivatives, some of which emerged as promising radiotracers in positron emission tomography (PET). Finally, it is notable that there are a significant number of FPhe derivatives which are nowadays incorporated into drug scaffolds of compounds either licensed or currently being studied in clinical trials.

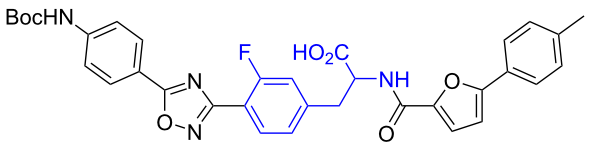

188

Figure 11: Structure of GLP1R (**188**).

Table 1: List of abbreviations.

Ada	adamantyl
Alloc	alloxycarbonyl
BNCT	boron neutron capture therapy
Boc	*tert*-butoxycarbonyl
Cbz	benzyloxycarbonyl
CCK	cholecystokinin
DAST	diethylaminosulfur trifluoride
DIBAL	diisobutylaluminium hydride
DMB	dimethoxybenzyl
DMAc	dimethylacetamide
DPP-4	dipeptidyl peptidase-4
DMPU	*N,N′*-dimethylpropyleneurea
FAAs	fluorinated amino acids
FPhe	fluorinated phenylalanine
Fmoc-Osu	*N*-(9-fluorenylmethoxycarbonyloxy)succinimide
GLP1R	glucagon-like peptide-1 receptor
kryptofix®222	4,7,13,16,21,24-hexaoxa-1,10-diazabicyclo[8.8.8]hexacosane
LAT1	L-type amino acid transporter1
LHMDS	lithium bis(trimethylsilyl)amide
LDA	lithium diisopropylamide
NaHDMS	sodium bis(trimethylsilyl)amide
NFSI	*N*-fluorobenzenesulfonimide
PAM	phenylalanine aminomutase
PET	positron emission tomography
PIP	2-(pyridin-2-yl)isopropylamine
Phth	phthalimido
RRMM	relapsed and refractory multiple myeloma
Selectfluor	1-chloromethyl-4-fluoro-1,4-diazoniabicyclo[2.2.2]octane bis(tetrafluoroborate)
SPhos	2-dicyclohexylphosphino-2′,6′-dimethoxybiphenyl
TBAF	tetrabutylammonium fluoride
TMSI	trimethylsilyl iodide
TMSCN	trimethylsilyl cyanide
TCE	trichloroethyl
TCB	1,2,4,5-tetracyanobenzene
Tr	triphenylmethyl
TEMPO	2,2,6,6-tetramethylpiperidin-1-yl)oxyl or (2,2,6,6-tetramethylpiperidin-1-yl)oxidanyl
TBTA	*tert*-butyl-2,2,2-trichloroacetimidate
TCNHPI	*N*-hydroxytetrachlorophthalimide
XtalFluor-E	*N,N*-diethylamino-*S*,*S*-difluorosulfinium tetrafluoroborate

Acknowledgements

L.F.A and M.S.A express sincere gratitude to Prof David O'Hagan for his support, also we are grateful to Faculty of Science, Alexandria University, Egypt.

ORCID® iDs

Laila F. Awad - https://orcid.org/0000-0001-9521-5511
Mohammed Salah Ayoup - https://orcid.org/0000-0001-6715-5478

References

1. Remete, A. M.; Nonn, M.; Fustero, S.; Fülöp, F.; Kiss, L. *Tetrahedron* **2018,** *74,* 6367–6418. doi:10.1016/j.tet.2018.09.021
2. Salwiczek, M.; Nyakatura, E. K.; Gerling, U. I. M.; Ye, S.; Koksch, B. *Chem. Soc. Rev.* **2012,** *41,* 2135–2171. doi:10.1039/c1cs15241f
3. Merkel, L.; Budisa, N. *Org. Biomol. Chem.* **2012,** *10,* 7241–7261. doi:10.1039/c2ob06922a
4. Purser, S.; Moore, P. R.; Swallow, S.; Gouverneur, V. *Chem. Soc. Rev.* **2008,** *37,* 320–330. doi:10.1039/b610213c

5. Odar, C.; Winkler, M.; Wiltschi, B. *Biotechnol. J.* **2015,** *10,* 427–446. doi:10.1002/biot.201400587
6. Gómez-Nuñez, M.; Haro, K. J.; Dao, T.; Chau, D.; Won, A.; Escobar-Alvarez, S.; Zakhaleva, V.; Korontsvit, T.; Gin, D. Y.; Scheinberg, D. A. *PLoS One* **2008,** *3,* e3938. doi:10.1371/journal.pone.0003938
7. Noren, C.; Anthony-Cahill, S.; Griffith, M.; Schultz, P. *Science* **1989,** *244,* 182–188. doi:10.1126/science.2649980
8. Ye, S.; Berger, A. A.; Petzold, D.; Reimann, O.; Matt, B.; Koksch, B. *Beilstein J. Org. Chem.* **2010,** *6,* No. 40. doi:10.3762/bjoc.6.40
9. Tang, Y.; Ghirlanda, G.; Petka, W. A.; Nakajima, T.; DeGrado, W. F.; Tirrell, D. A. *Angew. Chem., Int. Ed.* **2001,** *40,* 1494–1496. doi:10.1002/1521-3773(20010417)40:8<1494::aid-anie1494>3.0.co;2-x
10. Bilgiçer, B.; Fichera, A.; Kumar, K. *J. Am. Chem. Soc.* **2001,** *123,* 4393–4399. doi:10.1021/ja002961j
11. Kohlmann, J.; Braun, T.; Laubenstein, R.; Herrmann, R. *Chem. – Eur. J.* **2017,** *23,* 12218–12232. doi:10.1002/chem.201700549
12. Hoffmann, W.; Langenhan, J.; Huhmann, S.; Moschner, J.; Chang, R.; Accorsi, M.; Seo, J.; Rademann, J.; Meijer, G.; Koksch, B.; Bowers, M. T.; von Helden, G.; Pagel, K. *Angew. Chem., Int. Ed.* **2019,** *58,* 8216–8220. doi:10.1002/anie.201813954
13. Firooznia, F.; Gude, C.; Chan, K.; Fink, C. A.; Qiao, Y.; Satoh, Y.; Marcopoulos, N.; Savage, P.; Beil, M. E.; Bruseo, C. W.; Trapani, A. J.; Jeng, A. Y. *Bioorg. Med. Chem. Lett.* **2001,** *11,* 375–378. doi:10.1016/s0960-894x(00)00657-0
14. Lee, K.-H.; Lee, H.-Y.; Slutsky, M. M.; Anderson, J. T.; Marsh, E. N. G. *Biochemistry* **2004,** *43,* 16277–16284. doi:10.1021/bi049086p
15. Jäckel, C.; Koksch, B. *Eur. J. Org. Chem.* **2005,** 4483–4503. doi:10.1002/ejoc.200500205
16. Jäckel, C.; Salwiczek, M.; Koksch, B. *Angew. Chem., Int. Ed.* **2006,** *45,* 4198–4203. doi:10.1002/anie.200504387
17. Salwiczek, M.; Samsonov, S.; Vagt, T.; Nyakatura, E.; Fleige, E.; Numata, J.; Cölfen, H.; Pisabarro, M. T.; Koksch, B. *Chem. – Eur. J.* **2009,** *15,* 7628–7636. doi:10.1002/chem.200802136
18. Budisa, N.; Wenger, W.; Wiltschi, B. *Mol. BioSyst.* **2010,** *6,* 1630–1639. doi:10.1039/c002256j
19. He, T.; Gershenson, A.; Eyles, S. J.; Lee, Y.-J.; Liu, W. R.; Wang, J.; Gao, J.; Roberts, M. F. *J. Biol. Chem.* **2015,** *290,* 19334–19342. doi:10.1074/jbc.m115.668343
20. Hammill, J. T.; Miyake-Stoner, S.; Hazen, J. L.; Jackson, J. C.; Mehl, R. A. *Nat. Protoc.* **2007,** *2,* 2601–2607. doi:10.1038/nprot.2007.379
21. Jackson, J. C.; Hammill, J. T.; Mehl, R. A. *J. Am. Chem. Soc.* **2007,** *129,* 1160–1166. doi:10.1021/ja064661t
22. Wiltschi, B. Expressed Protein Modifications: Making Synthetic Proteins. In *Synthetic Gene Networks: Methods and Protocols;* Weber, W.; Fussenegger, M., Eds.; Humana Press: Totowa, NJ, USA, 2012; pp 211–225. doi:10.1007/978-1-61779-412-4_13
23. Furter, R. *Protein Sci.* **1998,** *7,* 419–426. doi:10.1002/pro.5560070223
24. Munier, R.; Cohen, G. N. *Biochim. Biophys. Acta* **1959,** *31,* 378–391. doi:10.1016/0006-3002(59)90011-3
25. Moschner, J.; Stulberg, V.; Fernandes, R.; Huhmann, S.; Leppkes, J.; Koksch, B. *Chem. Rev.* **2019,** *119,* 10718–10801. doi:10.1021/acs.chemrev.9b00024
26. Andra, K. K. *Biochem. Anal. Biochem.* **2015,** *4,* No. 1000235. doi:10.4172/2161-1009.1000235
27. Mallareddy, J. R.; Tóth, G.; Fazakas, C.; Molnár, J.; Nagyőszi, P.; Lipkowski, A. W.; Krizbai, I. A.; Wilhelm, I. *Chem. Biol. Drug Des.* **2012,** *79,* 507–513. doi:10.1111/j.1747-0285.2011.01306.x
28. Mallareddy, J. R.; Borics, A.; Keresztes, A.; Kövér, K. E.; Tourwé, D.; Tóth, G. *J. Med. Chem.* **2011,** *54,* 1462–1472. doi:10.1021/jm101515v
29. Piepenbrink, K. H.; Borbulevych, O. Y.; Sommese, R. F.; Clemens, J.; Armstrong, K. M.; Desmond, C.; Do, P.; Baker, B. M. *Biochem. J.* **2009,** *423,* 353–361. doi:10.1042/bj20090732
30. Doubrovina, E. S.; Doubrovin, M. M.; Lee, S.; Shieh, J.-H.; Heller, G.; Pamer, E.; O'Reilly, R. J. *Clin. Cancer Res.* **2004,** *10,* 7207–7219. doi:10.1158/1078-0432.ccr-04-1040
31. Dominguez, M. A., Jr.; Thornton, K. C.; Melendez, M. G.; Dupureur, C. M. *Proteins: Struct., Funct., Genet.* **2001,** *45,* 55–61. doi:10.1002/prot.1123
32. Pace, C. J.; Gao, J. *Acc. Chem. Res.* **2013,** *46,* 907–915. doi:10.1021/ar300086n
33. Dougherty, D. A. *Acc. Chem. Res.* **2013,** *46,* 885–893. doi:10.1021/ar300265y
34. Oswald, C. L.; Carrillo-Márquez, T.; Caggiano, L.; Jackson, R. F. W. *Tetrahedron* **2008,** *64,* 681–687. doi:10.1016/j.tet.2007.11.031
35. Jackson, R. F. W.; Moore, R. J.; Dexter, C. S.; Elliott, J.; Mowbray, C. E. *J. Org. Chem.* **1998,** *63,* 7875–7884. doi:10.1021/jo981133u
36. Ross, A. J.; Lang, H. L.; Jackson, R. F. W. *J. Org. Chem.* **2010,** *75,* 245–248. doi:10.1021/jo902238n
37. Ayoup, M. S.; Cordes, D. B.; Slawin, A. M. Z.; O'Hagan, D. *Org. Biomol. Chem.* **2015,** *13,* 5621–5624. doi:10.1039/c5ob00650c
38. Ayoup, M. S.; Cordes, D. B.; Slawin, A. M. Z.; O'Hagan, D. *Beilstein J. Org. Chem.* **2015,** *11,* 2671–2676. doi:10.3762/bjoc.11.287
39. Liu, S.; Dockendorff, C.; Taylor, S. D. *Org. Lett.* **2001,** *3,* 1571–1574. doi:10.1021/ol0158664
40. Hill, B.; Ahmed, V.; Bates, D.; Taylor, S. D. *J. Org. Chem.* **2006,** *71,* 8190–8197. doi:10.1021/jo061496r
41. Bosshard, H. R.; Berger, A. *Helv. Chim. Acta* **1973,** *56,* 1838–1845. doi:10.1002/hlca.19730560603
42. Zheng, H.; Comeforo, K.; Gao, J. *J. Am. Chem. Soc.* **2009,** *131,* 18–19. doi:10.1021/ja8062309
43. Li, X.; Xiao, W.; He, G.; Zheng, W.; Yu, N.; Tan, M. *Colloids Surf., A* **2012,** *408,* 79–86. doi:10.1016/j.colsurfa.2012.05.034
44. Kim, D.; Wang, L.; Beconi, M.; Eiermann, G. J.; Fisher, M. H.; He, H.; Hickey, G. J.; Kowalchick, J. E.; Leiting, B.; Lyons, K.; Marsilio, F.; McCann, M. E.; Patel, R. A.; Petrov, A.; Scapin, G.; Patel, S. B.; Roy, R. S.; Wu, J. K.; Wyvratt, M. J.; Zhang, B. B.; Zhu, L.; Thornberry, N. A.; Weber, A. E. *J. Med. Chem.* **2005,** *48,* 141–151. doi:10.1021/jm0493156
45. Setty, S. C.; Horam, S.; Pasupuleti, M.; Haq, W. *Int. J. Pept. Res. Ther.* **2017,** *23,* 213–225. doi:10.1007/s10989-016-9553-5
46. Castillo Meleán, J.; Ermert, J.; Coenen, H. H. *Org. Biomol. Chem.* **2011,** *9,* 765–769. doi:10.1039/c0ob00440e
47. Vukelić, S.; Ushakov, D. B.; Gilmore, K.; Koksch, B.; Seeberger, P. H. *Eur. J. Org. Chem.* **2015,** 3036–3039. doi:10.1002/ejoc.201500300
48. Samet, A. V.; Coughlin, D. J.; Buchanan, A. C., III; Gakh, A. A. *Synth. Commun.* **2002,** *32,* 941–946. doi:10.1081/scc-120002709
49. FILLER, R.; NOVAR, H. *J. Org. Chem.* **1960,** *25,* 733–736. doi:10.1021/jo01075a015
50. Yu, H.; Richey, R. N.; Stout, J. R.; LaPack, M. A.; Gu, R.; Khau, V. V.; Frank, S. A.; Ott, J. P.; Miller, R. D.; Carr, M. A.; Zhang, T. Y. *Org. Process Res. Dev.* **2008,** *12,* 218–225. doi:10.1021/op700235c

51. Liu, J.; Deng, X.; Fitzgerald, A. E.; Sales, Z. S.; Venkatesan, H.; Mani, N. S. *Org. Biomol. Chem.* **2011,** *9,* 2654–2660. doi:10.1039/c0ob01004a
52. Coenen, H. H.; Franken, K.; Kling, P.; Stöcklin, G. *Int. J. Radiat. Appl. Instrum., Part A* **1988,** *39,* 1243–1250. doi:10.1016/0883-2889(88)90107-4
53. Ishiwata, K.; Ido, T.; Mejia, A. A.; Ichihashi, M.; Mishima, Y. *Int. J. Radiat. Appl. Instrum., Part A* **1991,** *42,* 325–328. doi:10.1016/0883-2889(91)90133-l
54. Makaravage, K. J.; Brooks, A. F.; Mossine, A. V.; Sanford, M. S.; Scott, P. J. H. *Org. Lett.* **2016,** *18,* 5440–5443. doi:10.1021/acs.orglett.6b02911
55. Geurink, P. P.; Liu, N.; Spaans, M. P.; Downey, S. L.; van den Nieuwendijk, A. M. C. H.; van der Marel, G. A.; Kisselev, A. F.; Florea, B. I.; Overkleeft, H. S. *J. Med. Chem.* **2010,** *53,* 2319–2323. doi:10.1021/jm9015685
56. Chiu, H.-P.; Suzuki, Y.; Gullickson, D.; Ahmad, R.; Kokona, B.; Fairman, R.; Cheng, R. P. *J. Am. Chem. Soc.* **2006,** *128,* 15556–15557. doi:10.1021/ja0640445
57. Panella, L.; Aleixandre, A. M.; Kruidhof, G. J.; Robertus, J.; Feringa, B. L.; de Vries, J. G.; Minnaard, A. J. *J. Org. Chem.* **2006,** *71,* 2026–2036. doi:10.1021/jo052451d
58. Verhoeven, J.; Hulpia, F.; Kersemans, K.; Bolcaen, J.; De Lombaerde, S.; Goeman, J.; Descamps, B.; Hallaert, G.; Van den Broecke, C.; Deblaere, K.; Vanhove, C.; Van der Eycken, J.; Van Calenbergh, S.; Goethals, I.; De Vos, F. *Sci. Rep.* **2019,** *9,* 2878. doi:10.1038/s41598-019-40013-x
59. Ando, M.; Kuzuhara, H. *Bull. Chem. Soc. Jpn.* **1990,** *63,* 1925–1928. doi:10.1246/bcsj.63.1925
60. Kukhar, V. P.; Belokon, Y. N.; Soloshonok, V.; Svistunova, N. Yu.; Rozhenko, A. B.; Kuz'mina, N. A. *Synthesis* **1993,** 117–120. doi:10.1055/s-1993-25812
61. Soloshonok, V. A.; Belokon', Yu. N.; Kukhar', V. P.; Chernoglazova, N. I.; Saporovskaya, M. B.; Bakhmutov, V. I.; Kolycheva, M. T.; Belikov, V. M. *Russ. Chem. Bull.* **1990,** *39,* 1479–1485. doi:10.1007/bf00957865
62. Drouet, F.; Noisier, A. F. M.; Harris, C. S.; Furkert, D. P.; Brimble, M. A. *Eur. J. Org. Chem.* **2014,** 1195–1201. doi:10.1002/ejoc.201301718
63. Szymanski, W.; Wu, B.; Weiner, B.; de Wildeman, S.; Feringa, B. L.; Janssen, D. B. *J. Org. Chem.* **2009,** *74,* 9152–9157. doi:10.1021/jo901833y
64. Okuda, K.; Hirota, T.; Kingery, D. A.; Nagasawa, H. *J. Org. Chem.* **2009,** *74,* 2609–2612. doi:10.1021/jo802611t
65. Davis, F. A.; Srirajan, V.; Titus, D. D. *J. Org. Chem.* **1999,** *64,* 6931–6934. doi:10.1021/jo990947n
66. Shi, G.-q.; Zhao, Z.-y.; Zhang, X.-b. *J. Org. Chem.* **1995,** *60,* 6608–6611. doi:10.1021/jo00125a060
67. Kollonitsch, J.; Marburg, S.; Perkins, L. *J. Org. Chem.* **1975,** *40,* 3808–3809. doi:10.1021/jo00913a900
68. Tsushima, T.; Kawada, K.; Nishikawa, J.; Sato, T.; Tori, K.; Tsuji, T.; Misaki, S. *J. Org. Chem.* **1984,** *49,* 1163–1169. doi:10.1021/jo00181a003
69. Tsushima, T.; Sato, T.; Tsuji, T. *Tetrahedron Lett.* **1980,** *21,* 3591–3592. doi:10.1016/0040-4039(80)80243-7
70. Wade, T. N.; Gaymard, F.; Guedj, R. *Tetrahedron Lett.* **1979,** *20,* 2681–2682. doi:10.1016/s0040-4039(01)86385-1
71. Bloom, S.; McCann, M.; Lectka, T. *Org. Lett.* **2014,** *16,* 6338–6341. doi:10.1021/ol503094m
72. Egami, H.; Masuda, S.; Kawato, Y.; Hamashima, Y. *Org. Lett.* **2018,** *20,* 1367–1370. doi:10.1021/acs.orglett.8b00133
73. Bume, D. D.; Pitts, C. R.; Jokhai, R. T.; Lectka, T. *Tetrahedron* **2016,** *72,* 6031–6036. doi:10.1016/j.tet.2016.08.018
74. Davies, S. G.; Fletcher, A. M.; Frost, A. B.; Roberts, P. M.; Thomson, J. E. *Org. Lett.* **2015,** *17,* 2254–2257. doi:10.1021/acs.orglett.5b00880
75. Davies, S. G.; Fletcher, A. M.; Frost, A. B.; Roberts, P. M.; Thomson, J. E. *Tetrahedron* **2014,** *70,* 5849–5862. doi:10.1016/j.tet.2014.06.057
76. Davies, S. G.; Fletcher, A. M.; Frost, A. B.; Lee, J. A.; Roberts, P. M.; Thomson, J. E. *Tetrahedron* **2013,** *69,* 8885–8898. doi:10.1016/j.tet.2013.08.007
77. Zhang, Q.; Yin, X.-S.; Chen, K.; Zhang, S.-Q.; Shi, B.-F. *J. Am. Chem. Soc.* **2015,** *137,* 8219–8226. doi:10.1021/jacs.5b03989
78. Zhu, R.-Y.; Tanaka, K.; Li, G.-C.; He, J.; Fu, H.-Y.; Li, S.-H.; Yu, J.-Q. *J. Am. Chem. Soc.* **2015,** *137,* 7067–7070. doi:10.1021/jacs.5b04088
79. Meyer, S. D.; Schreiber, S. L. *J. Org. Chem.* **1994,** *59,* 7549–7552. doi:10.1021/jo00103a067
80. Dess, D. B.; Martin, J. C. *J. Org. Chem.* **1983,** *48,* 4155–4156. doi:10.1021/jo00170a070
81. Schlosser, M.; Brügger, N.; Schmidt, W.; Amrhein, N. *Tetrahedron* **2004,** *60,* 7731–7742. doi:10.1016/j.tet.2004.06.086
82. Harada, K.; Fox, S. W. *Naturwissenschaften* **1964,** *51,* 106–107. doi:10.1007/bf00629604
83. Schlosser, M. The Chemical and Physiological size of Fluorine. In *Enantiocontrolled Synthesis of Fluoro-organic Compounds: Stereochemical Challenges and Biomedicinal Targets;* Soloshonok, V. A., Ed.; John Wiley & Sons: Chichester, UK, 1999; pp 613–659.
84. Wei, Q.; Ma, Y.; Li, L.; Liu, Q.; Liu, Z.; Liu, G. *Org. Lett.* **2018,** *20,* 7100–7103. doi:10.1021/acs.orglett.8b03044
85. Vandenberghe, S.; Marsden, P. K. *Phys. Med. Biol.* **2015,** *60,* R115–R154. doi:10.1088/0031-9155/60/4/r115
86. Martarello, L.; Schaffrath, C.; Deng, H.; Gee, A. D.; Lockhart, A.; O'Hagan, D. *J. Labelled Compd. Radiopharm.* **2003,** *46,* 1181–1189. doi:10.1002/jlcr.779
87. Deng, H.; Cobb, S. L.; Gee, A. D.; Lockhart, A.; Martarello, L.; McGlinchey, R. P.; O'Hagan, D.; Onega, M. *Chem. Commun.* **2006,** 652–654. doi:10.1039/b516861a
88. Snyder, H. R.; Reedy, A. J.; Lennarz, W. J. *J. Am. Chem. Soc.* **1958,** *80,* 835–838. doi:10.1021/ja01537a021
89. Ishiwata, K.; Ido, T.; Kawamura, M.; Kubota, K.; Ichihashi, M.; Mishima, Y. *Int. J. Radiat. Appl. Instrum., Part B* **1991,** *18,* 745–751. doi:10.1016/0883-2897(91)90013-b
90. Ishiwata, K. *Ann. Nucl. Med.* **2019,** *33,* 223–236. doi:10.1007/s12149-019-01347-8
91. Ishiwata, K.; Ido, T.; Honda, C.; Kawamura, M.; Ichihashi, M.; Mishima, Y. *Int. J. Radiat. Appl. Instrum., Part B* **1992,** *19,* 311–318. doi:10.1016/0883-2897(92)90116-g
92. Chandra, S.; Kabalka, G. W.; Lorey, D. R.; Smith, D. R.; Coderre, J. A. *Clin. Cancer Res.* **2002,** *8,* 2675–2683.
93. Tscherpel, C.; Dunkl, V.; Ceccon, G.; Stoffels, G.; Judov, N.; Rapp, M.; Meyer, P. T.; Kops, E. R.; Ermert, J.; Fink, G. R.; Shah, N. J.; Langen, K.-J.; Galldiks, N. *Neuro-Oncology (Cary, NC, U. S.)* **2017,** *19,* 710–718. doi:10.1093/neuonc/now243

94. Verhoeven, J.; Bolcaen, J.; Kersemans, K.; De Meulenaere, V.; Deblaere, K.; Kalala, J.; Van den Broecke, C.; Vanhove, C.; Goethals, I.; De Vos, F. *Neuro-Oncology (Cary, NC, U. S.)* **2017,** *19* (Suppl. 3), iii46. doi:10.1093/neuonc/nox036.166
95. Chiaravalloti, A.; Filippi, L.; Ricci, M.; Cimini, A.; Schillaci, O. *Cancers* **2019,** *11,* 1853. doi:10.3390/cancers11121853
96. Moreau, A.; Febvey, O.; Mognetti, T.; Frappaz, D.; Kryza, D. *Front. Oncol.* **2019,** *9,* No. 1134. doi:10.3389/fonc.2019.01134
97. Lahoutte, T.; Caveliers, V.; Camargo, S. M.; Franca, R.; Ramadan, T.; Veljkovic, E.; Mertens, J.; Bossuyt, A.; Verrey, F. *J. Nucl. Med.* **2004,** *45,* 1591–1596.
98. Bolcaen, J.; Descamps, B.; Deblaere, K.; Boterberg, T.; De Vos Pharm, F.; Kalala, J.-P.; Van den Broecke, C.; Decrock, E.; Leybaert, L.; Vanhove, C.; Goethals, I. *Nucl. Med. Biol.* **2015,** *42,* 38–45. doi:10.1016/j.nucmedbio.2014.07.006
99. Feral, C. C.; Tissot, F. S.; Tosello, L.; Fakhry, N.; Sebag, F.; Pacak, K.; Taïeb, D. *Eur. J. Nucl. Med. Mol. Imaging* **2017,** *44,* 812–821. doi:10.1007/s00259-016-3586-z
100. Sun, A.; Liu, X.; Tang, G. *Front. Chem. (Lausanne, Switz.)* **2018,** *5,* No. 124. doi:10.3389/fchem.2017.00124
101. Chiotellis, A.; Müller Herde, A.; Rössler, S. L.; Brekalo, A.; Gedeonova, E.; Mu, L.; Keller, C.; Schibli, R.; Krämer, S. D.; Ametamey, S. M. *J. Med. Chem.* **2016,** *59,* 5324–5340. doi:10.1021/acs.jmedchem.6b00057
102. Strese, S. *Anticancer Activity of Melflufen: Preclinical Studies of a Novel Peptidase-Potentiated Alkylator;* Acta Universitatis Upsaliensis, 2015.
103. Carlier, C.; Strese, S.; Viktorsson, K.; Velander, E.; Nygren, P.; Uustalu, M.; Juntti, T.; Lewensohn, R.; Larsson, R.; Spira, J.; De Vlieghere, E.; Ceelen, W. P.; Gullbo, J. *Oncotarget* **2016,** *7,* 59322–59335. doi:10.18632/oncotarget.11163
104. Ormerod, D.; Willemsens, B.; Mermans, R.; Langens, J.; Winderickx, G.; Kalindjian, S. B.; Buck, I. M.; McDonald, I. M. *Org. Process Res. Dev.* **2005,** *9,* 499–507. doi:10.1021/op0500638
105. Chau, I.; Cunningham, D.; Russell, C.; Norman, A. R.; Kurzawinski, T.; Harper, P.; Harrison, P.; Middleton, G.; Daniels, F.; Hickish, T.; Prendeville, J.; Ross, P. J.; Theis, B.; Hull, R.; Walker, M.; Shankley, N.; Kalindjian, B.; Murray, G.; Gillbanks, A.; Black, J. *Br. J. Cancer* **2006,** *94,* 1107–1115. doi:10.1038/sj.bjc.6603058
106. Harper, E. A.; Roberts, S. P.; Kalindjian, S. B. *Br. J. Pharmacol.* **2007,** *151,* 1352–1367. doi:10.1038/sj.bjp.0707355
107. McDonald, I. M.; Black, J. W.; Buck, I. M.; Dunstone, D. J.; Griffin, E. P.; Harper, E. A.; Hull, R. A. D.; Kalindjian, S. B.; Lilley, E. J.; Linney, I. D.; Pether, M. J.; Roberts, S. P.; Shaxted, M. E.; Spencer, J.; Steel, K. I. M.; Sykes, D. A.; Walker, M. K.; Watt, G. F.; Wright, L.; Wright, P. T.; Xun, W. *J. Med. Chem.* **2007,** *50,* 3101–3112. doi:10.1021/jm070139l
108. Harper, E. A.; Mitchell, E. A.; Griffin, E. P.; Kalindjian, S. B. *Eur. J. Pharmacol.* **2008,** *581,* 1–12. doi:10.1016/j.ejphar.2007.11.055
109. Mei, H.; Han, J.; Klika, K. D.; Izawa, K.; Sato, T.; Meanwell, N. A.; Soloshonok, V. A. *Eur. J. Med. Chem.* **2020,** *186,* 111826. doi:10.1016/j.ejmech.2019.111826
110. Roberts, S.; Griffin, E.; Harper, E.; Hull, R; Kalindjian, S.; Lilley, E.; Kotecha, A.; Shankley, N.; Sykes, D.; Watt, G. *Pharmacologist* **2002,** *44* (Suppl. 1), 30.
111. Herranz, R. *Med. Res. Rev.* **2003,** *23,* 559–605. doi:10.1002/med.10042
112. Berna, M. J.; Tapia, J. A.; Sancho, V.; Jensen, R. T. *Curr. Opin. Pharmacol.* **2007,** *7,* 583–592. doi:10.1016/j.coph.2007.09.011
113. Pippel, M.; Boyce, K.; Venkatesan, H.; Phuong, V. K.; Yan, W.; Barrett, T. D.; Lagaud, G.; Li, L.; Morton, M. F.; Prendergast, C.; Wu, X.; Shankley, N. P.; Rabinowitz, M. H. *Bioorg. Med. Chem. Lett.* **2009,** *19,* 6376–6378. doi:10.1016/j.bmcl.2009.09.065
114. Herman, G. A.; Stevens, C.; Van Dyck, K.; Bergman, A.; Yi, B.; De Smet, M.; Snyder, K.; Hilliard, D.; Tanen, M.; Tanaka, W.; Wang, A. Q.; Zeng, W.; Musson, D.; Winchell, G.; Davies, M. J.; Ramael, S.; Gottesdiener, K. M.; Wagner, J. A. *Clin. Pharmacol. Ther. (Hoboken, NJ, U. S.)* **2005,** *78,* 675–688. doi:10.1016/j.clpt.2005.09.002
115. Kushwaha, R. N.; Haq, W.; Katti, S. *Chem. Biol. Interface* **2014,** *4,* 137–162.
116. Baksh, S. N.; McAdams-DeMarco, M.; Segal, J. B.; Alexander, G. C. *Pharmacoepidemiol. Drug Saf.* **2018,** *27,* 660–667. doi:10.1002/pds.4437
117. Kaihong, Y.; Piaoyang, S. Pharmaceutical composition for treatment of type 2 diabetes. U.S. Patent US 8,476,272 B2, July 2, 2013.
118. Drugbank, Retagliptin. https://www.drugbank.ca/drugs/DB14898 (accessed Feb 25, 2020).
119. Notte, G. T. *Annu. Rep. Med. Chem.* **2014,** *49,* 417–436. doi:10.1016/b978-0-12-800167-7.00026-2
120. Yong, X.; Hu, T.; Feng, S.; Du, X.; Shi, H.; Feng, W. *Trop. J. Pharm. Res.* **2015,** *14,* 1481–1486. doi:10.4314/tjpr.v14i8.22
121. McCormack, P. L. *Drugs* **2015,** *75,* 2045–2049. doi:10.1007/s40265-015-0496-5
122. Flick, A. C.; Ding, H. X.; Leverett, C. A.; Kyne, R. E., Jr.; Liu, K. K.-C.; Fink, S. J.; O'Donnell, C. J. *J. Med. Chem.* **2017,** *60,* 6480–6515. doi:10.1021/acs.jmedchem.7b00010
123. Oh, J.; Kim, A. H.; Lee, S.; Cho, H.; Kim, Y. S.; Bahng, M. Y.; Yoon, S. H.; Cho, J.-Y.; Jang, I.-J.; Yu, K.-S. *Diabetes Obes. Metab.* **2017,** *19,* 294–298. doi:10.1111/dom.12813
124. Zhao, W. *Handbook for Chemical Process Research and Development;* CRC Press: Boca Raton, FL, USA, 2016. doi:10.1201/9781315367316
125. Fraser, G. L.; Hoveyda, H. R.; Tannenbaum, G. S. *Endocrinology* **2008,** *149,* 6280–6288. doi:10.1210/en.2008-0804
126. Lasseter, K. C.; Shaughnessy, L.; Cummings, D.; Pezzullo, J. C.; Wargin, W.; Gagnon, R.; Oliva, J.; Kosutic, G. *J. Clin. Pharmacol.* **2008,** *48,* 193–202. doi:10.1177/0091270007310380
127. Hoveyda, H. R.; Marsault, E.; Gagnon, R.; Mathieu, A. P.; Vézina, M.; Landry, A.; Wang, Z.; Benakli, K.; Beaubien, S.; Saint-Louis, C.; Brassard, M.; Pinault, J.-F.; Ouellet, L.; Bhat, S.; Ramaseshan, M.; Peng, X.; Foucher, L.; Beauchemin, S.; Bhérer, P.; Veber, D. F.; Peterson, M. L.; Fraser, G. L. *J. Med. Chem.* **2011,** *54,* 8305–8320. doi:10.1021/jm2007062
128. Gallwitz, B. *Drugs* **2011,** *71,* 1675–1688. doi:10.2165/11592810-000000000-00000
129. Trujillo, J. M.; Nuffer, W. *Pharmacotherapy* **2014,** *34,* 1174–1186. doi:10.1002/phar.1507
130. Gallwitz, B. Glucagon-like peptide-1 receptor agonists. In *Handbook of Incretin-based Therapies in Type 2 Diabetes;* Gough, S., Ed.; Springer International Publishing: Cham, Switzerland, 2016; pp 31–43. doi:10.1007/978-3-319-08982-9_3
131. Theile, J. W.; Cummins, T. R. *Front. Pharmacol.* **2011,** *2,* No. 54. doi:10.3389/fphar.2011.00054
132. Hoyt, S. B.; London, C.; Abbadie, C.; Felix, J. P.; Garcia, M. L.; Jochnowitz, N.; Karanam, B. V.; Li, X.; Lyons, K. A.; McGowan, E.; Priest, B. T.; Smith, M. M.; Warren, V. A.; Thomas-Fowlkes, B. S.; Kaczorowski, G. J.; Duffy, J. L. *Bioorg. Med. Chem. Lett.* **2013,** *23,* 3640–3645. doi:10.1016/j.bmcl.2013.03.121

133. Hoyt Scott, B.; London, C.; Ok, D.; Parsons, W. H. Benzaepinones as sodium channel blockers. U.S. Patent US 7,888,345 B2, Feb 15, 2011.
134. Hoyt, S. B.; London, C.; Gorin, D.; Wyvratt, M. J.; Fisher, M. H.; Abbadie, C.; Felix, J. P.; Garcia, M. L.; Li, X.; Lyons, K. A.; McGowan, E.; MacIntyre, D. E.; Martin, W. J.; Priest, B. T.; Ritter, A.; Smith, M. M.; Warren, V. A.; Williams, B. S.; Kaczorowski, G. J.; Parsons, W. H. *Bioorg. Med. Chem. Lett.* **2007,** *17,* 4630–4634. doi:10.1016/j.bmcl.2007.05.076
135. Hoyt, S. B.; London, C.; Ok, H.; Gonzalez, E.; Duffy, J. L.; Abbadie, C.; Dean, B.; Felix, J. P.; Garcia, M. L.; Jochnowitz, N.; Karanam, B. V.; Li, X.; Lyons, K. A.; McGowan, E.; MacIntyre, D. E.; Martin, W. J.; Priest, B. T.; Smith, M. M.; Tschirret-Guth, R.; Warren, V. A.; Williams, B. S.; Kaczorowski, G. J.; Parsons, W. H. *Bioorg. Med. Chem. Lett.* **2007,** *17,* 6172–6177. doi:10.1016/j.bmcl.2007.09.032

License and Terms

This is an Open Access article under the terms of the Creative Commons Attribution License (http://creativecommons.org/licenses/by/4.0). Please note that the reuse, redistribution and reproduction in particular requires that the authors and source are credited.

The license is subject to the *Beilstein Journal of Organic Chemistry* terms and conditions: (https://www.beilstein-journals.org/bjoc)

The definitive version of this article is the electronic one which can be found at: doi:10.3762/bjoc.16.91

BEILSTEIN JOURNAL OF ORGANIC CHEMISTRY

Development of fluorinated benzils and bisbenzils as room-temperature phosphorescent molecules

Shigeyuki Yamada*[1], Takuya Higashida[1], Yizhou Wang[1], Masato Morita[1], Takuya Hosokai[2], Kaveendra Maduwantha[2,3], Kaveenga Rasika Koswattage[2,3] and Tsutomu Konno[1]

Full Research Paper

Open Access

Address:
[1]Faculty of Molecular Chemistry and Engineering, Kyoto Institute of Technology, Matsugasaki, Sakyo-ku, Kyoto 606-8585, Japan, [2]National Metrology Institute of Japan, National Institute of Advanced Industrial Science and Technology, 1-1-1 Umezono, Tsukuba 305-8560, Japan and [3]Faculty of Technology, Sabaragamuwa University of Sri Lanka, P.O. Box 02, Belihuloya 70140, Sri Lanka

Email:
Shigeyuki Yamada* - syamada@kit.ac.jp

* Corresponding author

Keywords:
alkyne oxidation; benzils; bistolanes; fluorinated compounds; phosphorescence

Beilstein J. Org. Chem. **2020,** *16,* 1154–1162.
doi:10.3762/bjoc.16.102

Received: 23 March 2020
Accepted: 20 May 2020
Published: 29 May 2020

This article is part of the thematic issue "Organo-fluorine chemistry V".

Guest Editor: D. O'Hagan

© 2020 Yamada et al.; licensee Beilstein-Institut.
License and terms: see end of document.

Abstract

Pure organic phosphorescent molecules are attractive alternatives to transition-metal-complex-based phosphores for biomedical and technological applications owing to their abundance and nontoxicity. This article discloses the design, synthesis, and photophysical properties of fluorinated benzil and bisbenzil derivatives as potential pure organic room-temperature phosphorescent molecules. These compounds were separately converted from the corresponding fluorinated bistolanes via $PdCl_2$-catalyzed oxidation by dimethyl sulfoxide, while nonfluorinated bistolane provided the corresponding bisbenzil derivatives exclusively in a similar manner. Intensive investigations of the photophysical properties of the benzil and bisbenzil derivatives in toluene at 25 °C showed both fluorescence with a photoluminescence (PL) band at a maximum wavelength (λ_{PL}) of around 400 nm and phosphorescence with a PL band at a λ_{PL} of around 560 nm. Interestingly, intersystem crossing effectively caused fluorinated benzils to emit phosphorescence, which may arise from immediate spin-orbit coupling involving the $^1(n, \pi) \rightarrow {}^3(\pi, \pi)$ transition, unlike the case of fluorinated or nonfluorinated bisbenzil analogues. These findings offer a useful guide for developing novel pure organic room-temperature phosphorescent materials.

Introduction

The development of organic light-emitting molecules is recognized as one of the most important studies because of the broad application of these compounds as fluorescence probes, bioimaging materials, and biosensors in biomedical diagnostics [1-4] and as organic light-emitting diodes in the technological field [5-8]. Among the organic light-emitting molecules de-

veloped thus far, extended π-conjugated compounds (e.g., pyrenes and perylenes) emit fluorescence, which is a radiative deactivation process from the lowest singlet (S_1) excited state to the ground (S_0) state [9]. Interestingly, for such π-conjugated molecules, suitable structural modifications can switch the radiative $S_1 \rightarrow S_0$ process to another radiative deactivation process from the triplet (T_1) excited state to S_0 via an $S_1 \rightarrow T_1$ intersystem crossing (ISC), resulting in the emission of phosphorescence [9].

Phosphorescent molecules generate two excitons (i.e., 25% S_1 excitons and 75% T_1 excitons) by application of an electric field, which is well known for organic light-emitting diodes. S_1 excitons are converted to T_1 excitons via an ISC process, finally achieving an excellent light-emitting efficiency (up to 100%) [10]. Therefore, extensive investigations to develop phosphorescent molecules have been performed thus far [11-13].

It has been established that transition metal complexes containing a heavy atom can promote ISC (e.g., Ru [14], Ir [15,16], Pt [17], and Au [18-21]) (Figure 1A), and this offers a molecular design approach for phosphorescence emission. However, it is becoming necessary to explore alternatives to rare metals because of the latter's scarcity and toxicity. Owing to recent considerable efforts, several molecular designs have been proposed as alternatives, particularly the use of pure organic phosphorescent molecules [22].

For example, methyl 4-bromobenzoate (Figure 1B) exhibits phosphorescence in the crystalline state via nonradiative ISC to the T_1 state owing to crystallization-induced restriction of intramolecular motions [23]. Moreover, crystalline 2,5-dihexyloxy-4-bromobenzaldehyde displays green phosphorescence, which stems from rapid ISC due to the heavy atom effect via halogen bonding (C=O···Br) [24]. Moreover, benzophenone- or benzil-

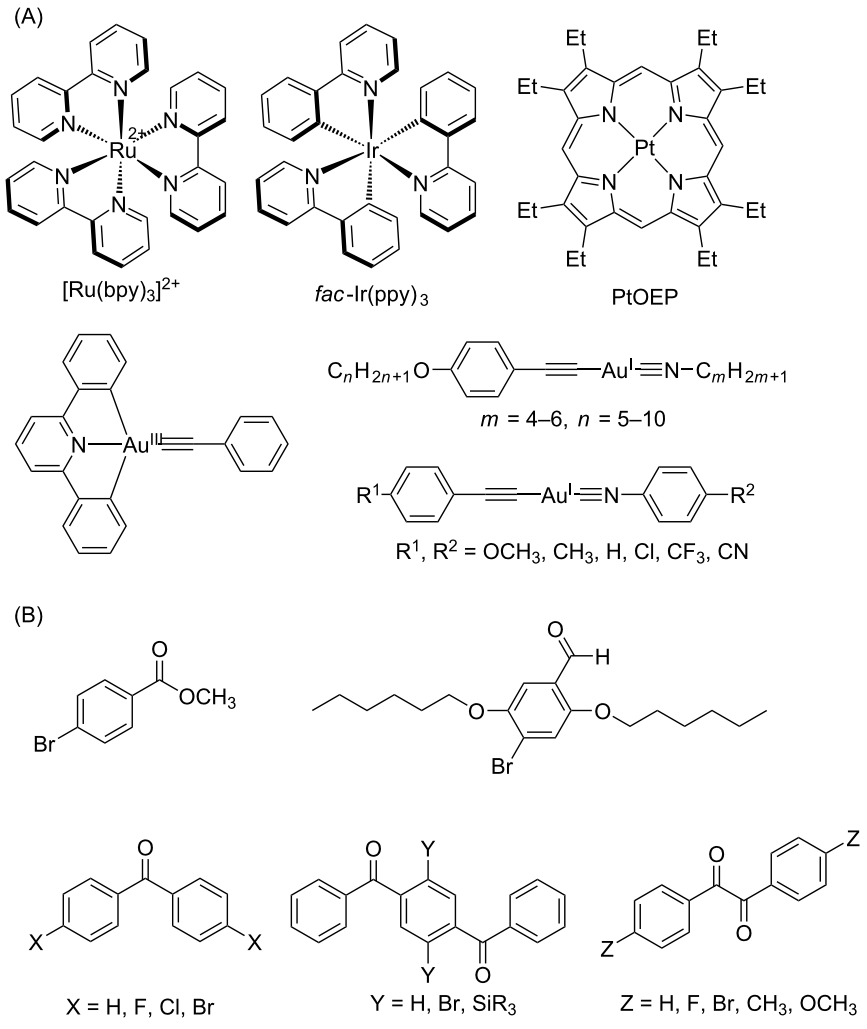

Figure 1: (A) Transition-metal-containing and (B) pure organic phosphorescent materials reported thus far (bpy: 2,2'-bipyridine, ppy: 2-phenylpyridine, OEP: octaethylporphyrin).

type molecules can achieve long-lived phosphorescence owing to a significant acceleration of spin-orbit coupling based on the El-Sayed rule involving the $^1(n, \pi) \rightarrow {}^3(\pi, \pi)$ transition [25,26].

Over the past few years, our group has intensively investigated fluorinated 1,4-bis(2-phenylethyn-1-yl)benzenes (**1**), a structural class known as bistolanes (Figure 2A), which show prominent fluorescence not only in dilute solution, but also in the crystalline state [27-31].

As a powerful tool to develop novel pure organic phosphorescent molecules, we envisioned the structural modification of the carbon–carbon triple (C≡C) bond in fluorinated bistolane **1** via oxidation to form the corresponding benzil **2** and/or bisbenzil **3** derivatives (Figure 2B). A literature review reveals that bisbenzil-type analogues have not received much attention, despite several publications on benzil-type phosphorescent molecules [25,26,32]. In this study, therefore, we examined the synthesis of novel benzil- and bisbenzil-type molecules via oxidation of fluorinated and nonfluorinated bistolane derivatives and evaluated their photophysical properties in detail.

Results and Discussion

Synthesis

This study was initiated with the synthesis of fluorinated bisbenzil derivatives. The $PdCl_2$-catalyzed oxidation of the C≡C bonds in **1** by dimethyl sulfoxide (DMSO) was performed according to a previously reported procedure (Scheme 1) [33,34].

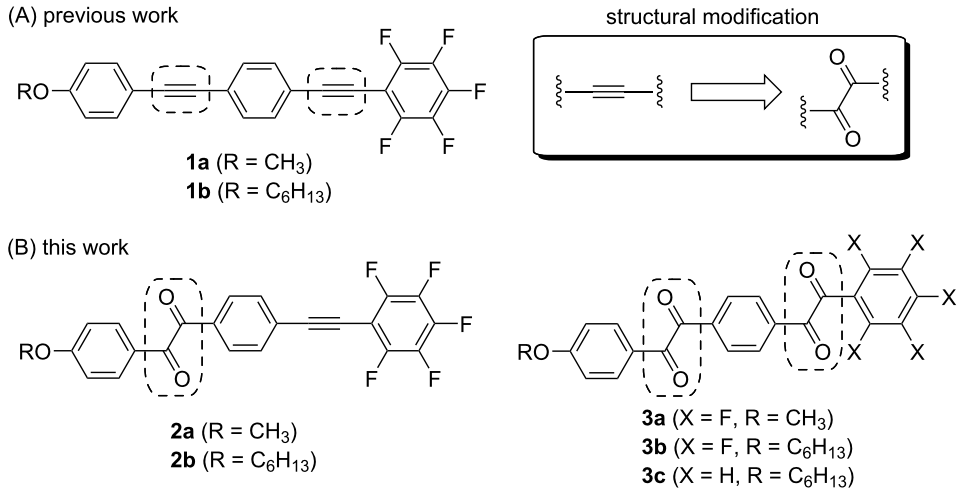

Figure 2: (A) Chemical structures of fluorescent bistolane derivatives previously developed by our group and (B) phosphorescent molecular structures intended for this work.

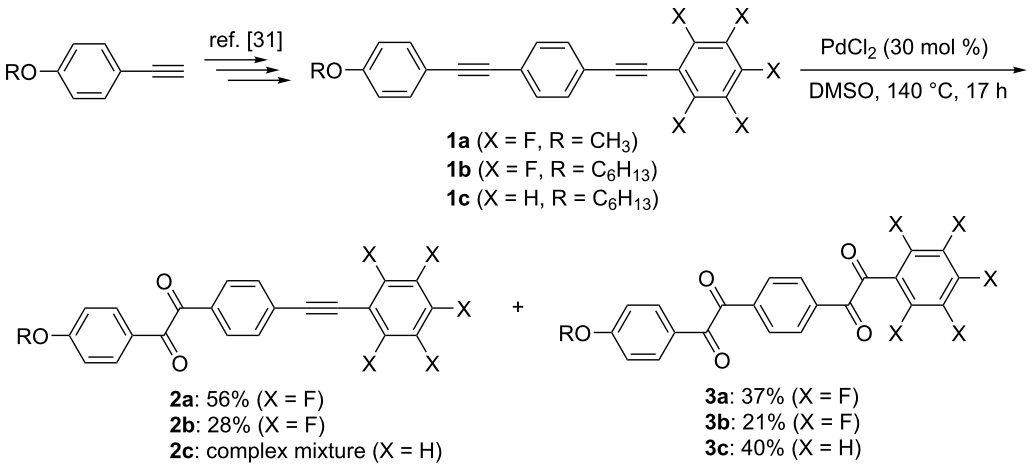

Scheme 1: Synthetic pathway for fluorinated benzil (**2**) and bisbenzil (**3**) derivatives.

The methoxy-substituted fluorinated bistolane **1a** was prepared from commercially available 4-ethynylanisole in four facile steps. Interestingly, stirring **1a** in DMSO solution in the presence of 30 mol % of $PdCl_2$ at 140 °C for 17 h produced two products (56% yield for the more polar product and 37% yield for the less polar product) after purification with column chromatography. Spectroscopic analyses (i.e., ^{1}H, ^{19}F, and ^{13}C nuclear magnetic resonance (NMR) spectroscopy, infrared spectroscopy, and high-resolution mass spectrometry) successfully identified the more polar product as the half-oxidized benzil **2a** and the less polar one as the fully oxidized bisbenzil **3a**. Fluorinated bistolane **1b**, bearing a hexyloxy chain, also underwent $PdCl_2$-catalyzed C≡C oxidation to give rise to the corresponding benzil **2b** and bisbenzil **3b** in 28% and 21% yield, respectively. When nonfluorinated bistolane **1c** was used as the substrate, the corresponding bisbenzil **3c** was obtained in 40% yield as the major product together with an inseparable mixture.

The proposed mechanism of Pd(II)-catalyzed C≡C oxidation is illustrated in Scheme 2 [33]: The catalytic cycle starts with the coordination of the electron-rich C≡C bond to the electron-deficient divalent Pd center, forming the corresponding π-complex (**Int-A**). **Int-A** smoothly undergoes nucleophilic attack by the oxygen atom in DMSO to construct a cationic vinyl-palladium(II) species (**Int-B**). Further nucleophilic attack of another DMSO molecule against **Int-B**, followed by elimination of dimethyl sulfide, furnishes a cationic intermediate (**Int-C**). Finally, immediate elimination of dimethyl sulfide and the Pd(II) catalyst gives rise to the corresponding benzil **2**, after which the eliminated Pd(II) catalyst is recycled to provide the oxidation products. The fully oxidized bisbenzil **3** is generated after further Pd(II)-catalyzed C≡C oxidation of the half-oxidized benzil **2** via the same catalytic cycle.

Considering the proposed reaction mechanism, the successful isolation of the half-oxidized benzil derivatives **2a** and **2b** from the oxidation of fluorinated bistolanes **1a** and **1b**, respectively, may be due to the decreased reactivity of the C≡C bond toward Pd(II)-catalyzed C≡C oxidation caused by the adjacent electron-deficient fluorinated aromatic ring. To confirm the electron-withdrawing effect of this fluorinated aromatic ring, the electronic charge at the adjacent C≡C bond was calculated by density functional theory (DFT) using the Gaussian 16 (Revision B.01) software package [35]. As typical examples, the molecular geometries of **1a** and **1c** were optimized at the CAM-B3LYP/6-31+G(d) level of theory. The absence of any imaginary frequency in the vibrational analysis proved that the calculated structures are the minima. Figure 3 shows the calculated Mulliken charge distributions of fluorinated **1a** and nonfluorinated **1c**.

The sp-hybridized carbon adjacent to the fluorinated aromatic ring of **1a** has a significant positive Mulliken charge (+0.472), while that adjacent to the nonfluorinated aromatic ring of **1c** has a negative charge (−0.304). This clearly indicates that the fluo-

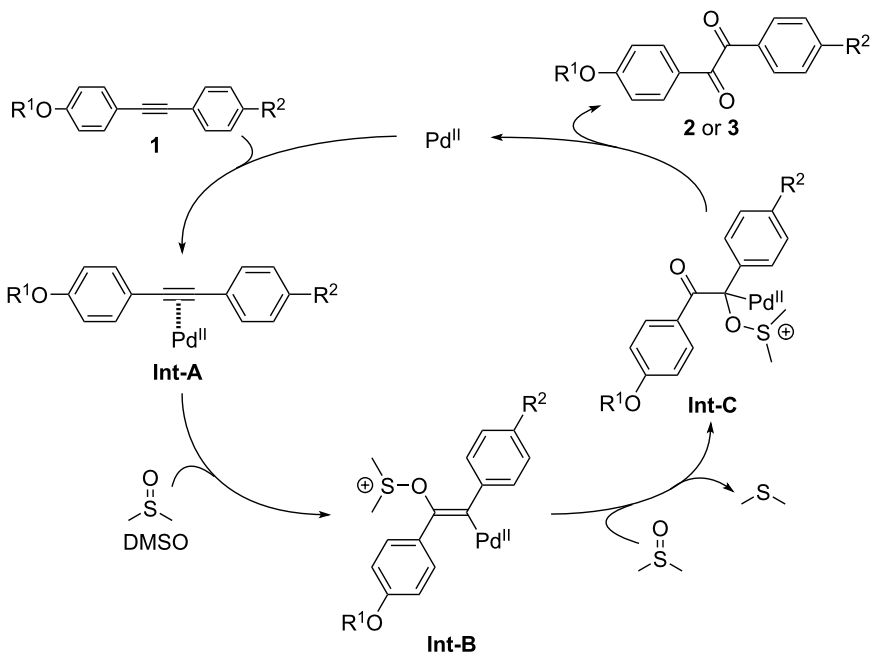

Scheme 2: Proposed mechanism of Pd(II)-catalyzed alkyne oxidation by dimethyl sulfoxide (DMSO).

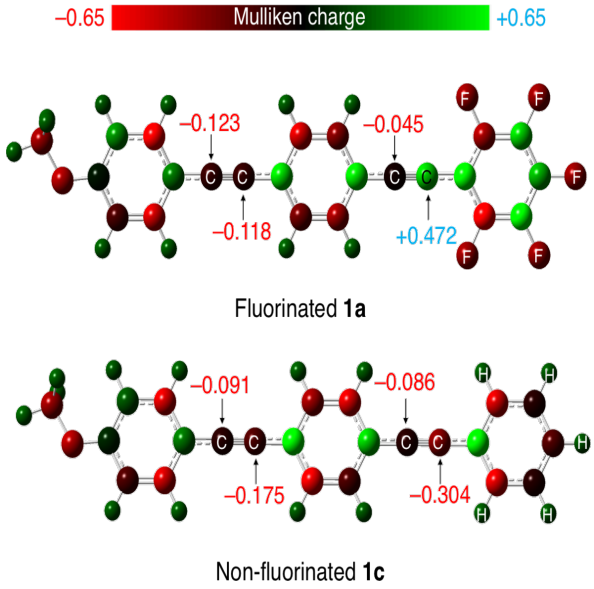

Figure 3: Mulliken charge distributions of fluorinated **1a** and nonfluorinated **1c** obtained from density functional theory calculations [CAM-B3LYP/6-31+G(d) level].

rinated aromatic ring retards the Pd(II)-catalyzed oxidation of the adjacent C≡C bond, thereby allowing the isolation of the half-oxidized benzil derivative **2a**. On the basis of this theoretical investigation, the unique reactivities of bistolanes with fluorinated and nonfluorinated aromatic rings toward oxidation by DMSO can be rationalized.

Photophysical behavior

Our interest was then directed toward the photophysical properties of benzil and bisbenzil derivatives, which were freshly purified by column chromatography (eluent: hexane/EtOAc = 5:1 for benzil and 10:1 for bisbenzil) and subsequently recrystallized from hexane. The sample solution concentrations in toluene were 1.0×10^{-5} and 1.0×10^{-3} M for the absorption and photoluminescence (PL) measurements, respectively, and the absorption and PL spectra are shown in Figure 4. The photophysical data obtained from these measurements are summarized in Table 1.

The methoxy-substituted fluorinated benzil **2a** in toluene absorbs UV light at 315 and 295 nm with molar extinction coefficients (ε) of 36500 and 28700 $M^{-1}\cdot cm^{-1}$, respectively (Figure 4A). Similarly, the toluene solution of the fluorinated benzil with a hexyloxy chain (**2b**) absorbs UV light at 314 (ε: 30400 $M^{-1}\cdot cm^{-1}$) and 293 nm (ε: 40500 $M^{-1}\cdot cm^{-1}$) (Figure 4B). Both **2a** and **2b** exhibit weak absorption at around 400 nm (ε: ≈170 $M^{-1}\cdot cm^{-1}$). As shown in Figure 4C–E, on the other hand, the bisbenzil derivatives **3a**–**c** show an absorption band at 290 nm (ε: 29600–51200 $M^{-1}\cdot cm^{-1}$) as the major signal, together with a quite weak absorption band at

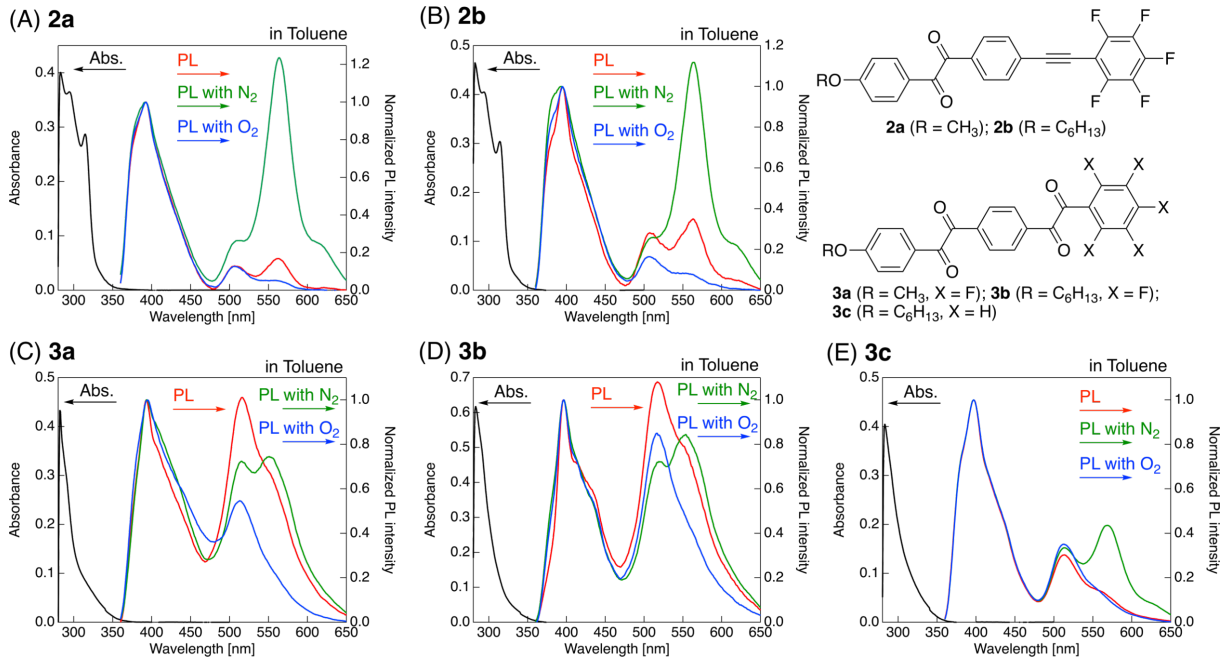

Figure 4: Absorption and photoluminescence (PL) spectra of (A) **2a**, (B) **2b**, (C) **3a**, (D) **3b**, and (E) **3c** in toluene solution. Concentrations: 1.0×10^{-5} and 1.0×10^{-3} M for absorbance and PL measurements, respectively. Color legend: black: absorption, red: PL as prepared, green: PL under N_2 atmosphere, and blue: PL under O_2 atmosphere.

Table 1: Photophysical data from ultraviolet (UV)-visible absorption and steady-state photoluminescence (PL) measurements[a].

	λ_{abs} [nm] (ε [M^{-1} cm^{-1}])	λ_{PL} [nm][b] (Φ_{PL})[c]	I_{560}/I_{395}		
			pristine	N_2	O_2
2a	295 (28700), 315 (36500), 407 (160)	395, 406 sh[d], 507, 563 (0.018)	0.17	1.24	0.05
2b	293 (40500), 314 (30400), 407 (180)	395, 406 sh, 507, 563 (0.015)	0.35	1.12	0.08
3a	290 (30500), 405 (180)	393, 406 sh, 516, 551 (<0.01)	0.61	0.74	0.19
3b	290 (51200), 405 (212)	396, 412, 517, 554 (<0.01)	0.79	0.84	0.50
3c	290 (29600), 402 (260)	397, 412, 514, 569 (<0.01)	0.14	0.44	0.14

[a]Toluene solution (concentrations: 1.0×10^{-5} and 1.0×10^{-3} M for UV-visible absorption and PL measurements, respectively); [b]Excitation wavelength: 350 nm; [c]Quantum yield measured using a calibrating sphere. Excitation wavelength: 290 nm. [d]Shoulder peak.

402–405 nm (ε: 180–260 $M^{-1}{\cdot}cm^{-1}$). To gain more information about the slight difference between the absorption behaviors of the benzil and bisbenzil derivatives, DFT and time-dependent DFT (TD-DFT) calculations at the CAM-B3LYP/6-31+G(d) level of theory were performed for fluorinated benzil **2a** and bisbenzil derivative **3a** as representative examples. Figure 5 shows the distributions of molecular orbitals involved in vertical electronic transitions in **2a** and **3a**.

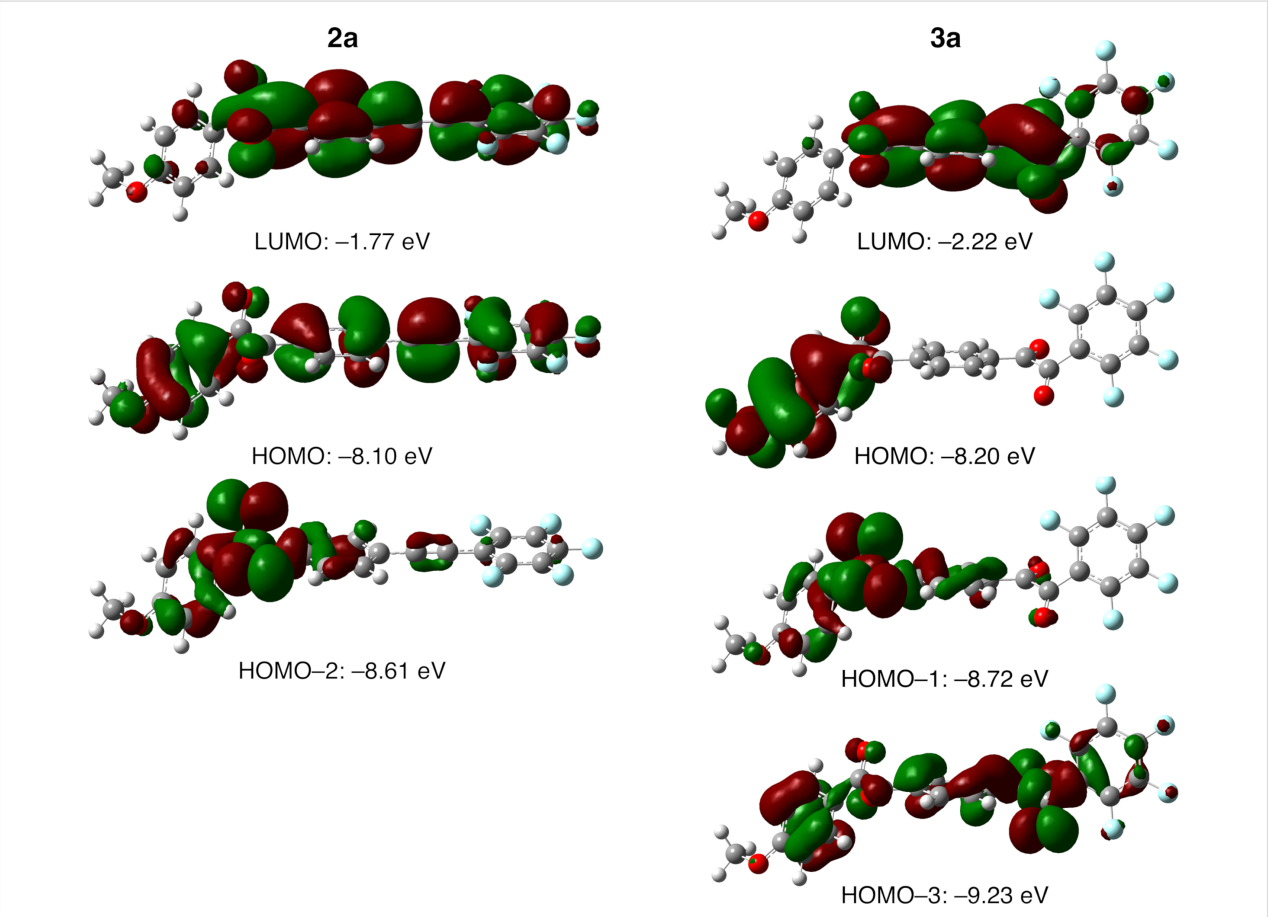

Figure 5: Distributions of molecular orbitals (isosurface value: 0.04 a.u.) involved in vertical electronic transitions in **2a** and **3a** calculated using density functional theory (DFT) and time-dependent DFT at the CAM-B3LYP/6-31+G(d) level (HOMO: highest occupied molecular orbital, LUMO: lowest unoccupied molecular orbital).

The main electronic transition with a relatively large oscillator strength (*f*) in both **2a** and **3a** is the highest occupied molecular orbital (HOMO)→lowest unoccupied molecular orbital (LUMO) transition. Focusing on the orbital distribution, the HOMO lobe of **2a** covers the entire molecule, while the LUMO lobe is localized at the tolane moiety. In the case of **3a**, the HOMO lobe is localized at the methoxy-substituted benzene ring, while the LUMO lobe is localized at the central benzene ring. Accordingly, it can be concluded that the absorption bands at the short-wavelength region (around 290–315 nm) stems from the π–π* transition. The TD-DFT calculation also reveals that n–π* transitions (e.g., HOMO–2→LUMO for **2a** and HOMO–3→LUMO for **3a**) have small values of *f*; thus, the small absorption band at around 400 nm can be safely attributed to an n–π* transition.

Upon irradiation of the toluene solutions of benzil derivatives **2a** and **2b** with a 350 nm UV light, three PL bands at 395, 507, and 563 nm, along with a shoulder signal at around 406 nm, are observed (Figure 4A and 4B). The bisbenzil derivatives, i.e., **3a**–**c**, also show similar PL behavior to the aforementioned benzil analogues: four PL bands with λ_{PL} of 393–397, 406–412, 514–517, and 551–569 nm are observed. To gain more information about the PL process in benzils and bisbenzils, the PL spectra of the toluene solutions (1.0×10^{-3} M) were acquired after bubbling with N_2 or O_2 gas for 30 min. In general, an O_2-saturated environment strongly deactivates the triplet states; thus, PL emission stems only from fluorescence. On the other hand, elimination of O_2 gas from a solution by bubbling with an inert gas (N_2 or Ar) allows the triplet states to survive for a long lifetime, which possibly leads to a phosphorescence emission. Hence, the elimination of O_2 gas from solutions by N_2 gas bubbling (or addition of O_2 gas in solutions) can judge the presence of phosphorescence, as well as the assignment of PL bands. The obtained PL spectra are superimposed on the PL spectra of a pristine sample (Figure 4). Upon bubbling the solution with N_2 gas for 30 min, a dramatic enhancement of the PL intensities of benzils **2a** and **2b** at λ_{PL} = 563 nm is observed. The PL intensities of bisbenzils **3a**–**c** at the long-wavelength region between 551 and 569 nm also increase, although the increment rates are not as high as those of **2a** and **2b**. On the contrary, bubbling the toluene solutions of benzil or bisbenzil derivatives with O_2 gas causes the intensity of the long-wavelength PL band to decrease compared with that of the pristine solution, while the other remaining PL bands in the short-wavelength region do not change. Judging from the PL behavior under N_2 or O_2 flow conditions, the PL bands at the short-wavelength region around 395 nm and long-wavelength region around 560 nm can be safely considered fluorescence via radiative deactivation from the S_1 excited state to the S_0 state and phosphorescence via electronic transition from the T_1 excited state to the S_0 state, respectively. Accordingly, fluorinated benzils and bisbenzils show room-temperature phosphorescence in the solution state.

To understand the effects of structural modification (i.e., the benzil structure with a tolane vs bisbenzil moiety) and incorporation of fluorine atoms on the phosphorescence, the ratio between the peak intensities at ≈395 and ≈560 nm (I_{560}/I_{395}) was quantitatively calculated, and the results are summarized in Table 1. The I_{560}/I_{395} values of benzils **2a** and **2b** under N_2 flow conditions increase up to sevenfold compared with those of the corresponding pristine solutions. On the other hand, the increase in the I_{560}/I_{395} values of fluorinated bisbenzil derivatives **3a** and **3b** is low (only 1.1 times) under N_2 flow conditions, although the PL intensity of nonfluorinated **3c** increases by approximately three times. Judging from these comprehensive observations, the benzil structure promotes ISC from S_1 to T_1, causing increment phosphorescence, unlike the corresponding bisbenzil scaffold. Moreover, fluorine substituents on the bisbenzil molecules cause significant retardation of ISC, leading to a weaker phosphorescence intensity.

Additionally, the quantum yields (Φ_{PL}) of the PL bands in the range of 350–600 nm were acquired using an absolute quantum yield measurement system with a calibrated integrating sphere. All samples have a low Φ_{PL} of less than 0.02 (Table 1), meaning that most of the excited states of all samples deactivate nonradiatively. At the moment, we cannot certify the origin of the low Φ_{PL} in terms of the molecular properties, for instance, the main pathway of nonradiative deactivation. Experiments are currently being conducted to better understand the photophysical mechanisms of the excited-state dynamics of these benzil and bisbenzil derivatives.

Conclusion

In this article, we described the design and synthesis of benzil- or bisbenzil-based room-temperature phosphorescent molecules via a simple oxidation protocol for fluorescent bistolane derivatives. Nonfluorinated bistolane derivatives exclusively gave the corresponding products with a bisbenzil scaffold, whereas the fluorinated bistolane derivatives generated not only mono-oxidized benzil derivatives bearing a fluorinated tolane scaffold, but also the corresponding bis-oxidized bisbenzil derivatives. Based on theoretical calculations, the selective formation of the fluorinated analogues stemmed from the slight modulation of the charge distribution at the alkyne moiety of the reactant induced by the electron-withdrawing fluorine atoms. Evaluation of the photophysical behavior of the benzils and bisbenzils through several PL measurements under N_2 and O_2 flow conditions probed the successful room-temperature phosphorescence of the compounds in toluene solution. A fuller

understanding of the excited-state dynamics of these benzil and bisbenzil derivatives will assist the development of environmentally benign, pure organic phosphorescent materials.

Supporting Information

Experimental procedures for the synthesis and characterization of fluorinated benzils **2a** and **2b**, fluorinated bisbenzils **3a** and **3b**, and nonfluorinated bisbenzil **3c**. ^{1}H, ^{13}C, and ^{19}F NMR spectra of **2a**, **2b**, and **3a**–**c**. Cartesian coordinates of the optimized geometries of **1a**, **1c**, **2a**, and **3a** obtained from DFT calculations.

Supporting Information File 1

Experimental preocedures, NMR spectra and Cartesian coordinates.
[https://www.beilstein-journals.org/bjoc/content/supplementary/1860-5397-16-102-S1.pdf]

Funding

The following sources of funding are acknowledged: Japan Society for the Promotion of Science (JSPS) KAKENHI Grant-in-Aid for Scientific Research (C) (Grant No. JP18K05262) and the AIST Nanocharacterization Facility (ANCF) platform as part of a program of the “Nanotechnology Platform” of the Ministry of Education, Culture, Sports, Science and Technology (MEXT), Japan.

ORCID® iDs

Shigeyuki Yamada - https://orcid.org/0000-0002-6379-0447
Takuya Hosokai - https://orcid.org/0000-0001-9164-4159
Kaveenga Rasika Koswattage - https://orcid.org/0000-0001-7183-406X

Preprint

A non-peer-reviewed version of this article has been previously published as a preprint doi:10.3762/bxiv.2020.31.v1

References

1. Singh, H.; Tiwari, K.; Tiwari, R.; Pramanik, S. K.; Das, A. *Chem. Rev.* **2019,** *119,* 11718–11760. doi:10.1021/acs.chemrev.9b00379
2. Mei, J.; Huang, Y.; Tian, H. *ACS Appl. Mater. Interfaces* **2018,** *10,* 12217–12261. doi:10.1021/acsami.7b14343
3. Chen, X.; Wang, F.; Hyun, J. Y.; Wei, T.; Qiang, J.; Ren, X.; Shin, I.; Yoon, J. *Chem. Soc. Rev.* **2016,** *45,* 2976–3016. doi:10.1039/c6cs00192k
4. Ma, Y.; Zhang, Y.; Yu, W. W. *J. Mater. Chem. C* **2019,** *7,* 13662–13679. doi:10.1039/c9tc04065j
5. Yersin, H., Ed. *Highly Efficient OLEDs: Materials Based on Thermally Activated Delayed Fluorescence;* Wiley-VCH: Weinheim, Germany, 2018. doi:10.1002/9783527691722
6. Gaspar, D. J.; Polikarpov, E., Eds. *OLED Fundamentals: Materials, Devices, and Processing of Organic Light-Emitting Diodes;* CRC Press: Boca Raton, FL, USA, 2015. doi:10.1201/b18485
7. Su, L.; Fan, X.; Yin, T.; Wang, H.; Li, Y.; Liu, F.; Li, J.; Zhang, H.; Xie, H. *Adv. Opt. Mater.* **2020,** *8,* 1900978. doi:10.1002/adom.201900978
8. Ostroverkhova, O. *Chem. Rev.* **2016,** *116,* 13279–13412. doi:10.1021/acs.chemrev.6b00127
9. Ronda, C. R. Emission and Excitation Mechanisms of Phosphors. In *Luminescence: From Theory to Applications;* Ronda, C. R., Ed.; Wiley-VCH: Weinheim, Germany, 2007; pp 1–34. doi:10.1002/9783527621064.ch1
10. Yersin, H.; Rausch, A. F.; Czerwieniec, R. Organometallic Emitters for OLEDs: Triplet Harvesting, Singlet Harvesting, Case Structures, and Trends. In *Physics of Organic Semiconductors;* Brütting, W.; Adachi, C., Eds.; Wiley-VCH: Weinheim, Germany, 2012; pp 371–424. doi:10.1002/9783527654949.ch13
11. Wang, W.; Zhang, Y.; Jin, W. J. *Coord. Chem. Rev.* **2020,** *404,* 213107. doi:10.1016/j.ccr.2019.213107
12. Zhan, G.; Liu, Z.; Bian, Z.; Huang, C. *Front. Chem. (Lausanne, Switz.)* **2019,** *7,* 305. doi:10.3389/fchem.2019.00305
13. Qu, G.; Zhang, Y.; Ma, X. *Chin. Chem. Lett.* **2019,** *30,* 1809–1814. doi:10.1016/j.cclet.2019.07.042
14. Crosby, G. A. *Acc. Chem. Res.* **1975,** *8,* 231–238. doi:10.1021/ar50091a003
15. Baldo, M. A.; Lamansky, S.; Burrows, P. E.; Thompson, M. E.; Forrest, S. R. *Appl. Phys. Lett.* **1999,** *75,* 4–6. doi:10.1063/1.124258
16. Adachi, C.; Baldo, M. A.; Forrest, S. R.; Thompson, M. E. *Appl. Phys. Lett.* **2000,** *77,* 904–906. doi:10.1063/1.1306639
17. Baldo, M. A.; O'Brien, D. F.; You, Y.; Shoustikov, A.; Sibley, S.; Thompson, M. E.; Forrest, S. R. *Nature* **1998,** *395,* 151–154. doi:10.1038/25954
18. Yam, V. W.-W.; Wong, K. M.-C.; Hung, L.-L.; Zhu, N. *Angew. Chem., Int. Ed.* **2005,** *44,* 3107–3110. doi:10.1002/anie.200500253
19. Yamada, S.; Yamaguchi, S.; Tsutsumi, O. *J. Mater. Chem. C* **2017,** *5,* 7977–7984. doi:10.1039/c7tc00728k
20. Fujisawa, K.; Kawakami, N.; Onishi, Y.; Izumi, Y.; Tamai, S.; Sugimoto, N.; Tsutsumi, O. *J. Mater. Chem. C* **2013,** *1,* 5359–5366. doi:10.1039/c3tc31105h
21. Seki, T.; Takamatsu, Y.; Ito, H. *J. Am. Chem. Soc.* **2016,** *138,* 6252–6260. doi:10.1021/jacs.6b02409
22. Kenry; Chen, C.; Liu, B. *Nat. Commun.* **2019,** *10,* 2111. doi:10.1038/s41467-019-10033-2
23. Yuan, W. Z.; Shen, X. Y.; Zhao, H.; Lam, J. W. Y.; Tang, L.; Lu, P.; Wang, C.; Liu, Y.; Wang, Z.; Zheng, Q.; Sun, J. Z.; Ma, Y.; Tang, B. Z. *J. Phys. Chem. C* **2010,** *114,* 6090–6099. doi:10.1021/jp909388y
24. Bolton, O.; Lee, K.; Kim, H.-J.; Lin, K. Y.; Kim, J. *Nat. Chem.* **2011,** *3,* 205–210. doi:10.1038/nchem.984
25. Zhao, W.; He, Z.; Lam, J. W. Y.; Peng, Q.; Ma, H.; Shuai, Z.; Bai, G.; Hao, J.; Tang, B. Z. *Chem* **2016,** *1,* 592–602. doi:10.1016/j.chempr.2016.08.010
26. Lower, S. K.; El-Sayed, M. A. *Chem. Rev.* **1966,** *66,* 199–241. doi:10.1021/cr60240a004
27. Morita, M.; Yamada, S.; Agou, T.; Kubota, T.; Konno, T. *Appl. Sci.* **2019,** *9,* 1905. doi:10.3390/app9091905
28. Yamada, S.; Miyano, K.; Agou, T.; Kubota, T.; Konno, T. *Crystals* **2019,** *9,* 195. doi:10.3390/cryst9040195
29. Yamada, S.; Tanaka, T.; Ichikawa, T.; Konno, T. *ACS Omega* **2019,** *4,* 3922–3932. doi:10.1021/acsomega.8b03543

30. Yamada, S.; Morita, M.; Agou, T.; Kubota, T.; Ichikawa, T.; Konno, T. *Org. Biomol. Chem.* **2018,** *16,* 5609–5617. doi:10.1039/c8ob01497c
31. Yamada, S.; Miyano, K.; Konno, T.; Agou, T.; Kubota, T.; Hosokai, T. *Org. Biomol. Chem.* **2017,** *15,* 5949–5958. doi:10.1039/c7ob01369h
32. Gong, Y. Y.; Tan, Y. Q.; Li, H.; Zhang, Y. R.; Yuan, W. Z.; Zhang, Y. M.; Sun, J. Z.; Tang, B. Z. *Sci. China: Chem.* **2013,** *56,* 1183–1186. doi:10.1007/s11426-013-4930-9
33. Muzart, J. *J. Mol. Catal. A: Chem.* **2011,** *338,* 7–17. doi:10.1016/j.molcata.2011.01.030
34. Chi, K.-W.; Yusubov, M. S.; Filimonov, V. D. *Synth. Commun.* **1994,** *24,* 2119–2122. doi:10.1080/00397919408010224
35. *Gaussian 16,* Revision B.01; Gaussian, Inc.: Wallingford, CT, USA, 2016.

License and Terms

This is an Open Access article under the terms of the Creative Commons Attribution License (http://creativecommons.org/licenses/by/4.0). Please note that the reuse, redistribution and reproduction in particular requires that the authors and source are credited.

The license is subject to the *Beilstein Journal of Organic Chemistry* terms and conditions: (https://www.beilstein-journals.org/bjoc)

The definitive version of this article is the electronic one which can be found at: doi:10.3762/bjoc.16.102

BEILSTEIN JOURNAL OF ORGANIC CHEMISTRY

Photoredox-catalyzed silyldifluoromethylation of silyl enol ethers

Vyacheslav I. Supranovich, Vitalij V. Levin and Alexander D. Dilman*

Letter

Open Access

Address:
N. D. Zelinsky Institute of Organic Chemistry, Leninsky prosp. 47, 119991 Moscow, Russian Federation

Email:
Alexander D. Dilman* - adil25@mail.ru

* Corresponding author

Keywords:
difluoroalkylation; organofluorine compounds; photocatalysis; radical addition; silicon reagents

Beilstein J. Org. Chem. **2020,** *16,* 1550–1553.
doi:10.3762/bjoc.16.126

Received: 15 April 2020
Accepted: 15 June 2020
Published: 29 June 2020

This article is part of the thematic issue "Organo-fluorine chemistry V".

Guest Editor: D. O'Hagan

© 2020 Supranovich et al.; licensee Beilstein-Institut.
License and terms: see end of document.

Abstract

A method for the light-mediated fluoroalkylation of silyl enol ethers with (bromodifluoromethyl)trimethylsilane followed by a reduction of the primary products with sodium borohydride is described. An 18 W, 375 nm LED was used as the light source. The reaction is performed in the presence of a gold photocatalyst, which effects the generation of a (trimethylsilyl)difluoromethyl radical via cleavage of the carbon–bromine bond.

Findings

Fluorinated silicon reagents have found widespread use for the introduction of fluorinated fragments [1-5]. Typically, these reagents work under strongly basic conditions required to activate inert C–Si bonds with the generation of carbanionic species. On the other hand, radical reactions offer different synthetic opportunities originating from the neutral character of the intermediates [6,7] and, accordingly, radical fluoroalkylation processes have been extensively investigated over the last decade [8-13].

Recently, (bromodifluoromethyl)trimethylsilane (**1**) which can be readily obtained from the Ruppert–Prakash reagent [14,15], has been introduced as a reagent for the synthesis of various difluorinated compounds [16-18]. This silane is very sensitive to Lewis bases and accordingly it was used as a precursor of difluorocarbene, which can react with enol ethers [19,20] (Scheme 1). We showed that this silane could be involved in the radical chain hydrofluoroalkylation of electron-deficient alkenes, using a boron hydride as a source of hydrogen [21]. We thought that silane **1** could couple with silyl enol ethers in the presence of a photocatalyst affording fluoroalkylation products. Indeed, silyl enol ethers were found to be good acceptors of fluorinated radicals, and the resultant silyloxy-substituted radicals underwent single-electron oxidation thereby supporting a photoredox cycle [22-24].

The silyl enol ether **2a** derived from acetophenone was selected as a model substrate and the reaction with silane **1** (1.5 equiv)

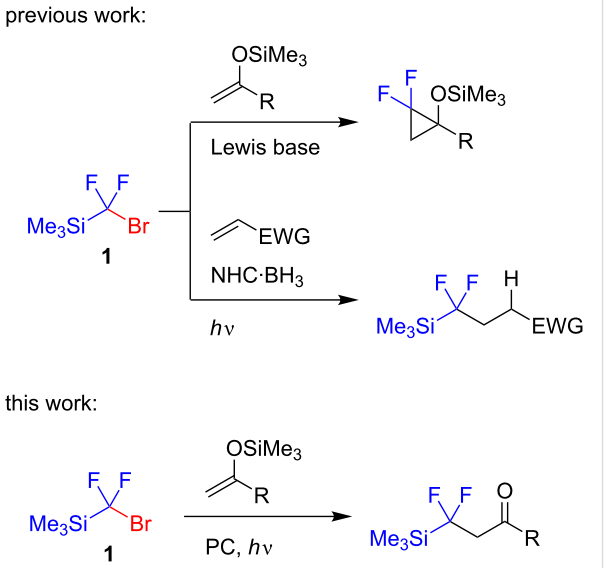

Scheme 1: Reactions of (bromodifluoromethyl)trimethylsilane (**1**).

was evaluated (Scheme 2). The reactions were performed in dichloromethane, and reaction mixtures were analyzed by ^{19}F NMR spectroscopy. A series of typical photocatalysts (for example, iridium catalysts) were ineffective in promoting the reaction. Rewardingly, a gold catalyst, [AuCl(μ-dppm)]$_2$ [25-27], provided reasonable yields of **3a** after one day of irradiation along with a full conversion of the starting enol ether. Moreover, a further increase in reaction time was accompanied by a decrease in the product yield. Finally, GC monitoring suggested complete consumption of the silyl enol ether within 6 hours. It should also be pointed out that the addition of basic additives, which are frequently employed in photoredox reactions to scavenge acidic byproducts [28,29], could not be employed. Silane **1** is easily destroyed by bases (even by the amide group [30]) followed by the rapid addition of difluorocarbene to silyl enol ethers [19,20]. Disappointingly, we were unable to isolate ketone **3a** using flash column chromatography on silica gel, presumably, owing to facile β-elimination of hydrogen fluoride. To isolate a stable product, the reaction mixture was treated with sodium borohydride in ethanol, which effected the reduction of the keto group affording the corresponding alcohol **4a** in 52% yield.

Under the optimized conditions, a series of silyl enol ethers **2** were reacted with silane **1** (Figure 1). The reaction worked well with enol ethers derived from aromatic ketones, while those obtained from aliphatic ketones were ineffective. This may be ascribed to the decreased radical-stabilizing effect of the alkyl group compared to that of an aryl group, which either makes radical addition reversible or attenuates the reactivity of the starting enol ether. Similarly, an aromatic substrate bearing an *ortho* substituent gave lower yields, which may be associated with the ability of the *ortho* group to disfavor the planar conformation needed to stabilize an intermediate benzyl radical. The complete conversions of the enol ethers were usually achieved within 6 hours, though to obtain products **4f**,**k** a longer time of 24 h was needed. Generally, higher yields were observed with substrates containing electron-donating functional groups. Substrates containing pyridine, furan, and thiophene as heterocyclic fragments were also successfully converted into the corresponding alcohols **4**. However, in the reaction of the enol ether derived from 2-acetyl-*N*-methylpyrrole, ketone **3p** did not undergo reduction with sodium borohydride, and the decreased reactivity of this ketone allowed its isolation.

A proposed mechanism for the photoredox fluoroalkylation reaction is shown in Scheme 3. The photoexcited catalyst converts silane **1** into difluoromethylsilyl-based radical. The efficiency of [AuCl(μ-dppm)]$_2$ compared to other strongly reducing catalysts may be associated with the ability of gold to interact with the bromine atom of silane **1** followed by inner-sphere electron transfer [27]. The radical then attacks silyl enol ether **2**, and the subsequent silyloxy-substituted radical is oxidized by the photocatalyst to generate the product with concomitant production of TMSBr.

Conclusion

In summary, a method for the introduction of the silyldifluoromethyl group was described by the coupling of a readily available silicon reagent with silyl enol ethers. The reaction is

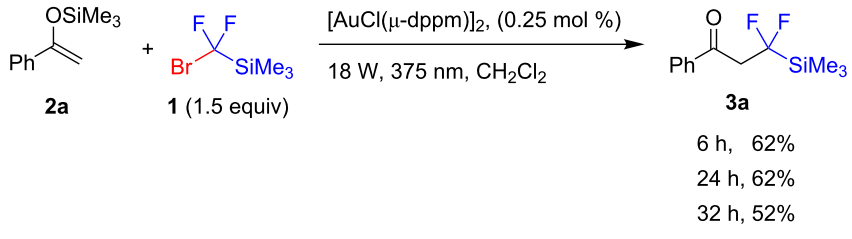

Scheme 2: Optimization studies. Yield determined by ^{19}F NMR spectroscopy using an internal standard.

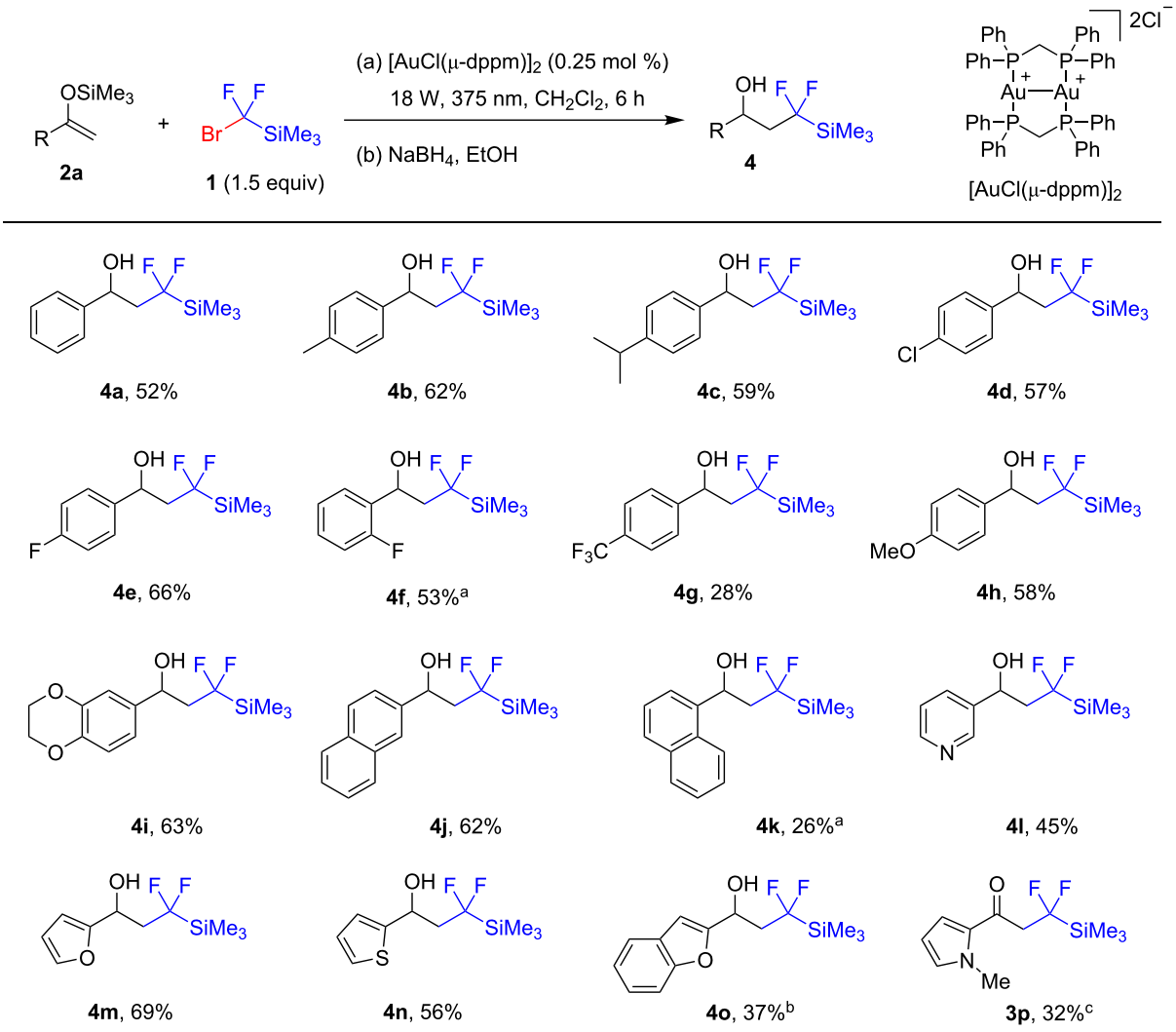

Figure 1: Reaction of silyl enol ethers. Yields refer to isolated yields. [a]Reaction time 24 h; [b]1.0 equiv of silane **1** was used; [c]ketone was isolated.

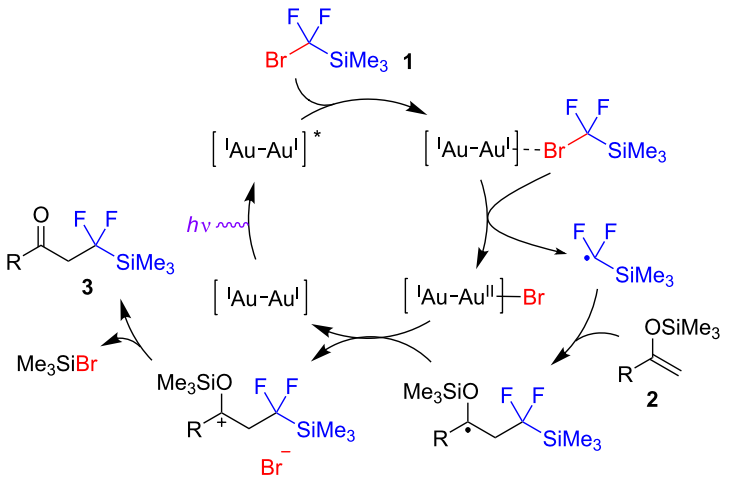

Scheme 3: Proposed mechanism of the fluoroalkylation reaction.

promoted by light and involves the generation of a fluorinated carbon-based radical via cleavage of the carbon–bromine bond by a gold photocatalyst.

Supporting Information

Supporting Information File 1

Full experimental details, compound characterization, and copies of NMR spectra.
[https://www.beilstein-journals.org/bjoc/content/supplementary/1860-5397-16-126-S1.pdf]

ORCID® iDs

Vitalij V. Levin - https://orcid.org/0000-0002-5606-8085
Alexander D. Dilman - https://orcid.org/0000-0001-8048-7223

References

1. Prakash, G. K. S.; Yudin, A. K. *Chem. Rev.* **1997,** *97,* 757–786. doi:10.1021/cr9408991
2. Liu, X.; Xu, C.; Wang, M.; Liu, Q. *Chem. Rev.* **2015,** *115,* 683–730. doi:10.1021/cr400473a
3. Krishnamoorthy, S.; Prakash, G. K. S. *Synthesis* **2017,** *49,* 3394–3406. doi:10.1055/s-0036-1588489
4. Uneyama, K. *J. Fluorine Chem.* **2008,** *129,* 550–576. doi:10.1016/j.jfluchem.2008.05.012
5. Dilman, A. D.; Levin, V. V. *Mendeleev Commun.* **2015,** *25,* 239–244. doi:10.1016/j.mencom.2015.07.001
6. Yan, M.; Lo, J. C.; Edwards, J. T.; Baran, P. S. *J. Am. Chem. Soc.* **2016,** *138,* 12692–12714. doi:10.1021/jacs.6b08856
7. Zard, S. Z. *Org. Lett.* **2017,** *19,* 1257–1269. doi:10.1021/acs.orglett.7b00531
8. Studer, A. *Angew. Chem., Int. Ed.* **2012,** *51,* 8950–8958. doi:10.1002/anie.201202624
9. Barata-Vallejo, S.; Cooke, M. V.; Postigo, A. *ACS Catal.* **2018,** *8,* 7287–7307. doi:10.1021/acscatal.8b02066
10. Koike, T.; Akita, M. *Acc. Chem. Res.* **2016,** *49,* 1937–1945. doi:10.1021/acs.accounts.6b00268
11. Koike, T.; Akita, M. *Org. Biomol. Chem.* **2019,** *17,* 5413–5419. doi:10.1039/c9ob00734b
12. Lemos, A.; Lemaire, C.; Luxen, A. *Adv. Synth. Catal.* **2019,** *361,* 1500–1537. doi:10.1002/adsc.201801121
13. Dagousset, G.; Carboni, A.; Masson, G.; Magnier, E. Visible Light–Induced (Per)fluoroalkylation by Photoredox Catalysis. In *Modern Synthesis Processes and Reactivity of Fluorinated Compounds;* Groult, H.; Leroux, F. R.; Tressaud, A., Eds.; Elsevier, 2017; pp 389–426. doi:10.1016/b978-0-12-803740-9.00014-7
14. Kosobokov, M. D.; Dilman, A. D.; Levin, V. V.; Struchkova, M. I. *J. Org. Chem.* **2012,** *77,* 5850–5855. doi:10.1021/jo301094b
15. Li, L.; Wang, F.; Ni, C.; Hu, J. *Angew. Chem., Int. Ed.* **2013,** *52,* 12390–12394. doi:10.1002/anie.201306703
16. Xie, Q.; Ni, C.; Zhang, R.; Li, L.; Rong, J.; Hu, J. *Angew. Chem., Int. Ed.* **2017,** *56,* 3206–3210. doi:10.1002/anie.201611823
17. Xie, Q.; Zhu, Z.; Li, L.; Ni, C.; Hu, J. *Angew. Chem., Int. Ed.* **2019,** *58,* 6405–6410. doi:10.1002/anie.201900763
18. Dilman, A. D.; Levin, V. V. *Acc. Chem. Res.* **2018,** *51,* 1272–1280. doi:10.1021/acs.accounts.8b00079
19. Kosobokov, M. D.; Levin, V. V.; Struchkova, M. I.; Dilman, A. D. *Org. Lett.* **2015,** *17,* 760–763. doi:10.1021/acs.orglett.5b00097
20. Fedorov, O. V.; Kosobokov, M. D.; Levin, V. V.; Struchkova, M. I.; Dilman, A. D. *J. Org. Chem.* **2015,** *80,* 5870–5876. doi:10.1021/acs.joc.5b00904
21. Supranovich, V. I.; Levin, V. V.; Struchkova, M. I.; Korlyukov, A. A.; Dilman, A. D. *Org. Lett.* **2017,** *19,* 3215–3218. doi:10.1021/acs.orglett.7b01334
22. Pham, P. V.; Nagib, D. A.; MacMillan, D. W. C. *Angew. Chem., Int. Ed.* **2011,** *50,* 6119–6122. doi:10.1002/anie.201101861
23. Panferova, L. I.; Tsymbal, A. V.; Levin, V. V.; Struchkova, M. I.; Dilman, A. D. *Org. Lett.* **2016,** *18,* 996–999. doi:10.1021/acs.orglett.6b00117
24. Chernov, G. N.; Levin, V. V.; Kokorekin, V. A.; Struchkova, M. I.; Dilman, A. D. *Adv. Synth. Catal.* **2017,** *359,* 3063–3067. doi:10.1002/adsc.201700423
25. Zidan, M.; Rohe, S.; McCallum, T.; Barriault, L. *Catal. Sci. Technol.* **2018,** *8,* 6019–6028. doi:10.1039/c8cy01765d
26. Revol, G.; McCallum, T.; Morin, M.; Gagosz, F.; Barriault, L. *Angew. Chem., Int. Ed.* **2013,** *52,* 13342–13345. doi:10.1002/anie.201306727
27. Li, D.; Che, C.-M.; Kwong, H.-L.; Yam, V. W.-W. *J. Chem. Soc., Dalton Trans.* **1992,** 3325–3329. doi:10.1039/dt9920003325
28. Prier, C. K.; Rankic, D. A.; MacMillan, D. W. C. *Chem. Rev.* **2013,** *113,* 5322–5363. doi:10.1021/cr300503r
29. Shaw, M. H.; Twilton, J.; MacMillan, D. W. C. *J. Org. Chem.* **2016,** *81,* 6898–6926. doi:10.1021/acs.joc.6b01449
30. Tsymbal, A. V.; Kosobokov, M. D.; Levin, V. V.; Struchkova, M. I.; Dilman, A. D. *J. Org. Chem.* **2014,** *79,* 7831–7835. doi:10.1021/jo501644m

License and Terms

This is an Open Access article under the terms of the Creative Commons Attribution License (http://creativecommons.org/licenses/by/4.0). Please note that the reuse, redistribution and reproduction in particular requires that the authors and source are credited.

The license is subject to the *Beilstein Journal of Organic Chemistry* terms and conditions: (https://www.beilstein-journals.org/bjoc)

The definitive version of this article is the electronic one which can be found at:
doi:10.3762/bjoc.16.126

BEILSTEIN JOURNAL OF ORGANIC CHEMISTRY

NHC-catalyzed enantioselective synthesis of β-trifluoromethyl-β-hydroxyamides

Alyn T. Davies, Mark D. Greenhalgh, Alexandra M. Z. Slawin and Andrew D. Smith*

Letter

Open Access

Address:
EaStCHEM, School of Chemistry, University of St Andrews, North Haugh, St Andrews, Fife KY16 9ST, United Kingdom

Email:
Andrew D. Smith* - ads10@st-andrews.ac.uk

* Corresponding author

Keywords:
enantioselective catalysis; formal [2 + 2] cycloaddition; N-heterocyclic carbene; ring opening; trifluoromethyl group

Beilstein J. Org. Chem. **2020,** *16,* 1572–1578.
doi:10.3762/bjoc.16.129

Received: 09 March 2020
Accepted: 05 June 2020
Published: 30 June 2020

This article is part of the thematic issue "Organo-fluorine chemistry V".

Guest Editor: D. O'Hagan

© 2020 Davies et al.; licensee Beilstein-Institut.
License and terms: see end of document.

Abstract

The N-heterocyclic carbene (NHC)-catalyzed formal [2 + 2] cycloaddition between α-aroyloxyaldehydes and trifluoroacetophenones, followed by ring opening with an amine or a reducing agent is described. The resulting β-trifluoromethyl-β-hydroxyamide and alcohol products are produced with reasonable diastereocontrol (typically ≈70:30 dr) and excellent enantioselectivity, and they can be isolated in moderate to good yield as a single diastereoisomer.

Introduction

The trifluoromethyl unit holds a prominent and privileged position within organic chemistry [1-6]. The incorporation of this motif is widely employed within the pharmaceutical, agrochemical, and materials industries as it can be used strategically to increase lipophilicity as well as to enhance metabolic stability and binding selectivity [7-9]. In this context, the generation of effective and practical methodologies capable of the enantioselective incorporation of the trifluoromethyl unit into organic molecules has been developed widely [10-12], with a series of elegant organocatalytic strategies utilized toward these aims [13]. One general strategy for the organocatalytic construction of stereogenic trifluoromethyl centers is through enantioselective addition of enolates or their equivalents to prochiral trifluoromethyl ketones (Figure 1A). Within this area, a common catalytic approach has utilized aliphatic ketones as enolate equivalents using prolinamide, cinchona, or hybrid catalysts that proceed via enamine intermediates (Figure 1B) [14-19]. The state of the art within this area has been recently demonstrated by Dixon and co-workers, who showed that bifunctional BIMP catalysts could promote the enantioselective addition of typically recalcitrant aryl ketones to trifluoromethyl ketones (Figure 1C) [20].

Over the last twenty years, NHCs have been widely exploited as highly efficient organocatalysts that have found use in numerous applications and were the subject of many extensive

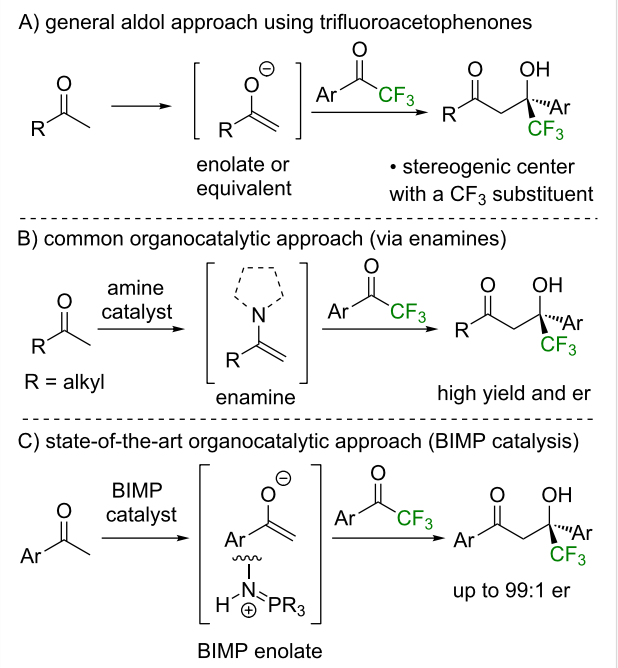

Figure 1: Organocatalytic enantioselective aldol approaches using trifluoroacetophenone derivatives.

reviews [21-26]. Among the most common reactive intermediates generated using NHCs, the azolium enolate has been widely used [27,28]. Methods to generate azolium enolates from a number of precursors have been reported, including the use of ketenes [29,30], α-functionalized aldehydes [31-35], enals [36-38], aryl esters [39-42], or aldehydes [43-45] in the presence of an oxidant. As representative examples of the use of azolium enolates in reactions with trifluoroacetophenone derivatives, Ye and co-workers have shown that using disubstituted ketenes as azolium enolate precursors and NHC precatalyst **1** allowed access to trifluoromethyl-substituted β-lactone products in a high yield, diastereo-, and enantioselectivity (Figure 2A) [46]. Chi and co-workers have reported limited examples of oxidative [2 + 2] cycloadditions using hydrocinnamaldehyde as an azolium enolate precursor and the NHC precatalyst **2**, giving β-lactone products in high enantioselectivity but requiring superstoichiometric quantities of quinone as an oxidant (Figure 2B) [47]. In our previous work, we have developed α-aroyloxyaldehydes as reactive, bench-stable precursors of azolium enolates [48-53], which can be synthesized in a single step from the desired aldehyde [54]. We have previously applied these precursors in the NHC-catalyzed formal [2 + 2]

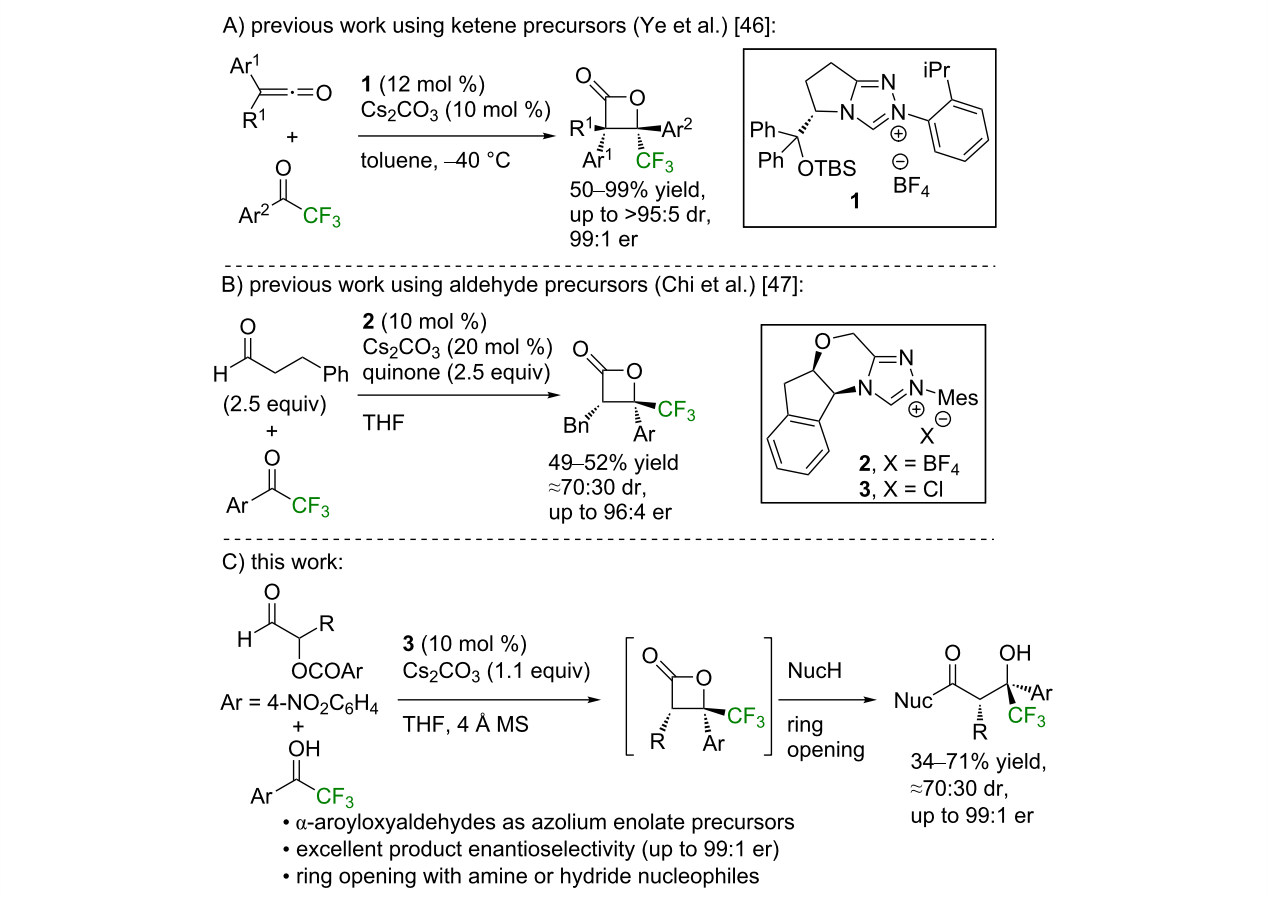

Figure 2: NHC-catalyzed approaches to β-lactones using trifluoroacetophenone derivatives.

cycloadditions between α-aroyloxyaldehydes and perfluoroalkyl-substituted ketones using NHC precatalyst **3** to produce polyfluorinated oxetanes and β-perfluoroalkyl-β-hydroxyamides after derivatization [55]. In this paper, this formal [2 + 2] protocol is extended to the use of trifluoroacetophenones to develop an enantioselective route to β-trifluoromethyl-β-hydroxy carboxylic acid derivatives (Figure 2C).

Results and Discussion

Optimization

Optimization of the NHC-catalyzed formal [2 + 2] cycloaddition using the α-aroyloxyaldehyde **4** and trifluoromethylacetophenone (**5**) as reactants began using the NHC precatalyst **3**, triethylamine as the base, and THF as the solvent (Table 1, entry 1). A moderate conversion (48%, as determined by NMR analysis) to the desired β-lactone product **6** as a 70:30 mixture of diastereoisomers was observed, which served as a basis for further optimization. Variation of the base showed caesium carbonate to be significantly more effective than the organic bases examined, giving 88% conversion to product **6** (Table 1, entries 2 and 3). Trialling a number of alternative solvents, including dichloromethane, diethyl ether, and toluene showed no improvement upon the yield obtained with THF (Table 1, entries 4–6). Unfortunately, attempts to isolate the desired β-lactone product **6** were unsuccessful, with **6** being unstable to chromatographic purification under a variety of different conditions. As such, following the NHC-catalyzed formal [2 + 2] cycloaddition in THF, a subsequent ring opening step with allylamine was investigated. Although the diastereomeric ratio of the resultant crude reaction mixture was 75:25 after chromatographic purification, as seen by NMR analysis, the corresponding β-trifluoromethyl-β-hydroxyamide **7** was isolated as a single diastereoisomer in 57% yield and >99:1 er (Table 1, entry 7).

Scope and limitations

Having optimized this process with a model system, further work probed the scope and limitations of this process through a sequential variation of the nucleophile used for the ring opening procedure, aryl and heteroaryl substitution of the trifluoromethylacetophenone, as well as variation of the α-aroyloxyaldehyde. Using α-aroyloxyaldehyde **4** and trifluoromethylacetophenone (**5**) as reactants, the variation of the nucleophile showed that a range of amine-based nucleophiles was readily tolerated in this process (Scheme 1). The use of benzylamine, pyrrolidine, and ammonia all gave the corresponding β-trifluoromethyl-β-hydroxyamide product in ≈75:25 dr, with purification giving **8**–**10**, respectively, as a single diastereoisomer in 42–55% yield and excellent enantioselectivity. Using methanol as a nucleophile gave the corresponding ester, however, this product proved unstable to purification. Generation of the ester in situ, followed by subsequent reduction with $LiAlH_4$, gave the diol **11** in 48% isolated yield as a single diastereoisomer in 96:4 er.

Table 1: Optimization of the NHC-catalyzed formal [2 + 2] cycoaddition.[a]

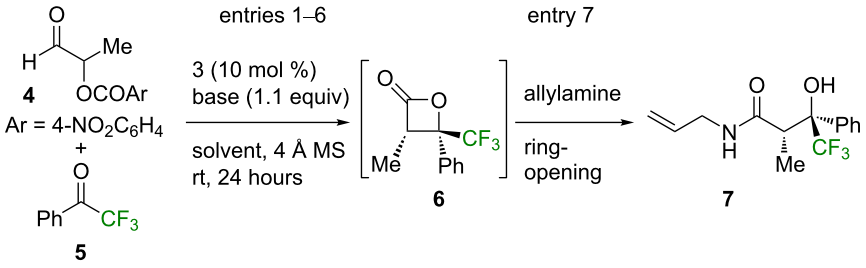

entry	solvent	base	dr[b]	yield (%)	er[c]
1	THF	Et_3N	70:30	48[d]	–
2	THF	iPr_2NEt	70:30	50[d]	–
3	THF	Cs_2CO_3	75:25	88[d]	–
4	CH_2Cl_2	Cs_2CO_3	80:20	61[d]	–
5	Et_2O	Cs_2CO_3	70:30	58[d]	–
6	toluene	Cs_2CO_3	70:30	55[d]	–
7	THF	Cs_2CO_3	75:25	57[e]	>99:1

[a]The data contained in this Table has previously been published as part of our previous communication in this area [55]. [b]Determined by ^{1}H NMR spectroscopic analysis of the crude reaction product mixture. [c]er of the major diastereoisomer (>95:5 dr), determined by GC analysis using a chiral support. [d]Combined yield of both diastereoisomers of **6**, determined by the analysis of the crude ^{1}H NMR spectra with reference to 2,5-dimethylfuran as an internal standard. [e]Isolated yield of product **7** (>95:5 dr).

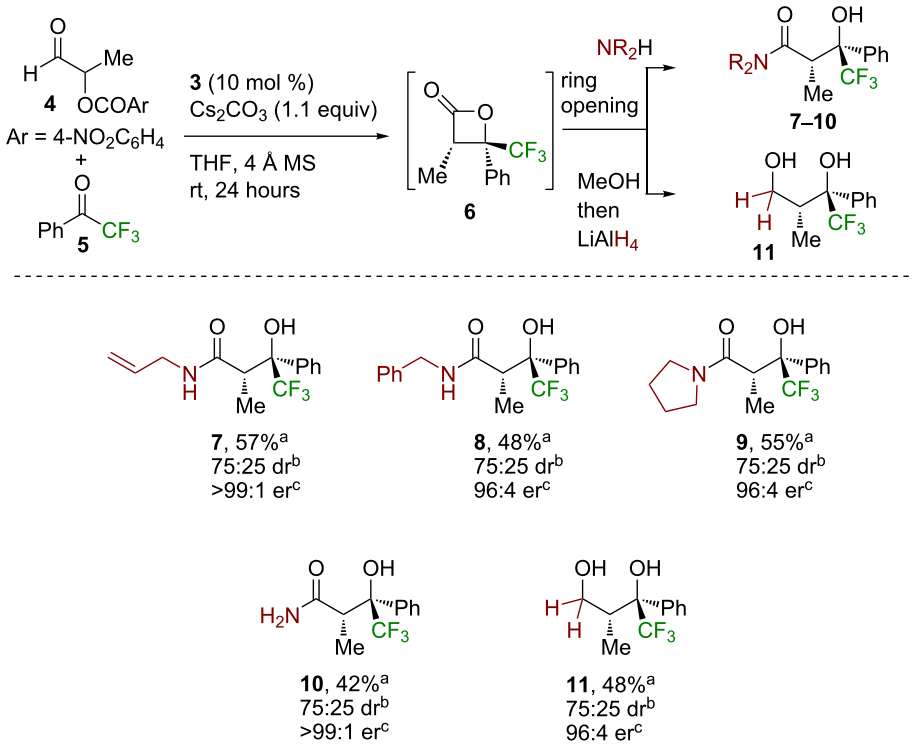

Scheme 1: Reaction scope with respect to the nucleophile. [a]Isolated yield of the product in >95:5 dr. [b]Determined by ^{1}H NMR spectroscopic analysis of the crude reaction product mixture. [c]Determined by HPLC analysis or GC analysis using a chiral support.

Subsequent variation of the electronic nature of the aromatic substituent within the trifluoroacetophenone component, followed by a ring opening with allylamine, showed that the introduction of electron-withdrawing groups (positive Hammett sigma constants) [56], such as *p*-bromo, *p*-fluoro, and *p*-trifluoromethyl groups, respectively, were well tolerated, giving a consistent diastereoselectivity of ≈75:25 dr (Scheme 2). Following chromatographic purification, the desired products **12**–**14**, respectively, were isolated in 59–71% yield as single diastereoisomers with excellent enantioselectivity (95:5 to >99:1 er). The relative and absolute configuration of (2*S*,3*S*)-β-trifluoromethyl-β-hydroxyamide **12** was confirmed by single crystal X-ray crystallographic analysis, with all other products in this series assigned by analogy to **12** [57]. The introduction of an electron-donating *p*-tolyl substituent was also tolerated in the system, providing the corresponding β-trifluoromethyl-β-hydroxyamide **15** in a moderate yield of 46%, although the er of **15** could not be determined by either GC or HPLC analysis. The trifluoroacetophenone derivatives with stronger electron-donating *p*-methoxy and *p*-dimethylamino substituents proved unreactive, consistent with the expected lower electrophilicity. A heterocyclic substituent could also be incorporated using this methodology, with thiophene-substituted β-trifluoromethyl-β-hydroxyamide **16** being produced in 80:20 dr, with purification giving **16** in 51% yield as a single diastereoisomer and 96:4 er. The substrate scope was further investigated by variation of the α-aroyloxyaldehyde component of the reaction. Functionalized α-aroyloxyaldehydes containing a C2-benzyl and a C2-benzyloxy derivative were tested, producing the corresponding β-trifluoromethyl-β-hydroxyamides **17** and **18**, respectively, in ≈70:30 dr after a ring opening with allylamine. Purification gave **17** and **18**, respectively, in a moderate yield as single diastereoisomers and with a good enantioselectivity.

The mechanism of this NHC redox process is believed to proceed through the following mechanism (Scheme 3): After deprotonation of the triazolium salt precatalyst **3** [58], reversible addition of the free NHC **I** to the aldehyde leads to adduct **II** [59]. A subsequent deprotonation allows access to Breslow intermediate **III**, which can eliminate *para*-nitrobenzoate to leave azolium enol **IV**. Deprotonation gives azolium enolate intermediate **V**, which undergoes a formal [2 + 2] cycloaddition with the trifluoroacetophenone derivative to give **VI** [60]. Elimination of the NHC catalyst completes the catalytic cycle and provides the corresponding β-lactone product. Subsequent ring opening with a suitable nucleophilic amine leads to the isolable β-trifluoromethyl-β-hydroxyamide (Scheme 3).

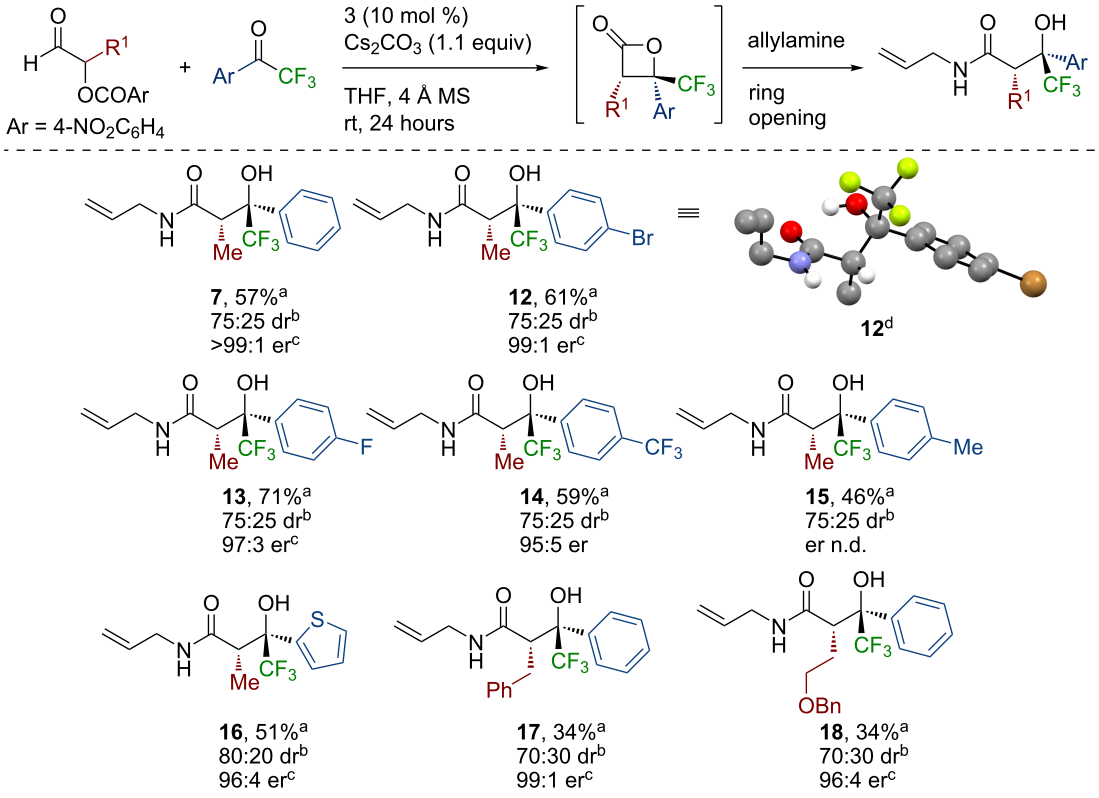

Scheme 2: Reaction scope with respect to the trifluoroacetophenone derivative and α-aroyloxyaldehyde. [a]Isolated yield of the product in >95:5 dr. [b]Determined by ^{1}H NMR spectroscopic analysis of the crude reaction product mixture. [c]er of the major diastereoisomer (>95:5 dr), determined by HPLC analysis or GC analysis using a chiral support. [d]Molecular representation of the X-ray crystal structure of **12**. The unit cell of **12** contained two molecules of **12**, with only one shown for clarity.

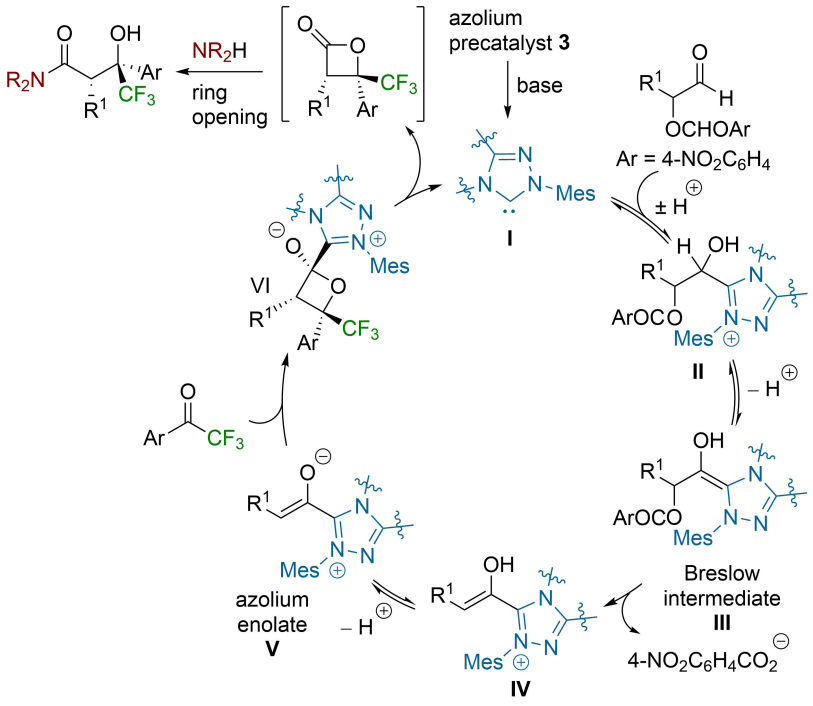

Scheme 3: Proposed mechanism.

Conclusion

In this paper, we showed that azolium enolates generated from α-aroyloxyaldehydes can undergo NHC-catalyzed formal [2 + 2] cycloadditions with trifluoroacetophenone derivatives. Although the β-lactone products proved unstable to chromatographic purification, ring opening with amine nucleophiles allowed access to β-trifluoromethyl-β-hydroxyamides in moderate to good yield as single diastereoisomers in excellent er following purification [61].

Supporting Information

Supporting Information File 1

Experimental procedures, product characterization data (mp, NMR, IR, HRMS, $[\alpha]_D$, HPLC), and spectra (^{1}H, ^{13}C, and ^{19}F NMR, HPLC).
[https://www.beilstein-journals.org/bjoc/content/supplementary/1860-5397-16-129-S1.pdf]

Supporting Information File 2

Crystallographic details for **12**.
[https://www.beilstein-journals.org/bjoc/content/supplementary/1860-5397-16-129-S2.cif]

Acknowledgements

We thank the EPSRC UK National Mass Spectrometry Facility at Swansea University.

Funding

We thank the European Research Council under the European Union's Seventh Framework Program (FP7/2007-2013) ERC grant agreement no. 279850 (A. T. D.)

ORCID® iDs

Mark D. Greenhalgh - https://orcid.org/0000-0002-4176-7633
Alexandra M. Z. Slawin - https://orcid.org/0000-0002-9527-6418
Andrew D. Smith - https://orcid.org/0000-0002-2104-7313

References

1. Purser, S.; Moore, P. R.; Swallow, S.; Gouverneur, V. *Chem. Soc. Rev.* **2008,** *37,* 320–330. doi:10.1039/b610213c
2. Müller, K.; Faeh, C.; Diederich, F. *Science* **2007,** *317,* 1881–1886. doi:10.1126/science.1131943
3. Studer, A. *Angew. Chem., Int. Ed.* **2012,** *51,* 8950–8958. doi:10.1002/anie.201202624
4. Tomashenko, O. A.; Grushin, V. V. *Chem. Rev.* **2011,** *111,* 4475–4521. doi:10.1021/cr1004293
5. Dilman, A. D.; Levin, V. V. *Eur. J. Org. Chem.* **2011,** 831–841. doi:10.1002/ejoc.201001558
6. Liu, H.; Gu, Z.; Jiang, X. *Adv. Synth. Catal.* **2013,** *355,* 617–626. doi:10.1002/adsc.201200764
7. Hagmann, W. K. *J. Med. Chem.* **2008,** *51,* 4359–4369. doi:10.1021/jm800219f
8. Sani, M.; Volonterio, A.; Zanda, M. *ChemMedChem* **2007,** *2,* 1693–1700. doi:10.1002/cmdc.200700156
9. Léger, S.; Bayly, C. I.; Black, W. C.; Desmarais, S.; Falgueyret, J.-P.; Massé, F.; Percival, M. D.; Truchon, J.-F. *Bioorg. Med. Chem. Lett.* **2007,** *17,* 4328–4332. doi:10.1016/j.bmcl.2007.05.024
10. Nie, J.; Guo, H.-C.; Cahard, D.; Ma, J.-A. *Chem. Rev.* **2011,** *111,* 455–529. doi:10.1021/cr100166a
11. Shibata, N.; Matsnev, A.; Cahard, D. *Beilstein J. Org. Chem.* **2010,** *6,* No. 65. doi:10.3762/bjoc.6.65
12. Ma, J.-A.; Cahard, D. *Chem. Rev.* **2004,** *104,* 6119–6146. doi:10.1021/cr030143e
13. Valero, G.; Companyó, X.; Rios, R. *Chem. – Eur. J.* **2011,** *17,* 2018–2037. doi:10.1002/chem.201001546
See for a review.
14. Yang, W.; Cui, Y.-M.; Zhou, W.; Li, L.; Yang, K.-F.; Zheng, Z.-J.; Lu, Y.; Xu, L.-W. *Synlett* **2014,** *25,* 1461–1465. doi:10.1055/s-0033-1341281
15. Vlasserou, I.; Sfetsa, M.; Gerokonstantis, D.-T.; Kokotos, C. G.; Moutevelis-Minakakis, P. *Tetrahedron* **2018,** *74,* 2338–2349. doi:10.1016/j.tet.2018.03.054
16. Duangdee, N.; Harnying, W.; Rulli, G.; Neudörfl, J.-M.; Gröger, H.; Berkessel, A. *J. Am. Chem. Soc.* **2012,** *134,* 11196–11205. doi:10.1021/ja302511t
17. Hara, N.; Tamura, R.; Funahashi, Y.; Nakamura, S. *Org. Lett.* **2011,** *13,* 1662–1665. doi:10.1021/ol2001039
18. Kokotos, C. G. *J. Org. Chem.* **2012,** *77,* 1131–1135. doi:10.1021/jo2020104
19. Qui, L.-H.; Shen, Z.-X.; Shi, C.-Q.; Liu, Y.-H.; Zhang, Y.-W. *Chin. J. Chem.* **2005,** *23,* 584–588. doi:10.1002/cjoc.200590584
20. Thomson, C. J.; Barber, D. M.; Dixon, D. J. *Angew. Chem., Int. Ed.* **2020,** *59,* 5359–5364. doi:10.1002/anie.201916129
21. Moore, J. L.; Rovis, T. *Top. Curr. Chem.* **2010,** *291,* 77–144.
22. Marion, N.; Díez-González, S.; Nolan, S. P. *Angew. Chem., Int. Ed.* **2007,** *46,* 2988–3000. doi:10.1002/anie.200603380
23. Enders, D.; Niemeier, O.; Henseler, A. *Chem. Rev.* **2007,** *107,* 5606–5655. doi:10.1021/cr068372z
24. Hopkinson, M. N.; Richter, C.; Schedler, M.; Glorius, F. *Nature* **2014,** *510,* 485–496. doi:10.1038/nature13384
25. Ryan, S. J.; Candish, L.; Lupton, D. W. *Chem. Soc. Rev.* **2013,** *42,* 4906–4917. doi:10.1039/c3cs35522e
26. Flanigan, D. M.; Romanov-Michailidis, F.; White, N. A.; Rovis, T. *Chem. Rev.* **2015,** *115,* 9307–9387. doi:10.1021/acs.chemrev.5b00060
27. Vora, H. U.; Wheeler, P.; Rovis, T. *Adv. Synth. Catal.* **2012,** *354,* 1617–1639. doi:10.1002/adsc.201200031
28. Douglas, J.; Churchill, G.; Smith, A. D. *Synthesis* **2012,** *44,* 2295–2309. doi:10.1055/s-0031-1289788
29. Zhang, Y.-R.; He, L.; Wu, X.; Shao, P.-L.; Ye, S. *Org. Lett.* **2008,** *10,* 277–280. doi:10.1021/ol702759b
30. Duguet, N.; Campbell, C. D.; Slawin, A. M. Z.; Smith, A. D. *Org. Biomol. Chem.* **2008,** *6,* 1108–1113. doi:10.1039/b800857b
31. He, M.; Uc, G. J.; Bode, J. W. *J. Am. Chem. Soc.* **2006,** *128,* 15088–15089. doi:10.1021/ja066380r
32. He, M.; Beahm, B. J.; Bode, J. W. *Org. Lett.* **2008,** *10,* 3817–3820. doi:10.1021/ol801502h
33. Kobayashi, S.; Kinoshita, T.; Uehara, H.; Sudo, T.; Ryu, I. *Org. Lett.* **2009,** *11,* 3934–3937. doi:10.1021/ol901544q

34. Yang, L.; Wang, F.; Chua, P. J.; Lv, Y.; Zhong, L.-J.; Zhong, G. *Org. Lett.* **2012,** *14,* 2894–2897. doi:10.1021/ol301175z
35. Jian, T.-Y.; Sun, L.-H.; Ye, S. *Chem. Commun.* **2012,** *48,* 10907–10909. doi:10.1039/c2cc35273g
36. Lv, H.; Chen, X.-Y.; Sun, L.-h.; Ye, S. *J. Org. Chem.* **2010,** *75,* 6973–6976. doi:10.1021/jo101318u
37. Jian, T.-Y.; Shao, P.-L.; Ye, S. *Chem. Commun.* **2011,** *47,* 2381–2383. doi:10.1039/c0cc04839a
38. Chen, X.; Fang, X.; Chi, Y. R. *Chem. Sci.* **2013,** *4,* 2613–2618. doi:10.1039/c3sc50666e
39. Hao, L.; Du, Y.; Lv, H.; Chen, X.; Jiang, H.; Shao, Y.; Chi, Y. R. *Org. Lett.* **2012,** *14,* 2154–2157. doi:10.1021/ol300676w
40. Lee, A.; Younai, A.; Price, C. K.; Izquierdo, J.; Mishra, R. K.; Scheidt, K. A. *J. Am. Chem. Soc.* **2014,** *136,* 10589–10592. doi:10.1021/ja505880r
41. Cheng, J.-T.; Chen, X.-Y.; Ye, S. *Org. Biomol. Chem.* **2015,** *13,* 1313–1316. doi:10.1039/c4ob02330g
42. Lee, A.; Scheidt, K. A. *Chem. Commun.* **2015,** *51,* 3407–3410. doi:10.1039/c4cc09590a
43. Zhao, X.; Ruhl, K. E.; Rovis, T. *Angew. Chem., Int. Ed.* **2012,** *51,* 12330–12333. doi:10.1002/anie.201206490
44. Dong, X.; Yang, W.; Hu, W.; Sun, J. *Angew. Chem., Int. Ed.* **2015,** *54,* 660–663. doi:10.1002/anie.201409961
45. Lin, L.; Yang, Y.; Wang, M.; Lai, L.; Guo, Y.; Wang, R. *Chem. Commun.* **2015,** *51,* 8134–8137. doi:10.1039/c5cc01587a
46. Wang, X.-N.; Shao, P.-L.; Lv, H.; Ye, S. *Org. Lett.* **2009,** *11,* 4029–4031. doi:10.1021/ol901290z
47. Mo, J.; Yang, R.; Chen, X.; Tiwari, B.; Chi, Y. R. *Org. Lett.* **2013,** *15,* 50–53. doi:10.1021/ol303035r
48. Ling, K. B.; Smith, A. D. *Chem. Commun.* **2011,** *47,* 373–375. doi:10.1039/c0cc02456b
49. Davies, A. T.; Taylor, J. E.; Douglas, J.; Collett, C. J.; Morrill, L. C.; Fallan, C.; Slawin, A. M. Z.; Churchill, G.; Smith, A. D. *J. Org. Chem.* **2013,** *78,* 9243–9257. doi:10.1021/jo401433q
50. Taylor, J. E.; Daniels, D. S. B.; Smith, A. D. *Org. Lett.* **2013,** *15,* 6058–6061. doi:10.1021/ol402955f
51. Davies, A. T.; Pickett, P. M.; Slawin, A. M. Z.; Smith, A. D. *ACS Catal.* **2014,** *4,* 2696–2700. doi:10.1021/cs500667g
52. Attaba, N.; Taylor, J. E.; Slawin, A. M. Z.; Smith, A. D. *J. Org. Chem.* **2015,** *80,* 9728–9739. doi:10.1021/acs.joc.5b01820
53. Kerr, R. W. F.; Greenhalgh, M. D.; Slawin, A. M. Z.; Arnold, P. L.; Smith, A. D. *Tetrahedron: Asymmetry* **2017,** *28,* 125–134. doi:10.1016/j.tetasy.2016.10.012
54. Uyanik, M.; Suzuki, D.; Yasui, T.; Ishihara, K. *Angew. Chem., Int. Ed.* **2011,** *50,* 5331–5334. doi:10.1002/anie.201101522
55. Davies, A. T.; Slawin, A. M. Z.; Smith, A. D. *Chem. – Eur. J.* **2015,** *21,* 18944–18948. doi:10.1002/chem.201504256
56. McDaniel, D. H.; Brown, H. C. *J. Org. Chem.* **1958,** *23,* 420–427. doi:10.1021/jo01097a026
57. Crystallographic data for **12** has been deposited with the Cambridge Crystallographic Data Centre (ascension number: CCDC 1987497).
58. Massey, R. S.; Collett, C. J.; Lindsay, A. G.; Smith, A. D.; O'Donoghue, A. C. *J. Am. Chem. Soc.* **2012,** *134,* 20421–20432. doi:10.1021/ja308420c
59. Collett, C. J.; Massey, R. S.; Maguire, O. R.; Batsanov, A. S.; O' Donoghue, A. C.; Smith, A. D. *Chem. Sci.* **2013,** *4,* 1514–1522. doi:10.1039/c2sc22137c
60. Barrios Antúnez, D.-J.; Greenhalgh, M. D.; Brueckner, A. C.; Walden, D. M.; Elías-Rodríguez, P.; Roberts, P.; Young, B. G.; West, T. H.; Slawin, A. M. Z.; Ha-Yeon Cheong, P.; Smith, A. D. *Chem. Sci.* **2019,** *10,* 6162–6173. doi:10.1039/c9sc00390h
61. The research data underpinning this publication can be accessed at doi:https://doi.org/10.17630/7bc9507c-e817-4da7-988a-02fcd1a6f4fa.

License and Terms

This is an Open Access article under the terms of the Creative Commons Attribution License (http://creativecommons.org/licenses/by/4.0). Please note that the reuse, redistribution and reproduction in particular requires that the authors and source are credited.

The license is subject to the *Beilstein Journal of Organic Chemistry* terms and conditions: (https://www.beilstein-journals.org/bjoc)

The definitive version of this article is the electronic one which can be found at: doi:10.3762/bjoc.16.129

BEILSTEIN JOURNAL OF ORGANIC CHEMISTRY

Fluorohydration of alkynes via I(I)/I(III) catalysis

Jessica Neufeld, Constantin G. Daniliuc§ and Ryan Gilmour*¶

Full Research Paper

Open Access

Address:
Organisch-Chemisches Institut, Westfälische Wilhelms-Universität Münster, Corrensstraße 40, 48149 Münster, Germany

Email:
Ryan Gilmour* - ryan.gilmour@uni-muenster.de

* Corresponding author
§ X-ray crystallographer
¶ https://www.uni-muenster.de/Chemie.oc/Gilmour

Keywords:
α-fluoroketone; alkyne; fluorination; hypervalent iodine; organocatalysis

Beilstein J. Org. Chem. **2020,** *16,* 1627–1635.
doi:10.3762/bjoc.16.135

Received: 07 May 2020
Accepted: 30 June 2020
Published: 10 July 2020

This article is part of the thematic issue "Organo-fluorine chemistry V".

Guest Editor: D. O'Hagan

© 2020 Neufeld et al.; licensee Beilstein-Institut.
License and terms: see end of document.

Abstract

Substrate specificity is ubiquitous in biological catalysis, but less pervasive in the realm of small-molecule catalysis. Herein, we disclose an intriguing example of substrate specificity that was observed whilst exploring catalysis-based routes to generate α-fluoroketones from terminal and internal alkynes under the auspices of I(I)/I(III) catalysis. Utilising *p*-TolI as an inexpensive organocatalyst with Selectfluor® and amine/HF mixtures, the formation of protected α-fluoroketones from simple alkynes was realised. Whilst the transient *p*-TolIF$_2$ species generated in situ productively engaged with pentynyl benzoate scaffolds to generate the desired α-fluoroketone motif, augmentation or contraction of the linker suppressed catalysis. The prerequisite for this substructure was established by molecular editing and was complemented with a physical organic investigation of possible determinants.

Introduction

The venerable role of fluorine as a powerful physicochemical modulator in small-molecule drug discovery is a compelling argument for the importance of sustained innovation to facilitate this form of structural editing [1-4]. Routinely employed as a bioisostere of hydrogen or hydroxy [5,6], substitution may enable inversion of the local electronic environment, or the precise deletion of hydrogen-bond donors, respectively, with minimal steric variation [7]. The latter aspect is a crucial determinant in enabling fluorinated materials to adopt intriguing conformations which are a manifest representation of stabilising non-covalent interactions [8-10]. These collective attributes render fluorination a valuable strategy in drug discovery [11] and agrochemical development [12]. In the conception of enabling fluorination technologies, the α-fluorocarbonyl motif has emerged as a prominent target scaffold [13]. Remarkable advances in the direct fluorination (F_2/N_2) of carbonyl compounds by Sandford and co-workers [14,15] are noteworthy in this regard, and mitigate the expense and poor atom economy associated with stoichiometric approaches. Moreover, this substructure provides a versatile entry point for subsequent C(sp^3)–C(sp^3) bond-forming reactions [16,17], and closely resembles one of the very few biological blueprints for the prep-

aration of fluorine-containing materials [18-21]. However, in translating the fluoroacetate-like building blocks to a laboratory paradigm, the intrinsic toxicity of these species in inhibiting aconitase [22] must be reconciled with synthetic utility. To that end, catalysis-based strategies to unmask the venerable α-fluorocarbonyl motif [23] from a terminal alkyne were considered (Figure 1). This general strategy was appealing given the commercial availability of the substrates and the plenum of methods available to activate π-bonds [24,25].

Confidence in this approach stemmed from our recent *vicinal* and *geminal* difluorination of alkenes [26-30], and contemporaneous studies from the Jacobsen laboratory [31-34], under the auspices of I(I)/I(III) catalysis [35-37]. Moreover, elegant studies by Hara and co-workers have demonstrated that α-fluoroketones could be prepared by exposing silyl enol ethers to stoichiometric *p*-ToIIF$_2$, in the presence of BF$_3$·OEt$_2$ and NEt$_3$/HF 1:2 [38]. A report by Kitamura and co-workers in which the direct fluorination of acetophenone derivatives was achieved using iodosylarenes and commercially available NEt$_3$/HF 1:5 to generate the ArIF$_2$ species in situ is also highly pertinent [39,40] (Figure 1A).

Elegant reports describing the conversion of internal alkynes to α-fluoroketones via π-acid catalysis were also disclosed (Figure 1B). Seminal reports by Nevado [41,42] and Gouverneur [43] enabled the synthesis of α-fluoroketones and -enones from terminal and internal alkynes, thereby mitigating difluoroketone formation: This is commonly observed in the fluorination of alkynes using stoichiometric electrophilic fluorinating reagents [44,45]. Developments by Hammond and Xu validated *N*-pyridine oxides as terminal oxidants to substitute Selectfluor® for the cationic Au(I)/Au(III) cycle, thereby enabling high functional group tolerance [46-49]. Inspired by these and other selected advances [50,51], in metal-based fluorination, a complementary organocatalytic variant [52], based on an I(I)/I(III) catalysis platform was explored (Figure 1C). It was envisaged that the in situ generation of *p*-TolIF$_2$ via oxidation of *p*-TolI with Selectfluor® in the presence of an amine/HF complex might enable the title transformation [53].

Results and Discussion

To explore the feasibility of generating α-fluoroketones from terminal alkynes via I(I)/I(III) catalysis, 4-pentynyl benzoate (**1**)

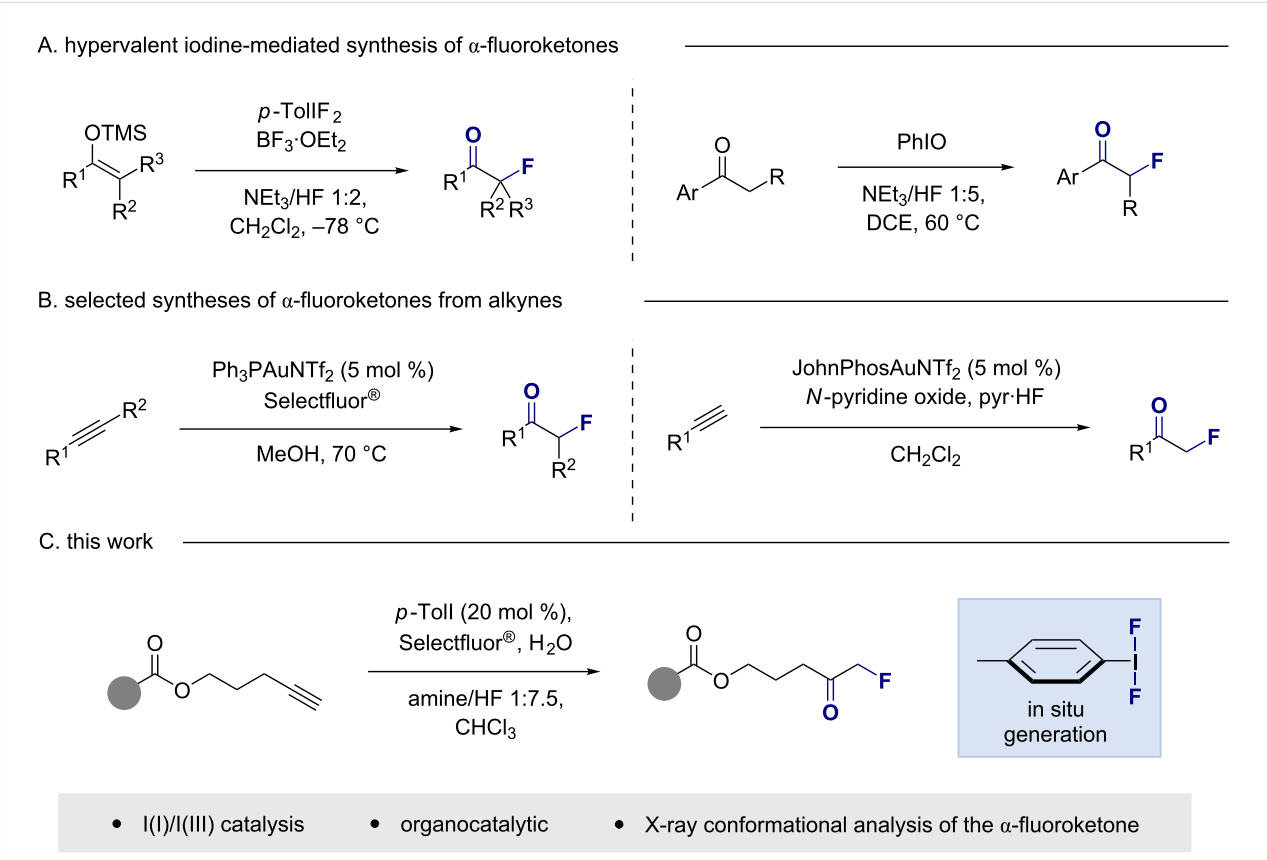

Figure 1: (A) Synthetic routes to α-fluoroketones from silyl enol ethers or acetophenone derivatives. (B) Selected Au-catalysed syntheses of α-fluoroketones from alkynes. (C) This work: synthesis of α-fluoroketones from pentynyl benzoates via I(I)/I(III) catalysis.

was selected as the substrate for optimisation studies (Table 1). The inexpensive, commercially available *p*-TolI was used as an organocatalyst, Selectfluor® was employed as the terminal oxidant, and an amine/HF complex enlisted as the fluoride source (please see Supporting Information File 1 for full details). The reaction was performed in $CHCl_3$ at ambient temperature and the crude reaction mixtures were analysed by ^{19}F NMR spectroscopy using ethyl fluoroacetate as the internal standard. Initially, the effect of Brønsted acidity was explored by varying the amine/HF ratio with mixtures of commercially available NEt_3/HF 1:3 and Olah's reagent (pyr/HF 1:9.23). Lower amine/HF ratios (1:4.5) resulted in poor conversion (9% yield, Table 1, entry 1), whereas increasing the Brønsted acidity to 1:7.5 furnished the desired α-fluoroketone **2** in 64% yield (Table 1, entry 2). However, employing Olah's reagent (1:9.23) had a negative impact on the efficiency (45% yield, Table 1, entry 3) thereby allowing a plateau to be established (vide infra).

Having established that an amine/HF ratio of 1:7.5 provides the optimal Brønsted acidity for catalysis, a solvent screen was conducted to assess the effect of the reaction medium. Chlorinated solvents proved to be most effective, with reactions performed in $CHCl_3$ slightly outperforming those in CH_2Cl_2 (64% and 56% yield, respectively, Table 1, entries 2 and 4). Fluorinated solvents such as hexafluoroisopropanol (HFIP) or ethyl trifluoroacetate (ETFA) led to similar results (52% and 50% yield, respectively, Table 1, entries 5 and 6). Switching to non-halogenated solvents such as acetonitrile or toluene proved to be detrimental (19% and 10%, respectively, Table 1, entries 7 and 8). A screen of common oxidants for I(I)/I(III) catalysis confirmed Selectfluor® as being ideally suited, in line with our previous observations [26-30]. Whereas *m*-CPBA generated the desired α-fluoroketone **2** (50% yield), ground Oxone® or *N*-pyridine oxide proved to be ineffective (Table 1, entries 9–11). Increasing the reaction temperature to 50 °C led to the same outcome as at ambient temperature (64% yield, Table 1, entry 12). Finally, the control reactions in the absence of catalyst, oxidant and HF source were performed and supported the involvement of the postulated I(I)/I(III) cycle (Table 1, entries 13–15).

Since the conditions described in Table 1, entry 2 furnished the desired α-fluoroketone **2** in a respectable yield without the addition of H_2O, efforts to establish the influence of rigorous exclusion and excess addition were conducted (Table 2). In both scenarios, comparable results were observed (without H_2O 64%, with addition of 1.0 equiv 64% yield, Table 2, entries 1

Table 1: Reaction optimisation for the synthesis of α-fluoroketone **2** from alkyne **1**.[a]

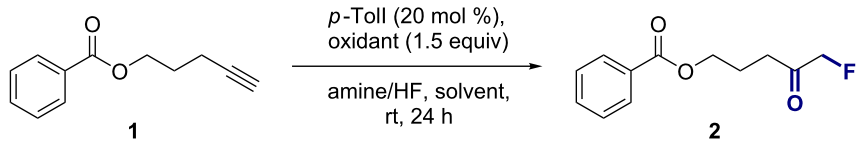

1 **2**

entry	oxidant	amine/HF[b]	solvent	yield[c]
1	Selectfluor®	1:4.5	$CHCl_3$	9%
2	**Selectfluor®**	**1:7.5**	**$CHCl_3$**	**64%**
3	Selectfluor®	1:9.23	$CHCl_3$	45%
4	Selectfluor®	1:7.5	CH_2Cl_2	56%
5	Selectfluor®	1:7.5	HFIP	52%
6	Selectfluor®	1:7.5	ETFA	50%
7	Selectfluor®	1:7.5	CH_3CN	19%
8	Selectfluor®	1:7.5	toluene	10%
9	*m*-CPBA	1:7.5	$CHCl_3$	50%
10	gr. Oxone®	1:7.5	$CHCl_3$	<5%
11	*N*-pyridine oxide	1:7.5	$CHCl_3$	<5%
12[d]	Selectfluor®	1:7.5	$CHCl_3$	64%
13[e]	Selectfluor®	1:7.5	$CHCl_3$	<5%
14	–	1:7.5	$CHCl_3$	<5%
15	Selectfluor®	–	$CHCl_3$	<5%

[a]Standard reaction conditions: alkyne **1** (0.2 mmol), *p*-TolI (20 mol %), oxidant (1.5 equiv), solvent (0.5 mL), amine/HF source (0.5 mL), ambient temperature, 24 h. [b]See Supporting Information File 1 for the exact calculation of the amine/HF mixtures. [c]Determined by ^{19}F NMR analysis of the crude reaction mixture using ethyl fluoroacetate as the internal standard. [d]Reaction was performed at 50 °C. [e]Control reaction without catalyst.

Table 2: Investigating the role of H_2O during the reaction.[a]

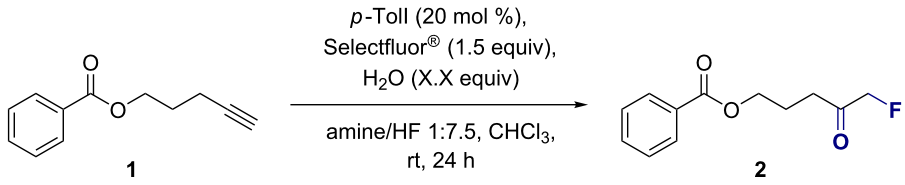

entry	equiv of H_2O	yield[b]	correlation of equiv H_2O versus yield[c]
1	–	64%	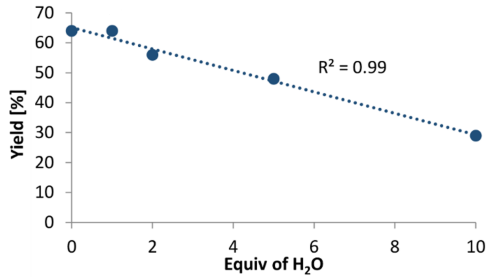
2	**1.0**	**64%**	
3	2.0	56%	
4	5.0	48%	
5	10	29%	

[a]Standard reaction conditions: alkyne **1** (0.2 mmol), *p*-TolI (20 mol %), Selectfluor® (1.5 equiv), H_2O (0–10 equiv), $CHCl_3$ (0.5 mL), amine/HF 1:7.5 (0.5 mL), ambient temperature, 24 h. See Supporting Information File 1 for the exact calculation of the amine/HF mixtures. [b]Determined by ^{19}F NMR analysis of the crude reaction mixture using ethyl fluoroacetate as internal standard. [c]Linear correlation of the equivalent of H_2O and the corresponding yield of **2**.

and 2). Further increasing the amount of H_2O from 2.0 equiv to 10 equiv suppressed reactivity (to 29% yield, Table 2, entries 3–5). In addition, a nearly linear correlation between the equivalents of added H_2O and the product yield was observed (Table 2 insert). Cognisant that H_2O is likely being introduced to the reaction via the HF source, and to prevent reproducibility issues due to variation of the H_2O content, 1.0 equiv was added in the general procedure to enable comparison.

With the optimised reaction conditions in hand (Table 2, entry 2), the scope and limitations of the title transformation were explored. Initially, the influence of modifying the aryl fragment of the 4-pentynyl benzoate motif was established (Scheme 1). Exposing the standard substrate **1** to the general reaction conditions furnished the desired product **2** in a synthetically useful isolated yield of 60%. Introduction of *para*-substituents was tolerated enabling formation of the chloro, methoxy, and nitro derivatives **3**–**5** with up to 54% yield. The exposure of a model internal alkyne to the standard conditions proved also successful affording **6** in 46% yield. Finally, replacement of the benzoate unit by a phthalimide moiety was possible and led to the protected amine derivative **7** (64% yield).

The structure of α-fluoroketone **2** was unequivocally established by single crystal X-ray diffraction (Figure 2). Interestingly, a study by Pattison has established that α-fluoroketones preferentially adopt a *cis*-conformation in polar solvents [54]. In the solid state, a dihedral angle of $\varphi = -3.7°$ was observed thereby placing the C–F bond in the same plane as the carbonyl group.

To establish the limitations of the title transformation, a process of substrate editing was initiated (Figure 3). However, efforts to contract or expand the alkynyl chain to four or six carbons, respectively, had a negative impact on the yield of the α-fluoroketone (16%, <5% for **8** and **9**, respectively, Figure 3A). Deletion of the ester carbonyl (**10**) and replacement of the phenyl group by methyl (**11**) was also detrimental. From these data it is tempting to speculate upon the involvement of a chair-like transition state in which the intramolecular interaction of the phenyl π-system, carbonyl and alkynyl group are optimally preorganised with a C5 linker. With this in mind, the amide derivatives **12** and **13** were exposed to the standard reaction conditions. Curiously, the reactions were extremely ineffective yielding the respective α-fluoroketones in only 15% yield as determined by ^{19}F NMR spectroscopy. This contrasts sharply with the phthalimide derivative **7** (64%). Doping a representative reaction (**14** → **9**) with methyl benzoate (**15**) (Figure 3B) to explore for potential activator effects also proved unsuccessful.

Finally, a stoichiometric reaction of alkynyl phthalimide **16** with freshly prepared *p*-TolIF_2 **17** demonstrated the importance of the exogenous amine·HF as a Brønsted acid activator

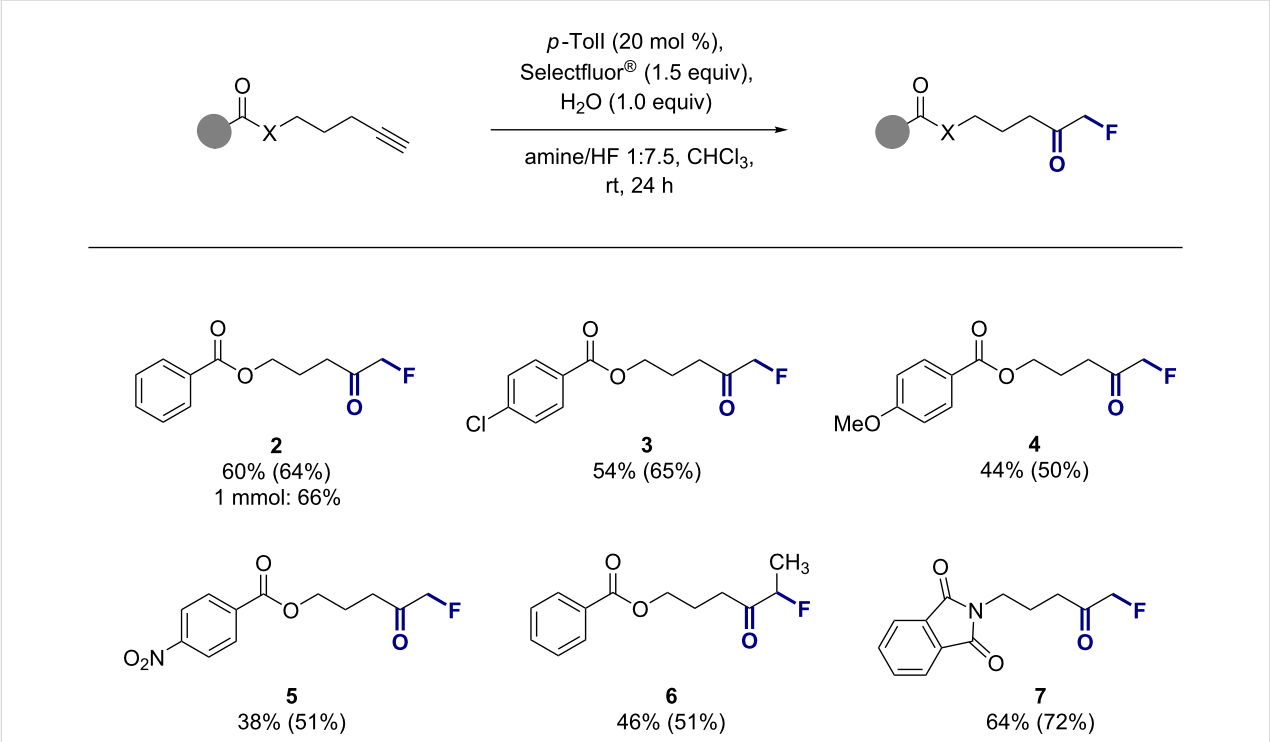

Scheme 1: Substrate scope with standard reaction conditions: alkyne (0.2 mmol), *p*-TolI (20 mol %), Selectfluor® (1.5 equiv), H_2O (1.0 equiv), $CHCl_3$ (0.5 mL), amine/HF 1:7.5 (0.5 mL), ambient temperature, 24 h. Yields refer to isolated products while ^{19}F NMR yields are given in parentheses (determined by ^{19}F NMR analysis of the crude reaction mixture using ethyl fluoroacetate as internal standard). See Supporting Information File 1 for the exact calculation of the amine/HF mixtures.

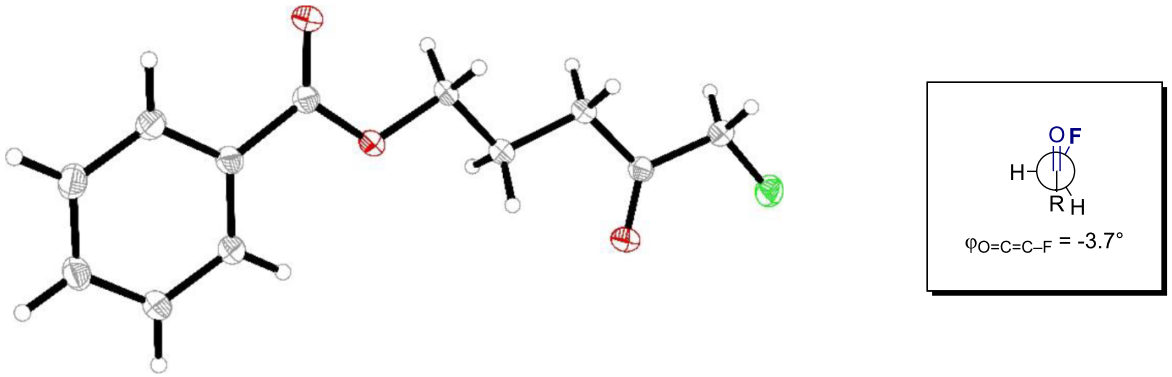

Figure 2: X-ray molecular structure of compound **2**. Conformation of the carbonyl group and the fluoride with a torsion angle of $\varphi_{O=C-C-F} = -3.7°$. CCDC number 2000136.

(Figure 3C). Similar yields were observed when comparing the stoichiometric reaction and the catalytic process using an amine/HF ratio of 1:7.5.

To interrogate the importance of the benzoate group in the substrate, a Hammett analysis was conducted. To that end, $\log(k_R/k_H)$ was plotted against the Hammett σ^-_p parameter for the *para*-substituted pentynyl benzoates with R = OMe, H, Cl, and NO_2 (Figure 4A). However, the resulting slope of the Hammett plot was essentially zero ($\rho \approx 0$). In contrast, a second Hammett analysis in which the substitution of the iodoarene catalyst was explored (R = Me, H, Cl, and Br) revealed a build-up of positive charge ($\rho < 0$) during the rate-determining step (Figure 4B).

From a methodological perspective, this study provides a conceptual platform to unmask the valuable α-fluoroketone motif from alkynes. Selectfluor®-mediated oxidation of *p*-TolI

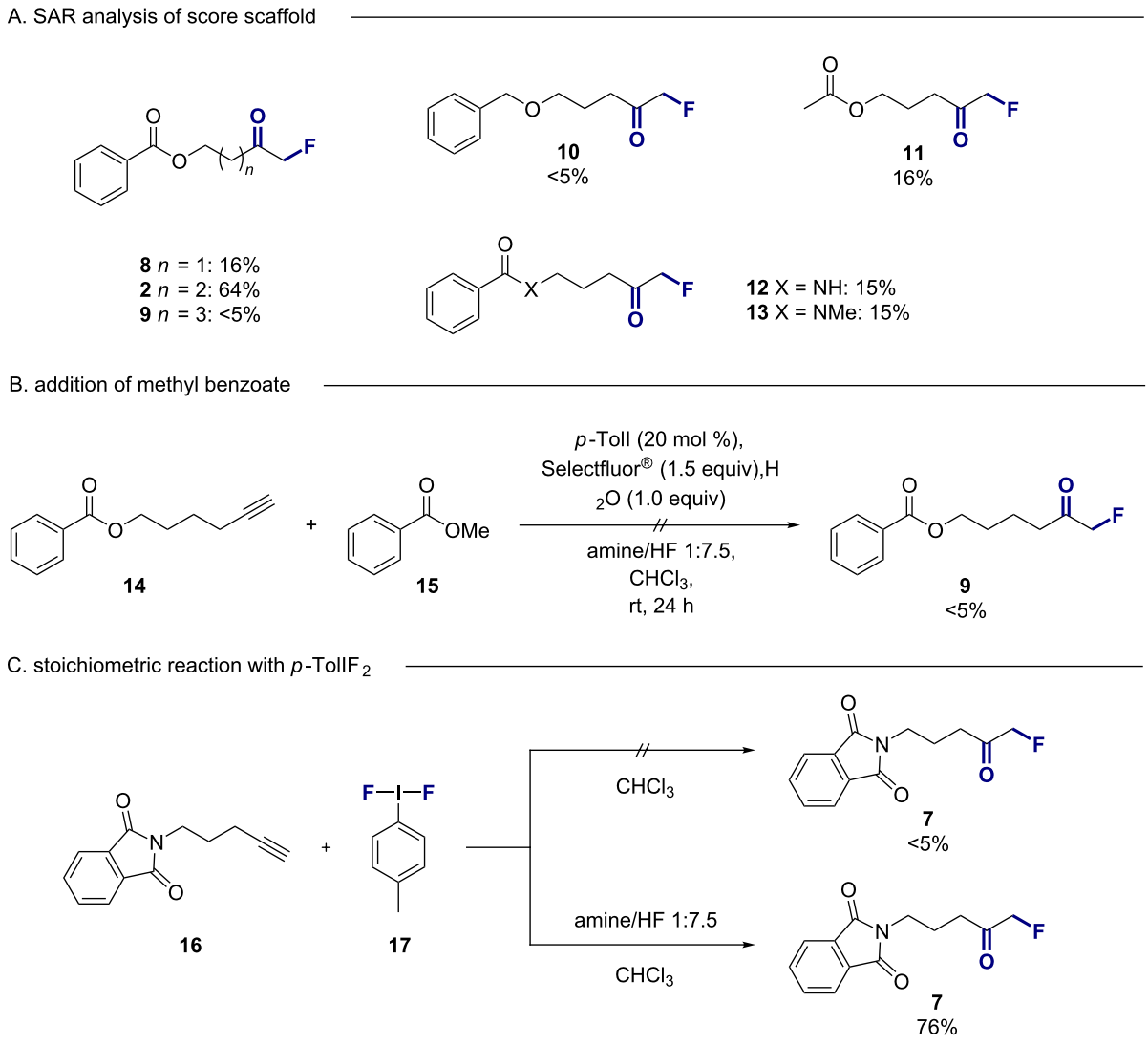

Figure 3: (A) Structure activity relationship of the core scaffold. (B) Exploring the effect of methyl benzoate as an activator. (C) Stoichiometric reaction with *p*-TolIF$_2$ **17** and alkyne **16**. Yields refer to spectroscopical yields determined by ^{19}F NMR analysis of the crude reaction mixtures using ethyl fluoroacetate as an internal standard.

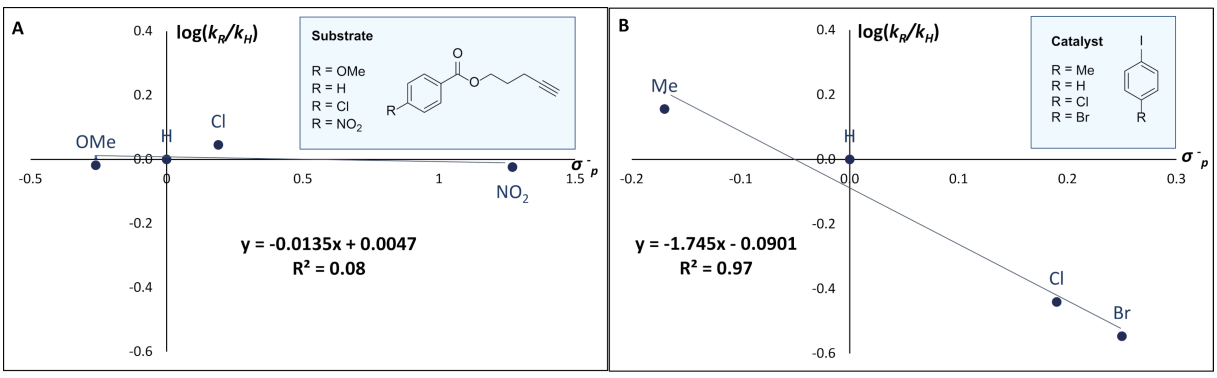

Figure 4: (A) Hammett plot varying the *para*-substitution on the alkyne ($\rho \approx 0$). (B) Hammett plot varying the *para*-substitution on the catalyst ($\rho < 0$).

in the presence of an amine/HF source, which plays a dual function as fluoride source and Brønsted acid activator, enables in situ generation of *p*-TolIF$_2$ (Figure 5). From these preliminary mechanistic investigations, conclusions regarding the extreme sensitivity of the fluorohydration towards changes in the substrate must be drawn with caution. The importance of the pentynyl linker, together with the requirement for the benzoyl ester, suggest a highly preorganised structure [55] in which the carbonyl group functions as a tempered Lewis base upon ligand exchange (Figure 5) [56]. This working hypothesis may also rationalise the deletion experiment (**10**), the recalcitrance of acetyl derivatives, and the striking reactivity disparity between amides (**12**/**13**) and the phthalimide derivative **16**. Finally, to investigate the fate of water in the transformation, the catalytic process was repeated in the presence of $H_2{}^{18}O$. Through isotope-shift experiments (please see Supporting Information File 1), it was possible to establish that the aryl ketone of the product contains the ^{18}O atom ($\Delta\delta_C$ = 4.42 Hz) [57-59]. Formation of the corresponding enol [60], tautomerisation and displacement liberates the α-fluoroketone and regenerates the ArI catalyst.

Preliminary mechanistic experiments, supported by Hammett analyses, have identified key determinants that are essential for reaction efficiency. X-ray crystal structure analysis of ketone **2** reveals a dihedral angle of $\varphi_{O=C-C-F}$ = −3.7°. Although the origin of this specificity requires clarification, this fluorohydration reaction constitutes a rare case of substrate specificity in small-molecule catalysis. It is envisaged that this organocatalytic variant of the venerable Kucherov reaction will find application in contemporary organofluorine chemistry [61] and contributes to the current interest in alkyne functionalisation via I(I)/I(III) catalysis [62,63].

Supporting Information

Supporting Information File 1

Experimental details, characterization data and copies of spectra.
[https://www.beilstein-journals.org/bjoc/content/supplementary/1860-5397-16-135-S1.pdf]

Conclusion

In conclusion, the synthesis of α-fluoroketones from 4-pentynyl benzoates based on an I(I)/I(III) catalysis manifold is disclosed.

Acknowledgements

We thank the analytical department of our institute for excellent support.

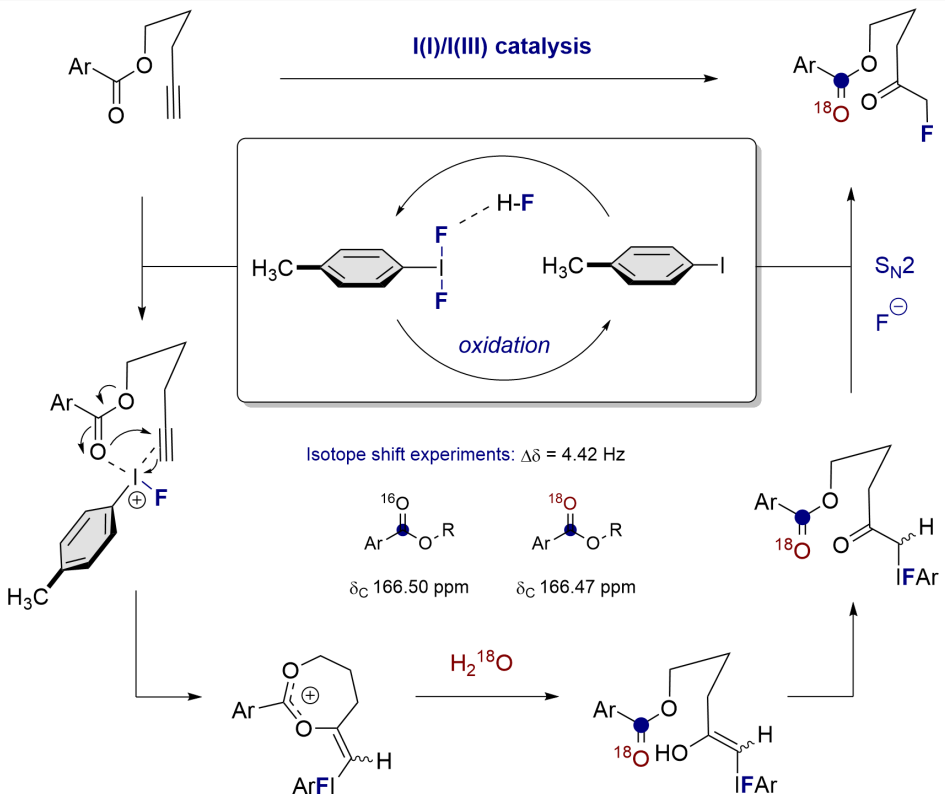

Figure 5: An overview of the I(I)/I(III)-catalysed fluorohydration of alkynes.

Funding

We acknowledge generous financial support from the WWU Münster and the Deutsche Forschungsgemeinschaft (SFB 858, fellowship to J.N.).

ORCID® iDs

Constantin G. Daniliuc - https://orcid.org/0000-0002-6709-3673
Ryan Gilmour - https://orcid.org/0000-0002-3153-6065

References

1. Böhm, H.-J.; Banner, D.; Bendels, S.; Kansy, M.; Kuhn, B.; Müller, K.; Obst-Sander, U.; Stahl, M. *ChemBioChem* **2004,** *5,* 637–643. doi:10.1002/cbic.200301023
2. Muller, K.; Faeh, C.; Diederich, F. *Science* **2007,** *317,* 1881–1886. doi:10.1126/science.1131943
3. Purser, S.; Moore, P. R.; Swallow, S.; Gouverneur, V. *Chem. Soc. Rev.* **2008,** *37,* 320–330. doi:10.1039/b610213c
4. Liang, T.; Neumann, C. N.; Ritter, T. *Angew. Chem., Int. Ed.* **2013,** *52,* 8214–8264. doi:10.1002/anie.201206566
5. Gillis, E. P.; Eastman, K. J.; Hill, M. D.; Donnelly, D. J.; Meanwell, N. A. *J. Med. Chem.* **2015,** *58,* 8315–8359. doi:10.1021/acs.jmedchem.5b00258
6. Meanwell, N. A. *J. Med. Chem.* **2018,** *61,* 5822–5880. doi:10.1021/acs.jmedchem.7b01788
7. O'Hagan, D. *Chem. Soc. Rev.* **2008,** *37,* 308–319. doi:10.1039/b711844a
8. Zimmer, L. E.; Sparr, C.; Gilmour, R. *Angew. Chem., Int. Ed.* **2011,** *50,* 11860–11871. doi:10.1002/anie.201102027
9. Aufiero, M.; Gilmour, R. *Acc. Chem. Res.* **2018,** *51,* 1701–1710. doi:10.1021/acs.accounts.8b00192
10. Thiehoff, C.; Rey, Y. P.; Gilmour, R. *Isr. J. Chem.* **2017,** *57,* 92–100. doi:10.1002/ijch.201600038
11. O'Hagan, D. *J. Fluorine Chem.* **2010,** *131,* 1071–1081. doi:10.1016/j.jfluchem.2010.03.003
12. Fujiwara, T.; O'Hagan, D. *J. Fluorine Chem.* **2014,** *167,* 16–29. doi:10.1016/j.jfluchem.2014.06.014
13. Harsanyi, A.; Sandford, G. *Green Chem.* **2015,** *17,* 3000–3009. doi:10.1039/c5gc00402k
14. Sandford, G. *J. Fluorine Chem.* **2007,** *128,* 90–104. doi:10.1016/j.jfluchem.2006.10.019
15. Breen, J. R.; Sandford, G.; Yufit, D. S.; Howard, J. A. K.; Fray, J.; Patel, B. *Beilstein J. Org. Chem.* **2011,** *7,* 1048–1054. doi:10.3762/bjoc.7.120
16. Erian, A. W.; Sherif, S. M.; Gaber, H. M. *Molecules* **2003,** *8,* 793–865. doi:10.3390/81100793
17. Dobson, L. S.; Pattison, G. *Chem. Commun.* **2016,** *52,* 11116–11119. doi:10.1039/c6cc05775f
18. O'Hagan, D.; Schaffrath, C.; Cobb, S. L.; Hamilton, J. T. G.; Murphy, C. D. *Nature* **2002,** *416,* 279. doi:10.1038/416279a
19. Dong, C.; Huang, F.; Deng, H.; Schaffrath, C.; Spencer, J. B.; O'Hagan, D.; Naismith, J. H. *Nature* **2004,** *427,* 561–565. doi:10.1038/nature02280
20. Zhu, X.; Robinson, D. A.; McEwan, A. R.; O'Hagan, D.; Naismith, J. H. *J. Am. Chem. Soc.* **2007,** *129,* 14597–14604. doi:10.1021/ja0731569
21. Chan, K. K. J.; O'Hagan, D. *Methods Enzymol.* **2012,** *516,* 219–235. doi:10.1016/b978-0-12-394291-3.00003-4
22. Murphy, C. D.; Schaffrath, C.; O'Hagan, D. *Chemosphere* **2003,** *52,* 455–461. doi:10.1016/s0045-6535(03)00191-7
23. Rozen, S.; Filler, R. *Tetrahedron* **1985,** *41,* 1111–1153. doi:10.1016/s0040-4020(01)96514-7
24. Yamamoto, Y.; Gridnev, I. D.; Patil, N. T.; Jin, T. *Chem. Commun.* **2009,** 5075–5087. doi:10.1039/b909978f
25. Kohlhepp, S. V.; Gulder, T. *Chem. Soc. Rev.* **2016,** *45,* 6270–6288. doi:10.1039/c6cs00361c
26. Molnár, I. G.; Gilmour, R. *J. Am. Chem. Soc.* **2016,** *138,* 5004–5007. doi:10.1021/jacs.6b01183
27. Scheidt, F.; Neufeld, J.; Schäfer, M.; Thiehoff, C.; Gilmour, R. *Org. Lett.* **2018,** *20,* 8073–8076. doi:10.1021/acs.orglett.8b03794
28. Scheidt, F.; Schäfer, M.; Sarie, J. C.; Daniliuc, C. G.; Molloy, J. J.; Gilmour, R. *Angew. Chem., Int. Ed.* **2018,** *57,* 16431–16435. doi:10.1002/anie.201810328
29. Molnár, I. G.; Thiehoff, C.; Holland, M. C.; Gilmour, R. *ACS Catal.* **2016,** *6,* 7167–7173. doi:10.1021/acscatal.6b02155
30. Scheidt, F.; Thiehoff, C.; Yilmaz, G.; Meyer, S.; Daniliuc, C. G.; Kehr, G.; Gilmour, R. *Beilstein J. Org. Chem.* **2018,** *14,* 1021–1027. doi:10.3762/bjoc.14.88
31. Banik, S. M.; Medley, J. W.; Jacobsen, E. N. *J. Am. Chem. Soc.* **2016,** *138,* 5000–5003. doi:10.1021/jacs.6b02391
32. Banik, S. M.; Medley, J. W.; Jacobsen, E. N. *Science* **2016,** *353,* 51–54. doi:10.1126/science.aaf8078
33. Mennie, K. M.; Banik, S. M.; Reichert, E. C.; Jacobsen, E. N. *J. Am. Chem. Soc.* **2018,** *140,* 4797–4802. doi:10.1021/jacs.8b02143
34. Haj, M. K.; Banik, S. M.; Jacobsen, E. N. *Org. Lett.* **2019,** *21,* 4919–4923. doi:10.1021/acs.orglett.9b00938
35. Arnold, A. M.; Ulmer, A.; Gulder, T. *Chem. – Eur. J.* **2016,** *22,* 8728–8739. doi:10.1002/chem.201600449
36. Yoshimura, A.; Zhdankin, V. V. *Chem. Rev.* **2016,** *116,* 3328–3435. doi:10.1021/acs.chemrev.5b00547
37. Lee, J. H.; Choi, S.; Hong, K. B. *Molecules* **2019,** *24,* 2634. doi:10.3390/molecules24142634
38. Sato, S.; Yoshida, M.; Hara, S. *Synthesis* **2005,** 2602–2605. doi:10.1055/s-2005-872105
39. Kitamura, T.; Muta, K.; Muta, K. *J. Org. Chem.* **2014,** *79,* 5842–5846. doi:10.1021/jo500691b
40. Nash, T. J.; Pattison, G. *Eur. J. Org. Chem.* **2015,** 3779–3786. doi:10.1002/ejoc.201500370
41. de Haro, T.; Nevado, C. *Adv. Synth. Catal.* **2010,** *352,* 2767–2772. doi:10.1002/adsc.201000559
42. de Haro, T.; Nevado, C. *Chem. Commun.* **2011,** *47,* 248–249. doi:10.1039/c002679d
43. Hopkinson, M. N.; Giuffredi, G. T.; Gee, A. D.; Gouverneur, V. *Synlett* **2010,** 2737–2742. doi:10.1055/s-0030-1258992
44. Zupan, M.; Iskra, J.; Stavber, S. *J. Org. Chem.* **1995,** *60,* 259–260. doi:10.1021/jo00106a045
45. Stavber, S.; Zupan, M. *Synlett* **1996,** 693–694. doi:10.1055/s-1996-5544
46. Wang, W.; Jasinski, J.; Hammond, G. B.; Xu, B. *Angew. Chem., Int. Ed.* **2010,** *49,* 7247–7252. doi:10.1002/anie.201003593
47. Xu, B.; Wang, W.; Hammond, G. B. *J. Fluorine Chem.* **2011,** *132,* 804–810. doi:10.1016/j.jfluchem.2011.05.006
48. Zeng, X.; Liu, S.; Shi, Z.; Liu, G.; Xu, B. *Angew. Chem., Int. Ed.* **2016,** *55,* 10032–10036. doi:10.1002/anie.201603914
49. Zeng, X.; Lu, Z.; Liu, S.; Hammond, G. B.; Xu, B. *Adv. Synth. Catal.* **2017,** *359,* 4062–4066. doi:10.1002/adsc.201701179
50. Li, F.-H.; Cai, Z.-J.; Yin, L.; Li, J.; Wang, S.-Y.; Ji, S.-J. *Org. Lett.* **2017,** *19,* 1662–1665. doi:10.1021/acs.orglett.7b00453

51. Chen, X.; Martini, S.; Michelet, V. *Adv. Synth. Catal.* **2019,** *361,* 3612–3618. doi:10.1002/adsc.201900268
52. Hummel, S.; Kirsch, S. F. *Beilstein J. Org. Chem.* **2011,** *7,* 847–859. doi:10.3762/bjoc.7.97
53. Sarie, J. C.; Thiehoff, C.; Mudd, R. J.; Daniliuc, C. G.; Kehr, G.; Gilmour, R. *J. Org. Chem.* **2017,** *82,* 11792–11798. doi:10.1021/acs.joc.7b01671
54. Pattison, G. *Beilstein J. Org. Chem.* **2017,** *13,* 2915–2921. doi:10.3762/bjoc.13.284
55. Boaventura, M. A.; Drouin, J.; Conia, J. M. *Synthesis* **1983,** 801–804. doi:10.1055/s-1983-30519
See for the cyclisation of ε-acetylenic carbonyl compounds.
56. Heinen, F.; Engelage, E.; Cramer, C. J.; Huber, S. M. *J. Am. Chem. Soc.* **2020,** *142,* 8633–8640. doi:10.1021/jacs.9b13309
57. Coplen, T. B.; Böhlke, J. K.; De Bièvre, P.; Ding, T.; Holden, N. E.; Hopple, J. A.; Krouse, H. R.; Lamberty, A.; Peiser, H. S.; Révész, K.; Rieder, S. E.; Rosman, K. J. R.; Roth, E.; Taylor, P. D. P.; Vocke, R. D.; Xiao, Y. K. *Pure Appl. Chem.* **2002,** *74,* 1987–2017. doi:10.1351/pac200274101987
58. Diakur, J.; Nakashima, T. T.; Vederas, J. C. *Can. J. Chem.* **1980,** *58,* 1311–1315. doi:10.1139/v80-204
59. Vederas, J. C. *Can. J. Chem.* **1982,** *60,* 1637–1642. doi:10.1139/v82-223
60. Ding, W.; Chai, J.; Wang, C.; Wu, J.; Yoshikai, N. *J. Am. Chem. Soc.* **2020,** *142,* 8619–8624. doi:10.1021/jacs.0c04140
See for the synthesis of β-λ3-iodanyl vinyl ethers.
61. Kutscheroff, M. *Ber. Dtsch. Chem. Ges.* **1881,** *14,* 1540–1542. doi:10.1002/cber.188101401320
62. Asari, N.; Takemoto, Y.; Shinomoto, Y.; Yagyu, T.; Yoshimura, A.; Zhdankin, V. V.; Saito, A. *Asian J. Org. Chem.* **2016,** *5,* 1314–1317. doi:10.1002/ajoc.201600383
63. Takahashi, S.; Umakoshi, Y.; Nakayama, K.; Okada, Y.; Zhdankin, V. V.; Yoshimura, A.; Saito, A. *Adv. Synth. Catal.* **2020**. doi:10.1002/adsc.202000381
See for a study on the fluorocyclization of *N*-propargyl carboxamides which appeared whilst this manuscript was under review.

License and Terms

This is an Open Access article under the terms of the Creative Commons Attribution License (http://creativecommons.org/licenses/by/4.0). Please note that the reuse, redistribution and reproduction in particular requires that the authors and source are credited.

The license is subject to the *Beilstein Journal of Organic Chemistry* terms and conditions: (https://www.beilstein-journals.org/bjoc)

The definitive version of this article is the electronic one which can be found at:
doi:10.3762/bjoc.16.135

BEILSTEIN JOURNAL OF ORGANIC CHEMISTRY

Pauson–Khand reaction of fluorinated compounds

Jorge Escorihuela[‡1], Daniel M. Sedgwick[‡1], Alberto Llobat[1], Mercedes Medio-Simón[1], Pablo Barrio[*2] and Santos Fustero[*1]

Review

Open Access

Address:
[1]Departamento de Química Orgánica, Facultad de Farmacia, Universitat de València, Av. Vicent Andrés Estellés s/n, 46100 Burjassot, Valencia, Spain, and [2]Departmento de Química Orgánica e Inorgánica, Facultad de Química, Universidad de Oviedo, Av. Julián Clavería 8, Campus Universitario de El Cristo, 33006 Oviedo, Spain

Email:
Pablo Barrio[*] - pablobarrio@iniovi.es; Santos Fustero[*] - santos.fustero@uv.es

* Corresponding author ‡ Equal contributors

Keywords:
alkene; alkyne; enyne; fluorine; Pauson–Khand

Beilstein J. Org. Chem. **2020,** *16,* 1662–1682.
doi:10.3762/bjoc.16.138

Received: 24 April 2020
Accepted: 02 July 2020
Published: 14 July 2020

This article is part of the thematic issue "Organo-fluorine chemistry V".

Guest Editor: D. O'Hagan

© 2020 Escorihuela et al.; licensee Beilstein-Institut.
License and terms: see end of document.

Abstract

The Pauson–Khand reaction (PKR) is one of the key methods for the construction of cyclopentenone derivatives, which can in turn undergo diverse chemical transformations to yield more complex biologically active molecules. Despite the increasing availability of fluorinated building blocks and methodologies to incorporate fluorine in compounds with biological interest, there have been few significant advances focused on the fluoro-Pauson–Khand reaction, both in the inter- and intramolecular versions. Furthermore, the use of vinyl fluorides as olefinic counterparts had been completely overlooked. In this review, we collect the advances both on the stoichiometric and catalytic intermolecular and intramolecular fluoro-Pauson–Khand reaction, with special attention to the PKR of enynes containing a fluoride moiety.

Introduction

The prevalence of fluorine-containing molecules in drug-discovery programs is nowadays unquestionable [1-3]. The presence of fluorine atoms or fluorine-containing units at strategic positions in a drug candidate may result in not only an increase in its potency, but also, perhaps more importantly, bring about an enhanced pharmacokinetic profile resulting in a more "drug-like" molecule [4]. Subtle changes in physicochemical properties such as acidity/basicity, lipophilicity, preferred conformation or hydrogen bond forming ability, among others, may result in a dramatic effect in the therapeutic potential of a drug candidate [5,6]. All these properties may be fine-tuned by the selective incorporation of fluorine into the structure of the molecule [7]. In addition to therapeutic use, fluorine-containing molecules have also found key applications in the field of medical diagnosis. Two of the most powerful imaging techniques used nowadays, positron-emission tomography (PET) and magnetic resonance imaging (MRI), are routinely carried out using fluorine-containing organic compounds [8,9]. The

former takes advantage of the superb properties of the ^{18}F-radioisotope as positron emitter ($t_{1/2}$ = 109 min, 97% β^+ emission), while the latter benefits from the excellent performance of the ^{19}F isotope in NMR (100% natural abundance, high sensitivity, lack of endogenous background signal). In addition, the use of fluorinated organic compounds in other key industrial fields is also of paramount importance. The agrochemical and materials industries, together with the aforementioned pharmaceutical industry, are perhaps the fields where organofluorinated compounds have exerted the most profound influence [10-12].

Regarding the development of new synthetic methodologies for the preparation of such molecules, these can be divided in two main categories: fluorination reactions [13-16] and the use of fluorinated building blocks [17]. The difference between them is that while in the former a fluorine atom or a fluorinated unit (e.g., a CF_3 group) is introduced into a non-fluorinated molecule, the latter takes advantage of a substrate that already contains fluorine in order to achieve more complex fluorinated structures. According to these definitions, the chemistry that will be discussed in this review belongs to the fluorinated building blocks category. More specifically, the participation of fluorine-containing olefins and alkynes in the Pauson–Khand cyclization, with a special focus on the intramolecular version using fluorinated enynes, which will be discussed in detail.

The focus of this review is to highlight the efforts made in the field of the Pauson–Khand reaction with fluorinated compounds for the preparation of bicyclic derivatives.

Review

The Pauson–Khand reaction

The Pauson–Khand reaction (PKR) formally consists of a [2 + 2 + 1]-cycloaddition between an alkyne, an olefin and carbon monoxide, resulting in the regioselective formation of a cyclopentenone derivative (Scheme 1) [18-22]. This cobalt-mediated reaction was initially discovered by Pauson and Khand in the early 70s [23-25] and has since become a powerful transformation widely used in the synthesis of polycyclic complex molecules. The intermolecular variant shows a wide alkyne scope, but in terms of the olefin counterpart is limited to the use of ethylene or strained alkenes, such as norbornene and norbornadiene. The high prevalence of five-membered ring systems in natural products, pharmaceuticals and other added-value compounds accounts for the great applicability that this reaction has found [26-32]. Despite the increasing demand of fluorinated compounds and the impressive development of the PKR, the combination of these two fields has been understudied, making it an exciting field of research.

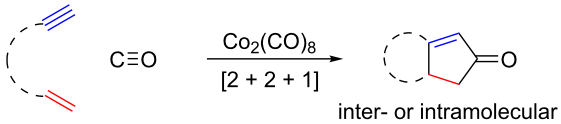

Scheme 1: Schematic representation of the Pauson–Khand reaction.

In order to study the influence on the reaction outcome, a fluorine atom or fluorine-containing group can be installed at either unsaturated counterpart, bound to either the olefin and/or the alkyne (vide infra) (Scheme 2). Of course, in the intramolecular version, the fluorine atom or fluorinated group can also form a part of the linker. The reaction yields are dependent on the degree of substitution, bulkiness, and electronic effects of the substituents of both the alkyne and alkene moieties. In general, electron-deficient alkynes are poor substrates for the PKR as they are deactivated in the cobalt-complexation step, and the highest yields are usually obtained with terminal alkynes. The scenario is similar in the case of fluorinated substrates, with the intramolecular version being much more developed than the intermolecular one.

The regio- and stereochemistry of this transformation is predictable, in most cases. Since this is an important issue throughout the review, a concise remark about the mechanism of this transformation is outlined below (Scheme 3). This mechanism was proposed by Magnus over 30 years ago and is still valid nowadays [33], although only the first intermediate (**I**) has been isolated and characterized [34]. However, contributions by Nakamura, Pericàs, and others support the initial proposal both

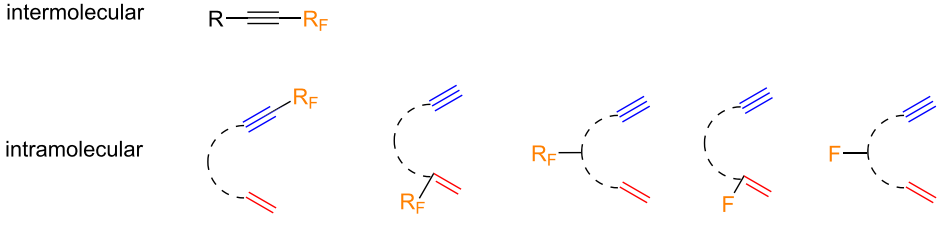

Scheme 2: Substrates included in this review.

experimentally and theoretically [35,36]. Firstly, two coordination vacancies are freed after the extrusion of two carbon monoxide ligands from the starting cobalt species, allowing the alkyne group to bind to the cobalt metal centers. The subsequent coordination of the olefin counterpart requires the extrusion of a third carbon monoxide ligand, leading to pentacarbonyl complex **II**. This highly endotermic process is the rate-limiting step and long reaction times are generally associated to this. However, the reaction can be accelerated in conditions that facilitate the dissociation of CO ligands such as heating, microwave irradiation [37,38], visible light, or ultrasonication [39]. Alternatively, mild oxidizing additives such as amine oxides, aminophosphines, phosphine oxides, and sulfoxides may be used as promoters to facilitate the dissociation step, by oxidatively removing one of the CO ligands in form of CO_2 [40]. The most common oxidants are *N*-morpholine *N*-oxide (NMO), trimethylamine *N*-oxide (TMANO), and dimethyl sulfoxide (DMSO). Once a new coordination vacancy has been opened on one of the cobalt centers, coordination of the olefin sets the stage for the subsequent C–C bond forming steps. The olefin is inserted into the less hindered Co–C bond, determining both the regio- and stereochemical outcome of the overall process. A carbon monoxide ligand then undergoes migratory insertion into one of the Co–C bonds in cobaltacycle **V**, followed by reductive elimination to release the final product (Scheme 3).

As mentioned above, the regiochemistry of this transformation is, in most cases, predictable for unsymmetrical alkynes (things are more complex regarding the olefin). Generally, the most sterically encumbered substituent of the alkyne occupies the proximal position in the enone system. This is dictated by the migratory insertion of the olefin into the most accessible Co–C bond (Scheme 3). This trend is strictly followed by terminal alkynes, for which exclusive formation of the α-substituted enone is observed, while mixtures are usually obtained with internal dissymmetric alkynes, although the major product follows the aforementioned trend [41]. On the other hand, for alkynes bearing groups of comparable steric demand at both ends of the alkyne, electronic effects come into play. Here, the more electron-rich substituent occupies the α position, and the more electron-poor the β position (Scheme 4). This selectivity could be rationalized by the insertion of the olefin into the weakest Co–C bond. These electronic effects have been shown to be less important than steric ones, and are often overcome by the latter. Regarding the stereochemistry, *exo*-products are almost exclusively obtained for norbornene and norbornadiene.

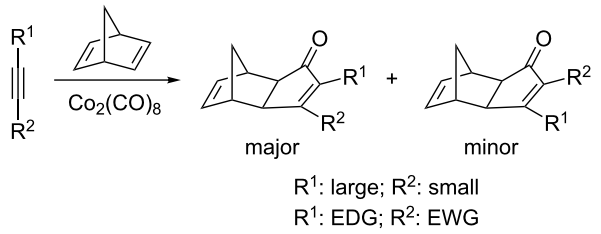

Scheme 4: Regioselectivity of the PKR.

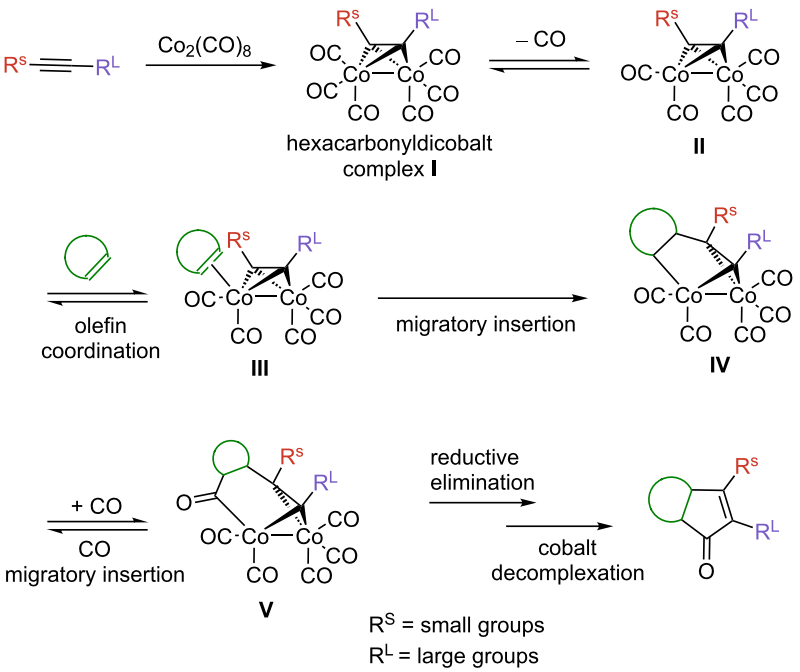

Scheme 3: Commonly accepted mechanism for the Pauson–Khand reaction.

Many deviations from the classic reaction conditions have been described, including the use of metals other than cobalt (such as rhodium, iridium, titanium, ruthenium, nickel, and palladium), or the use of CO surrogates such as aldehydes, alcohols and formates. Recently, its utility in flow chemistry has also been described [42].

Intramolecular Pauson–Khand reactions of fluorine-containing compounds

The utility of the Pauson–Khand reaction in the preparation of polycyclic compounds bearing both nitrogenated and cyclopentenone rings, two ubiquitous domains in drugs and natural products, has been reported in various contributions using 1,*n*-enynes, particularly 4-aza-1,7-enynes as starting materials [43-45]. However, the synthesis of fluorinated 1,*n*-enynes as well as the corresponding Pauson–Khand adducts has, until recently, scarcely been described in the literature. The intramolecular version of this reaction has recently gained recognition since it facilitates the synthesis of cyclopentenone-fused ring systems, which tend to be difficult to construct. The Pauson–Khand reaction has also been used as a key step in the synthesis of a number of biologically-relevant compounds, including fluorine-containing piperidine-fused cycles. Of course, where the fluorinated group is positioned in the final compound depends on whether it is attached to the alkene or alkyne counterpart of the substrate (Scheme 5).

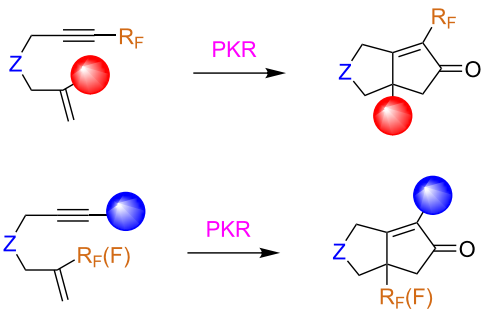

Scheme 5: Variability at the acetylenic and olefinic counterpart.

Regarding the intramolecular PKR of fluorinated enynes, only a few examples have been described. The first example was reported in 2001 by Ishizaki and co-workers [46]. In this study, a wide variety of 1,6-enynes bearing fluorine atoms or fluorine-containing groups at the alkenyl or alkynyl positions were synthesized and evaluated as substrates in the intramolecular PKR with dicobalt octacarbonyl [$Co_2(CO)_8$] in CH_2Cl_2 and promoted by NMO. In general, the presence of fluorinated groups on the alkenyl moiety of the 1,6-enyne resulted in low yields (lower than 35%) of the corresponding cyclized products, due to the poor reactivity of the fluorinated olefin (Scheme 6). For example, difluoroalkene-containing compound **1** decomposed and no cyclized product was formed. In this NMO-promoted PKR, monofluoroolefinic enyne **2** afforded the defluorinated cyclopentenone **7** in 37% yield. Similarly, trifluoromethyl-substituted olefin **3** also lost the chlorine atom upon cyclization to give **8** as a single diastereoisomer, albeit in a low 14% yield. The reaction of trifluoromethyl-substituted allylic alcohols **4** and **5** afforded the corresponding cyclized products **9** and **10** (31% and 34% yield, respectively) as inseparable mixtures of diastereoisomers. Finally, 1,6-enyne **6**, bearing a 4-fluorophenyl group on the olefin, stereoselectively produced *trans*-oriented arylcyclopentenone **11** in 23% yield.

When investigating the intramolecular PKR of enynes bearing fluorine groups on alkynyl moiety (**12**, **14**, **16**), several trends could be observed (Scheme 7). Firstly, fluoroaromatic enynes **12a–c** afforded the corresponding cyclized products **13a–c** in low yields (14–42%). However, no cyclized product was observed when using the trifluoromethyl ketone derivative **12d**.

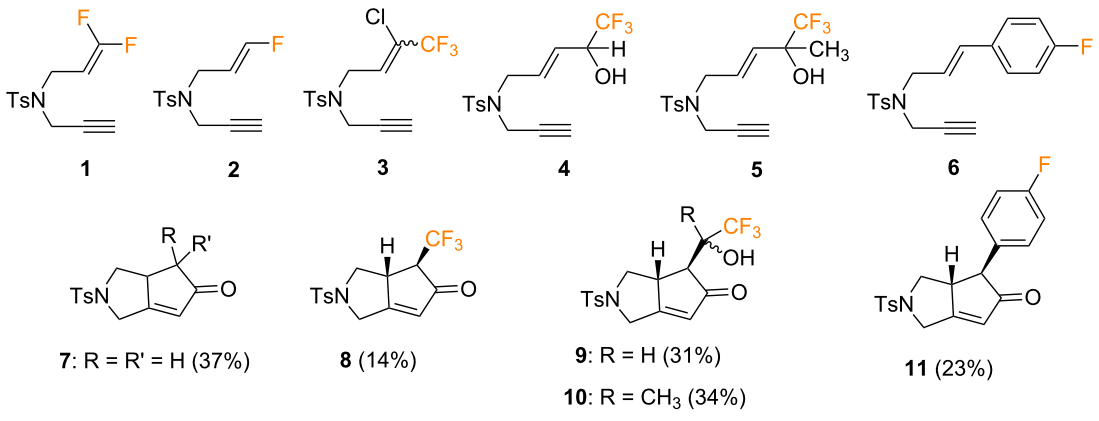

Scheme 6: Pauson–Khand reaction of fluoroolefinic enynes reported by the group of Ishizaki [46].

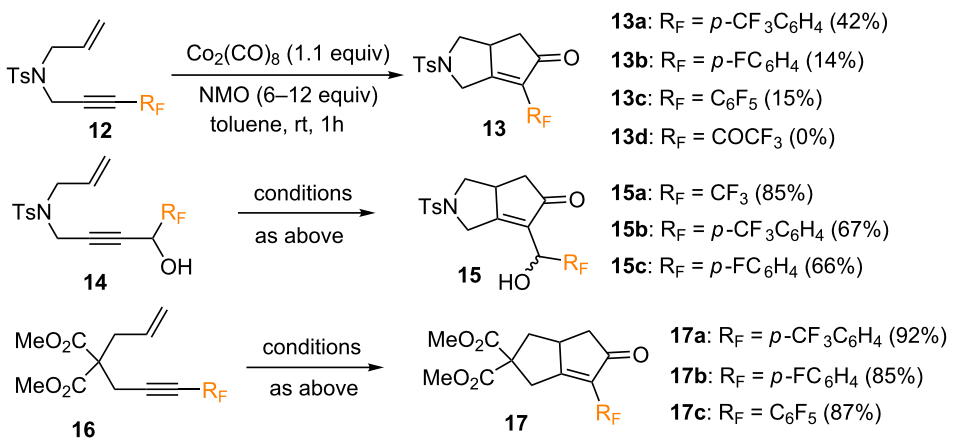

Scheme 7: PKR of enynes bearing fluorinated groups on the alkynyl moiety, reported by the group of Ishizaki [46]. Reaction conditions: i) $Co(CO)_8$ (1.1 equiv), toluene, rt, 1 h; ii) NMO (6–12 equiv), rt, 1 h.

Secondly, PKR with enynes **14** containing fluorinated propargyl alcohol groups yielded diastereoisomeric mixtures of pyrrolidine ring-fused cyclopentenones **15** in good yields (67–85%) but low diastereoselectivities. Finally, the reaction of dimethyl malonate-derived fluoroaromatic enynes **16** afforded the corresponding cyclopentenone products **17** in higher yields (85–92%). Thus, the reaction of enynes bearing fluorinated groups attached to the alkyne moiety was found to afford the corresponding cyclized products in moderate to high yields, except for those bearing marked electron withdrawing groups (Scheme 7).

In 2005, Billard and co-workers reported the PKR of α-trifluoromethylated homoallylamine derivatives (Scheme 8) [47]. Both 1,7-enynes **18a** and **18b** (n = 1) underwent PKR in the presence of 1 equiv of $Co_2(CO)_8$ and 10 equiv of NMO, yielding bicyclic derivatives **19** in moderate yields and high diastereoselectivity (de > 95%). The observed diastereoselectivity was rationalized considering two transition states of the PKR, and assuming the CF_3 group occupies an axial position due to the steric and electrostatic repulsions that occur in the equatorial position. Consequently, in the most favorable transition state there is no steric hindrance between the CF_3 group and the ethylenic hydrogen, leading to the observed diastereoisomer. On the other hand, the use of 1,9-enyne **18c** (n = 3) did not afford the corresponding bicyclic compound since the double and triple bonds are too distant.

In a following paper by Billard and co-workers, the PKR of oxygen-containing 1,7-enynes was assayed, affording trifluoromethylated oxygenated bicyclic enones (Scheme 9) [48]. Under classical stoichiometric conditions (reaction with $Co_2(CO)_8$ fol-

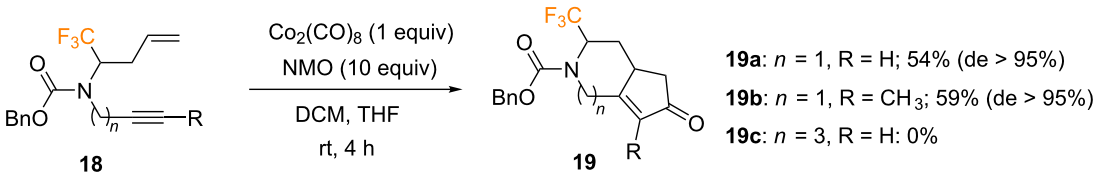

Scheme 8: Intramolecular PKR of 1,7-enynes reported by the group of Billard [47].

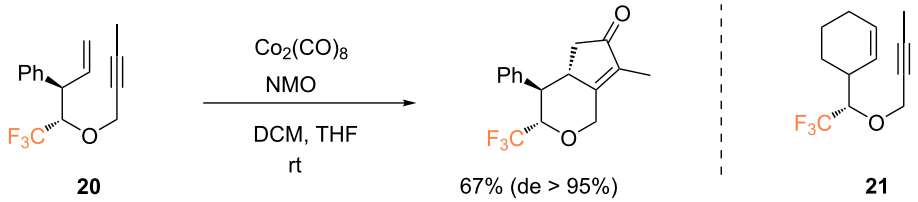

Scheme 9: Intramolecular PKR of 1,7-enynes reported by the group of Billard [48].

lowed by the addition of NMO), and starting from the pure *anti* diastereoisomer of 1,7-enyne **20**, the expected bicyclic enone was obtained in good yield and high diastereoselectivity (de > 95%). An attempt to extend the PKR to the formation of a fused tricyclic structure, starting from 1,7-enyne **21**, was unsuccessful and no tricyclic product was formed.

Bonnet-Delpon and co-workers reported the one-pot synthesis of several CF_3-containing *N*-tethered amines in good yields (54–86% over 2 steps) [49]. These products were subjected to metathesis reactions in the presence of Grubbs catalyst affording the corresponding CF_3-containing dehydropiperidine derivatives in excellent yields. Additionally, enynes **22** and **23** were evaluated as substrates in the intramolecular PKR, yielding the corresponding CF_3-containing heterobicyclic derivatives in 68% (85:15 ratio of *trans*/*cis* stereoisomers) and 80% yield (18:82 ratio of *trans*/*cis* stereoisomers), respectively (Scheme 10).

Ichikawa and co-workers described an attractive route to synthesize pyrrolidine ring-fused fluorinated cyclopentenone analogs via intramolecular PKR starting from 2-bromo-3,3,3-trifluoroprop-1-ene [50,51]. To this end, *N*-propargyl-*N*-[2-(trifluoromethyl)allyl]amides **24** were treated with dicobalt octacarbonyl to afford the cobalt alkyne complex, which was then heated in CH_3CN. Under these conditions, trifluoromethylated cyclopentenone **25a** was obtained in high yield (81%) and diastereoselectivity (*anti*/*syn* = 94:6) (Scheme 11). The cyclization of internal alkyne substrate **24b** yielded pyrrolidine ring-fused cyclopentenone **25b** in similar yield but lower diastereoselectivity. Finally, *N*-propargyl-*N*-[2-(trifluoromethyl)allyl] ether **24d**, containing an ether linkage instead of the aforementioned sulfonamide linkage, gave furan ring-fused cyclopentenone **25d** in both lower yield (53%) and lower diastereoselectivity.

A catalytic PKR of fluorinated 1,7-enyne amides **26** using catalytic amounts of $[Rh(COD)Cl]_2$ was reported in 2008 by Hammond and co-workers [52]. The authors concluded that the reaction was highly sensitive to experimental parameters such as solvent, concentration, temperature, catalyst and silver salt. Under standard reaction conditions, no reaction was observed in the absence of a silver salt, and the best results were obtained in the presence of AgOTf (20 mol %), giving the corresponding *gem*-difluorinated bicyclic lactam **27** in 43% yield (Scheme 12). This reaction was limited to unsubstituted alkynes, as the PKR did not occur with a phenyl-substituted alkyne. Unfortunately, no asymmetric induction was observed.

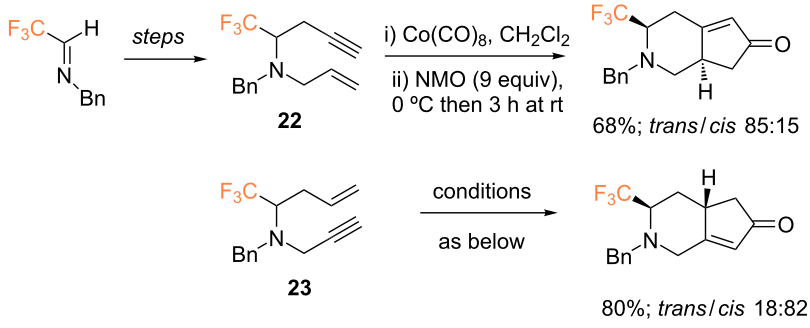

Scheme 10: Intramolecular PKR of 1,7-enynes by the group of Bonnet-Delpon [49]. Reaction conditions: i) $Co(CO)_8$ (1.2 equiv), CH_2Cl_2, 30 min; ii) NMO (9 equiv), 0 °C then 3 h at rt.

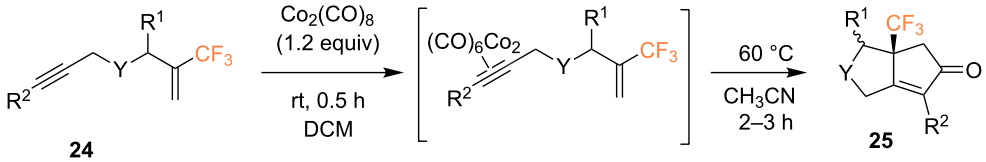

25a: Y = NTs; R^1 = Ph; R^2 = H; 81%; *anti*/*syn* 94:6
25b: Y = NTs; R^1 = Ph; R^2 = Et; 85%; *anti*/*syn* 83:17
25c: Y = NTs; R^1 = Pr; R^2 = H; 71%; *anti*/*syn* 86:14
25d: Y = O; R^1 = Ph; R^2 = H; 53%; *anti*/*syn* 64:36

Scheme 11: Intramolecular PKR of 1,6-enynes reported by the group of Ichikawa [50].

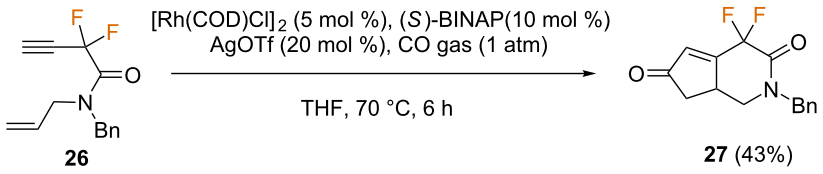

Scheme 12: Intramolecular Rh(I)-catalyzed PKR reported by the group of Hammond [52].

In 2011, Osipov and co-workers investigated the cobalt-mediated PKR of allenynes **28** in order to synthesize trifluoromethylated nitrogen- and sulfur-based bicyclic compounds (Scheme 13) [53]. Using this methodology, the corresponding cyclopentenones **29** were isolated in generally good yields, except for sulfur-containing derivative **29c**, due to the oxidation of the sulfide under the reaction conditions. In contrast, the phosphorus analog **29d** was obtained in 45% yield, which could be explained by favorable electronic and steric effects of the phosphonate group.

In the same work, the authors also evaluated the PKR of CF_3-substituted enynes **30**. In this case, bicyclic products **31** were formed as mixtures of separable diastereoisomers, which could be isolated in higher yields than the products of the corresponding reaction with allenynes (Scheme 14).

In 2012, Konno and co-workers studied the intramolecular PKR using fluorine-containing 1,6-enynes **32** (Scheme 15) [54]. The PKR of fluorinated propargyl allyl ether **32a** afforded the corresponding *cis* bicyclic product **33a** in moderate yield and high diastereoselectivity (dr > 20:1). Other fluorinated allyl propargyl ethers **32b–d** afforded the corresponding bicyclic PK-adducts **33** in moderate chemical yields but with high *cis*-selectivity. On the other hand, spirocyclic derivative **33e** was formed in a significantly lower yield. Surprisingly, a subtle change of the fluoroalkyl group from a CF_3 group to a CHF_2 group completely inhibited the reaction.

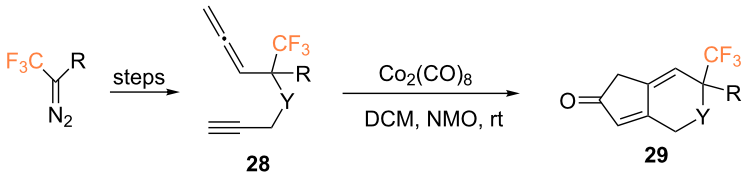

29a: Y = NMe; R = CO_2Me; 52%
29b: Y = NMe; R = $P(O)(OEt)_2$; 48%
29c: Y = S; R = CO_2Me; 5%
29d: Y = S; R = $P(O)(OEt)_2$; 45%

Scheme 13: Intramolecular PKR of allenynes reported by the group of Osipov [53].

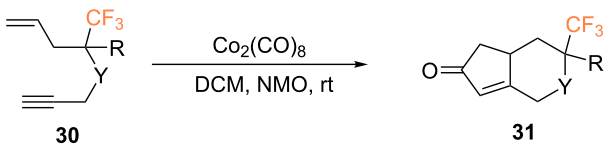

31a: Y = NMe; R = CO_2Me; 68%; *syn/anti* 83:17
31b: Y = NMe; R = $P(O)(OEt)_2$; 81%; *syn/anti* 35:65
31c: Y = S; R = CO_2Me; 40%; *syn/anti* 62:38
31d: Y = S; R = $P(O)(OEt)_2$; 59%; *syn/anti* 75:25

Scheme 14: Intramolecular PKR of 1,7-enynes reported by the group of Osipov [53].

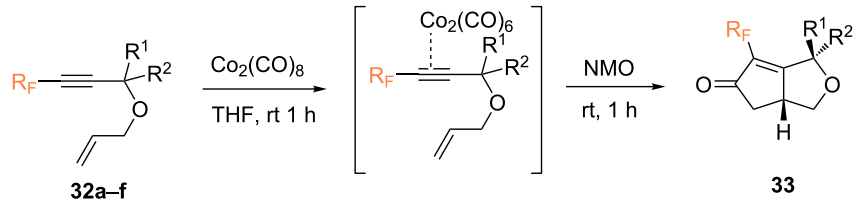

33a: $R_F = CF_3$; R^1 = *n*-Hex; R^2 = H; 50%
33b: $R_F = CF_3$; $R^1 = PhCH_2CH_2$; R^2 = H; 45%
33c: $R_F = CF_3$; R^1 = *c*-Hex; R^2 = H; 35%
33d: $R_F = CF_3$; $R^1 = Et_2CH$; R^2 = H; 51%
33e: $R_F = CF_3$; R^1,R^2 = -$(CH_2)_5$-; 28%
33f: $R_F = CHF_2$; R^1 = *n*-Hex; R^2 = H; 0%

Scheme 15: Intramolecular PKR of fluorine-containing 1,6-enynes reported by the Konno group [54].

Within the frame of a broader study, our group reported a single example of an intramolecular PKR using an Ellman's imine-derived CF_3-containing enyne, bearing the trifluoromethylethynyl group at the *ortho* position (Scheme 16) [55]. One of the key steps in the preparation of the starting 1,*n*-enynes was a highly diastereoselective allylation reaction of chiral Ellman's sulfinylimines. Based on this strategy, chiral 1,7-enynes **34** were prepared in three steps from sulfinylimines derived of *o*-iodobenzaldehydes. A variety of fluorinated compounds bearing fluorine or fluoroalkyl groups attached to the aryl moieties were efficiently prepared (Scheme 15). In this report, the suitability of enynes bearing CF_3-substituted alkyne moieties ($R = CF_3$) to participate in intramolecular PK reactions was also demonstrated. Furthermore, several other substrates bearing fluorine at different positions were included (Scheme 16). The process took place with moderate to high chemical yields and diastereoselectivities. This transformation can be performed on a multigram scale, and is characterized by a broad substrate scope, functional group compatibility, and high chemo- and diastereoselectivity.

Martínez-Solorio and co-workers reported an intramolecular PKR of Si–O tethered 1,7-enynes **35**, affording cyclopentaoxasilinones **36** with high diastereoselectivity [56]. In contrast to

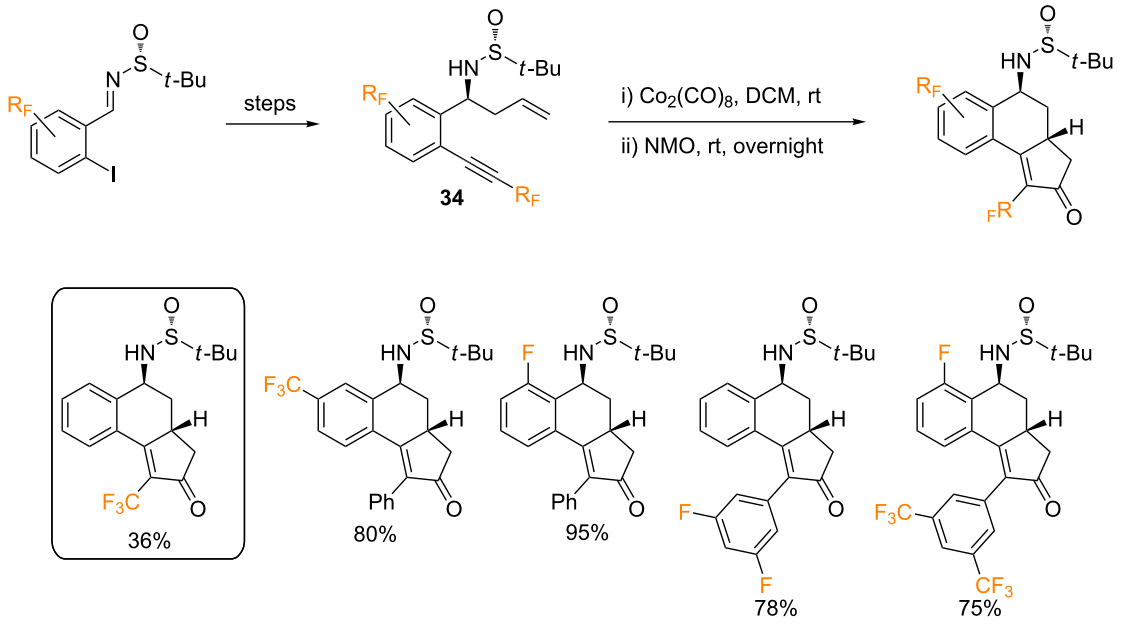

Scheme 16: Diastereoselective PKR with enantioenriched fluorinated enynes **34** [55].

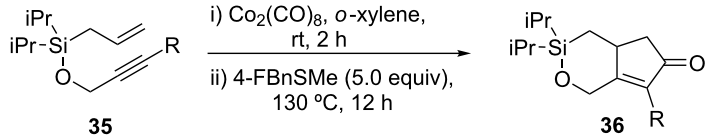

36a: R = CH_3; 81% **36e**: R = *p*-$MeOC_6H_4$; 65%
36b: R = H; 25% **36f**: R = *p*-NCC_6H_4; 72%
36c: R = iPr; 74% **36g**: R = *p*-$MeO_2CC_6H_4$; 76%
36d: R = Ph; 79% **36h**: R = *p*-$CF_3C_6H_4$; 77%

Scheme 17: Intramolecular PKR reported by the group of Martinez-Solorio [56].

previous silicon-based tethers, which reacted in low yields and resulted in unexpected byproducts, this transformation could be performed on a multigram scale and showed a wide substrate scope and functional group compatibility, as well as high diastereoselectivity [57,58]. In this work, Si–O tethered 1,7-enynes underwent the PKR after treatment with 1.05 equiv of $Co_2(CO)_8$ using 4-fluorobenzyl(methyl)sulfide (4-FBnSMe) as an additive, which is commercially available and can be easily recovered by flash chromatography. Under the aforementioned conditions, cyclopentaoxasilinone **36a** was isolated in 81% yield. A systematic study of the scope showed that unsubstituted enyne **35b** only afforded the desired product in 25% yield. In contrast, isopropyl and phenyl substituted enynes yielded cyclopentaoxasilinone **36c**,**d** in 74 and 79% yield, respectively. Furthermore, electron-withdrawing *para*-substituted arenes were obtained in good yields and demonstrate excellent functional group compatibility; MeO– (**36e**, 65%), −CN (**36f**, 72%), $-CO_2Me$ (**36g**, 76%) and fluorinated groups such as *p*-$CF_3C_6H_4$ (**36h**, 77%) (Scheme 17).

Concerning the intramolecular PKR with fluorine atoms or fluorinated groups at the vinylic position, very few examples have been described to date. In this context, our group recently explored the reactivity of 1,*n*-enynes bearing a vinyl fluoride moiety as the olefin counterpart in the intramolecular PKR [59] (Scheme 18).

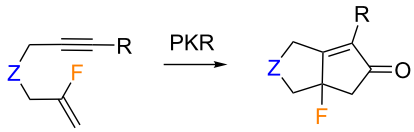

Scheme 18: Fluorine substitution at the olefinic counterpart.

The study of the behavior of this kind of compounds in the PK reaction started with fluorinated enynes derived from malonates and those containing heteroatoms as linkers. The synthesis of the starting enynes **37** was accomplished following various approaches (Scheme 19).

The first of these (via a) was based on a report by Hammond and co-workers, in which they detailed the Markovnikov hydrofluorination of alkynes using HF·DMPU coupled with a gold

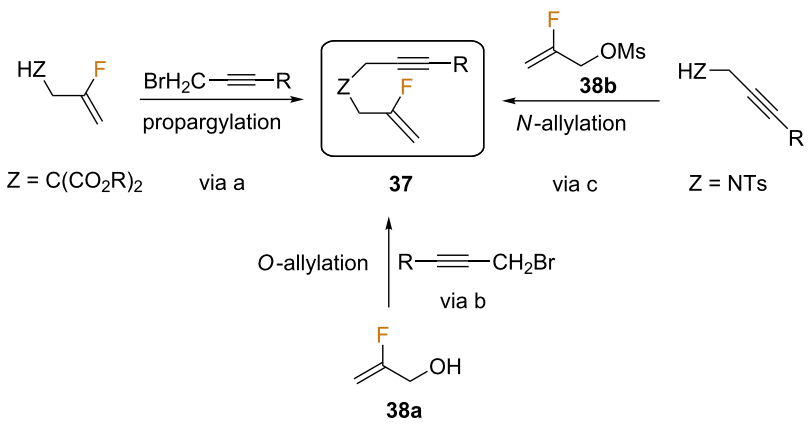

Scheme 19: Synthesis of fluorinated enynes **37** [59].

catalyst [60]. Accordingly, the appropriate propargylmalonate derivatives were fluorinated to give fluoroalkene intermediates, which were then converted into malonate-based enynes **37** (Z = CO_2R) through a simple propargylation procedure. In addition, the fluoroallyl alcohol **38a** was employed as a starting material to obtain the corresponding propargyl ethers **37** (Z = O) by Williamson's synthesis using propargyl bromides in moderate yields (via b). Activation of the fluoroallyl alcohol by conversion into the corresponding mesylate **38b** proved sufficient for the synthesis of *N*-tethered substrates **37** (Z = NTs), through simple nucleophilic substitution (via c).

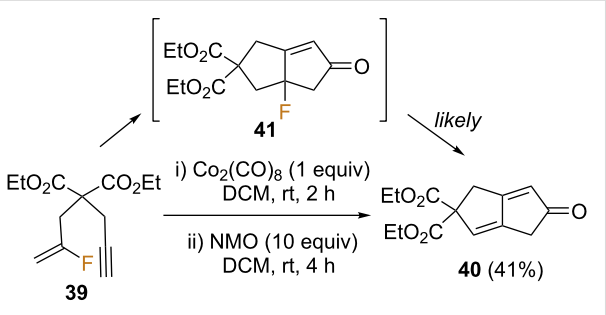

Scheme 20: Fluorine-containing substrates in PKR [59].

It is noteworthy that under standard PK reaction conditions, fluoroenyne **39** evolves to diene **40**. The formation of compound **40** is possible by elimination of HF from the PK product **41**, meaning that the fluoro-PKR does initially take place and that the desired product **41** could be isolated by avoiding the subsequent elimination reaction. This hypothesis was confirmed when the less basic DMSO was used as the promoter instead of NMO, allowing the successful isolation of **41** (Scheme 20) [59].

Under the optimized conditions, using stoichiometric $Co_2(CO)_8$ and DMSO as the promoter, the process worked well and moderate to good yields were obtained for derivatives **42** bearing aryl substituents at the propargyl moiety, regardless of their electronic nature (Scheme 21). Alkyl-substituted derivatives proved to be similarly successful substrates; however, the TMS-substituted derivative was obtained in a significantly lower yield. In terms of linkers, heteroatoms were well-tolerated, although the use of malononitrile resulted exclusively in the elim-

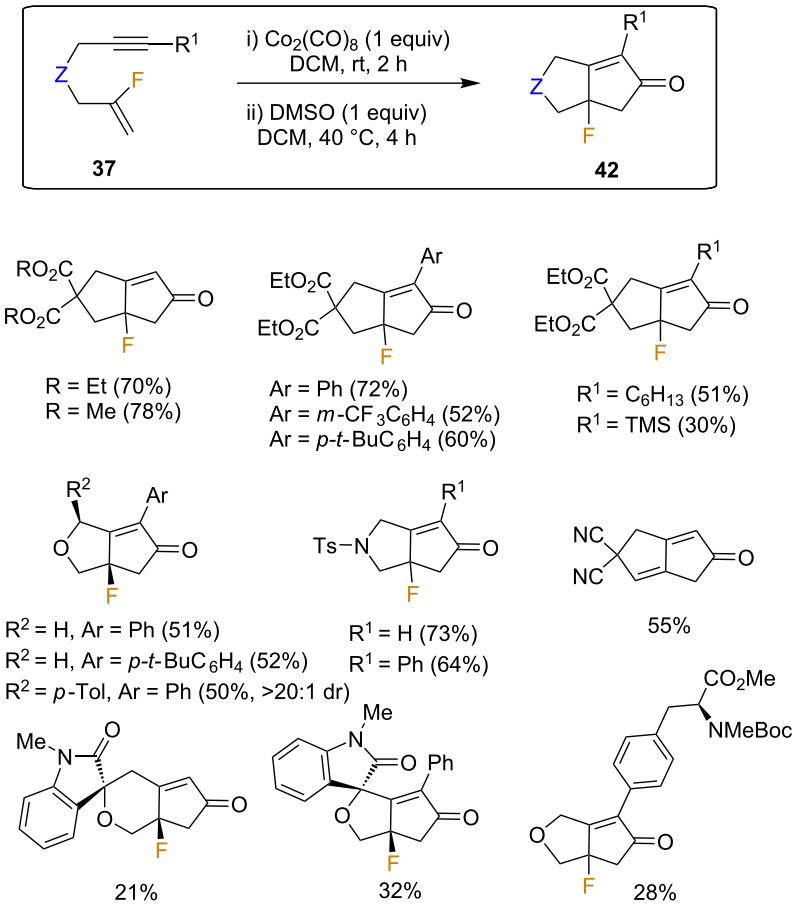

Scheme 21: Pauson Khand reaction for fluorinated enynes by the Fustero group: scope and limitations [59].

ination product despite testing a variety of reaction conditions. More complex biorelevant examples such as isatin derivatives were also suitable substrates, affording the corresponding spirocyclic derivatives, albeit in low yields (Scheme 21) [59]. Unfortunately, thioether and sulfone-based linkers were unsuitable in this reaction, and the starting materials were recovered in all cases.

As a comparison, the same authors also explored the reactivity of the corresponding chloro- and bromoenynes **43** as olefinic counterparts for the intramolecular PKR (Scheme 22) [59].

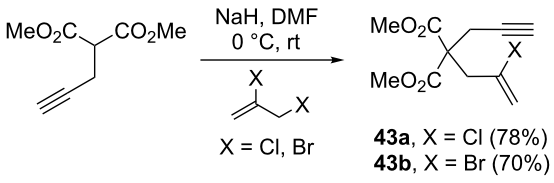

Scheme 22: Synthesis of chloro and bromo analogues [59].

In these cases, the corresponding halogenated PKR adducts **44** could not be detected in the crude reaction mixtures. Instead, the major isolated species was dimer **45**. However, the fact that **45** bears the cyclopentenone core suggests that the desired PKR does indeed take place, albeit as an intermediate before a secondary transformation to form the final dimer (Scheme 23) [59]. The authors rationalized the formation of **45** by considering that the inherent weakening of the C—X bond going down the halogen series may favor the generation of radical **A** with chloride and bromide derivatives, especially given the tertiary position of the halide and the stoichiometric quantities of cobalt present in the reaction mixture.

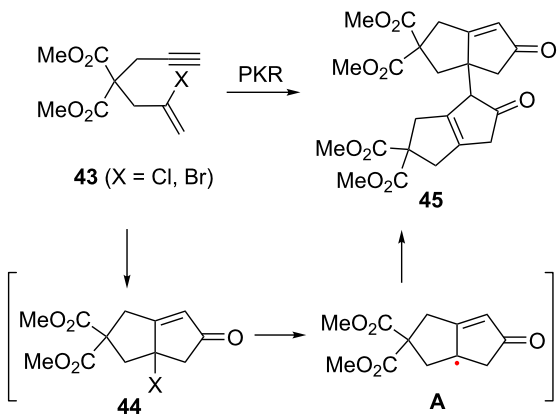

Scheme 23: Dimerization pathway [59].

The same group also studied the intramolecular PKR of chiral fluorine-containing *N*-tethered 1,7-enynes **48** for the stereoselective construction of enantioenriched bicyclic alkaloid analogues **49**, containing a fluorine atom in the bridge position [61]. For this purpose, 1,7-enynes **48** were prepared from Ellman's *tert*-butane sulfinylimines, followed by a diastereoselective addition of propargylmagnesium bromide to obtain a variety of sulfinyl amide intermediates **46** in good yields and high diastereoselectivities. Subsequent oxidation to the corresponding sulfonamides **47**, followed by the introduction of the fluoroallyl group via *N*-alkylation with previously described mesylate **38** provided fluorinated enynes **48** (Scheme 24).

The enantioenriched starting materials **48** were then evaluated in the Co-mediated PKR to yield the bicyclic products **49** in moderate to good yields and excellent diastereoselectivities (dr > 20:1) (Scheme 25). The substrate scope revealed that the reaction was tolerant of a wide range of substituents at the

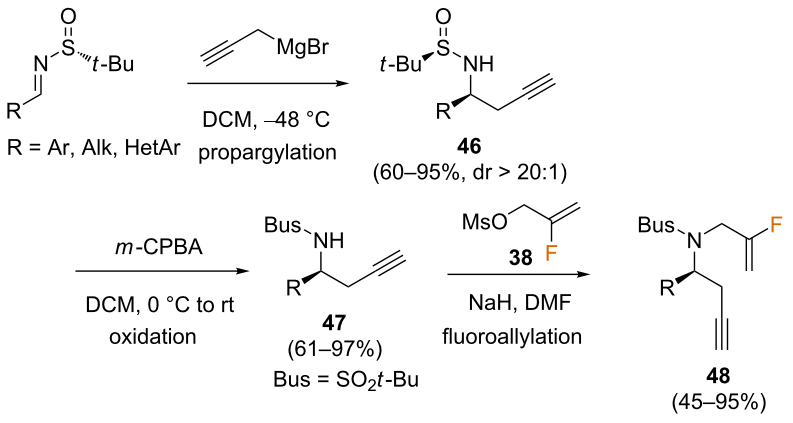

Scheme 24: Synthesis of fluorine-containing *N*-tethered 1,7-enynes [61].

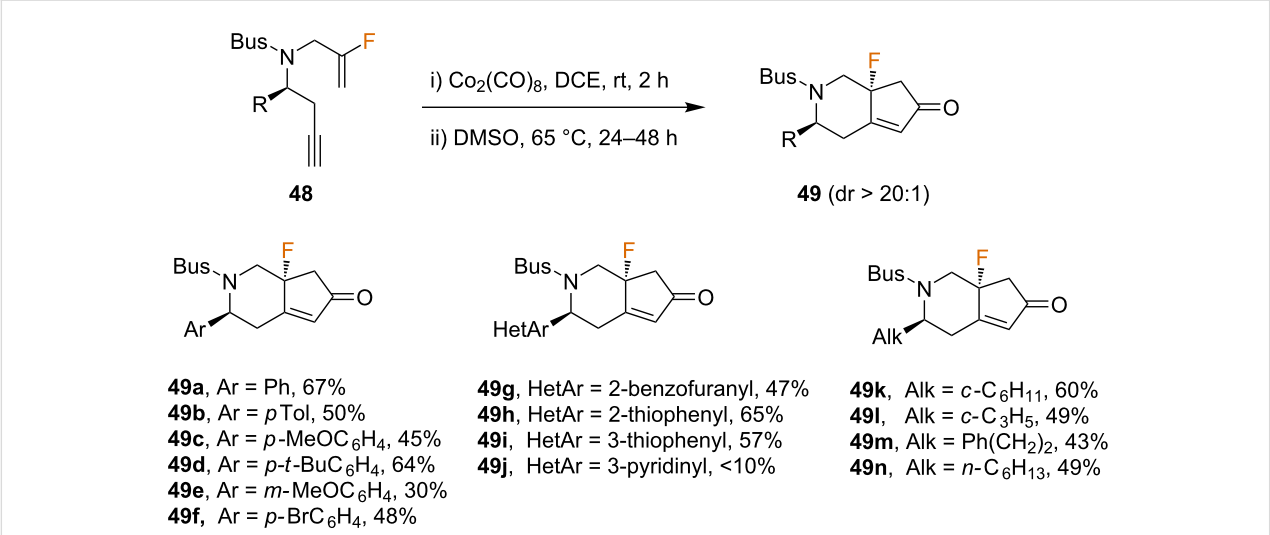

Scheme 25: Intramolecular PKR of chiral *N*-tethered fluorinated 1,7-enynes [61].

stereogenic center, such as heteroaromatic, aromatic, and aliphatic substituents (both linear and cyclic). Regarding aromatic substituents, electron-neutral and electron-rich rings with several substitution patterns performed well. However, pyridine-based **48j** resulted in a low yield. Noteworthy, the PKR of chiral enynes **48** led to a bridgehead quaternary stereocenter containing a C–F bond in a single step. Besides the intrinsic difficulty in generating quaternary stereocenters, the goal achieved is even more significant given the attention that the asymmetric introduction of fluorine at sp^3 carbon centers has received in recent years [62,63]. A gram-scale synthesis was also successfully performed in five steps starting from the corresponding aldehyde in a 41% global yield.

Bicyclic product **49a** underwent diastereoselective (dr > 20:1) hydrogenation using palladium over activated charcoal under an atmosphere of hydrogen to afford saturated derivative **50** (Scheme 26). On the other hand, the *tert*-butanesulfonyl group could be removed through treatment of **49a** with trifluoromethanesulfonic acid in the presence of anisole to form **51**.

In a recent report, Fustero and co-workers synthesized a series of *N*-tethered 1,7-enynes **53** bearing fluorinated substituents starting from fluorinated *tert*-butanesulfinyl imines **52** (Scheme 27), which were later evaluated in the cobalt-mediated PKR [64].

Scheme 27: Asymmetric synthesis the fluorinated enynes **53**.

The chiral enynes were treated with a stoichiometric amount of $Co_2(CO)_8$ in CH_2Cl_2 affording the corresponding cobalt complexes that, upon addition of an excess of NMO, underwent an efficient intramolecular PKR to afford the corresponding bicyclic cyclopentenones **54** as single diastereoisomers (Scheme 28). In general, yields were moderate to good, and high diastereoselectivities were observed in almost all cases.

The PKR tolerated both mono- and disubstituted olefins well, but when a trisubstituted olefin was assayed in the PKR, the initial enyne was recovered, in agreement with previous prece-

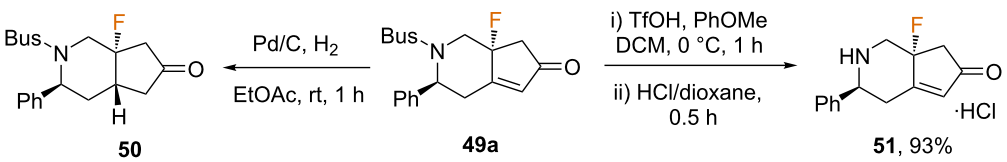

Scheme 26: Examples of further modifications to the Pauson–Khand adducts [61].

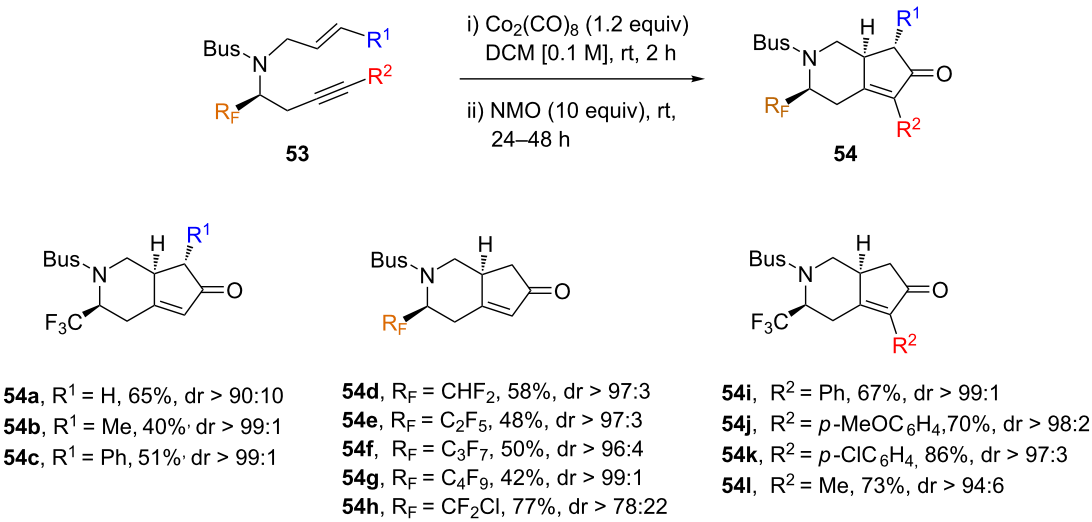

Scheme 28: Intramolecular PKR of chiral *N*-tethered 1,7-enynes **53** [64].

dents describing that trisubstituted alkenes are very unreactive substrates in this kind of process (Scheme 28) [65]. The influence of the introduction a vinyl fluoride moiety on the PKR was also investigated (Scheme 29). The resulting cyclopentenones **57** were obtained in a lower yield (52%) but high diastereoselectivity, similar to those previously reported [59,61].

The authors also explored the PKR in a catalytic version based on a biphasic system of ethylene glycol/toluene, which generally enhanced both yields and stereoselectivities, as well as simplifying purification of the products [66]. This methodology (7 mol % catalyst, atmospheric CO pressure, and 15% v/v of ethylene glycol in toluene) was shown to be suitable for substrates bearing differing fluorinated groups, as well as one example with a phenyl-substituted alkyne, giving rise to products **54** in good yields and diastereoselectivities (Scheme 30).

Intermolecular Pauson–Khand reactions of fluorine-containing compounds

In contrast to the previously discussed intramolecular PKR of fluorinated enynes, the study of intermolecular PKR reactions is far scarcer, and is limited by the poor reactivity and selectivity

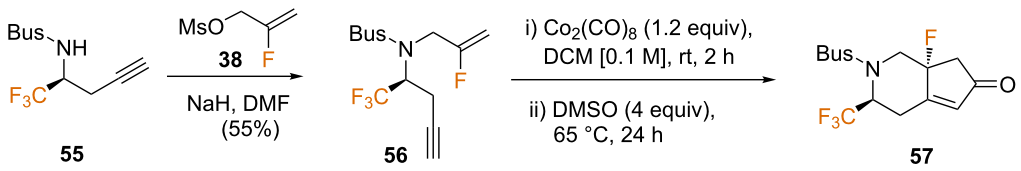

Scheme 29: Intramolecular PKR of chiral *N*-tethered 1,7-enyne bearing a vinyl fluoride [64].

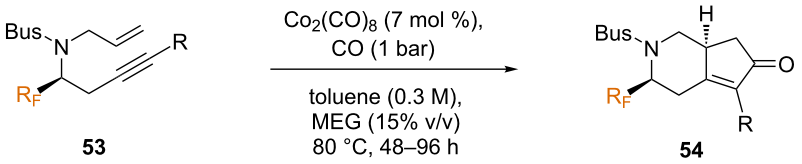

Scheme 30: Catalytic intramolecular PKR of chiral *N*-tethered 1,7-enynes [64].

of simple alkenes. In this regard, most examples have been restricted to the use of ethylene or strained alkenes such as cyclopropene, norbornene, norbornadiene, (*E*)-cyclooctene, or bicyclo[3.2.0]hept-6-ene [67-69]. The first example of an intermolecular version of fluorinated compounds was reported by Riera, Fustero and co-workers in 2010 [70]. In this seminal study, four model fluorinated alkyne precursors **58** were synthesized (Scheme 31).

With this small family of fluorinated alkynes, the authors studied the PKR using norbonadiene as the olefin partner under thermal conditions using a stoichiometric amount of $Co_2(CO)_8$. Products **59** were obtained in moderate to excellent yields, as single regioisomers, and **59c** as a 1:1 mixture of diastereoisomers. The most striking feature was the unexpected regiochemical outcome of this study; the fluorinated moiety occupied the α-position in the final cyclopentenone ring in all cases (Scheme 32). This was expected for terminal alkyne **58a**, since this is the substitution pattern always found (see Scheme 4). On the other hand, for alkynes bearing substituents of similar steric bulk, the electron withdrawing group is expected to occupy the β-position. However, for alkynes **58b,c** the opposite regiochemistry was found. Finally, the use of alkyne **58d** with two electron-withdrawing groups resulted in the regioselective formation of product **59d** in excellent yield, indicating an inherent trend of the fluoroalkyl group to occupy the α-position regardless of the steric or electronic nature of the other substituent. These results contrast with those obtained for non-fluorinated analogue (ethyl 2-butynoate) for which the expected regioisomer **60** was formed, bearing the methyl group at the α-position and the electron-withdrawing ester group in the β-position. These results may suggest that fluoroalkyl groups behave as bulky substituents rather than as electron-withdrawing ones, perhaps due to the purely inductive nature of the latter [71].

In the same work, the authors described the conjugated addition of several nucleophiles to model substrate **59d** (Scheme 33). In this sense, while the addition of hard organometallic nucleophiles, such as lithium dialkylcuprates or Grignard reagents, failed, softer nucleophiles such as nitroalkanes cleanly added to the β-position, providing the Michael adduct **61**. Unexpectedly, the conjugate addition reaction resulted in concomitant detrifluoromethylation. Furthermore, the Lewis acid-mediated retro Diels–Alder reaction was carried out uneventfully on product **61**, affording the corresponding cyclopentenone **62** in moderate yield (Scheme 33).

In order to rationalize the unexpected loss of the trifluoromethyl group upon nucleophilic addition, the authors suggested the tentative mechanism depicted in Scheme 34. As shown, γ-fluoride loss from enolate **I**, formed after the conjugate Michael addition, would lead to the formation of difluoroenone **II**. This could in turn undergo a nucleophilic addition of water, followed by a retro-aldol reaction affording the final product (Scheme 34). This mechanism was experimentally supported by the beneficial effect of water and the observation of HF-loss by ^{19}F NMR.

The catalytic version of this process was also studied. The best results in terms of efficiency and stereoselectivity were ob-

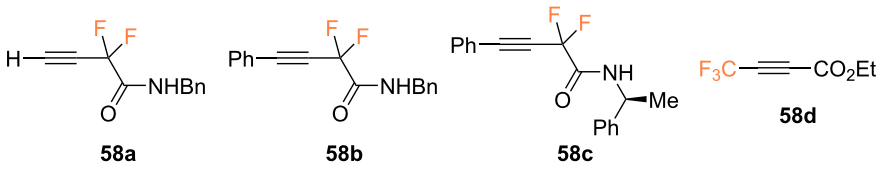

Scheme 31: Model fluorinated alkynes used by Riera and Fustero [70].

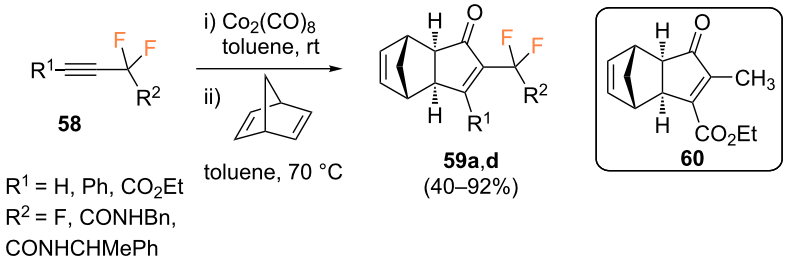

Scheme 32: PKR with norbornadiene and fluorinated alkynes **58** [71].

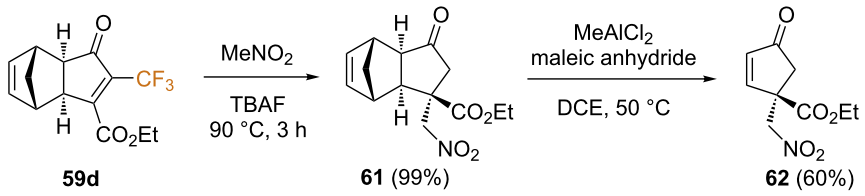

Scheme 33: Nucleophilic addition/detrifluoromethylation and retro Diels-Alder reactions [70].

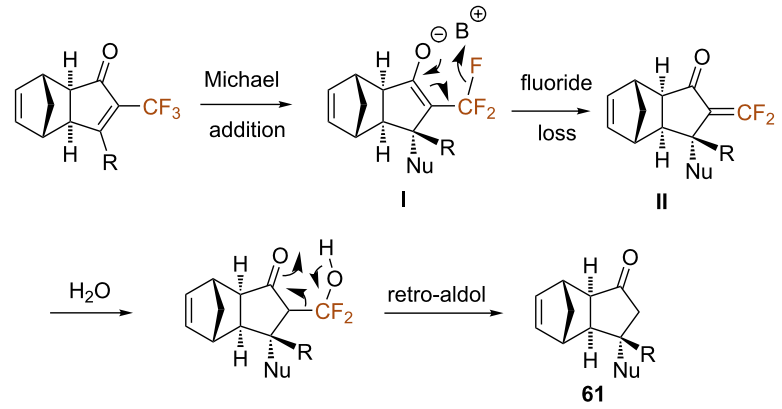

Scheme 34: Tentative mechanism for the nucleophilic addition/retro-aldol reaction sequence.

tained using the less reactive triphenylphosphine dicobaltpentacarbonyl complex **63** as the catalyst (Scheme 35).

In a later study [72], Riera and Fustero generalized the use of trifluoromethylalkynes as substrates for the PKR. The copper-catalyzed trifluoromethylation of terminal alkynes described by Qing and co-workers [73] allowed the efficient preparation of a small library of substrates bearing aryl, alkyl, and alkenyl substitutents. These were isolated after complexation to $Co_2(CO)_8$ as the corresponding adducts **64**, due to difficulties in their isolation. Subsequent heating with norbornadiene afforded the corresponding products **59** in good to excellent yields (Scheme 36).

The authors then studied the elimination of the trifluoromethyl group from this library of PK adducts, building upon their own experience in the field (vide supra, Scheme 34). Thus, by subjecting enones **59** to treatment with DBU in wet nitromethane under reflux, clean conjugate addition/detrifluoromethylation was observed, in this case followed by retro-Michael reaction of nitromethane achieving enones **65** in moderate to good yields (Scheme 37). Interestingly, the overall reaction sequence results in the formal inversion of the regiochemistry for terminal alkynes, affording the products substituted at the β-position. This regiochemistry switch might be regarded as the Holy Grail in Pauson–Khand chemistry.

The synthetic potential of this methodology was demonstrated by the formal total synthesis of α-cuparenone [74,75], a bicyclic sesquiterpene that belongs to the cuparene family isolated from *Thuja orientalis* [76]. More specifically, the authors designed a simple route to enone **67**, a key intermediate in several previous

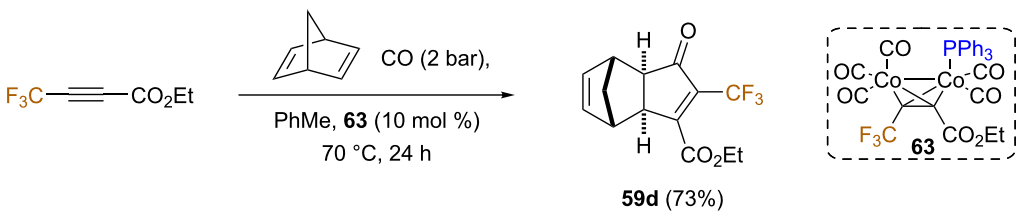

Scheme 35: Catalytic PKR with norbornadiene [70].

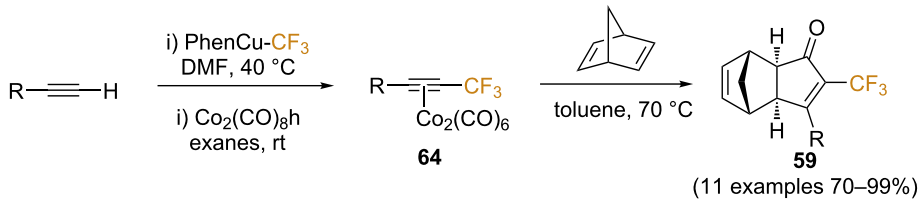

Scheme 36: Scope of the PKR of trifluoromethylalkynes with norbornadiene [72].

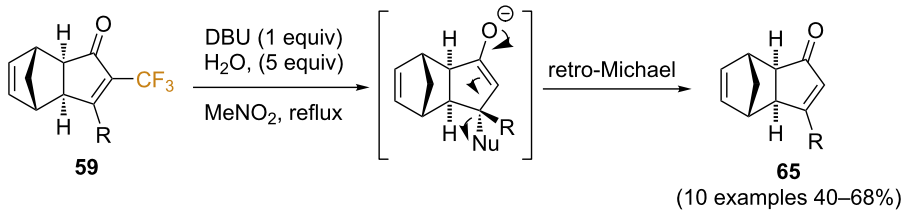

Scheme 37: DBU-mediated detrifluoromethylation [72].

total syntheses [77,78]. Its synthesis was achieved in two steps, namely a nickel-catalyzed conjugated addition of trimethylaluminum to form **66**, followed by Lewis acid-mediated retro Diels–Alder reaction (Scheme 38).

In another study by Riera and co-workers, they studied the influence of the olefin counterpart on the regioselectivity of the reaction [79]. Two olefins other than norbornadiene were used in this study, namely norbornene and ethylene (Scheme 39).

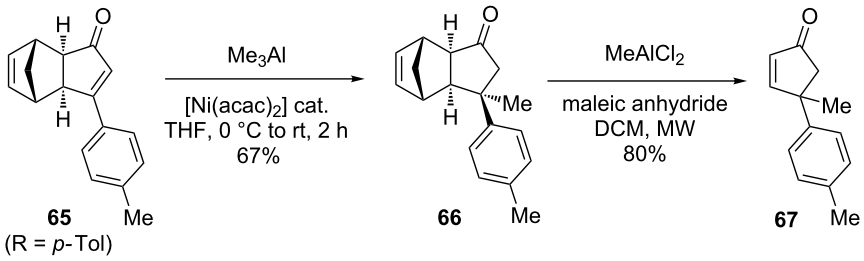

Scheme 38: A simple route to enone **67**, a common intermediate in the total synthesis of α-cuparenone.

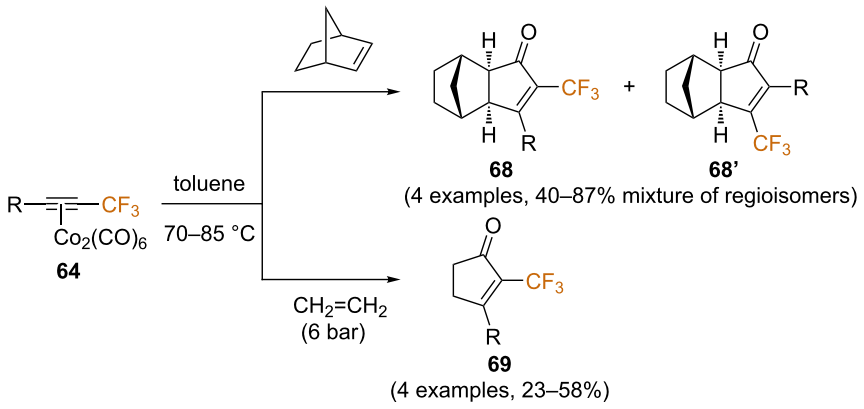

Scheme 39: Effect of the olefin partner in the regioselectivity of the PKR with trifluoromethyl alkynes [79].

Contrary to the results observed with norbonadiene and ethylene, which both furnished a single regioisomer, the use of norbornene afforded mixtures of regioisomers, although the same α-CF_3 isomer was favored in all cases. The aforementioned DBU-mediated detrifluoromethylation (Scheme 37) was achieved for substrates **68** in most cases with low to moderate yields, while the corresponding products could not be isolated starting from substrates **69**.

In 2012, Konno and co-workers reported the synthesis of 2-fluoralkyl-2-cyclopentenones through an intermolecular Co-mediated PKR of various trifluoromethyl alkynes with 2-norbornene (Scheme 40) [54]. In this process, the authors did not use NMO as a promoter due to its negative effect on the reaction yield. Under the described conditions, the cyclized products **70** were obtained as regioisomeric mixtures in moderate to high yields. The influence of alkyne substitution was studied, and alkynes bearing an electron-withdrawing or electron-donating group on the benzene ring afforded the corresponding cyclopentenones in high yields but as regioisomeric mixtures (ratio **A**/**B** ca. 70:30). Interestingly, a notable improvement of the regioselectivity was observed for trifluoromethyl alkynes bearing an alkyl substituent (R = Alk) or an ethoxycarbonyl group (R= CO_2Et). When a difluoromethylated alkyne (R_F = CF_2H) was used, the reaction took place very smoothly to preferentially afford the cyclopentenone with opposite regioselectivity (ratio **A**/**B** 31:69) to that observed for the other examples. This result contrasts with the lack of reactivity observed for CF_2H-substituted enynes in the intramolecular version (see Scheme 15). Although the PKR was also investigated for other alkenes such as cyclohexene, maleic anhydride, ethylene carbonate, and 1-octene, the desired products were not formed under the reaction conditions.

In the same year, Helaja and co-workers examined the electronic effects of the alkyne substituent on the regioselectivity of the microwave-assisted PKR with norbornene [80]. The electronic effects were evaluated by altering one functional group in the *para*-position of the starting diarylalkynes (Scheme 41). In this regard, electron-donating substituents such as, methoxy, dimethylamine, and methyl favored the α-position in the final cycloadduct (**71A**), whereas electron-withdrawing substituents such as dimethylaminium, trifluoromethyl, and acetyl favored the β-regioisomer (**71B**). The 4-fluorine substituted diarylalkynes had a very weak EWG effect yielding an equimolar mixture of both regioisomers. The experimental results were confirmed by a DFT study of the NBO charges of the α-alkyne carbons, which also showed a correlation with the regioselectivity.

In 2016, León and Fernández reported the first intermolecular PKR of internal alkynylboronic esters with norbornadiene [81].

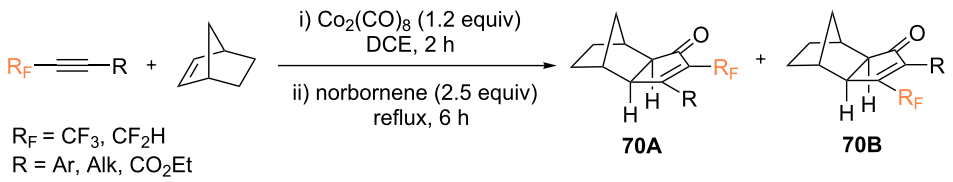

Scheme 40: Intermolecular PKR of trifluoromethylalkynes with 2-norbornene reported by the group of Konno [54].

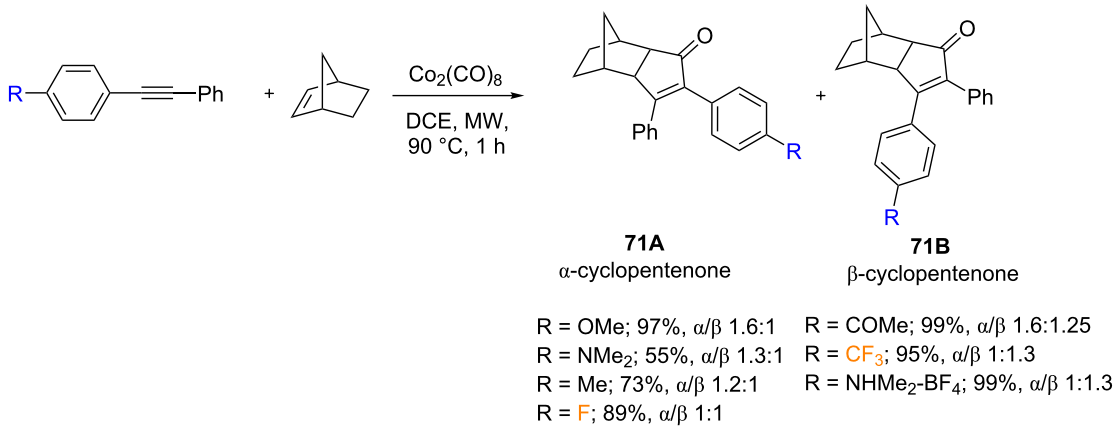

Scheme 41: Intermolecular PKR of diarylalkynes with 2-norbornene reported by the group of Helaja [80].

For this purpose, terminal alkynes were converted into their corresponding alkynylboronic pinacol esters, and evaluated in the intermolecular PKR with norbornadiene. Under the optimal reaction conditions, $Co_2(CO)_8$ (1 equiv), norbornadiene (3 equiv) and NMO (6 equiv) in dichloromethane, the internal alkynes afforded the corresponding α,β-substituted cyclopentenones with total stereo- and regioselectivity; the *exo*-stereoisomer with the B(pin) substituent in the β-position was obtained exclusively. The PKR was compatible with aromatic groups containing substituents with differing electronic properties, heteroaryl groups, benzopinacol, 1,8-diaminonaphthalene, olefinic, and aliphatic groups. However, the PKR failed when hindered alkynes were used. The authors reported two examples of fluorine-containing alkynylboronic pinacol esters, which afforded the corresponding β-substituted cyclopentenones **72** in good yields (Scheme 42).

In a recent report, Marek, Zhang, Ma and co-workers described a Rh^{II}-catalyzed cyclopropenation reaction of internal alkynes with a difluorodiazoethane reagent, offering efficient access to a broad range of enantioenriched difluoromethylated cyclopropenes with almost quantitative yields and up to 97% ee [82]. This asymmetric carbene transfer reaction was performed using chiral Rh^{II} complexes, more specifically the Hashimoto catalyst ($[Rh_2(S\text{-TCPTTL})_4]$) was found to be the most efficient in terms of yield and enantioselectivity. In this study, the authors described an example of an intermolecular PKR using the strained difluoromethylated cyclopropene **73** which, upon reaction with the hexacarbonyldicobalt complex prepared by treatment of the 1-butyne with $Co_2(CO)_8$, afforded the corresponding bicyclic cyclopropane-fused cyclopentenone **74** in high yield and high enantioselectivity (Scheme 43).

Conclusion

In conclusion, as highlighted in this review, the PKR is still a hot area of chemical research as it provides access to cyclopentenones from accessible starting materials under relatively mild conditions. The increasing demand of fine chemicals bearing fluorine atoms at strategic positions, together with the ubiquitous presence of the cyclopentenone ring in added-value compounds, has attracted researchers' interest throughout the past decades. Since its discovery, numerous research groups have devoted their efforts to develop alternative ways to expand the scope of the PKR and the combination of fluorinated building blocks with this [2 + 2 + 1] cycloaddition has been efficiently applied in the preparation of fluorinated compounds of biological interest. The addition of fluorine-containing olefins and alkynes to the arsenal of substrates for the PKR has resulted in a major contribution in the field. Not only has the scope of accessible products been significantly expanded, but a better understanding of the factors governing the regioselectivity has been achieved, including the possibility to formally reverse the regiochemistry in some cases. Despite the important advances highlighted in this review, there remains room for improvement in the scope of this useful reaction with fluorinated compounds. Nowadays, most described protocols for the fluorinated PKR are based on the cobalt-catalyzed version, and only a few examples have used other transition metal complexes. In this regard, significant advances can come from the careful selection of the metal complex and the CO source. The encouraging results de-

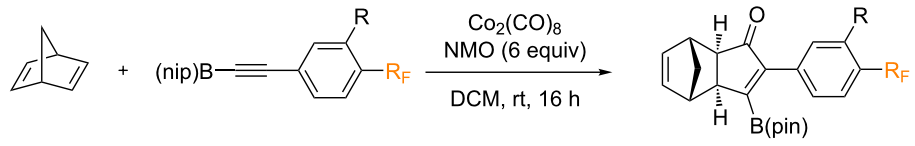

72
$R_F = OCF_3$; R = F; 55%
R_F = F; R = H; 65%

Scheme 42: Intermolecular PKR reported by León and Fernández [81].

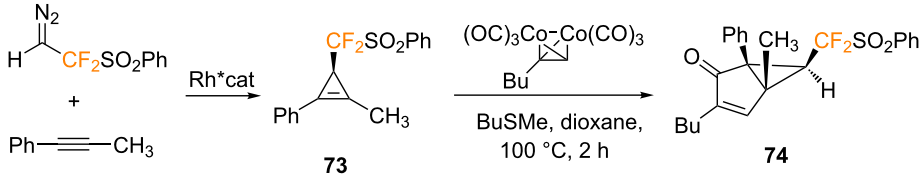

73

74
93% (dr 10:1, 96% ee)

Scheme 43: PKR reported with cyclopropene **73** [82].

scribed in this review will definitely pave the way for future applications in the fluoro-PKR, and put this emerging reaction at the forefront of drug design.

Acknowledgements

We thank the authors of the papers collected here for the hard work that made this review possible. The authors also thank Joel Navarro and Marta Pons for their help with this review.

Funding

The authors thank the Spanish Ministerio de Ciencia, Innovación y Universidades (MICINN) and Agencia Estatal de Investigación (AEI) for financial support (CTQ2017-84249-P)

ORCID® iDs

Jorge Escorihuela - https://orcid.org/0000-0001-6756-0991
Daniel M. Sedgwick - https://orcid.org/0000-0003-3902-6171
Mercedes Medio-Simón - https://orcid.org/0000-0001-9149-9350
Pablo Barrio - https://orcid.org/0000-0001-7101-4037
Santos Fustero - https://orcid.org/0000-0002-7575-9439

References

1. Mei, H.; Han, J.; Fustero, S.; Medio-Simon, M.; Sedgwick, D. M.; Santi, C.; Ruzziconi, R.; Soloshonok, V. A. *Chem. – Eur. J.* **2019,** *25,* 11797–11819. doi:10.1002/chem.201901840
2. Zhou, Y.; Wang, J.; Gu, Z.; Wang, S.; Zhu, W.; Aceña, J. L.; Soloshonok, V. A.; Izawa, K.; Liu, H. *Chem. Rev.* **2016,** *116,* 422–518. doi:10.1021/acs.chemrev.5b00392
3. Wang, J.; Sánchez-Roselló, M.; Aceña, J. L.; del Pozo, C.; Sorochinsky, A. E.; Fustero, S.; Soloshonok, V. A.; Liu, H. *Chem. Rev.* **2014,** *114,* 2432–2506. doi:10.1021/cr4002879
4. Shultz, M. D. *J. Med. Chem.* **2019,** *62,* 1701–1714. doi:10.1021/acs.jmedchem.8b00686
5. O'Hagan, D. *Chem. Soc. Rev.* **2008,** *37,* 308–319. doi:10.1039/b711844a
6. Hiyama, T. In *Organofluorine Compounds: Chemistry and Applications;* Yamamoto, H., Ed.; Springer: New York, NY, USA, 2000. doi:10.1007/978-3-662-04164-2
7. Liang, T.; Neumann, C. N.; Ritter, T. *Angew. Chem., Int. Ed.* **2013,** *52,* 8214–8264. doi:10.1002/anie.201206566
8. Tredwell, M.; Gouverneur, V. *Angew. Chem., Int. Ed.* **2012,** *51,* 11426–11437. doi:10.1002/anie.201204687
9. Chen, H.; Viel, S.; Ziarelli, F.; Peng, L. *Chem. Soc. Rev.* **2013,** *42,* 7971–7982. doi:10.1039/c3cs60129c
10. Fujiwara, T.; O'Hagan, D. *J. Fluorine Chem.* **2014,** *167,* 16–29. doi:10.1016/j.jfluchem.2014.06.014
11. Vincent, J.-M. *Chem. Commun.* **2012,** *48,* 11382–11391. doi:10.1039/c2cc34750d
12. Berger, R.; Resnati, G.; Metrangolo, P.; Weber, E.; Hulliger, J. *Chem. Soc. Rev.* **2011,** *40,* 3496–3508. doi:10.1039/c0cs00221f
13. Wu, J. *Tetrahedron Lett.* **2014,** *55,* 4289–4294. doi:10.1016/j.tetlet.2014.06.006
    See for nucleophilic fluorination.
14. Hollingworth, C.; Gouverneur, V. *Chem. Commun.* **2012,** *48,* 2929–2942. doi:10.1039/c2cc16158c
    See for nucleophilic fluorination.
15. Baudoux, J.; Cahard, D. *Org. React.* **2008,** *69,* 1–326. doi:10.1002/0471264180.or069.02
    See for nucleophilic fluorination.
16. Sibi, M. P.; Landais, Y. *Angew. Chem., Int. Ed.* **2013,** *52,* 3570–3572. doi:10.1002/anie.201209583
    See for radical fluorination.
17. Kuehnel, M. F.; Lentz, D.; Braun, T. *Angew. Chem., Int. Ed.* **2013,** *52,* 3328–3348. doi:10.1002/anie.201205260
18. Ricker, J. D.; Geary, L. M. *Top. Catal.* **2017,** *60,* 609–619. doi:10.1007/s11244-017-0741-0
    See for a review on the Pauson–Khand reaction.
19. Ríos Torres, R., Ed. *The Pauson-Khand Reaction. Scope, Variations and Applications;* John Wiley & Sons: Chichester, UK, 2012. doi:10.1002/9781119941934
20. Lee, H.-W.; Kwong, F.-Y. *Eur. J. Org. Chem.* **2010,** 789–811. doi:10.1002/ejoc.200900892
    See for a review on the Pauson–Khand reaction.
21. Park, J. H.; Chang, K.-M.; Chung, Y. K. *Coord. Chem. Rev.* **2009,** *253,* 2461–2480. doi:10.1016/j.ccr.2009.08.005
    See for a review on the Pauson–Khand reaction.
22. Blanco-Urgoiti, J.; Añorbe, L.; Pérez-Serrano, L.; Domínguez, G.; Pérez-Castells, J. *Chem. Soc. Rev.* **2004,** *33,* 32–42. doi:10.1039/b300976a
    See for a review on the Pauson–Khand reaction.
23. Khand, I. U.; Knox, G. R.; Pauson, P. L.; Watts, W. E. *J. Chem. Soc. D* **1971,** 36a. doi:10.1039/c2971000036a
24. Khand, I. U.; Knox, G. R.; Pauson, P. L.; Watts, W. E. *J. Chem. Soc., Perkin Trans. 1* **1973,** 975–977. doi:10.1039/p19730000975
25. Khand, I. U.; Knox, G. R.; Pauson, P. L.; Watts, W. E.; Foreman, M. I. *J. Chem. Soc., Perkin Trans. 1* **1973,** 977–981. doi:10.1039/p19730000977
26. García-Lacuna, J.; Domínguez, G.; Blanco-Urgoiti, J.; Pérez-Castells, J. *Org. Biomol. Chem.* **2019,** *17,* 9489–9501. doi:10.1039/c9ob02124h
27. Hugelshofer, C. L.; Palani, V.; Sarpong, R. *J. Am. Chem. Soc.* **2019,** *141,* 8431–8435. doi:10.1021/jacs.9b03576
28. Zhao, N.; Xie, S.; Tian, P.; Tong, R.; Ning, C.; Xu, J. *Org. Chem. Front.* **2019,** *6,* 2014–2022. doi:10.1039/c9qo00384c
29. Hu, N.; Dong, C.; Zhang, C.; Liang, G. *Angew. Chem., Int. Ed.* **2019,** *58,* 6659–6662. doi:10.1002/anie.201902043
30. Kaneko, H.; Takahashi, S.; Kogure, N.; Kitajima, M.; Takayama, H. *J. Org. Chem.* **2019,** *84,* 5645–5654. doi:10.1021/acs.joc.9b00586
31. Cabré, A.; Khaizourane, H.; Garçon, M.; Verdaguer, X.; Riera, A. *Org. Lett.* **2018,** *20,* 3953–3957. doi:10.1021/acs.orglett.8b01525
32. Huang, Z.; Huang, J.; Qu, Y.; Zhang, W.; Gong, J.; Yang, Z. *Angew. Chem., Int. Ed.* **2018,** *57,* 8744–8748. doi:10.1002/anie.201805143
33. Magnus, P.; Principe, L. M. *Tetrahedron Lett.* **1985,** *26,* 4851–4854. doi:10.1016/s0040-4039(00)94968-2
34. Banide, E. V.; Müller-Bunz, H.; Manning, A. R.; Evans, P.; McGlinchey, M. J. *Angew. Chem., Int. Ed.* **2007,** *46,* 2907–2910. doi:10.1002/anie.200605171
35. Yamanaka, M.; Nakamura, E. *J. Am. Chem. Soc.* **2001,** *123,* 1703–1708. doi:10.1021/ja005565+
36. Pericàs, M. A.; Balsells, J.; Castro, J.; Marchueta, I.; Moyano, A.; Riera, A.; Vázquez, J.; Verdaguer, X. *Pure Appl. Chem.* **2002,** *74,* 167–174. doi:10.1351/pac200274010167
37. Iqbal, M.; Vyse, N.; Dauvergne, J.; Evans, P. *Tetrahedron Lett.* **2002,** *43,* 7859–7862. doi:10.1016/s0040-4039(02)01912-3

38. Rodríguez, A. M.; Prieto, P. *Tetrahedron* **2016,** *72,* 7443–7448. doi:10.1016/j.tet.2016.09.048
39. Son, S. U.; Lee, S. I.; Chung, Y. K.; Kim, S.-W.; Hyeon, T. *Org. Lett.* **2002,** *4,* 277–279. doi:10.1021/ol017043k
40. Jeong, N.; Chung, Y. K.; Lee, B. Y.; Lee, S. H.; Yoo, S.-E. *Synlett* **1991,** 204–206. doi:10.1055/s-1991-20681
41. Fager-Jokela, E.; Muuronen, M.; Khaizourane, H.; Vázquez-Romero, A.; Verdaguer, X.; Riera, A.; Helaja, J. *J. Org. Chem.* **2014,** *79,* 10999–11010. doi:10.1021/jo502035t
42. Lam, F. L.; Lee, H. W.; Wang, J.; Kwong, F. Y. Recent Advancement of Catalytic Pauson–Khand-type Reactions. In *Pauson Khand Reaction. Scope, Variations and Applications;* Ríos Torres, R., Ed.; John Wiley & Sons: Chichester, UK, 2012; pp 181–210. doi:10.1002/9781119941934.ch7
43. Ockey, D. A.; Lewis, M. A.; Schore, N. E. *Tetrahedron* **2003,** *59,* 5377–5381. doi:10.1016/s0040-4020(03)00779-8
44. Mukai, C.; Yoshida, T.; Sorimachi, M.; Odani, A. *Org. Lett.* **2006,** *8,* 83–86. doi:10.1021/ol052562z
45. Miller, K. A.; Shanahan, C. S.; Martin, S. F. *Tetrahedron* **2008,** *64,* 6884–6900. doi:10.1016/j.tet.2008.02.066
46. Ishizaki, M.; Suzuki, D.; Hoshino, O. *J. Fluorine Chem.* **2001,** *111,* 81–90. doi:10.1016/s0022-1139(01)00436-5
47. Ferry, A.; Billard, T.; Langlois, B. R. *Synlett* **2005,** 1027–1029. doi:10.1055/s-2005-864812
48. Harthong, S.; Billard, T.; Langlois, B. R. *Synthesis* **2005,** 2253–2263. doi:10.1055/s-2005-872076
49. Magueur, G.; Legros, J.; Meyer, F.; Ourévitch, M.; Crousse, B.; Bonnet-Delpon, D. *Eur. J. Org. Chem.* **2005,** 1258–1265. doi:10.1002/ejoc.200400719
50. Nadano, R.; Ichikawa, J. *Chem. Lett.* **2007,** *36,* 22–23. doi:10.1246/cl.2007.22
51. Nadano, R.; Fuchibe, K.; Ikeda, M.; Takahashi, H.; Ichikawa, J. *Chem. – Asian J.* **2010,** *5,* 1875–1883. doi:10.1002/asia.201000139
52. Arimitsu, S.; Bottom, R. L.; Hammond, G. B. *J. Fluorine Chem.* **2008,** *129,* 1047–1051. doi:10.1016/j.jfluchem.2008.05.010
53. Vorobyeva, D. V.; Mailyan, A. K.; Peregudov, A. S.; Karimova, N. M.; Vasilyeva, T. P.; Bushmarinov, I. S.; Bruneau, C.; Dixneuf, P. H.; Osipov, S. N. *Tetrahedron* **2011,** *67,* 3524–3532. doi:10.1016/j.tet.2011.03.031
54. Konno, T.; Kida, T.; Tani, A.; Ishihara, T. *J. Fluorine Chem.* **2012,** *144,* 147–156. doi:10.1016/j.jfluchem.2012.08.006
55. Fustero, S.; Lázaro, R.; Aiguabella, N.; Riera, A.; Simón-Fuentes, A.; Barrio, P. *Org. Lett.* **2014,** *16,* 1224–1227. doi:10.1021/ol500142c
56. Gallagher, A. G.; Tian, H.; Torres-Herrera, O. A.; Yin, S.; Xie, A.; Lange, D. M.; Wilson, J. K.; Mueller, L. G.; Gau, M. R.; Carroll, P. J.; Martinez-Solorio, D. *Org. Lett.* **2019,** *21,* 8646–8651. doi:10.1021/acs.orglett.9b03255
57. Dobbs, A. P.; Miller, I. J.; Martinović, S. *Beilstein J. Org. Chem.* **2007,** *3,* No. 21. doi:10.1186/1860-5397-3-21
58. Ishaq, S.; Porter, M. J. *Synth. Commun.* **2006,** *36,* 547–557. doi:10.1080/00397910500406120
59. Román, R.; Mateu, N.; López, I.; Medio-Simón, M.; Fustero, S.; Barrio, P. *Org. Lett.* **2019,** *21,* 2569–2573. doi:10.1021/acs.orglett.9b00509
60. Okoromoba, O. E.; Han, J.; Hammond, G. B.; Xu, B. *J. Am. Chem. Soc.* **2014,** *136,* 14381–14384. doi:10.1021/ja508369z
61. Llobat, A.; Román, R.; Mateu, N.; Sedgwick, D. M.; Barrio, P.; Medio-Simón, M.; Fustero, S. *Org. Lett.* **2019,** *21,* 7294–7297. doi:10.1021/acs.orglett.9b02557
62. Champagne, P. A.; Desroches, J.; Hamel, J.-D.; Vandamme, M.; Paquin, J.-F. *Chem. Rev.* **2015,** *115,* 9073–9174. doi:10.1021/cr500706a
63. Zhu, Y.; Han, J.; Wang, J.; Shibata, N.; Sodeoka, M.; Soloshonok, V. A.; Coelho, J. A. S.; Toste, F. D. *Chem. Rev.* **2018,** *118,* 3887–3964. doi:10.1021/acs.chemrev.7b00778
64. Llobat, A.; Sedgwick, D. M.; Cabré, A.; Román, R.; Mateu, N.; Escorihuela, J.; Medio-Simón, M.; Soloshonok, V.; Han, J.; Riera, A.; Fustero, S. *Adv. Synth. Catal.* **2020,** *362,* 1378–1384. doi:10.1002/adsc.201901504
65. Pérez-Serrano, L.; Blanco-Urgoiti, J.; Casarrubios, L.; Domínguez, G.; Pérez-Castells, J. *J. Org. Chem.* **2000,** *65,* 3513–3519. doi:10.1021/jo0001232
66. Cabré, A.; Verdaguer, X.; Riera, A. *Synthesis* **2018,** *50,* 3891–3896. doi:10.1055/s-0037-1610441
67. Gibson, S. E.; Mainolfi, N. *Angew. Chem., Int. Ed.* **2005,** *44,* 3022–3037. doi:10.1002/anie.200462235
68. Lledó, A.; Fuster, A.; Revés, M.; Verdaguer, X.; Riera, A. *Chem. Commun.* **2013,** *49,* 3055–3057. doi:10.1039/c3cc41005f
69. Marchueta, I.; Verdaguer, X.; Moyano, A.; Pericàs, M. A.; Riera, A. *Org. Lett.* **2001,** *3,* 3193–3196. doi:10.1021/ol016505r
70. Kizirian, J.-C.; Aiguabella, N.; Pesquer, A.; Fustero, S.; Bello, P.; Verdaguer, X.; Riera, A. *Org. Lett.* **2010,** *12,* 5620–5623. doi:10.1021/ol102283c
71. For a systematic study on the effect of electron-withdrawing groups of different nature (inductive vs mesomeric effect) on the regioseectivity of the PKR see reference [41].
72. Aiguabella, N.; del Pozo, C.; Verdaguer, X.; Fustero, S.; Riera, A. *Angew. Chem., Int. Ed.* **2013,** *52,* 5355–5359. doi:10.1002/anie.201300907
73. Chu, L.; Qing, F.-L. *J. Am. Chem. Soc.* **2010,** *132,* 7262–7263. doi:10.1021/ja102175w
74. Matsuda, T.; Tsuboi, T.; Murakami, M. *J. Am. Chem. Soc.* **2007,** *129,* 12596–12597. doi:10.1021/ja0732779
75. Hodgson, D. M.; Chung, Y. K.; Nuzzo, I.; Freixas, G.; Kulikiewicz, K. K.; Cleator, E.; Paris, J.-M. *J. Am. Chem. Soc.* **2007,** *129,* 4456–4462. doi:10.1021/ja0672932
76. Chetty, G. L.; Dev, S. *Tetrahedron Lett.* **1964,** *5,* 73–77. doi:10.1016/s0040-4039(00)90332-0
77. Zhang, P.; Le, H.; Kyne, R. E.; Morken, J. P. *J. Am. Chem. Soc.* **2011,** *133,* 9716–9719. doi:10.1021/ja2039248
78. Nakashima, H.; Sato, M.; Taniguchi, T.; Ogasawara, K. *Tetrahedron Lett.* **2000,** *41,* 2639–2642. doi:10.1016/s0040-4039(00)00235-5
79. Aiguabella, N.; Arce, E. M.; del Pozo, C.; Verdaguer, X.; Riera, A. *Molecules* **2014,** *19,* 1763–1774. doi:10.3390/molecules19021763
80. Fager-Jokela, E.; Muuronen, M.; Patzschke, M.; Helaja, J. *J. Org. Chem.* **2012,** *77,* 9134–9147. doi:10.1021/jo3016902
81. León, T.; Fernández, E. *Chem. Commun.* **2016,** *52,* 9363–9366. doi:10.1039/c6cc04717c
82. Zhang, Z.-Q.; Zheng, M.-M.; Xue, X.-S.; Marek, I.; Zhang, F.-G.; Ma, J.-A. *Angew. Chem., Int. Ed.* **2019,** *58,* 18191–18196. doi:10.1002/anie.201911701

License and Terms

This is an Open Access article under the terms of the Creative Commons Attribution License (http://creativecommons.org/licenses/by/4.0). Please note that the reuse, redistribution and reproduction in particular requires that the authors and source are credited.

The license is subject to the *Beilstein Journal of Organic Chemistry* terms and conditions: (https://www.beilstein-journals.org/bjoc)

The definitive version of this article is the electronic one which can be found at: doi:10.3762/bjoc.16.138

BEILSTEIN JOURNAL OF ORGANIC CHEMISTRY

Polarity effects in 4-fluoro- and 4-(trifluoromethyl)prolines

Vladimir Kubyshkin

Full Research Paper

Open Access

Address:
University of Manitoba, Dysart Rd. 144, Winnipeg, R3T 2N2, Canada

Email:
Vladimir Kubyshkin - vladimir.kubyshkin@umanitoba.ca

Keywords:
amino acids; *cis–trans* isomerism; fluorine; polarity; proline

Beilstein J. Org. Chem. **2020,** *16,* 1837–1852.
doi:10.3762/bjoc.16.151

Received: 18 May 2020
Accepted: 06 July 2020
Published: 23 July 2020

This article is part of the thematic issue "Organo-fluorine chemistry V".

Guest Editor: D. O'Hagan

© 2020 Kubyshkin; licensee Beilstein-Institut.
License and terms: see end of document.

Abstract

Fluorine-containing analogues of proline are valuable tools in engineering and NMR spectroscopic studies of peptides and proteins. Their use relies on the fundamental understanding of the interplay between the substituents and the main chain groups of the amino acid residue. This study aims to showcase the polarity-related effects that arise from the interaction between the functional groups in molecular models. Properties such as conformation, acid–base transition, and amide-bond isomerism were examined for diastereomeric 4-fluoroprolines, 4-(trifluoromethyl)prolines, and 1,1-difluoro-5-azaspiro[2.4]heptane-6-carboxylates. The preferred conformation on the proline ring originated from a preferential axial positioning for a single fluorine atom, and an equatorial positioning for a trifluoromethyl- or a difluoromethylene group. This orientation of the substituents explains the observed trends in the pK_a values, lipophilicity, and the kinetics of the amide bond rotation. The study also provides a set of evidences that the transition state of the amide-bond rotation in peptidyl-prolyl favors C^4-*exo* conformation of the pyrrolidine ring.

Introduction

Polarity is among the key features essential for understanding the behavior of organic molecules of biological origin. In particular, there is a set of polarity-related issues in the chemistry of amino acids, while the latter are key actors in multiple biochemical processes. In protein translation, for example, 20 (+2) amino acids are utilized for polymerizing them into a primary structure of a protein. Most of these structures share the same key elements with the structure of alanine, which constitute the backbone features. The classification of the amino acid residues by hydrophobic/hydrophilic usually refers to the variable part, which locates in the side chain. The introduction of an aliphatic or an aromatic group into the side chain usually renders an amino acid hydrophobic, while the introduction of a polar or an ionizable group makes it hydrophilic.

Two amino acids stand out from the dualistic hydrophilic/hydrophobic classification: glycine and proline (Figure 1A) [1]. The origin of their effect onto the structure polarity is not due to the presence of additional functional groups, but due to the altered backbone folding and solvation. For example, a proline

residue cannot be considered hydrophobic, even though, it contains the same number of carbon atoms as valine, which is evidently hydrophobic [2]. In fact, a proline contribution to the peptide polarity can be ambivalent and mainly depends on the underlying secondary structure. The lack of a polar N–H bond in peptidyl-prolyl can decrease the polarity in one case, and increase in another. The first scenario may occur if a free N–H bond would otherwise be exposed to the solvent. Proline lacks an N–H bond, thus the polarity drops down. The second scenario would occur if there was an N–H···O=C hydrogen bond in the structure. Thus, the presence of proline would leave an unsolvated carbonyl group, and its appearance leads to a polarity rise. Finally, a proline residue usually prefers extended secondary fold and may identify structural breaks in a sequence. This fact contributes to the reputation of proline as a polar residue [3-5].

There is a rich portfolio of fluorine-containing proline analogues that have been developed to date (Figure 1B): fluorinated [6-12], trifluoromethylated [13-23], chimeric [16,19,24-29], conformationally restricted [30-33] having variations in the ring size [34-39], non-α [40-44], and other analogues [45-48]. The fluorine-containing functional groups are usually chemically inert under most biologically relevant conditions. The presence of these groups adjacent to the proline structure helps to modulate the conformational landscape of the parent amino acid, and this effectively alters the folding of the peptide chain when an analogue is included in it as a residue [49,50]. The presence of a fluorine-rich group in the structure is also beneficial for the NMR studies based on the detection of the ^{19}F nucleus [51-53]. Limited attention has been given to the polarity effects in the proline analogues though. Few studies reported peptides containing proline analogues with distinct hydrophobic properties can impact their ability to pass biomembranes [54-56]. A crystallographic study has shown that when included into a protein structure, a fluorine atom exhibits a network of interaction within a protein core [57]. Another recent study showed that the substitution of proline with analogues can result in the conformational stabilization and polarity effects competing with each other [58]. Finally, it has been shown that fluoroprolines can alter donor–acceptor interactions of the proline ring with a tryptophan residue [59].

All these findings indicate that polarity effects should be taken into account in the characterization of proline analogues containing fluorinated groups. Nonetheless, most studies focus on conformational properties of the analogues, and much less is known about their polarity. This study aims to shed light on the polarity-related phenomena in two typical examples: 4-fluoroprolines and 4-(trifluoromethyl)prolines (Figure 2). The study aims to provide experimental characterization of these amino acids in the context of simple molecular models. Thereby, it may help to build predictions for the amino acid use in the context of more complex structures: peptides and proteins.

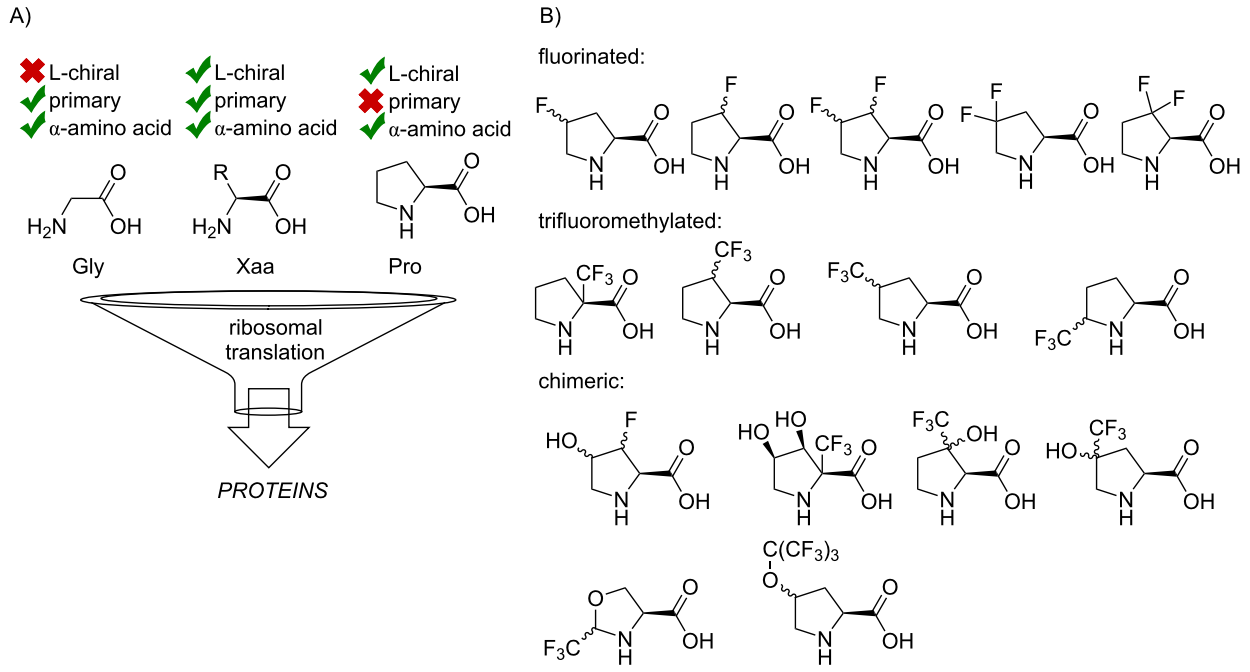

Figure 1: A) Three types of the backbone amino acid structures that are included in protein translation: glycine, alanine, and the set of its structural derivatives, proline. B) The portfolio of the fluorinated amino acids developed to date.

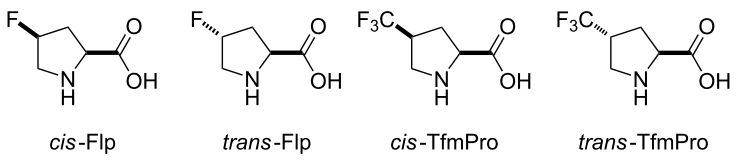

Figure 2: The set of amino acids examined in this study.

Results and Discussion

Model compounds

The study was originally set up following an assumption that a peptide containing a proline analogue would form a system of three dipoles. The peptide bond itself creates a strong dipole, with a direction that roughly aligns the direction of the carbonyl bond (see Figure S1 in Supporting Information File 1 for the estimation of dipole size and orientation). A proline residue is surrounded by two such dipoles originated from the up- and downstream peptide bonds. The strength of the dipoles can be estimated as 4–5 D. A fluorine-containing substituent adds a new dipole to the system. A C–F dipole is estimated as 1.9 D, whereas a CF_3-group dipole is about 2.4 D [60]. Thus, a proline analogue that contains these substituents would form a system of three mutually interacting dipoles (Figure 3).

To mimic this situation, a conventional model was chosen: the methyl ester of an *N*-acetylated amino acid. This model is very convenient, because it maintains the set of the dipoles. At the same time, it lacks the N–H bonds, which would otherwise disturb the measurements in nonpolar solvents due to the formation of specific hydrogen-bonded structures, such as γ- and δ-turns (also called C7- and C5-bonds, respectively) [61,62]. Thus, it was decided to examine the model compounds **1**–**4** and molecular effects therein.

Conformation of the proline ring

Due to its cyclic nature, the pyrrolidine ring in proline can adopt a few distinct conformational states [61,63]. The envelope conformation of the 5-membered pyrrolidine ring is commonly assumed to transit between two situations: 1) the one in which the C^4-atom is displaced from the main plain in the same direction as the carboxylic group (C^4-*endo* or *down* pucker), and 2) the one with the displacement in the opposite direction (C^4-*exo* or *up* pucker). Unsubstituted proline does not have a distinct preference towards either form, and the transition between them occurs in a relatively fast kinetic mode (barrier 10–13 kJ mol^{-1}) [64,65]. The 2-CH multiplicity in the ^{1}H NMR spectrum is indicative of the conformation adopted by the ring. A C^4-*endo* conformation exhibits two vicinal *J* couplings with one value being large and one being small, whereas a C^4-*exo* conformation displays two large *J* couplings [66] (Figure 4).

A substituent at the C^4-atom creates a certain preference towards one or another conformation. An electron-withdrawing substituent tends to adopt an axial position due to an orbital effect called the *gauche*-effect (stereoelectronic effect) [67,68]. Conversely, a bulky substituent adopts an equatorial position (steric effect) [69,70]. At the same time, there has been no evidence that a direct dipole–dipole interaction between the sub-

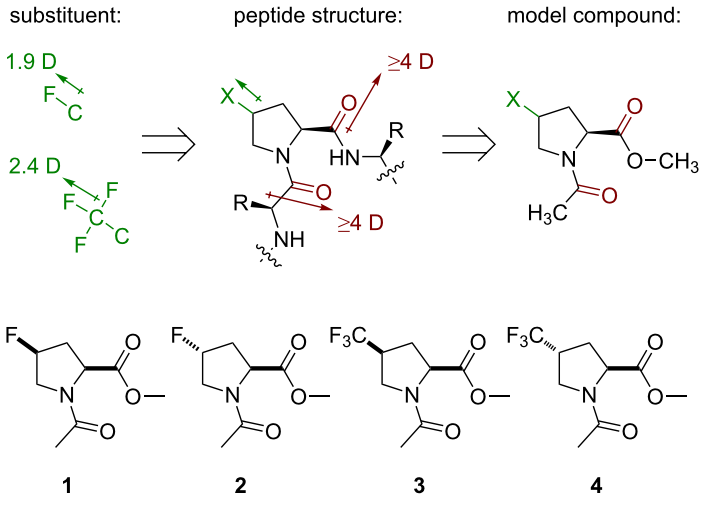

Figure 3: Design of the model system.

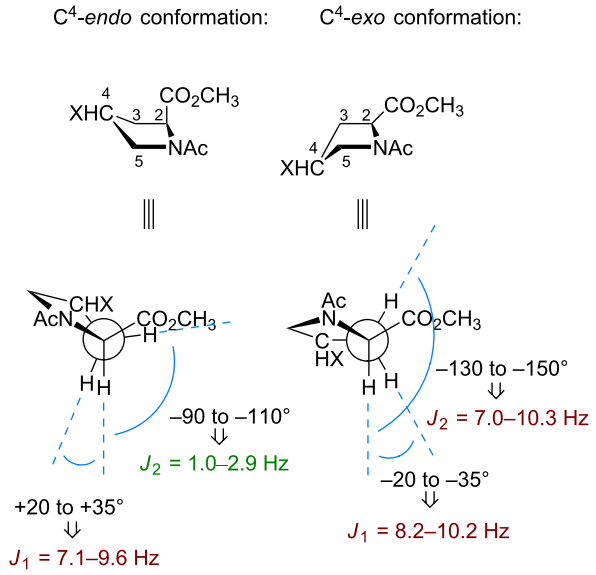

Figure 4: Propagation of the C^4-conformation into the values of the *J* coupling in the $C^2H–C^3H_2$ fragments.

stituent and the main chain groups could have an effect onto the conformation.

Here, the NMR data for the model compounds **1**–**4** were collected in three solvents with distinct dielectric properties (Table 1). The results were interpreted by comparing the experimental 2-CH multiplicity with the one predicted for the pure conformers (Figure 4). As can be seen from the data, both fluoroprolines exhibited stabilization of certain side-chain conformers: the *cis*-isomer **1** stabilized the C^4-*endo* envelope, whereas the *trans*-isomer **2** stabilized the C^4-*exo* (Figure 5). The major ring conformation (C^4-*endo* for **1** and C^4-*exo* for **2**) persisted in all three examined solvents and in both amide rotameric states. This outcome is fully consistent with the literature data [68], and it agrees with two conclusions: 1) the fluorine atom adopts an axial conformation and 2) the origin of the effect is orbital (the *gauche*-effect) rather than through space dipolar interaction (assuming that an interaction of dipoles would be attenuated in polar solvents, which was not observed).

Table 1: 2-CH multiplicity data and the conclusions regarding the C^4 conformation in the model compounds.[a]

compound	^{1}H NMR multiplicity of 2-CH[b]								
	in $CDCl_3$, ε 4.8			in CD_2Cl_2, ε 8.9			in D_2O, ε 80.1		
	J_1, Hz	J_2, Hz	C^4-	J_1, Hz	J_2, Hz	C^4-	J_1, Hz	J_2, Hz	C^4-
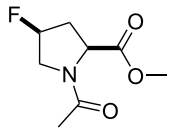 **1**	9.8 (9.4)	1.0 (n.d.)[c]	*endo* (*endo*)	9.8 (9.5)	1.0 (n.d.)[c]	*endo* (*endo*)	8.8 (9.6)	2.9 (n.d.)[c]	*endo* (*endo*)
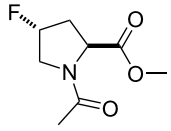 **2**	8.5 (8.4)	8.5 (8.4)	*exo* (*exo*)	8.5 (8.0)	8.5 (8.0)	*exo* (*exo*)	10.0 (8.4)	7.8 (8.4)	*exo* (*exo*)
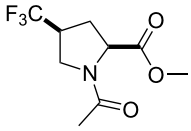 **3**	8.3 (9.0)	8.3 (5.4)	*exo* (*mix*)[d]	8.3 (9.2)	8.3 (5.2)	*exo* (*mix*)[d]	8.3 (9.9)	8.3 (4.1)	*exo* (*mix*)[d]
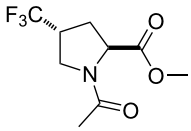 **4**	9.0 (8.7)	2.3 (1.7)	*endo* (*endo*)	9.0 (8.5)	2.5 (1.6)	*endo* (*endo*)	9.2 (8.6)	4.0 (2.6)	*mix*[d] (*endo*)

[a]Read out from 1D ^{1}H NMR spectra recorded at 700 or 500 MHz frequency at 298 K; [b]the s-*trans* (major) amide rotamer data is shown first; the results in parentheses are for the s-*cis* (minor) amide rotamer; [c]n.d. not detected, the resonance appears as a doublet; [d]mix = a mixture of two conformations.

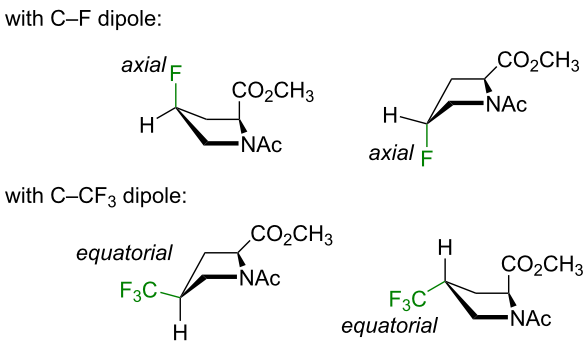

Figure 5: Preferred side-chain conformations according to the multiplicity data.

A stabilization of certain side-chain conformers was also observed in the trifluoromethylated analogues, **3** and **4**. However, the effect was not entirely clean. For example, in the *cis*-isomer **3**, the *exo*-C^4 envelope was only preferred in the major amide rotamer, whereas in the minor one, a mixture of two envelopes was observed. In the *trans*-isomer **4**, the C^4-*endo* envelope was found in all cases, except for the major amide rotamer in water, where the conformer was less defined. Overall, these outcomes demonstrate that the CF_3 group favors an equatorial placement, but the preference is notably weaker as compared to the monofluoroprolines (Figure 5).

It could be speculated that if the dipolar interaction of the polar substituents with the main chain groups would impact the side-chain conformation, this effect would be sensitive to the polarity of the solvent. The fact that the solvent plays only a minor role demonstrates that stronger determinants exist in the structure, namely, the stereoelectronic (C–F) and steric (C–CF_3) effects from the substituents.

Acid–base transition

The orientation of the substituents can also be inferred from the data on basicity of the ammonium group in free amino acids. It has been already mentioned that both, C–F and CF_3 groups introduce dipoles of similar sizes into the molecules. The latter one is slightly larger, but it is also one bond more distant to the main chain groups (Figure 3). Effectively, these dipoles reduce the basicity due to the interaction with the ammonium dipole through bond and through space [71] (Figure 6A). It can be seen from the experimental data that the basicity reduction from substituents that are parallel and perpendicular to the pyrrolidine ring are different. There are examples showing that the C–F or C–CF_3 fragment in plane with the ammonium dipole reduces the basicity by about $\Delta pK_a \approx 2.2$ [72,73]. The same value was obtained for (trifluoromethyl)prolines ($\Delta pK_a \approx 2.3$) with equatorially placed C–CF_3. In the fluoroprolines, there is a distinctly different orientation of the C–F dipoles, and the basicity reduction is notably smaller ($\Delta pK_a \approx 1.6$). Here, the substituent dipole is nearly perpendicular to the ammonium one, and this weakens their interaction.

Similar considerations can be applied to the acidity of the carboxylic group (Figure 6B), where the mutual orientation of the C–X dipole and the carboxylate -CO_2^- charge has an effect [74]. In diastereomeric fluoroprolines there is a large difference in the mutual orientation of the groups, while in the (trifluoromethyl)prolines the orientation is similar. This is reflected in the acidity values.

Lipophilicity

Another parameter, which may be sensitive to the orientation of the dipoles within a molecule is the lipophilicity. It is well known that single aliphatic fluorination usually increases polarity of a molecule due the newly introduced polar C–F bond. A CF_3 group introduces a dipole of a similar size (see Figure 2), however, due to its high molar volume it increases the hydrophobicity of a molecule [75]. The overall outcome may appear paradoxical: a CF_3 group can make a molecule more polar, but also more lipophilic at the same time. In addition, interactions of these dipoles with the ones preexisting in the parent molecule should always be considered for predicting the molecular polarity [60,76].

Experimental lipophilicity values found for the model compounds **1**–**4** fully corroborate the expectations: the monofluorinated compounds **1** and **2** exhibited a slightly lower log*P* compared to unsubstituted reference ($\Delta\log P_{H/F} \approx -0.2$ to -0.4), whereas in the trifluoromethylated compounds **3** and **4** the log*P* was notably higher ($\Delta\log P_{H/CF3} \approx +0.7$). Interestingly, the diastereomers exhibited some differences. The *cis*-diastereomer **1** with the C–F bond pointing in the same direction as the carboxymethyl group, appeared more polar compared to the *trans*-isomer **2**, where the direction was opposite ($\Delta\log P_{cis/trans} \approx -0.18$). The same effect was observed in 4-hydroxyprolines as well [13] ($\Delta\log P_{cis/trans} \approx -0.19$).

In contrast to **1** and **2**, the trifluoromethylated compounds **3** and **4** showed no difference between the lipophilicity of the diastereomers. This is due to the fact that the C–CF_3 substituent orientation is equatorial, thus nearly perpendicular to the CH–CO_2CH_3, and the dipoles do not sufficiently interact in this situation. However, minor conformations with axial CF_3 substituents do exist in the model compounds **3** and **4** (Figure 7). For example, both species were quite well separable using standard silica gel chromatography settings, where **4** appeared less polar than **3**. The existence of the minor conformations will also be relevant in the explanation of the amide-rotation barriers (vide infra).

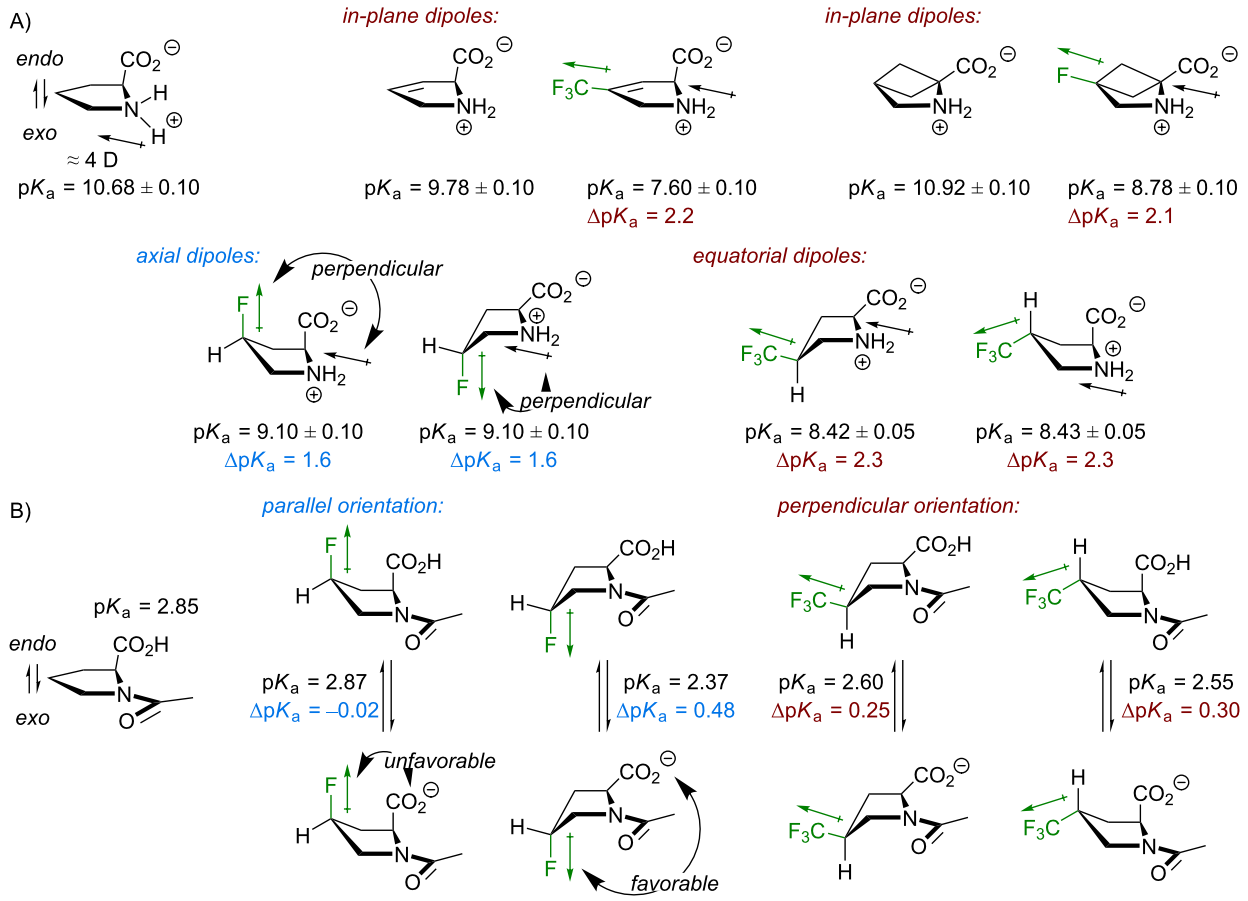

Figure 6: A) The basicity reduction from the introduction of the dipoles reflects the preferred conformation of the side chains. The positive end of the ammonium dipole is on the hydrogen atoms attached to the nitrogen. The nitrogen atom is the negative end. B) The acidity of the carboxylic group depends on the relative orientation of the substituent dipole with respect to the charged carboxylate. Only the s-*cis* rotamer data is shown. The error is ±0.05.

It should be noted that calculation of the net dipole is of little aid when accessing polarity of the model compounds **1**–**4** [77]. For example, the dipole moment calculated for compound **1** (μ_1 = 4.1–4.9 D) appeared smaller compared to the one of compound **2** (μ_2 = 5.4–5.9 D), although an entirely opposite outcome would be expected looking at the lipophilicity data. At the same time, the relatively low net dipole for the compounds **3** and **4** ($\mu_{3,4}$ = 1.4–2.1 D) predicts that there is an additional polarity drop associated with partial mutual compensation of the CF_3 and the amide dipoles (Figure 7). Indeed, this occurs experimentally. In fact, the lipophilicity contribution from the CF_3 group in **3** and **4** ($\Delta\log P_{H/CF3}$ +0.7) is notably larger compared to an isolated CF_3 group in a hydrocarbon chain ($\Delta\log P_{H/CF3}$ +0.3 – +0.4) [78]. In spite of this outcome, the model system seems too complex to be described by a single polarity parameter such as net dipole. This is due to the fact that the system maintains some degree of conformational flexibility (e.g., rotation of the carboxymethyl group), which creates a conformational landscape rather than a single conformation. At the same time, a net dipole calculation fully neglects the distance between individual interacting dipoles, which is a very important parameter by itself (e.g., the energy of the dipole–dipole interaction is reverse proportional to the cubic distance).

Discussions based on the net (molecular) dipole have become quite popular in the recent literature. Indeed, this parameter is critically relevant for the understanding of relatively small and simple molecular fragments [60,75,76,78], e.g., an axially rotating CF_3 group. Nonetheless, it is barely conclusive to approach interaction of complex molecules with solvents using net dipole alone. For example, even for the relatively simple molecules like **1**–**4**, the net dipole would not adequately represent neither the complexity of the interaction network within the molecule, nor probing of the molecular sites with relatively small dipoles of the solvent. This is why here it seems more reasonable to adhere to simple schematic descriptions such as the one shown in Figure 7.

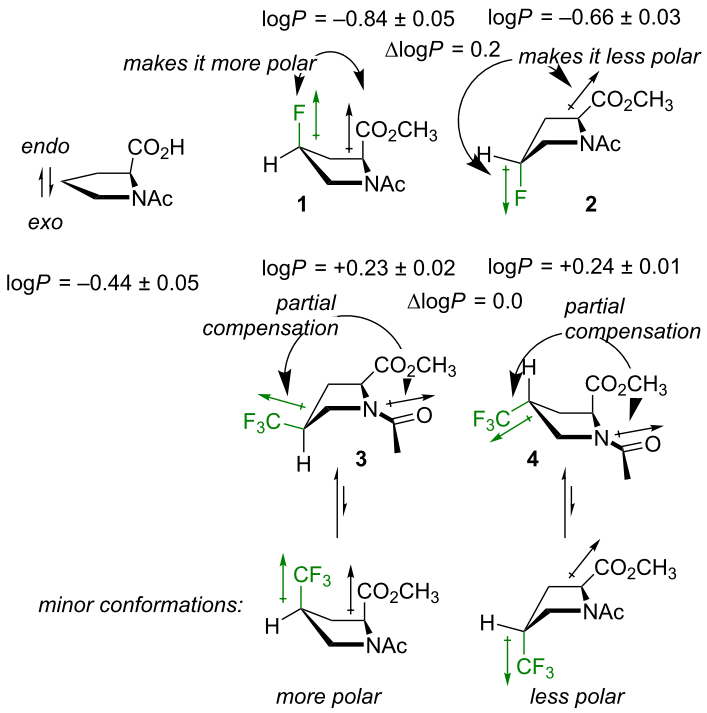

Figure 7: The lipophilicity data of the model compounds.

Amide-bond rotation: thermodynamics

Isomerization of the amide (peptide) bond is an important issue in protein chemistry. The peptide bond can exist in two discrete states, commonly designated as *trans*- and *cis*-rotamers (ω = 180 and 0°, respectively). The *cis*-peptide bond is very rare in natural proteins [79], except for the cases when it precedes a proline residue. The secondary amino group of proline forms a tertiary amide bond, which can often be found in either rotameric state. The peptide-bond isomerism in the peptidyl-prolyl fragments is involved in numerous biological processes in natural proteins [80].

Model compounds have been utilized to characterize the intrinsic propensity of proline and its analogues towards *trans*- and *cis*-amides [81]. An unsubstituted proline residue usually exhibits a preference to form a *trans*-amide. Fluoroprolines are notorious for the relative stabilization of the amide rotamers depending on the stereochemistry at the C^4-atom. This is known as the chiral bias. The effect occurs indirectly due to the impact onto the side-chain envelope conformation: the C^4-*exo* conformation creates a favorable relative arrangement of the main-chain groups. This energetic favorability is typically attributed to the n→π* donative interaction between the carbonyl groups, although the exact nature of this interaction (orbital or dipolar) is debatable [82]. Result of this effect though, is that the *trans*-fluoroproline shifts the equilibrium towards a higher abundance of the *trans*-amide, while *cis*-fluoroproline promotes the *cis*-amide (Figure 8). This was indeed found in the experimental data for the compounds **1** and **2** [83].

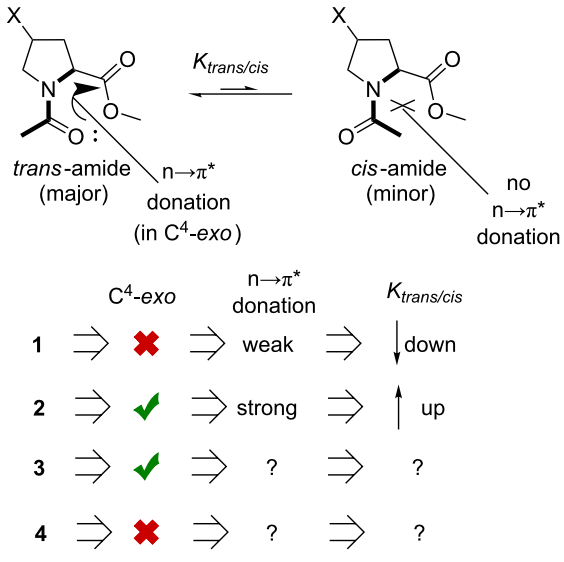

Figure 8: The expectations regarding the amide-bond rotation preferences in **1**–**4**.

The expectation was that the trifluoromethylated amino acids would exhibit similar effects with an opposite chiral bias. However, experimentally it was found that the *trans/cis* ratio in both compounds **3** and **4** is quite similar to the one in the unsubsti-

tuted reference (Table 2). The value $K_{trans/cis}$ decreased in a row: unsubstituted > **3** > **4**. Nonetheless, these differences were rather small and did not exceed 1.1 kJ mol^{-1}. Thus, (trifluoromethyl)prolines represent a peculiar case, where the C^4-conformational stabilization is so weak, that it only has a minor influence onto the *trans/cis* ratio. In contrast, the *gauche*-effect in fluoroprolines causes a much stronger stabilization of the C^4-conformations, as this propagates into stronger effects in the

Table 2: Amide-rotation equilibrium in the model compounds.[a]

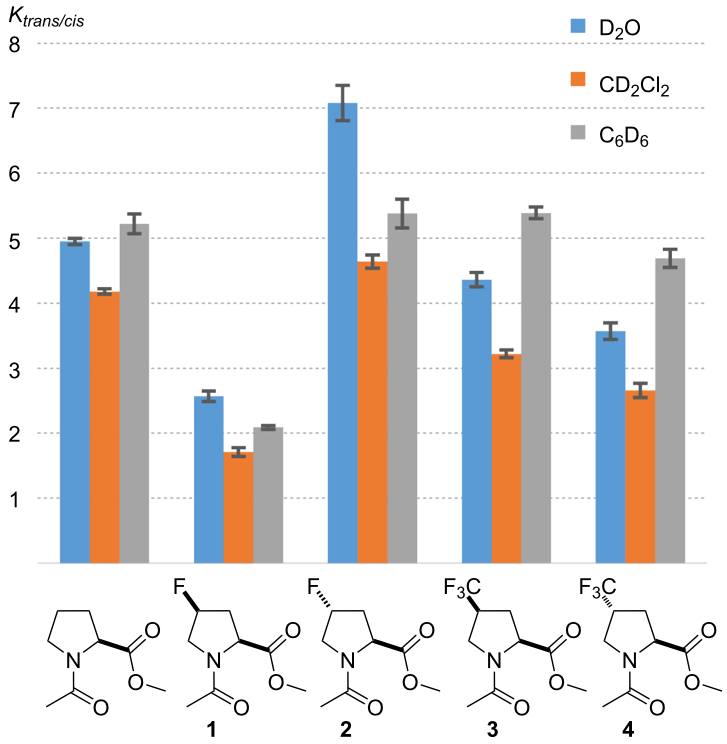

compound	$K_{trans/cis}$ in D_2O, ε 80.1	in CD_2Cl_2, ε 8.9	in C_6D_6, ε 2.3
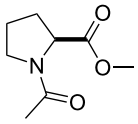	4.95 ± 0.05	4.18 ± 0.04	5.22 ± 0.15
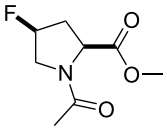 **1**	2.57 ± 0.08	1.71 ± 0.07	2.09 ± 0.03
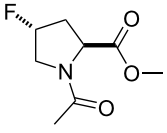 **2**	7.08 ± 0.27	4.64 ± 0.10	5.38 ± 0.22
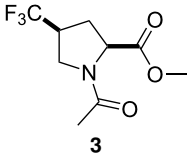 **3**	4.36 ± 0.11	3.22 ± 0.06	5.39 ± 0.09

Table 2: Amide-rotation equilibrium in the model compounds.[a] (continued)

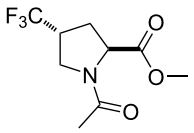 **4**	3.57 ± 0.13	2.66 ± 0.11	4.69 ± 0.14

[a]Measured by ^{1}H and ^{19}F NMR at 298 K. The values are provided with the standard deviation.

trans/cis equilibrium. In addition, there is a weak but systematic modulation in the *trans/cis* equilibrium caused by the solvent ($K_{benzene} \approx K_{water} > K_{dichloromethane}$). These are, however, still poorly understood and will not be further addressed here (see [74,77,84] for some discussions).

It is very well known that a proline-to-fluoroproline substitution alters protein folding. Predominantly, the effect onto the stability has been observed, and not the structure. The intrinsic preferences of the fluoroprolines translate into the differences in the folding energy and associated parameters such as melting points [81,85-90]. This study suggests that the analogous effect from (trifluoromethyl)prolines would be much weaker. The effects of their presence is a polypeptide structure should rather be associated with the increase in the molecular volume and hydrophobicity, and less with the backbone folding.

Amide-bond rotation: kinetics

Amide-bond rotation is known as an intrinsically slow process, which contributes to the rate-limiting steps in the protein folding [91] and molecular timing phenomena [92]. In peptidyl-prolyl bonds, the transition between the rotational states *cis*-amide and *trans*-amide usually occurs in the mHz scale, with the barriers of rotation around 80–90 kJ mol^{-1} (in water). At the same time, the amide rotation is a simple process with only one (prevalent) transition state and two ground states [93]. The high level of the energetic barrier implies that there is only a negligible subpopulation of molecules that may be involved in the transition, and therefore the rotation should not necessarily proceed from the major conformation. This is an important precaution that should be kept in mind in the analysis of the data. In model compounds, the barrier of rotation can be determined relatively accurately with the experimental methods such as EXSY NMR [94]. However, the interpretation is not always straightforward. In fact, the barrier of rotation is perhaps the most complex parameter among all those presented in this work.

In the next step, the amide rotation was measured in compounds **1**–**4** in three solvents with different polarities (for a detailed procedure see Supporting Information File 1). To make the interpretation easier, only *cis*-to-*trans* barrier is presented (Table 3). The analysis shows that this parameter decreased in a row: unsubstituted > **1** > **2** > **4** > **3** in all examined solvents.

Three interesting observations should be analyzed based on the presented data. First, the order unsubstituted > fluoroproline > (trifluoromethyl)proline reflects the increasing electron-withdrawing effect of the substituents H > –F > –CF_3, and it recapitulates the basicity trends observed previously (see Figure 6). Second, the solvation by polar solvents such as water substantially increases the stability of the ground-state amide bond, thereby elevating the rotation barrier [84,95]. Interestingly, the increase of the barrier when going from benzene to water ($\Delta_{water/benzene} = E^{\neq}_{in\ water} - E^{\neq}_{in\ benzene}$) was found larger in **1** compared to **2**, whereas in the diastereomeric couple **3** and **4** only a negligible difference was observed. This behavior can be explained by suggesting that the solvation of the diastereomers is also different. Because **1** is more polar than **2**, its desolvation in the course of the rotation process produces higher energetic costs. This can be seen from the fact that the energetic difference (1.5 kJ mol^{-1}) is similar do the difference in the lipophilicity values for the diastereomers **1** and **2** (see Figure 7: $\Delta \log P$ = 0.18 ~ 1.0 kJ mol^{-1}). In contrast, the lipophilicity in **3** and **4** is the same (see Figure 7), indicating that their solvation by water is also close to identical. Therefore, no difference was found in the solvation effects contributing to the rotation barriers in these molecules.

Finally, the difference between the barriers in the diastereomers calls for an explanation. It is clear from the presented data that the stereochemistry at the C^4-atom has an effect on the rotation velocity. The difference was especially prominent in the trifluoromethylated species, **3** and **4** (see Table 3). Curiously, it is not possible to explain this finding by considering the ground state, thus the so-called *syn/exo* transition state [96] should be analyzed instead. The data make sense, if one considers that the transition state proceeds through the C^4-*exo* conformation, as shown in Figure 9A. In this scenario, the *cis*-diastereomer **3** 1) readily favors the needed conformational state (vide supra), at the same time, 2) the CF_3-group dipole is oriented perpendicular to the carbonyl-group dipole, and creates no repulsion. As the result, the transition state is energetically favored, and the rotation becomes faster. Conversely, in the other diastereomer

Table 3: Amide-rotation velocity in the model compounds.[a]

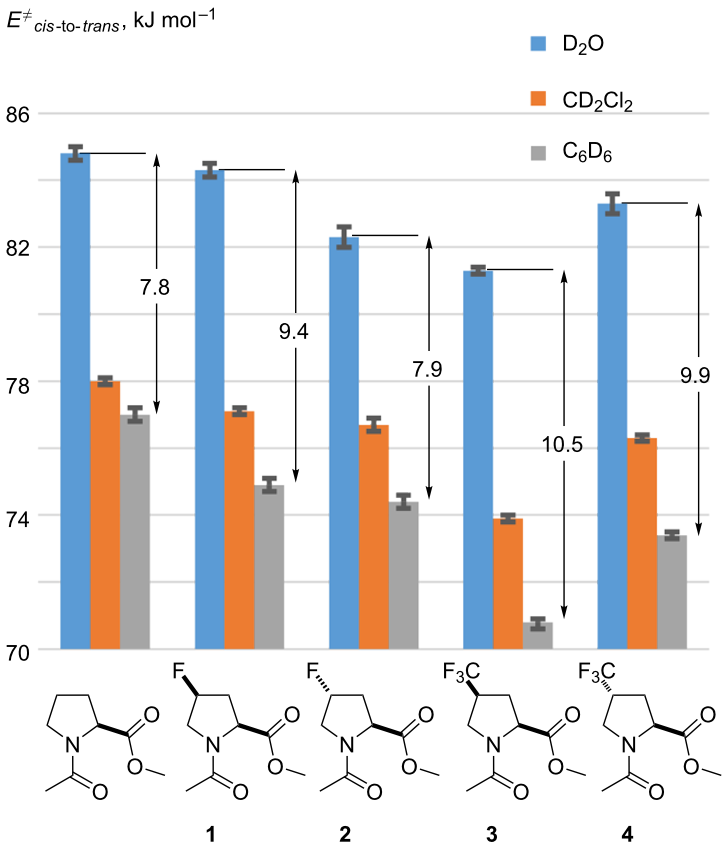

compound	$k_{cis\text{-to-}trans}$, Hz in D_2O, ε 80.1 (310 K)	in CD_2Cl_2, ε 8.9 (298 K)	in C_6D_6, ε 2.3 (298 K)
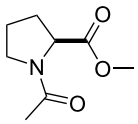	0.033 ± 0.002	0.033 ± 0.002[b]	0.043 ± 0.004
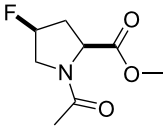 **1**	0.041 ± 0.004	0.187 ± 0.003	0.463 ± 0.034
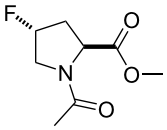 **2**	0.087 ± 0.009	0.220 ± 0.016	0.556 ± 0.027
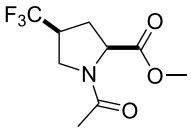 **3**	0.131 ± 0.008	0.690 ± 0.019	2.44 ± 0.07

Table 3: Amide-rotation velocity in the model compounds.[a] (continued)

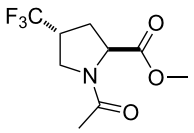 **4**	0.060 ± 0.006	0.265 ± 0.007	0.855 ± 0.031

[a]Measured by ^{1}H and ^{19}F EXSY NMR. Few spectra with different mixing times were measured. The exchange rate values were calculated from various exchange resonances and averaged. Their root mean deviation from the mean value is provided. The *k* values were converted to the energy barriers using the Eyring equation. The error in $E^{\neq}$ takes into account the standard deviation in the *k* values, and does not take into account the temperature calibration error. [b]The value is for $CDCl_3$, ε 4.8.

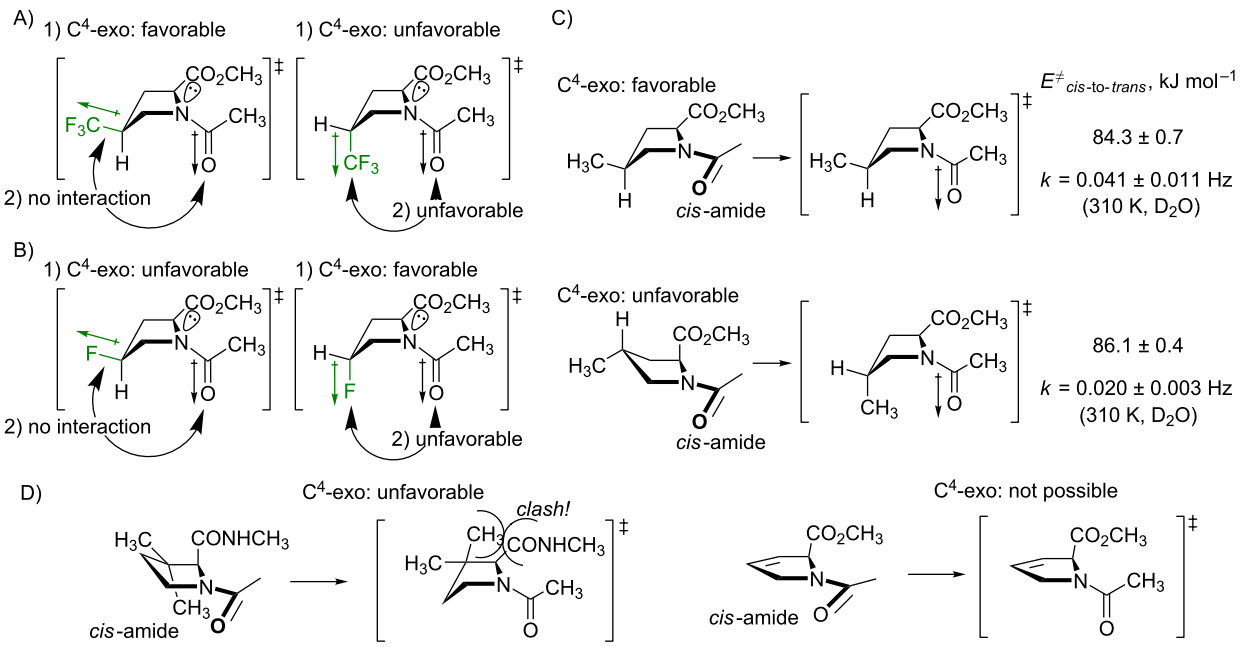

Figure 9: The explanation for the difference in the rotation barriers in the diastereomeric (A), 4-(trifluoromethyl)prolines (B) 4-fluoroprolines, and (**C**) 4-methylprolines. D) The two known cases with the increase of the barrier of rotation in proline analogues.

4, both factors disfavor the transition state: 1) the ring should adopt the disfavored C^4-*exo* conformation with an axial CF_3 group, and 2) this group forms an unfavorable dipole–dipole interaction with the carbonyl group. As the result, the rotation process slows down. Eventually, these differences translate into the observed 2.0–2.6 kJ mol^{-1} energetic difference in the barriers.

The same considerations can be applied to the fluoroprolines, **1** and **2** (Figure 9B). However, in this case, the two arguments, 1) and 2) contradict each other. As a result, it was observed that the rotation in **2** is faster, but only by a small number: 0.4 and 0.5 kJ mol^{-1} in dichloromethane and benzene, respectively [97] (note that in water the ground-state solvation effect increases this difference).

The explanation proposed in Figure 9 relies on the assumption that the C^4-*exo* conformation is favored by the transition state. This hypothesis should be further examined. This can be done by considering the rotation barriers in diastereomeric 4-methylprolines. In these species, the methyl group does not introduce any new dipoles to the parent system, therefore only the conformational preferences should have an effect. Indeed, it was found that the *cis*-to-*trans* transition in 4-*cis*-methylproline (favors C^4-*exo*) is faster compared to 4-*trans*-methylproline (disfavors C^4-*exo*) by 1.8 kJ mol^{-1} (Figure 9C). This observation agrees with the calculation predictions [98], and it fully confirms the hypothesis.

It is interesting to note, that there are only two types of analogues reported to date, where the barriers of the amide-bond

rotation are higher compared to proline. These are 3,3-dimethylprolines [99] and 3,4-dehydroprolines [72]. It has not been clear however, why these analogues show such an effect, considering that the modifications are quite distant to the rotating amide bond. The inability of the analogues to adopt the C^4-*exo* conformation in the transition state would explain the energy penalty in the rotation barriers (Figure 9D). In 3,3-dimethylprolines, the isomerization into the C^4-*exo* envelope would lead to a steric clash between one of the methyl groups and the backbone carbonyl (*k* decreases by a factor of 2–6) [99]; in 3,4-dehydroprolines, the ring is unable to adopt an envelope conformation due to an endocyclic double bond (*k* decreases by factor 3) [72].

Overall, the conclusions regarding the ring conformation preference in the transition state provides an entirely new insight onto the peptide-bond isomerization, and can be helpful for better understanding of this fundamental process in natural and engineered systems.

Effects in difluorinated spirocyclic analogues

In the final step, the proposed understanding of the molecular system was tested on a new set of proline analogues, **5** and **6** (Figure 10A). The synthesis of these amino acids was reported very recently [100]. The reference compound **7** was also analyzed. It should be noted that the difluorinated compounds **5** and **6** resemble the trifluoromethylated analogues **3** and **4** by the number of bonds separating the fluorine atoms from the main chain functional groups. A critical difference is, however, that the CF_2 group present in **5** and **6** does not undergo a rotational averaging of the dipoles, as this happens in the C–CF_3 system. This in principle may create even more complex situations compared to the presented so far.

In spite of this expectation, the results show that the model compounds **5** and **6** follow generally similar chiral bias to **3** and **4**. The pK_a data for the free amino acids shows that there is an identical reduction of the pK_a values from fluorination (Figure 10B and C). It was then found that neither the side-chain conformation markers (*J* coupling at 2-CH) nor the *trans/cis* equilibrium values ($K_{trans/cis}$) were different in **5** compared to the non-fluorinated reference **7**. Likewise, the *trans/cis* equilibrium in **3** is similar to the unsubstituted proline. Conversely, in compound **6**, there was a higher content of the C^4-*endo* conformation, a lower *trans/cis* equilibrium ratio, and the amide-bond rotation barrier was higher compared to the other diastereomer, **5**. The lack of rotational averaging in **5** and **6** leads to the interesting fact that the lipophilicity was different for these two diastereomers ($\Delta\log P$ = 0.15). This suggests that the solvation by water slightly differs between the diastereomeric species. Indeed, this conclusion was further corroborated by the rotation barrier data, which showed higher $\Delta_{water/benzene}$ for the less lipophilic diastereomer, **6** (Table 4).

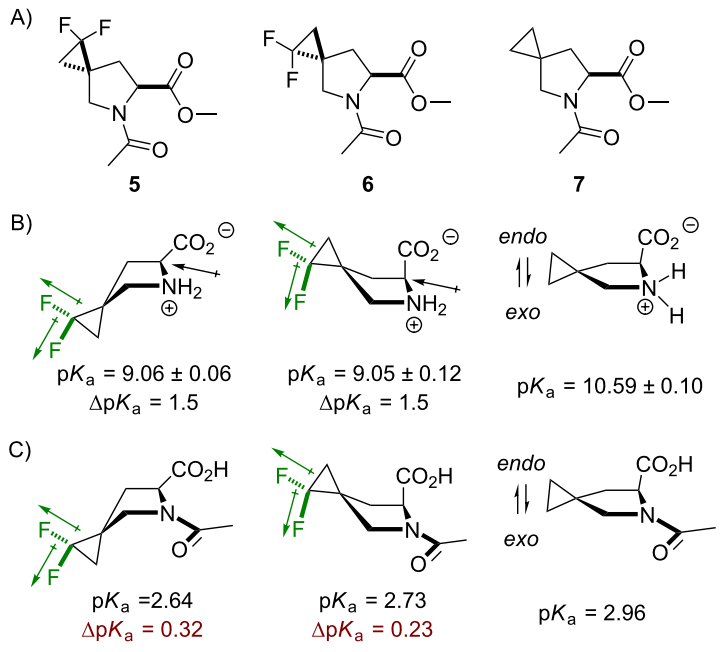

Figure 10: A) The structures of difluorinated model compounds **5** and **6**, and the fluorine-free reference **7**. B) Basicity data for the corresponding amino acids. C) Acidity data for the s-*cis* *N*-acetylamino acids. The error is ± 0.05.

Table 4: Experimental data for compounds **5**–**7**.

compound	^{1}H NMR multiplicity of 2-CH[a,b]						$E^{\neq}_{cis\text{-to-}trans}$[c] kJ mol^{-1}		log*P*
	in CD_2Cl_2			in D_2O			in D_2O	in C_6D_6	
	^1J, Hz	^2J, Hz	C^4-	^1J, Hz	^2J, Hz	C^4-			
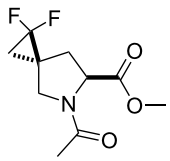 **5**	$K_{trans/cis}$ = 3.13 ± 0.07			$K_{trans/cis}$ = 3.94 ± 0.03			82.4 ± 0.4 $\Delta_{water/benzene}$ = 9.0	73.4 ± 0.1	+0.18 ± 0.03
	8.8 (8.7)	5.0 (2.8)	mix[d] *(endo)*	8.8 (8.8)	5.4 (2.3)	mix[d] *(endo)*			
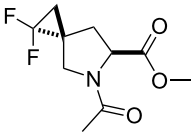 **6**	$K_{trans/cis}$ = 2.47 ± 0.02			$K_{trans/cis}$ = 3.15 ± 0.05			84.5 ± 0.2 $\Delta_{water/benzene}$ = 10.3	74.2 ± 0.2	+0.03 ± 0.02
	8.9 (8.5)	1.8 (1.0)	*endo* *(endo)*	9.1 (8.6)	1.2 (n.d.)[e]	*endo* *(endo)*			
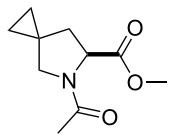 **7**	$K_{trans/cis}$ = 3.35 ± 0.02			$K_{trans/cis}$ = 3.92 ± 0.04			85.6 ± 1.1 $\Delta_{water/benzene}$ = 9.5	76.3 ± 0.1	+0.19 ± 0.03
	8.6 (8.5)	4.4 (2.4)	mix[d] *(endo)*	8.8 (8.4)	3.6 (n.d.)[e]	mix[d] *(endo)*			

[a]Read out from 1D ^{1}H NMR spectra recorded at 700 MHz frequency at 298 K; [b]the s-*trans* (major) amide rotamer data is shown first; the results in parentheses are for the s-*cis* (minor) amide rotamer; [c]measured by ^{1}H EXSY NMR at 298 K for C_6D_6 and 310 K for D_2O; [d]mix = a mixture of two conformations; [e]n.d. not detected.

Overall, the effects from fluorination in both diastereomeric compounds, **5** and **6**, were found to be weak relative to what has been observed in monofluoroprolines, for instance. Nonetheless, the trends in the molecular properties come in a good agreement with analogous trends found in (trifluoromethyl)prolines, with some exceptions in lipophilicity and solvation.

Conclusion

In summary, this study aimed to expose the impact of polar substituents in position 4 of the proline ring onto the physicochemical properties of the parent amino acid residue. Two molecular systems were examined to mimic such situation: 4-fluoroproline and 4-(trifluoromethyl)proline. In the first one, the substituent C^4–F bond tends to adopt an axial position, due to a F–C–C–N *gauche* effect. In the second one, the C^4–CF_3 bond favors an equatorial position due to its large steric size. The resulting orientation of the substituent dipoles with respect to the main chain groups has an impact onto molecular properties such as lipophilicity, acid–base transition, and kinetics of the amide-bond rotation. Interestingly it was found that the side-chain conformational preferences translate differently into the energy of the *trans/cis* amide equilibrium. While in the monofluoroprolines the effect was relatively strong, in the trifluoromethylated species it was notably weaker. Thus, it is expected that (trifluoromethyl)prolines should impact polypeptide structures by altering the bulkiness and hydrophobicity of the residue site, and not the backbone folding. The conclusions derived from the trifluoromethylated species were further corroborated by the examination of 1,1-difluoro-5-azaspiro[2.4]heptane-6-carboxylate based models, which showed similar trends in properties.

Finally, the study provides a set of experimental evidences that reveal details of the transition state for the *cis/trans* amide rotation. Namely, it follows from the presented data that the transition state prefers the C^4-*exo* conformation of the proline ring. This creates a chiral bias of the C^4-substitution in the amide-rotation barrier, that has not been highlighted so far in the experimental literature. These findings will be helpful for the design and the use of proline analogues in complex biological systems such as peptides and proteins, especially in ^{19}F NMR labelling, where fluorinated prolines can serve as spectroscopic probes. Potential areas for the application of fluorinated prolines are numerous, and include the design of molecular recognition systems [101], organocatalysis [102], drug discovery [103] and more.

Supporting Information

Supporting Information File 1

Data on acid–base transition and amide bond isomerism and NMR characterization of compounds **1**–**7**.
[https://www.beilstein-journals.org/bjoc/content/supplementary/1860-5397-16-151-S1.pdf]

Funding

The author would like to acknowledge Canadian federal government for funding the research chair for chemical synthetic biology (lead Dr. Budisa) at the University of Manitoba.

ORCID® iDs

Vladimir Kubyshkin - https://orcid.org/0000-0002-4467-4205

References

1. Kubyshkin, V.; Budisa, N. *Curr. Opin. Biotechnol.* **2019,** *60,* 242–249. doi:10.1016/j.copbio.2019.05.006
2. Li, S.-C.; Deber, C. M. *Nat. Struct. Mol. Biol.* **1994,** *1,* 368–373. doi:10.1038/nsb0694-368
3. Kay, B. K.; Williamson, M. P.; Sudol, M. *FASEB J.* **2000,** *14,* 231–241. doi:10.1096/fasebj.14.2.231
4. Theillet, F.-X.; Kalmar, L.; Tompa, P.; Han, K.-H.; Selenko, P.; Dunker, A. K.; Daughdrill, G. W.; Uversky, V. N. *Intrinsically Disord. Proteins* **2013,** *1,* e24360. doi:10.4161/idp.24360
5. Kubyshkin, V.; Budisa, N. *J. Pept. Sci.* **2018,** *24,* e3076. doi:10.1002/psc.3076
6. Newberry, R. W.; Raines, R. T. 4-Fluoroprolines: Conformational Analysis and Effects on the Stability and Folding of Peptides and Proteins. *Peptidomimetics;* Topics in Heterocyclic Chemistry, Vol. 48; Springer: Cham, Switzerland, 2017; pp 1–25. doi:10.1007/7081_2015_196
7. Kim, W.; Hardcastle, K. I.; Conticello, V. P. *Angew. Chem., Int. Ed.* **2006,** *45,* 8141–8145. doi:10.1002/anie.200603227
8. Thomas, C. A.; Talaty, E. R.; Bann, J. G. *Chem. Commun.* **2009,** 3366–3368. doi:10.1039/b821952d
9. Hofman, G.-J.; Ottoy, E.; Light, M. E.; Kieffer, B.; Kuprov, I.; Martins, J. C.; Sinnaeve, D.; Linclau, B. *Chem. Commun.* **2018,** *54,* 5118–5121. doi:10.1039/c8cc01493k
10. Hofman, G.-J.; Ottoy, E.; Light, M. E.; Kieffer, B.; Martins, J. C.; Kuprov, I.; Sinnaeve, D.; Linclau, B. *J. Org. Chem.* **2019,** *84,* 3100–3120. doi:10.1021/acs.joc.8b02920
11. Shoulders, M. D.; Kamer, K. J.; Raines, R. T. *Bioorg. Med. Chem. Lett.* **2009,** *19,* 3859–3862. doi:10.1016/j.bmcl.2009.03.168
12. Doebelin, C.; He, Y.; Kamenecka, T. M. *Tetrahedron Lett.* **2016,** *57,* 5658–5660. doi:10.1016/j.tetlet.2016.11.012
13. Kubyshkin, V.; Pridma, S.; Budisa, N. *New J. Chem.* **2018,** *42,* 13461–13470. doi:10.1039/c8nj02631a
14. Chaume, G.; Van Severen, M.-C.; Marinkovic, S.; Brigaud, T. *Org. Lett.* **2006,** *8,* 6123–6126. doi:10.1021/ol062593+
15. Huang, G.; Yin, Z.; Zhang, X. *Chem. – Eur. J.* **2013,** *19,* 11992–11998. doi:10.1002/chem.201301479
16. Tolmachova, N. A.; Kondratov, I. S.; Dolovanyuk, V. G.; Pridma, S. O.; Chernykh, A. V.; Daniliuc, C. G.; Haufe, G. *Chem. Commun.* **2018,** *54,* 9683–9686. doi:10.1039/c8cc05912h
17. Del Valle, J. R.; Goodman, M. *Angew. Chem., Int. Ed.* **2002,** *41,* 1600–1602. doi:10.1002/1521-3773(20020503)41:9<1600::aid-anie1600>3.0.co;2-v
18. Qiu, X.-l.; Qing, F.-l. *J. Chem. Soc., Perkin Trans. 1* **2002,** 2052–2057. doi:10.1039/b206719f
19. Qiu, X.-l.; Qing, F.-l. *J. Org. Chem.* **2002,** *67,* 7162–7164. doi:10.1021/jo0257400
20. Kubyshkin, V.; Afonin, S.; Kara, S.; Budisa, N.; Mykhailiuk, P. K.; Ulrich, A. S. *Org. Biomol. Chem.* **2015,** *13,* 3171–3181. doi:10.1039/c5ob00034c
21. Kondratov, I. S.; Dolovanyuk, V. G.; Tolmachova, N. A.; Gerus, I. I.; Bergander, K.; Fröhlich, R.; Haufe, G. *Org. Biomol. Chem.* **2012,** *10,* 8778–8785. doi:10.1039/c2ob26176f
22. Ortial, S.; Dave, R.; Benfodda, Z.; Bénimélis, D.; Meffre, P. *Synlett* **2014,** *25,* 569–573. doi:10.1055/s-0033-1340553
23. Lubin, H.; Pytkowicz, J.; Chaume, G.; Sizun-Thomé, G.; Brigaud, T. *J. Org. Chem.* **2015,** *80,* 2700–2708. doi:10.1021/jo502885v
24. Testa, A.; Lucas, X.; Castro, G. V.; Chan, K.-H.; Wright, J. E.; Runcie, A. C.; Gadd, M. S.; Harrison, W. T. A.; Ko, E.-J.; Fletcher, D.; Ciulli, A. *J. Am. Chem. Soc.* **2018,** *140,* 9299–9313. doi:10.1021/jacs.8b05807
25. Caupene, C.; Chaume, G.; Ricard, L.; Brigaud, T. *Org. Lett.* **2009,** *11,* 209–212. doi:10.1021/ol8024567
26. Chaume, G.; Barbeau, O.; Lesot, P.; Brigaud, T. *J. Org. Chem.* **2010,** *75,* 4135–4145. doi:10.1021/jo100518t
27. Feytens, D.; Chaume, G.; Chassaing, G.; Lavielle, S.; Brigaud, T.; Byun, B. J.; Kang, Y. K.; Miclet, E. *J. Phys. Chem. B* **2012,** *116,* 4069–4079. doi:10.1021/jp300284u
28. Chaume, G.; Simon, J.; Lensen, N.; Pytkowicz, J.; Brigaud, T.; Miclet, E. *J. Org. Chem.* **2017,** *82,* 13602–13608. doi:10.1021/acs.joc.7b01944
29. Tressler, C. M.; Zondlo, N. J. *J. Org. Chem.* **2014,** *79,* 5880–5886. doi:10.1021/jo5008674
30. Jenkins, C. L.; Lin, G.; Duo, J.; Rapolu, D.; Guzei, I. A.; Raines, R. T.; Krow, G. R. *J. Org. Chem.* **2004,** *69,* 8565–8573. doi:10.1021/jo049242y
31. Mykhailiuk, P. K.; Afonin, S.; Palamarchuk, G. V.; Shishkin, O. V.; Ulrich, A. S.; Komarov, I. V. *Angew. Chem., Int. Ed.* **2008,** *47,* 5765–5767. doi:10.1002/anie.200801022
32. Tkachenko, A. N.; Radchenko, D. S.; Mykhailiuk, P. K.; Grygorenko, O. O.; Komarov, I. V. *Org. Lett.* **2009,** *11,* 5674–5676. doi:10.1021/ol902381w
33. Kubyshkin, V. S.; Mykhailiuk, P. K.; Afonin, S.; Ulrich, A. S.; Komarov, I. V. *Org. Lett.* **2012,** *14,* 5254–5257. doi:10.1021/ol302412a
34. Ouerfelli, O.; Simon, J.; Chelain, E.; Pytkowicz, J.; Besbes, R.; Brigaud, T. *Org. Lett.* **2020,** *22,* 2946–2949. doi:10.1021/acs.orglett.0c00645
35. Kenis, S.; D'hooghe, M.; Verniest, G.; Reybroeck, M.; Dang Thi, T. A.; Pham The, C.; Thi Pham, T.; Törnroos, K. W.; Van Tuyen, N.; De Kimpe, N. *Chem. – Eur. J.* **2013,** *19,* 5966–5971. doi:10.1002/chem.201204485
36. Jiang, J.; Shah, H.; DeVita, R. J. *Org. Lett.* **2003,** *5,* 4101–4103. doi:10.1021/ol030099p
37. Lensen, N.; Marais, J.; Brigaud, T. *Org. Lett.* **2015,** *17,* 342–345. doi:10.1021/ol503448w

38. Jatoi, W. B.; Bariau, A.; Esparcieux, C.; Figueredo, G.; Troin, Y.; Canet, J.-L. *Synlett* **2008,** 1305–1308. doi:10.1055/s-2008-1072768
39. Gulevich, A. V.; Shevchenko, N. E.; Balenkova, E. S.; Röschenthaler, G.-V.; Nenajdenko, V. G. *Synlett* **2009,** 403–406. doi:10.1055/s-0028-1087529
40. Yarmolchuk, V. S.; Mykhailiuk, P. K.; Komarov, I. V. *Tetrahedron Lett.* **2011,** *52,* 1300–1302. doi:10.1016/j.tetlet.2011.01.070
41. Hao, J.; Milcent, T.; Retailleau, P.; Soloshonok, V. A.; Ongeri, S.; Crousse, B. *Eur. J. Org. Chem.* **2018,** 3688–3692. doi:10.1002/ejoc.201800255
42. Jatoi, W. B.; Desiront, A.; Job, A.; Troin, Y.; Canet, J.-L. *J. Fluorine Chem.* **2013,** *145,* 8–17. doi:10.1016/j.jfluchem.2012.11.006
43. Kudryavtsev, K. V.; Mantsyzov, A. B.; Ivantcova, P. M.; Sokolov, M. N.; Churakov, A. V.; Bräse, S.; Zefirov, N. S.; Polshakov, V. I. *Org. Lett.* **2016,** *18,* 4698–4701. doi:10.1021/acs.orglett.6b02327
44. Jurica, E. A.; Wu, X.; Williams, K. N.; Hernandez, A. S.; Nirschl, D. S.; Rampulla, R. A.; Mathur, A.; Zhou, M.; Cao, G.; Xie, C.; Jacob, B.; Cai, H.; Wang, T.; Murphy, B. J.; Liu, H.; Xu, C.; Kunselman, L. K.; Hicks, M. B.; Sun, Q.; Schnur, D. M.; Sitkoff, D. F.; Dierks, E. A.; Apedo, A.; Moore, D. B.; Foster, K. A.; Cvijic, M. E.; Panemangalore, R.; Flynn, N. A.; Maxwell, B. D.; Hong, Y.; Tian, Y.; Wilkes, J. J.; Zinker, B. A.; Whaley, J. M.; Barrish, J. C.; Robl, J. A.; Ewing, W. R.; Ellsworth, B. A. *J. Med. Chem.* **2017,** *60,* 1417–1431. doi:10.1021/acs.jmedchem.6b01559
45. Mykhailiuk, P. K.; Shishkina, S. V.; Shishkin, O. V.; Zaporozhets, O. A.; Komarov, I. V. *Tetrahedron* **2011,** *67,* 3091–3097. doi:10.1016/j.tet.2011.02.082
46. Malquin, N.; Rahgoshay, K.; Lensen, N.; Chaume, G.; Miclet, E.; Brigaud, T. *Chem. Commun.* **2019,** *55,* 12487–12490. doi:10.1039/c9cc05771d
47. Soloshonok, V. A.; Cai, C.; Hruby, V. J.; Van Meervelt, L.; Mischenko, N. *Tetrahedron* **1999,** *55,* 12031–12044. doi:10.1016/s0040-4020(99)00711-5
48. Rabasa-Alcañiz, F.; Hammerl, D.; Sánchez-Merino, A.; Tejero, T.; Merino, P.; Fustero, S.; del Pozo, C. *Org. Chem. Front.* **2019,** *6,* 2916–2923. doi:10.1039/c9qo00525k
49. Constantini, N. V.; Ganguly, H. K.; Martin, M. I.; Wenzell, N. A.; Yap, G. P. A.; Zondlo, N. J. *Chem. – Eur. J.* **2019,** *25,* 11356–11364. doi:10.1002/chem.201902382
50. Ganguly, H. K.; Basu, G. *Biophys. Rev.* **2020,** *12,* 25–39. doi:10.1007/s12551-020-00621-8
51. Verhoork, S. J. M.; Killoran, P. M.; Coxon, C. R. *Biochemistry* **2018,** *57,* 6132–6143. doi:10.1021/acs.biochem.8b00787
52. Kubyshkin, V.; Grage, S. L.; Ulrich, A. S.; Budisa, N. *Phys. Chem. Chem. Phys.* **2019,** *21,* 22396–22408. doi:10.1039/c9cp02996f
53. Tressler, C. M.; Zondlo, N. J. *ACS Chem. Biol.* **2020,** *15,* 1096–1103. doi:10.1021/acschembio.0c00131
54. Fillon, Y. A.; Anderson, J. P.; Chmielewski, J. *J. Am. Chem. Soc.* **2005,** *127,* 11798–11803. doi:10.1021/ja052377g
55. Pujals, S.; Fernández-Carneado, J.; Kogan, M. J.; Martinez, J.; Cavelier, F.; Giralt, E. *J. Am. Chem. Soc.* **2006,** *128,* 8479–8483. doi:10.1021/ja060036c
56. Oliver, M.; Gadais, C.; García-Pindado, J.; Teixidó, M.; Lensen, N.; Chaume, G.; Brigaud, T. *RSC Adv.* **2018,** *8,* 14597–14602. doi:10.1039/c8ra02511h
57. Holzberger, B.; Obeid, S.; Welte, W.; Diederichs, K.; Marx, A. *Chem. Sci.* **2012,** *3,* 2924–2931. doi:10.1039/c2sc20545a
58. Dietz, D.; Kubyshkin, V.; Budisa, N. *ChemBioChem* **2015,** *16,* 403–406. doi:10.1002/cbic.201402654
59. Huang, K.-Y.; Horng, J.-C. *Biochemistry* **2015,** *54,* 6186–6194. doi:10.1021/acs.biochem.5b00880
60. Müller, K. *Chimia* **2014,** *68,* 356–362. doi:10.2533/chimia.2014.356
61. Cabezas, C.; Varela, M.; Alonso, J. L. *ChemPhysChem* **2013,** *14,* 2539–2543. doi:10.1002/cphc.201300250
62. Newberry, R. W.; Raines, R. T. *Nat. Chem. Biol.* **2016,** *12,* 1084–1088. doi:10.1038/nchembio.2206
63. León, I.; Alonso, E. R.; Cabezas, C.; Mata, S.; Alonso, J. L. *Commun. Chem.* **2019,** *2,* No. 3. doi:10.1038/s42004-018-0103-2
64. Kang, Y. K.; Young Choi, H. *Biophys. Chem.* **2004,** *111,* 135–142. doi:10.1016/j.bpc.2004.05.006
65. Kang, Y. K. *J. Phys. Chem. B* **2007,** *111,* 10550–10556. doi:10.1021/jp073411b
66. Cai, M.; Huang, Y.; Liu, J.; Krishnamoorthi, R. *J. Biomol. NMR* **1995,** *6,* 123–128. doi:10.1007/bf00211775
67. Improta, R.; Benzi, C.; Barone, V. *J. Am. Chem. Soc.* **2001,** *123,* 12568–12577. doi:10.1021/ja010599i
68. Hodges, J. A.; Raines, R. T. *J. Am. Chem. Soc.* **2003,** *125,* 9262–9263. doi:10.1021/ja035881z
69. Shoulders, M. D.; Hodges, J. A.; Raines, R. T. *J. Am. Chem. Soc.* **2006,** *128,* 8112–8113. doi:10.1021/ja061793d
70. Cadamuro, S. A.; Reichold, R.; Kusebauch, U.; Musiol, H.-J.; Renner, C.; Tavan, P.; Moroder, L. *Angew. Chem., Int. Ed.* **2008,** *47,* 2143–2146. doi:10.1002/anie.200704310
71. Hansch, C.; Leo, A.; Taft, R. W. *Chem. Rev.* **1991,** *91,* 165–195. doi:10.1021/cr00002a004
72. Kubyshkin, V.; Budisa, N. *Beilstein J. Org. Chem.* **2016,** *12,* 589–593. doi:10.3762/bjoc.12.57
73. Mykhailiuk, P. K.; Kubyshkin, V.; Bach, T.; Budisa, N. *J. Org. Chem.* **2017,** *82,* 8831–8841. doi:10.1021/acs.joc.7b00803
74. Kubyshkin, V.; Durkin, P.; Budisa, N. *New J. Chem.* **2016,** *40,* 5209–5220. doi:10.1039/c5nj03611a
75. Huchet, Q. A.; Kuhn, B.; Wagner, B.; Fischer, H.; Kansy, M.; Zimmerli, D.; Carreira, E. M.; Müller, K. *J. Fluorine Chem.* **2013,** *152,* 119–128. doi:10.1016/j.jfluchem.2013.02.023
76. Huchet, Q. A.; Trapp, N.; Kuhn, B.; Wagner, B.; Fischer, H.; Kratochwil, N. A.; Carreira, E. M.; Müller, K. *J. Fluorine Chem.* **2017,** *198,* 34–46. doi:10.1016/j.jfluchem.2017.02.003
77. Siebler, C.; Maryasin, B.; Kuemin, M.; Erdmann, R. S.; Rigling, C.; Grünenfelder, C.; Ochsenfeld, C.; Wennemers, H. *Chem. Sci.* **2015,** *6,* 6725–6730. doi:10.1039/c5sc02211h
78. Jeffries, B.; Wang, Z.; Felstead, H. R.; Le Questel, J.-Y.; Scott, J. S.; Chiarparin, E.; Graton, J.; Linclau, B. *J. Med. Chem.* **2020,** *63,* 1002–1031. doi:10.1021/acs.jmedchem.9b01172
79. Jabs, A.; Weiss, M. S.; Hilgenfeld, R. *J. Mol. Biol.* **1999,** *286,* 291–304. doi:10.1006/jmbi.1998.2459
80. Craveur, P.; Joseph, A. P.; Poulain, P.; de Brevern, A. G.; Rebehmed, J. *Amino Acids* **2013,** *45,* 279–289. doi:10.1007/s00726-013-1511-3
81. Shoulders, M. D.; Raines, R. T. *Annu. Rev. Biochem.* **2009,** *78,* 929–958. doi:10.1146/annurev.biochem.77.032207.120833
82. Muchowska, K. B.; Pascoe, D. J.; Borsley, S.; Smolyar, I. V.; Mati, I. K.; Adam, C.; Nichol, G. S.; Ling, K. B.; Cockroft, S. L. *Angew. Chem., Int. Ed.* **2020,** in press. doi:10.1002/anie.202005739
83. Renner, C.; Alefelder, S.; Bae, J. H.; Budisa, N.; Huber, R.; Moroder, L. *Angew. Chem., Int. Ed.* **2001,** *40,* 923–925. doi:10.1002/1521-3773(20010302)40:5<923::aid-anie923>3.0.co;2-%23

84. Eberhardt, E. S.; Loh, S. N.; Hinck, A. P.; Raines, R. T. *J. Am. Chem. Soc.* **1992,** *114,* 5437–5439. doi:10.1021/ja00039a072
85. Steiner, T.; Hess, P.; Bae, J. H.; Wiltschi, B.; Moroder, L.; Budisa, N. *PLoS One* **2008,** *3,* e1680. doi:10.1371/journal.pone.0001680
86. Edwardraja, S.; Sriram, S.; Govindan, R.; Budisa, N.; Lee, S.-G. *Mol. BioSyst.* **2011,** *7,* 258–265. doi:10.1039/c0mb00154f
87. Crespo, M. D.; Rubini, M. *PLoS One* **2011,** *6,* e19425. doi:10.1371/journal.pone.0019425
88. Rubini, M.; Schärer, M. A.; Capitani, G.; Glockshuber, R. *ChemBioChem* **2013,** *14,* 1053–1057. doi:10.1002/cbic.201300178
89. Arnold, U.; Raines, R. T. *Org. Biomol. Chem.* **2016,** *14,* 6780–6785. doi:10.1039/c6ob00980h
90. Nadarajan, S. P.; Deepankumar, K.; Seo, J.-H.; Yun, H. *Biotechnol. Bioprocess Eng.* **2017,** *22,* 504–511. doi:10.1007/s12257-017-0257-2
91. Masiero, A.; Nelly, L.; Marianne, G.; Christophe, S.; Florian, L.; Ronan, C.; Claire, B.; Cornelia, Z.; Grégoire, B.; Eric, L.; Ludovic, L.; Dominique, B.; Sylvie, A.; Marie, G.; Francis, D.; Fabienne, S.; Cécile, C.; Isabelle, A.; Jacques, D.; Jérôme, D.; Bruno, G.; Katarina, R.; Jean-Michel, M.; Catherine, P. *mAbs* **2020,** *12,* 1698128. doi:10.1080/19420862.2019.1698128
92. Mosesso, R.; Dougherty, D. A.; Lummis, S. C. R. *ACS Chem. Neurosci.* **2019,** *10,* 3327–3333. doi:10.1021/acschemneuro.9b00315
93. Fischer, G. *Chem. Soc. Rev.* **2000,** *29,* 119–127. doi:10.1039/a803742f
94. Nikitin, K.; O'Gara, R. *Chem. – Eur. J.* **2019,** *25,* 4551–4589. doi:10.1002/chem.201804123
95. Radzicka, A.; Acheson, S. A.; Wolfenden, R. *Bioorg. Chem.* **1992,** *20,* 382–386. doi:10.1016/0045-2068(92)90048-8
96. Kubyshkin, V.; Budisa, N. *Org. Biomol. Chem.* **2017,** *15,* 6764–6772. doi:10.1039/c7ob01421j
97. Note that the transition in **2** is faster than in **1**, only when considering the *cis*-to-*trans* rotation. The order is reverse in the *trans*-to-*cis* rotation, because the *trans*-amide ground state in **2** is stabilized through the n→p* donation, and in **1** – not.
98. Kang, Y. K.; Byun, B. J.; Park, H. S. *Biopolymers* **2011,** *95,* 51–61. doi:10.1002/bip.21534
99. Beausoleil, E.; Sharma, R.; Michnick, S. W.; Lubell, W. D. *J. Org. Chem.* **1998,** *63,* 6572–6578. doi:10.1021/jo980673o
100. Bychek, R. M.; Levterov, V. V.; Sadkova, I. V.; Tolmachev, A. A.; Mykhailiuk, P. K. *Chem. – Eur. J.* **2018,** *24,* 12291–12297. doi:10.1002/chem.201705708
101. Guo, L.-E.; Tang, Y.-X.; Zhang, S.-Y.; Hong, Y.; Yan, X.-S.; Li, Z.; Jiang, Y.-B. *Org. Biomol. Chem.* **2020,** *18,* 4590–4598. doi:10.1039/d0ob00493f
102. Myers, E. L.; Palte, M. J.; Raines, R. T. *J. Org. Chem.* **2019,** *84,* 1247–1256. doi:10.1021/acs.joc.8b02644
103. Johnson, B. M.; Shu, Y.-Z.; Zhuo, X.; Meanwell, N. A. *J. Med. Chem.* **2020,** *63,* 6315–6386. doi:10.1021/acs.jmedchem.9b01877

License and Terms

This is an Open Access article under the terms of the Creative Commons Attribution License (http://creativecommons.org/licenses/by/4.0). Please note that the reuse, redistribution and reproduction in particular requires that the authors and source are credited.

The license is subject to the *Beilstein Journal of Organic Chemistry* terms and conditions: (https://www.beilstein-journals.org/bjoc)

The definitive version of this article is the electronic one which can be found at: doi:10.3762/bjoc.16.151

BEILSTEIN JOURNAL OF ORGANIC CHEMISTRY

Selective preparation of tetrasubstituted fluoroalkenes by fluorine-directed oxetane ring-opening reactions

Clément Q. Fontenelle, Thibault Thierry, Romain Laporte, Emmanuel Pfund and Thierry Lequeux*

Full Research Paper

Open Access

Address:
Normandie Université, Laboratoire de Chimie Moléculaire et Thioorganique LCMT UMR 6507, ENSICAEN, UNICAEN, CNRS, 6 Bd. du Maréchal Juin, 14050 Caen, France

Email:
Thierry Lequeux* - Thierry.Lequeux@ensicaen.fr

* Corresponding author

Keywords:
acyclonucleotide; fluorine; monofluoroalkene; oxetane; selective ring-opening reaction; tetrasubstituted alkene

Beilstein J. Org. Chem. **2020,** *16,* 1936–1946.
doi:10.3762/bjoc.16.160

Received: 27 May 2020
Accepted: 23 July 2020
Published: 07 August 2020

This article is part of the thematic issue "Organo-fluorine chemistry V".

Guest Editor: D. O'Hagan

© 2020 Fontenelle et al.; licensee Beilstein-Institut.
License and terms: see end of document.

Abstract

The selective ring-opening reaction of fluoroalkylidene-oxetanes was directed by the presence of the fluorine atom, enabling a two-step access to tetrasubstituted fluoroalkenes with excellent geometry control. Despite its small van der Waals radii electronic, rather than steric influences of the fluorine atom governed the ring-opening reaction with bromide ions, even in the presence of bulky substituents.

Introduction

The introduction of fluorine atoms into organic compounds is known to modify their biological and physiological properties and can enhance the half-life of drugs in vivo [1-4]. During the last decade, fluorinated nucleoside analogues have received increasing interest, as is illustrated by the two pharmaceutical leads gemcitabine (**I**) and sofosbuvir (**II**), potent anticancer or antiviral agents, respectively (Figure 1) [5,6]. The field of acyclonucleotides (ACN) has been explored less, however, the introduction of fluorine atoms showed remarkable effects. The most representative examples are phosphate analogues such as the nucleoside phosphorylase inhibitor **III** and acyclic nucleotides such as the antiviral agent FPMPA (**IV**) [7-9]. Other main structural modifications of ACN relied on the introduction of a hydroxy group into the aliphatic chain to improve hydrogen bonding with enzymes [10], or of a carbon–carbon double bond to constrain the aliphatic chain and to limit conformational changes [11-13]. For the latter, nucleoside analogues (Figure 2, **VI**) containing a *trans*-butenyl moiety where the endocyclic C–O bond was replaced by a C=C bond are recognized by kinases as dUMP surrogate (**V**) [11]. However, there is no existing data for the corresponding fluoroalkene (**VII**), as the latter was not yet synthetized. It is expected that the introduction of fluorine into the carbon–carbon double bond, in a position equivalent to the ring oxygen of the naturally occurring

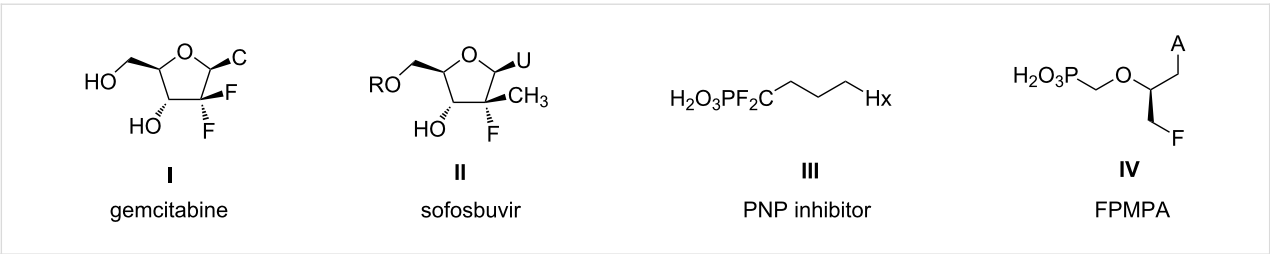

Figure 1: Representative fluorinated nucleos(t)ides and acyclonucleotides.

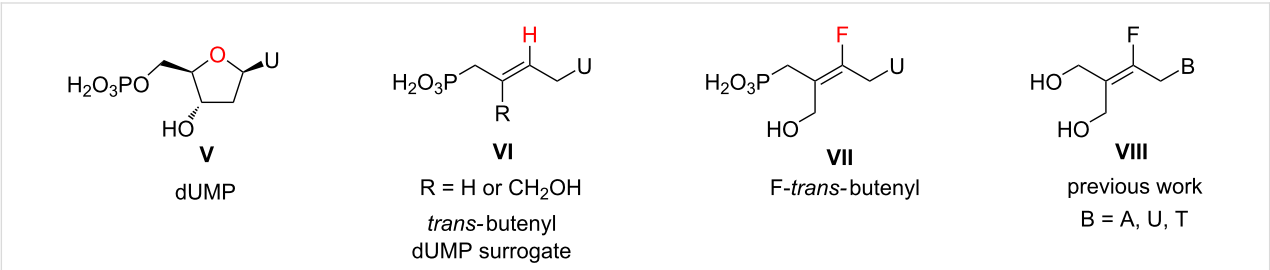

Figure 2: Acyclonucleotides as nucleotide surrogates.

nucleotide, will improve molecular recognition and activity. In addition, the polarity of the nucleotide and hydrogen-bond accepting capacity with proteins or enzymes would be restored [14].

The synthesis of fluoroalkene precursors of modified acyclonucleosides (**VIII**) has been explored by Choi, and more recently by us [15-17]. Nevertheless, it was reported that no antiviral activity for compounds of series **VIII** was observed due to the difficulty of phosphorylation of the substrate by kinases [16]. The first kinase phosphorylation step is generally rate limiting, and the prior introduction of a phosphate or phosphonate function can circumvent this problem. The preparation of diols **VIII** was realized by olefination of a protected 1,3-dihydroxypropanone (Figure 3). However, the selective introduction of functional groups is not possible in these diols as the two hydroxy groups present similar chemical reactivity. Other approaches are available for a selective preparation of monofluoroalkenes including olefination or defluorination reactions or a sigmatropic rearrangement, but these approaches are limited and do not allow the synthesis of tetrasubstituted fluoroalkenes with good control of their geometry [18-21]. In order to develop a selective synthesis for tetrasubstituted fluoroalkenes we envisioned an alternative approach starting from fluoroalkylidene-oxetane derivatives and to the end we have studied the selectivity of the oxetane ring-opening reaction (Figure 3).

Results and Discussion

The preparation of a series of fluoroalkylidene-oxetanes **1–3** was previously reported from 3-oxetanone through an olefination reaction with benzothiazoyl sulfones (Scheme 1) [22]. With these fluoroalkylidene-oxetanes in hands, we studied the selectivity of ring-opening reactions with heteroatom nucleophiles in order to access tetrasubstituted fluoroalkenes. A control of the geometry of these reactions would allow ready access to novel fluorinated ACN precursors.

At the outset the opening of the oxetane ring of **1** by a range of nucleophiles was trialed under acidic conditions. Inspired by Yadav et al. [23], methanol (20 equiv) was used as nucleophile in the presence of camphorsulfonic acid (CSA, 1 equiv) in dichloromethane. The reaction was slow and required heating

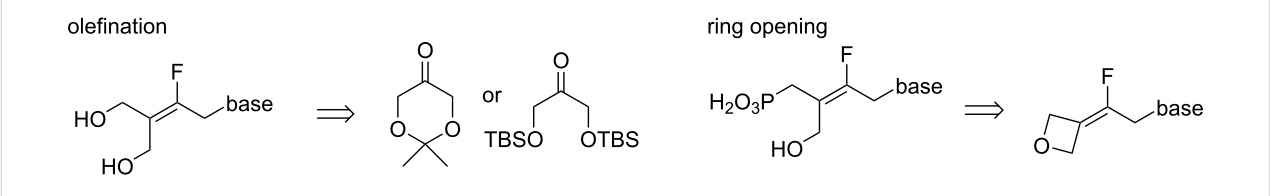

Figure 3: Olefination approaches and ring-opening of oxetane derivatives.

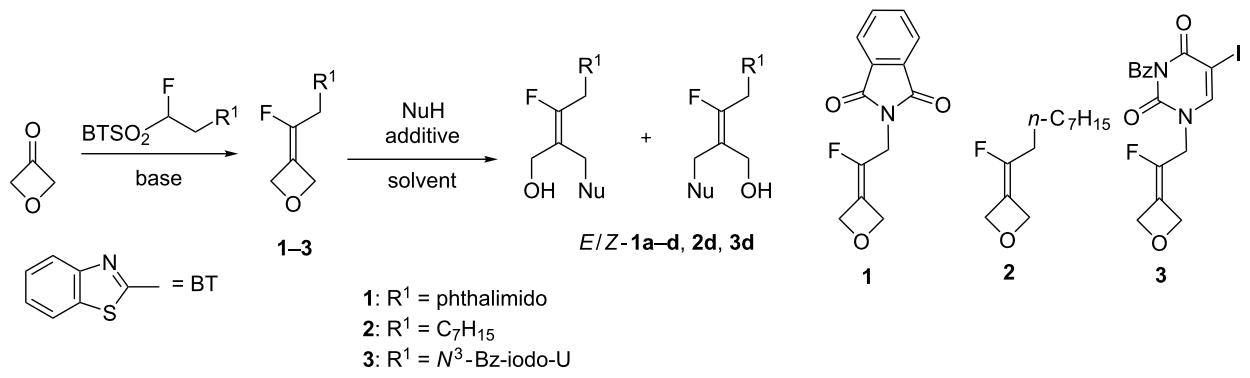

Scheme 1: Preparation of fluoroakylidene-oxetanes and their ring-opening reactions.

(50–65 °C) for 26 h to reach a 75% conversion and afforded a mixture of *E*/*Z*-**1a** in 60% yield. However, a low *E*/*Z* selectivity (40:60) was observed (Table 1, entry 1). When using neat benzylic alcohol, completion was achieved after 20 h at 80 °C but again no substantial selectivity could be observed for product **1b** (Table 1, entry 2). Inspired by the work of Müller and Wang [24,25], substitution by the more nucleophilic 2-mercaptobenzothiazol (BTSH, 1.4 equiv) was also possible in the presence of CSA (1 equiv) at 20 °C and an 80% conversion was reached after 24 h. An improved *E*/*Z* ratio of 25:75 was determined for this reaction and compound **1c** was isolated in 65% yield (Table 1, entry 3). In this case the nucleophilic ring-opening reaction appeared to be controlled by steric repulsions between the bulky benzothiazolyl and phthalimidoyl substituents affording preferentially the *Z*-isomer of **1c**. However, heteronucleophiles such as sodium azide, secondary amine and cesium fluoride were unsuccessfully tested. Finally, using the conditions developed by Burkhard and Carreira [26], the opening of the fluoroalkylidene-oxetane ring was investigated with hydrobromic acid (HBr 33 wt % in AcOH, 2.3 equiv) in diethyl ether (Table 1, entry 4). This reaction proved faster and reached completion after 45 min at 20 °C, giving product **1d** with an excellent yield of 94% and an *E*/*Z* selectivity of 89:11. The isomers could be separated and crystals of the major isomer were obtained by recrystallization. The X-ray diffraction analysis clearly showed that the bromine atom was located on the carbon *trans* to the fluorine atom resulting in the major product with the *E*-geometry (see Supporting Information File 1). It should be noted that longer reaction times resulted in slow solvolysis of alcohol **1d** with acetic acid giving mainly the corresponding acetate (not shown). Product **1d** was also obtained in a similar *E*/*Z* ratio (88:12) when the ring-opening reaction

Table 1: Oxetane opening by various nucleophiles.

entry	oxetane	Nu (equiv)	additive (equiv)	*t* (h)	*T* (° C)	solvent	product	*E*/*Z* ratio[a]	Yield (%)[b]
1	**1**	MeOH (20)	CSA (1)	26	40	CH_2Cl_2	**1a**	40:60	60
2	**1**	BnOH (24)	CSA (1)	20	80	neat	**1b**	45:55	n.a.
3	**1**	BTSH (1.4)	CSA (1)	24	20	CH_2Cl_2	**1c**	25:75	65
4	**1**	HBr (2.3)	AcOH[c]	0.75	20	Et_2O	**1d**	89:11	94
5	**1**	TBAB (2.5)	$BF_3{\cdot}Et_2O$ (1.1)	2	–20	CH_2Cl_2	**1d**	88:12	71
6	**2**	HBr (2.3)	AcOH[c]	0.75	20	CH_2Cl_2	**2d**	94:6	53
7	**3**	HBr (2.3)	AcOH[c]	0.75	20	CH_2Cl_2	–	–	–
8	**3**	TBAB (2.5)	$BF_3{\cdot}Et_2O$ (1.1)	2	–20	CH_2Cl_2	**3d**	96:4	76

[a]Determined by ^{19}F NMR of the crude mixture; [b]yield of isolated product; [c]HBr 33 wt % in AcOH solution.

was performed in dichloromethane with tetrabutylammonium bromide (TBAB) as the bromide source and boron trifluoride diethyl etherate as an activator (Table 1, entry 5). Nevertheless, the isolated yield of the product decreased to 71%. Next, the reaction performed with HBr/AcOH was extended to alkylidene oxetanes substituted by an alkyl chain, and a pyrimidine base. The presence of the alkyl chain in place of the phthalimido group did not affect the selectivity observed with **1**. The ring opening reaction of the *n*-octyl substituted oxetane **2** resulted in an excellent selectivity of 94:6 towards the *E*-isomer of bromoalkylated product **2d** (Table 1, entry 6). The *E/Z* mixture of **2d** was isolated in moderate yield (53%). In this case the corresponding acetate was observed as a minor product (15%) but with a similar selectivity of 92:8, although it could not be isolated in pure form. Unfortunately, the introduction of a nucleic base such as N^3-benzoyliodouracil instead of the phthalimido group gave a complex mixture of products (Table 1, entry 7). In contrast, the ring-opening reaction was successful when performed in the presence of TBAB and $BF_3{\cdot}Et_2O$ and afforded the *E*-alkene product **3d** with good selectivity (*E*/*Z* ratio > 96:4) and 76% yield (Table 1, entry 8). The geometric assignment of compound **3d** was corroborated by 1D NOESY experiments in which after selective irradiation of the protons α to the nitrogen atom, a response was observed only for the protons α to the bromine atom, thus indicating their spatial proximity.

In order to elucidate the selectivity control in this ring-opening reaction displayed by bromide ion despite the presence of bulky substituents (phthalimido and alkyl groups), a comparative study was initiated using non-fluorinated alkylidene oxetanes as substrates. Since the oxetane ring was attacked from the side of the bulky phthalimide or alkyl chain, it appeared plausible that the selectivity observed for the reaction did not originate from steric hindrance. Accordingly, the electronic influence of fluorine was explored. Thus, the non-fluorinated analogues bearing a phthalimido group (**4**) and an alkyl chain (**5**) were synthesized, and submitted to the ring-opening reaction [27,28]. Pleasingly, when subjecting compound **4** to the previous reaction conditions, a single isomer of bromoalcohol **4d** formed (determined by ^{1}H NMR of the crude) and the product was isolated in an excellent yield of 94% (Table 2, entry 3). The geometry of the product was confirmed to be *E*-**4d** by X-ray diffraction analysis (see Supporting Information File 1). The attack of the bromide ion this time occurred from the side of the alkene hydrogen atom (*cis* attack) and away from the bulky phthalimido group giving solely product *E*-**4d**. Likewise, the reaction of the alkyl-substituted substrate **5** proceeded with excellent *E*-selectivity (as determined by ^{1}H NMR of the crude). As in case of the fluorinated analogue, a substantial part of the newly formed alcohol **5d** reacted with acetic acid forming the corresponding acetate **5d'**. Interestingly, it appeared that only the *E*-isomer of **5d** reacted with AcOH giving pure *E*-**5d'** in 44% isolated yield. This left an 81:19 *E*/*Z* mixture of **5d** from which the pure alcohol *E*-**5d** could be isolated in 34% yield (Table 2, entry 4). The overall *E*/*Z* ratio for the ring-opening reaction of **5** was 91:9. 1D NOESY experiments were performed with alcohol **5d** and the outcome indicated that the bromide attack took place away from the bulky alkyl chain, resulting in the observed *E*-selectivity. These outcomes were opposite to those obtained

Table 2: Selectivity in the presence or absence of the fluorine atom.

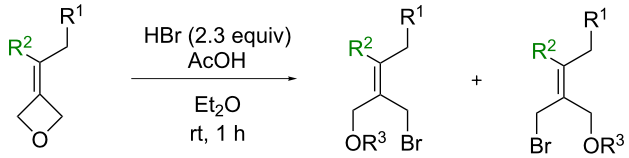

R^2 = H or F
R^1 = phthalimido, C_7H_{15} or C_8H_{17}
R^3 = H, Ac

entry	substrate	R^2	R^1	R^3	product	*E*/*Z* ratio[a]	yield (%)[b]
1	**1**	F	phthalimido	H	**1d**	89:11	94
2	**2**	F	C_7H_{15}	H	**2d**	94:6	53
3	**4**[c]	H	phthalimido	H	**4d**	100:0	94
4	**5**	H	C_8H_{17}	H	**5d**	81:19	34[d]
				Ac	**5d'**	100:0	44

[a]Determined by ^{19}F NMR (**1**, **2**) or ^{1}H NMR (**4**, **5**) of the crude mixture; [b]yield of isolated product; [c]substrate **4** was contaminated with 1 molar equivalent of phthalimide; [d]yield of isolated *E*-**5d**.

with the fluorinated substrate series, consistent with steric hindrance governing the non-fluorine containing oxetane reactions but electronics influencing and reversing the regioselectivity of the fluoro-oxetane reactions.

The reaction was then extended to fluoroalkylidene-oxetane **8** to expand the range of tetrasubstituted fluoroalkenes accessible via this method (Scheme 2). A variety of conditions were explored to prepare the protected alcohol **8** including an unsuccessful reduction of the corresponding ethyl ester (vide infra, **12**). Then we turned our attention to the modified Julia reaction since the reduction of the ester functionality could be achieved at the sulfide stage [29], prior to its oxidation to give **6**. Alcohol **6** was not stable in basic medium, as a Smiles rearrangement occurred leading to fluoroethylene and benzothiazolone. Therefore, its benzylation was explored under acidic conditions with benzyl trichloroacetimidate (1.5 equiv) and a catalytic amount of trifluoromethanesulfonic acid. This gave benzyl ether **7** as a 2.5:1 mixture with *N*-benzylbenzothiazolone (not shown, Scheme 2). After purification, benzyl ether **7** was successfully subjected to the modified Julia olefination conditions with 3-oxetanone, to give the corresponding alkene **8** in 79% yield.

With alkene **8** in hand, the ring-opening reaction was explored in the presence of hydrobromic acid (HBr 33 wt % in AcOH) in diethyl ether (Table 3). As observed with the phthalimido group, the reaction led to alkene *E*-**9** as the major product, together with alkene *Z*-**9** and a third product that was identified as the 2,5-dihydrofuran derivative **10**.

Using the standardized conditions, but at a temperature of 0 °C instead of 20 °C, for 30 min, complete conversion was achieved and the three products *E*,*Z*-**9** and **10** were present in a 62:8:26 ratio as determined by ^{19}F NMR, the remaining 4% being attributed to acetylated analogues of **9** (Table 3, entry 1). After purification, two products were obtained as a 95:5 mixture and identified by NMR as the desired bromoalcohols *E*-**9** and *Z*-**9**, respectively. The selectivity of the oxetane ring opening (crude *E*/*Z* ratio: 89:11) was again governed by the presence of the fluorine atom and not by steric hindrance.

In order to limit the competitive formation of the heterocyclic ether **10**, the addition of TBAB as a bromide source was explored. To our delight, after 30 min at 0 °C, the crude ^{19}F NMR showed that only 4% of **10** and 96% of **9** as an 84:16

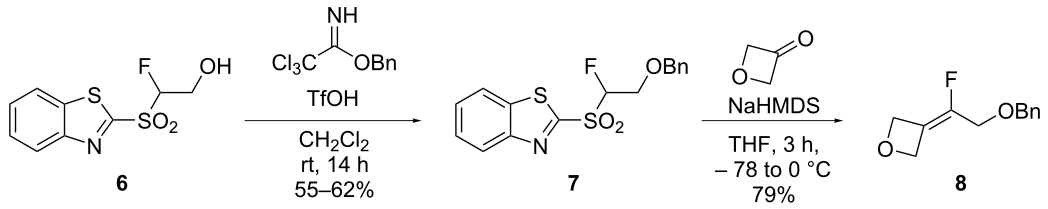

Scheme 2: Synthesis of benzyloxy-substituted fluoroethylidene-oxetane derivative **8**.

Table 3: Opening of the benzyloxy-substituted fluoroethylideneoxetane derivative **8**.

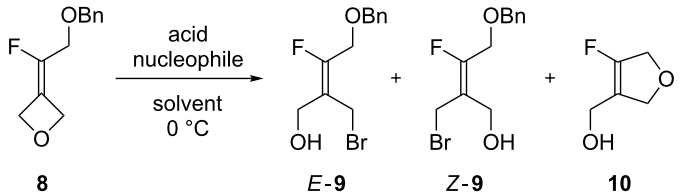

Entry	Nu (equiv)	Additive (equiv)	Solvent	Reaction time (h)	Selectivity[a]			Yield of **9** (%)
					E-**9**	*Z*-**9**	**10**	
1	HBr (2.3)	AcOH	Et_2O	0.5	62	8	26	45
2	HBr (1.2) TBAB (2.5)	AcOH	CH_2Cl_2	0.5	81	15	4	74[b]
3	TBAB (2.5)	$BF_3{\cdot}OEt_2$ (1.1)	CH_2Cl_2	1	90	10	0	66

[a]Determined by ^{19}F NMR of the crude mixture; [b]yield for the 92:8 *E*/*Z* mixture.

E/*Z* mixture had formed (Table 3, entry 2). Separation of the two *E*/*Z* isomers proved challenging by column chromatography and a 92:8 mixture of *E*/*Z*-**9** was obtained in 74% yield. Finally, the reaction performed with TBAB in the presence of $BF_3{\cdot}Et_2O$ afforded only alkenes **9** with an excellent *E*-selectivity and in 66% yield (Table 3, entry 3). In this case, we presume **10** was not obtained because the benzyl ether is not nucleophilic enough to react due to it complexation by $BF_3{\cdot}OEt_2$.

To understand in more detail the competitive formation of linear versus cyclic products in the reaction, methanol was explored as the nucleophile instead of bromide ion (Scheme 3). The reaction (43 h, 20 °C) realized in MeOH as a solvent and in the presence of CSA (1 equiv) afforded a mixture of **10** (85%) and the expected methoxyalcohols **11** (10%, 1:1 *E*/*Z* ratio) in addition to starting fluoroalkylidene-oxetane **8** (5%). After purification, compound **10** was isolated in 75% yield.

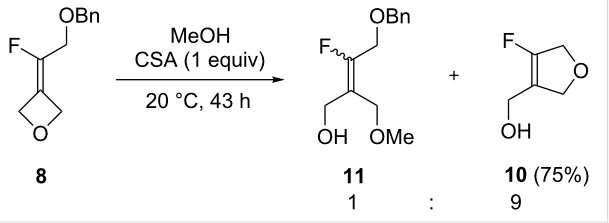

Scheme 3: Effect of the medium on the selective formation of derivative **10**.

The results from the acid-catalyzed results support the reaction outcomes which depended on the nucleophile (methanol or bromide ion) (Scheme 4). In the presence of excess bromide ions, the direct intermolecular nucleophilic attack of the oxetane (path a) is preferred leading to bromoalcohol **9** (path a). On the other hand, in the presence of the weaker methanol nucleophile, an intramolecular ring-opening reaction by the benzyl ether oxygen is preferred leading to the 2,5–dihydrofuran **10** (path b).

Finally, we turned our attention to a last series of reactions exploring the ring-opening reaction of fluoroalkylidene-oxetane **12** (Table 4).

Given the previous results, in the presence of the ester function we expected the ring-opening reaction to proceed with the formation of additional products to alkenes *E*-**13** and *Z*-**13**. In fact, two byproducts formed and were identified as β-hydroxymethyl-α-fluorolactone **14** and β-bromomethyl-α-fluorolactone **15** (Table 4) [30]. This ring expansion has been already reported in the literature from oxetane-containing α,β-unsaturated carbonyl derivatives through a Lewis acid-catalyzed rearrangement [31]. When the previous conditions (HBr/AcOH) were tried (3.5 h, 0 °C to 20 °C), hydroxymethyllactone **14** (87%, Table 4, entry 1) was the main product with traces of the corresponding acetate (4%, not shown), the bromomethyllactone **15** (8%), and alkene *Z*-**13** (1%). Only lactone **14** could be isolated in a pure form (58% yield). The amount of HBr/AcOH had little influence on the selectivity (Table 4, entry 2) of the reaction. However, in the presence of TBAB (2.5 equiv) and CSA (2 equiv) an 84% conversion into mainly brominated lactone **15** (79%) with traces of hydroxylated lactone **14**, and of bromoalkene *Z*-**13** was determined by crude ^{19}F NMR. The remaining 8% appeared to be the β-chloromethyllactone **19** (see Scheme 7 below), an analogue of **15** as determined by NMR analysis and supported by HRMS. All three halogenated products were purified and isolated as a mixture (≈61% determined by NMR). The contrasting result observed with HBr/AcOH and TBAB/CSA highlighted the importance of the acidity of the medium on the reaction course of the ring-opening reaction (Scheme 5). The former, using an excess of acid (33% HBr in AcOH solution) favored the direct nucleophilic attack (path b) leading to lactone **14**, whereas the latter in the presence of TBAB/CSA allowed bromide addition on the same side of the fluorine atom (path a) leading to lactone **15** [31]. However, the reaction can be stopped at the alcohol stage when performed in the presence of $BF_3{\cdot}Et_2O$ instead of CSA to afford alkene *Z*-**13** as the major product. The use of boron trifluoride etherate as an activator combined with TBAB afforded exclusively alkene Z-**13** as evidenced by TLC, but after work-up, 22% of the bromomethyllactone **15** was observed (Table 4, entry 4). It appeared obvious that *Z*-**13** could cyclize under acidic conditions and during the purification gave β-bromomethyllactone **15**. This was later confirmed when various ester/lactone mixtures obtained after the ring-opening reaction were treated with

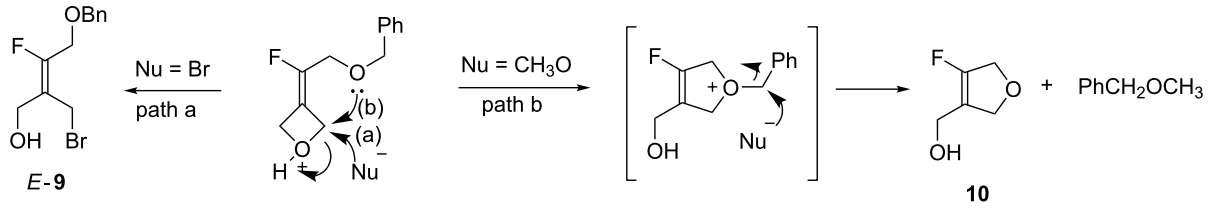

Scheme 4: Mechanism for the formation of dihydrofuran **10**.

Table 4: Ring-opening reaction from acetate derivative **12**.

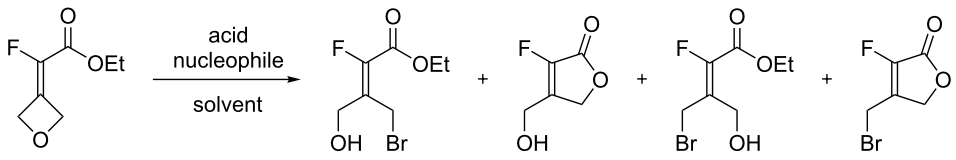

12 *E*-**13** **14** *Z*-**13** **15**

entry	Nu (equiv)	additive	solvent	*t* (h)	*T* (°C)	selectivity[a]				product (yield)[b]
						E-**13**	**14**	*Z*-**13**	**15**	
1	HBr (2.5)	AcOH	Et_2O	3.5	20	–	87	1	8	**14** (58)
2	HBr (1.2)	AcOH	Et_2O	3.5	0	3	76	7	10	–
3	TBAB (2.5)	CSA (2)[c]	CH_2Cl_2	30	20	–	7	6	79 (8)[d]	**15** (61)[e]
4	TBAB (2)	$BF_3.OEt_2$ (1.5)	CH_2Cl_2	4	–20	–	–	78	22	*Z*-**13** (72)[f] **15** (21)[f]
5	TBAB (1.5)	–	CH_2Cl_2	16	20	–	–	–	–	–
6	–	$BF_3{\cdot}OEt_2$ (1)	CH_2Cl_2	2	20	–	100	–	–	**14** (67)

[a]Determined by ^{19}F NMR of the crude mixture; [b]isolated yield; [c]the 2nd equivalent of CSA was added after 24 h; [d]chlorinated instead of brominated products; [e]yield of an 87:8:5 mixture of products **15**/**19**/*Z*-**13**; [f]*Z*-**13** and **15** were obtained as a crude mixture, yields were calculated from the crude mass and ^1H NMR.

acid (PTSA) in Et_2O giving pure lactone **15** or at least enriched mixtures depending on the reaction times (Scheme 5).

As a control, **12** was shown to be unreactive to TBAB on its own (Table 4, entry 5). Once again, the effect of the fluorine atom was highlighted by an investigation with the non-fluorinated alkylidene oxetane **16**. The latter was subjected to the HBr/AcOH ring-opening reaction conditions (Scheme 6). Remarkably, the cyclic products β-hydroxymethyl and β-bromomethyl-γ-lactones **17** and **18** were obtained in an 8:92 ratio [32]. This complete reversal of selectivity in comparison with fluoroalkylidene-oxetane **12**, where the β-hydroxymethyl-γ-lactone **14** was obtained, confirmed an electronic influence of the fluorine atom on these ring-opening reactions (Table 3, entries 1 and 2). In the case of fluoroalkylidene-oxetane **12** and, in contrast with **16**, when subjected to HBr/AcOH, the electronic repulsion induced between fluorine and bromine limited the intermolecular ring-opening reaction by bromide in favor of a faster intramolecular reaction involving the ester group leading to **14**. Indeed, a competitive cyclization reaction occurred forming **14** with HBr/AcOH and confirmed when the reaction was performed in the presence of $BF_3{\cdot}Et_2O$ only

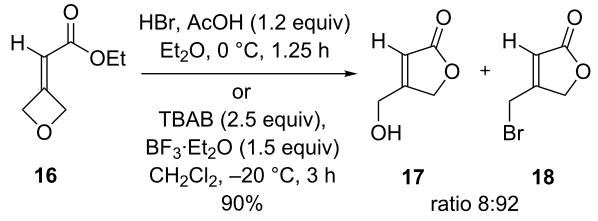

16 **17** **18**
ratio 8:92

Scheme 6: Opening reaction of ethyl 2-(oxetanyl-3-idene)acetate (**16**).

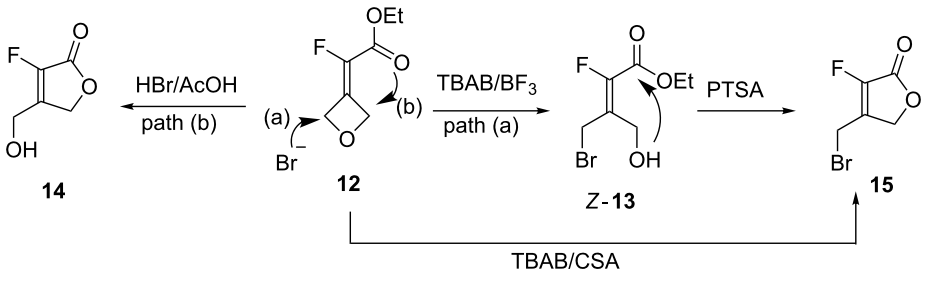

14 **12** *Z*-**13** **15**

Scheme 5: Mechanism for the formation of unsaturated lactones **14** and **15**.

(Table 4, entries 1, 2, and 6). Of note in contrast to **8**, when TBAB/BF_3·Et_2O was added we cannot exclude a control by steric or electronic repulsions between bromide ions and the ester function leading to *Z*-**13** and **15** instead of expected alkene *E*-**13** and to the lactone **18** from alkylidene oxetanes **12** and **16**, respectively.

Having established selective approaches for the preparation of halogenated allylic fluoroalkenes, their use in the synthesis of highly functionalized tetrasubstituted fluoroalkenes was explored. The derivatization of the three brominated products, lactone **15** and alkenes *E*-**1d** and *E*-**9**, was studied either on the bromomethyl (CH_2Br) or on the hydroxymethyl (CH_2OH) arm, when applicable.

First, from a mixture of lactones **15** and **19** substitution on the bromomethyl arm was performed using sodium azide (Scheme 7). The reaction proceeded smoothly in DMF but it proved difficult to extract product **20** from water. When the reaction was performed in acetone this allowed for a simple filtration of the sodium chloride and bromide salts formed and resulted in very satisfactory yields (91–97%) after column chromatography. An Arbuzov phosphonylation was performed on the crude lactone product **15** (containing 10% of ester *Z*-**13**) and proved successful with phosphonolactone **21** being isolated in 77% yield after column chromatography (Scheme 7). To access tetrasubstituted alkenes, reduction of **21** to generate diol **22** was explored with lithium borohydride in Et_2O. However, the reaction was slow at 20 °C and did not progress beyond 50% conversion even after the addition of excess $LiBH_4$. After purification by flash chromatography starting lactone **21** was obtained in 49% yield and the desired diol **22** in 47% yield. When the reaction was carried out in refluxing THF, a complete conversion was achieved but also with impurities. This route was not investigated further, and instead functionalization of alkene *E*-**1d** was explored.

Direct ring-opening reactions of fluoroalkylidene-oxetane **1** with heteronucleophiles were previously explored and success was only possible with thiols, such as mercaptobenzothiazole (Table 1). However, the reaction was not selective and afforded a mixture of *E*/*Z* alkenes **1c**. The functionalization of alkene *E*-**1d** via displacement of the bromine atom (Scheme 8), with nucleophiles such as CsF and NaN_3 was then studied. When the reaction was performed in DMF products *E*-**23** and *Z*-**24** were generated in 92% and 93% yield, respectively. Reactions with amines and thiols such as pyrrolidine and 2-mercaptobenzothiazole, gave rise to the products *Z*-**25** and *E*-**1c** in 96% yield, respectively. These reactions were carried out in dichloromethane in the presence of Et_3N. It should be noted that following this two-step method, pure *E*-**1c** could be obtained while direct ring opening of **1** with BTSH and CSA resulted in a 25:75 mixture of *E*/*Z*-**1c**. A crystallographic analysis of crystals of *Z*-**25** confirmed the nature and geometry of the obtained product (see Supporting Information File 2). Addition of carbanions or alcoholates was also attempted but the starting bromide *E*-**1d** degraded under these conditions.

Finally, this expeditious synthesis of tetrasubstituted fluoroalkenes by sequential ring-opening and nucleophilic substitution reactions was applied to test the robustness of a selective preparation of precursors of ACN (**VII**) bearing different functional groups (Scheme 9). A particular focus was applied to the preparation of the phosphonate **29**, a precursor of **VII** that is not accessible from diol **VIII**.

First, starting from pure alkene *E*-**9**, the introduction of a protected alcohol as a mimic of the naturally occurring

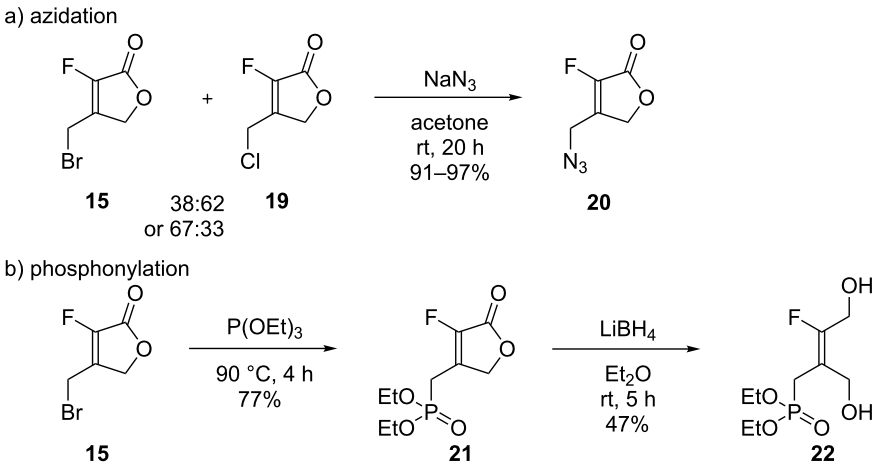

Scheme 7: Functionalization of bromomethyllactone **15** and its analogues.

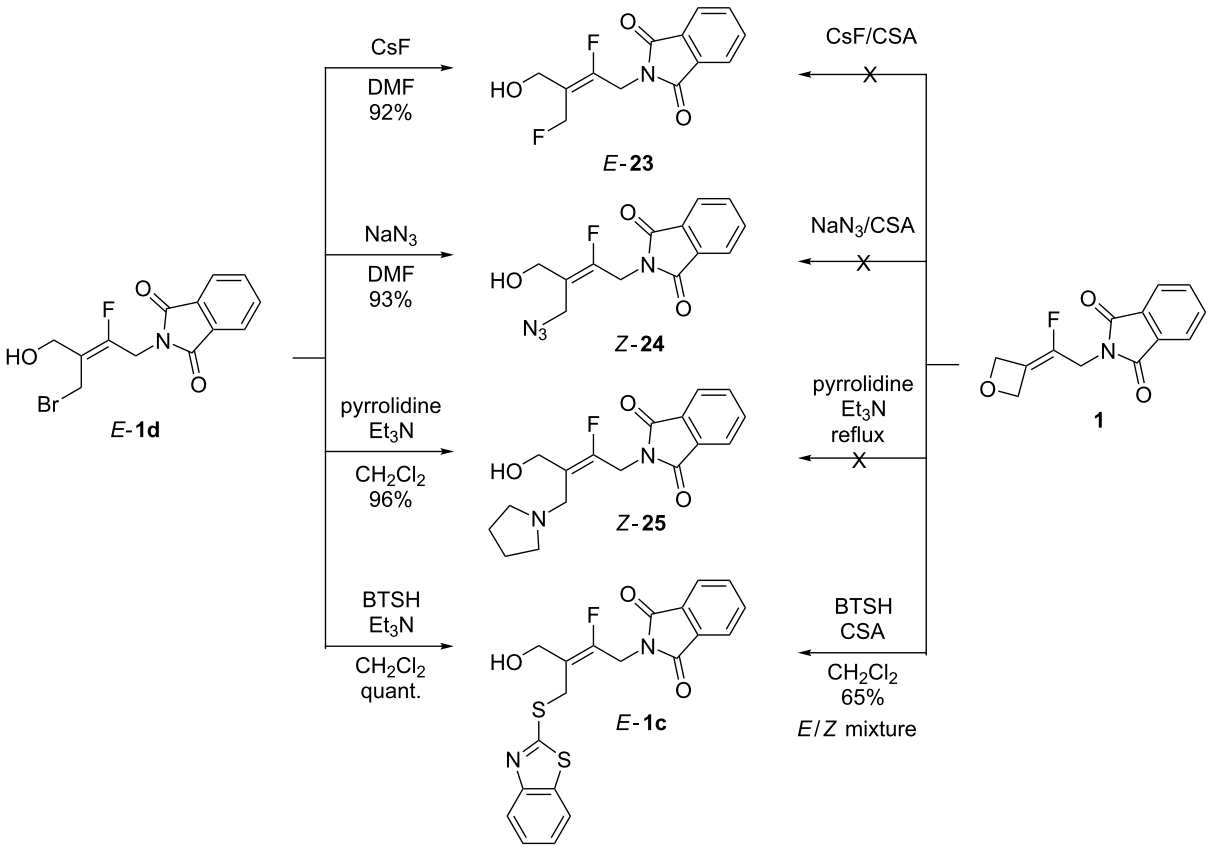

Scheme 8: Functionalization by substitution reaction of the bromide *E*-**1d** vs ring-opening reaction of the oxetane **1**.

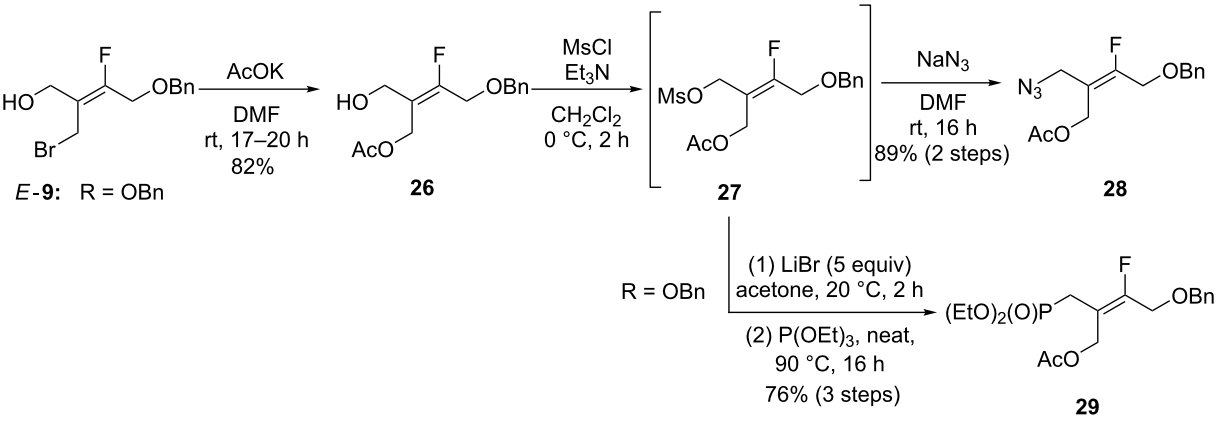

Scheme 9: Preparation of tetrasubstituted fluoroalkenes.

3'-hydroxy group was achieved by allylic bromine displacement with AcOK to efficiently afford alkene **26**. The phosphonate was introduced in three steps through the formation of intermediate mesylate **27**. This mesylate was progressed without purification, albeit contaminated (10%) with the corresponding chloride (not shown). An Arbuzov reaction was performed directly on the allylic bromide obtained by treatment of **27** with LiBr (5 equiv), to give the phosphonate **29** in 76% overall yield. Finally, azide **28** was obtained in 89% yield in two steps from the non-isolated intermediate mesylate **27**. After deacetylation, **28** was readily converted to *E*-**24** (see Scheme 8). These transformations of alkene *E*-**9** illustrated how the geometry can be controlled for the preparation of tetrasubstituted fluoroalkenes. The synthesis of nucleotide mimics from either

phosphonate **29** or azide **28** is underway and will be reported in due course.

Conclusion

The selective synthesis of tetrasubstituted *E*- or *Z*-fluoroalkenes was achieved by ring-opening reactions of fluoroalkylidene-oxetanes, with the presence of the fluorine atom governing regioisomeric attack of the bromide ion. Functionalization of the resultant bromoalcohols with nucleophiles led, in two steps from oxetanes, to a series of highly functionalized tetra-substituted fluoroalkenes with excellent geometric control. This method offers ready access to novel fluoroalkenes as potential precursors of important drug mimics.

Supporting Information

The experimental section describing the preparation of all new compounds, the copies of the NMR data (^{1}H NMR, ^{13}C NMR, ^{19}F NMR), HOESY and NOESY experiments and crystallographic data for compounds **1d**, **4d** and **25**. The CIF files of **1d**, **4d** and **25**.

Supporting Information File 1

Experimental section and copies of spectra.
[https://www.beilstein-journals.org/bjoc/content/supplementary/1860-5397-16-160-S1.pdf]

Supporting Information File 2

Crystallographic data (cif) for compounds *E*-**1d**, *E*-**4d**, and *Z*-**25**.
[https://www.beilstein-journals.org/bjoc/content/supplementary/1860-5397-16-160-S2.zip]

Funding

This work was supported by the excellence laboratory LabEx SYNORG (ANR-11-LABX-0029), ANR funding DALATAR (ANR-19-CE18-0008-03) the Conseil Régional de Normandie and the European FEDER funding.

ORCID® iDs

Clément Q. Fontenelle - https://orcid.org/0000-0002-1630-3407
Thibault Thierry - https://orcid.org/0000-0003-0342-2391
Romain Laporte - https://orcid.org/0000-0002-5984-6794
Emmanuel Pfund - https://orcid.org/0000-0003-1896-0109
Thierry Lequeux - https://orcid.org/0000-0003-3783-4458

References

1. Zhou, Y.; Wang, J.; Gu, Z.; Wang, S.; Zhu, W.; Aceña, J. L.; Soloshonok, V. A.; Izawa, K.; Liu, H. *Chem. Rev.* **2016,** *116,* 422–518. doi:10.1021/acs.chemrev.5b00392
2. Purser, S.; Moore, P. R.; Swallow, S.; Gouverneur, V. *Chem. Soc. Rev.* **2008,** *37,* 320–330. doi:10.1039/b610213c
3. Gillis, E. P.; Eastman, K. J.; Hill, M. D.; Donnelly, D. J.; Meanwell, N. A. *J. Med. Chem.* **2015,** *58,* 8315–8359. doi:10.1021/acs.jmedchem.5b00258
4. O'Hagan, D. *J. Fluorine Chem.* **2010,** *131,* 1071–1081. doi:10.1016/j.jfluchem.2010.03.003
5. Len, C.; Mackenzie, G. *Tetrahedron* **2006,** *62,* 9085–9107. doi:10.1016/j.tet.2006.07.050
6. Bassetto, M.; Slusarczyk, M. *Pharm. Pat. Anal.* **2018,** *7,* 277–299. doi:10.4155/ppa-2018-0028
7. Xie, M.-S.; Niu, H.-Y.; Qu, G.-R.; Guo, H.-M. *Tetrahedron Lett.* **2014,** *55,* 7156–7166. doi:10.1016/j.tetlet.2014.11.060
8. De Clercq, E. *Med. Res. Rev.* **2013,** *33,* 1278–1303. doi:10.1002/med.21283
9. Schramm, V. L. *Chem. Rev.* **2018,** *118,* 11194–11258. doi:10.1021/acs.chemrev.8b00369
10. Kasthuri, M.; El Amri, C.; Lefort, V.; Périgaud, C.; Peyrottes, S. *New J. Chem.* **2014,** *38,* 4736–4742. doi:10.1039/c4nj00813h
11. Topalis, D.; Pradère, U.; Roy, V.; Caillat, C.; Azzouzi, A.; Broggi, J.; Snoeck, R.; Andrei, G.; Lin, J.; Eriksson, S.; Alexandre, J. A. C.; El-Amri, C.; Deville-Bonne, D.; Meyer, P.; Balzarini, J.; Agrofoglio, L. A. *J. Med. Chem.* **2011,** *54,* 222–232. doi:10.1021/jm1011462
12. Amblard, F.; Nolan, S. P.; Schinazi, R. F.; Agrofoglio, L. A. *Tetrahedron* **2005,** *61,* 537–544. doi:10.1016/j.tet.2004.11.019
13. Varada, M.; Erande, N. D.; Kumar, V. A. *RSC Adv.* **2015,** *5,* 97824–97830. doi:10.1039/c5ra15673d
14. Champagne, P. A.; Desroches, J.; Paquin, J.-F. *Synthesis* **2015,** *47,* 306–322. doi:10.1055/s-0034-1379537
15. Choi, M.-H.; Lee, C.-K.; Jeong, L. S.; Chun, M. W.; Kim, H.-D. *Nucleosides, Nucleotides Nucleic Acids* **2001,** *20,* 681–684. doi:10.1081/ncn-100002350
16. Choi, M.-H.; Kim, H.-D. *Arch. Pharmacal Res.* **1997,** *20,* 501–506. doi:10.1007/bf02973948
17. Prunier, A.; Calata, C.; Legros, J.; Maddaluno, J.; Pfund, E.; Lequeux, T. *J. Org. Chem.* **2013,** *78,* 8083–8097. doi:10.1021/jo401356j
18. Drouin, M.; Hamel, J.-D.; Paquin, J.-F. *Synthesis* **2018,** *50,* 881–955. doi:10.1055/s-0036-1591867
19. Landelle, G.; Bergeron, M.; Turcotte-Savard, M.-O.; Paquin, J.-F. *Chem. Soc. Rev.* **2011,** *40,* 2867–2908. doi:10.1039/c0cs00201a
20. Yanai, H.; Taguchi, T. *Eur. J. Org. Chem.* **2011,** 5939–5954. doi:10.1002/ejoc.201100495
21. Pfund, E.; Lequeux, T.; Gueyrard, D. *Synthesis* **2015,** *47,* 1534–1546. doi:10.1055/s-0034-1380548
22. Laporte, R.; Prunier, A.; Pfund, E.; Roy, V.; Agrofoglio, L. A.; Lequeux, T. *Eur. J. Org. Chem.* **2015,** 3121–3128. doi:10.1002/ejoc.201500172
23. Yadav, J. S.; Singh, V. K.; Srihari, P. *Org. Lett.* **2014,** *16,* 836–839. doi:10.1021/ol403604u
24. Burkhard, J. A.; Wuitschik, G.; Rogers-Evans, M.; Müller, K.; Carreira, E. M. *Angew. Chem., Int. Ed.* **2010,** *49,* 9052–9067. doi:10.1002/anie.200907155
25. Wang, Z.; Chen, Z.; Sun, J. *Angew. Chem., Int. Ed.* **2013,** *52,* 6685–6688. doi:10.1002/anie.201300188
26. Burkhard, J.; Carreira, E. M. *Org. Lett.* **2008,** *10,* 3525–3526. doi:10.1021/ol801293f
27. Jaśkowska, J.; Kowalski, P. *J. Heterocycl. Chem.* **2008,** *45,* 1371–1375. doi:10.1002/jhet.5570450519

28. Wolin, R.; Connolly, M.; Afonso, A.; Hey, J. A.; She, H.; Rivelli, M. A.; Willams, S. M.; West, R. E., Jr. *Bioorg. Med. Chem. Lett.* **1998,** *8,* 2157–2162. doi:10.1016/s0960-894x(98)00379-5
29. Calata, C.; Pfund, E.; Lequeux, T. *J. Org. Chem.* **2009,** *74,* 9399–9405. doi:10.1021/jo901540c
30. Fort, D. A.; Woltering, T. J.; Alker, A. M.; Bach, T. *Heterocycles* **2014,** *88,* 1079–1100. doi:10.3987/com-13-s(s)67
31. White, A. R.; Kozlowski, R. A.; Tsai, S.-C.; Vanderwal, C. D. *Angew. Chem., Int. Ed.* **2017,** *56,* 10525–10529. doi:10.1002/anie.201704119
32. Fort, D. A.; Woltering, T. J.; Nettekoven, M.; Knust, H.; Bach, T. *Chem. Commun.* **2013,** *49,* 2989–2991. doi:10.1039/c3cc40757h

License and Terms

This is an Open Access article under the terms of the Creative Commons Attribution License (http://creativecommons.org/licenses/by/4.0). Please note that the reuse, redistribution and reproduction in particular requires that the authors and source are credited.

The license is subject to the *Beilstein Journal of Organic Chemistry* terms and conditions: (https://www.beilstein-journals.org/bjoc)

The definitive version of this article is the electronic one which can be found at: doi:10.3762/bjoc.16.160

BEILSTEIN JOURNAL OF ORGANIC CHEMISTRY

Controlling the stereochemistry in 2-oxo-aldehyde-derived Ugi adducts through the cinchona alkaloid-promoted electrophilic fluorination

Yuqing Wang[1], Gaigai Wang[1], Anatoly A. Peshkov[2,3], Ruwei Yao[1], Muhammad Hasan[1], Manzoor Zaman[1], Chao Liu[1], Stepan Kashtanov[4], Olga P. Pereshivko[*1,2] and Vsevolod A. Peshkov[*1,2,5]

Full Research Paper

Open Access

Address:
[1]College of Chemistry, Chemical Engineering and Materials Science, Soochow University, Dushu Lake Campus, Suzhou, 215123, P.R. China, [2]Department of Chemistry, School of Science and Technology, Nazarbayev University, 53 Kabanbay Batyr Ave, Block 7, Nur-Sultan 010000, Republic of Kazakhstan, [3]Saint Petersburg State University, Saint Petersburg 199034, Russian Federation, [4]Department of Chemistry, Xi'an Jiaotong-Liverpool University, Suzhou, 215123, P.R. China and [5]The Environment and Resource Efficiency Cluster (EREC), Nazarbayev University, Nur-Sultan, Republic of Kazakhstan

Email:
Olga P. Pereshivko[*] - olga.pereshivko@nu.edu.kz;
Vsevolod A. Peshkov[*] - vsevolod.peshkov@nu.edu.kz

* Corresponding author

Keywords:
cinchona alkaloids; electrophilic fluorination; enantioselective synthesis; 2-oxo-aldehydes; Ugi reaction

Beilstein J. Org. Chem. **2020,** *16,* 1963–1973.
doi:10.3762/bjoc.16.163

Received: 06 June 2020
Accepted: 30 July 2020
Published: 11 August 2020

This article is part of the thematic issue "Organo-fluorine chemistry V".

Guest Editor: D. O'Hagan

© 2020 Wang et al.; licensee Beilstein-Institut.
License and terms: see end of document.

Abstract

In this report, we introduce a new strategy for controlling the stereochemistry in Ugi adducts. Instead of controlling stereochemistry directly during the Ugi reaction we have attempted to stereodefine the chiral center at the peptidyl position through the post-Ugi functionalization. In order to achieve this, we chose to study 2-oxo-aldehyde-derived Ugi adducts many of which partially or fully exist in the enol form that lacks the aforementioned chiral center. This in turn led to their increased nucleophilicity as compared to the standard Ugi adducts. As such, the stereocenter at the peptidyl position could be installed and stereodefined through the reaction with a suitable electrophile. Towards this end, we were able to deploy an asymmetric cinchona alkaloid-promoted electrophilic fluorination producing enantioenriched post-Ugi adducts fluorinated at the peptidyl position.

Introduction

Multicomponent reactions (MCRs) [1-13] in general and isocyanide-based MCRs [14-18] in particular represent powerful tools of modern synthetic chemistry that allow to generate structurally diverse and complex products in a step and atom-economic manner from simple and accessible precursors. Three-component Passerini [19-22] and four-component Ugi

[23,24] reactions that rely on the ability of organic isocyanides to participate in the nucleophilic attack onto the carbonyl or imine group are among the most studied MCRs. Accordingly, a wide range of post-MCR transformations have been elaborated allowing to upgrade the Passerini and Ugi adducts into potentially bioactive heterocycles [25-32]. While both Passerini and Ugi reactions proved to be quite robust towards different classes of substrates and possess broad functional group tolerance, the difficulties associated with controlling their stereochemical outcome [33-35] severely restrict their applicability in medicinal chemistry [36].

The typical Passerini three-component reaction (P-3CR) of a carboxylic acid **1**, an aldehyde **2**, and an isocyanide **3** being conducted in a polar-aprotic solvent such as THF or dichloromethane results in the assembly of an α-acyloxyamide adduct **4**. Just a few protocols for the asymmetric P-3CR [37-40] and its modifications [41-47] have been reported over the course of the last two decades (Table 1). In the majority of those protocols [37-39], the stereocontrol was achieved with the aid of different Lewis acid promoters bearing chiral ligands, while the most recent and at the same time the most general procedure developed by Liu, Tan and co-workers relied on the stereoinduction by a chiral phosphoric acid (Table 1) [40].

In the standard Ugi four-component reaction (U-4CR) a carboxylic acid **1**, an aldehyde **2**, and an isocyanide **3** are complemented by a primary amine **5** that altogether undergo a

Table 1: Asymmetric protocols for Passerini three-component reaction (P-3CR).

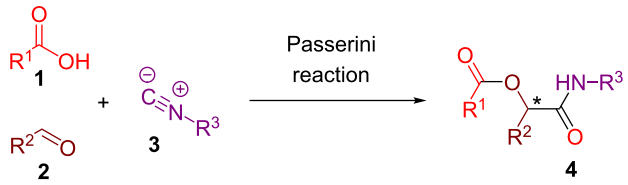

Asymmetric protocol	Catalytic system	Conditions	Yield range, %	ee range, %
Dömling and co-workers, 2003 [37]	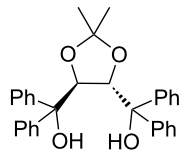 (1 equiv) $Ti(OiPr)_4$ (1.35 equiv)	THF (0.5 M), overnight	12–48	32–42
Schreiber and co-workers, 2004 [38]	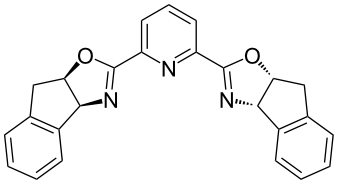 (20 mol %) $Cu(OTf)_2$ (20 mol %)	DCM (0.04 M), molecular sieves, 18–48 h	75–98	62–98
Wang, Zhu and co-workers, 2008 [39]	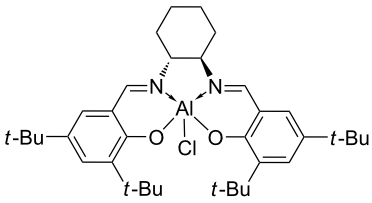 (10 mol %)	toluene (0.33 M), argon, −40 °C, 48 h	51–70	63 to >99
Liu, Tan and co-workers, 2015 [40]	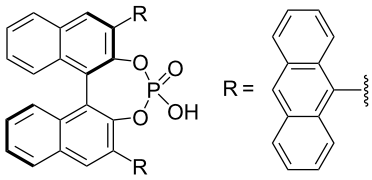 (10–20 mol %)	$CHCl_3$ (0.033 M or 0.05 M), argon, $MgSO_4$, rt or −20 °C or −35 °C, 36 h	41–99	84–99

condensation into a peptide-like adduct **6**. These reactions are typically conducted in polar protic solvents such as methanol or water. Several examples of diastereoselective U-4CR have been described [48-54]. Yet, the Ugi reaction turned out to be a rather challenging chemical transformation in terms of establishing the asymmetric version [33-35]. Apart from the two asymmetric three-component modifications lacking the acid component [55,56], no general asymmetric protocol for the four-component mode has been developed until very recently. In 2018, Houk, Tan and co-workers described an efficient enantioselective procedure operating in the presence of catalytic amounts of chiral phosphoric acids (Table 2) [57]. Two synthetic protocols have been elaborated allowing the engagement of different classes of substrates (Table 2). In addition, the group of Tan adapted their findings to the chiral phosphoric acid-catalyzed three-component Ugi reaction of an aldehyde **2**, an isocyanide **3**, and a primary amine **5** [58].

As a part of our ongoing research, we have been involved in the synthesis and utilization of 2-oxo-aldehyde-derived Ugi adducts **8** (Scheme 1). These products possess an increased nucleophilicity of the peptidyl position compared to the standard Ugi adducts owing to an additional electron-withdrawing group introduced with the 2-oxo-aldehyde **7**. For example, we have explored the potential of the peptidyl reactive site in a number of enolization-driven post-Ugi cyclizations leading to the assembly of pyrrol-2-ones **9** and **10** [59,60]. We have also taken advantage of a 1,3-dicarbonyl moiety present in **8** by engaging them in an enolization-triggered complexation with boron trifluoride diethyl etherate. The resulting *O*,*O*-chelated boron complexes **11** turned out to be strong solid-state emitters featuring clear aggregation-induced emission (AIE) characteristics [61].

Encouraged by these results, we decided to attempt the reaction of 2-oxo-aldehyde-derived Ugi adducts **8** with suitable electrophiles in the presence of chiral catalyst or promotor. In this way, the peptidyl position of **8** could be simultaneously functionalized and stereodefined leading to the formation of enantioenriched products **12** (Scheme 1). Towards this goal, we have

Table 2: Asymmetric protocols for Ugi four-component reaction (U-4CR) by Houk, Tan and co-workers.

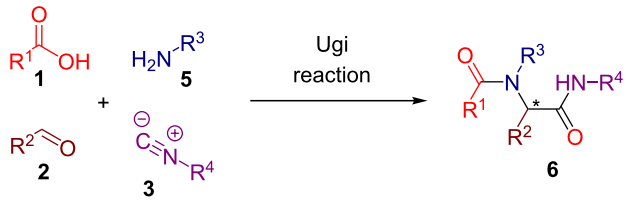

Substrate scope	Catalytic system	Conditions	Yield range, %	ee range, %
R^2 = Alk; R^3 = Ar	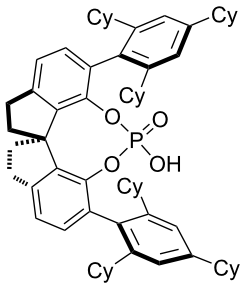 (5 mol %) Cy = cyclohexyl	DCM (0.05 M), argon, 5 Å MS, –20 °C, 12 h	43–96	75–97
R^2 = Ar; R^3 = Alk	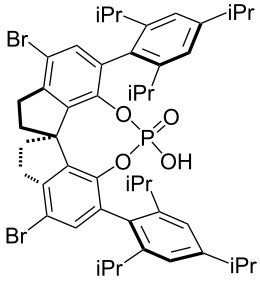 (10 mol %)	cyclohexane (0.025 M), argon, 5 Å MS, 20 °C, 36 h–7 d	60–96	80–94

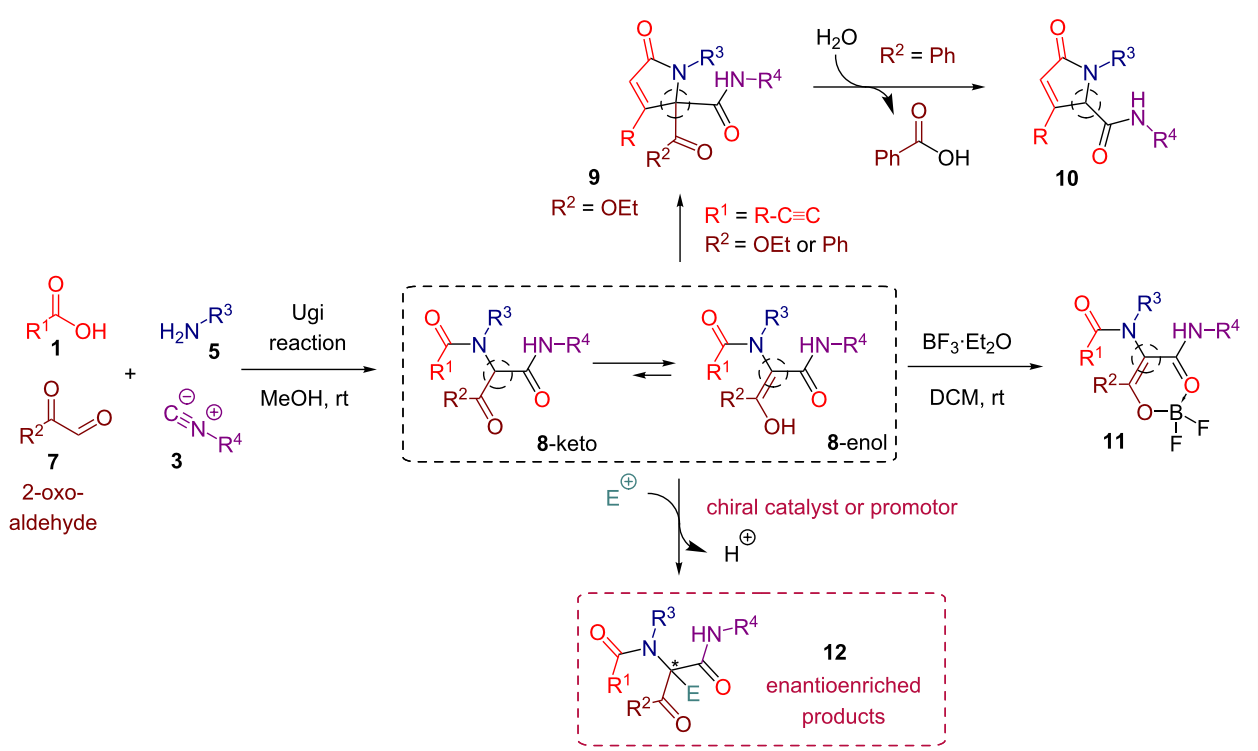

Scheme 1: Post-transformations of 2-oxo-aldehyde-derived Ugi adducts **8**.

previously tested the reactivity of **8** in the intermolecular aldol addition to ethyl glyoxalate [62]. As these attempts met with failure, we have turned our attention to enantioselective fluorination reactions [63-65]. Specifically, we decided to explore the enantioselective electrophilic fluorination of carbonyl compounds promoted by cinchona alkaloid derivatives developed independently by Shibata, Takeuchi and co-workers [65,66] and by the group of Cahard [67-70]. The method proved to be applicable to a broad range of substrates under a variety of conditions [71-78] and was successfully utilized for the synthesis of several bioactive molecules [79-81]. Herein we present its adaptation for the enantioselective fluorination of 2-oxo-aldehyde-derived Ugi adducts **8** leading to the installment of a fluorine-bound quaternary stereocenter at the peptidyl position. It should be stressed that the exploration of methods for the enantioselective fluorination continues to be an important topic considering the ever-growing role of fluorine derivatives in drug design and development [82,83]. An alternative strategy to prepare related quaternary carbon-containing adducts bearing fluorine and nitrogen atoms involves the asymmetric addition of α-fluoro-β-ketoesters or α-fluoro-α-nitro esters to appropriate electrophiles [84-89].

Results and Discussion

Initially, we prepared a series of Ugi adducts **8** by varying acid, 2-oxo-aldehyde, amine, and isocyanide components (Scheme 2). The product **8a** obtained from benzoic acid, phenylglyoxal, benzylamine, and *tert*-butyl isocyanide was selected for the screening of the reaction parameters (Table 3). The overall process was conducted in a two-step one-pot fashion as was originally designed by Shibata. In the first step, a cinchona alkaloid derivative was allowed to react with an electrophilic fluorinating agent to afford an *N*-fluoroammonium salt of the cinchona alkaloid via transfer fluorination. In the second step, the Ugi adduct **8a** was added to this in situ generated *N*-fluorocinchona intermediate to afford the desired fluorinated product **12a**. Thus, according to this synthetic and mechanistic path, the *N*-fluorocinchona intermediate acted as an asymmetric electrophilic fluorinating agent.

Conducting the fluorination of **8a** with a quinine (Q)/Selectfluor combination in different solvents revealed chloroform as a preferred reaction medium for this process with acetonitrile, tetrahydrofuran, and dichloromethane being less efficient in terms of ee of the obtained product **12a** (Table 3, entries 1–5). Using catalytic quantities of quinine led to a prolonged reaction time and diminished yield and ee of **12a** compared to the analogous reaction with stoichiometric amounts of quinine (Table 3, entry 4 versus entry 3). Thus, we focused on the exploration of a stoichiometric version considering that most of cinchona alkaloid derivatives are readily accessible and recoverable. The original Shibata's protocol also relied on the use of stoichio-

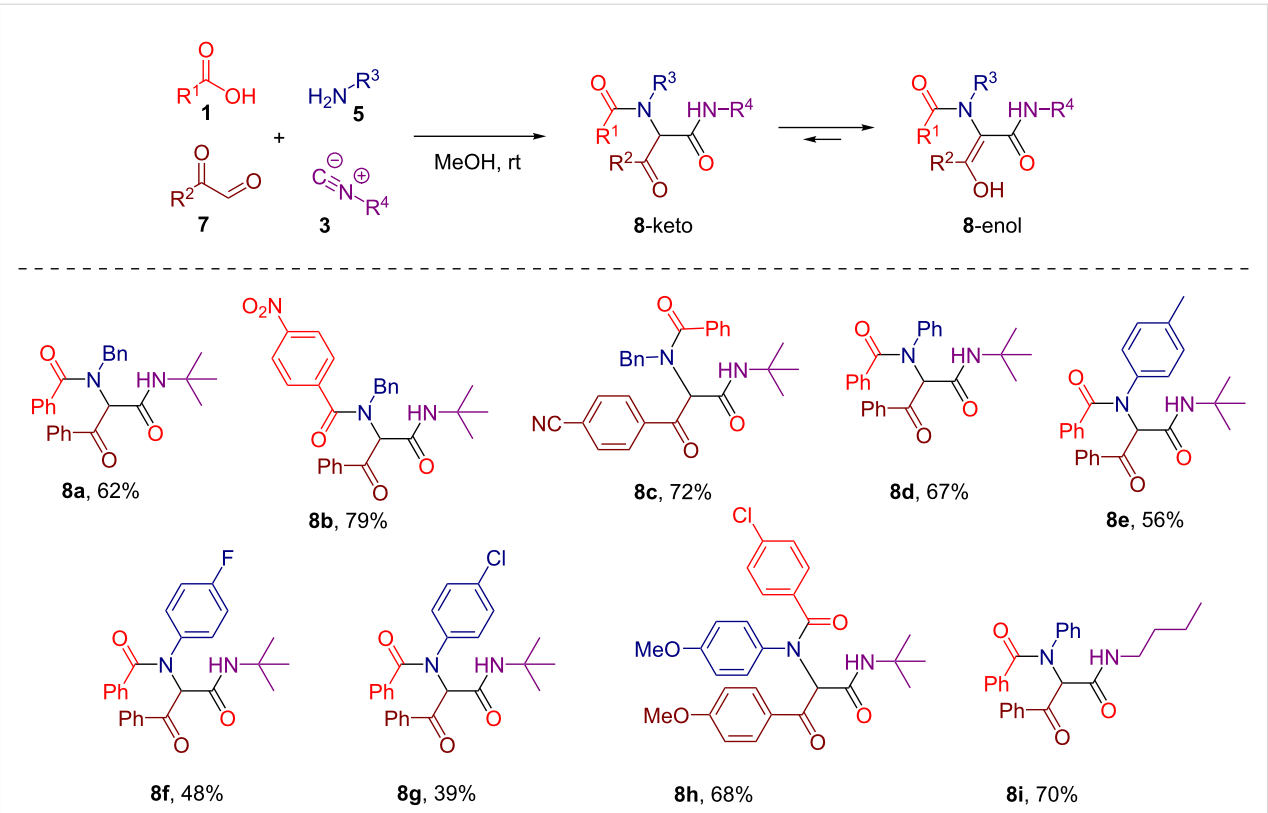

Scheme 2: Synthesis of 2-oxo-aldehyde-derived Ugi adducts.

metric amounts of the chiral promotor that was in an agreement with a two-step reaction mode requiring the initial formation of the asymmetric fluorinating agent. An attempt to use cupreine, a member of the cinchona family featuring free phenolic hydroxy group, met with failure producing no desired product **12a** (Table 3, entry 6). Using dihydroquinine (DHQ) led to an improved ee of **12a** compared to the analogous reactions with quinine (Table 3, entries 7 and 8 versus entries 5 and 2, respectively). Testing ether and ester derivatives of Q and DHQ (Table 3, entries 9–12) led to further improvement allowing to obtain **12a** with up to 73% ee through the reaction with dihydroquinine benzyl ether (DHQ-Bn, Table 3, entry 12). Switching to quinidine (QD), dihydroquinidine (DHQD), and their derivatives allowed to alter the stereoselectivity of the process leading to the preferred formation of another enantiomer of **12a** (Table 3, entries 13–18) with the QD-promoted reaction affording the best ee value (Table 3, entry 13). Additionally, we tested *N*-fluorobenzenesulfonimide (NFSI) as an alternative fluorinating agent in a combination with DHQ-Bn and QD with the outcome being indistinguishable with the analogous reactions with Selectfluor.

Having these results in hand, we moved to investigating the scope and limitation of this procedure with the Ugi adducts **8** obtained previously (Table 4). In order to have a more balanced representation we decided to test most of these substrates **8** with eight different cinchona alkaloid derivatives including Q, DHQ, QD, DHQD, and their benzyl ether derivatives. To assure reproducibility, some of these reactions were repeated two to five times. In all such cases a range for the yield and ee value is reported in Table 4. Testing Ugi adducts **8b** and **8c** that similarly to **8a** were obtained from benzylamine and *tert*-butyl isocyanide by varying either acid or 2-oxo-aldehyde components revealed that it was difficult to achieve high enantioselectivity for such substrates. Specifically, none of the studied chiral promoters could afford the desired products **12b** and **12c** with the ee value consistently higher than 50%. Turning to the substrates **8d–g** derived from aromatic amines we were able to achieve improved enantioselectivity. The best results were obtained with Q-Bn, DHQ-Bn, DHQD, and QD-Bn that performed consistently well with each of the substrates **8d–g** delivering the corresponding fluorinated products **12d–g** with the ee values higher than 50% and in some cases close or even over 70%. Furthermore, it was possible to divert the selectivity of these reactions towards the preferred formation of either of the enantiomers by choosing an appropriate chiral promotor. Testing Ugi adduct **8h** allowed us to highlight the possibility of simultaneous variation of acid, 2-oxo-aldehyde, and amine compo-

Table 3: Screening of the conditions for enantioselective fluorination of Ugi adduct **8a**.[a]

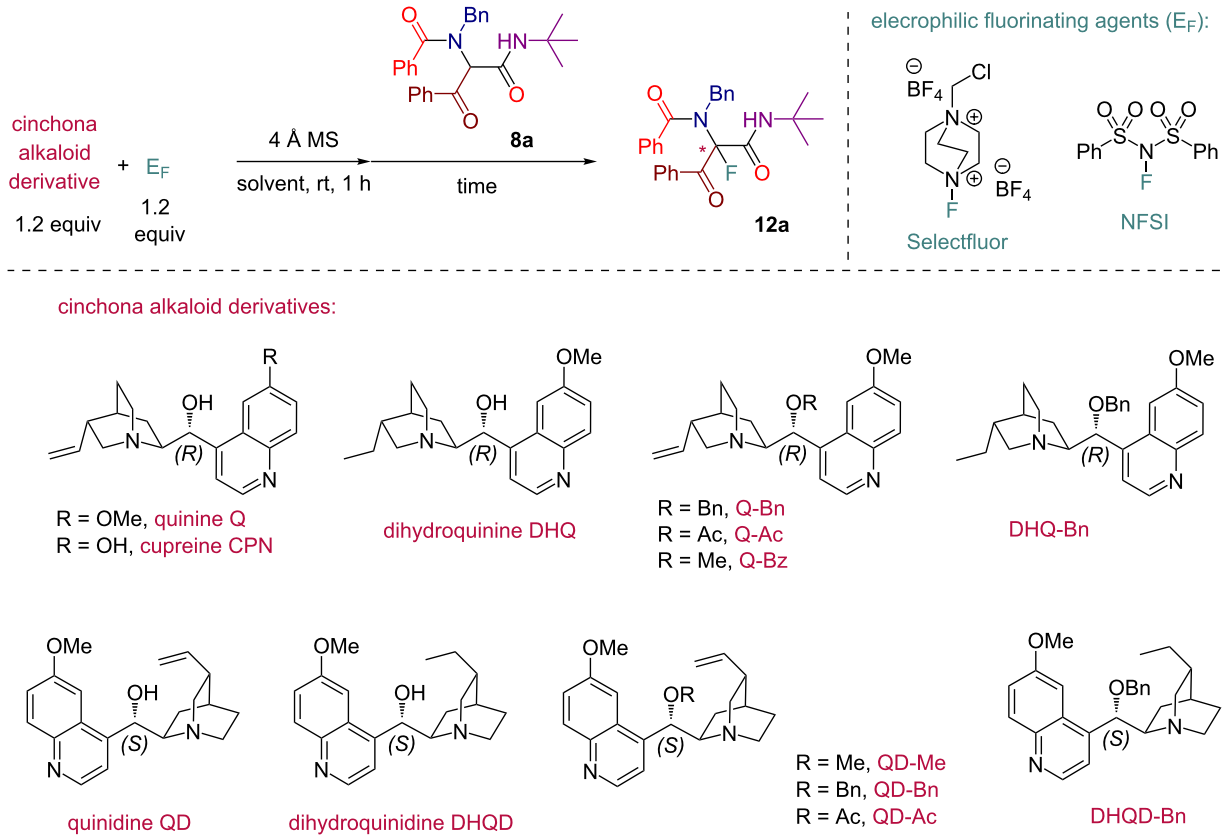

Entry	Cinchona alkaloid derivative	Fluorinating agent	Solvent	Time, h	Yield,[b] %	ee (major enantiomer),[c] %
1	Q	Selectfluor	MeCN	23	88	19 (F)
2	Q	Selectfluor	THF	19	94	21 (F)
3	Q	Selectfluor	DCM	21	74	26 (F)
4[d]	Q	Selectfluor	DCM	70	42	20 (F)
5	Q	Selectfluor	$CHCl_3$	21	71–79	31–44 (F)
6	CPN	Selectfluor	$CHCl_3$	21	–[e]	–[e]
7	DHQ	Selectfluor	$CHCl_3$	16-21	85–90	46–57 (F)
8	DHQ	Selectfluor	THF	12	76	43 (F)
9	Q-Bn	Selectfluor	$CHCl_3$	21	78–83	39–41 (F)
10	Q-Ac	Selectfluor	$CHCl_3$	21–24	35–59	42–51 (F)
11	Q-Bz	Selectfluor	$CHCl_3$	20	62	32 (F)
12	DHQ-Bn	Selectfluor or NFSI	$CHCl_3$	16–22	60–81	57–73 (F)
13	QD	Selectfluor or NFSI	$CHCl_3$	21–23	83–94	51–69 (S)
14	DHQD	Selectfluor	$CHCl_3$	21	86–92	15–21 (S)
15	QD-Me	Selectfluor	$CHCl_3$	23	75	14 (S)
16	QD-Ac	Selectfluor	$CHCl_3$	20	29	27 (S)
17	QD-Bn	Selectfluor	$CHCl_3$	21	80	29 (S)
18	DHQD-Bn	Selectfluor	$CHCl_3$	21	87	23 (S)

[a]The reactions were run on a 0.15–0.2 mmol scale; [b]isolated yield; [c]determined by chiral HPLC analysis, S: slower enantiomer, F: faster enantiomer; [d]the reaction was conducted with 0.2 equiv of Q; [e]no product **12a** was formed.

nents. Overall, four cinchona derivatives were screened with **8h** producing the fluorinated product **12h** with moderate to good enantioselectivity, which was consistent with the performance of other arylamine-derived Ugi adducts **8d**–**g**. The last investigated Ugi adduct **8i** featured the variation of the isocyanide component. Conducting fluorinations with this *n*-butyl isocyanide-derived Ugi adduct **8i**, the desired product **12i** could be successfully obtained. However, the degree of enantioselective induction was lower than in the reactions with the analogous *tert*-butyl isocyanide-derived substrate **8d**. This could probably be ascribed to a reduced rigidity and bulkiness of the *n*-butyl group as compared to *tert*-butyl.

For the substrates **8a**–**g** tested with eight cinchona alkaloid derivatives fluorinations with QD and DHQD led to the reversed stereoselectivity as compared to the reactions with Q and DHQ. For the benzylamine-derived substrates **8a**–**c** benzyl ether derivatives of cinchona alkaloids favored the formation of the same enantiomer of **12** as their free alcohol counterparts (e.g., both Q-Bn and Q favored the formation of the same enantiomer of **12**). In contrast, for the substrates **8d**–**g** derived from aromatic amines a reversed trend was observed. In case of **8d**–**g**, benzyl ether derivatives of cinchona alkaloids favored the formation of the opposite enantiomer of **12** as compared to the one favored by the parent alkaloids featuring free alcohol

Table 4: Scope and limitations of the asymmetric electrophilic fluorination of 2-oxo-aldehyde-derived Ugi adducts **8**.[a]

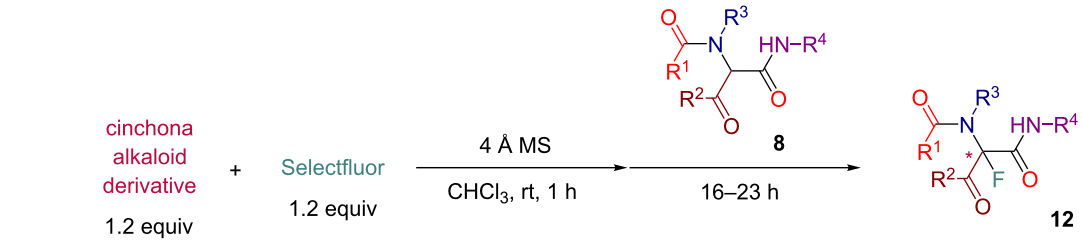

		Q	DHQ	Q-Bn	DHQ-Bn	QD	DHQD	QD-Bn	DHQD-Bn
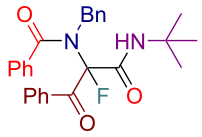 **12a**	yield,[b] %	71–79	85–90	78–83	60–81	83–94	86–92	80	87
	ee,[c] %	31–44 (F)	46–57 (F)	39–41 (F)	57–73 (F)	51–69 (S)	15–21 (S)	29 (S)	23 (S)
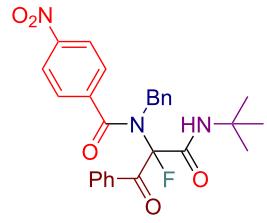 **12b**	yield,[b] %	78–85	84–97	79	76–90	83–89	95–97	67–80	81
	ee,[c] %	23–34 (S)	29–39 (S)	39 (S)	38–51 (S)	24–28 (F)	9–15 (F)	20–24 (F)	21 (F)
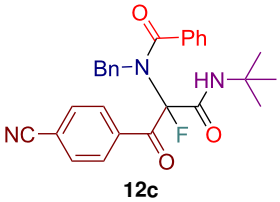 **12c**	yield,[b] %	59–81	60–81	83	74–89	68–85	72–78	81	78
	ee,[c] %	39–46 (S)	39–47 (S)	35 (S)	36 (S)	30–43 (F)	23–25 (F)	25 (F)	23 (F)
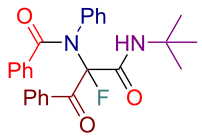 **12d**	yield,[b] %	91	81	78	96	71–91	84	85	82
	ee,[c] %	24 (F)	22 (F)	66 (S)	71 (S)	47–60 (S)	57 (S)	59 (F)	38 (F)

Table 4: Scope and limitations of the asymmetric electrophilic fluorination of 2-oxo-aldehyde-derived Ugi adducts **8**.[a] (continued)

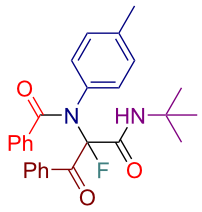 **12e**	yield,[b] %	68–78	91–97	78–82	86–97	89–98	84–91	95–98	85
	ee,[c] %	18–30 (F)	19–23 (F)	65–69 (S)	71–74 (S)	49–50 (S)	58–65 (S)	61–67 (F)	42 (F)
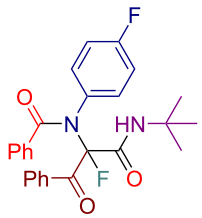 **12f**	yield,[b] %	88–89	91–92	84–88	85–86	71–78	89–98	89	79
	ee,[c] %	23–27 (F)	18–19 (F)	66–67 (S)	69-72 (S)	50–55 (S)	53–64 (S)	57–58 (F)	40 (F)
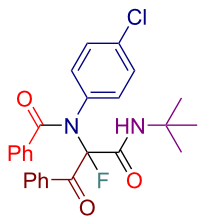 **12g**	yield,[b] %	74–85	90	82–84	86–87	82–88	75–76	75–84	78–81
	ee,[c] %	25–37 (F)	18–24 (F)	65–66 (S)	63–70 (S)	48–59 (S)	51–61 (S)	59–60 (F)	37–54 (F)
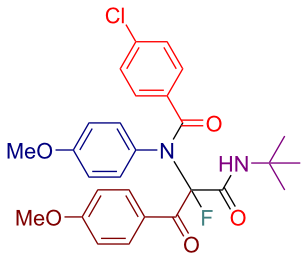 **12h**	yield,[b] %	–[d]	–[d]	64	86	84	–[d]	75	–[d]
	ee,[c] %	–[d]	–[d]	71 (F)	73 (F)	54 (F)	–[d]	55 (S)	–[d]
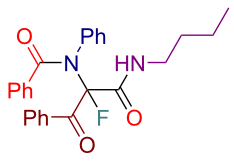 **12i**	yield,[b] %	–[d]	–[d]	51	54	67	–[d]	49	–[d]
	ee,[c] %	–[d]	–[d]	44 (F)	48 (F)	55 (F)	–[d]	29 (S)	–[d]

[a]The reactions were run on a 0.15–0.2 mmol scale; [b]isolated yield; [c]determined by chiral HPLC analysis, S: slower enantiomer, F: faster enantiomer; [d]not conducted.

moiety (e.g., Q-Bn favored the formation of the enantiomer of **12** with the absolute configuration opposite to the one favored by Q). Substrates **8h** and **8i** were tested with only four cinchona alkaloid derivatives, but the observed stereochemical trends appeared to be consistent with those established for the rest of arylamine-derived Ugi adducts **8d**–**g**.

Finally, we attempted to determine the absolute configuration of a stereocenter for the major enantiomer of the representative fluorinated product. Using a sample of product **12e** with the ee value of 74% we were able to obtain crystals suitable for the structure determination via X-ray crystallographic analysis. It was found that a part of the substance crystallized in a racemic

form while the rest crystallized in an enantiopure form. By resolving both types of crystals [90], the configuration of the major slow enantiomer was successfully established as *S* (Figure 1).

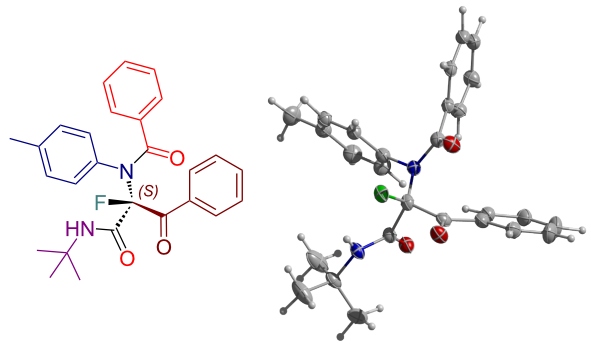

Figure 1: Molecular representation of the X-ray crystal structure of (*S*)-**12e** (slow enantiomer).

Conclusion

In summary, we have explored a new strategy for controlling the stereochemistry in the Ugi adducts through the enantioselective post-Ugi functionalization. Specifically, we have adapted the cinchona alkaloid-promoted asymmetric electrophilic fluorination for derivatizing the 2-oxo-aldehyde-derived Ugi adducts. This allowed us to obtain the post-Ugi products fluorinated at the peptidyl position with the enantiomeric excess values in several instances reaching more than 70%.

Supporting Information

Supporting Information File 1

Experimental procedures, characterization data and copies of spectra.
[https://www.beilstein-journals.org/bjoc/content/supplementary/1860-5397-16-163-S1.pdf]

Supporting Information File 2

Crystallographic data (CIF) for compound (*S*)-**12e**.
[https://www.beilstein-journals.org/bjoc/content/supplementary/1860-5397-16-163-S2.cif]

Supporting Information File 3

Crystallographic data (CIF) for compound (rac)-**12e**.
[https://www.beilstein-journals.org/bjoc/content/supplementary/1860-5397-16-163-S3.cif]

Acknowledgements

We thank Prof. Xingwang Wang for his advice to explore the electrophilic fluorination as a tool for the enantioselective post-Ugi functionalization.

Funding

This work was supported by the start-up fund from Soochow University (grant Q410900714), National Natural Science Foundation of China (grant 21650110445), Natural Science Foundation of Jiangsu Province of China (grant BK20160310), the Priority Academic Program Development of Jiangsu Higher Education Institutions (PAPD) and the project of scientific and technologic infrastructure of Suzhou (grant SZS201708). M.H. and M.Z. are grateful to the Chinese Scholarship Council (CSC) for providing doctoral scholarships.

References

1. Bienaymé, H.; Hulme, C.; Oddon, G.; Schmitt, P. *Chem. – Eur. J.* **2000,** *6,* 3321–3329. doi:10.1002/1521-3765(20000915)6:18<3321::aid-chem3321>3.0.co;2-a
2. Zhu, J.; Bienaymé, H., Eds. *Multicomponent Reactions,* 1st ed.; Wiley-VCH: Weinheim, Germany, 2005. doi:10.1002/3527605118
3. Sunderhaus, J. D.; Martin, S. F. *Chem. – Eur. J.* **2009,** *15,* 1300–1308. doi:10.1002/chem.200802140
4. Ganem, B. *Acc. Chem. Res.* **2009,** *42,* 463–472. doi:10.1021/ar800214s
5. Orru, R. V. A.; Ruijter, E., Eds. *Synthesis of Heterocycles via Multicomponent Reactions I;* Topics in Heterocyclic Chemistry; Springer: Heidelberg, Germany, 2010. doi:10.1007/978-3-642-12675-8
6. Orru, R. V. A.; Ruijter, E., Eds. *Synthesis of Heterocycles via Multicomponent Reactions II;* Topics in Heterocyclic Chemistry; Springer: Heidelberg, Germany, 2010. doi:10.1007/978-3-642-15455-3
7. Jiang, B.; Rajale, T.; Wever, W.; Tu, S.-J.; Li, G. *Chem. – Asian J.* **2010,** *5,* 2318–2335. doi:10.1002/asia.201000310
8. Dömling, A.; Wang, W.; Wang, K. *Chem. Rev.* **2012,** *112,* 3083–3135. doi:10.1021/cr100233r
9. Zhu, J.; Wang, Q.; Wang, M.-X., Eds. *Multicomponent Reactions in Organic Synthesis;* Wiley-VCH: Weinheim, Germany, 2014. doi:10.1002/9783527678174
10. Banfi, L.; Basso, A.; Moni, L.; Riva, R. *Eur. J. Org. Chem.* **2014,** 2005–2015. doi:10.1002/ejoc.201301715
11. Cioc, R. C.; Ruijter, E.; Orru, R. V. A. *Green Chem.* **2014,** *16,* 2958–2975. doi:10.1039/c4gc00013g
12. Levi, L.; Müller, T. J. J. *Chem. Soc. Rev.* **2016,** *45,* 2825–2846. doi:10.1039/c5cs00805k
13. Murlykina, M. V.; Morozova, A. D.; Zviagin, I. M.; Sakhno, Y. I.; Desenko, S. M.; Chebanov, V. A. *Front. Chem. (Lausanne, Switz.)* **2018,** *6,* 527. doi:10.3389/fchem.2018.00527
14. Dömling, A.; Ugi, I. *Angew. Chem., Int. Ed.* **2000,** *39,* 3168–3210. doi:10.1002/1521-3773(20000915)39:18<3168::aid-anie3168>3.0.co;2-u
15. Akritopoulou-Zanze, I. *Curr. Opin. Chem. Biol.* **2008,** *12,* 324–331. doi:10.1016/j.cbpa.2008.02.004
16. Koopmanschap, G.; Ruijter, E.; Orru, R. V. A. *Beilstein J. Org. Chem.* **2014,** *10,* 544–598. doi:10.3762/bjoc.10.50

17. Váradi, A.; Palmer, T. C.; Notis Dardashti, R.; Majumdar, S. *Molecules* **2016,** *21,* 19. doi:10.3390/molecules21010019
18. Bode, M. L.; Gravestock, D.; Rousseau, A. L. *Org. Prep. Proced. Int.* **2016,** *48,* 89–221. doi:10.1080/00304948.2016.1138072
19. Passerini, M. *Gazz. Chim. Ital.* **1921,** *51,* 126–129.
20. Banfi, L.; Riva, R. *Org. React.* **2005,** *65,* 1–140. doi:10.1002/0471264180.or065.01
21. Kazemizadeh, A. R.; Ramazani, A. *Curr. Org. Chem.* **2012,** *16,* 418–450. doi:10.2174/138527212799499868
22. Chandgude, A. Multicomponent Reactions: Development, Scope, and Applications. Ph.D. Thesis, University of Groningen, Groningen, Netherlands, 2017.
23. Ugi, I.; Meyr, R.; Fetzer, U.; Steinbrückner, C. *Angew. Chem.* **1959,** *71,* 386. doi:10.1002/ange.19590711110
24. Ugi, I.; Steinbrückner, C. *Angew. Chem.* **1960,** *72,* 267–268. doi:10.1002/ange.19600720709
25. Banfi, L.; Basso, A.; Riva, R. Synthesis of Heterocycles Through Classical Ugi and Passerini Reactions Followed by Secondary Transformations Involving One or Two Additional Functional Groups. In *Synthesis of Heterocycles via Multicomponent Reactions I;* Orru, R. V. A.; Ruijter, E., Eds.; Topics in Heterocyclic Chemistry, Vol. 23; Springer: Berlin, Germany, 2010; pp 1–39. doi:10.1007/7081_2009_23
26. Sharma, U. K.; Sharma, N.; Vachhani, D. D.; Van der Eycken, E. V. *Chem. Soc. Rev.* **2015,** *44,* 1836–1860. doi:10.1039/c4cs00253a
27. Zhang, Z.; Zheng, X.; Guo, C. *Chin. J. Org. Chem.* **2016,** *36,* 1241–1265. doi:10.6023/cjoc201511004
28. Li, X.; Jia, X.; Yin, L. *Chin. J. Org. Chem.* **2017,** *37,* 2237–2249. doi:10.6023/cjoc201704026
29. Banfi, L.; Basso, A.; Lambruschini, C.; Moni, L.; Riva, R. *Chem. Heterocycl. Compd.* **2017,** *53,* 382–408. doi:10.1007/s10593-017-2065-1
30. Heravi, M. M.; Mohammadkhani, L. Synthesis of various N-heterocycles using the four-component Ugi reaction. *Advances in Heterocyclic Chemistry;* Elsevier: Amsterdam, Netherlands, 2020; Vol. 131, pp 351–403. doi:10.1016/bs.aihch.2019.04.001
31. Bariwal, J.; Kaur, R.; Voskressensky, L. G.; Van der Eycken, E. V. *Front. Chem. (Lausanne, Switz.)* **2018,** *6,* 557. doi:10.3389/fchem.2018.00557
32. Mohammadi-Khanaposhtani, M.; Jalalimanesh, N.; Saeedi, M.; Larijani, B.; Mahdavi, M. *Mol. Diversity* **2020,** *24,* 855–887. doi:10.1007/s11030-019-09975-y
33. Wang, Q.; Wang, D.-X.; Wang, M.-X.; Zhu, J. *Acc. Chem. Res.* **2018,** *51,* 1290–1300. doi:10.1021/acs.accounts.8b00105
34. Shaabani, S.; Dömling, A. *Angew. Chem., Int. Ed.* **2018,** *57,* 16266–16268. doi:10.1002/anie.201811129
35. Riva, R. *Science* **2018,** *361,* 1072–1073. doi:10.1126/science.aau7497
36. Huang, Y.; Wolf, S.; Koes, D.; Popowicz, G. M.; Camacho, C. J.; Holak, T. A.; Dömling, A. *ChemMedChem* **2012,** *7,* 49–52. doi:10.1002/cmdc.201100428
37. Kusebauch, U.; Beck, B.; Messer, K.; Herdtweck, E.; Dömling, A. *Org. Lett.* **2003,** *5,* 4021–4024. doi:10.1021/ol035010u
38. Andreana, P. R.; Liu, C. C.; Schreiber, S. L. *Org. Lett.* **2004,** *6,* 4231–4233. doi:10.1021/ol0482893
39. Wang, S.-X.; Wang, M.-X.; Wang, D.-X.; Zhu, J. *Angew. Chem., Int. Ed.* **2008,** *47,* 388–391. doi:10.1002/anie.200704315
40. Zhang, J.; Lin, S.-X.; Cheng, D.-J.; Liu, X.-Y.; Tan, B. *J. Am. Chem. Soc.* **2015,** *137,* 14039–14042. doi:10.1021/jacs.5b09117
41. Denmark, S. E.; Fan, Y. *J. Org. Chem.* **2005,** *70,* 9667–9676. doi:10.1021/jo050549m
42. Wang, S.; Wang, M.-X.; Wang, D.-X.; Zhu, J. *Eur. J. Org. Chem.* **2007,** 4076–4080. doi:10.1002/ejoc.200700340
43. Wang, S.-X.; Wang, M.-X.; Wang, D.-X.; Zhu, J. *Org. Lett.* **2007,** *9,* 3615–3618. doi:10.1021/ol7014658
44. Yue, T.; Wang, M.-X.; Wang, D.-X.; Zhu, J. *Angew. Chem., Int. Ed.* **2008,** *47,* 9454–9457. doi:10.1002/anie.200804213
45. Yue, T.; Wang, M.-X.; Wang, D.-X.; Masson, G.; Zhu, J. *J. Org. Chem.* **2009,** *74,* 8396–8399. doi:10.1021/jo9017765
46. Mihara, H.; Xu, Y.; Shepherd, N. E.; Matsunaga, S.; Shibasaki, M. *J. Am. Chem. Soc.* **2009,** *131,* 8384–8385. doi:10.1021/ja903158x
47. Zeng, X.; Ye, K.; Lu, M.; Chua, P. J.; Tan, B.; Zhong, G. *Org. Lett.* **2010,** *12,* 2414–2417. doi:10.1021/ol1007789
48. Gulevich, A. V.; Balenkova, E. S.; Nenajdenko, V. G. *J. Org. Chem.* **2007,** *72,* 7878–7885. doi:10.1021/jo071030o
49. Nenajdenko, V. G.; Gulevich, A. V.; Chernichenko, K. Y.; Sokolova, N. V.; Balenkova, E. S. *Mendeleev Commun.* **2011,** *21,* 245–246. doi:10.1016/j.mencom.2011.09.004
50. Banfi, L.; Basso, A.; Cerulli, V.; Rocca, V.; Riva, R. *Beilstein J. Org. Chem.* **2011,** *7,* 976–979. doi:10.3762/bjoc.7.109
51. Banfi, L.; Basso, A.; Chiappe, C.; De Moliner, F.; Riva, R.; Sonaglia, L. *Org. Biomol. Chem.* **2012,** *10,* 3819–3829. doi:10.1039/c2ob25060h
52. Zhu, D.; Xia, L.; Pan, L.; Li, S.; Chen, R.; Mou, Y.; Chen, X. *J. Org. Chem.* **2012,** *77,* 1386–1395. doi:10.1021/jo2021967
53. Caputo, S.; Basso, A.; Moni, L.; Riva, R.; Rocca, V.; Banfi, L. *Beilstein J. Org. Chem.* **2016,** *12,* 139–143. doi:10.3762/bjoc.12.15
54. Lambruschini, C.; Moni, L.; Banfi, L. *Eur. J. Org. Chem.* **2020,** 3766–3778. doi:10.1002/ejoc.202000016
55. Hashimoto, T.; Kimura, H.; Kawamata, Y.; Maruoka, K. *Angew. Chem., Int. Ed.* **2012,** *51,* 7279–7281. doi:10.1002/anie.201201905
56. Zhao, W.; Huang, L.; Guan, Y.; Wulff, W. D. *Angew. Chem., Int. Ed.* **2014,** *53,* 3436–3441. doi:10.1002/anie.201310491
57. Zhang, J.; Yu, P.; Li, S.-Y.; Sun, H.; Xiang, S.-H.; Wang, J.; Houk, K. N.; Tan, B. *Science* **2018,** *361,* eaas8707. doi:10.1126/science.aas8707
58. Zhang, J.; Wang, Y.-Y.; Sun, H.; Li, S.-Y.; Xiang, S.-H.; Tan, B. *Sci. China: Chem.* **2020,** *63,* 47–54. doi:10.1007/s11426-019-9606-2
59. Nechaev, A. A.; Peshkov, A. A.; Peshkov, V. A.; Van der Eycken, E. V. *Synthesis* **2016,** *48,* 2280–2286. doi:10.1055/s-0035-1561422
60. Peshkov, A. A.; Peshkov, V. A.; Li, Z.; Pereshivko, O. P.; Van der Eycken, E. V. *Eur. J. Org. Chem.* **2014,** 6390–6393. doi:10.1002/ejoc.201402723
61. Wei, H.; Wang, G.; Wang, Y.; Li, B.; Huang, J.; Kashtanov, S.; Van Hecke, K.; Pereshivko, O. P.; Peshkov, V. A. *Chem. – Asian J.* **2017,** *12,* 825–829. doi:10.1002/asia.201700051
62. Hasan, M.; Zaman, M.; Peshkov, A. A.; Amire, N.; Les, A.; Nechaev, A. A.; Wang, Y.; Kashtanov, S.; Van der Eycken, E. V.; Pereshivko, O. P.; Peshkov, V. A. *Eur. J. Org. Chem.* **2020,** 3378–3389. doi:10.1002/ejoc.202000015
63. Shibata, N.; Ishimaru, T.; Nakamura, S.; Toru, T. *J. Fluorine Chem.* **2007,** *128,* 469–483. doi:10.1016/j.jfluchem.2006.12.014
64. Lectard, S.; Hamashima, Y.; Sodeoka, M. *Adv. Synth. Catal.* **2010,** *352,* 2708–2732. doi:10.1002/adsc.201000624
65. Shibatomi, K.; Narayama, A.; Soga, Y.; Muto, T.; Iwasa, S. *Org. Lett.* **2011,** *13,* 2944–2947. doi:10.1021/ol201007e
66. Shibata, N.; Suzuki, E.; Takeuchi, Y. *J. Am. Chem. Soc.* **2000,** *122,* 10728–10729. doi:10.1021/ja002732x

67. Shibata, N.; Suzuki, E.; Asahi, T.; Shiro, M. *J. Am. Chem. Soc.* **2001,** *123,* 7001–7009. doi:10.1021/ja010789t
68. Cahard, D.; Audouard, C.; Plaquevent, J.-C.; Roques, N. *Org. Lett.* **2000,** *2,* 3699–3701. doi:10.1021/ol006610l
69. Cahard, D.; Audouard, C.; Plaquevent, J.-C.; Toupet, L.; Roques, N. *Tetrahedron Lett.* **2001,** *42,* 1867–1869. doi:10.1016/s0040-4039(01)00017-x
70. Mohar, B.; Baudoux, J.; Plaquevent, J.-C.; Cahard, D. *Angew. Chem., Int. Ed.* **2001,** *40,* 4214–4216. doi:10.1002/1521-3773(20011119)40:22<4214::aid-anie4214>3.0.co;2-b
71. Baudequin, C.; Plaquevent, J.-C.; Audouard, C.; Cahard, D. *Green Chem.* **2002,** *4,* 584–586. doi:10.1039/b208817g
72. Baudequin, C.; Loubassou, J.-F.; Plaquevent, J.-C.; Cahard, D. *J. Fluorine Chem.* **2003,** *122,* 189–193. doi:10.1016/s0022-1139(03)00085-x
73. Thierry, B.; Audouard, C.; Plaquevent, J.-C.; Cahard, D. *Synlett* **2004,** 856–860. doi:10.1055/s-2004-817781
74. Mohar, B.; Sterk, D.; Ferron, L.; Cahard, D. *Tetrahedron Lett.* **2005,** *46,* 5029–5031. doi:10.1016/j.tetlet.2005.05.074
75. Fukuzumi, T.; Shibata, N.; Sugiura, M.; Nakamura, S.; Toru, T. *J. Fluorine Chem.* **2006,** *127,* 548–551. doi:10.1016/j.jfluchem.2006.01.004
76. Ramírez, J.; Huber, D. P.; Togni, A. *Synlett* **2007,** 1143–1147. doi:10.1055/s-2007-973897
77. Yi, W.-B.; Huang, X.; Zhang, Z.; Zhu, D.-R.; Cai, C.; Zhang, W. *Beilstein J. Org. Chem.* **2012,** *8,* 1233–1240. doi:10.3762/bjoc.8.138
78. Wang, M.; Wang, B. M.; Shi, L.; Tu, Y. Q.; Fan, C.-A.; Wang, S. H.; Hu, X. D.; Zhang, S. Y. *Chem. Commun.* **2005,** 5580–5582. doi:10.1039/b510004f
79. Shibata, N.; Ishimaru, T.; Suzuki, E.; Kirk, K. L. *J. Org. Chem.* **2003,** *68,* 2494–2497. doi:10.1021/jo026792s
80. Zoute, L.; Audouard, C.; Plaquevent, J.-C.; Cahard, D. *Org. Biomol. Chem.* **2003,** *1,* 1833–1834. doi:10.1039/b303113f
81. Shibata, N.; Ishimaru, T.; Nakamura, M.; Toru, T. *Synlett* **2004,** 2509–2512. doi:10.1055/s-2004-834810
82. Gillis, E. P.; Eastman, K. J.; Hill, M. D.; Donnelly, D. J.; Meanwell, N. A. *J. Med. Chem.* **2015,** *58,* 8315–8359. doi:10.1021/acs.jmedchem.5b00258
83. Inoue, M.; Sumii, Y.; Shibata, N. *ACS Omega* **2020,** *5,* 10633–10640. doi:10.1021/acsomega.0c00830
84. Huber, D. P.; Stanek, K.; Togni, A. *Tetrahedron: Asymmetry* **2006,** *17,* 658–664. doi:10.1016/j.tetasy.2006.01.035
85. Mang, J.-Y.; Kim, D.-Y. *Bull. Korean Chem. Soc.* **2008,** *29,* 2091–2092. doi:10.5012/bkcs.2008.29.11.2091
86. Mang, J. Y.; Kwon, D. G.; Kim, D. Y. *J. Fluorine Chem.* **2009,** *130,* 259–262. doi:10.1016/j.jfluchem.2008.11.001
87. Han, X.; Zhong, F.; Lu, Y. *Adv. Synth. Catal.* **2010,** *352,* 2778–2782. doi:10.1002/adsc.201000562
88. Cui, H.-F.; Li, P.; Wang, X.-W.; Chai, Z.; Yang, Y.-Q.; Cai, Y.-P.; Zhu, S.-Z.; Zhao, G. *Tetrahedron* **2011,** *67,* 312–317. doi:10.1016/j.tet.2010.11.041
89. Kwiatkowski, J.; Lu, Y. *Org. Biomol. Chem.* **2015,** *13,* 2350–2359. doi:10.1039/c4ob02486a
90. Crystallographic data for rac-**12e** (CCDC 2015756) and (S)-**12e** (CCDC 2015755) have been deposited with the Cambridge Crystallographic Data Centre.

License and Terms

This is an Open Access article under the terms of the Creative Commons Attribution License (http://creativecommons.org/licenses/by/4.0). Please note that the reuse, redistribution and reproduction in particular requires that the authors and source are credited.

The license is subject to the *Beilstein Journal of Organic Chemistry* terms and conditions: (https://www.beilstein-journals.org/bjoc)

The definitive version of this article is the electronic one which can be found at: doi:10.3762/bjoc.16.163

BEILSTEIN JOURNAL OF ORGANIC CHEMISTRY

Synthesis of 6,13-difluoropentacene

Matthias W. Tripp and Ulrich Koert*

Full Research Paper

Open Access

Address:
Department of Chemistry, Philipps-Universität Marburg, Hans-Meerwein-Straße 4, 35034 Marburg, Germany

Email:
Ulrich Koert* - koert@chemie.uni-marburg.de

* Corresponding author

Keywords:
fluorinated acenes; Friedel–Crafts reaction; *ortho*-lithiation; synthesis

Beilstein J. Org. Chem. **2020,** *16,* 2136–2140.
https://doi.org/10.3762/bjoc.16.181

Received: 16 July 2020
Accepted: 25 August 2020
Published: 02 September 2020

This article is part of the thematic issue "Organo-fluorine chemistry V".

Guest Editor: D. O'Hagan

© 2020 Tripp and Koert; licensee Beilstein-Institut.
License and terms: see end of document.

Abstract

6,13-Difluoropentacene was synthesized from 1,4-difluorobenzene. Friedel–Crafts annulation of the latter with phthalic anhydride and subsequent reduction of the anthraquinone gave 1,4-difluoroanthracene. After *ortho*-lithiation and reaction with phthalic anhydride a carboxylic acid was obtained whose Friedel–Crafts acylation and subsequent reductive removal of the oxygen-functionalities resulted in the formation of the target compound. The HOMO–LUMO gap of 6,13-difluoropentacene was determined via UV–vis spectroscopy and compared to other fluorinated pentacenes.

Introduction

Pentacenes are a prototype in the field of organic semiconductors due to their expanded π-systems and low HOMO–LUMO gaps with applications in different molecular-based organic electronics like OFETs, OLEDs or organic photovoltaics [1-3]. An advantage of organic molecular electronics over inorganic alternatives is the versatility in design of new molecular materials by derivatization of known compounds [4]. Since the performance of these devices is strongly dependent on the optoelectronic solid-state properties of the pentacenes, predictable control of the electronic structure is desirable. A common strategy to influence the electronic properties of pentacenes, without significant effect on the molecular shape, is fluorination [5]. Suzuki et al. showed in 2004 the strong effect of perfluorination on the electronic properties [6]. While unsubstituted pentacene (**1**, PEN, Figure 1) is known to be a p-type semiconductor, the perfluorinated counterpart perfluoropentacene (**2**, PFP) showed an n-type behavior. In their synthesis and structural as well as electronic characterization of F4PEN **3**, Bettinger et al. showed that the electronic properties of pentacenes are not a simple linear function of the degree of fluorination [7,8]. They reported that the fluorination in the 2,3,9,10-positions resulted in a larger HOMO–LUMO gap compared to PEN, while PFP showed a smaller gap than PEN. Another example for a partially fluorinated pentacene is the F6PEN **4** [9]. Its unilateral substitution pattern leads to a disctinct electronic structure and a criss-cross packing motif, unlike the herringbone structure of **1**–**3**.

Here, the synthesis and characterization of 6,13-difluoropentacene (**5**, F2PEN) is reported. Since the central ring of

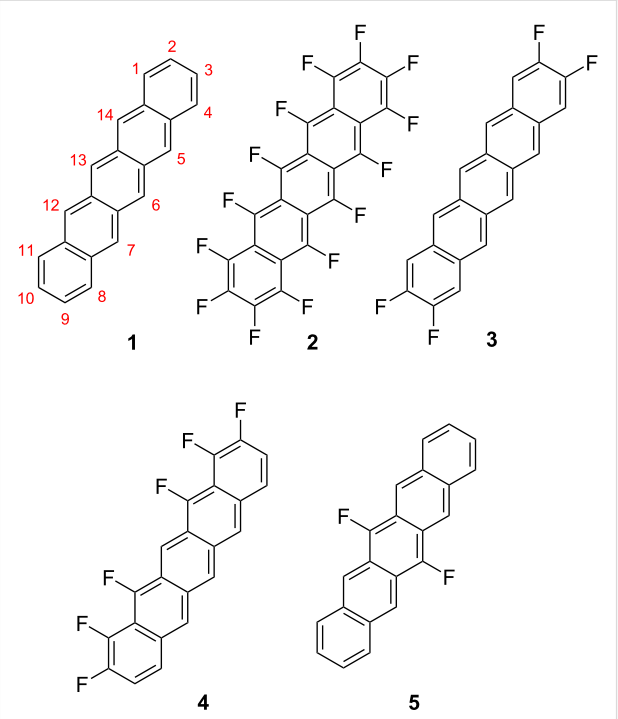

Figure 1: Structures of pentacene and fluorinated pentacenes.

pentacenes is known to be a weak spot (because of light-induced dimerization or oxidation) [2] the effects of fluorination in these positions are of interest.

Results and Discussion

6,13-Disubstituted pentacenes are often synthesized starting from 6,13-pentacenedione [2,3,10-12]. Initial attempts to prepare 6,13-difluoropentacene (**5**) along this route failed [13]. Therefore, an alternative route that commences with the central ring already carrying the two fluorine substituents was investigated. The retrosynthetic analysis for this strategy is shown in Scheme 1. The formation of the C5,5a-bond colored in red could be accomplished by an intramolecular Friedel–Crafts type acylation with the acylium-cation intermediate **6**. The corresponding carboxylic acid precursor could be prepared by reaction of the anthracenyllithium **7** with phthalic anhydride (**8**). Intermediate **7** could be accessed by *ortho*-lithiation of anthracene **9**. The synthesis of **9** by two consecutive Friedel–Crafts acylation reactions and reduction of the resulting anthraquinone could start from **8** and 1,4-difluorobenzene (**10**).

Starting point of the synthesis was the conversion of 1,4-difluorobenzene (**10**) to 1,4-difluoroanthraquinone (**11**, Scheme 2) [14]. The first Friedel-Crafts acylation of phthalic anhydride was achieved using $AlCl_3$ in boiling 1,4-difluorobenzene (**10**). The second Friedel–Crafts acylation is then performed in polyphosphoric acid at 140 °C, giving anthraquinone **11** in 53% yield over two steps. Reduction of **11** to the anthracene **9** proceeded smoothly using zinc powder in 1,4-dioxane and aqueous ammonia under copper catalysis [15]. To achieve good

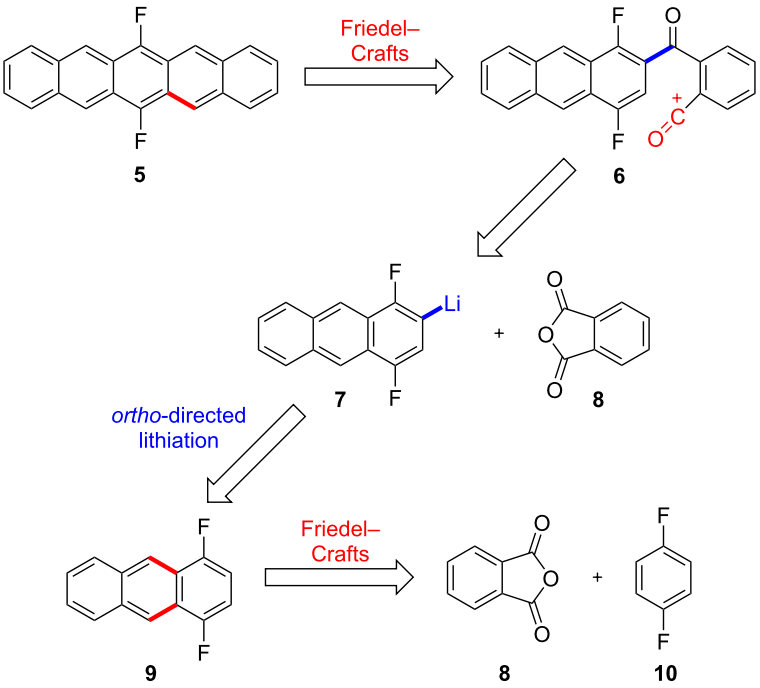

Scheme 1: Retrosynthetic analysis of F2PEN **5**.

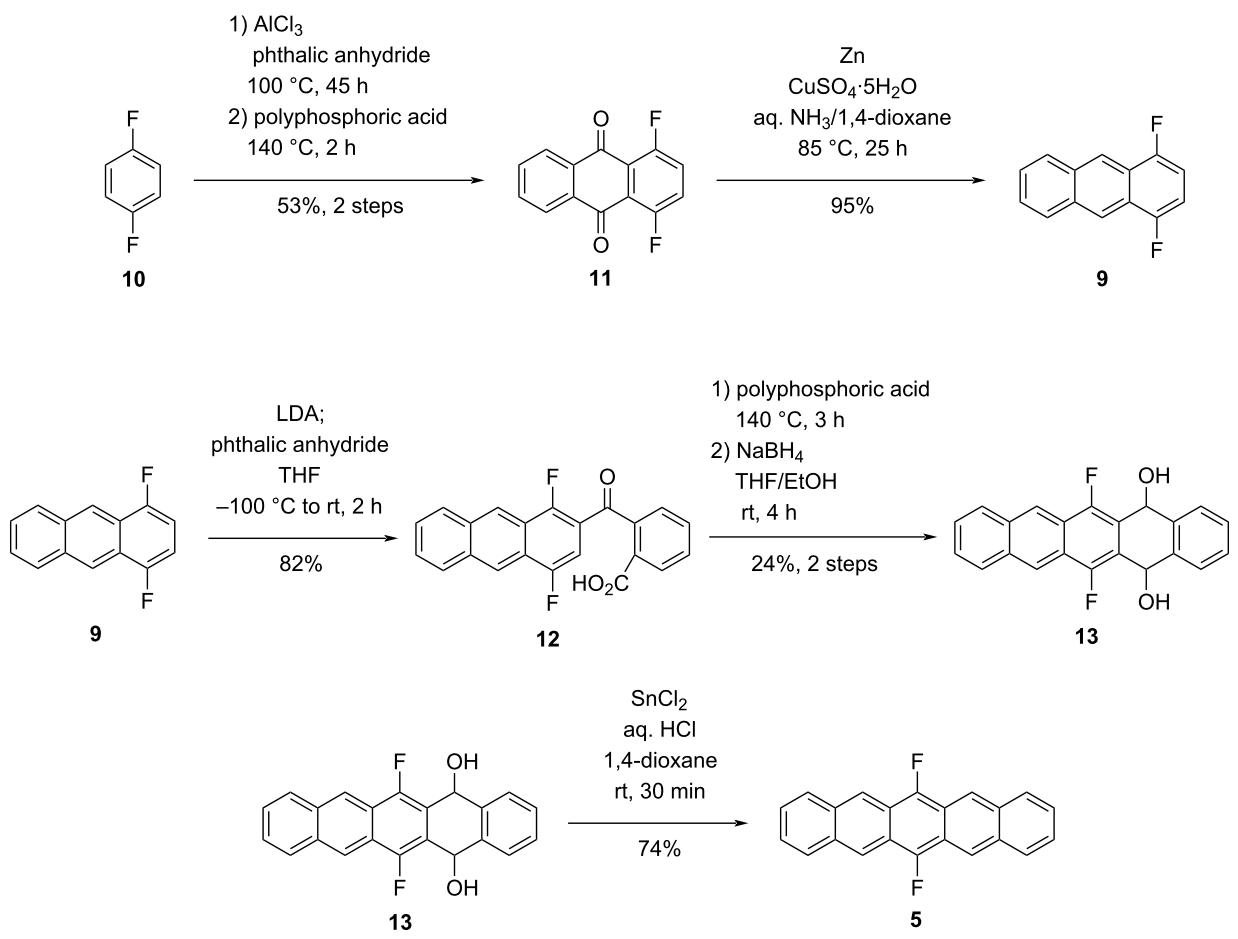

Scheme 2: Synthesis of F2PEN **5**.

yields, it was crucial to perform the reaction in a sealed pressure tube to prevent ammonia from degassing.

Different bases, temperatures and reaction times were screened to optimize the *ortho*-lithiation of **9**. The best results were achieved using LDA as a base at –78 °C for 15 min and then rapidly adding the lithiated species **7** to phthalic anhydride in THF precooled to –100 °C [16]. Using these conditions, the carboxylic acid **12** was isolated in 82% yield.

The subsequent Friedel–Crafts acylation proofed to be challenging. Using reagents like PCl_5 resulted in a quantitative substitution of the fluorine substituents in the corresponding pentacenequinone by chloride. This side reaction could be avoided using polyphosphoric acid as Friedel–Crafts reagent. The pentacenequinone showed very low solubility, which complicated a chromatographic isolation. However, the crude ^{1}H NMR showed sufficiently clean conversion, hence the subsequent reduction step using $NaBH_4$ to diol **13** was performed without further purification of the quinone.

The low yield for the formation of **13** seems to be an intrinsic instability of its *ortho*-fluorobenzylic alcohol moiety. Moreover, the compound quantitatively decomposes to 6,13-pentacenequinone **15** in CD_2Cl_2 solution at room temperature within 2 h. A possible reaction pathway for this degradation in the presence of moisture is an intermolecular attack of water, leading to a fluorohydrine **14** (Scheme 3). In absence of water, this reaction might take place in an intramolecular manner. The fluorohydrine **14** then rapidly decomposes to 6,13-pentacenequinone (**15**) after elimination of HF.

The final aromatization of diol **13** to the target molecule **5** proceeded smoothly in 74% yield using $SnCl_2$ in 1,4-dioxane and aqueous HCl [11,12]. F2PEN **5** can be stored under inertgas atmosphere at −20 °C for a month without noticeable decomposition. However, in solution under ambient atmosphere and sunlight decomposition takes place quickly, which is indicated by decolorization of a purple solution in CH_2Cl_2 within 3 min. ^{1}H NMR analysis showed 6,13-pentacenequinone (**15**) as the degradation product. The rate of degradation in degassed C_6D_6

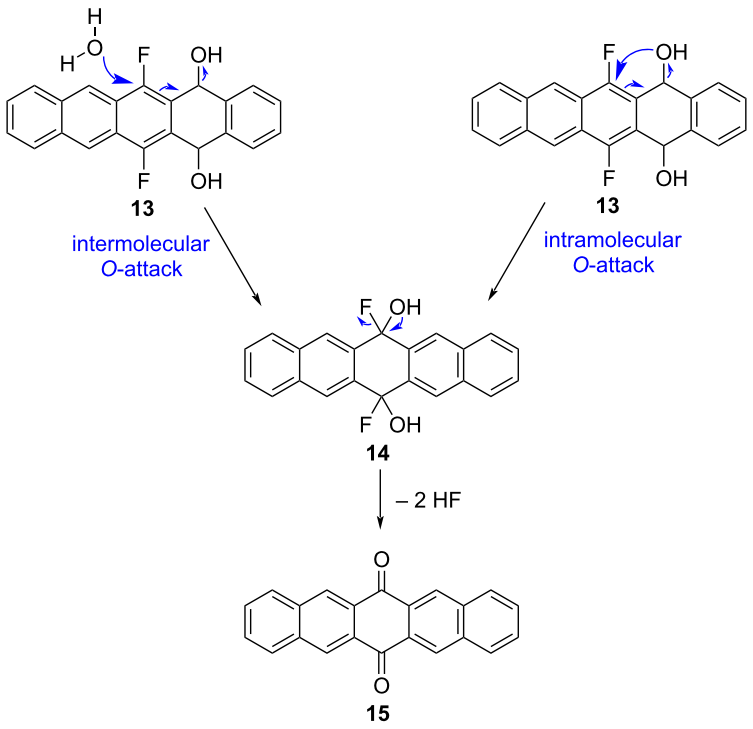

Scheme 3: Decomposition of diol **13** in solution.

was slow enough to obtain a clean ^{1}H NMR spectrum (see Supporing Information File 1) [17].

Next, the HOMO–LUMO gap of **5** was investigated via UV–vis spectroscopy in solution (Figure 2). The λ_{max} was determined to be at 597 nm, which corresponds to a HOMO–LUMO gap of ΔE = 2.08 eV. Comparison with the values of PEN (ΔE = 2.13 eV) [9] and PFP (ΔE = 1.99 eV) [9] shows that the electronic structure of F2PEN **5** lies in between these two.

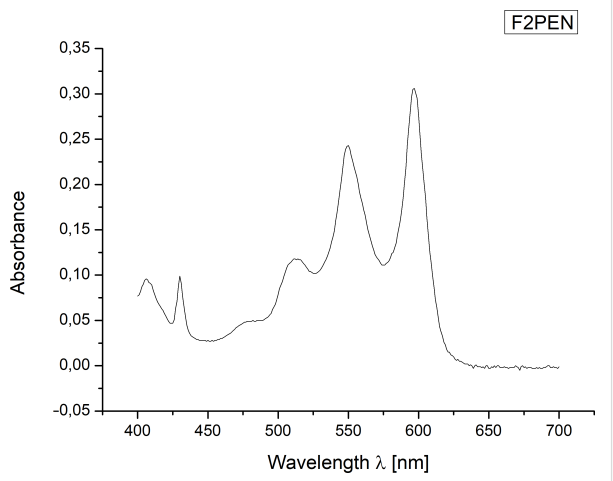

Figure 2: UV–vis spectrum of F2PEN **5** in CH_2Cl_2.

While fluorine substituents in 2,3,9,10-positions (F4PEN **3**) result in a larger HOMO–LUMO gap compared to PEN [7,8], substitution in the 6,13-positions leads to smaller band-gaps, similar to the unilaterally substituted F6PEN **4** [9].

Conclusion

Starting from 1,4-difluorobenzene a synthetic route to 6,13-difluoropentacene was established (7% over seven steps). Key steps are Friedel–Crafts acylation reactions and an *ortho*-directed lithiation of 1,4-difluoroanthracene. This strategy could be applicable for the synthesis of differently substituted 6,13-difluoropentacenes as well.

Supporting Information

Supporting Information File 1

Experimental details, spectroscopic and analytical data of all new compounds.
[https://www.beilstein-journals.org/bjoc/content/supplementary/1860-5397-16-181-S1.pdf]

Funding

Financial support by the Deutsche Forschungsgemeinschaft (SFB 1083, project A8) is gratefully acknowledged.

ORCID® iDs

Ulrich Koert - https://orcid.org/0000-0002-4776-8549

References

1. Ruiz, R.; Choudhary, D.; Nickel, B.; Toccoli, T.; Chang, K.-C.; Mayer, A. C.; Clancy, P.; Blakely, J. M.; Headrick, R. L.; Iannotta, S.; Malliaras, G. G. *Chem. Mater.* **2004,** *16,* 4497–4508. doi:10.1021/cm049563q
2. Anthony, J. E. *Angew. Chem., Int. Ed.* **2008,** *47,* 452–483. doi:10.1002/anie.200604045
3. Bunz, U. H. F. *Acc. Chem. Res.* **2015,** *48,* 1676–1686. doi:10.1021/acs.accounts.5b00118
4. Hains, A. W.; Liang, Z.; Woodhouse, M. A.; Gregg, B. A. *Chem. Rev.* **2010,** *110,* 6689–6735. doi:10.1021/cr9002984
5. Tang, M. L.; Bao, Z. *Chem. Mater.* **2011,** *23,* 446–455. doi:10.1021/cm102182x
6. Sakamoto, Y.; Suzuki, T.; Kobayashi, M.; Gao, Y.; Fukai, Y.; Inoue, Y.; Sato, F.; Tokito, S. *J. Am. Chem. Soc.* **2004,** *126,* 8138–8140. doi:10.1021/ja0476258
7. Shen, B.; Geiger, T.; Einholz, R.; Reicherter, F.; Schundelmeier, S.; Maichle-Mössmer, C.; Speiser, B.; Bettinger, H. F. *J. Org. Chem.* **2018,** *83,* 3149–3158. doi:10.1021/acs.joc.7b03241
8. Geiger, T.; Schundelmeier, S.; Hummel, T.; Ströbele, M.; Leis, W.; Seitz, M.; Zeiser, C.; Moretti, L.; Maiuri, M.; Cerullo, G.; Broch, K.; Vahland, J.; Leo, K.; Maichle-Mössmer, C.; Speiser, B.; Bettinger, H. F. *Chem. – Eur. J.* **2020,** *26,* 3420–3434. doi:10.1002/chem.201905843
9. Hofmann, P. E.; Tripp, M. W.; Bischof, D.; Grell, Y.; Schiller, A. L. C.; Breuer, T.; Ivlev, S. I.; Witte, G.; Koert, U. *Angew. Chem., Int. Ed.* **2020,** in press. doi:10.1002/anie.202006489
10. Tykwinski, R. R. *Acc. Chem. Res.* **2019,** *52,* 2056–2069. doi:10.1021/acs.accounts.9b00216
11. Schwaben, J.; Münster, N.; Klues, M.; Breuer, T.; Hofmann, P.; Harms, K.; Witte, G.; Koert, U. *Chem. – Eur. J.* **2015,** *21,* 13758–13771. doi:10.1002/chem.201501399
12. Schwaben, J.; Münster, N.; Breuer, T.; Klues, M.; Harms, K.; Witte, G.; Koert, U. *Eur. J. Org. Chem.* **2013,** 1639–1643. doi:10.1002/ejoc.201201714
13. Preparations of alkyl-disubstituted 6,13-difluoropentacenes via the corresponding pentacenequinone are reported in a patent: Okamoto, K; *Jpn. Kokai Tokkyo Koho*, JP 2008024684, 07.02.2008.
14. Krapcho, A. P.; Getahun, Z. *Synth. Commun.* **1985,** *15,* 907–910. doi:10.1080/00397918508063889
15. Wang, J.; Leung, L. M. *Dyes Pigm.* **2013,** *99,* 105–115. doi:10.1016/j.dyepig.2013.04.021
16. Parham, W. E.; Piccirilli, R. M. *J. Org. Chem.* **1976,** *41,* 1268–1269. doi:10.1021/jo00869a046
17. Because of the low solubility and decomposition in solution, no ^{13}C NMR spectrum could be obtained.

License and Terms

This is an Open Access article under the terms of the Creative Commons Attribution License (https://creativecommons.org/licenses/by/4.0). Please note that the reuse, redistribution and reproduction in particular requires that the authors and source are credited.

The license is subject to the *Beilstein Journal of Organic Chemistry* terms and conditions: (https://www.beilstein-journals.org/bjoc)

The definitive version of this article is the electronic one which can be found at: https://doi.org/10.3762/bjoc.16.181

BEILSTEIN JOURNAL OF ORGANIC CHEMISTRY

Lipophilicity trends upon fluorination of isopropyl, cyclopropyl and 3-oxetanyl groups

Benjamin Jeffries[1], Zhong Wang[1], Robert I. Troup[1], Anaïs Goupille[2], Jean-Yves Le Questel[2], Charlene Fallan[3], James S. Scott[3], Elisabetta Chiarparin[3], Jérôme Graton[2] and Bruno Linclau[*1]

Full Research Paper

Open Access

Address:
[1]School of Chemistry, University of Southampton, Highfield, Southampton SO17 1BJ, UK, [2]Université de Nantes, CNRS, CEISAM UMR 6230, F-44000 Nantes, France and [3]Medicinal Chemistry, Oncology R&D, AstraZeneca, Cambridge CB4 0WG, UK

Email:
Bruno Linclau[*] - bruno.linclau@soton.ac.uk

* Corresponding author

Keywords:
aliphatic fluorination; cyclopropane; isopropyl; isostere; lipophilicity; oxetane

Beilstein J. Org. Chem. **2020,** *16,* 2141–2150.
https://doi.org/10.3762/bjoc.16.182

Received: 19 July 2020
Accepted: 20 August 2020
Published: 02 September 2020

This article is part of the thematic issue "Organo-fluorine chemistry V".

Guest Editor: D. O'Hagan

© 2020 Jeffries et al.; licensee Beilstein-Institut.
License and terms: see end of document.

Abstract

A systematic comparison of lipophilicity modulations upon fluorination of isopropyl, cyclopropyl and 3-oxetanyl substituents, at a single carbon atom, is provided using directly comparable, and easily accessible model compounds. In addition, comparison with relevant linear chain derivatives is provided, as well as lipophilicity changes occurring upon chain extension of acyclic precursors to give cyclopropyl containing compounds. For the compounds investigated, fluorination of the isopropyl substituent led to larger lipophilicity modulation compared to fluorination of the cyclopropyl substituent.

Introduction

The introduction of small alkyl groups onto bioactive compounds as space filling groups is a common strategy in the drug optimization process. It is typically employed to ensure proper fitting of the part(s) of a ligand that interact with a receptor [1,2]. Apart from volume considerations, shape complementarity is regarded as important as well [3-5]. Hence, the modification of existing appendages is also commonly employed. For example, an isopropyl and a trifluoromethyl group have very similar volumes, but a very different shape [6].

However, even the introduction of relatively small methyl groups can impart profound consequences (“the magic methyl effect”) [7-9] on the activity and conformational profile, which can be very beneficial if this promotes the population of the

desired bioactive conformation(s). The introduction or extension of alkyl groups generally leads to an increase in lipophilicity, which is more often than not undesired. Hence, this has led to an interest in how to add volume without adding lipophilicity, i.e., how to extend a carbon chain without a concomitant increase in log*P*.

A much-used isosteric replacement is the change of an isopropyl group, or more commonly an α,α-disubstituted geminal dimethyl group [10], into a cyclopropyl group [11,12]. Apart from a slight shape/volume alteration caused by the significant change in bond angles and the deletion of two hydrogen atoms, this bioisosteric modification also usually results in improved metabolic stability, increased rigidity and, due to its electron-withdrawing nature, pK_a modulation of adjacent acid/base groups. Importantly, it also leads to a lipophilicity reduction, as illustrated by the Hansch π-values of isopropyl (1.53) [13] and cyclopropyl (1.14) [14]. This compares to π = 1.98 for a *tert*-butyl group [13]. However, exceptions are known, as illustrated for **1** and **2** (Figure 1) [15]. In this case, the expected lipophilicity reducing effect is offset by the electron-withdrawing effect on the nitrogen (Δlog*P* +0.34). The reduction in amine basicity also shifts the distribution of free base and protonated species, resulting in a higher proportion of free base in solution at pH 7.4, which leads to a large log$D_{7.4}$ increase (Δlog$D_{7.4}$ +0.73).

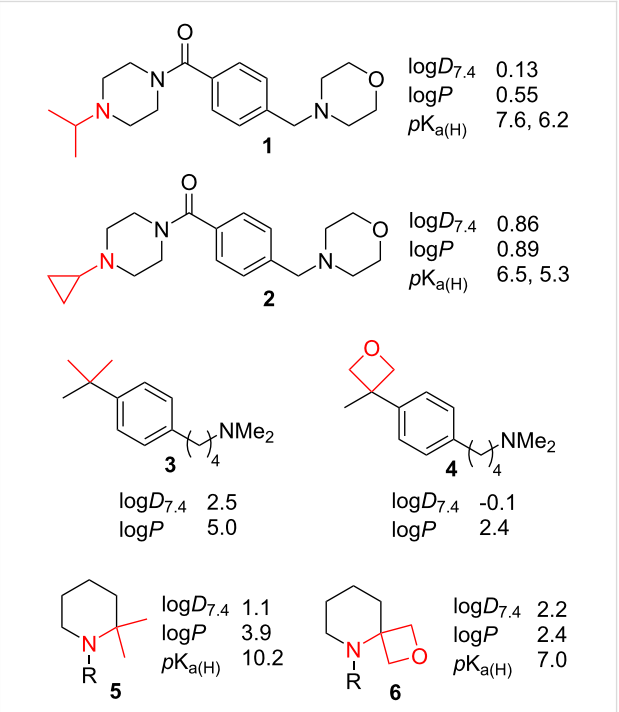

Figure 1: Examples of lipophilicity modulation for geminal dimethyl to cyclopropyl and oxetane modifications (measured experimentally via shake-flask method).

The modification of a geminal dimethyl moiety to an oxetanyl group has also proven to be a useful biomimetic replacement leading to a significant log*P* decrease (compare **3** with **4**) [16-18]. However, when an amino group is located in the α-position (**5**), the introduction of the oxetanyl group leading to **6** induces a significant p$K_{a(H)}$ decrease. While the reduction in log*P* is still observed, the larger proportion of unprotonated substrate leads to a log$D_{7.4}$ increase.

Aliphatic fluorination can also be employed to decrease lipophilicities [6,19-22]. However, there is comparatively less precedence of lipophilicity comparisons between fluorinated isopropyl groups, cyclopropanes and oxetanes. Examples of bioactive compounds are given in Figure 2.

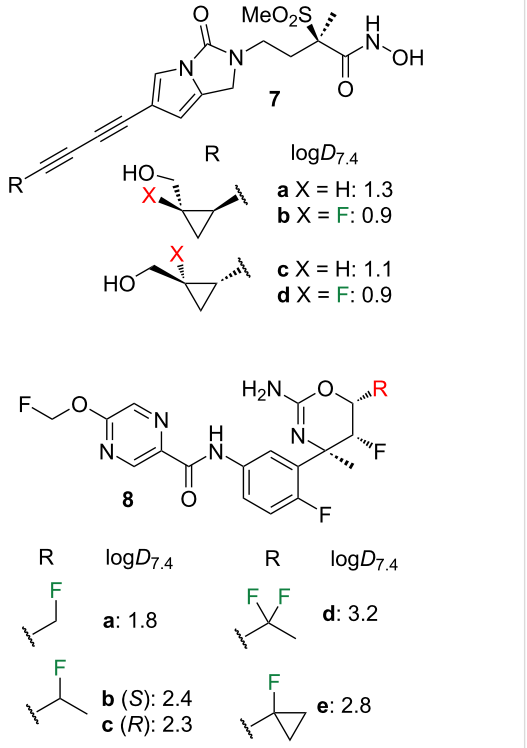

Figure 2: Lipophilicity modulation examples involving fluorinated cyclopropane derivatives (measured experimentally via shake-flask method).

During the optimization of the LpxC inhibitor **7a** [23], it was shown that fluorination to give analogue **7b** reduced the lipophilicity. Interestingly, while the nonfluorinated **7a** and **7c** diastereomers have different log$D_{7.4}$ values, this is not the case for their fluorinated analogues **7b** and **7d**. Oxazine derivative **8** featured in the development of centrally active β-secretase (BACE1) inhibitors [24]. Although the log$D_{7.4}$ of the unsubstituted cyclopropyl containing analogue was not provided, it can be seen that two-carbon extension of **8a**, and one-carbon exten-

sion of **8b**,**c** to give the cyclopropyl derivative **8e**, cause a lipophilicity increase. Conversely, changing a CF_2Me for a cPrF group (**8d** to **8e**) gives a lipophilicity reduction.

Finally, a number of model compound series have been reported (Figure 3). In the isopropanol series **A** [22], monofluorination led to a 0.4 log*P* decrease, which is further extended upon a second monofluorination at the other methyl group (compare **A1** with **A2**, **A3**). With one (**A4**) and two (**A5**) trifluoromethyl groups, large increases in lipophilicity are observed. An interesting series (**B**) of phenylcyclopropanes was reported by O'Hagan [25,26]. All-*cis* vicinal trifluorination as in **B2** led to a significant reduction in lipophilicity compared to the nonfluorinated **B1**, which was explained by the facially polar motif caused by the C–F dipoles present on the same side of the ring. Consequently, the diastereomer **B4** possessed a higher lipophilicity, although the lipophilicity of the vicinally difluorinated diastereomers **B3** and **B5** was identical, and also the same as the trifluorinated **B4**. Geminal difluorination caused an increase in lipophilicity compared to vicinal fluorination (compare **B6** with **B3** and **B5**, and **B7** with **B4** and **B2**). Interestingly, in analogy with the same lipophilicity of **B3**–**B4**, **B6** and **B7** also were equivalent in lipophilicity. Finally, the 3-fluorinated oxetanyl derivative **C2** has a lower log*D* value than the nonfluorinated parent **C1** [16,17].

In this contribution, we describe a systematic study on the lipophilicity modulations of the isopropyl, cyclopropyl and 3-oxetanyl groups and their various possible analogues, featuring fluorination at a single carbon atom (Figure 4), using the directly comparable isobutanol, cyclopropylmethanol and 3-oxetanylmethanol scaffolds. All compounds are either commercially available or are easily synthesized from available fluorinated building blocks. In addition, comparison of

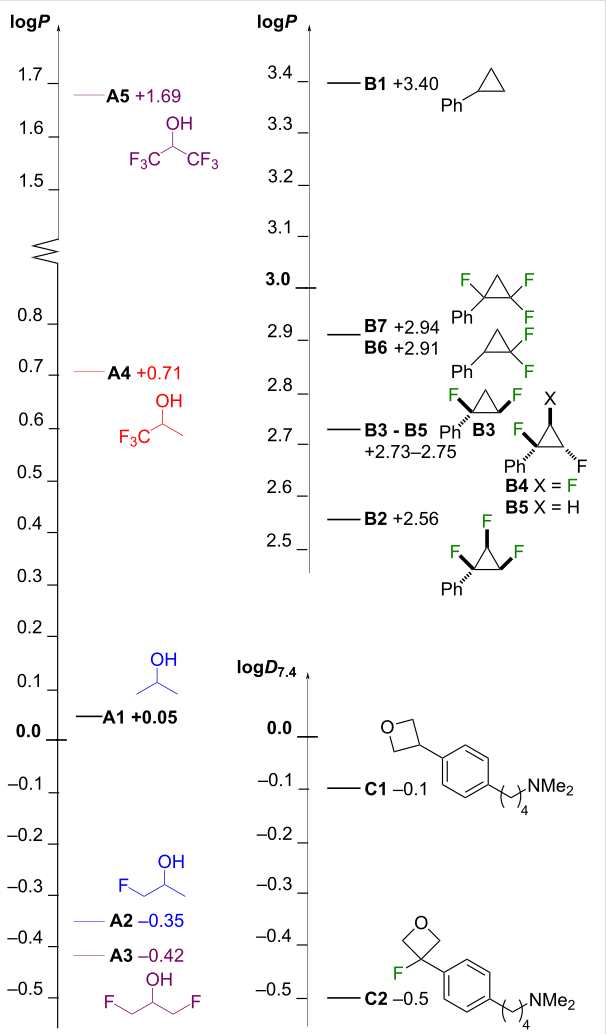

Figure 3: Lipophilicity changes upon fluorination of isopropyl, cyclopropane and oxetane rings (Series **A**, **C**: measured experimentally via shake-flask method; series **B**: measured experimentally by reversed-phase HPLC).

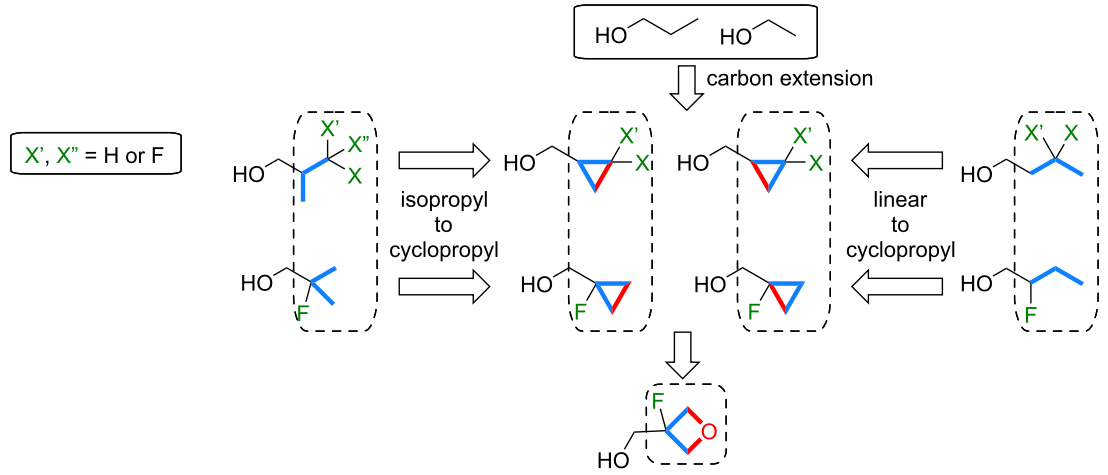

Figure 4: Lipophilicity modulations discussed in this contribution.

lipophilicities of relevant linear butanol derivatives is discussed, as well as that of the introduction of an isopropyl/cyclopropyl/oxetanyl group from 1-propanol and ethanol, which represents carbon extensions (volume increase).

Results and Discussion

Lipophilicity data and discussion

The lipophilicities of the nonfluorinated **E1** and **F1** have not been reported, and have been estimated by a range of calculation methods as described in Supporting Information File 1 (section 2). The average log*P* value of the data from those estimation approaches for **E1** was determined to be 0.24 ± 0.03, and for **F1** −0.80 ± 0.23. The experimental lipophilicity values of the fluorinated isobutanol, cyclopropylmethanol and 3-oxetanylmethanol derivatives are given in Figure 5. They were measured by a ^{19}F NMR-based method developed by our group [22,27], which is suitable for measuring the octanol/water partition coefficients *P* of (fluorinated) non-UV active substrates.

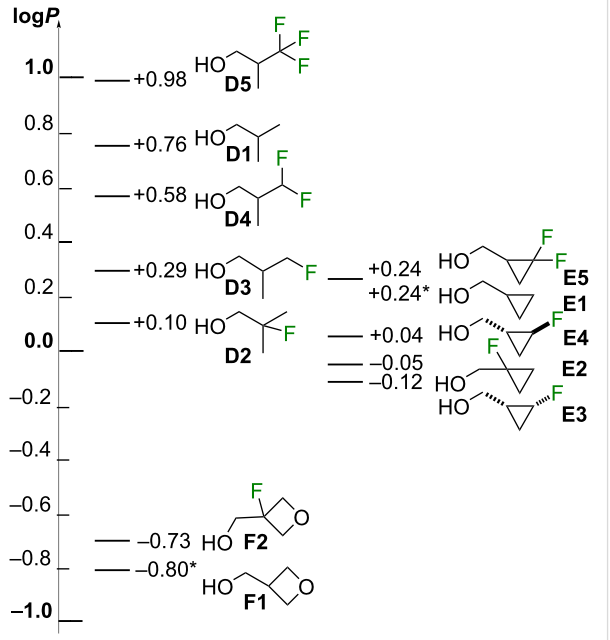

Figure 5: Distribution of the experimental lipophilicity values of series **D**, **E** and **F** (* denotes an estimated value, see Supporting Information File 1).

As expected, monofluorination decreases the lipophilicity compared to the nonfluorinated parent **D1**, with a much larger decrease for the β-fluorohydrin **D2** than for the γ-fluorohydrin **D3**. Interestingly, for the linear propanol, β-fluorination and γ-fluorination lead to a similar log*P* decrease (−0.29 vs −0.26 for 2- and 3-fluoropropanol) [22], while for the higher alkanols, β-fluorination leads to more lipophilic compounds than γ-fluorination [28]. The higher log*P* of β-fluorinated alcohols has been explained both by the occurrence of conformations with opposing dipole moments of the C–F and C–O bonds, as well as the reduction of polarizability of the oxygen lone pairs due to the fluorine electronegativity. However, while **D2** is a β-fluorohydrin, its fluorine is substituted at a tertiary position, with the C–F bond able to polarize the six C–H bonds of the methyl groups, which has a lipophilicity lowering effect. The electron-withdrawing effect of the fluorine is evident from the ^{1}H NMR chemical shift values of the CH_3 groups in **D1** (0.91 ppm) [29], **D3** (0.98 ppm), and **D2** (1.37 ppm) [30].

Compared to the monofluorinated **D3**, difluorination (**D4**) and trifluorination (**D5**) at the same carbon atom increases lipophilicity. There is a notable difference in lipohilicity between **D4** and **D5**. Aliphatic compounds containing a CF_2H group are frequently less lipophilic than to their nonfluorinated equivalent [20,31] (except in presence of a vicinal C–O bond [22,32]), which is what is found here for **D4**. The CF_3-containing **D5** is more lipophilic than the parent **D1**, and these values are consistent with the trends seen for 1-propanol [22].

For cyclopropylmethanol **E1**, β-fluorination (**E2**) leads to a smaller lipophilicity decrease compared to that seen for **D1**→**D2**, leading to a log*P* value in between those of the two γ-fluorinated diastereomers **E3** and **E4**. The decrease seen for **E2** is in accord with the observations for the β-fluorinated analogues of **7a** and **7c** (see above, Figure 2). The *cis*-isomer **E3** has a slightly lower lipophilicity than the *trans*-isomer **E4**. The lower lipophilicity decrease upon monofluorination in series **E** compared to series **F** could be related to the hybridization state of cyclopropyl carbon atoms. However, β-fluorination of the oxetanyl derivative **F1** led to a lipophilicity increase. With the caveat that the value for **F1** is not a measured value and the difference is well within the standard deviation (0.23 log*P* units), this increase is in contrast to the result observed for **C1** (see above, Figure 3).

As discussed in the Introduction, converting acyclic alkanes to cyclopropane equivalents is a frequently used tactic in medicinal chemistry. The pairwise comparison of the isopropyl with the cyclopropyl substructures is best discussed via Figure 6, with the bold red bond emphasizing the structural change (cf **D1** vs **E1**). For completion, the change observed from the corresponding linear 1-butanol equivalents with equidistant alcohol and fluorine groups, by connecting C2 and C4 as shown (cf **G1** to **E1**), is also considered (see Supporting Information File 1, Figure S1 for a summary figure showing changes in log*P* between linear alkanols and cyclopropylmethanols).

Firstly, the isobutanol (**D**) and their corresponding 1-butanol (**G**) series are compared. It is known that branching causes a

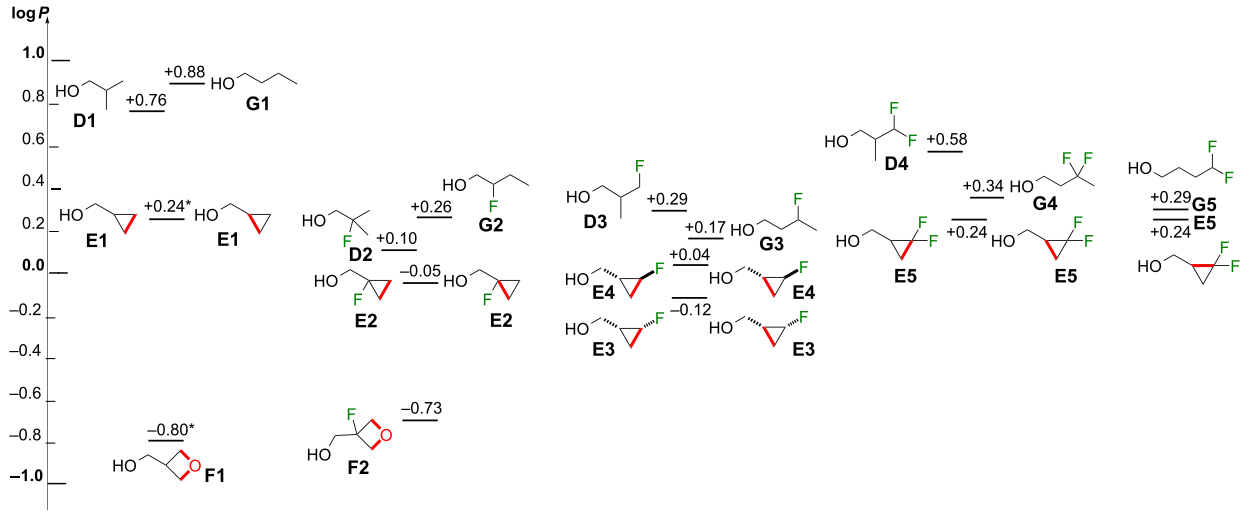

Figure 6: Comparison of lipophilicities between the linear alkyl, isopropyl, cyclopropyl, and 3-oxetanyl substituents by fluorination level (exchange two C–H bonds by a C–C bond or C–O–C bonds, same carbon count).

reduction in log*P*, which has been explained by a less energetically unfavorable contact with water due to the resulting reduction in hydrophobic surface [33] (compare **D1** with **G1**, Δ 0.12). This difference is similar upon β-fluorination (**D2** vs **G2**, Δ 0.16) with a slightly greater magnitude which, as discussed above, is potentially due to the polarization of C–H bonds by fluorine. Interestingly, for γ-mono- and γ,γ-difluorination the linear butanol derivatives **G3** and **G4** are now less lipophilic than the branched **D3** and **D4**, respectively. A possible explanation is that branching in **D3** and **D4** results in shielding of the polar C–F bonds preventing dipolar interactions.

Regarding the conversion of the iso- and *n*-butyl chains to the cyclopropylmethyl arrangement, as expected a significant lipophilicity decrease is observed for the nonfluorinated derivatives (compare **D1**, **G1** with **E1**), with another large decrease when converting the cyclopropyl group to an oxetanyl moiety (compare **E1** with **F1**). A much lower lipophilicity decrease is seen when converting the acyclic β-fluorinated compounds **D2** and **G2** to the cyclopropyl analogue **E2**, but an appreciable log*P* decrease is still seen going from **E2** to the oxetanyl derivative **F2**. With γ-fluorination, the log*P* decreases are similarly small, both for monofluorination (compare **D3**, **G3** with **E3**, **E4**) and for geminal difluorination (compare **D4**, **G4** with **E5**). Finally, converting the linear 4,4-difluorobutan-1-ol (**G5**) to the corresponding difluorinated cyclopropylmethanol **E5** only results in a minor lipophilicity decrease. Nevertheless, in all cases, for the same fluorination motif, the cyclopropane derivatives have a lower lipophilicity compared to their acyclic equivalents.

It is also useful to compare lipophilicities of acyclic and cyclopropane derivatives in which the isosterism represents conversion of a C–H and C–F bond into a C–C bond (Figure 7), hence transforming an acyclic to a cyclic group. Some interesting trends are identified. When the chain ring is closed with the loss of a C–F that was part of a single fluorine motif (Figure 7A), only very minimal lipophilicity differences were then observed. For 4-fluorobutan-1-ol (**G6**), and 3,4-difluorobutan-1-ol (**G7**), which have the lowest lipophilicities of the linear butanol series measured so far [28], the corresponding cyclopropyl isosteres **E1** and **E4** have a slightly higher lipophilicity, while **E3** has the same lipophilicity as **G7**. The lipophilicity-reducing power of the vicinal 1,2-difluoromotif in **G7** is well-described [34,35], but at least for series **D**, the motif present in **E3** is another efficient candidate when a log*P* reduction operation is in order. In contrast, other such ring closures (e.g., starting from **G2**, **D3**, and **G8**) lead to a minute log*P* decrease.

The situation is different when the "cyclisation" operation is achieved from geminal motifs (Figure 7B). Significant log*P* reductions are observed, especially from the internal geminal fluorination motif as in **G9** to **E2** (0.72 log*P* units). Starting from a trifluoromethyl group (Figure 7C), similar log*P* reductions are achieved (e.g., **D5**→**E5** and **G10**→**E5**) which interestingly, are of the same magnitude as for the nonfluorinated derivatives (compare **D1**, **G1** to **E1**, Figure 6). It is worth noting that "cyclisation" to give cyclopropanol derivatives substituted with a fluorinated methyl group (not shown) can also be considered. Marketed drugs with such substructures include Voxilaprevir and Glecaprevir.

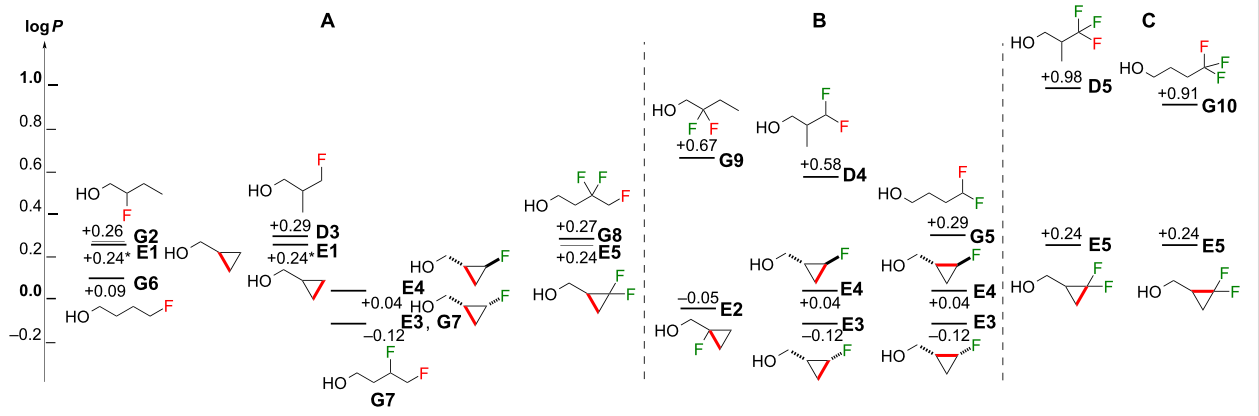

Figure 7: Comparison of lipophilicities between isopropyl and cyclopropyl substituents grouped by exchange of C–H/C–F bonds by a C–C bond (same carbon count). Organised by the exchanged fluorine being the only fluorine substituent on the carbon involved (**A**) or as part of a CF_2 (**B**) or CF_3 (**C**) group.

Finally, it is useful to consider the lipophilicity changes upon extending a propyl or ethyl chain to a cyclopropylmethyl moiety, which represents a one-carbon and a two-carbon extension, respectively. It is known that adding a spiro-cyclopropyl moiety onto a methylene group of an aliphatic chain, which represents a two-carbon extension, can lead to a lipophilicity reduction [16,17].

The one-carbon extension from **H1** to give **E1** results in a small lipophilicity decrease (Figure 8), which is slightly extended with further β-fluorination (**E2**). In contrast, the one-carbon introduction of a cyclopropyl group in **H2** to give **E2** leads to a lipophilicity increase. Replacing the fluorine substituent by a cyclopropyl carbon (compare **H2** with **E1**) also leads to a lipophilicity increase, but not when starting from a geminal difluoro motif (compare **C4** with **E2**).

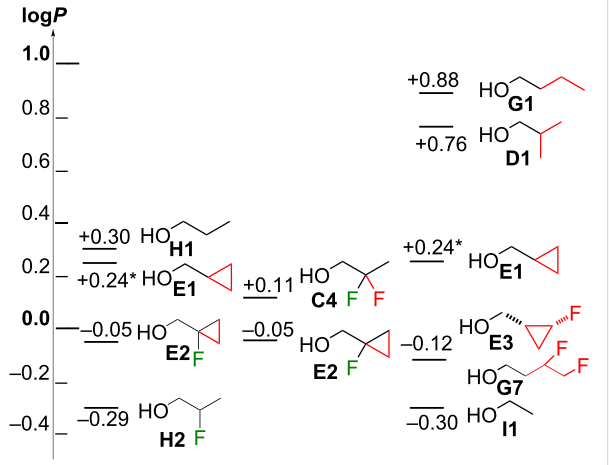

Figure 8: Carbon extensions.

The two-carbon extension from **I1** to the acyclic derivatives **D1** and **G1** leads to a large lipophilicity increase, which is much smaller for a two-carbon cyclopropyl extension (**E1**). This lipophilicity increase is somewhat attenuated with concomitant β-fluorination (**E2**) and γ-fluorination (**E3**). Interestingly, a two-carbon extension of **I1** with concomitant vicinal difluorination (**G7** [28]) or fluorinated cyclopropyl (**E3**) leads to a much smaller increase in log*P* compared to two-carbon extension as a cyclopropyl (**E1**).

Computational results

A number of open-access fragment-based calculation methods, as well as the internal AstraZeneca method, were used to obtain clog*P* values of the fluorinated butanol, isobutanol, cyclopropylmethanol and 3-oxetanylmethanol derivatives mentioned above (Supporting Information File 1, Table S6). For each method, the correlations with the experimental data were obtained (Supporting Information File 1, Figures S7–S11). Three methods gave excellent correlations (with r^2 between 0.86 and 0.91, Supporting Information File 1, Table S7), but other methods gave only low correlations (r^2 = 0.36, 0.49). This is perhaps due to the training sets used, but it clearly demonstrates that even for a set of relatively simple compounds, fragment-based clog*P* calculations are not guaranteed to give reliable lipophilicity data.

Next, theoretical lipophilicities were obtained using DFT calculations, based on the notion that the partition coefficient of a given solute between two phases relates to the difference in Gibbs energy of the free ligand conformations of this solute in the respective solvents. Quantum chemistry calculations of Gibbs energies in octanol and water thus provide theoretical estimations of lipophilicities. Such estimations require systematic conformational analyses and geometry optimizations. Ho

and co-worker showed that the use of the lowest-energy conformations as calculated in the respective solvents gave more accurate lipophilicities than the use of the lowest energy conformations in the gas phase [36]. Somewhat surprisingly, implicit solvent models proved superior than explicit models, despite their shorter calculation times, with the SMD implicit solvent model being superior compared to the IEF-PCM and C-PCM models [36,37]. However, the implicit octanol solvent model does not take into account the large amount of water present in saturated octanol [36].

We have previously used the SMD implicit solvation model with the MN15 functional in theoretical lipophilicity predictions of linear fluorohydrins [27,28], which gave an excellent correlation with the experimental values (r^2 = 0.957), although the absolute values were much higher (a slope of >2 was obtained).

Unfortunately, the theoretical lipophilicity values computed in the present work using the same methodology for series **D**, **E**, and **F**, as well as for the linear butanols **G1**–**G4**, **G7**, **G8**, pictured in Supporting Information File 1, Figure 9 and given in Supporting Information File 1, Table S11, did not provide any useful approximation in terms of rank order or absolute magnitude of effect.

For series **D**, **E**, **G**, the DFT-log*P* values cluster together with minimal lipophilicity differences, and within mean absolute error limits (estimated to be around 0.8 log*P* units), making detailed considerations meaningless. This was a surprise, as series **D** and **E** are relatively rigid, which simplifies conformational analysis. The remarkably similar DFT-log*P* values suggest that the influence of the fluorination is underrepresented in the calculations. The following observations are noteworthy. The trifluorinated **D5** was calculated to have the largest log*P* value, in accord with the experiment. The geminally difluorinated derivatives are calculated to be more lipophilic than the monofluorinated derivatives, except in series **G**: **G4** was calculated to be less lipophilic than **G2**. The **E3**/**E4** diastereomers were calculated to have essentially the same lipophilicities.

The correlation with the experimental values shows a coefficient of determination value of 0.776 (Figure 10A), which is worse than many of the investigated fragment-based clog*P* methods (see above), for which such clustering is not observed. When these values are combined with the full available set of fluorohydrins calculated with the MN15 functional (Figure 10B), the correlation is now reduced from r^2 = 0.957 to 0.860.

Interestingly, the theoretical and experimental values, while much different in absolute value and in relative difference, correspond almost perfectly regarding lipophilicity order when arranged by motif (Figure 11). As a point of interest, the calculations correctly estimate a lower lipophilicity for the branched **D1** and **D2** vs **G1** and **G2**, but cannot significantly distinguish between the linear and branched γ-mono- and difluorinated **G3**/**D3** and **G4**/**D4**. Cyclopropyl structures are always less lipophilic than their corresponding acyclic counterparts.

Conclusion

Monofluorination of isobutanol significantly decreased the lipophilicity, with β-fluorination leading to a lower log*P* value than γ-fluorination. As expected, geminal difluorination also decreased the log*P*, but to a lesser extent compared to monofluorination. For the corresponding cyclopropyl derivative, cyclopropylmethanol, monofluorination at the β or γ position only led to a minor decrease in log*P*, and no log*P* difference is observed

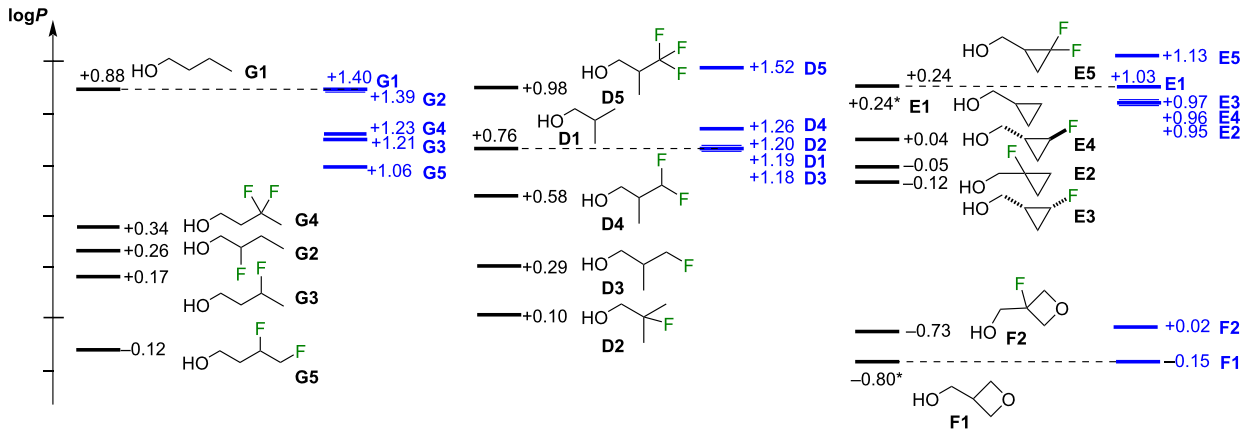

Figure 9: Experimental and theoretical (in blue) values (calculated at the MN15/aug-cc-pVTZ//MN15/cc-pVTZ level of theory). Values for **G1**, **G4**, **G7**, **G8** taken from the literature [28]. The distance between the lines relate to the relative lipophilicity differences. Experimental and theoretical data sets normalized towards the parent compound.

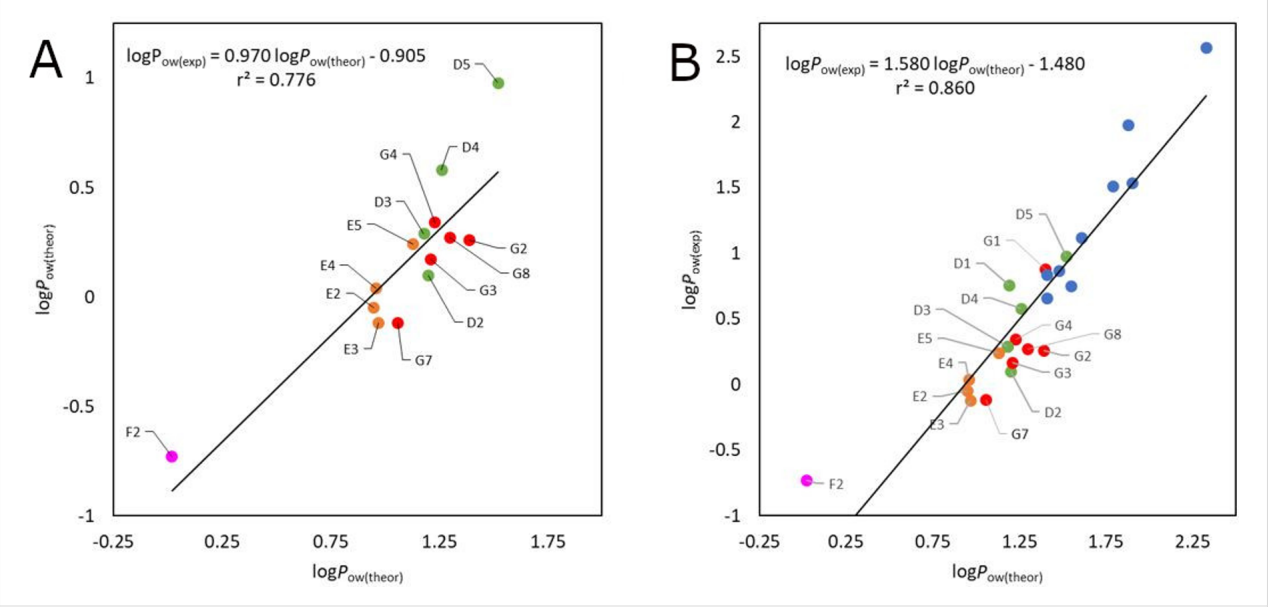

Figure 10: Correlation of the DFT-calculated lipophilicities with the experimental values. A) fluorinated series **D**, **E**, **F**, **G2–4**, **G7**, **G8**, B) Compilation with other fluorohydrins (taken from reference [28]).

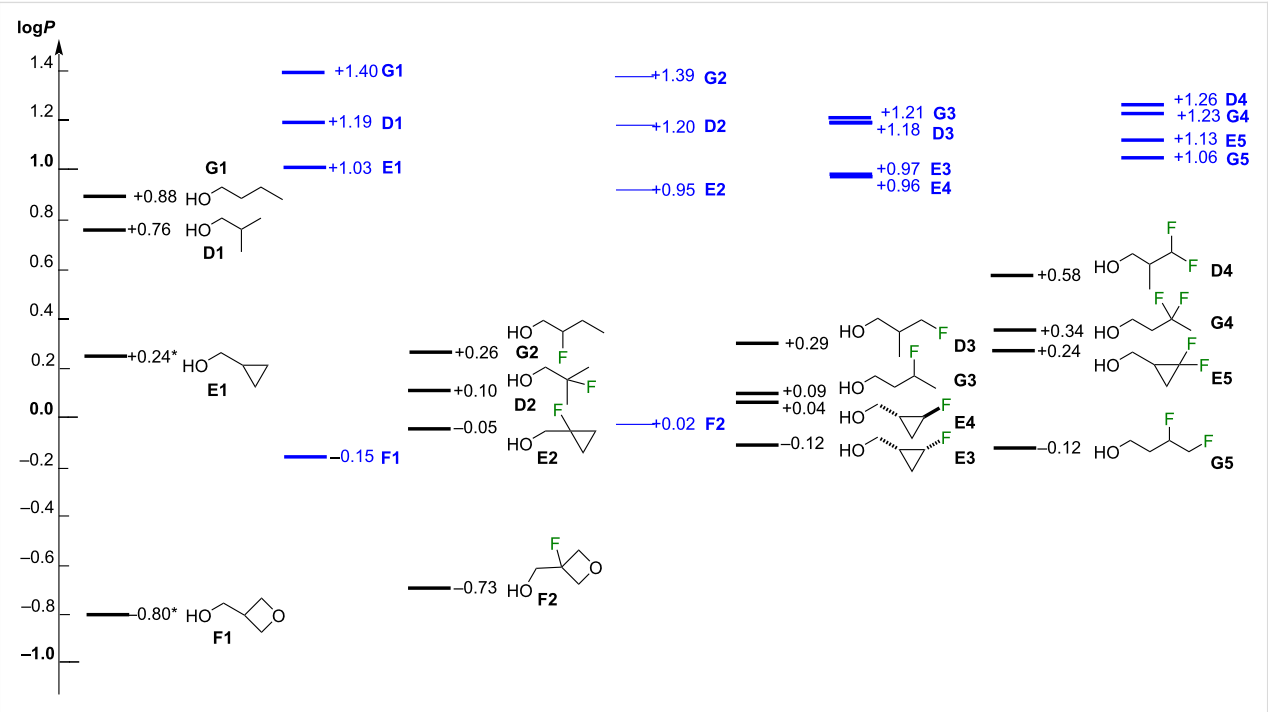

Figure 11: Experimental (in black) and theoretical (in blue) values (calculated at the MN15/aug-cc-pVTZ//MN15/cc-pVTZ level of theory) of all compounds, organized by motif.

with the geminal difluorinated analogue. The typically observed lower lipophilicities of branched isomers vs their linear isomers are also observed for β-fluorohydrin containing compounds, but not when γ-mono- or difluorinated. Equally, converting (acyclic) alkyl groups to the corresponding cyclopropane equivalents (C–H/C–H→C–C) typically leads to a lipophilicity decrease, which remains the case when fluorination is present. For a C–F/C–H→C–C 'cyclisation', only minimal lipophilicity differences are observed (in either direction) when the C–F moiety was part on a monofluorinated motif. However, when the C–F moiety was part of a geminal (CF_2 or CF_3) motif, a large log*P* reduction is observed.

Fragment based clog*P* methods show great variation in their ability to estimate the lipophilicities of the small alkanol compounds described herein. To our surprise, theoretical lipophilicity predictions using the MN15 functional with the SMD implicit solvation model also performed poorly, despite the fact that most of the substrates are small and relatively rigid compounds. It was found that for a given series, the DFT-log*P* values are clustered together, indicating the influence of the fluorination is underrepresented in the calculations. This clearly indicates that further research towards theoretical lipophilicity prediction based in relative Gibbs energies in water and (wet) octanol is required.

Supporting Information

Supporting Information File 1

Synthesis, characterisation and copies of spectra of the novel compounds, details of the calculations, log*P* determinations of the nonfluorinated parents **E1** and **F1**, and experimental measurements of the lipophilicities of the fluorinated derivatives.
[https://www.beilstein-journals.org/bjoc/content/supplementary/1860-5397-16-182-S1.pdf]

Funding

We are grateful to AstraZeneca for a CASE award, and to the EPSRC for a CASE Conversion grant (EP/M508147/1), a standard grant (EP/P019943/1), and a core capability grant (EP/K039466/1). The CCIPL (Centre de Calcul Intensif des Pays de Loire) is acknowledged for provision of computer time.

ORCID® iDs

Anaïs Goupille - https://orcid.org/0000-0003-2715-9495
Jean-Yves Le Questel - https://orcid.org/0000-0001-5307-2137
Charlene Fallan - https://orcid.org/0000-0002-5964-1465
James S. Scott - https://orcid.org/0000-0002-2263-7024
Bruno Linclau - https://orcid.org/0000-0001-8762-0170

References

1. Persch, E.; Dumele, O.; Diederich, F. *Angew. Chem., Int. Ed.* **2015,** *54,* 3290–3327. doi:10.1002/anie.201408487
2. Mecozzi, S.; Rebek, J., Jr. *Chem. – Eur. J.* **1998,** *4,* 1016–1022. doi:10.1002/(sici)1521-3765(19980615)4:6<1016::aid-chem1016>3.0.co;2-b
3. Bissantz, C.; Kuhn, B.; Stahl, M. *J. Med. Chem.* **2010,** *53,* 5061–5084. doi:10.1021/jm100112j
4. Zauhar, R. J.; Moyna, G.; Tian, L.; Li, Z.; Welsh, W. J. *J. Med. Chem.* **2003,** *46,* 5674–5690. doi:10.1021/jm030242k
5. Kumar, A.; Zhang, K. Y. J. *Front. Chem. (Lausanne, Switz.)* **2018,** *6,* 315. doi:10.3389/fchem.2018.00315
6. Smart, B. E. *J. Fluorine Chem.* **2001,** *109,* 3–11. doi:10.1016/s0022-1139(01)00375-x
7. Schönherr, H.; Cernak, T. *Angew. Chem., Int. Ed.* **2013,** *52,* 12256–12267. doi:10.1002/anie.201303207
8. Kuntz, K. W.; Campbell, J. E.; Keilhack, H.; Pollock, R. M.; Knutson, S. K.; Porter-Scott, M.; Richon, V. M.; Sneeringer, C. J.; Wigle, T. J.; Allain, C. J.; Majer, C. R.; Moyer, M. P.; Copeland, R. A.; Chesworth, R. *J. Med. Chem.* **2016,** *59,* 1556–1564. doi:10.1021/acs.jmedchem.5b01501
9. Barreiro, E. J.; Kümmerle, A. E.; Fraga, C. A. M. *Chem. Rev.* **2011,** *111,* 5215–5246. doi:10.1021/cr200060g
10. Talele, T. T. *J. Med. Chem.* **2018,** *61,* 2166–2210. doi:10.1021/acs.jmedchem.7b00315
11. Talele, T. T. *J. Med. Chem.* **2016,** *59,* 8712–8756. doi:10.1021/acs.jmedchem.6b00472
12. Novakov, I. A.; Babushkin, A. S.; Yablokov, A. S.; Nawrozkij, M. B.; Vostrikova, O. V.; Shejkin, D. S.; Mkrtchyan, A. S.; Balakin, K. V. *Russ. Chem. Bull.* **2018,** *67,* 395–418. doi:10.1007/s11172-018-2087-6
13. Hansch, C.; Leo, A.; Unger, S. H.; Kim, K. H.; Nikaitani, D.; Lien, E. J. *J. Med. Chem.* **1973,** *16,* 1207–1216. doi:10.1021/jm00269a003
14. Skagerberg, B.; Bonelli, D.; Clementi, S.; Cruciani, G.; Ebert, C. *Quant. Struct.-Act. Relat.* **1989,** *8,* 32–38. doi:10.1002/qsar.19890080105
15. Letavic, M. A.; Aluisio, L.; Apodaca, R.; Bajpai, M.; Barbier, A. J.; Bonneville, A.; Bonaventure, P.; Carruthers, N. I.; Dugovic, C.; Fraser, I. C.; Kramer, M. L.; Lord, B.; Lovenberg, T. W.; Li, L. Y.; Ly, K. S.; Mcallister, H.; Mani, N. S.; Morton, K. L.; Ndifor, A.; Nepomuceno, S. D.; Pandit, C. R.; Sands, S. B.; Shah, C. R.; Shelton, J. E.; Snook, S. S.; Swanson, D. M.; Xiao, W. *ACS Med. Chem. Lett.* **2015,** *6,* 450–454. doi:10.1021/ml5005156
16. Wuitschik, G.; Carreira, E. M.; Wagner, B.; Fischer, H.; Parrilla, I.; Schuler, F.; Rogers-Evans, M.; Müller, K. *J. Med. Chem.* **2010,** *53,* 3227–3246. doi:10.1021/jm9018788
17. Wuitschik, G.; Rogers-Evans, M.; Müller, K.; Fischer, H.; Wagner, B.; Schuler, F.; Polonchuk, L.; Carreira, E. M. *Angew. Chem., Int. Ed.* **2006,** *45,* 7736–7739. doi:10.1002/anie.200602343
18. Bull, J. A.; Croft, R. A.; Davis, O. A.; Doran, R.; Morgan, K. F. *Chem. Rev.* **2016,** *116,* 12150–12233. doi:10.1021/acs.chemrev.6b00274
19. Böhm, H.-J.; Banner, D.; Bendels, S.; Kansy, M.; Kuhn, B.; Müller, K.; Obst-Sander, U.; Stahl, M. *ChemBioChem* **2004,** *5,* 637–643. doi:10.1002/cbic.200301023
20. Huchet, Q. A.; Kuhn, B.; Wagner, B.; Fischer, H.; Kansy, M.; Zimmerli, D.; Carreira, E. M.; Müller, K. *J. Fluorine Chem.* **2013,** *152,* 119–128. doi:10.1016/j.jfluchem.2013.02.023
21. Müller, K. Fluorination patterns in small alkyl groups: their impact on properties relevant to drug discovery. In *Fluorine in Life Sciences: Pharmaceuticals, Medicinal Diagnostics, and Agrochemicals;* Haufe, G.; Leroux, F., Eds.; Academic Press: London, U.K., 2018; pp 91–140. doi:10.1016/b978-0-12-812733-9.00002-7
22. Linclau, B.; Wang, Z.; Compain, G.; Paumelle, V.; Fontenelle, C. Q.; Wells, N.; Weymouth-Wilson, A. *Angew. Chem., Int. Ed.* **2016,** *55,* 674–678. doi:10.1002/anie.201509460
23. Panchaud, P.; Surivet, J.-P.; Diethelm, S.; Blumstein, A.-C.; Gauvin, J.-C.; Jacob, L.; Masse, F.; Mathieu, G.; Mirre, A.; Schmitt, C.; Enderlin-Paput, M.; Lange, R.; Gnerre, C.; Seeland, S.; Herrmann, C.; Locher, H. H.; Seiler, P.; Ritz, D.; Rueedi, G. *J. Med. Chem.* **2020,** *63,* 88–102. doi:10.1021/acs.jmedchem.9b01605

24. Nakahara, K.; Fuchino, K.; Komano, K.; Asada, N.; Tadano, G.; Hasegawa, T.; Yamamoto, T.; Sako, Y.; Ogawa, M.; Unemura, C.; Hosono, M.; Ito, H.; Sakaguchi, G.; Ando, S.; Ohnishi, S.; Kido, Y.; Fukushima, T.; Dhuyvetter, D.; Borghys, H.; Gijsen, H. J. M.; Yamano, Y.; Iso, Y.; Kusakabe, K.-i. *J. Med. Chem.* **2018,** *61,* 5525–5546. doi:10.1021/acs.jmedchem.8b00011
25. Fang, Z.; Cordes, D. B.; Slawin, A. M. Z.; O'Hagan, D. *Chem. Commun.* **2019,** *55,* 10539–10542. doi:10.1039/c9cc05749h
26. Thomson, C. J.; Zhang, Q.; Al-Maharik, N.; Bühl, M.; Cordes, D. B.; Slawin, A. M. Z.; O'Hagan, D. *Chem. Commun.* **2018,** *54,* 8415–8418. doi:10.1039/c8cc04964e
27. Wang, Z.; Jeffries, B. F.; Felstead, H. R.; Wells, N. J.; Chiarparin, E.; Linclau, B. *J. Visualized Exp.* **2019,** No. 143, e58567. doi:10.3791/58567
28. Jeffries, B.; Wang, Z.; Felstead, H. R.; Le Questel, J.-Y.; Scott, J. S.; Chiarparin, E.; Graton, J.; Linclau, B. *J. Med. Chem.* **2020,** *63,* 1002–1031. doi:10.1021/acs.jmedchem.9b01172
29. Siebum, A. H. G.; Woo, W. S.; Lugtenburg, J. *Eur. J. Org. Chem.* **2003,** 4664–4678. doi:10.1002/ejoc.200300410
30. Scott, J. S.; Bailey, A.; Buttar, D.; Carbajo, R. J.; Curwen, J.; Davey, P. R. J.; Davies, R. D. M.; Degorce, S. L.; Donald, C.; Gangl, E.; Greenwood, R.; Groombridge, S. D.; Johnson, T.; Lamont, S.; Lawson, M.; Lister, A.; Morrow, C. J.; Moss, T. A.; Pink, J. H.; Polanski, R. *J. Med. Chem.* **2019,** *62,* 1593–1608. doi:10.1021/acs.jmedchem.8b01837
31. Zafrani, Y.; Sod-Moriah, G.; Yeffet, D.; Berliner, A.; Amir, D.; Marciano, D.; Elias, S.; Katalan, S.; Ashkenazi, N.; Madmon, M.; Gershonov, E.; Saphier, S. *J. Med. Chem.* **2019,** *62,* 5628–5637. doi:10.1021/acs.jmedchem.9b00604
32. Kubyshkin, V.; Budisa, N. *Beilstein J. Org. Chem.* **2017,** *13,* 2442–2457. doi:10.3762/bjoc.13.241
33. Bazzini, P.; Wermuth, C. G. Substituents and Functions: Qualitative and Quantitative Aspects of Structure–Activity Relationships. In *The Practice of Medicinal Chemistry,* 3rd ed.; Wermuth, C. G., Ed.; Academic Press: New York, NY, USA, 2008; pp 429–463. doi:10.1016/b978-0-12-374194-3.00020-2
34. Huchet, Q. A.; Kuhn, B.; Wagner, B.; Kratochwil, N. A.; Fischer, H.; Kansy, M.; Zimmerli, D.; Carreira, E. M.; Müller, K. *J. Med. Chem.* **2015,** *58,* 9041–9060. doi:10.1021/acs.jmedchem.5b01455
35. Erdeljac, N.; Kehr, G.; Ahlqvist, M.; Knerr, L.; Gilmour, R. *Chem. Commun.* **2018,** *54,* 12002–12005. doi:10.1039/c8cc05643a
36. Kundi, V.; Ho, J. *J. Phys. Chem. B* **2019,** *123,* 6810–6822. doi:10.1021/acs.jpcb.9b04061
37. Michalík, M.; Lukeš, V. *Acta Chim. Slovaca* **2016,** *9,* 89–94. doi:10.1515/acs-2016-0015

License and Terms

This is an Open Access article under the terms of the Creative Commons Attribution License (https://creativecommons.org/licenses/by/4.0). Please note that the reuse, redistribution and reproduction in particular requires that the authors and source are credited.

The license is subject to the *Beilstein Journal of Organic Chemistry* terms and conditions: (https://www.beilstein-journals.org/bjoc)

The definitive version of this article is the electronic one which can be found at: https://doi.org/10.3762/bjoc.16.182

BEILSTEIN JOURNAL OF ORGANIC CHEMISTRY

Photosensitized direct C–H fluorination and trifluoromethylation in organic synthesis

Shahboz Yakubov and Joshua P. Barham*

Review

Open Access

Address:
Fakultät für Chemie und Pharmazie, Universität Regensburg, Universitätsstraße 31, 93040 Regensburg, Germany

Email:
Joshua P. Barham* - Joshua-Philip.Barham@chemie.uni-regensburg.de

* Corresponding author

Keywords:
C–H activation; energy transfer; fluorination; photocatalysis; photosensitization; visible light

Beilstein J. Org. Chem. **2020,** *16,* 2151–2192.
https://doi.org/10.3762/bjoc.16.183

Received: 18 May 2020
Accepted: 17 August 2020
Published: 03 September 2020

This article is part of the thematic issue "Organo-fluorine chemistry V".

Guest Editor: D. O'Hagan

© 2020 Yakubov and Barham; licensee Beilstein-Institut.
License and terms: see end of document.

Abstract

The importance of fluorinated products in pharmaceutical and medicinal chemistry has necessitated the development of synthetic fluorination methods, of which direct C–H fluorination is among the most powerful. Despite the challenges and limitations associated with the direct fluorination of unactivated C–H bonds, appreciable advancements in manipulating the selectivity and reactivity have been made, especially via transition metal catalysis and photochemistry. Where transition metal catalysis provides one strategy for C–H bond activation, transition-metal-free photochemical C–H fluorination can provide a complementary selectivity via a radical mechanism that proceeds under milder conditions than thermal radical activation methods. One exciting development in C–F bond formation is the use of small-molecule photosensitizers, allowing the reactions i) to proceed under mild conditions, ii) to be user-friendly, iii) to be cost-effective and iv) to be more amenable to scalability than typical photoredox-catalyzed methods. In this review, we highlight photosensitized C–H fluorination as a recent strategy for the direct and remote activation of C–H (especially C(sp^3)–H) bonds. To guide the readers, we present the developing mechanistic understandings of these reactions and exemplify concepts to assist the future planning of reactions.

Review

1 Introduction

1.1 Importance of direct C–H fluorination/trifluoromethylation and photosensitization in organic synthesis

1.1.1 Importance of fluorine atoms in organic molecules: Here, we briefly summarize the importance of fluorine atoms in organic molecules in the context of medicinal chemistry, materials chemistry, analytical chemistry and in the mechanistic studies of synthetic reactions. The importance of fluorination reactions in organic synthesis is reviewed exhaustively

elsewhere, and the readers are referred to the relevant reviews [1-5].

Over the last two decades, introducing fluorine atoms into molecules has become a crucial aspect in contemporary synthesis of pharmaceuticals. Extraordinarily, about half of the so-called "blockbuster drugs" contain fluorine atoms, including drugs used to treat cancer, HIV, smallpox and malarial infections (Figure 1) [5,6]. Moreover, fluorine atoms and trifluoromethyl groups have dramatic effects on the biological activity of agrochemicals, such as herbicides, insecticides and fungicides, as reflected by a plethora of fluorinated agrochemicals (Figure 2) [7,8]. Fluorine possesses some unique properties, such as the highest atomic electronegativity [9] and, in its molecular form (F_2), the most positive standard reduction potential (E^0) of +2.87 V [10], as predictable from its position in the periodic table. The C–F bond length is ≈1.35 Å and is one of the strongest bonds known (bond dissociation enthalpy (BDE) of ≈130 kcal·mol^{-1}) [11,12]. By C(sp^3)–H/C(sp^3)–F substitution, adjacent C–C bonds are strengthened while allylic C–C double bonds are weakened [13]. Due to the similar size to the hydrogen atom (r_F = 1.47 Å, r_H = 1.20 Å) [9,14], the fluorine atom is often used as a bioisostere for the hydrogen atom. Furthermore, the trifluoromethyl group was recently identified as a bioisostere for the nitro (NO_2) group, which is important due to the strong binding ability of the nitro group and the high reactivity, which is speculated to raise toxicity issues [15].

Despite their similar size to hydrogen atoms, fluorine atoms possess a very different chemical reactivity and exert very different influences on neighboring atoms. C–H/C–F substitution in organic molecules influences practically all physical, pharmacokinetic, metabolic stability, adsorption and excretion properties of the compound [16,17]. For example, the pharmacokinetics of drugs are mostly regulated by the balance of the lipophilicity, hydrophilicity and ionization state. Since C–H/

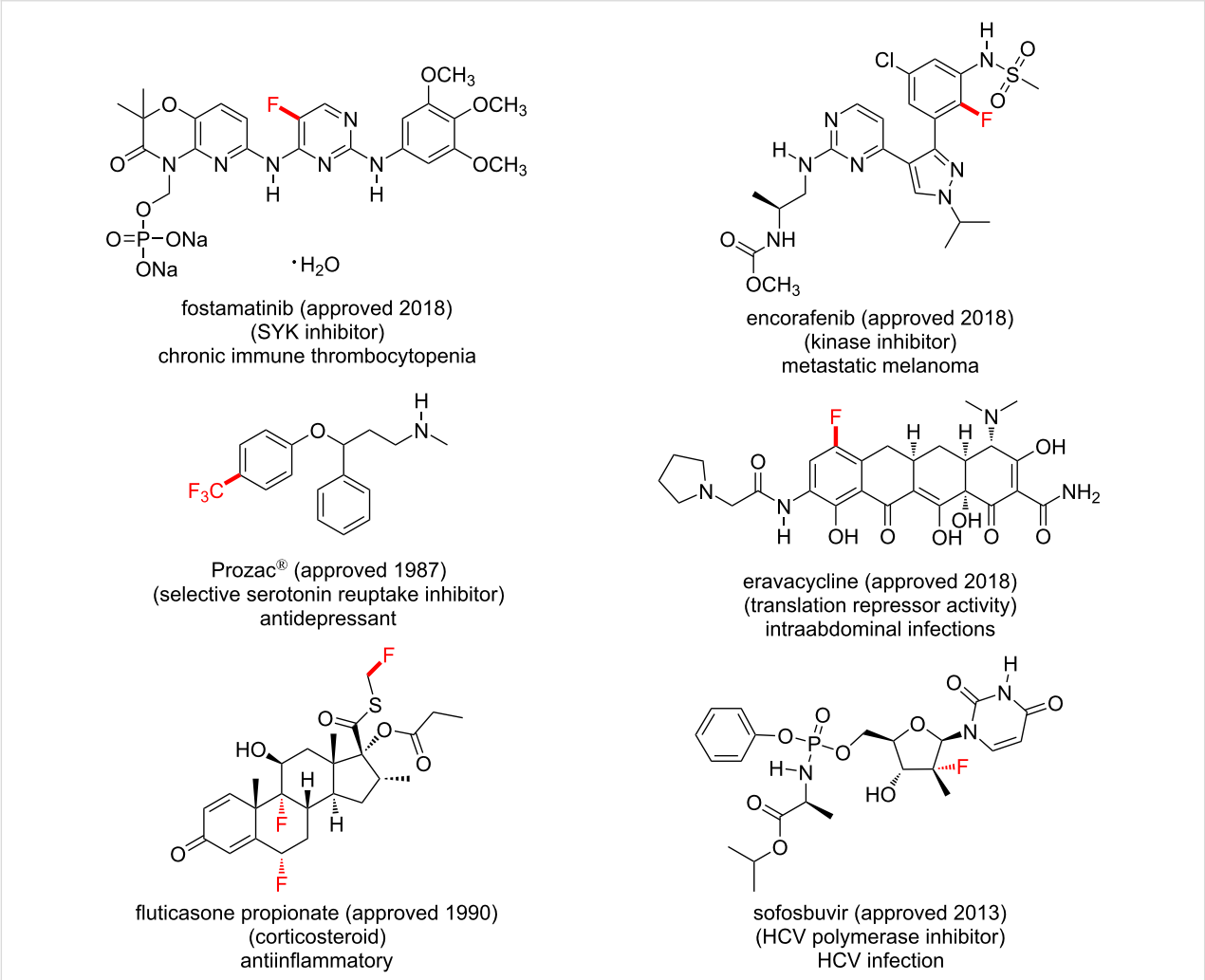

Figure 1: Fluorine-containing drugs.

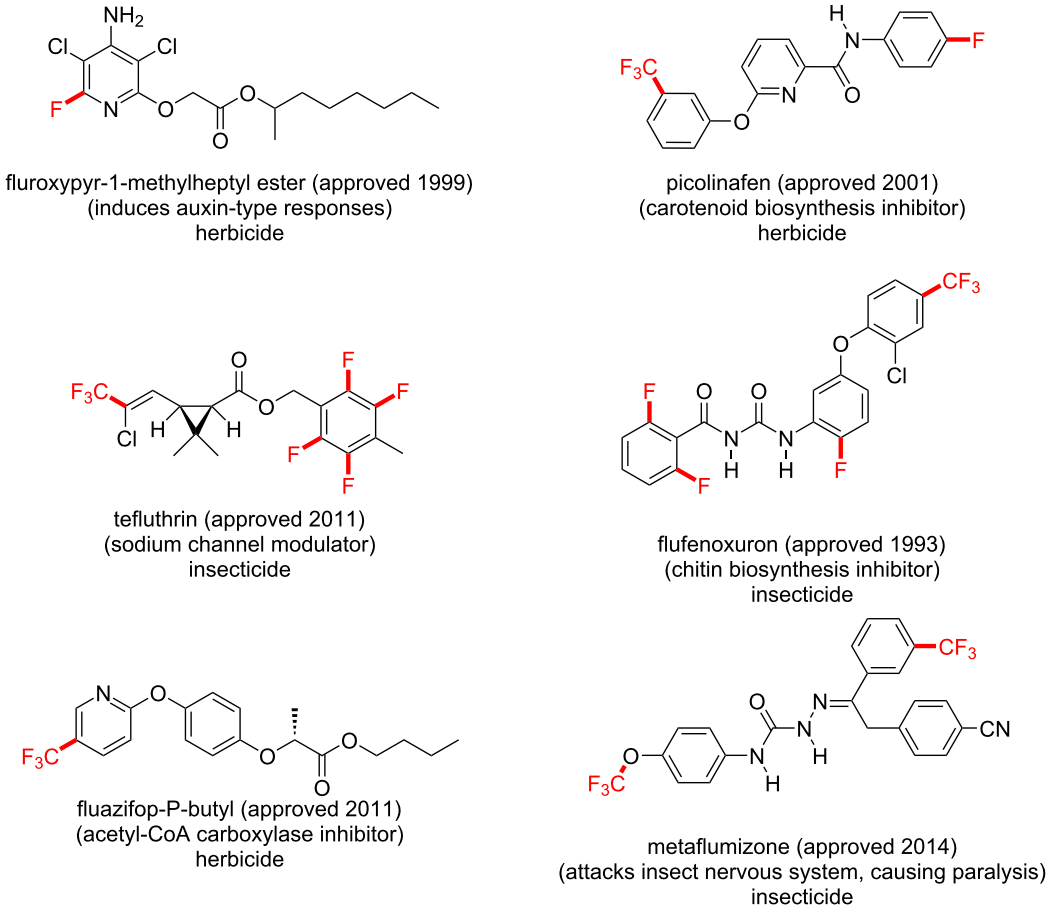

Figure 2: Fluorinated agrochemicals.

C–F substitution in a drug molecule enhances the lipophilicity [18], this has a positive impact on the biological absorption and distribution. Moreover, C–H/C–F substitution strongly decreases the basicity of neighboring amines (and lowers the pK_a by a similar increment) due to the σ-inductive effect of F. This results in i) a higher oral bioavailability [19], ii) a potential liability for phospholipidosis [20], iii) an increased membrane permeability [21] and iv) the mitigation of undesired binding to the human ether a-go-go-related gene (hERG) K^+ channel associated with cardiovascular toxicity [22]. Moreover, the radiochemical properties of the ^{18}F nucleus render them crucial isotopes for positron emission tomography (PET) due to their suitable half-life ($t_{1/2}$ = 110 min) and low positron energy, which allows the production of high-resolution images [23]. Therefore, radiopharmaceuticals that contain fluorine substituents are in high demand. Fluorine enhances important properties of polymers for their applications as water-repellent, chemical-proof, lubricant and thermally- and electrically-insulating materials [24]. The importance of fluorine atoms in chemical crop protection agents is well-acknowledged because fluorine improves the biological activity and user safety, decreases the environmental impact, and has new modes of action. In analytical chemistry, fluorine nuclei (^{19}F) are ideal for quantitative integration in NMR spectroscopy, comparable to ^{1}H NMR spectroscopy [25,26]. In contrast to ^{13}C signals, fluorine signals are well-resolved, and the nuclear spin of fluorine (I = 1/2) allows the coupling with nearby carbon and hydrogen atoms to be resolved [27].

1.1.2 Relevance of direct C–H fluorination methods:

Remarkable developments in synthetic chemistry over the last several decades have allowed the transformation of almost every organic functional group into another, paving the synthetic roadmap to many natural and unnatural compounds. While C–H bonds are not normally considered as functional groups, these are, however, ubiquitous, for example, in hydrocarbon fuels and in alkyl groups of countless organic molecules. The modification of unactivated C–H (especially C(sp^3)–H) bonds into other functional groups would not only enormously expand the synthetic maneuverability but would also intensify the use

of hydrocarbon feedstocks in organic synthesis. In this context, the advantage of direct C–H fluorination over traditional fluorination methods is that it does not require the introduction of other functional groups.

Although many methods have been developed for fluorination reactions [3,28-46], including the addition of electrophilic fluorine to alkenes [1,28,32], the fluorination of aryl triflates [29] and arylpalladium complexes [2,47], few permit a one-step transformation of unactivated C(sp^3)–H bonds to C(sp^3)–F bonds [1,3,36,38,48]. Such a transformation would be highly valuable for the late-stage functionalization (LSF) of complex molecules, such as those in Scheme 1.

The lack of sophisticated methods for direct C(sp^3)–H fluorinations is attributed to the challenges of regio- and chemoselectivity in C(sp^3)–H activation. Compounds that possess several C(sp^3)–H bonds will form several regioisomeric or polyfluorinated products that may be challenging to separate. Moreover, the inertness of C(sp^3)–H bonds due to their high homolytic bond dissociation energy and low polarity necessitate highly reactive reagents/intermediates for their activation, which may encourage off-site activity with other functional groups present in the target molecule and lead to a poor chemoselectivity. Overall, chemo- and regioselective C(sp^3)–H fluorinations continue to challenge chemists.

Most direct C(sp^3)–H fluorinations are reported to proceed under radical pathways involving hydrogen atom transfer (HAT), although proton-coupled electron transfer (PCET) has also been reported [44,49-57]. Accordingly, the reactivity and selectivity correlate with the homolytic C–H bond dissociation enthalpy and polarity matching principles [58-64]. One of the advantages of polarity matching is that it enables C(sp^3)–H bond activations that are not dictated by the thermodynamic driving force of the hydrogen atom transfer step (which depends on the stability of the resulting radical) or by the relative BDE of C–H bonds. Thus, it is possible to homolytically cleave stronger C–H bonds in the presence of weaker C–H bonds if the polarity of the stronger C–H bond is matched to the HAT catalyst. For example, an electrophilic radical abstracts H atoms selectively from the most electron-rich or "hydridic" C–H bond [65].

1.1.3 Importance of visible light and visible-light photosensitization in synthesis: Unlike many other traditional energy resources, light is inexpensive, nontoxic, noncontaminating, ample (or "limitless" in the case of sunlight) and a renewable source of energy for environmentally-friendly and "green" chemical synthesis. As a consequence of comprehending the detrimental impact of human industry on the environment, new methods to effectively utilize solar energy have represented a key scientific movement in the last two decades [66-68], especially after the oil crisis in the 1970s and the increasing solicitude about environmental pollution by chemical factories [69]. The attention on the solar generation of fuel brought unprecedented attention to photochemistry [70,71].

Increasing interest in photochemistry is often attributed to the ability to access radical intermediates that are otherwise difficult or impossible to obtain by classical chemistry but that can achieve unique chemical reactions complementary to two-electron processes [72-77]. However, the adoption of photochemistry into the toolbox of the synthetic organic chemist has been hindered by three phenomena: i) simple organic-molecule targets typically do not absorb (or have very small extinction coefficients for) visible light, which is among the most abundant in the solar distribution [78,79], instead absorbing only short wavelengths of UV light, ii) the photoexcitation of simple organic molecules by requisite high-energy UV photons populates higher-order excited states that undergo uncontrolled photodecomposition, such as Norrish-type cleavage reactions [80] and 1,5-HAT [81] and iii) the excited state of the simple organic molecule target can possess an ultrashort lifetime [82] that precludes photochemistry in favor of photophysical or nonradiative deactivation, e.g., fluorescence or internal conversion (IC).

Instead of direct UV excitation of the target substrate, one solution is the use of visible-light-harvesting photocatalysts that transfer their excitation energy to the target substrate. Over the last few decades, the field of visible-light photocatalysis has proven itself as a highly effective, versatile and "green" strategy for inducing different organic transformations under extremely mild conditions without threatening reagents and conditions [83-85]. There are three commonly observed and distinct mechanisms of photocatalytic activation [86] in the context of organic synthesis:

i) Most reported photocatalytic reactions proceed under photoredox catalysis (PRC), involving Dexter electron transfer. Such photoredox reactions begin with the excitation of the photocatalyst (PC) by visible light, followed by a single-electron transfer (SET) between the excited photocatalyst and another molecule (quencher, Scheme 2A). An unfortunate consequence of this is that there are many organic molecules with redox potentials that lie beyond the range of those of the excited photocatalyst [87]. The transiently generated (ultralow concentration of) the excited-state catalyst does not persist long enough even for slightly endergonic SET, so no reaction occurs. Moreover, C–H bonds are not redox-active. To circumvent those issues, SET can be leveraged to generate an HAT agent to

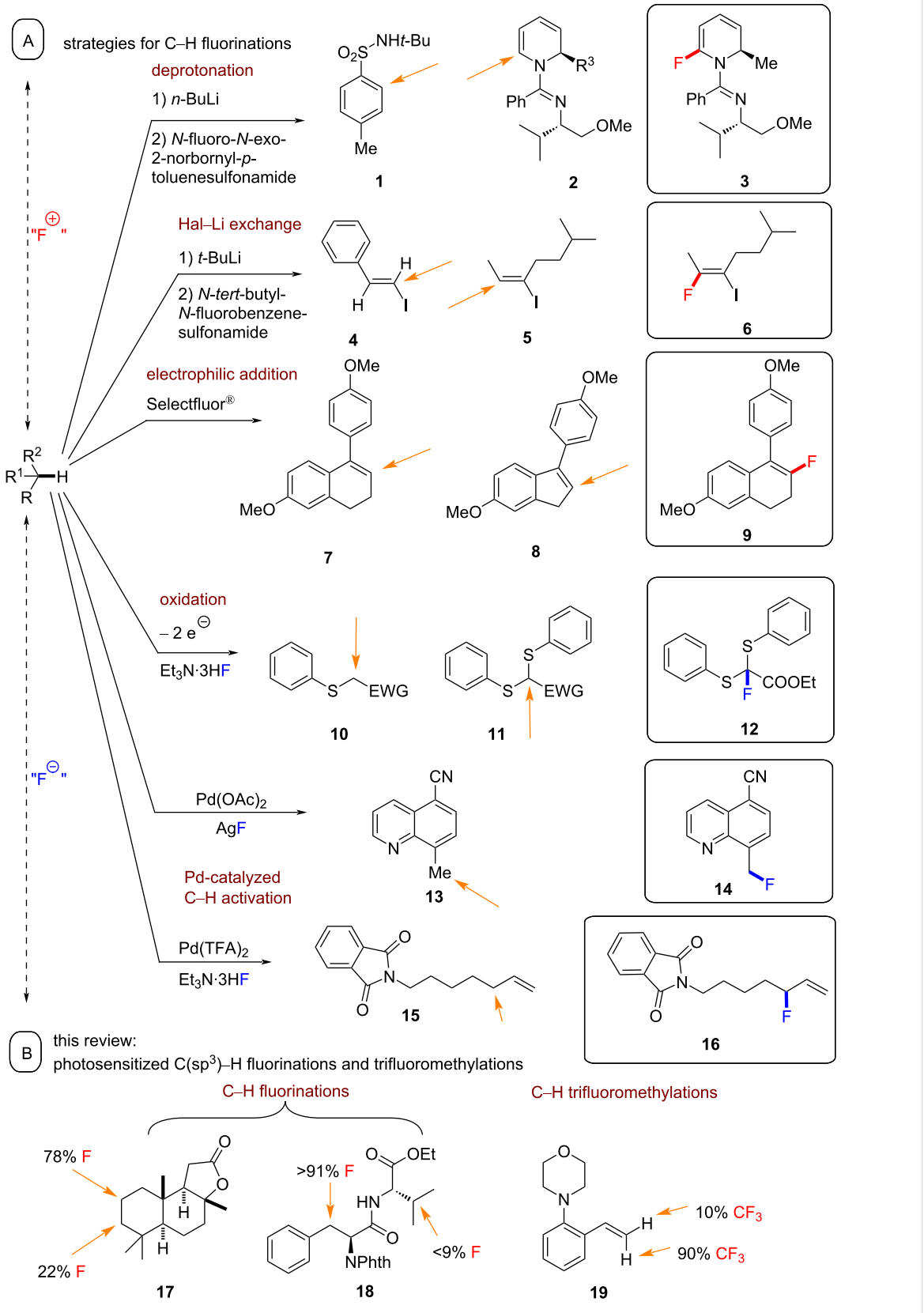

Scheme 1: Selectivity of fluorination reactions.

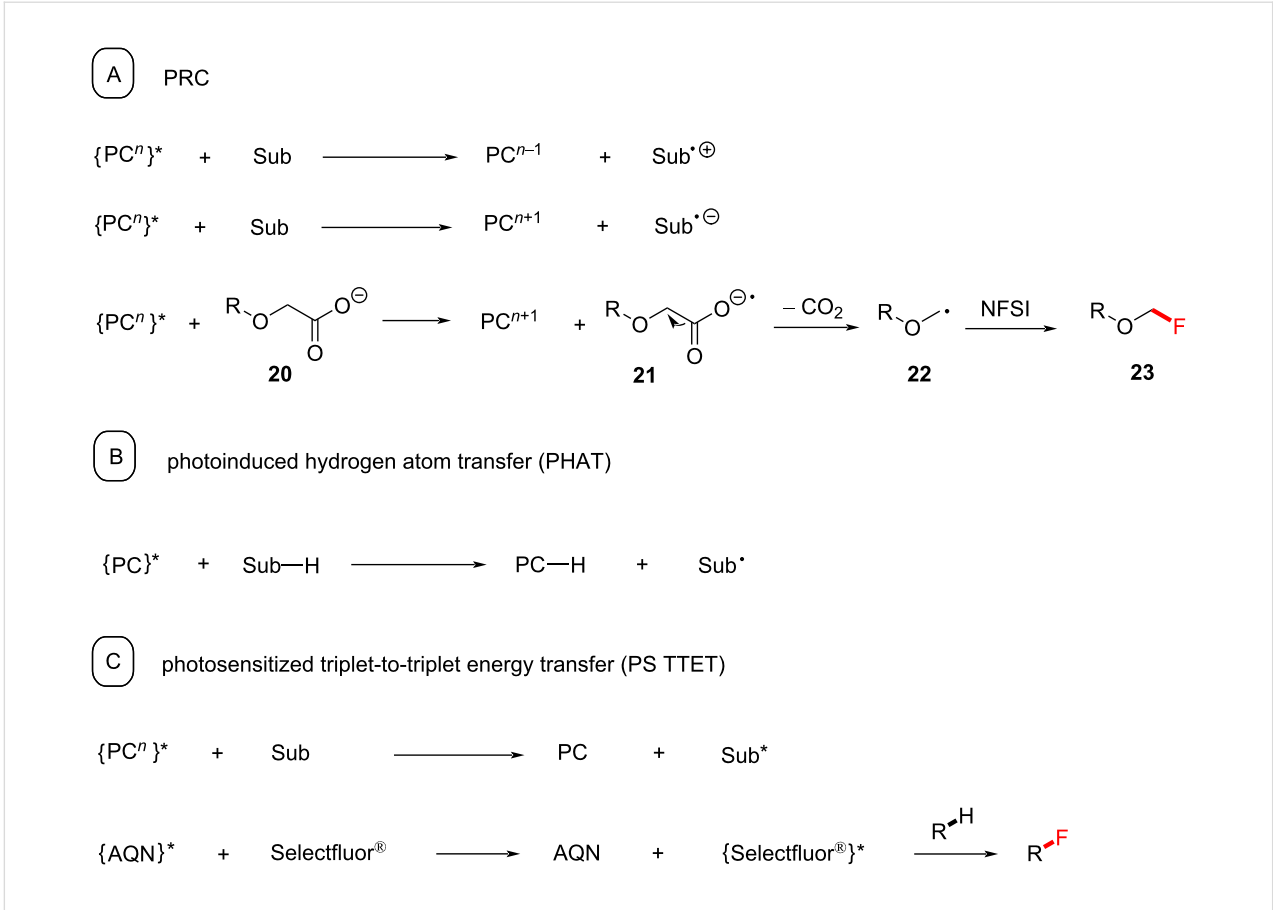

Scheme 2: Different mechanisms of photocatalytic activation. Sub = substrate.

activate C–H bonds. For the purposes of this review, we label this reaction class involving redox processes as PRC.

ii) Photochemical reactions in which the excited state photocatalyst participates directly in HAT with the substrate (Scheme 2B), herein termed PHAT [88].

iii) Photochemical reactions where the photosensitization catalyst (PSCat) engages in Dexter energy transfer (typically TTET) with the substrate (or fluorinating reagent) to induce a chemical reaction (Scheme 2C). This mechanistic class of PS TTET reactions is the focus of our review. PRC and PHAT processes are commonly grouped under the umbrella term "photocatalysis" in the literature, while PS TTET processes are often referred to as "energy transfer" [86].

1.1.4 PRC vs photosensitized energy transfer: Photocatalysis, photochemical sensitization and photosensitization are very similar terms. The IUPAC gold book defines photosensitization as follows: "The process by which a photochemical or photophysical alteration occurs in one molecular entity as a result of the initial absorption of radiation by another molecular entity called a photosensitizer. In mechanistic photochemistry, the term is limited to cases in which the photosensitizer is not consumed in the reaction" [89].

One can appreciate the close connection of this definition to that of photocatalysis, defined by the IUPAC as follows: "Change in the rate of a chemical reaction or its initiation under the action of ultraviolet, visible or infrared radiation in the presence of a substance – the photocatalyst – that absorbs light and is involved in the chemical transformation of the reaction partners" [90].

In principle, the photosensitizer is regenerated and therefore functions in a very similar way to a catalyst and can be deemed a photocatalyst. A common example of this concept is triplet photosensitization. The excited photocatalyst has a relatively high triplet-state energy and a long lifetime, such that it can function as an energy donor to activate the relatively lower triplet energy of the energy acceptor through an overall PS TTET process [91-100]. In contrast to PRC, the mechanism of TTET occurs in a way that does not depend on the redox potential of the molecules or on polar aprotic solvents, which are typ-

ically required for SET processes. Photosensitization also permits the facile and complementary access to radical intermediates via homolytic cleavage, without the need for SET [101,102].

1.1.5 Justification and scope of the review: Considering these advantages of photosensitization, it is clear that this field has attracted less attention than PRC methods. Moreover, PS TTET is a powerful method for the fluorination and trifluoromethylation of C–H bonds. We believe this may stem from the lack of dedicated reviews grouping together the theory [103-105], applications and mechanistic understanding that would enable researchers with a platform to plan photochemical reactions, as has been available for PRC [106-115]. Therefore, we present this review in the context of C–H fluorination and trifluoromethylation.

Section 2 equips readers with the basic theory of PS TTET and provides detailed property information tables on commonly utilized PSCats in organic synthesis and especially in C–H fluorinations, grouped by their properties relevant to PS TTET. Due to the importance of moving away from transition metal-based catalysts in organic synthesis and due to the exhaustive coverage of transition metal-based photosensitizers in the literature, we focus on detailing the properties of small-organic-molecule photosensitizers. Section 2 also highlights common fluorinating reagents, especially those used in C–H fluorinations. Section 3 groups the applications of direct C(sp^3)–H fluorination by their achievement, either using PSCats or photosensitization auxiliaries (PSXs), while Section 4 presents the applications of trifluoromethylations involving photosensitization.

In order to guide the readers and to help with the planning of future reactions, throughout Sections 3 and 4, we present the developing mechanistic understanding of these reactions in the literature, including considerations such as triplet-to-triplet energy matching for photosensitization, polarity matching and directing groups for HAT. It is not our purpose to provide a detailed review on photosensitized energy transfer in organic synthesis, including a detailed account of the photophysical phenomena [105,116] nor is it our purpose to review C–H fluorinations accomplished by nonphotochemical methods or by photochemical methods deemed to proceed via SET.

2 Principles of photosensitization; selection of the photosensitizer and fluorinating reagent in C–H fluorinations

2.1 Photosensitization and appropriate photosensitizer

The general mechanism of photosensitization is described in Figure 3 [86]. Initially, the PS absorbs visible light and is excited from the ground singlet state S_0{PS} to the excited singlet state S_1{PS}. Intersystem crossing (ISC) transforms S_1{PS} to its more stable triplet state, T_1{PS}. ISC is a process in which a nonradiative transition of a singlet excited electronic state to a triplet excited state takes place at a point where the potential energy curves of these two states interset, which requires spin–orbit coupling [117]. In the absence of spin–orbit

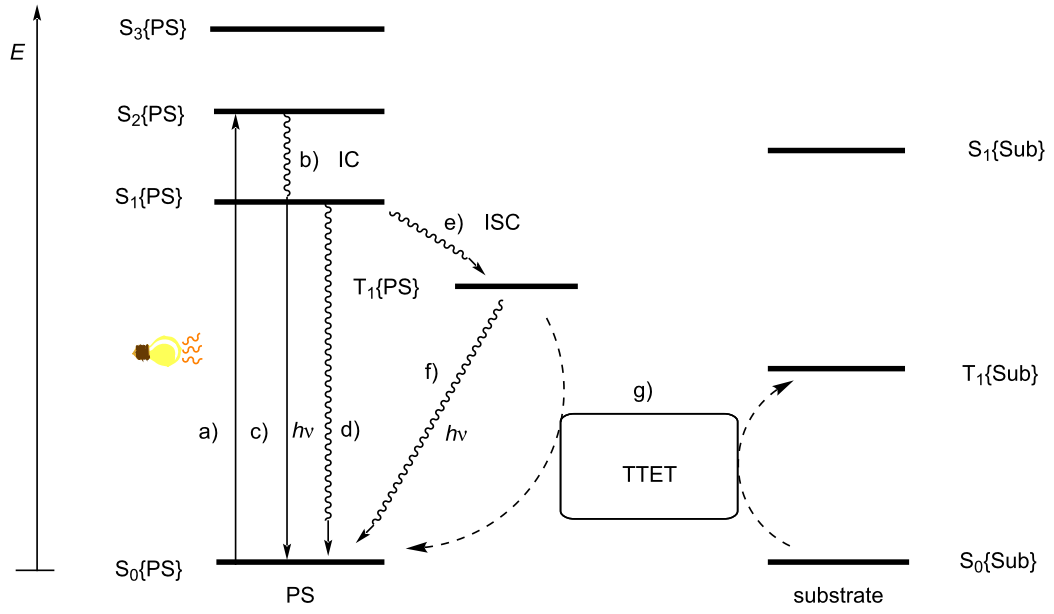

Figure 3: Jablonski diagram showing visible-light-induced energy transfer pathways: a) absorption, b) IC, c) fluorescence, d) radiationless transitions, e) ISC, f) phosphorescence and g) TTET.

coupling, it is a forbidden transition according to the Pauli exclusion principle. The resulting triplet state, $T_1\{PS\}$ is in an excited vibrational state that collides with nearby molecules to reach its lowest vibrational energy state.

Another fate of $T_1\{PS\}$, permitted by spin–orbit coupling, is the radiative process of phosphorescence. If a molecule exhibits a high triplet quantum yield (rapid ISC and slow phosphorescence), this state is long-lived and can exist beyond the timeframe of diffusion, to be leveraged in photosensitization. Intermolecular energy transfer from $T_1\{PS\}$ to the substrate excites it from its ground singlet state $S_0\{Sub\}$ to its excited triplet state $T_1\{Sub\}$. This intermolecular energy transfer process, known as TTET, involves the exchanges of two electrons with different spin and energy between two molecules (Figure 4). Therefore, it can be termed a Dexter energy transfer mechanism, not a Forster resonance energy transfer (FRET) mechanism. The generated triplet state of the substrate then undergoes further chemical transformation.

There are four prerequisites for TTET to be effective: i) The PS must have a chromophore that can absorb light, 2) the energy gap between $S_1\{PS\}$ and $T_1\{PS\}$ must be higher in energy than the energy gap between $S_1\{Sub\}$ and $T_1\{Sub\}$, iii) ISC between $S_1\{PS\}$ and $T_1\{PS\}$ must be rapid to ensure a high quantum yield of the triplet state and iv) the energy transfer from the PS to the substrate must, overall, be exergonic. An ideal PS is a single, well-characterized pure substance of known composition that is stable at room temperature. In the presence of light, it is not toxic or degrades to toxic byproducts. It is inexpensive, sustainable (ideally not ruthenium or iridium complexes) and commercially available. Due to their comparatively high triplet energies and the long lifetime of their triplet states; organic dyes and various ruthenium and iridium complexes are well-suited photosensitizers [118-122].

There are many approaches to photosensitized fluorination that do not involve direct C–H activation, which are reviewed elsewhere [123-125], such as C–C bond fragmentation/C–F bond formation [126], aminofluorination of cyclopropanes [127] and decarboxylative fluorination [128]. These employ photosensitizers such as 9-fluorenone [127], 1,2,4,5-tetracyanobenzene (TCB) [129,130], 1,4-dicyanobenzene (CB) [126,131] and benzophenone [128] and proceed in low (23%) to excellent (96%) yields [126,128]. One of the most efficient and high-energy (79.4 kcal·mol^{-1}) triplet photosensitizers is acetone. Frequently, it is used as a solvent or in high concentration where its optical density allows light absorption at approximately 300 nm, even though λ_{max} is about 270 nm [132]. Benzil, 9-fluorenone and 9,10-phenanthrenequinone are also well-established visible light triplet PSCats that are very cost-effective, commercially available and easy to handle [133-135]. Xanthone is capable of absorbing visible light (>400 nm) and has a triplet energy of about 74.1 kcal·mol^{-1} [136-139]. Figure 5 and Figure 6 as well as Table 1 show the structures and documented absorbance, triplet state energies and lifetimes of several small organic molecule/dye PSCats. Figure 7 shows the corresponding information for selected prototypical transition metal complexes.

2.2 Fluorination reagents

An extensive discussion on the different types of fluorination reagents is beyond the scope of this review, and readers are directed to relevant reviews on the topic [8,173,174]. Here, we present a brief overview.

Fluorine gas is the most fundamental electrophilic source of fluorine atoms; however, it is highly toxic, reactive and explosive, which severely limits its applicability in synthetic chemistry [175]. Despite the utility of (diethylamino)sulfur trifluoride (DAST) [176], morpholinosulfur trifluoride and tetrabutyl-

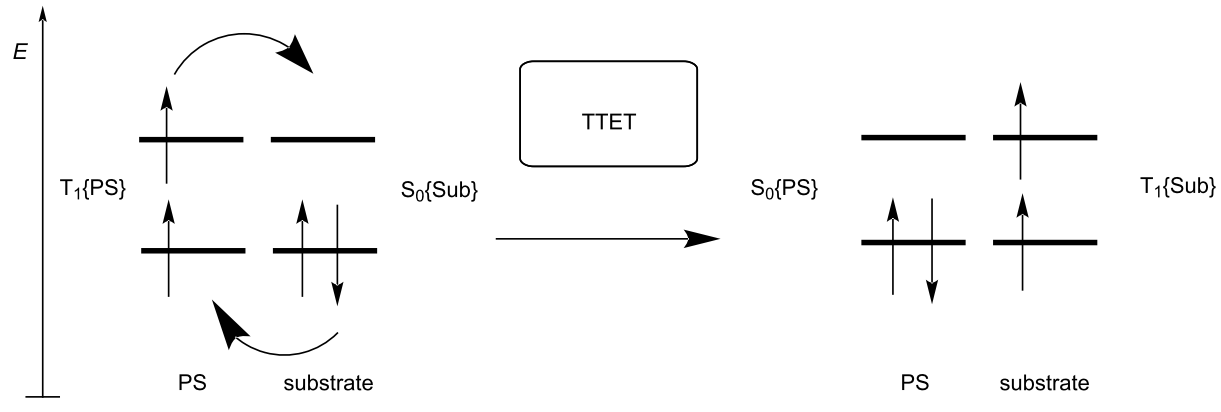

Figure 4: Schematic illustration of TTET.

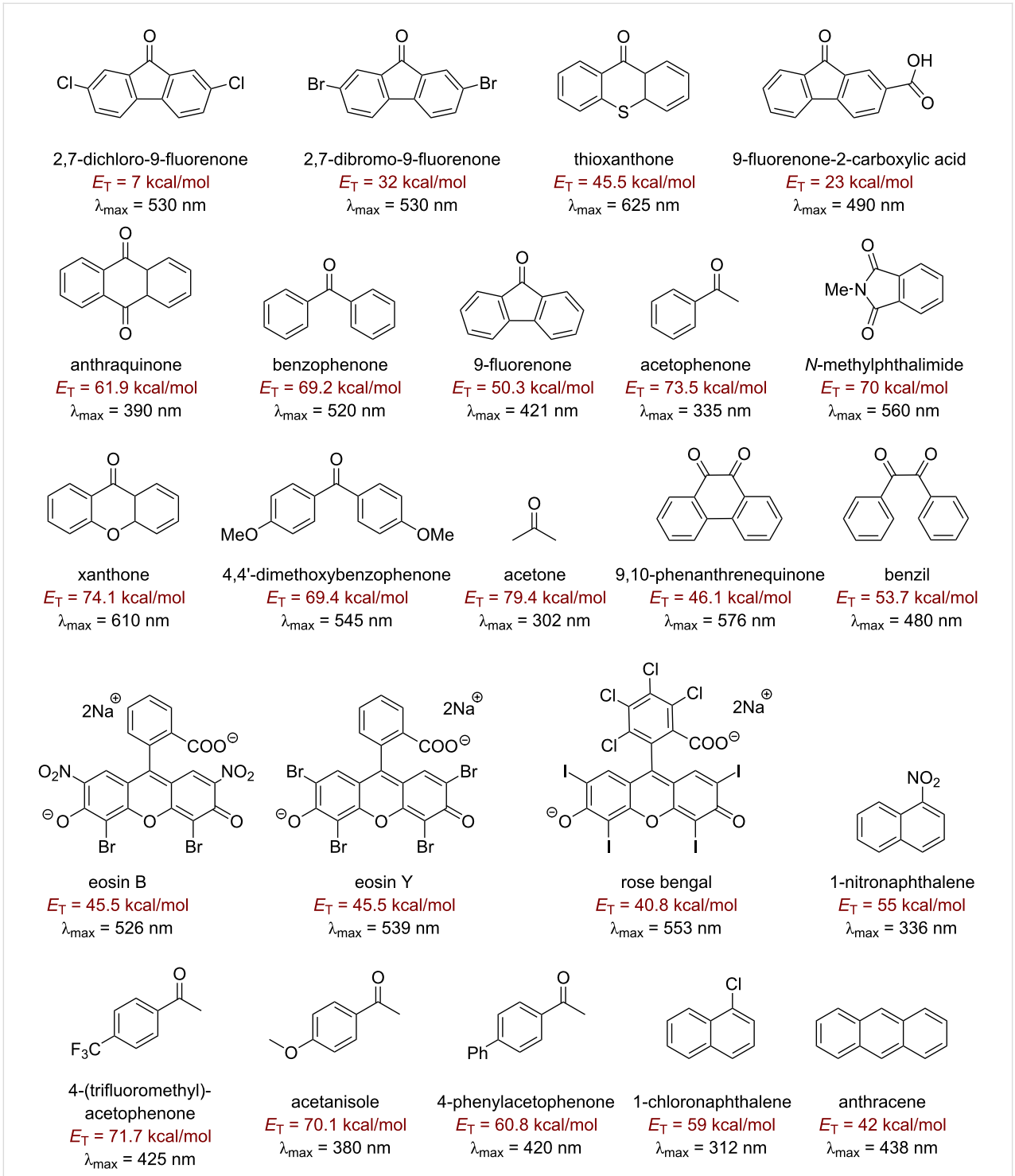

Figure 5: Organic triplet PSCats.

ammonium fluoride (TBAF) [4] as nucleophilic fluorine sources, the high reactivity of alternative electrophilic fluorine sources, such as fluoroxysulfates and hypofluorites [177-179], renders their employment in synthesis problematic. The high demand for a safe, stable and highly reactive electrophilic fluorinating reagent prompted researchers to synthesize the first generation of electrophilic fluorination reagents, including fluoroxytrifluoromethane [180], fluorine perchlorate [181], xenon difluoride [182], nitrogen oxide fluorides [183] and several other hypofluorides [184,185] (Figure 8A).

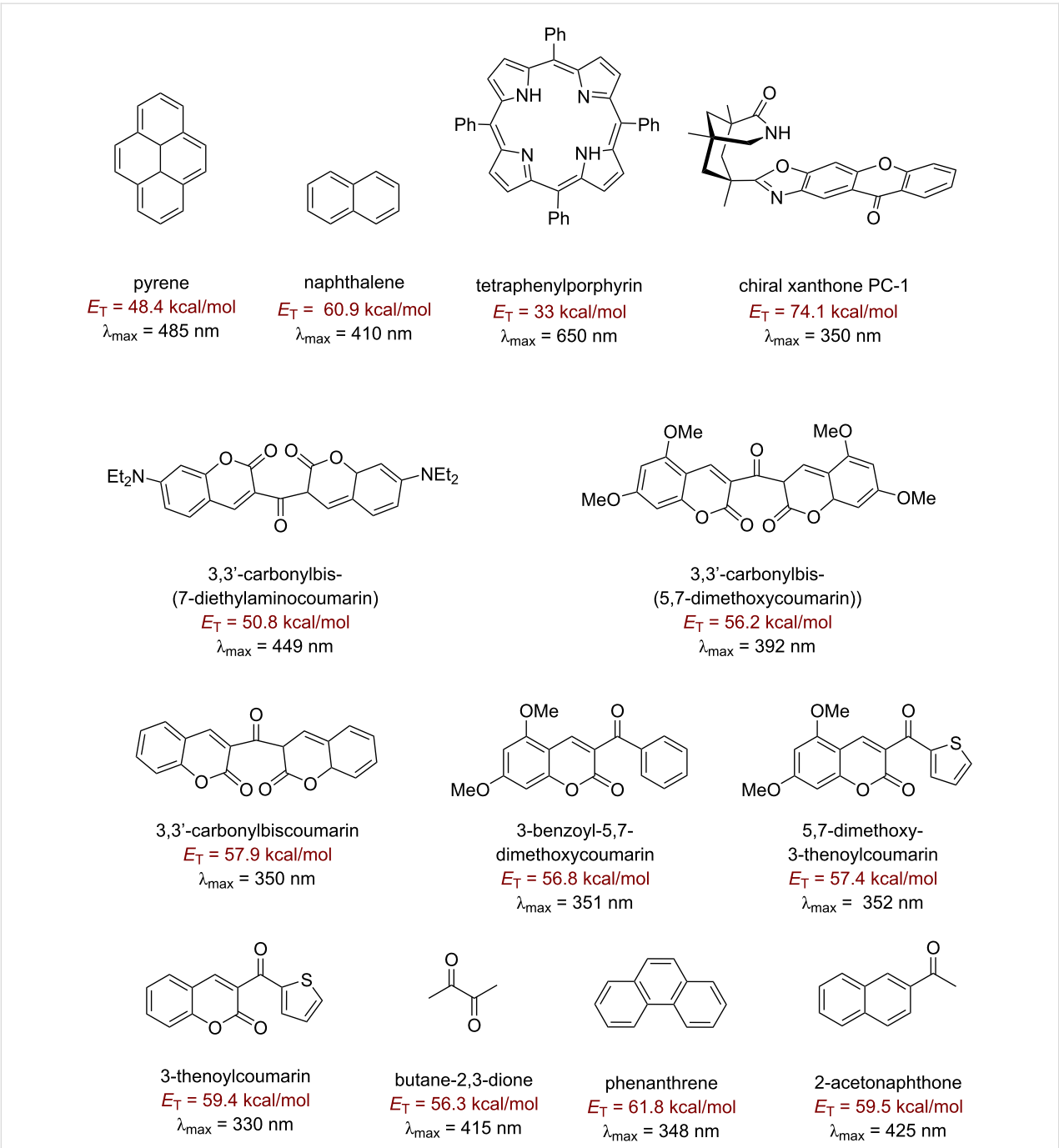

Figure 6: Additional organic triplet PSCats.

The second generation of fluorine reagents were the *N*-fluoro reagents (Figure 8B). These possessed selectivity, functional group tolerance, were safer and less expensive. Umemoto and co-workers first synthesized the NFPYs [186]. Further synthesis of similar compounds resulted in the synthesis of *N*-fluorobis(phenyl)sulfonimide (NFSI) [187], *N*-fluorobis[(trifluoromethyl)sulfonyl]imide [188,189], *N*-fluoropyridinium salts [186], *N*-fluorosaccharinsultam and 4-nitro-substituted *N*-fluorosaccharinsultam. The most recent discovery of an advanced electrophilic fluorinating agent was Selectfluor® (1-chloromethyl-4-fluoro-1,4-diazoniabicyclo[2.2.2]octane bis(tetrafluoroborate)) [190].

Selectfluor® [190,191] is a nonhygroscopic, crystalline solid, stable at temperatures up to 195 °C, nonhazardous [192], reliable and commercially available [193]. Selectfluor® is synthe-

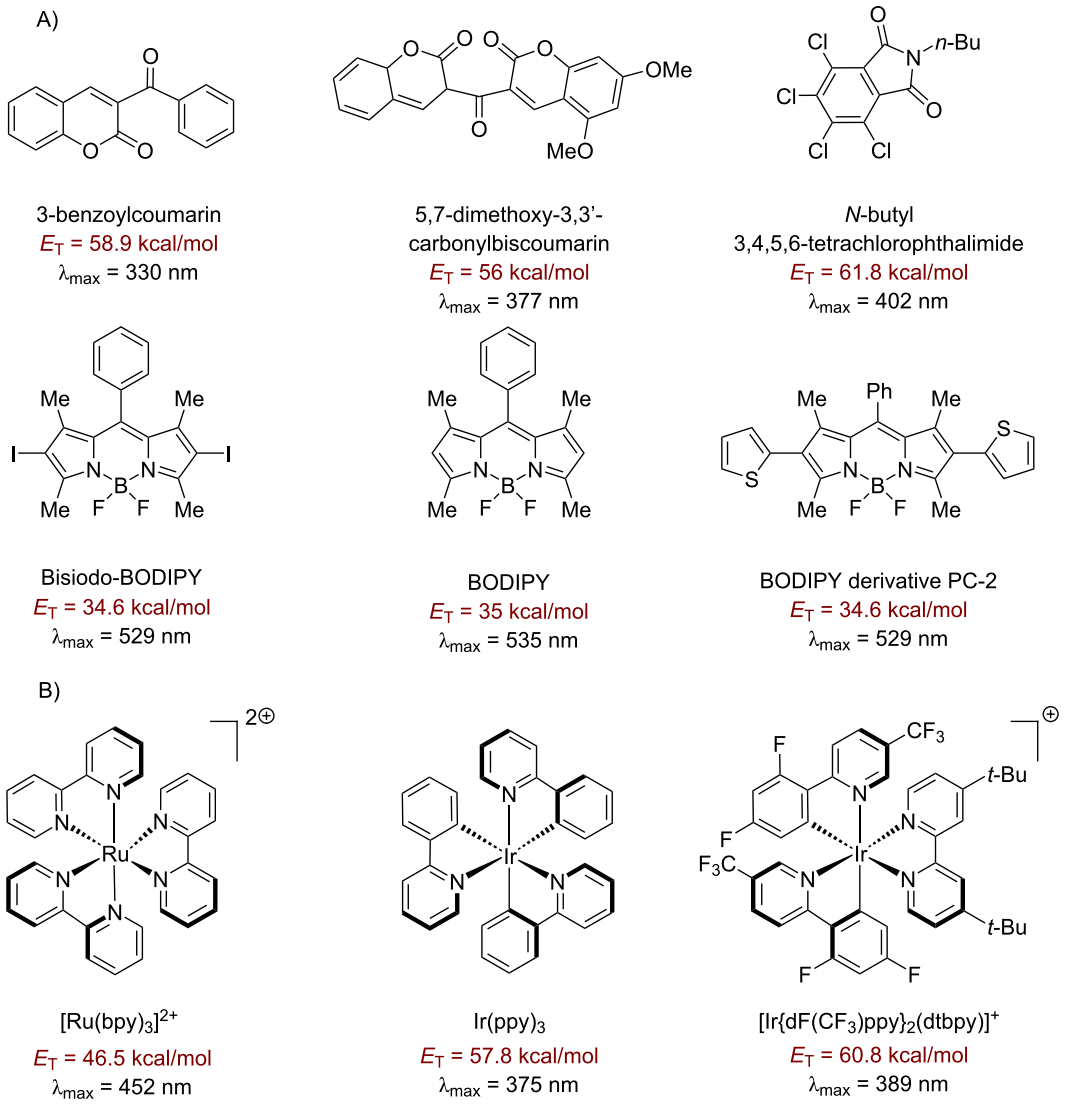

Figure 7: A) Further organic triplet PSCats and B) transition metal triplet PSCats.

sized on a multiton p.a. scale in a simple and efficient method (Scheme 3) [193]. The precursor **24** is prepared by alkylation of DABCO (1,4-diazabicyclo[2.2.2]octane) with DCM. A counter-ion exchange with $NaBF_4$ causes NaCl precipitation in MeCN, and the fluorination with F_2 in the presence of sodium tetrafluoroborate affords Selectfluor®. Moreover, by variation of these conditions, different derivatives of Selectfluor® (e.g., a methyl derivative: Selectfluor® II and a 2,2,2-trifluoroethyl derivative) with different physical properties and reactivity can be synthesized on an industrial scale (Scheme 3) [194].

2.3 General mechanism of photosensitized C–H fluorination

Generally, the mechanism of photocatalytic activation induced by energy transfer involves the simultaneous photoinduced electron exchange between the photosensitizer and the substrate. It is necessary to note that this process does not imply any net redox chemistry. For this reason, it is difficult to predict the reactivity of these processes by the electrochemical potentials of the compounds. On the contrary, the triplet state energy of the photocatalyst and the reactant are very useful to determine the possibility of an energy transfer process.

At the first stage of the mechanism, the photocatalyst is excited from the singlet ground state to the excited singlet state (Scheme 4) [86]. Ordinarily, most organic molecules do not undergo effective ISC to the triplet state, consequently they relax quickly to the ground state. However, triplet photosensitizers undergo rapid ISC and successfully generate long-lived triplet states. After an energy transfer between the triplet excited

Table 1: Absorption maxima, triplet energies and lifetimes of common PSCats.

Entry	PSCat	λ_{max} (nm)	E_T (kcal·mol^{-1})	Lifetime of the triplet excited state (τ)	Reference
1	2,7-dibromo-9-fluorenone[a]	530	32.0	2.7 ns	[140,141]
2	2,7-dichloro-9-fluorenone[a]	530	7.0	8.5 ns	[141]
3	thioxanthone[a]	625	45.5	4.0 µs	[136,142]
4	9-fluorenone-2-carboxylic acid[a]	490	23.0	9.1 ns	[141]
5	anthraquinone[b]	390	61.9	0.2 µs	[137,143,144]
6	benzophenone[a]	520	69.2	0.7 µs	[136,137]
7	9-fluorenone[a]	421	50.3	16.5 ns	[136,137,141]
8	acetophenone[a]	335	73.5	0.2 µs	[136,137,145]
9	*N*-methylphthalimide[a]	350	70.0	5.0 µs	[146-148]
10	xanthone[b]	610	74.1	8.3 µs	[136-138,149]
11	4,4'-dimethoxybenzophenone[a]	545	69.4	–	[136,137]
12	acetone[a]	302	79.4	47.0 µs	[132,137,150]
13	9,10-phenanthrenequinone[a]	576	46.1	7.3 µs	[151]
14	benzil[a]	480	53.7	–	[137,152,153]
15	eosin B[c]	526	45.5	–	[154,155]
16	eosin Y[c]	539	45.5	–	[107,155-157]
17	rose bengal[d]	553	40.8	30.0 µs[a]	[107,137,158,159]
18	1-nitronaphthalene[e]	580	55.0	–	[137,160]
19	4-(trifluoromethyl)acetophenone[a]	425	71.7	–	[136,137]
20	acetanisole[a]	380	70.1	–	[136,137]
21	4-phenylacetophenone[a]	420	60.8	–	[136]
22	tetraphenylporphyrin[a]	650	33.0	–	[161]
23	1-chloronaphthalene[f]	312	59.0	–	[160,162]
24	anthracene[a]	438	42.0	–	[137,163]
25	pyrene[a]	485[g]	48.4	–	[160,164]
26	naphthalene[a]	410[g]	60.9	38 µs	[137,144,163,164]
27	chiral xanthone PC-1	350	74.1	–	[157]
28	3,3'-carbonylbis(7-diethylaminocoumarin)[a]	449	50.8	–	[165,166]
29	3,3'-carbonylbis(5,7-dimethoxycoumarin)[a]	392	56.2	–	[165,166]
30	5,7-dimethoxy-3,3'-carbonylbiscoumarin[a]	377	56.0	–	[165,166]
31	3,3'-carbonylbiscoumarin[a]	350	57.9	–	[165,166]
32	3-benzoyl-5,7-dimethoxycoumarin[a]	351	56.8	–	[165,166]
33	5,7-dimethoxy-3-thenoylcoumarin[a]	352	57.4	–	[165,166]
34	3-benzoylcoumarin[a]	330	58.9	–	[165,166]
35	3-thenoylcoumarin[a]	330	59.4	–	[165,166]
36	$[Ru(bpy)_3]^{2+}$[a]	452	46.5	1100–850 ns	[108,157,167]
37	$Ir(ppy)_3$[a]	375	57.8	1.9 µs	[108,157]
38	$[Ir\{dF(CF_3)ppy\}_2(dtbpy)]^+$[a]	389	60.8	2.3 µs	[108,157]
39	butane-2,3-dione	415	56.0	–	[160,168]
40	phenanthrene[a]	348	61.8	–	[160,169]
41	2-acetonaphthone[a]	425	59.5	–	[136]
42	bisiodo-BODIPY[a]	529	34.6[h]	57.1 µs	[170]
43	BODIPY[a]	503	35.0[h]	0.02 µs	[170]
44	BODIPY derivative PC-2[i]	529	34.6[h]	390 µs	[171]
45	*N*-butyl-4,5,6,7-tetrachlorophthalimide	402[j,k]	61.8[j,l]	–	[172]

The absorption maximum λ_{max} refers to the longest-shifted maximum towards, or in the visible region. [a]In MeCN or MeCN (aq). [b]In C_6H_6. [c]In EtOH/MeOH 9:1. [d]In DMF. [e]EPA (77 K). [f]In H_2O. [g]Chemisorbed onto alumina. [h]Calculated E_T. [i]In PhMe. [j]In cyclohexane. [k]λ_{max} assumed from an *N*-substituted analog. [l]Triplet energy assumed from phosphorescence.

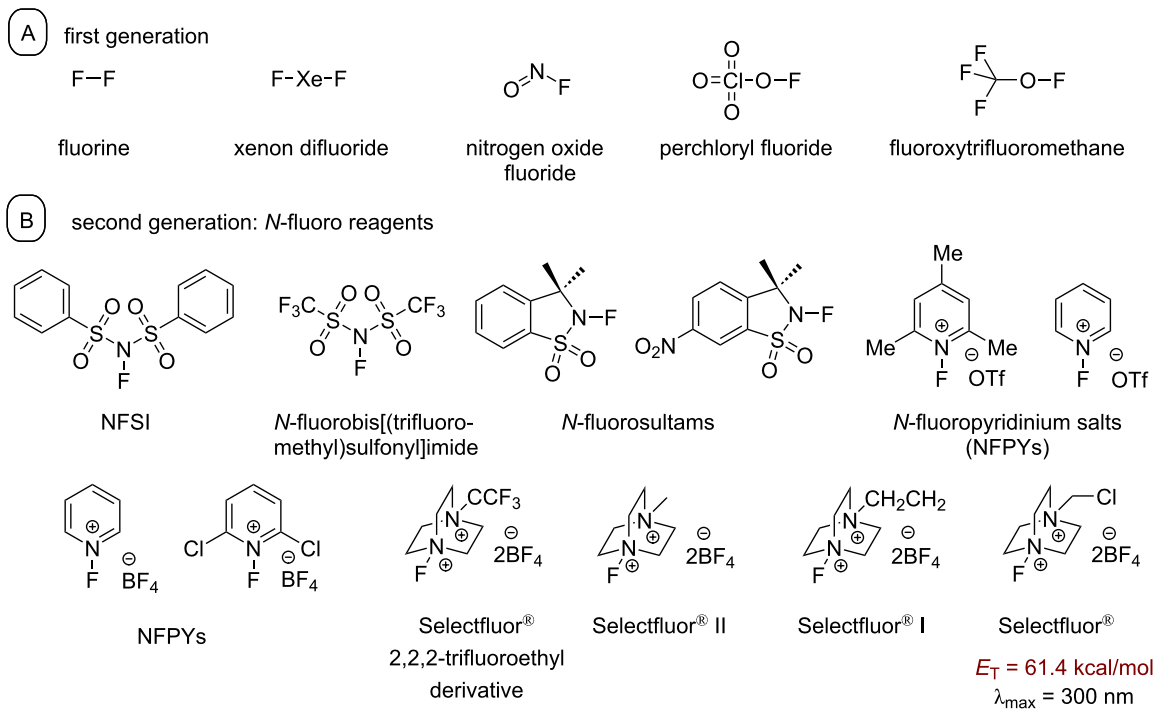

Figure 8: Different fluorination reagents grouped by generation.

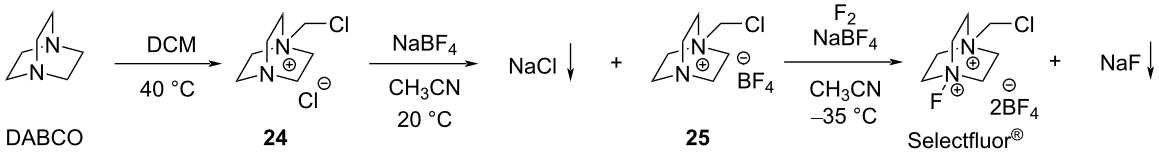

Scheme 3: Synthesis of Selectfluor®.

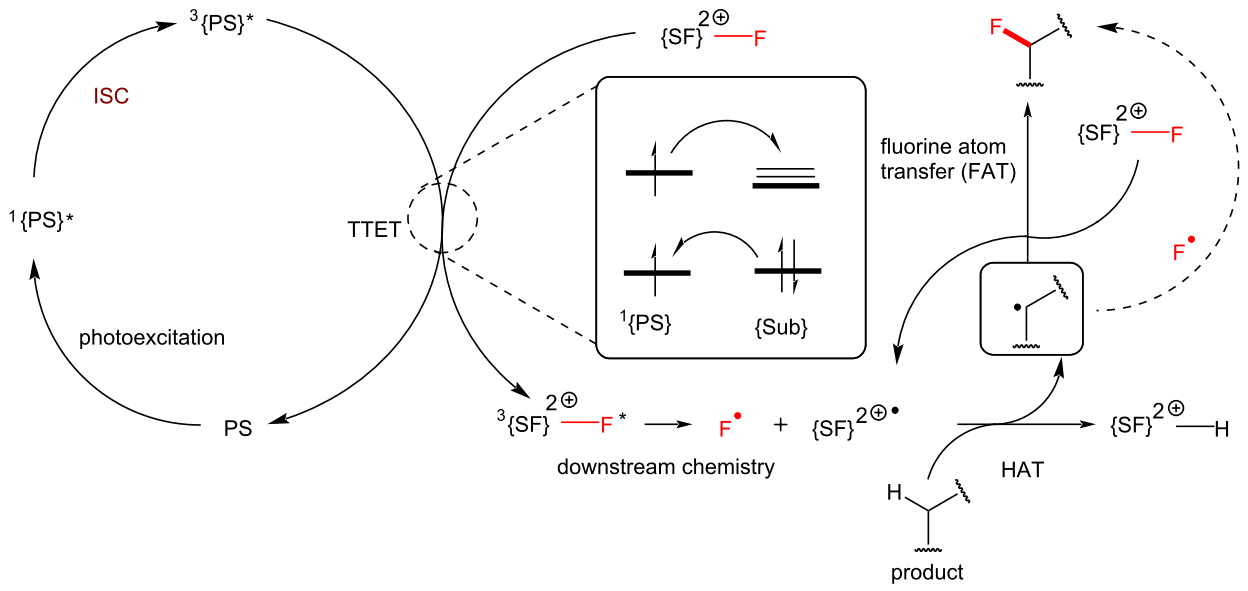

Scheme 4: General mechanism of PS TTET C(sp^3)–H fluorination.

photosensitizer and the substrate (e.g., Selectfluor®), the photocatalyst is relaxed to the ground state and the substrate is excited to its triplet excited state to undergo downstream chemistry. In the case of triplet Selectfluor®, plausible mechanisms for the downstream chemistry are shown in Scheme 4 and discussed in more detail in the following section.

3 C–H fluorination of visible-light-inactive molecules using PSCats

3.1 Benzylic C–H fluorination

A seminal paper in the field of transition-metal-free direct C–H fluorination comes from Chen and co-workers, who applied aryl ketones as PSCats [135]. They discovered that the choice of the PS impacted the selective formation of mono- vs difluorinated products at the benzylic position; 9-fluorenone affords benzylic monofluorination and xanthone affords benzylic difluorination (Scheme 5). Importantly, this metal-free direct C–H fluorination proceeded without the need for any specialized photochemical equipment; under visible-light irradiation by a household (19 W) compact fluorescent light (CFL) bulb (emitting variable wavelengths in the range of ≈365–625 nm) [195] and under mild conditions. Control reactions revealed that both the PS and light were essential for the reaction to occur. According to their report, benzylic C–H monofluorination photosensitized by 9-fluorenone demonstrated a remarkable scope and reaction efficiency.

A range of different photosensitizers (acetone, benzophenone, 9-fluorenone and $Ir(ppy)_3$) were investigated. Acetone as a PSCat gave no product, likely due to its absorption bands (≈280 nm) well out of reach of even the lowest emission wavelength range of the CFL bulb. $Ir(ppy)_3$ also gave no reaction. This was interesting, considering that its triplet energy (T_1 = 57.8 kcal·mol^{-1}) was similar to Selectfluor® (T_1 = 61.4 kcal·mol^{-1}). Benzophenone (T_1 = 69.1 kcal·mol^{-1}) and 9-fluorenone (T_1 = 50.3 kcal·mol^{-1}) were most effective, affording 83% and 86% yield of the monofluorinated product **27a**, respectively (Scheme 6). A range of electrophilic fluorine sources was evaluated (for example, NFSI and *N*-fluoropyridinium salts), but Selectfluor® was chosen for giving the highest yield of **27a**. Electroneutral and electron-poor compounds were successfully monofluorinated in modest to excellent (36–93%) yield of **27b–i** (Scheme 6). The functional group tolerance included bromoarenes, esters and unprotected benzoic acids.

Chen's photosensitized approach represents the first photochemical C–H *gem*-difluorination. *gem*-Difluorination is particularly challenging since the first introduced fluorine atom will electronically hinder the second fluorination at the same position. For difluorination, xanthone was employed as the PC and Selectfluor® II as the fluorine source (Scheme 7). The higher T_1 energy may have been responsible for generating more Selectfluor®-derived radical cations that drove the reaction towards difluorination to afford the product **28a**. However, it is important to note that only difluorinated products were detected and no monofluorinated products were observed, regardless of whether Selectfluor® or Selectfluor® II was employed. Were mono- and difluorination to proceed via the same mechanism, one would expect to see traces of the monofluorinated product **27a** unless the reaction of **27a** was faster than the reaction of the starting material **26**. Interestingly, NFSI gave exclusive monofluorination, albeit in a low (26%) yield, despite its lower BDE (calculated BDE = 63.4 kcal·mol^{-1}) than Selectfluor® [196]. *gem*-Difluorinations using xanthone gave a higher conversion of **26** and a higher yield of **28a** with Selectfluor® II rather than

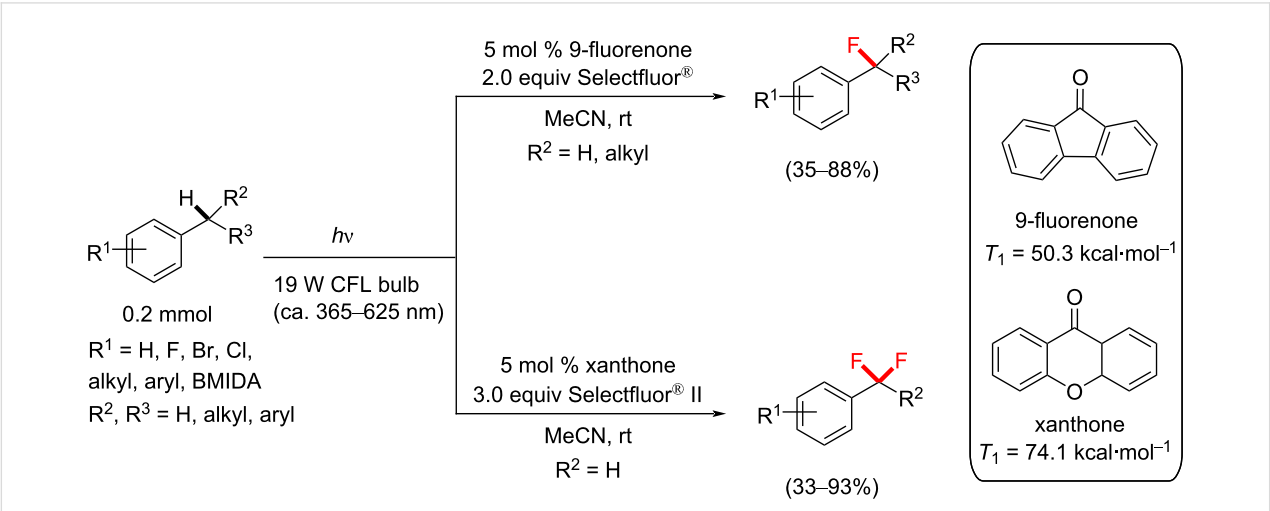

Scheme 5: Selective benzylic mono- and difluorination using 9-fluorenone and xanthone PSCats, respectively.

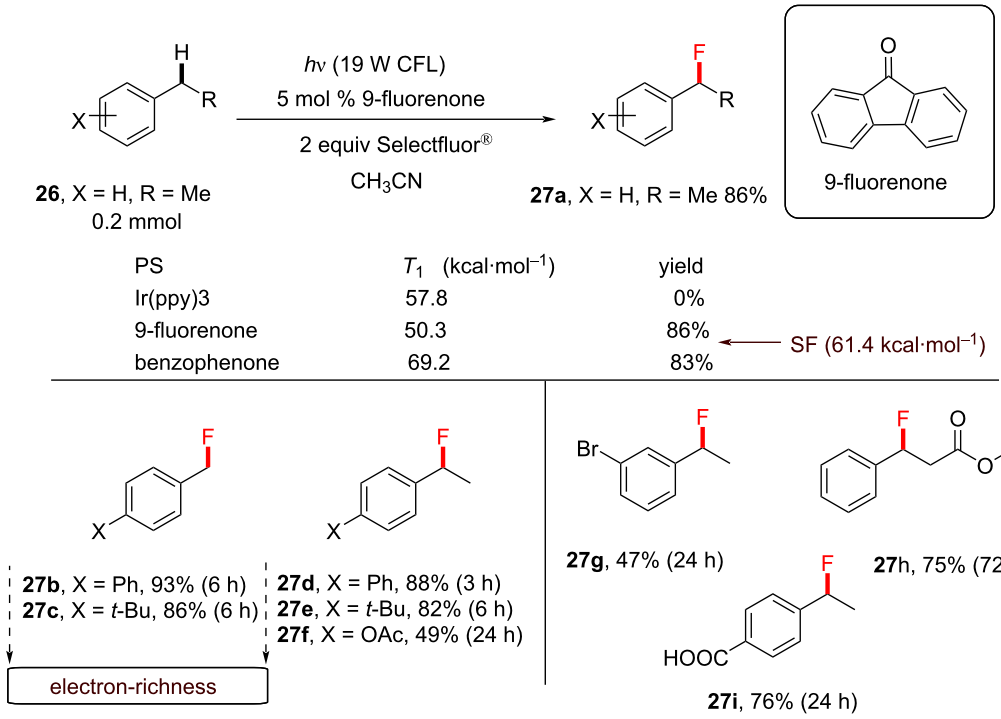

Scheme 6: Chen's photosensitized monofluorination: reaction scope.

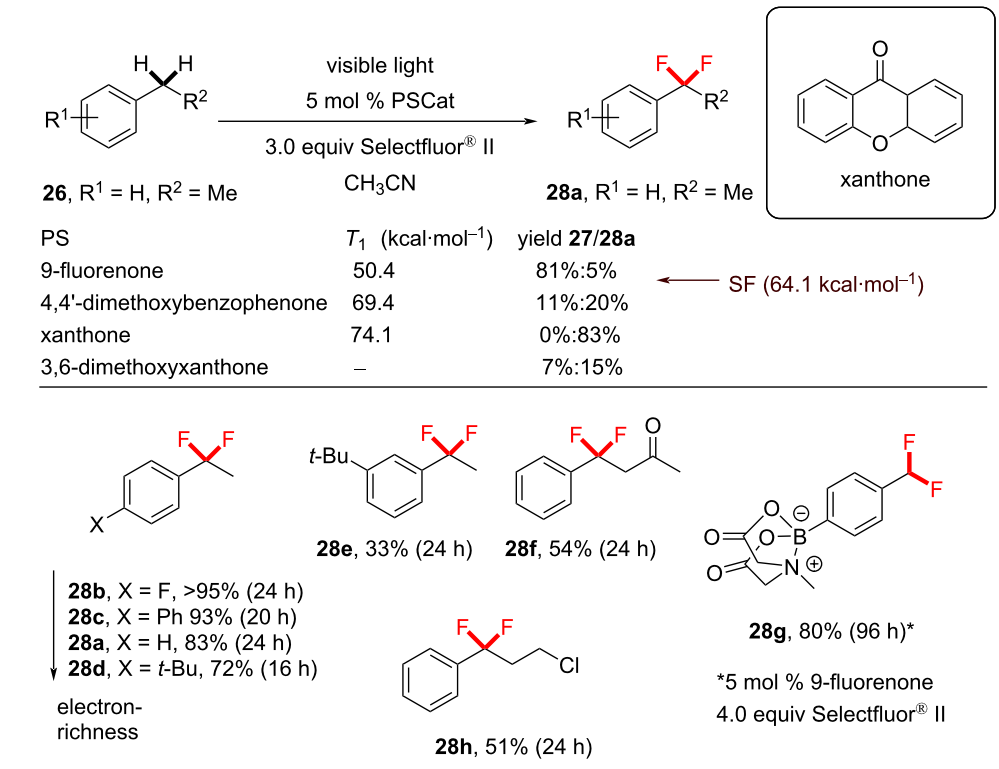

Scheme 7: Chen's photosensitized benzylic difluorination reaction scope.

with Selectfluor® (Scheme 7), despite their identical N–F bond dissociation enthalpies (calculated BDEs = 64.0 kcal·mol^{-1}) [196].

While the T_1 energy of Selectfluor® II is not reported to our knowledge, it is possible that the greater reactivity towards *gem*-difluorination could stem from it having a T_1 energy closer to xanthone. The reaction conditions tolerated various electron-rich and electron-poor substituents, affording exclusively benzylic C(sp^3)–H *gem*-difluorinated products in modest to excellent (33–95%) yield of **28b**–**h**. The functional group tolerance was demonstrated by successful reactions of alkyl chlorides, ketones and a *para*-substituted MIDA ester. A common trend between mono- and difluorination was that increasing the electron-releasing ability of a substituent *para* to the benzylic position decreased the product yield. It is known that polarity matching effects are negligible for benzylic HAT and that BDEs do not correlate with Hammett parameters of *para* substituents [197], and therefore the reaction success could relate to the transition state of the benzylic radical's fluorination step.

Given later studies [147,198,199], it cannot be ruled out that this reaction could be interpreted as a photosensitized C–H fluorination involving the complexation of the PSCat with Selectfluor® and TTET. The practicality of this photosensitized monofluorination was demonstrated using ethylbenzene on gram scale (Scheme 8) [135]. Ethylbenzene (2.12 g) was monofluorinated to give the desired fluorinated product (2.11 g) in 85% isolated yield, almost identical to the 83% yield under the standard conditions. This reaction was also demonstrated in continuous flow under similar conditions [139].

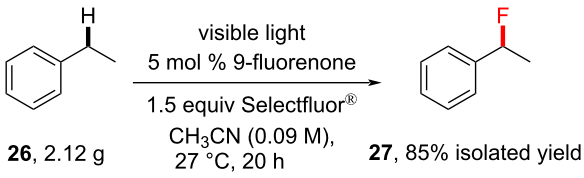

Scheme 8: Photosensitized monofluorination of ethylbenzene on a gram scale.

3.2 Polarity matching-guided unactivated C(sp^3)–H fluorination

3.2.1 Synthetic applications: In another seminal paper, Tan and co-workers [198] discovered the photocatalytic direct fluorination of unactivated C(sp^3)–H bonds by employing Selectfluor® and anthraquinone (AQN, T_1 = 61.9 kcal·mol^{-1}) as a photosensitizer. Control experiments showed that, under their conditions, both light and AQN were necessary for the reaction to proceed. A variety of different compounds containing multiple C(sp^3)–H bonds and different functional groups were successfully fluorinated (Scheme 9). Free amide NH_2 groups were tolerated with good yield (as for **43**). Although free amine groups were not tolerated, their protection with a trifluoroacetyl group enabled monofluorination, for example, to give **34** (34%). The monofluorination of butyramide on a 25 mmol scale successfully afforded 1.0 g of **37** in 40% yield, compared to 47% on a 3.0 mmol scale (Scheme 10).

Tan and co-workers noticed the selectivity difference in Chen's previous report when NFSI and Selectfluor® were employed [198], which led them to propose that Selectfluor® is not only a fluorine source but that its radical cation participates as a HAT

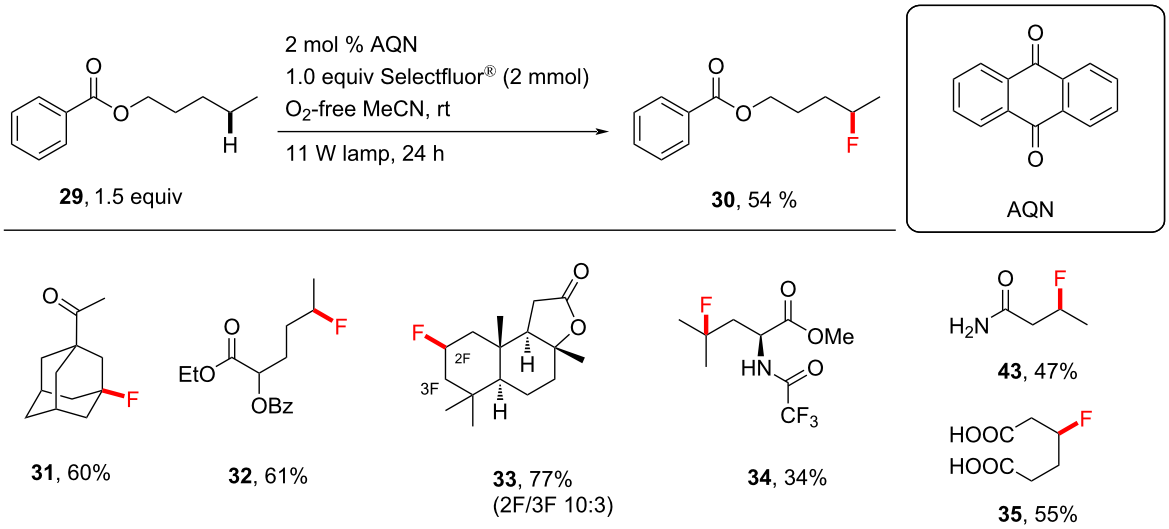

Scheme 9: Substrate scope of Tan's AQN-photosensitized C(sp^3)–H fluorination.

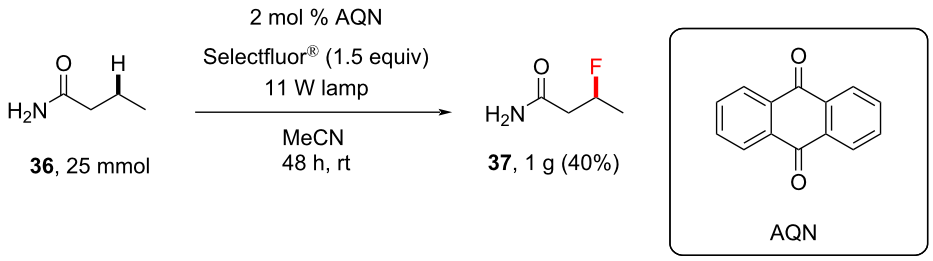

Scheme 10: AQN-photosensitized C–H fluorination reaction on a gram scale.

agent. When they substituted AQN (T_1 = 61.9 kcal·mol^{-1}) for 9-fluorenone (T_1 = 50.3 kcal·mol^{-1}) or alizarin red S (T_1 = 34.0 kcal·mol^{-1}), insignificant amounts of the fluorinated amyl benzoate **38** were formed. Since the triplet energy of AQN (2.7 eV) [200] is greater than/matched to the singlet–triplet energy gap of Selectfluor® (2.66 eV) but the triplet energy of 9-fluorenone (2.36 eV) [137] and alizarin red S are not, they proposed, for the first time, that TTET between AQN and Selectfluor® was the operating mechanism.

According to Tan's proposed mechanism at that time (Scheme 11), AQN is photoexcited by visible light and triplet ^{3}AQN* is generated upon ISC. TTET occurs between ^{3}AQN* and Selectfluor® to afford triplet ^{3}[Selectfluor®]* that has a notably longer N–F bond (2.73 Å) compared to singlet Selectfluor® (N–F = 1.37 Å, Figure 9). After the immediate dissociation of triplet Selectfluor®, the formed Selectfluor® *N*-radical cation undergoes HAT with the substrate to afford an alkyl radical. The authors deemed a complex between AQN and fluorine (AQN + F) more plausible than the formation of fluorine radicals. The generated alkyl radical could abstract fluorine atoms either from i) the AQN–F complex to regenerate AQN or ii) Selectfluor® to regenerate the Selectfluor® radical cation and thereby propagate a chain reaction.

Following shortly after Tan's report, Chen and co-workers disclosed the direct C–H fluorination [201] of unactivated alkyl C(sp^3)–H bonds using acetophenone as a PSCat, which was

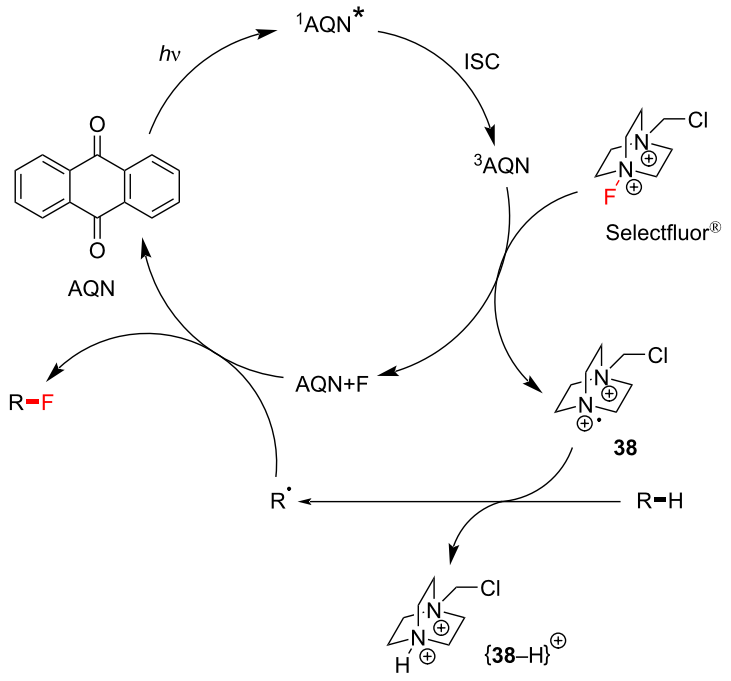

Scheme 11: Reaction mechanism of the AQN-assisted fluorination.

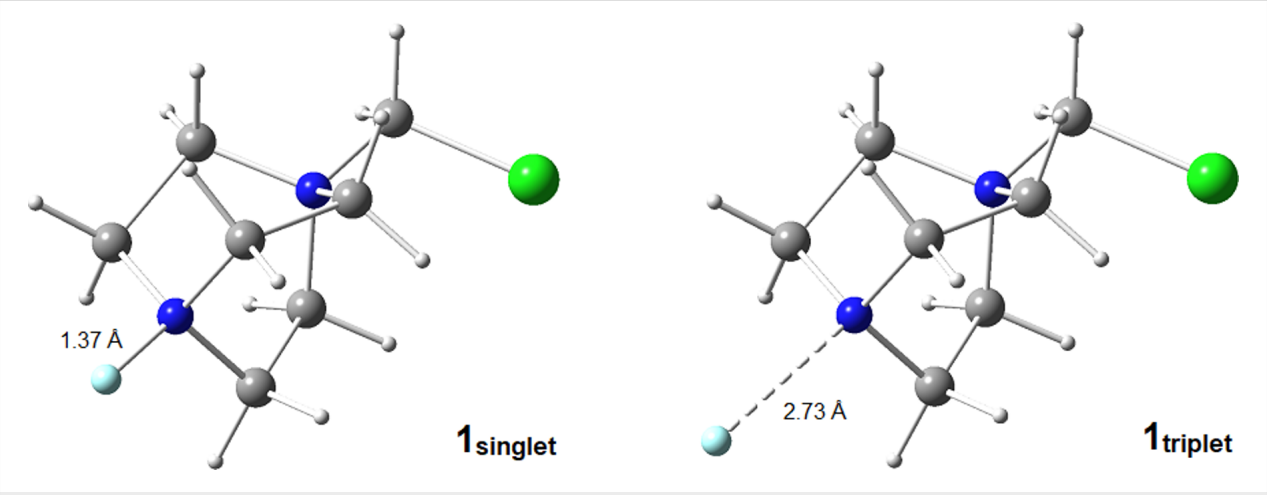

Figure 9: 3D structures of the singlet ground and triplet excited states of Selectfluor®.

photoexcited by near-UV light (375–400 nm, Scheme 12). In the absence of a PSCat and using dedicated UV-light irradiation (275–375 nm), the product was observed together with numerous decomposition products (Scheme 13). No reaction was observed using a 19 W CFL bulb in the absence of a PSCat. Despite acetophenone being a colorless oil with only trace absorption above 375 nm (an n–π* transition corresponding to a photon of 325 nm), it successfully functioned as a PSCat, undergoing photoexcitation by a CFL to afford the C(sp^3)–H fluorinated product in 85% yield (Scheme 13). Through the use of longpass filters, the authors found that wavelengths between 370–400 nm were necessary for the reaction to proceed.

The authors then subjected cyclohexane (**39**) to similar conditions to examine the choice of the PSCat. Acetophenone derivatives as well as benzaldehyde, 9-fluorenone, benzophenone derivatives and xanthone were all examined with respect to catalytic loadings (5 mol %), and acetophenone remained the most effective. Despite having stronger absorption bands than acetophenone at visible wavelengths (>400 nm), 9-fluorenone and

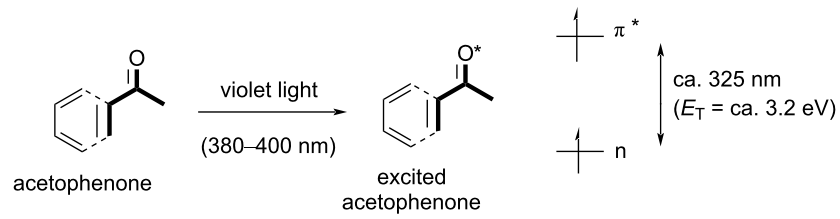

Scheme 12: Associated transitions for the activation of acetophenone by violet light.

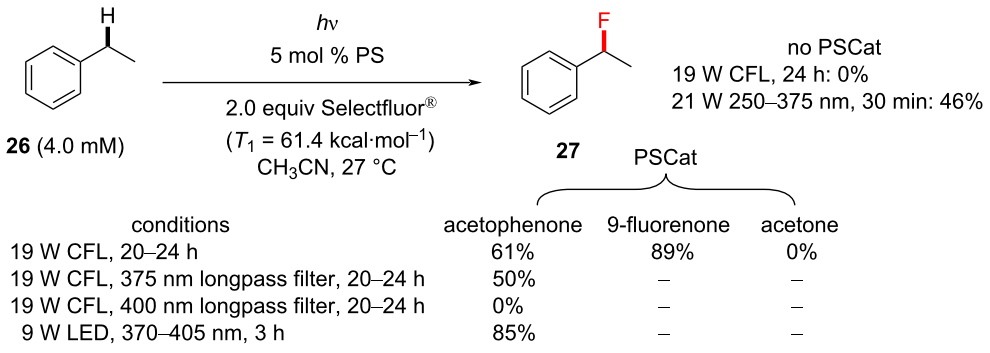

Scheme 13: Ethylbenzene C–H fluorination with various PSCats and conditions.

benzophenone were in fact less effective. The authors rationalized the different efficacies of the PSCats by their different n–π* energy gaps, of which acetophenone was among the largest and gave the highest yield of **40**. Scheme 14 shows the influence of T_1 on the increasing yield of **40**. It was found that decreasing the substrate loading below 1.5 equiv was detrimental to the yield, so 1.5 equiv of the substrate was chosen as optimal. A variety of unactivated C(sp^3)–H-containing substrates were monofluorinated in good to excellent yields (55–85%), obtaining the products **41**–**44** (Scheme 15).

Chen and co-workers maintained that their reaction proceeded via HAT between the excited-state ketone and the C(sp^3)–H-containing substrate. However, a PS TTET mechanism still could not be ruled out when Selectfluor® is present. That 9-fluorenone gave no reaction in Tan's initial report [198] indeed presents a challenge to rationalizing Chen's fluorinations of benzylic or unactivated C(sp^3)–H bonds as PS TTET processes, giving credibility to a photoexcited HAT process. Herein, we note the convincing trend between the T_1 energy and the reaction yield in their screening of PSCats (Scheme 14). However, the differences in the light sources and a radical-chain mechanism [202], which is initiated by PS TTET, cannot be conclusively ruled out.

3.2.2 C(sp^3)–H fluorination selectivity: Another facet that suggests a similar general mechanism is the C(sp^3)–H fluorination selectivity. One might expect excited triplet states to be much more reactive and less selective than the Selectfluor® radical cation. The selectivity in both Chen's and Tan's report is depicted in Figure 10. In both reaction conditions, employing either acetophenone or AQN as PSCat, the most electron-rich, or "hydridic" C(sp^3)–H bond that forms a secondary radical is predominantly fluorinated. This indicates that these reactions

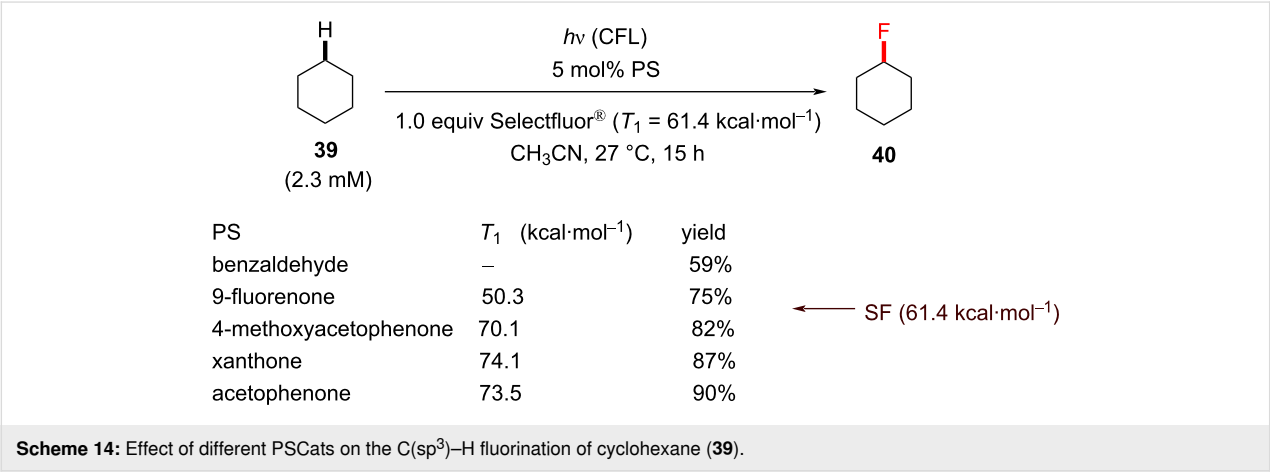

Scheme 14: Effect of different PSCats on the C(sp^3)–H fluorination of cyclohexane (**39**).

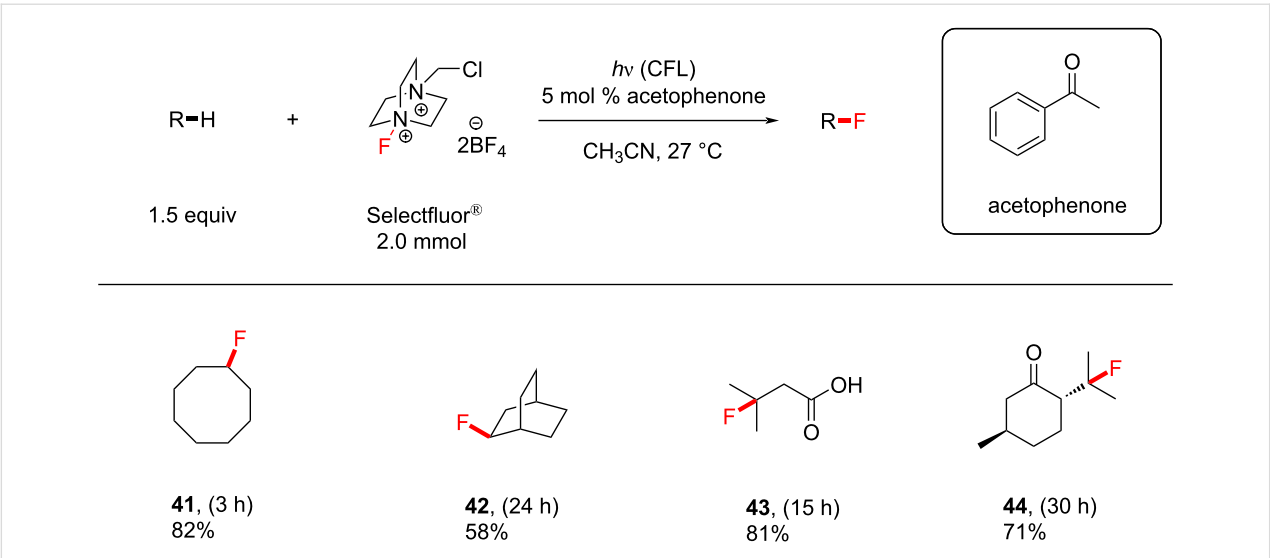

Scheme 15: Reaction scope of Chen's acetophenone-photosensitized C(sp^3)–H fluorination reaction.

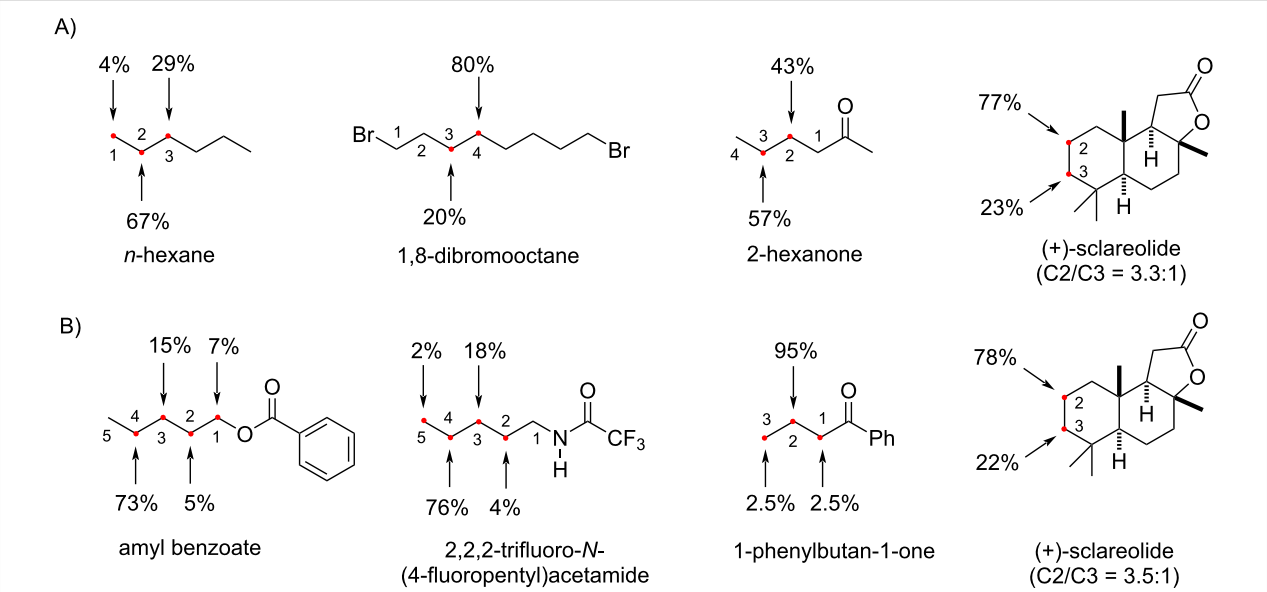

Figure 10: a) Site-selectivity of Chen's acetophenone-photosensitized C–H fluorination reaction [201]. b) Site-selectivity of Tan's AQN-photosensitized C–H fluorination reaction [198].

operate by HAT, which is directed by polarity matching effects [58-60]. For example, *n*-hexane is mainly fluorinated at its C2 position (67%) and only 4% fluorination at C1 occurs [201], due to the instability of the primary radical (Figure 10). The selective fluorination of C2 over C3 may be rationalized by steric effects (rather than polarity matching), which are reported for quinuclidinium radical cations [203].

A similar selectivity for the most hydridic C(sp^3)–H bond was observed for amyl benzoate, a trifluoroacetylated pentylamine [198] and 1,8-dibromooctane [201]. 2-Hexanone was fluorinated with a slightly higher selectivity for C3 over C2 fluorination [201]. Interestingly, 1-phenylbutan-1-one gave nearly exclusive C2 fluorination [198]. Both fluorination positions of (+)-sclareolide (C2 and C3) are remote from the lactone EWG and both form secondary radicals. Thus, the fluorination of these positions is presumably dictated by hindrance, given that the C3 position is neighbored by a *gem*-dimethyl group and is fluorinated to a lesser extent (22%). In both reports, the C2/C3 selectivity for the photochemical monofluorination of (+)-sclareolide was identical, suggesting a similar mechanism behind the HAT and FAT processes. This parallels the C2/C3 selectivity for the electrochemical fluorination of (+)-sclareolide, proposed to involve a Selectfluor® radical cation [204].

3.2.3 C(sp^3)–H fluorination mechanistic studies: In order to unearth a greater understanding of their previously-reported photosensitized C(sp^3)–H fluorination, Tan, Lu, Soo and co-workers employed a nanosecond-scale transient absorption (TA) spectroscopy and time-dependent density functional theory (TDDFT) calculations [199]. They were able to experimentally demonstrate, for the first time, that the reaction between photoexcited AQN and Selectfluor® afforded a transient AQN–Selectfluor® triplet exciplex species by calculating the predicted TDDFT absorption spectrum that matched with the experimentally obtained TA spectra. The direct reaction between AQN and the substrate was not observed by TAS. The authors' DFT calculations revealed reaction pathways that were thermodynamically and kinetically plausible. Initially, AQN and Selectfluor® (S_0 in Scheme 16) form a van der Waals complex RC1, which is markedly more stable than its two individual components. Instead of the photoexcitation of AQN, photoexcitation of RC1 by a 369 nm photon (77.5 kcal·mol^{-1}) affords the short-lived excited singlet state of RC1, S_1 (Scheme 16). Nonradiative ISC occurs from S_1 to yield the excited triplet state of RC1 (T_1), and a spontaneous intramolecular reorganization process affords the AQN–Selectfluor® exciplex Int1.

The AQN–Selectfluor® exciplex Int 1 possesses a longer N–F bond distance (1.98 Å) compared to the N–F bond distance (1.37 Å) of Selectfluor® (Scheme 17). This indicates that the fluorine atom in the exciplex is stabilized by the aromatic system of AQN and that the N–F bond becomes more labile. In this exciplex, the spin density is delocalized mostly over the AQN–F moiety (61%), and the absorption band depends mainly on the AQN–F interactions. Thus, the authors concluded that the TA spectra should not depend on the electrophilic fluorinating source. Thereafter, the AQN–Selectfluor® exciplex abstracts a hydrogen atom from the C3 position of pentane to

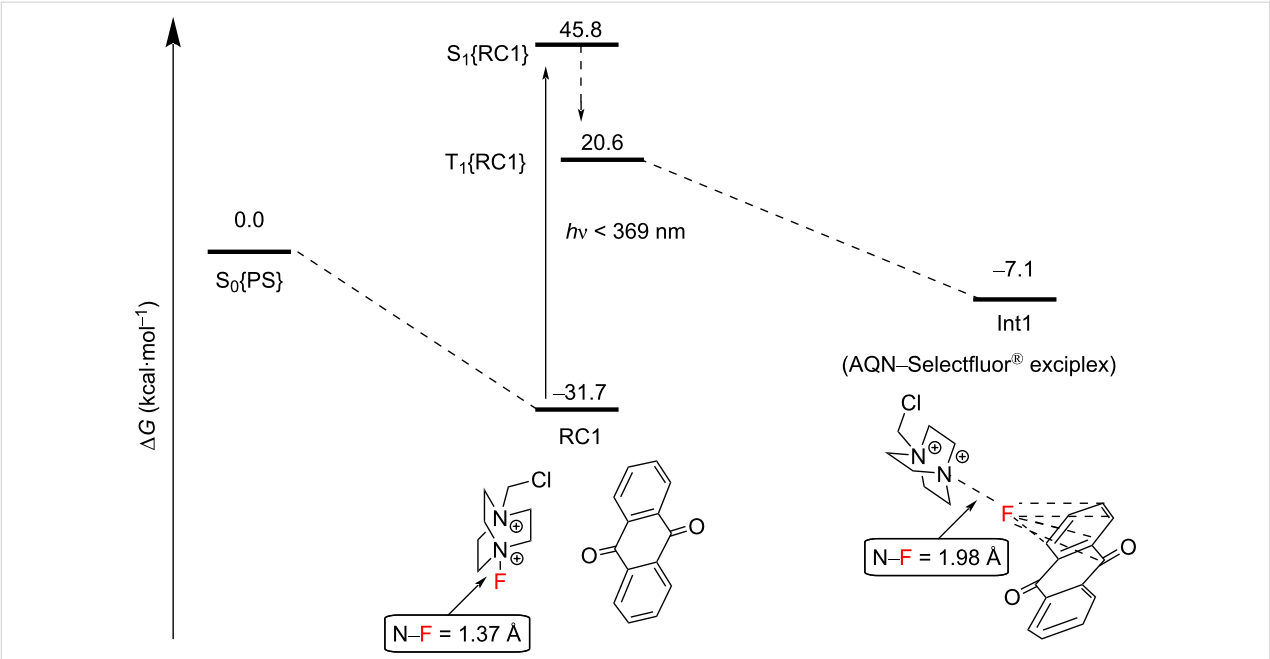

Scheme 16: Formation of the AQN–Selectfluor® exciplex Int1.

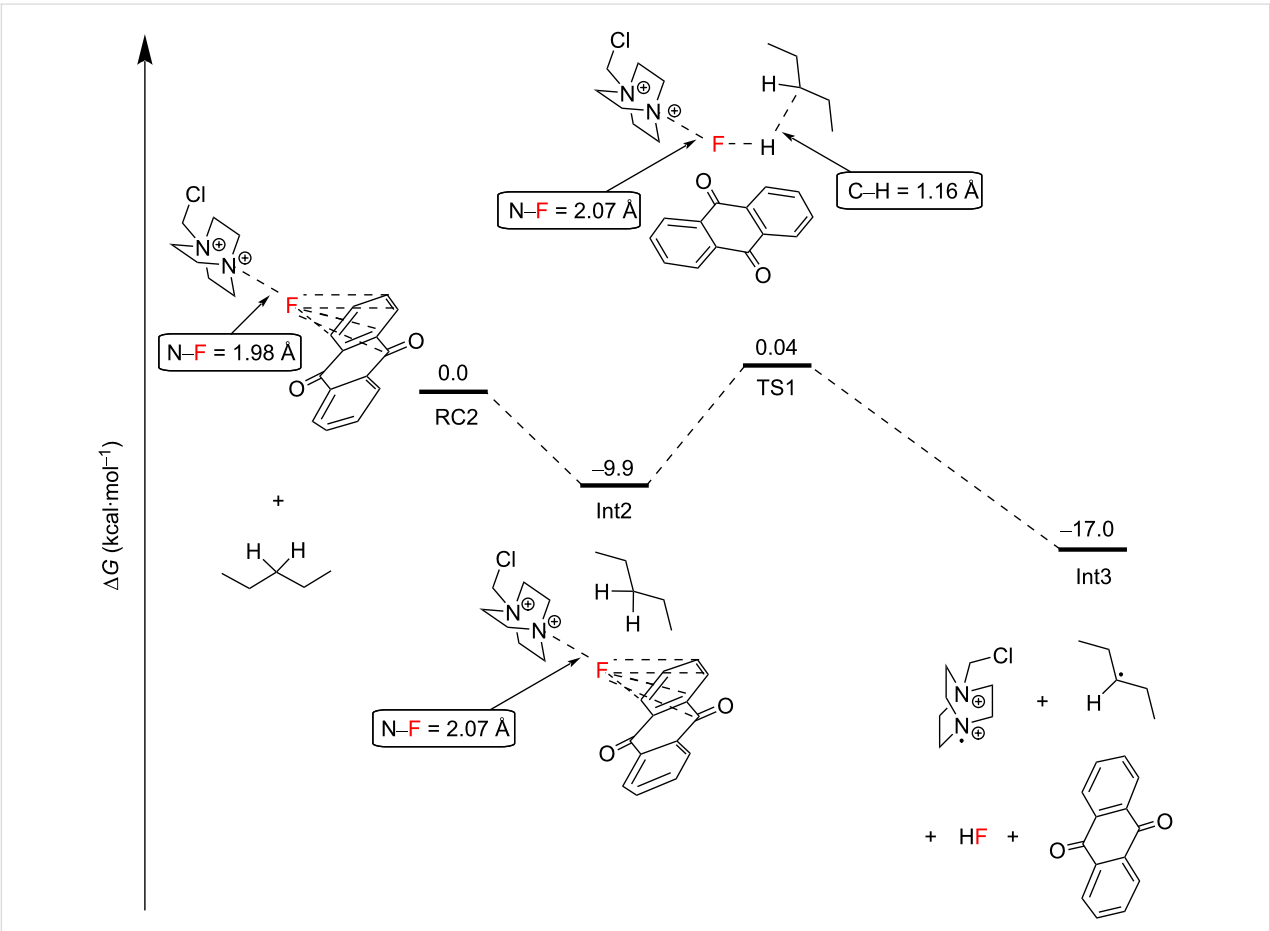

Scheme 17: Generation of the C3 2° pentane radical and the Selectfluor® *N*-radical cation from the exciplex.

form a secondary radical, a Selectfluor® *N*-radical cation, HF and AQN. The activation energy barrier relative to RC2 was only 9.9 kcal·mol^{-1} (Scheme 17).

The Selectfluor® *N*-radical cation can abstract a hydrogen atom from the C3 2° C–H bond of another pentane molecule in an overall exergonic process with an activation energy barrier of 2.0 kcal·mol^{-1} from Int4 to afford Int5 and ultimately Int6 (Scheme 18). The authors did not mention the possibility of a mechanism whereby the excitation of the complex RC1 directly allowed N–F cleavage to form the Selectfluor® radical cation. The reaction of the C3 2° pentane radical with Selectfluor® in an FAT was exergonic, with an energy barrier of 7.6 kcal·mol^{-1} relative to Int7, affording Int8 (Scheme 19). Since the Select-

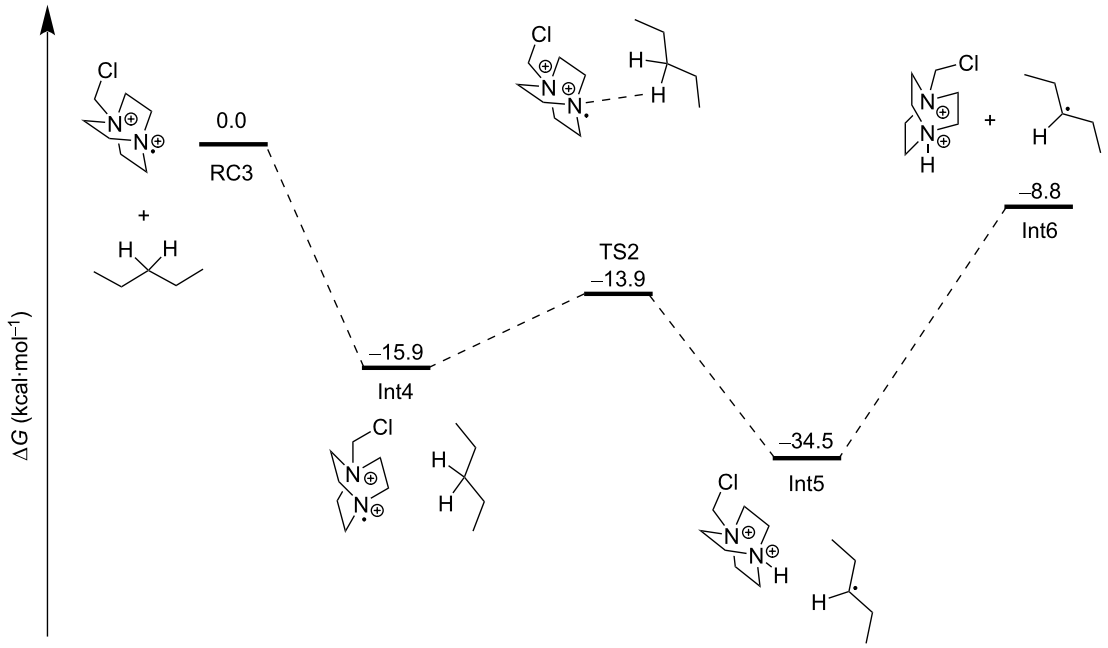

Scheme 18: Hydrogen atom abstraction by the Selectfluor® *N*-radical cation from pentane to give the C3 2° pentane radical.

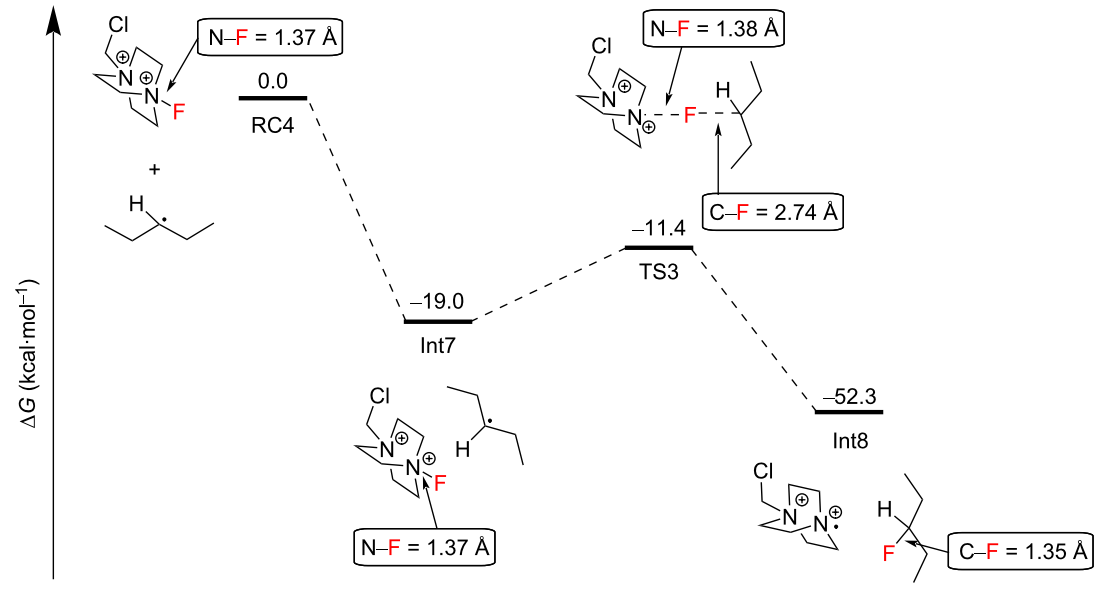

Scheme 19: Fluorine atom transfer from Selectfluor® to the C3 2° pentane radical to yield 3-fluoropentane and the Selectfluor® *N*-radical cation.

fluor® radical cation is regenerated here upon FAT, the authors considered the candidacy of the Selectfluor® radical cation as a chain carrier.

However, the quantum yield of the reaction was found to be only Φ = 0.13, strongly evidencing against a radical chain mechanism. The complexation of Selectfluor® with the PSCat in these reactions may inhibit its ability to participate in the propagation of a radical chain mechanism proposed for a complementary C(sp^3)–H fluorination method [204]. Alternatively, FAT between the AQN–Selectfluor® exciplex and the pentane C3 2° radical was found to be a highly exergonic process and could not be ruled out (Scheme 20).

3.3 Directing-group-guided C(sp^3)–H fluorination

3.3.1 Ketones as directing groups: Related to the curious near-exclusive C2 selectivity of 1-phenylbutan-1-one as reported by Tan and co-workers [198], Lectka and co-workers reported highly selective monofluorination of C(sp^3)–H bonds that are proximal (β- or γ-) to a carbonyl group [153] (Scheme 21); such selectivity was previously difficult to achieve with PS TTET fluorinations.

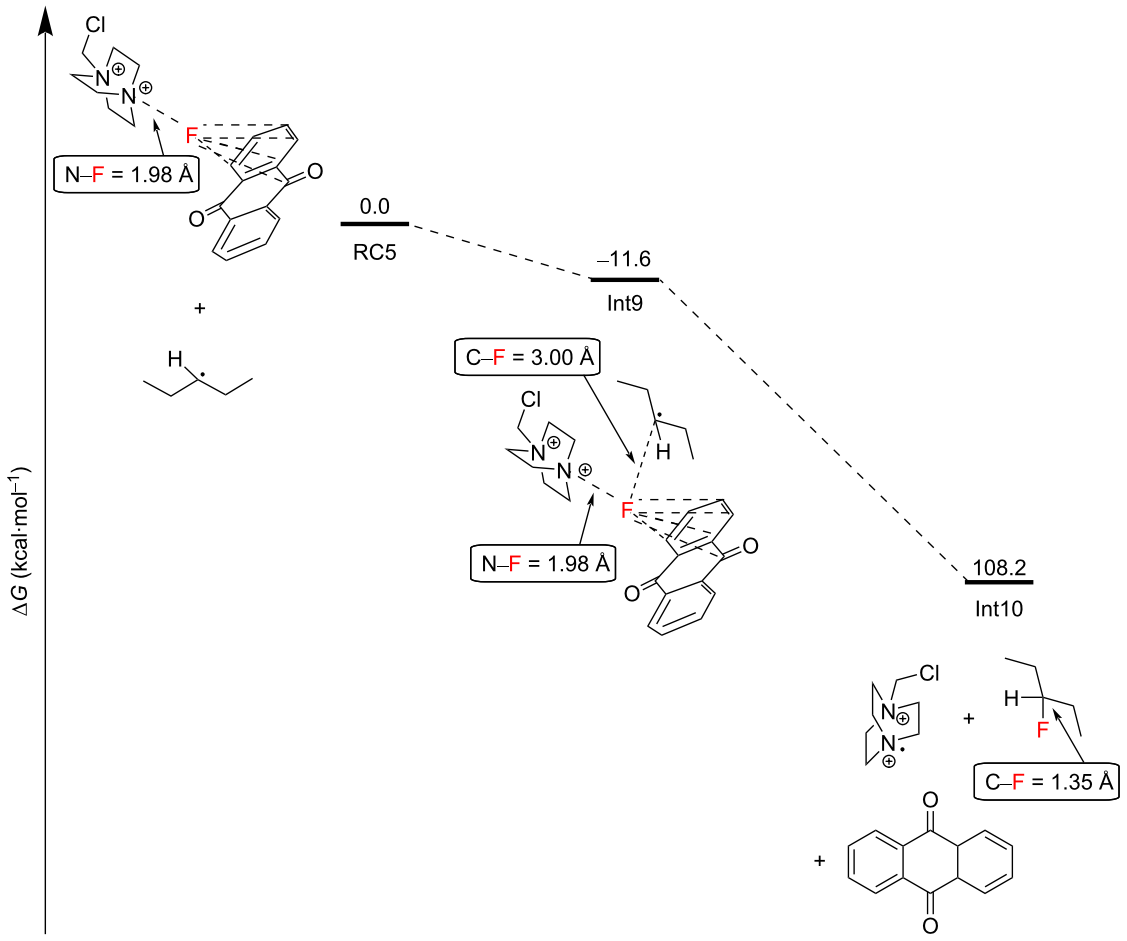

Scheme 20: Barrierless fluorine atom transfer from Int1 to the C3 2° pentane radical to yield 3-fluoropentane, AQN and the Selectfluor® *N*-radical cation.

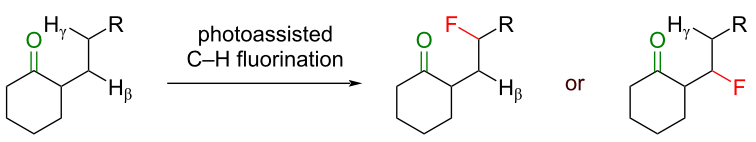

Scheme 21: Ketone-directed C(sp^3)–H fluorination.

The ketones, acting as directing groups, served as an elegant method to override the typical polarity matching-governed C(sp^3)–H fluorination [46,205]. The selectivity for β- or γ-fluorination could be attributed to an interaction of the breaking C(sp^3)–H bond and the neighboring ketone, which is part of the proposed 5- and 6-membered transition state, respectively. When the 5- and the 6-membered transition state is possible, the free rotation of the σ-bond between the carbonyl group and the α-position allows the fluorination of the β- or γ-position. A good practical example of such a competitive fluorination is progesterone, which was fluorinated at both the C12 (see **45**) and the C16 (see **46**) position in a 1.0:3.1 ratio (Scheme 22). Ideally, to achieve the best selectivity, the β- and the γ-position must be distinctive based on their geometric constraints. We note that the nature of the transition states in this ketone-directed C(sp^3)–H fluorination (and the subsequent carbonyl-directed C–H fluorinations) is not well-characterized, and we are tentative to draw firm conclusions on the regioselectivity of the C(sp^3)–H fluorination at this stage.

After screening several PSCats that absorb light >400 nm, such as benzophenone, 9-fluorenone, xanthone, 9,10-phenanthrenequinone and benzil, the highest yield (82%) was achieved with benzil (T_1 = 53.7 kcal·mol^{-1}, Scheme 23). Control reac-

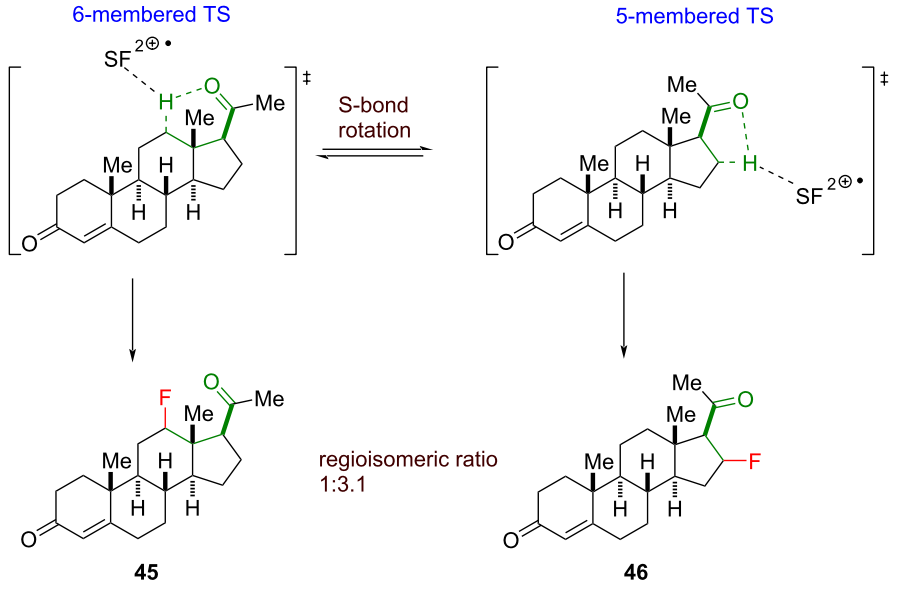

Scheme 22: Ketone-directed fluorination through a 5- and a 6-membered transition state, respectively.

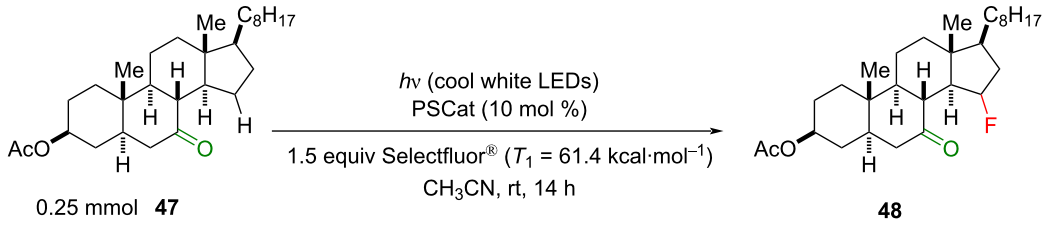

PSCat	T_1 (kcal·mol^{-1})	yield
9,10-phenanthrenequinone	46.1	54%
9-fluorenone	50.3	trace
benzil	53.7	82% ← SF (61.4 kcal·mol^{-1})
benzophenone	69.2	trace
xanthone	74.1	trace

Scheme 23: Effect of different PSCats on the photosensitized C(sp^3)–H fluorination of **47**.

tions revealed that Selectfluor® as the fluorinating agent gave the highest product yield, and light was essential for the reaction. To demonstrate the importance of the ketone directing group, ethylbenzene was employed under the same reaction conditions and no fluorinated product was observed, contrary to Chen's previous report [201].

The monofluorination of different classes of ketones, including 3° alkyl compounds or benzylic cyclohexanones, bicyclic ketones and steroidal ketones was achieved in moderate to excellent (43–85%) yield (**48**–**55**, Scheme 24), demonstrating the power of this method for LSF, especially given the biological activity and prevalence of steroids, such as cholesterol, progesterone and testosterone. Interestingly, under their conditions, 2-heptanone, 2-decanone and 2-dodecanone as the substrates gave in each case a distribution of fluorinated products, with a large preference for fluorination at the penultimate carbon (that would form a secondary radical), consistent with the polarity matching selectivity shown previously (Figure 10) [198,201].

Lectka and co-workers pointed out that the triplet energy of aliphatic ketones (79.4 kcal·mol^{-1} for acetone, Table 1) is too high to allow TTET from benzil and therefore triplet excited state intramolecular HAT of the substrate. They rationalized the distribution of the fluorinated products as a result of a radical chain reaction and suggested that linear ketones may promote cage escape of the Selectfluor® radical cation to participate in this mechanism, in contrast to cyclic ketones. Under light-free conditions initiated by triethylborane (BEt_3), they observed an identical monofluorination selectivity, which suggested the same intermediate (Selectfluor® radical cation) in each case. Since these BEt_3-initiated conditions are known to effect SET, they justified that the mechanism may occur through a PRC mechanism involving SET from the benzil triplet state to Selectfluor®. Given the lack of relationship between the T_1 energy of the PSCats and the product yield in their optimization, this is a plausible suggestion. However, the lack of reactivity of certain PSCats due to them absorbing different visible (white LED) wavelengths cannot be ruled out.

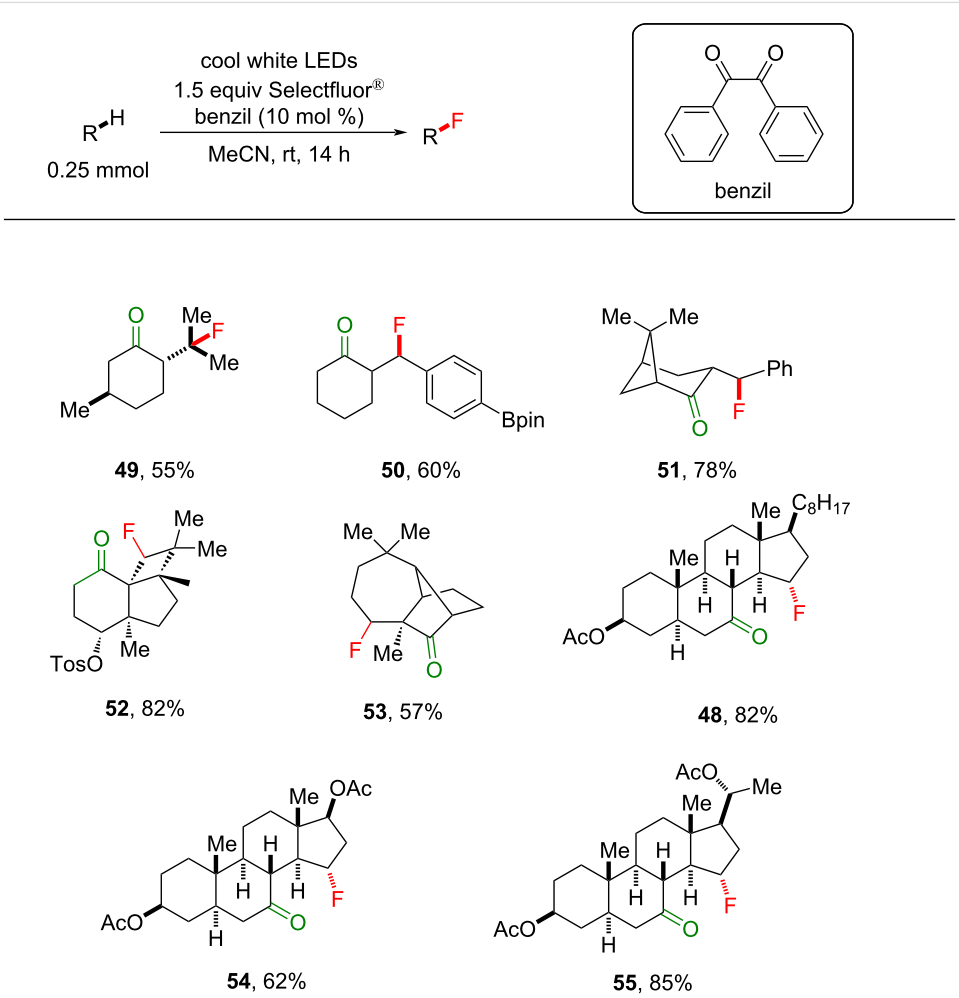

Scheme 24: Substrate scope of benzil-photoassisted C(sp^3)–H fluorinations.

3.3.2 Enones as directing groups: Related to, and following their observations with cyclic ketone-containing substrates, Lectka and co-workers reported that enones also served as directing groups for PS TTET fluorinations [206]. C(sp^3)–H bonds that were proximal (5 or 6 carbon atoms away) or distal (5 or 6 carbon atoms away) from the enone underwent C(sp^3)–H fluorination to afford the products **56**–**59** in modest to very good yield (40–86%), with a high selectivity (Scheme 25). As before, a nonphotochemical reaction with Selectfluor® and BEt_3 provided a similar selectivity, corroborating the Selectfluor® radical cation as an intermediate and suggesting that an SET mechanism may be possible.

3.3.3 Ketals as directing groups: Very recently, Lectka, Dudding and co-workers reported the regioselective C(sp^3)–H fluorination of acetonide ketals (Scheme 26A) [205]. C(sp^3)–H bonds α to ketal oxygen atoms were fluorinated with surprisingly high selectivity to afford the products **60**–**63** in moderate to excellent yield (41–91%, Scheme 26B). The reaction conditions were also amenable to carbamates, affording the products **64**–**67** in moderate to good yield (42–58%). That the carbamate oxygen atom could direct the fluorination α to itself instead of α to the amide nitrogen atom provided an inverted, complementary selectivity as expected from the electrochemical oxidation (Scheme 26C).

When the ketals were not fused to a central ring, the least-hindered C(sp^3)–H bond reacted, as in the products **61** and **62**. When the ketals were fused to a central ring, as in galactose acetonide, the C2 position underwent a selective C(sp^3)–H fluorination. The authors demonstrated that the transition state for Selectfluor® undergoing HAT at this position (see **TS1**)

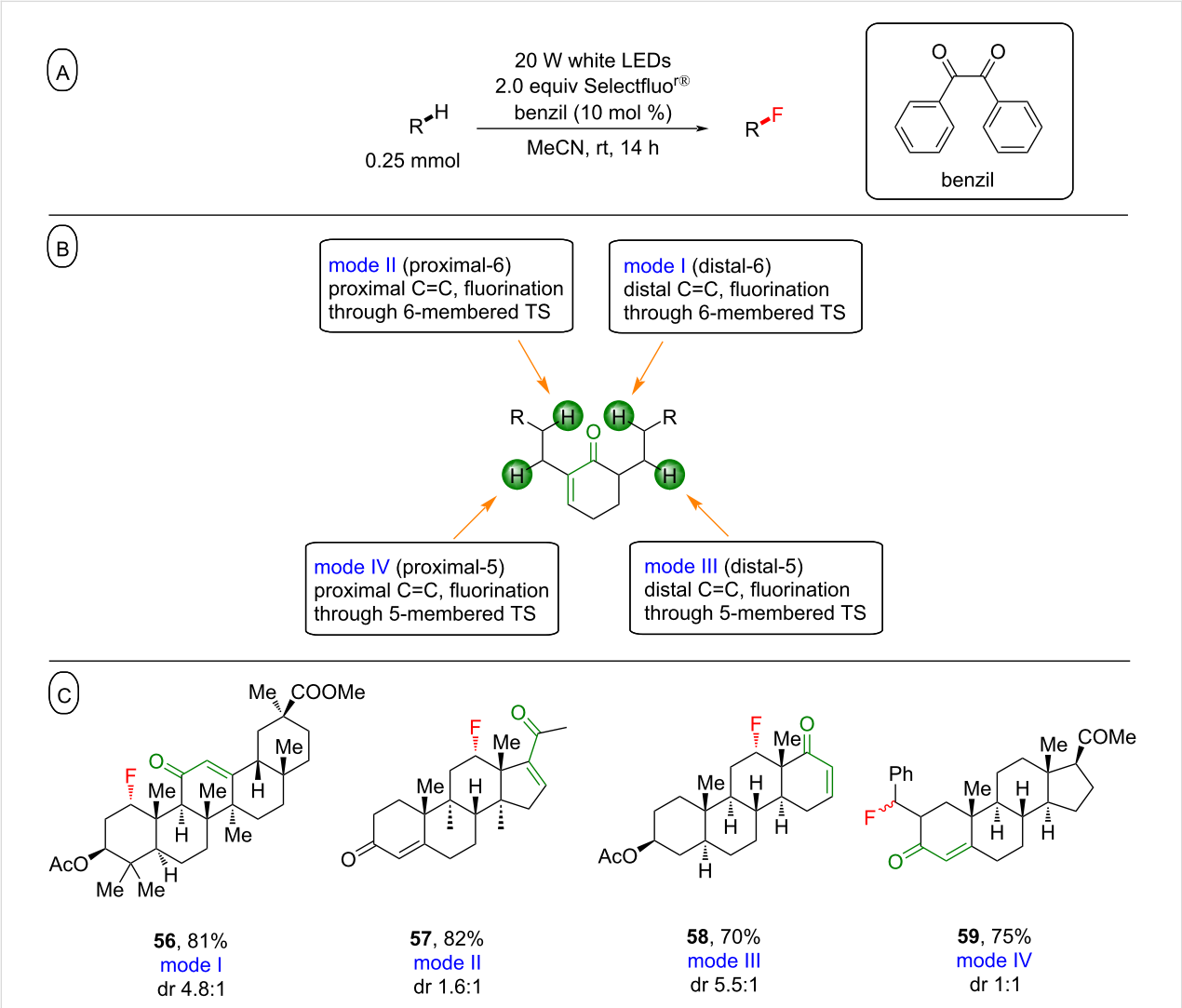

Scheme 25: A) Benzil-photoassisted enone-directed C(sp^3)–H fluorination. B) Classification of the reaction modes and transition states to rationalize the site-selectivity. C) C–H fluorination site-selectivity.

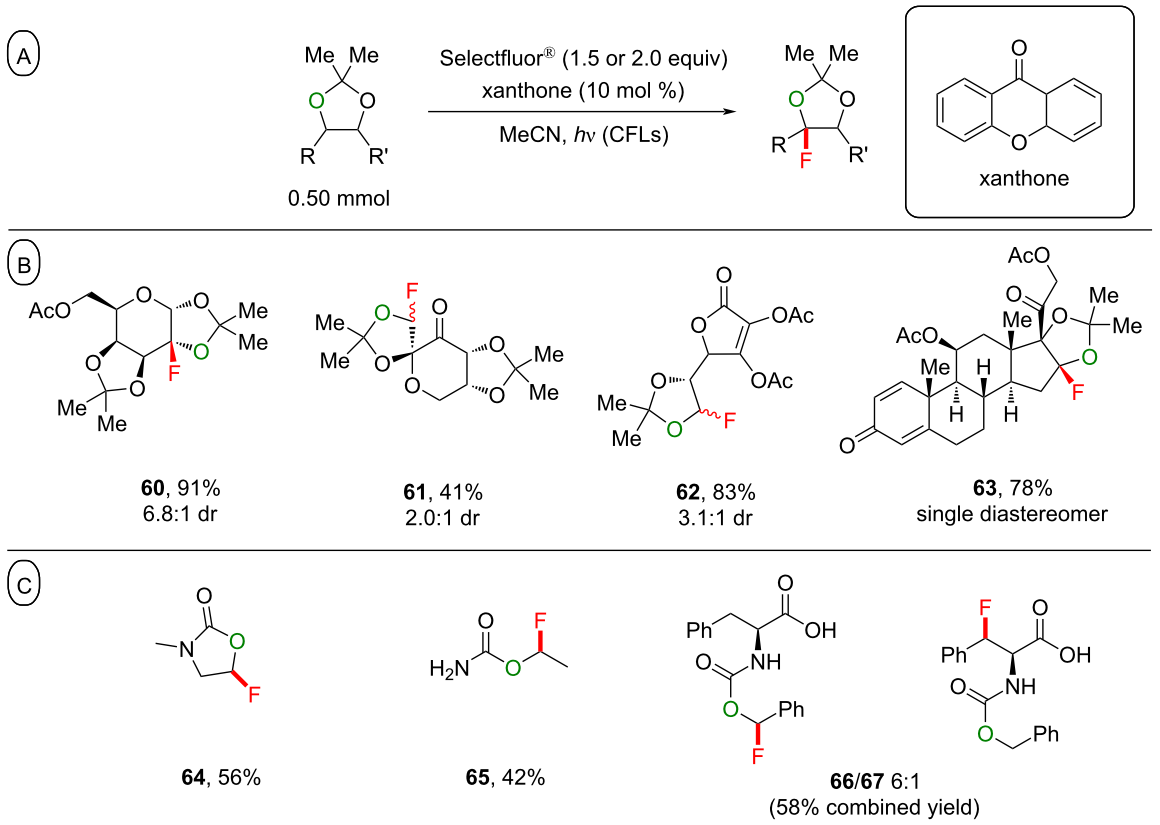

Scheme 26: A) Xanthone-photoassisted ketal-directed C(sp^3)–H fluorination. B) Substrate scope. C) C–H fluorination site-selectivity.

was more kinetically accessible, despite the bond dissociate free energies (BDFEs) suggesting C3 functionalization (Scheme 27).

3.4 Directing-group-guided benzylic C–H fluorination

In another report [207], Lectka and co-workers achieved selective monofluorination of the benzylic C–H bonds of phenylalanine- and tyrosine-like residues in peptides under visible-light photosensitization. After screening a variety of sensitizers, such as 1,2,4,5-tetracyanobenzene, AQN, 1,4-dicyanobenzene, 1-cyanonaphthalene, 9,10-phenanthrenequinone, xanthone, 2,7-dichloro-9-fluorenone, 9-fluorenone, benzophenone, 2-bromo-9-fluorenone and 2-chlorothioxanthone, 5-debenzosuberenone afforded the best yield of **69** (73%, Scheme 28).

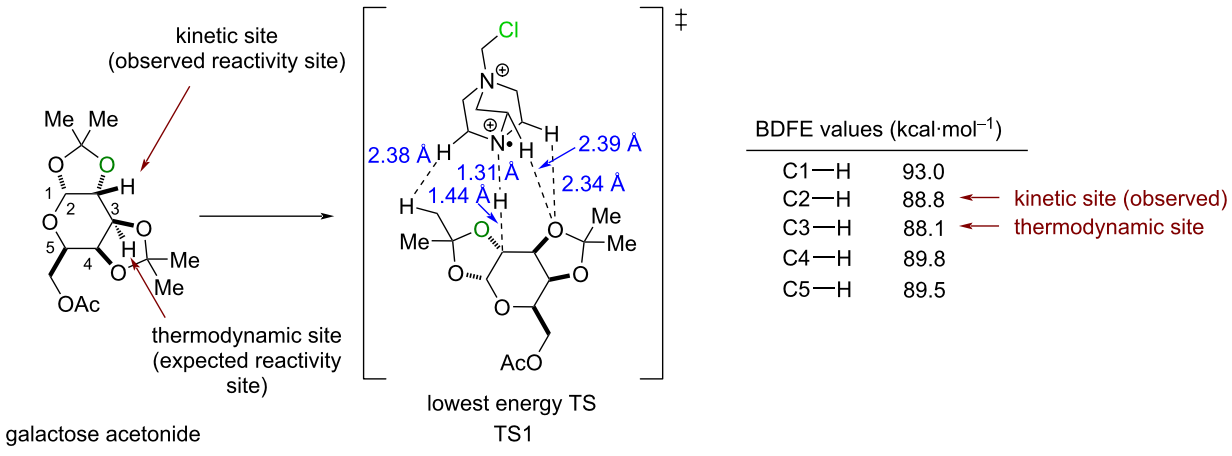

Scheme 27: Rationale for the selective HAT at the C2 C–H bond of galactose acetonide.

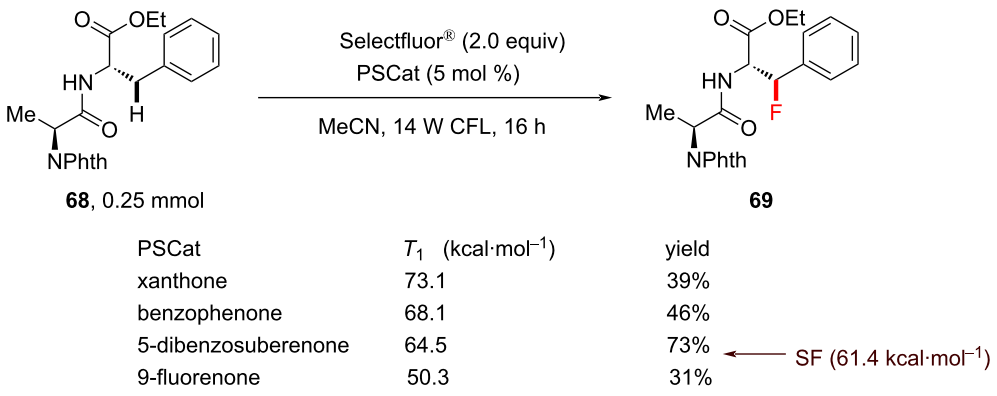

Scheme 28: Photosensitized C(sp^3)–H benzylic fluorination of a peptide using different PSCats.

In the presence of protected basic, acidic and nonpolar side chains, benzylic fluorination was achieved with exclusive regioselectivity in peptides, with modest to moderate diastereomeric ratios of the fluorinated products (Scheme 29). With the optimum PSCat in hand, it was necessary to find a protecting group (PG) for the amine that would not undergo fluorination or oxidation when treated with Selectfluor® [153]. The authors justified the use of protecting groups due to their extensive use in peptide synthesis. Of all the PGs tested, phthalimide (Phth)- and trifluoroacetate (TFA)-protected substrates underwent photosensitized C–H fluorination to give the highest yield of 80% and 71% of the respective products. Employing the optimum reaction conditions, Lectka and co-workers fluorinated phenylalanine-containing di- and tripeptides to give the products **70a–f** in modest to excellent yield (34–84%, Scheme 29). The carboxylic acid function could be free or pro-

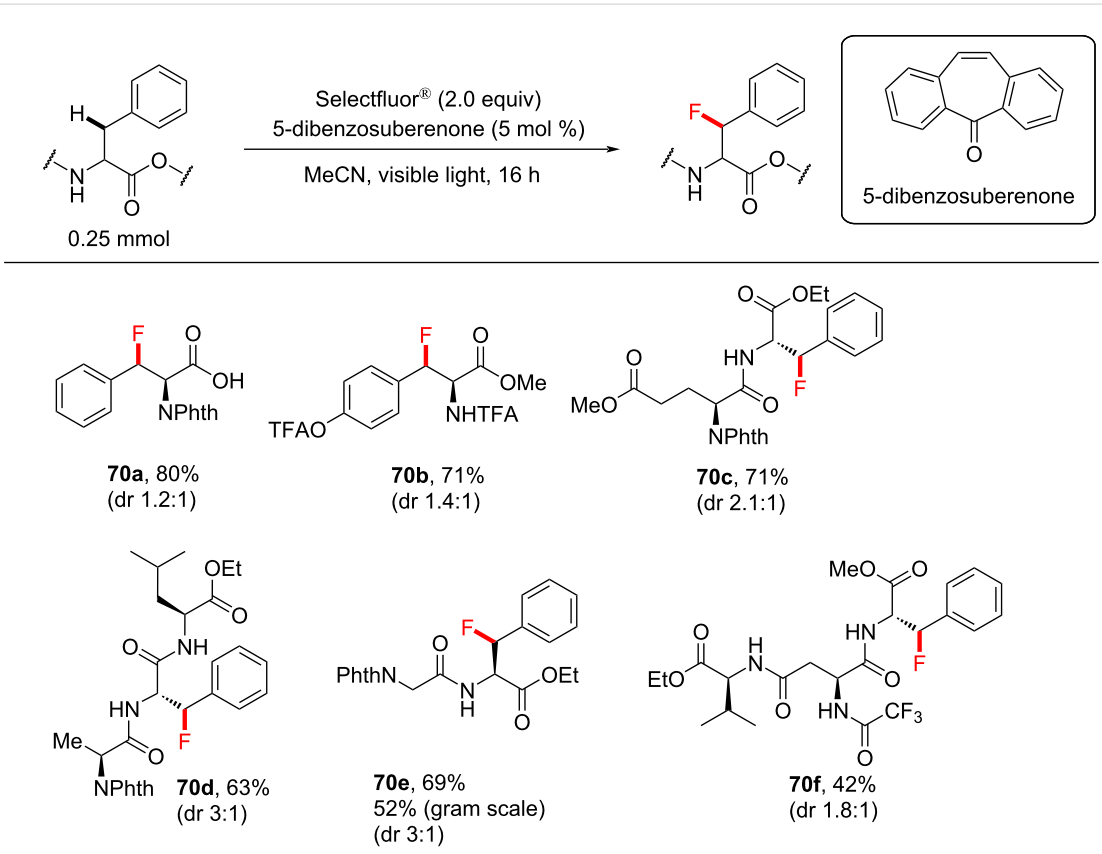

Scheme 29: Peptide scope of 5-benzosuberenone-photoassisted C(sp^3)–H fluorinations.

tected as an ester without noticeable differences in the product yield.

A mechanism was not proposed in this study. The highest yield was obtained when the T_1 energy of the PSCats and Selectfluor® matched closely, suggesting that PS TTET may occur. However, a PRC mechanism involving SET cannot be ruled out, which the authors reported previously for benzylic fluorination [130]. In a later perspective [36], the authors speculated that the amide served as a directing group. Indeed, in situ-formed ammonium carbamates were recently identified to direct the HAT of a quinuclidinium radical cation [208].

3.5 Scalability of C–H fluorinations

That the yields of gram-scale photosensitized C(sp^3)–H fluorinations (Scheme 8 and Scheme 10) did not decrease indicates a fundamental advantage of PS TTET chemistry vs PRC; the low extinction coefficients of small-molecule PSCats in the near-UV to visible region (380–420 nm). In this respect, PS TTET photochemistry with near-UV behaves similar to UV photochemistry. On the other hand, photocatalysts typically used in PRC possess very high extinction coefficients, leading to a strong visible light absorption and reactions that suffer more on a scale-up due to the exponential relationship between the transmitted intensity of the light and the extinction coefficient, as described by the Beer–Lambert law (Equation 1).

$$A = \log_{10} \cdot \frac{I_0}{I} = \varepsilon \cdot l \cdot c \qquad (1)$$

Rearranging for I (Equation 2) and solving for a typical PSCat concentration (a reaction mixture of 0.1 M with 5 mol % PSCat; c = 5.0 mM) and the molar extinction coefficient for 9-fluorenone (ε = 270 $M^{-1}{\cdot}cm^{-1}$ at 383 nm) [209,210] reveals a path length of l = 0.74 cm at which distance (from the surface) 90% of the light is absorbed. In comparison, a PRC reaction at the same concentration (c = 5.0 mM) involving the prototypical catalyst $[Ru(bpy)_3]Cl_2$ (ε = 11280 $M^{-1}{\cdot}cm^{-1}$ at 452 nm) gives a path length of l = 17.7 mm at which distance (from the surface) 90% of the light is absorbed.

$$l = \frac{\log_{10} \cdot \frac{I_0}{I}}{\varepsilon \cdot c} \qquad (2)$$

Flow chemistry provides an elegant means for scaling photochemical reactions [211-214], primarily due to the shorter path lengths for light transmission provided by flowing the reaction mixture through small-diameter (μm–mm) channels. Lectka and co-workers reported the processing of their benzil-photosensitized enone-directed C(sp^3)–H fluorination in a custom-built flow reactor, comprised of a syringe pump, a coil of fluorinated ethylene propylene (FEP) tubing (7.5 m; inner diameter 1.6 mm; outer diameter 3.2 mm; representing a 15 mL internal volume) and 6 × 20 W 72-LED work light sources (white LEDs, Scheme 30). The reaction mixture (a 12 mL slug) was pumped through. After 4 h, the coil was flushed through with MeCN to collect all of the reaction mixture.

In the synthesis of **71**, the flow method gave, after 4 h, a similar (if slightly lower) yield vs the batch method after 14 h, reflecting a ≈ 3 times higher mass productivity. The benefit of flow photochemistry was not as obvious here compared to the batch due to the tolerance of the PS TTET batch reactions to scale-up on a laboratory scale (thanks to the low extinction coefficients as mentioned above). However, batch reactors larger than having centimeter-order diameters would begin to suffer issues, and the benefits of flow photochemistry are expected to manifest toward industrial-scale applications.

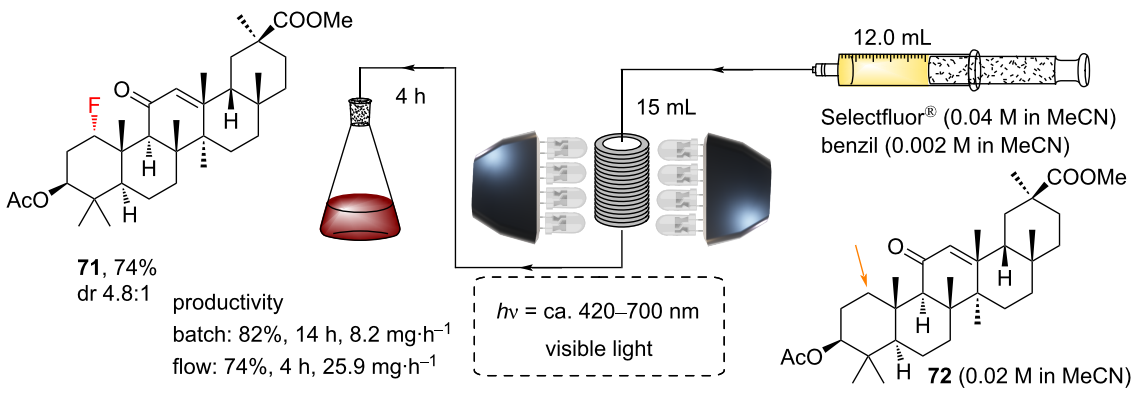

Scheme 30: Continuous flow PS TTET monofluorination of **72**.

4 C–H fluorination of visible-light-active molecules via photosensitization auxiliaries (PSXs)

Egami, Hamashima and co-workers discovered the photoinduced fluorination of phthalimide derivatives without an exogenous PSCat (Scheme 31) [147]. Here, phthalimide serves as a PSX by absorbing 320–360 nm light, corresponding to its n–π* transition [215] and a triplet energy of T_1 = 3.1 eV = 71.5 kcal·mol^{-1} [148]. The authors found that 365 nm LEDs and Selectfluor® facilitated the direct C–H fluorination of *N*-butylphthalimide (**73**) in MeCN without an exogenous PSCat to give a 78% yield of the fluorinated product **74** (Scheme 31). While 395 nm was still effective, 425 nm and the absence of light gave no product.

N-substituted phthalimides with alkyl chains underwent monofluorination at the most "hydridic" C(sp^3)–H position, including 3° alkyl and benzylic positions, in moderate to near-quantitative (42–98%) yield. The functional group tolerance was not explored to a large extent; esters tolerated the reaction conditions (Scheme 32). The success and selectivity of the C–H fluorination of the *N*-alkylphthalimides depended strongly on the alkyl chain length. *N*-Pentylphthalimide gave the compounds **75a** and **75b** in a 3.2:1 ratio of the C4-/C3-monofluorinated product, *N*-propylphthalimide reacted to give a moderate yield of **75g** (47%) at the β-position, and *N*-ethylphthalimide (**75h**) gave no reaction (Scheme 32). The authors suggested that the C–H BDFE could explain the direction of the selectivity to the position furthest from the phthalimide, which formed the

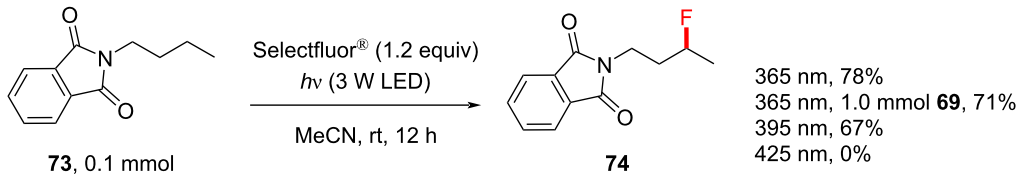

Scheme 31: Photosensitized C–H fluorination of *N*-butylphthalimide as a PSX.

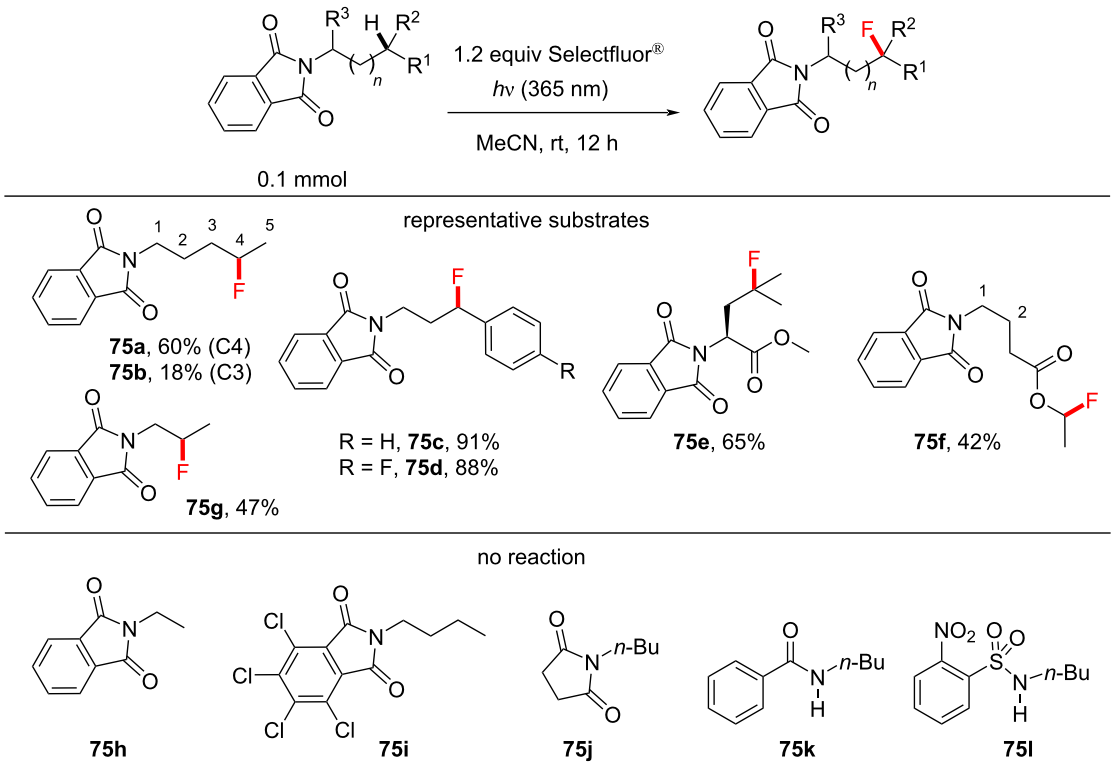

Scheme 32: Substrate scope and limitations of the PSX C(sp^3)–H monofluorination.

most stable radical, although we note that the selectivity in the fluorination of *N*-pentylphthalimide mirrored the selectivity of previous reports [198,201], which could be explained by polarity matching of the most "hydridic" C–H bond.

One notable difference was the product **75f**, where fluorination occurred α to the ester oxygen atom, in contrast to the aforementioned PS TTET fluorination of the amyl benzoate **29**. One could speculate that an initial polarity matching-favored HAT at the C2 position might facilitate an intramolecular 1,5-HAT to generate a more stable radical for FAT. In order to examine the necessity of the phthalimide moiety in such reactions, the authors substituted it with nosyl, benzamide and succinimide groups, yet none of these molecules underwent a C(sp^3)–H fluorination of the *n*-butyl chain. Although the 4,5,6,7-tetrachlorophthalimide **76** can easily be deprotected and employed in synthesis as a formal ammonia equivalent [147,216-218], the photosensitized C(sp^3)–H fluorination of the substrate **76** was unsuccessful. However, when **76** was treated under the reaction conditions in the presence of *N*-ethylphthalimide, C–H fluorination of the former was observed (Scheme 33), clearly indicating that phthalimide is crucial for the fluorination reaction. Presumably, the triplet energy [172] of **76** (for 4,5,6,7-tetrachlorophthalimide: T_1 = 61.8 kcal·mol^{-1}) was too low to allow the successful reaction with Selectfluor® (T_1 = 2.6 eV, 61.4 kcal·mol^{-1}). Although this energy is very similar to that of Selectfluor®, it is possible that a certain amount of energy is lost during the reorganization/solvation of the excited state and complexation with Selectfluor®, such that **76** becomes an ineffective PSX.

Hamashima, Egami and co-workers proposed a PS TTET reaction mechanism consistent with that reported by Tan and co-workers [147,198] (Scheme 34), which leads to the exciplex

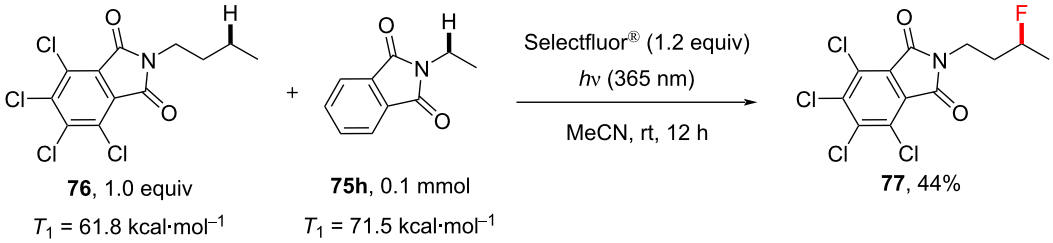

Scheme 33: Substrate crossover monofluorination experiment.

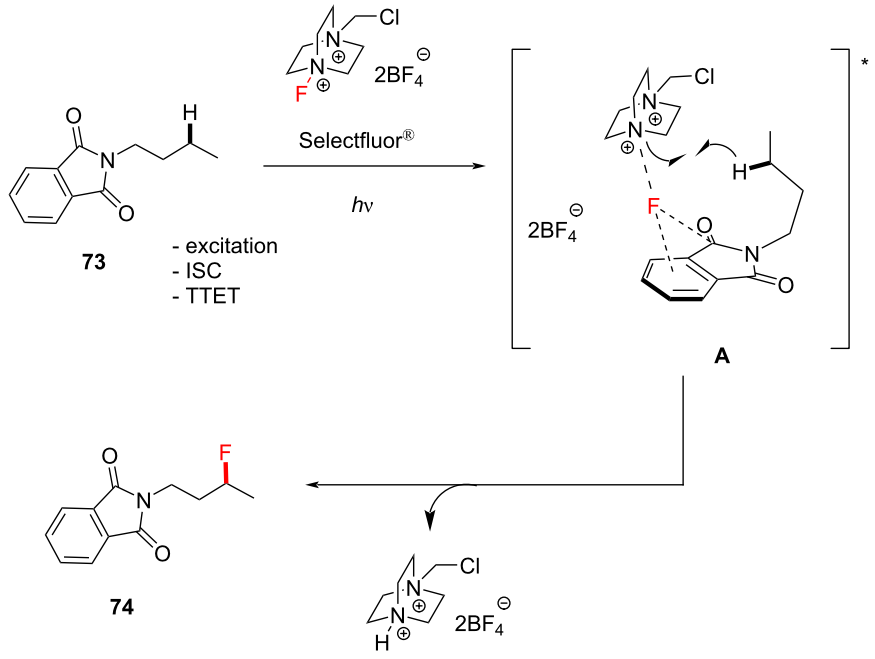

Scheme 34: PS TTET mechanism proposed by Hamashima and co-workers.

A. Intramolecular HAT then occurs between the developing nitrogen radical cation of the Selectfluor® moiety and the most hydridic C–H bond, which also benefits from the greatest thermodynamic stability of the generated radical. The authors then proposed that FAT occurs within the complex or between the formed radical and Selectfluor® to afford the fluorinated product. In contrast to previous methods involving PSCats, one fundamental advantage of this PSX approach is the ability to deconvolute the triplet energy matching of the PSCat and the fluorination source. One can simply use the same auxiliary to activate the substrate to fluorination and direct its selectivity before cleaving (for *N*-substituted phthalimides, by means of base hydrolysis or hydrazine [147]).

5 Trifluoromethylations involving photosensitization

While most reported trifluoromethylation (TFM) methods involve PRC (SET) [219-224], limited examples of TFM involve photosensitization (energy transfer), and these will now be presented. A developing sub-class of PRC reactions involve the use of electron donor–acceptor (EDA) complexes [219,222], and these have been employed in TFMs. However, the reaction of the EDA complex in these methods is proposed to proceed via SET, and so these are beyond the scope of this review. Although the following example is not technically a C–H fluorination but rather an addition of a trifluoromethyl radical to an olefin, it includes a photosensitized energy transfer process. Li, Wang and co-workers achieved the TFM of simple styrenes to afford α-CF_3-substituted ketones under mild conditions without using an external PSCat [225]. Their optimal reaction conditions employ CF_3SO_2Na (**79**, Langlois reagent) as a commercial and straightforward-to-handle CF_3 source, air atmosphere and LED irradiation of 380–385 nm at rt (Scheme 35).

Control reactions revealed that 380–385 nm light and acetone as a solvent are optimal for the reaction. Reactions in the dark or under an inert atmosphere did not proceed. Under the optimal conditions, a variety of styrenes substituted with EDG (such as Me, *t*-Bu, MeO) and EWG (such as Cl, Br, CF_3, Ph, CN, CO_2Me) on the aromatic ring were tolerated, giving the products **80a**–**h** in moderate to excellent product yield (45–84%, Scheme 36), with higher yields observed for electron-poor

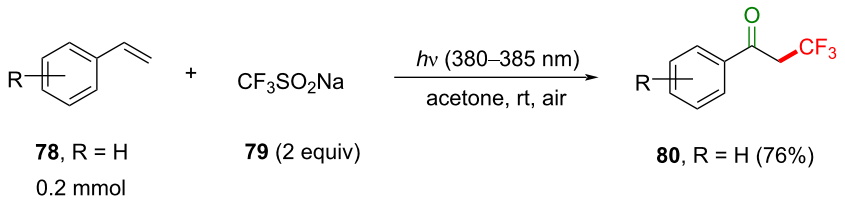

Scheme 35: Photosensitized TFM of **78** to afford α-trifluoromethylated ketone **80**.

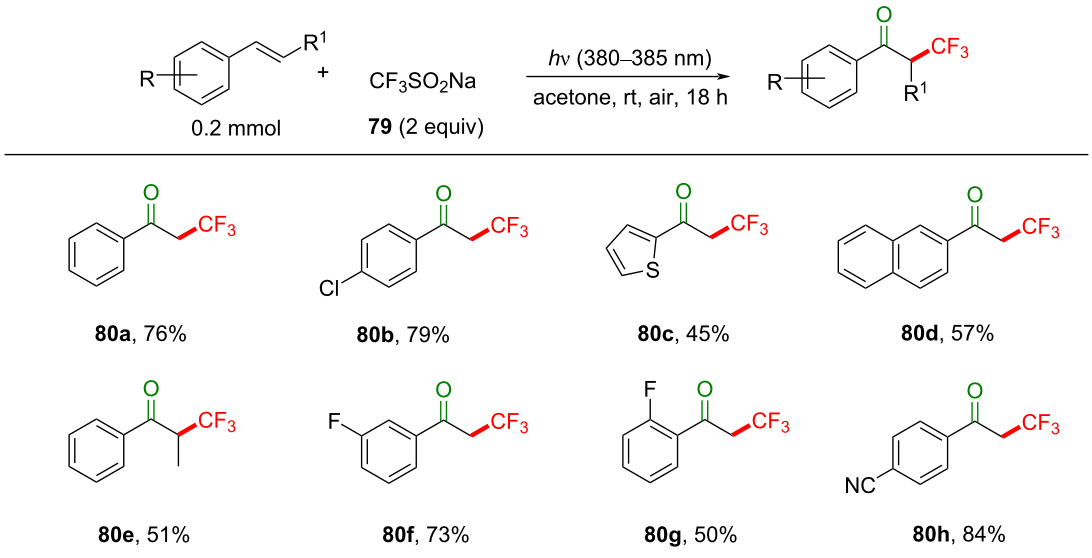

Scheme 36: Substrate scope for photosensitized styrene TFM to give α-trifluoromethylated ketones.

styrenes. Presumably due to steric effects, *meta*-substituted styrenes gave a higher product yield than *ortho*-substituted congeners. Nonstyrenic alkenes, such as cyclopentene, cyclooctene and benzyl vinyl ether gave no reaction.

Control reactions were chosen to provide mechanistic information on the TFM reaction (Scheme 37). In the presence of 1.5 equiv of (2,2,6,6-tetramethylpiperidin-1-yl)oxyl (TEMPO), the TFM reaction did not proceed, corroborating radical intermediates in the mechanism. Moreover, 1,1-diphenylethylene was subjected under the reaction conditions and reacted to afford the radical coupling product **82** (35%), implicating that CF_3 radicals are generated (Scheme 37). We note that this control experiment constitutes a formal C(sp^2)–H TFM.

Electron paramagnetic resonance (EPR) in the presence of 5,5-dimethylpyrroline-*N*-oxide (DMPO) and light (380–385 nm) revealed a signal corresponding to the superoxide ion ($O_2^{\bullet-}$), while the presence of 2,2,6,6-tetramethylpiperidine (TEMP) and light (380–385 nm) revealed a signal corresponding to singlet oxygen ($^1O_2$). Importantly, the fact that the products (α-trifluoromethylated ketones) can absorb light (380–385 nm) suggest their role in PS TTET in combination with O_2, and thus the TFM reaction occurs by an autocatalytic manifold (Scheme 38). The mechanism starts with the excitation of the product by visible-light irradiation (380–385 nm, Scheme 38), which transfers its triplet energy to ground state triplet oxygen ($^3O_2$) to afford excited $^1O_2$. This does not follow the previous definition of TTET and instead constitutes an example of a

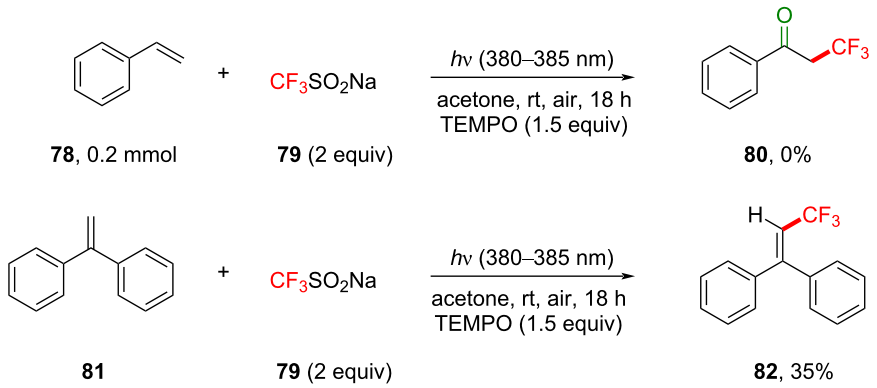

Scheme 37: Control reactions for photosensitized TFM of styrenes.

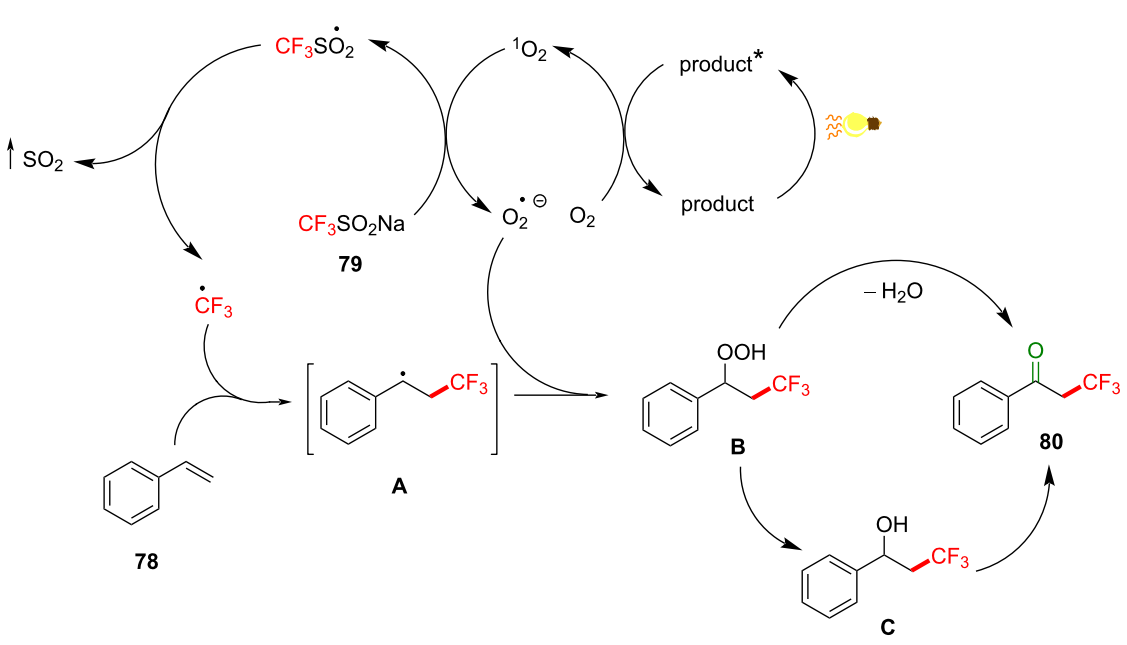

Scheme 38: Reaction mechanism for photosensitized TFM of styrenes to afford α-trifluoromethylated ketones.

singlet–triplet energy transfer (STET) [226,227] or type II photosensitized oxygenation reaction [228].

Singlet oxygen reacts with **79** through SET to afford a superoxide ion ($O_2^{\bullet-}$) and a $CF_3SO_2^{\bullet}$ radical, the latter of which decomposes to liberate SO_2 gas and to release the $CF_3^{\bullet}$ radical, which adds to the terminal styrene carbon atom to yield the intermediate **A**. The superoxide ion is then proposed to react with the intermediate **A** to yield the hydroperoxide intermediate **B**, which, after losing water, gives the product **80**. The authors proposed that the benzylic alcohol **C** might also serve as an intermediate en route to the product **80**. However, the initial generation of the product in the first place is unclear.

Although the following example involves SET processes, it also includes a PS TTET process. A stereoinducing PS TTET trifluoromethylation was performed by Qing and co-workers [229]. They conducted direct and regioselectivity-controllable C(sp^2)–H TFMs of electron-donating-group-substituted styrenes by employing either i) Togni's reagent in the presence of catalytic $[Ru(bpy)_3]Cl_2{\cdot}6H_2O$ and visible-light irradiation or ii) Umemoto's reagent in the presence of catalytic $Ir(ppy)_3$ and visible-light irradiation. The former proceeds under an SET mechanism to stereoselectively afford trifluoromethylated (*E*)-styrene, while the latter proceeds following both an SET and a TTET mechanism to afford a trifluoromethylated (*Z*)-styrene (Scheme 39).

Notable byproducts were observed when styrene (**78**) itself was exposed to the reaction conditions. Attaching an EDG on the *ortho*-position suppressed the byproduct formation. Consequently, *N*,*N*-dimethyl-2-vinylaniline was subjected to TFM conditions and afforded *trans*-**85a** (72%) without any detectable byproduct after 10 h. The optimum set of conditions targeting *E*-isomers were: blue LEDs [230], room temperature and Togni's reagent in DMF for 20 h (Scheme 40). Under these conditions, various EDG-substituted styrenes were tolerated in good to very good yield (50–78%). The synthesis of the

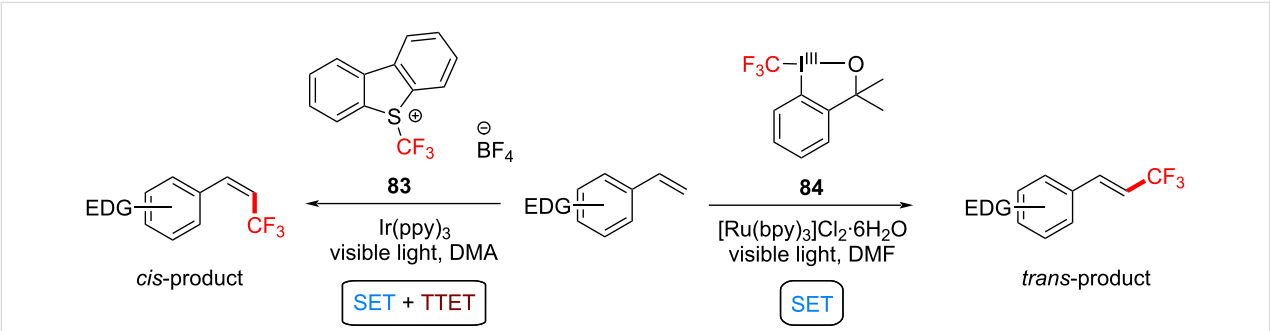

Scheme 39: Reaction conditions for TFMs to yield the *cis*- and the *trans*-product, respectively.

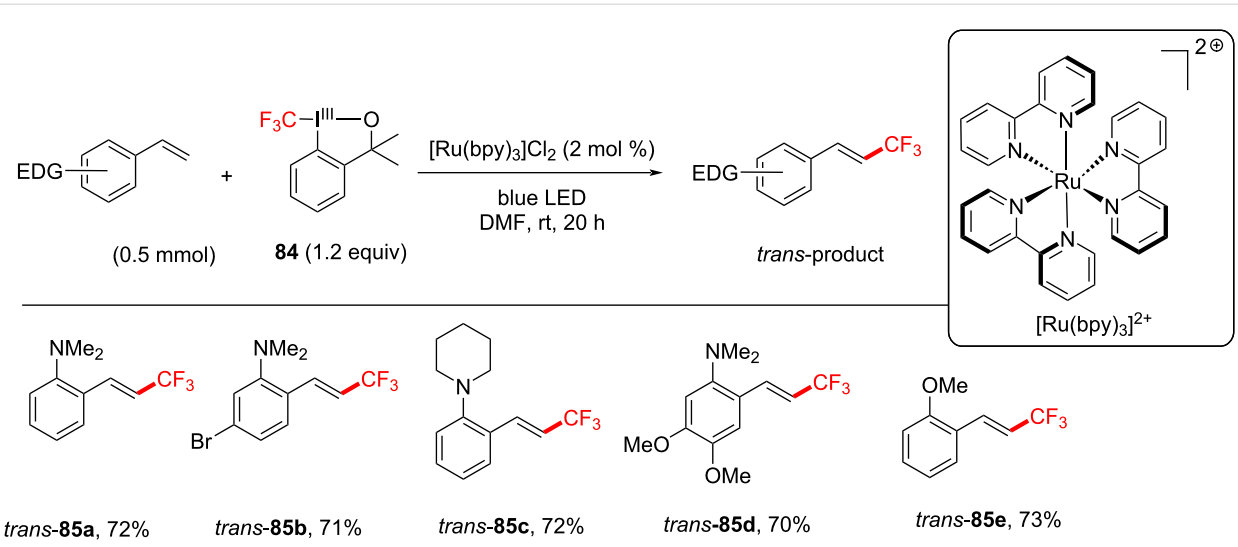

Scheme 40: Substrate scope of trifluoromethylated (*E*)-styrenes.

Z-isomer could be performed in two ways (Scheme 41). Firstly, by reacting the isolated *E*-isomer with $Ir(ppy)_3$ under blue LED irradiation in dimethylacetamide (DMA). Secondly (more elegantly), by reacting styrenes directly with Umemoto's reagent, $Ir(ppy)_3$ (3 mol %) as a catalyst under blue LED irradiation in DMA. Under the optimized conditions, in the latter case, various EDG-substituted styrenes, including steroid and amino acid-derived substrates were tolerated in good to very good yield (55–75%, Scheme 42), demonstrating the potential opportunities of this method in the LSF of bioactive molecules.

According to the mechanistic study of their first set of conditions, $[Ru(bpy)_3]^{2+}$ is excited by visible light to its excited state $[Ru(bpy)_3]^{2+*}$ (T_1 = 48.9 kcal·mol^{-1}), which is oxidatively

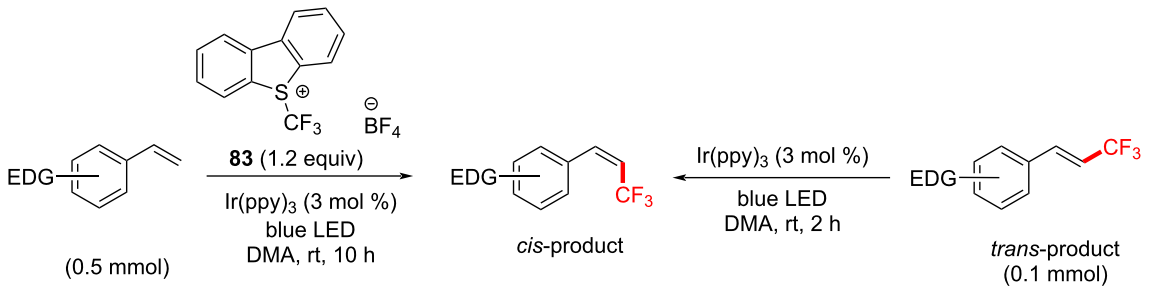

Scheme 41: Strategies toward trifluoromethylated (*Z*)-styrenes.

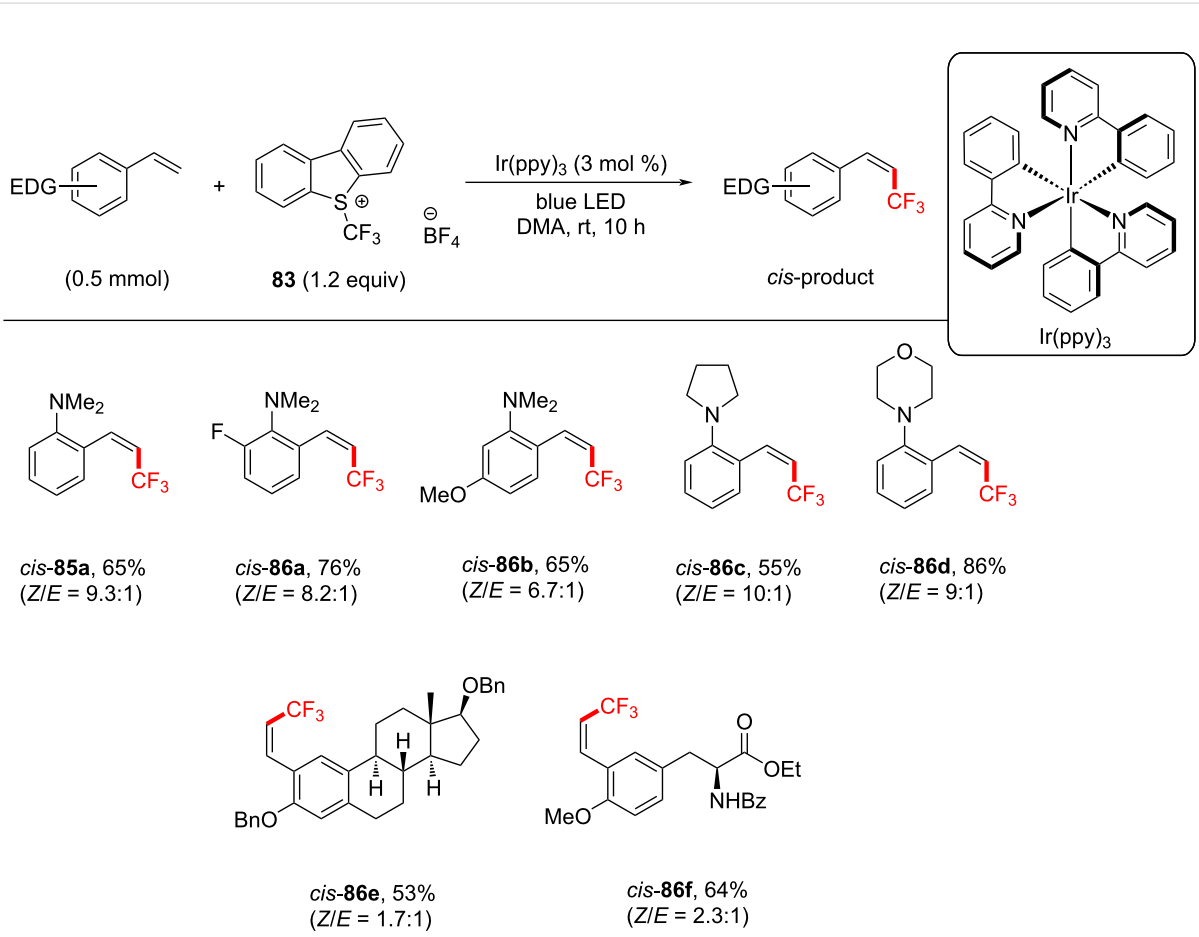

Scheme 42: Substrate scope of trifluoromethylated (*Z*)-styrenes.

quenched by the electrophilic trifluoromethylating reagent (Scheme 43), affording $[Ru(bpy)_3]^{2+}$ and the trifluoromethyl radical. The latter radical reacts with the aromatic olefin to afford the stable, benzylic radical intermediate. SET oxidation of this radical by $[Ru(bpy)_3]^{2+}$ affords a β-CF_3-substituted benzylic carbocation, which is deprotonated to furnish the (thermodynamically favored) *E*-isomer of the olefin. The authors rationalized that the EDG was required to increase the reactivity of intermediates and to suppress the formation of byproducts.

Previous studies on PS TTET involving transition metal complexes that promote olefinic *E*-to-*Z* isomerization [231] inspired Qing and co-workers to choose a PSCat with a higher triplet energy; $Ir(ppy)_3$ (T_1 = 55.6 kcal·mol^{-1}) [232]. Here, $Ir(ppy)_3$ facilitates the same oxidative quenching SET mechanism as $[Ru(bpy)_3]^{2+}$ to afford the *E*-isomer of the product. Thereafter, PS TTET between $Ir(ppy)_3$ and product generates the triplet state of **C**, which is relieved of its π-bond and can freely rotate. Contrary to classical *cis*/*trans* isomerism of olefins under UV irradiation, where the thermodynamic preference for the *trans*-isomer is overridden by the higher extinction coefficient of the *trans*-isomer [233], herein, the styrene products do not absorb light at the wavelengths employed. The authors proposed that the driving force for the isomerism to the (*Z*)-olefin product may be due to a more efficient TTET between $Ir(ppy)_3$* and the (*E*)-olefin. This is a reasonable argument since the triplet energy of the related (*cis*)-stilbene (T_1 = 55.5 kcal·mol^{-1}) is less accessible than that of the related (*trans*)-stilbene (T_1 = 51.0 kcal·mol^{-1}) [234]. Moreover, such triplet energies are likely out of the range of $[Ru(bpy)_3]^{2+}$ (T_1 = 49.4 kcal·mol^{-1}) but are likely within the range of $Ir(ppy)_3$.

6 Future challenges

6.1 Selectivity challenges

Despite the elegant efforts described herein, thus far, a key challenge that remains to be fully addressed in photosensitized C–H fluorinations (and direct C–H fluorinations in general) is the selectivity. Polarity matching-guided HAT is limited in scope not due to the PS TTET step but due to the inherent natural selectivity of the HAT step. Firstly, it provides a mixture of products despite the predictability of C–H fluorinations. Moreover, C–H bonds in proximity to functional groups such as alcohols and ketones are more reactive than the C–H bonds in alkyl chains elsewhere in the molecule. Finally, these methods are unable to functionalize the terminal positions of alkanes, which are oftentimes the desired positions of C–H fluorinations, due to the instability of the derived primary radicals. Directing groups for the HAT step, as elegantly identified by Lectka and co-workers [46,205-207], represent a complementary, if more valuable handle to direct selective C(sp^3)–H fluorinations.

6.2 Mechanistic understanding and precomplexation

More detailed studies are required to unearth the general reaction mechanisms in these PS TTET fluorinations. Comparing triplet energies is a useful guide but as can be seen comparing

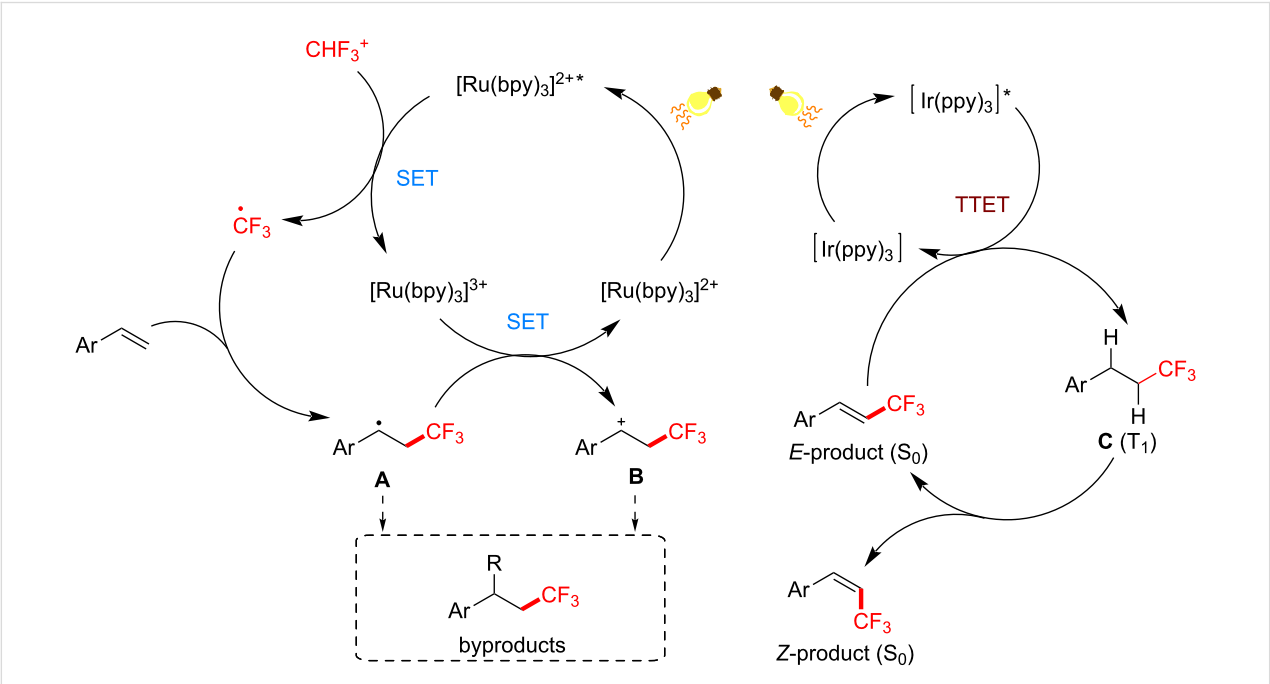

Scheme 43: Reaction mechanism for photosensitized TFM of styrenes to afford *E*- or *Z*-products.

the reports on C(sp^3)–H fluorinations of visible-light-inactive molecules using PSCats (Schemes 13, 21 and 26), this is not always an accurate predictor of the reactivity/success. The fact that the fluorination source (Selectfluor®) and light sources (generally 365–420 nm LEDs or CFL bulbs) are common themes but that different PSCats are optimal in different reactions suggests that the substrates themselves may play a role in the precomplexation with Selectfluor® and the PSCat in order to module the UV–visible absorption or T_1 energies [235,236]. Such behavior has been observed in other photochemical reactions [237,238].

6.3 Applicability of the methods to industrial processes

Finally, the activity remains a general challenge in photochemical fluorinations. Industry demands that reactions proceed at a sufficient rate. While most reactions discussed herein require multiple hours reaction time, in radiolabeling applications, for example, the incorporation of ^{18}F must be rapid, high-yielding and easily purifiable in order to synthesize, purify and characterize labeled molecules and get them into cells/organisms before the radioisotope decays away [97,239].

Conclusion

In conclusion, we presented an account of PS TTET as an emerging and important method for the direct fluorination and trifluoromethylation of unactivated C–H bonds. This method provides a complementary selectivity to C–H fluorinations using classical methods or transition metal catalysis. It is also distinct from fluorination methods under PRC because it can be used to directly activate C(sp^3)–H bonds instead of relying on the generation of radical intermediates by other methods (decarboxylation, addition of radicals to olefins). Moreover, it represents a highly practical and cost-effective method that can be scaled up without an erosion of the yield (at least to a multigram scale). The most promising facet of PS TTET fluorinations is the ability to directly functionalize C(sp^3)–H bonds selectively, within complex molecules and under very mild conditions. Given the prevalence of C–F bonds in bioactive molecules, this method proves to be a powerful tool in LSF. Its scalability in batch thanks to the low extinction coefficient of the reaction mixtures renders this method rather amenable to production, with opportunities for further scale-up via flow photochemistry. This review should serve as a platform for the discovery of future PS TTET reactions and the mechanistic understanding thereof. We are particularly excited by the developments in directing-group-guided C(sp^3)–H fluorinations of complex molecules and future investigations on the role of precomplexation and exciplex formation in the mechanisms of these reactions.

List of Abbreviations

Table 2: Abbreviations

Abbreviation	Explanation
BDE	bond-dissociation enthalpy
BDFE	bond-dissociation free energy
CFL	compact fluorescence lamp
DCM	dichloromethane
EDA	electron donor acceptor (complex)
EPR	electron paramagnetic resonance
EWG	electron-withdrawing group
HAT	hydrogen atom abstraction
IC	internal conversion
ISC	intersystem crossing
LED	light-emitting diode
MeCN	acetonitrile
PC	photocatalyst
PHAT	photoexcited hydrogen atom transfer
PRC	photoredox catalysis
SET	single-electron transfer
SF	Selectfluor®
TFA	trifluoroacetic acid
TFM	trifluoromethylation
TM	transition metal
T.S.	transition state
TTET	triplet-triplet energy transfer
UV–vis	ultraviolet/visible
λ_{max}	absorption maxima
τ	triplet-state lifetime
ns	nanosecond
μs	microsecond

Funding

S. Y. is grateful for funding provided by a DAAD Scholarship, the University of Regensburg and the SynCat programme of the Elite Network of Bavaria. J. P. B. acknowledges funding provided by the Alexander von Humboldt Foundation within the framework of the Sofja Kovalevskaja Award endowed by the German Federal Ministry of Education and Research.

ORCID® iDs

Shahboz Yakubov - https://orcid.org/0000-0003-4040-7967
Joshua P. Barham - https://orcid.org/0000-0003-1675-9399

References

1. Liang, T.; Neumann, C. N.; Ritter, T. *Angew. Chem., Int. Ed.* **2013,** *52,* 8214–8264. doi:10.1002/anie.201206566
2. Lee, E.; Kamlet, A. S.; Powers, D. C.; Neumann, C. N.; Boursalian, G. B.; Furuya, T.; Choi, D. C.; Hooker, J. M.; Ritter, T. *Science* **2011,** *334,* 639–642. doi:10.1126/science.1212625

3. Campbell, M. G.; Ritter, T. *Chem. Rev.* **2015,** *115,* 612–633. doi:10.1021/cr500366b
4. Hollingworth, C.; Gouverneur, V. *Chem. Commun.* **2012,** *48,* 2929–2942. doi:10.1039/c2cc16158c
5. Purser, S.; Moore, P. R.; Swallow, S.; Gouverneur, V. *Chem. Soc. Rev.* **2008,** *37,* 320–330. doi:10.1039/b610213c
6. Mei, H.; Han, J.; Fustero, S.; Medio-Simon, M.; Sedgwick, D. M.; Santi, C.; Ruzziconi, R.; Soloshonok, V. A. *Chem. – Eur. J.* **2019,** *25,* 11797–11819. doi:10.1002/chem.201901840
7. Theodoridis, G. Fluorine-Containing Agrochemicals: An Overview of Recent Developments. *Advances in Fluorine Science;* Elsevier: Amsterdam, Netherlands, 2006; Vol. 2, pp 121–175. doi:10.1016/s1872-0358(06)02004-5
8. Harsanyi, A.; Sandford, G. *Green Chem.* **2015,** *17,* 2081–2086. doi:10.1039/c4gc02166e
9. Shah, P.; Westwell, A. D. *J. Enzyme Inhib. Med. Chem.* **2007,** *22,* 527–540. doi:10.1080/14756360701425014
10. Bard, A. J.; Parsons, R.; Jordan, J.; International Union of Pure and Applied Chemistry. *Standard potentials in aqueous solution;* Marcel Dekker Inc.: New York, NY, USA, 1985.
11. Biffinger, J. C.; Kim, H. W.; DiMagno, S. G. *ChemBioChem* **2004,** *5,* 622–627. doi:10.1002/cbic.200300910
12. Dean, J. A. *Lange's Handbook of Chemistry;* McGraw-Hill Education: New York, NY, USA, 1999.
13. Banks, R. E.; Smart, B. E.; Tatlow, J. C., Eds. *Organofluorine Chemistry: Principles and Commercial Applications;* Springer US: New York, NY, USA, 1994. doi:10.1007/978-1-4899-1202-2
14. Bondi, A. *J. Phys. Chem.* **1964,** *68,* 441–451. doi:10.1021/j100785a001
15. Tseng, C.-C.; Baillie, G.; Donvito, G.; Mustafa, M. A.; Juola, S. E.; Zanato, C.; Massarenti, C.; Dall'Angelo, S.; Harrison, W. T. A.; Lichtman, A. H.; Ross, R. A.; Zanda, M.; Greig, I. R. *J. Med. Chem.* **2019,** *62,* 5049–5062. doi:10.1021/acs.jmedchem.9b00252
16. Müller, K.; Faeh, C.; Diederich, F. *Science* **2007,** *317,* 1881–1886. doi:10.1126/science.1131943
17. Hagmann, W. K. *J. Med. Chem.* **2008,** *51,* 4359–4369. doi:10.1021/jm800219f
18. Böhm, H.-J.; Banner, D.; Bendels, S.; Kansy, M.; Kuhn, B.; Müller, K.; Obst-Sander, U.; Stahl, M. *ChemBioChem* **2004,** *5,* 637–643. doi:10.1002/cbic.200301023
19. van Niel, M. B.; Collins, I.; Beer, M. S.; Broughton, H. B.; Cheng, S. K. F.; Goodacre, S. C.; Heald, A.; Locker, K. L.; MacLeod, A. M.; Morrison, D.; Moyes, C. R.; O'Connor, D.; Pike, A.; Rowley, M.; Russell, M. G. N.; Sohal, B.; Stanton, J. A.; Thomas, S.; Verrier, H.; Watt, A. P.; Castro, J. L. *J. Med. Chem.* **1999,** *42,* 2087–2104. doi:10.1021/jm981133m
20. Kruhlak, N. L.; Choi, S. S.; Contrera, J. F.; Weaver, J. L.; Willard, J. M.; Hastings, K. L.; Sancilio, L. F. *Toxicol. Mech. Methods* **2008,** *18,* 217–227. doi:10.1080/15376510701857262
21. Wang, J.; Sánchez-Roselló, M.; Aceña, J. L.; del Pozo, C.; Sorochinsky, A. E.; Fustero, S.; Soloshonok, V. A.; Liu, H. *Chem. Rev.* **2014,** *114,* 2432–2506. doi:10.1021/cr4002879
22. Alberati, D.; Hainzl, D.; Jolidon, S.; Krafft, E. A.; Kurt, A.; Maier, A.; Pinard, E.; Thomas, A. W.; Zimmerli, D. *Bioorg. Med. Chem. Lett.* **2006,** *16,* 4311–4315. doi:10.1016/j.bmcl.2006.05.058
23. Schirrmacher, R.; Wangler, C.; Schirrmacher, E. *Mini-Rev. Org. Chem.* **2007,** *4,* 317–329. doi:10.2174/157019307782411699
24. Imae, T. *Curr. Opin. Colloid Interface Sci.* **2003,** *8,* 307–314. doi:10.1016/s1359-0294(03)00050-5
25. Martino, R.; Gilard, V.; Desmoulin, F.; Malet-Martino, M. *J. Pharm. Biomed. Anal.* **2005,** *38,* 871–891. doi:10.1016/j.jpba.2005.01.047
26. Gakh, Y. G.; Gakh, A. A.; Gronenborn, A. M. *Magn. Reson. Chem.* **2000,** *38,* 551–558. doi:10.1002/1097-458x(200007)38:7<551::aid-mrc686>3.0.co;2-q
27. Dolbier, W. D., Jr. *Guide to Fluorine NMR for Organic Chemists;* John Wiley & Sons: Hoboken, NJ, USA, 2016.
28. McMurtrey, K. B.; Racowski, J. M.; Sanford, M. S. *Org. Lett.* **2012,** *14,* 4094–4097. doi:10.1021/ol301739f
29. Barnette, W. E. *J. Am. Chem. Soc.* **1984,** *106,* 452–454. doi:10.1021/ja00314a050
30. Pelletier, G.; Constantineau-Forget, L.; Charette, A. B. *Chem. Commun.* **2014,** *50,* 6883–6885. doi:10.1039/c4cc02220c
31. Lee, S. H.; Schwartz, J. *J. Am. Chem. Soc.* **1986,** *108,* 2445–2447. doi:10.1021/ja00269a052
32. Chang, M.-Y.; Lee, M.-F.; Lin, C.-H.; Lee, N.-C. *Tetrahedron Lett.* **2011,** *52,* 826–829. doi:10.1016/j.tetlet.2010.12.041
33. Adlington, R. M.; Barrett, A. G. M. *Acc. Chem. Res.* **1983,** *16,* 55–59. doi:10.1021/ar00086a004
34. Yin, B.; Inagi, S.; Fuchigami, T. *Beilstein J. Org. Chem.* **2015,** *11,* 85–91. doi:10.3762/bjoc.11.12
35. Wang, X.; Mei, T.-S.; Yu, J.-Q. *J. Am. Chem. Soc.* **2009,** *131,* 7520–7521. doi:10.1021/ja901352k
36. Szpera, R.; Moseley, D. F. J.; Smith, L. B.; Sterling, A. J.; Gouverneur, V. *Angew. Chem., Int. Ed.* **2019,** *58,* 14824–14848. doi:10.1002/anie.201814457
37. Yan, H.; Zhu, C. *Sci. China: Chem.* **2017,** *60,* 214–222. doi:10.1007/s11426-016-0399-5
38. Lin, A.; Huehls, C. B.; Yang, J. *Org. Chem. Front.* **2014,** *1,* 434–438. doi:10.1039/c4qo00020j
39. Li, Y.; Wu, Y.; Li, G.-S.; Wang, X.-S. *Adv. Synth. Catal.* **2014,** *356,* 1412–1418. doi:10.1002/adsc.201400101
40. Koperniku, A.; Liu, H.; Hurley, P. B. *Eur. J. Org. Chem.* **2016,** 871–886. doi:10.1002/ejoc.201501329
41. Ishida, S.; Sheppard, T.; Nishikata, T. *Tetrahedron Lett.* **2018,** *59,* 789–798. doi:10.1016/j.tetlet.2018.01.044
42. Chen, H.; Liu, Z.; Lv, Y.; Tan, X.; Shen, H.; Yu, H.-Z.; Li, C. *Angew. Chem., Int. Ed.* **2017,** *56,* 15411–15415. doi:10.1002/anie.201708197
43. Egami, H.; Hamashima, Y. Recent Advancements in Monofluorination Reactions. In *Frontiers of Organofluorine Chemistry;* Ojima, I., Ed.; World Scientific: Singapore, 2020; pp 3–91. doi:10.1142/9781786347336_0001
44. Field, M. J.; Sinha, S.; Warren, J. J. *Phys. Chem. Chem. Phys.* **2016,** *18,* 30907–30911. doi:10.1039/c6cp06418c
45. Barker, T. J.; Boger, D. L. *J. Am. Chem. Soc.* **2012,** *134,* 13588–13591. doi:10.1021/ja3063716
46. Bume, D. D.; Harry, S. A.; Lectka, T.; Pitts, C. R. *J. Org. Chem.* **2018,** *83,* 8803–8814. doi:10.1021/acs.joc.8b00982
47. Braun, M.-G.; Doyle, A. G. *J. Am. Chem. Soc.* **2013,** *135,* 12990–12993. doi:10.1021/ja407223g
48. Rueda-Becerril, M.; Chatalova Sazepin, C.; Leung, J. C. T.; Okbinoglu, T.; Kennepohl, P.; Paquin, J.-F.; Sammis, G. M. *J. Am. Chem. Soc.* **2012,** *134,* 4026–4029. doi:10.1021/ja211679v
49. Bloom, S.; Pitts, C. R.; Miller, D. C.; Haselton, N.; Holl, M. G.; Urheim, E.; Lectka, T. *Angew. Chem., Int. Ed.* **2012,** *51,* 10580–10583. doi:10.1002/anie.201203642

50. Pitts, C. R.; Bloom, S.; Woltornist, R.; Auvenshine, D. J.; Ryzhkov, L. R.; Siegler, M. A.; Lectka, T. *J. Am. Chem. Soc.* **2014,** *136,* 9780–9791. doi:10.1021/ja505136j
51. Amaoka, Y.; Nagatomo, M.; Inoue, M. *Org. Lett.* **2013,** *15,* 2160–2163. doi:10.1021/ol4006757
52. Xu, P.; Guo, S.; Wang, L.; Tang, P. *Angew. Chem., Int. Ed.* **2014,** *53,* 5955–5958. doi:10.1002/anie.201400225
53. Zhang, X.; Guo, S.; Tang, P. *Org. Chem. Front.* **2015,** *2,* 806–810. doi:10.1039/c5qo00095e
54. Danahy, K. E.; Cooper, J. C.; Van Humbeck, J. F. *Angew. Chem., Int. Ed.* **2018,** *57,* 5134–5138. doi:10.1002/anie.201801280
55. Pitts, C. R.; Ling, B.; Woltornist, R.; Liu, R.; Lectka, T. *J. Org. Chem.* **2014,** *79,* 8895–8899. doi:10.1021/jo501520e
56. Hua, A. M.; Mai, D. N.; Martinez, R.; Baxter, R. D. *Org. Lett.* **2017,** *19,* 2949–2952. doi:10.1021/acs.orglett.7b01188
57. Liu, W.; Huang, X.; Cheng, M.-J.; Nielsen, R. J.; Goddard, W. A.; Groves, J. T. *Science* **2012,** *337,* 1322–1325. doi:10.1126/science.1222327
58. Okada, M.; Fukuyama, T.; Yamada, K.; Ryu, I.; Ravelli, D.; Fagnoni, M. *Chem. Sci.* **2014,** *5,* 2893–2898. doi:10.1039/c4sc01072h
59. Salamone, M.; Bietti, M. *Acc. Chem. Res.* **2015,** *48,* 2895–2903. doi:10.1021/acs.accounts.5b00348
60. Jeffrey, J. L.; Terrett, J. A.; MacMillan, D. W. C. *Science* **2015,** *349,* 1532–1536. doi:10.1126/science.aac8555
61. Shaw, M. H.; Shurtleff, V. W.; Terrett, J. A.; Cuthbertson, J. D.; MacMillan, D. W. C. *Science* **2016,** *352,* 1304–1308. doi:10.1126/science.aaf6635
62. O'Reilly, R. J.; Chan, B.; Taylor, M. S.; Ivanic, S.; Bacskay, G. B.; Easton, C. J.; Radom, L. *J. Am. Chem. Soc.* **2011,** *133,* 16553–16559. doi:10.1021/ja205962b
63. Twilton, J.; Christensen, M.; DiRocco, D. A.; Ruck, R. T.; Davies, I. W.; MacMillan, D. W. C. *Angew. Chem., Int. Ed.* **2018,** *57,* 5369–5373. doi:10.1002/anie.201800749
64. Russell, G. A. In *Free Radicals;* Kochi, J. K., Ed.; John Wiley & Sons: New York, NY, USA, 1973; Vol. 1, pp 275–331.
65. Le, C.; Liang, Y.; Evans, R. W.; Li, X.; MacMillan, D. W. C. *Nature* **2017,** *547,* 79–83. doi:10.1038/nature22813
66. Morton, O. *Nature* **2006,** *443,* 19–22. doi:10.1038/443019a
67. Nocera, D. G. *Daedalus (Boston)* **2006,** *135,* 112–115. doi:10.1162/daed.2006.135.4.112
68. Lewis, N. S. *Science* **2007,** *315,* 798–801. doi:10.1126/science.1137014
69. Šima, J. *Acta Chim. Slov.* **2017,** *10,* 84–90. doi:10.1515/acs-2017-0015
70. Serpone, N.; Pelizzetti, E. *Photocatalysis: Fundamentals and Applications;* John Wiley & Sons: New York, NY, USA, 1989.
71. Serpone, N.; Emeline, A. V. *Int. J. Photoenergy* **2002,** *4,* 91–131. doi:10.1155/s1110662x02000144
72. Douglas, J. J.; Albright, H.; Sevrin, M. J.; Cole, K. P.; Stephenson, C. R. J. *Angew. Chem., Int. Ed.* **2015,** *54,* 14898–14902. doi:10.1002/anie.201507369
73. Pac, C.; Miyauchi, Y.; Ishitani, O.; Ihama, M.; Yasuda, M.; Sakurai, H. *J. Org. Chem.* **1984,** *49,* 26–34. doi:10.1021/jo00175a006
74. Ishitani, O.; Ihama, M.; Miyauchi, Y.; Pac, C. *J. Chem. Soc., Perkin Trans. 1* **1985,** 1527–1531. doi:10.1039/p19850001527
75. Fukuzumi, S.; Mochizuki, S.; Tanaka, T. *J. Phys. Chem.* **1990,** *94,* 722–726. doi:10.1021/j100365a039
76. Hironaka, K.; Fukuzumi, S.; Tanaka, T. *J. Chem. Soc., Perkin Trans. 2* **1984,** 1705–1709. doi:10.1039/p29840001705
77. Narayanam, J. M. R.; Tucker, J. W.; Stephenson, C. R. J. *J. Am. Chem. Soc.* **2009,** *131,* 8756–8757. doi:10.1021/ja9033582
78. Yoon, T. P.; Ischay, M. A.; Du, J. *Nat. Chem.* **2010,** *2,* 527–532. doi:10.1038/nchem.687
79. Abe, R. *J. Photochem. Photobiol., C* **2010,** *11,* 179–209. doi:10.1016/j.jphotochemrev.2011.02.003
80. Cui, G.; Sun, Z.; Fang, W. *J. Phys. Chem. A* **2011,** *115,* 10146–10153. doi:10.1021/jp2053025
81. Nechab, M.; Mondal, S.; Bertrand, M. P. *Chem. – Eur. J.* **2014,** *20,* 16034–16059. doi:10.1002/chem.201403951
82. Demas, J. *Excited State Lifetime Measurements;* Academic Press: New York, NY, USA, 1983.
83. Roth, H. D. *Angew. Chem., Int. Ed. Engl.* **1989,** *28,* 1193–1207. doi:10.1002/anie.198911931
84. Albini, A.; Fagnoni, M. *Green Chem.* **2004,** *6,* 1–6. doi:10.1039/b309592d
85. Albini, A.; Fagnoni, M. *ChemSusChem* **2008,** *1,* 63–66. doi:10.1002/cssc.200700015
86. Skubi, K. L.; Blum, T. R.; Yoon, T. P. *Chem. Rev.* **2016,** *116,* 10035–10074. doi:10.1021/acs.chemrev.6b00018
87. Barham, J. P.; König, B. *Angew. Chem., Int. Ed.* **2020,** *59,* 11732–11747. doi:10.1002/anie.201913767
88. West, J. G.; Bedell, T. A.; Sorensen, E. J. *Angew. Chem., Int. Ed.* **2016,** *55,* 8923–8927. doi:10.1002/anie.201603149
89. Photosensitization. In *IUPAC Compendium of Chemical Terminology (the "Gold Book"),* 2nd ed.; McNaught, A. D.; Wilkinson, A., Eds.; Blackwell Scientific Publications: Oxford, U.K., 1997. doi:10.1351/goldbook.p04652
90. Photocatalysis. In *IUPAC Compendium of Chemical Terminology (the "Gold Book"),* 2nd ed.; McNaught, A. D.; Wilkinson, A., Eds.; Blackwell Scientific Publications: Oxford, U.K., 1997. doi:10.1351/goldbook.p04580
91. Alonso, R.; Bach, T. *Angew. Chem., Int. Ed.* **2014,** *53,* 4368–4371. doi:10.1002/anie.201310997
92. Hurtley, A. E.; Lu, Z.; Yoon, T. P. *Angew. Chem., Int. Ed.* **2014,** *53,* 8991–8994. doi:10.1002/anie.201405359
93. Blum, T. R.; Miller, Z. D.; Bates, D. M.; Guzei, I. A.; Yoon, T. P. *Science* **2016,** *354,* 1391–1395. doi:10.1126/science.aai8228
94. Adam, W.; Griesbeck, A.; Staab, E. *Tetrahedron Lett.* **1986,** *27,* 2839–2842. doi:10.1016/s0040-4039(00)84656-0
95. Krief, A.; Colaux-Castillo, C. *Tetrahedron Lett.* **1999,** *40,* 4189–4192. doi:10.1016/s0040-4039(99)00721-2
96. Heitz, D. R.; Tellis, J. C.; Molander, G. A. *J. Am. Chem. Soc.* **2016,** *138,* 12715–12718. doi:10.1021/jacs.6b04789
97. Welin, E. R.; Le, C.; Arias-Rotondo, D. M.; McCusker, J. K.; MacMillan, D. W. C. *Science* **2017,** *355,* 380–385. doi:10.1126/science.aal2490
98. Kim, T.; McCarver, S. J.; Lee, C.; MacMillan, D. W. C. *Angew. Chem., Int. Ed.* **2018,** *57,* 3488–3492. doi:10.1002/anie.201800699
99. Brachet, E.; Ghosh, T.; Ghosh, I.; König, B. *Chem. Sci.* **2015,** *6,* 987–992. doi:10.1039/c4sc02365j
100. Das, A.; Banerjee, T.; Hanson, K. *Chem. Commun.* **2016,** *52,* 1350–1353. doi:10.1039/c5cc08081a
101. Lu, Z.; Yoon, T. P. *Angew. Chem., Int. Ed.* **2012,** *51,* 10329–10332. doi:10.1002/anie.201204835
102. Cho, J.-D.; Hong, J.-W. *J. Appl. Polym. Sci.* **2004,** *93,* 1473–1483. doi:10.1002/app.20597

103. For relevant reviews on photosensitization in organic synthesis see [104] and [105].
104. Sideri, I. K.; Voutyritsa, E.; Kokotos, C. G. *Org. Biomol. Chem.* **2018,** *16,* 4596–4614. doi:10.1039/c8ob00725j
105. Strieth-Kalthoff, F.; James, M. J.; Teders, M.; Pitzer, L.; Glorius, F. *Chem. Soc. Rev.* **2018,** *47,* 7190–7202. doi:10.1039/c8cs00054a
106. Koike, T.; Akita, M. *Inorg. Chem. Front.* **2014,** *1,* 562–576. doi:10.1039/c4qi00053f
107. Romero, N. A.; Nicewicz, D. A. *Chem. Rev.* **2016,** *116,* 10075–10166. doi:10.1021/acs.chemrev.6b00057
108. Prier, C. K.; Rankic, D. A.; MacMillan, D. W. C. *Chem. Rev.* **2013,** *113,* 5322–5363. doi:10.1021/cr300503r
109. Xi, Y.; Yi, H.; Lei, A. *Org. Biomol. Chem.* **2013,** *11,* 2387–2403. doi:10.1039/c3ob40137e
110. Reckenthäler, M.; Griesbeck, A. G. *Adv. Synth. Catal.* **2013,** *355,* 2727–2744. doi:10.1002/adsc.201300751
111. Larsen, C. B.; Wenger, O. S. *Chem. – Eur. J.* **2018,** *24,* 2039–2058. doi:10.1002/chem.201703602
112. Narayanam, J. M. R.; Stephenson, C. R. J. *Chem. Soc. Rev.* **2011,** *40,* 102–113. doi:10.1039/b913880n
113. König, B. *Eur. J. Org. Chem.* **2017,** 1979–1981. doi:10.1002/ejoc.201700420
114. Meggers, E. *Chem. Commun.* **2015,** *51,* 3290–3301. doi:10.1039/c4cc09268f
115. Twilton, J.; Le, C.; Zhang, P.; Shaw, M. H.; Evans, R. W.; MacMillan, D. W. C. *Nat. Rev. Chem.* **2017,** *1,* 0052. doi:10.1038/s41570-017-0052
116. Albini, A. *Synthesis* **1981,** 249–264. doi:10.1055/s-1981-29405
117. Marian, C. M. *Wiley Interdiscip. Rev.: Comput. Mol. Sci.* **2012,** *2,* 187–203. doi:10.1002/wcms.83
118. Yoo, W.-J.; Tsukamoto, T.; Kobayashi, S. *Org. Lett.* **2015,** *17,* 3640–3642. doi:10.1021/acs.orglett.5b01645
119. Ikezawa, H.; Kutal, C.; Yasufuku, K.; Yamazaki, H. *J. Am. Chem. Soc.* **1986,** *108,* 1589–1594. doi:10.1021/ja00267a032
120. Zou, Y.-Q.; Duan, S.-W.; Meng, X.-G.; Hu, X.-Q.; Gao, S.; Chen, J.-R.; Xiao, W.-J. *Tetrahedron* **2012,** *68,* 6914–6919. doi:10.1016/j.tet.2012.06.011
121. Skubi, K. L.; Kidd, J. B.; Jung, H.; Guzei, I. A.; Baik, M.-H.; Yoon, T. P. *J. Am. Chem. Soc.* **2017,** *139,* 17186–17192. doi:10.1021/jacs.7b10586
122. Oba, M.; Okada, Y.; Nishiyama, K.; Ando, W. *Org. Lett.* **2009,** *11,* 1879–1881. doi:10.1021/ol900240s
123. Lantaño, B.; Postigo, A. *Org. Biomol. Chem.* **2017,** *15,* 9954–9973. doi:10.1039/c7ob02402a
124. Rehm, T. H. *Chem. Eng. Technol.* **2016,** *39,* 66–80. doi:10.1002/ceat.201500195
125. Chatalova-Sazepin, C.; Hemelaere, R.; Paquin, J.-F.; Sammis, G. M. *Synthesis* **2015,** *47,* 2554–2569. doi:10.1055/s-0034-1378824
126. Pitts, C. R.; Bloom, M. S.; Bume, D. D.; Zhang, Q. A.; Lectka, T. *Chem. Sci.* **2015,** *6,* 5225–5229. doi:10.1039/c5sc01973g
127. Pitts, C. R.; Ling, B.; Snyder, J. A.; Bragg, A. E.; Lectka, T. *J. Am. Chem. Soc.* **2016,** *138,* 6598–6609. doi:10.1021/jacs.6b02838
128. Leung, J. C. T.; Sammis, G. M. *Eur. J. Org. Chem.* **2015,** 2197–2204. doi:10.1002/ejoc.201500038
129. Bloom, S.; Knippel, J. L.; Lectka, T. *Chem. Sci.* **2014,** *5,* 1175–1178. doi:10.1039/c3sc53261e
130. Bloom, S.; McCann, M.; Lectka, T. *Org. Lett.* **2014,** *16,* 6338–6341. doi:10.1021/ol503094m
131. Arnold, D. R.; Lamont, L. J.; Perrott, A. L. *Can. J. Chem.* **1991,** *69,* 225–233. doi:10.1139/v91-036
132. Montalti, M.; Credi, A.; Prodi, L.; Gandolfi, M. T. *Handbook of Photochemistry,* 3rd ed.; CRC Press: Boca Raton, FL, USA, 2006. doi:10.1201/9781420015195
133. Herkstroeter, W. G.; Lamola, A. A.; Hammond, G. S. *J. Am. Chem. Soc.* **1964,** *86,* 4537–4540. doi:10.1021/ja01075a005
134. Herkstroeter, W. G.; Hammond, G. S. *J. Am. Chem. Soc.* **1966,** *88,* 4769–4777. doi:10.1021/ja00973a001
135. Xia, J.-B.; Zhu, C.; Chen, C. *J. Am. Chem. Soc.* **2013,** *135,* 17494–17500. doi:10.1021/ja410815u
136. Lathioor, E. C.; Leigh, W. J. *Photochem. Photobiol.* **2006,** *82,* 291–300. doi:10.1562/2005-06-20-ra-581
137. Carmichael, I.; Hug, G. L. *J. Phys. Chem. Ref. Data* **1986,** *15,* 1–250. doi:10.1063/1.555770
138. Ley, C.; Morlet-Savary, F.; Fouassier, J. P.; Jacques, P. *J. Photochem. Photobiol., A* **2000,** *137,* 87–92. doi:10.1016/s1010-6030(00)00374-9
139. Cantillo, D.; de Frutos, O.; Rincón, J. A.; Mateos, C.; Kappe, C. O. *J. Org. Chem.* **2014,** *79,* 8486–8490. doi:10.1021/jo5016757
140. Eakins, G. L.; Alford, J. S.; Tiegs, B. J.; Breyfogle, B. E.; Stearman, C. J. *J. Phys. Org. Chem.* **2011,** *24,* 1119–1128. doi:10.1002/poc.1864
141. Murphy, R. S.; Moorlag, C. P.; Green, W. H.; Bohne, C. *J. Photochem. Photobiol., A* **1997,** *110,* 123–129. doi:10.1016/s1010-6030(97)00191-3
142. Ferreira, G. C.; Schmitt, C. C.; Neumann, M. G. *J. Braz. Chem. Soc.* **2006,** *17,* 905–909. doi:10.1590/s0103-50532006000500013
143. Meyer, A. Y.; Goldblum, A. *Isr. J. Chem.* **1973,** *11,* 791–804. doi:10.1002/ijch.197300077
144. Kemp, T. J.; Parker, A. W.; Wardman, P. *Photochem. Photobiol.* **1987,** *45,* 663–666. doi:10.1111/j.1751-1097.1987.tb07395.x
145. Clark, L. B.; Tinoco, I., Jr. *J. Am. Chem. Soc.* **1965,** *87,* 11–15. doi:10.1021/ja01079a003
146. Horvat, M.; Mlinarić-Majerski, K.; Griesbeck, A. G.; Basarić, N. *Photochem. Photobiol. Sci.* **2011,** *10,* 610–617. doi:10.1039/c0pp00357c
147. Egami, H.; Masuda, S.; Kawato, Y.; Hamashima, Y. *Org. Lett.* **2018,** *20,* 1367–1370. doi:10.1021/acs.orglett.8b00133
148. Griesbeck, A. G.; Görner, H. *J. Photochem. Photobiol., A* **1999,** *129,* 111–119. doi:10.1016/s1010-6030(99)00180-x
149. Scaiano, J. C. *J. Am. Chem. Soc.* **1980,** *102,* 7747–7753. doi:10.1021/ja00546a018
150. Fakhfakh, N.; Cognet, P.; Cabassud, M.; Lucchese, Y.; de Los Ríos, M. D. *Chem. Eng. Process.* **2008,** *47,* 349–362. doi:10.1016/j.cep.2007.01.015
151. Togashi, D. M.; Nicodem, D. E. *Spectrochim. Acta, Part A* **2004,** *60,* 3205–3212. doi:10.1016/j.saa.2004.03.003
152. Rajalakshmi, M.; Shyju, T. S.; Indirajith, R.; Gopalakrishnan, R. *Spectrochim. Acta, Part A* **2012,** *86,* 27–32. doi:10.1016/j.saa.2011.09.049
153. Bume, D. D.; Pitts, C. R.; Ghorbani, F.; Harry, S. A.; Capilato, J. N.; Siegler, M. A.; Lectka, T. *Chem. Sci.* **2017,** *8,* 6918–6923. doi:10.1039/c7sc02703f
154. Vera, F.; Schrebler, R.; Muñoz, E.; Suarez, C.; Cury, P.; Gómez, H.; Córdova, R.; Marotti, R. E.; Dalchiele, E. A. *Thin Solid Films* **2005,** *490,* 182–188. doi:10.1016/j.tsf.2005.04.052
155. Chambers, R. W.; Kearns, D. R. *Photochem. Photobiol.* **1969,** *10,* 215–219. doi:10.1111/j.1751-1097.1969.tb05681.x
156. Chakraborty, M.; Panda, A. K. *Spectrochim. Acta, Part A* **2011,** *81,* 458–465. doi:10.1016/j.saa.2011.06.038

157. Zhou, Q.-Q.; Zou, Y.-Q.; Lu, L.-Q.; Xiao, W.-J. *Angew. Chem., Int. Ed.* **2019,** *58,* 1586–1604. doi:10.1002/anie.201803102
158. Kapoor, R. C.; Jain, M. K.; Mishra, V. N. *J. Lumin.* **1981,** *22,* 429–439. doi:10.1016/0022-2313(81)90018-1
159. Islam, S. D.-M.; Ito, O. *J. Photochem. Photobiol., A* **1999,** *123,* 53–59. doi:10.1016/s1010-6030(99)00042-8
160. Sandros, K.; Bäckström, H. L. J.; Havanka, R.; Briggs, T.; Haslewood, G. A. D.; Flood, H. *Acta Chem. Scand.* **1962,** *16,* 958–968. doi:10.3891/acta.chem.scand.16-0958
161. Gratz, H.; Penzkofer, A. *Chem. Phys.* **2000,** *254,* 363–374. doi:10.1016/s0301-0104(00)00049-5
162. Hamai, S. *J. Mater. Chem.* **2005,** *15,* 2881–2888. doi:10.1039/b501119a
163. Kuzmin, V. A.; Tatikolov, A. S. *Chem. Phys. Lett.* **1978,** *53,* 606–610. doi:10.1016/0009-2614(78)80080-3
164. Kessler, R. W.; Wilkinson, F. *J. Chem. Soc., Faraday Trans. 1* **1981,** *77,* 309–320. doi:10.1039/f19817700309
165. Zhao, J.; Wu, W.; Sun, J.; Guo, S. *Chem. Soc. Rev.* **2013,** *42,* 5323–5351. doi:10.1039/c3cs35531d
166. Specht, D. P.; Martic, P. A.; Farid, S. *Tetrahedron* **1982,** *38,* 1203–1211. doi:10.1016/0040-4020(82)85104-1
167. Rillema, D. P.; Allen, G.; Meyer, T. J.; Conrad, D. *Inorg. Chem.* **1983,** *22,* 1617–1622. doi:10.1021/ic00153a012
168. Bayrakçeken, F. *Spectrochim. Acta, Part A* **2007,** *66,* 1267–1270. doi:10.1016/j.saa.2006.06.018
169. Renge, I. *J. Chem. Phys.* **2007,** *127,* 034504. doi:10.1063/1.2751170
170. Wu, W.; Guo, H.; Wu, W.; Ji, S.; Zhao, J. *J. Org. Chem.* **2011,** *76,* 7056–7064. doi:10.1021/jo200990y
171. Ji, S.; Ge, J.; Escudero, D.; Wang, Z.; Zhao, J.; Jacquemin, D. *J. Org. Chem.* **2015,** *80,* 5958–5963. doi:10.1021/acs.joc.5b00691
172. Barlow, J. H.; Davidson, R. S.; Lewis, A.; Russell, D. R. *J. Chem. Soc., Perkin Trans. 2* **1979,** 1103–1109. doi:10.1039/p29790001103
173. Lal, G. S.; Pez, G. P.; Syvret, R. G. *Chem. Rev.* **1996,** *96,* 1737–1756. doi:10.1021/cr941145p
174. Meyer, D.; Jangra, H.; Walther, F.; Zipse, H.; Renaud, P. *Nat. Commun.* **2018,** *9,* 4888. doi:10.1038/s41467-018-07196-9
175. Sandford, G. *J. Fluorine Chem.* **2007,** *128,* 90–104. doi:10.1016/j.jfluchem.2006.10.019
176. Middleton, W. J. *J. Org. Chem.* **1975,** *40,* 574–578. doi:10.1021/jo00893a007
177. Barton, D. H. R.; Ganguly, A. K.; Hesse, R. H.; Loo, S. N.; Pechet, M. M. *Chem. Commun.* **1968,** 806–808. doi:10.1039/c19680000806
178. Barton, D. H. R.; Hesse, R. H.; Pechet, M. M.; Tarzia, G.; Toh, H. T.; Westcott, N. D. *J. Chem. Soc., Chem. Commun.* **1972,** 122–123. doi:10.1039/c39720000122
179. Airey, J.; Barton, D. H. R.; Ganguly, A. K.; Hesse, R. H.; Pechet, M. M. *An. Quim.* **1974,** *70,* 871–875.
180. Barton, D. H. R.; Godinho, L. S.; Hesse, R. H.; Pechet, M. M. *Chem. Commun.* **1968,** 804–806. doi:10.1039/c19680000804
181. Schack, C. J.; Christe, K. O. *Inorg. Chem.* **1979,** *18,* 2619–2620. doi:10.1021/ic50199a056
182. Tius, M. A. *Tetrahedron* **1995,** *51,* 6605–6634. doi:10.1016/0040-4020(95)00362-c
183. Schmutzler, R. *Angew. Chem., Int. Ed. Engl.* **1968,** *7,* 440–455. doi:10.1002/anie.196804401
184. Rozen, S. *Chem. Rev.* **1996,** *96,* 1717–1736. doi:10.1021/cr941147+
185. Navarrini, W.; Tortelli, V.; Russo, A.; Corti, S. *J. Fluorine Chem.* **1999,** *95,* 27–39. doi:10.1016/s0022-1139(98)00296-6
186. Umemoto, T.; Kawada, K.; Tomita, K. *Tetrahedron Lett.* **1986,** *27,* 4465–4468. doi:10.1016/s0040-4039(00)84980-1
187. Differding, E.; Ofner, H. *Synlett* **1991,** 187–189. doi:10.1055/s-1991-20673
188. Resnati, G.; DesMarteau, D. D. *J. Org. Chem.* **1991,** *56,* 4925–4929. doi:10.1021/jo00016a022
189. DesMarteau, D. D.; Xu, Z. Q.; Witz, M. *J. Org. Chem.* **1992,** *57,* 629–635. doi:10.1021/jo00028a042
190. Banks, R. E.; Mohialdin-Khaffaf, S. N.; Lal, G. S.; Sharif, I.; Syvret, R. G. *J. Chem. Soc., Chem. Commun.* **1992,** 595–596. doi:10.1039/c39920000595
191. Banks, R. E.; Besheesh, M. K.; Mohialdin-Khaffaf, S. N.; Sharif, I. *J. Chem. Soc., Perkin Trans. 1* **1996,** 2069–2076. doi:10.1039/p19960002069
192. It was revealed by toxicologists that the oral LD_{50} (the dose of the compound that kills 50% of the subjects) is 640 mg per 1 kg of male adult rats. Studies with rabbits and guinea pigs disclosed only mild eye and skin irritation and no mutagenic or carcinogenic properties [194].
193. Hart, J. J.; Syvret, R. G. *J. Fluorine Chem.* **1999,** *100,* 157–161. doi:10.1016/s0022-1139(99)00199-2
194. Nyffeler, P. T.; Durón, S. G.; Burkart, M. D.; Vincent, S. P.; Wong, C.-H. *Angew. Chem., Int. Ed.* **2005,** *44,* 192–212. doi:10.1002/anie.200400648
195. Bonfield, H. E.; Knauber, T.; Lévesque, F.; Moschetta, E. G.; Susanne, F.; Edwards, L. J. *Nat. Commun.* **2020,** *11,* 804. doi:10.1038/s41467-019-13988-4
196. Yang, J.-D.; Wang, Y.; Xue, X.-S.; Cheng, J.-P. *J. Org. Chem.* **2017,** *82,* 4129–4135. doi:10.1021/acs.joc.7b00036
197. Singh, N. K.; Popelier, P. L. A.; O'Malley, P. J. *Chem. Phys. Lett.* **2006,** *426,* 219–221. doi:10.1016/j.cplett.2006.06.008
198. Kee, C. W.; Chin, K. F.; Wong, M. W.; Tan, C.-H. *Chem. Commun.* **2014,** *50,* 8211–8214. doi:10.1039/c4cc01848f
199. Kee, J. W.; Shao, H.; Kee, C. W.; Lu, Y.; Soo, H. S.; Tan, C.-H. *Catal. Sci. Technol.* **2017,** *7,* 848–857. doi:10.1039/c6cy02484j
200. Zalesskaya, G. A. *J. Appl. Spectrosc.* **2002,** *69,* 328–336. doi:10.1023/a:1019782628427
201. Xia, J.-B.; Zhu, C.; Chen, C. *Chem. Commun.* **2014,** *50,* 11701–11704. doi:10.1039/c4cc05650g
202. Cismesia, M. A.; Yoon, T. P. *Chem. Sci.* **2015,** *6,* 5426–5434. doi:10.1039/c5sc02185e
203. Barham, J. P.; John, M. P.; Murphy, J. A. *J. Am. Chem. Soc.* **2016,** *138,* 15482–15487. doi:10.1021/jacs.6b09690
204. Takahira, Y.; Chen, M.; Kawamata, Y.; Mykhailiuk, P.; Nakamura, H.; Peters, B. K.; Reisberg, S. H.; Li, C.; Chen, L.; Hoshikawa, T.; Shibuguchi, T.; Baran, P. S. *Synlett* **2019,** *30,* 1178–1182. doi:10.1055/s-0037-1611737
205. Capilato, J. N.; Pitts, C. R.; Rowshanpour, R.; Dudding, T.; Lectka, T. *J. Org. Chem.* **2020,** *85,* 2855–2864. doi:10.1021/acs.joc.9b03047
206. Pitts, C. R.; Bume, D. D.; Harry, S. A.; Siegler, M. A.; Lectka, T. *J. Am. Chem. Soc.* **2017,** *139,* 2208–2211. doi:10.1021/jacs.7b00335
207. Bume, D. D.; Pitts, C. R.; Jokhai, R. T.; Lectka, T. *Tetrahedron* **2016,** *72,* 6031–6036. doi:10.1016/j.tet.2016.08.018
208. Ye, J.; Kalvet, I.; Schoenebeck, F.; Rovis, T. *Nat. Chem.* **2018,** *10,* 1037–1041. doi:10.1038/s41557-018-0085-9
209. The molar extinction coefficient of 9-fluorenone was measured in *n*-heptane at a temperature of 4 K, see [210].
210. Zwarich, R.; Bree, A. *J. Mol. Spectrosc.* **1974,** *52,* 329–343. doi:10.1016/0022-2852(74)90183-0

211. Gilmore, K.; Seeberger, P. H. *Chem. Rec.* **2014,** *14,* 410–418. doi:10.1002/tcr.201402035
212. Elliott, L. D.; Knowles, J. P.; Koovits, P. J.; Maskill, K. G.; Ralph, M. J.; Lejeune, G.; Edwards, L. J.; Robinson, R. I.; Clemens, I. R.; Cox, B.; Pascoe, D. D.; Koch, G.; Eberle, M.; Berry, M. B.; Booker-Milburn, K. I. *Chem. – Eur. J.* **2014,** *20,* 15226–15232. doi:10.1002/chem.201404347
213. Noël, T. *J. Flow Chem.* **2017,** *7,* 87–93. doi:10.1556/1846.2017.00022
214. Cambié, D.; Bottecchia, C.; Straathof, N. J. W.; Hessel, V.; Noël, T. *Chem. Rev.* **2016,** *116,* 10276–10341. doi:10.1021/acs.chemrev.5b00707
215. Gawronski, J.; Kazmierczak, F.; Gawronska, K.; Rychlewska, U.; Nordén, B.; Holmén, A. *J. Am. Chem. Soc.* **1998,** *120,* 12083–12091. doi:10.1021/ja982131u
216. Kelterer, A.-M.; Mansha, A.; Iftikhar, F. J.; Zhang, Y.; Wang, W.; Xu, J.-H.; Grampp, G. *J. Mol. Model.* **2014,** *20,* 2344. doi:10.1007/s00894-014-2344-z
217. Munday, R. H.; Goodman, L.; Noonan, G. M. *Tetrahedron Lett.* **2019,** *60,* 606–609. doi:10.1016/j.tetlet.2019.01.037
218. Myszka, H.; Grzywacz, D.; Zdrowowicz, M.; Spisz, P.; Butowska, K.; Rak, J.; Piosik, J.; Jaśkiewicz, M.; Kamysz, W.; Liberek, B. *Bioorg. Chem.* **2020,** *96,* 103568. doi:10.1016/j.bioorg.2020.103568
219. Postigo, A. *Eur. J. Org. Chem.* **2018,** 6391–6404. doi:10.1002/ejoc.201801079
220. Woźniak, Ł.; Murphy, J. J.; Melchiorre, P. *J. Am. Chem. Soc.* **2015,** *137,* 5678–5681. doi:10.1021/jacs.5b03243
221. Beatty, J. W.; Douglas, J. J.; Miller, R.; McAtee, R. C.; Cole, K. P.; Stephenson, C. R. J. *Chem* **2016,** *1,* 456–472. doi:10.1016/j.chempr.2016.08.002
222. Xie, J.; Li, J.; Wurm, T.; Weingand, V.; Sung, H.-L.; Rominger, F.; Rudolph, M.; Hashmi, A. S. K. *Org. Chem. Front.* **2016,** *3,* 841–845. doi:10.1039/c6qo00158k
223. Pham, P. V.; Nagib, D. A.; MacMillan, D. W. C. *Angew. Chem., Int. Ed.* **2011,** *50,* 6119–6122. doi:10.1002/anie.201101861
224. Tomita, R.; Yasu, Y.; Koike, T.; Akita, M. *Angew. Chem., Int. Ed.* **2014,** *53,* 7144–7148. doi:10.1002/anie.201403590
225. Zhao, L.; Li, P.; Zhang, H.; Wang, L. *Org. Chem. Front.* **2019,** *6,* 87–93. doi:10.1039/c8qo01079j
226. To, T.-L.; Fadul, M. J.; Shu, X. *Nat. Commun.* **2014,** *5,* 4072. doi:10.1038/ncomms5072
227. Martinez, G. R.; Ravanat, J.-L.; Cadet, J.; Miyamoto, S.; Medeiros, M. H. G.; Di Mascio, P. *J. Am. Chem. Soc.* **2004,** *126,* 3056–3057. doi:10.1021/ja039111z
228. Baptista, M. S.; Cadet, J.; Di Mascio, P.; Ghogare, A. A.; Greer, A.; Hamblin, M. R.; Lorente, C.; Nunez, S. C.; Ribeiro, M. S.; Thomas, A. H.; Vignoni, M.; Yoshimura, T. M. *Photochem. Photobiol.* **2017,** *93,* 912–919. doi:10.1111/php.12716
229. Lin, Q.-Y.; Xu, X.-H.; Qing, F.-L. *J. Org. Chem.* **2014,** *79,* 10434–10446. doi:10.1021/jo502040t
230. The authors did not specify the power or wavelength of their LEDs. One assumes “blue” could mean anywhere in the range of 380–470 nm.
231. Wrighton, M.; Markham, J. *J. Phys. Chem.* **1973,** *77,* 3042–3044. doi:10.1021/j100644a002
232. Chen, F.-C.; He, G.; Yang, Y. *Appl. Phys. Lett.* **2003,** *82,* 1006–1008. doi:10.1063/1.1544658
233. Calvin, M.; Alter, H. W. *J. Chem. Phys.* **1951,** *19,* 765–767. doi:10.1063/1.1748349
234. Ni, T.; Caldwell, R. A.; Melton, L. A. *J. Am. Chem. Soc.* **1989,** *111,* 457–464. doi:10.1021/ja00184a008
235. Kawahara, S.-i.; Tsuzuki, S.; Uchimaru, T. *J. Phys. Chem. A* **2004,** *108,* 6744–6749. doi:10.1021/jp047646o
236. Li, P.; Maier, J. M.; Vik, E. C.; Yehl, C. J.; Dial, B. E.; Rickher, A. E.; Smith, M. D.; Pellechia, P. J.; Shimizu, K. D. *Angew. Chem., Int. Ed.* **2017,** *56,* 7209–7212. doi:10.1002/anie.201702950
237. Eisenhofer, A.; Hioe, J.; Gschwind, R. M.; König, B. *Eur. J. Org. Chem.* **2017,** 2194–2204. doi:10.1002/ejoc.201700211
238. Nitschke, P.; Lokesh, N.; Gschwind, R. M. *Prog. Nucl. Magn. Reson. Spectrosc.* **2019,** *114–115,* 86–134. doi:10.1016/j.pnmrs.2019.06.001
239. Liu, W.; Huang, X.; Placzek, M. S.; Krska, S. W.; McQuade, P.; Hooker, J. M.; Groves, J. T. *Chem. Sci.* **2018,** *9,* 1168–1172. doi:10.1039/c7sc04545j

License and Terms

This is an Open Access article under the terms of the Creative Commons Attribution License (https://creativecommons.org/licenses/by/4.0). Please note that the reuse, redistribution and reproduction in particular requires that the authors and source are credited.

The license is subject to the *Beilstein Journal of Organic Chemistry* terms and conditions: (https://www.beilstein-journals.org/bjoc)

The definitive version of this article is the electronic one which can be found at: https://doi.org/10.3762/bjoc.16.183

BEILSTEIN JOURNAL OF ORGANIC CHEMISTRY

Regioselective cobalt(II)-catalyzed [2 + 3] cycloaddition reaction of fluoroalkylated alkynes with 2-formylphenylboronic acids: easy access to 2-fluoroalkylated indenols

Tatsuya Kumon, Miroku Shimada, Jianyan Wu, Shigeyuki Yamada and Tsutomu Konno*

Full Research Paper

Open Access

Address:
Faculty of Molecular Chemistry and Engineering, Kyoto Institute of Technology, Matsugasaki, Sakyo-ku, Kyoto 606-8585, Japan

Email:
Tsutomu Konno* - konno@kit.ac.jp

* Corresponding author

Keywords:
[2 + 3] cycloaddition; cobalt catalyst; fluorine-containing; indenols; regioselective

Beilstein J. Org. Chem. **2020,** *16,* 2193–2200.
https://doi.org/10.3762/bjoc.16.184

Received: 13 July 2020
Accepted: 25 August 2020
Published: 04 September 2020

This article is part of the thematic issue "Organo-fluorine chemistry V".

Guest Editor: D. O'Hagan

© 2020 Kumon et al.; licensee Beilstein-Institut.
License and terms: see end of document.

Abstract

[2 + 3] cycloaddition reactions of fluorinated alkynes with 2-formylphenylboronic acids under the influence of $Co(acac)_2{\cdot}2H_2O$ in two-component solvents of acetonitrile/2-propanol at reflux temperature for 18 h took place smoothly, affording the corresponding fluoroalkylated indenol derivatives in good yields. This reaction shows excellent regioselectivity, giving 2-fluoroalkylated indenols, together with a very small amount of 3-fluoroalkylated indanones as side products.

Introduction

2,3-Disubstituted indenol derivatives are important compounds possessing high potential due to the insecticidal, myorelaxation, and antiproliferative properties (Figure 1) [1-12]. Thus, enormous attention has been paid to 2- or 3-fluoroalkylated indenol derivatives in the field of medicinal and agrochemical drug design since a fluorine atom can very often bring about an increasing effect on the pharmacological activity owing to the unique nature of the fluorine atom(s) [13-18]. However, reports on a synthetic protocol for 2- or 3-fluoroalkylated indenols are very limited [19-22]. Recently, Yamazaki et al. have reported the reaction of the CF_3-containing phthalide **B** prepared from the 1,2-diester **A** with the Ruppert–Prakash reagent ($TMSCF_3$) in the presence of a catalytic amount of CsF (Scheme 1a). According to this paper, phthalide **B** reacted smoothly with phenylthiomethyllithium to give the corresponding CF_3-containing indanone **C**. Then, dehydration of **C** using *p*-$TsOH{\cdot}H_2O$, followed by a 1,2-reduction led to 3-fluoroalky-

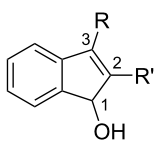

Figure 1: Indenol skeleton.

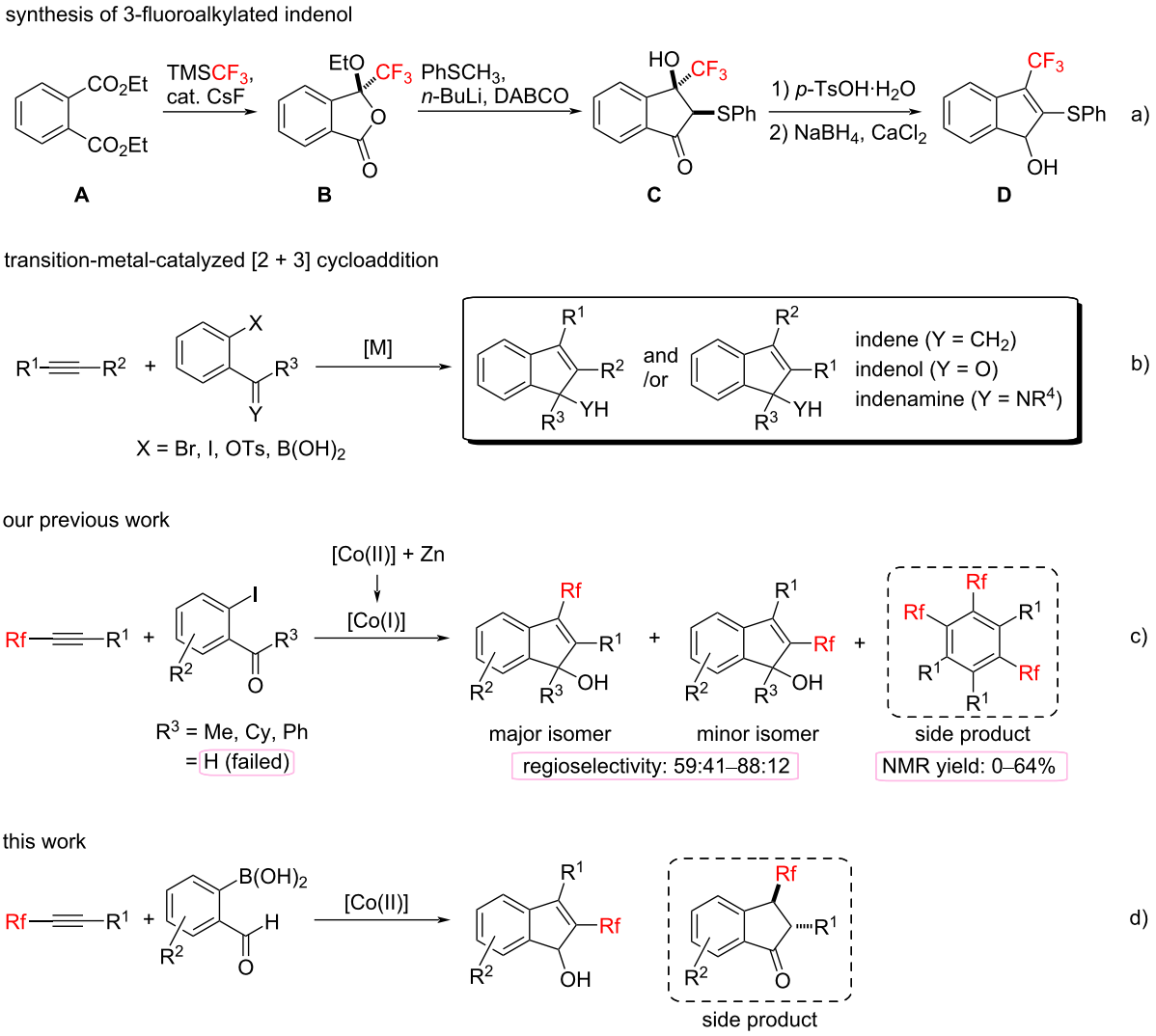

Scheme 1: Synthesis of 2,3-disubstituted indene derivatives.

lated indenol **D**. All of these reactions produced the desired products in good yield, however, this protocol is limited to the introduction of a trifluoromethyl group at the 3-position of the indenol. To the best of our knowledge, there are no reports on the practical synthesis of disubstituted 2-fluoroalkylated indenols so far.

Transition-metal-catalyzed carbocyclization reactions of alkynes with benzene derivatives having a leaving group X (X = Br, I, OTs, $B(OH)_2$) have been widely considered as one of the most efficient and convenient protocols for the construction of various 2,3-disubstituted indene derivatives, such as indenols and indenamines (Scheme 1b) [23-25]. There have been numerous studies on the reaction with nonfluorinated alkynes under the influence of various transition metals. Despite their effective advantages, on the other hand, the reports on cycloaddition reactions with fluorine-containing alkynes for the construction of fluoroalkylated indene derivatives are rare [21,26].

Recently, our group has reported the first practical synthesis of fluoroalkylated indenol derivatives using various fluoroalkylated alkynes with 2-iodoaryl ketones via cobalt-catalyzed carbocyclizations (Scheme 1c) [21]. Although our previous work was practical to produce interesting fluoroalkylated indenol derivatives, some drawbacks still remain unsolved. Initially, the reaction showed a low regioselectivity, leading to a mixture of 3-fluoroalkylated and 2-fluoroalkylated indenols, which was difficult to separate. Secondly, a trimer of fluoroalkylated alkynes was obtained as a side product since the cobalt(I) species produced by the cobalt(II)/Zn system worked as a suitable catalyst, leading to the corresponding trimer of the

fluoroalkylated alkyne, as reported by our group [27]. Finally, only 2-iodoaryl ketones (R^3 = Me, Cy, Ph) were applicable in this catalytic reaction, whereas the cycloaddition using 2-iodobenzaldehyde (R^3 = H) did not work at all. Therefore, the development of practical protocols for [2 + 3] cycloaddition reactions with a broader substrate scope for the synthesis of fluoroalkylated indenols is still required. Herein we present a synthesis of 2-fluoroalkylated indenols via [2 + 3] cycloadditions of various fluorinated alkynes with 2-formylphenylboronic acids in the presence of cobalt(II) species as a catalyst to suppress the trimerization products (Scheme 1d).

Results and Discussion

Initially, we carried out the screening of the reaction conditions for the cobalt-catalyzed [2 + 3] cycloaddition using fluoroalkylated alkyne **1a** and 2-formylphenylboronic acid (**2A**) [28]. The results are summarized in Table 1.

The cycloaddition of the fluoroalkylated alkyne **1a** with 2.0 equiv of 2-formylphenylboronic acid (**2A**) in the presence of 10 mol % each of $Co(acac)_2{\cdot}2H_2O$ and 1,2- bis(diphenylphosphino)ethane (dppe) in CH_3CN at 80 °C for 18 h proceeded to afford the corresponding cyclic products **3aA** and **4aA** in 76% yield as a regioisomeric 66:34 mixture (Table 1, entry 1). Intriguingly, a small amount of the undesired *trans*-3-fluoroalkylated indanone **5aA** was obtained as a side product, whereas the *cis*-3-fluoroalkylated and *cis/trans*-2-fluoroalkylated indanones were not observed. As shown in Table 1, entries 2–4, changing the solvent from CH_3CN to DCE, iPrOH, or 1,4-dioxane caused an appreciable decrease in the yield. It should be noted that the use of a mixed solvent of CH_3CN and iPrOH significantly improved the isomeric ratio of **3aA** and **4aA** (>99:1), although 48% of the indanone **5aA** was also obtained (Table 1, entry 5). The cycloaddition reaction in the presence of $CoCl_2$ instead of $Co(acac)_2{\cdot}2H_2O$ produced the desired **3aA** and **4aA** in 81% yield, with a lower selectivity of 66:34 (Table 1, entry 6), while the other cobalt catalysts, such as $Co(OAc)_2{\cdot}4H_2O$, $Co(acac)_3$, and $Co(OH)_2$ resulted in the sluggish formation of the fluoroalkylated indenols or indanone (Table 1, entries 7–9). When 1,3-bis(diphenylphosphino)propane (dppp) was used as a phosphine ligand, the desired indenol **3aA** was obtained in a moderate yield and with high regioselectivity of 98:2, together with a very small amount of the fluoroalkylated indanone **5aA** (Table 1, entry 10). On the other hand, 1,4-bis(diphenylphosphino)butane (dppb) was not a suitable ligand for this reaction, leading only to trace amount of the indanone **5aA** (Table 1, entry 11). Finally, the desired cyclization product was produced in a good yield at the reflux tem-

Table 1: Screening for the reaction conditions of the cobalt-catalyzed [2 + 3] cycloaddition using the fluoroalkylated alkyne **1a** and 2-formylphenylboronic acid (**2A**).

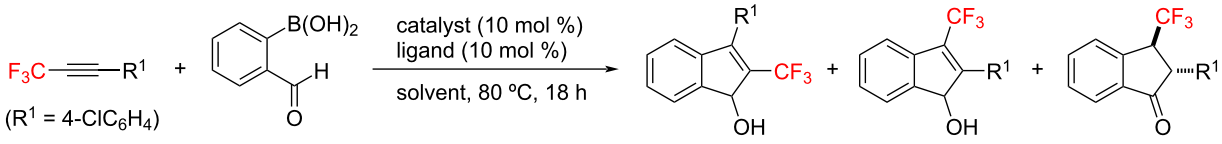

1a **2A** (2.0 equiv) **3aA** **4aA** **5aA**

entry	solvent	catalyst	ligand	yield[a]/% **3aA** + **4aA**	ratio[a] **3aA**/**4aA**	yield[a]/% **5aA**
1	CH_3CN	$Co(acac)_2{\cdot}2H_2O$	dppe	76	66:34	12
2	DCE	$Co(acac)_2{\cdot}2H_2O$	dppe	8	49:51	0
3	iPrOH	$Co(acac)_2{\cdot}2H_2O$	dppe	6	>99:1	3
4	1,4-dioxane	$Co(acac)_2{\cdot}2H_2O$	dppe	14	64:36	1
5	CH_3CN/iPrOH 3:1, v/v	$Co(acac)_2{\cdot}2H_2O$	dppe	48	>99:1	48
6	CH_3CN/iPrOH 3:1, v/v	$CoCl_2$	dppe	81	66:34	16
7	CH_3CN/iPrOH 3:1, v/v	$Co(OAc)_2{\cdot}4H_2O$	dppe	24	>99:1	24
8	CH_3CN/iPrOH 3:1, v/v	$Co(acac)_3$	dppe	15	70:30	11
9	CH_3CN/iPrOH 3:1, v/v	$Co(OH)_2$	dppe	8	39:61	3
10	CH_3CN/iPrOH 3:1, v/v	$Co(acac)_2{\cdot}2H_2O$	dppp	59	98:2	3
11	CH_3CN/iPrOH 3:1, v/v	$Co(acac)_2{\cdot}2H_2O$	dppb	trace	>99:1	2
12[b]	CH_3CN/iPrOH 3:1, v/v	$Co(acac)_2{\cdot}2H_2O$	dppp	75	>99:1	6
13[c]	CH_3CN/iPrOH 3:1, v/v	$Co(acac)_2{\cdot}2H_2O$	dppp	49	73:27	–

[a]Determined by ^{19}F NMR spectroscopy. [b]Carried out at the reflux temperature. [c]2-Acetylphenylboronic acid was used.

perature while maintaining the selectivity (>99:1, Table 1, entry 12). Unfortunately, 2-acetylphenylboronic acid instead of 2-formylphenylboronic acid (**2A**) showed a lower reactivity and a poor regioselectivity (73:27, Table 1, entry 13) [29].

With the optimized reaction conditions (Table 1, entry 12), we explored the substrate scope for the [2 + 3] cycloaddition of various fluoroalkylated alkynes **1** and 2-formylphenylboronic acids **2**. The results are summarized in Scheme 2.

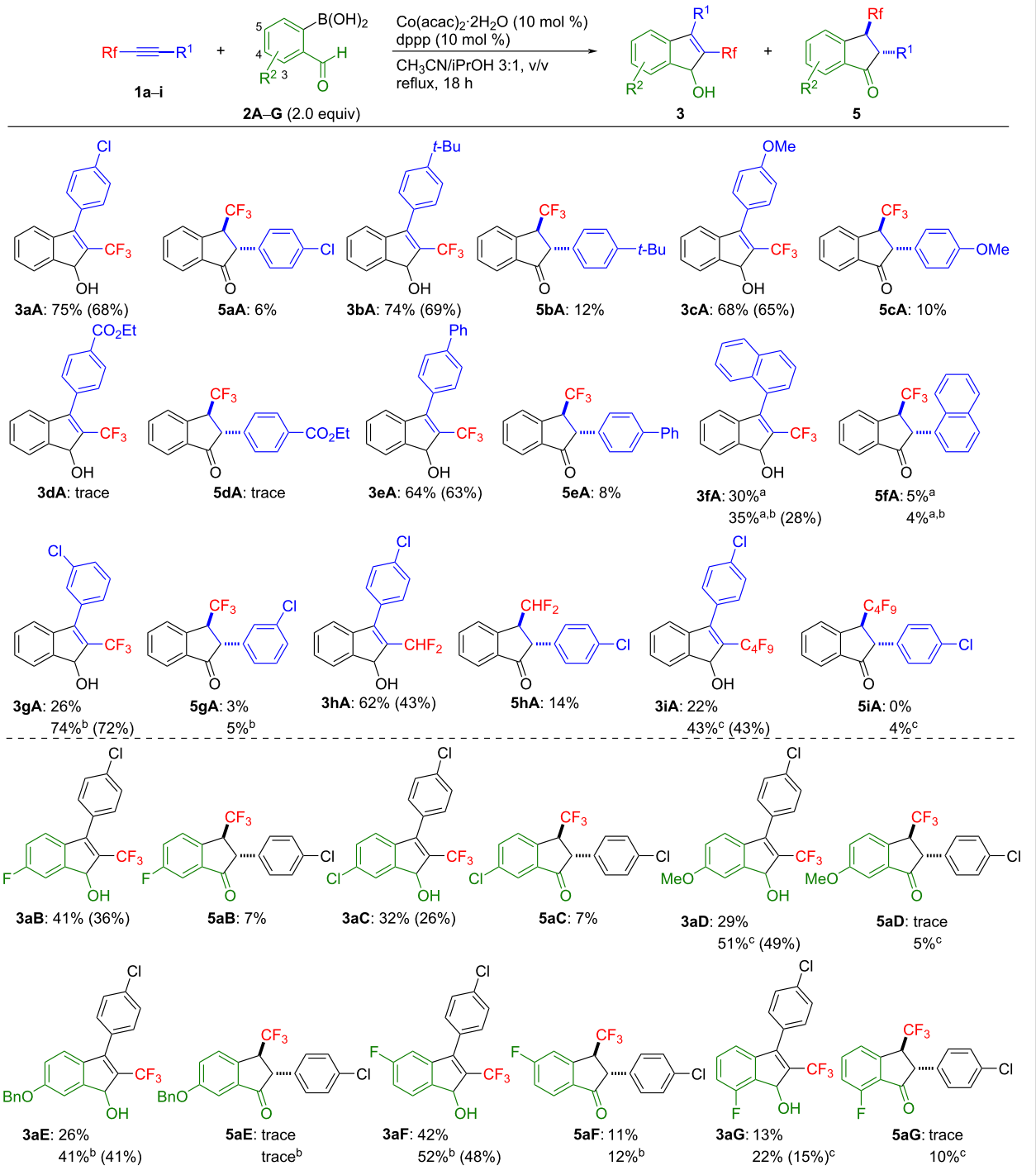

Scheme 2: Cobalt-catalyzed [2 + 3] cycloaddition reaction of the fluorinated alkynes **1** with various 2-formylphenylboronic acids **2**. The yields were determined by ^{19}F NMR spectroscopy. The values in parentheses are the isolated yield of **3**. [a]Atropisomers of **3fA** and **5fA** were detected. [b]3.0 equiv of **2** were used. [c]The reaction was carried out using 3.0 equiv of **2** in the presence of 20 mol % each of $Co(acac)_2{\cdot}2H_2O$ and dppp at 110 °C in a sealed tube.

The substrates **1**, having an electron-donating substituent on the benzene ring of the fluoroalkylated alkyne, such as *t*-Bu or MeO, reacted efficiently, leading to the desired fluoroalkylated indenols **3bA** and **3cA** in 74% and 68% yield, respectively. However, the substrate containing the electron-withdrawing group CO_2Et on the benzene ring of **1** showed a lower reactivity in this reaction (see **3dA**). The cycloaddition reaction using a fluoroalkylated alkyne having a 4-biphenyl group as R^1 took place smoothly, giving the corresponding indenol **3eA** in a good yield. Though bulkier groups as R^1, such as 1-naphthyl or 3-chlorophenyl, reduced the reactivity (see **3fA** and **3gA**), an excess loading of the boronic acid improved the yield appreciably. For the difluoromethylated alkyne **1h**, the desired indenol **3hA** was obtained in 62% yield under optimal conditions. However, the nonafluorobutylated alkyne **1i** showed a lower reactivity, giving the corresponding indenol **3iA** in 22% yield. Therefore, when the reaction was carried out using 3.0 equiv of the boronic acid **2A** and 20 mol % each of $Co(acac)_2{\cdot}2H_2O$ and dppp at 110 °C, the desired 2-fluoroalkylated indenol **3iA** was obtained in 43% yield.

Subsequently, we investigated the [2 + 3] cycloaddition reaction of the fluoroalkylated alkyne **1a** (R^1 = 4-ClC_6H_4) with variously substituted 2-formylphenylboronic acids **2**. Electron-deficient formylphenylboronic acids possessing a fluorine or chlorine atom on the benzene ring gave the corresponding indenols **3aB** and **3aC** in 41% and 32% yield, respectively, which could not be improved even when an excess loading of the reagents, prolonging the reaction time, and a higher reaction temperature were applied. However, the exposure of the fluoroalkylated alkynes **1a** to electron-rich substrates, e.g., **2D** and **2E**, lead to the indenols in approximately 30% yield, and the use of an excessive amount of boronic acid, $Co(acac)_2{\cdot}2H_2O$, or dppp improved the yields of the desired indenols, forming **3aD** in 51% and **3aE** in 41% yield. Changing the substituent position on the aromatic ring of the phenylboronic acid from the 4- to the 5-position did not affect the result, giving the indenol **3aF** in 52% yield. However, a boronic acid with a fluorine atom at the 3-position did not lead to a satisfactory result, with the cyclic product **3aG** being formed in only 22% yield.

Substituted indenones and indanones widely exist in nature, and these skeletons are important classes of organic compounds due to diverse biological and pharmacological activities [30-32]. Therefore, we also accomplished the synthesis of 2-fluoroalkylated indenone and indanone by simple reactions (Scheme 3). An allylic oxidation was carried out with 10 equiv of manganese dioxide in dichloromethane as the solvent at 0 °C for 30 minutes, leading to the corresponding 2-fluoroalkylated indenone **6** in 98% yield. Subsequently, a hydrogenolysis with 1 mol % of Pd/C under a hydrogen atmosphere in methanol at room temperature for 15 h produced the desired 2-fluoroalkylated indanone **7** as the *trans*-isomer in 69% yield [33-35].

The stereochemical assignment of **5aA** and **7** was carried out based on NMR techniques, as shown in Scheme 4 [36]. A strong correlation between the carbonyl carbon atom and H_a was obtained, whereas the cross-peak between the carbonyl carbon atom and H_b was not observed, strongly indicating that the indanone **5aA** possessed a CF_3 group at the 3-position. On the other hand, the cross-peak between the carbonyl carbon atom and H_c of the indanone **7** was obtained, but there was no cross-peak between the carbonyl carbon atom and H_d, meaning that the indanone **7** has a CF_3 group at the 2-position. This result indicated that the indenol **3aA**, which is the precursor of the 2-fluoroalkylated indanone **7**, also possess a trifluoromethyl group at the 2-position. Each H_a–H_b coupling of **5aA** and each H_c–H_d coupling of **7** appeared as a doublet, with J = 4.0 Hz and 4.6 Hz, respectively. These NMR results suggested that the fluoroalkylated indanones **5aA** and **7** were *trans*-isomers, and previous results showed that the J value of the nonfluoroalkylated *trans*-2,3-disubstituted indanone **8** is 5.0 Hz, whereas the J value of the *cis*-isomer **9** is 8.0 Hz [37].

The proposed catalytic cycles for the cobalt-catalyzed [2 + 3] cycloaddition process leading to 2-fluoroalkylated indenols and

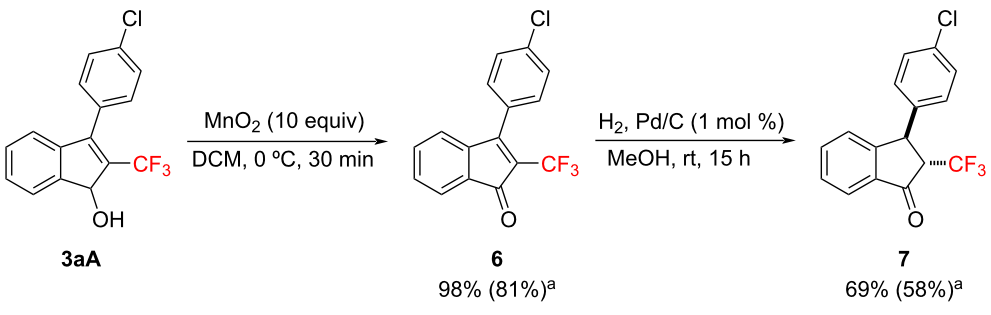

Scheme 3: Synthesis of the fluoroalkylated indenone **6** and the indanone **7** from the indenol **3aA**. The yields were determined by ^{19}F NMR spectroscopy. The values in parentheses are the isolated yields.

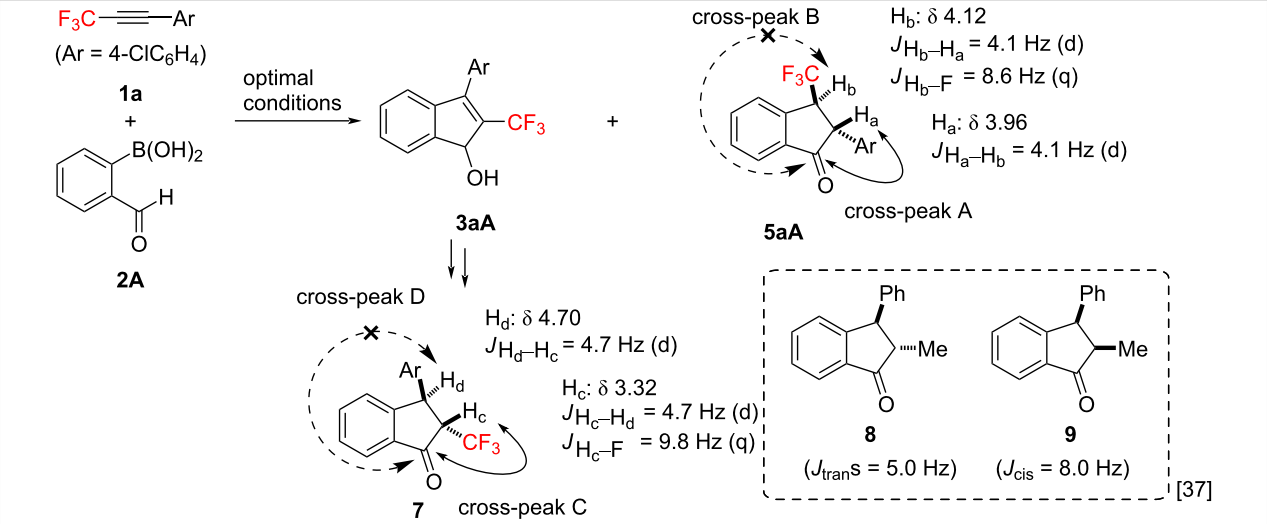

Scheme 4: Stereochemical assignment of **5aA** and **7** based on NMR techniques. The cross-peaks were observed through HMBC measurements.

3-fluoroalkylated indanones are shown in Scheme 5 [28,38]. Thus, the reaction presumably proceeds as follows: (1) transmetalation of the cobalt catalyst with 2-formylphenylboronic acids (**2**) gives the arylcobalt species **Int-1**, (2) insertion of the alkyne **1** into the [Co]–Ar bond (see **Int-2a**) [39], (3) migration insertion into the formyl moiety to afford the corresponding cobalt alkoxide **Int-3a**, (4) protonation of **Int-3a** with HX (X = acac, OiPr, or OH), giving rise to the desired 2-fluoroalkylated indenol **3**.

The formation of the 3-fluoroalkylated indanones as a side product may be explained based on the previous literature

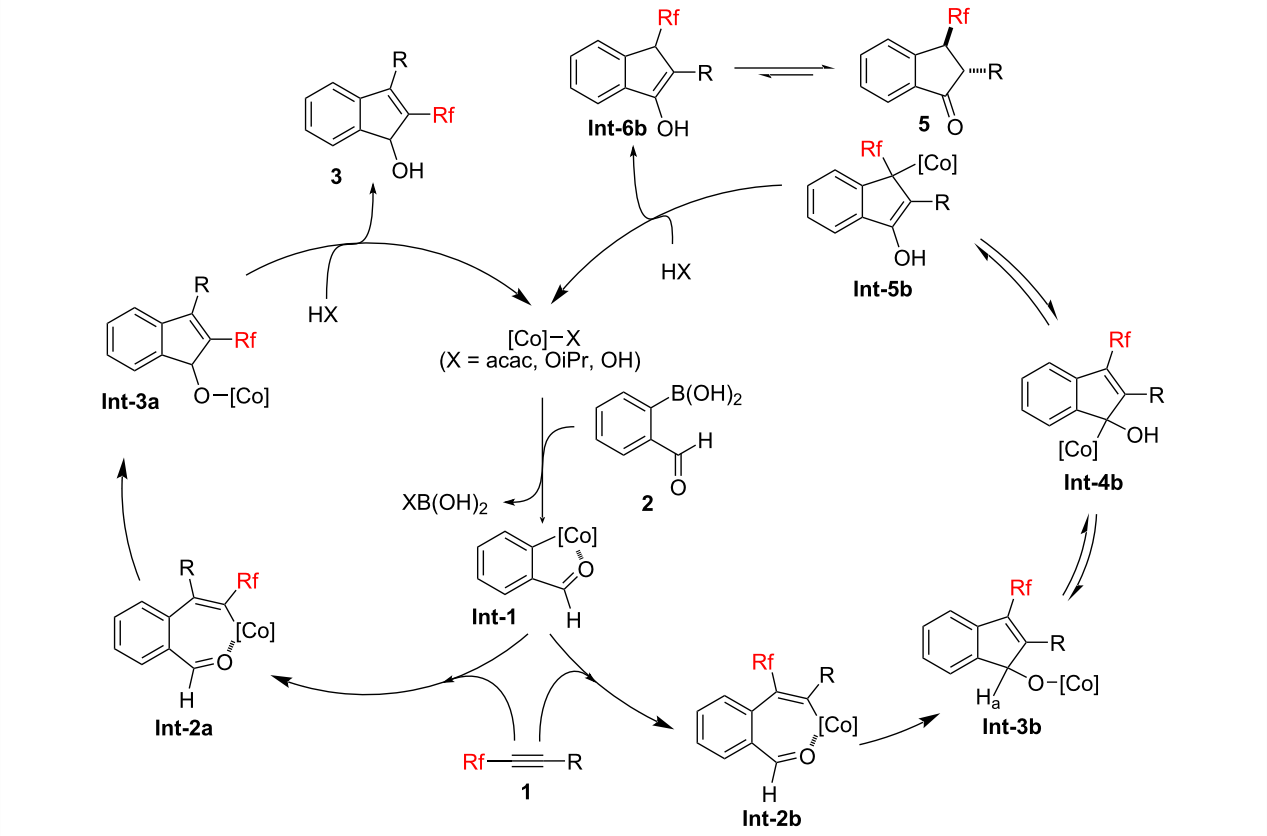

Scheme 5: Proposed reaction mechanism.

[20,40]. The reaction of **Int-1** with the alkynes **1** also gives **Int-2b** as a regioisomeric intermediate of **Int-2a**, leading to the 3-fluoroalkylated cobalt alkoxide **Int-3b**. Subsequently, the proton shift of the cobalt alkoxide **Int-3b** provides the allylcobalt species **Int-4b** because the acidity of the proton H_a of **Int-3b** is the same as, or higher than the hydroxy group of **Int-4b** due to the electron-withdrawing effect of the fluoroalkyl group. It should be noted that this process is probably accelerated by 2-propanol or H_2O, which is explained by the results that the most 3-fluoroalkylated indenol **4aA** was converted into the indanone **5aA** in the reaction, using 2-propanol as the solvent and a cobalt hydrate as a catalyst, such as $Co(acac)_2{\cdot}2H_2O$ and $Co(OAc)_2{\cdot}4H_2O$, respectively (Table 1, entries 3, 5, and 7).

The compound **Int-4b** produced the allylcobalt species **Int-5b** with a stabilized C–[Co] bond due to the electron-withdrawing ability of the fluoroalkyl group. The **Int-5b** species undergoes protonation at the carbon bonded to the fluoroalkyl group, giving the enol **Int-6b**. Finally, the enol **Int-6b** produces the 3-fluoroalkylated indanone **5** via keto–enol tautomerism.

Conclusion

In conclusion, we developed a practical and efficient synthetic protocol for 2-fluoroalkylated indenol derivatives via a cobalt-catalyzed [2 + 3] cycloaddition reaction using fluorinated alkynes and 2-formylphenylboronic acids. It was revealed that the reaction using dppp as a ligand showed a high regioselectivity, leading to 2-fluoroalkylated indenols in good yield. Moreover, the side product was a small amount of 3-fluoroalkylated indanones, which was easily separated from the 2-fluoroalkylated indenols due to the lower polarity of indanones compared to indenols. Finally, 2-fluoroalkylated indenol was simply converted into the corresponding 2-fluoroalkylated indenone and indanone in good to excellent yield.

Supporting Information

Supporting Information File 1

Experimental procedures, characterization data (^1H, ^{13}C, ^{19}F NMR, IR, and HRMS), copies of ^1H, ^{13}C, and ^{19}F NMR spectra.
[https://www.beilstein-journals.org/bjoc/content/supplementary/1860-5397-16-184-S1.pdf]

Acknowledgements

We sincerely thank the Tosoh Finechem Corp. for a generous gift of 2-bromo-3,3,3-trifluoroprop-1-ene.

ORCID® iDs

Tatsuya Kumon - https://orcid.org/0000-0003-0862-1218
Shigeyuki Yamada - https://orcid.org/0000-0002-6379-0447
Tsutomu Konno - https://orcid.org/0000-0002-5146-9840

References

1. Ishiguro, Y.; Okamoto, K.; Ojima, F.; Sonoda, Y. *Chem. Lett.* **1993,** *22,* 1139–1140. doi:10.1246/cl.1993.1139
2. Clark, W. M.; Tickner-Eldridge, A. M.; Huang, G. K.; Pridgen, L. N.; Olsen, M. A.; Mills, R. J.; Lantos, I.; Baine, N. H. *J. Am. Chem. Soc.* **1998,** *120,* 4550–4551. doi:10.1021/ja973882j
3. Jiang, Z.-H.; Hwang, G.-S.; Xi, Z.; Goldberg, I. H. *J. Am. Chem. Soc.* **2002,** *124,* 3216–3217. doi:10.1021/ja0176292
4. Upadhayaya, R. S.; Shinde, P. D.; Kadam, S. A.; Bawane, A. N.; Sayyed, A. Y.; Kardile, R. A.; Gitay, P. N.; Lahore, S. V.; Dixit, S. S.; Földesi, A.; Chattopadhyaya, J. *Eur. J. Med. Chem.* **2011,** *46,* 1306–1324. doi:10.1016/j.ejmech.2011.01.053
5. Liebeskind, L. S.; Gasdaska, J. R.; McCallum, J. S.; Tremont, S. J. *J. Org. Chem.* **1989,** *54,* 669–677. doi:10.1021/jo00264a030
6. Robinson, N. P.; Main, L.; Nicholson, B. K. *J. Organomet. Chem.* **1989,** *364,* C37–C39. doi:10.1016/0022-328x(89)87157-8
7. Quan, L. G.; Gevorgyan, V.; Yamamoto, Y. *J. Am. Chem. Soc.* **1999,** *121,* 3545–3546. doi:10.1021/ja983645w
8. Chang, K.-J.; Rayabarapu, D. K.; Cheng, C.-H. *J. Org. Chem.* **2004,** *69,* 4781–4787. doi:10.1021/jo049506g
9. Singh, P. P.; Reddy, P. B.; Sawant, S. D.; Koul, S.; Taneja, S. C.; Kumar, H. M. S. *Tetrahedron Lett.* **2006,** *47,* 7241–7243. doi:10.1016/j.tetlet.2006.07.126
10. Chinnagolla, R. K.; Jeganmohan, M. *Eur. J. Org. Chem.* **2012,** 417–423. doi:10.1002/ejoc.201101364
11. Zhang, C.; Li, H.; Pei, C.; Qiu, L.; Hu, W.; Bao, X.; Xu, X. *ACS Catal.* **2019,** *9,* 2440–2447. doi:10.1021/acscatal.8b04144
12. Gu, C.-X.; Chen, W.-W.; Xu, M.-H. *J. Org. Chem.* **2020,** *85,* 3887–3893. doi:10.1021/acs.joc.9b02958
13. Meanwell, N. A. *J. Med. Chem.* **2018,** *61,* 5822–5880. doi:10.1021/acs.jmedchem.7b01788
14. Zhou, Y.; Wang, J.; Gu, Z.; Wang, S.; Zhu, W.; Aceña, J. L.; Soloshonok, V. A.; Izawa, K.; Liu, H. *Chem. Rev.* **2016,** *116,* 422–518. doi:10.1021/acs.chemrev.5b00392
15. Wang, J.; Sánchez-Roselló, M.; Aceña, J. L.; del Pozo, C.; Sorochinsky, A. E.; Fustero, S.; Soloshonok, V. A.; Liu, H. *Chem. Rev.* **2014,** *114,* 2432–2506. doi:10.1021/cr4002879
16. Kirk, K. L. *J. Fluorine Chem.* **2006,** *127,* 1013–1029. doi:10.1016/j.jfluchem.2006.06.007
17. Bégué, J.-P.; Bonnet-Delpon, D. *J. Fluorine Chem.* **2006,** *127,* 992–1012. doi:10.1016/j.jfluchem.2006.05.006
18. Isanbor, C.; O'Hagan, D. *J. Fluorine Chem.* **2006,** *127,* 303–319. doi:10.1016/j.jfluchem.2006.01.011
19. Allen, A. D.; Fujio, M.; Mohammed, N.; Tidwell, T. T.; Tsuji, Y. *J. Org. Chem.* **1997,** *62,* 246–252. doi:10.1021/jo961387k
20. Mitobe, K.; Terashima, K.; Kawasaki-Takasuka, T.; Agou, T.; Kubota, T.; Yamazaki, T. *Eur. J. Org. Chem.* **2018,** 6944–6951. doi:10.1002/ejoc.201801384
21. Kumon, T.; Yoshida, K.; Yamada, S.; Agou, T.; Kubota, T.; Konno, T. *Tetrahedron* **2019,** *75,* 3713–3721. doi:10.1016/j.tet.2019.05.042
22. Ghavtadze, N.; Fröhlich, R.; Bergander, K.; Würthwein, E.-U. *Synthesis* **2008,** 3397–3406. doi:10.1055/s-0028-1083188
23. Chinchilla, R.; Nájera, C. *Chem. Rev.* **2014,** *114,* 1783–1826. doi:10.1021/cr400133p

24. Gandeepan, P.; Cheng, C.-H. *Acc. Chem. Res.* **2015,** *48,* 1194–1206. doi:10.1021/ar500463r
25. Boyarskiy, V. P.; Ryabukhin, D. S.; Bokach, N. A.; Vasilyev, A. V. *Chem. Rev.* **2016,** *116,* 5894–5986. doi:10.1021/acs.chemrev.5b00514
26. Jeon, S. L.; Kim, J. K.; Son, J. B.; Kim, B. T.; Jeong, I. H. *Tetrahedron Lett.* **2006,** *47,* 9107–9111. doi:10.1016/j.tetlet.2006.10.088
27. Kumon, T.; Yamada, S.; Agou, T.; Kubota, T.; Konno, T. *J. Fluorine Chem.* **2018,** *213,* 11–17. doi:10.1016/j.jfluchem.2018.06.004
28. Ueda, M.; Ueno, T.; Suyama, Y.; Ryu, I. *Tetrahedron Lett.* **2017,** *58,* 2972–2974. doi:10.1016/j.tetlet.2017.06.049
29. The lower regioselectivity when using 2-acetylphenylboronic acid instead of 2-formylphenylboronic (**2A**) still remains unclear. However, a similar tendency for the regioselectivity has been observed in the cobalt-catalyzed [2 + 3] cycloaddition using an unsymmetrical internal alkyne for the construction of indenol derivatives, see [8].
30. Ernst-Russell, M. A.; Chai, C. L. L.; Wardlaw, J. H.; Elix, J. A. *J. Nat. Prod.* **2000,** *63,* 129–131. doi:10.1021/np9903245
31. Morrell, A.; Placzek, M.; Parmley, S.; Grella, B.; Antony, S.; Pommier, Y.; Cushman, M. *J. Med. Chem.* **2007,** *50,* 4388–4404. doi:10.1021/jm070307+
32. Turek, M.; Szczęsna, D.; Koprowski, M.; Bałczewski, P. *Beilstein J. Org. Chem.* **2017,** *13,* 451–494. doi:10.3762/bjoc.13.48
33. It is well-known that α-trifluoromethylated carbonyl compounds have a strongly acidic α-hydrogen atom due to the highly electron-withdrawing trifluoromethyl and carbonyl groups and are easily enolized. In the present study, it is therefore highly possible that the *cis*-isomer generated through the catalytic hydrogenation of the indenone **6** isomerized to the much more thermally stable *trans*-isomer **7** via enolization.
34. Cooke, E.; Paradellis, T. C.; Edward, J. T. *Can. J. Chem.* **1982,** *60,* 29–34. doi:10.1139/v82-006
35. Barth, W.; Paquette, L. A. *J. Org. Chem.* **1985,** *50,* 2438–2443. doi:10.1021/jo00214a008
36. Generally, the signal of the 2-fluoroalkylated indenols **3** appeared at −56 ppm and that of the 3-fluoroalkylated indenols **4** appeared at −59 ppm.
37. Minatti, A.; Zheng, X.; Buchwald, S. L. *J. Org. Chem.* **2007,** *72,* 9253–9258. doi:10.1021/jo701741y
38. Lin, P.-S.; Jeganmohan, M.; Cheng, C.-H. *Chem. – Eur. J.* **2008,** *14,* 11296–11299. doi:10.1002/chem.200801858
39. Since a fluoroalkyl group has a very strong electron-withdrawing ability, the Rf–Cα–[Co] bond may be stronger than the Cβ–[Co] bond, which stabilizes the transition state of the insertion step. Therefore, **Int-2a** was produced as the major regioisomeric intermediate.
40. Hamada, Y.; Kawasaki-Takasuka, T.; Yamazaki, T. *Beilstein J. Org. Chem.* **2017,** *13,* 1507–1512. doi:10.3762/bjoc.13.149

License and Terms

This is an Open Access article under the terms of the Creative Commons Attribution License (https://creativecommons.org/licenses/by/4.0). Please note that the reuse, redistribution and reproduction in particular requires that the authors and source are credited.

The license is subject to the *Beilstein Journal of Organic Chemistry* terms and conditions: (https://www.beilstein-journals.org/bjoc)

The definitive version of this article is the electronic one which can be found at: https://doi.org/10.3762/bjoc.16.184

BEILSTEIN JOURNAL OF ORGANIC CHEMISTRY

Chan–Evans–Lam *N*1-(het)arylation and *N*1-alkenylation of 4-fluoroalkylpyrimidin-2(1*H*)-ones

Viktor M. Tkachuk[1], Oleh O. Lukianov[1], Mykhailo V. Vovk[1], Isabelle Gillaizeau[2] and Volodymyr A. Sukach[*1,3]

Full Research Paper

Open Access

Address:
[1]Institute of Organic Chemistry, National Academy of Sciences of Ukraine, [2]Institute of Organic and Analytical Chemistry, ICOA UMR 7311 CNRS, Université d'Orléans, rue de Chartres, 45100 Orléans, France and [3]Enamine LTD, 78 Chervonotkats'ka str., Kyiv 02094, Ukraine

Email:
Volodymyr A. Sukach[*] - vsukach@gmail.com

* Corresponding author

Keywords:
C–N cross-coupling; Chan–Evans–Lam reaction; pyrimidin-2(1*H*)-ones; fluoroalkyl group; boronic acids

Beilstein J. Org. Chem. **2020,** *16,* 2304–2313.
https://doi.org/10.3762/bjoc.16.191

Received: 11 July 2020
Accepted: 04 September 2020
Published: 17 September 2020

This article is part of the thematic issue "Organo-fluorine chemistry V".

Guest Editor: D. O'Hagan

© 2020 Tkachuk et al.; licensee Beilstein-Institut.
License and terms: see end of document.

Abstract

The Chan–Evans–Lam reaction of 1-unsubstituted 4-fluoroalkylpyrimidin-2(1*H*)-ones with arylboronic acids is reported as a facile synthetic route to hitherto unavailable *N*1-(het)aryl and *N*1-alkenyl derivatives of the corresponding pyrimidines. An efficient C–N bond-forming process is also observed by using boronic acid pinacol esters as coupling partners in the presence of Cu(II) acetate and boric acid. The 4-fluoroalkyl group on the pyrimidine ring significantly assists in the formation of the target *N*1-substituted products, in contrast to the 4-methyl and 4-unsubstituted substrates which do not undergo *N*1-arylation under similar reaction conditions.

Introduction

The catalytic formation of C–N bonds in the presence of transition metal salts is an essential transformation that permits the preparation *N*-(het)aryl-substituted amines and their derivatives including various nitrogen-containing heterocycles [1-5], an important class of compounds throughout chemical research. The copper-catalyzed arylation of the nucleophilic nitrogen atom, known as the Ullmann [6,7] reaction, and its modification by Chan and Lam [8] are favored due to the several advantages they offer versus the Pd counterpart (i.e., the Buchwald–Hartwig reaction) such as the lower cost and lower toxicity of the metal as well as their tolerance of aerobic conditions [2,9]. The efficiency of the Ullmann arylation has recently been greatly improved through extensive mechanistic investigation, ligand/precatalyst design and optimization studies [10-13]. As a result, the reaction has become feasible under milder conditions, whereas originally it required very high temperatures, and some

limitations including mostly low yields and intolerance of sensitive functional groups have been partially overcome [14]. A search for new efficient reagents for copper-catalyzed *N*-arylation has led to the recognition of arylboronic acids as uniquely advantageous means to perform C–N cross-coupling reactions [15-17]. The corresponding Ullmann-type reaction currently known as Chan–Evans–Lam (CEL) coupling is characterized by the combination of two nucleophilic reactants which implies that oxidative processes with atmospheric oxygen play a significant role in the generation of active copper-organic intermediates from boron-organic precursors [18-20].

Our interest in the development of *N*-arylation methods resonated with recent studies focused on the addition of various C-nucleophilic reagents to 4-trifluoromethylpyrimidin-2(1*H*)-ones I, heterocyclic analogues of activated ketimines (Figure 1), thus offering potential applications in the design of new heterocyclic chemotypes [21-25]. Compounds **I** are precursors of trifluoromethyl-substituted dihydropyrimidine derivatives which appear as original and potent scaffolds in medicinal chemistry, given the great importance of fluorinated groups in drug discovery [26-29]. On the strength of these results, herein we aim at extending the range of available compounds **I** by the introduction of (het)aryl and alkenyl substituents at the N1 position of the pyrimidine ring. Such derivatives have been hitherto unknown due to their synthetic inaccessibility by the conventional approach based on the formation of the pyrimidine moiety. For example, the attempted heterocyclization of ethoxyenones **II** (e.g., 4-ethoxy-1,1,1-trifluorobut-3-en-2-one) with *N*-arylureas, unlike the reaction with most *N*-alkylureas **III** (see Figure 1a, method A) [30], led to a complex mixture of products (unpublished data), which may be attributed to the decreased nucleophilicity of the nitrogen atom bound to the aryl group. On the other hand, a previously developed synthetic nontrivial method involving the cyclocondensation of *N*-(trifluorochloroethylidene) carbamates **IV** with β-amino crotonates **V** led only to 4-trifluoromethylpyrimidin-2(1*H*)-ones **I** bearing a 5-alkoxycarbonyl substituent ($R^{3/6}$ = CO_2Alk) due to the strong structural limitations of the nucleophilic enamine component (see Figure 1a, method **B**) [31]. The access to other *C5*-substituted and *C5*-unsubstituted pyrimidin-2(1*H*)-ones is beyond the synthetic scope of this approach.

At the same time, simple *N*1-unsubstituted pyrimidin-2(1*H*)-ones **1** (see Figure 1b) are readily available on a multigram scale from inexpensive reagents [32-34] and can serve as promising building blocks for further functionalization, including (het)aryl or alkenyl substitution at the N1 atom. However, direct arylation of **1** with aryl halides under Ullmann reaction conditions is a low-efficiency process giving only complex mixtures. It is likely that the harsh thermal conditions required for the coupling are not tolerated with the highly electrophilic ketimine moiety of 4-trifluoromethylpyrimidin-2(1*H*)-ones. The CEL reaction was successfully applied in the *N*-arylation of many heterocyclic systems [35-37] including non-fluorinated pyrimidin-2(1*H*)-ones [38,39] under mild conditions. There are a few thorough studies on this reaction with pyrimidine and purine nucleoside bases and their derivatives which are most closely

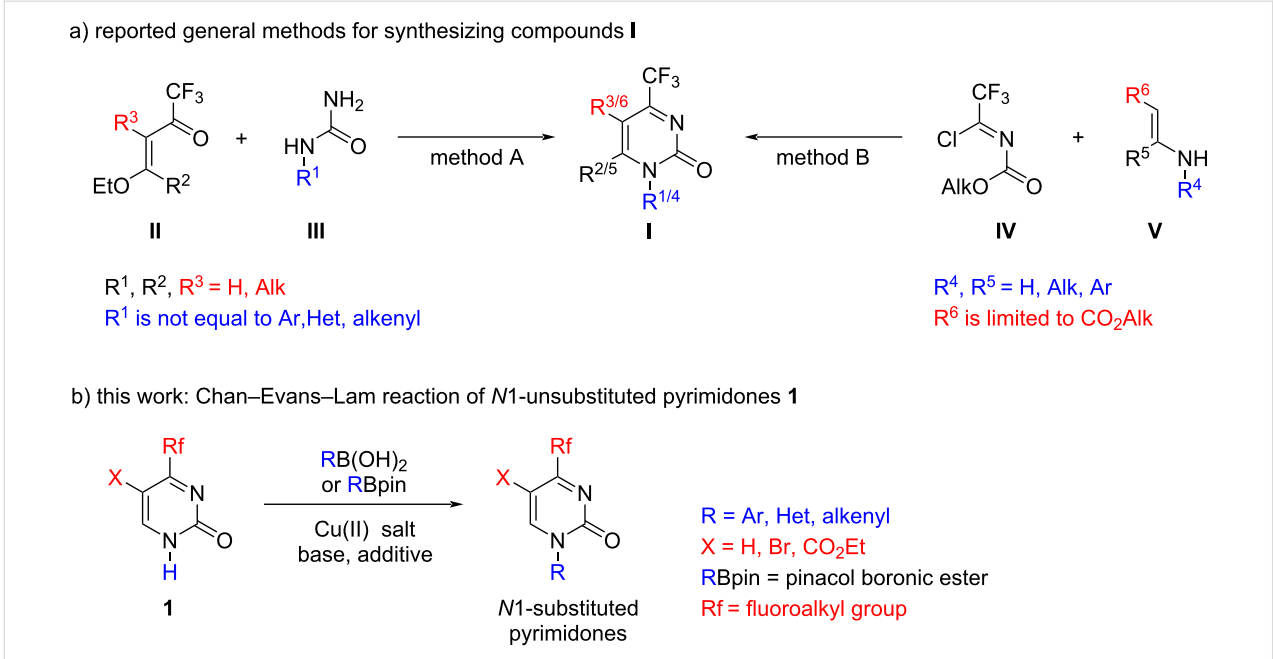

Figure 1: Summary of the previous and present studies.

related to fluorine-containing substrates **1** [40-42]. However, considering the high sensitivity and capricious nature of CEL reaction, we wish to report herein a general set that promotes the effective coupling of *N*1-unsubstituted 4-fluoroalkylpyrimidin-2(1*H*)-ones **1** with (het)aryl- and alkenylboronic acids as well as with their pinacol esters. As the main synthetic result of the study, we have obtained the first representatives of hitherto unavailable 4-fluoroalkylpyrimidin-2(1*H*)-ones bearing (het)aryl and alkenyl substituents, respectively, at the N1 position (see Figure 1b).

Results and Discussion

Our investigation started with 4-trifluoromethylpyrimidin-2(1*H*)-one (**1a**) as a model substrate in the presence of phenylboronic acid (**2a**) to study the effect of solvent, base, and temperature on the course of the CEL arylation in the presence of copper(II) acetate monohydrate (Table 1). As observed for dichloromethane medium, the reaction proceeded very efficiently, with a product **3a** yield of 88%, and reached completion within 48 h upon the addition of 2 equiv of pyridine (as a base and ligand), and 1 equiv of copper acetate at room temperature (see Table 1, entry 1). The product yield decreased slightly to 80% with 1 equiv of pyridine (Table 1, entry 2) and dropped dramatically to below 5% under pyridine-free conditions (Table 1, entry 3). With decreased amounts of both pyridine and copper acetate (0.4 and 0.2 equiv, respectively), the yield was reduced insignificantly to 81% suggesting, however, the catalytic nature of the conversion (Table 1, entry 4). Boiling the reaction mixture for 10 h led to a markedly reduced yield of 45% (Table 1, entry 5). The replacement of pyridine by other

Table 1: Effect of the solvent, base, and temperature on the CEL reaction of 4-trifluoromethylpyrimidin-2(1*H*)-one (**1a**) with phenylboronic acid (**2a**).

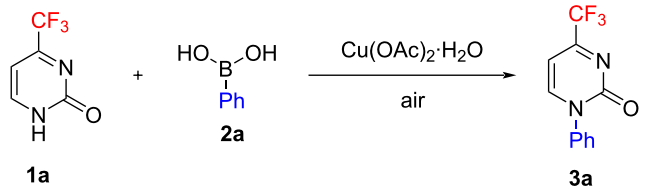

Entry	Solvent[a]	Additive, equiv	$Cu(OAc)_2 \cdot H_2O$, equiv	*t*, °C	Time, h	Yield **3a**,[b] %
1	CH_2Cl_2	Py, 2	1	rt	48	88
2	CH_2Cl_2	Py,1	1	rt	48	80
3	CH_2Cl_2	–	1	rt	48	<5
4	CH_2Cl_2	Py, 0.4	0.2	rt	48	81
5	CH_2Cl_2	Py, 2	1	40	10	45
6	CH_2Cl_2	4-DMAP, 2	0.2	rt	48	19
7	CH_2Cl_2	2,2'-bipy, 2	0.2	rt	48	15
8	CH_2Cl_2	Et_3N, 2	1	rt	48	61
9	CH_2Cl_2	TMEDA, 2	1	rt	48	44
10	CH_2Cl_2	8-hydroxy-quinoline, 2	1	rt	48	18
11	CH_2Cl_2	Py, 2	CuF_2 (1 equiv)	rt	48	86
12	CH_2Cl_2	Py, 2	$Cu(OTf)_2$ (1 equiv)	rt	48	27
13	MeOH	Py, 2	1	rt	48	40
14	MeOH/H_2O 9:1	Py, 2	1	rt	16	38
15	DCE	Py, 2	1	rt	48	69
16	MeCN	Py, 2	1	rt	48	83
17	**MeCN**	**Py, 2**	**1**	**rt**	**96**	**92**
18	**MeCN**	**Py, 2**	**1**	**80**	**8**	**90**
19	MeCN	Py, 0.4	0.2	80	8	79
20	THF	Py, 2	1	rt	48	38
21	EtOAc	Py, 2	1	rt	48	65
22	DMC	Py, 2	1	rt	48	4
23	DMSO	Py, 2	1	rt	48	11

[a]The reaction was conducted in an open flask (with an air condenser) and was vigorously stirred; [b]yields monitored by ^{1}H NMR analysis of the isolated crude samples.

organic bases/ligands (4-DMAP, 2,2'-bipy, Et_3N, TMEDA, 8-hydroxyquinoline) resulted in poorer yields of the target product in all cases (Table 1, entries 6–10). The use of copper(II) fluoride (in contrast to triflate) instead of acetate had practically no effect on the reaction course under the same conditions (Table 1, entries 11 and 12). Therefore, further solvent screening was carried out using pyridine (2 equiv) and copper acetate (1 equiv) as the efficient and most available system. The conversion under study proved to be sensitive to the nature of the solvent. Average product yields of 38–69% were observed for the reaction run in methanol, dichloroethane, tetrahydrofuran, and ethyl acetate (Table 1, entries 13–15, 20 and 21). In dimethyl carbonate and DMSO solutions, the yields were reduced to 4 and 11%, respectively (Table 1, entries 22 and 23). In contrast, with acetonitrile used as a solvent, the yield of product **3a** reached 83%. When the reaction in acetonitrile was prolonged to 96 h, the yield improved to 92% (Table 1, entries 16 and 17). Unlike the experiment in dichloromethane at 40 °C (Table 1, entry 5), heating to 80 °C and reduction of the reaction time to 8 h did not reduce the yield, which remained essentially the same, about 90% (Table 1, entry 18). Heating the reaction mixture also allowed the copper salt and pyridine to be used in substantially lower (catalytic) amounts, though sacrificing the yield to some extent (79%, Table 1, entry 19). Structural determination of compound **3a** was performed by IR and ^1H, ^{13}C, and ^{19}F NMR spectroscopy as well as by LCMS and HRMS analysis.

Performing the reaction with substrate **1a** under the optimum conditions (see Table 1, entry 18), we examined a variety of (het)aryl- and alkenylboronic acids **2b**–**w** as coupling partners. As established in the first experiments, stirring the reaction mixture at room temperature for 24 h followed by heating at 80 °C in acetonitrile results in a considerably increased yield of the corresponding pyrimidones **3**. The thus optimized reaction conditions were applied to obtain a series of otherwise difficult to access and hitherto unknown *N*1-aryl-substituted 4-trifluoromethylpyrimidin-2(1*H*)-ones **3b**–**w** (Scheme 1). The product yields were found to depend on the electronic nature of the substituents on the phenyl ring. A number of commercially available phenylboronic acids with electron-donating or electron-withdrawing *para*-substituents on the aromatic ring were reacted with substrate **1a** to give pyrimidones **3** in satisfactory and high yields of 66–90%. Boronic acids containing *p*-$CONH_2$, *p*-SO_2Me and *p*-CH_2OH substituents, respectively, provided the correspondingly *N*1-substituted pyrimidones **3i**,**j**,**n** in moderate to satisfactory yields of 43–60%.

It is notable that in our case, the Chan–Evans–Lam arylation is tolerant to many sensitive functional groups contained in boronic acids, thereby providing a synthetic entry to products **3** with the aldehyde (in compound **3k**), phenolic *meta*- and *para*-hydroxy (**3l**,**m**), and hydroxymethyl (**3n**) substituents. At the same time, the reaction with *para*-*N*,*N*-dimethylaminomethylphenylboronic acid failed to produce the desired arylated product due to the oxidation of the substituent to the aldehyde group and, probably, some other related side processes. As might be expected, the *ortho*-substituent on the phenyl ring of the boronic acid impeded *N*1-arylation by steric hindrance. However, the methoxy and methyl groups at the *ortho* position did not prevent the formation of the corresponding products **3o** and **3p**, which were isolated in moderate yields of 52 and 35%, respectively. In contrast, the fluorine *ortho*-substituent drastically inhibited the reaction, which is evidently attributed more to electronic than to steric effects.

The formation of alternative *O*-arylated products was ruled out by conducting a NOE NMR experiment with compound **3b** as an example. Saturation of the signal from the pyrimidine H^6 proton resulted in a significantly enhanced resonance of the *ortho* protons in the *para*-methoxyphenyl group (see Scheme 2 and Supporting Information File 1).

As the next step of the study, substrate **1a** was reacted with hetarylboronic acids containing various heterocyclic moieties to obtain the first representatives of hetaryl-substituted 4-trifluoromethylpyrimidin-2(1*H*)-ones **3**. The simplest 3- and 4-pyridylboronic acids provided the corresponding products **3q**,**r**, which were isolated and completely characterized in spite of tthe low yields (13–17%). Electron-donating substituents (a methoxy or 1-pyrrolidinyl group) at position 4 of 3-pyridylboronic acid enabled increased yields of the target products **3s** and **3t** thus opening a preparative pathway to a wide variety of 4-alkoxy-3-pyridyl and 4-dialkylamino-3-pyridyl derivatives. Hetarylboronic acids containing a more electron-deficient pyrimidyl instead of the pyridyl residue was completely unreactive to *N*1-hetarylation of substrate **1a** under the conditions used. Contrary to this case, the method developed allowed electron-rich heterocyclic nuclei including the 3-thienyl (but not isomeric 2-thienyl), 5-trifluoromethyl-3-thienyl, and 3-furyl residues, respectively, to be introduced at the N1 position of the pyrimidone ring, affording compounds **3u**–**w**.

Stimulated by the reported examples of the copper-catalyzed *N*-alkenylation of heterocycles [40,43-48], we extended the reaction scope to β-styrylboronic acid (**4**) as a reagent; the thus obtained *N*1-styryl-substituted 4-trifluoromethylpyrimidin-2(1*H*)-one **5a** obviously has considerable synthetic potential [49,50]. The stereochemistry of compound **5a** was confirmed by a NOE NMR experiment, which demonstrated significant spatial interaction between the H^6 and H^b protons (see Scheme 1) and therefore suggested the preferred *s-trans* confor-

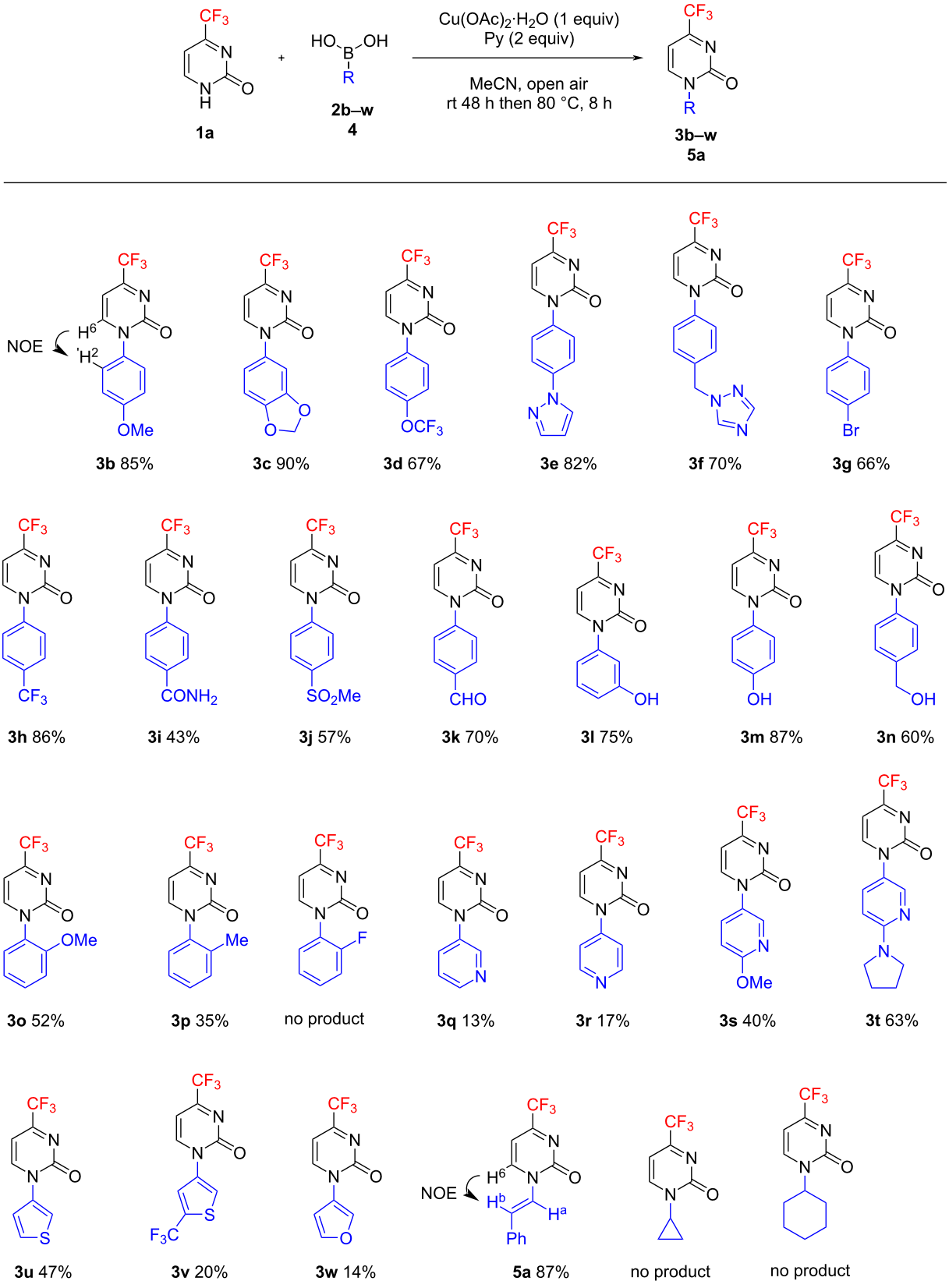

Scheme 1: Chan–Evans–Lam reaction of 4-trifluoromethylpyrimidin-2(1*H*)-one **1a** with (het)aryl boronic acid **2b–w** and β-styrylboronic acid **4**.

mation of the β-styryl substituent in a $CDCl_3$ solution (see Supporting Information File 1). It should be noted that the attempted *N*1-cycloalkylation did not proceed with cyclopropyl- and cyclohexylboronic acids.

Aiming at extending further the range of reagents, we subjected phenylboronic acid pinacol ester (**6a**) to a similar model conversion. Boronic acid pinacol esters are generally known to be much less reactive than the corresponding boronic acids in the Chan–Evans–Lam reaction having, on the other hand, the important advantage of being more available and stable [20,51,52]. A recently reported combined synthetic and spectroscopic study optimized the conditions for the C–N-coupling of NH compounds of various kinds (amines and NH-heterocycles) with boronic acid pinacol esters [20]. The use of acetonitrile as a solvent, with the addition of boric acid as a promoter, was shown to be most efficient. As found by us, starting from pyrimidone **1a**, when reacted with pinacol boronate **6a** (1.5 equiv), provided only a minor amount of product **3a** (about 9%) under the optimum conditions for the reactions with boronic acids (Table 2, entry 1). However, the addition of 2 equiv of boric acid drastically increased the arylation efficiency, with the yield of pyrimidone **3a** reaching 86% (Table 2, entry 2). We assume that the boric acid added triggers the transesterification of phenylboronic acid pinacol ester **6a** thereby leading to the in situ generation of reactive phenylboronic acid (**2a**). The reaction attempted at the lower (room) temperature and with lower amounts of copper acetate and pyridine practically failed to occur (Table 2, entries 3–5).

In view of the availability of boronic acid pinacol esters, and particularly of synthetically attractive pinacol alkenylboronates [53,54], we studied the reaction of **1a** with a series of such reagents **6b–d** and **7a–h** (Scheme 2). The yields of (het)aryl-substituted products **3g**,**q**,**s** obtained from **6b–d** were found to be much the same as in the analogous reactions of substrate **1a** with the corresponding boronic acids **2g**,**q**,**s**. Pinacol alkenyl boronates **7a–h** smoothly furnished the corresponding *N*1-alkenyl-substituted pyrimidones **5a–h**. Product **5f** obtained from the simplest vinylboronic acid pinacol ester (**7f**) appears to be of special value [55,56]. However, we did not succeed in reacting substrate **1a** with pinacol 2-phenylethynyl boronate. The *meta*-methoxystyryl derivative **5c** was found to easily undergo photodimerization in solid state upon sunlight exposure, leading to the formation of compound **8** with a central cyclobutane ring (see Supporting Information File 1). As proved previously for analogous enamides [57], the facile [2 + 2] photocycloaddition process likely occurred due to favorable orientation of the interacting molecules and close contacts between alkene carbon atoms in the crystal structure. Consequently, the synthesis of product **5c** was performed in darkness. *N*1-Styryl-substituted pyrimidin-2(1*H*)-ones **5a–e** exhibit fluorescence properties with emission of λ_{max} = 490–532 nm in CH_2Cl_2 solution.

In order to analyze the effect exerted on the Chan–Evans–Lam arylation by 4-, 5-, and 6-substituents on the pyrimidine ring and also aiming at the further functionalization of pyrimidin-2(1*H*)-one, we studied various substrates **1b–h** in the reaction

Table 2: Effect of boric acid and pyridine additives on the Chan–Evans–Lam reaction of 4-trifluoromethylpyrimidin-2(1*H*)-one (**1a**) with phenylboronic acid pinacol ester (**6a**).

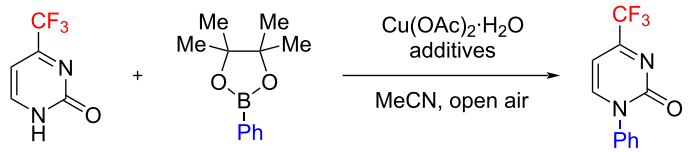

1a (1 equiv) **6a** (1.5 equiv) **3a**

Entry[b]	Additive, equiv	$Cu(OAc)_2·H_2O$ equiv	*t*, °C	Time, h	Yield **3a**, %
1	Py, 2	1	80	8	9
2	Py, 2 H_3BO_3, 2	1	80	8	86
3	Py, 2 H_3BO_3, 2	1	20	48	7
4	Py, 0.4 H_3BO_3, 2	0.2	80	8	9
5	H_3BO_3, 2	1	80	8	<5

[a]The reaction was conducted in an open flask (with an air condenser) and was vigorously stirred; [b]yields monitored by ^{1}H NMR analysis of the isolated crude samples.

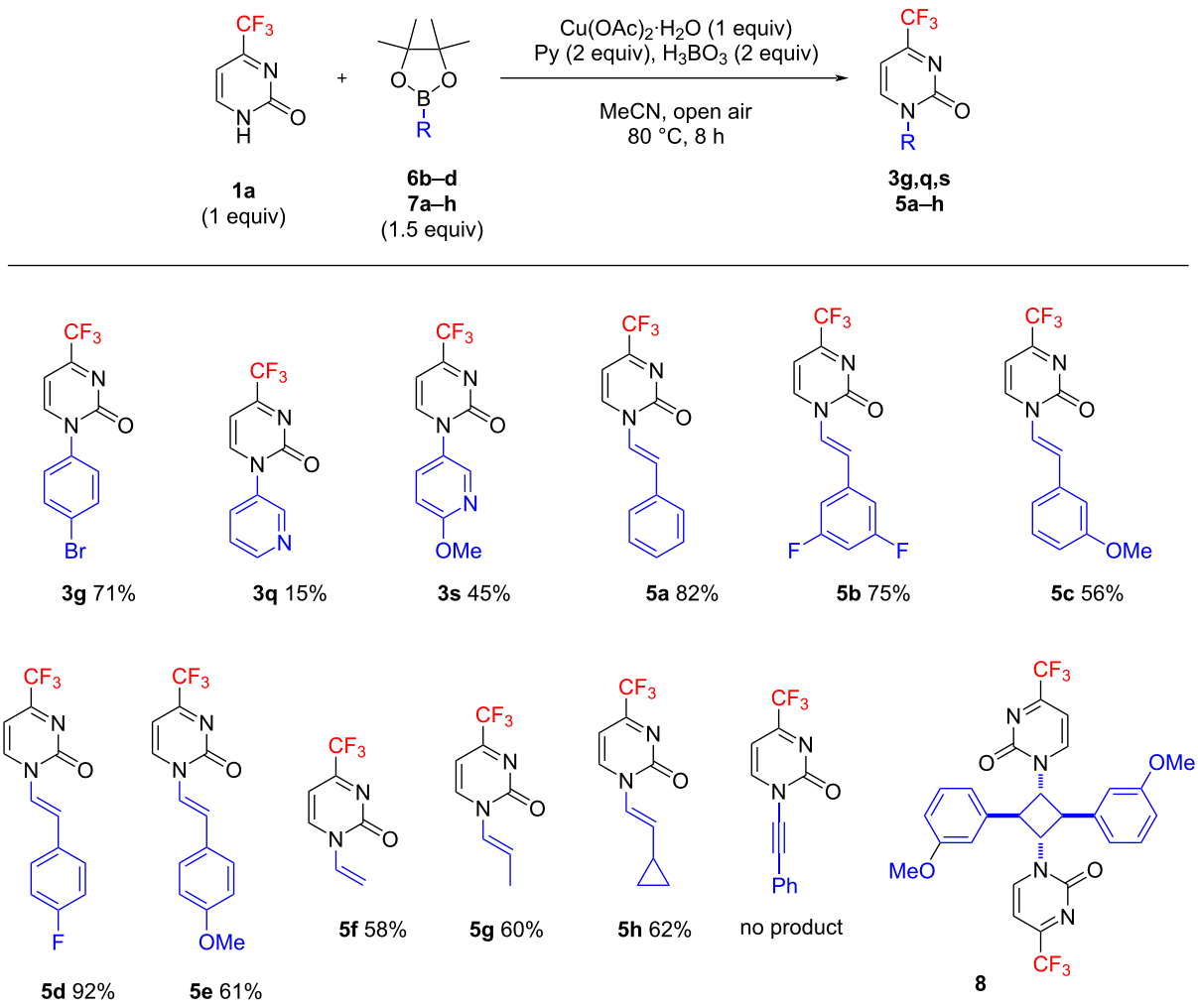

Scheme 2: Chan–Evans–Lam reaction of 4-trifluoromethylpyrimidin-2(1*H*)-one (**1a**) with (het)aryl- and alkenylboronic acid pinacol esters **4b–d** and **7a–h**.

with phenylboronic acid (**2a**, Scheme 3). It was found that 4-difluoromethylpyrimidin-2(1*H*)-one (**1b**) produced the corresponding *N*1-phenyl derivative **9a** in a moderate yield of 40%, whereas its 4-difluorochloromethyl and 4-pentafluoroethyl-substituted analogues **1c,d** afforded products **9b,c** in high yields of 74 and 78%, respectively (see Supporting Information File 1). Unexpectedly, 4-methyl-substituted and 4-unsubstituted pyrimidin-2(1*H*)-ones **1e,f**, when reacted under similar conditions, gave complex mixtures containing no more than 5% of target products **9d**,**e**. Thus, the presence of the electron-withdrawing 4-fluoroalkyl group in pyrimidones **1** is a significant structural factor playing a major role in the overall success of the Chan–Evans–Lam reaction, most likely due to related increase in NH-acidity of the heterocyclic system. The ester group and the bromine atom at position 5 of the 4-trifluoromethylpyrimidin-2(1*H*)-ones **1g**,**h** did not disturb the course of the reaction and the products **9f**,**g** bearing the corresponding functionalities are applicable as building blocks in further syntheses. The 6-methyl substituent had a negative effect on the *N*-arylation process. As evidenced by LCMS analysis, the reaction with 6-methyl-4-(trifluoromethyl)pyrimidin-2(1*H*)-one provided a mixture of three cross-coupling products (not separated), with a total yield of no more than 18%, which suggests a poor regioselectivity.

Conclusion

We have optimized the reaction conditions for the efficient and facile Chan–Evans–Lam *N*1-(het)arylation and *N*1-alkenylation of 4-fluoroalkylpyrimidin-2(1*H*)-ones. It has been shown that with the addition of boric acid, high yields of the target products are also obtained when the reaction is carried out with boronic acid pinacol esters as an organoboron component,

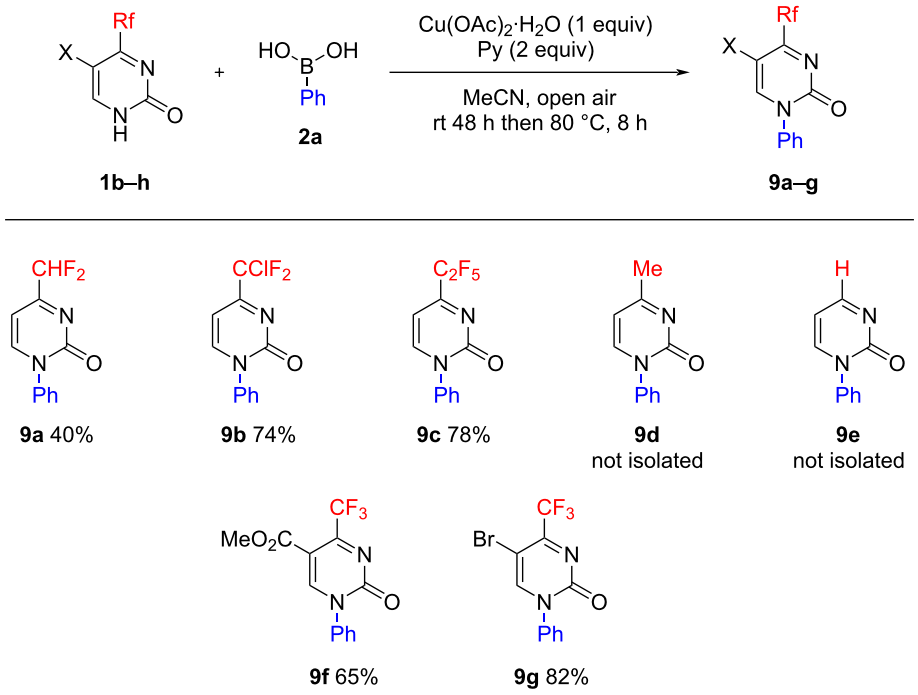

Scheme 3: Chan–Evans–Lam reaction of pyrimidin-2(1*H*)-ones **1b–h** with phenylboronic acid (**2a**).

instead of the conventionally used boronic acids. Among the newly-synthesized compounds are the first representatives of *N*1-(het)aryl-4-fluoroalkylpyrimidin-2(1*H*)-ones as well as their synthetically promising *N*1-alkenyl-substituted analogues. The success of the reaction has been found to depend on the presence of the 4-fluoroalkyl group in the starting pyrimidone.

Supporting Information

Supporting Information File 1

Experimental procedures, characterization data, copies of the ^{1}H and ^{13}C NMR spectra.
[https://www.beilstein-journals.org/bjoc/content/supplementary/1860-5397-16-191-S1.pdf]

Acknowledgements

The authors are very grateful to Dr. V. Polovinko for NOE experiments and A. Skreminskij for HRMS analytical data.

ORCID® iDs

Viktor M. Tkachuk - https://orcid.org/0000-0002-7978-464X
Oleh O. Lukianov - https://orcid.org/0000-0002-2651-8196
Mykhailo V. Vovk - https://orcid.org/0000-0003-1753-3535
Isabelle Gillaizeau - https://orcid.org/0000-0002-7726-3592
Volodymyr A. Sukach - https://orcid.org/0000-0002-2891-343X

References

1. Bariwal, J.; Van der Eycken, E. *Chem. Soc. Rev.* **2013,** *42,* 9283–9303. doi:10.1039/c3cs60228a
2. Ruiz-Castillo, P.; Buchwald, S. L. *Chem. Rev.* **2016,** *116,* 12564–12649. doi:10.1021/acs.chemrev.6b00512
3. Monnier, F.; Taillefer, M. *Angew. Chem., Int. Ed.* **2008,** *47,* 3096–3099. doi:10.1002/anie.200703209
4. Senra, J. D.; Aguiar, L. C. S.; Simas, A. B. C. *Curr. Org. Synth.* **2011,** *8,* 53–78. doi:10.2174/157017911794407683
5. Ricci, A., Ed. *Modern Amination Methods;* Wiley-VCH: Weinheim, Germany, 2000. doi:10.1002/9783527613182
6. Monnier, F.; Taillefer, M. *Angew. Chem., Int. Ed.* **2009,** *48,* 6954–6971. doi:10.1002/anie.200804497
7. Sambiagio, C.; Marsden, S. P.; Blacker, A. J.; McGowan, P. C. *Chem. Soc. Rev.* **2014,** *43,* 3525–3550. doi:10.1039/c3cs60289c
8. Qiao, J. X.; Lam, P. Y. S. Recent Advances in Chan–Lam Coupling Reaction: Copper-Promoted C–Heteroatom Bond Cross-Coupling Reactions with Boronic Acids and Derivatives. In *Boronic Acids: Preparation and Applications in Organic Synthesis, Medicine and Materials;* Hall, D. G., Ed.; Wiley-VCH: Weinheim, Germany, 2011; pp 315–361. doi:10.1002/9783527639328.ch6
9. Hartwig, J. F. *Acc. Chem. Res.* **1998,** *31,* 852–860. doi:10.1021/ar970282g
10. Altman, R. A.; Buchwald, S. L. *Nat. Protoc.* **2007,** *2,* 2474–2479. doi:10.1038/nprot.2007.364
11. Jia, X.; Peng, P. *Asian J. Org. Chem.* **2019,** *8,* 1548–1554. doi:10.1002/ajoc.201900273
12. Lo, Q. A.; Sale, D.; Braddock, D. C.; Davies, R. P. *ACS Catal.* **2018,** *8,* 101–109. doi:10.1021/acscatal.7b03664
13. Surry, D. S.; Buchwald, S. L. *Chem. Sci.* **2010,** *1,* 13. doi:10.1039/c0sc00107d

14. Quivelli, A. F.; Vitale, P.; Perna, F. M.; Capriati, V. *Front. Chem. (Lausanne, Switz.)* **2019,** *7,* 723. doi:10.3389/fchem.2019.00723
15. Chan, D. M. T.; Monaco, K. L.; Wang, R.-P.; Winters, M. P. *Tetrahedron Lett.* **1998,** *39,* 2933–2936. doi:10.1016/s0040-4039(98)00503-6
16. Evans, D. A.; Katz, J. L.; West, T. R. *Tetrahedron Lett.* **1998,** *39,* 2937–2940. doi:10.1016/s0040-4039(98)00502-4
17. Lam, P. Y. S.; Clark, C. G.; Saubern, S.; Adams, J.; Winters, M. P.; Chan, D. M. T.; Combs, A. *Tetrahedron Lett.* **1998,** *39,* 2941–2944. doi:10.1016/s0040-4039(98)00504-8
18. Qiao, J.; Lam, P. *Synthesis* **2011,** 829–856. doi:10.1055/s-0030-1258379
19. Lam, P. Y. S. *Chan–Lam Coupling Reaction: Copper-promoted C–Element Bond Oxidative Coupling Reaction with Boronic Acids*. *Synthetic Methods in Drug Discovery;* The Royal Society of Chemistry: Cambridge, UK, 2016; Vol. 1, pp 242–273. doi:10.1039/9781782622086-00242
20. Vantourout, J. C.; Miras, H. N.; Isidro-Llobet, A.; Sproules, S.; Watson, A. J. B. *J. Am. Chem. Soc.* **2017,** *139,* 4769–4779. doi:10.1021/jacs.6b12800
21. Sukach, V. A.; Tkachuk, V. M.; Shoba, V. M.; Pirozhenko, V. V.; Rusanov, E. B.; Chekotilo, A. A.; Röschenthaler, G.-V.; Vovk, M. V. *Eur. J. Org. Chem.* **2014,** 1452–1460. doi:10.1002/ejoc.201301542
22. Sukach, V. A.; Resetnic, A. A.; Tkachuk, V. M.; Lin, Z.; Kortz, U.; Vovk, M. V.; Röschenthaler, G.-V. *Eur. J. Org. Chem.* **2015,** 1290–1301. doi:10.1002/ejoc.201403495
23. Tkachuk, V. M.; Sukach, V. A.; Kovalchuk, K. V.; Vovk, M. V.; Nenajdenko, V. G. *Org. Biomol. Chem.* **2015,** *13,* 1420–1428. doi:10.1039/c4ob02233e
24. Melnykov, S. V.; Pataman, A. S.; Dmytriv, Y. V.; Shishkina, S. V.; Vovk, M. V.; Sukach, V. A. *Beilstein J. Org. Chem.* **2017,** *13,* 2617–2625. doi:10.3762/bjoc.13.259
25. Tkachuk, V. M.; Melnykov, S. V.; Vorobei, A. V.; Sukach, V. A.; Vovk, M. V. *Chem. Heterocycl. Compd.* **2019,** *55,* 66–71. doi:10.1007/s10593-019-02420-w
26. Zhou, Y.; Wang, J.; Gu, Z.; Wang, S.; Zhu, W.; Aceña, J. L.; Soloshonok, V. A.; Izawa, K.; Liu, H. *Chem. Rev.* **2016,** *116,* 422–518. doi:10.1021/acs.chemrev.5b00392
27. Wang, J.; Sánchez-Roselló, M.; Aceña, J. L.; del Pozo, C.; Sorochinsky, A. E.; Fustero, S.; Soloshonok, V. A.; Liu, H. *Chem. Rev.* **2014,** *114,* 2432–2506. doi:10.1021/cr4002879
28. Bassetto, M.; Ferla, S.; Pertusati, F. *Future Med. Chem.* **2015,** *7,* 527–546. doi:10.4155/fmc.15.5
29. Gillis, E. P.; Eastman, K. J.; Hill, M. D.; Donnelly, D. J.; Meanwell, N. A. *J. Med. Chem.* **2015,** *58,* 8315–8359. doi:10.1021/acs.jmedchem.5b00258
30. Zanatta, N.; Faoro, D.; da S. Fernandes, L.; Brondani, P. B.; Flores, D. C.; Flores, A. F. C.; Bonacorso, H. G.; Martins, M. A. P. *Eur. J. Org. Chem.* **2008,** 5832–5838. doi:10.1002/ejoc.200800822
31. Sukach, V. A.; Tkachuk, V. M.; Rusanov, E. B.; Röschenthaler, G.-V.; Vovk, M. V. *Tetrahedron* **2012,** *68,* 8408–8415. doi:10.1016/j.tet.2012.07.099
32. Gerus, I. I.; Vdovenko, S. I.; Gorbunova, M. G.; Kukhar', V. P. *Chem. Heterocycl. Compd.* **1991,** *27,* 398–406. doi:10.1007/bf00480838
33. Bonacorso, H. G.; Martins, M. A. P.; Bittencourt, S. R. T.; Lourega, R. V.; Zanatta, N.; Flores, A. F. C. *J. Fluorine Chem.* **1999,** *99,* 177–182. doi:10.1016/s0022-1139(99)00146-3
34. Gorbunova, M. G.; Gerus, I. I.; Kukhar, V. P. *Synthesis* **2000,** 738–742. doi:10.1055/s-2000-6386
35. Farahat, A. A.; Boykin, D. W. *Synth. Commun.* **2015,** *45,* 245–252. doi:10.1080/00397911.2014.961196
36. Hardouin Duparc, V.; Bano, G. L.; Schaper, F. *ACS Catal.* **2018,** *8,* 7308–7325. doi:10.1021/acscatal.8b01881
37. Sanjeeva Rao, K.; Wu, T.-S. *Tetrahedron* **2012,** *68,* 7735–7754. doi:10.1016/j.tet.2012.06.015
38. Chua, G. N. L.; Wassarman, K. L.; Sun, H.; Alp, J. A.; Jarczyk, E. I.; Kuzio, N. J.; Bennett, M. J.; Malachowsky, B. G.; Kruse, M.; Kennedy, A. J. *ACS Med. Chem. Lett.* **2019,** *10,* 180–185. doi:10.1021/acsmedchemlett.8b00474
39. James, C. A.; DeRoy, P.; Duplessis, M.; Edwards, P. J.; Halmos, T.; Minville, J.; Morency, L.; Morin, S.; Simoneau, B.; Tremblay, M.; Bethell, R.; Cordingley, M.; Duan, J.; Lamorte, L.; Pelletier, A.; Rajotte, D.; Salois, P.; Tremblay, S.; Sturino, C. F. *Bioorg. Med. Chem. Lett.* **2013,** *23,* 2781–2786. doi:10.1016/j.bmcl.2013.02.021
40. Jacobsen, M. F.; Knudsen, M. M.; Gothelf, K. V. *J. Org. Chem.* **2006,** *71,* 9183–9190. doi:10.1021/jo061694i
41. Yue, Y.; Zheng, Z.-G.; Wu, B.; Xia, C.-Q.; Yu, X.-Q. *Eur. J. Org. Chem.* **2005,** 5154–5157. doi:10.1002/ejoc.200500589
42. Tao, L.; Yue, Y.; Zhang, J.; Chen, S.-Y.; Yu, X.-Q. *Helv. Chim. Acta* **2008,** *91,* 1008–1014. doi:10.1002/hlca.200890107
43. Bolshan, Y.; Batey, R. A. *Tetrahedron* **2010,** *66,* 5283–5294. doi:10.1016/j.tet.2010.03.076
44. Janíková, K.; Jedinák, L.; Volná, T.; Cankař, P. *Tetrahedron* **2018,** *74,* 606–617. doi:10.1016/j.tet.2017.12.042
45. Bolshan, Y.; Batey, R. A. *Angew. Chem., Int. Ed.* **2008,** *47,* 2109–2112. doi:10.1002/anie.200704711
46. Jiao, J.-W.; Bi, H.-Y.; Zou, P.-S.; Wang, Z.-X.; Liang, C.; Mo, D.-L. *Adv. Synth. Catal.* **2018,** *360,* 3254–3259. doi:10.1002/adsc.201800718
47. Chen, C.-H.; Liu, Q.-Q.; Ma, X.-P.; Feng, Y.; Liang, C.; Pan, C.-X.; Su, G.-F.; Mo, D.-L. *J. Org. Chem.* **2017,** *82,* 6417–6425. doi:10.1021/acs.joc.7b00620
48. Ohata, J.; Minus, M. B.; Abernathy, M. E.; Ball, Z. T. *J. Am. Chem. Soc.* **2016,** *138,* 7472–7475. doi:10.1021/jacs.6b03390
49. Carbery, D. R. *Org. Biomol. Chem.* **2008,** *6,* 3455. doi:10.1039/b809319a
50. Gopalaiah, K.; Kagan, H. B. *Chem. Rev.* **2011,** *111,* 4599–4657. doi:10.1021/cr100031f
51. Liu, S.; Xu, L. *Asian J. Org. Chem.* **2018,** *7,* 1856–1863. doi:10.1002/ajoc.201800371
52. Vantourout, J. C.; Law, R. P.; Isidro-Llobet, A.; Atkinson, S. J.; Watson, A. J. B. *J. Org. Chem.* **2016,** *81,* 3942–3950. doi:10.1021/acs.joc.6b00466
53. Coombs, J. R.; Zhang, L.; Morken, J. P. *Org. Lett.* **2015,** *17,* 1708–1711. doi:10.1021/acs.orglett.5b00480
54. Kovalenko, M.; Yarmoliuk, D. V.; Serhiichuk, D.; Chernenko, D.; Smyrnov, V.; Breslavskyi, A.; Hryshchuk, O. V.; Kleban, I.; Rassukana, Y.; Tymtsunik, A. V.; Tolmachev, A. A.; Kuchkovska, Y. O.; Grygorenko, O. O. *Eur. J. Org. Chem.* **2019,** 5624–5635. doi:10.1002/ejoc.201900648
55. Hill, M.; Movassaghi, M. *Synthesis* **2007,** 1115–1119. doi:10.1055/s-2007-965940
56. Hansen, A. L.; Skrydstrup, T. *J. Org. Chem.* **2005,** *70,* 5997–6003. doi:10.1021/jo050669u
57. Song, F.; Snook, J. H.; Foxman, B. M.; Snider, B. B. *Tetrahedron* **1998,** *54,* 13035–13044. doi:10.1016/s0040-4020(98)00806-0

License and Terms

This is an Open Access article under the terms of the Creative Commons Attribution License (https://creativecommons.org/licenses/by/4.0). Please note that the reuse, redistribution and reproduction in particular requires that the authors and source are credited.

The license is subject to the *Beilstein Journal of Organic Chemistry* terms and conditions: (https://www.beilstein-journals.org/bjoc)

The definitive version of this article is the electronic one which can be found at: https://doi.org/10.3762/bjoc.16.191

BEILSTEIN JOURNAL OF ORGANIC CHEMISTRY

Catalytic trifluoromethylation of iodoarenes by use of 2-trifluoromethylated benzimidazoline as trifluoromethylating reagent

Tatsuhiro Uchikura, Nanami Kamiyama, Taisuke Ishikawa and Takahiko Akiyama*

Letter

Open Access

Address:
Department of Chemistry, Faculty of Science, Gakushuin University, Mejiro, Toshima-ku, Tokyo, 171-8588, Japan

Email:
Takahiko Akiyama* - takahiko.akiyama@gakushuin.ac.jp

* Corresponding author

Keywords:
benzimidazoline; catalysis; copper; fluorine chemistry; trifluoromethylation

Beilstein J. Org. Chem. **2020,** *16,* 2442–2447.
https://doi.org/10.3762/bjoc.16.198

Received: 31 July 2020
Accepted: 15 September 2020
Published: 30 September 2020

This article is part of the thematic issue "Organo-fluorine chemistry V".

Guest Editor: D. O'Hagan

© 2020 Uchikura et al.; licensee Beilstein-Institut.
License and terms: see end of document.

Abstract

The trifluoromethylation of iodoarenes was accomplished by use of a 2-trifluoromethylbenzimidazoline derivative as the trifluoromethylating reagent and a catalytic amount of Cu(I) in the presence of 2,2'-bipyridyl as the ligand. Through a mechanistic study, we found that the oxidative addition of the iodoarene to the Cu(I)–CF_3 species is the rate-determining step.

Introduction

The introduction of a trifluoromethyl group is one of the most attractive reactions in drug discovery [1,2]. In the past decade, trifluoromethylation reactions of aryl halides in the presence of transition-metal complexes were reported [3-21]. $CuCF_3$ is a useful species for the trifluoromethylation of aryl halides and there are a number of precursors of $CuCF_3$ for trifluoromethylation reactions. In contrast, the catalytic generation of $CuCF_3$ was less investigated [15-21]. For example, R_3SiCF_3, a fluoral derivative, and trifluoroacetates were employed as precursors of $CuCF_3$ species for the catalytic trifluoromethylation of iodoarenes (Figure 1a) and the development of novel types of trifluoromethylating reagents is still desired. We have recently reported the trifluoromethylation of iodoarenes by use of 2-aryl-2-trifluoromethylbenzimidazoline as the trifluoromethylating reagent in the presence of 3 equiv of a copper salt [22]. The benzimidazoline derivatives could be readily prepared from relatively cheap materials, namely, trifluoromethylacetophenone and phenylenediamine derivatives (Figure 1b). Herein we report a catalytic trifluoromethylation of iodoarenes by use of benzimidazoline derivatives in the presence of a catalytic amount of copper salts and a bipyridyl ligand (Figure 1c).

Results and Discussion

We first investigated the reaction conditions by use of *p*-iodonitrobenzene (**1a**) and 2-phenyl-2-trifluoromethyl-1-methylbenzimidazoline (**2**) (Table 1). Using 3 equiv of CuI gave 4-trifluoromethyl-1-nitrobenzene (**3a**) quantitatively, as

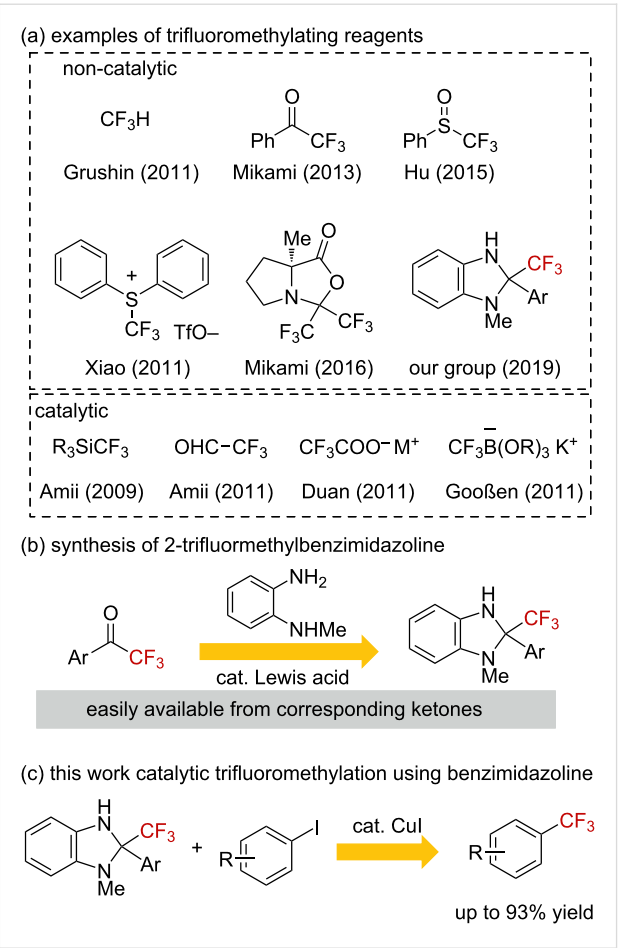

Figure 1: Trifluoromethylation of aryl halides.

we had reported previously (Table 1, entry 1) [22]. Decreasing the CuI catalyst loading to 20 mol % lowered the yield of **3a** even at a high temperature (Table 1, entries 2 and 3). In order to stabilize the copper(I) catalyst, a bipyridyl ligand was employed in the reaction [23]. By this, the trifluoromethylation proceeded with a catalytic amount of CuI in the presence of 0.8 equiv of 2,2'-bipyridyl to furnish product **3a** in 80% yield (Table 1, entry 4). However, smaller amounts of CuI (10 mol %) and 2,2'-bipyridyl (20 mol %) gave compound **3a** in lower yields (Table 1, entries 5 and 6). Benzonitrile was the solvent of choice (Table 1, entries 7 and 8). Replacing CuI by CuBr or CuCl gave similar results (Table 1, entries 9 and 10). However, we selected the most stable and readily available CuI as the catalyst for further investigations. Thus, the trifluoromethylation of *p*-iodonitrobenzene proceeded by use of 2-phenyl-2-trifluoromethyl-1-methylbenzimidazoline in the presence of catalytic amounts of CuI and 2,2'-bipyridyl as ligand.

We next screened for 2,2'-bipyridyl ligands to be used with CuI (Table 2). 4,4'-Dimethyl-2,2'-bipyridyl (**4b**) gave product **3a** in a higher yield than 2,2'-bipyridyl (**4a**), whereas 5,5'- and 6,6'-dimethylbipyridyl (**4c** and **4d**) were not effective. From these results, the substituents at 4,4'-positions were expected to be beneficial for the reaction, and other 4,4'-substituted bipyridyl ligands were investigated. We found that 4,4'-di-*tert*-butyl-2,2'-bipyridyl (**4e**) afforded the best result (91% yield). On the other hand, 2,2'-bipyridyl ligands bearing electron-donating (–OMe, **4f**) and -withdrawing (–CF_3, **4g**) groups furnished **3a** in low

Table 1: Screening for reaction conditions[a].

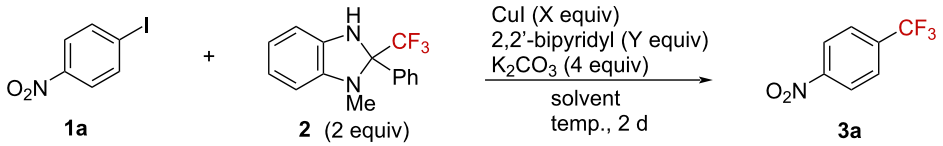

1a + **2** (2 equiv) → **3a**

entry	X	Y	solvent	temp.	yield[b]
1	3	0	PhCN	60 °C	quant
2	0.2	0	PhCN	60 °C	36%
3	0.2	0	PhCN	90 °C	40%
4	0.2	0.8	PhCN	90 °C	80%
5	0.1	0.8	PhCN	90 °C	59%
6	0.2	0.2	PhCN	90 °C	63%
7	0.2	0.8	MeCN	90 °C	32%
8	0.2	0.8	DMF	90 °C	30%
9[c]	0.2	0.8	PhCN	90 °C	72%
10[d]	0.2	0.8	PhCN	90 °C	79%

[a]Performed with **2a** (0.050 mmol) and **1a** (0.10 mmol) in solvent (1.0 mL). [b]Determined by ^{19}F NMR spectroscopy (benzotrifluoride was used as the internal standard). [c]CuBr was used instead of CuI. [d]CuCl was used instead of CuI.

Table 2: Screening for diamine ligands[a].

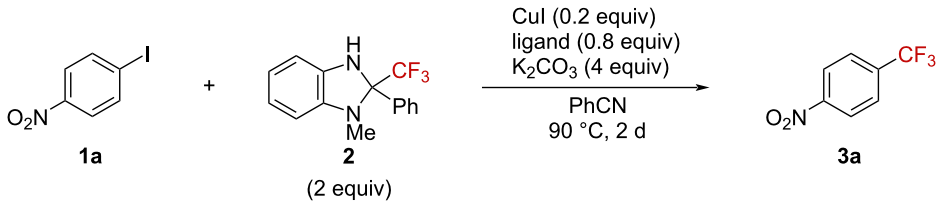

ligand	yield[b]	ligand	yield[b]
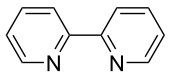 **4a**	80%	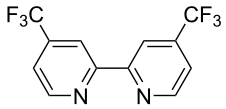 **4g**	56%
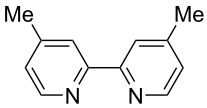 **4b**	82%	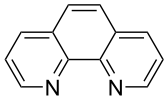 **4h**	64%
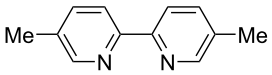 **4c**	72%	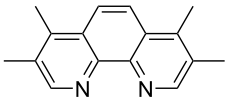 **4i**	57%
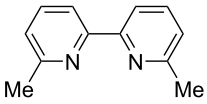 **4d**	19%	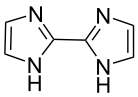 **4j**	trace
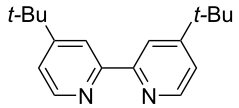 **4e**	91%	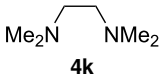 **4k**	26%
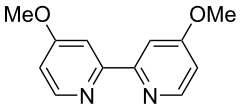 **4f**	73%	–	40%

[a]Performed with **2a** (0.050 mmol) and **1a** (0.10 mmol) in solvent (1.0 mL). [b]Determined by ^{19}F NMR spectroscopy (benzotrifluoride was used as the internal standard).

yields. Moreover, other electron-withdrawing ligands, i.e., phenanthroline derivatives (**4h** and **4i**), and electron-donating ligands such as 2,2'-biimidazole (**4j**) and tetramethylethylenediamine (**4k**) gave inferior results.

We next screened for the generality of the reaction towards various substrates under the optimized conditions (Figure 2). Electron-deficient aryl iodides were well tolerated furnishing the corresponding trifluoromethylation products in high yields. Among the tested nitrophenyl derivatives, *p*- and *o*-nitrophenyliodide gave the products in highest yields. In contrast, *m*-iodonitrobenzene afforded the trifluoromethylated product in a decreased yield of 35% due to the higher electron density of the *meta*-position compared to the *ortho*- and *para*-positions. Iodoarenes bearing other electron-withdrawing substituents, such as *p*-cyano, *p*-acetyl, and *p*-methoxycarbonyl, were also suitable and gave products **3d**–**f** in moderate to high yields. Furthermore, the presence of a formyl group was also tolerated in the reaction, and *p*-formyltrifluoromethylbenzene (**3g**) was obtained in 40% yield. However, the electron-rich substrate 2-methoxyiodobenzene (**1h**) gave product **3h** in only a modest yield (30%).

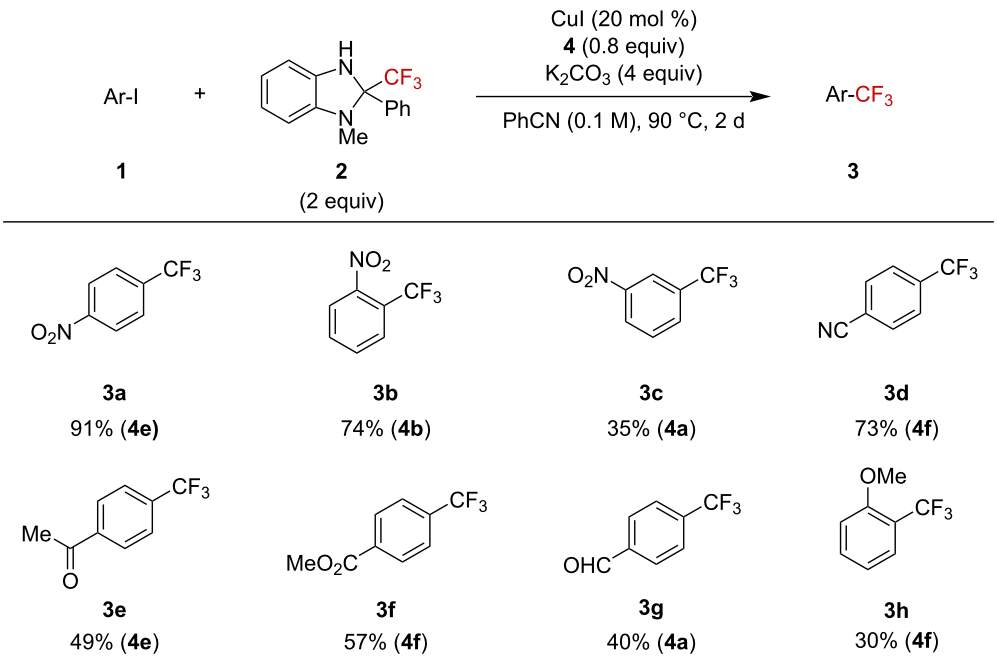

Figure 2: Scope of aryl iodides. Yields determined by ^{19}F NMR spectroscopy and used ligand is given in parenthesis.

Heteroaryl iodides were also suitable substrates (Figure 3). 2-Iodopyridine (**5a**) gave the expected trifluoromethylation product **6a** in 80% yield. 2-Iodoquinoline (**5b**) and 1-iodoisoquinoline (**5c**) were also suitable substrates to furnish desired products **6b** and **6c** in high yields. Furthermore, iodopyrazine was applicable to furnish **6d** in 63% yield.

Finally, a mechanistic study of the reaction was carried out. First, the active species of the reaction was investigated by NMR analysis. The generation of Cu(I)–CF_3 was observed by mixing benzimidazoline **2** and CuI in EtCN at 90 °C (Figure S1, in Supporting Information File 1). Therefore, CuI and **2** generated $CuCF_3$ species as the active species for the trifluoromethylation [24].

Then, the dependence of the conversion on the reaction time was estimated (Figure 4) and no induction period was observed. Although benzimidazoline **2** was completely consumed after 24 h, the yield of the trifluoromethylation product continued to increase up to 48 h. This suggests that product generation proceeded slower than the cleavage of the C–CF_3 bond of benzimidazoline.

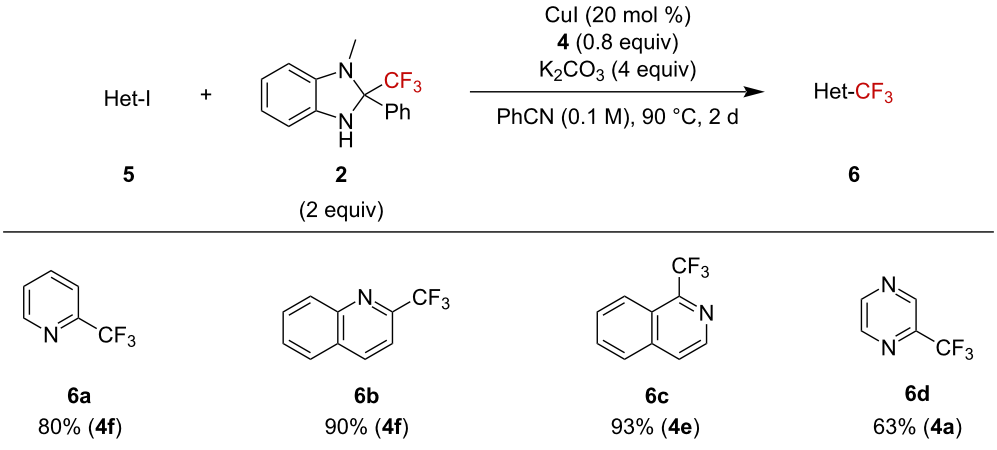

Figure 3: Scope of heteroaryl iodides. Yields determined by ^{19}F NMR spectroscopy and used ligand is given in parenthesis.

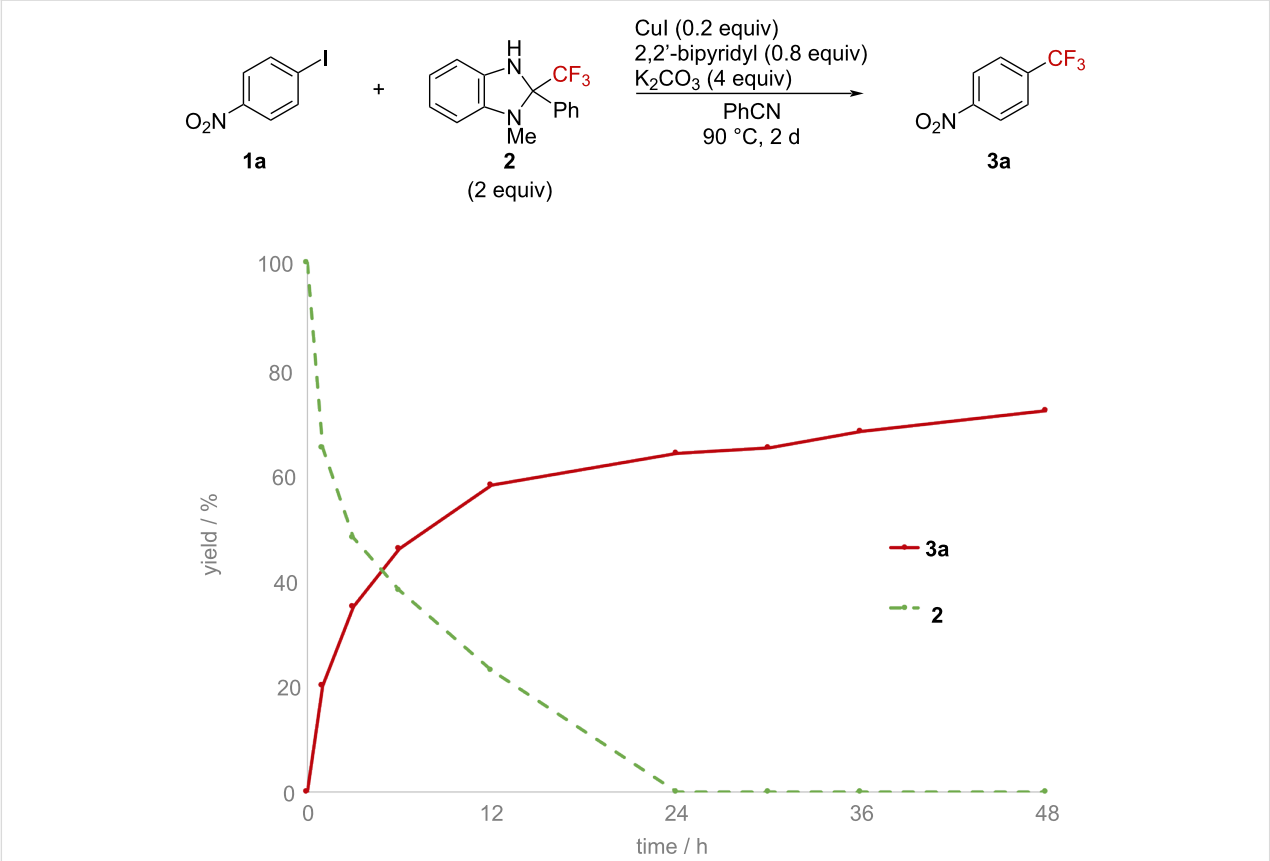

Figure 4: Time course of the trifluoromethylation reaction.

We propose a mechanism for the reaction, as shown in Figure 5. The Cu(I)–CF_3 species, generated through the reaction of benzimidazoline **2** with CuI under basic conditions, underwent an oxidative addition reaction with the aryl iodide to generate a Cu(III) complex. A subsequent reductive elimination furnished the trifluoromethylarene and Cu(I). Because an electron-donating ligand was more effective than an electron-deficient one (Table 2), and the reaction with benzimidazoline proceeded rapidly (Figure 4), the oxidative addition was suggested to be the rate-determining step.

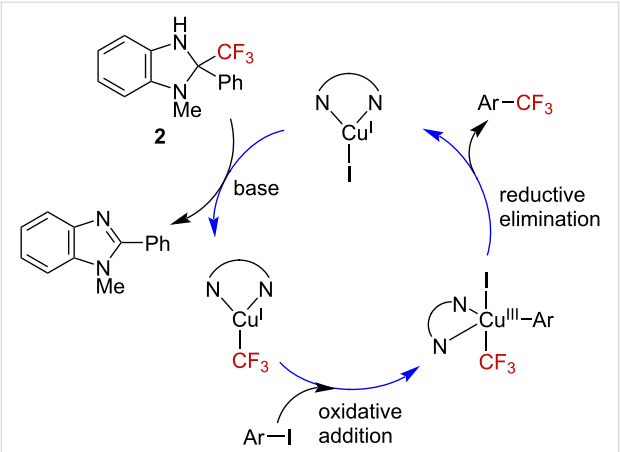

Figure 5: Proposed mechanism of the catalytic cycle.

Conclusion

In conclusion, we have developed a catalytic trifluoromethylation of aryl iodides by using trifluoromethylated benzimidazoline derivatives. The mechanistic study revealed that the oxidative addition was the rate-determining step of this reaction. 2-Phenyl-2-trifluoromethyl-1-methylbenzimidazoline is a novel type of trifluoromethylating reagents that might be useful for organic synthesis.

Experimental

General procedure of trifluoromethylation: Aryl iodide **1** (0.1 mmol), **2** (56 mg, 0.2 mmol), CuI (3.8 mg, 0.02 mmol), 2,2'-bipyridyl (12.5 mg, 0.08 mmol), and potassium carbonate (55.6 mg, 0.4 mmol) were mixed in benzonitrile (1.0 mL), and the mixture heated to 90 °C. After 48 h, hexafluorobenzene was added as an internal standard and the mixture analyzed by ^{19}F NMR spectroscopy for the calculation of the NMR yield. Then, the crude products were purified by preparative TLC to give pure products **3**.

Supporting Information

Supporting Information File 1

Details of screening experiments, synthetic procedures and characterization data of new compounds, and copies of spectra.
[https://www.beilstein-journals.org/bjoc/content/supplementary/1860-5397-16-198-S1.pdf]

Funding

JSPS KAKENHI Grant Numbers JP17H03060, JP20H00380, and JP20H04826 (Hybrid Catalysis)

ORCID® iDs

Tatsuhiro Uchikura - https://orcid.org/0000-0002-0327-3675
Takahiko Akiyama - https://orcid.org/0000-0003-4709-4107

References

1. Wang, J.; Sánchez-Roselló, M.; Aceña, J. L.; del Pozo, C.; Sorochinsky, A. E.; Fustero, S.; Soloshonok, V. A.; Liu, H. *Chem. Rev.* **2014,** *114,* 2432–2506. doi:10.1021/cr4002879
2. Zhou, Y.; Wang, J.; Gu, Z.; Wang, S.; Zhu, W.; Aceña, J. L.; Soloshonok, V. A.; Izawa, K.; Liu, H. *Chem. Rev.* **2016,** *116,* 422–518. doi:10.1021/acs.chemrev.5b00392
3. Alonso, C.; Martínez de Marigorta, E.; Rubiales, G.; Palacios, F. *Chem. Rev.* **2015,** *115,* 1847–1935. doi:10.1021/cr500368h
4. Li, G.-b.; Zhang, C.; Song, C.; Ma, Y.-d. *Beilstein J. Org. Chem.* **2018,** *14,* 155–181. doi:10.3762/bjoc.14.11
5. Liu, X.; Xu, C.; Wang, M.; Liu, Q. *Chem. Rev.* **2015,** *115,* 683–730. doi:10.1021/cr400473a
6. Oishi, M.; Kondo, H.; Amii, H. *Chem. Commun.* **2009,** 1909–1911. doi:10.1039/b823249k
7. Zhang, C. *Org. Biomol. Chem.* **2014,** *12,* 6580. doi:10.1039/c4ob00671b
8. Umemoto, T.; Zhang, B.; Zhu, T.; Zhou, X.; Zhang, P.; Hu, S.; Li, Y. *J. Org. Chem.* **2017,** *82,* 7708–7719. doi:10.1021/acs.joc.7b00669
9. Zanardi, A.; Novikov, M. A.; Martin, E.; Benet-Buchholz, J.; Grushin, V. V. *J. Am. Chem. Soc.* **2011,** *133,* 20901–20913. doi:10.1021/ja2081026
10. Chen, M.; Buchwald, S. L. *Angew. Chem., Int. Ed.* **2013,** *52,* 11628–11631. doi:10.1002/anie.201306094
11. Lin, X.; Hou, C.; Li, H.; Weng, Z. *Chem. – Eur. J.* **2016,** *22,* 2075–2084. doi:10.1002/chem.201504306
12. Zhang, C.-P.; Wang, Z.-L.; Chen, Q.-Y.; Zhang, C.-T.; Gu, Y.-C.; Xiao, J.-C. *Angew. Chem., Int. Ed.* **2011,** *50,* 1896–1900. doi:10.1002/anie.201006823
13. Li, X.; Zhao, J.; Zhang, L.; Hu, M.; Wang, L.; Hu, J. *Org. Lett.* **2015,** *17,* 298–301. doi:10.1021/ol5034018
14. Negishi, K.; Aikawa, K.; Mikami, K. *Eur. J. Org. Chem.* **2016,** 4099–4104. doi:10.1002/ejoc.201600711
15. Chen, Q.-Y.; Wu, S.-W. *J. Chem. Soc., Chem. Commun.* **1989,** 705–706. doi:10.1039/c39890000705
16. Kondo, H.; Oishi, M.; Fujikawa, K.; Amii, H. *Adv. Synth. Catal.* **2011,** *353,* 1247–1252. doi:10.1002/adsc.201000825
17. Knauber, T.; Arikan, F.; Röschenthaler, G.-V.; Gooßen, L. J. *Chem. – Eur. J.* **2011,** *17,* 2689–2697. doi:10.1002/chem.201002749
18. Li, Y.; Chen, T.; Wang, H.; Zhang, R.; Jin, K.; Wang, X.; Duan, C. *Synlett* **2011,** 1713–1716. doi:10.1055/s-0030-1260930
19. Nakamura, Y.; Fujiu, M.; Murase, T.; Itoh, Y.; Serizawa, H.; Aikawa, K.; Mikami, K. *Beilstein J. Org. Chem.* **2013,** *9,* 2404–2409. doi:10.3762/bjoc.9.277
20. Aikawa, K.; Nakamura, Y.; Yokota, Y.; Toya, W.; Mikami, K. *Chem. – Eur. J.* **2015,** *21,* 96–100. doi:10.1002/chem.201405677
21. Shimizu, N.; Kondo, H.; Oishi, M.; Fujikawa, K.; Komada, K.; Amii, H. *Org. Synth.* **2016,** *93,* 147–162. doi:10.15227/orgsyn.093.0147
22. Miyagawa, M.; Ishikawa, T.; Shinkai, K.; Akiyama, T. *J. Fluorine Chem.* **2019,** *219,* 29–31. doi:10.1016/j.jfluchem.2018.12.006
23. The bipyridyl ligands stabilize the copper(I) catalyst for catalytic reaction (see ref. [6]).
24. From the examination of an aryl group at the 2-position of benzimidazolines, electron-rich moieties were more reactive than electron-deficient ones (Table S5, see Supporting Information File 1). These results suggest that an oxidative addition step proceeds by nucleophilic process.

License and Terms

This is an Open Access article under the terms of the Creative Commons Attribution License (https://creativecommons.org/licenses/by/4.0). Please note that the reuse, redistribution and reproduction in particular requires that the authors and source are credited.

The license is subject to the *Beilstein Journal of Organic Chemistry* terms and conditions: (https://www.beilstein-journals.org/bjoc)

The definitive version of this article is the electronic one which can be found at:
https://doi.org/10.3762/bjoc.16.198

BEILSTEIN JOURNAL OF ORGANIC CHEMISTRY

Conformational preferences of fluorine-containing agrochemicals and their implications for lipophilicity prediction

Daniela Rodrigues Silva‡, Joyce K. Daré‡ and Matheus P. Freitas*

Full Research Paper

Open Access

Address:
Department of Chemistry, Federal University of Lavras, 37200–900, Lavras–MG, Brazil

Email:
Matheus P. Freitas* - matheus@ufla.br

* Corresponding author ‡ Equal contributors

Keywords:
dipole moment; fluorinated compounds; *gauche* effect; herbicides; log *P*

Beilstein J. Org. Chem. **2020,** *16,* 2469–2476.
https://doi.org/10.3762/bjoc.16.200

Received: 30 May 2020
Accepted: 23 September 2020
Published: 05 October 2020

This article is part of the thematic issue "Organo-fluorine chemistry V".

Guest Editor: D. O'Hagan

© 2020 Silva et al.; licensee Beilstein-Institut.
License and terms: see end of document.

Abstract

Molecular polarity governs lipophilicity, which in turn determines important agrochemical and environmental properties, such as soil sorption and bioconcentration of organic compounds. Since the C–F bond is the most polar in organic chemistry, the orientation of fluorine substituents originating from the rotation around C–C(F) bonds should affect the polarity and, consequently, the physicochemical and biological properties of fluorine-containing agrochemicals. Accordingly, this study aims to determine the most likely conformers of some fluorine-containing agrochemicals and to correlate their molecular dipole moments with the respective *n*-octanol/water partition coefficients (log *P*), in order to investigate the dependence of the lipophilicity with the molecular conformation.

Introduction

Whilst in the last years the agrochemical industry has encountered a period of downturn affected by new regulations, low crop prices, biochemical resistance, among other variables, recent events have shown signs of recovery [1]. Currently, the agrochemical industry focuses on introducing new efficient and more environmentally friendly products, that attend the new regulation requirements, for replacing those agrochemicals that were banned due to either their hazard or inefficiency in fighting persistent weeds and pathogens [1]. However, the process for designing, developing, and introducing new agrochemicals to the market is considerably challenging, since it involves many steps and the optimization of a range of properties. Furthermore, it is also an expensive and time-consuming procedure [2].

Fluorination is a common strategy employed as part of the optimization process during the design of new chemical compounds, which includes the modulation of a variety of proper-

ties such as lipophilicity, biological half-life, and biosorption [3,4]. This role helps in explaining the expressive amount of fluorine-containing agrochemical candidates (around 30%) as well as pharmaceuticals (around 20%) [5,6]. In this sense, the chemistry of fluorine-containing compounds has been extensively investigated in order to better understand the effects of fluorination on conformation, membrane permeation, pharmacokinetic properties, among other parameters [7].

From a conformational analysis point of view, the fluorine atom presents minimal steric effects; on the other hand, due to its high electronegativity, the C–F bond is highly polarized, which characterizes it as a site for electrostatic and hyperconjugative interactions [8]. Additionally, Juaristi and Notario [9] and O'Hagan and co-workers [10] have highlighted the crucial role of hyperconjugative interactions involving the fluorine lone pair in explaining the chemical behavior of organofluorine molecules and their unusual physicochemical properties. Lastly, Müller [11] explained that these features along with fluorine's strict monovalent binding mode and little polarizability, when covalently bound, guarantee fluorination the well-known ability of modulating physicochemical properties.

Although the stereochemical effects of fluorination, responsible for specific interactions and conformational preferences of several groups of compounds, have become increasingly well understood [12], their direct implication on physicochemical properties has not been fully investigated yet. The orientation of fluorine substituents originated from the rotation of fluorine-containing C–C bonds should affect the polarity and, therefore, the physicochemical and biological properties of organofluorine compounds. However, there is a lack of studies that explain how these well-known conformational effects directly alter macroscopic observed properties, such as lipophilicity [13].

Accordingly, the main goal of this work is to investigate the relationship between lipophilicity and molecular conformation on a set of organofluorine agrochemicals. To this end, this study has been divided in two parts. First, we have analyzed the conformational equilibrium of penoxsulam (**I**, Figure 1). This compound has a 1,2–disubstituted ethane motif that could adopt three main staggered conformations, namely $\mathbf{I_{gg}}$, $\mathbf{I_{ag}}$ and $\mathbf{I_{ga}}$ (g = *gauche* and a = *anti*; see Figure 1), thus we have explored the intramolecular interactions governing its conformational preferences. It is worth mentioning that $\mathbf{I_{gg}}$ has two *gauche* relationships between C–F and C–O bonds, which is stabilized by $\sigma_{CH} \rightarrow \sigma_{CF/CO}$ hyperconjugative interactions [14]. Second, we have searched for the implications of the relative conformational stabilities for log *P* prediction, the most common parameter employed to describe lipophilicity. It has been previously established that the lipophilicity of a compound depends greatly on the overall molecular polarity [15], which is often expressed as the molecular dipole moment (μ). In turn, the orientation of polar bonds also influences the overall polarity of an organic molecule, as above mentioned. Therefore, this work also seeks to assess a correlation between calculated μ values and experimental log *P* measures, in order to unveil the dependence of lipophilicity with molecular conformation.

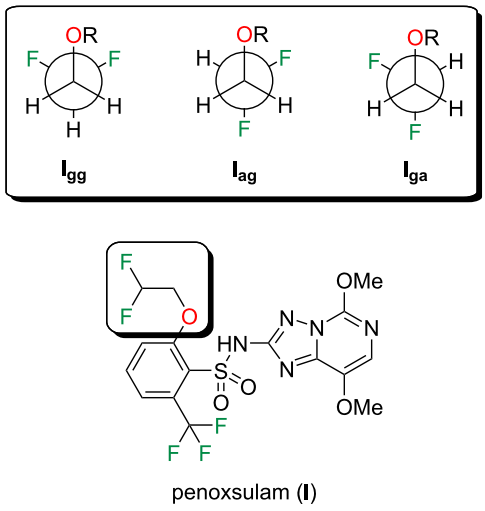

Figure 1: Chemical structure of penoxsulam (**I**) and the main staggered conformations along the two F–C–C–O torsional angles (i.e., $\mathbf{I_{gg}}$, $\mathbf{I_{ag}}$, and $\mathbf{I_{ga}}$; g = *gauche* and a = *anti*).

Results and Discussion

Conformational analysis of penoxsulam

Given the high degree of freedom in the chemical structure of penoxsulam (**I**), the conformational analysis started with a Monte Carlo conformational search at the ωB97X-D/6-31G(d,p) [16,17] level of the density functional theory (DFT). The global energy minimum conformation was then re-optimized in a higher level of theory, ωB97X-D/6-311++G(d,p) [16,18], resulting in conformer $\mathbf{I_{ag}}$ (Figure 2). This conformer has one fluorine atom in an *anti*-orientation and the other one in a *gauche*-orientation relative to the vicinal oxygen atom (pointing towards the amine hydrogen atom). To evaluate the other possible conformations along the 1,2-disubstituted ethane motif, the C–C(F) bond was rotated to additionally obtain conformers $\mathbf{I_{gg}}$ and $\mathbf{I_{ga}}$, and the corresponding geometries were then optimized. The resulting geometries and relative conformational energies are summarized in Figure 2.

At first, we observe that the overall geometry is quite similar among the three conformers. Only for $\mathbf{I_{ga}}$, where the *gauche* fluorine atom points to the opposite direction of the amine group, the triazole ring was farther away from the 1,2-disubstituted ethane moiety. Note that the gas-phase relative conforma-

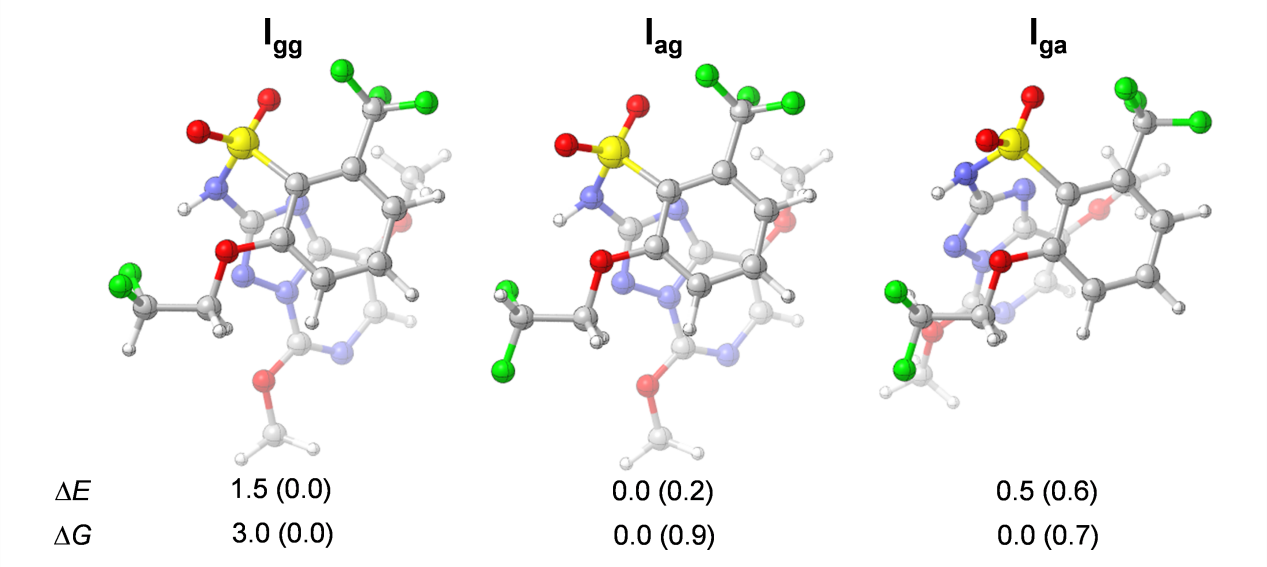

Figure 2: Optimized structures of conformers $\mathbf{I_{gg}}$ (left), $\mathbf{I_{ag}}$ (middle), and $\mathbf{I_{ga}}$ (right), along with the relative electronic and Gibbs free energies (in kcal mol^{-1}) in the gas phase and in water solution (in parentheses), computed at the ωB97X-D/6-311++G(d,p) level of theory.

tional energy Δ*E* increases, i.e., becomes less stabilizing, in the order $\mathbf{I_{ag}} < \mathbf{I_{ga}} < \mathbf{I_{gg}}$. The difference in energy between $\mathbf{I_{ag}}$ and $\mathbf{I_{ga}}$ is somehow small (0.5 kcal mol^{-1}), and these conformers are equally stable according to the relative Gibbs free energy Δ*G* (Boltzmann populations of 50% and 49%, respectively). The inclusion of an implicit polar solvent (e.g. water), however, decreases the difference in energy among conformers and $\mathbf{I_{gg}}$ becomes the most stable conformer in solution, i.e., a double *gauche* effect takes place (see data in parentheses in Figure 2). This is not surprising, since $\mathbf{I_{gg}}$ has the highest dipole moment (data shown in the next section) and is naturally more stabilized by polar solvents. Therefore, further analysis will consider the gas phase, since in this way we are accounting for the intrinsic intramolecular interactions without the influence of solvent as an external factor.

To better understand the relative conformational stabilities, we performed a numerical experiment in which the C–C(F) bond is rotated from conformer $\mathbf{I_{ag}}$ keeping other geometrical parameters fixed. In this way, we can specifically investigate the intramolecular interactions governing conformational preferences in the 1,2–disubstituted ethane motif. Furthermore, we decomposed the conformational energy along rotation around the C–C(F) bond within the framework of the natural bond orbital (NBO) analysis [19] into the Lewis (ΔE_L, which accounts for classical interactions) and non-Lewis (ΔE_{NL}, which accounts for delocalization energy) contributions (Figure 3). Note that all energy terms are represented relative to the conformation with the $\varphi_{O-C-C-H}$ torsional angle of 0°, thus positive values mean that the energy becomes less stabilizing and negative values mean that the energy becomes more stabilizing.

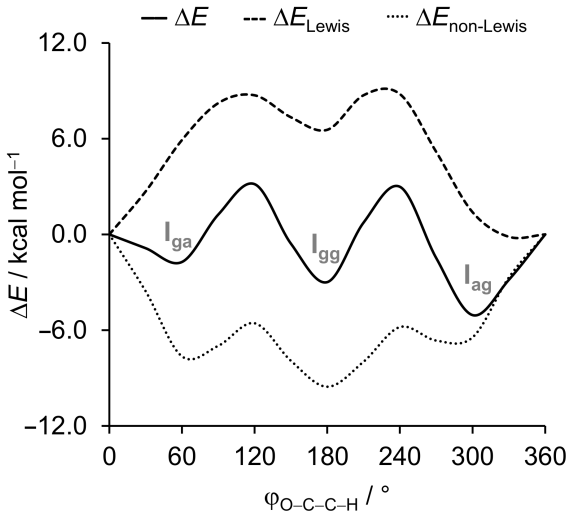

Figure 3: Energy profile for the rotation around the C–C(F) bond and NBO analysis project onto the $\varphi_{O-C-C-H}$ torsional angle (step size of 30°) at the ωB97X-D/6-311G(d,p) level of theory.

From Figure 3, it can be observed that conformer $\mathbf{I_{gg}}$ is the most stabilized by the ΔE_{NL} term, which can be attributed to the stabilizing interactions featured in the *gauche* effect [14,20], due to the *gauche* arrangement along the two F–C–C–O pathways. The charge transfer from the filled σ_{CH} orbital to the empty σ^*_{CF} or σ^*_{CO} orbitals amounts to 4.6/4.5 and 3.3 kcal mol^{-1}, respectively, which are more stabilizing than the corresponding $\sigma_{CF/CO} \rightarrow \sigma^*_{CO/CF}$ and $n_{F/O} \rightarrow \sigma^*_{CO/CF}$ in the *anti*-orientation (Table 1). Note that the $n_F \rightarrow \sigma^*_{CO}$ charge transfer is slightly more stabilizing than the $\sigma_{CF} \rightarrow \sigma^*_{CO}$, which

is in agreement with the findings of Juaristi and Notario [9], and O'Hagan and co-workers [10]. Besides, there is also an interaction between the fluorine electron lone pair n_F and the σ^*_{NH} orbital of the amine group (of 3.2 kcal mol^{-1}, see Table 1). **I_{ga}** also experiences this stabilizing hydrogen bond-like intramolecular interaction ($n_F \rightarrow \sigma_{NH}$ of 2.8 kcal mol^{-1}, see Table 1). Yet, conformer **I_{gg}** is not the global energy minimum. This is surprising, because all-*gauche* conformations in fluoropropanediol are strongly preferred [21], while the double *gauche* effect in difluoroethylamine and its hydrochloride salt stabilizes the gg over ag conformations [22]. Therefore, **I_{ag}** is the global energy minimum because it experiences a more stabilizing ΔE_L term. Among the three conformers, **I_{gg}** has the least stabilizing ΔE_L energy, and this can be ascribed to the closer proximity between the F and O electronegative atoms. Thus, the least stabilizing ΔE_L term overcomes the stabilization from hyperconjugation interactions (ΔE_{NL}), and classical electrostatic and steric interactions are the main factors governing conformational preferences of penoxsulam (**I**).

It is worth mentioning that the structure of penoxsulam in the biological environment is already known in the literature [23] and, accordingly, it differs from the energy minimum conformations computed in this work. However, a conformational search in the gas phase, as performed herein, is necessary to fully understand the intramolecular interactions and to establish the correlation between μ and log *P*, since this physicochemical property does not depend on the geometry of penoxsulam inside a biological receptor.

Effect of molecular conformation on log *P*

Herein, we aim at evaluating the correlation of molecular conformation with lipophilicity, described in terms of the *n*-octanol/water partition coefficient – log *P*, through molecular dipole moment (μ). The molecular dipole moment, μ is a relatively simple parameter that can inform on subtle intramolecular interactions that favor one structural arrangement over another, as previously mentioned. Therefore, by using a weighted average μ over the most likely conformations to correlate with experimental log *P*, one can assess the dependence of log *P* with molecular conformation.

Accordingly, a consistent set of fluorine-containing agrochemicals (Figure 4) with experimentally available log *P* data was selected from a single database [24], which comprises: penoxsulam (**I**), pyroxsulam (**II**), cloransulam-methyl (**III**), flumioxazin (**IV**), fluroxypyr-1-methylheptyl ester (**V**), ethalfluralin (**VI**), and trifluralin (**VII**). The data set contains compounds without rotatable C–C(F) bonds (**III**–**V**), with a rotatable C–C(F) bond that does not generate different conformers (**II**, **VI**, and **VII**), and with a rotatable C–C(F) bond that generates

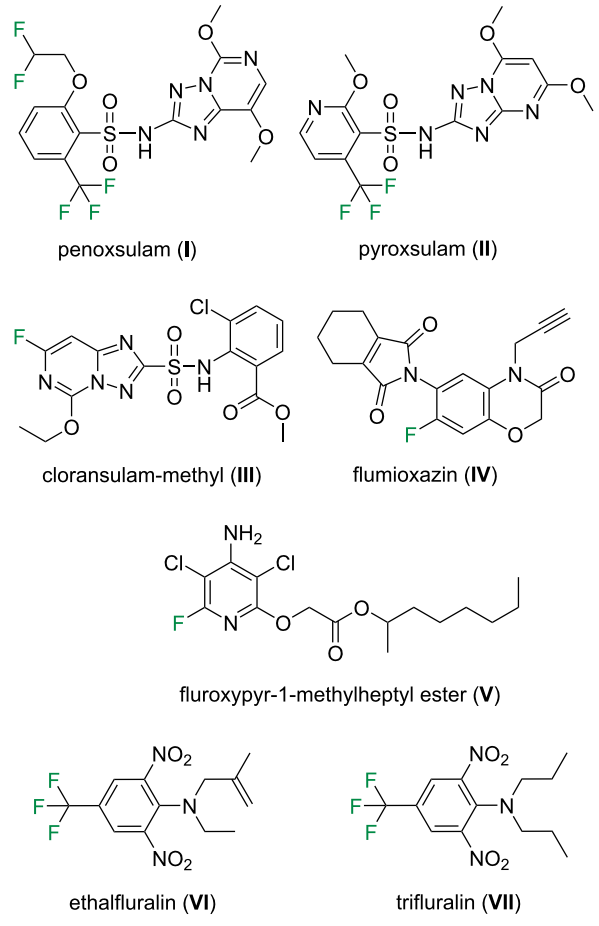

Figure 4: Chemical structure of the agrochemicals **I**–**VII** analyzed herein.

Table 1: Second order perturbation energy *E*(2) of the main hyperconjugation interactions (in kcal mol^{-1}) computed at the ωB97X-D/6-311G(d,p) level of theory.

Conf.	$\sigma_{CH} \rightarrow \sigma^*_{CF}$	$\sigma_{CH} \rightarrow \sigma^*_{CO}$	$\sigma_{CO} \rightarrow \sigma^*_{CF}$	$\sigma_{CF} \rightarrow \sigma^*_{CO}$	$n_F \rightarrow \sigma^*_{CO}$	$n_O \rightarrow \sigma^*_{CF}$	$n_F \rightarrow \sigma^*_{NH}$
I_{gg}	4.6/4.5	3.3	–	–	–	–	3.2
I_{ag}	4.7	–	1.5	1.5	1.8	0.8	2.8
I_{ga}	4.3	–	1.7	1.4	1.6	0.8	–

different conformers (**I**). The μ values for all herbicides were computed through theoretical calculations (see computational details section) and are presented in Table 2 along with their respective experimental log *P* data.

Table 2: Experimental log *P*, dipole moment (μ, in Db), and predicted log *P* of agrochemicals **I**–**VII**.

Compd.	log *P*[a]	μ[b]	milog *P*[c]
I_{gg} [0.01]	–0.60	11.56	2.74
I_{ag} [0.50]	–0.60	9.61	2.74
I_{ga} [0.49]	–0.60	9.50	2.74
II	–1.01	7.24	1.44
III	1.12	7.76	3.09
IV	2.55	4.27	2.12
V	5.04	0.68	5.43
VI	5.11	2.32	4.28
VII	5.27	2.85	4.47

[a]Experimental log *P* obtained from the Dow AgroSciences database [24]; [b]dipole moments computed at the ωB97X-D/6-311++G(d,p) level of theory, see computational section for details; [c]predicted log *P* calculated in the Molinspiration Cheminformatics server [25].

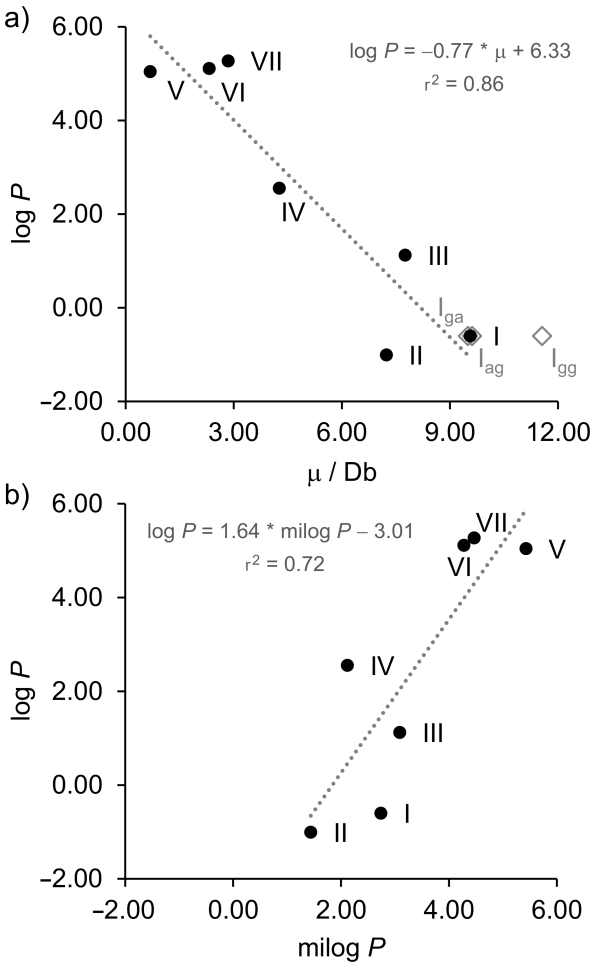

Figure 5: Correlation between the experimental log *P* of agrochemicals **I**–**VII** and a) dipole moment (for **I**, μ is used as a weighted average of the conformers $\mathbf{I_{gg}}$, $\mathbf{I_{ag}}$, and $\mathbf{I_{ga}}$), and b) predicted log *P* (milog *P*).

Penoxsulam (**I**) has a rotatable C–C(F) bond (as analyzed in the previous section) and, consequently, has the dependence of the molecular dipole moment μ with the rotation around this bond. It is well-known that μ is influenced by two main factors: the molecular dimensions and the electron distribution [26]. Thus, a different μ was calculated for each of the three staggered conformers of **I** and a weighted average μ was obtained from the calculated μ of the three conformers $\mathbf{I_{gg}}$, $\mathbf{I_{ag}}$, and $\mathbf{I_{ga}}$. Then, the calculated μ values were plotted against the experimental log *P* (Figure 5a) in order to quantitatively analyze the correlation between the two parameters. The resulting linear regression coefficient (r^2) was 0.86, which can be considered a suitable correlation coefficient. A hypothesis test for the significance of the observed correlation, based on the *p*-value (at a significance level of 95%, $\alpha = 0.05$), was also carried out. A *p*-value of 0.00264 was obtained, which is much smaller than the critical value of 0.05. Therefore, the null hypothesis (that considers the correlation coefficient as 0) is rejected, which reinforces the dependence of lipophilicity on the total molecular polarity.

In another attempt to demonstrate the importance of μ (a conformational dependent parameter) for estimating log *P*, we employed the Molinspiration Cheminformatics tool [25] to predict log *P*, and the results are displayed in Table 2. The predicted outcomes were also plotted against the experimental values (see Figure 5b). Most tools for predicting physicochemical properties are based on the additive contributions of polarity from atoms or chemical groups instead of considering the overall molecular polarity (μ) [27]. The predictive ability of these methods for compounds with higher structural complexity have been questioned in the literature [28]. Indeed, the obtained r^2 (0.72) exhibits a considerably higher discrepancy than that correlation obtained from μ when compared to the optimal value of 1. A linear regression of experimental log *P* against calculated log *P* values obtained from another source (the ChemSketch module of the ACD/Labs program) yields a similar result ($r^2 = 0.71$, see Figure S1 in Supporting Information File 1). Moreover, from Figure 5b, due to the high slope and the resulting intercept, one can assume the existence of a systematic error associated with the prediction of log *P*. This finding reinsures the issues with additive methods for predicting lipophilicity of complex structures as those analyzed herein.

Nevertheless, a reservation should be considered for small organofluorine compounds, for which well-parameterized models for log *P* prediction are usually available.

Regarding the use of calculated molecular dipole moments as a descriptor of lipophilicity for small molecules, a more detailed analysis is required. Accordingly, a series of structurally simpler organofluorine compounds were retrieved (Figure 6), all from the same source [29], and a similar computational routine was carried out (see computational details section for a full description).

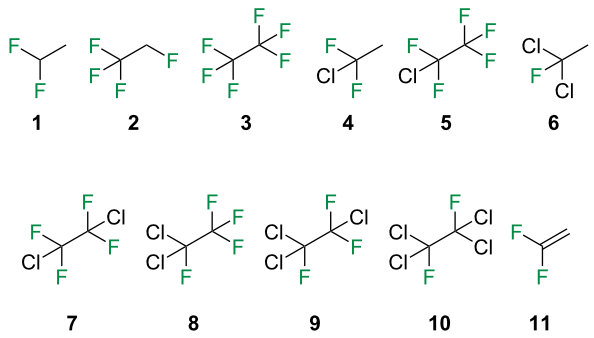

Figure 6: Chemical structure of the compounds **1**–**11** analyzed herein.

Compounds **7**, **9**, and **10** have the dependence of the molecular dipole moment μ with the rotation around the C–C bond. The correlation plots between the experimental log *P* of compounds **1**–**11** and a) dipole moment and b) predicted log *P* are shown in Figure 7.

From Figure 7a one can observe an r^2 value of 0.53, which indicates a rough correlation between μ and log *P*. However, when applying the same hypothesis test, as for the first data set, a *p*-value of 0.0115 was obtained, which suggests that, although smaller than the first correlation, there is also a dependence between the calculated dipole moment and lipophilicity for small molecules. The considerably lower correlation may be explained by the fact that, in a small molecule, subtle structural changes strongly influence the overall molecular dipole and, sometimes, the introduction of a polar bond in a molecule decreases the overall molecular dipole moment. For instance, carbon tetrafluoride has four polar bonds, but it is apolar, while the other fluorinated methanes are all polar. Thus, the use of calculated molecular dipole moments as descriptors for lipophilicity in these small organofluorines should be used with caution. On the other hand, Figure 7b reveals a satisfactory correlation between the predicted and experimental values of log *P*, which reinforces that for simple molecules there are well-

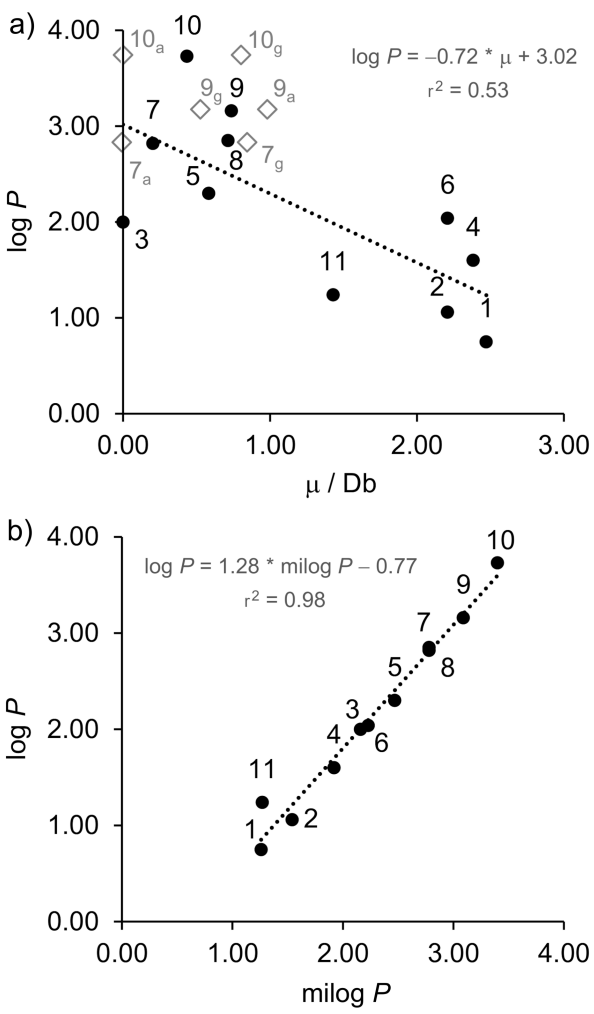

Figure 7: Correlation between the experimental log *P* of compounds **1**–**11** and a) dipole moment (for **7**, **9**, and **10**, μ is used as a weighted average of the *gauche* and *anti*-conformers), and b) predicted log *P* (milog *P*).

parameterized models for log *P* prediction, in spite of the remarkable systematic error.

Conclusion

In summary, the overall molecular polarity is influenced not only by the nature of the substituent group (as considered by additive techniques of prediction), but also by the orientation of the neat molecular dipole moment vector. In this sense, methods that ignore such influences result in reduced accuracy when predicting physicochemical properties of complex structures, such as the herbicides presented herein. Taking into account the correlation between lipophilicity and molecular conformation contributes to rationalize the effect of fluorine introduction on lipophilicity. Furthermore, the use of the molecular dipole moment that considers information on the molecular conforma-

tion, as presented herein, is a simple and straightforward parameter that can be valuable as a descriptor in quantitative structure–property relationships (QSPR). This could contribute significantly in studies involving organofluorine agrochemicals, for example, towards modeling herbicidal activity, and/or for environmental risk assessment.

Computational Details

The conformational search of agrochemicals **I**–**VII** was performed at the ωB97X-D/6-31G(d,p) [16,17] level of theory using the Spartan'18 software [30]. The lowest energy minimum conformation of each compound was then reoptimized and the dipole moment determined using a higher level of theory, ωB97X-D/6-311++G(d,p) [16,18], in the Gaussian 09 software [31]. The geometries and dipole moments for compounds **1**–**11** were calculated at the same level, which has been successfully applied to predict the conformational energies of other fluorine-containing compounds [32-34]. Frequency calculations were performed to confirm that the optimized geometries were true energy minima (no imaginary frequency) and to estimate thermodynamic energies, at 298.15 K. Solvent effects were accounted for by geometry optimization using the integral equation formalism variant of the polarizable continuum model (IEFPCM) [35]. Insights into the intramolecular interactions governing conformational preferences were obtained through the natural bond orbital (NBO) analysis [19,36]. The predicted log *P* was calculated using the Molinspiration Cheminformatics tool [25] and molecular structures were illustrated using CYLview [37].

Supporting Information

Supporting Information File 1

Additional linear correlation, main conformers from the Monte Carlo conformational search, Cartesian coordinates and energies of the conformers of agrochemicals **I**–**VII** and compounds **1**–**11** analyzed herein.
[https://www.beilstein-journals.org/bjoc/content/supplementary/1860-5397-16-200-S1.pdf]

Funding

The authors are grateful to the Conselho Nacional de Desenvolvimento Científico e Tecnológico (CNPq, fellowship and scholarship grant numbers 301371/2017-2 and 140955/2017-8, respectively), the Coordenação de Aperfeiçoamento de Pessoal de Nível Superior (CAPES, funding code 001) and the Fundação de Amparo à Pesquisa do Estado de Minas Gerais (FAPEMIG, grant number APQ-00383/15) for financial support.

ORCID® iDs

Matheus P. Freitas - https://orcid.org/0000-0002-7492-1801

Preprint

A non-peer-reviewed version of this article has been previously published as a preprint: https://doi.org/10.3762/bxiv.2020.66.v1

References

1. Phillips, M. W. A. *Pest Manage. Sci.* **2020,** *76,* 3348–3356. doi:10.1002/ps.5728
2. Sparks, T. C.; Lorsbach, B. A. *Pest Manage. Sci.* **2017,** *73,* 672–677. doi:10.1002/ps.4457
3. Jeffries, B.; Wang, Z.; Felstead, H. R.; Le Questel, J.-Y.; Scott, J. S.; Chiarparin, E.; Graton, J.; Linclau, B. *J. Med. Chem.* **2020,** *63,* 1002–1031. doi:10.1021/acs.jmedchem.9b01172
4. Zhou, Y.; Wang, J.; Gu, Z.; Wang, S.; Zhu, W.; Aceña, J. L.; Soloshonok, V. A.; Izawa, K.; Liu, H. *Chem. Rev.* **2016,** *116,* 422–518. doi:10.1021/acs.chemrev.5b00392
5. Fujiwara, T.; O'Hagan, D. *J. Fluorine Chem.* **2014,** *167,* 16–29. doi:10.1016/j.jfluchem.2014.06.014
6. O'Hagan, D. *J. Fluorine Chem.* **2010,** *131,* 1071–1081. doi:10.1016/j.jfluchem.2010.03.003
7. Gillis, E. P.; Eastman, K. J.; Hill, M. D.; Donnelly, D. J.; Meanwell, N. A. *J. Med. Chem.* **2015,** *58,* 8315–8359. doi:10.1021/acs.jmedchem.5b00258
8. Hunter, L. *Beilstein J. Org. Chem.* **2010,** *6,* No. 38. doi:10.3762/bjoc.6.38
9. Juaristi, E.; Notario, R. *J. Org. Chem.* **2016,** *81,* 1192–1197. doi:10.1021/acs.joc.5b02718
10. Keddie, N. S.; Slawin, A. M. Z.; Lebl, T.; Philp, D.; O'Hagan, D. *Nat. Chem.* **2015,** *7,* 483–488. doi:10.1038/nchem.2232
11. Müller, K. *Chimia* **2014,** *68,* 356–362. doi:10.2533/chimia.2014.356
12. O'Hagan, D. *Chem. Soc. Rev.* **2008,** *37,* 308–319. doi:10.1039/b711844a
13. O'Hagan, D.; Young, R. J. *Angew. Chem., Int. Ed.* **2016,** *55,* 3858–3860. doi:10.1002/anie.201511055
Angew. Chem. **2016,** *128,* 3922–3924. doi:10.1002/ange.201511055
14. Buissonneaud, D. Y.; van Mourik, T.; O'Hagan, D. *Tetrahedron* **2010,** *66,* 2196–2202. doi:10.1016/j.tet.2010.01.049
15. Huchet, Q. A.; Kuhn, B.; Wagner, B.; Fischer, H.; Kansy, M.; Zimmerli, D.; Carreira, E. M.; Müller, K. *J. Fluorine Chem.* **2013,** *152,* 119–128. doi:10.1016/j.jfluchem.2013.02.023
16. Chai, J.-D.; Head-Gordon, M. *Phys. Chem. Chem. Phys.* **2008,** *10,* 6615–6620. doi:10.1039/b810189b
17. Francl, M. M.; Pietro, W. J.; Hehre, W. J.; Binkley, J. S.; Gordon, M. S.; DeFrees, D. J.; Pople, J. A. *J. Chem. Phys.* **1982,** *77,* 3654–3665. doi:10.1063/1.444267
18. Krishnan, R.; Binkley, J. S.; Seeger, R.; Pople, J. A. *J. Chem. Phys.* **1980,** *72,* 650–654. doi:10.1063/1.438955
19. Glendening, E. D.; Landis, C. R.; Weinhold, F. *J. Comput. Chem.* **2013,** *34,* 1429–1437. doi:10.1002/jcc.23266
20. Goodman, L.; Gu, H.; Pophristic, V. *J. Phys. Chem. A* **2005,** *109,* 1223–1229. doi:10.1021/jp046290d
21. Andrade, L. A. F.; Silla, J. M.; Duarte, C. J.; Rittner, R.; Freitas, M. P. *Org. Biomol. Chem.* **2013,** *11,* 6766–6771. doi:10.1039/c3ob41207e
22. Silla, J. M.; Duarte, C. J.; Cormanich, R. A.; Rittner, R.; Freitas, M. P. *Beilstein J. Org. Chem.* **2014,** *10,* 877–882. doi:10.3762/bjoc.10.84

23. Lonhienne, T.; Garcia, M. D.; Pierens, G.; Mobli, M.; Nouwens, A.; Guddat, L. W. *Proc. Natl. Acad. Sci. U. S. A.* **2018,** *115,* E1945–E1954. doi:10.1073/pnas.1714392115
24. SDS Finder – Dow Safety Data Sheets. https://www.dow.com/en-us/support/sds-finder.html.
25. Molinspiration Cheminformatics 2020; Calculation of Molecular Properties and Bioactivity Score. https://www.molinspiration.com/cgi-bin/properties.
26. Carey, F.; Sundberg, R. *Chemical Bonding and Molecular Structure. In Advanced Organic Chemistry: Part A: Structure and Mechanisms,* 5th ed.; Springer: New York, NY, USA, 2008; p 52.
27. Matter, H.; Barighaus, K.-H.; Naumann, T.; Klabunde, T.; Pirard, B. *Comb. Chem. High Throughput Screening* **2001,** *4,* 453–475. doi:10.2174/1386207013330896
28. Mannhold, R.; van de Waterbeemd, H. *J. Comput.-Aided Mol. Des.* **2001,** *15,* 337–354. doi:10.1023/a:1011107422318
29. Mackay, D.; Shiu, W.; Ma, K.-C.; Lee, S. *Handbook of Physical-Chemical Properties and Environmental Fate for Organic Chemicals,* 2nd ed.; CRC Press: Boca Raton, FL, USA, 2006. doi:10.1201/9781420044393
30. *Spartan'18,* Version 1.3.0; Wavefunction, Inc.: Irvine, CA, USA, 2018.
31. *Gaussian 09,* Revision D.01; Gaussian, Inc.: Wallingford, CT, 2013.
32. Silla, J. M.; Freitas, M. P. *J. Fluorine Chem.* **2019,** *217,* 8–12. doi:10.1016/j.jfluchem.2018.10.018
33. Martins, F. A.; Silla, J. M.; Freitas, M. P. *Beilstein J. Org. Chem.* **2017,** *13,* 1781–1787. doi:10.3762/bjoc.13.172
34. Andrade, L. A. F.; Freitas, M. P. *New J. Chem.* **2017,** *41,* 11672–11678. doi:10.1039/c7nj02463k
35. Tomasi, J.; Mennucci, B.; Cammi, R. *Chem. Rev.* **2005,** *105,* 2999–3094. doi:10.1021/cr9904009
36. *NBO 6.0;* Theoretical Chemistry Institute: University of Wisconsin, Madison, USA, 2013.
37. *CYLview,* 1.0b; Legault, C. Y.: Université de Sherbrooke, 2009, http://www.cylview.org.

License and Terms

This is an Open Access article under the terms of the Creative Commons Attribution License (https://creativecommons.org/licenses/by/4.0). Please note that the reuse, redistribution and reproduction in particular requires that the authors and source are credited.

The license is subject to the *Beilstein Journal of Organic Chemistry* terms and conditions: (https://www.beilstein-journals.org/bjoc)

The definitive version of this article is the electronic one which can be found at: https://doi.org/10.3762/bjoc.16.200

BEILSTEIN JOURNAL OF ORGANIC CHEMISTRY

Synthesis of novel fluorinated building blocks via halofluorination and related reactions

Attila Mário Remete[1,2], Tamás T. Novák[1], Melinda Nonn[1,2,3], Matti Haukka[4], Ferenc Fülöp[1,2,3] and Loránd Kiss[*1,2]

Full Research Paper

Open Access

Address:
[1]Institute of Pharmaceutical Chemistry, University of Szeged, H-6720 Szeged, Eötvös u. 6, Hungary, [2]Interdisciplinary Excellence Centre, Institute of Pharmaceutical Chemistry, University of Szeged, H-6720 Szeged, Eötvös u. 6, Hungary, [3]MTA-SZTE Stereochemistry Research Group, Hungarian Academy of Sciences, H-6720 Szeged, Eötvös u. 6, Hungary and [4]Department of Chemistry, University of Jyväskylä, FIN-40014, Jyväskylä, Finland

Email:
Loránd Kiss[*] - kiss.lorand@szte.hu

* Corresponding author

Keywords:
fluorine; fluoroselenation; functionalization; halofluorination; stereocontrol

Beilstein J. Org. Chem. **2020,** *16,* 2562–2575.
https://doi.org/10.3762/bjoc.16.208

Received: 30 June 2020
Accepted: 06 October 2020
Published: 16 October 2020

This article is part of the thematic issue "Organo-fluorine chemistry V".

Guest Editor: D. O'Hagan

© 2020 Remete et al.; licensee Beilstein-Institut.
License and terms: see end of document.

Abstract

A study exploring halofluorination and fluoroselenation of some cyclic olefins, such as diesters, imides, and lactams with varied functionalization patterns and different structural architectures is described. The synthetic methodologies were based on electrophilic activation through halonium ions of the ring olefin bonds, followed by nucleophilic fluorination with Deoxo-Fluor®. The fluorine-containing products thus obtained were subjected to elimination reactions, yielding various fluorine-containing small-molecular entities.

Introduction

The effects of fluorine on lipophilicity, metabolism, binding, and bioavailability are often beneficial [1-9]. Fluorinated organic compounds are common amongst drugs [8,9], and the synthesis of fluorinated compounds has become a rapidly developing area [9-18]. In addition to discovering new reagents and conditions for the introduction of fluorine and fluorine-containing groups into a certain organic molecule [11-18], several known methods have been studied and improved over the past decade.

One such long-known method is halofluorination. During this process, an alkene reacts with a halogen cation to form a halonium ion, which immediately undergoes ring opening by fluoride to form a vicinal halofluoride (see Scheme 1). The overall result is an *anti*-addition of the XF moiety (X = Cl, Br, I) across the double bond. Since many nucleophilic fluorine sources (e.g., $Et_3N{\cdot}3HF$ and HF–pyridine) and halonium ion sources (e.g., *N*-halosuccinimides) are relatively cheap and easily available, halofluorination might be an economic way to obtain vicinal

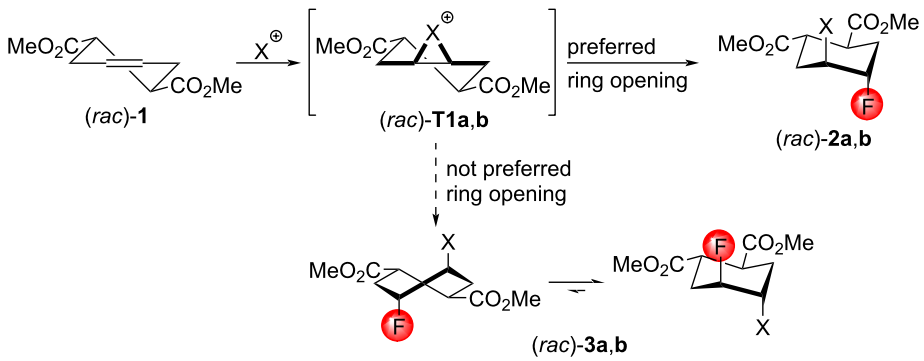

Scheme 1: Proposed outcome of the halofluorination of (rac)-**1**. Only the main conformers of (rac)-**1** and (rac)-**T1a**,**b** are shown. (rac)-**2a**: X = Br; (rac)-**2b**: X = I.

halofluorides that can be transformed further in various ways thanks to the different leaving group abilities of halogens [19]. Halofluorinaton-related reactions, such as fluorosulfuration, fluoroselenation, nitrofluorination, and nitriminofluorination, in contrast, are much less studied [20].

Deoxyfluorination, that is fluorine introduction accompanied by oxygen removal (subtypes: OH→F exchange, C=O→CF_2 transformation, and COOH→CF_3 transformation), is also an important nucleophilic fluorination method [2-5,10,11,18]. The synthesis of fluorinated compounds via deoxyfluorination [21-30] or utilizing sulfur fluoride deoxyfluorinating reagents [31,32] is a highlighted topic. It is notable that halofluorination reactions applying sulfur fluoride deoxyfluorinating reagents as fluoride sources are practically unknown [33], but analogous reactions with α-fluoroamines (another class of deoxyfluorinating reagents) were reported [20]. As a result, our main aim was to investigate the use of bis(2-methoxyethyl)aminosulfur trifluoride (Deoxo-Fluor®) as a fluoride source in halofluorination reactions. We also intended to study fluoroselenations with Deoxo-Fluor® and phenylselenyl bromide (a previously unreported reagent combination).

Results and Discussion

As starting compounds, we selected some functionalized (to obtain valuable building blocks), cyclic (to obtain better insight into the stereochemistry), and usually symmetrical olefins (to eliminate regioselectivity issues). The first substrate, the cyclohexene diester (*rac*)-**1**, has a twofold rotational symmetry, that is the formation of only a single halonium ion intermediate is possible. According to the Fürst–Plattner rule (ring-opening into a chair conformation is preferred over a twist boat conformation), the formation of the products (*rac*)-**2a**,**b** is expected (Scheme 1).

Indeed, halofluorinations of (*rac*)-**1** with NBS/Deoxo-Fluor® and NIS/Deoxo-Fluor® systems in anhydrous CH_2Cl_2 afforded the compounds (*rac*)-**2a** and (*rac*)-**2b** as single products. The stereochemistry of (*rac*)-**2a** and (*rac*)-**2b** was determined using NOESY experiments. The reactions proceeded smoothly, although the yields were moderate (Scheme 2).

Our experiments were continued with compound **4**, the *cis* isomer of the diester (*rac*)-**1**. In this case, two different halonium ion intermediates can be formed, leading to the possible

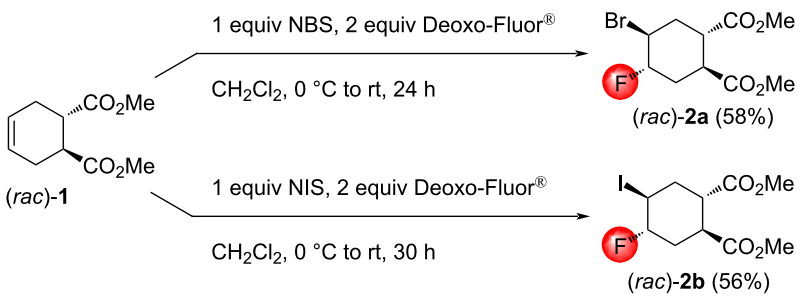

Scheme 2: Halofluorination reactions of the *trans*-diester (*rac*)-**1**.

products (*rac*)-**5a**,**b** and (*rac*)-**6a**,**b** (Scheme 3). Since the axial ester group somewhat hinders the attack of the large halonium ion on that side of the ring, the preferred formation of (*rac*)-**6a**,**b** was expected.

Contrary to our expectations, the bromofluorination of **4** led to the product (*rac*)-**5a** in 32% yield. The iodofluorination proceeded differently since the reaction was more effective and resulted in a product mixture. As originally expected, a mixture of the main product (*rac*)-**6b** and the minor product (*rac*)-**5b** was formed. The stereochemistry was assigned on the basis of NOESY cross-peaks (Scheme 4).

In subsequent studies, halofluorinations of some less symmetrically functionalized cyclohexenes were attempted. Upon treatment with 1 equiv NBS and 2 equiv Deoxo-Fluor® (CH_2Cl_2, 0 °C to rt, 2.5 h), benzyl cyclohex-3-ene-1-ylcarbamate quickly produced a multicomponent mixture. Unfortunately, however, no halofluorination product could be isolated. Under similar conditions (1 equiv NBS, 2 equiv Deoxo-Fluor®, CH_2Cl_2, 0 °C to rt, 24 h), benzyl cyclohex-3-ene-1-carboxylate yielded a mixture of two isomeric bromofluorinated products (≈12:10 ratio, combined yield 66%), with the separation being unsuccessful. Methyl cyclohex-3-ene-1-carboxylate behaved similarly, resulting in an inseparable mixture (1 equiv NBS, 2 equiv Deoxo-Fluor®, CH_2Cl_2, 0 °C to rt, 27 h, 61% yield of two isomeric bromofluorinated products in a ≈11:10 ratio).

We continued our synthetic explorations with unsaturated fused ring systems. Our first choice was the easily accessible N-benzylated *cis*-tetrahydrophthalic imide **7**. Unfortunately, both bromo- and iodofluorination of **7** yielded a mixture of two isomeric halofluorinated products for which the separation failed (Scheme 5).

Since halofluorinations of the *trans*-diester (*rac*)-**1** proceeded more selectively than analogous reactions of the stereoisomeric *cis*-diester **4**, it seemed reasonable to prepare the N-benzylated

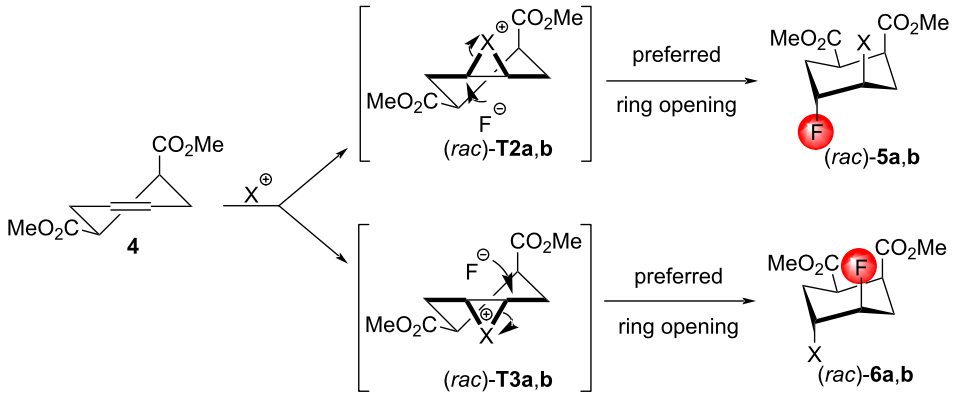

Scheme 3: Probable outcomes of the halofluorination of **4**. Both conformers of the compounds **4**, (*rac*)-**T2a**,**b**, and (*rac*)-**T3a**,**b**, respectively, have an equal energy. (*rac*)-**5a** and (*rac*)-**6a**: X = Br; (*rac*)-**5b** and (*rac*)-**6b**: X = I.

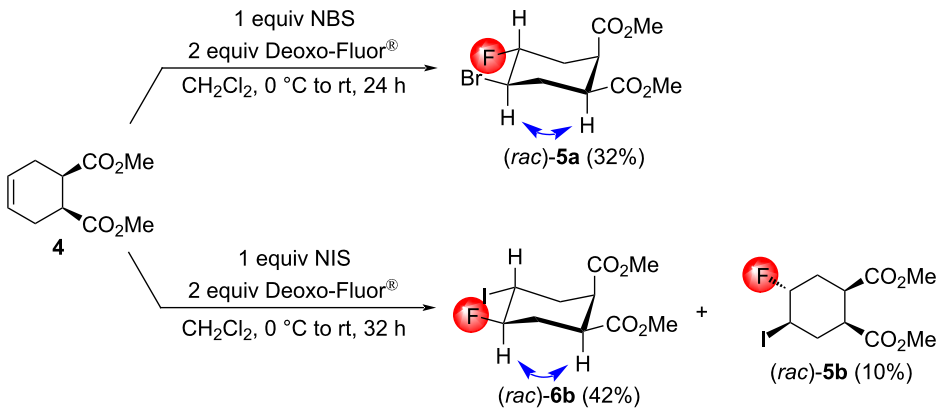

Scheme 4: Halofluorination reactions of the *cis*-diester **4**. Important NOESY interactions are indicated by two-headed arrows.

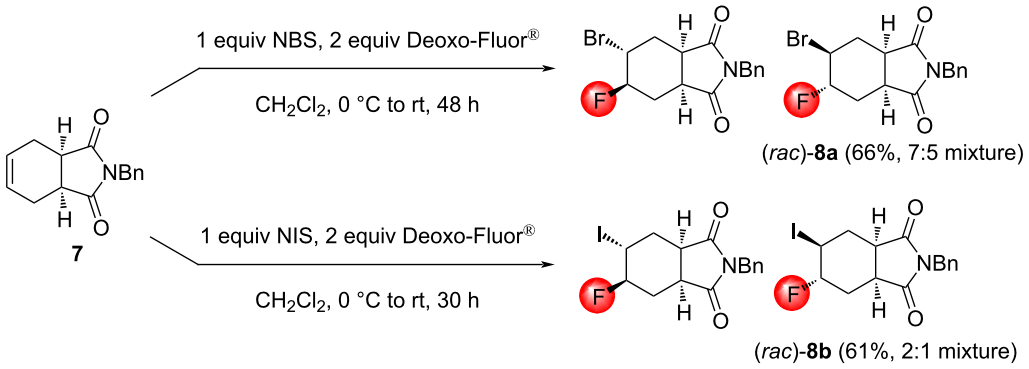

Scheme 5: Halofluorination reactions of the *cis*-tetrahydrophthalic imide derivative **7**.

trans-fused tetrahydrophthalic imide (*rac*)-**10** that was previously unknown in the literature. The synthesis started from the *trans*-tetrahydrophthalic anhydride (*rac*)-**9** [34], and the reaction of (*rac*)-**9** with $BnNH_2$ in the presence of Et_3N in toluene under reflux [35] gave the desired product (*rac*)-**10** in 42% yield. Halofluorinations of the compound (*rac*)-**10** proceeded smoothly and, according to our expectations, afforded (*rac*)-**11a** and (*rac*)-**11b**, respectively, as single products (Scheme 6). The stereochemistry of these products was originally determined by NOESY measurements. In addition, the structure of (*rac*)-**11b** was unequivocally established by single-crystal X-ray diffraction (Figure 1).

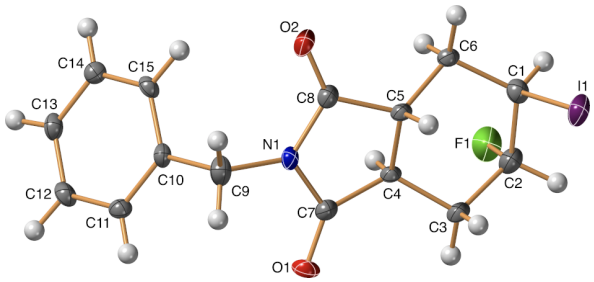

Figure 1: Crystal structure of (*rac*)-**11b**.

Then, the preparation of another model compound, the *trans*-annelated bicyclic carbamide derivative (*rac*)-**13**, was attempted. This compound was also unknown in the literature. In the reaction of commercially available *trans*-4-cyclohexene-1,2-diamine dihydrochloride and 1,1'-carbonyldiimidazole (CDI), through a slightly modified literature protocol [36], the desired product was isolated in only 10% yield (Scheme 7). Increasing the reaction temperature considerably decreased the

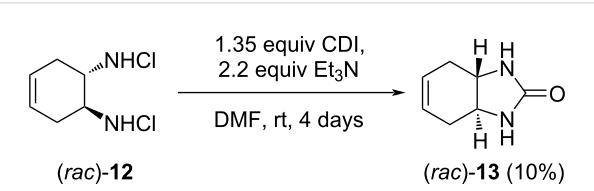

Scheme 7: Synthesis of the cyclic carbamide (*rac*)-**13**.

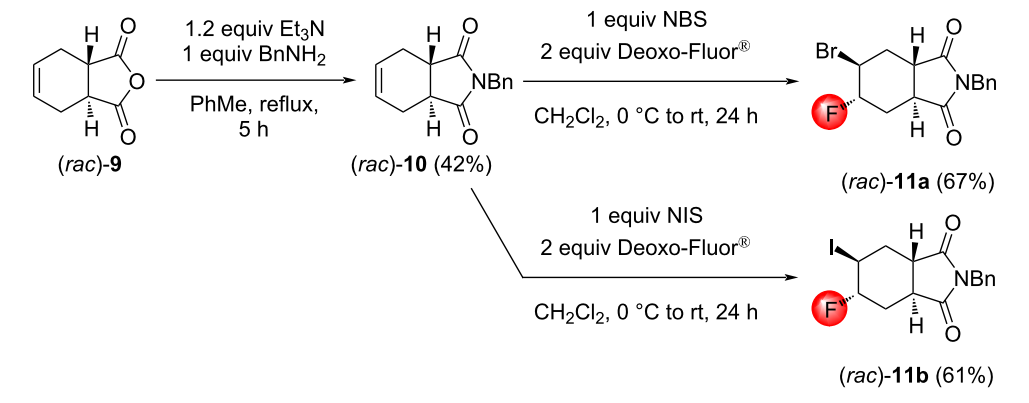

Scheme 6: Synthesis and halofluorination of the *trans*-imide (*rac*)-**10**.

product purity. With the low yield in mind, further plans concerning compound (*rac*)-**13** were abandoned.

We continued our studies with strained, rigid bicyclic systems. First, the *N*-Boc-protected Vince lactam (*rac*)-**14** was subjected to halofluorination reactions. Despite the asymmetric nature of the olefin, the compounds (*rac*)-**15a** and (*rac*)-**15b** were formed as single products, without any regio- or stereoselectivity issues (Scheme 8). However, repeated *N*-halosuccinimide addition was necessary, and the yield of the bromofluorination reaction was still mediocre. The stereochemistry of the products (*rac*)-**15a** and (*rac*)-**15b** was determined by both NOESY measurements and single-crystal X-ray diffraction (Figure 2 and Figure 3).

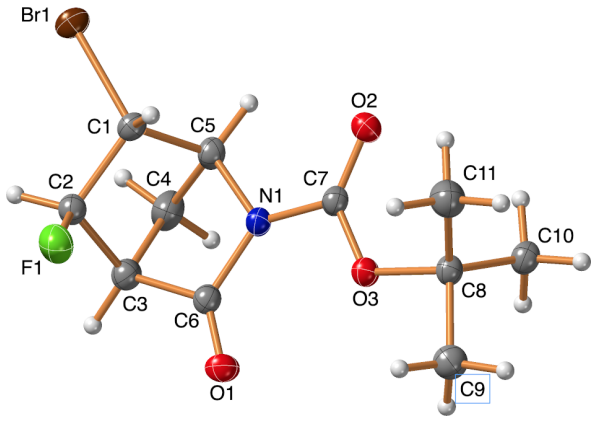

Figure 2: Crystal structure of the product (*rac*)-**15a**.

The next rigid bicyclic system studied was the methyl diendo norbornene dicarboxylate **16**. The treatment of **16** with NBS/Deoxo-Fluor® yielded the bromolactone (*rac*)-**17a** [37]. The

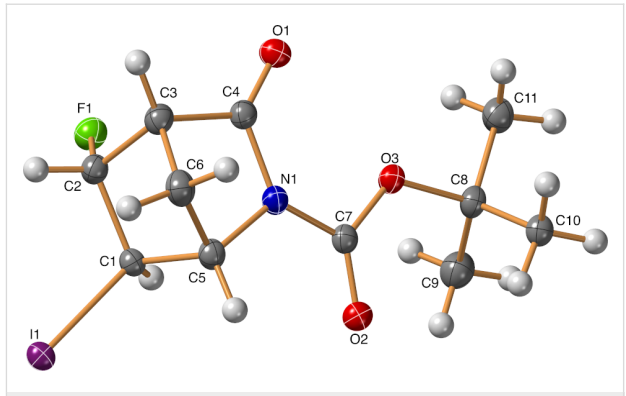

Figure 3: Crystal structure of the product (*rac*)-**15b**.

reaction, when repeated only with NBS (without a fluoride source), gave the same product. Similarly, subjecting the diester **16** to NIS or NIS/Deoxo-Fluor® resulted in the iodolactone (*rac*)-**17b** (Scheme 9) [37]. Interestingly, the bromolactonization was more efficient in the presence of Deoxo-Fluor®, while the iodofluorination worked better in the absence of the reagent. It is also worth mentioning that the bromolactone (*rac*)-**17a** was surprisingly stable against lactone ring-opening: the compound remained intact after 20 hours of reflux in methanol in the presence of a catalytic amount of H_2SO_4.

Presumably, the halogen cation attacks from the less-hindered side of the carbon–carbon double bond, yielding the halonium ion **T4a**,**b** (Scheme 10). In a subsequent nucleophilic attack, the carbonyl oxygen atom, as an intramolecular nucleophile, competes successfully with the external nucleophilic fluoride ion, resulting in the intermediate (*rac*)-**T5a**,**b**, followed by the transfer of a methyl group to a nearby nucleophile (for example, F^- or the succinimidate anion).

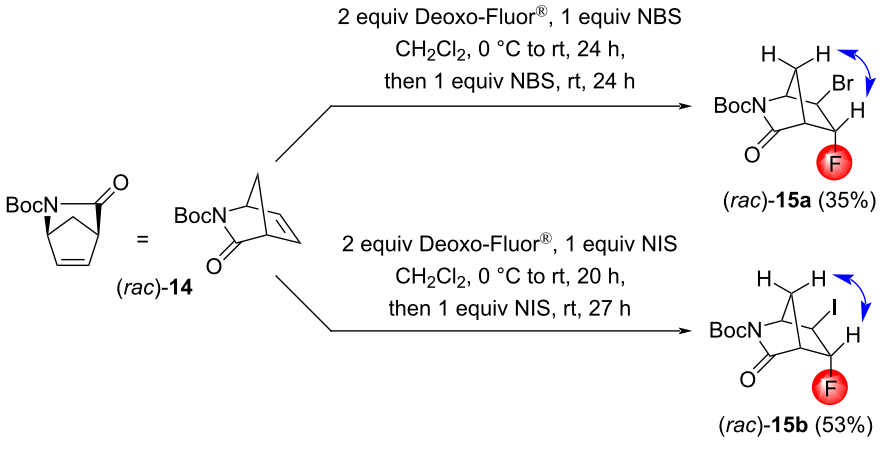

Scheme 8: Halofluorination reactions of the γ-lactam (*rac*)-**14**. Relevant NOESY interactions are indicated by two-headed arrows.

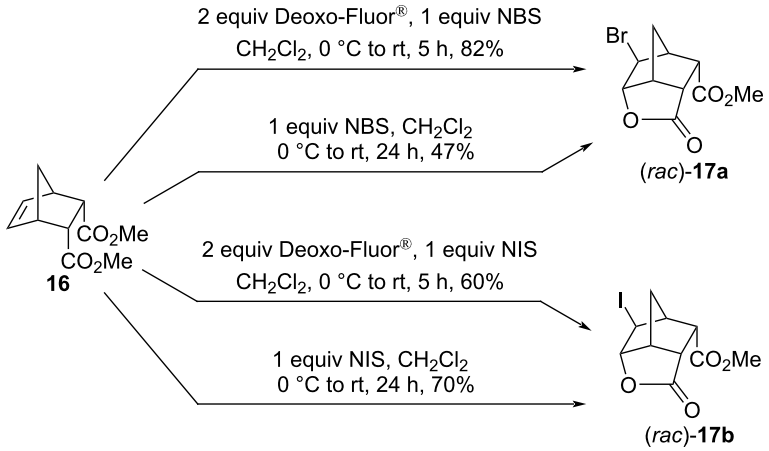

Scheme 9: Reactions of the diester **16** with NBS or NIS in the presence or absence of Deoxo-Fluor®.

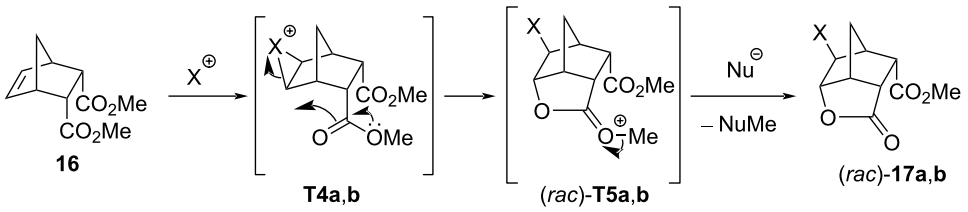

Scheme 10: Formation of the halolactons (*rac*)-**17a**,**b**. The initial attack of the halogen cation occurs at the sterically more accessible side of the C=C bond; (*rac*)-**17a**: X = Br; (*rac*)-**2a**: X = I.

We assumed that changing the arrangement of the ester groups from *endo* to *exo* (increasing the distance between the C=C bond and the carbonyl oxygen atom) would render an intramolecular cyclization impossible. Therefore, we attempted the bromofluorination of the easily accessible oxabicycloheptene derivative **18**. Unfortunately, the reaction led to a complex mixture, without any halofluorinated product (Scheme 11).

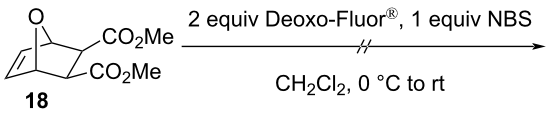

Scheme 11: Unsuccessful halofluorination of the bicyclic diester **18**.

As an alternative approach, the *N*-benzyl imide **19** was investigated under halofluorination conditions. We expected that the imide moiety of this molecule would fix the carbonyl oxygen atom in a position remote to the C=C bond to avoid cyclization. Indeed, the bromofluorination of tricyclic **19** was successful. However, the process required repeated reagent addition and involved a rearrangement, providing the isomeric products (*rac*)-**20a** and (*rac*)-**21a** (Scheme 12). We also observed the formation of the dibrominated compound **22**, which became the sole product when the reaction was performed under reflux conditions. Iodofluorination was much less effective: even after repeated reagent addition and a prolonged reaction time, 46% of the unreacted starting material could be retrieved, together with 11% of the iodofluorinated product (*rac*)-**20b**. Another halofluorinated product was also formed, but the isolation of the compound in a pure form failed. Attempts to perform this iodofluorination at reflux afforded only unreacted starting material. Since iodofluorination is usually more efficient than bromofluorination [19], the decreased yield of (*rac*)-**20b** compared to that of (*rac*)-**20a** is possibly caused by steric hindrance around the olefin bond, which affects the electrophilic attack of the larger iodine cation to a greater extent. With this in mind, we also tried the chlorofluorination of compound **19**. Again, two chlorofluorinated products were formed, but only (*rac*)-**20c** could be isolated in a pure form (Scheme 12). Chlorofluorination is usually inferior in terms of the yield when compared to bromo- and iodofluorination. However, since Cl^+ is smaller and less sensitive to steric hindrance than Br^+ or I^+, the yield of chloro- and iodofluorination were comparable in this case. The stereochemistry of the above products was determined using NOESY measurements.

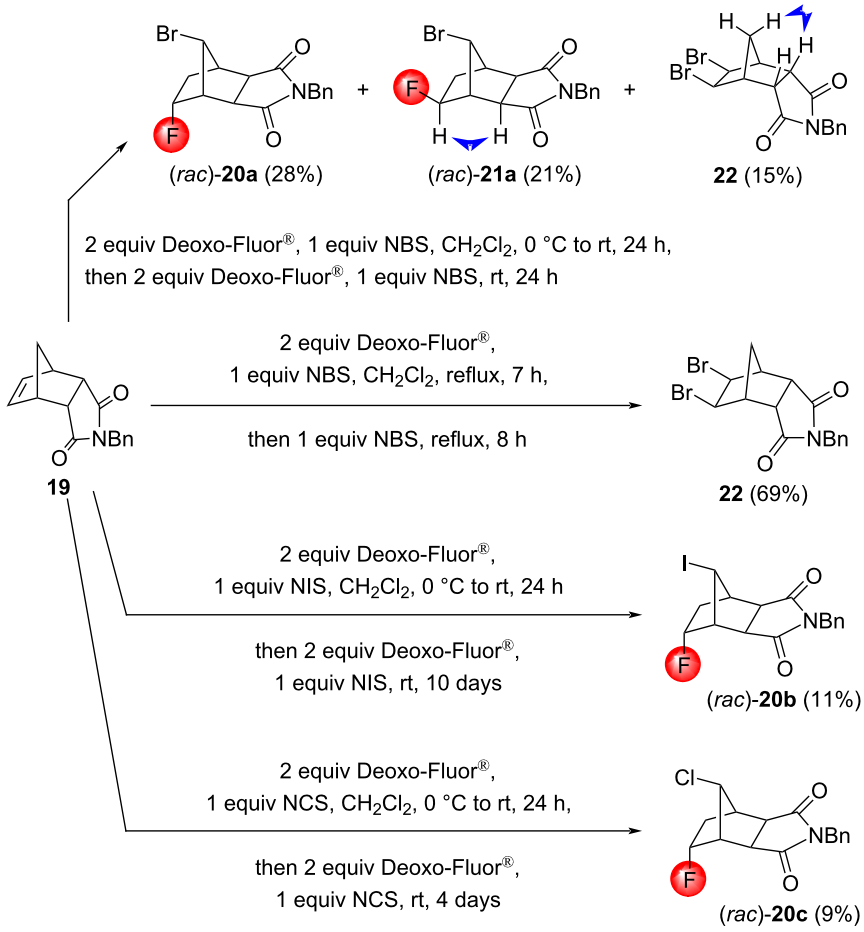

Scheme 12: Halofluorination reactions of the rigid tricyclic imine **19**. The relevant NOESY interactions are marked with two-headed arrows.

The formation of two isomeric halofluorination products can be explained by the preferred formation of the halonium ions **T6a**–**c**, respectively, since the halogen cation attacks the C=C bond of the imide **19** from the less hindered side, followed by rearrangement into the intermediates (*rac*)-**T7a**–**c**, respectively. For epoxides and bromonium ions of norbornene systems, such rearrangements are not uncommon [38-40]. Then, the carbenium ion motif of (*rac*)-**T7a**–**c** can be attacked from both sides to give the products (*rac*)-**20a**–**c** and (*rac*)-**21a**–**c** (Scheme 13). The formation mechanism of the product **22**, however, is still an open question. Since the treatment of the reaction mixture at reflux conditions significantly increased the yield, the formation of **22** may follow a radical pathway.

Using a modified literature protocol [35], the tricyclic imide **24** was also prepared and investigated. In halofluorination reactions, the behavior of **24** was similar to the *N*-benzyl analogue **19**. The treatment of **24** with Deoxo-Fluor®/NBS yielded two bromofluorinated products and the dibrominated compound **26**. Unfortunately, from the two bromofluorinated products, only (*rac*)-**25a** could be isolated in a pure form (Scheme 14). The reaction of **24** with NIS/Deoxo-Fluor® gave two iodofluorinated products, but only (*rac*)-**25b** could be isolated in a pure form. The stereochemistry of the products (*rac*)-**25a**,**b** was determined using NOESY measurements. It is worth noting that the iodofluorination was less effective than the bromofluorination – presumably because of steric hindrance – and 33% unreacted starting material was recovered from the iodofluorination reaction mixture.

In order to study the synthetic usefulness of the halofluorinated products, E2 hydrogen halide elimination was attempted. Since bromide and iodide are much better leaving groups than fluoride, the selective elimination of the former halogens was expected. Taking into account the stereochemical requirements of the E2 elimination (the halide group and the β-hydrogen atom should be antiperiplanar relative to each other), the limited availability of the compound (*rac*)-**5b**, and Bredt's rule (bridge-

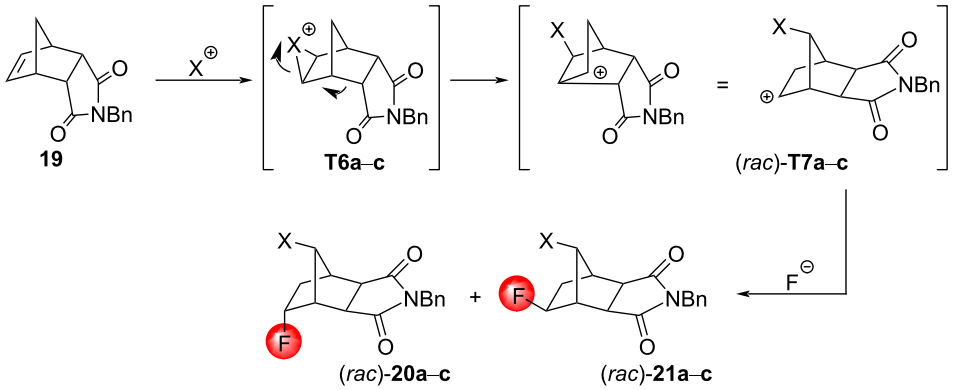

Scheme 13: Mechanism of the halofluorination reactions of the substrate **19**. X = Br (compounds a), I (compounds b), Cl (compounds c).

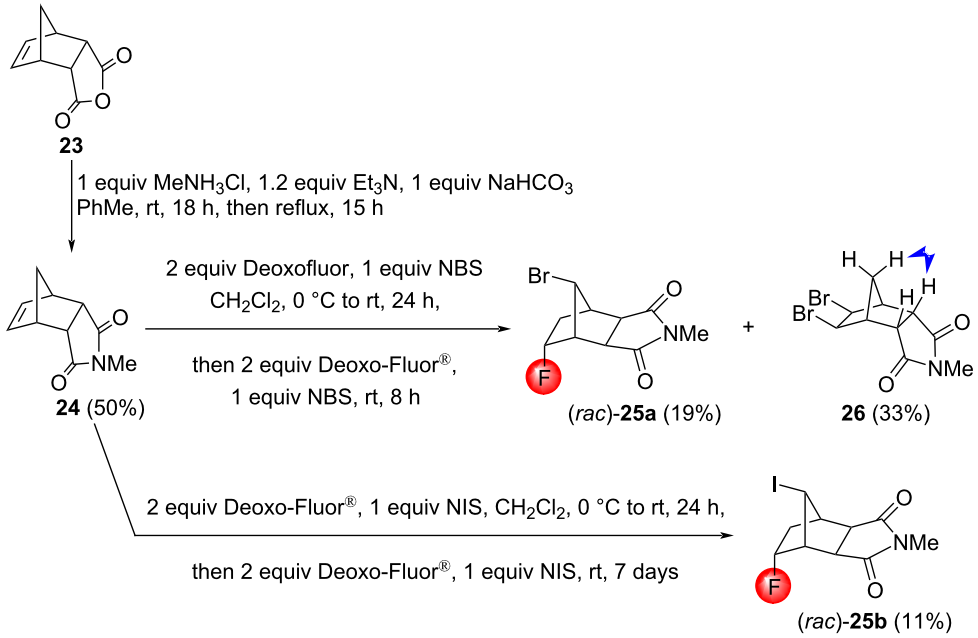

Scheme 14: Synthesis and halofluorination of the imide **24**.

head alkenes are only stable in large ring systems), elimination was attempted only with (*rac*)-**2a**,**b**, (*rac*)-**5a**, (*rac*)-**6b**, (*rac*)-**8a**,**b**, and (*rac*)-**11a**,**b**.

DBU in THF under reflux was insufficient to promote the elimination of the halofluorinated diesters (*rac*)-**2a**,**b**, (*rac*)-**5a**, and (*rac*)-**6b**. In contrast, the treatment with *t*-BuOK in THF under reflux was effective. Unexpectedly, all four halofluorinated diesters produced the same condensed ring cyclopropane derivative (*rac*)-**27** (Scheme 15). The stereochemistry of (*rac*)-**27** was determined using NOESY measurements.

Regarding the compounds (*rac*)-**2a**,**b** and (*rac*)-**5a**, the mechanism is relatively straightforward. Instead of an E2 elimination, these compounds are deprotonated next to the ester group, which is closer to the CHBr unit. Then, the carbanion motif of the formed enolates (*rac*)-**T8a** and **T8b** afford the cyclopropane-fused cyclopentane dicarboxylate (*rac*)-**27** upon the intramolecular nucleophilic attack by the alkyl halide (Scheme 16).

The reaction of the compound (*rac*)-**6b** is less direct. According to the above pathway, the formation of the compound (*rac*)-**T10** would be expected (Scheme 17). In order to generate the final product (*rac*)-**27**, a base-catalyzed epimerization is required. The requirement of additional reaction steps may explain the lower yield (31%) of this reaction. Note, that from the other three substrates, the product (*rac*)-**27** was obtained in

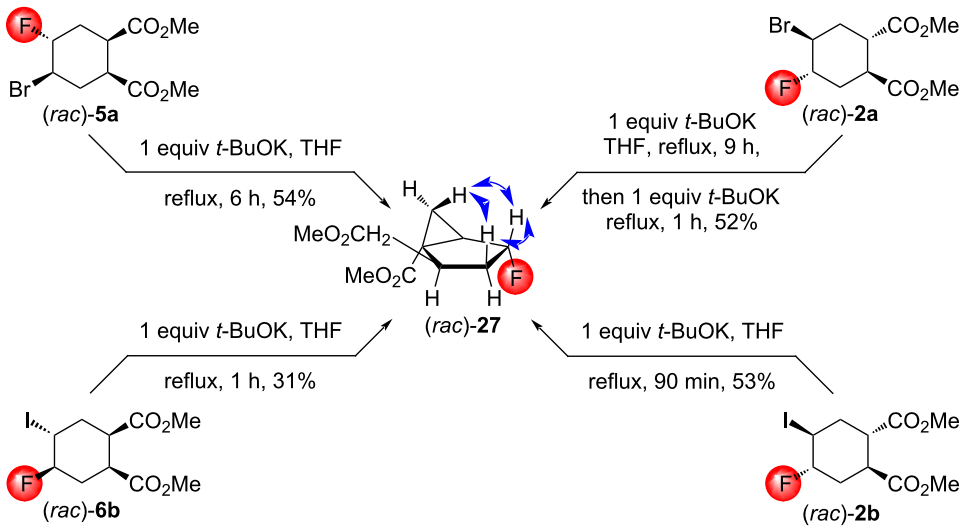

Scheme 15: Cyclizations of halofluorinated diesters with potassium *tert*-butoxide. Relevant NOESY interactions are marked with blue two-headed arrows.

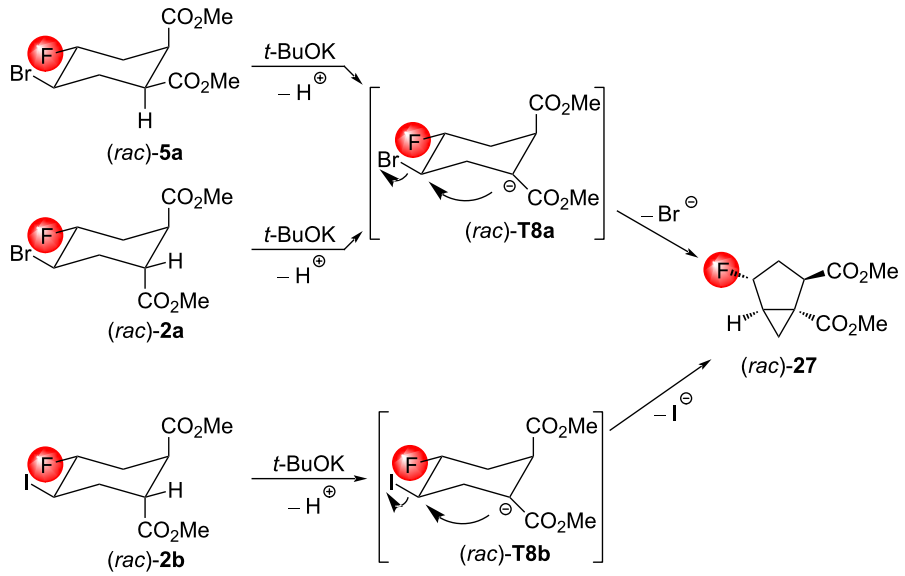

Scheme 16: Mechanism of the reaction of the cyclopropanation of the compounds (*rac*)-**2a**,**b** and (*rac*)-**5a** with *t*-BuOK.

a yield of 52–54%. Since the enolate (*rac*)-**T9** is all-equatorial, and consequently, the energy is lower than that of the corresponding stereoisomers, it is more likely that the epimerization occurs after the formation of (*rac*)-**T10**.

Concerning (*rac*)-**8a** and **8b** as well as (*rac*)-**11a** and **11b**, the reagent preference was exactly the opposite: DBU in THF under reflux was effective, while *t*-BuOK in THF under reflux was inferior. Interestingly, the same type of tricyclic compound (*rac*)-**28** was formed from all four substrates (Scheme 18). The stereochemistry of the product was determined using NOESY measurements.

Since the structures of the substances in the mixture of (*rac*)-**8a**,**b** are unknown, a possible mechanism for the formation can be written only from the imides (*rac*)-**11a**,**b**. Apparently, the first step involves a base-catalyzed epimerization into a less-strained *cis*-annelated system, which undergoes ring inversion, enabling the large halogen atom to be equatorial. This is followed by a deprotonation next to the carbonyl group of the

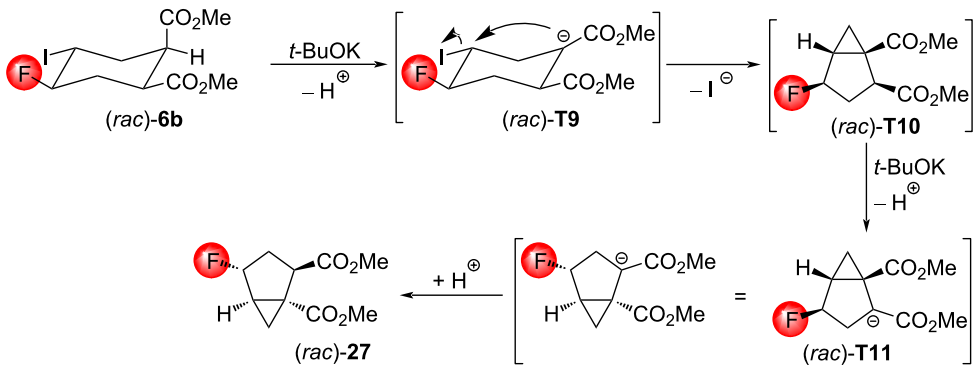

Scheme 17: Presumed mechanism of the reaction of the compound (*rac*)-**6b** with *t*-BuOK.

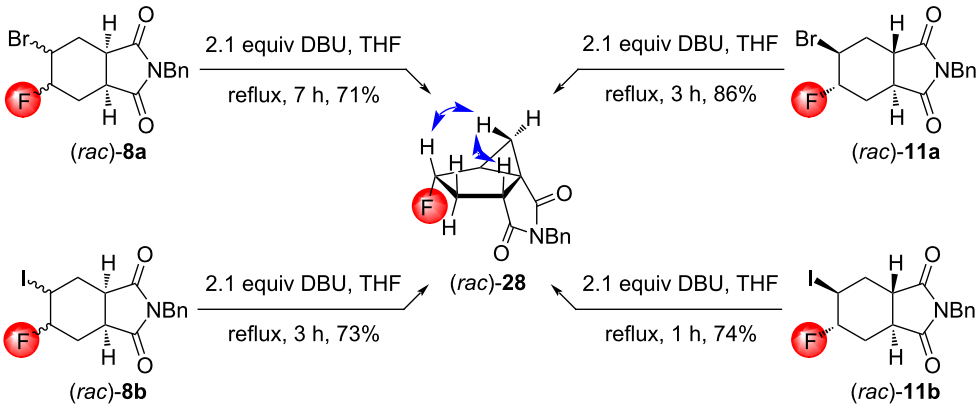

Scheme 18: Cyclizations of halofluorinated tetrahydrophthalimides with DBU. Relevant NOESY interactions are marked with two-headed arrows.

imide ring closer to the CHX moiety. Finally, an intramolecular nucleophilic attack of the carbanion on the CHX motif closes the cyclopropane ring. Of the two possible pathways, only one is observed, which starts with the removal of the sterically less-hindered proton and ends with (*rac*)-**28**, containing *cis*-annulated cyclopentane rings. Note, that the cyclopentane rings in (*rac*)-**29** have a more strained *trans*-annulated attachment (Scheme 19).

After finishing the study of the halofluorinations with NBS/Deoxo-Fluor® and NIS/Deoxo-Fluor® systems, our attention shifted to the utilization of Deoxo-Fluor® in fluoroselenations. PhSeBr was selected to provide the phenylselenyl cation serving as the required electrophilic selenium species. This reagent combination was previously unknown in the literature. Preliminary experiments with the diester **4** demonstrated that the reaction is much more efficient in anhydrous CH_3CN than in anhydrous CH_2Cl_2; therefore, the reactions were conducted in this medium at room temperature.

Similar to halofluorinations, the treatment of the diester (*rac*)-**1** with PhSeBr/Deoxo-Fluor® gave a single product (Scheme 20). The stereochemistry of the cyclohexane (*rac*)-**30** was determined using NOESY analysis. From the diester **4**, however, a mixture of two fluoroselenides was formed, and the separation failed. The use of PhSeBr/$Et_3N{\cdot}3HF$ for the fluoroselenation – another reagent combination that was previously unknown in the literature – gave similar results, although these reactions required twice as much PhSeBr (Scheme 20).

Using the above conditions (1 equiv PhSeBr, 2 equiv Deoxo-Fluor®, CH_3CN, rt), the *N*-benzylated *cis*-tetrahydrophthalic imide **7** gave a multicomponent mixture, and no fluoroselenated product was isolated. From the stereoisomeric imide (*rac*)-**10** and the bicyclic lactam (*rac*)-**14**, the formation of fluoroselenated products in low amounts could be detected, but the isolation in a pure form failed.

The treatment of the diester **16** with PhSeBr caused lactonization regardless of the presence or absence of Deoxo-Fluor®. The yield was better when phenylselenyl bromide was used alone (Scheme 21). The stereochemistry of the product (*rac*)-**32** was determined using NOESY data.

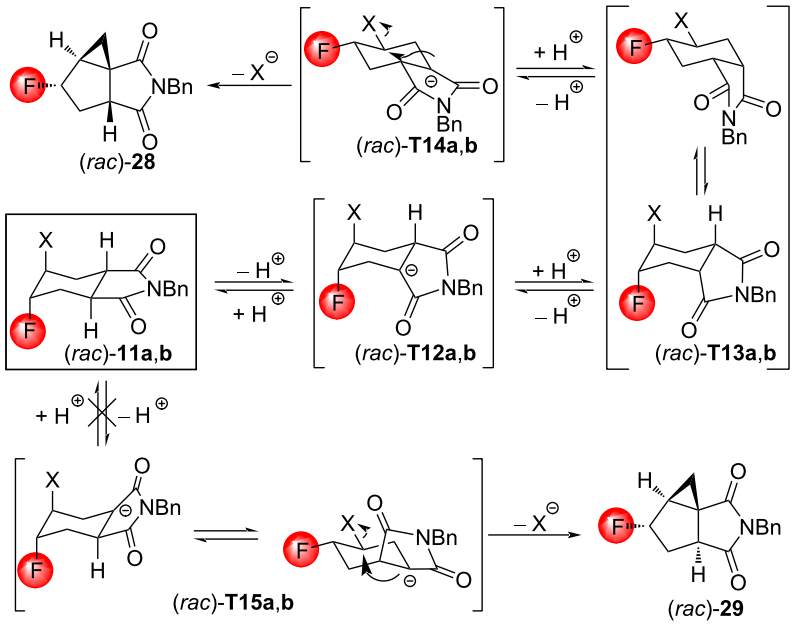

Scheme 19: Mechanism for the formation of (*rac*)-**28** from (*rac*)-**11a**,**b**. Although the formation of the compound (*rac*)-**29** is theoretically also possible, this product was not observed. X = Br (compounds a), I (compounds b).

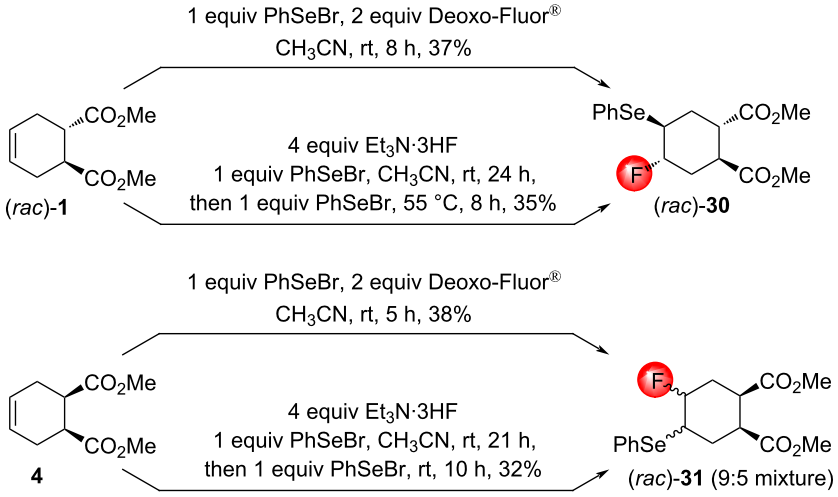

Scheme 20: Fluoroselenations of the cyclohexenedicarboxylates (*rac*)-**1** and **4**.

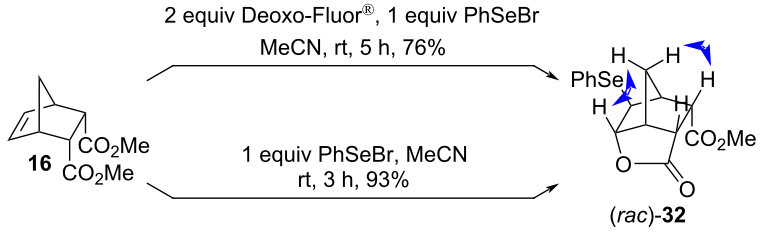

Scheme 21: $PhSe^+$-induced lactonization of the diester **16**. Relevant NOESY interactions are marked with two-headed arrows.

The tricyclic imides **19** and **24** failed to react with PhSeBr/Deoxo-Fluor®, and only unreacted starting compounds could be recovered from the reaction mixtures. Since these imides showed a decreased reactivity towards the larger I^+ cation in comparison to the smaller Br^+ cation (see Scheme 12 and Scheme 14), the absolute lack of reactivity with the even larger $PhSe^+$ cation is not surprising.

To study the synthetic utility of the obtained fluoroselenides, oxidative elimination of the phenylselenyl group was attempted. In the case of (*rac*)-**32**, this reaction would lead to a bridgehead olefin, violating Bredt's rule. Consequently, only (*rac*)-**30** and (*rac*)-**31** were used as starting compounds. On the basis of literature data [20,41,42], we expected the preferred formation of allylic fluorides over fluoroalkenes. Note, that fluoroselenation and subsequent oxidative deselenation can be performed efficiently as a one-pot procedure to transform an olefin directly into an allylic fluoride [41,42].

The oxidation of (*rac*)-**30** with MCPBA in CH_2Cl_2 was ineffective at room temperature and led to decomposition upon reflux. In contrast, the treatment with trifluoroperacetic acid formed in situ in THF resulted in the expected allylic fluoride (*rac*)-**33**. Oxidative treatment under basic conditions, however, yielded the highly unsaturated diester (*rac*)-**34**, presumably via a base-promoted E1cB elimination of (*rac*)-**33** formed primarily (Scheme 22). A possible driving force of this reaction is the extended conjugation.

Interestingly, the treatment of a mixture of (*rac*)-**31** with H_2O_2/CF_3COOH resulted in single allylic fluoride, (*rac*)-**35** (Scheme 23). Unfortunately, the determination of the stereochemistry via NOESY was unsuccessful. The reason is that cyclohexenes have a half-chair conformation, and the hydrogen atoms to undergo important NOESY interactions are simply too far away from each other. To solve this problem, the olefin bond of (*rac*)-**35** was hydrogenated to a cyclohexane, affording the fluorinated dimethyl cyclohexanedicarboxylate (*rac*)-**36**. The change of the conformation from a half-chair to an ordinary chair enabled the determination of the stereochemistry of (*rac*)-**36** by NOESY measurements. Since the saturation of (*rac*)-**35** did not affect the configuration

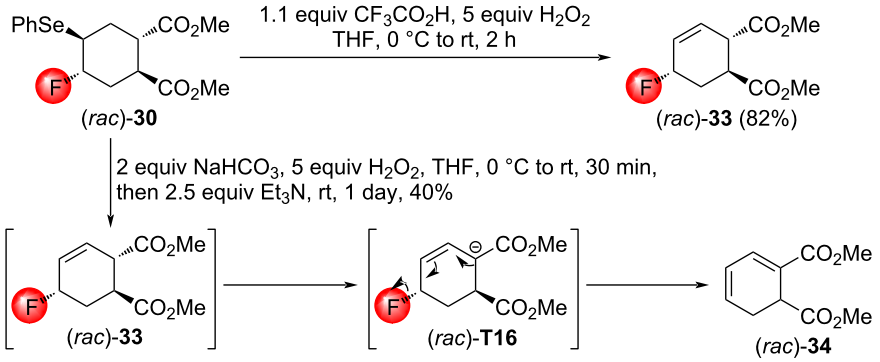

Scheme 22: Oxidation of the fluoroselenide (*rac*)-**30** under acidic and basic conditions.

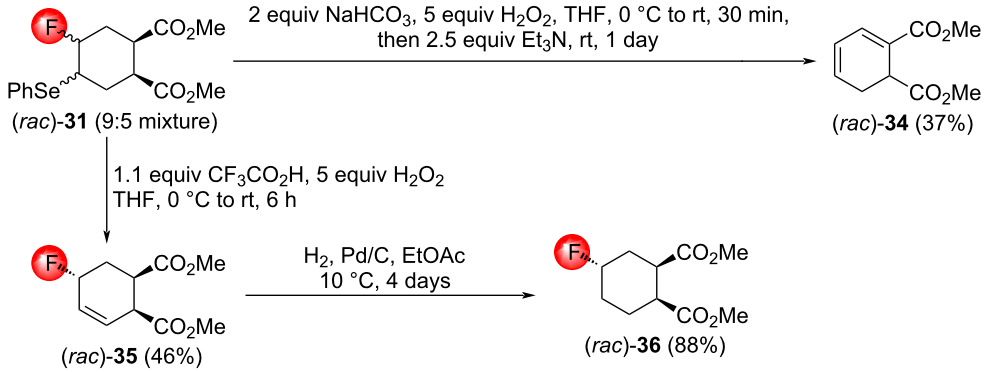

Scheme 23: Oxidation of the fluoroselenide mixture (*rac*)-**31** under acidic and basic conditions.

of the CHF motif, that structure was uncovered, too. The oxidation of (*rac*)-**31** under basic conditions delivered the conjugated diene (*rac*)-**34**, possibly through a deselenation/E1cB elimination sequence similar to the one shown in Scheme 22.

Conclusion

In conclusion, novel fluorine-containing, functionalized small-molecular scaffolds have been accessed through halofluorination or selenofluorination protocols. Deoxo-Fluor® proved to be a suitable fluoride source in the halofluorination and fluoroselenation reactions. Bromo- and iodofluorinations were the most useful for symmetric olefins. Regarding cyclohexene derivatives, the extent of selectivity can be predicted by considering the differences of steric shielding on the two sides of the double bond and applying the Fürst–Plattner rule to the halonium ion intermediates. The presence of electron-withdrawing carbonyl groups with α-hydrogen atoms enabled E2 elimination of the halofluorinated products and subsequent cyclization into fused-ring cyclopropanes.

Two new fluoroselenation protocols using PhSeBr/Deoxo-Fluor® and PhSeBr/$Et_3N{\cdot}3HF$, respectively, have been described, but the substrate scope of this reaction was more limited. The transformation of the obtained fluoroselenides into allyl fluorides via oxidation succeeded only in an acidic environment. Presumably, the presence of ester groups enabled the base-promoted E1cB elimination, driven by the extension of the conjugation. Further studies of other functionalized cyclic olefin substrates possessing varied architectural structures, and fine-tuning the reaction conditions of other halofluorination and fluoroselenation reactions are currently being studied in our research group.

Supporting Information

Supporting Information File 1

Characterization and NMR data of the new compounds.
[https://www.beilstein-journals.org/bjoc/content/supplementary/1860-5397-16-208-S1.pdf]

Funding

We are grateful to the Hungarian Research Foundation (NKFIH No K 119282) for financial support. Fnancial support of the GINOP-2.3.2-15-2016-00038 project is also acknowledged. This research was supported by the EU-funded Hungarian grant EFOP-3.6.1-16-2016-00008. The Ministry of Human Capacities, Hungary (grant 20391-3/2018/FEKUSTRAT) is also acknowledged.

ORCID® iDs

Matti Haukka - https://orcid.org/0000-0002-6744-7208

References

1. Purser, S.; Moore, P. R.; Swallow, S.; Gouverneur, V. *Chem. Soc. Rev.* **2008,** *37,* 320–330. doi:10.1039/b610213c
2. Ojima, I., Ed. *Fluorine in Medicinal Chemistry and Chemical Biology;* Wiley-Blackwell: Hoboken, NJ, USA, 2009. doi:10.1002/9781444312096
3. Wang, J.; Sánchez-Roselló, M.; Aceña, J. L.; del Pozo, C.; Sorochinsky, A. E.; Fustero, S.; Soloshonok, V. A.; Liu, H. *Chem. Rev.* **2014,** *114,* 2432–2506. doi:10.1021/cr4002879
4. Zhou, Y.; Wang, J.; Gu, Z.; Wang, S.; Zhu, W.; Aceña, J. L.; Soloshonok, V. A.; Izawa, K.; Liu, H. *Chem. Rev.* **2016,** *116,* 422–518. doi:10.1021/acs.chemrev.5b00392
5. O'Hagan, D.; Al-Maharik, D. *Aldrichimica Acta* **2011,** *44,* 65–75.
6. Böhm, H.-J.; Banner, D.; Bendels, S.; Kansy, M.; Kuhn, B.; Müller, K.; Obst-Sander, U.; Stahl, M. *ChemBioChem* **2004,** *5,* 637–643. doi:10.1002/cbic.200301023
7. Müller, K.; Faeh, C.; Diederich, F. *Science* **2007,** *317,* 1881–1886. doi:10.1126/science.1131943
8. O'Hagan, D. *J. Fluorine Chem.* **2010,** *131,* 1071–1081. doi:10.1016/j.jfluchem.2010.03.003
9. Hagmann, W. K. *J. Med. Chem.* **2008,** *51,* 4359–4369. doi:10.1021/jm800219f
10. Kirsch, P. *Modern Fluoroorganic Chemistry: Synthesis, Reactivity, Applications;* Wiley-VCH: Weinheim, Germany, 2004. doi:10.1002/352760393x
11. Liang, T.; Neumann, C. N.; Ritter, T. *Angew. Chem., Int. Ed.* **2013,** *52,* 8214–8264. doi:10.1002/anie.201206566
12. Fustero, S.; Sedgwick, D. M.; Román, R.; Barrio, P. *Chem. Commun.* **2018,** *54,* 9706–9725. doi:10.1039/c8cc05181j
13. Bykova, T.; Al-Maharik, N.; Slawin, A. M. Z.; Bühl, M.; Lebl, T.; O'Hagan, D. *Chem. – Eur. J.* **2018,** *24,* 13290–13296. doi:10.1002/chem.201802166
14. Zhu, W.; Wang, J.; Wang, S.; Gu, Z.; Aceña, J. L.; Izawa, K.; Liu, H.; Soloshonok, V. A. *J. Fluorine Chem.* **2014,** *167,* 37–54. doi:10.1016/j.jfluchem.2014.06.026
15. Ishida, S.; Sheppard, T.; Nishikata, T. *Tetrahedron Lett.* **2018,** *59,* 789–798. doi:10.1016/j.tetlet.2018.01.044
16. Jaroschik, F. *Chem. – Eur. J.* **2018,** *24,* 14572–14582. doi:10.1002/chem.201801702
17. Yerien, D. E.; Bonesi, S.; Postigo, A. *Org. Biomol. Chem.* **2016,** *14,* 8398–8427. doi:10.1039/c6ob00764c
18. Dykstra, K. D.; Ichiishi, N.; Krska, S. W.; Richardson, P. F. Emerging fluorination methods in organic chemistry relevant for life science application. In *Fluorine in Life Sciences: Pharmaceuticals, Medicinal Diagnostics, and Agrochemicals;* Haufe, G.; Leroux, F. G., Eds.; Academic Press: London, U.K., 2019. doi:10.1016/b978-0-12-812733-9.00001-5
19. Marciniak, B.; Walkowiak-Kulikowska, J.; Koroniak, H. *J. Fluorine Chem.* **2017,** *203,* 47–61. doi:10.1016/j.jfluchem.2017.09.001
20. Haufe, G. Synthesis by addition to alkenes. In *Fluorine;* Percy, J. M., Ed.; Science of Synthesis, Vol. 37; Georg Thieme Verlag KG: Stuttgart, Germany, 2006; pp 169–224.
21. Kiss, L.; Forró, E.; Fustero, S.; Fülöp, F. *Org. Biomol. Chem.* **2011,** *9,* 6528–6534. doi:10.1039/c1ob05648d

22. Kiss, L.; Forró, E.; Fustero, S.; Fülöp, F. *Eur. J. Org. Chem.* **2011,** 4993–5001. doi:10.1002/ejoc.201100583
23. Kiss, L.; Nonn, M.; Sillanpää, R.; Fustero, S.; Fülöp, F. *Beilstein J. Org. Chem.* **2013,** *9,* 1164–1169. doi:10.3762/bjoc.9.130
24. Kiss, L.; Nonn, M.; Forró, E.; Sillanpää, R.; Fustero, S.; Fülöp, F. *Eur. J. Org. Chem.* **2014,** 4070–4076. doi:10.1002/ejoc.201402121
25. Nonn, M.; Kiss, L.; Hänninen, M. M.; Sillanpää, R.; Fülöp, F. *Chem. Biodiversity* **2012,** *9,* 2571–2581. doi:10.1002/cbdv.201200323
26. Kiss, L.; Nonn, M.; Sillanpää, R.; Haukka, M.; Fustero, S.; Fülöp, F. *Chem. – Asian J.* **2016,** *11,* 3376–3381. doi:10.1002/asia.201601046
27. Kiss, L.; Remete, A. M.; Nonn, M.; Fustero, S.; Sillanpää, R.; Fülöp, F. *Tetrahedron* **2016,** *72,* 781–787. doi:10.1016/j.tet.2015.12.017
28. Kiss, L.; Petrovszki, Á.; Vass, C.; Nonn, M.; Sillanpää, R.; Haukka, M.; Fustero, S.; Fülöp, F. *ChemistrySelect* **2017,** *2,* 3049–3052. doi:10.1002/slct.201700403
29. Remete, A. M.; Nonn, M.; Fustero, S.; Haukka, M.; Fülöp, F.; Kiss, L. *Beilstein J. Org. Chem.* **2017,** *13,* 2364–2371. doi:10.3762/bjoc.13.233
30. Remete, A. M.; Nonn, M.; Fustero, S.; Haukka, M.; Fülöp, F.; Kiss, L. *Eur. J. Org. Chem.* **2018,** 3735–3742. doi:10.1002/ejoc.201800057
31. Nonn, M.; Kiss, L.; Haukka, M.; Fustero, S.; Fülöp, F. *Org. Lett.* **2015,** *17,* 1074–1077. doi:10.1021/acs.orglett.5b00182
32. Remete, A. M.; Nonn, M.; Fustero, S.; Fülöp, F.; Kiss, L. *Molecules* **2016,** *21,* 1493. doi:10.3390/molecules21111493
33. Bohlmann, R. *Tetrahedron Lett.* **1994,** *35,* 85–88. doi:10.1016/0040-4039(94)88168-5
34. Bernáth, G.; Stájer, G.; Szabó, A. E.; Fölöp, F.; Sohár, P. *Tetrahedron* **1985,** *41,* 1353–1365. doi:10.1016/s0040-4020(01)96537-8
35. Camm, K. D.; Martinez Castro, N.; Liu, Y.; Czechura, P.; Snelgrove, J. L.; Fogg, D. E. *J. Am. Chem. Soc.* **2007,** *129,* 4168–4169. doi:10.1021/ja071047o
36. Adams, J. L.; Meek, T. D.; Mong, S.-M.; Johnson, R. K.; Metcalf, B. W. *J. Med. Chem.* **1988,** *31,* 1355–1359. doi:10.1021/jm00402a018
37. Windmon, N.; Dragojlovic, V. *Beilstein J. Org. Chem.* **2008,** *4,* No. 29. doi:10.3762/bjoc.4.29
38. Gültekin, D. D.; Taşkesenligil, Y.; Daştan, A.; Balci, M. *Tetrahedron* **2008,** *64,* 4377–4383. doi:10.1016/j.tet.2008.02.067
39. Faith, W. C.; Booth, C. A.; Foxman, B. M.; Snider, B. B. *J. Org. Chem.* **1985,** *50,* 1983–1985. doi:10.1021/jo00211a041
40. Crandall, J. K. *J. Org. Chem.* **1964,** *29,* 2830–2833. doi:10.1021/jo01033a005
41. Bloom, S.; Knippel, J. L.; Holl, M. G.; Barber, R.; Lectka, T. *Tetrahedron Lett.* **2014,** *55,* 4576–4580. doi:10.1016/j.tetlet.2014.05.093
42. Guo, R.; Huang, J.; Zhao, X. *ACS Catal.* **2018,** *8,* 926–930. doi:10.1021/acscatal.7b03829

License and Terms

This is an Open Access article under the terms of the Creative Commons Attribution License (https://creativecommons.org/licenses/by/4.0). Please note that the reuse, redistribution and reproduction in particular requires that the authors and source are credited.

The license is subject to the *Beilstein Journal of Organic Chemistry* terms and conditions: (https://www.beilstein-journals.org/bjoc)

The definitive version of this article is the electronic one which can be found at: https://doi.org/10.3762/bjoc.16.208

BEILSTEIN JOURNAL OF ORGANIC CHEMISTRY

Activation of pentafluoropropane isomers at a nanoscopic aluminum chlorofluoride: hydrodefluorination versus dehydrofluorination

Maëva-Charlotte Kervarec, Thomas Braun*, Mike Ahrens and Erhard Kemnitz

Full Research Paper

Open Access

Address:
Department of Chemistry, Humboldt-Universität zu Berlin, Brook-Taylor-Straße 2, 12489 Berlin, Germany

Email:
Thomas Braun* - thomas.braun@cms.hu-berlin.de

* Corresponding author

Keywords:
aluminum fluoride; C–F bond activation; dehydrofluorination; hydrodefluorination; hydrofluorocarbons

Beilstein J. Org. Chem. **2020,** *16,* 2623–2635.
https://doi.org/10.3762/bjoc.16.213

Received: 27 July 2020
Accepted: 09 October 2020
Published: 23 October 2020

This article is part of the thematic issue "Organo-fluorine chemistry V".

Guest Editor: D. O'Hagan

© 2020 Kervarec et al.; licensee Beilstein-Institut.
License and terms: see end of document.

Abstract

The hydrofluorocarbon 245 isomers, 1,1,1,3,3-pentafluoropropane, 1,1,1,2,2- pentafluoropropane, and 1,1,1,2,3-pentafluoropropane (HFC-245fa, HFC-245cb, and HFC-245eb) were activated through C–F bond activations using aluminium chlorofluoride (ACF) as a catalyst. The addition of the hydrogen source Et_3SiH is necessary for the activation of the secondary and tertiary C–F bonds. Multiple C–F bond activations such as hydrodefluorinations and dehydrofluorinations were observed, followed by hydroarylation and Friedel–Crafts-type reactions under mild conditions.

Introduction

Hydrofluorocarbons (HFCs) have been intensively used in daily life, mainly due to their excellent properties in refrigeration applications [1-3]. In the past, HFCs were considered as replacements that do not deplete ozone for chlorofluorocarbons (CFCs) and hydrochlorofluorocarbons (HCFCs), which have been strictly regulated by the Montreal protocol [4-6]. However, due to the high global warming potential (GWP), HFCs have also been included in the Montreal protocol in 2019 (Kigali amendment) and have to be phased out [7-10].

On the other hand, HFCs are valuable starting compounds or intermediate products for the synthesis of hydrofluoroolefins (HFOs), which have been regarded as the next generation of refrigerants, exhibiting zero ozone depletion potential (ODP) and a negligible GWP [11-13]. A considerable amount of studies has been carried out to synthesize HFOs under mild conditions [11,14-16]. Among them are routes to access 2,3,3,3-tetrafluoropropene and 1,3,3,3-tetrafluoropropene (HFO-1234yf and HFO-1234ze), for which numerous patents suggest synthetic pathways and showcase the reactivity [12,13,15]. One possibility for the preparation includes the conversion of pentafluoropropanes (HFC-245 isomers) using chromia-based catalysts, or metal chloride/fluoride (AlF_3, MgF_2)-supported catalysts at elevated temperatures (350 °C) [11,14,15,17,18]. The group of

Lu recently reported the gas-phase transformation of 1,1,1,3,3-pentafluoropropane (HFC-245eb) into 1,3,3,3-tetrafluoropropene (HFO-1234ze) using mesoporous nanoscopic aluminum fluoride-based catalysts [19]. The catalysts were prepared via a sol–gel process in the presence of polyols, allowing for the evolution of a large surface area and improved acidic properties when compared to fluorinated Cr_2O_3 or traditional β-AlF_3 catalysts. At a reaction temperature set at 280 °C, the conversion of 1,1,1,2,2- pentafluoropropane (HFC-245fa) into the 1,3,3,3-tetrafluoropropene (HFO-1234ze) varied between 50 and 60%, depending on the conditions used to synthesize the catalyst, reaching almost full selectivity. The harsh conditions are in part needed due to the high dissociation energy of C–F bonds, and in general, C–F activation steps are considered to be challenging [20-27].

Solid Lewis acids with a high fluoride ion affinity as catalysts are useful tools for C–F bond activation reactions since the Lewis acidic centers can induce dehydrofluorination reactions, involving the abstraction of a fluoride ion by heterolytic bond cleavage [28-31]. AlF_3-based catalysts are among the strongest Lewis acidic materials. They exhibit an effective activity in C–F bond conversion reactions and are widely investigated [16,28,32-39]. Especially microporous aluminum chlorofluoride (ACF, $AlCl_xF_{3-x}$; x = 0.05–0.3), which has a large surface area (>200 m^2g^{-1}) and was patented by Dupont in 1992, has been extensively studied [40-46]. It is an amorphous aluminum fluoride doped with chlorine atoms which causes a distortion of the structure resulting in the amorphicity and high Lewis acidity of the compound. The reactivity of ACF towards C–F bond activations was deeply investigated. For instance, the activation of fluoromethanes was observed at ACF in the presence of $HSiEt_3$ as a hydrogen source to produce, in the presence of benzene as the solvent, Friedel–Crafts products as main compounds [47]. In contrast, the hydrodefluorination products were generated in the absence of benzene. Thermodynamically, the generation of strong H–F, Al–F, or Si–F bonds can enforce an activation of C–F bonds under mild conditions, and hence the addition of the silane $HSiEt_3$ as a hydrogen source [27,48,49]. More recently, ACF was shown to efficiently convert the fluoroalkenes HFO-1234yf (**1**) and HFO-1234ze (**4a**) in the presence of the hydrogen source $HSiEt_3$ into the hydrodefluorination or Friedel–Crafts products (Scheme 1) [16].

The activation of fluoropentane was achieved using a modified ACF, loaded with germane or silane [39]. When silane was immobilized at the surface of ACF in the presence of benzene, Friedel–Crafts products were again generated. In comparison, when ACF was loaded with germane, dehydrofluorination products were detected. Besides, 2-chloro-1,1,1,2-tetrafluoropropane (HCFC-244bb) was as well effectively activated at ACF to yield the corresponding dehydrofluorination product 2-chloro-3,3,3-trifluoropropene (HFO-1233xf) without the use of any additional hydrogen source [50]. In the presence of silane and ACF, HFO-1233xf was further activated via allylic hydrodefluorination.

In this paper, we report on the reactivity of ACF towards hydrofluorocarbons, and in particular, the pentafluoropropane isomers (HFC-245). Effective hydrodefluorination and dehydrofluorina-

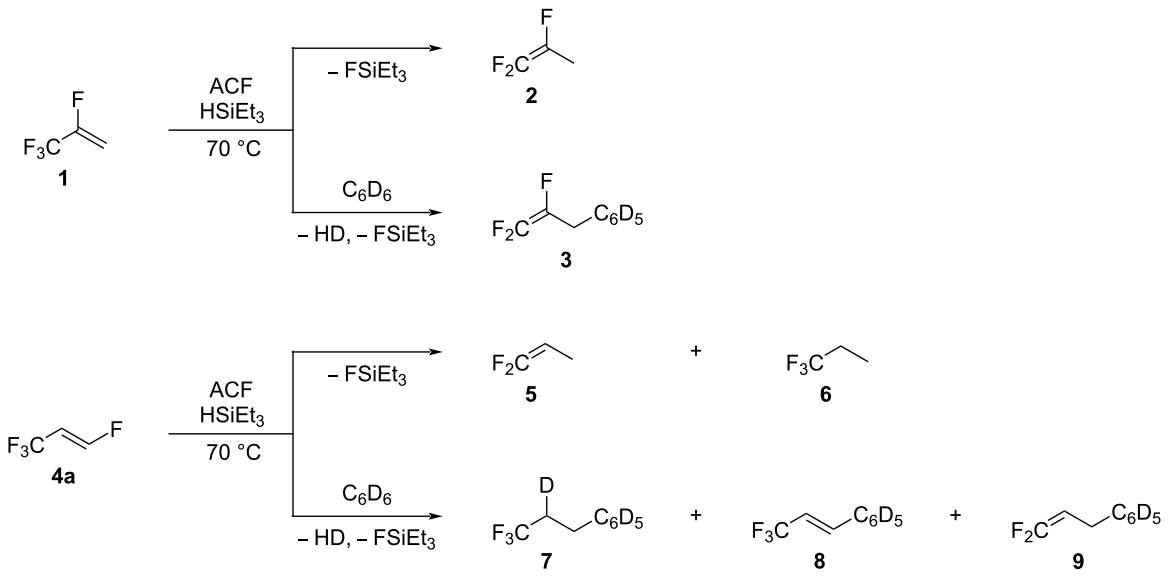

Scheme 1: Reactivity of tetrafluoropropanes HFO-1234yf (**1**) (top) and HFO-1234ze (**4a**) (bottom) in the presence of ACF as the catalyst and $HSiEt_3$ as a hydrogen source [16].

tion steps of pentafluoropropane isomers in the presence of Et_3SiH as a hydrogen source at mild conditions are described.

Results and Discussion

Activation of 1,1,1,2,3-pentafluoropropane (HFC-245eb, **10a**)

The treatment of 1,1,1,2,3-pentafluoropropane (**10a**) with ACF at 70 °C in C_6D_{12} gave the dehydrofluorination product 2,3,3,3-tetrafluoropropene (HFO-1234yf, **1**) and the isomerization product 1,1,1,2,2-pentafluoropropane (HFC-245cb, **10b**) in a 1:2 ratio (Scheme 2, top) with almost full conversion. The group of Kemnitz previously showed that **1** and **10b** can be in an equilibrium when HF is present in the reaction mixture [33]. It was demonstrated that starting from 2-chloro-3,3,3-trifluoropropene (HFO-1233xf) in the presence of fluorinated Cr_2O_3 as a catalyst and HF, 2,3,3,3-tetrafluoropropene (HFO-1234yf, **1**) is generated by the replacement of the chlorine substituent with a fluorine atom, and is further transformed by HF addition into 1,1,1,2,2-pentafluoropropane (HFC-245cb, **10b**) [33].

When the aromatic solvent C_6D_6 was used instead of C_6D_{12}, **10a** was once more transformed into **1** as the main compound, together with traces of the Friedel–Crafts product $CF_3CFHCH_2C_6D_5$ (**11**) and the hydroarylation product $CF_3CFDCH_2C_6D_5$ (**12**) (Scheme 2, bottom), with only 22% conversion. The low conversion in C_6D_6 could be a consequence of a possible interaction of the aromatic solvent with the surface of ACF, which would result in the blocking of the acidic sites, and thus hamper the adsorption of the substrates. Indeed, in a previous study, a pulse TA experiment suggested the presence of a strong interaction between benzene and the surface of ACF [38]. This result was further confirmed by ^1H MAS NMR spectroscopy.

Note, that **10a** was activated under mild conditions without the use of an additional hydrogen source, which often has been added for the activation of C–F bonds at ACF [16,39,47]. Several patents cover the transformation of **10a** by dehydrofluorination at chromia-based catalysts, but the reaction temperatures were above 200 °C [17,51,52].

Mechanistically, an abstraction of a fluorine from the CH_2F group by the surface of ACF can occur, generating carbenium-like species and surface fluorides (Scheme 3). Via HF elimination, the olefin **1** can be produced, followed by a refluorination of the double bond by the released HF, generating **10b** (Scheme 3, left). In the presence of C_6D_6, the hydroarylation product **12** can be generated from **1** at the ACF surface. Alternatively, the aromatic solvent can also attack the carbenium-like species, producing a zwitterionic Wheeland intermediate, which can release the Friedel–Crafts product **11** and DF to regenerate the catalyst (Scheme 3, right).

Although a hydrogen source was not needed to accomplish the activation of **10a**, it was of interest to introduce a silane, because as mentioned above, recent reports showed that the activation of various substrates treated with ACF was indeed promoted by the presence of silanes [16,39,47]. Thus, the experiments were also conducted in the presence of $HSiEt_3$, either in a solvent (C_6D_6 or C_6D_{12}), or in neat silane under similar conditions (all reactions were carried out at 70 °C and monitored for 7 days).

The treatment of **10a** and $HSiEt_3$ in C_6D_{12} generated **1** and **10b** again, in addition to traces of 1,1,2-trifluoropropene (**2**, Scheme 4, top). The ratio between the olefin **1** and the refluorination product **10b** observed in the presence of $HSiEt_3$ was 3:1, whereas, without the silane, a ratio of 1:2 was detected. This difference in the ratio might relate to the amount of HF present in the reaction mixture, which would be lower in the presence of silane because the latter can convert with HF into fluorosilane and H_2 [39,50,53]. Consequently, less refluorination takes place, and a higher selectivity towards the formation of the olefin **1** is observed. In C_6D_6, the activation of **10a** gave comparable results as when no $HSiEt_3$ was introduced (Scheme 4,

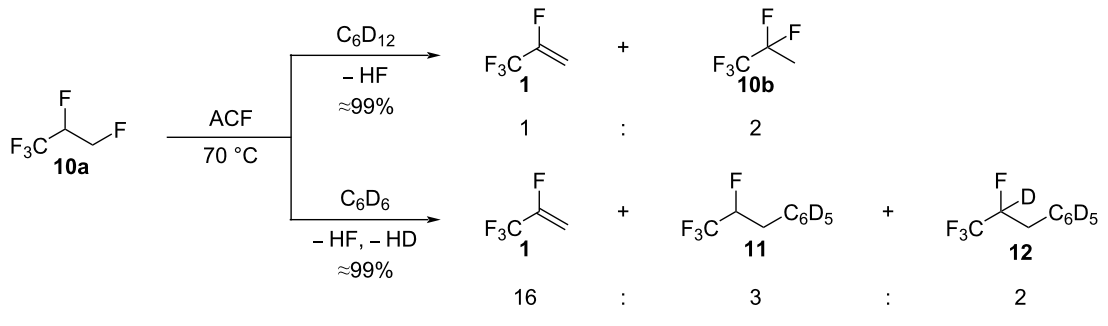

Scheme 2: Reactivity of **10a** in the presence of ACF as the catalyst in C_6D_{12} (top) or C_6D_6 (bottom) as solvents.

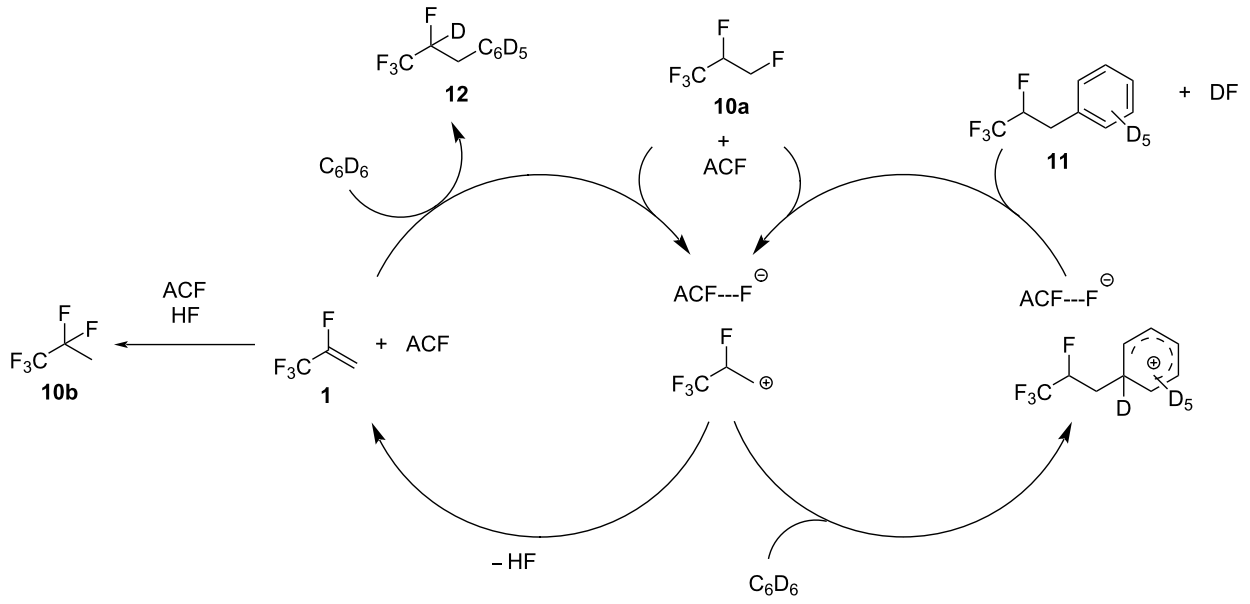

Scheme 3: Proposed catalytic cycle of the transformation of **10a** in C_6D_{12} and C_6D_6 in the presence of ACF as the catalyst.

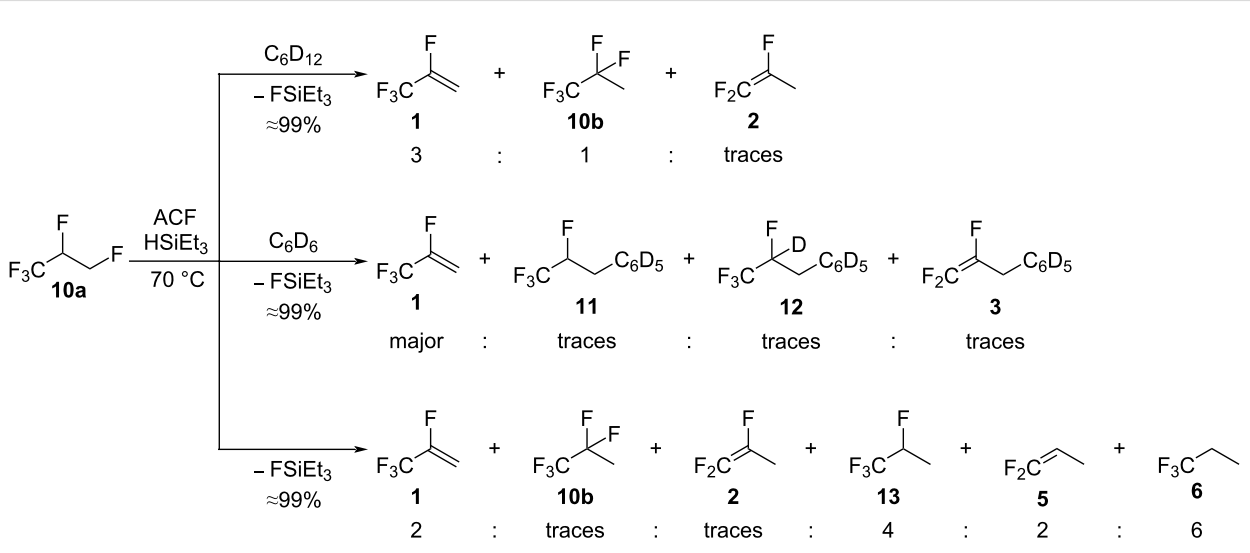

Scheme 4: Reactivity of **10a** in the presence of ACF as the catalyst and $HSiEt_3$ as a hydrogen source in C_6D_{12} (top) or C_6D_6 (middle) as solvents or in neat silane (bottom).

middle). Compound **10a** is transformed into **1**, **11**, and **12** with the additional presence of traces of the Friedel–Crafts product CF_2=$CFCH_2C_6D_5$ (**3**). However, in neat silane, **10a** was converted into **1**, **10b**, **2**, 1,1,1,2-tetrafluoropropane (**13**), 1,1-difluoropropene (**5**), and 1,1,1-trifluoropropane (**6**, Scheme 4, bottom). Thus, by having a large excess of silane, a consecutive reactivity was observed, which led to the formation of the hydrodefluorination product **6** as the main compound. However, the reaction is unselective, and various intermediates are still present in considerable amounts (Scheme 4).

Note, that for the transformation in the presence of silane, the conversions reached over 99% after 7 days at 70 °C, which underlines the significant role of the silane in the reaction mixture. The improved conversion can generally arise from an interaction of silane with the surface of ACF, also competing with the above-mentioned benzene interaction. Furthermore, in the presence of silane, additional mechanistic C–F activation steps have to be considered (Scheme 5). Basically, the immobilization of silane at the Lewis-acidic surface might result in silylium-like species, which subsequently initiate the C–F bond

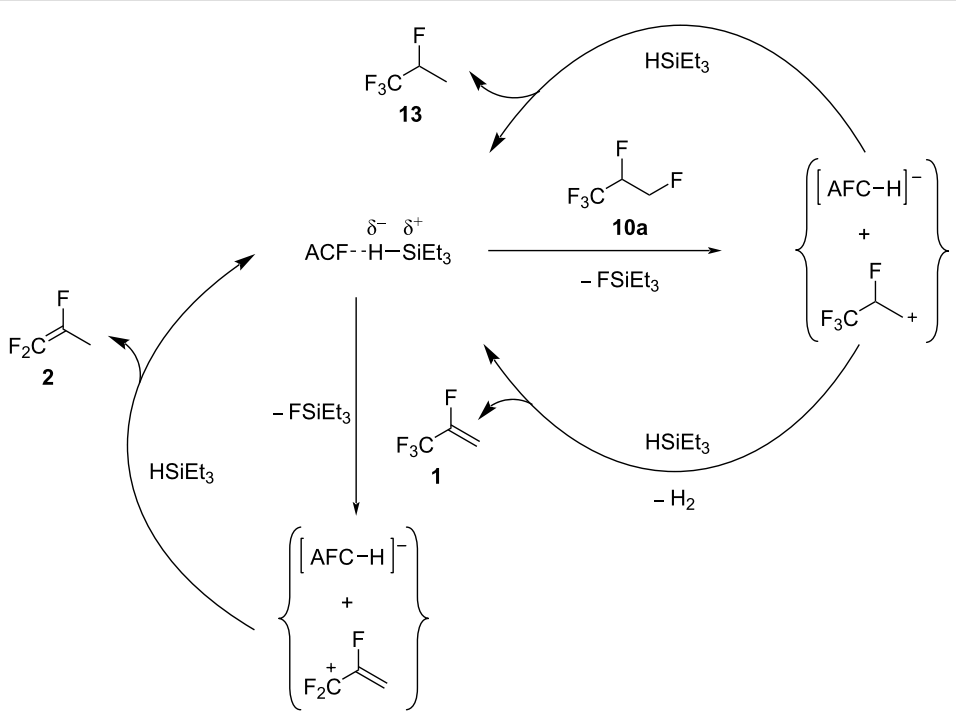

Scheme 5: Proposed catalytic cycle for sylilium-mediated hydrodefluorinations and dehydrofluorinations from **10a** at the surface of ACF.

activation at the primary carbon–fluorine bond in **10a**, generating $FSiEt_3$, the corresponding carbenium-like species, and a surface-bound hydride. At this stage, either the hydrodefluorination product **13** can be generated, or dehydrofluorination occurs to furnish the olefin **1** and H_2, both in the presence of silane. Additionally, **1** can further react with any silylium ion species at the surface of ACF, resulting in a C–F bond cleavage at the CF_3 group, yielding once again a surface hydride and the corresponding carbenium ion. Subsequently, the allylic hydrodefluorination product **2** is formed. Allylic hydrodefluorination reactions were previously observed at ACF. Indeed, in the presence of silane and ACF, the CF_3 group in tetrafluoropropenes (HFO-1234yf, **1** and HFO-1234ze, **4**) was transformed into an olefinic CF_2 group (Scheme 1) [16]. Previous MAS NMR studies also gave evidence for the existence of silylium species at an ACF surface [39,47]. In addition, silylium species that are stabilized by weakly coordinating anions can also catalyze hydrodefluorination reactions in a homogeneous phase with silanes as hydrogen source [54-57]. In contrast, silylium-mediated dehydrofluorination reactions have not been found in a homogeneous phase, but germylium ions can promote such reaction pathways [58]. Nevertheless, the formation of the compounds **1**, **10b**, **11**, and **12** can alternatively be initiated by the Lewis acidity of ACF itself, as outlined above without the presence of silane (see Scheme 3). Therefore, as an alternative to the initial formation of the surface silylium ion species at ACF, it is in principle also conceivable that carbenium species can be initially produced by an abstraction of a fluoride ion from a fluorinated group by the surface of the catalyst. Then, carbenium ions can react with silane to yield hydrodefluorination products, or after dehydrofluorination, HF that in the presence of silane, produces $FSiEt_3$ and H_2 [39,50]. Furthermore, any intermediate carbenium species, generated directly at the ACF surface or via interaction with a silylium species, can be engaged in Friedel–Crafts-like reactions to give with C_6D_6 **11** or **3**, which is consistent with previous studies [16].

The formation of the products described above (Scheme 4) involves consecutive reaction steps, such as dehydrofluorination, hydrodefluorination, hydrofluorination, allylic defluorination, hydroarylation, and Friedel–Crafts reactions. In the presence of an excess of silane, the dehydrofluorination product **1** and the hydrodefluorination intermediate **13** are generated simultaneously to further lead to **2**, **5**, and **6** as the main compounds. To get further insight, independent reactions were performed to elucidate reaction patterns and to demonstrate the conceivable transformations between certain products, which were observed in the activation of **10a** in the presence of ACF and $HSiEt_3$.

It turned out that the tetrafluoropropene **13** reacts in the presence of silane with ACF as the catalyst in C_6D_{12} or neat silane to give **5** and **6** (ratio 1:2, Scheme 6, top). When C_6D_6 was used

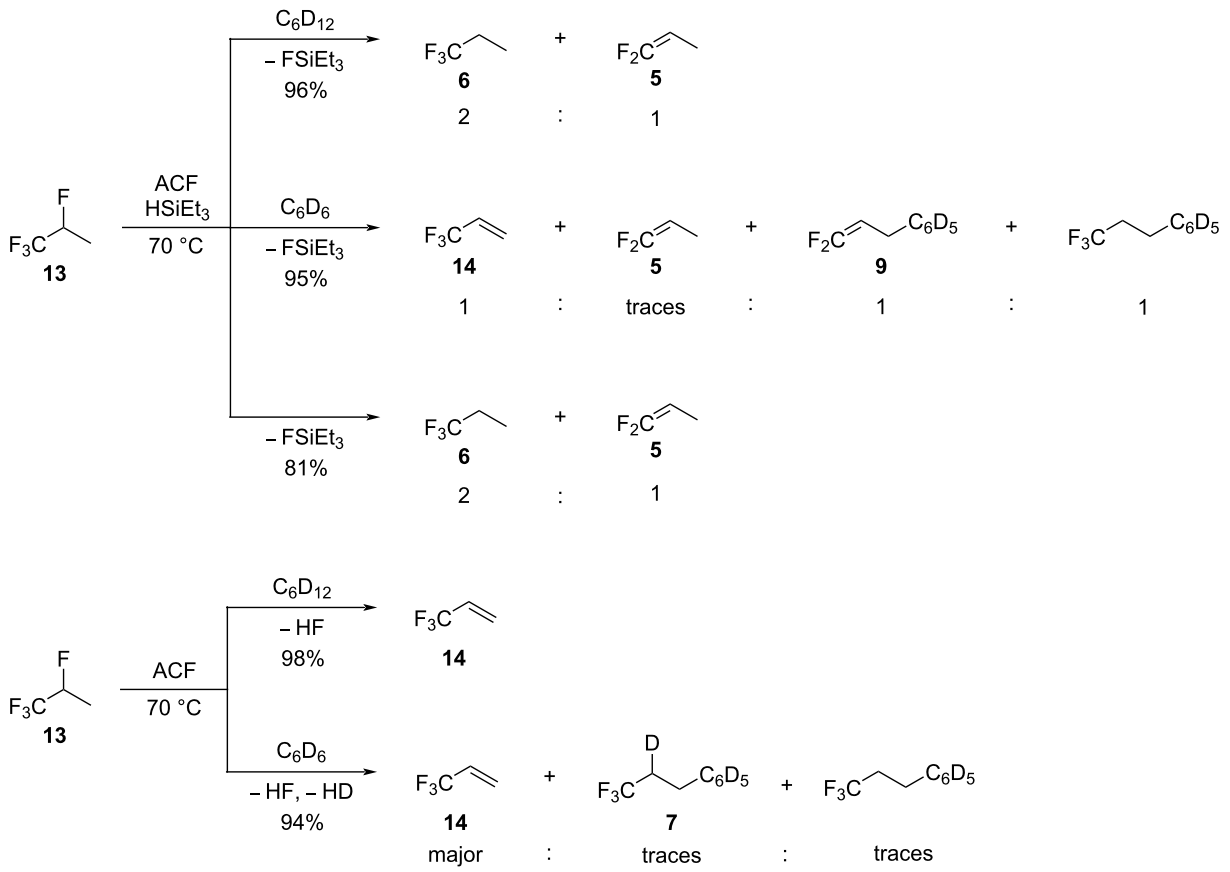

Scheme 6: Reactivity of **13** in the presence of ACF as the catalyst, with (top) or without (bottom) $HSiEt_3$ as a hydrogen source.

as a solvent in the presence of silane, **5**, **14**, **9**, and the Friedel–Crafts product $CF_3CH_2CH_2C_6D_5$ were generated. Note, that in this context, in the absence of silane and in C_6D_{12}, the selective formation of **14** was detected (Scheme 6, bottom). In benzene, **14** was also formed as the main compound, together with the corresponding Friedel–Crafts and hydroarylation products, both observed in traces. This suggests that silane promotes the generation of **5** and **6**, but for the formation of **14** it is not essential.

Furthermore, another independent reaction by treating **5** with HF was performed (Scheme 7, top), but the hydrofluorination product **6** was only detected in small amounts. In accordance with this result, the treatment of **6** in the presence of silane and ACF gave the dehydrofluorination product **5**. The observations nevertheless suggest the presence of an equilibrium between **5** and **6**, that depends on the amount of HF or $HSiEt_3$ present in the reaction mixture.

Additionally, it is conceivable that **14** can further react to form **5** via allylic hydrodefluorination [16]. Therefore, the reactivity of **14** was tested in the presence of ACF and silane in C_6D_{12} or C_6D_6 (Scheme 7, bottom). Indeed, in C_6D_{12}, allylic defluorination to yield **5** was observed, together with **6** and traces of 2-chloro-1,1,1-trifluoropropene (**15**). The chlorinated product **15** could stem from a plausible HCl formation if the substrate is fluorinating ACF [41]. It should be noted that the synthesis of ACF itself consists of the fluorination of $AlCl_3$ by chlorofluoroalkanes [40,41]. Nevertheless, in C_6D_6, the formation of **5** and **6** and the Friedel–Crafts product $CF_2{=}CHCH_2C_6D_5$ (**9**) was observed from **14**.

Based on these findings, a general scheme can be drafted to illustrate the sequential generation of products starting from **10a** for the conversions in the presence of silane at ACF (Scheme 8). Note, that the reaction of **1** in the presence of silane, ACF, and solvents was repeated under the same conditions as for the activation of **10a**, and the generation of **2** and **3** was confirmed similarly as reported (see above, Scheme 1) [16].

Overall, the reactivity study on **10a** in the presence of ACF and $HSiEt_3$ suggests that the formation of **1** described in the top part of the mechanism is favored when no silane is present in the

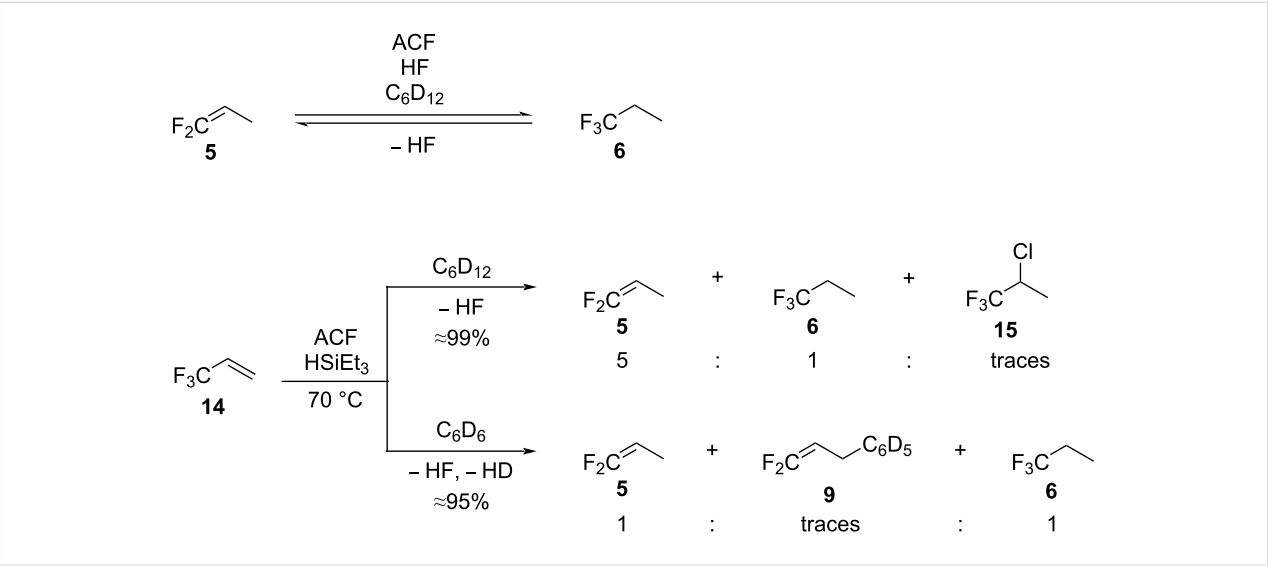

Scheme 7: Independent reactions starting from **5**, **6**, or **14** in the presence of ACF as the catalyst.

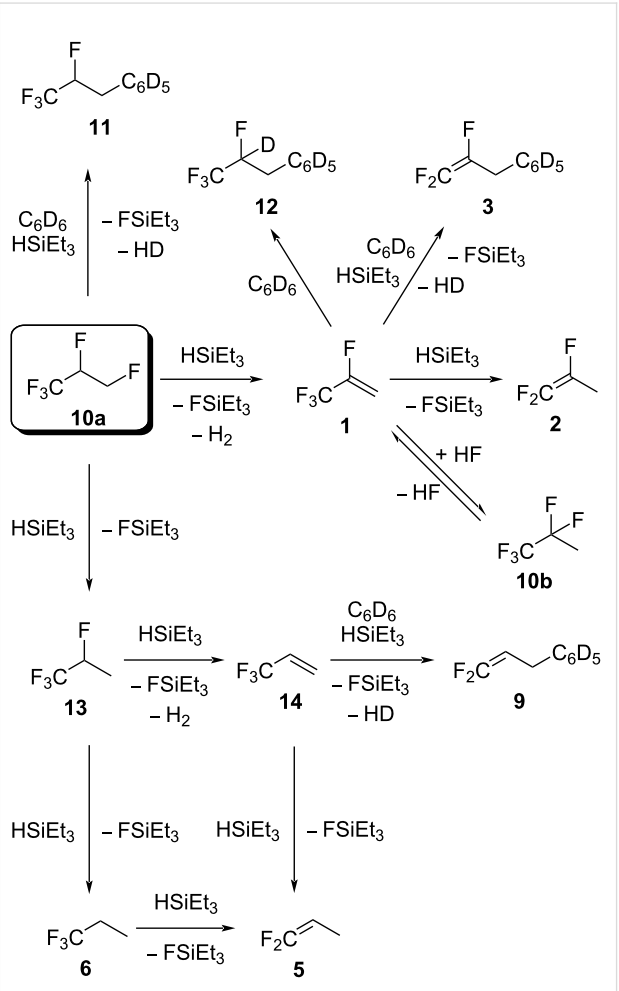

Scheme 8: Proposed reaction pathways starting from **10a** in the presence of ACF and silane.

reaction mixture or when only a small amount of silane is present (Scheme 8). In contrast, in neat silane, the bottom part of Scheme 8 is preferred, leading to the formation of **6**.

Activation of 1,1,1,3,3-pentafluoropropane (HFC-245fa, **10c**)

The reactivity of 1,1,1,3,3-pentafluoropropane (**10c**) at ACF was compared with the one of the isomer 1,1,1,2,3-pentafluoropropane (**10a**), again to elucidate conceivable reaction pathways and to understand potential similarities in their reactivity. In contrast to the findings for **10a**, no conversion was observed without the use of $HSiEt_3$ as a hydrogen source, indicating that for the activation of CHF_2 groups, silane might be required.

When **10c** was treated with 0.5 equivalents of $HSiEt_3$ with respect to the substrate in the presence of ACF at 70 °C, the selective generation of the 1,3,3,3-tetrafluoropropenes (HFO-1234ze, **4a** and **4b**) was detected with an *E:Z* ratio of 10:1 and 43% conversion (Scheme 9). The transformation of **10c** into **4a** and **4b** is remarkable since other catalytic conversions at chromia-based catalysts require elevated temperatures [11,19,59-62].

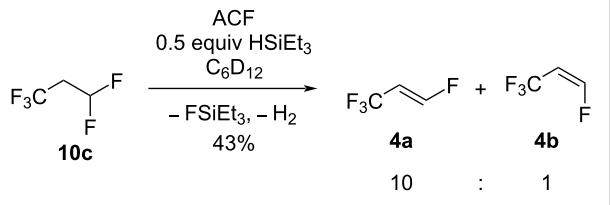

Scheme 9: Reactivity of **10c** in the presence of ACF as the catalyst and 0.5 equivalents of $HSiEt_3$ as a hydrogen source in C_6D_{12}.

The mechanisms for the C−F bond cleavage starting from **10c** to yield the isomers **4** are similar to the ones proposed in the activation of **10a** in the presence of silane (see above, Scheme 5). It is likely that silylium species are involved in the C–F activation steps at the ACF surface since $HSiEt_3$ is needed to initiate any reactivity. On the one hand, an initial C–F bond activation at **10c** by some silylium ion species will produce $FSiEt_3$ and the corresponding carbenium species (Scheme 10). The latter can generate **4a** and **4b** together with H_2, leading to the regeneration of the catalyst. When only 0.5 equivalents of silane are present, the reaction does not pursue further, as shown above (Scheme 9). On the other hand, as for **10a**, an alternative mechanism can be proposed where the carbenium species is initially generated by an abstraction of a fluoride ion at the CHF_2 group by the surface of the catalyst. Via HF elimination, **4a** and **4b** are produced, and the conversion is driven by the HF reaction with $HSiEt_3$ to give $FSiEt_3$.

When the amount of silane was increased to one equivalent, further reactivity was observed (Scheme 11). In C_6D_{12}, **6** was generated as the main compound, with traces of **5** and **14** (Scheme 11, top). When C_6D_6 was used as the solvent, **5** as the main product, **6** as a minor product, and **14** in traces were again generated, together with the Friedel–Crafts products CF_2=$CHCH_2C_6D_5$ (**9**) and CF_3CH=CHC_6D_5 (**8**, Scheme 11, middle). In neat silane, **5** and **6** were detected in a ratio of 1:4 (Scheme 11, bottom).

Notably, for all conversions (C_6D_6 and silane, C_6D_{12} and silane, or in neat silane), monitoring of the reaction by

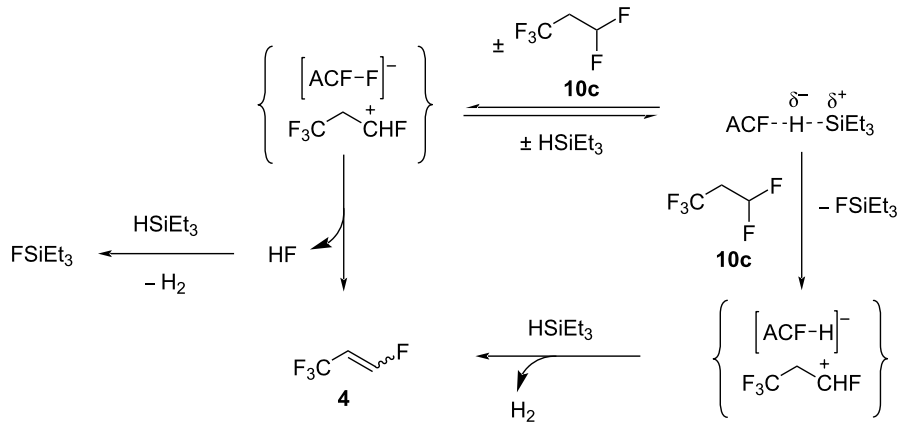

Scheme 10: Proposed catalytic cycles for the transformation of **10c** in C_6D_{12} and in the presence of 0.5 equivalents of silane and ACF as the catalyst.

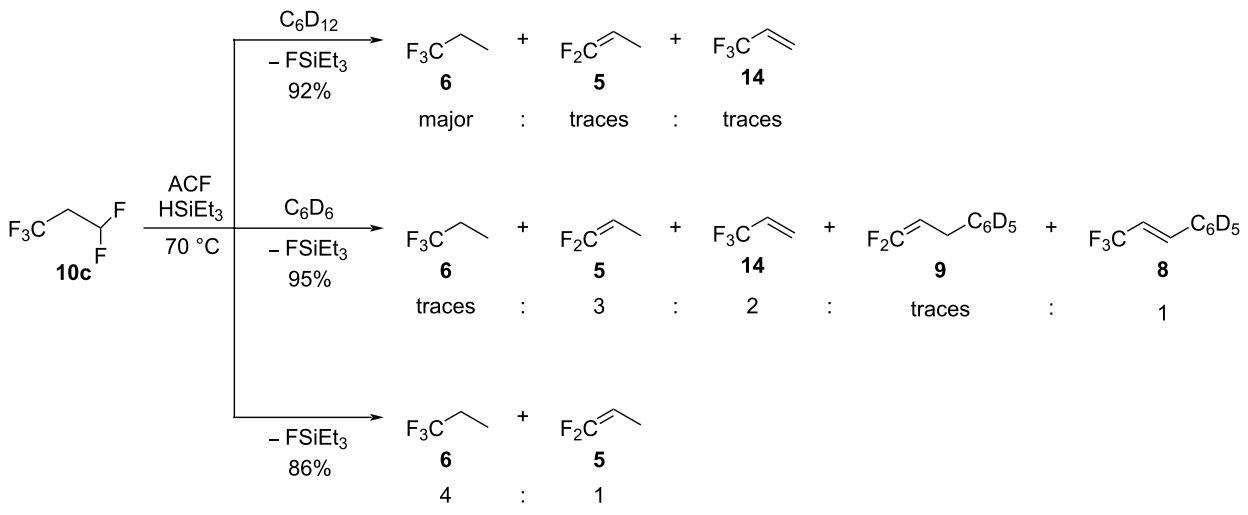

Scheme 11: Reactivity of **10c** in the presence of ACF as the catalyst and $HSiEt_3$ as a hydrogen source in C_6D_{12} (top) or C_6D_6 (middle) as solvents or in neat silane (bottom).

^{19}F NMR spectroscopy led to the observation of the early generation of **4a** and **4b** after 24 hours reaction time at 70 °C. After 3 days at 70 °C, the transformation into the different products described above could be detected. Moreover, the continuous formation of $FSiEt_3$ over time was observed for all reactions, which underlines the crucial role of the hydrogen source at each reaction step. As stated, it has been reported before that for the activation of 1,3,3,3-tetrafluoropropene (HFO-1234ze, **4**) at ACF in neat $HSiEt_3$ 1,1-difluoropropene (**5**) and 1,1,1-trifluoropropane (**6**) are furnished (Scheme 1) [16]. In the presence of C_6D_6 and silane, the Friedel–Crafts products $CF_2{=}CHCH_2C_6D_5$ (**9**) and $CF_3CH{=}CHC_6D_5$ (**8**) were observed, together with the hydroarylation product $CF_3CHDCH_2C_6D_5$ (**7**) [16]. To note, in neat silane, a distinct selectivity was detected, depending on the substrates used. Indeed, starting from **10c**, the product ratio between **5** and **6** was 1:4, whereas it was reported to be 1:0.8 starting from **4a** [16]. This observation might be the result of a hydrofluorination reaction from **5** to **6**. Moreover, in neat silane, **14** was not detected, whereas when less silane and a solvent was present, this product was observed. Due to a large amount of silane present, a more considerable amount of the silylium species can be generated compared to when only one equivalent of silane is used. Therefore, the rate of the reaction from **10c** to **6** might be increased in neat silane favoring two subsequent hydrodefluorination steps from **10c** to yield **6**.

As observed in the study on the reactivity of **10a**, the variety of products for a larger amount of silane can be explained by several consecutive reactions, which include C–F bond activation steps (Scheme 12). Via hydrodefluorination, **10c** can produce the intermediate 1,1,1,3-tetrafluoropropane (not observed). This intermediate could give **6** via a second hydrodefluorination. Alternatively, 1,1,1,3-tetrafluoropropane could also produce **14**, which was shown to give **6** via the intermediate **5** by independent reactions. However, pathways to yield **6** are also required from the olefins **4**, because they were detected as intermediates. This implies HF addition to **4** or **5**. In the presence of benzene, **14** can also generate the Friedel–Crafts product **9**; however, product **9** can also be generated from **4** by hydrodefluorination followed by a Friedel–Crafts reaction. The Friedel–Crafts product **8** can as well be formed from **10c** directly, via a Friedel–Crafts reaction followed by HF elimination.

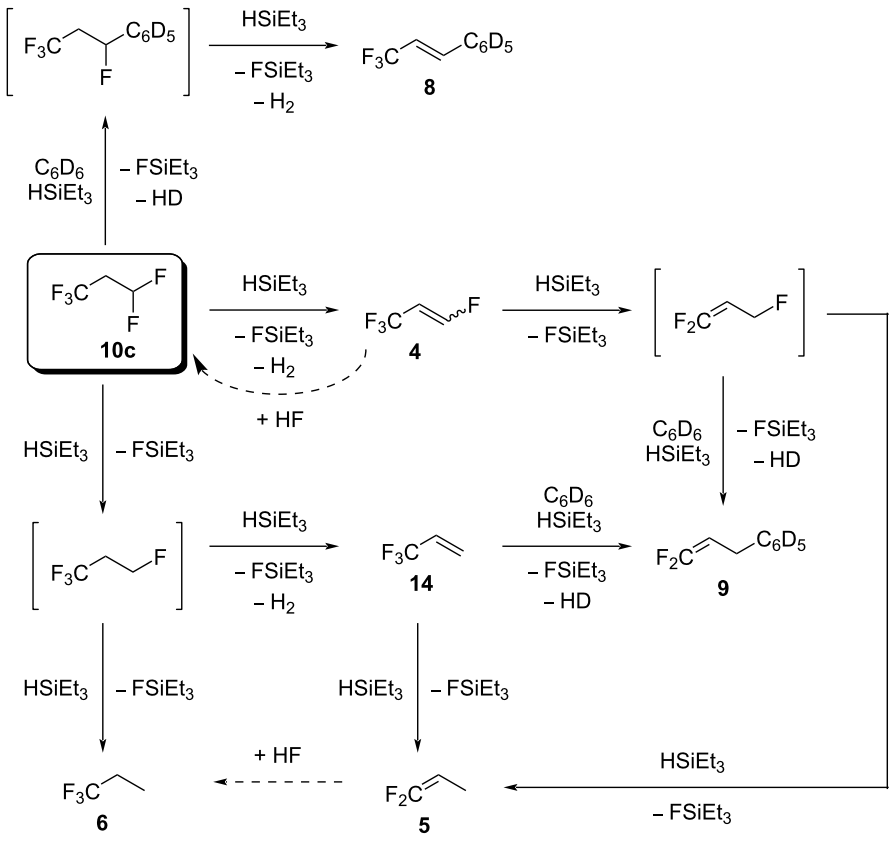

Scheme 12: Proposed reaction pathways starting from **10c** in the presence of ACF and silane.

Comparable to the reaction patterns of **10a**, the reactivity study on **10c** reveals that with a small amount of silane, the dehydrofluorination to **4** is favored, and with more silane, the conversions in Scheme 12 end up favorably in the formation of **6**.

Activation of 1,1,1,2,2-pentafluoropropane (HFC-245fa, **10b**)

As observed for **10c**, the isomeric 1,1,1,2,2-pentafluoropropane (HFC-245fa, **10b**) could also not be activated without the presence of $HSiEt_3$ as a hydrogen source. The treatment of **10b** in C_6D_{12} in the presence of silane at 70 °C gave the allylic hydrodefluorination product **2** as well as **5** in a ratio of 1:1 with 38% conversion (Scheme 13, top). When benzene was used as a solvent together with silane, the Friedel–Crafts products **3** and **9** were observed in a ratio of 1:1, but the conversion reached only 18% (Scheme 13, middle). In neat silane, **2** and **5** were again observed, but this time the conversion did not exceed 10% (Scheme 13, bottom).

As for the activation of **10c**, it is plausible that surface silylium ion species are formed at ACF. Therefore, a reaction pathway can be suggested, starting with the initial generation of **1**, $FSiEt_3$, and H_2. Subsequently, **2** can be generated via an allylic hydrodefluorination as it was observed in the study of tetrafluoropropenes at ACF [16]. Additionally, **5** can stem from several C–F bond activations at **10b**, starting with a hydrodefluorination to generate the intermediate **13**, which further undergoes an HF elimination, followed by an allylic hydrodefluorination to give **5**. In the presence of benzene, at **1**, a Friedel–Crafts reaction can generate **3**, which further supports the formation as an intermediate of **1**. Moreover, the intermediate **14** can also produce **9** via a Friedel–Crafts reaction, which again supports the pathway proposed to achieve **5**.

Overall, for the reactivity of the pentafluoropropane isomer **10b**, two different pathways seem to compete. The upper part of the reaction patterns in Scheme 14 leads to the formation of **2**, and the bottom part provides pathways to **5**. Thus, the hydrodefluorination step at **10b** to form **13** seems to be more difficult than for the other isomers **10a** and **10c**.

Conclusion

This study on the reactivity of pentafluoropropane isomers has revealed that ACF is a suitable catalyst for dehydrofluorination and hydrodefluorination reactions of polyfluorinated compounds under mild conditions. It was elaborated that the single C–F bond in **10a** does not require the use of $HSiEt_3$ as a hydrogen source to be activated via dehydrofluorination. However, when silane was introduced, further reactivity was observed, leading to the formation of subsequent defluorination products. In contrast, CF_2, CHF_2, and CF_3 groups need the presence of a hydrogen source in order to promote the activation of at least one C–F bond by the formation of the thermodynamically stable Si–F bond. This observation is consistent with a decrease of the bond dissociation energies of C–F bonds from trifluoromethyl via difluoromethyl to monofluoromethyl groups [63]. Additionally, the C–F bond at the CHF_2 group in **10c** was easier to activate than the C–F bond in the CF_3CF_2 group in **10c**, resulting in an order of reactivity of **10a** > **10c** > **10b**. When only a small amount of silane was introduced for the reaction of **10a** or **10c**, the major products are due to dehydrofluorination, whereas in neat silane, formally hydrodefluorination products are gener-

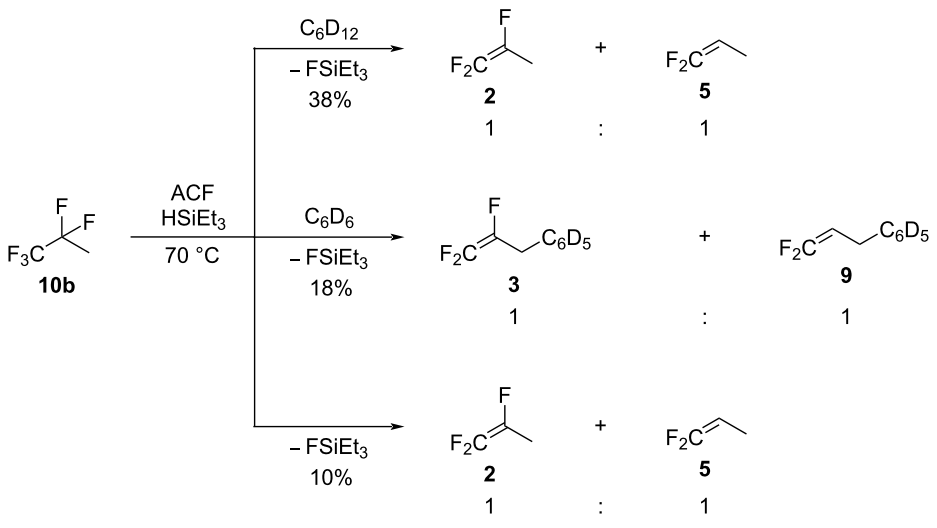

Scheme 13: Reactivity of **10b** in the presence of ACF as the catalyst and $HSiEt_3$ as a hydrogen source in C_6D_{12} (top) or C_6D_6 (middle) as solvents or in neat silane (bottom).

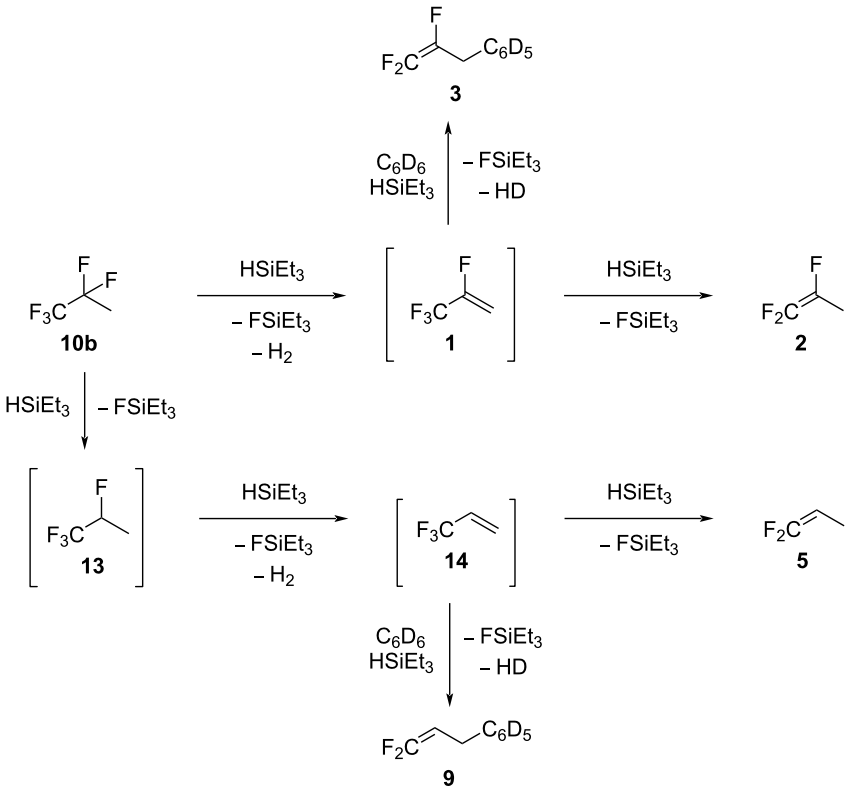

Scheme 14: Proposed reaction pathway starting from **10b** in the presence of ACF and silane.

ated mainly. By using C_6D_6, various Friedel–Crafts products can be further generated. For **10b**, the conversions are very low, but dehydrofluorination and hydrodefluorination pathways compete with each other.

Mechanistically, the C–F bonds of the fluorinated substrates can be activated by Lewis-acidic sites at the ACF surface. In the presence of silane, it can be assumed that preferentially silylium surface species initiate the C–F bond cleavage. For both, the generated carbenium species show further reactivity to result in dehydrofluorination, hydrodefluorination, or Friedel–Crafts products. Notably, the conversion in neat silane was lower in the case of **10c** and **10b**, possibly because of a certain blocking of the acidic sites of ACF by silane. Note in that context that there are reports showing that silylium species can interact with more silane to generate larger entities [56,58,64].

Experimental

Material and methods

The reactions were carried out using Schlenk techniques as well as JYoung NMR tubes. The solvents were purchased from Eurisotop. C_6D_{12} was dried over molecular sieves and purged with argon prior to use. C_6D_6 was dried with K-Solvona and distilled prior to use. Et_3SiH (99%) was purchased from Sigma–Aldrich in a sure seal bottle and stored under argon. 1,1,1,2,3-Pentafluoropropane (HFC-245eb, **10a**), 1,1,1,3,3-pentafluoropropane (HFC-245fa, **10c**), and 1,1,1,2,2-pentafluoropropane (HFC-245cb, **10b**) were gifted by Arkema and used without further purification. 3,3,3-Trifluoropropene (**14**, 99%), 1,1,1-trifluoropropane (**6**), and 1,1,1,2-tetrafluoropropane (**13**) were purchased from abcr and used without further purification. 1,1-Difluoropropene (**5**) was bought from Apollo Scientific and used without further purification. ACF was synthesized according to the literature and stored in a glove box. The number of active sites (1 mmol acidic sites/g of catalyst) was determined by temperature programmed desorption of ammonia (NH_3-TPD) [34,65]. NMR spectra were recorded at room temperature using a Bruker DPX 300 spectrometer. A capillary of trifluorotoluene was employed as an external standard for quantification purposes. The ^{19}F NMR spectra were referenced to $PhCF_3$ ($\delta = -63.5$ ppm) and the chemical shifts in ^1H NMR were referenced to residual C_6D_5H ($\delta = 7.16$ ppm) or $C_6D_{11}H$ ($\delta = 1.38$ ppm).

Procedure for reactions with gaseous substrates

A JYoung NMR tube was loaded with 25 mg of ACF inside a glovebox. In experiments involving a solvent (C_6D_6 or C_6D_{12}),

0.4 mL of the solvent was added under Schlenk conditions, together with the corresponding amount of $HSiEt_3$. In the reactions without solvent, 0.5 mL of $HSiEt_3$ was added using Schlenk techniques to the JYoung NMR tube loaded with ACF. The gases were then condensed using a small glass bulb filled with 0.5 atm of the corresponding gas (0.1 mmol). The reactions were monitored by ^1H and ^{19}F NMR spectroscopy. The tubes were kept at 70 °C for 7 days. $PhCF_3$ was used as an external standard in a closed capillary to calculate the conversion based on the consumed substrate by the integration of the ^{19}F NMR spectra.

Supporting Information

Supporting Information File 1

Analytical data and copies of spectra.
[https://www.beilstein-journals.org/bjoc/content/supplementary/1860-5397-16-213-S1.pdf]

Acknowledgements

Special thanks to Dr. Clara Patricia Marshall for the fruitful discussion on the topic.

Funding

Financial support by the CRC 1349 “Fluorine-Specific Interactions” funded by the Deutsche Forschungsgemeinschaft (gefördert durch die Deutsche Forschungsgemeinschaft (DFG)–Projektnummer 387284271–SFB 1349) is gratefully acknowledged.

ORCID® iDs

Thomas Braun - https://orcid.org/0000-0003-1629-5352

References

1. Velders, G. J. M.; Andersen, S. O.; Daniel, J. S.; Fahey, D. W.; McFarland, M. *Proc. Natl. Acad. Sci. U. S. A.* **2007,** *104,* 4814–4819. doi:10.1073/pnas.0610328104
2. Ko, M.; Shia, R.-L.; Sze, N.-D.; Magid, H.; Bray, R. G. *J. Geophys. Res.: Atmos.* **1999,** *104,* 8173–8181. doi:10.1029/1998jd100097
3. Bolaji, B. O.; Huan, Z. *Renewable Sustainable Energy Rev.* **2013,** *18,* 49–54. doi:10.1016/j.rser.2012.10.008
4. United Nations Environment Programme; *Handbook for the Montreal Protocol on Substances That Deplete the Ozone Layer*; 2018.
5. United Nations Environment Programme; *The Montreal Protocol on Substances That Deplete the Ozone Layer*; 2000. doi:10.1163/15718069620847781
6. United Nations Environment Programme; *Production and Consumption of Ozone Depleting Substances under the Montreal Protocol*; Nairobi, 2005.
7. United Nations Environment Programme; *Amendment to the Montreal Protocol on Substances That Deplete the Ozone Layer*; 2016.
8. United Nations Environment Programme; *Ratification of the Kigali Amendment*; 2017.
9. United Nations Environment Programme; *The Kigali Amendment to the Montreal Protocol: HFC Phase-Down*; 2016.
10. Velders, G. J. M.; Ravishankara, A. R.; Miller, M. K.; Molina, M. J.; Alcamo, J.; Daniel, J. S.; Fahey, D. W.; Montzka, S. A.; Reimann, S. *Science* **2012,** *335,* 922–923. doi:10.1126/science.1216414
11. Wang, H.; Tung, H. S. Process for the Production of HFO Trans-1234ze from HFC-245fa. U.S. Patent US8,067,650 B2, July 10, 2011.
12. Light, B. A.; Phillips, S. D.; Fleming, K. M.; Ferguson, S. A.; Ma, J. J.; Bortz, C. L.; Van Der Puy, M.; Merkel, D. C.; Tung, H. S.; Mukhopadhyay, S. Method for Producing Fluorinated Organic Compounds. U.S. Patent US9102579 B2, Jan 3, 2007.
13. Righetti, G.; Zilio, C.; Longo, G. A. *Int. J. Refrig.* **2015,** *54,* 1–9. doi:10.1016/j.ijrefrig.2015.02.010
14. Fang, X.-X.; Wang, Y.; Jia, W.-Z.; Song, J.-D.; Wang, Y.-J.; Luo, M.-F.; Lu, J.-Q. *Appl. Catal., A* **2019,** *576,* 39–46. doi:10.1016/j.apcata.2019.02.035
15. Van Der Puy, M. Process for the Preparation of 2,3,3,3-Tetrafluoropropene (HFO-1234yf). U.S. Patent US8,071,826 B2, Dec 6, 2011.
16. Meißner, G.; Kretschmar, K.; Braun, T.; Kemnitz, E. *Angew. Chem., Int. Ed.* **2017,** *56,* 16338–16341. doi:10.1002/anie.201707759
17. Lim, S.; Kim, M. S.; Choi, J.-W.; Kim, H.; Ahn, B. S.; Lee, S. D.; Lee, H.; Kim, C. S.; Suh, D. J.; Ha, J.-M.; Song, K. H. *Catal. Today* **2017,** *293–294,* 42–48. doi:10.1016/j.cattod.2016.11.017
18. Wang, F.; Zhang, W.; Liang, Y.; Wang, Y.; Lu, J.; Luo, M. *Chem. Res. Chin. Univ.* **2015,** *31,* 1003–1006. doi:10.1007/s40242-015-5190-3
19. Mao, W.; Bai, Y.; Jia, Z.; Yang, Z.; Hao, Z.; Lu, J. *Appl. Catal., A* **2018,** *564,* 147–156. doi:10.1016/j.apcata.2018.07.028
20. Shen, Q.; Huang, Y.-G.; Liu, C.; Xiao, J.-C.; Chen, Q.-Y.; Guo, Y. *J. Fluorine Chem.* **2015,** *179,* 14–22. doi:10.1016/j.jfluchem.2015.07.007
21. Müller, K.; Faeh, C.; Diederich, F. *Science* **2007,** *317,* 1881–1886. doi:10.1126/science.1131943
22. Ni, C.; Hu, J. *Chem. Soc. Rev.* **2016,** *45,* 5441–5454. doi:10.1039/c6cs00351f
23. Gilles, P. W.; Margrave, J. L. *J. Chem. Phys.* **1953,** *21,* 381–382. doi:10.1063/1.1698915
24. Mazurek, U.; Schwarz, H. *Chem. Commun.* **2003,** 1321–1326. doi:10.1039/b211850e
25. Braun, T.; Wehmeier, F. *Eur. J. Inorg. Chem.* **2011,** 613–625. doi:10.1002/ejic.201001184
26. Amii, H.; Uneyama, K. *Chem. Rev.* **2009,** *109,* 2119–2183. doi:10.1021/cr800388c
27. O'Hagan, D. *Chem. Soc. Rev.* **2008,** *37,* 308–319. doi:10.1039/b711844a
28. Krahl, T.; Kemnitz, E. *Catal. Sci. Technol.* **2017,** *7,* 773–796. doi:10.1039/c6cy02369j
29. Stahl, T.; Klare, H. F. T.; Oestreich, M. *ACS Catal.* **2013,** *3,* 1578–1587. doi:10.1021/cs4003244
30. Fuchibe, K.; Hatta, H.; Oh, K.; Oki, R.; Ichikawa, J. *Angew. Chem., Int. Ed.* **2017,** *56,* 5890–5893. doi:10.1002/anie.201701985

31. Yagupolskii, Yu. L.; Pavlenko, N. V.; Shelyazhenko, S. V.; Filatov, A. A.; Kremlev, M. M.; Mushta, A. I.; Gerus, I. I.; Peng, S.; Petrov, V. A.; Nappa, M. *J. Fluorine Chem.* **2015,** *179,* 134–141. doi:10.1016/j.jfluchem.2015.08.001
32. Teinz, K.; Wuttke, S.; Börno, F.; Eicher, J.; Kemnitz, E. *J. Catal.* **2011,** *282,* 175–182. doi:10.1016/j.jcat.2011.06.013
33. Teinz, K.; Manuel, S. R.; Chen, B. B.; Pigamo, A.; Doucet, N.; Kemnitz, E. *Appl. Catal., B* **2015,** *165,* 200–208. doi:10.1016/j.apcatb.2014.09.076
34. Prechtl, M. H. G.; Teltewskoi, M.; Dimitrov, A.; Kemnitz, E.; Braun, T. *Chem. – Eur. J.* **2011,** *17,* 14385–14388. doi:10.1002/chem.201102853
35. Calvo, B.; Braun, T.; Kemnitz, E. *ChemCatChem* **2018,** *10,* 403–406. doi:10.1002/cctc.201701327
36. Calvo, B.; Wuttke, J.; Braun, T.; Kemnitz, E. *ChemCatChem* **2016,** *8,* 1945–1950. doi:10.1002/cctc.201600257
37. Siwek, A. K.; Ahrens, M.; Feist, M.; Braun, T.; Kemnitz, E. *ChemCatChem* **2017,** *9,* 839–845. doi:10.1002/cctc.201601238
38. Meißner, G.; Feist, M.; Braun, T.; Kemnitz, E. *J. Organomet. Chem.* **2017,** *847,* 234–241. doi:10.1016/j.jorganchem.2017.04.030
39. Meißner, G.; Dirican, D.; Jäger, C.; Braun, T.; Kemnitz, E. *Catal. Sci. Technol.* **2017,** *7,* 3348–3354. doi:10.1039/c7cy00845g
40. Krahl, T.; Kemnitz, E. *J. Fluorine Chem.* **2006,** *127,* 663–678. doi:10.1016/j.jfluchem.2006.02.015
41. Krahl, T.; Stösser, R.; Kemnitz, E.; Scholz, G.; Feist, M.; Silly, G.; Buzaré, J.-Y. *Inorg. Chem.* **2003,** *42,* 6474–6483. doi:10.1021/ic034106h
42. Krespan, C. G. Process for Production of Polyfluoroolefins. U.S. Pat. Appl. US 5,162,594 A, Nov 11, 1992.
43. Calvo, B.; Marshall, C. P.; Krahl, T.; Kröhnert, J.; Trunschke, A.; Scholz, G.; Braun, T.; Kemnitz, E. *Dalton Trans.* **2018,** *47,* 16461–16473. doi:10.1039/c8dt03279c
44. Petrov, V. A.; Krespan, C. G.; Smart, B. E. *J. Fluorine Chem.* **1998,** *89,* 125–130. doi:10.1016/s0022-1139(98)00098-0
45. Petrov, V. A.; Krespan, C. G.; Smart, B. E. *J. Fluorine Chem.* **1996,** *77,* 139–142. doi:10.1016/0022-1139(96)03391-x
46. Petrov, V. A.; Krespan, C. G. *J. Fluorine Chem.* **2000,** *102,* 199–204. doi:10.1016/s0022-1139(99)00279-1
47. Ahrens, M.; Scholz, G.; Braun, T.; Kemnitz, E. *Angew. Chem., Int. Ed.* **2013,** *52,* 5328–5332. doi:10.1002/anie.201300608
48. Luo, Y. *Comprehensive Handbook of Chemical Bond Energies;* CRC Press: Boca Raton, FL, USA, 2007.
49. Kuehnel, M. F.; Lentz, D.; Braun, T. *Angew. Chem., Int. Ed.* **2013,** *52,* 3328–3348. doi:10.1002/anie.201205260
50. Kervarec, M.-C.; Marshall, C. P.; Braun, T.; Kemnitz, E. *J. Fluorine Chem.* **2019,** *221,* 61–65. doi:10.1016/j.jfluchem.2019.04.001
51. Xie, Z.; Fan, J.; Cheng, Y.; Jin, L.; Hu, G.; Lu, J.; Luo, M. *Ind. Eng. Chem. Res.* **2013,** *52,* 3295–3299. doi:10.1021/ie303067d
52. Wang, H.; Tung, H. S.; Singh, R. R.; Shankland, I. Process for Producing 2,3,3,3-Tetrafluoropropene. U.S. Patent US8,766,020 B2, July 1, 2014.
53. Braun, T.; Wehmeier, F.; Altenhöner, K. *Angew. Chem., Int. Ed.* **2007,** *46,* 5321–5324. doi:10.1002/anie.200700711
54. Douvris, C.; Ozerov, O. V. *Science* **2008,** *321,* 1188–1190. doi:10.1126/science.1159979
55. Douvris, C.; Nagaraja, C. M.; Chen, C.-H.; Foxman, B. M.; Ozerov, O. V. *J. Am. Chem. Soc.* **2010,** *132,* 4946–4953. doi:10.1021/ja100605m
56. Scott, V. J.; Çelenligil-Çetin, R.; Ozerov, O. V. *J. Am. Chem. Soc.* **2005,** *127,* 2852–2853. doi:10.1021/ja0426138
57. Panisch, R.; Bolte, M.; Müller, T. *J. Am. Chem. Soc.* **2006,** *128,* 9676–9682. doi:10.1021/ja061800y
58. Talavera, M.; Meißner, G.; Rachor, S. G.; Braun, T. *Chem. Commun.* **2020,** *56,* 4452–4455. doi:10.1039/d0cc01420f
59. Song, J.-D.; Song, T.-Y.; Zhang, T.-T.; Wang, Y.; Luo, M.-F.; Lu, J.-Q. *J. Catal.* **2018,** *364,* 271–281. doi:10.1016/j.jcat.2018.04.014
60. Wang, F.; Liang, Y.; Zhang, W.-X.; Wang, Y.-J.; Lu, J.-Q.; Meng-Fei, L. *Indian J. Chem.* **2015,** *54,* 1192–1197.
61. Tung, H. S.; Johnson, R. C.; Merkel, D. C. Process for the Manufacture of 1,3,3,3-Tetrafluoropropene. U.S. Patent US7,592,494 B2, Sept 22, 2009.
62. Pen, S.; Nappa, M. J. Dehydrofluorination of 245fa to 1234ze. U.S. Patent US9,302,962 B2, April 5, 2016.
63. Burdeniuc, J.; Jedicka, B.; Crabtree, R. H. *Chem. Ber./Recl.* **1997,** *130,* 145–154. doi:10.1002/cber.19971300203
64. Müller, T. Silylium Ions. In *Functional Molecular Silicon Compounds I. Structure and Bonding;* Scheschkewitz, D., Ed.; Springer: Cham, Switzerland, 2013; Vol. 155, pp 107–162. doi:10.1007/430_2013_132
65. Murthy, J. K.; Gross, U.; Rüdiger, S.; Rao, V. V.; Kumar, V. V.; Wander, A.; Bailey, C. L.; Harrison, N. M.; Kemnitz, E. *J. Phys. Chem. B* **2006,** *110,* 8314–8319. doi:10.1021/jp0601419

License and Terms

This is an Open Access article under the terms of the Creative Commons Attribution License (https://creativecommons.org/licenses/by/4.0). Please note that the reuse, redistribution and reproduction in particular requires that the authors and source are credited.

The license is subject to the *Beilstein Journal of Organic Chemistry* terms and conditions: (https://www.beilstein-journals.org/bjoc)

The definitive version of this article is the electronic one which can be found at: https://doi.org/10.3762/bjoc.16.213

BEILSTEIN JOURNAL OF ORGANIC CHEMISTRY

Vicinal difluorination as a C=C surrogate: an analog of piperine with enhanced solubility, photostability, and acetylcholinesterase inhibitory activity

Yuvixza Lizarme-Salas[1], Alexandra Daryl Ariawan[1], Ranjala Ratnayake[2], Hendrik Luesch[2], Angela Finch[3] and Luke Hunter[*1]

Full Research Paper

Open Access

Address:
[1]School of Chemistry, University of New South Wales (UNSW), Sydney NSW 2052, Australia, [2]Department of Medicinal Chemistry and Center for Natural Products, Drug Discovery and Development (CNPD3), University of Florida, Gainesville FL 32610, United States and [3]School of Medical Sciences, University of New South Wales (UNSW), Sydney NSW 2052, Australia

Email:
Luke Hunter[*] - l.hunter@unsw.edu.au

* Corresponding author

Keywords:
Alzheimer's disease; bioisostere; conformational analysis; gauche effect; stereoselective synthesis

Beilstein J. Org. Chem. **2020,** *16,* 2663–2670.
https://doi.org/10.3762/bjoc.16.216

Received: 12 August 2020
Accepted: 16 October 2020
Published: 28 October 2020

This article is part of the thematic issue "Organo-fluorine chemistry V".

Guest Editor: D. O'Hagan

© 2020 Lizarme-Salas et al.; licensee Beilstein-Institut.
License and terms: see end of document.

Abstract

Piperine, a natural product derived from peppercorns, has a variety of biological activities that make it an attractive lead compound for medicinal chemistry. However, piperine has some problematic physicochemical properties including poor aqueous solubility and a susceptibility to UV-induced degradation. In this work, we designed an analog of piperine in which the central conjugated hydrocarbon chain is replaced with a vicinal difluoroalkane moiety. We show that this fluorinated analog of piperine has superior physicochemical properties, and it also has higher potency and selectivity towards one particular drug target, acetylcholinesterase. This work highlights the potential usefulness of the *threo*-difluoroalkane motif as a surrogate for *E*-alkenes in medicinal chemistry.

Introduction

Piperine (**1**, Figure 1) is a well-known natural product that is derived from peppercorns [1-3]. Many biological studies of **1** have been carried out, and these studies have led to a diverse array of biological activities being claimed for this compound [4-9]. For example, **1** is reported to exhibit inhibitory activity towards both acetylcholinesterase (AChE) and β-secretase (BACE-1), which suggests that **1** could hold promise as a dual mechanism-of-action treatment for Alzheimer's disease [4,10-13].

However, piperine (**1**) has some limitations as a drug lead. For example, it has poor solubility, and it is susceptible to photo-

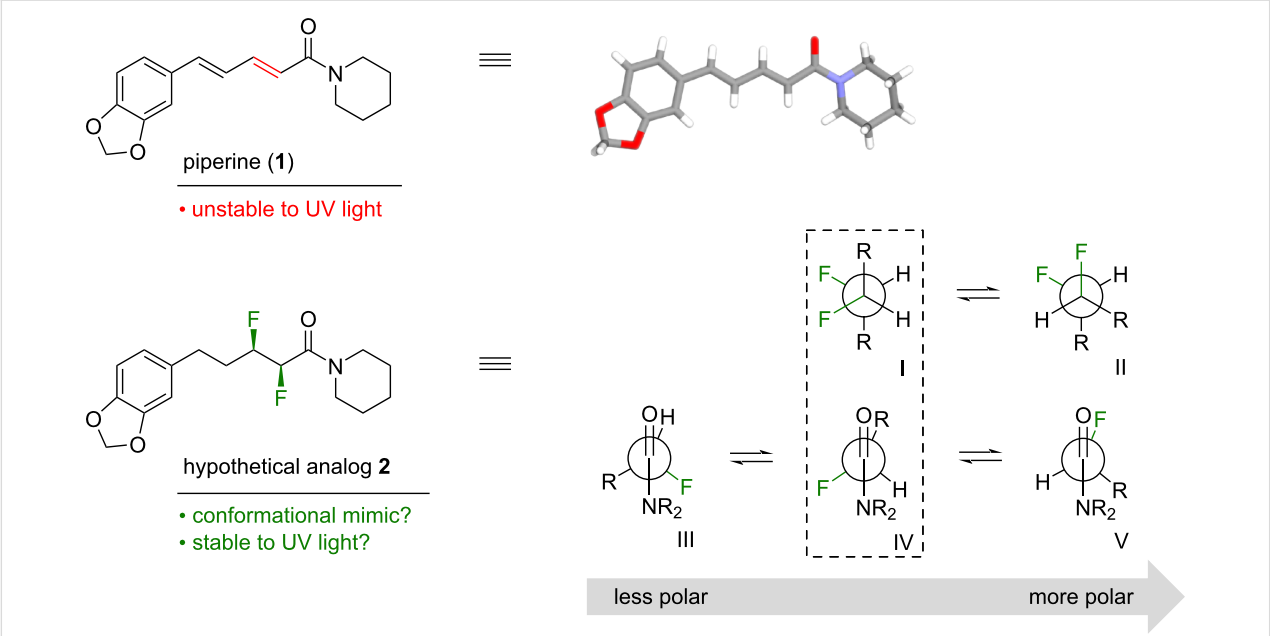

Figure 1: The natural product piperine (**1**) is the inspiration for this work; the crystal structure is shown [14]. In this work, a hypothetical analog **2** was designed to mimic parent compound **1**. The predicted low-energy rotamers of **2** about the F–C–C–F and F–C–C=O bonds are shown; rotamers I and IV give the best mimicry of **1**.

isomerization of the conjugated system [15-17]. This prompted us to consider whether there was another structural motif that could (i) mimic the extended geometry of an *E*-alkene, (ii) impart better solubility, and (iii) be more stable in the presence of UV light. Such a C=C surrogate might offer an improved lead compound for the development of drugs to treat Alzheimer's disease.

Stereoselective fluorination is an emerging strategy for controlling the conformations of organic molecules. The highly polarized C–F bond tends to align in predictable ways with adjacent functional groups, due to a combination of hyperconjugative and/or dipolar interactions [18-21]. This knowledge led us to propose the hypothetical analog **2** (Figure 1) as a potential mimic of **1**. The analog **2** contains a saturated alkyl chain with two vicinal C–F bonds in the α/β positions relative to the amide moiety. The presence of a vicinal difluoride moiety within an alkyl chain is known to favour rotamers in which the C–F bonds align *gauche* (I and II, Figure 1) [22]. Separately, the presence of fluorine on the α-carbon of a tertiary amide is known to restrict the $C_α$–C(O) bond to a small set of low-energy rotamers (III–V, Figure 1) [23]. Intriguingly, studies of simple molecules containing either F–C–C–F or F–C–C=O motifs have shown that the rotamer populations can change, depending on the polarity of the solvent [22,23]. The rotamers I and IV (Figure 1, boxed) would appear to provide the closest structural match with compound **1**, but in a highly polar medium the more polar rotamers II and V might predominate. Of course, the contiguous positioning of the F–C–C–F and F–C–C=O moieties within the same molecule (**2**) means that these moieties would not function independently, but rather would likely influence one another, adding another layer of complexity. Finally, it is interesting to consider whether the microenvironment of a protein binding site could also change the relative energies of the various F–C–C–F and F–C–C=O rotamers, offering the possibility that analog **2** might be an effective conformational mimic of **1** in some environments but not in others.

Herein, we describe the optimisation of a synthetic route to compound **2**, the conformational analysis of this molecule by NMR and molecular modelling studies, a comparison of the photostabilities of parent compound **1** vs derivative **2**, and a comparison of the inhibitory activities of **1** vs **2** towards both AChE and BACE-1.

Results and Discussion

Synthesis

Jacobsen and co-workers have recently described a method for the one-step, diastereoselective 1,2-difluorination of alkenes, mediated by a hypervalent iodine catalyst [24]. The substrate scope of the Jacobsen method has certain constraints but their original report did include some examples of α,β-unsaturated amides, and so we were motivated to investigate the method in this work, using compound **3** [25] as the substrate (Scheme 1). We recognized that the product of this reaction would most likely be the unwanted *erythro*-isomer **6** but we nevertheless

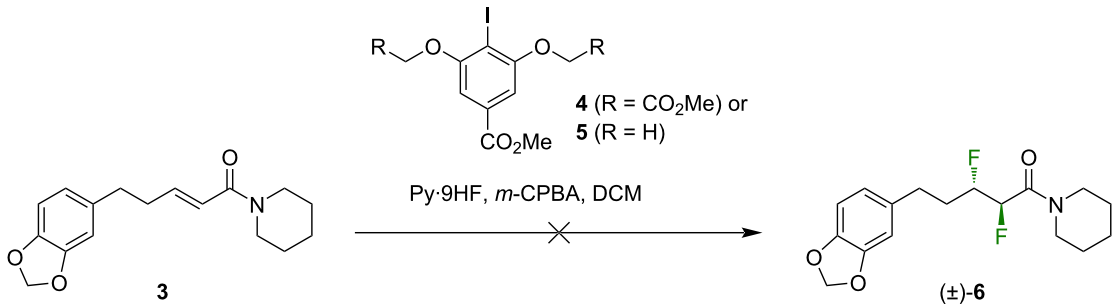

Scheme 1: The attempted synthesis of **6** (a diastereoisomer of **2**) via a one-step 1,2-difluorination reaction [24]. Py = pyridine; *m*-CPBA = *m*-chloroperbenzoic acid, DCM = dichloromethane.

deemed it a worthwhile preliminary investigation. Disappointingly, the treatment of the precursor **3** with pyridine·HF and either catalyst **4** or **5** at room temperature for two days gave no discernible reaction, and the starting material **3** was recovered intact. Warming the reaction mixture to 50 °C caused the disappearance of **3** but the formation of an intractable mixture of products. We were forced to conclude that the rather complex structure of **3** was incompatible with the Jacobsen catalytic system.

Since the one-step difluorination method (Scheme 1) was unsuccessful, we decided to pursue a stepwise fluorination approach [26,27] (Scheme 2). Thus, the allylic alcohol **7** [28] was protected as the benzyl ether then subjected to a Sharpless asymmetric dihydroxylation reaction to furnish the diol **8** in modest yield. The diol **8** was then converted into the cyclic sulfate **9**, which was ring-opened using TBAF to furnish the fluorohydrin **10**. A Mosher ester analysis of the fluorohydrin **10** suggested that the earlier dihydroxylation reaction had proceeded with 90% ee. The deoxyfluorination of **10** was then attempted using several reagents including DeoxoFluor, DeoxoFluor in combination with TMS-morpholine [29], and PyFluor [30]. The optimal yield of the *threo*-difluoroalkane **11** was obtained with DeoxoFluor at elevated temperature (Scheme 2). A side-product in this fluorination reaction was the tricyclic compound **12**, which presumably formed through an electrophilic aromatic substitution reaction of the activated alcohol intermediate. The inclusion of TMS-morpholine [29] reduced the formation of this side-product but did not lead to an overall increase in the yield of **11**. Despite the modest optimised yield of the difluoroalkane **11**, a sufficient quantity of this material was secured to continue with the synthesis. The hydrogenolysis

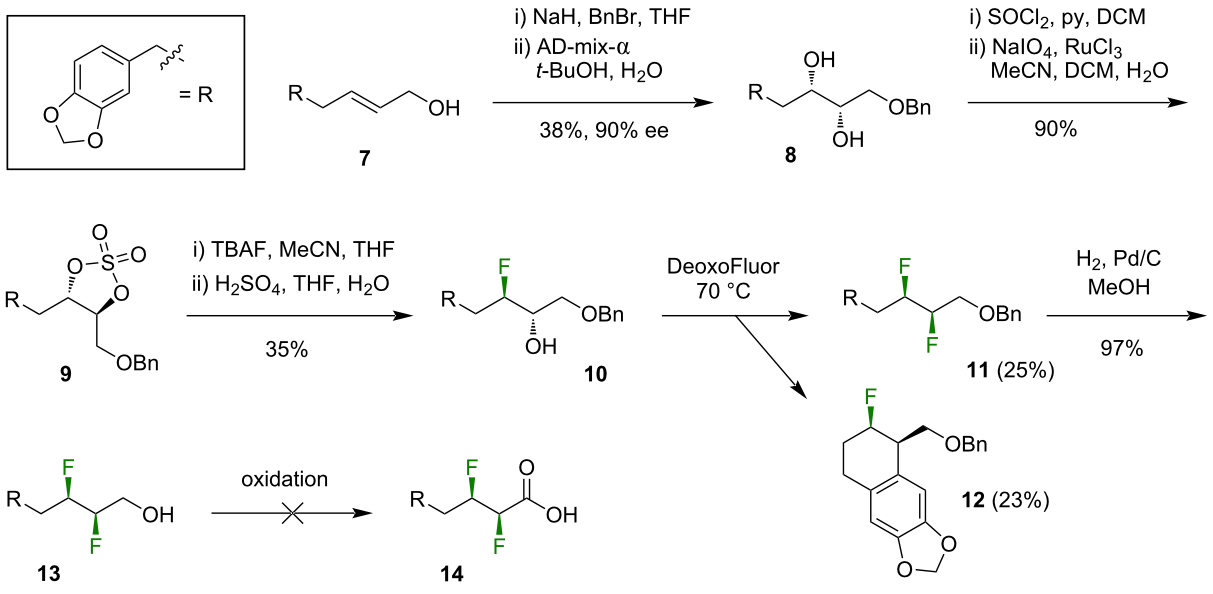

Scheme 2: The attempted synthesis of **2** via a stepwise fluorination approach (ether series). THF = tetrahydrofuran, AD-mix-α = commercially available asymmetric dihydroxylation reagent, TBAF = tetrabutylammonium fluoride, DeoxoFluor = bis(2-methoxyethyl)aminosulfur trifluoride.

of the benzyl ether of **11** provided the primary alcohol **13**, which only needed to be oxidised to the carboxylic acid **14** then coupled to piperidine in order to deliver the target compound, **2**. However, the oxidation of **13** proved to be unexpectedly troublesome. Mild oxidising agents caused incomplete consumption of **13**, while vigorous conditions led to the oxidation not only of the primary alcohol of **13** but also of the electron-rich aryl moiety (see Supporting Information File 1).

In order to circumvent the troublesome oxidation reaction (i.e., **13**→**14**, Scheme 2), and to seek higher enantiopurity of the target, we modified the synthetic plan to include an ester moiety throughout (Scheme 3). Thus, the α,β-unsaturated ester **15** [25] was carried through a similar sequence to that previously described, i.e., dihydroxylation, cyclic sulfate formation, ring-opening with TBAF (although note the regioselectivity [31]), deoxyfluorination, and deprotection to deliver the difluorinated acid **20**. Finally, coupling of the acid **20** with piperidine afforded the target compound **2** in moderate yield (Scheme 3). The enantiopurity of **2** was investigated using chiral HPLC. From a spectroscopically pure sample of **2**, two HPLC peaks were observed, with an integral ratio of 99:1. It is assumed that the two peaks correspond to the two enantiomers of **2** and, if that assumption is true, then the optical purity of this sample is 98% ee.

Conformational analysis

Having completed the synthesis of the target molecule **2**, the next task was to investigate the conformational behavior of this molecule. This was achieved by performing a DFT study in the Gaussian software, using the M06-2X level of theory with the 6-311+G(d,p) basis set, parameters similar to those employed by Linclau and co-workers for their studies of vicinal difluoro systems [22]. A set of starting structures of **2** was generated by systematically rotating three bonds (i.e., F–C–C–F, F–C–C=O, and O=C–N–C) in 120° increments and the starting structures were then geometry optimised and their energies calculated. To enable benchmarking against experiment, NMR spin–spin coupling constants were calculated for the lowest-energy final structures of **2** using the GIAO method with the B3LYP/6-311+G(d,p) level of theory. Chloroform was used as the solvent for both the NMR experiments and the SMD calculations.

The three lowest-energy structures to emerge from the computational analysis (i.e., **2a**–**c**) are shown in Figure 2. The global minimum structure **2a** has a F–C–C–F dihedral angle of 73°, giving an extended zigzag carbon chain. This approximates rotamer I (Figure 1) and in this regard **2a** is a good conformational mimic of **1**. However, **2a** has a F–C–C=O dihedral angle of 152°, approximating rotamer III (Figure 1) and in this regard **2a** is a poorer conformational mimic of **1**. The next-higher energy structure (**2b**, Figure 2) is related to **2a** through a ring-flip of the piperidine moiety (equivalent to a 180° rotation of the amide bond). The structures **2a**,**b** are close in energy, suggesting that both puckers of the piperidine moiety would be substantially populated in solution. A similar situation occurs for piperine itself; an indirect evidence for this comes from the crystal structure of **1** (Figure 1), where there is a second molecule in the unit cell (not shown) that has the alternative ring pucker [14]. The next-higher energy calculated structure of **2**

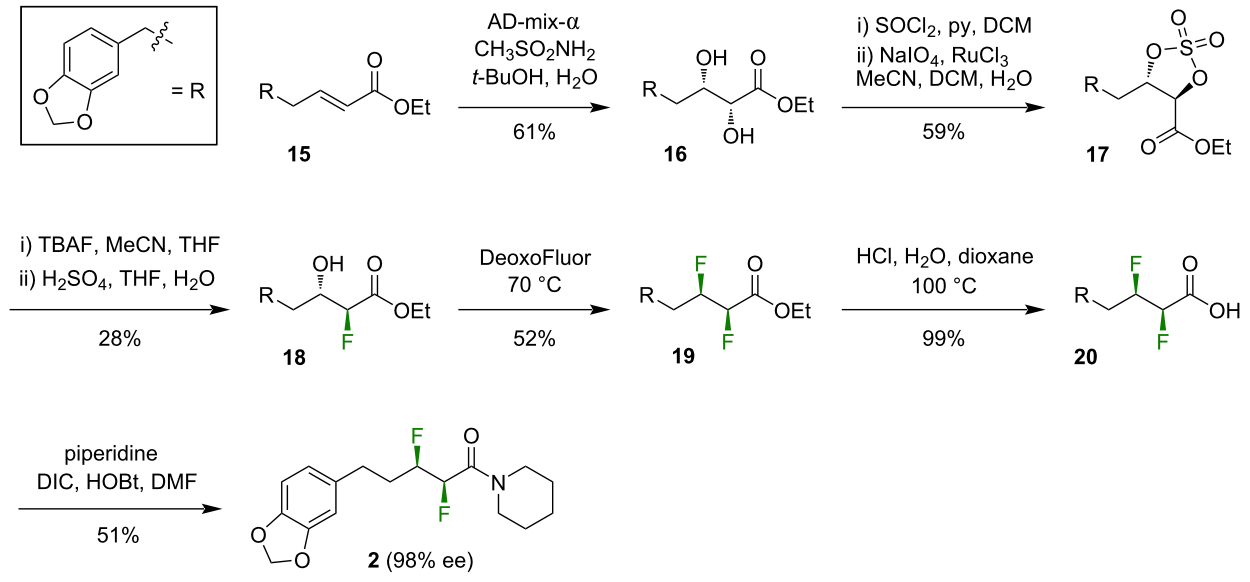

Scheme 3: Synthesis of compound **2** via a stepwise fluorination approach (ester series). DIC = diisopropylcarbodiimide, HOBt = hydroxybenzotriazole, DMF = *N*,*N*-dimethylformamide.

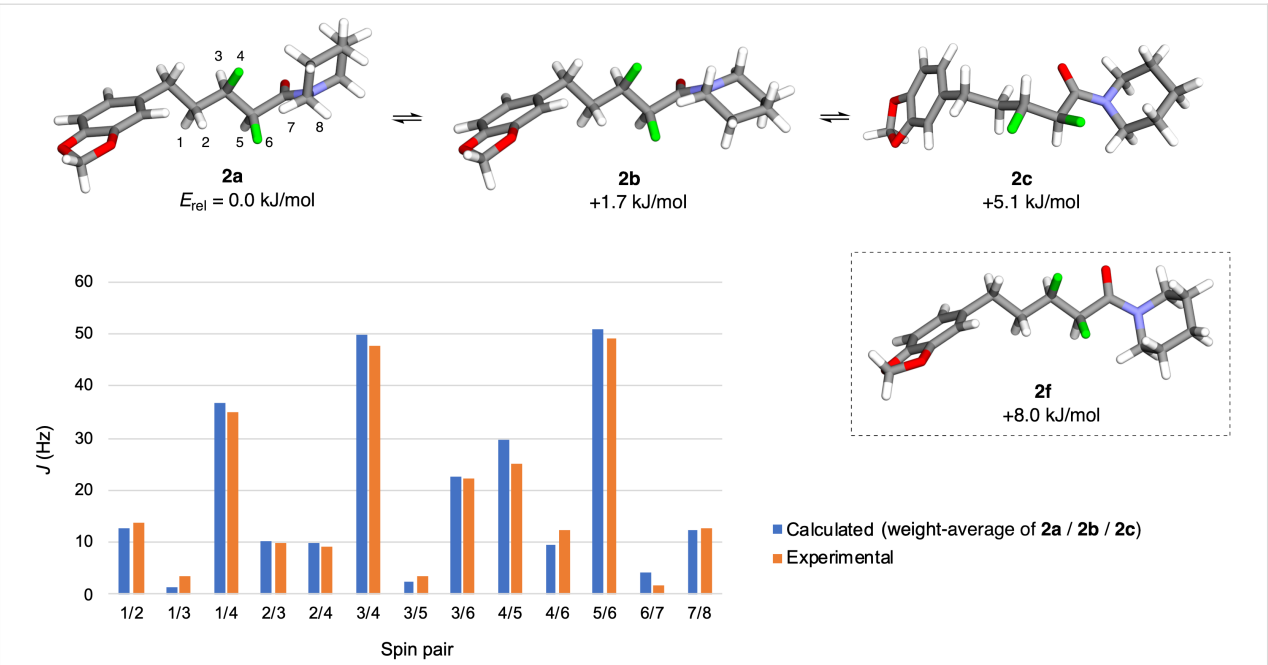

Figure 2: Conformational analysis of **2** by DFT and NMR. The numbering scheme for NMR spins is given on structure **2a**.

(i.e., **2c**, Figure 2) has a F–C–C–F dihedral angle of −52°. This approximates rotamer II (Figure 1), giving a bent carbon chain that contrasts with the extended chains of **2a**,**b**. The structure **2c** has a F–C–C=O dihedral angle of −118°; this approximates rotamer IV (Figure 1). Together, the structures **2a**–**c** seem to dominate the conformer population distribution of **2** in chloroform solution, because the weight-averaged calculated *J*-values of **2a**–**c** match the experimentally-measured *J*-values quite well (Figure 2). But none of the structures **2a**–**c** are a close conformational match with piperine (**1**).

A noteworthy feature of structures **2a**,**b** (Figure 2) is that both, the α-fluorine and the β-fluorine atoms of each structure make close contacts with the hydrogen atoms on the piperidine ring (2.08–2.34 Å). This manifests in the observation of a through-space coupling (J = 1.9 Hz) between the α-fluorine and a piperidine hydrogen in the experimental NMR spectrum of **2** (i.e., spins 6/7, Figure 2). The attractive F···H interactions might explain why the amide bond is twisted by 11–20° from planarity in **2a**,**b**. In structure **2c**, only the α-fluorine makes close contacts with hydrogens on the piperidine ring, and the amide is twisted to a lesser degree in that case (8° away from planarity). It is interesting that in the crystal structure of piperine itself (**1**, Figure 1) [14], the amide bond is also twisted by 15° away from planarity. In this case the distortion might be attributable to a H···H clash (1.99 Å).

Structure **2f** (Figure 2), which was among the higher-energy calculated conformers of **2** (see Supporting Information File 1), bears a close resemblance to the solid-state conformation of piperine (**1**, Figure 1). The structure **2f** has a F–C–C–F dihedral angle of 57° and a F–C–C=O dihedral angle of –133°. These angles approximate rotamers I and IV, respectively (Figure 1). The unexpectedly high relative energy that was calculated for compound **2f** might be partially attributable to the fact that it features only a single F···H contact within 2.50 Å. The calculations suggest that the conformer **2f** is not significantly populated in chloroform solution but it was not possible to verify this by NMR measurements, because **2f** is essentially superimposable with **2a**,**b** within the fluoroalkyl segment. In more polar solvents such as water, the intramolecular F···H interactions would be expected to decrease in significance [32] and this might increase the accessibility of conformer **2f**. We reasoned that comparing the biological activities of **1** vs **2** might shed light on this possibility (vide infra).

Photostability

A limitation of piperine (**1**) as a drug lead is its instability under UV light. The conjugated system of **1** is well-known to undergo facile *E*/*Z* isomerization upon the absorption of UV photons, leading rapidly to a mixture of all four possible geometric isomers of **1** [15-17]. In the present work, this phenomenon was confirmed by exposing an ethanolic solution of **1** to sunlight for 2.5 h (Figure 3). The analysis of the product by ^{1}H NMR spectroscopy revealed a multitude of new signals in the alkenyl region. In contrast, the analog **2** lacks conjugation in the central portion of the molecule and was therefore expected to be more stable to UV light. Indeed, the exposure of **2** to sunlight in an

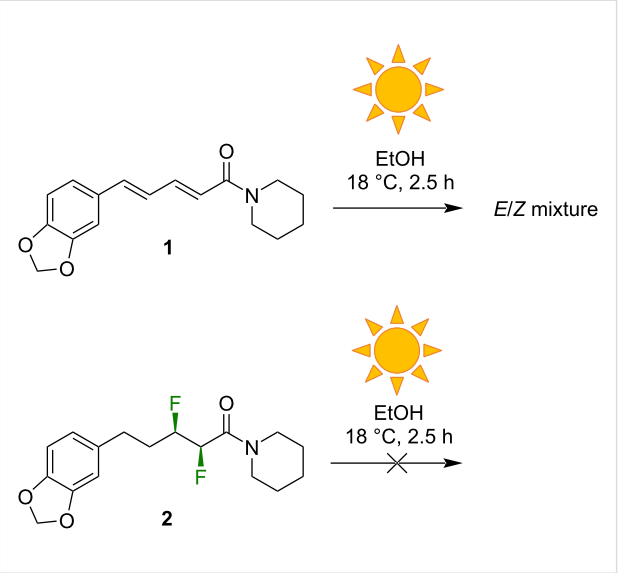

Figure 3: Analog **2** has greater stability to UV light than does piperine (**1**).

identical manner to that described for **1** led to no detectable decomposition (Figure 3, Supporting Information File 1).

Biological activity and solubility

The biological activities of piperine (**1**) and the analog **2** were compared using two different assays, namely the inhibition of either acetylcholinesterase (AChE) or β-secretase (BACE-1).

The inhibition of AChE was measured using a modification of a previously described colorimetric assay (Figure 4a) [33]. It quickly became apparent that the limited solubility of piperine (**1**) in 50 mM Tris-HCl buffer, even in the presence of methanol as a co-solvent, was a major problem in this assay. We observed cloudiness or the appearance of a precipitate at higher concentrations of **1**, which affected the reproducibility of the assay, and prevented complete inhibition from being achieved (Figure 4a). The estimated IC_{50} of **1** was >1,000 μM. In contrast, analog **2** posed no solubility problems in this assay, generating a reproducible curve all the way to complete inhibition and returning an IC_{50} value of 51.7 μM. Thus, the replacement of the C=C fragment in **1** with a *threo*-difluoroalkane motif in **2** appears to preserve or enhance the AChE-binding ability, while simultaneously offering the advantage of improved aqueous solubility.

The inhibition of BACE-1 was measured using a fluorogenic peptide substrate according to an established method (Figure 4b) [34]. Intriguingly, the relative activities of **1** vs **2** were reversed in comparison with the AChE assay. The lead compound **1** achieved the complete inhibition of BACE-1 under the conditions of the assay, giving an IC_{50} value of 59.2 μM. In contrast, analog **2** was a much weaker inhibitor of BACE-1, failing to achieve complete inhibition, and giving an estimated IC_{50} value of >1,000 μM.

There are several conceivable explanations for the reversed relative activities of **1** vs **2** in the AChE vs BACE-1 assays. One possibility is that analog **2** is induced to adopt the "correct" conformation when binding to both targets (i.e., **2f**, Figure 2), and this structure fits well within the AChE active site but poorly within the BACE-1 active site, perhaps due to unfavourable interactions of the fluorine substituents of **2** with BACE-1 active site residues. A second possibility is that **2** adopts an "incorrect" conformation upon binding to both targets (e.g., **2a**,

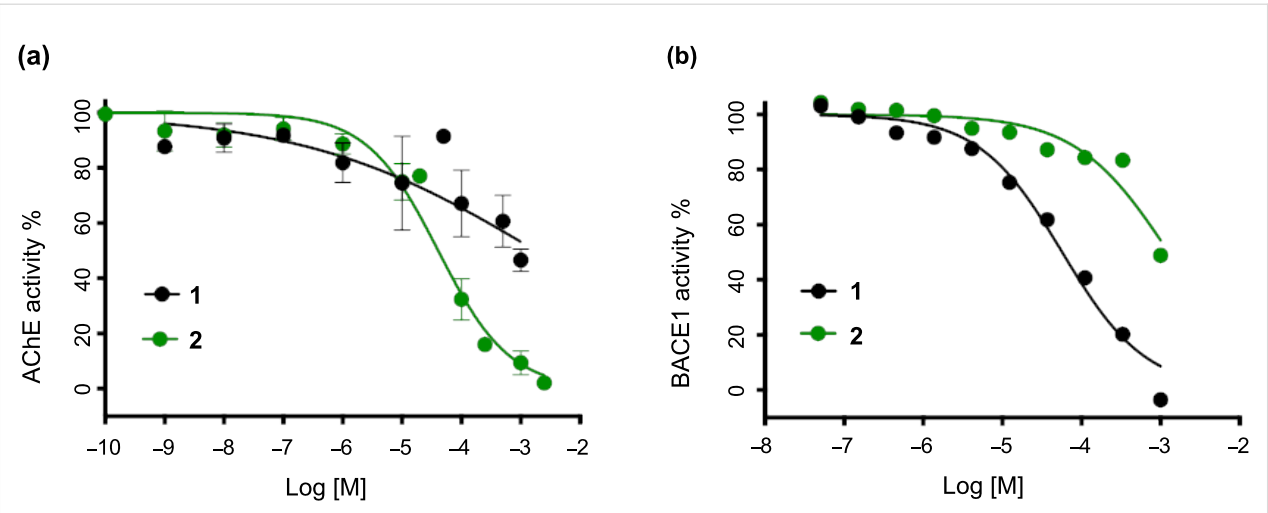

Figure 4: Biological activity of piperine (**1**) and derivative **2**. (a) Inihbition of AChE by **1** (IC_{50} >1000 μM) and **2** (IC_{50} = 51.7 μM) and (b) inhibition of BACE-1 by **1** (IC_{50} = 59.2 μM) and **2** (IC_{50} > 1000 μM).

Figure 2), and this novel molecular shape is readily accommodated by AChE [35] but not by BACE-1, perhaps due to different levels of flexibility within the enzyme active sites. A third possibility is that the analog **2** adopts different conformations upon binding to AChE vs BACE-1, since the microenvironments within the enzymes' active sites could be different (e.g., more/less polar), the "correct" binding geometry of **2** might be favoured in AChE but not in BACE-1. These possibilities all remain speculative in the absence of high-resolution structural data of the enzyme–ligand complexes.

Conclusion

A *threo*-difluorinated piperine analog (**2**) was successfully synthesised through a stepwise route. The physicochemical properties of compound **2** were found to be superior to piperine (**1**) itself in two key respects, namely photostability and aqueous solubility. The conformational analysis of **2** by DFT and NMR spectroscopy revealed that the lowest-energy conformations **2a**–**c** are imperfect mimics of **1** but that a somewhat higher-energy conformation (**2f**) is a close match for **1**. A preliminary biological investigation revealed that the analog **2** displays superior inhibitory activity towards AChE but inferior activity towards BACE-1, relative to **1**. While the inhibition of both AChE and BACE-1 is potentially desirable for the purpose of treating Alzheimer's disease, it should be noted that problems have been encountered in clinical trials with BACE-1 as the target [36], suggesting that the analog **2** might still have relevance in the context of an Alzheimer's treatment. More generally, our finding that the *threo*-difluoroalkane motif is sometimes but not always an effective surrogate for *E*-alkenes suggests that this bioisosteric switch could be exploited more widely in medicinal chemistry as a means of increasing the selectivity of a lead compound towards its desired target.

Supporting Information

Supporting Information File 1

Synthetic procedures, characterization data for novel compounds and copies of spectra; photostability assessment, conformational analysis of compound **2**, and biological assays.
[https://www.beilstein-journals.org/bjoc/content/supplementary/1860-5397-16-216-S1.pdf]

ORCID® iDs

Yuvixza Lizarme-Salas - https://orcid.org/0000-0001-6964-8129
Ranjala Ratnayake - https://orcid.org/0000-0002-5980-2070
Angela Finch - https://orcid.org/0000-0002-4598-6745
Luke Hunter - https://orcid.org/0000-0002-8678-3602

Preprint

A non-peer-reviewed version of this article has been previously published as a preprint: https://doi.org/10.3762/bxiv.2020.93.v1

References

1. Ørsted, H. C. *J. Chem. Phys.* **1820,** *29,* 80–82.
2. Ladenburg, A.; Scholtz, M. *Ber. Dtsch. Chem. Ges.* **1894,** *27,* 2958–2960. doi:10.1002/cber.18940270356
3. Epstein, W. W.; Netz, D. F.; Seidel, J. L. *J. Chem. Educ.* **1993,** *70,* 598–599. doi:10.1021/ed070p598
4. Meghwal, M.; Goswami, T. K. *Phytother. Res.* **2013,** *27,* 1121–1130. doi:10.1002/ptr.4972
5. Srinivasan, K. *Crit. Rev. Food Sci. Nutr.* **2007,** *47,* 735–748. doi:10.1080/10408390601062054
6. Manayi, A.; Nabavi, S. M.; Setzer, W. N.; Jafari, S. *Curr. Med. Chem.* **2018,** *25,* 4918–4928. doi:10.2174/0929867324666170523120656
7. Yadav, V.; Krishnan, A.; Vohora, D. *J. Ethnopharmacol.* **2020,** *247,* 112255. doi:10.1016/j.jep.2019.112255
8. Smilkov, K.; Ackova, D. G.; Cvetkovski, A.; Ruskovska, T.; Vidovic, B.; Atalay, M. *Curr. Pharm. Des.* **2019,** *25,* 1729–1739. doi:10.2174/1381612825666190701150803
9. Butt, M. S.; Pasha, I.; Sultan, M. T.; Randhawa, M. A.; Saeed, F.; Ahmed, W. *Crit. Rev. Food Sci. Nutr.* **2013,** *53,* 875–886. doi:10.1080/10408398.2011.571799
10. Chonpathompikunlert, P.; Wattanathorn, J.; Muchimapura, S. *Food Chem. Toxicol.* **2010,** *48,* 798–802. doi:10.1016/j.fct.2009.12.009
11. Okello, E. J.; Coleman, A.; Seal, C. J. *Int. J. Pharm. Sci. Res.* **2015,** *6,* 3726–3732.
12. Pai, V.; Chandrashekar, K. S.; Shreedhara, C. S.; Pai, A. *Res. J. Pharm. Technol.* **2017,** *10,* 3506–3510. doi:10.5958/0974-360x.2017.00628.x
13. Čolović, M. B.; Krstić, D. Z.; Lazarević-Pašti, T. D.; Bondžić, A. M.; Vasić, V. M. *Curr. Neuropharmacol.* **2013,** *11,* 315–335. doi:10.2174/1570159x11311030006
14. He, H.; Zhang, Q.; Wang, J.-R.; Mei, X. *CrystEngComm* **2017,** *19,* 6154–6163. doi:10.1039/c7ce01468f
15. Grewe, R.; Freist, W.; Neumann, H.; Kersten, S. *Chem. Ber.* **1970,** *103,* 3752–3770. doi:10.1002/cber.19701031204
16. Hashimoto, K.; Yaoi, T.; Koshiba, H.; Yoshida, T.; Maoka, T.; Fujiwara, Y.; Yamamoto, Y.; Mori, K. *Food Sci. Technol. Int., Tokyo* **1996,** *2,* 24–29. doi:10.3136/fsti9596t9798.2.24
17. Kozukue, N.; Park, M.-S.; Choi, S.-H.; Lee, S.-U.; Ohnishi-Kameyama, M.; Levin, C. E.; Friedman, M. *J. Agric. Food Chem.* **2007,** *55,* 7131–7139. doi:10.1021/jf070831p
18. O'Hagan, D. *Chem. Soc. Rev.* **2008,** *37,* 308–319. doi:10.1039/b711844a
19. Hunter, L. *Beilstein J. Org. Chem.* **2010,** *6,* No. 38. doi:10.3762/bjoc.6.38
20. Meanwell, N. A. *J. Med. Chem.* **2018,** *61,* 5822–5880. doi:10.1021/acs.jmedchem.7b01788
21. Gillis, E. P.; Eastman, K. J.; Hill, M. D.; Donnelly, D. J.; Meanwell, N. A. *J. Med. Chem.* **2015,** *58,* 8315–8359. doi:10.1021/acs.jmedchem.5b00258
22. Fox, S. J.; Gourdain, S.; Coulthurst, A.; Fox, C.; Kuprov, I.; Essex, J. W.; Skylaris, C.-K.; Linclau, B. *Chem. – Eur. J.* **2015,** *21,* 1682–1691. doi:10.1002/chem.201405317
23. Tormena, C. F.; Rittner, R.; Abraham, R. J.; Basso, E. A.; Pontes, R. M. *J. Chem. Soc., Perkin Trans. 2* **2000,** 2054–2059. doi:10.1039/b004685j

24. Banik, S. M.; Medley, J. W.; Jacobsen, E. N. *J. Am. Chem. Soc.* **2016,** *138,* 5000–5003. doi:10.1021/jacs.6b02391
25. de Araújo Júnior, J. X.; Barreiro, E. J.; Parente, J. P.; Fraga, C. A. M. *Synth. Commun.* **1999,** *29,* 263–273. doi:10.1080/00397919908085766
26. Nicoletti, M.; O'Hagan, D.; Slawin, A. M. Z. *J. Am. Chem. Soc.* **2005,** *127,* 482–483. doi:10.1021/ja045299q
27. Hunter, L.; Jolliffe, K. A.; Jordan, M. J. T.; Jensen, P.; Macquart, R. B. *Chem. – Eur. J.* **2011,** *17,* 2340–2343. doi:10.1002/chem.201003320
28. de Araújo-Júnior, J. X.; de M. Duarte, C.; de O. Chaves, M. C.; Parente, J. P.; Fraga, C. A. M.; Barreiro, E. J. *Synth. Commun.* **2001,** *31,* 117–123. doi:10.1081/scc-100000187
29. Bresciani, S.; O'Hagan, D. *Tetrahedron Lett.* **2010,** *51,* 5795–5797. doi:10.1016/j.tetlet.2010.08.104
30. Nielsen, M. K.; Ugaz, C. R.; Li, W.; Doyle, A. G. *J. Am. Chem. Soc.* **2015,** *137,* 9571–9574. doi:10.1021/jacs.5b06307
31. Gao, Y.; Sharpless, K. B. *J. Am. Chem. Soc.* **1988,** *110,* 7538–7539. doi:10.1021/ja00230a045
32. Yamamoto, I.; Jordan, M. J. T.; Gavande, N.; Doddareddy, M. R.; Chebib, M.; Hunter, L. *Chem. Commun.* **2012,** *48,* 829–831. doi:10.1039/c1cc15816c
33. Mathew, M.; Subramanian, S. *PLoS One* **2014,** *9,* e86804. doi:10.1371/journal.pone.0086804
34. Liu, Y.; Zhang, W.; Li, L.; Salvador, L. A.; Chen, T.; Chen, W.; Felsenstein, K. M.; Ladd, T. B.; Price, A. R.; Golde, T. E.; He, J.; Xu, Y.; Li, Y.; Luesch, H. *J. Med. Chem.* **2012,** *55,* 10749–10765. doi:10.1021/jm301630s
35. Abdul Manap, A. S.; Wei Tan, A. C.; Leong, W. H.; Yin Chia, A. Y.; Vijayabalan, S.; Arya, A.; Wong, E. H.; Rizwan, F.; Bindal, U.; Koshy, S.; Madhavan, P. *Front. Aging Neurosci.* **2019,** *11,* 10.3389/fnagi.2019.00206. doi:10.3389/fnagi.2019.00206
36. Moussa-Pacha, N. M.; Abdin, S. M.; Omar, H. A.; Alniss, H.; Al-Tel, T. H. *Med. Res. Rev.* **2020,** *40,* 339–384. doi:10.1002/med.21622

License and Terms

This is an Open Access article under the terms of the Creative Commons Attribution License (https://creativecommons.org/licenses/by/4.0). Please note that the reuse, redistribution and reproduction in particular requires that the authors and source are credited.

The license is subject to the *Beilstein Journal of Organic Chemistry* terms and conditions: (https://www.beilstein-journals.org/bjoc)

The definitive version of this article is the electronic one which can be found at: https://doi.org/10.3762/bjoc.16.216

BEILSTEIN JOURNAL OF ORGANIC CHEMISTRY

Asymmetric Mannich reactions of (*S*)-*N*-*tert*-butylsulfinyl-3,3,3-trifluoroacetaldimines with yne nucleophiles

Ziyi Li[1], Li Wang[1], Yunqi Huang[1], Haibo Mei[1], Hiroyuki Konno[2], Hiroki Moriwaki[3], Vadim A. Soloshonok[4,5] and Jianlin Han[*1]

Full Research Paper

Open Access

Address:
[1]Jiangsu Co-Innovation Center of Efficient Processing and Utilization of Forest Resources, College of Chemical Engineering, Nanjing Forestry University, Nanjing 210037, Jiangsu, China, [2]Department of Biological Engineering, Graduate School of Science and Engineering, Yamagata University, Yonezawa, Yamagata 992-8510, Japan, [3]Hamari Chemical Ltd., 1-4-29 Kunijima, Higashi-Yodogawa-ku, Osaka 533-0024, Japan, [4]Department of Organic Chemistry I, Faculty of Chemistry, University of the Basque Country UPV/EHU, Paseo Manuel Lardizábal 3, 20018 San Sebastián, Spain and [5]IKERBASQUE, Basque Foundation for Science, Alameda Urquijo 36-5, Plaza Bizkaia, 48011 Bilbao, Spain

Email:
Jianlin Han[*] - hanjl@njfu.edu.cn

* Corresponding author

Keywords:
arylethynes; asymmetric Mannich reaction; C-nucleophile; CF_3-aldimine; fluorinated propargylamine

Beilstein J. Org. Chem. **2020,** *16,* 2671–2678.
https://doi.org/10.3762/bjoc.16.217

Received: 30 July 2020
Accepted: 20 October 2020
Published: 29 October 2020

This article is part of the thematic issue "Organo-fluorine chemistry V".

Guest Editor: D. O'Hagan

© 2020 Li et al.; licensee Beilstein-Institut.
License and terms: see end of document.

Abstract

In the present work, arylethynes were studied as new C-nucleophiles in the asymmetric Mannich addition reactions with (*S*)-*N*-*tert*-butylsulfinyl-3,3,3-trifluoroacetaldimine. The reactions were conducted under operationally convenient conditions affording the corresponding Mannich adducts with up to 87% yield and 70:30 diastereoselectivity. The isomeric products can be separated using regular column chromatography to afford diastereomerically pure compounds. The purified Mannich addition products were deprotected to give the target enantiomerically pure trifluoromethylpropargylamines. A mechanistic rationale for the observed stereochemical outcome is discussed.

Introduction

In recent years, substitution of hydrogen by fluorine atoms or fluorine-containing groups usually provides unexpected biological and physicochemical properties, which thus has become an established approach for the development of pharmaceuticals [1-9], agrochemicals [10-14], and advanced materials [15-19]. On the other hand, chiral propargylamine represents a very important type of organic intermediates, which has been successfully used in the synthesis of natural products and biologically

relevant heterocyclic compounds [20-24]. Thus, fluorinated propargylamine, in particular, chiral trifluoromethylpropargylamine, should be considered of great research interest due to the apparently advantageous pharmaceutical profile of CF_3-containing drugs [25,26]. For example, DPC 961 contains the trifluoromethylpropargylamine moiety and has been developed as the inhibitor against non-nucleoside reverse transcriptase for the treatment of human immunodeficiency virus [27] (Figure 1).

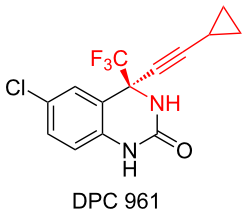

Figure 1: Anti-HIV compound containing a trifluoromethylpropargylamine moiety.

Thus, the development of synthetic methods for the preparation of these compounds, featuring trifluoromethylpropargylamine is of general research interest [28-32]. The asymmetric Ru/(*R*)-CPA-catalyzed chemoselectivie biomimetic reduction [33] and the organocatalytic transfer hydrogenation [34] of fluorinated alkynylketimines have been developed for the synthesis of fluorinated propargylamines in good yields and high enantioselectivities by the groups of Zhou and Peng, respectively (Scheme 1a). It should be mentioned that the Qing group also reported a method for the synthesis of α-trifluoromethylated α-propargylamines via a Ti-promoted addition reaction between acetylide and chiral CF_3-ketimines (Scheme 1b) [35]. Based on our experience in the preparation of trifluoromethylated amino compounds [36-40] and the chemistry of *N*-*tert*-butylsulfinyl-3,3,3-trifluoroacetaldimine (**1**) [41-54], we noticed that the reactions of chiral imine **1** with yne nucleophiles have never been reported thus far. Accordingly, intrigued by this methodological deficiency, we decided to dedicate a special research project to this objective; herein, we report Mannich reactions between yne nucleophiles and aldimine **1** (Scheme 1c). The results reported in this work expand our knowledge of the reactivity of imines and the origins of stereocontrol, as well as provide synthetic access to a series of trifluoromethylpropargylamine of high biological interest.

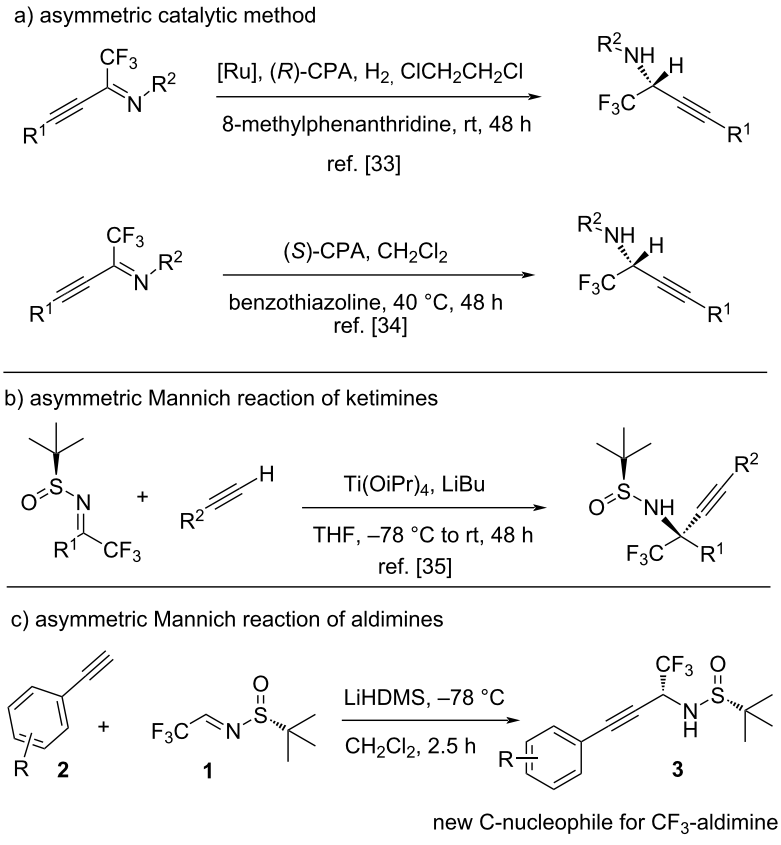

Scheme 1: Literature-known methods (a and b) and the here reported (c) approach for the synthesis of α-trifluoromethylated α-propargylamines.

Results and Discussion

Drawing from our previous studies on the chemistry of trifluoromethylated sulfinylimine **1** [41-54], the initial reaction conditions focused on the use of 1.3 equiv of 1-ethynyl-4-methoxybenzene (**2a**) in the presence of *n*-BuLi with CH_2Cl_2 as a solvent at −78 °C. The desired product **3a** was obtained after 2.5 hours in 46% yield as a mixture of two diastereomers (55:45 dr, Table 1, entry 1). Fortunately, the diastereomeric products can be quite easily separated by regular column chromatography using hexane/EtOAc (4:1, v/v) as an eluent. Further optimization of the reaction conditions was then carried out to improve both the yield and diastereoselectivity. First, a series of pilot experiments in dichloromethane were performed to scan the base in the reaction. When using LDA and LiHMDS instead of *n*-BuLi, the yields were noticeably increased to 83% and 87%, respectively (Table 1, entries 2 and 3). In particular, the use of LiHMDS resulted in improved diastereoselectivity (69:31 dr, Table 1, entry 3). On the other hand, the solvent was found to show a significant effect on this transformation (Table 1, entries 4–6) and the results indicated dichloromethane was the best choice. Variation of the loading amount of 1-ethynyl-4-methoxybenzene (**2a**) did not provide any improvement on the chemical yield and the stereochemical outcome (Table 1, entries 7 and 8). We also observed a noticeable temperature effect on the reaction yield (Table 1, entries 9 and 10) and −78 °C was proved to be the best choice. Screening of the reaction time revealed that 2.5 hours were necessary for the completion of this transformation (Table 1, entries 11 and 12). Finally, we found that the use of Lewis acids $BF_3{\cdot}Et_2O$ and $Ti(OiPr)_4$ as additives for this reaction was unsuccessful and the same level of chemical yield and diastereoselectivity was observed (Table 1, entries 13 and 14).

With the optimized reaction conditions in hand, we examined the generality of these asymmetric Mannich reactions by using various arylethynes **2** (Scheme 2). Under standard reaction conditions, all the tested substrates worked well to generate the corresponding Mannich adducts in moderate to good yields. In particular, ethynylbenzenes bearing electron-donating substituents on the aromatic ring were more compatible with this reaction, resulting in higher chemical yields (53–87%) and better diastereoselectivities (**3a**–**g**). The ethynylbenzene **2g** featuring a long alkyl chain on *para*-position was also a suitable substrate, which was converted into product **3g** in 77% yield. On the other hand, arylethynes bearing electron-withdrawing groups on the aromatic ring showed lower reactivity along with lower yields (31–55%) as well as poorer diastereoselectivities (**3i**–**m**), except for **3n** which gave 70:30 dr. It should be mentioned that the po-

Table 1: Optimization of reaction conditions.[a]

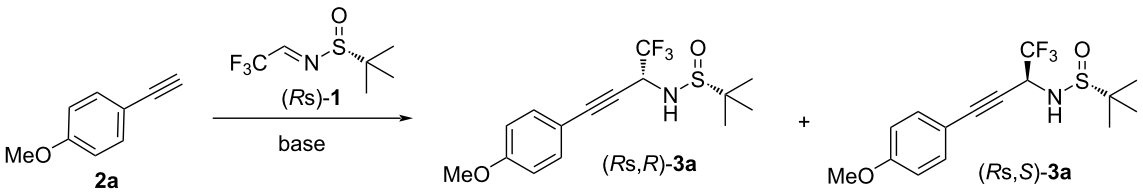

Entry	Base	Solvent	**2a** (equiv)	*T* (°C)	Time (h)	Yield[b] (%)	dr[c]
1	*n*-BuLi	CH_2Cl_2	1.3	−78	2.5	46	55:45
2	LDA	CH_2Cl_2	1.3	−78	2.5	83	66:34
3	LiHMDS	CH_2Cl_2	1.3	−78	2.5	87	69:31
4	LiHMDS	THF	1.3	−78	2.5	57	56:44
5	LiHMDS	$CHCl_3$	1.3	−60	2.5	trace	–
6	LiHMDS	$PhCH_3$	1.3	−78	2.5	45	63:37
7	LiHMDS	CH_2Cl_2	1.1	−78	2.5	85	66:34
8	LiHMDS	CH_2Cl_2	1.6	−78	2.5	79	68:32
9	LiHMDS	CH_2Cl_2	1.3	0	2.5	52	68:32
10	LiHMDS	CH_2Cl_2	1.3	rt	2.5	38	63:37
11	LiHMDS	CH_2Cl_2	1.3	−78	1.0	62	67:33
12	LiHMDS	CH_2Cl_2	1.3	−78	1.5	82	67:33
13[d]	LiHMDS	CH_2Cl_2	1.3	−78	2.5	65	66:34
14[e]	LiHMDS	CH_2Cl_2	1.3	−78	2.5	66	70:30

[a]Reaction conditions: **1** (0.3 mmol), base (1.3 equiv of **2a**), solvent (3 mL), under nitrogen. [b]Isolated yield of two isomers. [c]Determined by ^{19}F NMR. [d]0.5 equiv of $BF_3{\cdot}Et_2O$ was added. [e]0.5 equiv of $Ti(OiPr)_4$ was added.

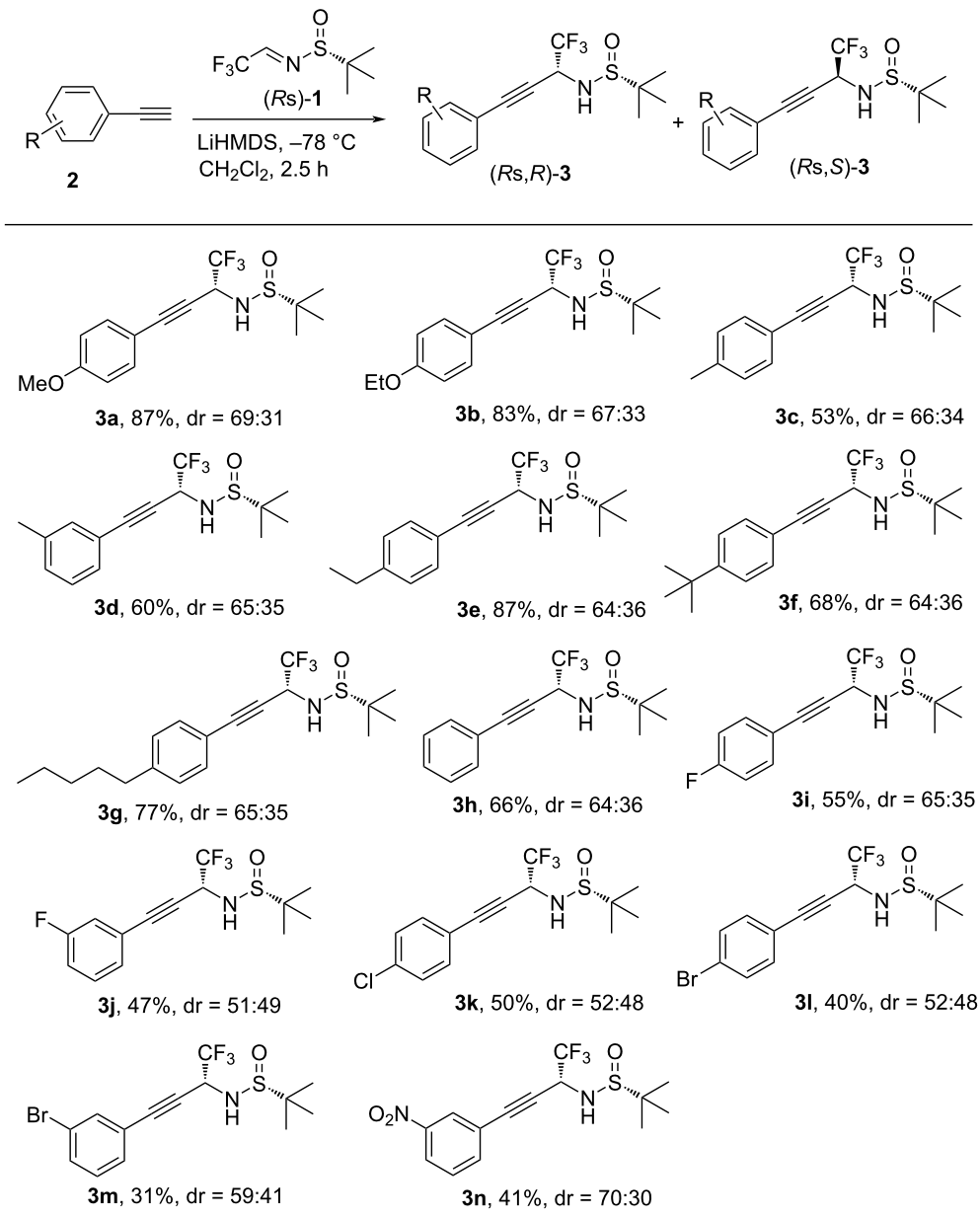

Scheme 2: Substrate scope study. Reaction conditions: arylethyne **2** (0.39 mmol), imine **1** (0.3 mmol), LiHMDS (0.51 mmol), CH_2Cl_2 (3 mL), –78 °C, under nitrogen, 2.5 h. Isolated yields of mixture of isomers. Diastereoselectivities were determined by ^{19}F NMR.

sition of substituents showed almost no effects on the reaction efficiency (**3c** vs **3d**, **3i** vs **3j**, **3l** vs **3m**). Also, importantly, two diastereomers, in all the cases **3a**–**n**, can be readily obtained in diastereomerically pure form by routine column chromatography, underscoring the value of this strategy for the synthesis of chiral α-trifluoromethylated propargylamines.

In order to determine the absolute configuration of the chiral addition products, we successfully performed a crystallographic analysis of the minor product **3a**. The structure is shown in Figure 2, the absolute configuration of the newly generated chiral center of the minor product **3a** is *S*, which demonstrates accordingly that the major one is *R*. The absolute configurations of other corresponding products were assigned by analogy.

In general, the low-to-moderate diastereoselectivity observed in this study was unexpected. In fact, considering the excellent level (>90% de) of stereocontrol reported for the Mannich additions of aldimine **1** with sp^3 [42,55] and sp^2 [56] nucleophiles, including lithiated aromatics [57] one would not anticipate such a dramatic drop in the selectivity in the reactions of sp nucleo-

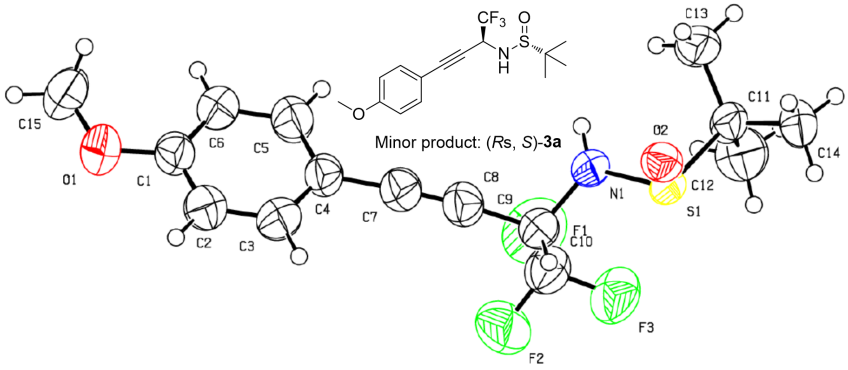

Figure 2: ORTEP diagram showing of the minor product of **3a**.

philes. Accordingly, we considered the mode of nucleophilic attack on the imine double bond in **1**. As presented in Figure 3, imine **1** might react in the most stable conformation with the bulky *tert*-butyl group pointing away from the imine double bond. In this case the only stereocontrolling factor in play is the difference between the sulfinyl oxygen and the oxygen electron lone pair. The latter presents a lesser steric obstacle rendering the corresponding nucleophilic attack the more probable event.

These ever-unexpected results strongly suggest that the origin of the stereocontrol in the reactions of imine **1** is not just the bulk of the *tert*-butyl group but, as a major factor, the corresponding chelated transition states.

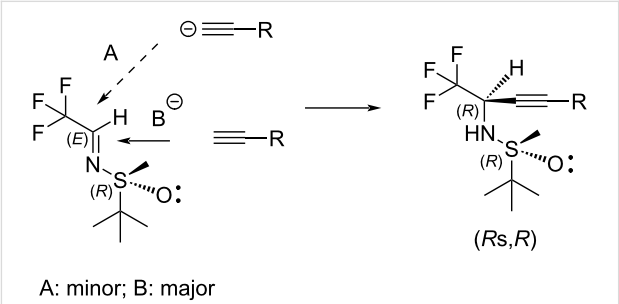

Figure 3: Mode of nucleophilic attacks A and B.

As all diastereomers **3** can be easily isolated in optical pure form by routine column chromatography, this reaction should be of certain value for biological studies. In this regard, we decided to demonstrate the reproducibility of this method for large-scale synthesis (Scheme 3) and the removal of the sulfinyl auxiliary to give the free amine (Scheme 4). To our delight,

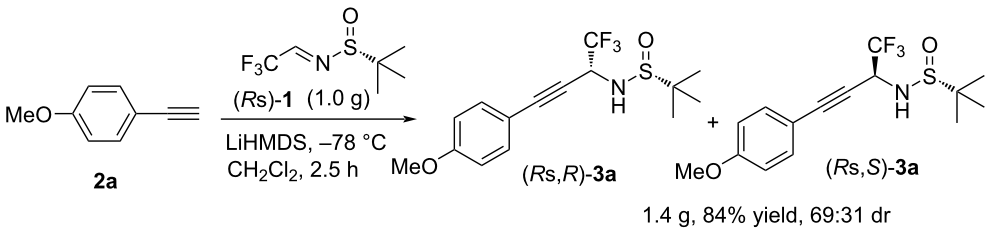

Scheme 3: Large-scale application of the reaction.

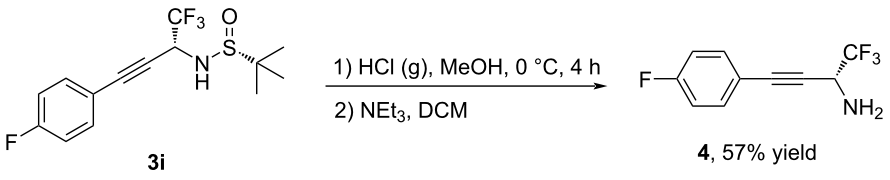

Scheme 4: Removal of the chiral auxiliary.

1.4 g of the desired product **3a** was obtained when the amount of sulfinylimine **1** was raised to 1.0 g (5.0 mmol). Comparing with reaction of 0.3 mmol scale, only a slight decrease in the yield was observed (84%) along with the same stereochemical outcome. Also, the chiral sulfinyl auxiliary can be easily removed under acidic conditions to give the free amine. Treating **3i** with HCl gas in methanol at 0 °C, the *tert*-butylsulfinyl group was cleaved under mild conditions and the target primary amine **4** was obtained with 57% yield.

Conclusion

In conclusion, we have explored arylethynes as new nucleophiles for the Mannich reactions of (*R*)-*N*-*tert*-butylsulfinyl-3,3,3-trifluoroacetaldimine. Quite unexpectedly, the diastereoselectivity of the reactions were noticeably lower when compared with the corresponding reactions of sp^3 and sp^2 nucleophiles. Nevertheless, the two diastereomers can be easily isolated in diastereomerically pure state by regular column chromatography. This method provides access to chiral trifluoromethylpropargylamines. The application of these compounds for the synthesis of biologically relevant targets and their self-disproportionation of enantiomers (SDE) properties [58-60] are currently under study and will be reported in due course.

Experimental

General procedure for the Mannich reaction of arylethynes with sulfinylimine: Into an oven-dried reaction vial flushed with N_2 were taken the respective arylethyne **2** (0.39 mmol) and anhydrous CH_2Cl_2 (2.0 mL). The reaction vial was cooled to −78 °C and LiHMDS (1 M in THF, 0.51 mmol) was added dropwise with stirring. After 1 h at −78 °C, sulfinylimine **1** (0.3 mmol), dissolved in anhydrous CH_2Cl_2 (1.0 mL), was added dropwise. Stirring was continued at −78 °C for 2.5 h, then the reaction was quenched with saturated NH_4Cl (2.0 mL), followed by H_2O (5.0 mL) and the mixture was brought to room temperature. The organic layer was taken and the aqueous layer was extracted with CH_2Cl_2 (3 × 15 mL). The combined organic layers were dried with anhydrous Na_2SO_4, filtered and the solvent was removed to give the crude product **3**, which was purified by column chromatography using hexane/EtOAc (4:1, v/v) as eluent.

Supporting Information

Supporting Information File 1

Experimental details and spectral data.
[https://www.beilstein-journals.org/bjoc/content/supplementary/1860-5397-16-217-S1.pdf]

Funding

We gratefully acknowledge the financial support from the National Natural Science Foundation of China (No. 21761132021) and Qing Lan Project of Jiangsu Province. IKERBASQUE, Basque Foundation for Science (for V. A. Soloshonok) is also acknowledged.

ORCID® iDs

Hiroyuki Konno - https://orcid.org/0000-0002-6629-6102
Hiroki Moriwaki - https://orcid.org/0000-0002-2028-2565
Vadim A. Soloshonok - https://orcid.org/0000-0003-0681-4526
Jianlin Han - https://orcid.org/0000-0002-3817-0764

References

1. Zhou, Y.; Wang, J.; Gu, Z.; Wang, S.; Zhu, W.; Aceña, J. L.; Soloshonok, V. A.; Izawa, K.; Liu, H. *Chem. Rev.* **2016,** *116,* 422–518. doi:10.1021/acs.chemrev.5b00392
2. Wang, J.; Sánchez-Roselló, M.; Aceña, J. L.; del Pozo, C.; Sorochinsky, A. E.; Fustero, S.; Soloshonok, V. A.; Liu, H. *Chem. Rev.* **2014,** *114,* 2432–2506. doi:10.1021/cr4002879
3. Kirk, K. L. *J. Fluorine Chem.* **2006,** *127,* 1013–1029. doi:10.1016/j.jfluchem.2006.06.007
4. Bégué, J.-P.; Bonnet-Delpon, D. *J. Fluorine Chem.* **2006,** *127,* 992–1012. doi:10.1016/j.jfluchem.2006.05.006
5. O'Hagan, D. *J. Fluorine Chem.* **2010,** *131,* 1071–1081. doi:10.1016/j.jfluchem.2010.03.003
6. Mei, H.; Remete, A. M.; Zou, Y.; Moriwaki, H.; Fustero, S.; Kiss, L.; Soloshonok, V. A.; Han, J. *Chin. Chem. Lett.* **2020,** *31,* 2401–2413. doi:10.1016/j.cclet.2020.03.050
7. Mei, H.; Han, J.; Klika, K. D.; Izawa, K.; Sato, T.; Meanwell, N. A.; Soloshonok, V. A. *Eur. J. Med. Chem.* **2020,** *186,* 111826. doi:10.1016/j.ejmech.2019.111826
8. Mei, H.; Han, J.; White, S.; Graham, D. J.; Izawa, K.; Sato, T.; Fustero, S.; Meanwell, N. A.; Soloshonok, V. A. *Chem. – Eur. J.* **2020,** *26,* 11349–11390. doi:10.1002/chem.202000617
9. Zhu, Y.; Han, J.; Wang, J.; Shibata, N.; Sodeoka, M.; Soloshonok, V. A.; Coelho, J. A. S.; Toste, F. D. *Chem. Rev.* **2018,** *118,* 3887–3964. doi:10.1021/acs.chemrev.7b00778
10. Fujiwara, T.; O'Hagan, D. *J. Fluorine Chem.* **2014,** *167,* 16–29. doi:10.1016/j.jfluchem.2014.06.014
11. Isanbor, C.; O'Hagan, D. *J. Fluorine Chem.* **2006,** *127,* 303–319. doi:10.1016/j.jfluchem.2006.01.011
12. Hagmann, W. K. *J. Med. Chem.* **2008,** *51,* 4359–4369. doi:10.1021/jm800219f
13. Aceña, J. L.; Sorochinsky, A. E.; Moriwaki, H.; Sato, T.; Soloshonok, V. A. *J. Fluorine Chem.* **2013,** *155,* 21–38. doi:10.1016/j.jfluchem.2013.06.004
14. Inoue, M.; Sumii, Y.; Shibata, N. *ACS Omega* **2020,** *5,* 10633–10640. doi:10.1021/acsomega.0c00830
15. Zhang, W. *Chem. Rev.* **2009,** *109,* 749–795. doi:10.1021/cr800412s
16. Berger, R.; Resnati, G.; Metrangolo, P.; Weber, E.; Hulliger, J. *Chem. Soc. Rev.* **2011,** *40,* 3496–3508. doi:10.1039/c0cs00221f
17. Hagiwara, R.; Ito, Y. *J. Fluorine Chem.* **2000,** *105,* 221–227. doi:10.1016/s0022-1139(99)00267-5
18. Fang, M.; Okamoto, Y.; Koike, Y.; He, Z.; Merkel, T. C. *J. Fluorine Chem.* **2016,** *188,* 18–22. doi:10.1016/j.jfluchem.2016.05.013

19. Amatucci, G. G.; Pereira, N. *J. Fluorine Chem.* **2007,** *128,* 243–262. doi:10.1016/j.jfluchem.2006.11.016
20. Hoepping, A.; Johnson, K. M.; George, C.; Flippen-Anderson, J.; Kozikowski, A. P. *J. Med. Chem.* **2000,** *43,* 2064–2071. doi:10.1021/jm0001121
21. Davidson, M. H.; McDonald, F. E. *Org. Lett.* **2004,** *6,* 1601–1603. doi:10.1021/ol049630m
22. Trost, B. M.; Chung, C. K.; Pinkerton, A. B. *Angew. Chem., Int. Ed.* **2004,** *43,* 4327–4329. doi:10.1002/anie.200460058
23. Fleming, J. J.; Du Bois, J. *J. Am. Chem. Soc.* **2006,** *128,* 3926–3927. doi:10.1021/ja0608545
24. Llobat, A.; Escorihuela, J.; Sedgwick, D. M.; Rodenes, M.; Román, R.; Soloshonok, V. A.; Han, J.; Medio-Simón, M.; Fustero, S. *Eur. J. Org. Chem.* **2020,** 4193–4207. doi:10.1002/ejoc.202000598
25. Zhu, W.; Wang, J.; Wang, S.; Gu, Z.; Aceña, J. L.; Izawa, K.; Liu, H.; Soloshonok, V. A. *J. Fluorine Chem.* **2014,** *167,* 37–54. doi:10.1016/j.jfluchem.2014.06.026
26. Huang, Y.-Y.; Yang, X.; Chen, Z.; Verpoort, F.; Shibata, N. *Chem. – Eur. J.* **2015,** *21,* 8664–8684. doi:10.1002/chem.201500361
27. Kauffman, G. S.; Harris, G. D.; Dorow, R. L.; Stone, B. R. P.; Parsons, R. L.; Pesti, J. A.; Magnus, N. A.; Fortunak, J. M.; Confalone, P. N.; Nugent, W. A. *Org. Lett.* **2000,** *2,* 3119–3121. doi:10.1021/ol006321x
28. Crucianelli, M.; Angelis, F. D.; Lazzaro, F.; Malpezzi, L.; Volonterio, A.; Zanda, M. *J. Fluorine Chem.* **2004,** *125,* 573–577. doi:10.1016/j.jfluchem.2003.11.034
29. Jiang, B.; Si, Y.-G. *Angew. Chem., Int. Ed.* **2004,** *43,* 216–218. doi:10.1002/anie.200352301
30. Zhang, F.-G.; Ma, H.; Nie, J.; Zheng, Y.; Gao, Q.; Ma, J.-A. *Adv. Synth. Catal.* **2012,** *354,* 1422–1428. doi:10.1002/adsc.201100926
31. Zhang, F.-G.; Ma, H.; Zheng, Y.; Ma, J.-A. *Tetrahedron* **2012,** *68,* 7663–7669. doi:10.1016/j.tet.2012.05.086
32. Morisaki, K.; Sawa, M.; Nomaguchi, J.-y.; Morimoto, H.; Takeuchi, Y.; Mashima, K.; Ohshima, T. *Chem. – Eur. J.* **2013,** *19,* 8417–8420. doi:10.1002/chem.201301237
33. Chen, M.-W.; Wu, B.; Chen, Z.-P.; Shi, L.; Zhou, Y.-G. *Org. Lett.* **2016,** *18,* 4650–4653. doi:10.1021/acs.orglett.6b02283
34. Chen, M.-W.; Yang, Q.; Deng, Z.; Zhou, Y.; Ding, Q.; Peng, Y. *J. Org. Chem.* **2018,** *83,* 8688–8694. doi:10.1021/acs.joc.8b00873
35. Xiao, H.; Huang, Y.; Qing, F.-L. *Tetrahedron: Asymmetry* **2010,** *21,* 2949–2955. doi:10.1016/j.tetasy.2010.11.028
36. Xie, C.; Wu, L.; Han, J.; Soloshonok, V. A.; Pan, Y. *Angew. Chem., Int. Ed.* **2015,** *54,* 6019–6023. doi:10.1002/anie.201500908
37. Han, J.; Sorochinsky, A. E.; Ono, T.; Soloshonok, V. A. *Curr. Org. Synth.* **2011,** *8,* 281–294. doi:10.2174/157017911794697277
38. Xie, C.; Zhang, L.; Sha, W.; Soloshonok, V. A.; Han, J.; Pan, Y. *Org. Lett.* **2016,** *18,* 3270–3273. doi:10.1021/acs.orglett.6b01516
39. Xie, C.; Dai, Y.; Mei, H.; Han, J.; Soloshonok, V. A.; Pan, Y. *Chem. Commun.* **2015,** *51,* 9149–9152. doi:10.1039/c5cc02256h
40. Xie, C.; Wu, L.; Mei, H.; Soloshonok, V. A.; Han, J.; Pan, Y. *Tetrahedron Lett.* **2014,** *55,* 5908–5910. doi:10.1016/j.tetlet.2014.09.001
41. Xie, C.; Wu, L.; Mei, H.; Soloshonok, V. A.; Han, J.; Pan, Y. *Org. Biomol. Chem.* **2014,** *12,* 7836–7843. doi:10.1039/c4ob01575d
42. Mei, H.; Xiong, Y.; Han, J.; Pan, Y. *Org. Biomol. Chem.* **2011,** *9,* 1402–1406. doi:10.1039/c0ob00586j
43. Xie, C.; Mei, H.; Wu, L.; Soloshonok, V. A.; Han, J.; Pan, Y. *RSC Adv.* **2014,** *4,* 4763–4768. doi:10.1039/c3ra45773g
44. Mei, H.; Xie, C.; Wu, L.; Soloshonok, V. A.; Han, J.; Pan, Y. *Org. Biomol. Chem.* **2013,** *11,* 8018–8021. doi:10.1039/c3ob41785a
45. Mei, H.; Xiong, Y.; Xie, C.; Soloshonok, V. A.; Han, J.; Pan, Y. *Org. Biomol. Chem.* **2014,** *12,* 2108–2113. doi:10.1039/c3ob42348d
46. Liu, Y.; Huang, Y.; Qing, F.-L. *Tetrahedron* **2012,** *68,* 4955–4961. doi:10.1016/j.tet.2012.04.070
47. Liu, Y.; Yang, Y.; Huang, Y.; Xu, X.-H.; Qing, F. L. *Synlett* **2015,** *26,* 67–72. doi:10.1055/s-0034-1379600
48. Shibata, N.; Nishimine, T.; Tokunaga, E.; Kawada, K.; Kagawa, T.; Sorochinsky, A. E.; Soloshonok, V. A. *Chem. Commun.* **2012,** *48,* 4124–4126. doi:10.1039/c2cc30627a
49. Mei, H.; Xie, C.; Han, J.; Soloshonok, V. A. *Eur. J. Org. Chem.* **2016,** 5917–5932. doi:10.1002/ejoc.201600578
50. Mei, H.; Han, J.; Fustero, S.; Román, R.; Ruzziconi, R.; Soloshonok, V. A. *J. Fluorine Chem.* **2018,** *216,* 57–70. doi:10.1016/j.jfluchem.2018.10.003
51. Robak, M. T.; Herbage, M. A.; Ellman, J. A. *Chem. Rev.* **2010,** *110,* 3600–3740. doi:10.1021/cr900382t
52. Liu, P.; Liu, Z.-J.; Wu, F. *Adv. Synth. Catal.* **2015,** *357,* 818–822. doi:10.1002/adsc.201400992
53. Boerth, J. A.; Hummel, J. R.; Ellman, J. A. *Angew. Chem., Int. Ed.* **2016,** *55,* 12650–12654. doi:10.1002/anie.201603831
54. Sanz-Vidal, Á.; Torres, J.; Soloshonok, V. A.; Zhu, Y.; Han, J.; Fustero, S.; del Pozo, C. *Adv. Synth. Catal.* **2018,** *360,* 366–373. doi:10.1002/adsc.201701284
55. Shevchuk, M. V.; Kukhar, V. P.; Röschenthaler, G.-V.; Bassil, B. S.; Kawada, K.; Soloshonok, V. A.; Sorochinsky, A. E. *RSC Adv.* **2013,** *3,* 6479. doi:10.1039/c3ra40687c
56. Wu, L.; Xie, C.; Mei, H.; Soloshonok, V. A.; Han, J.; Pan, Y. *J. Org. Chem.* **2014,** *79,* 7677–7681. doi:10.1021/jo5012009
57. Mei, H.; Dai, Y.; Wu, L.; Soloshonok, V. A.; Han, J.; Pan, Y. *Eur. J. Org. Chem.* **2014,** 2429–2433. doi:10.1002/ejoc.201400118
58. Sorochinsky, A. E.; Katagiri, T.; Ono, T.; Wzorek, A.; Aceña, J. L.; Soloshonok, V. A. *Chirality* **2013,** *25,* 365–368. doi:10.1002/chir.22180
59. Sorochinsky, A. E.; Aceña, J. L.; Soloshonok, V. A. *Synthesis* **2013,** *45,* 141–152. doi:10.1055/s-0032-1316812
60. Han, J.; Nelson, D. J.; Sorochinsky, A. E.; Soloshonok, V. A. *Curr. Org. Synth.* **2011,** *8,* 310–317. doi:10.2174/157017911794697303

License and Terms

This is an Open Access article under the terms of the Creative Commons Attribution License (https://creativecommons.org/licenses/by/4.0). Please note that the reuse, redistribution and reproduction in particular requires that the authors and source are credited.

The license is subject to the *Beilstein Journal of Organic Chemistry* terms and conditions: (https://www.beilstein-journals.org/bjoc)

The definitive version of this article is the electronic one which can be found at: https://doi.org/10.3762/bjoc.16.217

BEILSTEIN JOURNAL OF ORGANIC CHEMISTRY

Synthesis of purines and adenines containing the hexafluoroisopropyl group

Viacheslav Petrov[*,‡1], Rebecca J. Dooley[‡2], Alexander A. Marchione[‡2], Elizabeth L. Diaz[3], Brittany S. Clem[‡2] and William Marshall[‡3]

Full Research Paper

Open Access

Address:
[1]Chemours Co. Fluoroproducts, Chemours Discovery Hub N2-136S, 201 Discovery Blvd, Newark, DE 19713, USA, [2]Chemours Co. Fluoroproducts, Chemours Discovery Hub, 201 Discovery Blvd, Newark, DE 19713, USA and [3]DuPont Corporate Center for Analytical Sciences, Experimental Station, P.O. Box 80500, Wilmington, DE 19880-0500, USA

Email:
Viacheslav Petrov[*] - viacheslav.petrov@chemours.com

* Corresponding author ‡ Equal contributors

Keywords:
adenine; caffeine; cyclic dimer of hexafluorothioacetone; hexafluoroisopropyl group; purine; 2,2,4,4-tetrakis(trifluoromethyl)-1,3-dithietane; theophylline

Beilstein J. Org. Chem. **2020,** *16,* 2739–2748.
https://doi.org/10.3762/bjoc.16.224

Received: 25 July 2020
Accepted: 27 October 2020
Published: 11 November 2020

This article is part of the thematic issue "Organo-fluorine chemistry V".

Guest Editor: D. O'Hagan

© 2020 Petrov et al.; licensee Beilstein-Institut.
License and terms: see end of document.

Abstract

Several new derivatives of adenine, purine, and theophylline containing the $(CF_3)_2CH$ group connected to a nitrogen atom of the imidazole ring were prepared by the reaction of 2,2,4,4-tetrakis(trifluoromethyl)-1,3-dithietane (**1**) with the corresponding substrates, resulting in the selective alkylation of one of the nitrogen atoms of the imidazole ring. The reaction proceeds under mild conditions in a polar solvent, giving the alkylated products in 47–78% yield. While for purine and 4- and 5-azabenzimidazole, the reaction led to a mixture of two isomers, the reaction of adenine and the corresponding 2-fluoro derivative was regioselective, resulting in the formation of only one isomer in each case. The alkylation of theophylline led to the formation of a new derivative of caffeine.

Introduction

Despite significant progress in the last 20–30 years, the selective introduction of fluorine and polyfluoroalkyl substituents into organic molecules remains a challenging problem in the synthesis of fluorinated biologically active compounds, especially larger moieties, such as C_2F_5, $CF(CF_3)_2$, and $CH(CF_3)_2$. With respect to the hexafluoroisopropyl group, the methods are limited to a relatively short list: the reduction of the OH group of the $C(CF_3)_2OH$ moiety (this protocol was employed in the synthesis of enantiomerically pure (*S*)-5,5,5,5',5',5'-hexafluoroleucine [1]); the Wittig reaction of $Ph_3P{=}C(O)C(O)OR$ with hexafluoroacetone, followed by the hydrogenation of the $CH{=}C(CF_3)_2$ unit, and the conversion of the ketoester into an

amino acid [2]; and the reaction of aldehydes with either $Ph_3P/(CF_3)_2CCl_2$ [3] or 2,2,4,4-tetrakis(trifluoromethyl)-1,3-dithietane [4,5]. The last method was employed in the synthesis of 16,16,16,17,17,17-hexafluororetinal, as reported by the Haas group [5].

Benzimidazoles are an important class of organic materials, and many derivatives of these group are biologically active [6-9]. The benzimidazole moiety " […] is isosteric with indole and purine nuclei, which are present in a number of fundamental cellular components and bioactive compounds. Indeed, a number of important drugs used in different therapeutic areas contain the benzimidazole ring […], such as proton pump inhibitors (omeprazole), antihypertensives (candesartan, telmisartan), antihistaminics (astemizole), antihelmintics (albendazole, mebendazole), as well as several other kinds of still investigational therapeutic agents, including antitumorals and antivirals […]" [8].

Interestingly, most fluorine-containing benzimidazoles contain the fluorinated substituent either on the aromatic ring or on a side chain connected to the aromatic ring; examples of benzimidazoles containing a fluoroalkyl group connected to a nitrogen atom of the imidazole segment are relatively rare. Known examples include benzimidazoles carrying NCF_3 [10], NCF_2H [11-13], NR_f (R_f = CF_2Cl, CF_2Br, CF_2CFClH, CF=CFClF) [14,15], and hexafluoroisopropyl groups attached to the nitrogen atom [16]. Recently, we reported a new method for the introduction of a hexafluoroisopropyl group based on the reaction of tetrakis(trifluoromethyl)-1,3-dithietane (**1**) with the corresponding azoles [17]. Since this methodology is simple and works for a wide variety of imidazoles, including benzimidazole, we decided to explore the applicability of this method to the modification of biologically active imidazoles, such as adenine and purine derivatives. The results of this study are reported in this article.

Results and Discussion

Despite the presence of two electron-withdrawing nitrogen atoms in the aromatic ring, purine (**2**) was found to react with tetrakis(trifluoromethyl)-1,3-dithietane (**1**) in a manner similar to benzimidazole [17]. The reaction proceeds without catalyst in DMSO solvent at ambient temperature, leading to the formation of 7- and 9-(hexafluoroisopropyl)purine (**2a** and **2b**), respectively, along with the formation of one equivalent of elemental sulfur (Scheme 1).

A crude mixture of **2a** and **2b** (ratio 70:30) was isolated in 78% yield. Since the minor isomer **2b** had a significantly higher solubility in hexane, washing of the crude mixture with hexane resulted in an enrichment of the major isomer **2a** (ratio **2a**/**2b** 95:5 after washing with hexane). Pure **2a** was isolated after recrystallization from hexane (see Experimental section), and the structure was established by X-ray diffraction (Figure 1).

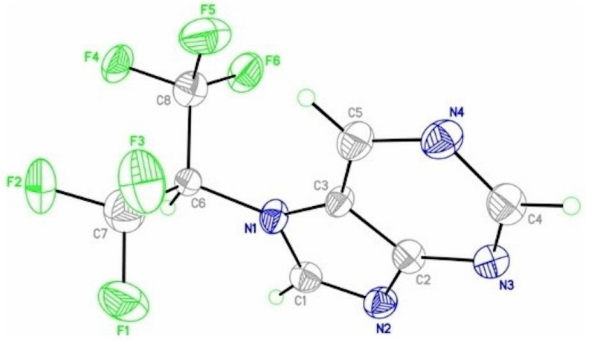

Figure 1: Crystal structure of **2a**, with the thermal ellipsoids drawn at 30% probability.

4-Azabenzimidazole (**3**) reacted with tetrakis(trifluoromethyl)-1,3-dithietane (**1**) under similar conditions, with the formation of the two isomeric products **3a** and **3b** (Scheme 2).

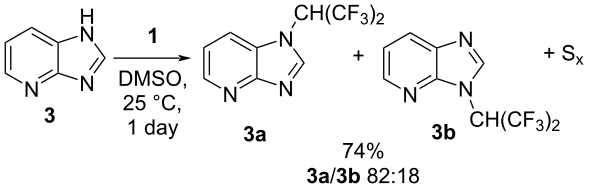

Scheme 2: Reaction of 4-azabenzimidazole (**3**) with tetrakis(trifluoromethyl)-1,3-dithietane (**1**).

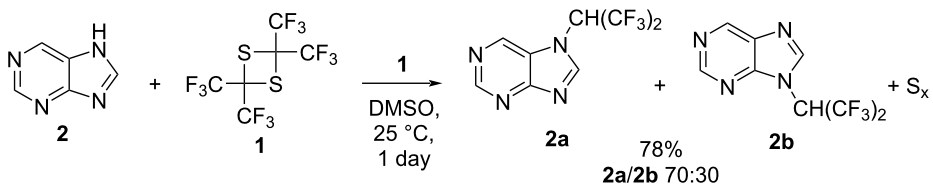

Scheme 1: Reaction of purine (**2**) with tetrakis(trifluoromethyl)-1,3-dithietane (**1**).

The major isomer **3a** was isolated in a pure form, and the structure was confirmed by X-ray diffraction. It should be pointed out that the ^{19}F NMR spectra of the two isomers were very different. While the resonance corresponding to the $CH(CF_3)_2$ group in the spectrum of **3b** was a sharp and well-resolved doublet (δ = −69.95 ppm, J_{FH} = 6.9 Hz in $CDCl_3$), the analogous resonance in the major isomer **3a** was significantly broadened (δ = −68.95 ppm, $\Delta\sqrt{}_{1/2}$ = 60Hz, $CDCl_3$), indicating a restricted rotation around the C–N bond, likely due to the steric interaction of the CF_3 groups of the hexafluoroisopropyl fragment with the neighboring hydrogen atom of the pyridine ring. A similar phenomenon was previously observed for *N*-(hexafluoroisopropyl)benzimidazole [17].

5-Azabenzimidazole (**4**) reacted similarly with tetrakis(trifluoromethyl)-1,3-dithietane (**1**), which also resulted in the formation of two regioisomers, **4a** and **4b** (Scheme 3).

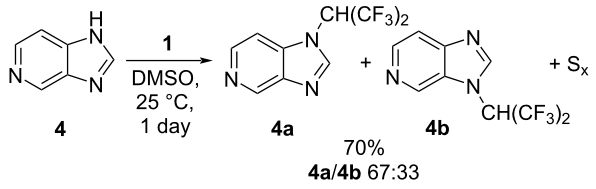

Scheme 3: Reaction of 5-azabenzimidazole (**4**) with **1**.

In this context, the isomers **4a** and **4b** were separated by column chromatography (see Experimental section), and the structure of both was established by X-ray diffraction. In the ^{19}F NMR spectra of both isomers **4a** and **4b**, the resonances corresponding to the $CH(CF_3)_2$ group were significantly broadened.

While all attempts to involve guanine in the reaction with **1** failed (DMSO, 25–70 °C, 4 d), the reaction of adenine (**5**) or 2-fluoroadenine (**6**) with tetrakis(trifluoromethyl)-1,3-dithietane (**1**) was found to proceed under mild conditions (DMSO, 25 °C, 1 d), leading (unexpectedly) to the formation of only one isomer (**5a** and **6a**, respectively) in each case (Scheme 4).

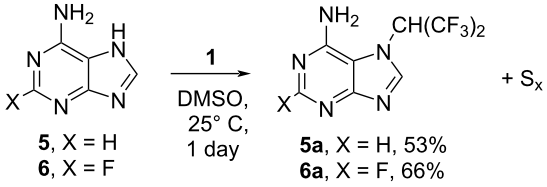

Scheme 4: Reaction of adenine (**5**) and 2-fluoroadenine (**6**) with tetrakis(trifluoromethyl)-1,3-dithietane (**1**).

Another surprising feature of these reactions was the selective alkylation of the nitrogen atoms of the imidazole ring rather than the amino group. This is in sharp contrast to the report by Ishikawa and Kitazume that the reaction of anilines with tetrakis(trifluoromethyl)-1,3-dithietane (**1**) results in the formation of the corresponding imines of hexafluoroacetone [18]. Unfortunately, we were not able to confirm the structures by X-ray diffraction, and the structural assignment for the compounds **5a** and **6a** relies solely on NMR data. In both cases, the data were consistent with the structures **5a** or **6a**, carrying NH_2 and $CH(CF_3)_2$ groups on the same side of the molecule. Indeed, in the ^{19}F NMR spectra of **5a** and **6a**, the resonance corresponding to $CH(CF_3)_2$ was significantly broadened (**5a**: $\Delta\sqrt{}_{1/2}$ = 150 Hz; **6a**: $\Delta\sqrt{}_{1/2}$ = 50 Hz), and in the ^{1}H NMR spectrum of **6a**, the ^{1}H nuclei of the NH_2 group were observed as two separate resonances, with significantly different chemical shifts (δ = 1.66 (br. s) and 5.98 ppm (1H, br. s) in $CDCl_3$ solvent, while in DMSO-d_6, only one broad resonance (δ = 7.69 ppm, 2H, br. s) was observed for the NH_2 group. We believe that these observations are consistent with the restricted rotation of the $CH(CF_3)_2$ group because of the proximity to the amino group.

Theobromine or caffeine both were found to be inert towards tetrakis(trifluoromethyl)-1,3-dithietane (**1**) – even at elevated temperature (65 °C, 4–6 d, DMSO or DMF) or in the presence of a catalyst (CsF, DMSO, 25 °C, 2 d), but the structurally similar theophylline (**7**) reacted with **1** in the presence of CsF catalyst, producing a mixture of the two isomers **7a** and **7b**, with a significant predominance of **7a** (Scheme 5).

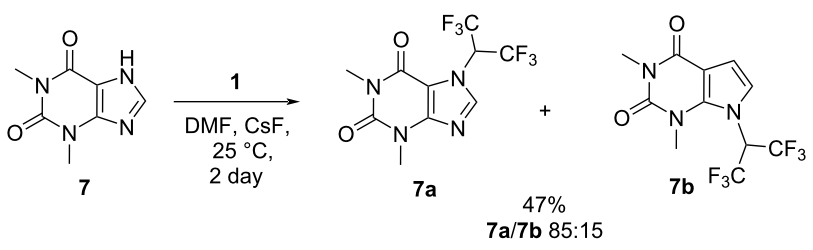

Scheme 5: Reaction of theophylline (**7**) with tetrakis(trifluoromethyl)-1,3-dithietane (**1**).

The major isomer **7a** was isolated by recrystallization from hexane, and the structure was unambiguously established by X-ray diffraction (Figure 2).

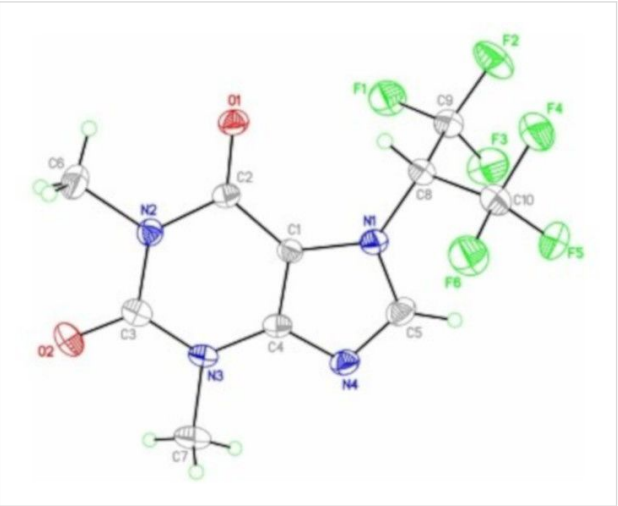

Figure 2: Crystal structure of **7a**, with the thermal ellipsoids drawn at 30% probability.

Exchange broadening of the resonances of the $(CF_3)_2CH$ group was not observed in the ^{19}F NMR spectra of **7a** and **7b**.

Compound **7a** can be viewed as a caffeine analogue, modified by the attachment of two CF_3 groups to the methyl group. This is the first example of an introduction of a fluoroalkyl group bigger than CF_3 or CF_2H into a theophylline (**7**) molecule, since known examples of fluorinated caffeine derivatives are limited to 7-trifluoromethyl caffeine, claimed in the patent literature [19,20] and 7-difluoromethyl caffeine, prepared by the insertion of difluorocarbene into the N–H bond of theophylline (**7**) [11,21,22]. Similar to the reaction of tetrakis(trifluoromethyl)-1,3-dithietane (**1**) and theophylline (**7**, Scheme 5), this process also led to the formation of two regioisomers, but interestingly, the ratio of the 7-CF_2H- and 9-CF_2H-isomers varied broadly from 1:2 [22] to 3:2, depending on the reaction conditions and the source of difluorocarbene [11].

Mechanism, regiochemistry, and rotation barriers of the $CH(CF_3)_2$ group

The mechanism of the reaction of tetrakis(trifluoromethyl)-1,3-dithietane (**1**) with the azoles **2**–**7** is not entirely clear. Although there are two similar reactions reported in the literature (the reaction of **1** with anilines [18] and azoles [17]), no satisfactory mechanism was suggested for these reactions. Recently, it was demonstrated that the majority of the reactions of **1** can involve monomeric hexafluorothioacetone (HFTA) as long as the reaction is carried out in a polar and nucleophilic solvent, such as DMF or DMSO [23]. One can speculate that an alternative mechanism may involve the interaction of monomeric HFTA and imidazole. In this case, the reaction can proceed through the attack of a nitrogen atom of the imidazole ring at the carbon atom of the C=S bond, leading to the formation of the zwitterion **B** (Scheme 6).

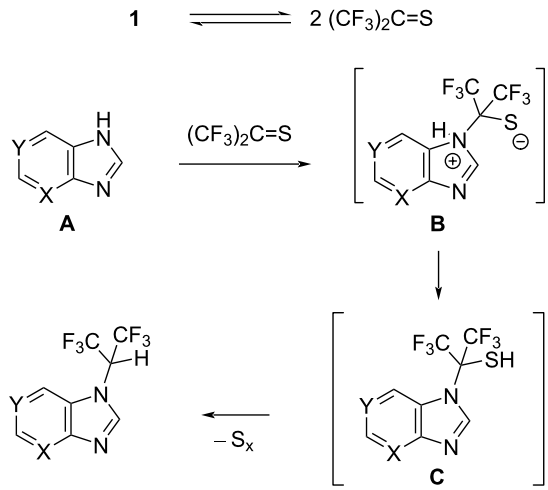

Scheme 6: Probable mechanism of the reaction of tetrakis(trifluoromethyl)-1,3-dithietane (**1**) with compounds **2**–**7**.

The transfer of a proton from the nitrogen atom to the sulfur atom leads to the formation of thiol **C**, which can lose sulfur, giving rise to the final product. Because of the unsymmetrical nature of substrate **A**, the attack on the C=S bond of HFTA proceeds by either nitrogen atom of the imidazole ring, resulting in the formation of two isomers for compounds **2**–**4** and **7**. The highly selective reaction of adenines **5** and **6** may reflect a significantly higher nucleophilicity of the nitrogen atom of the imidazole ring versus that of the NH_2 group.

It should be pointed out that the mechanism depicted in Scheme 6 is highly speculative since the nature of the last step (the conversion of intermediate **C** into the final product, with extrusion of elemental sulfur) is not well understood and may be more complex, involving additional steps. The mechanism clarification of the reaction of tetrakis(trifluoromethyl)-1,3-dithietane (**1**) with azoles (and anilines) does require further investigation.

As was mentioned above, the broadening of the resonances corresponding to the CF_3 group as observed in the ^{19}F NMR spectra of derivatives **3a**, **4a**, and **4b** at ambient temperature is likely to be related to a restricted rotation around the C–N bond as a result of the steric interaction between the fluorine atoms of the $(CF_3)_2CH$ group and a neighboring hydrogen of an aromatic ring. Indeed, a similar phenomenon was observed for benz-

imidazole carrying a $CH(CF_3)_2$ group at a nitrogen atom of the imidazole ring [17]. Another argument in favor of this explanation is the absence of any evidence for the restricted rotation in the isomer **3b** (Scheme 2), which has a nitrogen atom in the β-position relative to the $CH(CF_3)_2$ group (see Table 1), while signal broadening was clearly present in the ^{19}F NMR spectra of both isomers **4a** and **4b**. All these data are consistent with the observed restricted rotation of the $(CF_3)_2CH$ group in compounds **5a** and **6a** (see Table 2) because of the presence in the β-position relative to the $CH(CF_3)_2$ unit of the amino group, which is substantially bigger than a hydrogen atom.

Dynamic NMR spectroscopy

The broadening of resonances corresponding to the hexafluoroisopropyl moieties in the ^{19}F NMR spectra described above was observed at near-ambient temperatures and at resonance frequencies from 376 to 564 MHz, consistent with a slow exchange between rotameric states on the NMR timescale under these conditions. The activation parameters of the hindered rotation were obtained for a subset of these compounds, **3a**, **4a**, **4b**, and **6a**, by NMR experiments similar to those used in recent studies [24]. In brief, solutions of each compound were made in *N*,*N*-dimethylformamide-d_7. A series of ^{19}F NMR spectra were acquired at subambient temperature: both simple one-dimensional spectra and selective inversion spectra, in which the resonance corresponding to one rotamer was selectively inverted, allowed to interconvert with the other site for a variable period and then converted to observable magnetization with an excitation pulse. The former experiments allowed an assay of the population of each site as a function of the temperature, which enabled an extrapolation of the population differences at an elevated temperature (via the van 't Hoff equation). The latter experiments provided information directly on the kinetics of the interconversion between the sites. A series of spectra were then acquired at elevated temperature; here, the kinetics of the interconversion between the sites could be derived directly from the linewidth. Figure 3 illustrates the spectra acquired over a range of temperatures using compound **3a** as an example. With the rate constants of the interconversion between the rotamers in hand, an Eyring plot was generated, and the enthalpy and entropy of activation were derived (Table 2).

The structural identification of the major and minor rotamers was not attempted by NMR, but in silico investigations of **3a** supported the intuitive notion that the rotamer of lower energy was that with the CF_3 moieties nearer the five-membered ring of the azabenzimidazole unit, and the rotamer of higher energy was that with the CF_3 moieties near the six-membered ring (see

Table 1: Reaction products, conditions, yield, ratio of isomers, and melting points for the new materials.

compound	solvent (cat.)	*T*, °C (time, d)	yield, %	ratio of isomers (crude product)	mp, °C (crude product)	mp, °C (recrystallized from hexane)
2a	DMSO	25 (1)	78	**2a**/**2b** 70:30	158–167	–
2b						**2b**, 122–123
3a,**b**	DMSO	25 (1)	74	**3a**/**3b** 82:18	137–163	**3a**, 164–165
4a,**b**	DMSO	25 (1)	70	**4a**/**4b** 67:33	–	**4a**, 157–158 **4b**, 110–111
5a	DMSO	25 (1)	53	one isomer	212–214 (dec.)	**5a**, 214–216 (dec.)
6a	DMSO	25 (1)	66	one isomer	–	**6a**, 220–222
7a,**b**	DMF (CsF)	25 (4)	47	**7a**/**7b** 85:15	86–88	**7a**, 95–95.5 (purity 98%)

Table 2: Enthalpy and entropy of activation for the rotameric interconversion of a subset of hexafluoroisopropyl azoles.

compound	$\Delta H^{\ddagger}$, major to minor (kcal·mol^{-1})	$\Delta S^{\ddagger}$, major to minor (cal·mol^{-1} K^{-1})	$\Delta H^{\ddagger}$, minor to major (kcal·mol^{-1})	$\Delta S^{\ddagger}$, minor to major (cal·mol^{-1} K^{-1})	population of the major rotamer at 298 K
3a	11.6	–5.38	11.1	–5.90	0.691
4a	12.0	–4.12	11.5	–3.67	0.760
4b	11.6	–5.91	10.6	–7.76	0.680
6a	12.0	–3.72	9.79	–7.09	0.862

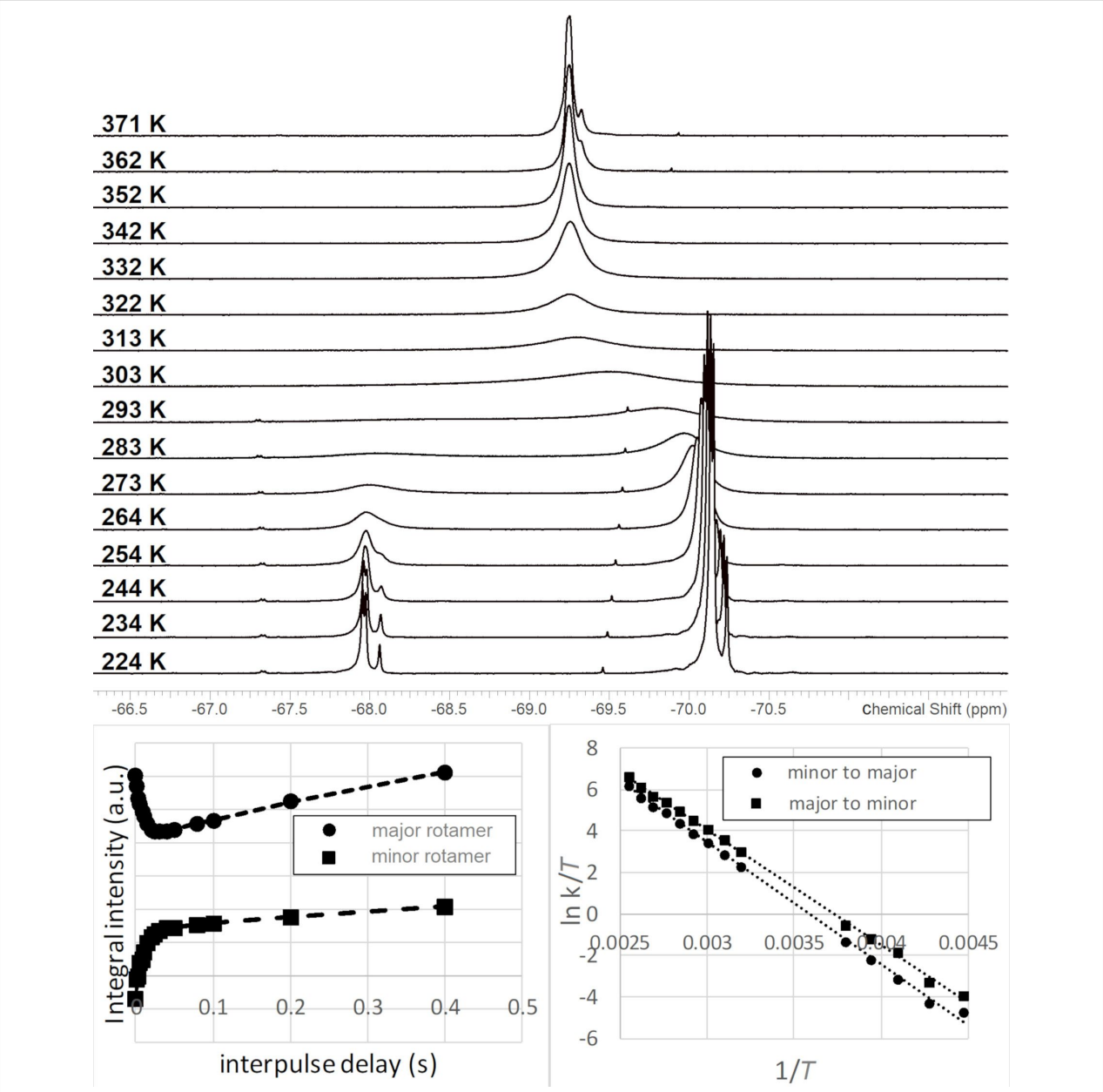

Figure 3: Top: ^{19}F NMR spectra of **3a** acquired over a sample temperature range of 223–373 K. Left: Fitted plot of integrated intensity vs interpulse delay time from the experiment inverting the minor rotamer of **3a** at 253 K. Right: Eyring plot of the interconversion of the rotamers of **3a**.

Figure 4). Density functional theory calculations predict an enthalpy difference of 0.48 kcal·mol^{-1} between the two rotamers. By comparison, ΔH between the two rotamers was obtained experimentally by fitting the van 't Hoff equation to the population differences observed in the ^{19}F NMR spectra between 224 and 264 K. 0.89 kcal·mol^{-1} is in tolerable agreement with the computation.

Comparing **3a**, **4a**, **4b**, and **6a** in Table 2, the enhanced imbalance in the population of the rotamers of **6a** is notable and consistent with the amino moiety imposing a greater steric

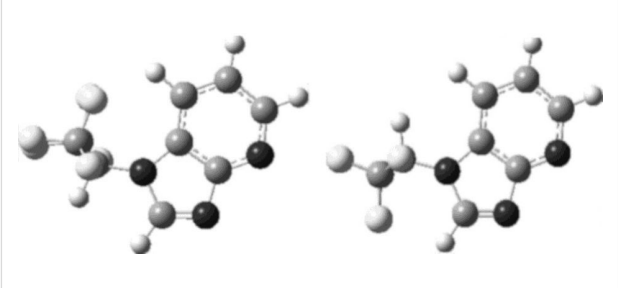

Figure 4: DFT-optimized structures of the two rotamers of **3a**. Left: Lower-energy rotamer. Right: Higher-energy rotamer.

hindrance. The differences among the other compounds are more modest. The small entropy of activation is consistent with a simple rotation over a steric barrier (with minimal contribution from such forces as hydrogen bonding or solvent interactions), and the relative enthalpy of activation for each compound (major to minor vs minor to major) are roughly similar to the difference in total enthalpy for the two rotamers for each compound.

Experimental

GC and GC–MS analyses were carried out on a HP-6890 instrument using a HP FFAP capillary column and either TCD (GC) or mass-selective detectors (GS–MS), respectively. Purine (**2**), 4-aza- and 5-azabenzimidazole (**3** and **4**), adenine (**5**), theophylline (**7**), dry DMF, and DMSO were obtained from commercial source (Sigma-Aldrich) and used without further purification. CsF (Sigma-Aldrich) was dried in vacuum and stored and handled inside a glove box. Compound **1** was prepared according to a literature procedure [24], purity 96–98% and was used without further purification. The purity of the new materials, determined by GC and NMR spectroscopy, was at least 99%, unless stated otherwise.

Standard NMR experiments

The NMR data presented in Table 2 and Table 3 were derived from spectra acquired on a Bruker Neo spectrometer with a 9.4 T magnetic field, equipped with a 5 mm $^{15}N,^{77}Se$, ^{31}P $\{^{19}F,^{1}H\}$ nitrogen cryoprobe. Chemical shifts are refer-

Table 3: NMR and MS data for the compounds **2a**,**b**, **3a**,**b**, **4a**,**b**, **5a**, **6a**, and **7a**,**b**.

compound	^{1}H NMR (in $CDCl_3$, δ, ppm; *J*, Hz)	^{19}F NMR (in $CDCl_3$, δ, ppm; *J*, Hz)	^{13}C NMR (δ, ppm; *J*, Hz)[a]	MS (*m*/*z*)[b]
2a	5.55 (1H, sept, 6.5), 8.40 (1H, s), 9.08 (1H, s), 9.28 (1H, s)	–68.75 (d, 6.6)	–	270 (M^+, $C_8H_4F_6N_4^+$)
2b	6.08 (1H, sept, 7.0), 8.33 (1H, s), 9.09 (1H, s), 9.30 (1H, s)	–69.75 (d, 7.0)	55.07 (sept, 33.7), 120.51 (q, 283.8), 133.87, 141.75 (sept, 1.5), 149.83, 151.43, 153.80	270 (M^+, $C_8H_4F_6N_4^+$)
3a	5.63 (1H, sept, 6.7), 7.40 (1H, dd, 8.4, 4.7), 7.89 (1H, d, 8.4), 8.37 (1H, s), 8.70 (1H, d, 4.7)	–68.95 (br. s, $\Delta\sqrt{}_{1/2}$ = 60 Hz)	52.50 (br. s), 118.99, 119.61, 121.61 (q, 287.00), 144.00, 146.01, 159.81, 205.22	269 (M^+, $C_9H_5F_6N_3^+$)
3b	6.18 (1H, sept), 7.40 (1H), 8.25 (1H), 8.37 (1H), 8.50 (1H)	–69.95 (d, 6.9)	–	–
4a	5.46 (sept, 6.7), 7.41 (1H, d, 5.7), 8.15 (1H, s), 8.61 (1H, d, 5.7), 9.24 (1H, s)	–69.15 (br. s)	58.38 (sept, 32.8), 115.74, 120.78 (q, 284.4), 131.28, 132.90, 143.65, 144.00, 148.35	269 (M^+, $C_9H_5F_6N_3^+$)
4b	5.46 (sept, 6.7), 7.41 (1H, d, 5.7), 8.15 (1H, s), 8.61 (1H, d, 5.7), 9.24 (1H, s)	–69.08 (br. s)	58.10 (sept, 33.2), 104.64, 120.77 (q, 284.4), 138.78, 139.97, 142.11, 144.06, 144.09	–
5a	5.67 (2H, br. s), 5.95 (1H, sept, 7.2), 8.02 (1H, s), 8.48 (1H, s); DMSO-d_6: 7.23 (1H, sept, 7.2 Hz), 7.64 (2H, s), 8.27 (1H, s), 8.42 (1H, s)	–69.08 (br. s, $\Delta\sqrt{}_{1/2}$ > 150 Hz); DMSO-d_6: –69.88 (br. s, $\Delta\sqrt{}_{1/2}$ > 150 Hz)	55.03 (sept, 33.0), 117.93, 121.44 (q, 282.0), 138.87, 150.41, 154.27, 156.20[c]	285 (M^+, $C_8H_5F_6N_5^+$)
6a	1.66 (1H, br. s), 5.81 (1H, sept, 7.2), 5.98 (1H, br. s), 7.98 (1H, s); DMSO-d_6: 6.48 (1H, sept, 7.1), 7.69 (2H, br. s), 7.96 (1H, s)	–69.84 (6F, br. s, $\Delta\sqrt{}_{1/2}$ = 50 Hz), –49.15 (1F, br. s); DMSO-d_6: –69.4 (6F, br. s, $\Delta\sqrt{}_{1/2}$ = 50 Hz), –50.42 (1F, br. s)	59.70 (sept, 32.0), 117.21, 121.51 (q, 283.8), 139.27, 151.88 (d, 20.4), 158.55 (d, 21.70), 159.68 (d, 205.9)[c]	303 (M^+, $C_8H_4F_7N_5^+$)
7a	3.40 (3H, s), 3.60 (3H, s), 6.74 (1H, sept, 7.0), 7.85 (1H, s)	–70.00 (d, 7.0)	–	330 (M^+, $C_{10}H_8F_6N_4O_2^+$)
7b	3.39 (3H, s), 3.59 (3H, s), 4.68 (1H, sept, 7.8), 7.80 (1H, s)	–65.02 (d, 7.8)	–	–

[a]$^{13}C\{^{1}H\}$ in $CDCl_3$, unless stated otherwise. [b]Mixture of isomers, solution in acetone. [c]In DMSO-d_6 as a solvent.

enced to internal tetramethylsilane or trichlorofluoromethane. The spectra were acquired at 298 K.

Dynamic NMR experiments

The dynamics of rotamer interconversion were studied on a Bruker AVIIIHD spectrometer with a 9.4 T magnetic field, equipped with a 10 mm F{H} probe suitable for high- and low-temperature operation. The sample temperature was calibrated against neat ethylene glycol and neat methanol standards. Selective inversion experiments at subambient temperature effected the selective inversion with iBURP shapes [25]. The spin–lattice relaxation time T_1 for each site was determined with nonselective inversion recovery experiments. The rate constant for the interconversion between the rotamers at each temperature was determined using numerical integration, minimizing the square of residuals, with the obtained T_1 relaxation time as an input to the model. The linewidths at elevated temperature were determined using the peak fitting utility in ACDLabs Spectrus Processor software (v. 2018.1.1).

X-ray diffraction

X-ray data for **7a**, **2a**, **3a**, **4a**, and **6a** were collected at −100 °C using a Bruker APEX-II CCD system equipped with a sealed tube molybdenum source and a graphite monochromator. The structures were solved and refined using the SHELXTL software package [26], refinement by full-matrix least squares on F2, scattering factors from [25]. Crystallographic data (excluding structure factors) for the structures in this paper have been deposited with the Cambridge Crystallographic Data Center as supplementary publication nos. CCDC #1998565−1998569.

Computational chemistry

Computational optimization of **8a** and **8b** structures was performed with Gaussian 9 software. Density functional theory at the B3LYP level, with a 6-311g++ basis set (Co phase) was employed.

Reaction of purine (**2**) and **1**

A mixture of 1.2 g (0.01 mol) of purine (**2**), 3 g (0.08 mol) of **1**, and 15 mL of DMSO was agitated for 24 h at ambient temperature. The precipitated sulfur was filtered and dried on a filter (isolated: 0.25 g, 78%). The filtrate was poured in 300 mL of water, and the mixture was extracted with hexane (50 mL × 2). The hexane layer was dried, and the solvent was removed under vacuum to leave 0.6 g of a white solid, which was found to be the 99% pure minor isomer **2b** (mp 122–123 °C after the second crystallization from hexane; this sample was used for X-ray diffraction studies). The rest of the reaction mixture was extracted with DCM (50 mL × 2). The DCM layer was washed with water (200 mL × 3) and dried, and the solvent was removed under vacuum to leave 1.5 g of a crude orange solid, which was found to be a mixture of **2a** and **2b** in the ratio 70:30 (GC, NMR), mp 158–167 °C. Total yield of **2a**,**b**: 78%.

A small sample of a mixture of **2a**,**b** was washed with cold hexane on a ceramic filter to give a material with a **2a**,**b** ratio of 95:5. Recrystallization of this sample from hexane gave the isomer **2b** (purity 99%, by NMR), and this sample was used for an X-ray diffraction experiment. The reaction conditions, mass spectrometry, and NMR data are given in Table 1 and Table 3.

Reaction of 4-azabenzimidazole (**3**) and **1**

A mixture of 1.2 g (0.01 mol) of 4-azabenzimidazole (**3**), 2 g (0.06 mol) of **1**, and 15 mL of DMSO was agitated at ambient temperature for 24 h. The precipitated sulfur was filtered, washed with hexane, and dried on a filter (isolated: 0.25 g, 78%). The reaction mixture was poured into 500 mL of water, and the solids were extracted with a 1:1 mixture of hexane/dichloromethane (50 mL × 2), washed with water (100 mL × 2), dried with $MgSO_4$, and filtered. The solvent was removed under reduced pressure to give 2 g (74%) of the crude product, which was found to be a mixture of two isomers (ratio 82:18, by NMR), mp 137–163 °C.

A small sample of this material was recrystallized from hot hexane to give a sample of the major isomer **3a** (purity 99.8%, mp 164–165 °C), which was used for an X-ray diffraction experiment. The reaction conditions, mass spectrometry, and NMR data are given in Table 1 and Table 3.

Reaction of 5-azabenzimidazole (**4**) and **1**

A mixture of 1.2 g (0.01 mol) of 5-azabenzimidazole (**4**), 2 g (0.06 mol) of **1**, and 15 mL of DMSO was agitated at ambient temperature for 24 h. The precipitated sulfur was filtered. The reaction mixture was poured in 500 mL of water, and the solids were filtered off to give 1.9 g (70%) of a crude product, which was found to be a mixture of the isomers **4a** and **4b** in a ratio of 67:33 (by NMR).

Pure isomers were isolated using column chromatography (Biotage instrument, hexane/ethyl acetate gradient, 100 mL/min, cartridge SNAP 340 g). The structure of each isomer was determined by X-ray diffraction. The reaction conditions, mass spectrometry, and NMR data are given in Table 1 and Table 3.

Reaction of adenine (**5**) and 2-fluoroadenine (**6**), respectively, and **1**

A mixture of 0.01 mol of the corresponding adenine (1.35 g of **5** or 1.53 g of **6**), 2 g (0.06 mol) of **1**, and 15 mL of DMSO was agitated at ambient temperature for 24 h. The precipitated sulfur

was filtered and dried on a filter (isolated: 0.25 and 0.30 g, 78–94%, respectively). The reaction mixture was poured in 500 mL of water, and the solids were filtered off, washed with water (100 mL × 2), and dried on a filter. The crude material was washed with cold hexane and dried to give 1.51 g of **5a** (yield 53%, purity 98%) and 1.99 g of **6a** (yield 66%, purity 97%). Pure samples (>99%, by GC and NMR) of **5a** and **5b** were obtained by recrystallization of small sample from hexane. The reaction conditions, mass spectrometry, and NMR data are given in Table 1 and Table 3.

Reaction of theophylline (**7**) and **1**

A mixture of 1.8 g (0.01 mol) of theophylline (**7**), 2 g (0.012 mol) of **1**, 0.5 g (0.003 mol) of dry CsF, and 15 mL of DMF was agitated for 4 d at ambient temperature. The reaction mixture was filtered to remove precipitated sulfur and the catalyst. The filtrate was poured in 300 mL of water, and the mixture was extracted by a dichloromethane/hexane mixture (3:1, 50 mL × 2). The organic layer was dried with $MgSO_4$, filtered, and the solvent was removed under reduced pressure to give 1.5 g of a slightly yellow solid. This was redissolved in 20 mL of 1:1 mixture of dichloromethane/hexane and kept at −15 °C. A yellow precipitate (0.1 g) was filtered off, and the solvent was removed to leave 1.2 g of the crude product (mp 86–88 °C), which was found to be a mixture of the two isomers **7a** and **7b** in a ratio of 85:15 (purity 98%, yield 47%). A small sample of this material was recrystallized from hot hexane to give a sample of **7a** (mp 95 °C, purity 99%), which was used for an X-ray diffraction experiment. The identity of a single crystal and the bulk of the material was confirmed by powder diffraction data and compared to simulated powder diffraction data from the single crystal diffraction experiment. The reaction conditions, mass spectrometry, and NMR data are given in Table 1 and Table 3.

Acknowledgements

P. V. A. would like to thank Joe Buriak for technical assistance and reviewers 1 and 2 for valuable suggestions.

ORCID® iDs

Alexander A. Marchione - https://orcid.org/0000-0002-6611-5076
Elizabeth L. Diaz - https://orcid.org/0000-0001-5352-0083

References

1. Anderson, J. T.; Toogood, P. L.; Marsh, E. N. G. *Org. Lett.* **2002,** *4,* 4281–4283. doi:10.1021/ol026922j
2. Chiu, H.-P.; Cheng, R. P. *Org. Lett.* **2007,** *9,* 5517–5520. doi:10.1021/ol702470j
3. Hanack, M.; Korhummel, C. *Synthesis* **1987,** 944–947. doi:10.1055/s-1987-28135
4. Burton, D. J.; Inouye, Y. *Tetrahedron Lett.* **1979,** *20,* 3397–3400. doi:10.1016/s0040-4039(01)95419-x
5. Abele, H.; Haas, A.; Lieb, M.; Zwingenberger, J. *Chem. Ber.* **1994,** *127,* 145–149. doi:10.1002/cber.19941270123
6. Tonelli, M.; Simone, M.; Tasso, B.; Novelli, F.; Boido, V.; Sparatore, F.; Paglietti, G.; Pricl, S.; Giliberti, G.; Blois, S.; Ibba, C.; Sanna, G.; Loddo, R.; La Colla, P. *Bioorg. Med. Chem.* **2010,** *18,* 2937–2953. doi:10.1016/j.bmc.2010.02.037
7. Tonelli, M.; Paglietti, G.; Boido, V.; Sparatore, F.; Marongiu, F.; Marongiu, E.; La Colla, P.; Loddo, R. *Chem. Biodiversity* **2008,** *5,* 2386–2401. doi:10.1002/cbdv.200890203
8. Tonelli, M.; Novelli, F.; Tasso, B.; Vazzana, I.; Sparatore, A.; Boido, V.; Sparatore, F.; La Colla, P.; Sanna, G.; Giliberti, G.; Busonera, B.; Farci, P.; Ibba, C.; Loddo, R. *Bioorg. Med. Chem.* **2014,** *22,* 4893–4909. doi:10.1016/j.bmc.2014.06.043
9. Akhtar, W.; Khan, M. F.; Verma, G.; Shaquiquzzaman, M.; Rizvi, M. A.; Mehdi, S. H.; Akhter, M.; Alam, M. M. *Eur. J. Med. Chem.* **2017,** *126,* 705–753. doi:10.1016/j.ejmech.2016.12.010
10. Engl, P. S.; Senn, R.; Otth, E.; Togni, A. *Organometallics* **2015,** *34,* 1384–1395. doi:10.1021/acs.organomet.5b00137
11. Prakash, G. K. S.; Krishnamoorthy, S.; Ganesh, S. K.; Kulkarni, A.; Haiges, R.; Olah, G. A. *Org. Lett.* **2014,** *16,* 54–57. doi:10.1021/ol403007j
12. Poludnenko, V. G.; Didinskaya, O. B.; Pozharskii, A. F.; Gil'burd, M. M. *Khim. Geterotsikl. Soedin.* **1982,** 1696.
13. Poludnenko, V. G.; Didinskaya, O. B.; Pozharskii, A. F. *Khim. Geterotsikl. Soedin.* **1984,** 520–523.
14. Yagupolskii, L. M.; Fedyuk, D. V.; Petko, K. I.; Troitskaya, V. I.; Rudyk, V. I.; Rudyuk, V. V. *J. Fluorine Chem.* **2000,** *106,* 181–187. doi:10.1016/s0022-1139(00)00321-3
15. Rudyuk, V. V.; Fedyuk, D. V.; Yagupolskii, L. M. *J. Fluorine Chem.* **2004,** *125,* 1465–1471. doi:10.1016/j.jfluchem.2004.05.003
16. Petko, K. I.; Vorobey, V. M. *Ukr. Khim. Zh. (Russ. Ed.)* **2015,** *81,* 106–110.
17. Petrov, V. A.; Marshall, W. *J. Fluorine Chem.* **2013,** *156,* 262–267. doi:10.1016/j.jfluchem.2013.07.004
18. Ishikawa, N.; Kitazume, T. *Chem. Lett.* **1972,** *1,* 169–170. doi:10.1246/cl.1972.169
19. Huang, W. 2,4-(1*H*,3*H*)-Pyrimidinedione derivatives and preparation method therefor. WO Patent WO2015106624A1, July 23, 2015.
20. Huang, W. 2,4-(1*H*,3*H*)-Pyrimidinedione derivatives and preparation method thereof. Chinese Patent CN103788095A, May 14, 2014.
21. Hao, X.; Chen, W.; Chen, M.; Lan, S.; Zhang, J.; Li, W. *J. Huazhong Univ. Sci. Technol., Nat. Sci.* **2007,** *41,* 546–548.
22. Mehta, V. P.; Greaney, M. F. *Org. Lett.* **2013,** *15,* 5036–5039. doi:10.1021/ol402370f
23. Petrov, V. A.; Marshall, W. *J. Fluorine Chem.* **2015,** *179,* 56–63. doi:10.1016/j.jfluchem.2015.04.003
24. Petrov, V. A.; Marshall, W. *J. Fluorine Chem.* **2010,** *131,* 1144–1155. doi:10.1016/j.jfluchem.2010.06.011
25. International Tables for Crystallography, Volume C, Tables 4.2.6.8 and 6.1.1.4.
26. *SHELXTL,* Version 6.0; Bruker AXS: Madison, WI, USA, 1996.

License and Terms

This is an Open Access article under the terms of the Creative Commons Attribution License (https://creativecommons.org/licenses/by/4.0). Please note that the reuse, redistribution and reproduction in particular requires that the authors and source are credited.

The license is subject to the *Beilstein Journal of Organic Chemistry* terms and conditions: (https://www.beilstein-journals.org/bjoc)

The definitive version of this article is the electronic one which can be found at: https://doi.org/10.3762/bjoc.16.224

BEILSTEIN JOURNAL OF ORGANIC CHEMISTRY

Fluorine effect in nucleophilic fluorination at C4 of 1,6-anhydro-2,3-dideoxy-2,3-difluoro-β-D-hexopyranose

Danny Lainé, Vincent Denavit, Olivier Lessard, Laurie Carrier, Charles-Émile Fecteau, Paul A. Johnson and Denis Giguère*

Full Research Paper

Open Access

Address:
Département de chimie, Université Laval, 1045 av. De la Médecine, Québec City, Qc, G1V 0A6, Canada

Email:
Denis Giguère* - denis.giguere@chm.ulaval.ca

* Corresponding author

Keywords:
deoxyfluorination; $Et_3N{\cdot}3HF$; fluorine effect; polyfluorinated carbohydrates; polyfluoroalditol analogues

Beilstein J. Org. Chem. **2020,** *16,* 2880–2887.
https://doi.org/10.3762/bjoc.16.237

Received: 24 September 2020
Accepted: 08 November 2020
Published: 25 November 2020

This article is part of the thematic issue "Organo-fluorine chemistry V".

Guest Editor: D. O'Hagan

© 2020 Lainé et al.; licensee Beilstein-Institut.
License and terms: see end of document.

Abstract

In this work, we have developed a simple synthetic approach using $Et_3N{\cdot}3HF$ as an alternative to the DAST reagent. We controlled the stereochemistry of the nucleophilic fluorination at C4 of 1,6-anhydro-2,3-dideoxy-2,3-difluoro-4-*O*-triflate-β-D-talopyranose using $Et_3N{\cdot}3HF$ or in situ generated $Et_3N{\cdot}1HF$. The influence of the fluorine atom at C2 on reactivity at C4 could contribute to a new fluorine effect in nucleophilic substitution. Finally, with the continuous objective of synthesizing novel multi-vicinal fluorosugars, we prepared one difluorinated and one trifluorinated alditol analogue.

Introduction

The biological significance of carbohydrates includes, but are not limited to, immune regulation, infection, and cancer metastasis. Research in the field of molecular biology allowed the discovery of glycomimetics to study various biochemical processes [1]. Therefore, the use of bioisosteres of carbohydrates functional groups is a popular approach in glycobiology [2]. As such, the synthesis of fluorosugars, including polyfluorinated analogues, is an interesting strategy to study biological systems [3-7]. The replacement of OH groups by fluorine atoms arise from their similarities in term of polarity and isosteric relationship [3,8]. For a long time, fluorinated carbohydrates have been used as a method to stabilize glycosidic bonds [9-11] or for epitope mapping [12,13]. More recently, heavily fluorinated carbohydrates were involved, among other things [5], in binding with UDP-Gal mutase [14], immunoglobulin [15,16], and glycogen phosphorylase [17].

The synthesis of complex polyfluorinated carbohydrates is challenging and new synthetic methods must be developed. Pioneering work by many groups brought significant progress to the development of innovative synthetic methodology to access polyfluorosugars [18]. For our part, we recently de-

scribed the preparation of multi-vicinal trifluorinated hexopyranose analogues **6–9** using the Chiron approach from levoglucosan (**1**, Figure 1) [19]. Various 1,6-anhydro-2,3-dideoxy-2,3-difluoro-β-D-hexopyranoses **2–5** were prepared as pivotal intermediates to access compounds **6–9**. We initially supposed that C4 deoxyfluorination of intermediates **2–5** could provide the corresponding trifluorinated product with inversion of configuration. Although that holds true for intermediates **2–4** (leading to products **6–8** after few synthetic steps), intermediate **5** failed to produce any significant results under various reaction conditions. Surprisingly, depending on the reaction conditions, C4 deoxyfluorination of compound **4** led to either the product with inversion or retention of configuration.

Recently, the group of Linclau proposed the involvement of an oxiranium intermediate for the C4 deoxyfluorination of compound **3** using diethylaminosulfur trifluoride (DAST) [20]. Moreover, in their report, they also rationalized our previous finding that a DAST-mediated deoxyfluorination of compound **4** occurs only with retention of configuration via a possible oxiranium intermediate [19]. Hence, we wish to complement this work by proposing an alternative to the DAST reagent for the selective C4 deoxyfluorination of intermediate **4**.

Our group is interested in the synthesis, physical properties and biological activities of heavily fluorinated carbohydrates [19,21-25]. With intermediates **2–5** in hand, we studied the reactivities of a small set of chirally distinct difluorinated 1,6-anhydro-β-D-hexopyranose analogues. We aimed to explore the difference in reactivities of compounds **2–5** under various deoxyfluorination reaction conditions. In our specific case, we were able to modulate the stereoselectivity of the nucleophilic fluorination at C4 with the use of $Et_3N{\cdot}3HF$. As proposed by the group of Linclau [20], we support the involvement of an oxiranium intermediate (results reinforced by density functional theory (DFT) calculations). Finally, we wish to report the preparation of novel multi-vicinal fluorinated alditol analogues using a simple reduction protocol.

Results and Discussion

We initially supposed that DAST, a commonly used reagent to install fluorine atoms on the carbohydrate core, would be suitable for the C4 deoxyfluorination of intermediates **2–5**. However, it is well documented that undesired rearrangement products with 1,2-aglycone migration [26-28] or skeletal rearrangements [29] have been observed during fluorodeoxygenation of glycopyranosides with DAST. Nevertheless, we investigated the preparation of 1,6-anhydro-2,3,4-trideoxy-2,3,4-trifluoro-β-D-hexopyranose analogues from previously described 1,6-anhydro-2,3-dideoxy-2,3-difluoro-β-D-hexopyranoses **2–5** using DAST (Table 1). We thus used 2 equivalents of DAST at 100 °C under microwave heating for 1 h and reactions were monitored using ^{19}F NMR spectroscopy with 2-fluoro-4-nitrotoluene as internal standard. Fluorodeoxygenation of glucopyranose **2** gave galactose **10** (inversion of configuration), as the only diastereoisomer (Table 1, entry 1). Interestingly, the

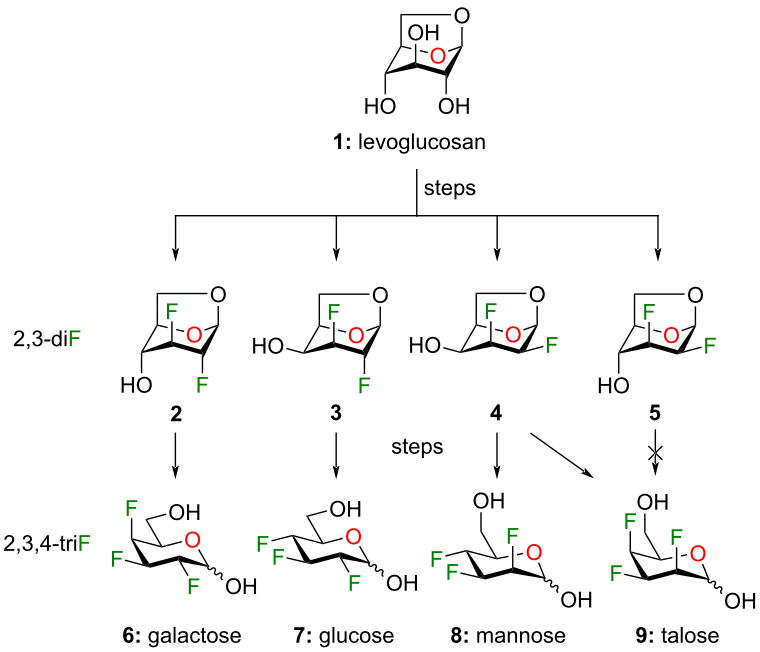

Figure 1: Previously described synthesis of 2,3,4-trifluorinated analogues of galactose **6**, glucose **7**, mannose **8**, and talose **9** from levoglucosan **1**.

Table 1: Synthesis of 1,6-anhydro-2,3,4-trideoxy-2,3,4-trifluoro-β-D-hexopyranoses **10–12** using DAST.

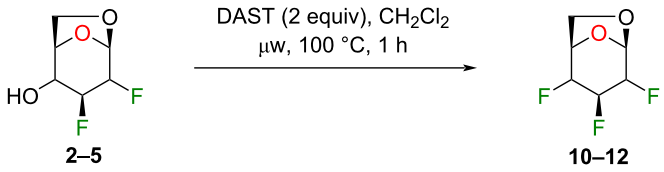

Entry	Starting materials	Conversion (%)[a]	Products (yield, %)[a]
1	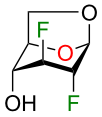 **2**	98	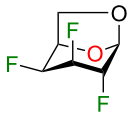 (47%) **10**
2	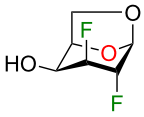 **3**	99	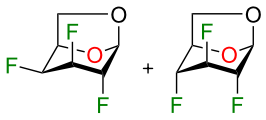 (39%) (31%) **10** + **11**
3	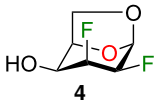 **4**	100	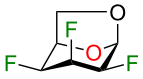 (47%) **12**
4	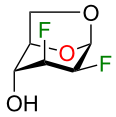 **5**	100	decomposition

[a]Conversions and yields were determined from the ^{19}F NMR (470 MHz, $CDCl_3$) using 2-fluoro-4-nitrotoluene as internal standard.

epimer at C4 (compound **3**) provided galactose **10** (retention of configuration) with a 39% yield along with glucose **11** (inversion of configuration) in 31% yield (Table 1, entry 2) [20,30]. Moreover, the use of the talose analogue **4** generated exclusively the product with retention of configuration **12**. This result was surprising since the only difference with **3** is the stereochemistry of the fluorine atom at C2. Finally, only decomposition originated from the use of mannose analogue **5** as substrate. The difference in terms of reactivity between **5** and **2** was unexpected since they only differ from the stereochemistry of the fluorine atom at C2 (distal to the reactive site at C4).

Although rather disappointing in terms of yields, these results shed some light on the fact that both the stereochemistry of the fluorine atom at C2 and the C4 hydroxy group could influence the outcome of the fluorodeoxygenation at C4 for 1,6-anhydrohexopyranose systems in the studied conditions. At this point, it became obvious to us that it would be difficult to selectively prepare 1,6-anhydro-2,3,4-trideoxy-2,3,4-trifluorohexopyranose analogues using DAST-mediated deoxyfluorination. Consequently, we turned our attention towards activation of the C4 hydroxy group as a triflate followed by exposure to a fluorine nucleophile [31]. We selected $Et_3N{\cdot}3HF$ as a simple, stable, and versatile nucleophilic reagent since it would be possible to modulate the nucleophilicity/basicity with addition of Et_3N [32]. Triflate **13** [19] was engaged as a good substrate model since the product arising from an inversion of configuration could generate the desired trifluorinated mannose analogue **14**, inaccessible from the DAST-mediated fluorodeoxygenation (Table 2) [33]. We first used 15 equivalents of $Et_3N{\cdot}3HF$ at 80 °C for 24 h with the addition of 50 equivalents of Et_3N as solvent (Table 2, entry 1). To our delight, mannose analogue **14** was formed as the major product (44% yield), along with 21% of the talose analogue **12** and the elimination product **15** in 20% yield, as determined after analysis of the ^{19}F NMR spectra of the crude reaction mixture. Figure 2 shows a representative

Table 2: Selective synthesis of trifluorotalose analogue **12** or trifluoromannose analogue **14** using $Et_3N{\cdot}3HF$.[a]

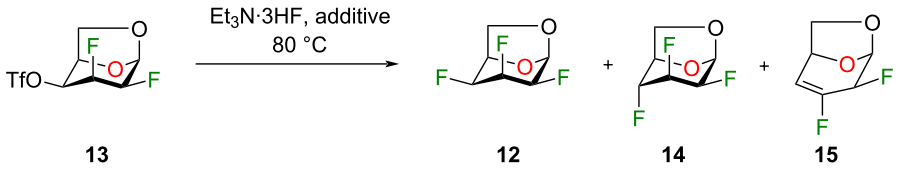

Entry	Additive (equiv)	Conversion[b] (%)	Yield (%)[b]		
			12	**14**	**15**
1[a]	Et_3N (50)	100	21	44	20
2	**Et_3N (30)**	**100**	**22**	**48**	**15**
3	Et_3N (15)	98	29	32	11
4	quinuclidine (30)	100	6	18	22
5	pyridine (30)	92	29	6	4
6	(–)-sparteine (30)	99	10	43	14
7[c]	pyridine (120)	46	1	0	2
8	**–**	**98**	**70**	**3**	**0**

[a]Reactions were carried out in a glass seal tube with 15 equivalents of $Et_3N{\cdot}3HF$ at 80 °C for 24 h. [b]Conversions and yields were determined with the ^{19}F NMR (470 MHz, $CDCl_3$) using 2-fluoro-4-nitrotoluene as internal standard. [c]Pyridine·9HF was used instead of $Et_3N{\cdot}3HF$.

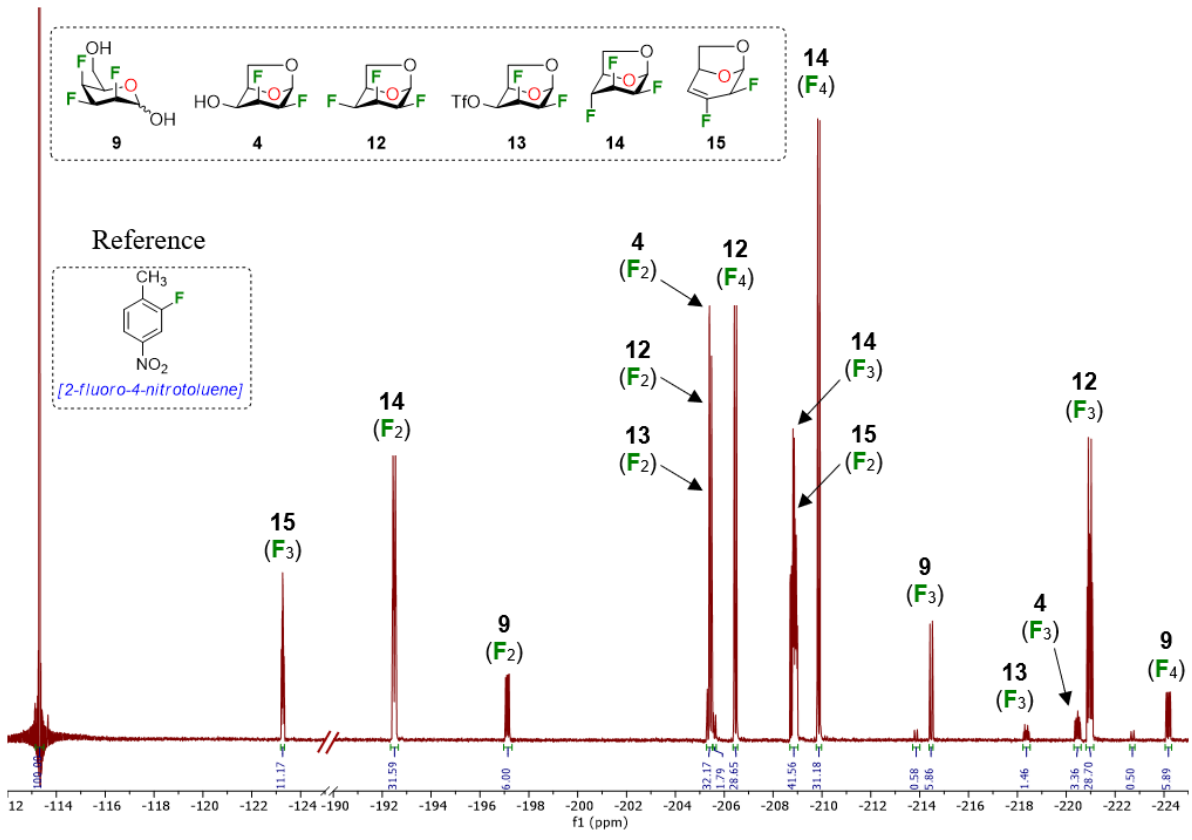

Figure 2: Typical ^{19}F NMR spectrum (470 MHz, $CDCl_3$) of the crude reaction mixture using $Et_3N{\cdot}3HF/Et_3N$ (entry 3 of Table 2).

^{19}F NMR spectrum (470 MHz, $CDCl_3$) of the crude reaction mixture of the fluorodeoxygenation using $Et_3N{\cdot}3HF$ (entry 3 of Table 2). Next, decreasing the amount of Et_3N allowed us to generate in situ $Et_3N{\cdot}1HF$ (Table 2, entry 2) and $Et_3N{\cdot}1.5HF$ (Table 2, entry 3). Using in situ generated $Et_3N{\cdot}1HF$, the mannose analogue **14** was formed in 48% yield and with $Et_3N{\cdot}1.5HF$, compound **14** was formed in 32% yield. It is known that $Et_3N{\cdot}3HF/Et_3N$ is more nucleophilic than $Et_3N{\cdot}3HF$ with a limited basicity that reduces the formation of elimination byproducts [32,34]. Then, screening other bases (Table 2, entries 4–6) did not furnish the mannose analogue **14** in higher yield and using pyridine·1HF as reagent (pyridine·9HF with 120 equivalents of pyridine) allowed only poor conversion of starting material. Finally, performing the reaction in neat $Et_3N{\cdot}3HF$ (no additive) provided almost exclusively talose analogue **12** with no elimination byproduct. These results suggest that addition of Et_3N dictates the selectivity for the C4 fluorination.

With the optimized conditions in hand, we investigated the use of other triflate analogues (Figure 3a). Under optimized conditions (Table 2, entry 2), triflate analogues **16–18** [19] gave exclusively products with inversion of configuration, although in a lower yield for compound **18**. These results highlighted the likely influence of the stereochemistry of the fluorine atom at C2 in particular when we compared the reactivity between compounds **13** and **16**. The nucleophilic substitution with retention of configuration was unexpected since the fluoride anion would have to approach the more sterically hindered β-face. To account for the retention of configuration (minor product) in the fluorination of compound **13**, we proposed the involvement of an oxiranium-like intermediate **A** (Figure 3b). Interestingly, oxiranium ions in carbohydrate chemistry have been proposed as intermediates in the course of various reactions [20,29,35,36]. An equatorial fluorine atom at C2 (antiperiplanar to the C1–O5 bond) reduces the endocyclic oxygen polarizability, but also destabilizes a possible carbocation at C4

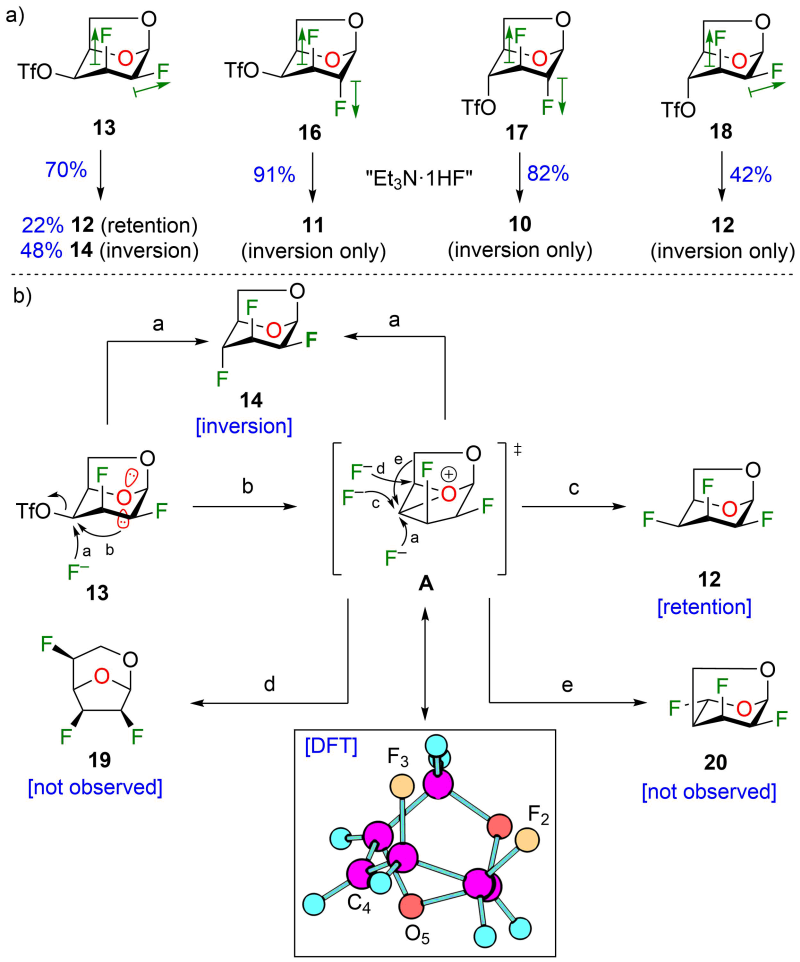

Figure 3: Fluorination at C4 of 1,6-anhydro-2,3-difluorohexopyranose analogues. a) Reactions on triflates **13**, **16–18**, dipole of C–F bonds are displayed in green arrows; b) Proposed mechanism for the formation of trifluorotalose analogue **12** and trifluoromannose analogue **14** via an oxiranium-like intermediate **A** from compound **13**.

(the C2–F2 bond is antiperiplanar to the C3–C4 bond) [37]. As a result, the oxiranium ion could be stabilized in the presence of triethylamine. A lone pair of electrons on the nitrogen atom from triethylamine overlaps with the antibonding σ* orbital of the O5–C4 bond of the oxirane, favoring the fluorine electron density to attack equatorially. Although we propose an oxiranium intermediate for the C4 deoxyfluorination of **13**, we did not observe any ring rearrangement, typically as a result of ring contraction (for example, compound **19**, step d) [26,29,38]. Also, we did not observe any 1,2-alkyl shift of C6 from C5 to C4 with enlargement of the dioxolane ring followed by fluorine introduction at C5 (compound **20**, step e) [33]. This known alkyl shift [29,39] is usually displayed by more carbocationic character of the intermediate species [40]. In our case, the polyfluoroalkyl group could destabilize the adjacent carbocation center [41-43], avoiding 1,2-alkyl shift, and thus formation of byproduct **20**. Similarly, the large dipole moment of the C–F bond at C2 influences the outcome of the deoxyfluorination at C4 [3]. For triflates **16** and **17**, both dipoles (green arrows, Figure 3a) are opposite to each other (dipolar relaxation) and consequently provided higher yields for the nucleophilic fluorination at C4 with inversion of configuration. In contrast, triflates **13** and **18** (both dipole in the same direction) led to lower yields for the fluorination with inversion of configuration.

Finally, DFT calculations were performed with Gaussian 09, revision E.01 [44] to evaluate the hypothesis for the formation of oxiranium ion **A**. Calculations were performed with the CAM-B3LYP functional [45-47] using Grimme's D3 dispersion correction [48] and the 6-31+G(d,p) basis set. The results of our modeling calculations showed a distance of 1.52 Å between the endocyclic oxygen and C4.

With the optimisation of the C4 deoxyfluorination successfully completed, and as a demonstration of the usefulness of our strategy, we completed the synthesis of two fluorinated alditol analogues (Scheme 1). We first evaluated reduction conditions on a simpler difluorinated hexopyranose analogue. Thus, difluoroglucose **21**, easily accessible in 3 steps from levoglucosan (**1**) [21], was subjected to lithium aluminium hydride ($LiAlH_4$) in THF (Scheme 1a) and difluoroglucitol **22** was isolated in 58% yield. The reaction was hardly reproducible because a thick gel was formed after neutralisation with an acidic resin, thus resulting in yield loss after a difficult filtration. Next, we evaluated sodium borohydride ($NaBH_4$) as reducing reagent. Difluoroglucose **21** was subjected to 5 equivalents of $NaBH_4$ in EtOH at rt and compound **22** was isolated in 71% yield. We then apply this strategy to the synthesis of trifluorohexitol analogue integrating fluorine atoms at C2, C3, and C4 (Scheme 1b). Compound **4**,

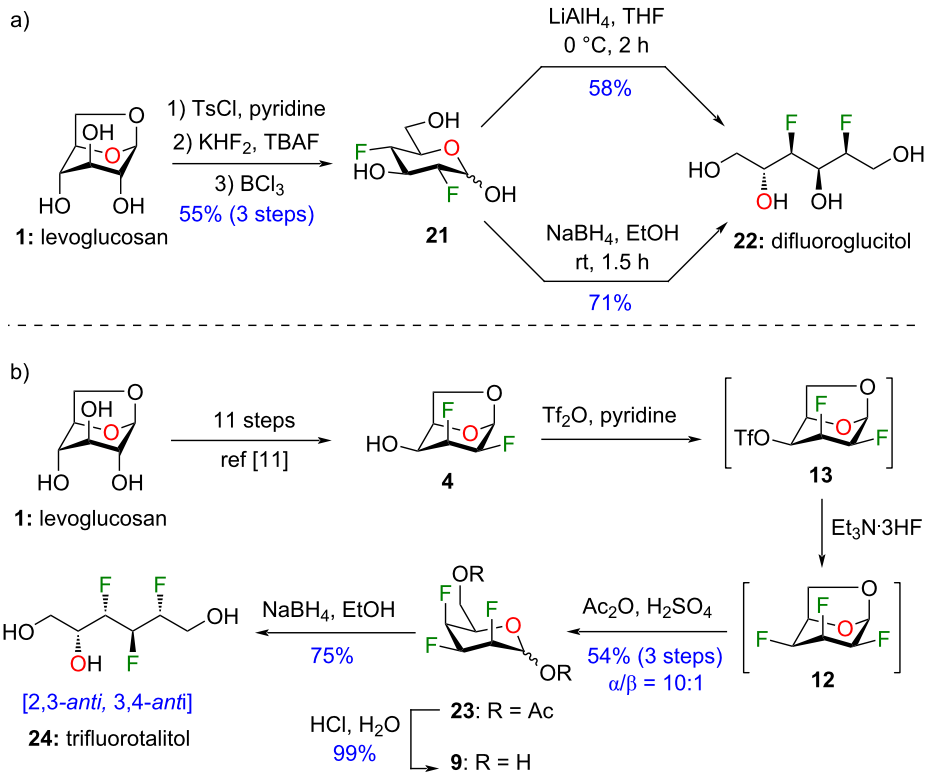

Scheme 1: Synthesis of polyfluorinated alditols from levoglucosan **1**: a) difluoroglucitol analogue **22**; b) trifluorotalitol analogue **24**.

also accessible from levoglucosan (**1**) [19], was activated as triflate and subjected to nucleophilic fluorination. The crude reaction mixture was treated under acidic conditions and furnished the desired acetylated analogue **23** in 54% over 3 steps. This synthetic sequence represents a useful alternative to DAST or TBAF (tetrabutylammonium fluoride) that lead to elimination byproducts. Finally, after acetates removal, reduction of compound **9** with sodium borohydride led to novel trifluorotalitol analogue **24** in 75% yield containing a 2,3-*anti*, 3,4-*anti* pattern for the integrated fluorine atoms.

Conclusion

Supporting evidence from numerous studies on various substrates indicated that predicting the selectivity of the DAST-mediated deoxyfluorination is a difficult task to achieve. The simple synthetic approach described herein and the use of $Et_3N{\cdot}3HF$ as an alternative to the unpredictable DAST looked promising. In the specific case of triflate **13**, we were able to modulate the stereoselectivity of the nucleophilic fluorination at C4 using simple $Et_3N{\cdot}3HF$ with or without addition of triethylamine. The role of the reagent and the remote influence of the fluorine atom at C2 on reactivity at C4 could concomitantly contribute to a new fluorine effect in nucleophilic substitution [49]. Finally, the synthesis of two distinct polyfluorinated alditol analogues was achieved. The strategy described herein will allowed us to achieve the synthesis of other polyfluorinated hexitol analogues in order to explore their physical properties.

Supporting Information

Supporting Information File 1

Detailed experimental procedures, characterization data, copies of ^{1}H, ^{13}C, ^{19}F, COSY, and HSQC NMR spectra of all new compounds, and optimization of the deoxyfluorination.
[https://www.beilstein-journals.org/bjoc/content/supplementary/1860-5397-16-237-S1.pdf]

Acknowledgements

The authors would like to thank Dr. Yoann M. Chabre for useful discussions and proof reading of this article.

Funding

This work was supported by the Natural Sciences and Engineering Research Council of Canada (NSERC) and Université Laval. D. L. and O. L. thank NSERC for a postgraduate fellowship. This research was enabled in part by Calcul Québec and Compute Canada.

ORCID® iDs

Denis Giguère - https://orcid.org/0000-0003-2209-1428

References

1. Hevey, R. *Pharmaceuticals* **2019,** *12,* 55. doi:10.3390/ph12020055
2. Hevey, R. *Biomimetics* **2019,** *4,* 53. doi:10.3390/biomimetics4030053
3. O'Hagan, D. *Chem. Soc. Rev.* **2008,** *37,* 308–319. doi:10.1039/b711844a
4. Dalvit, C.; Invernizzi, C.; Vulpetti, A. *Chem. – Eur. J.* **2014,** *20,* 11058–11068. doi:10.1002/chem.201402858
5. Linclau, B.; Ardá, A.; Reichardt, N.-C.; Sollogoub, M.; Unione, L.; Vincent, S. P.; Jiménez-Barbero, J. *Chem. Soc. Rev.* **2020,** *49,* 3863–3888. doi:10.1039/c9cs00099b
6. Biffinger, J. C.; Kim, H. W.; DiMagno, S. G. *ChemBioChem* **2004,** *5,* 622–627. doi:10.1002/cbic.200300910
7. Hevey, R. *Chem. – Eur. J.* **2020**. doi:10.1002/chem.202003135
8. Hunter, L. *Beilstein J. Org. Chem.* **2010,** *6,* No. 38. doi:10.3762/bjoc.6.38
9. Withers, S. G.; Street, I. P.; Percival, M. D. Fluorinated Carbohydrates as Probes of Enzyme Specificity and Mechanism. *Fluorinated Carbohydrates;* ACS Symposium Series, Vol. 374; American Chemical Society: Washington, DC, USA, 1988; pp 59–77. doi:10.1021/bk-1988-0374.ch005
10. Lee, S. S.; Greig, I. R.; Vocadlo, D. J.; McCarter, J. D.; Patrick, B. O.; Withers, S. G. *J. Am. Chem. Soc.* **2011,** *133,* 15826–15829. doi:10.1021/ja204829r
11. Namchuk, M. N.; McCarter, J. D.; Becalski, A.; Andrews, T.; Withers, S. G. *J. Am. Chem. Soc.* **2000,** *122,* 1270–1277. doi:10.1021/ja992044h
12. Glaudemans, C. P. J. *Chem. Rev.* **1991,** *91,* 25–33. doi:10.1021/cr00001a002
13. Lemieux, R. U. *Chem. Soc. Rev.* **1989,** *18,* 347–374. doi:10.1039/cs9891800347
14. van Straaten, K. E.; Kuttiyatveetil, J. R. A.; Sevrain, C. M.; Villaume, S. A.; Jiménez-Barbero, J.; Linclau, B.; Vincent, S. P.; Sanders, D. A. R. *J. Am. Chem. Soc.* **2015,** *137,* 1230–1244. doi:10.1021/ja511204p
15. Hoffmann-Röder, A.; Johannes, M. *Chem. Commun.* **2011,** *47,* 9903–9905. doi:10.1039/c1cc13184b
16. Oberbillig, T.; Mersch, C.; Wagner, S.; Hoffmann-Röder, A. *Chem. Commun.* **2012,** *48,* 1487–1489. doi:10.1039/c1cc15139h
17. Street, I. P.; Armstrong, C. R.; Withers, S. G. *Biochemistry* **1986,** *25,* 6021–6027. doi:10.1021/bi00368a028
18. Uhrig, M. L.; Lantaño, B.; Postigo, A. *Org. Biomol. Chem.* **2019,** *17,* 5173–5189. doi:10.1039/c9ob00405j
19. Denavit, V.; Lainé, D.; St-Gelais, J.; Johnson, P. A.; Giguère, D. *Nat. Commun.* **2018,** *9,* 4721. doi:10.1038/s41467-018-06901-y
20. Quiquempoix, L.; Wang, Z.; Graton, J.; Latchem, P. G.; Light, M.; Le Questel, J.-Y.; Linclau, B. *J. Org. Chem.* **2019,** *84,* 5899–5906. doi:10.1021/acs.joc.9b00310
21. St-Gelais, J.; Côté, É.; Lainé, D.; Johnson, P. A.; Giguère, D. *Chem. – Eur. J.* **2020,** *26,* 13499–13506. doi:10.1002/chem.202002825
22. Denavit, V.; Lainé, D.; Bouzriba, C.; Shanina, E.; Gillon, É.; Fortin, S.; Rademacher, C.; Imberty, A.; Giguère, D. *Chem. – Eur. J.* **2019,** *25,* 4478–4490. doi:10.1002/chem.201806197
23. Denavit, V.; St-Gelais, J.; Tremblay, T.; Giguère, D. *Chem. – Eur. J.* **2019,** *25,* 9272–9279. doi:10.1002/chem.201901346
24. St-Gelais, J.; Bouchard, M.; Denavit, V.; Giguère, D. *J. Org. Chem.* **2019,** *84,* 8509–8522. doi:10.1021/acs.joc.9b00795

25. Lainé, D.; Denavit, V.; Giguère, D. *J. Org. Chem.* **2017,** *82,* 4986–4992. doi:10.1021/acs.joc.7b00543
26. Dax, K.; Albert, M.; Hammond, D.; Illaszewicz, C.; Purkarthofer, T.; Tscherner, M.; Weber, H. *Monatsh. Chem.* **2002,** *133,* 427–448. doi:10.1007/s007060200019
27. Borrachero, P.; Cabrera-Escribano, F.; Carmona, A. T.; Gómez-Guillén, M. *Tetrahedron: Asymmetry* **2000,** *11,* 2927–2946. doi:10.1016/s0957-4166(00)00252-4
28. Faghih, R.; Escribano, F. C.; Castillon, S.; Garcia, J.; Lukacs, G.; Olesker, A.; Thang, T. T. *J. Org. Chem.* **1986,** *51,* 4558–4564. doi:10.1021/jo00374a013
29. Karban, J.; Císařová, I.; Strašák, T.; Šťastná, L. Č.; Sýkora, J. *Org. Biomol. Chem.* **2012,** *10,* 394–403. doi:10.1039/c1ob06336g
30. Sarda, P.; Escribano, F. C.; Alves, R. J.; Olesker, A.; Lukacs, G. *J. Carbohydr. Chem.* **1989,** *8,* 115–123. doi:10.1080/07328308908047996
31. Liang, S.; Hammond, G. B.; Xu, B. *Chem. – Eur. J.* **2017,** *23,* 17850–17861. doi:10.1002/chem.201702664
32. Giudicelli, M. B.; Picq, D.; Veyron, B. *Tetrahedron Lett.* **1990,** *31,* 6527–6530. doi:10.1016/s0040-4039(00)97108-9
33. See Supporting Information File 1 for full details related to optimization reactions.
34. Other fluorinating reagent such as $R_4N^+HF_2^-$ or R_4NF were too basic and generated compound **15** as major side product.
35. Lin, T.-S.; Tsai, W.-T.; Liang, P.-H. *Tetrahedron* **2016,** *72,* 5571–5577. doi:10.1016/j.tet.2016.06.075
36. Chan, W.-P.; Gross, P. H. *J. Org. Chem.* **1980,** *45,* 1369–1373. doi:10.1021/jo01296a005
37. An axial fluorine at C-2 could prevent anchimeric assistance as a result of electrostatic repulsion with the axial oxygen lone pair.
38. Mori, Y.; Morishima, N. *Chem. Pharm. Bull.* **1992,** *40,* 826–828. doi:10.1248/cpb.40.826
39. Karban, J.; Sykora, J.; Kroutil, J.; Cisarova, I.; Padelkova, Z.; Budesinsky, M. *J. Org. Chem.* **2010,** *75,* 3443–3446. doi:10.1021/jo1000912
40. Alexander, M. S.; Horton, D. *Carbohydr. Res.* **2007,** *342,* 31–43. doi:10.1016/j.carres.2006.11.003
41. Creary, X. *Chem. Rev.* **1991,** *91,* 1625–1678. doi:10.1021/cr00008a001
42. Jansen, M. P.; Koshy, K. M.; Mangru, N. N.; Tidwell, T. T. *J. Am. Chem. Soc.* **1981,** *103,* 3863–3867. doi:10.1021/ja00403a040
43. McCarter, J. D.; Adam, M. J.; Withers, S. G. *Biochem. J.* **1992,** *286,* 721–727. doi:10.1042/bj2860721
44. *Gaussian 09,* Revision E.01; Gaussian, Inc.: Wallingford, CT, USA, 2016.
45. Yanai, T.; Tew, D. P.; Handy, N. C. *Chem. Phys. Lett.* **2004,** *393,* 51–57. doi:10.1016/j.cplett.2004.06.011
46. Becke, A. D. *J. Chem. Phys.* **1993,** *98,* 5648–5652. doi:10.1063/1.464913
47. Lee, C.; Yang, W.; Parr, R. G. *Phys. Rev. B* **1988,** *37,* 785–789. doi:10.1103/physrevb.37.785
48. Grimme, S.; Antony, J.; Ehrlich, S.; Krieg, H. *J. Chem. Phys.* **2010,** *132,* 154104. doi:10.1063/1.3382344
49. Ni, C.; Hu, J. *Chem. Soc. Rev.* **2016,** *45,* 5441–5454. doi:10.1039/c6cs00351f

License and Terms

This is an Open Access article under the terms of the Creative Commons Attribution License (https://creativecommons.org/licenses/by/4.0). Please note that the reuse, redistribution and reproduction in particular requires that the authors and source are credited.

The license is subject to the *Beilstein Journal of Organic Chemistry* terms and conditions: (https://www.beilstein-journals.org/bjoc)

The definitive version of this article is the electronic one which can be found at: https://doi.org/10.3762/bjoc.16.237

BEILSTEIN JOURNAL OF ORGANIC CHEMISTRY

Controlled decomposition of SF_6 by electrochemical reduction

Sébastien Bouvet[1], Bruce Pégot[1], Stéphane Sengmany[2], Erwan Le Gall[2], Eric Léonel[2], Anne-Marie Goncalves[*1] and Emmanuel Magnier[*1]

Full Research Paper

Open Access

Address:
[1]Université Paris-Saclay, UVSQ, CNRS, UMR 8180, Institut Lavoisier de Versailles, 78035 Versailles Cedex, France and [2]Electrosynthèse, Catalyse et Chimie Organique, Université Paris-Est Créteil, CNRS, ICMPE, UMR 7182, 2 rue Henri Dunant, 94320 Thiais, France

Email:
Anne-Marie Goncalves[*] - anne-marie.goncalves@uvsq.fr;
Emmanuel Magnier[*] - emmanuel.magnier@uvsq.fr

* Corresponding author

Keywords:
electroreduction; fluoride anion; redox potential; sulfur hexafluoride

Beilstein J. Org. Chem. **2020,** *16,* 2948–2953.
https://doi.org/10.3762/bjoc.16.244

Received: 09 October 2020
Accepted: 18 November 2020
Published: 01 December 2020

This article is part of the thematic issue "Organo-fluorine chemistry V".

Guest Editor: D. O'Hagan

© 2020 Bouvet et al.; licensee Beilstein-Institut.
License and terms: see end of document.

Abstract

The electroreduction of SF_6 is shown at ambient temperature in acetonitrile using an array of platinum microelectrodes to improve the electrical detection. Its half reduction potential occurs at −2.17 V vs Fc^+/Fc. The exact number of electrons for the full consumption of sulfur hexafluoride was determined and this gas further quantitatively transformed into environmentally benign fluoride anion and sulfur by electrochemical reduction.

Introduction

Sulfur hexafluoride (SF_6) is a fluorinated gas firstly identified in 1900 by Henry Moissan [1]. The strategy applied at industrial level to obtain SF_6 uses sulfur in the presence of molecular fluorine. Sulfur hexafluoride possesses the particularity of being an inert gas both chemically and physiologically, it is non-flammable, has a high density and a high dielectric constant (2.5 times greater than that of air) [2-5]. These properties explain that this compound is widely used industrially as an electrical insulating gas in circuit breakers or in electrical substations [6,7]. On the other hand, SF_6 is a greenhouse gas [8]. It has indeed a global warming potential (GWP) 22,000 times greater than CO_2 [9]. From an industrial point of view, this requires efficient methods of recycling or destroying SF_6. This last point implies, because of its great stability, the use of expensive methods requiring a large input of energy (high temperature, high pressure). Many SF_6 decomposition strategies so far developed use photoreduction, plasma discharges or even photolysis processes [10,11]. Beyond the energetic high cost of such processes, they produce side products that are highly reactive, corrosive and toxic [12]. Recent and really impressive works were devoted to the decomposition of sulfur hexafluoride using stoichiometric or catalytic amounts of metals (Rh, Ni, Pt) [13-16]. Organic derivatives (phosphines or bipyridine) proved efficient tools for the selective degradation of SF_6 [17,18]. Other elegant approaches have described the use of SF_6 as precursor of reagent for fluorination or pentafluorosulfanyla-

tion. Very interestingly, the photochemical activation of this gas was described and allowed the in situ transformation of alcohols into alkyl fluorides [19,20]. The modern and green photoredox catalytic activation of SF_6 was recently performed for the fluoro- and alkoxypentafluorosulfanylation of styrenes [21,22]. The same type of transformation was also described through the reductive activation of sulfur hexafluoride with TEMPO [23].

To the best of our knowledge, electrochemical reduction of SF_6 has not yet been disclosed. The decomposition of sulfur hexafluoride by electrochemistry can nevertheless be a suitable answer and interesting alternative to the previous expensive options. In this article, we describe the electrochemical behavior of sulfur hexafluoride dissolved in various organic solvents. After combining an analytical approach of electrochemistry and ^{19}F NMR spectroscopy, we have succeeded in the total consumption of SF_6 in an electrochemical cell.

Results and Discussion

The first step of this work began with the measurement of the solubility of sulfur hexafluoride in an organic solvent. This data was not available in the literature but was however crucial for the implementation of the electrochemical experiences. Two solvents (DMF and acetonitrile) were selected for their good dissolution abilities and their large electroactivity area. The solubility of SF_6 was measured, at 20 °C, by ^{19}F NMR with chlorodifluoromethoxybenzene as internal standard probe. The concentration value for DMF was quite low (0.17 g/L) whereas the one for acetonitrile (2.48 g/L) was convenient for further studies. Acetonitrile is a common nonaqueous solvent in electrochemistry. Having a dielectric constant relatively high ($\varepsilon = 38$), acetonitrile allows a good dissociation of several salts providing the conductivity of the medium. The concentration of SF_6 in the following studies was then around 1.7×10^{-2} M.

We then turned our attention to the determination of the reduction potential of SF_6. To allow its electroreduction feasibility in acetonitrile, an electrochemical analytical approach was required [24]. This crucial step was supported by sensors which are based on a micro-disc-array of platinum ultramicroelectrodes (20 µm diameter) acting as multi-probe channels.

Due to their small size, microelectrodes provide electrochemical studies of very low concentrations of electroactive substances contained in a small amount of solvent. As a consequence, a conductive solvent is not required and a low concentration of conducting salt is sufficient. In contrast to macroelectrodes, the current density on microelectrodes is very high. This allows a better current sensitivity in electrochemical measurements (cyclic voltametrics, polarization curve …) providing the study of rapid electron and coupled chemical reactions. In comparison to macroelectrodes, their small size leads to a large decrease of the capacitive current and avoids IR drop effects. The array of Pt microdiscs offers the advantage of summing the current intensity of each microelectrode, thus increasing the sensitivity of the resulting current [25].

Whereas a planar diffusion is observed onto classical electrode (size >0.1 cm^2), a hemispherical diffusion is expected with a microdisc electrode due to the contribution of the current diffusion by edge effects. The mass transport regime is then drastically modified on microdisc electrodes and can be adjusted in accordance with the polarization time by monitoring the potential scan rate. By cyclic voltametry, unlike macroelectrodes, the polarization of microelectrodes with a low potential scan rate (≤25 mV/s) leads to a drastic decrease of Cottrel contribution which involves the disappearance of current waves. The resulting current becomes a stationary current of diffusion (*id*), which is directly proportional to the bulk concentration of the electroactive substance (C^{∞}), its diffusion coefficient in the solvent (D), the number of electrons exchanged in the electrochemical process (n), and the radius of the microelecrode (r) and F the Faraday constant, in accordance with the following relation [26]:

$$id = 4nFD\,C^{\infty}r \quad (1)$$

To the half limiting current (*id*/2) can be associated the half wave potential noted $E_{1/2}$. For reversible electrons exchanged at the interface electrode/electrolyte, the half wave potential can be assimilated to the reversible formal potential redox couple noted $E°$ox/red [27]. After the addition of SF_6, a stationary current is clearly observed before the acetonitrile reduction [28]. The electrochemial response of SF_6 is related to a reproducible stationnary cathodic current. The intensity of the limiting current (plateau intensity) directly depends on SF_6 concentration. From the voltamogram, the half wave potential of SF_6 reduction is deduced and corresponds to −2.17 V vs Fc^+/Fc (Figure 1).

To the best of our knowledge, this was the first determination of the redox potential of sulfur hexafluoride. Pleasingly, this value was compatible with the employed solvent and offered the opportunity to reduce this gas in solution. In order to reach our target, i.e., the total consumption of SF_6 into stable and nontoxic species, the next step was the determination of the number of electrons. It was determined by using two controlled size (S) of Pt electrodes: Pt ultramicroelectrode (∅ 20 µm, $S_1 = 3.14 \times 10^{-6}$ cm^2) and Pt macroelectrode (∅ 0.76 mm, $S_2 = 4.5 \times 10^{-3}$ cm^2). Using Pt ultramicroelectrode, the stationary current density (j_1) is deduced from Equation 2:

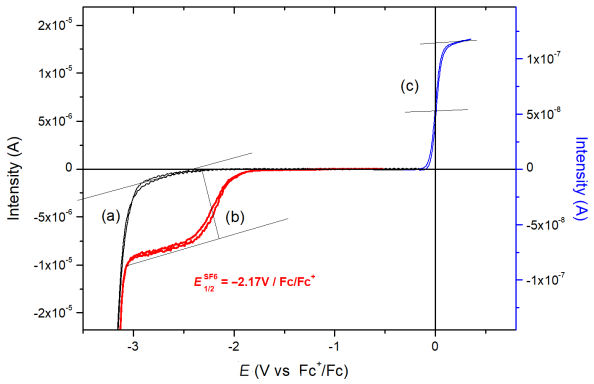

Figure 1: (a) Cyclic voltammetry onto microelectrode arrays (Ø = 20 µm) in acetonitrile freshly distilled after the addition of $TBAClO_4$ (0.1 M) at room temperature, under slight argon stream, v = 20 mV/s. (b) Same conditions as for (a) after addition of SF_6. (c) Same conditions than (a) after addition of ferrocene (10^{-3} M).

$$j_1 = \frac{4 \times n_e_FD[SF_6]}{\pi \times r} \quad (2)$$

Assuming a rapid electron transfer, the current (j_2) decreases exponentially with time (t) according to the Cottrell law (Equation 3) onto a Pt macroelectrode, under sufficient electrochemical polarization [29].

$$j_2 = \frac{n_e_FD^{\frac{1}{2}}S_2[SF_6](\pi t^{-\frac{1}{2}})}{S_2} \quad (3)$$

From a combination of Equation 2 and Equation 3, the determination of the number of electrons exchanged is given by Equation 4 [30]:

$$n_{e-} = \frac{4 \times t \times j_2^2}{F \times [SF_6] \times r \times j_1} \quad (4)$$

The number of electrons exchanged (Equation 4) only depends on the validity of the Cottrell equation onto the macroelectrode (j_2) since a constant current density (j_1) is detected onto the microelectrode. The validity of the Cottrell equation requires a linear variation of the current density (j_2) with $t^{-1/2}$. This linear variation gives the upper limit on time. From this straight line the maximum duration (t) and the corresponding value of j_2 are determined. These two values (t and j_2) are then included in Equation 4 for the determination of the number of electrons exchanged. The macroelectrode (Ø = 0.76 mm) was polarized at −2.3 V vs Fc^+/Fc after saturation of SF_6 in the electrolyte. The chronoamperogram was reported in Figure 2. As it was expected, an exponential decrease of the current was indeed observed just before reaching a stationary current which was related to a constant layer thickness of SF_6 diffusion. Indeed, the decrease in current comes from the consumption of SF_6 at the interface electrode/acetonitrile. The current intensity depends on the SF_6 flow in agreement with the 1st Fick's Law from which the Cottrell equation is originated [29].

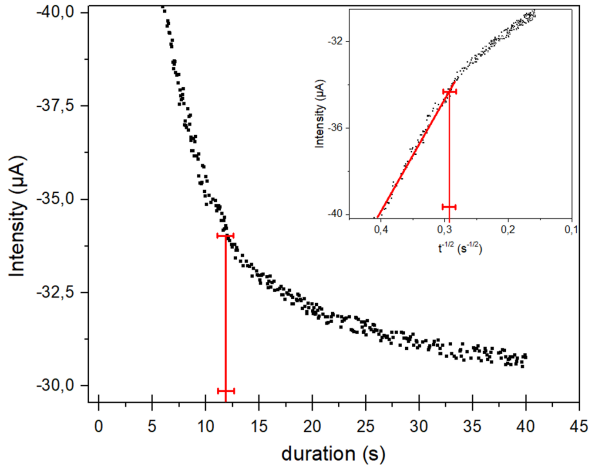

Figure 2: Variation of the current reduction (i_2) of SF_6 onto Pt macroelectrode (Ø = 0.76 mm) at –2.3 V vs Fc^+/Fc in acetonitrile freshly distilled after addition of $TBAClO_4$ (0.1 M) at room temperature, under slight argon stream. Insert figure: Determination of the upper limit on time of Cottrell law from the straight line $i_2 = f(t^{-1/2})$.

The upper limit on time was determined from the straight line reported in the insert figure (Figure 2). A value of 11.9 ± 0.7 s was deduced and the corresponding value of i_2 (−34.2 µA ± 0.5) was determined from the chronoamperogram (Figure 2). Based on these values, the number of electron (ne^- = 7.8 ± 0.3) was deduced from Equation 4. The reduction mechanism of SF_6 can then involve 8 electrons per molecule:

$$SF_6 + 8e^- \rightarrow S^{2-} + 6F^-$$

This preliminary study is an important step to determine the best conditions for the SF_6 electrolysis (the choice of potential polarization, the understanding of current decrease). With these analytical data in hands, the large scale decomposition of SF_6 was then undertaken. The reactions were carried out in a single compartment with a conventional three-electrode arrangement: two platinum electrodes and one silver reference electrode, SRE (Figure 3). The electrolysis is performed at constant potential (−2.3 V vs Fc^+/Fc) with a continuous supply of SF_6 placed in a rubber balloon (constant bubbling).

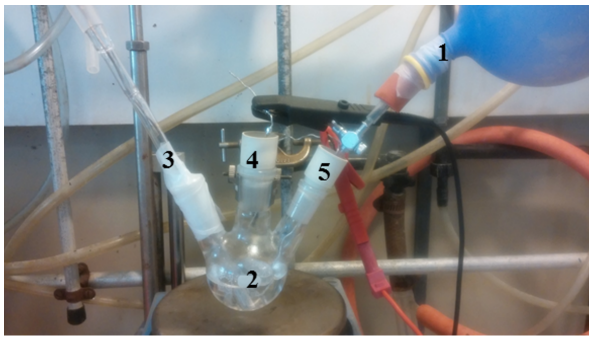

Figure 3: Single compartment three-electrode experiment. 1: Balloon of SF_6, 2: electrochemical cell, 3: reference electrode (silver wire), 4: counter-electrode (platinum), 5: working electrode (platinum).

The electrolysis was investigated on the same electrolyte but with larger surface of Pt electrode (15 cm^2) (Figure 4). Figure 4b clearly highlights the consumption of the gas by the decrease of the electrochemical waves.

The control of the decomposition of the sulfur hexafluoride was also monitored by ^{19}F NMR (Figure 5). After 3 hours experience, unidentified side-products were detected by NMR. Identification of these fleeting species as well as their potential reactivity are under current investigation in our laboratory. The left part of Figure 5 clearly demonstrates the total disappearance of SF_6 after 6 hours as well as all the fluorinated organic compounds. The only peak detected by ^{19}F NMR is around −153 ppm. This value corresponds to the classical chemical shift range of a fluoride anion. Due to its broad appearance, we

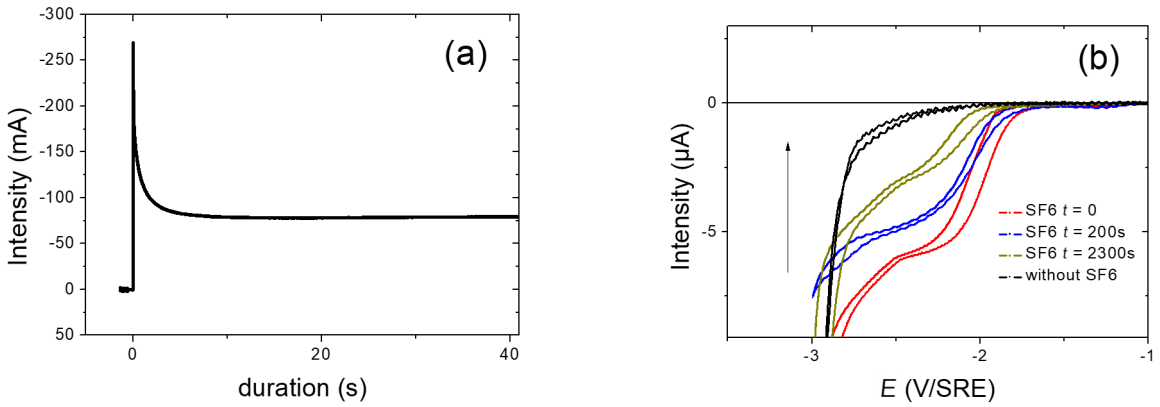

Figure 4: Electrolysis of SF_6 at −2.3 V vs Fc^+/Fc in acetonitrile freshly distilled after addition of $TBAClO_4$ (0.1 M) at room temperature under slight argon stream. (a) Exponential decrease of the cathodic current according to the electrolysis duration onto a smooth Pt electrode (15 cm^2). (b) Decrease of the cathodic current during the electrolysis duration which is detected onto an array of Pt microelectrodes (Ø = 20 µm).

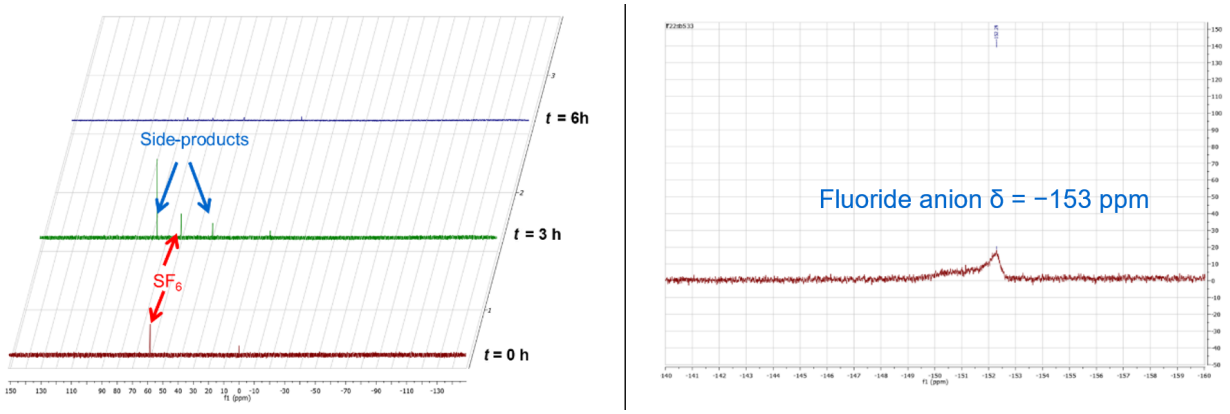

Figure 5: ^{19}F NMR evolution of the crude mixture along the time after electrolysis realized at constant potential of −2.3 V/SRE; (left). ^{19}F NMR expansion of the final mixture.

can postulate the association with cations coming from the supporting electrolytes based on tetrabutylammonium (TBA) structures after anion exchange. This poor resolved signal is quite classical for such species due to hydrogen bonds. Another important point is the production of H^+ ions at the counter electrode because of the oxidation of acetonitrile [31,32]:

$$2CH_3CN \rightarrow NC–CH_2–CH_2–CN + 2H^+ + 2e^-$$

They can associate themselves with the F^- anions and generate bifluoride HF_2 anions or even polyfluorides F(HF). The presence of fluoride anions can produce a Hoffman elimination on the alkyl chain of TBA giving rise to tributylamine, butene, and HF. We can suppose that the anion S_2^- could also be react with these hydrogen sources and become H_2S. Nevertheless, in spite of our efforts it is very difficult to clearly identify all these decomposition compounds. A comprehensive analytical study could be of interest but it falls down the scope of the present article.

Conclusion

The smooth and controlled decomposition of sulfur hexafluoride was described under electroreduction. The reduction potential was firstly determined and used for preparative studies. The extrapolation on large scale of this methodology is under current development in our laboratory.

Experimental

Acetonitrile (HPLC grade, Mallinckrodt) was distilled from CaH_2 and then degassed using three freeze-pump-thaw cycles before use. An electrochemical cell filled up with 40 mL of acetonitrile with TBABr (0.1 M) or $TBAClO_4$ (0.1 M) as conducting salt at room temperature. The degassing of the medium was performed under an argon stream before the bubbling of SF_6 to reach a saturated concentration that is 1.7×10^{-2} M. A balloon filled with 8 g of SF_6 (0.055 mmol) is connected to the device (see Figure 3) and the electrolysis is carried out until the balloon is empty. The electrochemical set-up was a classical three electrodes device. All potentials were measured against a pseudo silver reference electrode (SRE). The addition of ferrocene in the electrolyte gives access to an internal reference [33]. In order to improve the current detection level of SF_6, platinum disk electrodes were used as working electrode (Pt ultramicroelectrode with a diameter of 20 µm, an array of eight Pt ultramicroelectrodes with a diameter of 20 µm and a Pt macroelectrode with a diameter of 1 mm). Platinum disk microelectrodes were made by sealing into very fine glass, one or eight platinum wires, with a diameter of 20 µm, into the same soft glass tubing [33]. The microelectrodes array was polished successively on finer grades sand paper. After the analytical approach, a Pt wire (15 cm^2) is used to allow SF_6 electrolysis.

Whatever the step of the study (analytical, electrolysis) a smooth platinum electrode with a larger surface was used as a counter electrode. Electrochemical measurements were covered by a wide range of a potentiostat for more effective current detection. A potentiostat–galvanostat such as Princeton Applied Research Model 263 was monitored by its front panel and analogue-to-digital conversion was provided by «Powerlab». A Parstat 2273 potentiostat was also used with its internal «Powersuite» software. For all cyclic voltammetries, the conventional representation of anodic currents is reported as positive values and cathodic currents as negative values.

SF_6 electrolysis was performed in acetonitrile with a constant potential in an undivided electrochemical cell.

The control of the decomposition of sulfur hexafluoride was monitored by ^{19}F NMR. The spectra were recorded with a Bruker AC-200 or AC-300 spectrometer. Reported chemical shifts are based on a first order analysis. Internal reference was the peak of $CFCl_3$ (δ = 0.00 ppm) for ^{19}F (188 or 282 MHz) NMR spectra. The ^{19}F NMR of the final mixture was recorded after concentration under vacuum to see a broad fluoride signal.

Funding

S.B. thanks the French Ministry of Research for a Ph.D. grant. The Rhodia-Solvay company is gratefully acknowledged for the gift of sulfur hexafluoride. The French Fluorine Network (GIS Fluor) is acknowledged for financial support.

ORCID® iDs

Bruce Pégot - https://orcid.org/0000-0001-5137-5548
Erwan Le Gall - https://orcid.org/0000-0002-8972-3971
Eric Léonel - https://orcid.org/0000-0002-2998-1004
Emmanuel Magnier - https://orcid.org/0000-0003-3392-3971

References

1. Moissan, H.; Lebeau, P. *C. R. Hebd. Seances Acad. Sci.* **1900,** *130,* 865–871.
2. Weston, R. E. *J. Phys. Chem.* **1995,** *99,* 13150–13155. doi:10.1021/j100035a017
3. Pola, J.; Engst, P.; Horák, M. *Collect. Czech. Chem. Commun.* **1979,** *44,* 2092–2095. doi:10.1135/cccc19792092
4. Hagen, A. P.; Jones, D. J.; Ruttman, S. R. *J. Inorg. Nucl. Chem.* **1974,** *36,* 1217–1219. doi:10.1016/0022-1902(74)80054-0
5. Case, J. R.; Nyman, F. *Nature* **1962,** *193,* 473. doi:10.1038/193473a0
6. Naidu, M. S. *Gas Insulated Substation;* I.K. International: New Delhi, India, 2008.
7. Christophorou, L. G.; Olthoff, J. K.; Van Brunt, R. J. *IEEE Electr. Insul. Mag.* **1997,** *13,* 20–24. doi:10.1109/57.620514
8. Huang, L.; Shen, Y.; Dong, W.; Zhang, R.; Zhang, J.; Hou, H. *J. Hazard. Mater.* **2008,** *151,* 323–330. doi:10.1016/j.jhazmat.2007.05.080

9. Maiss, M.; Brenninkmeijer, C. A. M. *Environ. Sci. Technol.* **1998,** *32,* 3077–3086. doi:10.1021/es9802807
10. Totterdill, A.; Kovács, T.; Gómez Martín, J. C.; Feng, W.; Plane, J. M. C. *J. Phys. Chem. A* **2015,** *119,* 2016–2025. doi:10.1021/jp5123344
11. Song, X.; Liu, X.; Ye, Z.; He, J.; Zhang, R.; Hou, H. *J. Hazard. Mater.* **2009,** *168,* 493–500. doi:10.1016/j.jhazmat.2009.02.047
12. Tsai, W.-T. *J. Fluorine Chem.* **2007,** *128,* 1345–1352. doi:10.1016/j.jfluchem.2007.06.008
13. Zámostná, L.; Braun, T.; Braun, B. *Angew. Chem., Int. Ed.* **2014,** *53,* 2745–2749. doi:10.1002/anie.201308254
14. Holze, P.; Horn, B.; Limberg, C.; Matlachowski, C.; Mebs, S. *Angew. Chem., Int. Ed.* **2014,** *53,* 2750–2753. doi:10.1002/anie.201308270
15. Zámostná, L.; Braun, T. *Angew. Chem., Int. Ed.* **2015,** *54,* 10652–10656. doi:10.1002/anie.201505462
16. Berg, C.; Braun, T.; Ahrens, M.; Wittwer, P.; Herrmann, R. *Angew. Chem., Int. Ed.* **2017,** *56,* 4300–4304. doi:10.1002/anie.201612417
17. Buß, F.; Mück-Lichtenfeld, C.; Mehlmann, P.; Dielmann, F. *Angew. Chem., Int. Ed.* **2018,** *57,* 4951–4955. doi:10.1002/anie.201713206
18. Rueping, M.; Nikolaienko, P.; Lebedev, Y.; Adams, A. *Green Chem.* **2017,** *19,* 2571–2575. doi:10.1039/c7gc00877e
19. McTeague, T. A.; Jamison, T. F. *Angew. Chem., Int. Ed.* **2016,** *55,* 15072–15075. doi:10.1002/anie.201608792
20. Tomar, P.; Braun, T.; Kemnitz, E. *Chem. Commun.* **2018,** *54,* 9753–9756. doi:10.1039/c8cc05494k
21. Rombach, D.; Wagenknecht, H.-A. *ChemCatChem* **2018,** *10,* 2955–2961. doi:10.1002/cctc.201800501
22. Rombach, D.; Wagenknecht, H.-A. *Angew. Chem., Int. Ed.* **2020,** *59,* 300–303. doi:10.1002/anie.201910830
23. Iakobson, G.; Pošta, M.; Beier, P. *J. Fluorine Chem.* **2018,** *213,* 51–55. doi:10.1016/j.jfluchem.2018.07.003
24. Vedel, J.; Trémillon, B. *J. Electroanal. Chem. (1959-1966)* **1960,** *1,* 241–247. doi:10.1016/0022-0728(60)85018-8
25. Montenegro, M. I.; Queiros, M. A.; Daschbach, J. L., Eds. *Microelectrodes: Theory and Applications;* Nato ASI Series. Series E: Applied Sciences 197; Springer Science + Business Media: Dordrecht, The Netherlands, 1991. doi:10.1007/978-94-011-3210-7
26. Berionni, G.; Gonçalves, A.-M.; Mathieu, C.; Devic, T.; Etchéberry, A.; Goumont, R. *Phys. Chem. Chem. Phys.* **2011,** *13,* 2857–2869. doi:10.1039/c0cp01282c
27. Jovené, C.; Jacquet, M.; Marrot, J.; Bourdreux, F.; Kletsky, M. E.; Burov, O. N.; Gonçalves, A.-M.; Goumont, R. *Eur. J. Org. Chem.* **2014,** 6451–6466. doi:10.1002/ejoc.201402692
28. Billon, J. P. *J. Electroanal. Chem. (1959-1966)* **1960,** *1,* 486–501. doi:10.1016/0022-0728(60)85295-3
29. Bard, A. J.; Faulkner, L. R. *Electrochimie Principes, méthodes et applications;* Masson, 1983.
30. Amatore, C.; Azzabi, M.; Calas, P.; Jutand, A.; Lefrou, C.; Rollin, Y. *J. Electroanal. Chem. Interfacial Electrochem.* **1990,** *288,* 45–63. doi:10.1016/0022-0728(90)80024-z
31. Vedel, J.; Trémillon, B. *J. Electroanal. Chem. (1959-1966)* **1960,** *1,* 241–247. doi:10.1016/0022-0728(60)85018-8
32. Billon, J. P. *J. Electroanal. Chem. (1959-1966)* **1960,** *1,* 486–501. doi:10.1016/0022-0728(60)85295-3
33. Gonçalves, A.-M.; Mathieu, C.; Herlem, M.; Etcheberry, A. *J. Electroanal. Chem.* **1999,** *477,* 140–145. doi:10.1016/s0022-0728(99)00398-8

License and Terms

This is an Open Access article under the terms of the Creative Commons Attribution License (https://creativecommons.org/licenses/by/4.0). Please note that the reuse, redistribution and reproduction in particular requires that the author(s) and source are credited and that individual graphics may be subject to special legal provisions.

The license is subject to the *Beilstein Journal of Organic Chemistry* terms and conditions: (https://www.beilstein-journals.org/bjoc/terms)

The definitive version of this article is the electronic one which can be found at: https://doi.org/10.3762/bjoc.16.244

BEILSTEIN JOURNAL OF ORGANIC CHEMISTRY

Metal-free nucleophilic trifluoromethylselenolation via an iodide-mediated umpolung reactivity of trifluoromethylselenotoluenesulfonate

Kevin Grollier[‡1], Alexis Taponard[‡1], Arnaud De Zordo-Banliat[2], Emmanuel Magnier[2] and Thierry Billard[*1,3]

Full Research Paper

Open Access

Address:
[1]Institute of Chemistry and Biochemistry (ICBMS-UMR CNRS 5246), Univ Lyon, Université Lyon 1, CNRS, CPE, INSA, 43 Bd du 11 novembre 1918, 69622 Villeurbanne, France, [2]Université Paris-Saclay, UVSQ, CNRS, UMR 8180, Institut Lavoisier de Versailles, 78035 Versailles Cedex, France and [3]CERMEP-In vivo imaging, Groupement Hospitalier Est, 59 Bd Pinel, 69677 Lyon, France

Email:
Thierry Billard* - Thierry.billard@univ-lyon1.fr

* Corresponding author ‡ Equal contributors

Keywords:
fluorine; nucleophilic substitution; perfluoroalkylselenolation; selenium; trifluoromethylselenolation

Beilstein J. Org. Chem. **2020,** *16,* 3032–3037.
https://doi.org/10.3762/bjoc.16.252

Received: 23 October 2020
Accepted: 02 December 2020
Published: 10 December 2020

This article is part of the thematic issue "Organo-fluorine chemistry V".

Guest Editor: D. O'Hagan

© 2020 Grollier et al.; licensee Beilstein-Institut.
License and terms: see end of document.

Abstract

We report herein a practical method to generate CF_3Se^- (and R_FSe^-) anions from shelf-stable reagents under iodide activation. Metal-free nucleophilic trifluoromethylselenolations have been then performed with this in situ-generated anion. Perfluoroalkylselenolations have also been described.

Introduction

Because of the peculiar properties of the fluorine atom, fluorinated compounds gained a growing interest over the last decades and found applications in a large panel of fields from materials to life sciences [1-15]. Fluorinated motifs bring to molecules specific and often unique electronic and physicochemical characteristics. In order to design new substrates with targeted properties, a modulation of the properties of the introduced substituents became fundamental. In this context, the development of innovative fluorinated groups recently emerged, in particular by combining heteroatoms, such as chalcogens, and fluorinated moieties [16].

Despite, the negative reputation of selenium due to its toxicity at high doses, it is an essential trace element for human physiology and biochemistry [17-20]. Furthermore, selenolated compounds found valuable applications in materials [21-23], life sciences [19,20,24-29], and drug design [30-33]. Consequently, the merging of fluorinated moieties, such as CF_3 with selenium

could constitute an interesting motif in the design of new molecules, in particular in medicinal chemistry or agrochemistry. Even if, to date, there are no CF_3Se-containing pharmaceuticals registered [15], a recent work has demonstrated the promising development of trifluoromethylselenolated nonsteroidal anti-inflammatory drugs as potential anticancer drugs [34].

Over the last years, trifluoromethylselenolation reactions have gained a rising infatuation but, despite this recent interest, methods to introduce the CF_3Se group into organic substrates remain limited [35,36].

One of the simplest ways to achieve trifluoromethylselenolated compounds is the direct nucleophilic substitution of suitable leaving groups to form the CF_3Se–$C(sp^3)$ bond. This chemistry is the prerogative of the CF_3Se^- anion (Scheme 1) [37-40]. However, the formation of this selenium species requires the tedious use of red elemental selenium [41] and also suffers from stability issues. To circumvent these drawbacks, a copper complex has been developed, but in this case the use of a stoichiometric amount of the metal is required [37-39].

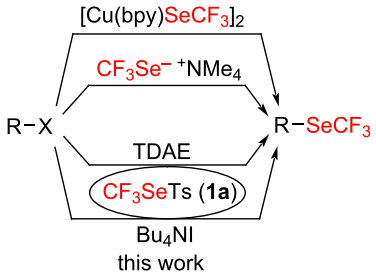

Scheme 1: State of the art concerning the direct nucleophilic trifluoromethylselenolation.

Only a few years ago, trifluoromethylselenotoluenesulfonate (**1a**) has been developed as an efficient reagent to perform electrophilic or radical trifluoromethylselenolations [42-47]. Very recently, we demonstrated that under reductive conditions, such compounds succeeded to perform nucleophilic substitutions [48]. In this reaction, the CF_3Se^- anion was in situ generated by reduction through a double electron transfer of **1a** with TDAE (tetrakis(dimethylamino)ethylene). Even though this umpolung strategy is efficient, the use of the sensitive TDAE, a strong reducing agent, could constitute a drawback for some applications. Consequently, we decided to develop a new umpolung method in non-reductive conditions.

Results and Discussion

A few years ago, we have demonstrated that trifluoromethanesulfenamides, electrophilic trifluoromethylthiolation reagents, could also perform nucleophilic trifluoromethylthiolations through the transient formation of a CF_3SI species which presented an inverted polarity [49,50]. Based on a similar approach, we hypothesized that the CF_3SeI species could also possess the $CF_3Se^{\delta-}$–$I^{\delta+}$ inverted polarity. Thus, based on the previously developed conditions, reagent **1a** was reacted with benzyl bromide (**2a**) in the presence of tetrabutylammonium iodide (TBAI) in acetone at 40 °C (Table 1, entry 1).

The observed result was moderate (Table 1, entry 1). Other solvents, which led also to satisfactory yields in the "sulfur series" were then tested. Acetonitrile did not improve the yield, howev-

Table 1: Reaction between **1a** and **2a**.

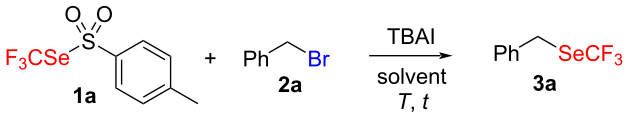

entry	**1a** (equiv)	TBAI (equiv)	**2a** (equiv)	solvent	*T* (°C)	*t* (h)	**3a** (%)[a]
1	1	2	1	acetone	40	15	52
2	1	2	1	CH_3CN	40	15	54
3	1	2	1	THF	40	15	61
4	1	2	1	THF	40	4	62
5	1	2	1	THF	50	4	59
6	1	2	1	THF	60	4	54
7	1	2	1	THF	25	4	47
8	1.5	3	1	THF	40	4	55
9	1	2	2	THF	40	4	89

[a]Yields determined by ^{19}F NMR spectroscopy with $PhOCF_3$ as an internal standard.

er, a better one was obtained in THF (Table 1, entries 2 and 3). Interestingly, a shorter reaction time (4 h instead of 15 h) provided similar results (Table 1, entries 3 and 4). At higher temperatures, the results were not improved and even a slight decrease of the yield was observed, possibly due to an increased degradation of CF_3SeI or CF_3Se^- (Table 1, entries 5 and 6). A lower temperature also decreased the yield (Table 1, entry 7). With an excess of reagents **1a** and TBAI, leading to an excess of the CF_3Se^- species, no significant improvement was observed (Table 1, entry 8). On contrary, the use of 2 equivalents of the electrophile **2a**, to ameliorate the CF_3Se^- anion trapping, had a significant effect and gave a very good yield of the product (Table 1, entry 9). With the optimal conditions in hand, the reaction was exemplified with various other electrophiles (Scheme 2).

The reaction gave generally good results with reactive electrophiles such as benzylic, allylic or propargylic ones (**3a**–**k**). Noteworthy, in the reaction with 2-(bromomethyl)pyridine (**2g**) only 1 equivalent was required, maybe due to a higher reactivity. Furthermore, the reaction seems to be very sensitive to steric hindrance as illustrated by the low yield obtained for **3b**. In contrast, in the aliphatic series, only low yields were observed (**3m**,**n**) except for the activated α-bromo acetophenone (**3l**). This led us to suppose that CF_3Se^- might be a poor nucleophile, which is confirmed by the medium yield observed with the propargylic substrate **3k**, where the chloride starting material was used instead of the bromide as for the other compounds. Noteworthy, because of the volatility of the obtained products, the isolated yields were sometimes significantly below the NMR yields.

Higher fluorinated homologs of **1a** were also synthesized. Consequently, an extension of this method was considered with pentafluoroethylated and tridecafluorohexylated reagents **1b** and **1c**. Good yields were obtained, in particular for **5a** which constitutes, to the best of our knowledge, the first example of a direct nucleophilic tridecafluorohexylselenolation.

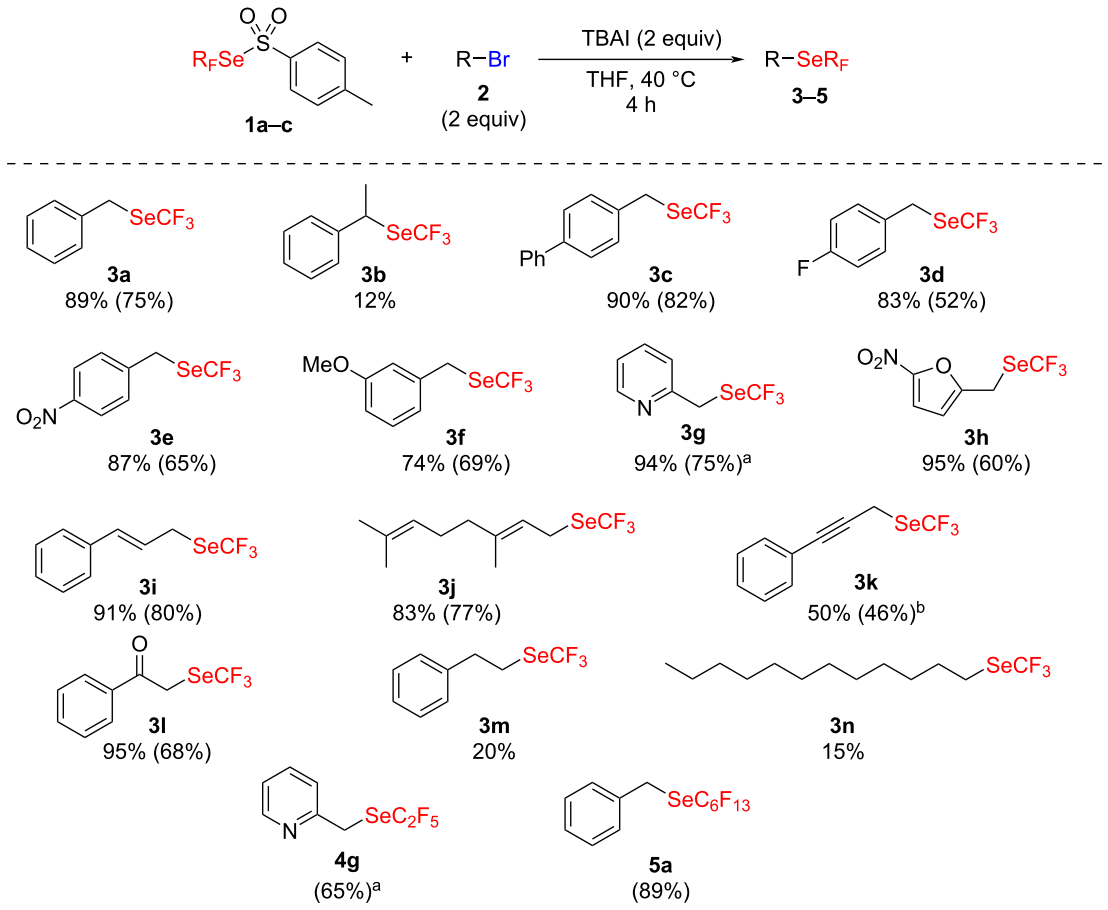

Scheme 2: The nucleophilic fluoroalkylselenolation of alkyl bromides. Yields were determined by ^{19}F NMR spectroscopy with $PhOCF_3$ as an internal standard and yields of isolated products are shown in parentheses. [a]With 1 equiv of electrophile **2**. [b]Starting from propargyl chloride.

From a mechanistic point of view, a pathway inspired by the reaction described with trifluoromethanesulfenamides was postulated (Scheme 3) [49].

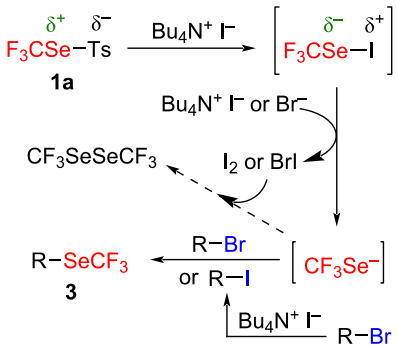

Scheme 3: Mechanism proposal.

The first equivalent of iodide (from TBAI) reacts with the reagent **1a** to produce the transient species CF_3SeI with an inverted polarity on the selenium atom. This compound then undergoes the attack of the second equivalent of iodide to generate the CF_3Se^- anion with releasing of I_2. Finally, the nucleophilic CF_3Se^- can substitute the leaving group onto the electrophilic substrate **2**. However, because of the release of I_2, as side reaction the oxidation of the CF_3Se^- anion can be also envisaged. This was confirmed by the formation of 25–30% of $CF_3SeSeCF_3$ when 1 equivalent of **2a** was used (Table 1, entries 3 and 4). Consequently, the nucleophilic substitution is in competition with this relatively fast oxidation. By adding an excess of the electrophile **2**, the substitution is favored detrimentally to the oxidation. Nevertheless, with weaker or hindered electrophiles, the oxidation reaction is favored compared to the slower substitution. This is adequate with the observed results. Noteworthy, the supposed formation of I_2 was strengthened by the appearance of a red-brown color of the reaction media which faded after the addition of sodium thiosulfate. As demonstrated in the sulfur series [49], the in situ formation of an alkyl iodide from **2**, through a Finkelstein reaction, can be also envisaged. This would not impact the reaction pathway since the released bromide can also activate the CF_3SeI species to provide the expected CF_3Se^- anion.

Conclusion

To conclude, trifluoromethylselenotoluenesulfonate confirmed to be a versatile reagent able to perform electrophilic, radical or nucleophilic reactions depending on the conditions. The iodide-mediated, metal-free method is complementary to the previous one using TDAE. Thus, the umpolung reactivity of trifluoromethylselenotoluenesulfonate can be performed under reductive or oxidative conditions. Furthermore, this method was extended to higher fluorinated homologs allowing the first nucleophilic tridecafluorohexylselenolation.

Experimental

Typical procedure: In a 10 mL flame-dried flask tube equipped with a magnetic stirring bar was added **1a–c** (0.2 mmol, 1 equiv) followed by 0.4 mL of dry THF. Then, compound **2a–n** (0.4 mmol, 2 equiv) was added followed by TBAI (0.4 mmol, 2 equiv). The tube is then sealed and the reaction mixture stirred at 40 °C for 4 h. The conversion was checked by ^{19}F NMR spectroscopy with $PhOCF_3$ as internal standard. After completion, the reaction mixture was partitioned between Et_2O or pentane and water. The aqueous layer was extracted with Et_2O and pentane and the combined organic layers were dried over $MgSO_4$, filtered and concentrated to dryness. The crude residue was purified by chromatography to afford the desired products **3**, **4**, or **5**.

Supporting Information

Supporting Information File 1

Additional experimental and analytical data.
[https://www.beilstein-journals.org/bjoc/content/supplementary/1860-5397-16-252-S1.pdf]

Funding

This work was supported by a grant from the French National Research Agency (ANR 18-CE07-0039-01). The authors are grateful to the CNRS and the French Ministry of Research for financial support. The French Fluorine Network is also acknowledged for its support.

ORCID® iDs

Kevin Grollier - https://orcid.org/0000-0003-0850-8653
Alexis Taponard - https://orcid.org/0000-0001-8008-2293
Emmanuel Magnier - https://orcid.org/0000-0003-3392-3971
Thierry Billard - https://orcid.org/0000-0002-2937-9523

References

1. Smart, B. E. *J. Fluorine Chem.* **2001,** *109,* 3–11. doi:10.1016/s0022-1139(01)00375-x
2. Kirsch, P. *Modern Fluoroorganic Chemistry;* Wiley-VCH: Weinheim, Germany, 2013. doi:10.1002/9783527651351
3. Zhou, Y.; Wang, J.; Gu, Z.; Wang, S.; Zhu, W.; Aceña, J. L.; Soloshonok, V. A.; Izawa, K.; Liu, H. *Chem. Rev.* **2016,** *116,* 422–518. doi:10.1021/acs.chemrev.5b00392
4. Meanwell, N. A. *J. Med. Chem.* **2018,** *61,* 5822–5880. doi:10.1021/acs.jmedchem.7b01788

5. Mei, H.; Han, J.; Fustero, S.; Medio-Simon, M.; Sedgwick, D. M.; Santi, C.; Ruzziconi, R.; Soloshonok, V. A. *Chem. – Eur. J.* **2019,** *25,* 11797–11819. doi:10.1002/chem.201901840
6. Han, J.; Remete, A. M.; Dobson, L. S.; Kiss, L.; Izawa, K.; Moriwaki, H.; Soloshonok, V. A.; O'Hagan, D. *J. Fluorine Chem.* **2020,** *239,* 109639. doi:10.1016/j.jfluchem.2020.109639
7. Cheng, M.; Guo, C.; Gross, M. L. *Angew. Chem., Int. Ed.* **2020,** *59,* 5880–5889. doi:10.1002/anie.201907662
8. Johnson, B. M.; Shu, Y.-Z.; Zhuo, X.; Meanwell, N. A. *J. Med. Chem.* **2020,** *63,* 6315–6386. doi:10.1021/acs.jmedchem.9b01877
9. Jeschke, P. *Pest Manage. Sci.* **2010,** *66,* 10–27. doi:10.1002/ps.1829
10. Ogawa, Y.; Tokunaga, E.; Kobayashi, O.; Hirai, K.; Shibata, N. *iScience* **2020,** *23,* 101467. doi:10.1016/j.isci.2020.101467
11. Fujiwara, T.; O'Hagan, D. *J. Fluorine Chem.* **2014,** *167,* 16–29. doi:10.1016/j.jfluchem.2014.06.014
12. Pagliaro, M.; Ciriminna, R. *J. Mater. Chem.* **2005,** *15,* 4981–4991. doi:10.1039/b507583c
13. Berger, R.; Resnati, G.; Metrangolo, P.; Weber, E.; Hulliger, J. *Chem. Soc. Rev.* **2011,** *40,* 3496–3508. doi:10.1039/c0cs00221f
14. Chopra, D.; Row, T. N. G. *CrystEngComm* **2011,** *13,* 2175–2186. doi:10.1039/c0ce00538j
15. Inoue, M.; Sumii, Y.; Shibata, N. *ACS Omega* **2020,** *5,* 10633–10640. doi:10.1021/acsomega.0c00830
16. Cahard, D.; Ma, J.-A., Eds. *Emerging Fluorinated Motifs: Synthesis, Properties and Applications;* Wiley-VCH: Weinheim, Germany, 2020. doi:10.1002/9783527824342
17. EFSA Panel on Dietetic Products, Nutrition and Allergies. *EFSA J.* **2014,** *12,* 3846. doi:10.2903/j.efsa.2014.3846
18. European Food Safety Authority (EFSA). *EFSA Supporting Publ.* **2017,** *14,* e15121E. doi:10.2903/sp.efsa.2017.e15121
19. Rayman, M. P. *Lancet* **2000,** *356,* 233–241. doi:10.1016/s0140-6736(00)02490-9
20. Mousa, R.; Notis Dardashti, R.; Metanis, N. *Angew. Chem., Int. Ed.* **2017,** *56,* 15818–15827. doi:10.1002/anie.201706876
21. Romashov, L. V.; Ananikov, V. P. *Chem. – Eur. J.* **2013,** *19,* 17640–17660. doi:10.1002/chem.201302115
22. Guo, W.; Fu, Y. *Chem. – Eur. J.* **2020,** *26,* 13322–13331. doi:10.1002/chem.202000878
23. Li, Q.; Zhang, Y.; Chen, Z.; Pan, X.; Zhang, Z.; Zhu, J.; Zhu, X. *Org. Chem. Front.* **2020,** *7,* 2815–2841. doi:10.1039/d0qo00640h
24. Mugesh, G.; du Mont, W.-W.; Sies, H. *Chem. Rev.* **2001,** *101,* 2125–2180. doi:10.1021/cr000426w
25. Rocha, J. B. T.; Piccoli, B. C.; Oliveira, C. S. *ARKIVOC* **2017,** No. ii, 457–491. doi:10.24820/ark.5550190.p009.784
26. Short, S. P.; Pilat, J. M.; Williams, C. S. *Free Radical Biol. Med.* **2018,** *127,* 26–35. doi:10.1016/j.freeradbiomed.2018.05.066
27. Solovyev, N.; Drobyshev, E.; Bjørklund, G.; Dubrovskii, Y.; Lysiuk, R.; Rayman, M. P. *Free Radical Biol. Med.* **2018,** *127,* 124–133. doi:10.1016/j.freeradbiomed.2018.02.030
28. Antoniadou, I.; Kouskou, M.; Arsiwala, T.; Singh, N.; Vasudevan, S. R.; Fowler, T.; Cadirci, E.; Churchill, G. C.; Sharp, T. *Br. J. Pharmacol.* **2018,** *175,* 2599–2610. doi:10.1111/bph.14179
29. Jain, V. K.; Priyadarsini, K. I., Eds. *Organoselenium Compounds in Biology and Medicine: Synthesis, Biological and Therapeutic Treatments;* Royal Society of Chemistry: Cambridge. U.K., 2018. doi:10.1039/9781788011907
30. Singh, N.; Halliday, A. C.; Thomas, J. M.; Kuznetsova, O. V.; Baldwin, R.; Woon, E. C. Y.; Aley, P. K.; Antoniadou, I.; Sharp, T.; Vasudevan, S. R.; Churchill, G. C. *Nat. Commun.* **2013,** *4,* 1332. doi:10.1038/ncomms2320
31. Thangamani, S.; Younis, W.; Seleem, M. N. *Sci. Rep.* **2015,** *5,* 11596. doi:10.1038/srep11596
32. Gandin, V.; Khalkar, P.; Braude, J.; Fernandes, A. P. *Free Radical Biol. Med.* **2018,** *127,* 80–97. doi:10.1016/j.freeradbiomed.2018.05.001
33. Alcolea, V.; Pérez-Silanes, S. *Eur. J. Med. Chem.* **2020,** *206,* 112673. doi:10.1016/j.ejmech.2020.112673
34. He, X.; Zhong, M.; Li, S.; Li, X.; Li, Y.; Li, Z.; Gao, Y.; Ding, F.; Wen, D.; Lei, Y.; Zhang, Y. *Eur. J. Med. Chem.* **2020,** *208,* 112864. doi:10.1016/j.ejmech.2020.112864
35. Tlili, A.; Ismalaj, E.; Glenadel, Q.; Ghiazza, C.; Billard, T. *Chem. – Eur. J.* **2018,** *24,* 3659–3670. doi:10.1002/chem.201704637
36. Billard, T.; Toulgoat, F. When Fluorine Meets Selenium. In *Emerging Fluorinated Motifs: Synthesis, Properties and Applications;* Cahard, D.; Ma, J.-A., Eds.; Wiley-VCH: Weinheim, Germany, 2020; pp 691–721. doi:10.1002/9783527824342.ch23
37. Chen, C.; Ouyang, L.; Lin, Q.; Liu, Y.; Hou, C.; Yuan, Y.; Weng, Z. *Chem. – Eur. J.* **2014,** *20,* 657–661. doi:10.1002/chem.201303934
38. Rong, M.; Huang, R.; You, Y.; Weng, Z. *Tetrahedron* **2014,** *70,* 8872–8878. doi:10.1016/j.tet.2014.09.091
39. Yang, Y.; Lin, X.; Zheng, Z.; Lin, G.; Zhang, Y.; You, Y.; Weng, Z. *J. Fluorine Chem.* **2017,** *204,* 1–5. doi:10.1016/j.jfluchem.2017.10.001
40. Dong, T.; He, J.; Li, Z.-H.; Zhang, C.-P. *ACS Sustainable Chem. Eng.* **2018,** *6,* 1327–1335. doi:10.1021/acssuschemeng.7b03673
41. Tyrra, W.; Naumann, D.; Yagupolskii, Y. L. *J. Fluorine Chem.* **2003,** *123,* 183–187. doi:10.1016/s0022-1139(03)00118-0
42. Glenadel, Q.; Ghiazza, C.; Tlili, A.; Billard, T. *Adv. Synth. Catal.* **2017,** *359,* 3414–3420. doi:10.1002/adsc.201700904
43. Ghiazza, C.; Tlili, A.; Billard, T. *Beilstein J. Org. Chem.* **2017,** *13,* 2626–2630. doi:10.3762/bjoc.13.260
44. Ghiazza, C.; Debrauwer, V.; Billard, T.; Tlili, A. *Chem. – Eur. J.* **2018,** *24,* 97–100. doi:10.1002/chem.201705231
45. Ghiazza, C.; Khrouz, L.; Monnereau, C.; Billard, T.; Tlili, A. *Chem. Commun.* **2018,** *54,* 9909–9912. doi:10.1039/c8cc05256e
46. Ghiazza, C.; Debrauwer, V.; Monnereau, C.; Khrouz, L.; Médebielle, M.; Billard, T.; Tlili, A. *Angew. Chem., Int. Ed.* **2018,** *57,* 11781–11785. doi:10.1002/anie.201806165
Angew. Chem. **2018,** *130,* 11955–11959. doi:10.1002/ange.201806165
47. Ghiazza, C.; Monnereau, C.; Khrouz, L.; Médebielle, M.; Billard, T.; Tlili, A. *Synlett* **2019,** *30,* 777–782. doi:10.1055/s-0037-1610347
48. Ghiazza, C.; Kataria, A.; Tlili, A.; Toulgoat, F.; Billard, T. *Asian J. Org. Chem.* **2019,** *8,* 675–678. doi:10.1002/ajoc.201900027
49. Glenadel, Q.; Bordy, M.; Alazet, S.; Tlili, A.; Billard, T. *Asian J. Org. Chem.* **2016,** *5,* 428–433. doi:10.1002/ajoc.201600003
50. Glenadel, Q.; Tlili, A.; Billard, T. *Eur. J. Org. Chem.* **2016,** 1955–1957. doi:10.1002/ejoc.201600197

License and Terms

This is an Open Access article under the terms of the Creative Commons Attribution License (https://creativecommons.org/licenses/by/4.0). Please note that the reuse, redistribution and reproduction in particular requires that the author(s) and source are credited and that individual graphics may be subject to special legal provisions.

The license is subject to the *Beilstein Journal of Organic Chemistry* terms and conditions: (https://www.beilstein-journals.org/bjoc/terms)

The definitive version of this article is the electronic one which can be found at: https://doi.org/10.3762/bjoc.16.252

BEILSTEIN JOURNAL OF ORGANIC CHEMISTRY

Deoxyfluorination of acyl fluorides to trifluoromethyl compounds by FLUOLEAD®/Olah's reagent under solvent-free conditions

Yumeng Liang[1], Akihito Taya[2], Zhengyu Zhao[2], Norimichi Saito[3] and Norio Shibata[*1,2,4]

Letter

Open Access

Address:
[1]Department of Nanopharmaceutical Sciences, Nagoya Institute of Technology, Gokiso, Showa-ku, Nagoya 466-5888, Japan, [2]Department of Life Science and Applied Chemistry, Nagoya Institute of Technology, Gokiso, Showa-ku, Nagoya 466-5888, Japan, [3]Pharmaceutical Division, Ube Industries, Ltd., Seavans North Bldg, 1-2-1 Shibaura, Minato-ku, Tokyo 105-8449, Japan and [4]Institute of Advanced Fluorine-Containing Materials, Zhejiang Normal University, 688 Yingbin Avenue, 321004 Jinhua, China

Email:
Norio Shibata* - nozshiba@nitech.ac.jp

* Corresponding author

Keywords:
acyl fluorides; deoxyfluorination; fluorine; solvent-free; trifluoromethyl group

Beilstein J. Org. Chem. **2020,** *16,* 3052–3058.
https://doi.org/10.3762/bjoc.16.254

Received: 25 October 2020
Accepted: 04 December 2020
Published: 14 December 2020

This article is part of the thematic issue "Organo-fluorine chemistry V".

Guest Editor: D. O'Hagan

© 2020 Liang et al.; licensee Beilstein-Institut.
License and terms: see end of document.

Abstract

A new protocol enabling the formation of trifluoromethyl compounds from acyl fluorides has been developed. The combination of FLUOLEAD® and Olah's reagent in solvent-free conditions at 70 °C initiated the significant deoxyfluorination of the acyl fluorides and resulted in the corresponding trifluoromethyl products with high yields (up to 99%). This strategy showed a great tolerance for various acyl fluorides containing aryloyl, (heteroaryl)oyl, or aliphatic acyl moieties, providing good to excellent yields of the trifluoromethyl products. Synthetic drug-like molecules were also transformed into the corresponding trifluoromethyl compounds under the same reaction conditions. A reaction mechanism is proposed.

Introduction

Due to an impressively wide effect of fluorine on the biological activity, the insertion of fluorine atoms or fluorine-containing functional groups into organic molecules has become a common strategy in pharmaceutical and agrochemical industries [1-5]. Among various fluorine-containing functional groups, the trifluoromethyl (CF_3) group has received countless attention in the design of novel drugs [6,7]. One utility of the CF_3 group is the replacement of a methyl group in biologically active molecules to avoid the metabolic oxidation of a reactive methyl group in the parent molecules [8]. It should be noted that 19% out of 340 marketed fluoro-pharmaceuticals [4] and 42% out of 424 registered fluoro-agrochemicals [5] contain a CF_3 moiety in their

structures (Figure 1), but this motif has never been found in nature [9]. Several notable examples of CF_3-containing pharmaceuticals and agrochemicals include cinacalcet, efavirenz, travoprost, pexidartinib, fluoxetine, and upadacitinib (Figure 2) [4,5].

Methodologies for the synthesis of trifluoromethyl compounds can be modestly divided into two general categories: the direct introduction of a CF_3 group into the target position by trifluoromethylation [10,11], and the construction of a CF_3 unit by transforming other functional groups [12,13]. Our group has developed various efficient methodologies for the electrophilic [14,15], nucleophilic [16], and radical [17] trifluoromethylation reactions for more than a decade. In recent years, we also reported the direct introduction of an acyl fluoride unit into aromatic compounds by the Pd-catalyzed cross-coupling reaction of aryl, vinyl, and heteroaryl iodides with 2-(difluoromethoxy)-5-nitropyridine [18]. A wide variety of acyl fluorides were efficiently obtained in high yields. We were fascinated by the synthetic versatility of acyl fluorides [19] to form other functional groups during our research on acyl fluorides. Acyl fluorides, which are one type of acyl halides, show distinct stability in the presence of moisture, indicating their suitable reactivity only in selected conditions [19].

In addition to our direct cross-coupling reaction method, several useful synthetic methods for the formation of acyl fluorides have become available in recent years [19-23]. In this context, we were interested in the functional transformation of an acyl fluoride unit into a CF_3 motif. Despite the current rich availability of acyl fluorides and a strong market demand for trifluoro-

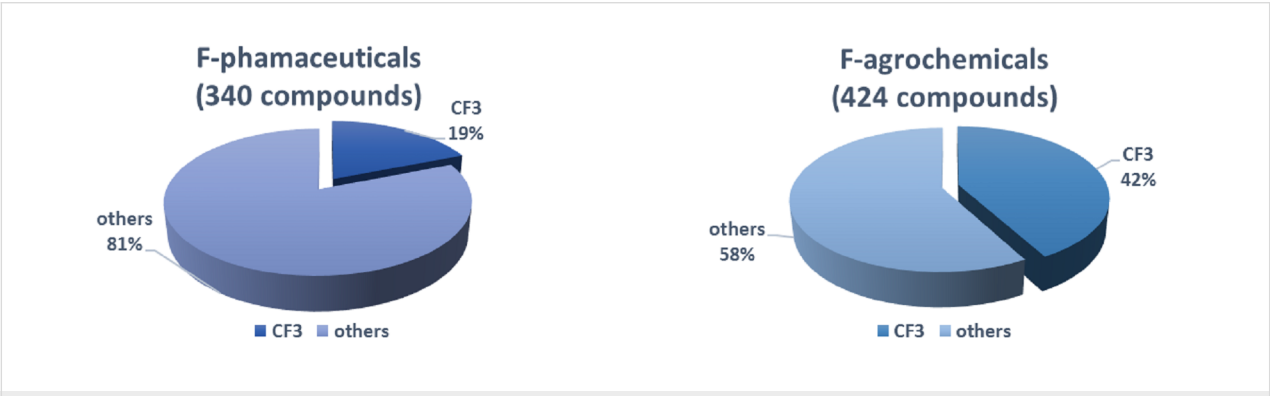

Figure 1: Ratios of CF_3-containing drugs in marketed fluoro-pharmaceuticals and registered fluoro-agrochemicals in the world.

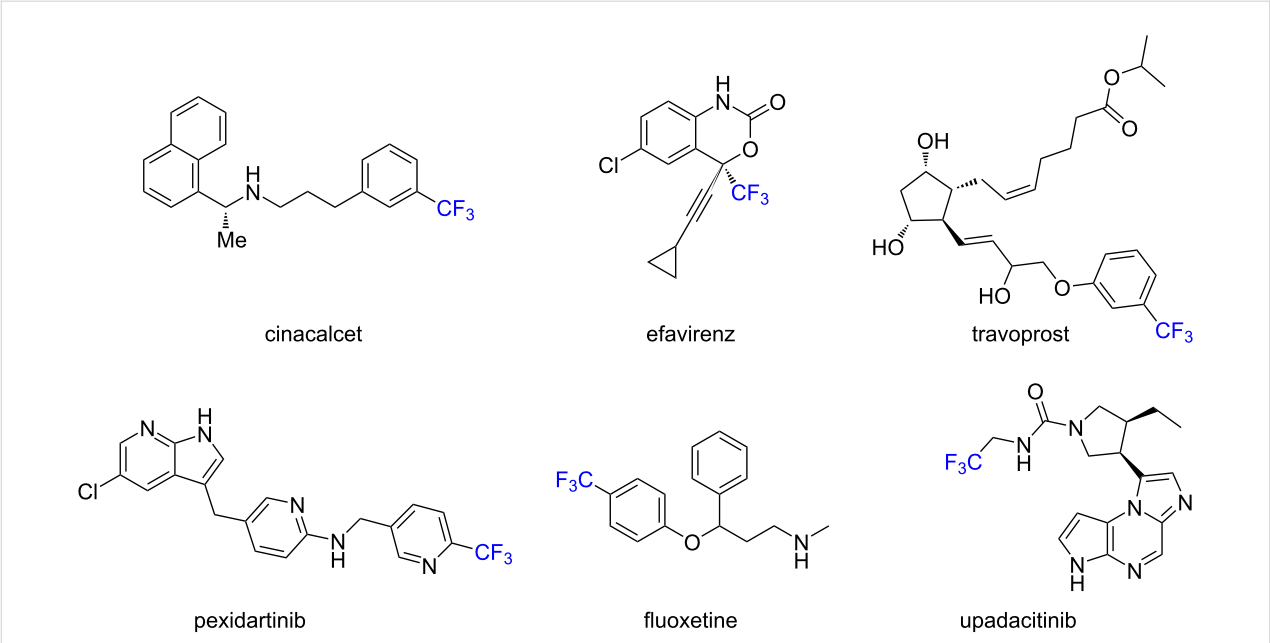

Figure 2: Selected examples of CF_3-containing biologically active molecules.

methyl compounds, synthetic methods for the direct transformation of acyl fluorides to trifluoromethyl compounds are rare [24-26]. A seminal example is the work by Lal and co-workers reported in 1999 (Scheme 1a) [24,25]. The acyl fluorides were converted into the trifluoromethyl compounds in good yields using Deoxo-Fluor®, but they only provided two examples. In 2018, Schoenebeck and co-workers reported the decarbonylative trifluoromethylation of acyl fluorides by trifluoromethyl triethylsilane (Et_3SiCF_3) under Pd catalysis at high temperature (Scheme 1b) [26], although the reaction was categorized as trifluoromethylation and not as fluorination of acyl fluorides. Thus, the acyl fluoride moiety is commonly sacrificed as a "leaving group" in reactions. On the other hand, the transformation to CF_3 derivatives from carboxylic acids are traditionally examined. In 1960, Engelhardt [27] performed the deoxyfluorination of carboxylic acids with sulfur tetrafluoride (SF_4) at 120 to 150 °C in liquid hydrogen fluoride (HF) (Scheme 1c). Very recently, Mykhailiuk [28,29] improved the method to use SF_4 for the deoxofluorination of carboxylic acids with or without HF in the gram scale (Scheme 1c). Although Mykhailiuk's

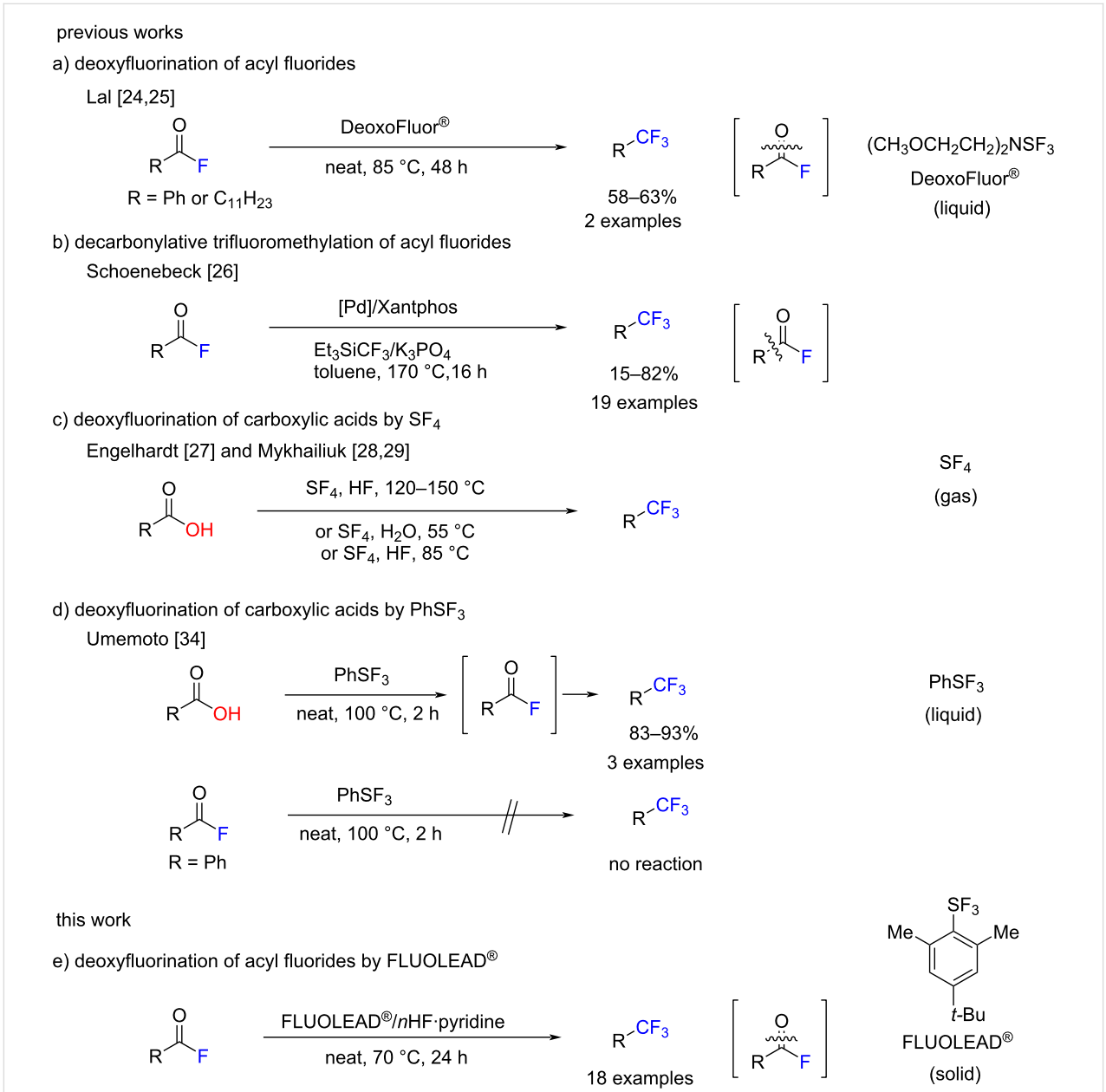

Scheme 1: Transformation of acyl fluorides to trifluoromethyl compounds. a) Deoxyfluorination of acyl fluorides by DeoxoFluor®. b) Decarbonylative trifluoromethylation of acyl fluorides by Et_3SiCF_3. c) Deoxyfluorination of carboxylic acids by SF_4. d) Deoxyfluorination of carboxylic acids by $PhSF_3$ via acyl fluoride intermediates. e) Deoxyfluorination of acyl fluorides by FLUOLEAD®.

protocol is beneficial even for industrial applications, the use of toxic SF_4 requires special apparatus with expert handling.

In 2010, Umemoto and co-workers developed a novel deoxyfluorinating agent, FLUOLEAD® [30]. FLUOLEAD® is a nucleophilic fluorinating agent that can be used as a broad and general substrate for the deoxyfluorination. FLUOLEAD® is a stable crystalline solid and has sufficient stability against moisture to be handled open to air without the emission of fumes, and it is available in quantities that can exceed 100 kg from Ube Industries, Ltd [31]. FLUOLEAD® is an attractive alternative to the toxic sulfur tetrafluoride [32] and the explosive (diethylamino)sulfur trifluoride (DAST) [33]. Although the 2010 report by Umemoto provided a method for the deoxyfluorination of a wide variety of substrates, including alcohols, ketones, and even carboxylic acids to the mono-, di-, and trifluoromethyl compounds using FLUOLEAD® [30], they did not show the direct transformation of an acyl fluoride moiety to a CF_3 unit. In 2012, Umemoto and Singh examined the deoxyfluorination of carboxylic acids to trifluoromethyl compounds by phenylsulfur trifluoride ($PhSF_3$) [34]. They suggested that the transformation of carboxylic acids to the trifluoromethyl units consisted of two steps, including the generation of acyl fluoride intermediates (Scheme 1d). However, the direct transformation of acyl fluorides to trifluoromethyl compounds by $PhSF_3$ did not occur. They explained the importance of the HF generation in the first step from acids to acyl fluorides and for the second step the transformation of the acyl fluorides to the trifluoromethyl compounds. Others have also suggested the critical role of HF for transforming the carboxylic acids to the trifluoromethyl compounds [27-29,35]. Based on these facts, we herein report the efficient deoxyfluorination protocol of acyl fluorides to the trifluoromethyl compounds using FLUOLEAD® (Scheme 1e). The key to the successful transformation is the use of FLUOLEAD® combined with Olah's reagent [36] in solvent-free conditions. A wide variety of acyl fluorides involving aryloyl, (heteroaryl)oyl, and even aliphatic acyl, as well as some drug-like molecules, were smoothly transformed into the corresponding trifluoromethyl compounds in good to excellent yields by FLUOLEAD®/Olah's reagent. Since both FLUOLEAD® and Olah's reagent are commercially available in industrial quantities, this would be an ideal method for the synthesis of trifluoromethyl compounds.

Results and Discussion

First, [1,1'-biphenyl]-4-carbonyl fluoride (**1a**) was selected as the benchmark substrate to optimize the reaction conditions (see Table S1 in Supporting Information File 1 for an extensive list of reaction conditions). The investigation of a range of parameters showed that the best results were achieved by the combination of 3 equiv FLUOLEAD® and 5 equiv *n*HF·pyridine in solvent-free conditions at 70 °C for 24 h, providing the product 4-(trifluoromethyl)-1,1'-biphenyl (**2a**) in 99% ^{19}F NMR yield (Table 1, entry 1). Control experiments conducted in the absence of either FLUOLEAD® or *n*HF·pyridine resulted in no desired product **2a** (Table 1, entries 2 and 3). Moreover, other fluorinating agents, such as DAST, DeoxoFluor, Xtalfluor-M®, and tetrabutylammonium difluorotriphenylsilicate (TBAT), were less effective (Table 1, entry 4). When $NEt_3·(HF)_3$ was used instead of *n*HF·pyridine, the yield decreased to 37%

Table 1: Optimizing the reaction conditions for the conversion of **1a**[a].

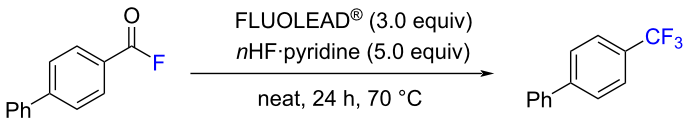

1a (0.3 mmol) **2a**

entry	deviation from the standard conditions	yield (%)[b]
1	none	>99 (91)
2	no FLUOLEAD®	0
3	no *n*HF·pyridine	0
4	using DAST, DeoxoFluor, Xtalfluor-M, TBAT instead of FLUOLEAD®	25, 0, 0, 0
5	using $NEt_3·(HF)_3$ instead of *n*HF·pyridine	37
6	using MeCN, DMF, THF, toluene, or DCM, instead of neat	0, 0, 0, 65,26
7	using 17 h, 3 h or 1 h instead 24 h	55, 22, 9
8	using 40 °C, 50 °C, 100 °C instead of 70 °C	9, 68, 85

[a]Standard conditions: **1a** (0.3 mmol), FLUOLEAD® (0.9 mmol) and *n*HF·pyridine (1.5 mmol) in neat conditions at 70 °C for 24 h. [b]Determined by ^{19}F NMR spectroscopy; the number in parentheses refers to the isolated yield.

(Table 1, entry 5). Using a solvent to participate in the reaction reduced the reaction yield or even resulted in no reaction (Table 1, entry 6). Testing different reaction times indicated that 24 h were necessary (Table 1, entry 7). Lowering the temperature resulted in a decrease in the solubility of substrate **1a**, while raising the temperature to 100 °C allowed a similar yield to be obtained (Table 1, entry 8).

With the optimized conditions in hand, the reaction scope was explored, and the results are summarized in Scheme 2. Various acyl fluorides were investigated in the presence of 3 equiv of FLUOLEAD® and 5 equiv of nHF·pyridine. We first examined the deoxyfluorination of biarylacyl fluorides **1a** and **1b** with a *para*- or *ortho*-substitution. Both substrates gave excellent yields of the desired product **2** (95–99%). Phenyl substrates with a functional group, such as bromo, butyl, cyclohexyl, and methyl at the *para*-position afforded the desired products **2c**–**f** in good to high yields (54–89%). Naphthoyl fluorides **1g** and **1h** gave the desired products **2g** and **2h** in excellent yields (99%). Benzoyl fluoride (**1i**) also furnished trifluoromethylbenzene (**2i**) in an excellent yield (99%). Substrates with two substituents, such as 3,5-dibutyl, 1-bromo-2-methyl, and 1,2-diethoxy groups (**1j**–**l**), furnished the desired products **2j**–**l** in good to excellent yields (66–99%). The heteroaryl group of 2-thiophene (**1m**), the alkyl substrates (**1n** and **1o**) and vinylacyl fluoride (**1p**) were attempted and gave the desired products **2m**–**p** in good to excellent yields (52–93%). Moreover, drug-like derivatives were next investigated as substrates to assess further the utility of this method. The acyl fluoride of the probenecid derivative **1q** was successfully transformed into the corresponding trifluoromethyl compound in an excellent yield of 97% under the same conditions. The deoxyfluorination of the acyl fluoride in febuxostat (**1r**) required a higher reaction temperature (100 °C), and gave the corresponding CF_3 product **2r** in a 73% yield. The gram-scale transformation of **1a** to **2a** was also performed under the same conditions providing a similar result (87% isolated yield). In all cases, the yields of the CF_3 products **2** were high to excellent, as determined by NMR, while the isolated yields decreased due to the high volatility of the products **2**.

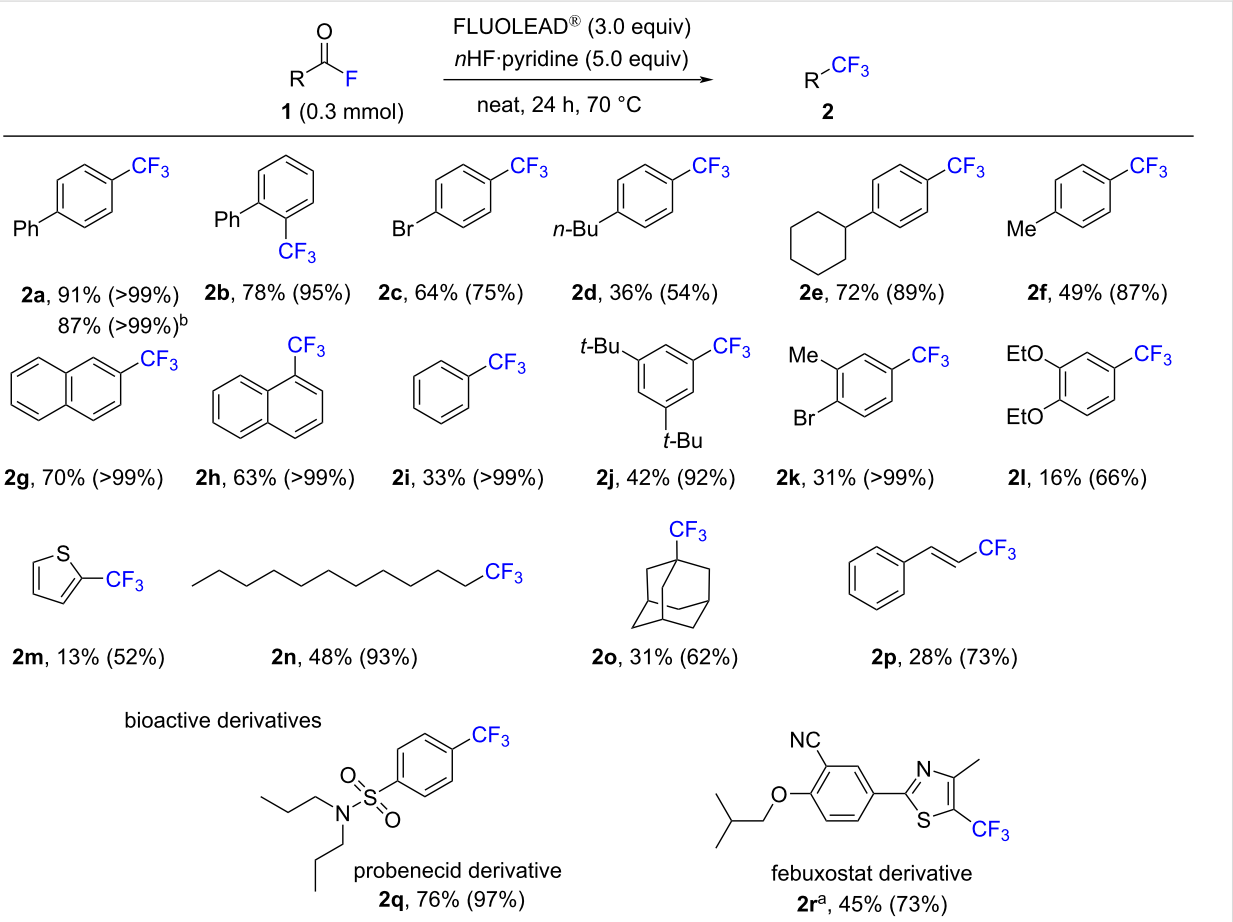

Scheme 2: The substrate scope of acyl fluorides. Reaction conditions: **1** (0.3 mmol), FLUOLEAD® (0.9 mmol, 3.0 equiv) and *n*HF·pyridine (1.5 mmol, 5.0 equiv) in neat conditions at 70 °C for 24 h. Yields in parentheses were determined by ^{19}F NMR spectroscopy. [a]At 100 °C. [b]Using **1a** (1.0 g, 5.0 mmol).

A mechanism of the deoxyfluorination of the acyl fluorides with FLUOLEAD®/*n*HF·pyridine is proposed in Scheme 3. First, FLUOLEAD® is activated with (HF)*n* via hydrogen bonding to provide an activated form **I**, which induces a nucleophilic attack from the carbonyl oxygen of **1** to **I** providing an intermediate **III** via transition state **II**. The intermediate **III** is further activated by (HF)*n* to form **IV**, which finally induces the deoxyfluorination via **V** furnishing the trifluoromethylated products **2** with the release of ArS(O)F and (HF)*n*.

Conclusion

We have reported an efficient protocol for the deoxyfluorination of acyl fluoride substrates, using FLUOLEAD® as the deoxofluorinating agent in the presence of Olah's reagent, to generate trifluoromethyl compounds. FLUOLEAD® combined with Olah's reagent, *n*HF·pyridine, was most effective for this functional transformation reaction. The reaction of acyl fluorides afforded the desired products smoothly in good to high yield in solvent-free conditions. An extension of this deoxyfluorination strategy to drug-like molecules was demonstrated to show the usefulness of this transformation. The present protocol also expands the utility of FLUOLEAD® in organic synthesis.

Experimental

General procedure: An oven-dried narrow-mouth FEP tube (Nalgene®, 10.0 mL) containing a magnetic stirring bar was charged with substrate **1** (0.3 mmol), FLUOLEAD® (225.3 mg, 0.9 mmol, 3.0 equiv) and the *n*HF·pyridine complex (HF 70%, pyridine 30%, 1.5 mmol, 5.0 equiv, neat). The tube was tightly sealed and the reaction mixture stirred at 70 °C for 24 h. Then the mixture was cooled to room temperature and ethanol (3.0 mL) was added to the mixture while stirring for an additional 30 min at room temperature. The mixture was then added to 1 M aqueous $NaHCO_3$ (3 mL) at 0 °C, extracted with Et_2O (3 × 5 mL), and the combined organic layer was dried over anhydrous Na_2SO_4, filtered, and concentrated under reduced pressure. The yield was determined by ^{19}F NMR analysis of the crude mixture by using $C_6H_5OCF_3$ (40.0 µL, 0.3 mmol, 1.0 equiv) as an internal standard. The residue was purified by silica gel flash chromatography (*n*-hexane) to afford the title compounds.

Supporting Information

Supporting Information File 1

Optimization of the reaction conditions, general procedure and product characterization data.
[https://www.beilstein-journals.org/bjoc/content/supplementary/1860-5397-16-254-S1.pdf]

Funding

This work was supported by JSPS KAKENHI grants JP 18H02553 (KIBAN B, NS).

ORCID® iDs

Yumeng Liang - https://orcid.org/0000-0002-2846-0792
Norio Shibata - https://orcid.org/0000-0002-3742-4064

References

1. Isanbor, C.; O'Hagan, D. *J. Fluorine Chem.* **2006,** *127,* 303–319. doi:10.1016/j.jfluchem.2006.01.011
2. Wang, J.; Sánchez-Roselló, M.; Aceña, J. L.; del Pozo, C.; Sorochinsky, A. E.; Fustero, S.; Soloshonok, V. A.; Liu, H. *Chem. Rev.* **2014,** *114,* 2432–2506. doi:10.1021/cr4002879
3. Zhu, Y.; Han, J.; Wang, J.; Shibata, N.; Sodeoka, M.; Soloshonok, V. A.; Coelho, J. A. S.; Toste, F. D. *Chem. Rev.* **2018,** *118,* 3887–3964. doi:10.1021/acs.chemrev.7b00778
4. Inoue, M.; Sumii, Y.; Shibata, N. *ACS Omega* **2020,** *5,* 10633–10640. doi:10.1021/acsomega.0c00830

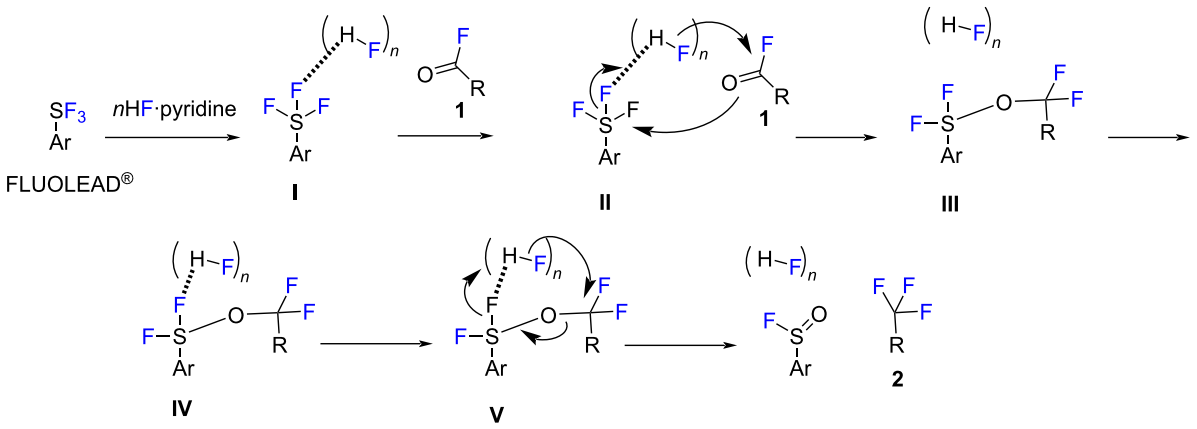

Scheme 3: Mechanism of deoxyfluorination of acyl fluorides **1** with FLUOLEAD®/Olah's reagent to trifluoromethyl compounds **2**.

5. Ogawa, Y.; Tokunaga, E.; Kobayashi, O.; Hirai, K.; Shibata, N. *iScience* **2020,** *23,* 101467. doi:10.1016/j.isci.2020.101467
6. Nie, J.; Guo, H.-C.; Cahard, D.; Ma, J.-A. *Chem. Rev.* **2011,** *111,* 455–529. doi:10.1021/cr100166a
7. Landelle, G.; Panossian, A.; Leroux, F. R. *Curr. Top. Med. Chem.* **2014,** *14,* 941–951. doi:10.2174/1568026614666140202210016
8. Park, B. K.; Kitteringham, N. R.; O'Neill, P. M. *Annu. Rev. Pharmacol. Toxicol.* **2001,** *41,* 443–470. doi:10.1146/annurev.pharmtox.41.1.443
9. O'Hagan, D.; Harper, D. B. *J. Fluorine Chem.* **1999,** *100,* 127–133. doi:10.1016/s0022-1139(99)00201-8
10. Ma, J.-A.; Cahard, D. *J. Fluorine Chem.* **2007,** *128,* 975–996. doi:10.1016/j.jfluchem.2007.04.026
11. Tomashenko, O. A.; Grushin, V. V. *Chem. Rev.* **2011,** *111,* 4475–4521. doi:10.1021/cr1004293
12. Cohen, O.; Mishani, E.; Rozen, S. *Tetrahedron* **2010,** *66,* 3579–3582. doi:10.1016/j.tet.2010.03.045
13. Boswell, G. A., Jr.; Ripka, W. C.; Scribner, R. M.; Tullock, C. W. *Org. React.* **1974,** *21,* 1–124. doi:10.1002/0471264180.or021.01
14. Shibata, N.; Mizuta, S.; Kawai, H. *Tetrahedron: Asymmetry* **2008,** *19,* 2633–2644. doi:10.1016/j.tetasy.2008.11.011
15. Shibata, N.; Matsnev, A.; Cahard, D. *Beilstein J. Org. Chem.* **2010,** *6,* No. 65. doi:10.3762/bjoc.6.65
16. Shibata, N. *Bull. Chem. Soc. Jpn.* **2016,** *89,* 1307–1320. doi:10.1246/bcsj.20160223
17. Matsuzaki, K.; Hiromura, T.; Tokunaga, E.; Shibata, N. *ChemistryOpen* **2017,** *6,* 226–230. doi:10.1002/open.201600172
18. Liang, Y.; Zhao, Z.; Shibata, N. *Commun. Chem.* **2020,** *3,* 59. doi:10.1038/s42004-020-0304-3
19. Ogiwara, Y.; Sakai, N. *Angew. Chem., Int. Ed.* **2020,** *59,* 574–594. doi:10.1002/anie.201902805
20. Munoz, S. B.; Dang, H.; Ispizua-Rodriguez, X.; Mathew, T.; Prakash, G. K. S. *Org. Lett.* **2019,** *21,* 1659–1663. doi:10.1021/acs.orglett.9b00197
21. Scattolin, T.; Deckers, K.; Schoenebeck, F. *Org. Lett.* **2017,** *19,* 5740–5743. doi:10.1021/acs.orglett.7b02516
22. Meanwell, M.; Lehmann, J.; Eichenberger, M.; Martin, R. E.; Britton, R. *Chem. Commun.* **2018,** *54,* 9985–9988. doi:10.1039/c8cc06375c
23. Gonay, M.; Batisse, C.; Paquin, J.-F. *J. Org. Chem.* **2020,** *85,* 10253–10260. doi:10.1021/acs.joc.0c01377
24. Lal, G. S.; Pez, G. P.; Pesaresi, R. J.; Prozonic, F. M.; Cheng, H. *J. Org. Chem.* **1999,** *64,* 7048–7054. doi:10.1021/jo990566+
25. Lal, G. S.; Pez, G. P.; Pesaresi, R. J.; Prozonic, F. M. *Chem. Commun.* **1999,** 215–216. doi:10.1039/a808517j
26. Keaveney, S. T.; Schoenebeck, F. *Angew. Chem., Int. Ed.* **2018,** *57,* 4073–4077. doi:10.1002/anie.201800644
27. Hasek, W. R.; Smith, W. C.; Engelhardt, V. A. *J. Am. Chem. Soc.* **1960,** *82,* 543–551. doi:10.1021/ja01488a012
28. Bugera, M.; Trofymchuk, S.; Tarasenko, K.; Zaporozhets, O.; Pustovit, Y.; Mykhailiuk, P. K. *J. Org. Chem.* **2019,** *84,* 16105–16115. doi:10.1021/acs.joc.9b02596
29. Trofymchuk, S.; Bugera, M. Y.; Klipkov, A. A.; Razhyk, B.; Semenov, S.; Tarasenko, K.; Starova, V. S.; Zaporozhets, O. A.; Tananaiko, O. Yu.; Alekseenko, A. N.; Pustovit, Y.; Kiriakov, O.; Gerus, I. I.; Tolmachev, A. A.; Mykhailiuk, P. K. *J. Org. Chem.* **2020,** *85,* 3110–3124. doi:10.1021/acs.joc.9b03011
30. Umemoto, T.; Singh, R. P.; Xu, Y.; Saito, N. *J. Am. Chem. Soc.* **2010,** *132,* 18199–18205. doi:10.1021/ja106343h
31. Ube Industries, Ltd. https://www.ube-ind.co.jp/ube/en/index.html (accessed Oct 25, 2020).
32. Wang, C. L. J. Sulfur Tetrafluoride. In *Encyclopedia of Reagents for Organic Synthesis.* [Online] Posted April 15, 2001.. https://onlinelibrary.wiley.com/doi/10.1002/047084289X.rs137 (accessed Oct 25, 2020). doi:10.1002/047084289x.rs137
33. Champagne, P. A.; Paquin, J.-F. Trifluoro(*N*-methylmethanaminato)sulfur. In *Encyclopedia of Reagents for Organic Synthesis.* [Online] Posted May 27, 2014. https://onlinelibrary.wiley.com/doi/10.1002/047084289X.rn01660 (accessed Oct 25, 2020). doi:10.1002/047084289x.rn01660
34. Umemoto, T.; Singh, R. P. *J. Fluorine Chem.* **2012,** *140,* 17–27. doi:10.1016/j.jfluchem.2012.03.008
35. Umemoto, T. 4-*tert*-Butyl-2,6-dimethylphenylsulfur trifluoride. In *Encyclopedia of Reagents for Organic Synthesis.* [Online] Posted May 15, 2013. https://onlinelibrary.wiley.com/doi/abs/10.1002/047084289X.rn01524 (accessed Oct 25, 2020). doi:10.1002/047084289x.rn01524
36. Kotun, S. P.; Prakash, G. S.; Hu, J. Pyridinium Poly(hydrogen fluoride). In *Encyclopedia of Reagents for Organic Synthesis.* [Online]; Posted March 15, 2007. https://onlinelibrary.wiley.com/doi/10.1002/9780470842898.rp293.pub2 (accessed Oct 25, 2020). doi:10.1002/9780470842898.rp293.pub2

License and Terms

This is an Open Access article under the terms of the Creative Commons Attribution License (https://creativecommons.org/licenses/by/4.0). Please note that the reuse, redistribution and reproduction in particular requires that the author(s) and source are credited and that individual graphics may be subject to special legal provisions.

The license is subject to the *Beilstein Journal of Organic Chemistry* terms and conditions: (https://www.beilstein-journals.org/bjoc/terms)

The definitive version of this article is the electronic one which can be found at: https://doi.org/10.3762/bjoc.16.254

BEILSTEIN JOURNAL OF ORGANIC CHEMISTRY

Amine–borane complex-initiated SF_5Cl radical addition on alkenes and alkynes

Audrey Gilbert[1], Pauline Langowski[1], Marine Delgado[2], Laurent Chabaud[2], Mathieu Pucheault[*2] and Jean-François Paquin[*1]

Full Research Paper

Open Access

Address:
[1]Département de chimie, Université Laval, Québec, QC, G1V 0A6, Canada and [2]Institut des Sciences Moléculaires - Groupe ORGA - UMR 5255, Université de Bordeaux, 351 Cours de la libération, 33405 Talence, France

Email:
Mathieu Pucheault[*] - mathieu.pucheault@u-bordeaux.fr;
Jean-François Paquin[*] - jean-francois.paquin@chm.ulaval.ca

* Corresponding author

Keywords:
amine-borane complex; pentafluorosulfanyl chloride; pentafluorosulfanyl substituent; radical addition; radical initiation

Beilstein J. Org. Chem. **2020,** *16,* 3069–3077.
https://doi.org/10.3762/bjoc.16.256

Received: 29 September 2020
Accepted: 03 December 2020
Published: 16 December 2020

This article is part of the thematic issue "Organo-fluorine chemistry V".

Guest Editor: D. O'Hagan

© 2020 Gilbert et al.; licensee Beilstein-Institut.
License and terms: see end of document.

Abstract

The SF_5Cl radical addition on unsaturated compounds was performed using an air-stable amine–borane complex as the radical initiator. This method showed to be complementary to the classic Et_3B-mediated SF_5Cl addition on alkenes and alkynes. A total of seven alkene and three alkyne derivatives were tested in the reaction, with yields ranging from 3% to 85%.

Introduction

The pentafluorosulfanyl (SF_5) substituent has been attracting its share of attention since its discovery in 1950 [1]. Often referred to as a "super CF_3", the SF_5 shows enhanced properties when compared to its trifluoromethylated (CF_3) analog [2]. Indeed, the SF_5 moiety is more electronegative, more lipophilic, bulkier, and more thermally and chemically stable than the CF_3 substituent [3-8]. Furthermore, it induces a stronger dipole moment, which can dramatically affect the properties of the neighboring functional groups on a molecule [3-8]. Considering the wide range of trifluoromethylated compounds of interest, the synthesis of their SF_5-analogs has become a trend to increase the properties of these valuable molecules [9]. Due to the unique properties, the SF_5 group has been used in various fields of chemistry, including pharmaceuticals [10-16], agrochemistry [17-20], and materials sciences [21-26]. The applications have, however, been limited by the poor synthetic accessibility of SF_5-containing molecules. As such, the development of alternative methods for the introduction of the SF_5 group is highly relevant.

Although the number of synthetic routes towards the SF_5 substituent remains limited, a few methods have been developed in

the past 20 years in order to include a SF_5 moiety on various organic substrates [27,28]. The main strategy towards pentafluorosulfanylated aliphatic compounds, reported for the first time by Dolbier and co-workers in 2002, is the Et_3B-mediated radical addition of SF_5Cl on alkenes and alkynes (Scheme 1) [29,30]. This strategy represented a tremendous step forward in the pentafluorosulfanyl aliphatic chemistry, since it addressed the drawbacks that were previously reported with the use of SF_5Cl as a reagent. It allows the SF_5Cl addition to occur in the liquid phase (SF_5Cl being a gas that boils at −21 °C) in milder reaction conditions and in normal glassware, instead of using special apparatus such as autoclaves and photochemical reactors [31]. Moreover, this method leads to significantly higher yields in shorter reaction times compared to the previous methods. Since this first report, this reaction has been extensively used to obtain a wide range of SF_5-containing aliphatic derivatives, and represents the most versatile route towards pentafluorosulfanylated aliphatic compounds [28].

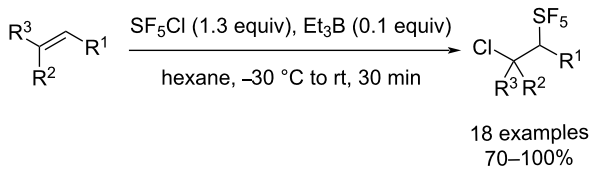

Scheme 1: Dolbier's protocol for the SF_5Cl radical addition on alkenes.

However, some limitations have emerged from the Dolbier protocol. The SF_5Cl addition on unsaturated compounds goes through a free-radical mechanism, and is promoted by the radical activation of SF_5Cl by Et_3B, which leads to the formation of the propagating species $SF_5^{\bullet}$ [32,33]. Trialkylboranes are common low-temperature radical initiators, and Et_3B is one of the most used in the literature [34,35]. The use of the reagent allows the radicals to form, even at very low temperature, due to its strong reactivity with oxygen. However, the disadvantage for the use of the reagent comes from the same property: Et_3B is an oxygen-sensitive and pyrophoric compound even at low temperatures, which requires the use of air-free techniques in the laboratory. Et_3B in the pure form has limited commercial availability and is known to spontaneously react with oxygen to produce a green flame [36]. To avoid the pyrophoric properties of triethylborane, this reagent is mostly sold in low-concentrated solutions (typically 1–2 M in hexane, THF or Et_2O). Another concern is the fluctuation in the quality/concentration in commercial solutions, even among the same batch from the same supplier. Finally, in some cases, the reaction yields can be poorly reproducible if the trialkylborane reagent is not freshly prepared [37]. It is therefore of interest to address this challenge in order to widen the scope of this transformation.

Compared to trialkylboranes, amine–borane complexes have shown to be more stable [38]. Indeed, they are usually air-stable, and their preparation from $NaBH_4$, H_2SO_4 and amines involves traditional mild acidic work-up without degradation. They are therefore much easier to handle on a laboratory scale and can be stored on the shelf for months without noticeable alteration of their properties and purity [39]. Amine–borane complexes have been extensively used in the literature as hydrogen reservoirs [40], as reducing agents in various transformations, including the reduction of aldehydes, amides and ketones, reductive aminations, alkene hydroboration, and carbon bond forming reaction [41,42], as well as various boronate and borinic acid precursors [43-47]. More recently, it has been shown that some of these common amine–borane complexes can also be used as radical initiators for atom transfer radical addition of alkyl halides to alkenes [48]. They were also used in the free-radical polymerization of alkene-containing monomers such as methyl methacrylate or styrene [48-50]. We envisioned that it could be possible to replace the Et_3B in Dolbier's protocol by a stable amine–borane complex that could perform the radical initiation of SF_5Cl on its addition on alkenes. This would address the drawbacks associated with the use of Et_3B as the radical initiator, and therefore facilitate the access to various pentafluorosulfanylated derivatives.

As shown in Scheme 2, we envisioned that the amine–borane complex-initiated reaction of SF_5Cl with alkenes would proceed following a mechanism similar to the amine–borane complex-initiated carbohalogenation of alkenes [48]. The first step would involve the formation of a trialkylborane species via the hydroboration of the alkene, as previously observed by ^{11}B NMR spectroscopy [48,49]. In the presence of oxygen, the trialkylborane would, similarly to Et_3B, generate an alkyl radical. The latter would react with SF_5Cl to produce a chloroalkane as well as the key $SF_5^{\bullet}$ radical. The propagation steps would occur exactly as reported by Dolbier and co-workers for the Et_3B-mediated radical addition of SF_5Cl on alkenes and alkynes [29,30]. Overall, while similar mechanistically, the use of an amine–borane complex as the initiator would avoid the need to manipulate an oxygen-sensitive and pyrophoric reagent.

Results and Discussion

Table 1 and Table 2 show the selected optimization results for the use of amine–borane complexes in the SF_5Cl radical addition on alkenes. We chose allyl benzyl ether (**1**) as the model substrate for our optimization, since it has been previously shown that this compound undergoes SF_5Cl radical addition following Dolbier's protocol in various solvents with high yields [51]. We started the optimization with 3 equivalents of SF_5Cl, 10 mol % of the amine–borane complex, with temperatures going from 30 °C to 60 °C for 3 hours. The addition of all

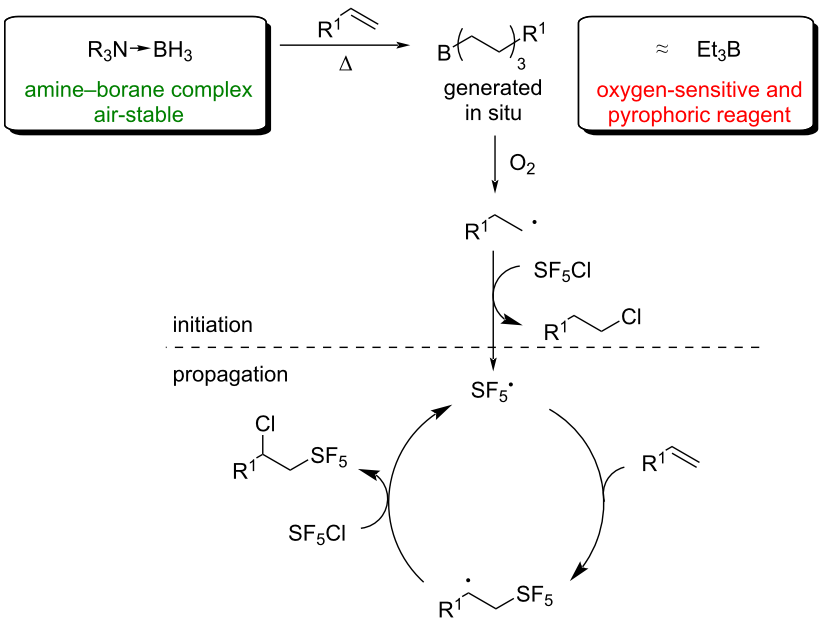

Scheme 2: Proposed mechanism for the amine–borane complex-initiated radical addition of SF_5Cl on alkenes.

reagents was performed at −40 °C, before the reaction vessel was hermetically sealed and heated to avoid evaporation of SF_5Cl, since it is gaseous above −21 °C. The reaction was performed in common organic solvents that remain liquid both at −40 °C and at the tested reaction temperatures. The results in hexane, ethyl acetate (EtOAc), and methyl *tert*-butyl ether (MTBE) are shown in Table 1 and Table 2, but more solvents were tested and did not lead to higher yields of the desired compound (see Supporting Information File 1 for the complete optimization results). Three commercially available borane complexes were tested in the reaction, i.e., diisopropylamine borane (DIPAB), dicyclohexylamine borane (DICAB), and *N,N*-diisopropylethylamine borane (DIPEA·BH_3) (Figure 1). The use of DIPAB and DICAB led to higher yields, and the results are respectively shown in Table 1 and Table 2 (see Supporting Information File 1 for the results with DIPEA·BH_3).

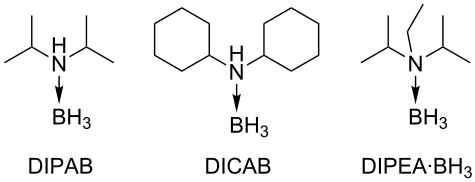

Figure 1: Structures and acronyms of the amine-borane complexes investigated.

We started the optimization with DIPAB as the amine–borane complex. To our delight, in all tested solvents and temperatures, we observed the formation of the desired product **2a**, which is in accordance with our hypothesis that the amine–borane complexes can indeed be used as radical initiators under thermal activation in the SF_5Cl addition on alkenes. DIPAB showed to be generally more productive at lower temperatures. Indeed, when performing the reaction in EtOAc, a full conversion was observed at all tested temperatures, but with a decrease in the yield when the reaction temperature was increased (Table 1, entries 5–8). The same effect was observed in MTBE, with the best results obtained at 30 °C and 50 °C, while 60 °C led to a low yield of 26% (Table 1, entries 9–12). Surprisingly, the intermediate temperature of 40 °C led to only 6% of the desired compound, and the reason for this result remains unclear (Table 1, entry 10). Moreover, the use of hexane as the solvent did not show to be compatible with DIPAB as the amine–borane complex, since it led to low yields at all tested temperatures (Table 1, entries 1–4). When using DIPAB as the radical initiator, the best result was obtained in EtOAc at 30 °C, with a yield of 72% of the desired addition product (Table 1, entry 5).

We next turned our attention to the amine–borane complex DICAB as the radical initiator for the addition of SF_5Cl on allyl benzyl ether (**1**) (Table 2). In this case, increasing the reaction temperature generally led to higher yields. When the reaction was performed in hexane, the yields went from 1–2% to 72% when heating the reaction at 50 °C, compared to 30 °C and 40 °C, while a low yield of 32% was obtained with the reaction temperature of 60 °C (Table 2, entries 1–4). This tendency was also observed when using EtOAc as the solvent (Table 2,

Table 1: Selected optimization results for the SF_5Cl addition on allyl benzyl ether (**1**) using DIPAB as the radical initiator.

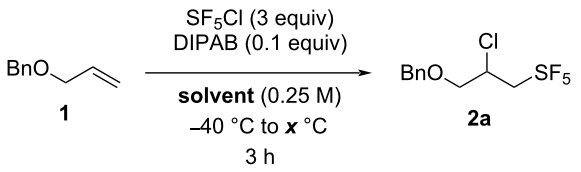

entry	solvent	*x* (°C)	conversion (%)[a]	yield (%)[b]
1	hexane	30	28	2
2	hexane	40	32	6
3	hexane	50	33	7
4	hexane	60	55	5
5	EtOAc	30	100	72
6	EtOAc	40	100	64
7	EtOAc	50	100	5
8	EtOAc	60	100	29
9	MTBE	30	77	40
10	MTBE	40	69	6
11	MTBE	50	79	41
12	MTBE	60	92	26

[a]Disappearance of the starting material, estimated by ^{1}H NMR analysis of the crude mixture using 2-fluoro-4-nitrotoluene as an internal standard. [b]Yield estimated by ^{19}F NMR analysis of the crude mixture using 2-fluoro-4-nitrotoluene as an internal standard.

Table 2: Selected optimization results for the SF_5Cl addition on allyl benzyl ether (**1**) using DICAB as the radical initiator.

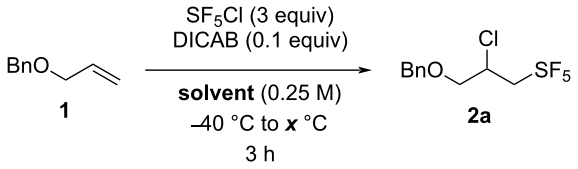

entry	solvent	*x* (°C)	conversion (%)[a]	yield (%)[b]
1	hexane	30	25	1
2	hexane	40	17	2
3	hexane	50	82	72
4	hexane	60	76	32
5	EtOAc	30	100	traces
6	EtOAc	40	100	4
7	EtOAc	50	100	62
8	EtOAc	60	100	56
9	MTBE	30	49	3
10	MTBE	40	100	65
11	MTBE	50	94	21
12	MTBE	60	100	86 (77)[c]

[a]Disappearance of the starting material, estimated by ^{1}H NMR analysis of the crude mixture using 2-fluoro-4-nitrotoluene as an internal standard. [b]Yield estimated by ^{19}F NMR analysis of the crude mixture using 2-fluoro-4-nitrotoluene as an internal standard. [c]Isolated yield.

entries 5–8), with the best yield of 62% obtained at 50 °C (Table 2, entry 7). We hypothesized that a higher temperature is necessary to activate the crystalline and more sterically hindered DICAB, compared to the liquid DIPAB, but that a too high reaction temperature such as 60 °C tends to increase the degradation pathways instead of the formation of the desired compound. However, this effect was not observed when performing the reaction in MTBE. A high yield of 86% was obtained at 60 °C (Table 2, entry 12), while performing the reaction at 40 °C led to a higher yield than at 50 °C (Table 2, entries 10 and 11). With the use of DICAB, the best result obtained was with MTBE as the solvent at 60 °C, affording the product with a yield of 86% (Table 2, entry 12).

At this point, we performed some control reactions in order to get more insight into the reaction (Table 3). We first increased the amount of the amine–borane complex added to the reaction mixture to evaluate if this would promote the desired reaction. Hexane and EtOAc were tested at 50 °C with 20 mol % instead of 10 mol % of DICAB (Table 3, entries 1 and 2). This showed to be slightly beneficial in the case of EtOAc (Table 3, entry 1), while it led to a low yield in the case of hexane (Table 3, entry 2). Moreover, increasing the reaction time from 3 to 6 hours led to higher yields of the desired SF_5-containing adduct, with yields of 80% and 89% with EtOAc and hexane, respectively (Table 3, entries 3 and 4). Finally, we performed the reaction in hexane with no amine–borane complex added, and only trace amounts of the final compound **2a** were detected (Table 3, entry 5).

Table 3: Effect of time and amount of the amine–borane complex on the SF_5Cl addition on allyl benzyl ether (**1**).

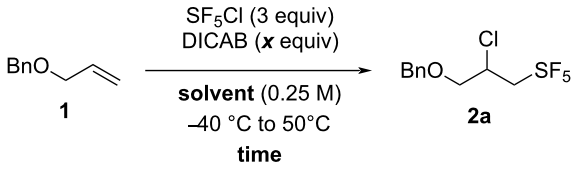

entry	solvent	DICAB (equiv)	time (h)	conversion (%)[a]	yield (%)[b]
1	EtOAc	0.2	3	100	80
2	hexane	0.2	3	61	37
3	EtOAc	0.1	6	100	86
4	hexane	0.1	6	94	89
5	hexane	0	6	20	traces

[a]Disappearance of the starting material, estimated by ^{1}H NMR analysis of the crude mixture using 2-fluoro-4-nitrotoluene as an internal standard. [b]Yield estimated by ^{19}F NMR analysis of the crude mixture using 2-fluoro-4-nitrotoluene as an internal standard.

We next wondered if it could be possible to start the reaction at a higher temperature than −40 °C without significantly affecting the reaction yield. We performed the reaction with 10 mol % of DICAB, using our standard conditions, but with the addition of all reagents at 0 °C or at room temperature (20–21 °C) before sealing the reaction vessel and heating the reaction mixture to 50 °C (Table 4). EtOAc, hexane, and MTBE were tested in these conditions, and with the exception of hexane when starting the reaction at 0 °C (Table 4, entry 3), all reactions led to the desired final compound in good to excellent yields (Table 4, entries 1, 2, and 4–6). Indeed, we obtained a 93% yield of the addition product **2a** when performing the reaction in EtOAc from 0 °C to 50 °C (Table 4, entry 1). The low yield of 2% that was obtained with hexane (Table 4, entry 3) is, however, rather surprising, since the reaction in that solvent from room temperature to 50 °C led to 81% of the desired compound (Table 4, entry 4). When repeating the reaction, we rapidly realized that these higher initial temperatures conditions were not reproducible, which we believe came from the fact that at 0 °C and room temperature, SF_5Cl is gaseous. Therefore, its addition to the reaction mixture might have been inefficient in some case, while getting added properly in some other cases, which would explain the reproducibility problems. Moreover, this effect was not observed when repeating some of the reactions where the initial temperature was −40 °C, which is in accordance with this hypothesis.

Table 4: Effect of the initial temperature on the SF_5Cl addition on allyl benzyl ether (**1**).

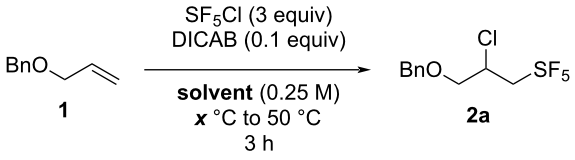

entry	solvent	*x* (°C)	conversion (%)[a]	yield (%)[b]
1	EtOAc	0	100	93
2	EtOAc	20	100	71
3	hexane	0	40	2
4	hexane	20	100	81
5	MTBE	0	100	75
6	MTBE	20	100	79

[a]Disappearance of the starting material, estimated by ^{1}H NMR analysis of the crude mixture using 2-fluoro-4-nitrotoluene as an internal standard. [b]Yield estimated by ^{19}F NMR analysis of the crude mixture using 2-fluoro-4-nitrotoluene as an internal standard.

Finally, we hypothesized that reducing the amount of the amine–borane complex in the reaction could increase the yield by avoiding a surge of the radical species early in the reaction. We performed the reactions with 3.3 mol % of the amine–borane complex in hexane, EtOAc, and MTBE and at 50 °C and 60 °C (Table 5). Unfortunately, the reaction yields

Table 5: Effect of the decreased amount of the amine-borane complex on the SF_5Cl addition on allyl benzyl ether (**1**).

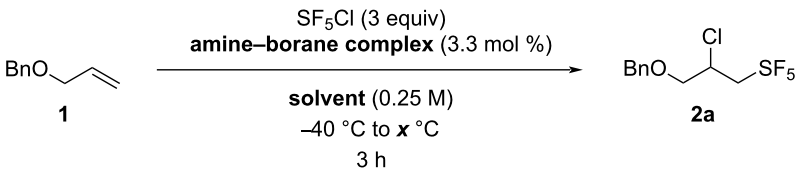

entry	solvent	amine–borane complex	*x* (°C)	conversion (%)[a]	yield (%)[b]
1	hexane	DIPAB	50	25	2
2	hexane	DICAB	50	93	86
3	hexane	DIPAB	60	65	41
4	hexane	DICAB	60	30	22
5	EtOAc	DIPAB	50	54	9
6	EtOAc	DICAB	50	66	2
7	EtOAc	DIPAB	60	100	6
8	EtOAc	DICAB	60	100	37
9	MTBE	DIPAB	50	67	20
10	MTBE	DICAB	50	100	73
11	MTBE	DIPAB	60	67	24
12	MTBE	DICAB	60	100	75

[a]Disappearance of the starting material, estimated by ^{1}H NMR analysis of the crude mixture using 2-fluoro-4-nitrotoluene as an internal standard. [b]Yield estimated by ^{19}F NMR analysis of the crude mixture using 2-fluoro-4-nitrotoluene as an internal standard.

did not increase, and these reaction conditions proved to be less efficient for the SF_5Cl addition on allyl benzyl ether than the ones previously discussed. The only case where the yield was promoted by a decreased amount of the amine–borane complex was when the reaction was performed in hexane at 50 °C and with the use of DICAB as the radical initiator (Table 5, entry 2). Indeed, this led to a product yield of 86%, which is equal to the best yield obtained so far, in MTBE with 10 mol % of DICAB at 60 °C (Table 2, entry 12). However, the latter led to a full conversion, which is not the case with the reaction in hexane, with a conversion of 93%. Considering the similar polarity of the starting material **1** and the final product **2a**, we chose the reaction conditions in MTBE as the optimal conditions, in order to facilitate the purification process.

With the optimal reaction conditions in hand, we evaluated the scope of the reaction. Both our DICAB-promoted and the Dolbier's protocol using Et_3B for the SF_5Cl radical addition on unsaturated compounds were performed on every substrate, in order to compare the two methods. First, a series of alkenes was assessed for the SF_5Cl radical addition using both protocols (Scheme 3). In most cases, the desired pentafluorosulfanylated compounds were obtained in comparable yields with both methods, with a slightly better yield for the Dolbier protocol. Indeed, compound **2a** was obtained with an 88% yield when the SF_5Cl addition was performed with Et_3B, while 77% of the desired final product was obtained with the DICAB-mediated protocol. Moreover, yields of 90% and 85% of compound **2b** were respectively obtained when using 4-phenyl-1-butene as the starting material. When performing the reactions on styrene, the desired addition product **2c** was only observed with a low NMR yield of 8% with the Et_3B-mediated reaction, while the DICAB protocol led to a 15% isolated yield of the 2:1 addition product **2d**, with no sign of the desired compound **2c**. Furthermore, as expected, a low yield of 15% of the corresponding addition product **2e** was obtained with Dolbier's protocol when performing the reaction on dec-9-en-1-ol, while protecting the alcohol group with an acetate significantly increased the yield, leading to the corresponding pentafluorosulfanylated derivative **2f** with a 92% yield. However, this effect was not observed when the DICAB protocol was performed on these two substrates. In both cases, while the final compounds could not be isolated from the reaction mixture, comparison of the NMR yields of both crude mixtures showed that the alcohol was more tolerated in the reaction with DICAB, albeit the final compound **2e** was obtained with the moderate NMR yield of 43%. The SF_5Cl addition on the acetate derivative led to only 3% NMR yield of the final compound **2f** and the reaction mixture showed the presence of various degradation compounds. Finally, the SF_5Cl addition was performed on two ester derivatives. When using vinyl benzoate as the starting material, the desired compound **2g** was obtained with a 75% yield with

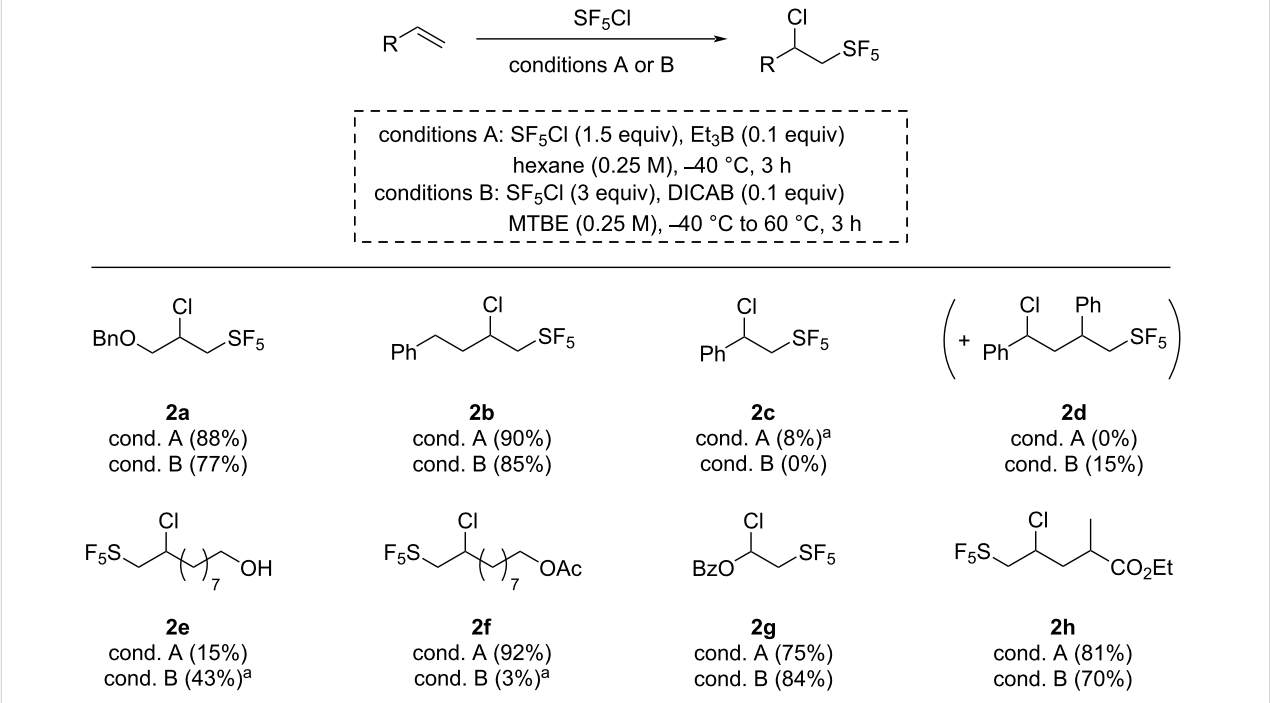

Scheme 3: Scope of the Et_3B and the DICAB-initiated SF_5Cl additions on alkenes. Unless noted otherwise, isolated yields are reported. [a]Yield estimated by ^{19}F NMR analysis of the crude mixture using 2-fluoro-4-nitrotoluene as an internal standard.

Dolbier's protocol and an 84% yield with the DICAB protocol, while the addition product **2h** was obtained with an 81% yield using Et_3B as the radical initiator and 70% when the reaction was performed with DICAB.

Next, the SF_5Cl radical additions on alkynes using both protocols were performed (Scheme 4). First, 4-phenyl-1-butyne was evaluated, and the desired pentafluorosulfanylated product **2i** was obtained with a 79% yield with the Et_3B-mediated reaction, and a higher yield of 88% when using DICAB as the radical initiator. In the case of the SF_5Cl addition on phenylacetylene, it has been reported in the initial report from Dolbier that the formation of the side-product **2k**, resulting from the 2:1 addition of the starting material on the intermediate radical, occurred with the Et_3B-mediated reaction [29]. In our hands, Dolbier's protocol led to only trace amounts of the compound **2k** and 18% of the desired addition product **2j**, while the reaction with the DICAB conditions led to 23% of the desired compound **2j**, and 5% of the 2:1 addition side product **2k**. Finally, the reaction was performed on the internal alkyne 6-dodecyne, and the Dolbier's protocol led to the moderate yield of 65% of the desired compound **2l**, while only a 17% NMR yield was obtained in the reaction using DICAB as the radical initiator.

Conclusion

In conclusion, we have shown that amine–borane complexes can be used as radical initiators under thermal conditions to perform the SF_5Cl radical addition on unsaturated compounds. These air-stable complexes can therefore be used as alternatives to the more unstable and pyrophoric Et_3B, in order to incorporate the SF_5 substituent on aliphatic derivatives. A total of 7 examples of alkene derivatives and 3 examples of alkyne derivatives were evaluated in the reaction, with yields ranging from 3% to 85%. Overall, this reaction represents a complementary method to the Et_3B-mediated SF_5Cl addition on unsaturated compounds.

Supporting Information

Supporting Information File 1

General information, synthetic procedures, additional optimization results, NMR spectra for known compounds (^1H, ^{19}F) and full characterization of all new compounds.
[https://www.beilstein-journals.org/bjoc/content/supplementary/1860-5397-16-256-S1.pdf]

Funding

We acknowledge the financial support of the Natural Sciences and Engineering Research Council of Canada (NSERC) and Université Laval.

ORCID® iDs

Laurent Chabaud - https://orcid.org/0000-0002-2590-8707
Jean-François Paquin - https://orcid.org/0000-0003-2412-3083

References

1. Silvey, G. A.; Cady, G. H. *J. Am. Chem. Soc.* **1950,** *72,* 3624–3626. doi:10.1021/ja01164a084
2. Thayer, A. M. *Chem. Eng. News* **2006,** *84* (23), 27–32. doi:10.1021/cen-v084n023.p027

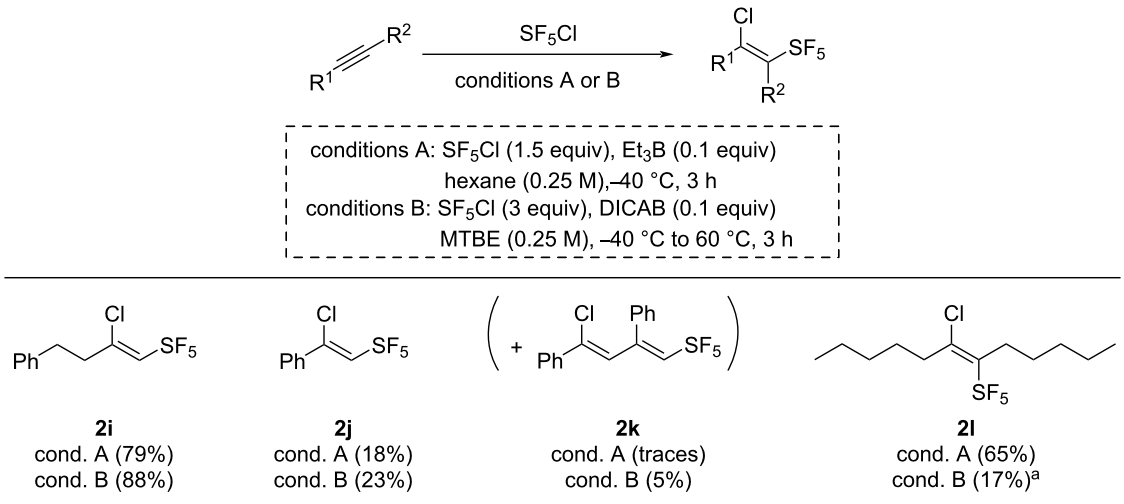

Scheme 4: Scope of the Et_3B and the DICAB-initiated SF_5Cl additions on alkynes. Unless noted otherwise, isolated yields are reported. [a]Yield estimated by ^{19}F NMR analysis of the crude mixture using 2-fluoro-4-nitrotoluene as an internal standard.

3. Matsuzaki, K.; Okuyama, K.; Tokunaga, E.; Saito, N.; Shiro, M.; Shibata, N. *Org. Lett.* **2015,** *17,* 3038–3041. doi:10.1021/acs.orglett.5b01323
4. Bassetto, M.; Ferla, S.; Pertusati, F. *Future Med. Chem.* **2015,** *7,* 527–546. doi:10.4155/fmc.15.5
5. Savoie, P. R.; Welch, J. T. *Chem. Rev.* **2015,** *115,* 1130–1190. doi:10.1021/cr500336u
6. Dalvit, C.; Ko, S. Y.; Vulpetti, A. *J. Fluorine Chem.* **2013,** *152,* 129–135. doi:10.1016/j.jfluchem.2013.01.017
7. Sheppard, W. A. *J. Am. Chem. Soc.* **1962,** *84,* 3064–3072. doi:10.1021/ja00875a006
8. Jackson, D. A.; Mabury, S. A. *Environ. Toxicol. Chem.* **2009,** *28,* 1866–1873. doi:10.1897/09-037.1
9. Sowaileh, M. F.; Hazlitt, R. A.; Colby, D. A. *ChemMedChem* **2017,** *12,* 1481–1490. doi:10.1002/cmdc.201700356
10. Welch, J. T.; Lim, D. S. *Bioorg. Med. Chem.* **2007,** *15,* 6659–6666. doi:10.1016/j.bmc.2007.08.012
11. Wipf, P.; Mo, T.; Geib, S. J.; Caridha, D.; Dow, G. S.; Gerena, L.; Roncal, N.; Milner, E. E. *Org. Biomol. Chem.* **2009,** *7,* 4163–4165. doi:10.1039/b911483a
12. Chia, P. W.; Brennan, S. C.; Slawin, A. M. Z.; Riccardi, D.; O'Hagan, D. *Org. Biomol. Chem.* **2012,** *10,* 7922–7927. doi:10.1039/c2ob26402a
13. Zhang, Y.; Wang, Y.; He, C.; Liu, X.; Lu, Y.; Chen, T.; Pan, Q.; Xiong, J.; She, M.; Tu, Z.; Qin, X.; Li, M.; Tortorella, M. D.; Talley, J. J. *J. Med. Chem.* **2017,** *60,* 4135–4146. doi:10.1021/acs.jmedchem.6b01484
14. Moraski, G. C.; Bristol, R.; Seeger, N.; Boshoff, H. I.; Tsang, P. S.-Y.; Miller, M. J. *ChemMedChem* **2017,** *12,* 1108–1115. doi:10.1002/cmdc.201700170
15. Mori, S.; Tsuemoto, N.; Kasagawa, T.; Nakano, E.; Fujii, S.; Kagechika, H. *Chem. Pharm. Bull.* **2019,** *67,* 1278–1283. doi:10.1248/cpb.c19-00522
16. Naclerio, G. A.; Abutaleb, N. S.; Onyedibe, K. I.; Seleem, M. N.; Sintim, H. O. *RSC Med. Chem.* **2020,** *11,* 102–110. doi:10.1039/c9md00391f
17. Banks, B. J. Parasiticidal pyrazoles. Eur. Pat. Appl. EP0933363A1, Aug 4, 1999.
18. Lim, D. S.; Choi, J. S.; Pak, C. S.; Welch, J. T. *J. Pestic. Sci. (Tokyo, Jpn.)* **2007,** *32,* 255–259. doi:10.1584/jpestics.g06-50
19. Kay, I. T.; Barton, J. E. D.; Collins, D. J.; Kowalczyk, B.; Mitchell, G.; Shribbs, J. M.; Cox, J. M.; Barnes, N. J.; Smith, S. C. Herbicides. WO Pat. Appl. WO/94/13652, June 23, 1994.
20. Alt, G. H.; Pratt, J. K.; Phillips, W. G.; Srouji, G. H. Substituted thiazoles and their use as fungicides. Eur. Pat. Appl. EP0371950A2, June 6, 1990.
21. Zhang, G.; Lee, Y.-J.; Gautam, P.; Lin, C.-C.; Liu, C.-L.; Chan, J. M. W. *J. Mater. Chem. C* **2019,** *7,* 7865–7871. doi:10.1039/c9tc00756c
22. Kirsch, P.; Bremer, M.; Heckmeier, M.; Tarumi, K. *Angew. Chem., Int. Ed.* **1999,** *38,* 1989–1992. doi:10.1002/(sici)1521-3773(19990712)38:13/14<1989::aid-anie1989>3.0.co;2-k
23. Henwood, A. F.; Webster, J.; Cordes, D.; Slawin, A. M. Z.; Jacquemin, D.; Zysman-Colman, E. *RSC Adv.* **2017,** *7,* 25566–25574. doi:10.1039/c7ra03190d
24. Iida, N.; Tanaka, K.; Tokunaga, E.; Mori, S.; Saito, N.; Shibata, N. *ChemistryOpen* **2015,** *4,* 698–702. doi:10.1002/open.201500165
25. Chan, J. M. W. *J. Mater. Chem. C* **2019,** *7,* 12822–12834. doi:10.1039/c9tc01949a
26. Pal, A. K.; Henwood, A. F.; Cordes, D. B.; Slawin, A. M. Z.; Samuel, I. D. W.; Zysman-Colman, E. *Inorg. Chem.* **2017,** *56,* 7533–7544. doi:10.1021/acs.inorgchem.7b01075
27. Beier, P. Pentafluorosulfanylation of Aromatics and Heteroaromatics. In *Emerging Fluorinated Motifs: Synthesis, Properties and Applications;* Ma, J.-A.; Cahard, D., Eds.; Wiley-VCH: Weinheim, Germany, 2020; pp 551–570. doi:10.1002/9783527824342.ch18
28. Haufe, G. Pentafluorosulfanylation of Aliphatic Substrates. In *Emerging Fluorinated Motifs: Synthesis, Properties and Applications;* Ma, J.-A.; Cahard, D., Eds.; Wiley-VCH: Weinheim, Germany, 2020; pp 571–609. doi:10.1002/9783527824342.ch19
29. Aït-Mohand, S.; Dolbier, W. R., Jr. *Org. Lett.* **2002,** *4,* 3013–3015. doi:10.1021/ol026483o
30. Dolbier, W. R., Jr.; Aït-Mohand, S.; Schertz, T. D.; Sergeeva, T. A.; Cradlebaugh, J. A.; Mitani, A.; Gard, G. L.; Winter, R. W.; Thrasher, J. S. *J. Fluorine Chem.* **2006,** *127,* 1302–1310. doi:10.1016/j.jfluchem.2006.05.003
31. Verma, R. D.; Kirchmeier, R. L.; Shreeve, J. M. *Adv. Inorg. Chem.* **1994,** *41,* 125–169. doi:10.1016/s0898-8838(08)60171-3
32. Sidebottom, H. W.; Tedder, J. M.; Walton, J. C. *Trans. Faraday Soc.* **1969,** *65,* 2103–2109. doi:10.1039/tf9696502103
33. Uematsu, R.; Saka, C.; Sumiya, Y.; Ichino, T.; Taketsugu, T.; Maeda, S. *Chem. Commun.* **2017,** *53,* 7302–7305. doi:10.1039/c7cc02541f
34. Ollivier, C.; Renaud, P. *Chem. Rev.* **2001,** *101,* 3415–3434. doi:10.1021/cr010001p
35. Renaud, P.; Beauseigneur, A.; Brecht-Forster, A.; Becattini, B.; Darmency, V.; Kandhasamy, S.; Montermini, F.; Ollivier, C.; Panchaud, P.; Pozzi, D.; Scanlan, E. M.; Schaffner, A.-P.; Weber, V. *Pure Appl. Chem.* **2007,** *79,* 223–233. doi:10.1351/pac200779020223
36. Frankland, E. *J. Chem. Soc.* **1862,** *15,* 363–381. doi:10.1039/js8621500363
37. Székely, A.; Klussmann, M. *Chem. – Asian J.* **2019,** *14,* 105–115. doi:10.1002/asia.201801636
38. Brotherton, R. J.; Weber, C. J.; Guibert, C. R.; Little, J. L. Boron Compounds. *Ullmann's Encyclopedia of Industrial Chemistry;* Wiley-VCH Verlag GmbH: Weinheim, Germany, 2000. doi:10.1002/14356007.a04_309
39. A ^{11}B NMR spectrum of the amino-borane complex DICAB was taken over one year after the reception of the compound (see Supporting Information File 1). The ^{11}B NMR spectrum shows a clean signal from the DICAB complex, with no sign of oxidation or degradation. This indicates that these complexes can be stored (without the need for argon) for a long time without noticeable degradation.
40. Staubitz, A.; Robertson, A. P. M.; Manners, I. *Chem. Rev.* **2010,** *110,* 4079–4124. doi:10.1021/cr100088b
41. Couturier, M.; Tucker, J. L.; Andresen, B. M.; Dubé, P.; Negri, J. T. *Org. Lett.* **2001,** *3,* 465–467. doi:10.1021/ol006969+
42. Marciasini, L. D.; Richard, J.; Cacciuttolo, B.; Sartori, G.; Birepinte, M.; Chabaud, L.; Pinet, S.; Pucheault, M. *Tetrahedron* **2019,** *75,* 164–171. doi:10.1016/j.tet.2018.11.036
43. Guerrand, H. D. S.; Marciasini, L. D.; Gendrineau, T.; Pascu, O.; Marre, S.; Pinet, S.; Vaultier, M.; Aymonier, C.; Pucheault, M. *Tetrahedron* **2014,** *70,* 6156–6161. doi:10.1016/j.tet.2014.04.036
44. Guerrand, H. D. S.; Vaultier, M.; Pinet, S.; Pucheault, M. *Adv. Synth. Catal.* **2015,** *357,* 1167–1174. doi:10.1002/adsc.201401153
45. Richard, J.; Birepinte, M.; Charbonnier, J. B.; Liautard, V.; Pinet, S.; Pucheault, M. *Synthesis* **2017,** *49,* 736–744. doi:10.1055/s-0036-1588345

46. Birepinte, M.; Liautard, V.; Chabaud, L.; Pucheault, M. *Chem. – Eur. J.* **2020,** *26,* 3236–3240. doi:10.1002/chem.201905772
47. Birepinte, M.; Liautard, V.; Chabaud, L.; Pucheault, M. *Org. Lett.* **2020,** *22,* 2838–2843. doi:10.1021/acs.orglett.0c00908
48. Liautard, V.; Delgado, M.; Colin, B.; Chabaud, L.; Michaud, G.; Pucheault, M. *ChemRxiv* **2020**. doi:10.26434/chemrxiv.13274543.v1
49. Delgado, M.; Michaud, G.; Colin, B.; Simon, F.; Fouquay, S.; Pucheault, M. Procédé de polymérisation d'au moins un composé polymérisable par voie radicalaire. Fr. Pat. Appl. FR2003811, 2020.
50. Michaud, G.; Simon, F.; Fouquay, S.; Liautard, V.; Pucheault, M.; Colin, B. Procédé de polymérisation avec un complexe de borane-amine. Fr. Pat. Appl. FR1908159, 2019.
51. Gilbert, A.; Paquin, J.-F. *J. Fluorine Chem.* **2019,** *221,* 70–74. doi:10.1016/j.jfluchem.2019.04.003

License and Terms

This is an Open Access article under the terms of the Creative Commons Attribution License (https://creativecommons.org/licenses/by/4.0). Please note that the reuse, redistribution and reproduction in particular requires that the author(s) and source are credited and that individual graphics may be subject to special legal provisions.

The license is subject to the *Beilstein Journal of Organic Chemistry* terms and conditions: (https://www.beilstein-journals.org/bjoc/terms)

The definitive version of this article is the electronic one which can be found at: https://doi.org/10.3762/bjoc.16.256

BEILSTEIN JOURNAL OF ORGANIC CHEMISTRY

Synthesis of tetrafluorinated piperidines from nitrones via a visible-light-promoted annelation reaction

Vyacheslav I. Supranovich[1], Igor A. Dmitriev[1,2] and Alexander D. Dilman[*1]

Letter

Open Access

Address:
[1]N. D. Zelinsky Institute of Organic Chemistry, 119991 Moscow, Leninsky prosp. 47, Russian Federation, and [2]Moscow State University, Department of Chemistry, 119991, Moscow, Leninskie Gory 1–3, Russian Federation

Email:
Alexander D. Dilman[*] - adil25@mail.ru

* Corresponding author

Keywords:
difluoroalkylation; nitrones; organofluorine compounds; photocatalysis; radical addition

Beilstein J. Org. Chem. **2020,** *16,* 3104–3108.
https://doi.org/10.3762/bjoc.16.260

Received: 16 October 2020
Accepted: 09 December 2020
Published: 29 December 2020

This article is part of the thematic issue "Organo-fluorine chemistry V".

Guest Editor: D. O'Hagan

© 2020 Supranovich et al.; licensee Beilstein-Institut.
License and terms: see end of document.

Abstract

A method for the one-step construction of 3,3,4,4-tetrafluorinated piperidines from nitrones and readily accessible tetrafluorinated iodobromobutane is described. The reaction requires an excess amount of ascorbic acid as the terminal reductant and is performed in the presence of an iridium photocatalyst activated by blue light. The annelation is a result of a radical addition at the nitrone, intramolecular nucleophilic substitution, and reduction of the N–O bond.

Introduction

Nitrogen-containing heterocyclic compounds play an important role in pharmaceutical industry and related areas [1,2]. Among the variety of aromatic and saturated structures, the piperidine ring has a special role, as it is the most widely occurring form of nitrogen in FDA-approved drugs [3]. The ability of fluorine atoms to modify basicity, lipophilicity, as well as the hydrogen-bonding properties of amines [4,5] makes fluorinated piperidines [6,7] attractive targets in medicinal chemistry [8,9]. Previous efforts were mainly focused on the synthesis of mono- and difluorinated compounds. A single fluorine atom is typically introduced into a saturated cycle by nucleophilic fluorination reactions [10-17]. For compounds bearing *gem*-difluorinated fragments, an alternative pathway based on the construction of the cycle from building blocks may be considered [18]. However, the latter frequently implies multistep protocols, since two distinct bond-forming reactions are necessary for the cycle formation. While mono- and difluorinated piperidines are well known, tetrafluorinated piperidines are rare [19]. At the same time, the chemistry of compounds containing the tetrafluoroethylene fragment (CF_2CF_2) has advanced considerably over the last decade [20], and the use of preformed tetrafluorinated building blocks [21] provides the most efficient way of making these molecules.

Recently, we disclosed a photoredox method for the reductive radical fluoroalkylation of nitrones [22-24]. We have also eval-

uated the construction of fluorinated tetrahydroisoquinoline structures starting from nitrones, but this required four consecutive reactions with different conditions and chromatographic separation at each step [25] (Scheme 1). Herein we report a single-step protocol for the construction of fluorinated piperidines based on an accidentally discovered annelation reaction proceeding under reductive conditions.

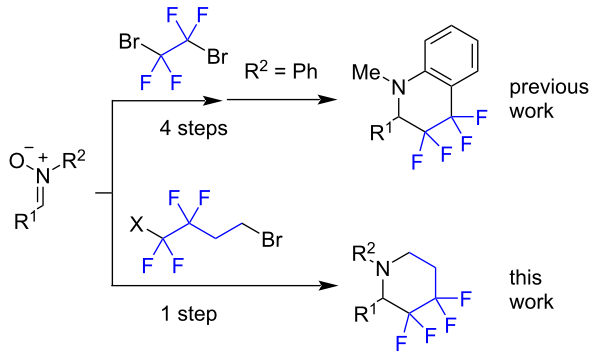

Scheme 1: The construction of tetrafluorinated piperidines from nitrones.

Results and Discussion

Nitrone **1a** was selected as a model substrate and it was combined with commercially available dibromide **2a** under blue light irradiation in the presence of an iridium photocatalyst and stoichiometric quantities (1.2 equiv) of a reducing system (ascorbic acid/collidine). In this reaction no products were formed with reactant **2a** remaining unconsumed (Table 1). To obtain a more reactive fluorinated halide, the bromine atom residing at the fluorinated moiety was exchanged for iodine by treatment with zinc, followed by the reaction with iodine monochloride. The iodide **2b** reacted quite rapidly with the nitrone but the expected fluoroalkylation product was not observed. Instead, the tetrafluorinated piperidine **3a** was obtained in a moderate yield (Table 1, entry 2). Apparently, after the fluoroalkylation event, the reduction of the N–O bond had occurred. The corresponding addition of an additional amount of the reductant and performing the reaction in DMF led to product **3a** in 84% isolated yield (Table 1, entry 4).

Under the optimized conditions, a series of nitrones were involved in the reductive annelation reaction (Scheme 2). The process worked with nitrones containing alkyl, halogen, and electron-donating groups in the aromatic ring. With ester and

Table 1: Optimization studies for the synthesis of **3a**.

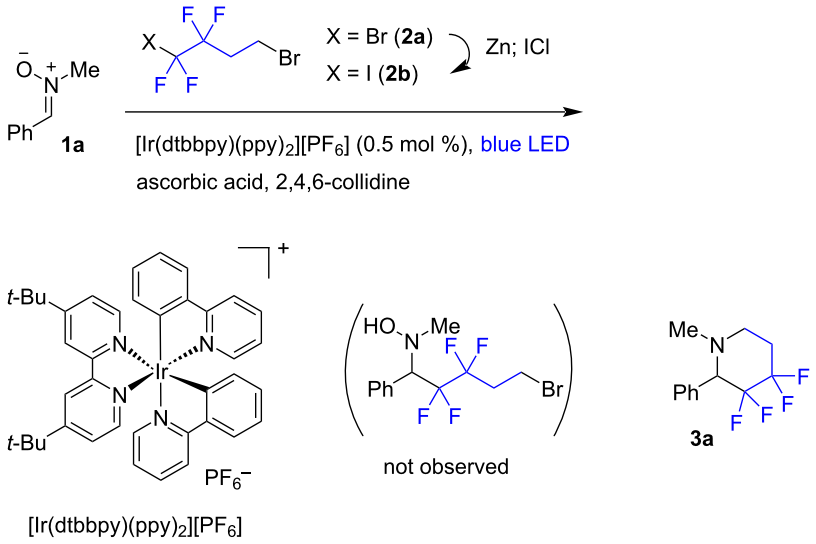

entry	2[a]	ascorbic acid[a]	collidine[a]	solvent	yield, %
1	**2a**, 1.2	1.2	1.2	DMSO	–
2	**2b**, 1.2	1.2	1.2	DMSO	56[b]
3	**2b**, 1.5	2.5	3.5	DMSO	70[b]
4	**2b**, 1.5	2.5	3.5	DMF	84[c]

[a]Equivalents are shown; [b]determined by ^{19}F NMR; [c]isolated yield.

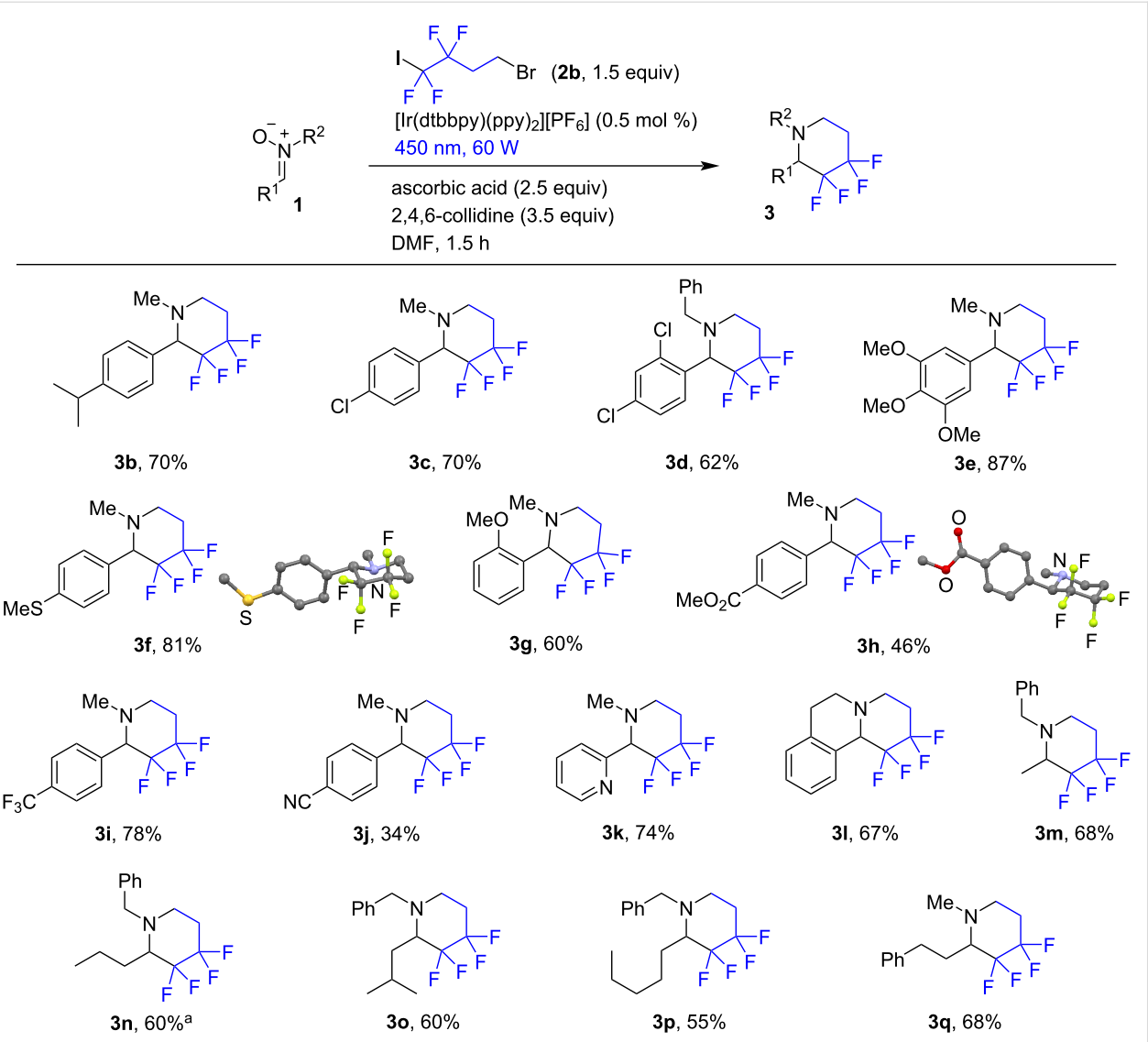

Scheme 2: The scope of the annelation reaction for the synthesis of piperidines. Isolated yields are shown. [a]1.0 equiv of **2b** was used.

cyano groups, the piperidines **3h** and **3j** were obtained in decreased yields, which may be tentatively attributed to a greater propensity of the corresponding nitrones towards nucleophilic addition of ascorbate. The nitrones derived from α-unbranched aliphatic aldehydes also provided the expected piperidines (products **3m–q**) in reasonable yields. In case of **3n** there was some unidentified side product formed under the standard conditions. In the previous research on the radical addition to nitrones we sometimes encountered a fluoroalkylation of the aromatic rings, if an excess of the fluorinated alkyl iodide was used [22-24]. This prompted us to attempt the reaction with an equimolar amount of the iodide **2b**, which resulted in a cleaner process. However, the reaction of a nitrone obtained from cyclohexyl carboxaldehyde gave a complex mixture containing unidentified products. The structures of compounds **3f** and **3h** were established by X-ray analysis (CCDC, **3f**: 2032382; **3h**: 2032383).

The proposed annelation mechanism is shown in Scheme 3. The iridium(III) photocatalyst under the action of light and ascorbic acid generates the iridium(II) species. The latter serves as a key reducing agent, and importantly, its formation is maintained throughout the process while an excess amount of ascorbate is present. The annelation likely starts from the addition of the fluorinated radical to the C=N bond followed by a conversion of the nitroxyl radical via hydrogen atom transfer [26,27] providing hydroxylamine **4**. At the next stage, the intramolecular N-alkylation occurs leading to an *N*-oxide. This step of nucleophilic substitution could be catalyzed by iodide anions accumulating in the reaction mixture. Finally, the deoxygenation of the

N-oxide fragment may proceed via consecutive protonation and electron-transfer steps [28].

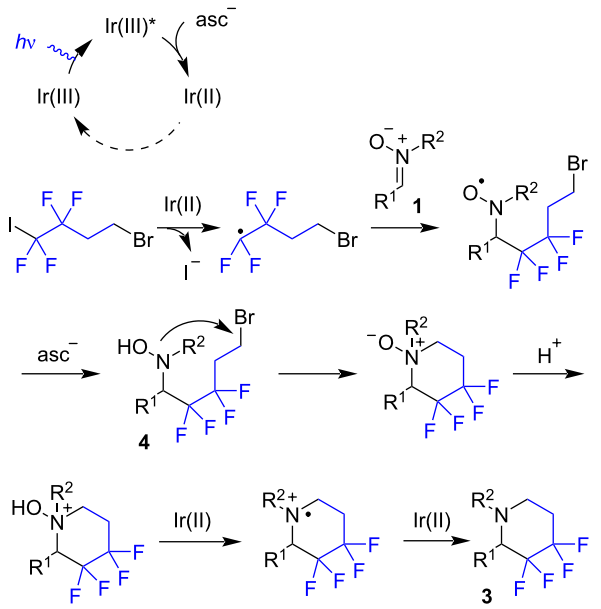

Scheme 3: The proposed mechanism of the photoredox annelation reaction (asc = ascorbic acid).

Conclusion

In summary, a one-step method for the synthesis of tetrafluorinated piperidines starting from nitrones and a fluorinated building block is described. The annelation is based on a sequence of visible-light-promoted redox processes and a substitution reaction, and involves the cleavage of the N–O bond.

Supporting Information

Supporting Information File 1

Full experimental details, compound characterization, X-ray data, and copies of NMR spectra.
[https://www.beilstein-journals.org/bjoc/content/supplementary/1860-5397-16-260-S1.pdf]

Supporting Information File 2

Crystallographic information file for compound **3f**.
[https://www.beilstein-journals.org/bjoc/content/supplementary/1860-5397-16-260-S2.cif]

Supporting Information File 3

Crystallographic information file for compound **3h**.
[https://www.beilstein-journals.org/bjoc/content/supplementary/1860-5397-16-260-S3.cif]

Acknowledgements

The crystal structure determination was performed in the Department of Structural Studies of the Zelinsky Institute of Organic Chemistry, Moscow.

Funding

This work was supported by the Russian Foundation for Basic Research (project 18-03-00320).

ORCID® iDs

Vyacheslav I. Supranovich - https://orcid.org/0000-0001-8703-0779
Igor A. Dmitriev - https://orcid.org/0000-0002-3630-8328
Alexander D. Dilman - https://orcid.org/0000-0001-8048-7223

References

1. Taylor, A. P.; Robinson, R. P.; Fobian, Y. M.; Blakemore, D. C.; Jones, L. H.; Fadeyi, O. *Org. Biomol. Chem.* **2016,** *14,* 6611–6637. doi:10.1039/c6ob00936k
2. Wu, Y. J.; Gribble, G. W.; Joule, J. Heterocycles and Medicine: A Survey of the Heterocyclic Drugs Approved by the U.S. FDA from 2000 to Present. *Progress in Heterocyclic Chemistry;* Elsevier: Oxford, U.K., 2012; Vol. 24, pp 1–53. doi:10.1016/b978-0-08-096807-0.00001-4
3. Vitaku, E.; Smith, D. T.; Njardarson, J. T. *J. Med. Chem.* **2014,** *57,* 10257–10274. doi:10.1021/jm501100b
4. Morgenthaler, M.; Schweizer, E.; Hoffmann-Röder, A.; Benini, F.; Martin, R. E.; Jaeschke, G.; Wagner, B.; Fischer, H.; Bendels, S.; Zimmerli, D.; Schneider, J.; Diederich, F.; Kansy, M.; Müller, K. *ChemMedChem* **2007,** *2,* 1100–1115. doi:10.1002/cmdc.200700059
5. Gillis, E. P.; Eastman, K. J.; Hill, M. D.; Donnelly, D. J.; Meanwell, N. A. *J. Med. Chem.* **2015,** *58,* 8315–8359. doi:10.1021/acs.jmedchem.5b00258
6. Bhuma, N.; Burade, S. S.; Louat, T.; Herman, J.; Kawade, S.; Doshi, P. J.; Dhavale, D. D. *Tetrahedron* **2018,** *74,* 852–858. doi:10.1016/j.tet.2017.12.059
7. Giacoboni, J.; Clausen, R. P.; Marigo, M. *Synlett* **2016,** *27,* 2803–2806. doi:10.1055/s-0036-1588313
8. Wang, J.; Sánchez-Roselló, M.; Aceña, J. L.; del Pozo, C.; Sorochinsky, A. E.; Fustero, S.; Soloshonok, V. A.; Liu, H. *Chem. Rev.* **2014,** *114,* 2432–2506. doi:10.1021/cr4002879
9. Purser, S.; Moore, P. R.; Swallow, S.; Gouverneur, V. *Chem. Soc. Rev.* **2008,** *37,* 320–330. doi:10.1039/b610213c
10. Zou, L.; Ruan, Y.; Jiang, W.; Yan, N.; Liu, D.-Y.; Yu, C.-Y.; Hu, X.-G. *ChemistrySelect* **2019,** *4,* 12683–12688. doi:10.1002/slct.201903403
11. Yan, N.; Fang, Z.; Liu, Q.-Q.; Guo, X.-H.; Hu, X.-G. *Org. Biomol. Chem.* **2016,** *14,* 3469–3475. doi:10.1039/c6ob00063k
12. Okoromoba, O. E.; Hammond, G. B.; Xu, B. *Org. Lett.* **2015,** *17,* 3975–3977. doi:10.1021/acs.orglett.5b01919
13. Al-Maharik, N.; O'Hagan, D. *Aldrichimica Acta* **2011,** *44,* 65–75.
14. Nielsen, M. K.; Ahneman, D. T.; Riera, O.; Doyle, A. G. *J. Am. Chem. Soc.* **2018,** *140,* 5004–5008. doi:10.1021/jacs.8b01523
15. Surmont, R.; Verniest, G.; De Weweire, A.; Thuring, J. W.; Macdonald, G.; Deroose, F.; De Kimpe, N. *Synlett* **2009,** 1933–1936. doi:10.1055/s-0029-1217533
16. González-Esguevillas, M.; Miró, J.; Jeffrey, J. L.; MacMillan, D. W. C. *Tetrahedron* **2019,** *75,* 4222–4227. doi:10.1016/j.tet.2019.05.043

17. Nairoukh, Z.; Wollenburg, M.; Schlepphorst, C.; Bergander, K.; Glorius, F. *Nat. Chem.* **2019,** *11,* 264–270. doi:10.1038/s41557-018-0197-2
18. Qing, F.-L.; Zheng, F. *Synlett* **2011,** 1052–1072. doi:10.1055/s-0030-1259947
19. Konno, T.; Hoshino, T.; Kida, T.; Takano, S.; Ishihara, T. *J. Fluorine Chem.* **2013,** *152,* 106–113. doi:10.1016/j.jfluchem.2013.02.013
20. Václavík, J.; Klimánková, I.; Budinská, A.; Beier, P. *Eur. J. Org. Chem.* **2018,** 3554–3593. doi:10.1002/ejoc.201701590
21. Dmowski, W. *J. Fluorine Chem.* **2012,** *142,* 6–13. doi:10.1016/j.jfluchem.2012.06.018
22. Supranovich, V. I.; Levin, V. V.; Struchkova, M. I.; Dilman, A. D. *Org. Lett.* **2018,** *20,* 840–843. doi:10.1021/acs.orglett.7b03987
23. Dmitriev, I. A.; Supranovich, V. I.; Levin, V. V.; Struchkova, M. I.; Dilman, A. D. *Adv. Synth. Catal.* **2018,** *360,* 3788–3792. doi:10.1002/adsc.201800802
24. Dmitriev, I. A.; Supranovich, V. I.; Levin, V. V.; Dilman, A. D. *Eur. J. Org. Chem.* **2019,** 4119–4122. doi:10.1002/ejoc.201900274
25. Supranovich, V. I.; Dilman, A. D. *Mendeleev Commun.* **2019,** *29,* 515–516. doi:10.1016/j.mencom.2019.09.012
26. Warren, J. J.; Mayer, J. M. *J. Am. Chem. Soc.* **2008,** *130,* 7546–7547. doi:10.1021/ja802055t
27. Warren, J. J.; Mayer, J. M. *J. Am. Chem. Soc.* **2010,** *132,* 7784–7793. doi:10.1021/ja102337n
28. Jeong, J.; Suzuki, K.; Hibino, M.; Yamaguchi, K.; Mizuno, N. *ChemistrySelect* **2016,** *1,* 5042–5048. doi:10.1002/slct.201601146

License and Terms

This is an Open Access article under the terms of the Creative Commons Attribution License (https://creativecommons.org/licenses/by/4.0). Please note that the reuse, redistribution and reproduction in particular requires that the author(s) and source are credited and that individual graphics may be subject to special legal provisions.

The license is subject to the *Beilstein Journal of Organic Chemistry* terms and conditions: (https://www.beilstein-journals.org/bjoc/terms)

The definitive version of this article is the electronic one which can be found at: https://doi.org/10.3762/bjoc.16.260

BEILSTEIN JOURNAL OF ORGANIC CHEMISTRY

Benzothiazolium salts as reagents for the deoxygenative perfluoroalkylthiolation of alcohols

Armin Ariamajd‡, Nils J. Gerwien‡, Benjamin Schwabe, Stefan Dix and Matthew N. Hopkinson*

Letter

Open Access

Address:
Institute of Chemistry and Biochemistry, Freie Universität Berlin, Fabeckstrasse 34–36, 14195 Berlin, Germany

Email:
Matthew N. Hopkinson* - matthew.hopkinson@fu-berlin.de

* Corresponding author ‡ Equal contributors

Keywords:
alcohols; benzothiazolium salts; deoxygenative reactions; fluorine; perfluoroalkylthiolation; thioethers

Beilstein J. Org. Chem. **2021,** *17,* 83–88.
https://doi.org/10.3762/bjoc.17.8

Received: 30 October 2020
Accepted: 11 December 2020
Published: 08 January 2021

This article is part of the thematic issue "Organo-fluorine chemistry V".

Guest Editor: D. O'Hagan

© 2021 Ariamajd et al.; licensee Beilstein-Institut.
License and terms: see end of document.

Abstract

A series of 2-(perfluoroalkylthio)benzothiazolium (BT-SR_F) salts have been synthesized that serve as convenient sources of hitherto underexplored perfluoroalkylthiolate anions. An investigation of their reactivity in a deoxygenative nucleophilic substitution reaction led to the development of an unprecedented process that provides pentafluoroethyl and heptafluoropropyl thioethers directly from readily available alcohols.

Introduction

The incorporation of fluorine-containing groups into organic molecules to modulate their biological or physical properties is nowadays a common strategy employed in the development of pharmaceuticals [1-4], agrochemicals [5] and materials [6]. Recent years have seen a surge in interest in emerging fluorinated motifs, which can offer improved performance over single fluorine atoms or perfluoroalkyl substituents. The trifluoromethylthio group (SCF_3), for example, is attracting considerable attention due to its strong lipophilicity-enhancing influence (Hansch constant $\pi = 1.44$) and electron-withdrawing properties (Hammett constants $\sigma_p = 0.50$ and $\sigma_m = 0.40$) [7-12]. On the other hand, longer-chain perfluoroalkylthio groups (SR_F, $R_F = C_nF_{2n+1}$) have received comparatively little attention despite promising applications in liquid crystal displays [13,14], as pharmaceuticals and agrochemicals [15]. For example, analogues of the drug losartan featuring SC_2F_5, SC_3F_7 and SC_4F_9 groups have shown promise as treatments for hypertensive disorders [16]. Furthermore, in a number of drug candidates, exchanging a CF_3 group with C_2F_5 has been shown to result in superior pharmacological properties; however, analogous studies comparing SCF_3 with SC_2F_5 are scarce [17-19].

Much of the recent interest in the SCF_3 group can be attributed to the development of several bench-stable and easily handled trifluoromethylthiolating reagents, which do not require specialist equipment or expertise [7-12]. Synthetic approaches towards longer-chain perfluoroalkylthio-substituted molecules, on the other hand, remain limited. In the vast majority of cases,

the SR_F group is not installed as an intact functional group but rather indirectly through perfluoroalkylation of a thiol or sulfide moiety already present on the substrate (Scheme 1a) [15,20-26]. By contrast, direct perfluoroalkylthiolation, which avoids pre-functionalization of the substrate, has been hindered by the lack of suitable reagents. In recent years, however, a selection of mostly electrophilic and radical sources has been introduced [27]. Nucleophilic perfluoroalkylthiolation is especially challenging due to the low nucleophilicity of heavily fluorinated thiolate anions and the potential for deleterious side-reactions resulting from β-fluoride elimination [28-34]. Only a handful of perfluoroalkylthiolate salts are known and, to the best of our knowledge, only one general direct nucleophilic perfluoroalkylthiolation of an alkyl electrophile has been reported to date [35]. This process used an umpolung strategy with activation of typically electrophilic perfluoroalkylsulfenamide reagents by iodide, releasing $^-SC_2F_5$ or $^-SC_3F_7$ anions in situ, which could then react with a selection of alkyl halides (Scheme 1b).

In 2019, we reported a new reagent for nucleophilic trifluoromethylthiolation based on the benzothiazolium motif: BT-SCF_3 [36-38]. This easily handled solid, which is stable at least over several months under ambient conditions, could be engaged in efficient deoxygenative trifluoromethylthiolation reactions of readily available aliphatic alcohols. Some features of this process led us to consider whether related benzothiazolium salts featuring longer-chain SR_F substituents could serve as practical reagents for investigating nucleophilic perfluoroalkylthiolation reactions. Firstly, the simple two-step synthesis of BT-SCF_3 from inexpensive 2-mercaptobenzothiazole (MBT) can be readily adapted to provide a wide range of different BT-SR_F reagents. Moreover, in situ activation of the benzothiazolium salt by the alcohol provides a highly reactive alkyl electrophile, which can compensate for the inherently low nucleophilicity of ^-SR_F anions [39]. Herein, we report the successful synthesis of several BT-SR_F reagents and provide insights into the reactivity of different perfluoroalkylthiolate anions in nucleophilic substitution reactions. This study led to the development of unprecedented deoxygenative pentafluoroethyl- and heptafluoropropylthiolation reactions directly from alcohols (Scheme 1c).

Results and Discussion

Five BT-SR_F reagents were selected to provide a good overview on the reactivity of different perfluoroalkylthio groups; four linear BT-SR_F derivatives (BT-SC_2F_5, BT-SC_3F_7,

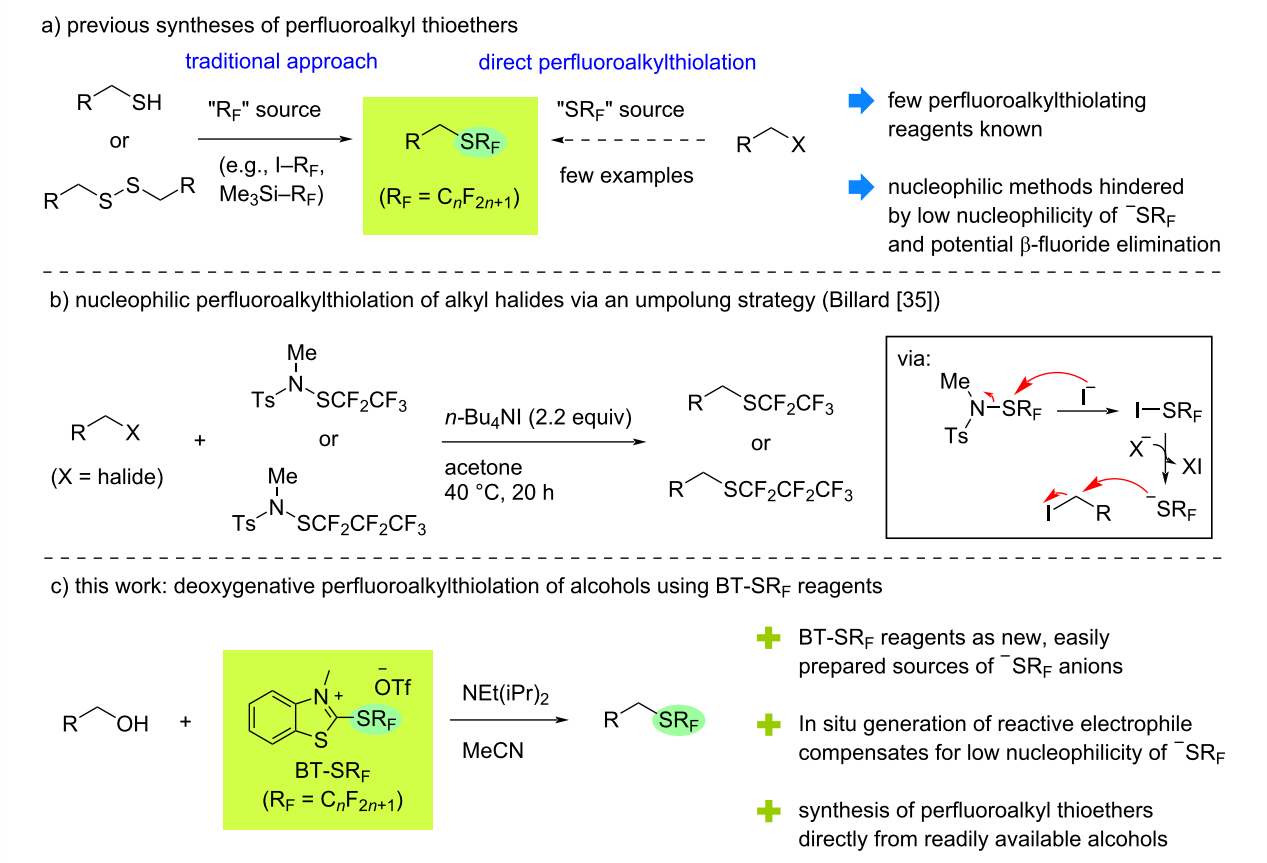

Scheme 1: Synthetic routes towards perfluoroalkyl thioethers.

$BT\text{-}SC_5F_{11}$ and $BT\text{-}SC_8F_{17}$) and the perfluoroisopropyl species $BT\text{-}SCF(CF_3)_2$. Each reagent was synthesized according to the two-step procedure shown in Scheme 2. Firstly, MBT was reacted with a perfluoroalkyl iodide and NaH in DMF under irradiation with UVA LEDs (λ_{max} = 365 nm). In all cases, efficient *S*-perfluoroalkylation was observed within 16 h at rt, and the heteroaromatic compounds **1a–e** could be isolated in good yields. Subsequent *N*-methylation with methyl trifluoromethanesulfonate in CH_2Cl_2 also proceeded smoothly with the $BT\text{-}SR_F$ reagents each being obtained after 48 h at rt in high yields upon precipitation with Et_2O. As with $BT\text{-}SCF_3$, further purification of the reagents was not required and each was found to be stable at least over several months when stored in a fridge.

With a selection of $BT\text{-}SR_F$ reagents in hand, we next sought to evaluate their relative reactivity in a benchmark nucleophilic perfluoroalkylthiolation. Thus, 4-nitrobenzyl alcohol (**2a**) was reacted with 1.25 equivalents of $BT\text{-}SC_2F_5$ and 2 equivalents of $NEt(iPr)_2$ in MeCN for 2 h at rt. The analysis of the crude reaction mixture by NMR revealed the formation of two products: the desired (pentafluoroethyl) thioether **3a** in 78% NMR yield and a second species with ^{19}F and ^1H spectra consistent with the trifluoromethyl thionoester **4a** (7% NMR yield, Table 1, entry 1). The formation of both species can be explained by the mechanism shown in Scheme 3 [36]. Nucleophilic attack of the alcohol in the presence of $NEt(iPr)_2$ at the C2-position of the BT reagent affords the key electrophilic 2-alkoxybenzothiazolium species **A** and the perfluoroalkylthiolate anion. Nucleophilic substitution then affords product **3** and thiocarbamate by-product **B**. As a side-reaction, β-fluoride elimination from the perfluoroalkylthiolate anion can occur, leading to a thiocarbonyl fluoride species, which can subsequently react with the alcohol, delivering thionoester **4**. β-Fluoride elimination is a known decomposition pathway of $^-SCF_3$ and has even been exploited in synthetic trifluoromethylthiolation and fluorination processes [32-34].

The formation of the side-product **4a** could be effectively suppressed by conducting the reaction at −40 °C. Under these

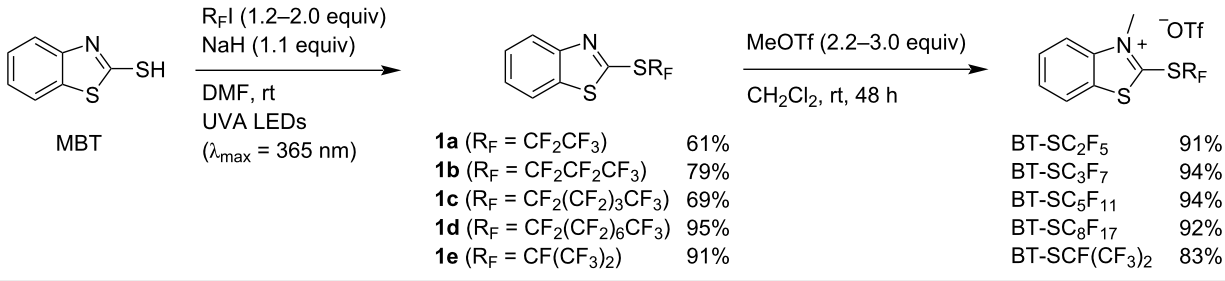

Scheme 2: Two-step synthesis of $BT\text{-}SR_F$ reagents from MBT.

Table 1: Deoxygenative perfluoroalkylthiolation of alcohol **2a** with $BT\text{-}SR_F$ reagents.[a]

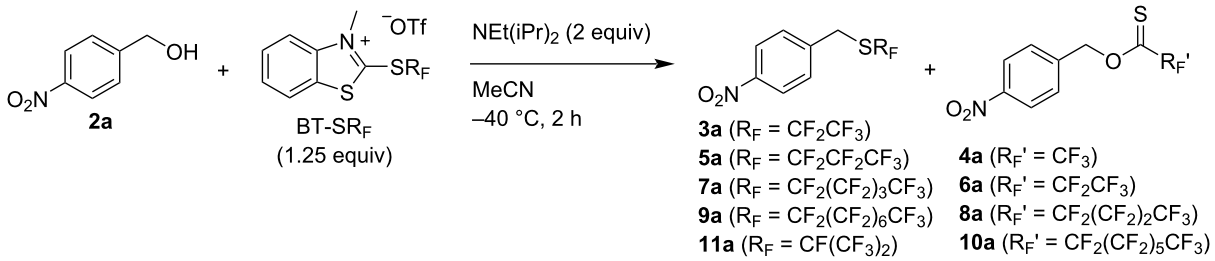

Entry	R_F	^1H NMR yield of thioether	^1H NMR yield of thionoester
1[b]	CF_2CF_3	**3a** (78%)	**4a** (7%)
2	CF_2CF_3	**3a** (99%)	**4a** (trace)
3	$CF_2CF_2CF_3$	**5a** (82%)	**6a** (15%)
4	$CF_2(CF_2)_3CF_3$	**7a** (74%)	**8a** (26%)
5	$CF_2(CF_2)_6CF_3$	**9a** (46%)	**10a** (47%)
6	$CF(CF_3)_2$	**11a** (trace)	–

[a]Reaction conditions: $BT\text{-}SR_F$ (1.25 equiv), $NEt(iPr)_2$ (2 equiv), MeCN (0.17 M), –40 °C, 2 h. [b]Reaction conducted at rt.

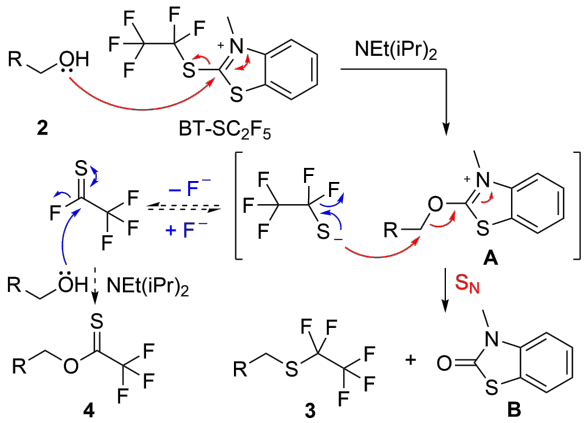

Scheme 3: Plausible mechanism for the formation of thioether **3** and thionoester **4**.

conditions, the desired (pentafluoroethyl) thioether **3a** was obtained in 99% NMR yield (91% isolated yield, Table 1, entry 2). At this stage, we were ready to evaluate the relative efficiency of different perfluoroalkylthiolate nucleophiles. Each of the other BT-SR_F reagents (1.25 equiv) was reacted with alcohol **2a** and $NEt(iPr)_2$ (2 equiv) in MeCN at −40 °C and, after 2 h, the crude mixture was analysed by ^1H and ^{19}F NMR. As shown in Table 1, a significant decrease in the nucleophilic perfluoroalkylthiolation efficiency was observed upon increasing the R_F chain length (Table 1, entries 2–5). For example, thionoester **8a** was generated as a significant side product (26% NMR yield) when using BT-SC_5F_{11}, while thioether **9a** and thionoester **10a** were provided in almost equal amounts when BT-SC_8F_{17} was reacted with **2a**. The increased prevalence of the β-fluoride elimination pathway with longer perfluoroalkylthio chains likely reflects the lower nucleophilicity of the increasingly fluorinated thiolate anions. Moreover, (perfluoroisopropyl) thioether **11a** was produced in only trace amounts in the reaction with BT-$SCF(CF_3)_2$, which is consistent with the expected lower nucleophilicity of the sterically more encumbered anion (Table 1, entry 6).

The efficient perfluoroalkylthiolation of **2a** observed with BT-SC_2F_5 led us to further investigate this approach as a route towards (pentafluoroethyl) thioethers. Deoxygenative substitution reactions of this type are synthetically appealing as they avoid pre-generation of an active electrophile such as an alkyl halide.

A selection of benzylic alcohols **2** was reacted under the standard conditions with BT-SC_2F_5 (1.25 equiv) and $NEt(iPr)_2$ (2 equiv) in MeCN at −40 °C, providing the corresponding (pentafluoroethyl) thioethers **3** in generally high yields

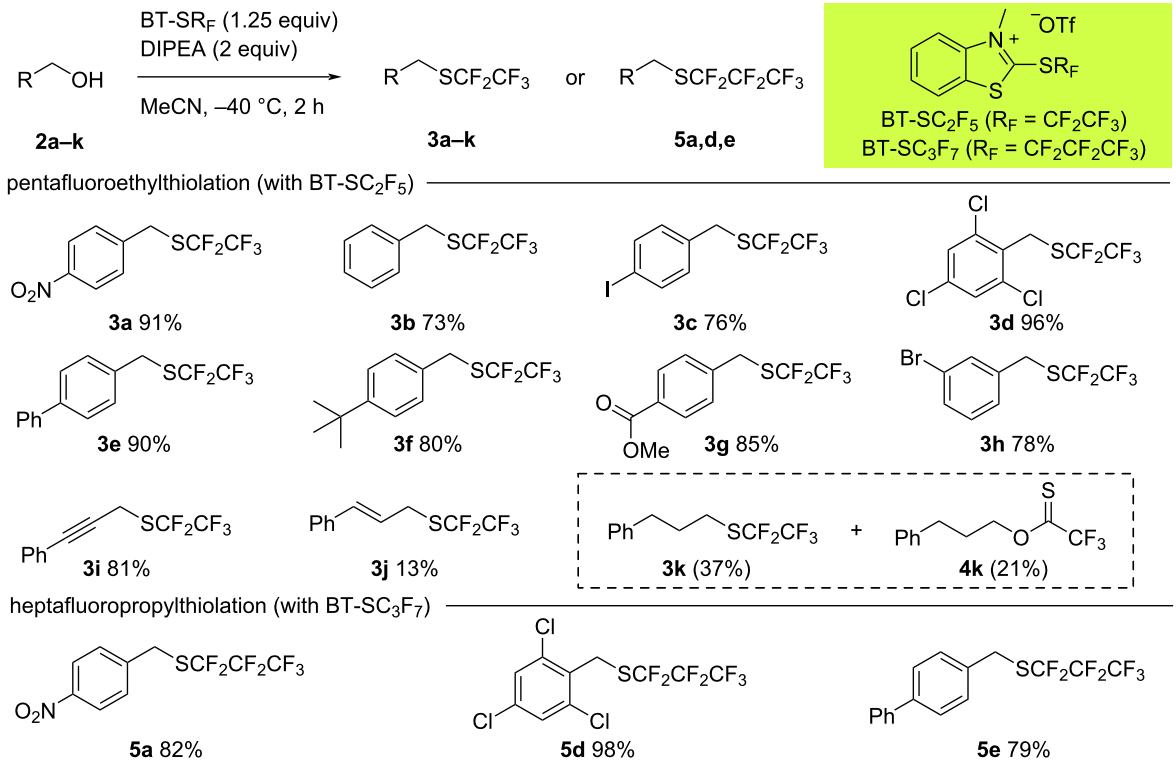

Scheme 4: Scope of the deoxygenative perfluoroalkylthiolation reaction using BT-SC_2F_5 and BT-SC_3F_7.

(Scheme 4). A wide range of functional groups were tolerated, including the halogens Cl, Br, and I, thus opening the door for further functionalization of the products via cross-coupling. The propargylic alcohol substrate **2i** could also be converted into thioether **3i** in 81% yield, although the allylic alcohol **2j** was less efficient (13% yield of **3j**). The primary aliphatic (pentafluoroethyl) thioether **3k** could also be obtained in the reaction between alcohol **2k** and BT-SC_2F_5, however, with this less activated substrate, the thionoester **4k** was generated as a significant side product. Finally, the suitability of this methodology for the preparation of (heptafluoropropyl) thioethers was investigated by reacting a selection of benzylic alcohols **2** with BT-SC_3F_7. As for the pentafluoroethylthiolation reactions, efficient conversion was observed with products **5** being obtained in high yields of up to 98%.

Conclusion

In conclusion, a series of bench-stable and easy to handle 2-(perfluoroalkylthio)benzothiazolium (BT-SR_F) salts have been synthesized and investigated as reagents for the direct nucleophilic perfluoroalkylthiolation of aliphatic alcohols. While β-fluoride elimination was a significant side reaction with longer-chain SR_F groups, efficient deoxygenative functionalization was observed with BT-SC_2F_5 and BT-SC_3F_7. This synthetically attractive reaction provides pentafluoroethyl and heptafluoropropyl thioethers directly from readily available alcohols, thus avoiding the pre-formation of an alkyl halide. This straight-forward route should inspire further investigations of perfluoroalkylthio groups in pharmaceutical, agrochemical and materials science.

Supporting Information

The Supporting Information contains experimental procedures, characterization data of all BT-SR_F reagents and isolated products as well as copies of NMR spectra.

Supporting Information File 1

Experimental section.
[https://www.beilstein-journals.org/bjoc/content/supplementary/1860-5397-17-8-S1.pdf]

Acknowledgements

We would like to acknowledge the assistance of the Core Facility BioSupraMol supported by the DFG.

Funding

Funded by the Daimler und Benz Stiftung (Postdoctoral Scholarship, Project No.: 32-04/18) and the Deutsche Forschungsgemeinschaft (DFG, German Research Foundation) – Project-ID 387284271 – SFB 1349 (gefördert durch die Deutsche Forschungsgemeinschaft (DFG) – Projektnummer 387284271 – SFB 1349)). Financial support from the Fonds der Chemischen Industrie (Sachkostenzuschuss) is also gratefully acknowledged.

ORCID® iDs

Armin Ariamajd - https://orcid.org/0000-0003-1563-6987
Nils J. Gerwien - https://orcid.org/0000-0003-2211-4829
Matthew N. Hopkinson - https://orcid.org/0000-0002-0183-0466

References

1. Müller, K.; Faeh, C.; Diederich, F. *Science* **2007,** *317,* 1881–1886. doi:10.1126/science.1131943
2. Purser, S.; Moore, P. R.; Swallow, S.; Gouverneur, V. *Chem. Soc. Rev.* **2008,** *37,* 320–330. doi:10.1039/b610213c
3. Wang, J.; Sánchez-Roselló, M.; Aceña, J. L.; del Pozo, C.; Sorochinsky, A. E.; Fustero, S.; Soloshonok, V. A.; Liu, H. *Chem. Rev.* **2014,** *114,* 2432–2506. doi:10.1021/cr4002879
4. Gillis, E. P.; Eastman, K. J.; Hill, M. D.; Donnelly, D. J.; Meanwell, N. A. *J. Med. Chem.* **2015,** *58,* 8315–8359. doi:10.1021/acs.jmedchem.5b00258
5. Fujiwara, T.; O'Hagan, D. *J. Fluorine Chem.* **2014,** *167,* 16–29. doi:10.1016/j.jfluchem.2014.06.014
6. Berger, R.; Resnati, G.; Metrangolo, P.; Weber, E.; Hulliger, J. *Chem. Soc. Rev.* **2011,** *40,* 3496–3508. doi:10.1039/c0cs00221f
7. Xu, X.-H.; Matsuzaki, K.; Shibata, N. *Chem. Rev.* **2015,** *115,* 731–764. doi:10.1021/cr500193b
8. Barata-Vallejo, S.; Bonesi, S.; Postigo, A. *Org. Biomol. Chem.* **2016,** *14,* 7150–7182. doi:10.1039/c6ob00763e
9. Xiong, H.-Y.; Pannecoucke, X.; Besset, T. *Chem. – Eur. J.* **2016,** *22,* 16734–16749. doi:10.1002/chem.201603438
10. Pannecoucke, X.; Besset, T. *Org. Biomol. Chem.* **2019,** *17,* 1683–1693. doi:10.1039/c8ob02995d
11. Mampuys, P.; McElroy, C. R.; Clark, J. H.; Orru, R. V. A.; Maes, B. U. W. *Adv. Synth. Catal.* **2020,** *362,* 3–64. doi:10.1002/adsc.201900864
12. Xiao, X.; Zheng, Z.-T.; Li, T.; Zheng, J.-L.; Tao, T.; Chen, L.-M.; Gu, J.-Y.; Yao, X.; Lin, J.-H.; Xiao, J.-C. *Synthesis* **2020,** *52,* 197–207. doi:10.1055/s-0039-1690714
13. Hein, M.; Miethchen, R.; Schwäbisch, D. *J. Fluorine Chem.* **1999,** *98,* 55–60. doi:10.1016/s0022-1139(99)00076-7
14. Miethchen, R.; Hein, M. *Carbohydr. Res.* **2000,** *327,* 169–183. doi:10.1016/s0008-6215(99)00317-1
15. Boiko, V. N. *Beilstein J. Org. Chem.* **2010,** *6,* 880–921. doi:10.3762/bjoc.6.88
16. Yagupolskii, L. M.; Maletina, I. I.; Petko, K. I.; Fedyuk, D. V.; Handrock, R.; Shavaran, S. S.; Klebanov, B. M.; Herzig, S. *J. Fluorine Chem.* **2001,** *109,* 87–94. doi:10.1016/s0022-1139(01)00382-7
17. Andrzejewska, M.; Yépez-Mulia, L.; Cedillo-Rivera, R.; Tapia, A.; Vilpo, L.; Vilpo, J.; Kazimierczuk, Z. *Eur. J. Med. Chem.* **2002,** *37,* 973–978. doi:10.1016/s0223-5234(02)01421-6
18. Johansson, A.; Poliakov, A.; Åkerblom, E.; Wiklund, K.; Lindeberg, G.; Winiwarter, S.; Danielson, U. H.; Samuelsson, B.; Hallberg, A. *Bioorg. Med. Chem.* **2003,** *11,* 2551–2568. doi:10.1016/s0968-0896(03)00179-2
19. Lishchynskyi, A.; Grushin, V. V. *J. Am. Chem. Soc.* **2013,** *135,* 12584–12587. doi:10.1021/ja407017j

20. Umemoto, T.; Kuriu, Y. *Chem. Lett.* **1982,** *11,* 65–66. doi:10.1246/cl.1982.65
21. Wakselman, C.; Tordeux, M. *J. Org. Chem.* **1985,** *50,* 4047–4051. doi:10.1021/jo00221a017
22. Boiko, V. N.; Shchupak, G. M. *J. Fluorine Chem.* **1994,** *69,* 207–212. doi:10.1016/0022-1139(94)03132-0
23. Roques, N. *J. Fluorine Chem.* **2001,** *107,* 311–314. doi:10.1016/s0022-1139(00)00374-2
24. Exner, B.; Bayarmagnai, B.; Matheis, C.; Goossen, L. J. *J. Fluorine Chem.* **2017,** *198,* 89–93. doi:10.1016/j.jfluchem.2016.12.006
25. Xiang, J.-X.; Xu, X.-H.; Qing, F.-L. *J. Fluorine Chem.* **2017,** *203,* 110–114. doi:10.1016/j.jfluchem.2017.07.008
26. Luo, Z.; Yang, X.; Tsui, G. C. *Org. Lett.* **2020,** *22,* 6155–6159. doi:10.1021/acs.orglett.0c02235
27. Baert, F.; Colomb, J.; Billard, T. *Angew. Chem., Int. Ed.* **2012,** *51,* 10382–10385. doi:10.1002/anie.201205156
28. Alazet, S.; Billard, T. *Synlett* **2015,** *26,* 76–78. doi:10.1055/s-0034-1379501
29. Jiang, L.; Qian, J.; Yi, W.; Lu, G.; Cai, C.; Zhang, W. *Angew. Chem., Int. Ed.* **2015,** *54,* 14965–14969. doi:10.1002/anie.201508495
30. Xu, B.; Li, D.; Lu, L.; Wang, D.; Hu, Y.; Shen, Q. *Org. Chem. Front.* **2018,** *5,* 2163–2166. doi:10.1039/c8qo00327k
31. Matheis, C.; Bayarmagnai, B.; Jouvin, K.; Goossen, L. J. *Org. Chem. Front.* **2016,** *3,* 949–952. doi:10.1039/c6qo00194g
32. Haszeldine, R. N.; Kidd, J. M. *J. Chem. Soc.* **1955,** 3871–3880. doi:10.1039/jr9550003871
33. Liu, J.-B.; Xu, X.-H.; Chen, Z.-H.; Qing, F.-L. *Angew. Chem., Int. Ed.* **2015,** *54,* 897–900. doi:10.1002/anie.201409983
34. Scattolin, T.; Pu, M.; Schoenebeck, F. *Chem. – Eur. J.* **2018,** *24,* 567–571. doi:10.1002/chem.201705240
35. Glenadel, Q.; Bordy, M.; Alazet, S.; Tlili, A.; Billard, T. *Asian J. Org. Chem.* **2016,** *5,* 428–433. doi:10.1002/ajoc.201600003
36. Dix, S.; Jakob, M.; Hopkinson, M. N. *Chem. – Eur. J.* **2019,** *25,* 7635–7639. doi:10.1002/chem.201901607
37. Hopkinson, M.; Dix, S. Fluorine-containing compounds for use as nucleophilic reagents for transferring functional groups onto high value organic compounds. Eur. Pat. Appl. EP19150201, Jan 3, 2019. International Pat. Appl. PCT/EP2020/050031, Jan 2, 2020.
38. Tironi, M.; Maas, L. M.; Garg, A.; Dix, S.; Götze, J. P.; Hopkinson, M. N. *Org. Lett.* **2020,** *22,* 8925–8930. doi:10.1021/acs.orglett.0c03328
39. Mukaiyama, T. *Angew. Chem., Int. Ed. Engl.* **1979,** *18,* 707–721. doi:10.1002/anie.197907073

License and Terms

This is an Open Access article under the terms of the Creative Commons Attribution License (https://creativecommons.org/licenses/by/4.0). Please note that the reuse, redistribution and reproduction in particular requires that the author(s) and source are credited and that individual graphics may be subject to special legal provisions.

The license is subject to the *Beilstein Journal of Organic Chemistry* terms and conditions: (https://www.beilstein-journals.org/bjoc/terms)

The definitive version of this article is the electronic one which can be found at: https://doi.org/10.3762/bjoc.17.8

BEILSTEIN JOURNAL OF ORGANIC CHEMISTRY

Synthesis of aryl 2-bromo-2-chloro-1,1-difluoroethyl ethers through the base-mediated reaction between phenols and halothane

Yukiko Karuo, Ayaka Kametani, Atsushi Tarui, Kazuyuki Sato, Kentaro Kawai and Masaaki Omote*

Full Research Paper

Open Access

Address:
Faculty of Pharmaceutical Sciences, Setsunan University, 45-1, Nagaotoge-cho, Hirakata, Osaka 573-0101, Japan

Email:
Masaaki Omote* - omote@pharm.setsunan.ac.jp

* Corresponding author

Keywords:
aryl 1,1-difluoroethyl ether; 1,1-difluoroethene; fluorine compound; halothane; phenol

Beilstein J. Org. Chem. **2021,** *17,* 89–96.
https://doi.org/10.3762/bjoc.17.9

Received: 19 October 2020
Accepted: 11 December 2020
Published: 11 January 2021

This article is part of the thematic issue "Organo-fluorine chemistry V".

Guest Editor: D. O'Hagan

© 2021 Karuo et al.; licensee Beilstein-Institut.
License and terms: see end of document.

Abstract

An efficient and convenient method for the synthesis of structurally unique and highly functionalized aryl 2-bromo-2-chloro-1,1-difluoroethyl ethers has been developed. This approach exhibits a broad reaction scope, a simple operation and without the need of any expensive transition-metal catalyst, highly toxic or corrosive reagents. Notably, we demonstrate the potential utility of halothane for the synthesis of aryl *gem*-difluoroalkyl ethers containing the bromochloromethyl group.

Introduction

Molecules containing fluoroalkyl groups are of interest in pharmaceutical and agrochemical sciences because deliberately incorporated fluorine atoms often change the chemical properties of the parent molecules by improving the absorption, resistance to metabolism, and pharmacological activities. To date, difluoromethyl or difluoromethylene compounds have been studied extensively as well as monofluorinated and trifluoromethylated arenes or aliphatics [1-4]. Recent progress in difluoromethylene chemistry successfully led to the finding of bioactive compounds such as pantoprazole, a proton pump inhibitor [5], and AFP-07, a prostaglandin I2 receptor-selective agonist [6-8], which suggests the importance of the difluoromethylene unit in drug discovery (Figure 1). There have been many reports for the construction of the difluoromethylene unit, such as the deoxygenating conversion of a carbonyl group to the difluoromethylene unit using *N*,*N*-diethylaminosulfur trifluoride (DAST) [9-14], the Reformatsky reaction of ethyl bromodifluoroacetate [15-23], and transformations of tetrafluoroethylene using suitable metal catalysts [24-31]. Additionally, recent advances in difluoromethylene chemistry have demon-

strated the synthesis of aryl fluoroalkyl ethers as shown in Scheme 1 [32-34]. For example, the reactions of phenols with "*gem*-difluorocarbene precursors (route (a))" or "bromodifluoroalkyl compounds (route (b))" have been typically used to obtain a variety of aryl *gem*-difluoromethyl ethers. Particularly, the latter approach is useful for obtaining liquid crystal materials [35-38]. In the case of using 2-chloro-3,3,3-trifluoroprop-1-ene (route (c), Scheme 1), the aryl enol ether with a trifluoromethyl group was obtained [39,40]. A further example for the formation of an aryl fluoroalkyl ether was the reaction of phenol with 2-chloro-1,1,1-trifluoroethane, also known as HCFC-133a, in the presence of potassium hydroxide (KOH) to give the *gem*-difluoromethyl ethers along with the formation of 1-fluoro-2-chlorovinyl ether (route (d), Scheme 1) [41]. On the basis of our previous reports, we focused on halothane, 2-bromo-2-chloro-1,1,1-trifluoroethane, because the treatment of this compound with several bases was found to provide the highly electrophilic 2-bromo-2-chloro-1,1-difluoroethene [42,43]. Additionally, another report discussed the carbocationic character of the *gem*-difluorovinyl carbon that was explained by an orbital interaction between the n orbital (fluorine) and the π orbital [44]. A literature survey revealed that Yagupol'skii et al. have achieved the first synthesis of aryl or alkyl 2-bromo-2-chloro-1,1-difluoroethyl ethers by the reaction of alcohols with halothane as shown in Scheme 2 [45]. This study had a large impact on fluorine chemistry in terms of the availability of halothane to build difluoroalkyl ethers. However, these reactions have significant drawbacks such as the need of harsh reaction conditions, low chemical yields, and in particular, very few examples to understand the reaction profile (Scheme 2). To address this issue, we

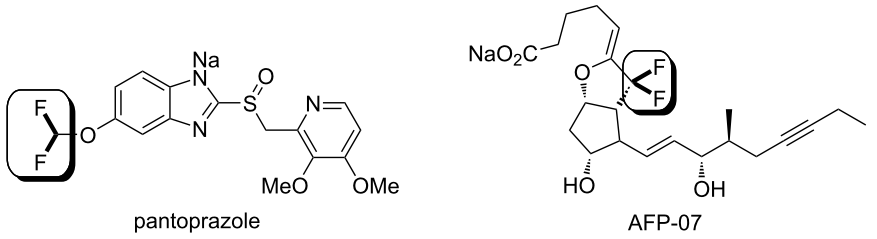

Figure 1: Medical compounds having a difluoromethyl group.

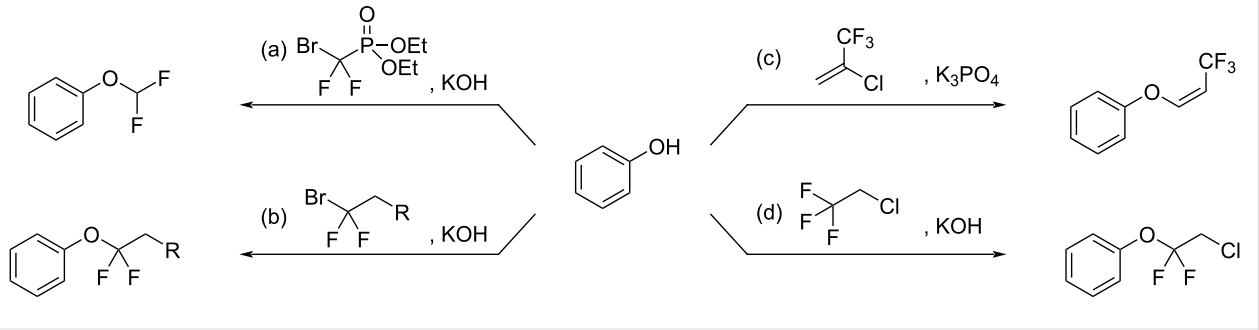

Scheme 1: Methods for the synthesis of ethers containing fluorine substituents.

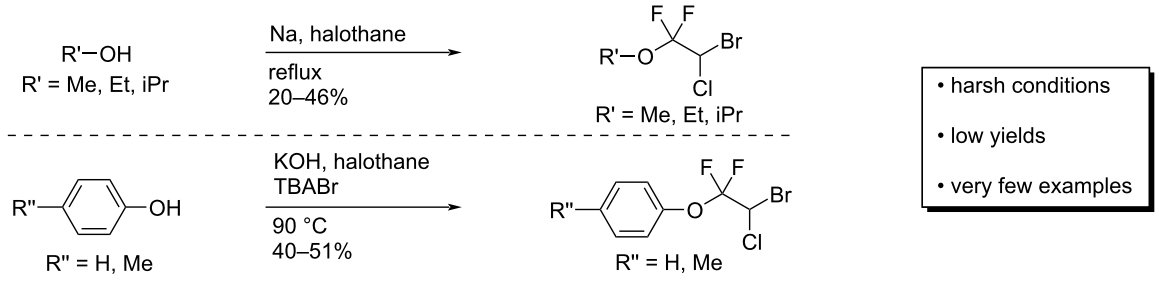

Scheme 2: The previous work reported by Yagupol'skii et al.

conducted extensive research to provide a general use of halothane for the construction of such difluoroalkyl ethers. In this paper, we discuss a new and practical synthetic approach to structurally unique and highly functionalized aryl 2-bromo-2-chloro-1,1-difluoroethyl ethers as well as several considerations of the reaction mechanism.

Results and Discussion

We began our study to optimize the reaction conditions (Table 1). When two equivalents of halothane and sodium hydride (NaH) were treated with phenol (**1a**) at room temperature for 20 h, the reaction provided the ether product **2a** in 39% yield (Table 1, entry 1). In this case, some of the substrate phenol remained in the reaction mixture. Therefore, the reactions were conducted with an increased amount of halothane (2.5 and 4.0 equivalents). However, in both reactions, the yield of the product **2a** was not improved in spite of a significant decrease of the starting material, phenol (Table 1, entries 2 and 3). Next, as shown in entry 4 of Table 1, when the reaction was conducted with a lower loading of NaH, the desired product **2a** was obtained in the same yield as that in entry 1 (Table 1). From the result of entry 5 (Table 1) in which the reaction time was prolonged to 52 h, the reaction was considered to be sluggish because the yield of **2a** was only slightly better (55%). On the other hand, when the reaction temperature was raised to 40 or 60 °C, the product yield was gradually improved (Table 1, entries 6 and 7). It is worth noting that when changing the base to KOH, a dramatic improvement of the reaction efficiency was observed giving product **2a** in 74% yield, even though the reaction time was remarkably short (Table 1, entry 8). On the contrary, the reaction did not occur at all when potassium carbonate was used as a base, because the deprotonation of phenol became slow due to the low basicity (Table 1, entry 9).

With the optimal reaction conditions (Table 1, entry 8) in hand, we next examined the scope of the reaction (Table 2). When an electron-rich phenol, *p*-methoxyphenol (**1b**) was used, the reaction proceeded to afford ether **2b** in 79% yield (Table 2, entry 1). An *ortho*-substitution with the bulkier *tert*-butyl group slightly affected the reaction giving product **2c** in still acceptable yield (47%, Table 2, entry 2). *p*-Nitrophenol (**1d**), which is an electron-poor phenol, was converted into the corresponding ether **2d** only in traces (Table 2, entry 3). By using 3.0 equivalents of KOH, *p*-trifluoromethylphenol (**1e**) provided the product **2e** in 48% yield (Table 2, entry 4). Also a phenol possessing a base-labile ester group (**1f**) afforded the product **2f** in 47% yield without the loss of the ester moiety (Table 2, entry 5). However, the reaction between *p*-hydroxybenzaldehyde (**1g**) and halothane did not proceed at all (Table 2, entry 6). A phenyl group in the *ortho* position (**1h**) did not affect the reaction and also the positional isomers **1i** and **1j**, gave the corresponding products in comparably high yields (Table 2, entries 7–9). Also, 1-naphthol (**1k**) was compatible with the reaction conditions giving the product **2k** in a good yield of 85% (Table 2, entry 10). As shown in entries 11–13 (Table 2), *o*-iodophenol (**1l**) and the alkenyl-substituted phenols **1m** and **1n**, all substrates that are susceptible to radical conditions, afforded the corresponding iodo- and alkenyl-substituted products, suggesting the reaction proceeds through an ionic process.

Table 1: Optimization of the reaction conditions with phenol (**1a**).

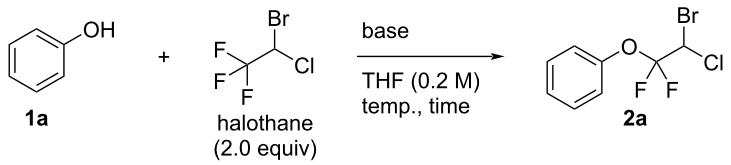

entry	base (equiv)	temp. (°C)	time (h)	yield (%)[a]
1	NaH (2.0)	rt	20	39
2[b]	NaH (2.0)	rt	23	37
3[c]	NaH (2.0)	rt	23	32
4	NaH (1.5)	rt	24	39
5	NaH (1.5)	rt	52	55
6	NaH (1.5)	40	25	54
7	NaH (1.5)	60	13	74
8	KOH (1.5)	60	1.5	74
9	K_2CO_3 (1.5)	60	24	0

[a]Isolated yields. [b]Halothane (2.5 equiv) was used. [c]Halothane (4.0 equiv) was used.

2-Hydroxychalcone (**1o**), which is a good Michael acceptor, also participated in the reaction to give the product **2o** in 56% yield, without byproduct formation from a Michael reaction (Table 2, entry 14). When *o*-aminophenol (**1p**) was used as the substrate, the coupling reaction occurred on the hydroxy group exclusively to give **2p** (Table 2, entry 15).

Table 2: The reaction scope with various phenols.

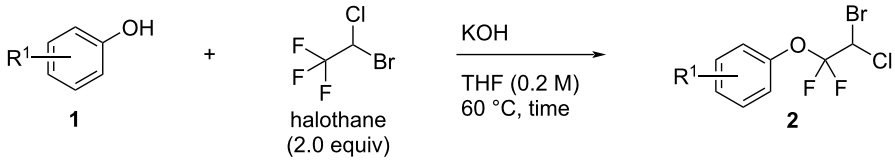

entry	phenol	products	time (h)	yield (%)[a]
1	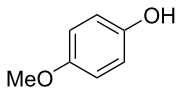 **1b**	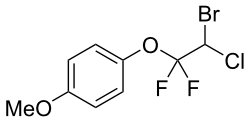 **2b**	2.5	79
2	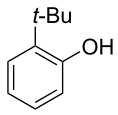 **1c**	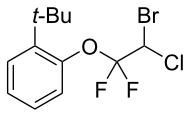 **2c**	0.5	47
3[b]	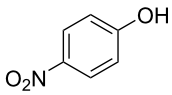 **1d**	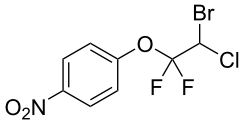 **2d**	20.5	3
4[b]	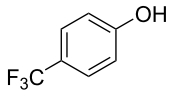 **1e**	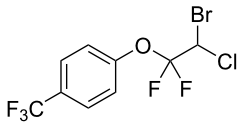 **2e**	7	48
5[b]	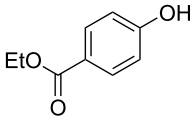 **1f**	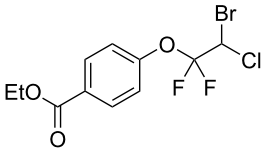 **2f**	13	47
6[b]	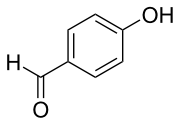 **1g**	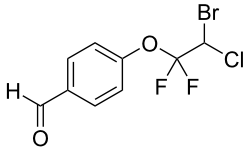 **2g**	24	no reaction
7	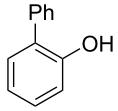 **1h**	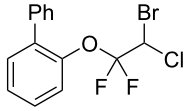 **2h**	3	71
8	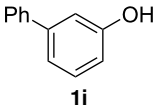 **1i**	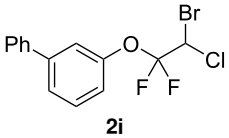 **2i**	1.5	79

Table 2: The reaction scope with various phenols. (continued)

9	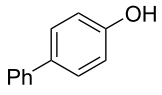 **1j**	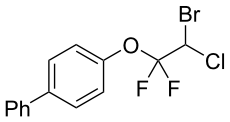 **2j**	5	88
10	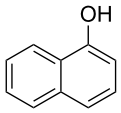 **1k**	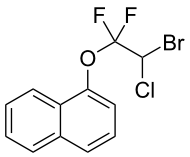 **2k**	3.5	85
11	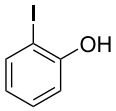 **1l**	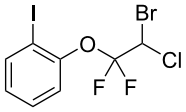 **2l**	6.5	67
12	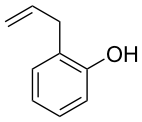 **1m**	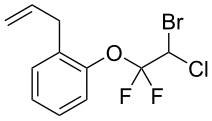 **2m**	1.5	81
13[c]	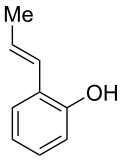 **1n**	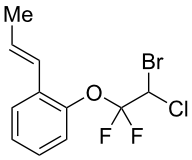 **2n**	1	71
14[b]	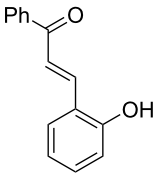 **1o**	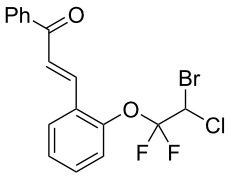 **2o**	20	56
15	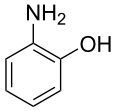 **1p**	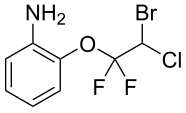 **2p**	19	51

[a]Isolated yield. [b]KOH (3.0 equiv) was used. [c]**1n** and **2n** were *cis–trans* mixtures.

To show the synthetic advantages of the obtained *gem*-difluoro ethers **2**, we examined the further application of compound **2o** in a cyclization reaction. Upon the treatment of **2o** with zinc and chlorotrimethylsilane (TMSCl), the intramolecular 1,4-addition reaction of **2o** proceeded to give the 2,2-*gem*-difluorochromane **3** in low yield (Scheme 3).

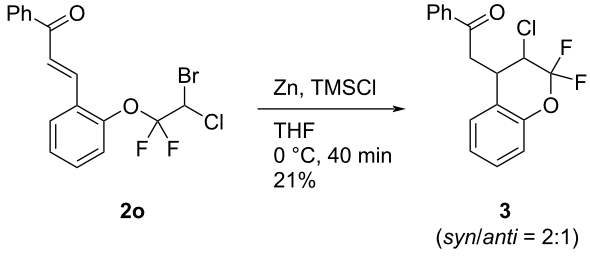

Scheme 3: Intramolecular 1,4-addition of **2o**.

Next, we moved on consideration of the reaction mechanism as shown in Scheme 4a. The reaction was carried out in a step-wise procedure in which the phenoxide was prepared by mixing equimolar amounts of phenol (**1a**) and NaH to consume all NaH

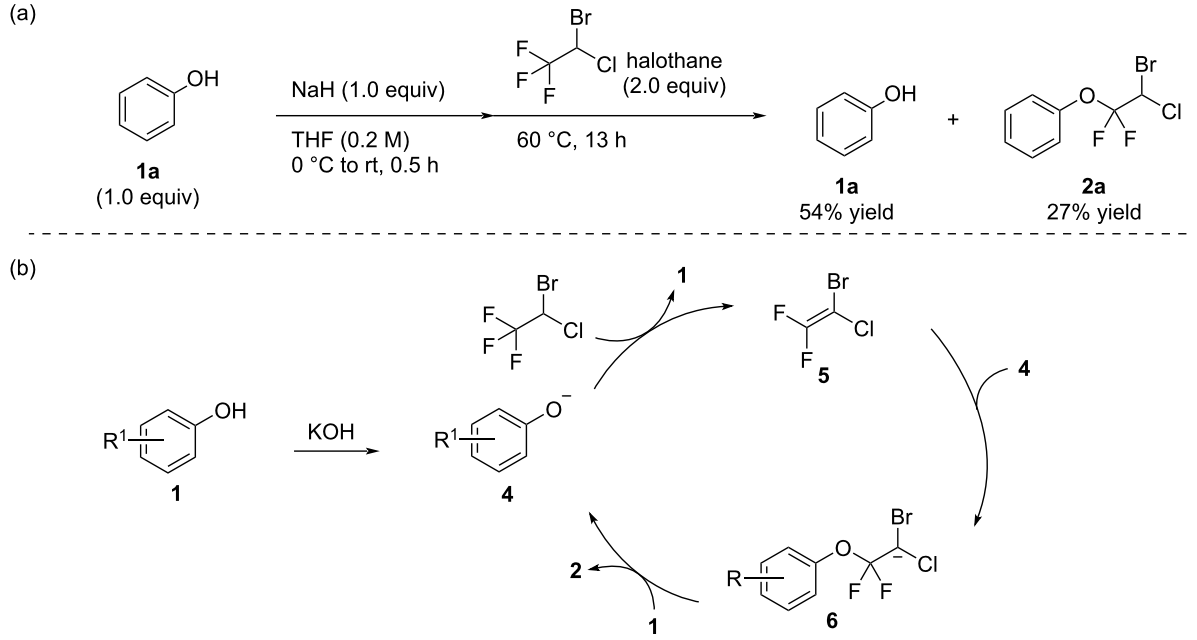

Scheme 4: Proposed reaction mechanism.

in the reaction mixture, and then halothane was added to the reaction mixture. The stepwise reaction gave the product **2a** in 27% yield and **1a** was recovered in 54% (Scheme 4a). Based on these results, we speculated that the initially generated phenoxide **4** or potassium hydroxide remaining in the reaction mixture could deprotonate halothane to provide the fully halogenated ethylene **5** (Scheme 4b) [32,33,45]. Recent studies demonstrated an electrophilic character of a *gem*-difluorovinyl carbon due to the overlapping of the fluorine lone pairs and the adjacent π orbital in favor of the generation of a difluoromethyl cation species [44]. Considering these reports, the phenoxide attack on the *gem*-difluorovinyl carbon atom is a reasonable process to forward the reaction with the generation of carbanion **6**. Finally, the protonation of **6** by **1** or other acidic compounds, such as water molecules present in the reaction medium, would provide **2**.

Conclusion

We exploited the reaction of various phenols with halothane to obtain aryl 2-bromo-2-chloro-1,1-difluoroethyl ethers. The products are structurally unique and represent highly functionalized compounds containing the *gem*-difluoroalkyl ether unit in addition to a bromochloromethyl group. The reaction proceeds under mild conditions and is compatible with variously substituted phenols giving the products in moderate to good yields. Additionally, the products are expected to undergo a variety of functionalization using ionic and radical processes. Further studies on the chemical transformations of the ether products are currently underway.

Experimental

General information

^{1}H NMR, ^{13}C NMR and ^{19}F NMR spectra were recorded on JEOL ECZ 400S spectrometers. Chemical shifts of ^{1}H NMR are reported in ppm from tetramethylsilane (TMS) as an internal standard. Chemical shifts of ^{13}C NMR are reported in ppm from the center line of the triplet at 77.16 ppm for deuteriochloroform. Chemical shifts of ^{19}F NMR are reported in ppm from $CFCl_3$ as an internal standard. All data are reported as follows: chemical shifts, multiplicity (s = singlet, d = doublet, t = triplet, q = quartet, sep = septet, br = broad, brd = broad-doublet, m = multiplet), coupling constants (Hz), relative integration value. Mass spectra were obtained on a JEOL JMS-700T spectrometer (EI).

Materials

All commercially available materials were used as received without further purification. All experiments were carried out under argon atmosphere in flame-dried glassware using standard inert techniques for introducing reagents and solvents unless otherwise noted.

Typical procedure for the reaction between various phenols and halothane

To a solution of the phenol (1.0 mmol) in THF (5.0 mL) was added previously ground KOH (1.5 mmol) and halothane (2.0 mmol) in small portions at 0 °C. The solution was heated to 60 °C until the reaction was completed. Then, the reaction mixture was quenched by the addition of sat. aq. NH_4Cl (20 mL) at

0 °C and extracted with AcOEt. The organic phase was washed with brine (30 mL), dried over Na_2SO_4, filtered, and concentrated under reduced pressure. The residue was purified by column chromatography to afford the products **2**.

2-Bromo-2-chloro-1,1-difluoroethyl phenyl ether (2a): The title product **2a** was purified by column chromatography and preparative TLC (hexane only) and obtained in 74% yield (199.6 mg). Pale yellow oil; ^{1}H NMR (400 MHz, $CDCl_3$) δ 5.91 (t, *J* = 5.2 Hz, 1H), 7.20–7.31 (m, 5H), 7.35–7.42 (m, 2H); ^{13}C NMR (100 MHz, $CDCl_3$) δ 53.5 (t, *J* = 41.7 Hz), 119.7 (t, *J* = 267.1 Hz), 121.8, 126.5, 129.7, 149.7; ^{19}F NMR (376 MHz, $CDCl_3$) δ −77.9 (dd, *J* = 136.9, 5.2 Hz, 1F), −78.2 (dd, *J* = 136.9, 5.2 Hz, 1F); EIMS (*m/z*): 270, 272 $[M]^+$; HRMS–EI (*m/z*): $[M]^+$ calcd for $C_8H_6BrClF_2O$, 269.9259, 271.9238; found, 269.9264, 271.9233.

4-Benzoylmethyl-3-chloro-2,2-difluorochromane (3): To a solution of **2o** (210.8 mg, 0.53 mmol) in THF (2.6 mL) was added zinc (42.1 mg, 0.64 mmol) and chlorotrimethylsilane (133 µL, 1.05 mmol) at 0 °C. After stirring for 40 min, the reaction mixture was quenched by the addition of 10% aq. HCl (40 mL) at 0 °C and extracted with AcOEt. The organic phase was dried over Na_2SO_4, filtered, and concentrated under reduced pressure. The residue was purified by column chromatography (hexane/$CHCl_3$ 4:1 to 1:1) and product **3** was obtained as a mixture of two diastereoisomers (*syn*/*anti* 2:1) in 21% yield (36.9 mg). Yellow oil; ^{1}H NMR (400 MHz, $CDCl_3$) δ 3.48 (ddd, *J* = 18.7, 5.2, 1.4 Hz, *anti*-isomer), 3.73 (ddd, *J* = 18.7, 7.0, 1.2 Hz, *anti*-isomer, 2H), 3.57–3.71 (m, *syn*-isomer, 2H), 4.04–4.18 (m, *anti*-isomer, 1H), 4.29–4.37 (m, *syn*-isomer, 1H), 4.66 (ddd, *J* = 7.0, 6.0, 1.0 Hz, *anti*-isomer, 1H), 4.82 (t, *J* = 4.1 Hz, *syn*-isomer, 1H), 7.01–7.22 (m, 3H), 7.24–7.33 (m, 1H), 7.49 (t, *J* = 7.3 Hz, *anti*-isomer, 2H), 7.52 (t, *J* = 7.3 Hz, *syn*-isomer, 2H), 7.58–7.67 (m, 1H), 7.97 (dd, *J* = 7.8, 1.3 Hz, *anti*-isomer, 2H), 8.05 (dd, *J* = 7.8, 1.3 Hz, *syn*-isomer, 2H); ^{13}C NMR (100 MHz, $CDCl_3$) δ 34.5 (*syn*-isomer), 38.4 (d, *J* = 2.2 Hz, *syn*-isomer), 39.3 (*anti*-isomer), 41.7 (d, *J* = 6.0 Hz, *anti*-isomer), 54.7 (d, *J* = 28.6 Hz, *anti*-isomer), 54.9 (d, *J* = 26.6 Hz, *syn*-isomer), 55.1 (d, *J* = 28.6 Hz, *anti*-isomer), 55.3 (d, *J* = 26.6 Hz, *syn*-isomer), 117.3 (*syn*-isomer), 117.4 (*anti*-isomer), 119.49 (d, *J* = 256.9 Hz, *anti*-isomer), 119.52 (d, *J* = 251.1 Hz, *syn*-isomer), 120.6 (*syn*-isomer), 121.5 (*anti*-isomer), 122.06 (d, *J* = 256.9 Hz, *anti*-isomer), 122.11 (d, *J* = 251.1 Hz, *syn*-isomer), 124.1 (*syn*-isomer), 124.3 (*anti*-isomer), 127.0 (*anti*-isomer), 128.2 (*syn*-isomer), 128.3, 129.0, 129.1 (*anti*-isomer), 129.3 (*syn*-isomer), 133.9, 136.4 (*anti*-isomer), 136.5 (*syn*-isomer), 149.2 (*anti*-isomer), 149.6 (d, *J* = 4.1 Hz, *syn*-isomer), 197.0 (*anti*-isomer), 197.3 (*syn*-isomer); ^{19}F NMR (376 MHz, $CDCl_3$) δ −69.0 (dd, *J* = 155.8, 4.1 Hz, *syn*-isomer, 1F), −70.8 (d, *J* = 157.3 Hz, *anti*-isomer, 1F), −77.6 (ddd, *J* = 157.6, 7.0, 4.2 Hz, *anti*-isomer, 1F), −79.0 (dd, *J* = 155.8, 3.1 Hz, *syn*-isomer, 1F); EIMS (*m/z*): 322 $[M]^+$; HRMS–EI (*m/z*): $[M]^+$ calcd for $C_{17}H_{13}ClF_2O_2$, 322.0572; found, 322.0565.

Supporting Information

Supporting Information File 1

Characterization data for **2b**–**p** and copies of ^{1}H, ^{13}C, and ^{19}F NMR spectra.
[https://www.beilstein-journals.org/bjoc/content/supplementary/1860-5397-17-9-S1.pdf]

ORCID® iDs

Kazuyuki Sato - https://orcid.org/0000-0001-6572-602X
Kentaro Kawai - https://orcid.org/0000-0002-6291-0558
Masaaki Omote - https://orcid.org/0000-0003-1210-1768

References

1. Wang, J.; Sánchez-Roselló, M.; Aceña, J. L.; del Pozo, C.; Sorochinsky, A. E.; Fustero, S.; Soloshonok, V. A.; Liu, H. *Chem. Rev.* **2014,** *114,* 2432–2506. doi:10.1021/cr4002879
2. Dreyer, G. B.; Metcalf, B. W. *Tetrahedron Lett.* **1988,** *29,* 6885–6888. doi:10.1016/s0040-4039(00)88466-x
3. Hamer, R. R. L.; Freed, B.; Allen, C. R. Alkylamino- and alkylamino alkyl diarylketones. U.S. Pat. Appl. US5,006,563A, April 9, 1991.
4. Han, C.; Salyer, A. E.; Kim, E. H.; Jiang, X.; Jarrard, R. E.; Powers, M. S.; Kirchhoff, A. M.; Salvador, T. K.; Chester, J. A.; Hockerman, G. H.; Colby, D. A. *J. Med. Chem.* **2013,** *56,* 2456–2465. doi:10.1021/jm301805e
5. Kohl, B.; Sturm, E.; Senn-Bilfinger, J.; Simon, W. A.; Krüger, U.; Schaefer, H.; Rainer, G.; Figala, V.; Klemm, K. *J. Med. Chem.* **1992,** *35,* 1049–1057. doi:10.1021/jm00084a010
6. Nakano, T.; Makino, M.; Morizawa, Y.; Matsumura, Y. *Angew. Chem., Int. Ed. Engl.* **1996,** *35,* 1019–1021. doi:10.1002/anie.199610191
7. Chang, C.-S.; Negishi, M.; Nakano, T.; Morizawa, Y.; Matsumura, Y.; Ichikawa, A. *Prostaglandins* **1997,** *53,* 83–90. doi:10.1016/s0090-6980(97)00003-8
8. Matsumura, Y.; Nakano, T.; Asai, T.; Morizawa, Y. Synthesis and Properties of Novel Fluoroprostacyclins. In *Biomedical Frontiers of Fluorine Chemistry;* Ojima, I.; McCarthy, J. R.; Welch, J. T., Eds.; ACS Symposium Series, Vol. 639; American Chemical Society: Washington, DC, USA, 1996; pp 83–94. doi:10.1021/bk-1996-0639.ch006
9. Middleton, W. J. *J. Org. Chem.* **1975,** *40,* 574–578. doi:10.1021/jo00893a007
10. Lal, G. S.; Pez, G. P.; Pesaresi, R. J.; Prozonic, F. M.; Cheng, H. *J. Org. Chem.* **1999,** *64,* 7048–7054. doi:10.1021/jo990566+
11. Lal, G. S.; Lobach, E.; Evans, A. *J. Org. Chem.* **2000,** *65,* 4830–4832. doi:10.1021/jo000020j
12. Singh, R. P.; Twamley, B.; Shreeve, J. M. *J. Org. Chem.* **2002,** *67,* 1918–1924. doi:10.1021/jo016245r

13. L'Heureux, A.; Beaulieu, F.; Bennett, C.; Bill, D. R.; Clayton, S.; LaFlamme, F.; Mirmehrabi, M.; Tadayon, S.; Tovell, D.; Couturier, M. *J. Org. Chem.* **2010,** *75,* 3401–3411. doi:10.1021/jo100504x
14. Umemoto, T.; Singh, R. P.; Xu, Y.; Saito, N. *J. Am. Chem. Soc.* **2010,** *132,* 18199–18205. doi:10.1021/ja106343h
15. Hallinan, E. A.; Fried, J. *Tetrahedron Lett.* **1984,** *25,* 2301–2302. doi:10.1016/s0040-4039(01)80239-2
16. Taguchi, T.; Kitagawa, O.; Suda, Y.; Ohkawa, S.; Hashimoto, A.; Iitaka, Y.; Kobayashi, Y. *Tetrahedron Lett.* **1988,** *29,* 5291–5294. doi:10.1016/s0040-4039(00)80740-6
17. Baldwin, J. E.; Lynch, G. P.; Schofield, C. J. *J. Chem. Soc., Chem. Commun.* **1991,** 736–738. doi:10.1039/c39910000736
18. Angelastro, M. R.; Bey, P.; Mehdi, S.; Peet, N. P. *Bioorg. Med. Chem. Lett.* **1992,** *2,* 1235–1238. doi:10.1016/s0960-894x(00)80220-6
19. Curran, T. T. *J. Org. Chem.* **1993,** *58,* 6360–6363. doi:10.1021/jo00075a033
20. Shen, Y.; Qi, M. *J. Fluorine Chem.* **1994,** *67,* 229–232. doi:10.1016/0022-1139(93)02961-d
21. Kanai, K.; Wakabayashi, H.; Honda, T. *Org. Lett.* **2000,** *2,* 2549–2551. doi:10.1021/ol006268c
22. Sato, K.; Tarui, A.; Matsuda, S.; Omote, M.; Ando, A.; Kumadaki, I. *Tetrahedron Lett.* **2005,** *46,* 7679–7681. doi:10.1016/j.tetlet.2005.09.031
23. Poisson, T.; Belhomme, M.-C.; Pannecoucke, X. *J. Org. Chem.* **2012,** *77,* 9277–9285. doi:10.1021/jo301873y
24. Saijo, H.; Ohashi, M.; Ogoshi, S. *J. Am. Chem. Soc.* **2014,** *136,* 15158–15161. doi:10.1021/ja5093776
25. Ohashi, M.; Kawashima, T.; Taniguchi, T.; Kikushima, K.; Ogoshi, S. *Organometallics* **2015,** *34,* 1604–1607. doi:10.1021/acs.organomet.5b00218
26. Ohashi, M.; Shirataki, H.; Kikushima, K.; Ogoshi, S. *J. Am. Chem. Soc.* **2015,** *137,* 6496–6499. doi:10.1021/jacs.5b03587
27. Kawashima, T.; Ohashi, M.; Ogoshi, S. *J. Am. Chem. Soc.* **2017,** *139,* 17795–17798. doi:10.1021/jacs.7b12007
28. Kawashima, T.; Ohashi, M.; Ogoshi, S. *J. Am. Chem. Soc.* **2018,** *140,* 17423–17427. doi:10.1021/jacs.8b11671
29. Ohashi, M.; Ishida, N.; Ando, K.; Hashimoto, Y.; Shigaki, A.; Kikushima, K.; Ogoshi, S. *Chem. – Eur. J.* **2018,** *24,* 9794–9798. doi:10.1002/chem.201802415
30. Shirataki, H.; Ohashi, M.; Ogoshi, S. *Eur. J. Org. Chem.* **2019,** 1883–1887. doi:10.1002/ejoc.201801721
31. Shirataki, H.; Ono, T.; Ohashi, M.; Ogoshi, S. *Org. Lett.* **2019,** *21,* 851–856. doi:10.1021/acs.orglett.8b03674
32. Tarrant, P.; Brown, H. C. *J. Am. Chem. Soc.* **1951,** *73,* 5831–5833. doi:10.1021/ja01156a111
33. Li, X.; Pan, H.; Jiang, X. *Tetrahedron Lett.* **1984,** *25,* 4937–4940. doi:10.1016/s0040-4039(01)91263-8
34. Ohashi, M.; Adachi, T.; Ishida, N.; Kikushima, K.; Ogoshi, S. *Angew. Chem., Int. Ed.* **2017,** *56,* 11911–11915. doi:10.1002/anie.201703923
35. Zafrani, Y.; Sod-Moriah, G.; Segall, Y. *Tetrahedron* **2009,** *65,* 5278–5283. doi:10.1016/j.tet.2009.04.082
36. Fuchibe, K.; Koseki, Y.; Sasagawa, H.; Ichikawa, J. *Chem. Lett.* **2011,** *40,* 1189–1191. doi:10.1246/cl.2011.1189
37. Sasada, Y.; Shimada, T.; Ushioda, M.; Matsui, S. *Liq. Cryst.* **2007,** *34,* 569–576. doi:10.1080/02678290701284279
38. Tanaka, H.; Endou, H. Liquid crystal compound, liquid crystal composition and liquid crystal display element. Japanese Patent JPWO2014/129268, Aug 28, 2014.
39. Hiraoka, Y.; Kawasaki-Takasuka, T.; Morizawa, Y.; Yamazaki, T. *J. Fluorine Chem.* **2015,** *179,* 71–76. doi:10.1016/j.jfluchem.2015.05.006
40. Dai, K.; Wang, K.; Li, Y.; Chen, J.-G.; Liu, Z.-W.; Lu, J.; Liu, Z.-T. *J. Org. Chem.* **2017,** *82,* 4721–4728. doi:10.1021/acs.joc.7b00396
41. Wu, K.; Chen, Q.-Y. *Tetrahedron* **2002,** *58,* 4077–4084. doi:10.1016/s0040-4020(02)00257-0
42. Nishihara, M.; Nakamura, Y.; Maruyama, N.; Sato, K.; Omote, M.; Ando, A.; Kumadaki, I. *J. Fluorine Chem.* **2003,** *122,* 247–249. doi:10.1016/s0022-1139(03)00053-8
43. Ando, A.; Takahashi, J.; Nakamura, Y.; Maruyama, N.; Nishihara, M.; Fukushima, K.; Moronaga, J.; Inoue, M.; Sato, K.; Omote, M.; Kumadaki, I. *J. Fluorine Chem.* **2003,** *123,* 283–285. doi:10.1016/s0022-1139(03)00148-9
44. Ichikawa, J.; Kaneko, M.; Yokota, M.; Itonaga, M.; Yokoyama, T. *Org. Lett.* **2006,** *8,* 3167–3170. doi:10.1021/ol060912r
45. Gerus, I. I.; Kolycheva, M. T.; Yagupol'skii, Y. L.; Kukhar, V. P. *Zh. Org. Khim.* **1989,** *25,* 2020–2021.

License and Terms

This is an Open Access article under the terms of the Creative Commons Attribution License (https://creativecommons.org/licenses/by/4.0). Please note that the reuse, redistribution and reproduction in particular requires that the author(s) and source are credited and that individual graphics may be subject to special legal provisions.

The license is subject to the *Beilstein Journal of Organic Chemistry* terms and conditions: (https://www.beilstein-journals.org/bjoc/terms)

The definitive version of this article is the electronic one which can be found at: https://doi.org/10.3762/bjoc.17.9

BEILSTEIN JOURNAL OF ORGANIC CHEMISTRY

Facile preparation and conversion of 4,4,4-trifluorobut-2-yn-1-ones to aromatic and heteroaromatic compounds

Takashi Yamazaki*, Yoh Nakajima, Minato Iida and Tomoko Kawasaki-Takasuka

Full Research Paper

Open Access

Address:
Division of Applied Chemistry, Institute of Engineering, Tokyo University of Agriculture and Technology, 2-24-16 Nakamachi, Koganei 184-8588, Japan

Email:
Takashi Yamazaki* - tyamazak@cc.tuat.ac.jp

* Corresponding author

Keywords:
CF_3-containing propargylic alcohols; CF_3-containing ynones; oxidation; pyrimidines; salicylate derivatives

Beilstein J. Org. Chem. **2021,** *17,* 132–138.
https://doi.org/10.3762/bjoc.17.14

Received: 20 October 2020
Accepted: 18 December 2020
Published: 15 January 2021

This article is part of the thematic issue "Organo-fluorine chemistry V".

Guest Editor: D. O'Hagan

© 2021 Yamazaki et al.; licensee Beilstein-Institut.
License and terms: see end of document.

Abstract

The concise preparation of 4,4,4-trifluorobut-2-yn-1-ones by the oxidation of the readily accessible corresponding propargylic alcohols as well as their utilization as Michael acceptors for the construction of aromatic and heteroaromatic compounds are reported.

Introduction

It is well known that the incorporation of a fluorine atom or a fluorine-containing group into organic compounds sometimes affects their original biological activities [1-3], and thus the development of methods for the construction of such molecules with this atom or group is an important task. During our research in the field of fluorine chemistry, we have previously developed methods to get convenient access to CF_3-containing propargylic alcohols **1** using 2-bromo-3,3,3-trifluoropropene [4,5] as well as 1-chloro-3,3,3-trifluoropropene [6] as a substrate and to utilize **1** by way of a variety of routes [7-14]. Recently, we turned our attention to oxidized propargyl alcohols, namely ynones **2**, because of the interesting structure with two strongly electron-withdrawing moieties, resulting in a high electrophilicity. However, only a few methods have been reported thus far for their preparation [15-20], including one that appeared in 2020 [21]. However, they suffer from problems, such as the formation of the desired product **2** only as regioisomeric mixtures [15,17] or the applicability to only one substrate without any extension to other related compounds [16,18-20]

Aromatic and heteroaromatic compounds are recognized as useful intermediates, and as pointed out above, the expected high electrophilicity of **2** was considered to allow the utilization as efficient Michael acceptors. Actually, this was the case, and the Sandford group clarified the high potency of these compounds for the conjugate addition of N- as well as O-nucleophiles [21]. On the basis of such an idea, we tried two routes to gain access to 1) 4-substituted 6-(trifluoromethyl)salicylate derivatives (C-nucleophiles) and 2) 6-substituted 4-(trifluoromethyl)pyrimidines (N-nucleophiles), both in a concise fashion, with the full details, including the preparation of **2**, being reported herein.

Results and Discussion

Investigations on the reaction conditions were carried out for the oxidation of propargylic alcohols **1**, which were readily accessible by our already reported procedure [4,19] as well as by the ones developed by other groups [22,23]. In spite of the previous unfavorable results for the oxidative transformation of **1a** by MnO_2 as well as other oxidants [18,23], MnO_2 was selected due to the low cost and convenient handling. After a number of trials aimed at optimizing the reaction conditions, the unexpectedly smooth conversion of **1a** to **2a** was realized. Although it was reported [18,23] that only a small amount of **2a** was confirmed after the reaction of **1a** with 10 equiv of MnO_2 at ambient temperature after 1 day, the same amount of oxidant actually led to the complete conversion after only 4 h at room temperature. In this instance, for the clean preparation of the desired compound **2a**, the important point was to initiate this oxidation process at 0 °C, followed by warming to ambient temperature. With this intriguing result in hand, the oxidation of the other substrates **1** was performed under similar reaction condition, the results of which are summarized in Table 1.

We reported the yield as determined by ^{19}F NMR spectroscopy rather than after purification because of the inherent instability of **2** on silica gel, causing partial decomposition. The crude mixture proved to be substantially pure, and thus **2c** and **2d** afforded appropriate analytical data, including NMR (^{1}H, ^{13}C, and ^{19}F), IR, as well as high-resolution MS data. This process allowed us to obtain the required ynones **2** as long as the residue R was aromatic, while with an aliphatic substituent in this position, a full conversion was not observed even after a prolonged reaction period and at a higher temperature, and such conditions seemed to evoke the degradation of the products **2** to some extent. This was not the case for the Dess–Martin periodinane oxidation and the propargylic alcohols with C_7H_{15} as the residue R^1 by Hoye et al. [15] and C_9H_{19} as the residue R^1 by the Sandford group [21], who recorded 80% and 76% isolated yield, respectively, of the corresponding ketones. Because these compounds were previously isolated inconveniently by preparative GLC [15] or distillation [17,19], we decided to employ them without further purification.

The Michael addition reactions were then carried out under basic conditions for the ynone **2a** thus obtained, which, to our astonishment, was found to be relatively rare even for the nonfluorinated counterparts (Table 2) [24-28].

As expected for this model system, a very efficient addition was observed within a period of 0.5 h at 0 °C, leading to an isolated yield of 69% for the adduct **3aa** when 1.5 equiv of acetylacetone and NaH in Et_2O were used (Table 2, entries 1−3), which unambiguously demonstrated the high potency of **2a** as a Michael acceptor. Stronger bases, such as NaH and *t*-BuOK seemed to be preferable (Table 2, entries 3 and 6), and amines such as DBU and 1,1,3,3-tetramethylguanidine (TMG) were found to be insufficient (Table 2, entries 10 and 11). Judging from the possible mechanism, this process was considered to proceed under the action of a catalytic amount of a base, and only 2 mol % of *t*-BuOK led to the formation of the desired adduct **3aa** as a sole stereoisomer in 84% isolated yield under the same reaction conditions (Table 2, entries 6−8). The *E*-stereochemistry of **3aa** was deduced from the NMR data of structurally similar compounds [29] on the basis of 1) comparison of the chemical shift of the CF_3 group and 2) the absence of a coupling between the vinylic and allylic protons. In order to explore other nucleophiles, we employed 1,3-diketones, such as 5-methylhexane-1,3-dione and 5,5-dimethylhexane-1,3-dione (that is, one of the two methyl groups in acetylacetone was formally substituted for an isopropyl or a *t*-Bu moiety, respective-

Table 1: Oxidation of propargylic alcohols **1**.[a]

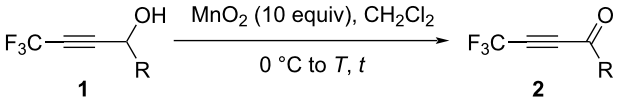

1 **2**

entry	R	*T* (°C)	*t* (h)	product	^{19}F NMR yield[b] (%)
1	Ph	rt	4	**2a**	95 (100)
2	4-(MeO)C_6H_4	rt	2.5	**2b**	93 (100)
3	4-MeC_6H_4	rt	3	**2c**	90 (100)
4	4-BrC_6H_4	rt	2	**2d**	58 (93)
5	$PhCH_2CH_2$	reflux	20	**2e**	35 (48)
6[c]	$PhCH_2CH_2$	reflux	20	**2e**	25 (80)

[a]**1** was added to a CH_2Cl_2 solution of MnO_2 at 0 °C, and the mixture was stirred with gradually warming to a defined temperature for a defined reaction time, as indicated. [b]The conversion of **1** as determined by ^{19}F NMR spectroscopy is shown in parentheses. [c]$CHCl_3$ was used instead of CH_2Cl_2.

Table 2: Michael addition of acetylacetone to **2a**.

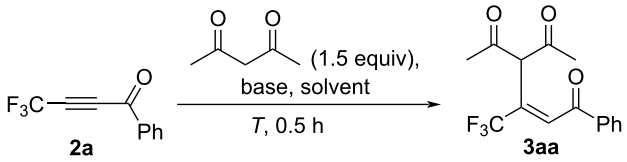

entry	base (equiv)	solvent	*T* (°C)	^{19}F NMR yield[a] (%)
1	NaH (1.5)	THF	0	53
2	NaH (1.5)	DMF	0	34
3	NaH (1.5)	Et_2O	0	76 (69)
4	NaH (1.5)	Et_2O	–40	72
5	NaH (1.5)	Et_2O	rt	61
6	*t*-BuOK (1.5)	Et_2O	0	68 (67)
7	*t*-BuOK (0.1)	Et_2O	0	77
8	*t*-BuOK (0.02)	Et_2O	0	94 (84)
9	*t*-BuOK (0.02)	*t*-BuOH	30	78
10	DBU (0.1)	Et_2O	0	33
11	TMG[b] (0.1)	Et_2O	0	14

[a]The isolated yield is shown in parentheses. [b]1,1,3,3-Tetramethylguanidine.

ly), but no reaction was observed at all. The conjugate addition of amines to this type of ynone has already been reported [21], where the authors pointed out the significant slowdown of the reaction rate when *tert*-butylamine was employed, which was considered to be a reflection of the sensitivity of ynones **2** towards steric hindrance.

Because appropriate conditions for the initial Michael addition reactions were thus determined, further conversion to the benzene derivative **4aa** was also performed (Table 3).

First of all, **3aa** was introduced to a *t*-BuOH solution of 2 equiv of *t*-BuOK to afford the desired product **4aa** in a high yield, and

Table 3: Investigation of the cyclization conditions for **3aa**.

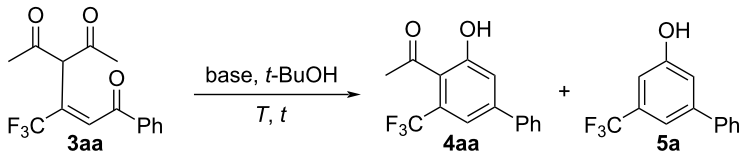

entry	base (equiv)	*T* (°C)	*t* (h)	^{19}F NMR yield of **4aa**[a] (%)
1	*t*-BuOK (0.5)	60	4	7 (49)
2	*t*-BuOK (1.0)	60	4	13 (81)[b] {8}
3	*t*-BuOK (2.0)	60	4	85 (<1)
4	*t*-BuOK (3.0)	60	4	>99 (0)
5	*t*-BuOK (3.0)	60	2	>99 (0)
6	*t*-BuOK (3.0)	30	2	>99 (0) {84}
7[c]	*t*-BuOK (3.0)	30	2	>99 (0)
8	*t*-BuONa (3.0)	30	2	58 (0)
9	*t*-BuOLi (3.0)	30	3	66 (3)
10[d]	EtONa (3.0)	30	2	0 (0)
11[d]	EtONa (3.0)	60	6	18 (15)

[a]The ^{19}F NMR yield of **5a** and the isolated yield of **4aa** are shown in parentheses and braces, respectively. [b]Isolated yield of **5a**. [c]Et_2O was used instead of *t*-BuOH. [d]EtOH was used instead of *t*-BuOH.

an increase in the amount of this base to 3 equiv led to the complete conversion of the substrate **3aa** (Table 3, entries 3 and 4). This trend was followed even when the temperature was decreased to 30 °C and the reaction time was 2 h, furnished **4aa** in a 84% yield (Table 3, entries 6 and 7). The use of the corresponding lithium and sodium *tert*-butoxides was found to afford a lower yield, which clarified the importance of the ionic character of the base (Table 3, entries 8 and 9).

For the present transformation, Hu and Guan already reported a similar type of ring closure of the substrate **3fa** [30], which allowed the conversion to the phenolic product **5f** as a result of the cyclization and was accompanied by deacetylation under the conditions depicted in Scheme 1 [31-33].

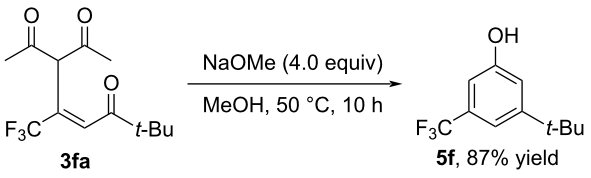

Scheme 1: Deacetylative cyclization of **3fa**.

In our case, it was quite interesting to note that the deacylated product **5a** was also obtained as the major product when an equimolar or lesser amount of *t*-BuOK was employed (Table 3, entries 1 and 2), along with formation of a minor amount of **4aa**. Moreover, when the isolated product **4aa** was subjected to the conditions shown in Table 3, entry 4, no reaction was observed at all, with recovery of **4aa**, which clearly demonstrated that the deacetylation step had occurred before the conversion to **4aa**. In the present cyclization, the ionic character of the alkoxide seemed to be an important factor, and the corresponding lithium and sodium salts did not aid the reaction satisfactory. Moreover, EtONa was found to be inappropriate for this protocol (Table 3, entries 10 and 11).

Determination of the appropriate conditions both for Michael addition as well as cyclization/aromatization reactions allowed us to explore a brief scope and limitation of the present reaction by using four representative types of crude ynones **2** starting from the conjugate addition step either with acetylacetone or ethyl acetoacetate (Table 4).

In all instances, the desired products **4** were obtained in good to excellent yield without contamination by the deacetylated products **5**.

With the success of the regiospecific formation of 4-substituted 6-(trifluoromethyl)salicylate derivatives **4**, as shown in Table 4, the application of ynones **2** was demonstrated at the next stage for the construction of a variety of pyrimidine derivatives, **6**, using amidines including guanidine [34]. First of all, various bases were employed for the reaction of the model substrate **2a**. During initial testing, guanidine hydrochloride at 25 °C for 4 h in acetonitrile (Table 5, entries 1–7) as well as sodium carbonate were found to be adequate (Table 5, entry 5).

A comparison of the results in Table 5, entries 8–11 vs entry 5 led to the determination that the adequate solvent was acetonitrile. After screening the reaction time and temperature (Table 5, entries 12–15 vs entry 5), we eventually selected the conditions as shown in Table 5, entry 14, which included heating the reaction mixture at 80 °C for 8 h in MeCN, furnishing the desired pyrimidine **6aa** in 60% isolated yield.

Table 4: Preparation of the trifluoromethylated salicylate derivatives **4**.

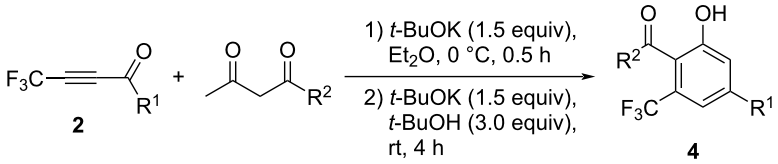

entry	R^1	R^2	product	isolated yield (%)
1	Ph	Me	**4aa**	74
2	Ph	EtO	**4ab**	80
3	4-(MeO)C_6H_4	Me	**4ba**	67
4	4-(MeO)C_6H_4	EtO	**4bb**	73
5	4-Me-C_6H_4	Me	**4ca**	68
6	4-Me-C_6H_4	EtO	**4cb**	75
7	4-Br-C_6H_4	Me	**4da**	70
8	4-Br-C_6H_4	EtO	**4db**	54

Table 5: Preparation of trifluoromethylated pyrimidine derivatives **6aa**.

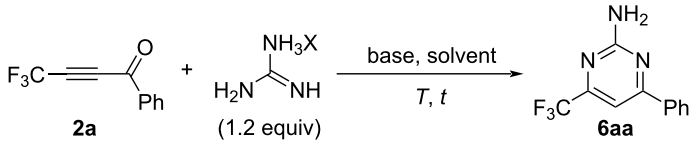

2a (1.2 equiv) **6aa**

entry	base	solvent	*T* (°C)	*t* (h)	^{19}F NMR yield[a] (%)	
					6aa	byproducts
1	KO*t*-Bu	CH_3CN	25	4	8	54
2	NaOEt	CH_3CN	25	4	15	9
3	DBU	CH_3CN	25	4	3	17
4	K_2CO_3	CH_3CN	25	4	28	4
5	Na_2CO_3	CH_3CN	25	4	33	17
6	$CaCO_3$	CH_3CN	25	4	25	39
7	Li_2CO_3	CH_3CN	25	4	27	29
8	Na_2CO_3	DME	25	4	19	24
9	Na_2CO_3	DMF	25	4	31	14
10	Na_2CO_3	DMSO	25	4	24	9
11	Na_2CO_3	THF	25	4	31	20
12	Na_2CO_3	CH_3CN	50	4	66	5
13	Na_2CO_3	CH_3CN	80	4	81 (57)	2
14	Na_2CO_3	CH_3CN	80	8	83 (60)	0
15	Na_2CO_3	CH_3CN	80	16	70 (56)	<1

[a]The isolated yield is shown in parentheses.

Then, four types of ynones, **2a**–**d**, were reacted with formamidine and acetamidine as well as guanidine under the optimized conditions outlined above, the results of which are summarized in Table 6. When the reactions were performed with acetamidine and guanidine, a good to high yield was recorded, while only a lower yield was obtained by the application of formami-

Table 6: Preparation of trifluoromethylated pyrimidine derivatives **6**.

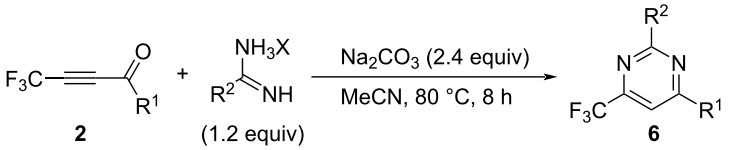

2 (1.2 equiv) **6**

entry	R^1	R^2	X	product	isolated yield (%)
1	Ph (**2a**)	NH_2	Cl	**6aa**	60
2	4-(MeO)C_6H_4 (**2b**)	NH_2	Cl	**6ab**	55
3	4-MeC_6H_4 (**2c**)	NH_2	Cl	**6ac**	52
4	4-BrC_6H_4 (**2d**)	NH_2	Cl	**6ad**	67
5	Ph (**2a**)	Me	Cl	**6ba**	67
6	4-(MeO)C_6H_4 (**2b**)	Me	Cl	**6bb**	75
7	4-MeC_6H_4 (**2c**)	Me	Cl	**6bc**	53
8	4-BrC_6H_4 (**2d**)	Me	Cl	**6bd**	57
9	Ph (**2a**)	H	AcO	**6ca**	21
10	4-(MeO)C_6H_4 (**2b**)	H	AcO	**6cb**	28
11	4-MeC_6H_4 (**2c**)	H	AcO	**6cc**	22
12	4-BrC_6H_4 (**2d**)	H	AcO	**6cd**	26

dine acetate, for which the reaction was not further elucidated at this point.

The unfavorable yield may be reasoned by the fact that there have been very limited reports for the syntheses of, for example, pyrimidine **6ca** [35-38], with such drawbacks as the formation of a regioisomeric mixture [35] and the requirement of harsh conditions [38]. At the same time, for the use of a substrate similar to **2a** where the CF_3 and Ph groups were formally exchanged, an isolated yield of 84% has been recorded for **6ca** [37]. Moreover, it is noteworthy that only one report dealt with the preparation of **6cb** [37], and **6cc** and **6cd** have not been previously reported. Thus, including **6aa** [37-40] and **6ba** [37,38,41,42], it is noteworthy to realize the construction of relatively rare pyrimidines in a concise fashion via the ynones **2** with a CF_3 group.

Conclusion

As described above, we succeeded in the construction of 4,4,4-trifluorobut-2-yn-1-ones **2** by way of a convenient MnO_2 oxidation of readily accessible propargylic alcohols **1**. In spite of the application of this method only to **1**, with an aromatic substituent at the propargylic position and the requirement of an excess amount of this oxidant, the practical convenience, low cost, as well as the clean conversion are notable features of this method, which is worthy of attention. Furthermore, the high electrophilicity of ynones **2** obtained was nicely demonstrated through two representative reactions, namely 1) Michael additions of β-keto carbonyl compounds and 2) amidines and guanidine for the construction of aromatic and heteroaromatic products, which successfully expanded this unique synthetic approach to compounds with a limited precedent. Further work is ongoing for the application of ynones **2**.

Supporting Information

The Supporting Information features the experimental part of this article.

Supporting Information File 1

General information, synthetic procedures, and spectral data.
[https://www.beilstein-journals.org/bjoc/content/supplementary/1860-5397-17-14-S1.pdf]

ORCID® iDs

Takashi Yamazaki - https://orcid.org/0000-0002-1460-3086
Tomoko Kawasaki-Takasuka - https://orcid.org/0000-0002-8468-7553

References

1. Inoue, M.; Sumii, Y.; Shibata, N. *ACS Omega* **2020,** *5,* 10633–10640. doi:10.1021/acsomega.0c00830
2. Mei, H.; Han, J.; Fustero, S.; Medio-Simon, M.; Sedgwick, D. M.; Santi, C.; Ruzziconi, R.; Soloshonok, V. A. *Chem. – Eur. J.* **2019,** *25,* 11797–11819. doi:10.1002/chem.201901840
3. Wang, J.; Sánchez-Roselló, M.; Aceña, J. L.; del Pozo, C.; Sorochinsky, A. E.; Fustero, S.; Soloshonok, V. A.; Liu, H. *Chem. Rev.* **2014,** *114,* 2432–2506. doi:10.1021/cr4002879
4. Mizutani, K.; Yamazaki, T.; Kitazume, T. *J. Chem. Soc., Chem. Commun.* **1995,** 51–52. doi:10.1039/c39950000051
5. Yamazaki, T.; Mizutani, K.; Kitazume, T. *J. Org. Chem.* **1995,** *60,* 6046–6056. doi:10.1021/jo00124a013
6. Miyagawa, A.; Naka, M.; Yamazaki, T.; Kawasaki-Takasuka, T. *Eur. J. Org. Chem.* **2009,** 4395–4399. doi:10.1002/ejoc.200900370
7. Yamazaki, T.; Ichige, T.; Kitazume, T. *Org. Lett.* **2004,** *6,* 4073–4076. doi:10.1021/ol048229x
8. Yamazaki, T.; Yamamoto, T.; Ichihara, R. *J. Org. Chem.* **2006,** *71,* 6251–6253. doi:10.1021/jo060909l
9. Yamazaki, T.; Kawasaki-Takasuka, T.; Furuta, A.; Sakamoto, S. *Tetrahedron* **2009,** *65,* 5945–5948. doi:10.1016/j.tet.2009.05.087
10. Watanabe, Y.; Yamazaki, T. *Synlett* **2009,** 3352–3354. doi:10.1055/s-0029-1218383
11. Watanabe, Y.; Yamazaki, T. *J. Fluorine Chem.* **2010,** *131,* 646–651. doi:10.1016/j.jfluchem.2010.01.003
12. Watanabe, Y.; Yamazaki, T. *J. Org. Chem.* **2011,** *76,* 1957–1960. doi:10.1021/jo102503s
13. Yamazaki, T.; Watanabe, Y.; Yoshida, N.; Kawasaki-Takasuka, T. *Tetrahedron* **2012,** *68,* 6665–6673. doi:10.1016/j.tet.2012.05.131
14. Ichikawa, T.; Kawasaki-Takasuka, T.; Yamada, S.; Yamazaki, T.; Kubota, T. *J. Fluorine Chem.* **2013,** *152,* 38–45. doi:10.1016/j.jfluchem.2012.10.013
15. Shen, Y.; Xin, Y.; Cen, W.; Huang, Y. *Synthesis* **1984,** 35–37. doi:10.1055/s-1984-30723
16. Bumgardner, C. L.; Bunch, J. E.; Whangbo, M. H. *J. Org. Chem.* **1986,** *51,* 4082–4083. doi:10.1021/jo00371a037
17. Chechulin, P. I.; Filyakova, V. I.; Pashkevich, K. I. *Bull. Acad. Sci. USSR, Div. Chem. Sci. (Engl. Transl.)* **1989,** *38,* 189–190. doi:10.1007/bf00953736
18. Tajammal, S.; Tipping, A. E. *J. Fluorine Chem.* **1990,** *47,* 45–57. doi:10.1016/s0022-1139(00)80446-7
19. Brisdon, A. K.; Crossley, I. R. *Chem. Commun.* **2002,** 2420–2421. doi:10.1039/b207979h
20. Wang, T.; Niu, D.; Hoye, T. R. *J. Am. Chem. Soc.* **2016,** *138,* 7832–7835. doi:10.1021/jacs.6b03786
21. Murray, B. J.; Marsh, T. G. F.; Yufit, D. S.; Fox, M. A.; Harsanyi, A.; Boulton, L. T.; Sandford, G. *Eur. J. Org. Chem.* **2020,** 6236–6244. doi:10.1002/ejoc.202001071
22. Ishihara, T.; Yamasaki, Y.; Ando, T. *Tetrahedron Lett.* **1985,** *26,* 79–82. doi:10.1016/s0040-4039(00)98472-7
23. Sibous, L.; Tipping, A. E. *J. Fluorine Chem.* **1993,** *62,* 39–49. doi:10.1016/s0022-1139(00)80079-2
24. Fouli, F. A.; Basyouni, M. N. *Acta Chim. Acad. Sci. Hung.* **1981,** *106,* 297–302.
25. Shankar, R.; Jha, A. K.; Singh, U. S.; Hajela, K. *Tetrahedron Lett.* **2006,** *47,* 3077–3079. doi:10.1016/j.tetlet.2006.03.008
26. Ramachary, D. B.; Venkaiah, C.; Murali Krishna, P. *Chem. Commun.* **2012,** *48,* 2252–2254. doi:10.1039/c2cc17219d

27. Tong, W.; Li, Q.-Y.; Xu, Y.-L.; Wang, H.-S.; Chen, Y.-Y.; Pan, Y.-M. *Adv. Synth. Catal.* **2017,** *359,* 4025–4035. doi:10.1002/adsc.201700830
28. Yuan, Y.; Guo, Z.; Mu, Y.; Wang, Y.; Xu, M.; Li, Y. *Adv. Synth. Catal.* **2020,** *362,* 1298–1302. doi:10.1002/adsc.201901631
29. Ramasamy, M.; Lin, H.-C.; Kuo, S.-C.; Hsieh, M.-T. *Synlett* **2019,** *30,* 356–360. doi:10.1055/s-0037-1611694
30. Guan, H.-P.; Hu, C.-M. *J. Fluorine Chem.* **1996,** *78,* 101–102. doi:10.1016/0022-1139(96)03407-0
31. Furuta, T.; Nakayama, M.; Suzuki, H.; Tajimi, H.; Inai, M.; Nukaya, H.; Wakimoto, T.; Kan, T. *Org. Lett.* **2009,** *11,* 2233–2236. doi:10.1021/ol900689m
32. Wang, X.-j.; Zhang, L.; Byrne, D.; Nummy, L.; Weber, D.; Krishnamurthy, D.; Yee, N.; Senanayake, C. H. *Org. Lett.* **2014,** *16,* 4090–4093. doi:10.1021/ol501755h
33. Matsuda, T.; Matsumoto, T. *Org. Biomol. Chem.* **2016,** *14,* 5023–5027. doi:10.1039/c6ob00734a
34. Nenajdenko, V. G., Ed. *Fluorine in Heterocyclic Chemistry;* Springer: Berlin, Germany, 2014; Vol. 1 and 2.
35. Gupta, S.; Melanson, J. A.; Vaillancourt, L.; Nugent, W. A.; Tanoury, G. J.; Schatte, G.; Snieckus, V. *Org. Lett.* **2018,** *20,* 3745–3748. doi:10.1021/acs.orglett.8b01300
36. Geri, J. B.; Wade Wolfe, M. M.; Szymczak, N. K. *Angew. Chem., Int. Ed.* **2018,** *57,* 1381–1385. doi:10.1002/anie.201711316
37. Romanov, A. R.; Rulev, A. Y.; Ushakov, I. A.; Muzalevskiy, V. M.; Nenajdenko, V. G. *Eur. J. Org. Chem.* **2017,** 4121–4129. doi:10.1002/ejoc.201700727
38. Saijo, R.; Watanabe, G.; Kurihara, K.-i.; Kawase, M. *Heterocycles* **2014,** *89,* 2334–2345. doi:10.3987/com-14-13075
39. Liu, C.; Cui, Z.; Yan, X.; Qi, Z.; Ji, M.; Li, X. *Molecules* **2016,** *21,* 828. doi:10.3390/molecules21070828
40. Rawal, R. K.; Tripathi, R.; Katti, S. B.; Pannecouque, C.; De Clercq, E. *Bioorg. Med. Chem.* **2007,** *15,* 3134–3142. doi:10.1016/j.bmc.2007.02.044
41. Funabiki, K.; Nakamura, H.; Matsui, M.; Shibata, K. *Synlett* **1999,** 756–758. doi:10.1055/s-1999-2741
42. Jeong, I. H.; Jeon, S. L.; Kim, M. S.; Kim, B. T. *J. Fluorine Chem.* **2004,** *125,* 1629–1638. doi:10.1016/j.jfluchem.2004.09.021

License and Terms

This is an Open Access article under the terms of the Creative Commons Attribution License (https://creativecommons.org/licenses/by/4.0). Please note that the reuse, redistribution and reproduction in particular requires that the author(s) and source are credited and that individual graphics may be subject to special legal provisions.

The license is subject to the *Beilstein Journal of Organic Chemistry* terms and conditions: (https://www.beilstein-journals.org/bjoc/terms)

The definitive version of this article is the electronic one which can be found at: https://doi.org/10.3762/bjoc.17.14

BEILSTEIN JOURNAL OF ORGANIC CHEMISTRY

Exploring the possibility of using fluorine-involved non-conjugated electron-withdrawing groups for thermally activated delayed fluorescence emitters by TD-DFT calculation

Dongyang Chen and Eli Zysman-Colman*§

Full Research Paper

Open Access

Address:
Organic Semiconductor Centre, EaStCHEM School of Chemistry, University of St Andrews, St Andrews, Fife, KY16 9ST, UK

Email:
Eli Zysman-Colman* - eli.zysman-colman@st-andrews.ac.uk

* Corresponding author
§ Fax: +44-1334 463808; Tel: +44-1334 463826

Keywords:
DFT calculation; pentafluorosulfanyl; spin-orbit coupling; TADF; trifluoromethoxy; trifluoromethylthio

Beilstein J. Org. Chem. **2021,** *17,* 210–223.
https://doi.org/10.3762/bjoc.17.21

Received: 11 November 2020
Accepted: 05 January 2021
Published: 21 January 2021

This article is part of the thematic issue "Organo-fluorine chemistry V".

Guest Editor: D. O'Hagan

© 2021 Chen and Zysman-Colman; licensee Beilstein-Institut.
License and terms: see end of document.

Abstract

The trifluoromethyl group has been previously explored as a non-conjugated electron-withdrawing group in donor–acceptor thermally activated delayed fluorescence (TADF) emitters. In the present study, we investigate computationally the potential of other fluorine-containing acceptors, trifluoromethoxy (OCF_3), trifluoromethylthio (SCF_3), and pentafluorosulfanyl (SF_5), within two families of donor–acceptor TADF emitters. Time-dependent density functional theory calculations indicate that when only two *ortho*-disposed carbazole donors are used (Type I molecules), the lowest-lying triplet state possesses locally excited (LE) character while the lowest-lying singlet state possesses charge-transfer character. When five carbazole donors are present in the emitter design (Type II molecules), now both S_1 and T_1 states possess CT character. For molecules **2CzOCF$_3$** and **5CzOCF$_3$**, the singlet energies are predicted to be 3.92 eV and 3.45 eV; however, the singlet-triplet energy gaps, ΔE_{ST}s, are predicted to be large at 0.46 eV and 0.37 eV, respectively. The compounds **2CzCF$_3$**, **2CzSCF$_3$**, and **2CzSF$_5$**, from Type I molecules, show significant promise as deep blue TADF emitters, possessing high calculated singlet energies in the gas phase (3.62 eV, 3.66 eV, and 3.51 eV, respectively) and small, ΔE_{ST}s, of 0.17 eV, 0.22 eV, and 0.07 eV, respectively. For compounds **5CzSCF$_3$** and **5CzSF$_5$**, from Type II molecules, the singlet energies are stabilized to 3.24 eV and 3.00 eV, respectively, while ΔE_{ST}s are 0.27 eV and 0.12 eV, respectively, thus both show promise as blue or sky-blue TADF emitters. All these six molecules possess a dense number of intermediate excited states between S_1 and T_1, thus likely leading to a very efficient reverse intersystem crossing in these compounds.

Introduction

Organic thermally activated delayed fluorescence (TADF) materials have generated significant attention recently, particularly for their use as emitters in organic light-emitting diodes (OLEDs). This is due to their ability to utilize both singlet excitons and triplet excitons, thereby increasing the theoretical internal quantum efficiency (IQE) to 100% from 25% for fluorescent compounds [1-4]. For TADF materials, a small energy gap between the lowest singlet and triplet excited states (ΔE_{ST}) is essential to permit the efficient up-conversion of triplet excitons to singlet excitons via reverse intersystem crossing (rISC) [5-7]. The rISC process can happen by hyperfine coupling when the ΔE_{ST} is sufficiently small (<10 meV) or spin orbit coupling (SOC), which requires different symmetry between the two states coupled with a relatively small singlet–triplet energy gap, ΔE_{ST}, (<300 meV) [8,9]. The ΔE_{ST} is directly dependent on the magnitude of the electron exchange energy J (Equation 1), which itself is dependent on the electron density overlap between the highest occupied molecular orbital (HOMO) and lowest unoccupied molecular orbital (LUMO) (Equation 2) [10,11]. Compounds possessing a donor–acceptor (D–A) structure could satisfy the requirements for efficient TADF if the donor and acceptor moieties are poorly conjugated with each other in order to minimize J. The HOMO/LUMO separation that controls J can be modulated by introducing strong and bulky electron donors and electron acceptors to produce large torsions between the donor and acceptor groups so as to localized the HOMO on the electron-donating moiety and to confine the LUMO on the electron-withdrawing moiety [12,13].

$$\Delta E_{ST} = E^{S}_{orb} + K + J - (E^{T}_{orb} + K - J) = 2J + (E^{S}_{orb} - E^{T}_{orb}) \quad (1)$$

$$J = \int\int \Phi_{LUMO}(r_2)\Phi_{HOMO}(r_1)\left(\frac{e^2}{(r_1 - r_2)}\right) \Phi_{LUMO}(r_1)\Phi_{HOMO}(r_2)\mathrm{d}r_1\mathrm{d}r_2 \quad (2)$$

According to the Fermi's golden rule, the reversed intersystem crossing rate (k_{rISC}) can be expressed as [14,15]:

$$k_{rISC} = \frac{2\pi}{\hbar} 2 |V_{SOC}|^2 \times \rho_{FCWD} \quad (3)$$

Where $|V_{SOC}|^2$ is the spin-orbit coupling matrix element between S_1 and T_1 and ρ_{FCWD} is the Franck–Condon-weighted density of states, which can be expressed as [16]:

$$\rho_{FCWD} = \frac{1}{\sqrt{4\pi\lambda k_B T}} \exp\left(-\frac{(\Delta E_{ST} + \lambda)^2}{4\lambda k_B T}\right) \quad (4)$$

where λ is the Marcus reorganization energy associated with the intermolecular and intramolecular low-frequency vibrations; k_B is Boltzmann's constant; and T is temperature. Combing Equation 3 and Equation 4, it is evident that k_{rISC} is proportional to $|V_{SOC}|^2 \times \exp[-(\Delta E_{ST}^2)]$. Further, judicious molecular design in terms of the identity, position, and number of donor to acceptor moieties can also contribute to the modulation of ΔE_{ST}, leading to faster rISC. Typical donors include a small group of structurally related *N*-heterocycles such as carbazole [5], dimethylacridine [13], phenoxazine [17], and phenothiazine [18].

Prior studies have shown that placing the donor groups *ortho* to the acceptor can lead to more limited conjugation between the two, resulting in emitters with relatively smaller ΔE_{ST} compared to analogous compounds where the donor is positioned *para* to the acceptor [19,20]. Duan et al. have investigated the properties of D–A TADF benzonitrile-based emitters containing two carbazole donors disposed at different positions about the phenylene bridge [19]. The results showed that when the carbazoles were both located *ortho* to the cyano acceptor the molecule (**2,6-2CzBN**) possessed a highly twisted structure and a corresponding small ΔE_{ST} (0.27 eV in toluene). The ΔE_{ST}s increased to 0.41 (**2,4-2CzBN**) and 0.40 eV (**3,5-2CzBN**) in toluene when at least one of the carbazoles was disposed *meta* or *para* to the cyano acceptor [19]. OLEDs fabricated using **2,6-2CzBN** as the emitter exhibited deep blue emission with λ_{EL} = 418 nm and CIE coordinate of (0.15, 0.05); however, due to the low photoluminescence quantum yields (Φ_{PL}s) (28% in 10 wt % DPEPO films) and relatively slow k_{rISC} (0.86×10^5 s^{-1}) in the DPEPO host, the EQE_{max} was only 2.5%, and showed significant efficiency roll-off, reducing to 0.1% at 50 cd·m^{-2} [21]. A similar study by Monkman, Lee and co-workers investigated the compound **2,6-2CzTRZ**, which possessed the smallest ΔE_{ST} (0.02 eV) amongst the family of emitters possessing a diphenyltriazine as the acceptor and different regiochemistry of the carbazole donors; the ΔE_{ST}s increased to 0.10 eV for **2,4-2CzTRZ** and 0.29 eV for **3,4-2CzTRZ**. The single crystal structure of **2,6-2CzTRZ** revealed a highly twisted structure with large torsions (81.0° and 76.3°) between the carbazole moieties and the central benzene ring; the same torsions are appreciably smaller at 45.6° and 69.6° for the molecule **2,4-2CzTRZ** where one of the carbazole donors is situated at the *para* position and another one situated at the *ortho* position [20]. Compound **2,6-2CzTRZ** possessed a very small ΔE_{ST} (0.02 eV) and short delayed fluorescence lifetime (τ_d = 16.4 μs) in zeonex [20]. These two studies illustrate that *ortho*-substituted D–A molecules possess highly twisted geometries, leading to spatially separated HOMO/LUMO distributions and, thus, small ΔE_{ST}s, while maintaining high energy excited states.

The presence of intermediate triplet states lying above T_1 and below S_1 have been shown to facilitate rISC and render TADF more efficient by opening up a reverse internal conversion (RIC) pathway that is mediated by spin-vibronic coupling between T_1 and one or more of the intermediate states, followed by rISC [22]. This situation typically occurs when there are multiple donors about a single acceptor as exists in the molecules **5CzBN** and **5CzTRZ**. For **5CzBN**, time-dependent density functional theory (TD-DFT) calculation revealed the existence of three intermediate triplet states [22]. The presence of these states helped to explain the short τ_d of 3.7 μs and the high EQE_{max} of 17% and good device stability with a T_{50} of 176 hours for the OLED [CIE coordinate (0.22, 0.40)] [23]. In an analogous manner, TD-DFT calculations predicted **5CzTRZ** to possess a small ΔE_{ST} (0.02 eV) as well as a small energy gap (≈0.24 eV) between T_2 and T_1 [24]. In an analogous manner, **5CzTRZ** showed very fast k_{rISC} of ≈1.5×10^7 s^{-1} in toluene, and the device based on **5CzTRZ** exhibited superior EQE_{max} = 29% with λ_{EL} = 486 nm and very low efficiency roll-off with the EQE at 5,000 cd·m^{-2} remaining high at 27% [24].

Huang et al. also adopted a multiple donor strategy in concert with the weak trifluoromethyl (CF_3) acceptor group in their TADF emitter design. The blue-emitting TADF emitter **5CzCF$_3$** possessed a miniscule measured ΔE_{ST} of 0.02 eV and Φ_{PL} of 43% in oxygen-free toluene [25]. The solution-processed device based on **5CzCF$_3$** exhibited sky-blue emission with CIE coordinates of (0.21, 0.33) and an EQE_{max} of 5.2% at 1 cd·m^{-2} [25].

The promising performance of emitters possessing a CF_3 acceptor group prompted us to investigate other fluorinated weakly-conjugated acceptor units in order to assess their potential within TADF emitter design (Figure 1) [25-27]. In the present study, we report on the impact of incorporating other fluorine-containing electron-withdrawing groups beyond trifluoromethyl (CF_3), including trifluoromethoxy (OCF_3), trifluoromethylthio (SCF_3), and pentafluorosulfanyl (SF_5) groups, and explore their potential computationally within TADF emitter design. We cross-compare their optoelectronic properties with analog materials using well-studied conjugated elec-

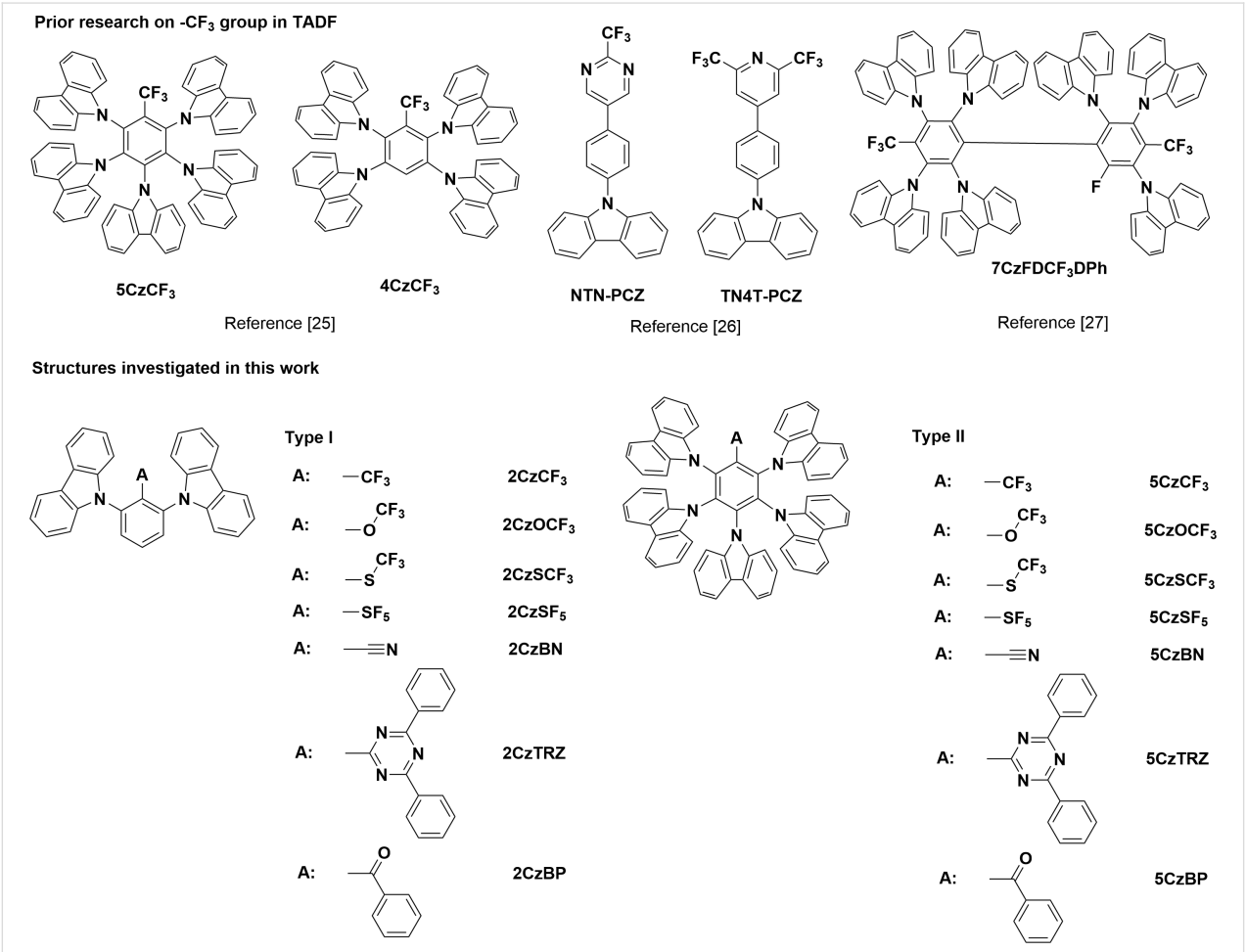

Figure 1: Molecular structures of emitters discussed in this work.

tron-withdrawing groups (cyano, benzophenone, and triazine). We investigated two families of structures. The first family consists of D–A–D (Type I) molecules containing two carbazole donors disposed each *ortho* to the acceptor group, while the second family consists of five carbazole donors substituted about a central benzene ring and the sixth position occupied by the acceptor moiety (Type II). Adachi et al. have shown that compounds that fall within the Type I family can simultaneously show high singlet and triplet energies and small ΔE_{ST} while compounds that are a part of Type II family possess a more dense number of low-lying excited states [22], the presence of which has been shown to assist in the rISC process through spin-vibronic coupling [23,24,27]. The energy levels and electronic configurations of S_1 and T_1 in these molecules were analysed and we found that compounds possessing either SCF_3 and SF_5 groups as acceptors (**2CzSCF$_3$**/**2CzSF$_5$** in Type I, **5CzSCF$_3$**/**5CzSF$_5$** in Type II), possessed LUMOs that are mainly located on the central benzene ring and the acceptor group while the HOMOs are mainly localized on the carbazoles, thereby leading to small ΔE_{ST}s. The calculated ΔE_{ST}s for **2CzSCF$_3$**/**2CzSF$_5$** are 0.22 eV and 0.07 eV, respectively, which are comparable to the calculated results for **2CzBN** (0.18 eV) and **2CzTRZ** (0.08 eV); likewise, the calculated ΔE_{ST}s for **5CzSCF$_3$**/**5CzSF$_5$** are 0.27 eV and 0.12 eV, respectively, which are close to the calculated results of **5CzBN** (0.20 eV) and **5CzTRZ** (0.17 eV). The molecules incorporating an OCF_3 acceptor (**2CzOCF$_3$** in Type I, **5CzOCF$_3$** in Type II), however, exhibited relatively larger ΔE_{ST}s (0.46 eV for **2CzOCF$_3$**, 0.37 eV for **5CzOCF$_3$**). The calculated S_1 energies of **2CzOCF$_3$** (3.92 eV), **2CzSCF$_3$** (3.62 eV), **2CzSF$_5$** (3.51 eV), and **5CzOCF$_3$** (3.45 eV) demonstrate that these molecules show potential as deep blue emitters as their S_1 states are higher in energy than that of **2CzBN** (3.34 eV calculated in gas phase in this work), which was reported as deep blue emitter with λ_{EL} = 418 nm and CIE coordinate of (0.15, 0.05) when doped in DPEPO [21]. DFT calculations for **5CzOCF$_3$**, **5CzSCF$_3$**, and **5CzSF$_5$** predicted dense populations of excited states between T_1 and S_1, which should assist in rISC process [28,29].

Results and Discussion

We employed density functional theory (DFT) and TD-DFT calculations to predict the photophysical properties of these emitters in order to assess their potential as TADF emitters for OLEDs. All ground-state calculations were performed using PBE0/6-31G(d,p) in the gas phase [30,31]. The lowest energy structures from these DFT calculations were used as input geometries for excited-state calculations using the Tamm–Dancoff approximation (TDA) to TD-DFT, which provide computed energies of the excited singlet and triplet states [32,33]. The nature of the lowest singlet and triplet states were ascertained by an analysis of the natural transition orbitals (NTO) obtained from the TDA-DFT calculations [34].

We first investigated the strength of the acceptor groups by modelling phenyl-substituted acceptors and compared their LUMO energies as well as the energies of the S_1 and T_1 states (Figure 2). Among the fluorinated electron-withdrawing groups in the study, **PhOCF$_3$** possesses the shallowest LUMO at −0.22 eV while **PhSF$_5$** possess the deepest LUMO at −0.90 eV, with **PhSCF$_3$** (−0.78 eV) and **PhCF$_3$** (−0.57 eV) possessing intermediate values. The LUMO energies of these four acceptors correlate linearly to the Hammett substituent constant, σ_p, (Figure 2c) [35]. All of these fluorinated acceptors are much weaker than the more commonly investigated benzonitrile (**BN**, −1.30 eV), triphenyltriazine (**TRZ**, −1.72 eV) and benzophenone (**BP**, −1.58 eV) acceptors. These results indicate that the use of the fluorinated acceptor groups in donor–acceptor TADF emitters should lead to a pronounced blue-shift in the emission, as reflected in the higher-energy singlet states of the model systems in Figure 2.

We next modelled the Type I emitters (Figure 3 and Figure 4). The DFT-calculated geometries indicate that the carbazoles adopt a significantly twisted conformation (dihedral angles > 50°) in order to minimize their interaction with the acceptor group. Specifically, for **2CzCF$_3$** the carbazoles are twisted to 60.2° and 70.5° with respect to the bridging phenyl ring while for **2CzSF$_5$**, due to the increased bulkiness of the SF_5 group, the corresponding twist angle increased to 78.5° and 78.7°. These highly twisted conformations contribute to the spatial separation of the HOMO and LUMO.

Figure 3 shows the energies of the HOMOs and LUMOs and the S_1 and T_1 states for the fluorinated acceptor-containing emitters **2CzCF$_3$**, **2CzOCF$_3$**, **2CzSCF$_3$**, and **2CzSF$_5$**. The HOMOs in these compounds are mainly located on the two carbazole moieties and a small part on the bridging central benzene ring. The LUMOs of **2CzCF$_3$**, **2CzSCF$_3$**, and **2CzSF$_5$** are mainly located on the benzene ring and a small distribution onto the electron-withdrawing group, whereas the LUMO of **2CzOCF$_3$** is localized essentially only on the central benzene. Emitters **2CzCF$_3$**, **2CzOCF$_3$**, and **2CzSCF$_3$** show similarly deep HOMO values at around −5.80 eV, while the HOMO level of **2CzSF$_5$** is more stabilized at −5.89 eV. The trend in LUMO energies matches that observed for the model acceptors (Figure 2) where **2CzOCF$_3$** possesses the shallowest LUMO of −0.95 eV while **2CzSF$_5$** possesses the deepest LUMO level of −1.46 eV. **2CzOCF$_3$** possesses the largest energy gap (ΔE_g) at 4.83 eV while the ΔE_g for **2CzSF$_5$** is the smallest at 4.43 eV amongst these four compounds. Figure 4 shows the correspond-

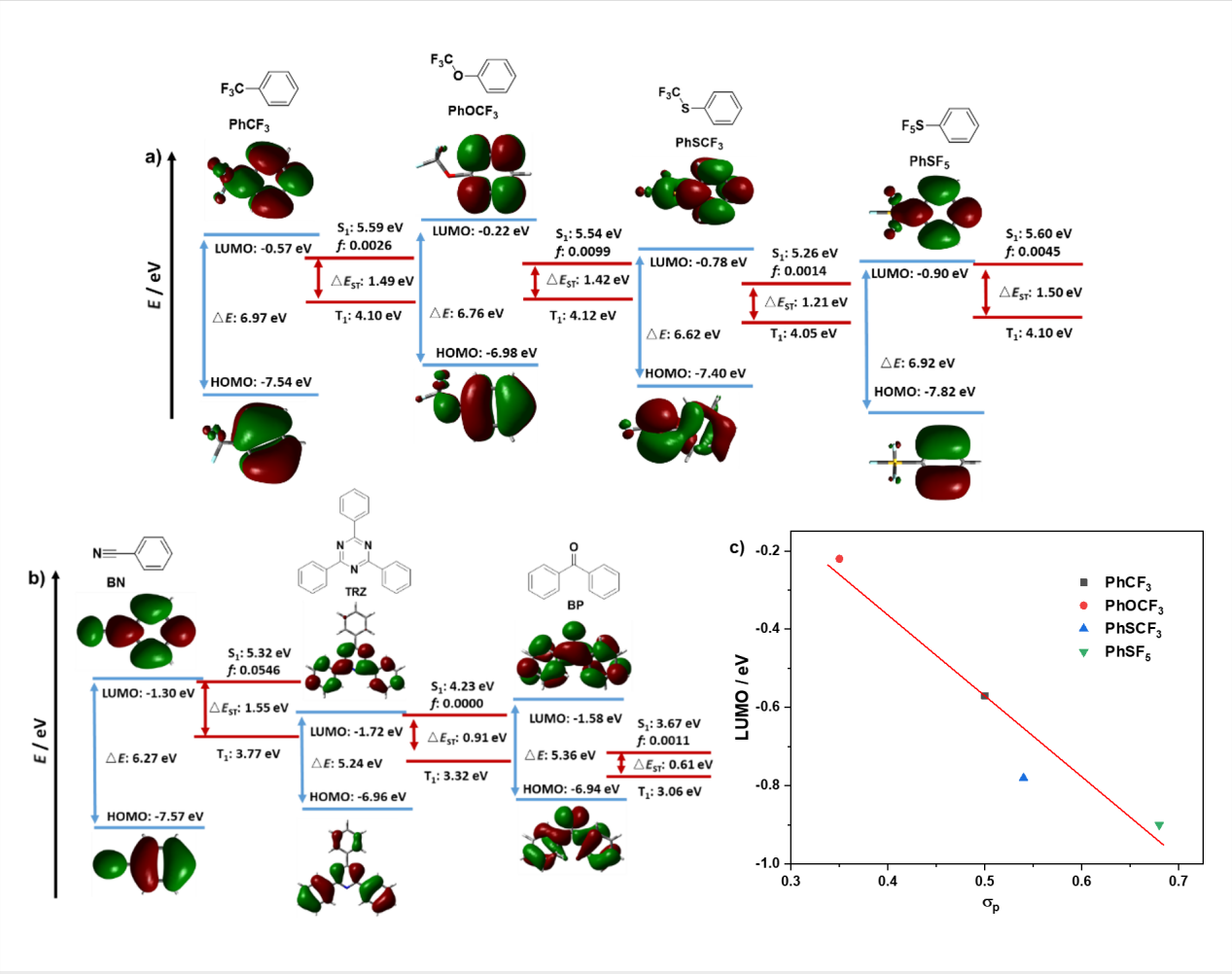

Figure 2: a) Calculated HOMO, LUMO, S_1 and T_1 energies, as well as HOMO and LUMO topologies of **$PhCF_3$**, **$PhOCF_3$**, **$PhOSCF_3$**, and **$PhSF_5$**, b) Calculated HOMO, LUMO, S_1 and T_1 energies, as well as HOMO and LUMO topologies of **BN**, **TRZ** and **BP** (isovalue = 0.02). c) Hammett *para* substituent values (σ_p) relationship with the calculated LUMO energies for fluorine-containing acceptors **$PhCF_3$**, **$PhOCF_3$**, **$PhOSCF_3$**, and **$PhSF_5$**.

ing data for the Type I reference compounds **2CzBN**, **2CzTRZ**, and **2CzBP**. In these three compounds the HOMOs are located mostly on the two carbazole moieties, with only a small contribution from the bridging benzene ring; this latter contribution is most pronounced for **2CzBN**, which leads to the greatest stabilization of the HOMO level at −5.89 eV. **2CzTRZ**, and **2CzBP** possess destabilized HOMO levels of −5.69 and −5.60 eV, respectively. The LUMOs of **2CzBN**, **2CzTRZ** and **2CzBP** are each located on the bridging benzene ring and the electron-acceptor groups. The LUMO levels for **2CzBN**, **2CzTRZ**, and **2CzBP** of −1.70 eV, −1.63 eV, and −1.67 eV, respectively, are much deeper those of the fluorine-containing emitters in Figure 3, which is a reflection of the greater conjugation length present in compounds with an extended π-accepting framework. The corresponding ΔE_g of **2CzBN** (4.19 eV), **2CzTRZ** (4.06 eV), and **2CzBP** (3.93 eV) are all significantly smaller compared to those of **$2CzCF_3$**, **$2CzOCF_3$**, **$2CzSCF_3$**, and **$2CzSF_5$**.

The emissive S_1 state for the seven Type I molecules is characterized mainly by a HOMO to LUMO transition, while the distribution of highest occupied natural transition orbitals (HONTOs) and the lowest unoccupied natural transition orbitals (LUNTOs) show good agreement with the HOMOs and LUMOs (Figure 5 and Figure 6). As the HOMOs and LUMOs of the seven molecules are sufficiently separated, the nature of the S_1 is charge-transfer (CT) in character. The S_1 energies of **$2CzCF_3$**, **$2CzOCF_3$**, **$2CzSCF_3$**, and **$2CzSF_5$** are much higher than those of **2CzBN**, **2CzTRZ**, and **2CzBP**. **$2CzOCF_3$** possesses the highest S_1 at 3.92 eV followed by **$2CzSCF_3$** (3.66 eV) and **$2CzCF_3$** (3.62 eV). The S_1 of **$2CzSF_5$** at 3.51 eV is relatively more stabilized due to the stronger electron-withdrawing ability of the SF_5 group. The S_1 states of **2CzBN**, **2CzTRZ**, and **2CzBP** are 3.34 eV, 3.22 eV, and 3.09 eV, respectively. The calculated S_1 values are slightly destabilized relative to the literature reported values for **2CzBN** (3.27 eV in toluene [19]) and **2CzTRZ** (3.12 eV in zeonex [20]).

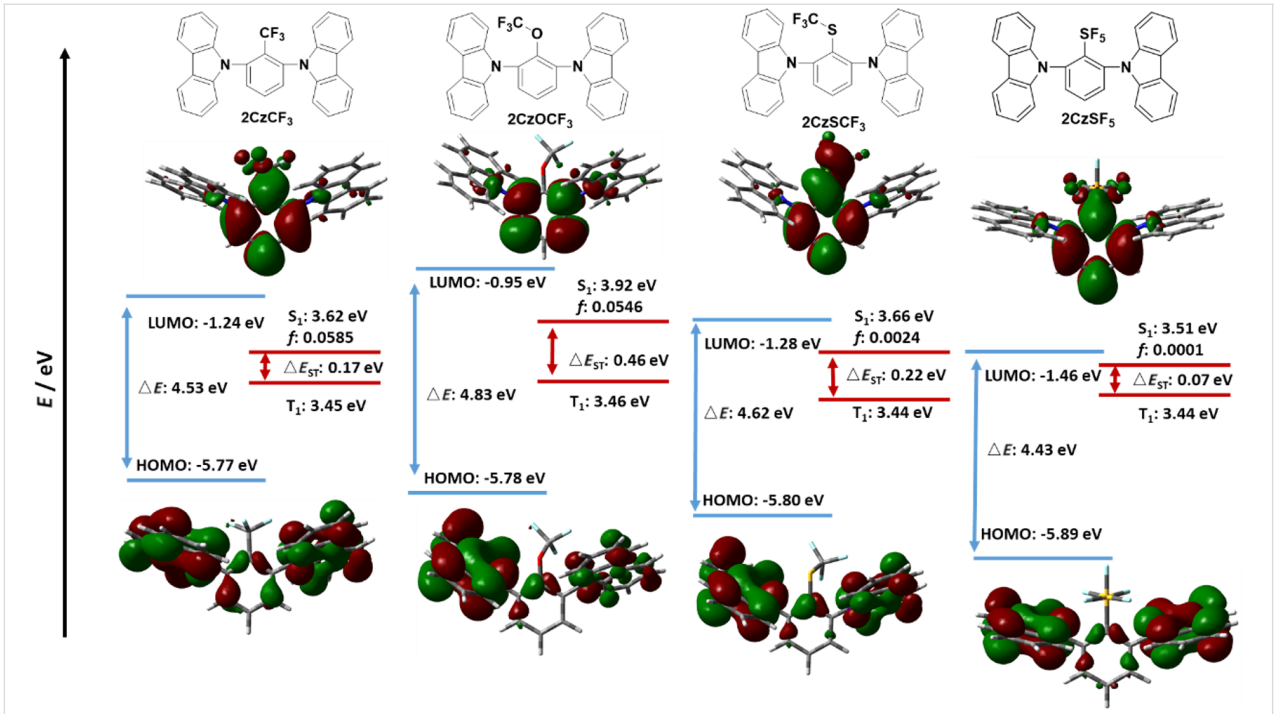

Figure 3: Calculated HOMO, LUMO, S_1 and T_1 energies, as well as HOMO and LUMO topologies of **2CzCF$_3$**, **2CzOCF$_3$**, **2CzSCF$_3$**, and **2CzSF$_5$** (isovalue = 0.02).

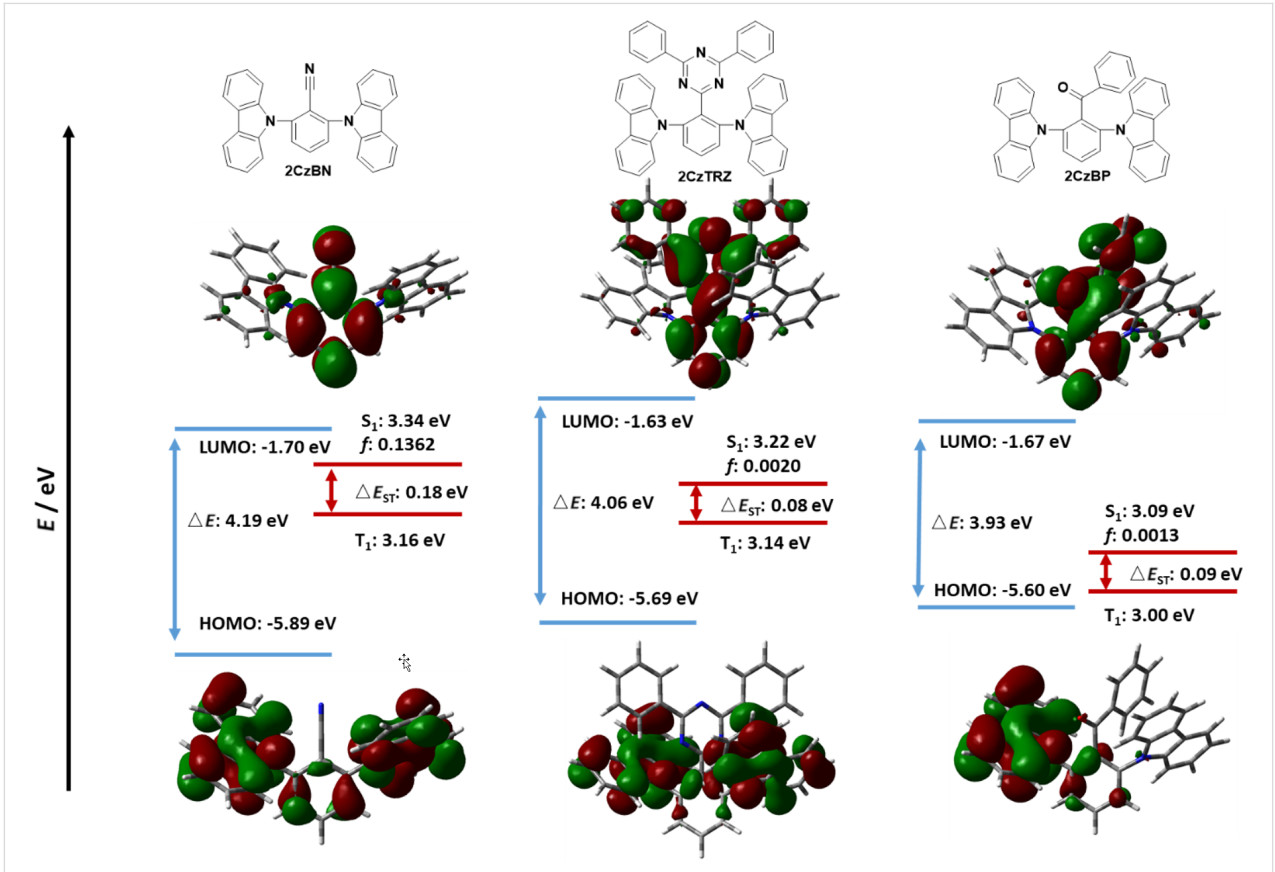

Figure 4: Calculated HOMO, LUMO, S_1 and T_1 energies, as well as HOMO and LUMO topologies of **2CzBN**, **2CzTRZ**, and **2CzBP** (isovalue = 0.02).

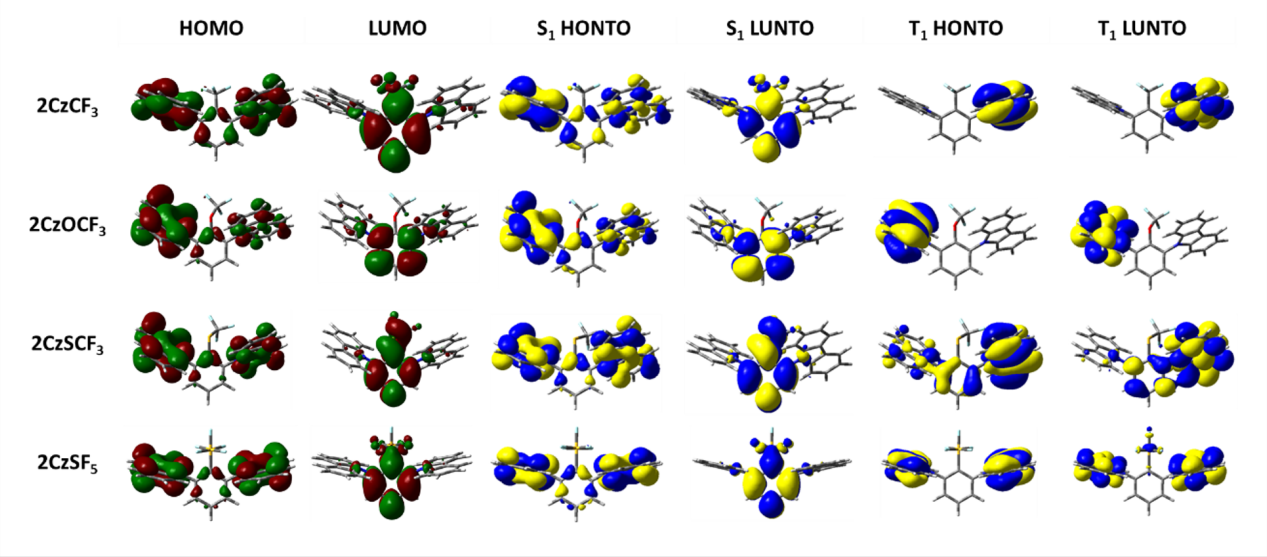

Figure 5: HOMO and LUMO distribution, HONTO and LUNTO of lowest singlet (S_1) and triplet excited (T_1) states for compounds **2CzCF$_3$**, **2CzOCF$_3$**, **2CzSCF$_3$**, and **2CzSF$_5$** (isovalue = 0.02).

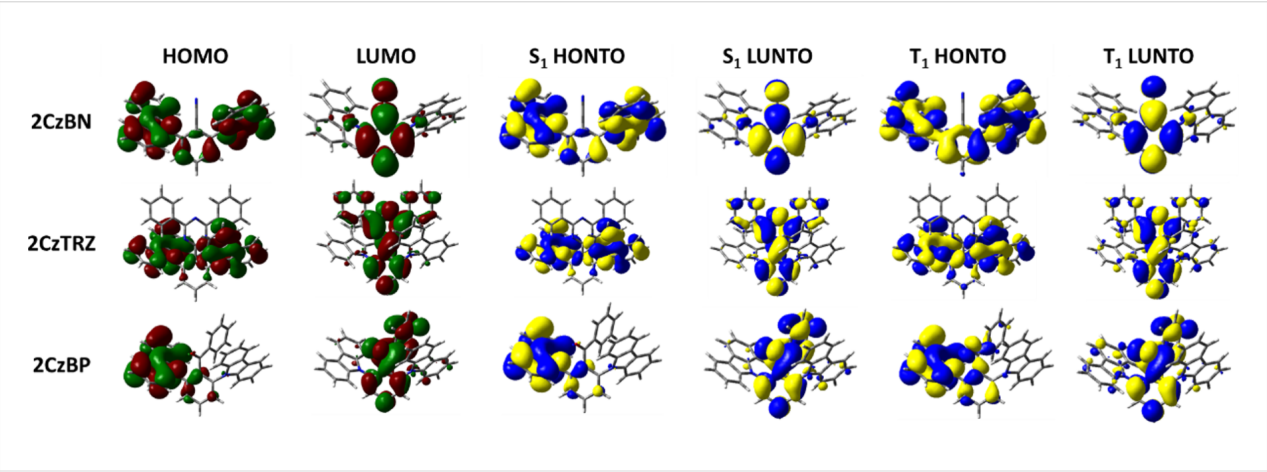

Figure 6: HOMO and LUMO distribution, HONTO and LUNTO of lowest singlet (S_1) and triplet excited (T_1) states for compounds **2CzBN**, **2CzTRZ**, and **2CzBP** (isovalue = 0.02).

The nature of the T_1 state of **2CzCF$_3$**, **2CzOCF$_3$**, and **2CzSF$_5$** is of locally excited (LE) character on the carbazole, while for **2CzSCF$_3$** the T_1 state is also LE, but also involving the bridging benzene ring. These assignments are reflected in very similar T_1 energies of around 3.45 eV. The corresponding ΔE_{ST} values are 0.17 eV for **2CzCF$_3$**, 0.46 eV for **2CzOCF$_3$**, 0.22 eV for 2**CzSCF$_3$** and 0.07 eV for **2CzSF$_5$**; thus, with the exception of **2CzOCF$_3$**, the small singlet-triplet energy gaps coupled with the large difference in symmetry between S_1 and T_1 augers well for efficient deep blue TADF emitters. By contrast, the triplet states of **2CzBN**, **2CzTRZ**, and **2CzBP** are best characterized by HOMO to LUMO CT-type transition. The calculated T_1 values for **2CzBN**, **2CzTRZ**, and **2CzBP** are 3.16 eV, 3.14 eV, and 3.00 eV, respectively. These values are slightly destabilized compared to the literature reported values for **2CzBN** (3.03 eV in toluene [19]) and **2CzTRZ** (3.05 eV in zeonex [20]). The corresponding ΔE_{ST} values are generally smaller than those of the Type I fluorinated compounds with values of 0.08 eV for **2CzTRZ**, 0.09 eV for **2CzBP** and 0.18 eV for **2CzBN**; however, the similar orbital symmetries between S_1 and T_1 would render rISC between these two states less efficient. The calculated ΔE_{ST} values are close to the literature reported values for **2CzBN** (0.27 eV in toluene [19]) and **2CzTRZ** (0.07 eV in zeonex [20]).

Inspired by these results, we next extended our theoretical study to Type II compounds where we increased the number of carbazole donor groups from two to five. We expect this design

to lead to improved spatial separation of the electron density distributions between the HOMO and LUMO, thereby strengthening the CT character of the S_1 state and leading to smaller ΔE_{ST} values, and thus more efficient TADF. The HOMO and LUMO distributions and energies for the Type II emitters are shown in Figure 7 and Figure 8. The HOMOs of **5CzCF$_3$**,

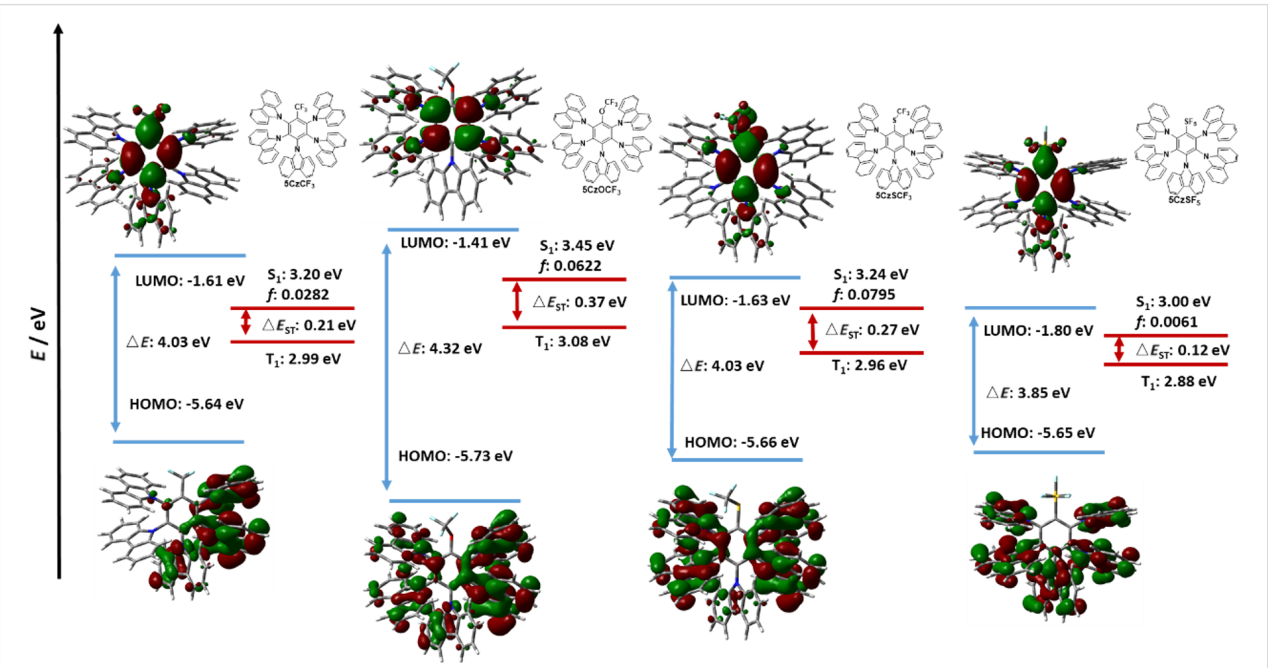

Figure 7: Calculated HOMO, LUMO, S_1 and T_1 energies, as well as HOMO and LUMO topologies of **5CzCF$_3$**, **5CzOCF$_3$**, **5CzSCF$_3$**, and **5CzSF$_5$** (isovalue = 0.02).

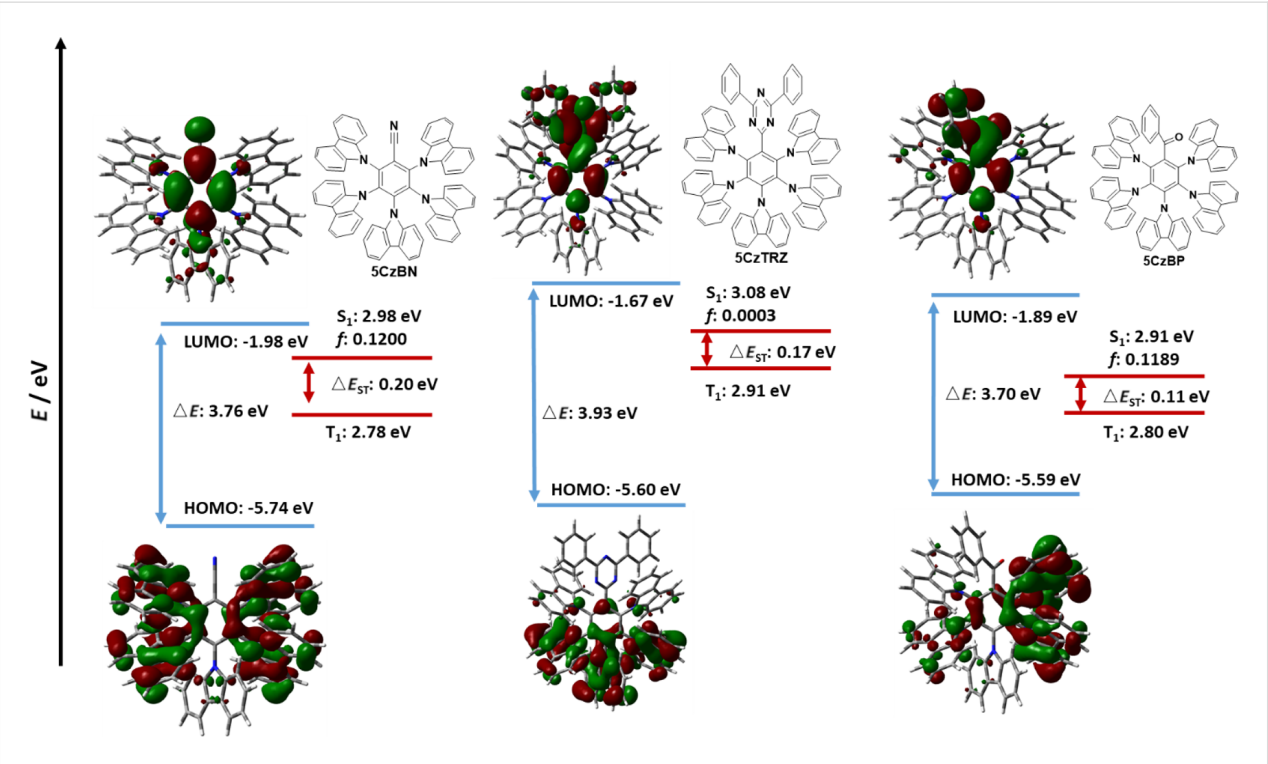

Figure 8: Calculated HOMO, LUMO, S_1 and T_1 energies, as well as HOMO and LUMO topologies of **5CzBN**, **5CzTRZ**, and **5CzBP** (isovalue = 0.02).

5CzOCF$_3$, and **5CzSCF$_3$** are mainly located on the carbazole moieties located *ortho* and *meta* to the acceptor group, with only a small distribution on the *para*-carbazole. For **5CzSF$_5$**, the HOMO is evenly distributed over the five carbazole moieties. The LUMOs of **5CzCF$_3$**, **5CzSCF$_3$**, and **5CzSF$_5$** are mainly located on the bridging benzene ring and the electron-withdrawing groups along with a small contribution from the *para*-disposed carbazole, whereas the LUMO of **5CzOCF$_3$** is located only on the central benzene ring, a similar behavior to **2CzOCF$_3$**. Compounds **5CzCF$_3$**, **5CzSCF$_3$**, and **5CzSF$_5$** showed similarly deep HOMO values of around −5.65 eV, while the HOMO value of **5CzOSF$_3$** is more stabilized at −5.73 eV. The **5CzOCF$_3$** possesses the most destabilized LUMO level at −1.41 eV, while **5CzSF$_5$** possesses the deepest LUMO level at −1.80 eV. The LUMO values for **5CzCF$_3$** and **5CzSCF$_3$** are −1.61 eV and −1.63 eV, respectively. **5CzOCF$_3$** has, therefore, the largest energy gap (ΔE_g) at 4.32 eV while **5CzSF$_5$** has the smallest at 3.85 eV; both **5CzCF$_3$** and **5CzOCF$_3$** possess ΔE_g of 4.03 eV. The trends for the HOMO and LUMO energies for these five Type II emitters mirror those observed for their Type I analogues; however, the HOMO and LUMO values in the Type II emitters are more stabilized and the energy gaps are reduced.

The HOMO of **5CzBN** is symmetrically distributed across the *ortho*- and *meta*-disposed carbazoles while the HOMO of **5CzTRZ** is located mostly on the *meta*- and *para*-carbazoles. For **5CzBP**, due to the asymmetric structure, the HOMO is located on one side of *ortho*- and *meta*-disposed carbazoles while the pseudo-degenerate HOMO−1 is located on the other *ortho*- and *meta*-disposed carbazoles. The LUMOs of **5CzBN**, **5CzBP**, and **5CzTRZ** are each located on the central benzene ring and extending onto the electron-withdrawing group. The HOMO of **5CzBN** is deepest at −5.74 eV, similar to that calculated for **5CzOCF$_3$**, while the HOMOs of **5CzBP** and **5CzTRZ** are −5.59 and −5.60 eV, respectively. The LUMO values of **5CzBN**, and **5CzBP** are −1.98 eV, and −1.89 eV, respectively, which are significantly more stabilized than the fluorinated Type II emitters while the LUMO of **5CzTRZ** at −1.67 eV is similar to those predicted for **5CzCF$_3$** (−1.61 eV) and **5CzSCF$_3$** (−1.63 eV). The ΔE_g values of **5CzBN** (3.76 eV), **5CzTRZ** (3.93 eV), and **5CzBP** (3.70 eV) are all slightly smaller than those of the fluorinated Type II emitters.

The HONTOs and LUNTOs for the Type II emitters are shown in Figure 9 and Figure 10. These generally reflect the HOMO and LUMO distributions, save for **5CzTRZ** where the HONTO of S_1 is located on the *ortho*-carbazoles. Due to the sufficiently large separation of the electron densities between the HOMO and LUMO of each of the seven Type II emitters, the S_1 state for each of these possesses CT character, analogously to those calculated for the Type I compounds. **5CzOCF$_3$** possesses the highest S_1 energy (3.45 eV) among Type II molecules, followed by **5CzSCF$_3$** (3.24 eV) and **5CzCF$_3$** (3.20 eV). The S_1 of **5CzSF$_5$** is 3.00 eV, which is close to the values of **5CzBN** (2.98 eV), **5CzTRZ** (3.08 eV) and **5CzBP** (2.91 eV). The

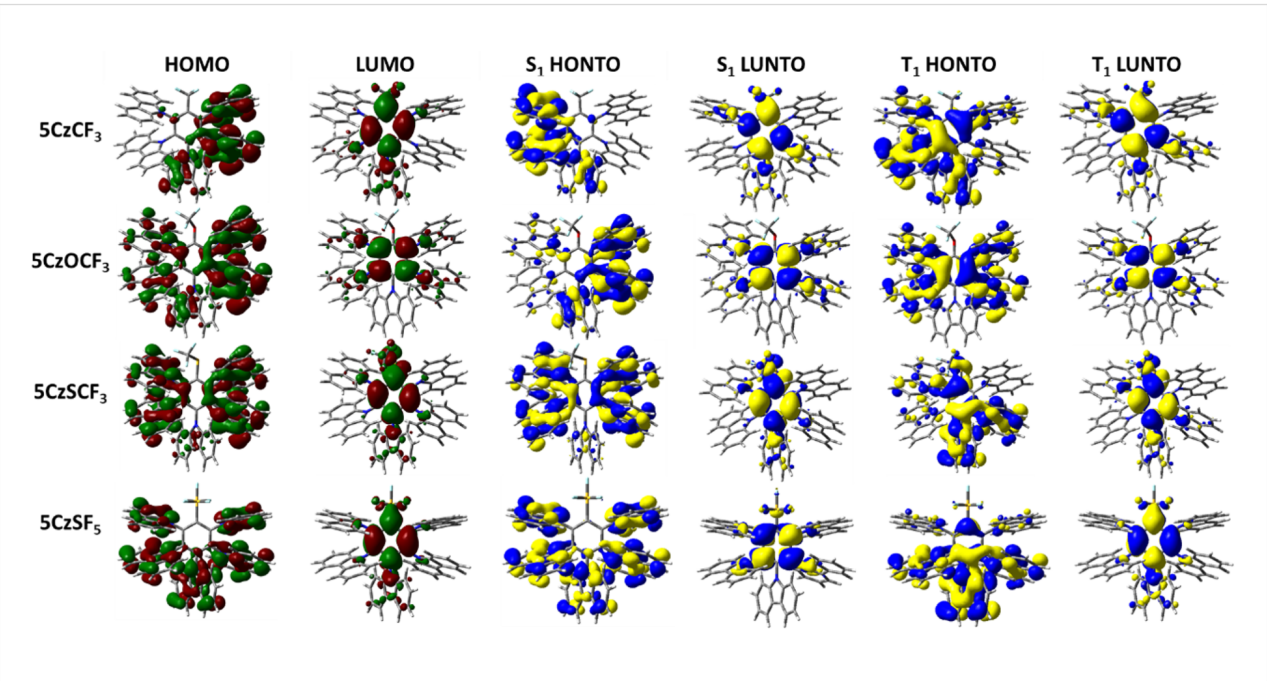

Figure 9: HOMO and LUMO distribution, HONTO and LUNTO of lowest singlet (S_1) and triplet excited (T_1) states for compounds **5CzCF$_3$**, **5CzOCF$_3$**, **5CzSCF$_3$**, and **5CzSF$_5$** (isovalue = 0.02).

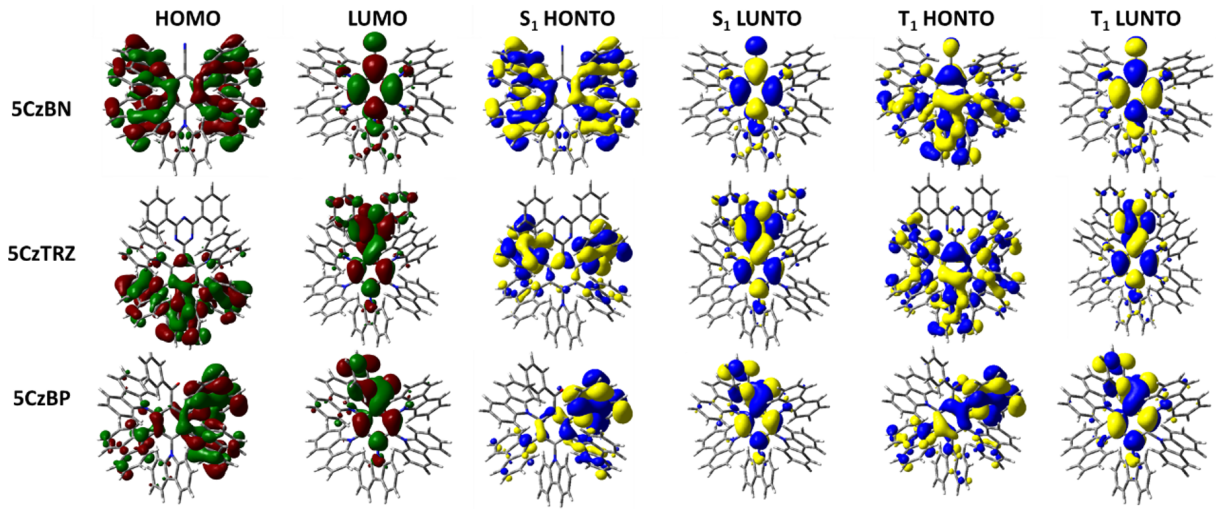

Figure 10: HOMO and LUMO distribution, HONTO and LUNTO of lowest singlet (S_1) and triplet excited (T_1) states for compounds **5CzBN**, **5CzTRZ**, and **5CzBP** (isovalue = 0.02).

calculated S_1 values are more destabilized than the literature reported values of **5CzBN** (2.90 eV in toluene [23]), **5CzTRZ** (2.85 eV in toluene [24]) and **5CzCF$_3$** (2.82 eV in toluene [25]). The nature of the T_1 state for each of these compounds is CT where the HONTOs of T_1 are mainly located on the carbazole moieties (and sometimes the central benzene) while the LUNTOs of T_1 are mainly located on the benzene ring and electron-withdrawing groups, except for **5CzOCF$_3$** where the LUNTO is located only on the benzene. **5CzOCF$_3$** possesses the highest T_1 energy (3.08 eV), while the T_1 energies of **5CzCF$_3$**, **5CzSCF$_3$**, and **5CzSF$_5$** are stabilized at 2.99 eV, 2.96 eV, and 2.88 eV, respectively. The T_1 energy of **5CzTRZ** is 2.91 eV while those of **5CzBN** and **5CzBP** are more stabilized at 2.78 eV and 2.80 eV, respectively. The calculated T_1 energies match the literature reported value of **5CzBN** (2.78 eV in toluene [23]) and are slightly destabilized relative to the literature reported value of **5CzTRZ** (2.79 eV in toluene [24]) and **5CzCF$_3$** (2.82 eV in toluene [25]). The corresponding ΔE_{ST} value of **5CzOCF$_3$** is 0.37 eV, which is reduced by 0.11 eV compared to **2CzOCF$_3$** (0.46 eV). This reduction results from the greater CT character in both S_1 and T_1. However, as the HOMO/LUMO overlap includes a small distribution on *para*-disposed carbazole in the Type II emitters with the exception of **5CzOCF$_3$**, the ΔE_{ST} values of Type II emitters are generally slightly larger compared to their Type I congeners. The ΔE_{ST}s of **5CzCF$_3$**, **5CzSCF$_3$** and **5CzSF$_5$** are 0.21 eV, 0.27 eV, and 0.12 eV, respectively, which are 0.04 eV, 0.05 eV, and 0.05 eV, respectively larger compared to **2CzCF$_3$** (0.17 eV), **2CzSCF$_3$** (0.22 eV), and 2**CzSF$_5$** (0.07 eV). The ΔE_{ST}s of **5CzBN** and **5CzBP** are 0.20 eV and 0.11 eV, which are only 0.02 eV larger compared to **2CzBN** (0.18 eV) and **2CzBP** (0.09 eV), while the ΔE_{ST} for **5CzTRZ** is 0.17 eV, which is 0.09 eV larger than that of **2CzTRZ** (0.08 eV). The calculated ΔE_{ST} values are slightly larger than the literature reported values for **5CzBN** (0.12 eV in toluene [23]) and **5CzTRZ** (0.06 eV in toluene [24]).

The spin-orbit coupling (SOC) values between excited singlet and triplets were calculated by considering the three T_1 substates (m = 0, ±1) are degenerate and the $|V_{SOC}|^2$ as the average of the three spin-orbit coupling matrix elements (SOCME) between singlet and the triplet states [36]. The results are summarized in Table 1. Among the Type I molecules, **2CzSCF$_3$** possesses the highest $|V_{SOC}|^2$ value as 0.148 cm^{-2}, followed by **2CzBP** (0.070 cm^{-2}) and **2CzSF$_5$** (0.053 cm^{-2}). The $|V_{SOC}|^2$ values for **2CzCF$_3$** and **2CzOCF$_3$** are 0.011 cm^{-2} and 0.019 cm^{-2}, respectively, which are still much higher than **2CzBN** (0.002 cm^{-2}) and **2CzTRZ** (3×10^{-4} cm^{-2}). The Type II molecules show an increase in $|V_{SOC}|^2$ values compared to their Type I counterparts. **5CzSCF$_3$** possesses the highest $|V_{SOC}|^2$ value at 0.750 cm^{-2} which is five times higher than **2CzSF$_5$**, and **5CzSF$_5$** possesses the second highest $|V_{SOC}|^2$ value as 0.718 cm^{-2}, which is more than thirteen times higher than **2CzSF$_5$**. The higher $|V_{SOC}|^2$ values of **2CzSCF$_3$**/**5CzSCF$_3$** and **2CzSF$_5$**/**5CzSF$_5$** can be ascribed to the presence of the relatively heavier chalcogen, which has also been attributed by Duan et al. to much higher SOCME values in a sulfur-containing emitter than in analogs without the sulfur atom present [37]. The $|V_{SOC}|^2$ values of **5CzBN** and **5CzBP** increased to 0.298 cm^{-2} and 0.267 cm^{-2}, respectively, which are more than one hundred times higher than **2CzBN** and four times higher than **2CzBP**. The $|V_{SOC}|^2$ values of **5CzCF$_3$** and **5CzOCF$_3$** are also higher at 0.090 cm^{-2} and 0.060 cm^{-2}, respectively. The

Table 1: S_1 and T_1 energies, ΔE_{ST}, and average $|V_{SOC}|^2$ values of Type I and Type II molecules.

Compound	S_1 [eV]	T_1 [eV]	ΔE_{ST} [eV]	$\lvert V_{SOC}\rvert^2$ [cm^{-2}]	$\lvert V_{SOC}\rvert^2 \times \exp[-(\Delta E_{ST}^2)]$
2CzCF$_3$	3.62	3.45	0.17	0.011	1.48×10^{-10}
2CzOCF$_3$	3.92	3.46	0.46	0.019	2.20×10^{-10}
2CzSCF$_3$	3.66	3.44	0.22	0.148	2.03×10^{-9}
2CzSF$_5$	3.51	3.44	0.07	0.053	7.54×10^{-10}
2CzBN	3.34	3.16	0.18	0.002	3.07×10^{-11}
2CzBP	3.22	3.14	0.08	0.070	1.00×10^{-9}
2CzTRZ	3.09	3.00	0.09	3×10^{-4}	4.29×10^{-12}
5CzCF$_3$	3.20	2.99	0.21	0.090	1.24×10^{-9}
5CzOCF$_3$	3.45	3.08	0.37	0.060	7.51×10^{-10}
5CzSCF$_3$	3.24	2.96	0.27	0.750	1.00×10^{-8}
5CzSF$_5$	3.00	2.88	0.12	0.718	1.02×10^{-8}
5CzBN	2.98	2.78	0.20	0.298	4.12×10^{-9}
5CzBP	3.08	2.91	0.17	0.267	3.74×10^{-9}
5CzTRZ	2.91	2.80	0.11	0.001	1.57×10^{-11}

$|V_{SOC}|^2$ value of **5CzTRZ** also increased to 0.001 cm^{-2} from 3×10^{-4} cm^{-2} for **2CzTRZ**; however, the predicted $|V_{SOC}|^2$ value between S_1 and T_2 (0.107 cm^{-2}) is much higher (Table **S**14, Supporting Information File 1). A measure of the magnitude of k_{rISC} can be ascertained from $|V_{SOC}|^2 \times \exp[-(\Delta E_{ST}^2)]$. The trends align here are consistent with the SOCME calculations. By comparison, the experimentally inferred k_{rISC} for **2CzBN**, **5CzBN** and **5CzTRZ** are 0.86×10^5 s^{-1} in DPEPO film [21], 2.2×10^5 s^{-1} in toluene [22], and 1.5×10^7 s^{-1} in toluene [24], respectively. The trend in experimental k_{rISC} for **2CzBN** and **5CzBN** match our SOCME calculations as **5CzBN** possesses the third highest $|V_{SOC}|^2 \times \exp[-(\Delta E_{ST}^2)]$ while **2CzBN** has the third lowest value. Clearly, for **5CzTRZ** there is a lack of correlation between the computed $|V_{SOC}|^2 \times \exp[-(\Delta E_{ST}^2)]$ and the experimentally determined k_{rISC} values. The significantly higher experimental k_{rISC} can be explained by the presence of intermediate triplet states leading to second order spin-vibronic coupling to mediate rISC in **5CzTRZ** [24]; indeed, the $|V_{SOC}|^2$ value was predicted to be much higher by the SOCME calculations between S_1 and T_2 at 0.107 cm^{-2}.

Prior studies on **5CzBN** and **5CzTRZ** showed that intermediate excited states between S_1 and T_1 can facilitate the rISC process by providing extra rISC transition channels from the higher intermediate excited triplet states to S_1 thereby improving the rISC rate [22,24]. The presence of multiple donors, each possessing slightly different conformations, and thereby presenting slightly different electronic coupling with the central acceptor guarantees a dense population of excited states [22,24]. We analysed the higher excited states of the fluorinated acceptor-containing emitters in both Type I and Type II structures. For **2CzCF$_3$**, the T_1 is locally excited; further, T_2 (3.46 eV) to T_6 (3.58 eV) all exhibited significant LE character. The lowest triplet state that exhibits charge transfer characteristics is T_7 at 3.72 eV (Figure 11). By contrast, the T_1 of **5CzCF$_3$** exhibited CT character and the higher triplet states from T_2 to T_6 also exhibited CT character, which is a similar picture to the literature reported calculated electronic structure of **5CzBN** using TD-DFT/ωB97XD [22] (Figure 12). This change from mostly low-lying LE triplet states in Type I emitters to mostly low-lying CT states in Type II emitters is prevalent in **2CzOCF$_3$**/**5CzOCF$_3$**, **2CzSCF$_3$**/**5CzSCF$_3$**, and **2CzSF$_5$**/**5CzSF$_5$** (Figures S1–S6, Supporting Information File 1). Both Type I and Type II molecules are predicted to possess multiple intermediate excited states between S_1 and T_1. For example, for **2CzCF$_3$** T_2 to T_6 lie between S_1 and T_1 and the energy gap between T_6 and S_1 (ΔE_{S1T6}) is 0.04 eV while for **5CzCF$_3$** the T_2 to T_4 are intermediate states with energies below S_1 and the energy gap between T_4 and S_1 (ΔE_{S1T4}) is 0.02 eV. This phenomenon is also observed in **2CzOCF$_3$** (ΔE_{S1T6} = 0.08 eV)/**5CzOCF$_3$** (ΔE_{S1T8} = 0.02 eV), and **2CzSCF$_3$** (ΔE_{S1T6} = 0.09 eV)/**5CzSCF$_3$** (ΔE_{S1T4} = 0.00 eV), **2CzSF$_5$** (ΔE_{S1T3} = 0.01 eV)/**5CzCF$_3$** (ΔE_{S1T4} = 0.00 eV). We thus contend that the intermediate excited states present in the fluorinated acceptor-containing emitters will assist in the rISC process, and improve the TADF characteristics, mitigating the somewhat larger ΔE_{ST} values in these compounds.

Conclusion

This computational study demonstrates the high potential of fluorinated acceptors in TADF emitter design. In particular, we

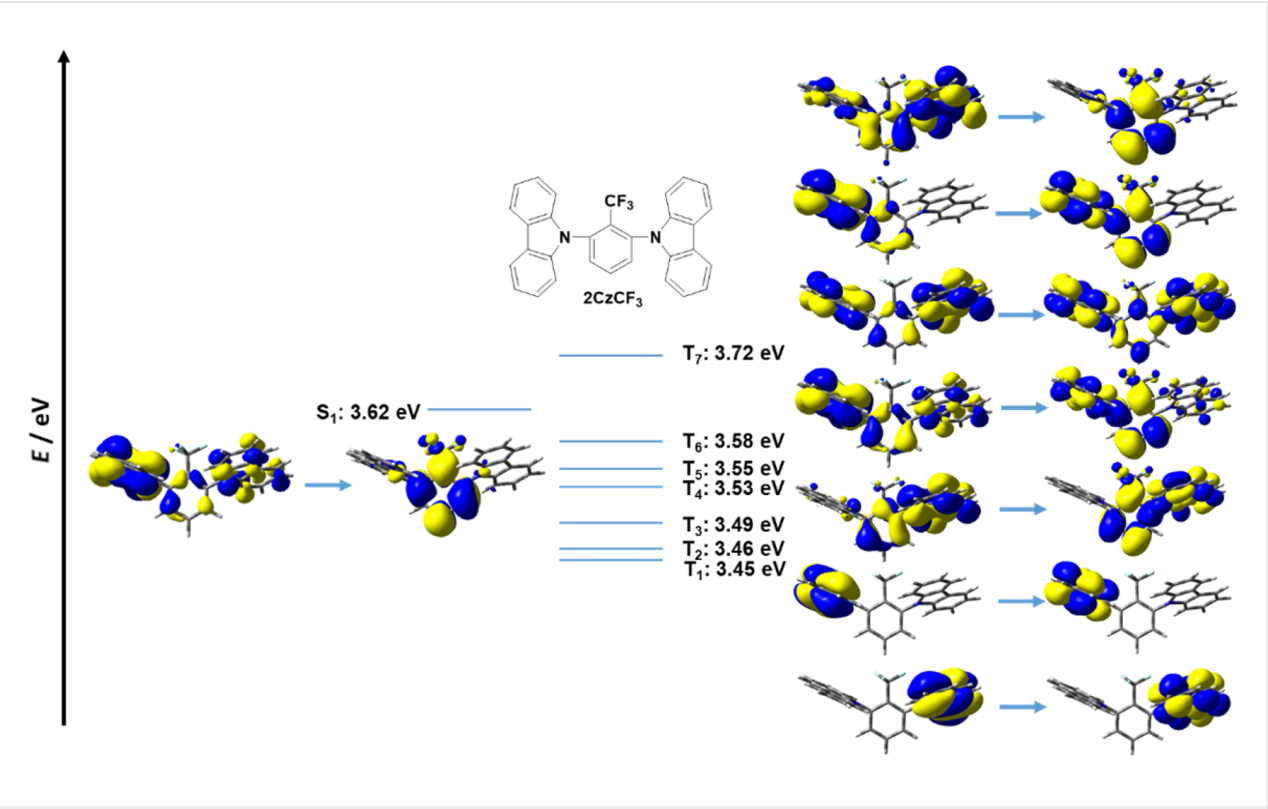

Figure 11: HONTOs and LUNTOs of **2CzCF$_3$** in higher excited states (isovalue = 0.02).

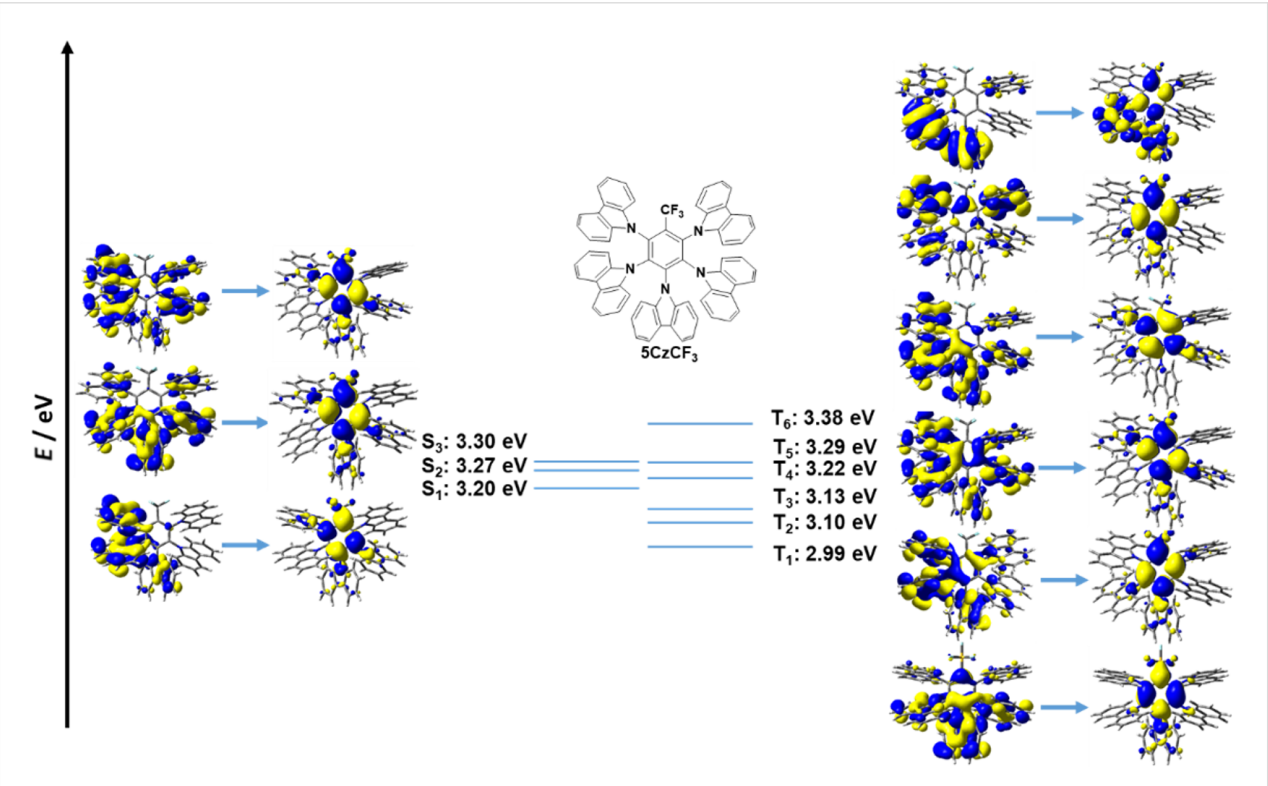

Figure 12: HONTOs and LUNTOs of **5CzCF$_3$** in higher excited states (isovalue = 0.02).

showed that OCF_3, SCF_3 and SF_5 groups should all be considered when designing deep blue TADF emitters. Type II emitters, with five carbazole donors, showed the most promise in terms of suitable small ΔE_{ST} values, high spin-orbit coupling values coupled with a relatively large density of intermediate excited triplet states that can be recruited to render TADF more efficient. Present efforts are ongoing to synthesize promising candidates from this theoretical study.

Supporting Information

The research data underpinning this publication can be accessed at https://doi.org/10.17630/b8f9f445-60a0-4c0a-808e-ce27cfcbf48a

Supporting Information File 1

Calculation details, Cartesian coordinates of all the molecules, SOCME calculation result, and HONTOs and LUNTOs of **2CzCF$_3$/5CzCF$_3$**, **2CzOCF$_3$/5CzOCF$_3$**, **2CzSCF$_3$/5CzSCF$_3$**, and **2CzSF$_5$/5CzSF$_5$** in higher-lying excited states are available in supporting information. [https://www.beilstein-journals.org/bjoc/content/supplementary/1860-5397-17-21-S1.pdf]

Acknowledgements

We thank Oliver Lee for help with the SOCME calculations.

Funding

Dongyang Chen thanks the China Scholarship Council (201603780001). We acknowledge support from the Engineering and Physical Sciences Research Council of the United Kingdom (grant EP/P010482/1).

ORCID® iDs

Eli Zysman-Colman - https://orcid.org/0000-0001-7183-6022

References

1. Wong, M. Y.; Zysman-Colman, E. *Adv. Mater.* **2017,** *29,* 1605444. doi:10.1002/adma.201605444
2. Liu, Y.; Li, C.; Ren, Z.; Yan, S.; Bryce, M. R. *Nat. Rev. Mater.* **2018,** *3,* 18020. doi:10.1038/natrevmats.2018.20
3. Cai, X.; Su, S.-J. *Adv. Funct. Mater.* **2018,** *28,* 1802558. doi:10.1002/adfm.201802558
4. Teng, J.-M.; Wang, Y.-F.; Chen, C.-F. *J. Mater. Chem. C* **2020,** *8,* 11340–11353. doi:10.1039/d0tc02682d
5. dos Santos, P. L.; Chen, D.; Rajamalli, P.; Matulaitis, T.; Cordes, D. B.; Slawin, A. M. Z.; Jacquemin, D.; Zysman-Colman, E.; Samuel, I. D. W. *ACS Appl. Mater. Interfaces* **2019,** *11,* 45171–45179. doi:10.1021/acsami.9b16952
6. Li, W.; Li, B.; Cai, X.; Gan, L.; Xu, Z.; Li, W.; Liu, K.; Chen, D.; Su, S.-J. *Angew. Chem., Int. Ed.* **2019,** *58,* 11301–11305. doi:10.1002/anie.201904272
7. Wang, Y.-K.; Huang, C.-C.; Ye, H.; Zhong, C.; Khan, A.; Yang, S.-Y.; Fung, M.-K.; Jiang, Z.-Q.; Adachi, C.; Liao, L.-S. *Adv. Opt. Mater.* **2020,** *8,* 1901150. doi:10.1002/adom.201901150
8. Gibson, J.; Monkman, A. P.; Penfold, T. J. *ChemPhysChem* **2016,** *17,* 2956–2961. doi:10.1002/cphc.201600662
9. Etherington, M. K.; Gibson, J.; Higginbotham, H. F.; Penfold, T. J.; Monkman, A. P. *Nat. Commun.* **2016,** *7,* 13680. doi:10.1038/ncomms13680
10. Agou, T.; Matsuo, K.; Kawano, R.; Park, I. S.; Hosoya, T.; Fukumoto, H.; Kubota, T.; Mizuhata, Y.; Tokitoh, N.; Yasuda, T. *ACS Mater. Lett.* **2020,** *2,* 28–34. doi:10.1021/acsmaterialslett.9b00433
11. Penfold, T. J.; Gindensperger, E.; Daniel, C.; Marian, C. M. *Chem. Rev.* **2018,** *118,* 6975–7025. doi:10.1021/acs.chemrev.7b00617
12. Sharma, N.; Spuling, E.; Mattern, C. M.; Li, W.; Fuhr, O.; Tsuchiya, Y.; Adachi, C.; Bräse, S.; Samuel, I. D. W.; Zysman-Colman, E. *Chem. Sci.* **2019,** *10,* 6689–6696. doi:10.1039/c9sc01821b
13. Meng, G.; Chen, X.; Wang, X.; Wang, N.; Peng, T.; Wang, S. *Adv. Opt. Mater.* **2019,** *7,* 1900130. doi:10.1002/adom.201900130
14. Robinson, G. W.; Frosch, R. P. *J. Chem. Phys.* **1963,** *38,* 1187–1203. doi:10.1063/1.1733823
15. Lawetz, V.; Orlandi, G.; Siebrand, W. *J. Chem. Phys.* **1972,** *56,* 4058–4072. doi:10.1063/1.1677816
16. Schmidt, K.; Brovelli, S.; Coropceanu, V.; Beljonne, D.; Cornil, J.; Bazzini, C.; Caronna, T.; Tubino, R.; Meinardi, F.; Shuai, Z.; Brédas, J.-L. *J. Phys. Chem. A* **2007,** *111,* 10490–10499. doi:10.1021/jp075248q
17. Chen, Z.; Wu, Z.; Ni, F.; Zhong, C.; Zeng, W.; Wei, D.; An, K.; Ma, D.; Yang, C. *J. Mater. Chem. C* **2018,** *6,* 6543–6548. doi:10.1039/c8tc01698d
18. Wang, K.; Shi, Y.-Z.; Zheng, C.-J.; Liu, W.; Liang, K.; Li, X.; Zhang, M.; Lin, H.; Tao, S.-L.; Lee, C.-S.; Ou, X.-M.; Zhang, X.-H. *ACS Appl. Mater. Interfaces* **2018,** *10,* 31515–31525. doi:10.1021/acsami.8b08083
19. Zhang, D.; Cai, M.; Bin, Z.; Zhang, Y.; Zhang, D.; Duan, L. *Chem. Sci.* **2016,** *7,* 3355–3363. doi:10.1039/c5sc04755b
20. Oh, C. S.; de Sa Pereira, D.; Han, S. H.; Park, H.-J.; Higginbotham, H. F.; Monkman, A. P.; Lee, J. Y. *ACS Appl. Mater. Interfaces* **2018,** *10,* 35420–35429. doi:10.1021/acsami.8b10595
21. Chan, C.-Y.; Cui, L.-S.; Kim, J. U.; Nakanotani, H.; Adachi, C. *Adv. Funct. Mater.* **2018,** *28,* 1706023. doi:10.1002/adfm.201706023
22. Noda, H.; Chen, X.-K.; Nakanotani, H.; Hosokai, T.; Miyajima, M.; Notsuka, N.; Kashima, Y.; Brédas, J.-L.; Adachi, C. *Nat. Mater.* **2019,** *18,* 1084–1090. doi:10.1038/s41563-019-0465-6
23. Zhang, D.; Cai, M.; Zhang, Y.; Zhang, D.; Duan, L. *Mater. Horiz.* **2016,** *3,* 145–151. doi:10.1039/c5mh00258c
24. Cui, L.-S.; Gillett, A. J.; Zhang, S.-F.; Ye, H.; Liu, Y.; Chen, X.-K.; Lin, Z.-S.; Evans, E. W.; Myers, W. K.; Ronson, T. K.; Nakanotani, H.; Reineke, S.; Bredas, J.-L.; Adachi, C.; Friend, R. H. *Nat. Photonics* **2020,** *14,* 636–642. doi:10.1038/s41566-020-0668-z
25. Mei, L.; Hu, J.; Cao, X.; Wang, F.; Zheng, C.; Tao, Y.; Zhang, X.; Huang, W. *Chem. Commun.* **2015,** *51,* 13024–13027. doi:10.1039/c5cc04126k
26. Liang, X.; Han, H.-B.; Yan, Z.-P.; Liu, L.; Zheng, Y.-X.; Meng, H.; Huang, W. *New J. Chem.* **2018,** *42,* 4317–4323. doi:10.1039/c7nj04482h

27. Yuan, W.; Yang, H.; Duan, C.; Cao, X.; Zhang, J.; Xu, H.; Sun, N.; Tao, Y.; Huang, W. *Chem* **2020,** *6,* 1998–2008. doi:10.1016/j.chempr.2020.04.021
28. Ward, J. S.; Kukhta, N. A.; dos Santos, P. L.; Congrave, D. G.; Batsanov, A. S.; Monkman, A. P.; Bryce, M. R. *Chem. Mater.* **2019,** *31,* 6684–6695. doi:10.1021/acs.chemmater.9b01184
29. dos Santos, P. L.; Ward, J. S.; Congrave, D. G.; Batsanov, A. S.; Eng, J.; Stacey, J. E.; Penfold, T. J.; Monkman, A. P.; Bryce, M. R. *Adv. Sci.* **2018,** *5,* 1700989. doi:10.1002/advs.201700989
30. Adamo, C.; Barone, V. *J. Chem. Phys.* **1999,** *110,* 6158–6170. doi:10.1063/1.478522
31. Pople, J. A.; Binkley, J. S.; Seeger, R. *Int. J. Quantum Chem.* **1976,** *10* (Suppl. 10), 1–19. doi:10.1002/qua.560100802
32. Grimme, S. *Chem. Phys. Lett.* **1996,** *259,* 128–137. doi:10.1016/0009-2614(96)00722-1
33. Hirata, S.; Head-Gordon, M. *Chem. Phys. Lett.* **1999,** *314,* 291–299. doi:10.1016/s0009-2614(99)01149-5
34. Jesser, A.; Rohrmüller, M.; Schmidt, W. G.; Herres-Pawlis, S. *J. Comput. Chem.* **2014,** *35,* 1–17. doi:10.1002/jcc.23449
35. Hansch, C.; Leo, A.; Taft, R. W. *Chem. Rev.* **1991,** *91,* 165–195. doi:10.1021/cr00002a004
36. Gao, X.; Bai, S.; Fazzi, D.; Niehaus, T.; Barbatti, M.; Thiel, W. *J. Chem. Theory Comput.* **2017,** *13,* 515–524. doi:10.1021/acs.jctc.6b00915
37. Cai, M.; Auffray, M.; Zhang, D.; Zhang, Y.; Nagata, R.; Lin, Z.; Tang, X.; Chan, C.-Y.; Lee, Y.-T.; Huang, T.; Song, X.; Tsuchiya, Y.; Adachi, C.; Duan, L. *Chem. Eng. J.* **2021,** 127591. doi:10.1016/j.cej.2020.127591

License and Terms

This is an Open Access article under the terms of the Creative Commons Attribution License (https://creativecommons.org/licenses/by/4.0). Please note that the reuse, redistribution and reproduction in particular requires that the author(s) and source are credited and that individual graphics may be subject to special legal provisions.

The license is subject to the *Beilstein Journal of Organic Chemistry* terms and conditions: (https://www.beilstein-journals.org/bjoc/terms)

The definitive version of this article is the electronic one which can be found at: https://doi.org/10.3762/bjoc.17.21

BEILSTEIN JOURNAL OF ORGANIC CHEMISTRY

Decarboxylative trifluoromethylthiolation of pyridylacetates

Ryouta Kawanishi, Kosuke Nakada and Kazutaka Shibatomi*

Full Research Paper

Open Access

Address:
Department of Applied Chemistry and Life Science, Toyohashi University of Technology, 1-1 Hibarigaoka, Tempaku-cho, Toyohashi 441-8580, Japan

Email:
Kazutaka Shibatomi* - shiba@chem.tut.ac.jp

* Corresponding author

Keywords:
decarboxylation; fluorinated compounds; pyridine compounds; trifluoromethylthiolation

Beilstein J. Org. Chem. **2021,** *17,* 229–233.
https://doi.org/10.3762/bjoc.17.23

Received: 31 October 2020
Accepted: 04 January 2021
Published: 25 January 2021

This article is part of the thematic issue "Organo-fluorine chemistry V".

Guest Editor: D. O'Hagan

© 2021 Kawanishi et al.; licensee Beilstein-Institut.
License and terms: see end of document.

Abstract

Decarboxylative trifluoromethylthiolation of lithium pyridylacetates was achieved using *N*-(trifluoromethylthio)benzenesulfonimide as the electrophilic trifluoromethylthiolation reagent. The reaction afforded the corresponding trifluoromethyl thioethers in good yield. Furthermore, the preparation of lithium pyridylacetates by saponification of the corresponding methyl esters and subsequent decarboxylative trifluoromethylthiolation were performed in a one-pot fashion.

Introduction

The pyridine ring is found in numerous biologically active compounds. Therefore, efficient methods for synthesizing substituted pyridines are in high demand in pharmaceutical and agricultural chemistry [1,2]. Because of the unique features of fluorine atoms, fluorinated functional groups have also been recognized as important substructures in the design of medicinally relevant compounds [3-6]. Introducing a trifluoromethylthio group (CF_3S–), which has high lipophilicity and strong electron-withdrawing properties, into medicinal compounds can improve their pharmacokinetic properties [7-11]. Hence, the development of a synthetic method for the preparation of trifluoromethyl thioethers has recently attracted much attention [12-15].

Previously, our research group achieved decarboxylative functionalization of tertiary β-ketocarboxylic acids by exploiting their special ability to readily undergo decarboxylation [16-21]. During the course of this study, we found that lithium pyridylacetates undergo decarboxylative fluorination upon treatment with an electrophilic fluorination reagent to afford fluoromethylpyridines under catalyst-free conditions. Furthermore, we demonstrated the one-pot synthesis of fluoromethylpyridines from methyl pyridylacetates by saponification of methyl esters and subsequent decarboxylative fluorination (Scheme 1a) [21]. Herein, we describe the application of this method to decarboxylative trifluoromethylthiolation with an electrophilic trifluoromethylthiolation reagent (Scheme 1b) [22], which enables easy installation of the trifluoromethylthio group at a pyridylic carbon.

Results and Discussion

First, we synthesized lithium 2-pyridylacetate **1a** according to our previously reported procedure [21] and subjected it to decarboxylative trifluoromethylthiolation with *N*-trifluoro-

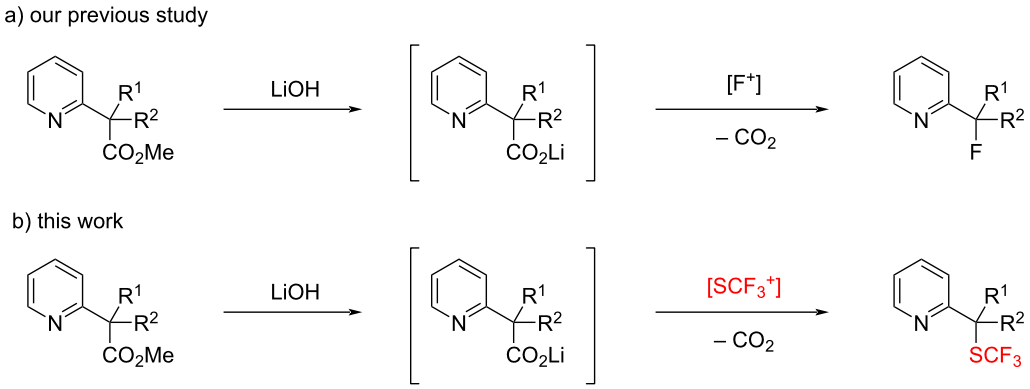

Scheme 1: Electrophilic decarboxylative functionalization of 2-pyridylacetates.

methylthiosuccinimide (**4**) in DMF at room temperature for 15 h. However, the desired product **2a** was not observed (Table 1, entry 1). The use of *N*-trifluoromethylthiophthalimide (**5**) did not afford **2a** either (Table 1, entry 2). Fortunately, the use of *N*-(trifluoromethylthio)dibenzenesulfonimide **6** [23] gave **2a** in 14% yield, along with the protonated product **3a** in 31% yield (Table 1, entry 3). The yield of **2a** could be improved to 30% by adding MS 4 Å to the reaction mixture (Table 1, entry 4). Screening of various solvents revealed that THF was the best choice for this reaction (Table 1, entries 4–11), and the yield of

Table 1: Screening of reaction conditions.

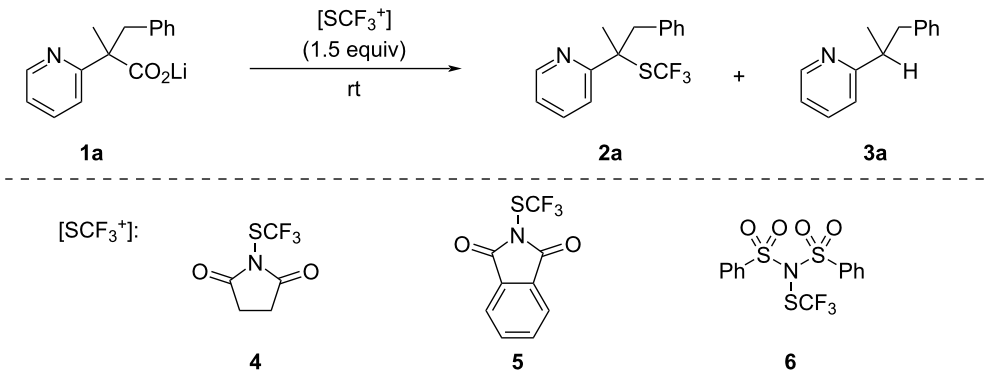

entry	[SCF_3^+]	solvent	time (h)	yield of **2a** (%)	yield of **3a** (%)
1	**4**	DMF	15	0	0
2	**5**	DMF	72	0	0
3	**6**	DMF	3	14	31
4[a]	**6**	DMF	5	30	34
5[a]	**6**	DMSO	5	64	21
6[a]	**6**	acetonitrile	8	77	0
7[a]	**6**	toluene	168	72	0
8[a]	**6**	CH_2Cl_2	72	54	0
9[a]	**6**	*t*-BuOMe	72	55	0
10[a]	**6**	1,4-dioxane	9	75	0
11[a]	**6**	THF	8	89	0
12	**6**	THF	8	63	26
13[a,b]	**6**	THF	8	70	0

[a]The reaction was carried out with MS 4 Å (180 mg/0.2 mmol); [b]1.1 equiv of **6** was used.

2a was dramatically improved to 89% (Table 1, entry 11). In the absence of MS 4 Å, the yield of **2a** was diminished even when the reaction was carried out in THF (Table 1, entry 12).

With the optimized reaction conditions in hand, we examined the one-pot synthesis of **2a** from methyl ester **7a**. Methyl 2-pyridylacetate **7a** were saponified with lithium hydroxide in a $MeOH/H_2O$ system. After completion of the reaction, the solvents were evaporated under reduced pressure. Then, THF, MS 4 Å, and **6** were added to the residue, and the mixture was stirred at room temperature for 8 h. This reaction successfully afforded the desired product **2a** in 85% yield over two steps (Scheme 2).

Encouraged by the aforementioned result, we applied this method to several 2-pyridylacetates (Scheme 3). Methyl 2-pyridylacetates **7b–d** with arylmethyl substituents furnished the corresponding trifluoromethylthiolated products **2b−d** in good yields. α,α-Dialkyl-2-pyridylacetates **7e–g** also gave the desired products **2e–g** in moderate yields. The method could also be applied to substrates with quinoline and isoquinoline backbones to afford the corresponding products **2h** and **2i**. In addition, the reaction of α-monosubstituted 2-pyridylacetate **8** was performed to yield the corresponding mono-trifluoromethylthiolated product **9** in 36% yield, along with 6% yield of disubstituted product **10** (Scheme 4). Increasing the amount of **6** did not improve the yield of products **9** and **10** significantly.

Based on the abovementioned results and our previous study on decarboxylative fluorination [21], we propose a plausible mechanism for this reaction, as outlined in Scheme 5. An electrophilic sulfur atom of **6** approaches the nitrogen atom on the pyridine ring to promote decarboxylation via the formation of *N*-trifluoromethylthio-2-alkylidene-1,2-dihydropyridine intermedi-

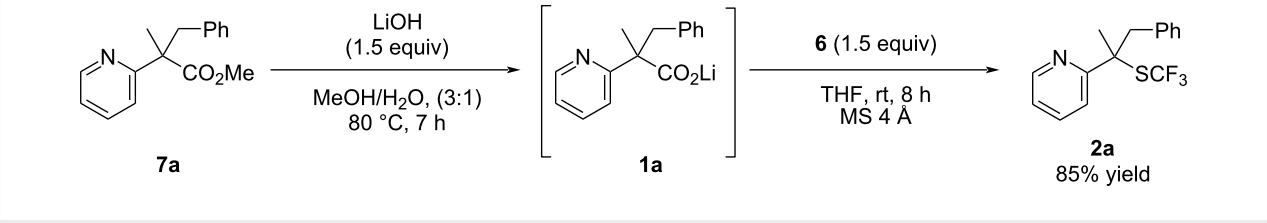

Scheme 2: One-pot procedure for the synthesis of **2a**.

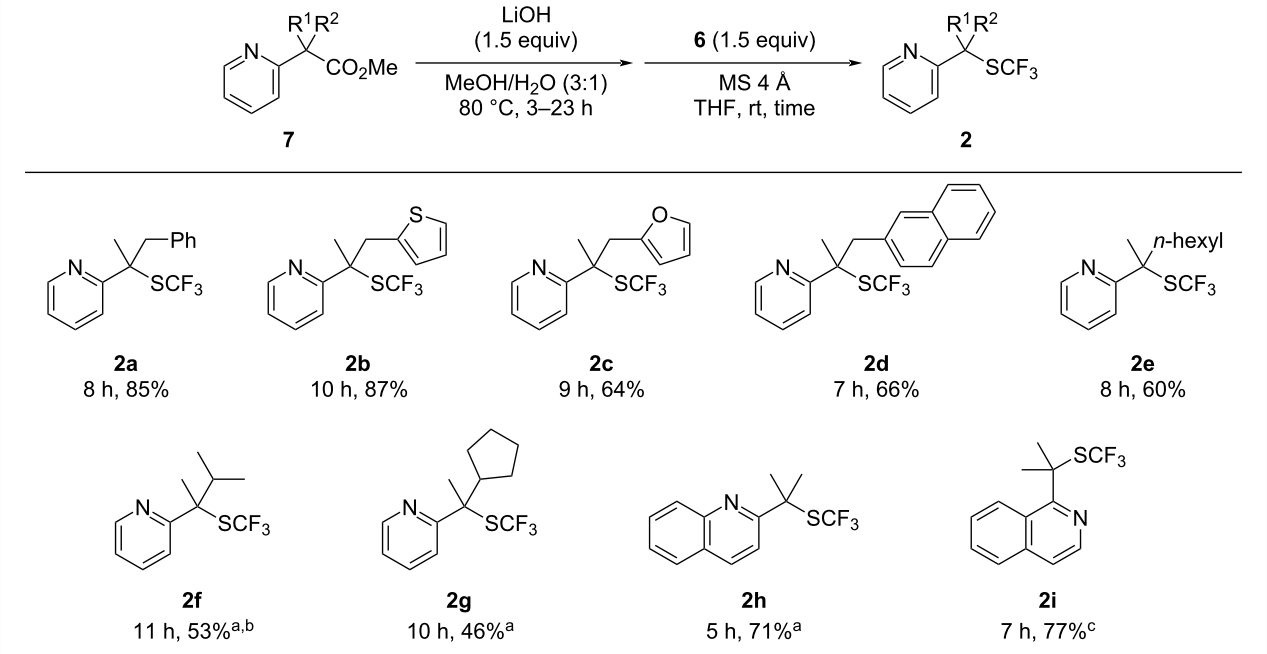

Scheme 3: Substrate scope. [a]Saponification was carried out with 2.5 equiv of LiOH, and 2.5 equiv of **6** was used for trifluoromethylthiolation. [b]Saponification of **7** was carried out for 39 h. [c]Saponification was carried out with 2.5 equiv of LiOH under reflux conditions, and 2.5 equiv of **6** was used for trifluoromethylthiolation.

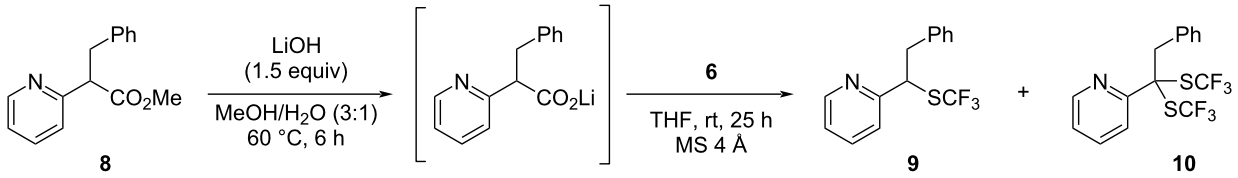

6	yield of 9	yield of 10
1.1 equiv	36%	6%
5.0 equiv	34%	11%

Scheme 4: Reaction of α-monosubstituted 2-pyridylacetates.

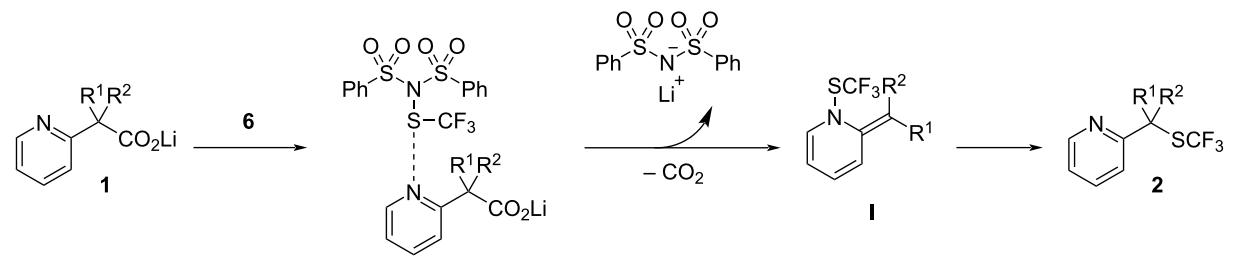

Scheme 5: Proposed reaction pathway.

ate **I**, which immediately isomerizes to afford **2** (Scheme 5). Methyl 4-pyridylacetate **11** also gave the corresponding trifluoromethylthiolated product **12** in 29% yield (Scheme 6), where the reaction was assumed to proceed via the *N*-trifluoromethylthio-4-alkylidene-1,4-dihydropyridine intermediate. In contrast, methyl 3-pyridylacetate **13** did not yield the trifluoromethylthiolated product at all, despite complete saponification of the methyl ester.

Conclusion

In conclusion, we demonstrated the decarboxylative trifluoromethylthiolation of lithium 2- and 4-pyridylacetates to synthesize pyridine derivatives with a trifluoromethylthio group at a tertiary carbon center adjacent to the pyridine ring. Furthermore, saponification of methyl pyridylacetates and subsequent decarboxylative trifluoromethylthiolation of the resulting lithium salts were performed in a one-pot fashion. This method can

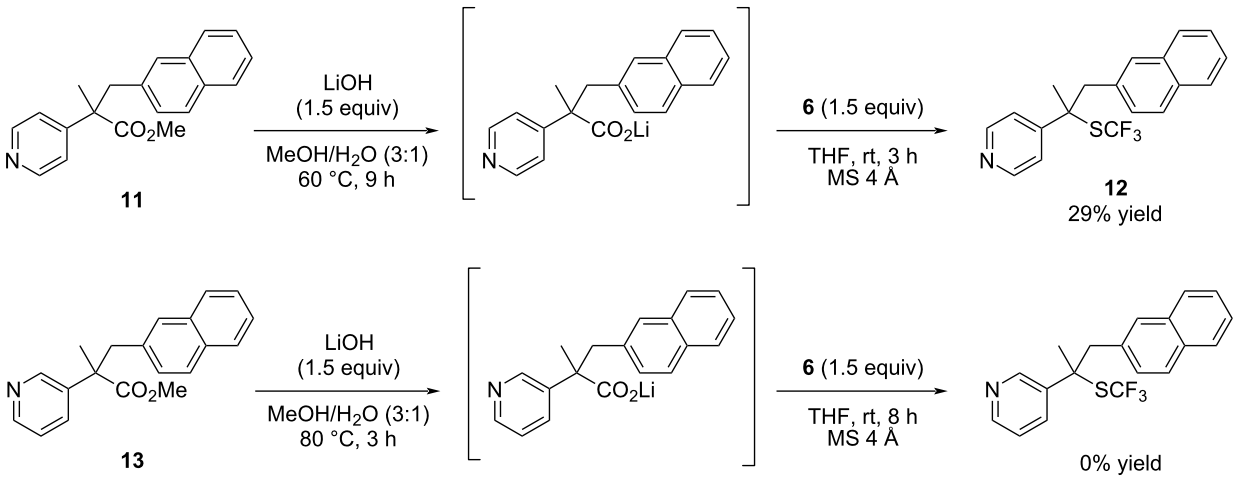

Scheme 6: Reaction of 3- and 4-pyridylacetates.

easily convert an ester group into a trifluoromethylthio group. The resulting trifluoromethyl thioethers would be useful for the preparation of various medicinally relevant compounds.

Supporting Information

Supporting Information File 1

Experimental procedures, characterization data, and copies of NMR spectra.
[https://www.beilstein-journals.org/bjoc/content/supplementary/1860-5397-17-23-S1.pdf]

Funding

This study was supported by the Grants-in-Aid for Scientific Research (B) (18H01974) from JSPS and the Toyota RIKEN Scholar Program from the Toyota Physical and Chemical Research Institute.

ORCID® iDs

Kazutaka Shibatomi - https://orcid.org/0000-0001-6368-4823

References

1. Taylor, R. D.; MacCoss, M.; Lawson, A. D. G. *J. Med. Chem.* **2014,** *57,* 5845–5859. doi:10.1021/jm4017625
2. Vitaku, E.; Smith, D. T.; Njardarson, J. T. *J. Med. Chem.* **2014,** *57,* 10257–10274. doi:10.1021/jm501100b
3. Müller, K.; Faeh, C.; Diederich, F. *Science* **2007,** *317,* 1881–1886. doi:10.1126/science.1131943
4. Purser, S.; Moore, P. R.; Swallow, S.; Gouverneur, V. *Chem. Soc. Rev.* **2008,** *37,* 320–330. doi:10.1039/b610213c
5. Wang, J.; Sánchez-Roselló, M.; Aceña, J. L.; del Pozo, C.; Sorochinsky, A. E.; Fustero, S.; Soloshonok, V. A.; Liu, H. *Chem. Rev.* **2014,** *114,* 2432–2506. doi:10.1021/cr4002879
6. Zhu, Y.; Han, J.; Wang, J.; Shibata, N.; Sodeoka, M.; Soloshonok, V. A.; Coelho, J. A. S.; Toste, F. D. *Chem. Rev.* **2018,** *118,* 3887–3964. doi:10.1021/acs.chemrev.7b00778
7. Leo, A.; Hansch, C.; Elkins, D. *Chem. Rev.* **1971,** *71,* 525–616. doi:10.1021/cr60274a001
8. Hansch, C.; Leo, A.; Taft, R. W. *Chem. Rev.* **1991,** *91,* 165–195. doi:10.1021/cr00002a004
9. Landelle, G.; Panossian, A.; Leroux, F. R. *Curr. Top. Med. Chem.* **2014,** *14,* 941–951. doi:10.2174/1568026614666140202210016
10. Leroux, F.; Jeschke, P.; Schlosser, M. *Chem. Rev.* **2005,** *105,* 827–856. doi:10.1021/cr040075b
11. Manteau, B.; Pazenok, S.; Vors, J.-P.; Leroux, F. R. *J. Fluorine Chem.* **2010,** *131,* 140–158. doi:10.1016/j.jfluchem.2009.09.009
12. Toulgoat, F.; Alazet, S.; Billard, T. *Eur. J. Org. Chem.* **2014,** 2415–2428. doi:10.1002/ejoc.201301857
13. Xu, X.-H.; Matsuzaki, K.; Shibata, N. *Chem. Rev.* **2015,** *115,* 731–764. doi:10.1021/cr500193b
14. Barata-Vallejo, S.; Bonesi, S.; Postigo, A. *Org. Biomol. Chem.* **2016,** *14,* 7150–7182. doi:10.1039/c6ob00763e
15. Barthelemy, A.-L.; Magnier, E.; Dagousset, G. *Synthesis* **2018,** *50,* 4765–4776. doi:10.1055/s-0037-1611278
16. Shibatomi, K.; Kitahara, K.; Sasaki, N.; Kawasaki, Y.; Fujisawa, I.; Iwasa, S. *Nat. Commun.* **2017,** *8,* 15600. doi:10.1038/ncomms15600
17. Katada, M.; Kitahara, K.; Iwasa, S.; Shibatomi, K. *Synlett* **2018,** *29,* 2408–2411. doi:10.1055/s-0037-1611019
18. Naruse, A.; Kitahara, K.; Iwasa, S.; Shibatomi, K. *Asian J. Org. Chem.* **2019,** *8,* 691–693. doi:10.1002/ajoc.201900072
19. Kawanishi, R.; Hattori, S.; Iwasa, S.; Shibatomi, K. *Molecules* **2019,** *24,* 2773. doi:10.3390/molecules24152773
20. Kitahara, K.; Mizutani, H.; Iwasa, S.; Shibatomi, K. *Synthesis* **2019,** *51,* 4385–4392. doi:10.1055/s-0039-1690009
21. Kawanishi, R.; Phongphane, L.; Iwasa, S.; Shibatomi, K. *Chem. – Eur. J.* **2019,** *25,* 7453–7456. doi:10.1002/chem.201900565
22. Shao, X.; Xu, C.; Lu, L.; Shen, Q. *Acc. Chem. Res.* **2015,** *48,* 1227–1236. doi:10.1021/acs.accounts.5b00047
23. Liu, X.; An, R.; Zhang, X.; Luo, J.; Zhao, X. *Angew. Chem., Int. Ed.* **2016,** *55,* 5846–5850. doi:10.1002/anie.201601713

License and Terms

This is an Open Access article under the terms of the Creative Commons Attribution License (https://creativecommons.org/licenses/by/4.0). Please note that the reuse, redistribution and reproduction in particular requires that the author(s) and source are credited and that individual graphics may be subject to special legal provisions.

The license is subject to the *Beilstein Journal of Organic Chemistry* terms and conditions: (https://www.beilstein-journals.org/bjoc/terms)

The definitive version of this article is the electronic one which can be found at:
https://doi.org/10.3762/bjoc.17.23

BEILSTEIN JOURNAL OF ORGANIC CHEMISTRY

Diels–Alder reaction of β-fluoro-β-nitrostyrenes with cyclic dienes

Savva A. Ponomarev[1], Roman V. Larkovich[1], Alexander S. Aldoshin[1], Andrey A. Tabolin[2], Sema L. Ioffe[2], Jonathan Groß[3], Till Opatz[3] and Valentine G. Nenajdenko[*1,§]

Full Research Paper

Open Access

Address:
[1]Department of Chemistry, Lomonosov Moscow State University, Leninskie gory 1, Moscow, 119991, Russian Federation, [2]N. D. Zelinsky Institute of Organic Chemistry, Russian Academy of Sciences Leninsky prosp. 47, Moscow 119991, Russian Federation and [3]Department of Chemistry Johannes Gutenberg-University, Duesbergweg 10–14, D-55128 Mainz, Germany

Email:
Valentine G. Nenajdenko[*] - nenajdenko@org.chem.msu.ru

* Corresponding author
§ Fax: (+)7-495-9328846

Keywords:
Diels–Alder reaction; fluorine; nitrostyrene; norbornene; stereochemistry

Beilstein J. Org. Chem. **2021,** *17,* 283–292.
https://doi.org/10.3762/bjoc.17.27

Received: 11 November 2020
Accepted: 13 January 2021
Published: 27 January 2021

This article is part of the thematic issue "Organo-fluorine chemistry V".

Guest Editor: D. O'Hagan

© 2021 Ponomarev et al.; licensee Beilstein-Institut.
License and terms: see end of document.

Abstract

The Diels–Alder reaction of β-fluoro-β-nitrostyrenes with cyclic 1,3-dienes was investigated. A series of novel monofluorinated norbornenes was prepared in up to 97% yield. The reaction with 1,3-cyclohexadiene permits the preparation of monofluorinated bicyclo[2.2.2]oct-2-enes. The kinetic data of the reactions with 1,3-cyclopentadiene and 1,3-cyclohexadiene were used to calculate activation parameters. Furthermore, the synthetic utility of the cycloadducts obtained was demonstrated.

Introduction

Organofluorine compounds play an exceptionally important role in various fields of science and technology. The incorporation of fluorine into molecules can significantly influence their pharmacokinetic and physicochemical properties and enhance their metabolic and chemical stability [1-5]. For instance, nearly a quarter of the currently manufactured agrochemical and pharmaceutical products contains at least one fluorine atom [6-8]. Fluorinated functional materials have also found wide application as durable ion exchange membranes, e.g., in fuel cells [9-11], as thermoplastic polymers [12-14], in electronic and optoelectronic technologies [15], and in liquid crystal display applications [16-21], etc [22]. The use of fluorinated building blocks is a very convenient approach and in many cases represents an indispensable alternative to late-stage fluorinations in the preparation of such unique materials [23].

The Diels–Alder reaction is considered a versatile and powerful tool for assembling a variety of fluorinated carbo- and

heterocycles using either the diene [24-30] or the dienophile component [31-39] as fluorine-containing building blocks. The application of [4 + 2] cycloadditions for the preparation of fluorinated bicyclic compounds has attracted much attention [40-47]. In this regard, the development of new protocols to relevant monofluorinated bicyclic molecules involving novel versatile fluorine-containing building blocks is of key importance. Fluoroalkenes are recognized to be one of the most widely used fluorine-containing building blocks [48,49]. Recently, we have developed an efficient stereoselective synthesis of β-fluoro-β-nitrostyrenes **1** based on the radical nitration of 2-bromo-2-fluorostyrenes [50]. This process takes place with simultaneous elimination of bromine, and gives the target structures solely in the Z-isomeric form in high yields (up to 92%). These fluorine-containing olefins activated by a nitro group proved to be the appealing building blocks for the construction of numerous monofluorinated compounds [51-56]. This paper is devoted to a new synthetic approach to novel monofluorinated bicyclic compounds, namely norbornenes and bicyclo[2.2.2]oct-2-enes and their subsequent functionalization. The present study is our follow-up work on the Diels–Alder reaction involving β-fluoro-β-nitrostyrenes [57].

A recent review reported that by 2018, the total number of publications and patents related to the production and use of norbornene and norbornadiene derivatives had exceeded 30,000 [58]. Indeed, norbornene and its derivatives have found application in medicine, agriculture, microelectronics, and rocket technology as well as in production of polymeric materials, efficient gas separation membranes and solar energy converters [58]. Considering the high interest in such structures and the unique role of fluorine, we believe that novel norbornene derivatives obtained in the framework of this study can become relevant compounds in practical use.

Results and Discussion

Initially, we studied the Diels–Alder reaction of β-fluoro-β-nitrostyrenes **1** with 1,3-cyclopentadiene (CPD) to prepare a series of novel monofluorinated norbornenes. The starting nitrostyrenes were prepared and used in the *Z*-isomer form. The transformations were conducted in screw-top vials in *o*-xylene at 110 °C using a fivefold excess of the diene (Scheme 1). The reaction proceeded smoothly under these conditions to give the target cycloadducts **2** as a mixture of *exo* and *endo*-isomers in high isolated yield (up to 97%). It should be noted that in the present work we indicate an isomer as e*xo* or *endo* according to the stereo-position of the fluorine atom. Thus *exo*-**2** and *endo*-**2** means 5-*exo*-fluoro-5-*endo*-nitro-6-*exo*-arylnorbornene and 5-*endo*-fluoro-5-*exo*-nitro-6-*endo*-arylnorbornene, respectively (Figure 1). Both diastereomers are formed in a nearly 1:1 ratio for the majority of the substituents on the aryl group of the nitrostyrenes **1**. However, a higher diastereoselectivity towards the *endo*-isomer was observed when strong electron-withdrawing groups (EWGs) were present in the dienophile. For example, in the case of the 4-cyano and the 3-nitro-substituted derivative, the ratio of *endo*/*exo* was 2:1.

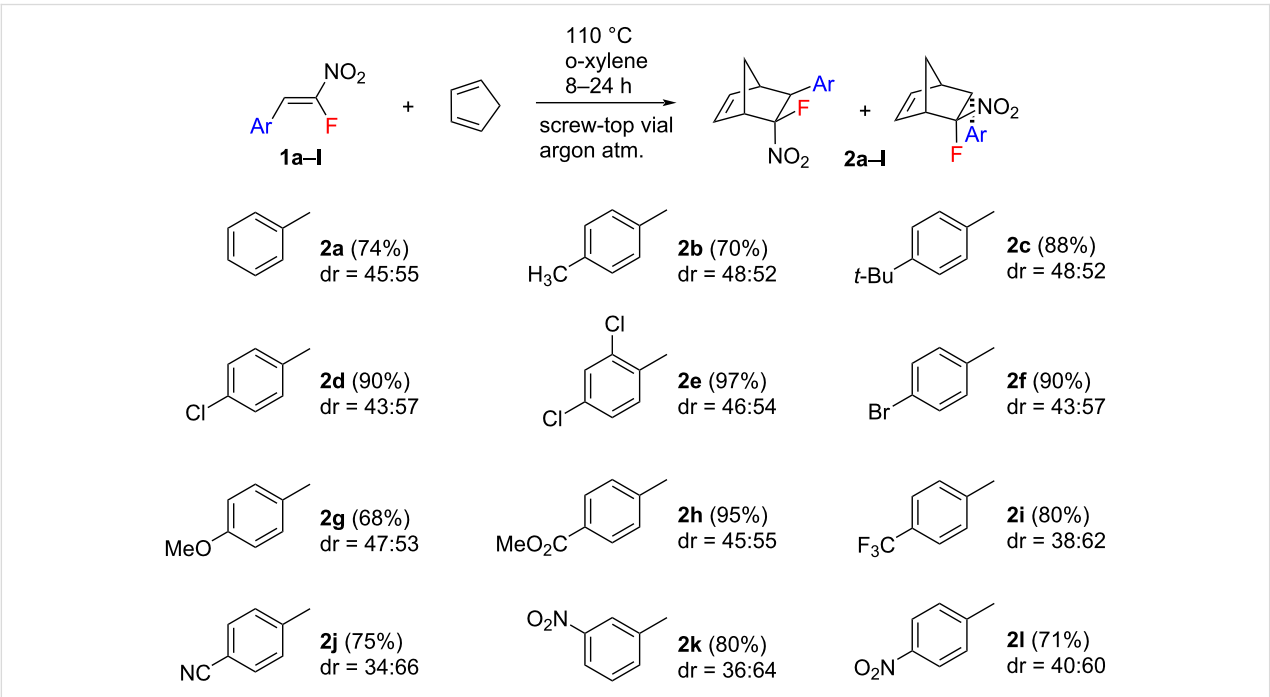

Scheme 1: Scope of the nitrostyrenes **1** in the Diels–Alder reaction with CPD (dr = *exo*:*endo*).

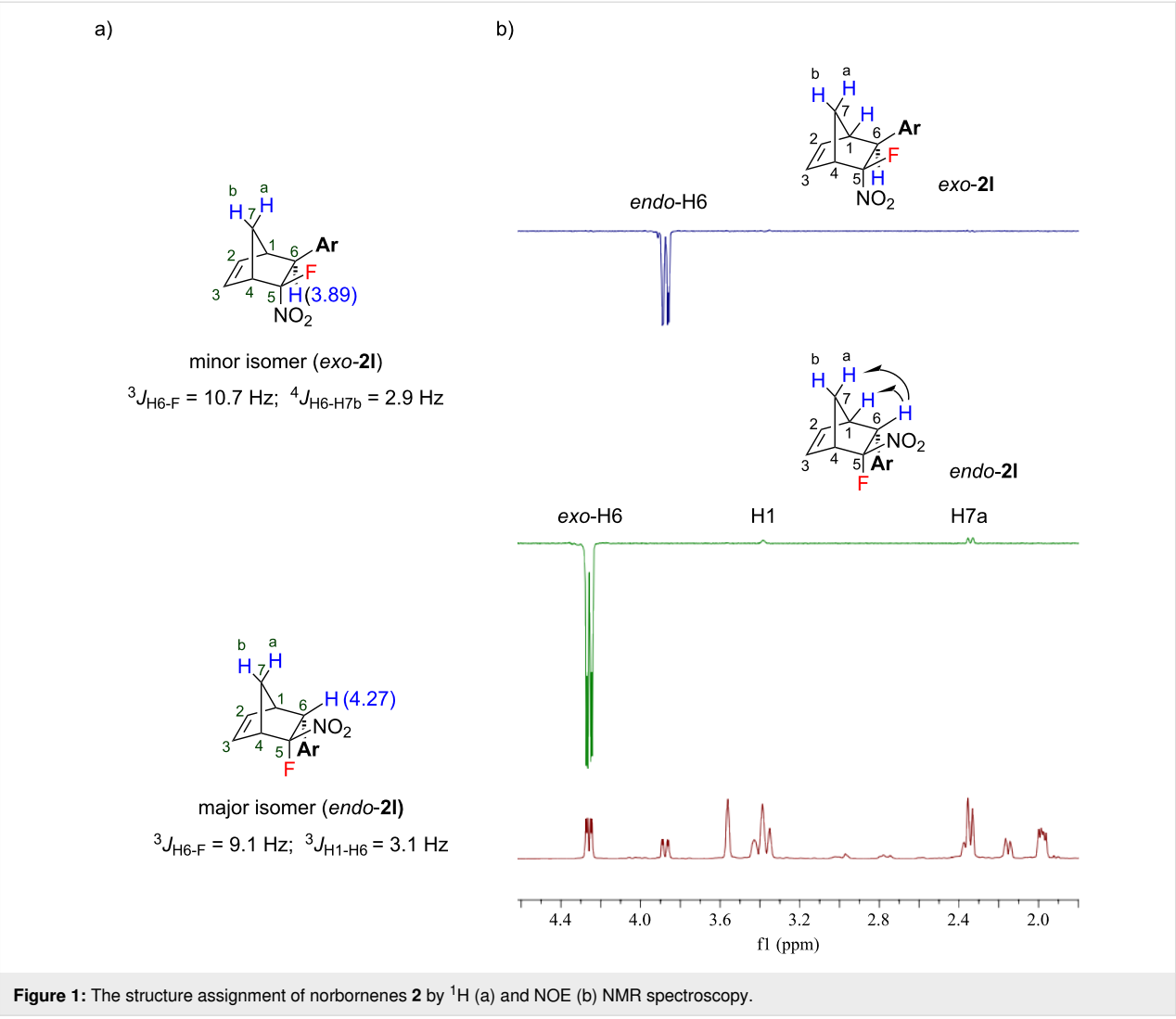

Figure 1: The structure assignment of norbornenes **2** by ^{1}H (a) and NOE (b) NMR spectroscopy.

The stereochemistry of the products **2a–l** can be unambiguously assigned using ^{1}H NMR spectroscopy. According to the literature data [59] the dienophile-derived proton at C6 resonates at lower field in the *exo*-form than the corresponding proton of the *endo*-isomer. For example, in the case of **2l**, the ^{1}H NMR spectrum shows a doublet of doublet signal for H6 at 3.89 ppm for the minor isomer and at 4.27 ppm for the major isomer (Figure 1a). A significant chemical shift difference is observed for the aryl proton signals of the *exo*- and *endo*-isomeric norbornenes **2**. Most probably such significant difference in the chemical shifts can be explained by the double bond anisotropy of the norbornene molecule [60]. The stereochemical assignments are in full accordance with the values of vicinal ($^3J_{H6-F}$ and $^3J_{H1-H6}$) and long-range coupling constants ($^4J_{H6-H7b}$). According to the literature data, the value of $^3J_{H1-H6}$ is larger than that of $^4J_{H6-H7b}$ [32,61-63]. For example, the ^{1}H NMR spectrum of the minor isomer of **2l** showed the coupling constants $^3J_{H6-F}$ = 10.7 Hz and $^4J_{H6-H7b}$ = 2.9 Hz consistent with an *exo*-geometry. In contrast, the major isomer having constants $^3J_{H6-F}$ = 9.1 Hz and $^3J_{H1-H6}$ = 3.1 Hz was ascribed to the *endo*-form (Figure 1). It should be noted that this observation applies for all cases investigated. The value of the coupling constant $^3J_{H6-F}$ between the *exo*-F and *endo*-H6 was always larger than the corresponding value between the *endo*-F and *exo*-H6. The stereochemical assignments were additionally confirmed by nuclear Overhauser effect spectroscopy (NOE). The peak of H6 was selected to be selectively excited for each isomer. As expected, in the case of *endo*-**2l** the NOE peaks resulted from the interaction of *exo*-H6 with H1 and H7a were observed. Whereas for *exo*-**2l** due to the opposite side position of *endo*-H6 there was no interaction observed. Thus, using these spectral data all the pairs of *exo*- and *endo*-isomers **2** obtained can be assigned unambiguously.

Moreover, the ^{13}C NMR spectra of the *exo* and *endo*-isomers exhibit a significant difference (approximately 3 ppm) in the

chemical shifts for some carbon atoms (Figure 2). A considerable difference in the chemical shifts was observed for C-7 of the methylene bridge (46.1 for the *exo*- vs 48.9 ppm for the *endo*-isomer), C-6 (51.3 for the *exo* vs 53.4 for the *endo*-isomer), C-4 (52.4 for the *exo*- vs 55.3 ppm for the *endo*-isomer), and C-2 (139.7 for the *endo*- vs 143.0 ppm for the *exo*-isomer). The same pattern in the chemical shifts and coupling constants was observed for all structures **2** synthesized.

For further insights into the mechanistic background of the *endo-exo* selectivity, the Diels–Alder reaction of CPD with the model nitrostyrene **1h** was simulated in silico to predict the reaction pathway, the reaction rate constants, and the activation enthalpies. Density functional theory calculations were conducted for the reactants, products, and transition states using the B3LYP [64-66] and M062X [67] level of theory in combination with a Pople basis set and the IEFPCM [68] solvation model for *o*-xylene. Both functionals are already known in the literature for the investigation of cycloadditions [69-72]. For the computational details the reader is referred to Supporting Information File 1.

The predicted reaction pathways for the formation of the *exo*- and *endo*-isomeric norbornene **2h** using M062X are displayed in Figure 3. For each isomer one transition state *exo*-**TS** and *endo*-**TS** was identified. The former transition state is higher in energy and leads to the less exergonic product *exo*-**2h**. The *exo* and *endo*-isomers were predicted to have free energies of activation ($\Delta G^{\ddagger}_{383.15}$) of 120.62 and 119.64 kJ mol^{-1}, respectively. The corresponding predicted reaction free energies ($\Delta G_{383.15}$) are −39.66 and −42.07 kJ mol^{-1}. With the former values of $\Delta G^{\ddagger}$, the reaction rate coefficient k can be calculated using the Eyring equation (Equation 1) [73,74]:

$$k(T) = \frac{k_B T}{hc_0} e^{-\Delta G^{\ddagger}_{383.15\mathrm{K}}/RT} \quad (1)$$

For T = 110 °C, the predicted ratio of k_{endo}/k_{exo} = 1.36 (1.68 for B3LYP) is in good accordance with the experimentally observed diastereomeric ratio of 1.22. The larger discrepancy in case of the B3LYP functional may be due to the fact that disper-

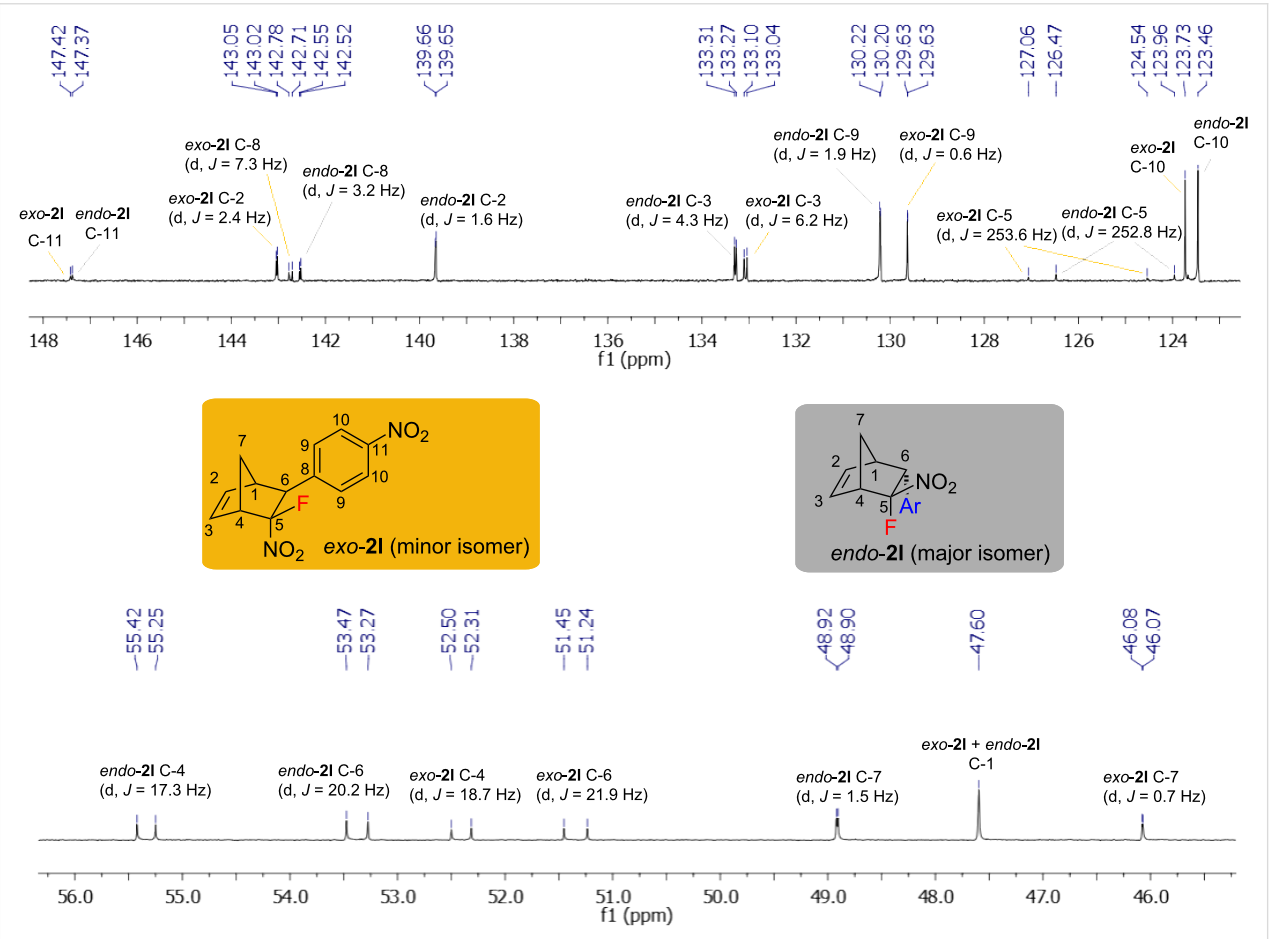

Figure 2: ^{13}C NMR spectrum of the mixture of *exo*- and *endo*-isomers of norbornene **2l**.

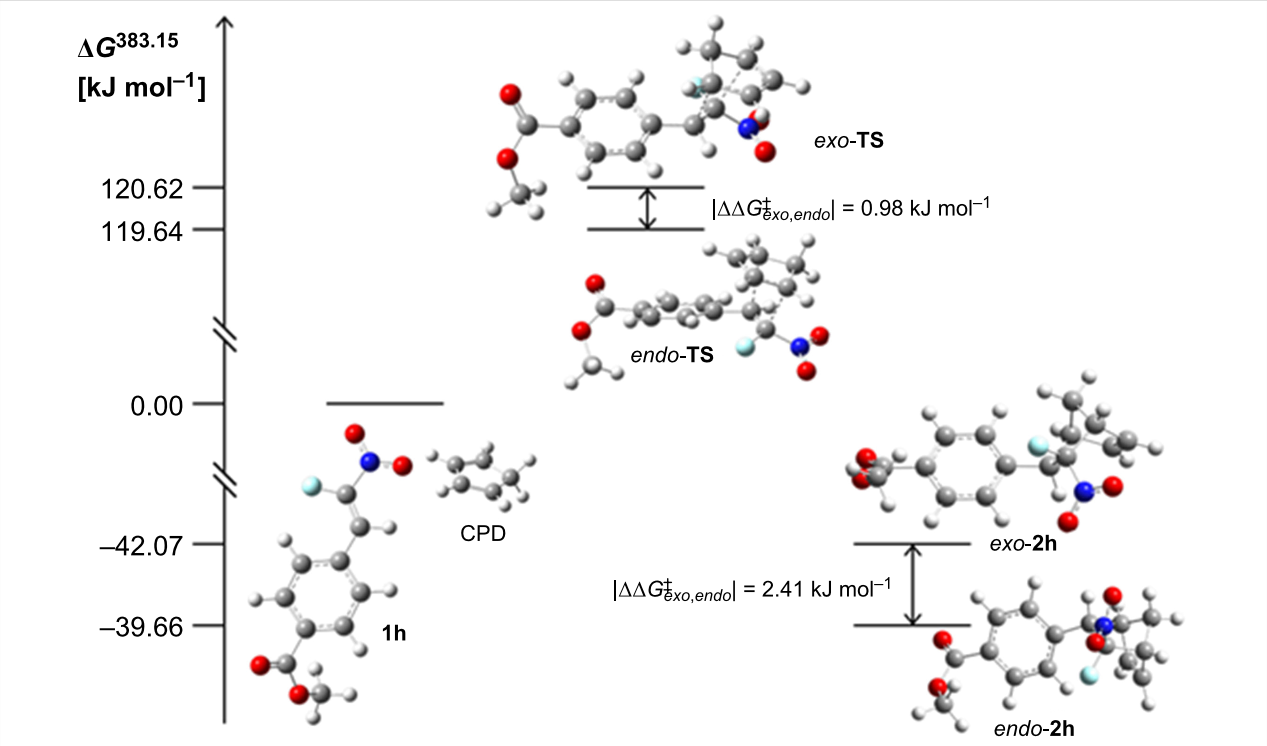

Figure 3: The predicted reaction pathway for the Diels–Alder reaction of nitrostyrene **1h** with CPD is displayed. The path leading to the *endo*-**2h** isomer has a lower lying transition state and is more exergonic than the path resulting in the *exo*-**2h** isomer. Energies are given in kJ mol^{-1} and were calculated with M062X/6-311+G(d,p) at 383.15 K in *o*-xylene (the corresponding B3LYP reaction pathway is not shown).

sion effects are not included, whereas M062X includes nonlocal effects of electronic dispersion [70,75].

We also demonstrate the preparation of norbornene structures substituted at the methylene bridge. The reaction of model nitrostyrene **1h** with spiro[2.4]hepta-4,6-diene was carried out (Scheme 2). As a result, the corresponding norbornene **2m** having a cyclopropane ring was obtained in moderate yield (44%). The cycloaddition proceeds much more slowly as a result of the high steric demand of the cyclopropyl ring of the spirodiene compared to the CH_2 group of cyclopentadiene. We believe that this is the reason of the lower yield in comparison to the reaction with CPD. The stereochemical assignment was performed using ^{1}H NMR spectroscopy (Scheme 2) to show similar peculiarities of the spectra. In contrast to the reaction with CPD, a slight prevalence in the formation of the *exo*-isomer (*exo*:*endo* = 56:44) was observed for the product **2m**.

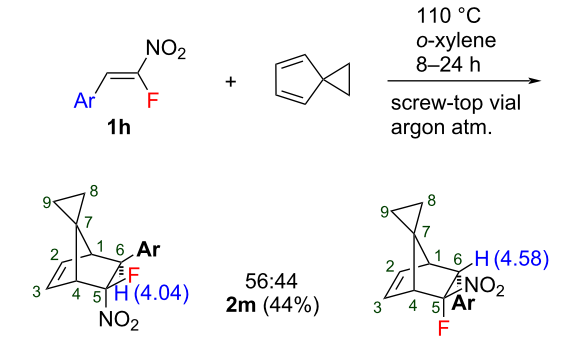

Scheme 2: The Diels–Alder reaction of nitrostyrene **1h** with spiro[2.4]hepta-4,6-diene.

Next, the reaction with 1,3-cyclohexadiene (CHD) was investigated. It was found that the reaction is very sensitive to the structure of starting diene and in the case of CHD proceeds much more slowly. Both thermal and microwave (MW) activation (Scheme 3) was investigated to accelerate the reaction with CHD. However, in all cases, the yields of the target cycloadducts **3** were below 35% despite the full conversion of the nitrostyrenes **1** which is common for this type of dienophiles (Scheme 3). The stereochemical assignment was made similarly to the norbornene structures using ^{1}H NMR spectroscopy (Scheme 3). Larger values of $^3J_{H6\text{-}F}$ were observed for the *exo*-F isomers. The presence of a strong EWG on the aryl substituent led to higher stereoselectivity. For example, approximately a 2:1 ratio was observed for the nitro- and carboxymethyl-substituted products **3b**, **3c**, whereas in the absence of a

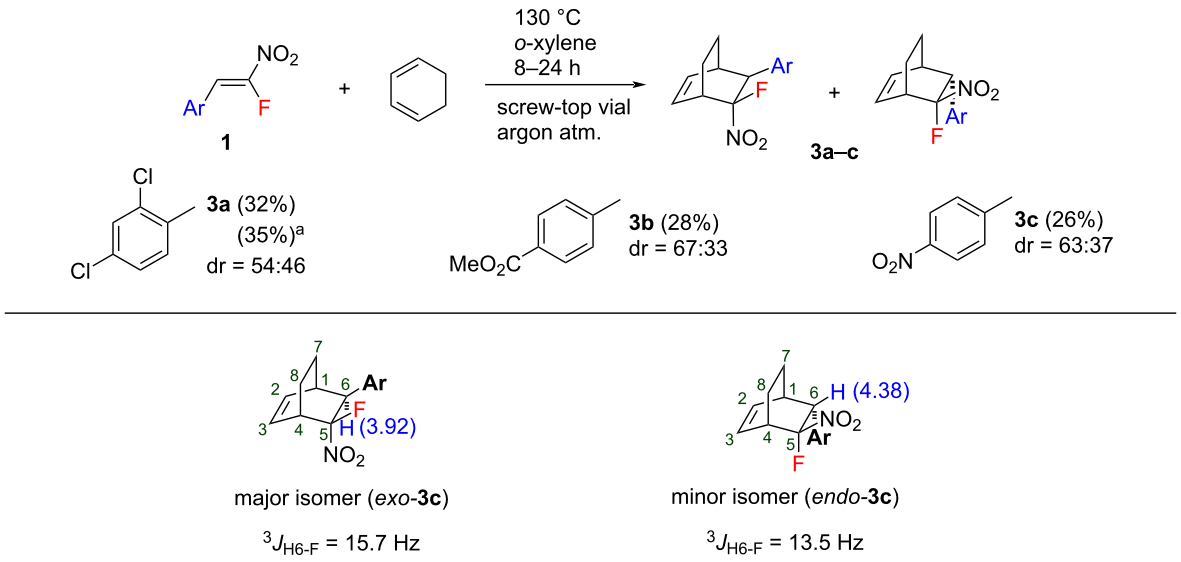

Scheme 3: Diels–Alder reaction of nitrostyrenes **1** with CHD (dr = *exo*:*endo*). (a) Reaction under microwave activation.

strong EWG, the ratio was about 1:1 (**3a**). However, in contrast to CPD derivatives, the major products formed in the reaction with CHD have *exo*-configuration.

To gain deeper insights into the reaction, we carried out some kinetic studies to evaluate and compare the reactivities of CHD and CPD in the reactions with model nitrostyrene **1h** (Scheme 4). All the kinetic runs were performed using a ≈43–49 molar excess of the diene in *o*-xylene (1:1) to provide pseudo-first order conditions. Conversions (*F*) of **1** were measured by ^{1}H NMR spectroscopy. The reactions were found to proceed under the kinetic control since the isomer ratio remained constant throughout the reaction course regardless of the temperature (Table 1).

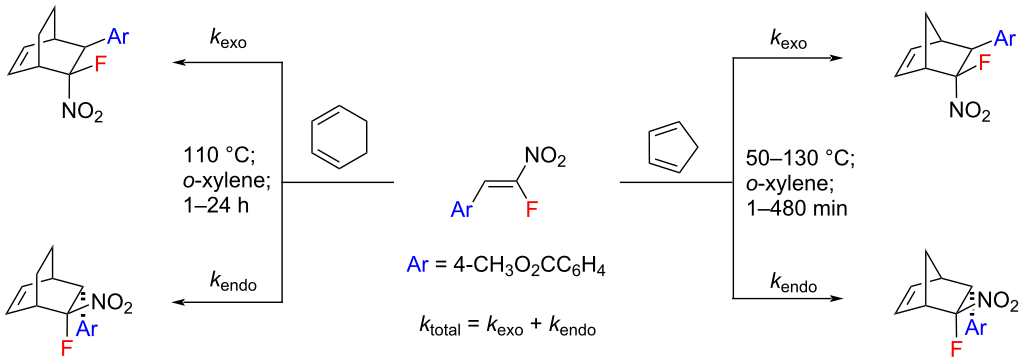

Scheme 4: Kinetic study of reactions of **1h** with CPD and CHD.

Table 1: Kinetic parameters for the reactions of **1h** with CPD and CHD.

entry	diene	*T*, °C	molar ratio *exo*/*endo*	$k^*\cdot10^4$ s^{-1}	$k_{total}\cdot10^5$ L/mol·s	$k_{exo}\cdot10^5$, L/mol·s	$k_{endo}\cdot10^5$, L/mol·s	R_{corr}
1	CPD	50	46:54	1.00	1.67	0.090	0.077	0.997
2	CPD	80	46:54	5.78	9.72	5.26	4.46	0.998
3	CPD	110	46:54	35.62	59.91	32.39	27.53	0.990
4	CPD	130	46:54	46.20	77.71	41.99	35.72	0.999
5	CHD	110	61:39	0.12	0.224	0.137	0.087	0.999

The total effective pseudo-first order rate constants k^* were obtained by plotting the experimental values of $\ln(c_0/c)$ versus time with good correlations (Table 1). The overall second-order rate total constants k_{total} were calculated from the effective k^* and initial concentration of the diene (Table 1). The individual constants for the *endo* and *exo*-isomers (k_{endo} and k_{exo}) were evaluated by multiplication of k_{total} with the molar fractions of the isomers (Table 1). The data obtained demonstrated that the overall reaction rate for CHD is 267 times lower than that for CPD at 110 °C (Figure 4, Table 1). Such a large difference in the reactivity of CHD and CPD was described in the literature. For example, in model reactions with tetracyanoethene, the difference was 2600-fold at 20 °C [76]. The activation parameters were estimated for the reaction of **1h** with CPD by plotting $\ln(k/T)$ versus $1/T$ according to the Eyring equation (Equations 2–4) [77].

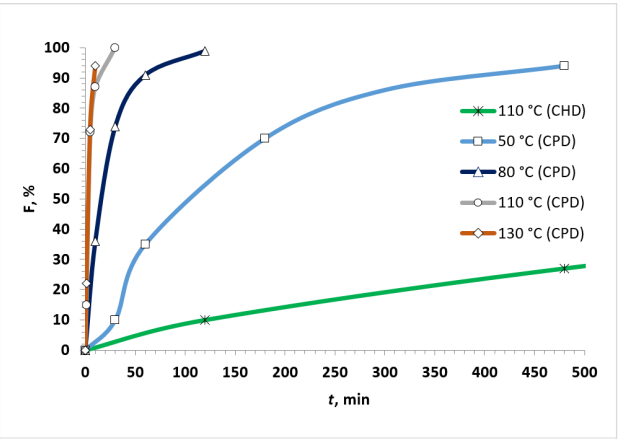

Figure 4: Kinetic curves for the reactions of nitrostyrene **1h** with CPD (50–130 °C) and CHD at 110 °C.

$$\ln(k/T) = \ln(k_b/\hbar) + \Delta S^{\neq}/R - \Delta H^{\neq}/RT \quad (2)$$

$$\ln(k_{endo}/T) = 1.89 - 6208/T \quad (R_{corr} = 0.989) \quad (3)$$

$$\ln(k_{exo}/T) = 1.72 - 6207/T \quad (R_{corr} = 0.989) \quad (4)$$

The activation enthalpies ($\Delta H^{\neq}$) for *exo*- and *endo*-**1h** were found to be identical for both reaction pathways (51.6 kJ mol^{-1}). Whereas the entropies of activation ($\Delta S^{\neq}$) were −181.8 and −183.1 J mol^{-1} K^{-1} for the formation of the *endo* and *exo*-isomers, respectively. The values obtained are typical for concerted [4 + 2]-cycloaddition reactions [60]. The free energies of activation ($\Delta G^{\ddagger}_{383.15}$) were calculated for 121.26 kJ mol^{-1} for *endo*-**1h** and 121.75 kJ mol^{-1} for *exo*-**1h** and were consistent with the predicted ones.

Next, the reaction with some other cyclic dienes was investigated. The reaction with the unsymmetrical 1-methoxy-1,3-cyclohexadiene (Scheme 5) led to the formation of a mixture of four products (regioisomers and stereoisomers, respectively) **3d** in 40% overall yield. Two pairs of regioisomers were partially separated by column chromatography with sufficiently slow elution and analyzed by ^{1}H NMR spectroscopy. The structure assignment was made as depicted in Scheme 5. The structures of two pairs of regioisomers were assigned by chemical shifts of the singlet of the methoxy group. The products having the MeO and NO_2 groups in the adjacent position have the signal of the methoxy protons shifted to a lower field. The assignment of the *exo*/*endo*-isomers was carried out by the position of the benzylic proton (H5 or H6) and its coupling constant to fluorine ($^3J_{H5\text{-}F}$ or $^3J_{H6\text{-}F}$).

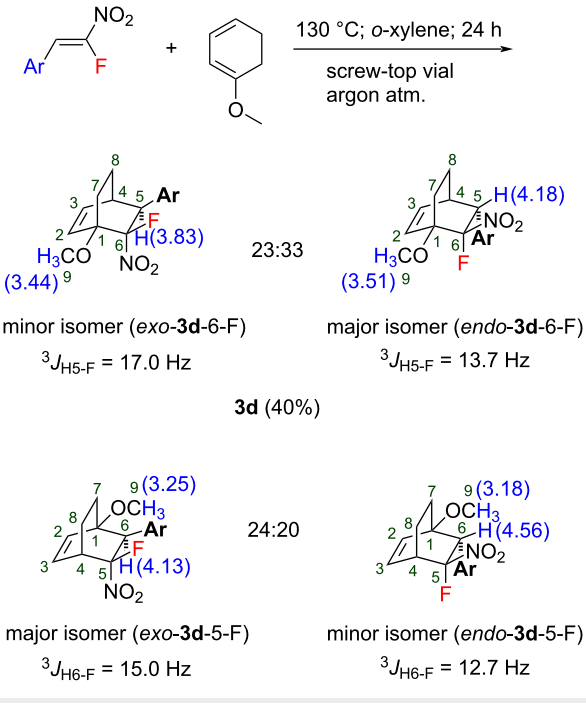

Scheme 5: The Diels–Alder reaction of the nitrostyrene **1h** with 1-methoxy-1,3-cyclohexadiene.

The reaction with 7- and 8-membered cyclic dienes (1,3-cycloheptadiene and 1,3-cyclooctadiene) did not result in the formation of the corresponding cycloadducts confirming that the reaction is very sensitive to the structure of the dienes. Moreover, it was found that furan did not react with nitrostyrenes **1**.

Furthermore, we performed some subsequent transformations of the fluorinated norbornenes prepared to investigate their chemical properties and to demonstrate their utility (Scheme 6). These reactions were carried out to involve either the double bond or the nitro group of the norbornene products. The treatment of cycloadducts **2** with *m*-chloroperbenzoic acid afforded a series of novel fluorinated epoxynorbornane derivatives **4** in high

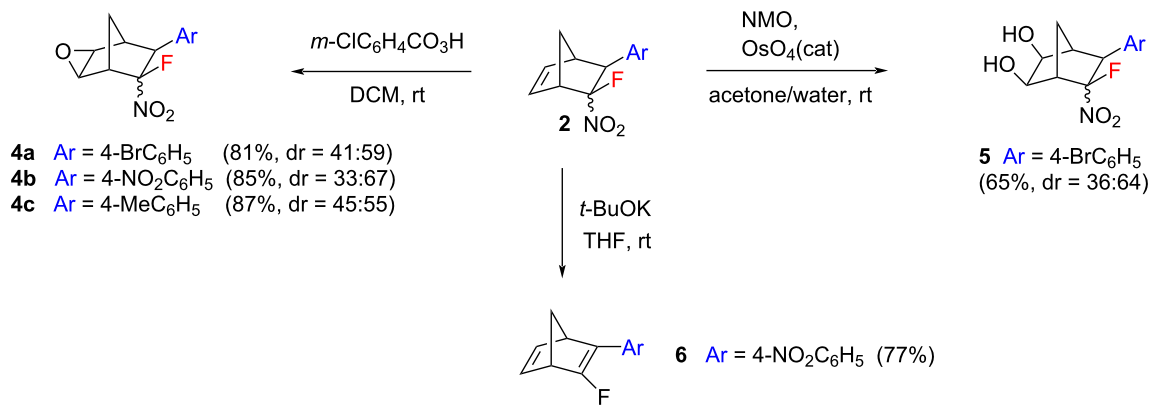

Scheme 6: Selected chemical transformations of norbornenes **2** (dr = *exo*:*endo*).

yields (up to 87%). In all cases, the formation of mixtures of only two products was observed in ratios similar to those of the starting mixture **2**. We believe that this is a result of an *exo*-epoxidation which is preferred in norbornene systems [78,79]. Such a functionalization is very attractive to produce new reactive building blocks bearing the norbornane scaffold. This approach can pave a straightforward way to numerous fluorine-containing bicyclic compounds not previously available. The *syn*-dihydroxylation of compound **2f** with the *N*-methylmorpholine-*N*-oxide (NMO)–OsO_4 system resulted in a mixture of the corresponding diols **5** in a 36:64 ratio in 65% yield. Again, *exo*-dihydroxylation is to be expected [80-82]. The treatment of norbornene **2l** with *t*-BuOK resulted in the selective elimination of nitrous acid to form the desired monofluorinated norbornadiene **6** in 77% yield. No competitive elimination of HF was observed. The Diels–Alder reaction–base-induced HNO_2 elimination sequence opens a straightforward way to novel fluorinated norbornadienes from β-fluoro-β-nitrostyrenes and CPD.

Conclusion

In summary, the Diels–Alder reaction of β-fluoro-β-nitrostyrenes with cyclic 1,3-dienes was investigated. A series of novel monofluorinated norbornenes was prepared in high yield up to 97%. A number of novel monofluorinated bicyclo[2.2.2]oct-2-enes was obtained in up to 40% yield. The reactivity of CPD and its homologues was evaluated and compared. The reaction rate for CHD proved to be 267 times lower than that for CPD in a model reaction, whereas 1,3-cycloheptadiene and 1,3-cyclooctadiene were found to be unable to react. The activation parameters of the reaction of nitrostyrene **1h** with CPD were estimated. In addition, the synthetic utility of the norbornenes obtained was demonstrated. All the structures obtained in this work were elucidated by NMR spectroscopy and elemental analysis or HRMS.

Supporting Information

Supporting Information File 1

Copies of spectra, experimental section, and computational details of DFT calculations.
[https://www.beilstein-journals.org/bjoc/content/supplementary/1860-5397-17-27-S1.pdf]

Acknowledgements

The authors acknowledge the partial support in measuring of NMR spectra from the M. V. Lomonosov Moscow State University Program of Development. We thank Jan Brauer and Paul Eckhardt for their assistance with the computational calculations and evaluations. Parts of this research were conducted using the supercomputer MOGON and/or advisory services offered by the Johannes Gutenberg University Mainz (hpc.uni-mainz.de), which is a member of the AHRP (Alliance for High Performance Computing in Rhineland Palatinate, http://www.ahrp.info) and the Gauss Alliance e.V. The authors gratefully acknowledge the computing time granted on the supercomputer MOGON at Johannes Gutenberg University Mainz.

Funding

This work was supported by RFBR, project number 20-33-70132.

ORCID® iDs

Savva A. Ponomarev - https://orcid.org/0000-0002-5667-4800
Alexander S. Aldoshin - https://orcid.org/0000-0003-3653-1439
Andrey A. Tabolin - https://orcid.org/0000-0003-3241-8279
Till Opatz - https://orcid.org/0000-0002-3266-4050
Valentine G. Nenajdenko - https://orcid.org/0000-0001-9162-5169

References

1. Purser, S.; Moore, P. R.; Swallow, S.; Gouverneur, V. *Chem. Soc. Rev.* **2008,** *37,* 320–330. doi:10.1039/b610213c
2. Shah, P.; Westwell, A. D. *J. Enzyme Inhib. Med. Chem.* **2007,** *22,* 527–540. doi:10.1080/14756360701425014
3. Wang, B.-C.; Wang, L.-J.; Jiang, B.; Wang, S.-Y.; Wu, N.; Li, X.-Q.; Shi, D.-Y. *Mini-Rev. Med. Chem.* **2017,** *17,* 683–692. doi:10.2174/1389557515666151016124957
4. Gillis, E. P.; Eastman, K. J.; Hill, M. D.; Donnelly, D. J.; Meanwell, N. A. *J. Med. Chem.* **2015,** *58,* 8315–8359. doi:10.1021/acs.jmedchem.5b00258
5. Meanwell, N. A. *J. Med. Chem.* **2018,** *61,* 5822–5880. doi:10.1021/acs.jmedchem.7b01788
6. Politanskaya, L. V.; Selivanova, G. A.; Panteleeva, E. V.; Tretyakov, E. V.; Platonov, V. E.; Nikul'shin, P. V.; Vinogradov, A. S.; Zonov, Y. V.; Karpov, V. M.; Mezhenkova, T. V.; Vasilyev, A. V.; Koldobskii, A. B.; Shilova, O. S.; Morozova, S. M.; Burgart, Y. V.; Shchegolkov, E. V.; Saloutin, V. I.; Sokolov, V. B.; Aksinenko, A. Y.; Nenajdenko, V. G.; Moskalik, M. Y.; Astakhova, V. V.; Shainyan, B. A.; Tabolin, A. A.; Ioffe, S. L.; Muzalevskiy, V. M.; Balenkova, E. S.; Shastin, A. V.; Tyutyunov, A. A.; Boiko, V. E.; Igumnov, S. M.; Dilman, A. D.; Adonin, N. Y.; Bardin, V. V.; Masoud, S. M.; Vorobyeva, D. V.; Osipov, S. N.; Nosova, E. V.; Lipunova, G. N.; Charushin, V. N.; Prima, D. O.; Makarov, A. G.; Zibarev, A. V.; Trofimov, B. A.; Sobenina, L. N.; Belyaeva, K. V.; Sosnovskikh, V. Y.; Obydennov, D. L.; Usachev, S. A. *Russ. Chem. Rev.* **2019,** *88,* 425–569. doi:10.1070/rcr4871
7. Inoue, M.; Sumii, Y.; Shibata, N. *ACS Omega* **2020,** *5,* 10633–10640. doi:10.1021/acsomega.0c00830
8. Han, J.; Remete, A. M.; Dobson, L. S.; Kiss, L.; Izawa, K.; Moriwaki, H.; Soloshonok, V. A.; O'Hagan, D. *J. Fluorine Chem.* **2020,** *239,* 109639. doi:10.1016/j.jfluchem.2020.109639
9. Mauritz, K. A.; Moore, R. B. *Chem. Rev.* **2004,** *104,* 4535–4586. doi:10.1021/cr0207123
10. Schmidt-Rohr, K.; Chen, Q. *Nat. Mater.* **2008,** *7,* 75–83. doi:10.1038/nmat2074
11. Kraytsberg, A.; Ein-Eli, Y. *Energy Fuels* **2014,** *28,* 7303–7330. doi:10.1021/ef501977k
12. Ferrari, M. C.; Galizia, M.; De Angelis, M. G.; Sarti, G. C. *Ind. Eng. Chem. Res.* **2010,** *49,* 11920–11935. doi:10.1021/ie100242q
13. Mastronardi, F.; Gutmann, B.; Kappe, C. O. *Org. Lett.* **2013,** *15,* 5590–5593. doi:10.1021/ol4027914
14. Kubota, T. *J. Synth. Org. Chem., Jpn.* **2013,** *71,* 196–206. doi:10.5059/yukigoseikyokaishi.71.196
15. Babudri, F.; Farinola, G. M.; Naso, F.; Ragni, R. *Chem. Commun.* **2007,** 1003–1022. doi:10.1039/b611336b
16. Hird, M. *Chem. Soc. Rev.* **2007,** *36,* 2070–2095. doi:10.1039/b610738a
17. Yokokoji, O.; Miyajima, T.; Irisawa, J.; Shimizu, T.; Inoue, S. *Liq. Cryst.* **2009,** *36,* 799–807. doi:10.1080/02678290903062986
18. Goodby, J. W.; Hindmarsh, P.; Hird, M.; Lewis, R. A.; Toyne, K. J. *Mol. Cryst. Liq. Cryst. Sci. Technol., Sect. A* **2001,** *364,* 889–898. doi:10.1080/10587250108025062
19. Ishigure, T.; Koike, Y. *Mol. Cryst. Liq. Cryst. Sci. Technol., Sect. A* **2000,** *353,* 451–469. doi:10.1080/10587250008025681
20. Kirsch, P. *J. Fluorine Chem.* **2015,** *177,* 29–36. doi:10.1016/j.jfluchem.2015.01.007
21. Al-Maharik, N.; Kirsch, P.; Slawin, A. M. Z.; Cordes, D. B.; O'Hagan, D. *Org. Biomol. Chem.* **2016,** *14,* 9974–9980. doi:10.1039/c6ob01986b
22. Pagliaro, M.; Ciriminna, R. *J. Mater. Chem.* **2005,** *15,* 4981–4991. doi:10.1039/b507583c
23. Kondratov, I. S.; Tolmachova, N. A.; Haufe, G. *Eur. J. Org. Chem.* **2018,** 3618–3647. doi:10.1002/ejoc.201800327
24. Hayashi, T.; Usuki, Y.; Wakamatsu, Y.; Iio, H. *Synlett* **2010,** 2843–2846. doi:10.1055/s-0030-1259013
25. Shi, G.-q.; Cottens, S.; Shiba, S. A.; Manfred, S. *Tetrahedron* **1992,** *48,* 10569–10574. doi:10.1016/s0040-4020(01)88354-x
26. Patrick, T. B.; Rogers, J.; Gorrell, K. *Org. Lett.* **2002,** *4,* 3155–3156. doi:10.1021/ol026512v
27. Patrick, T. B.; Gorrell, K.; Rogers, J. *J. Fluorine Chem.* **2007,** *128,* 710–713. doi:10.1016/j.jfluchem.2007.03.010
28. Jin, F.-q.; Xu, Y.-y.; Huang, W.-y. *J. Fluorine Chem.* **1995,** *71,* 1–4. doi:10.1016/0022-1139(94)03186-4
29. Shi, G.-q.; Schlosser, M. *Tetrahedron* **1993,** *49,* 1445–1456. doi:10.1016/s0040-4020(01)90196-6
30. Amii, H.; Kobayashi, T.; Terasawa, H.; Uneyama, K. *Org. Lett.* **2001,** *3,* 3103–3105. doi:10.1021/ol0163631
31. Hanamoto, T.; Korekoda, K.; Nakata, K.; Handa, K.; Koga, Y.; Kondo, M. *J. Fluorine Chem.* **2002,** *118,* 99–101. doi:10.1016/s0022-1139(02)00198-7
32. Sridhar, M.; Leela Krishna, K.; Madhusudana Rao, J. *Tetrahedron* **2000,** *56,* 3539–3545. doi:10.1016/s0040-4020(00)00242-8
33. de Meijere, A.; Teichmann, S.; Seyed-Mahdavi, F.; Kohlstruk, S. *Liebigs Ann.* **1996,** 1989–2000. doi:10.1002/jlac.199619961208
34. Ito, H.; Saito, A.; Taguchi, T. *Tetrahedron: Asymmetry* **1998,** *9,* 1979–1987. doi:10.1016/s0957-4166(98)00195-5
35. Arany, A.; Crowley, P. J.; Fawcett, J.; Hursthouse, M. B.; Kariuki, B. M.; Light, M. E.; Moralee, A. C.; Percy, J. M.; Salafia, V. *Org. Biomol. Chem.* **2004,** *2,* 455–465. doi:10.1039/b314314g
36. Crowley, P. J.; Percy, J. M.; Stansfield, K. *Tetrahedron Lett.* **1996,** *37,* 8237–8240. doi:10.1016/0040-4039(96)01877-1
37. Yamada, S.; Noma, M.; Konno, T.; Ishihara, T.; Yamanaka, H. *Org. Lett.* **2006,** *8,* 843–845. doi:10.1021/ol052897g
38. Yamada, S.; Hondo, K.; Konno, T.; Ishihara, T. *RSC Adv.* **2016,** *6,* 28458–28469. doi:10.1039/c6ra00569a
39. Shastin, A. V.; Nenajdenko, V. G.; Muzalevskiy, V. M.; Balenkova, E. S.; Fröhlich, R.; Haufe, G. *Tetrahedron* **2008,** *64,* 9725–9732. doi:10.1016/j.tet.2008.07.097
40. Crowley, P. J.; Percy, J. M.; Stansfield, K. *Tetrahedron Lett.* **1996,** *37,* 8233–8236. doi:10.1016/0040-4039(96)01876-x
41. Petrov, V.; Marchione, A. A.; Dooley, R. *Chem. Commun.* **2018,** *54,* 9298–9300. doi:10.1039/c8cc05075a
42. Chanteau, F.; Essers, M.; Plantier-Royon, R.; Haufe, G.; Portella, C. *Tetrahedron Lett.* **2002,** *43,* 1677–1680. doi:10.1016/s0040-4039(02)00107-7
43. Baum, K.; Archibald, T. G.; Tzeng, D.; Gilardi, R.; Flippen-Anderson, J. L.; George, C. *J. Org. Chem.* **1991,** *56,* 537–539. doi:10.1021/jo00002a011
44. Percy, J. M.; Stansfield, K.; Crowley, P. J.; Stansfield, K. *Chem. Commun.* **1997,** 2033–2034. doi:10.1039/a704717g
45. Petrov, V.; Dooley, R. J.; Marchione, A. A.; Diaz, E. L.; Clem, B. S. *J. Fluorine Chem.* **2019,** *225,* 1–10. doi:10.1016/j.jfluchem.2019.06.003
46. Ernet, T.; Maulitz, A. H.; Würthwein, E.-U.; Haufe, G. *J. Chem. Soc., Perkin Trans. 1* **2001,** 1929–1938. doi:10.1039/b102684b
47. Bogachev, A. A.; Kobrina, L. S.; Meyer, O. G. J.; Haufe, G. *J. Fluorine Chem.* **1999,** *97,* 135–143. doi:10.1016/s0022-1139(99)00040-8

48. Konev, A. S.; Khlebnikov, A. F. *Collect. Czech. Chem. Commun.* **2008,** *73,* 1553–1611. doi:10.1135/cccc20081553
49. Yanai, H.; Taguchi, T. *Eur. J. Org. Chem.* **2011,** 5939–5954. doi:10.1002/ejoc.201100495
50. Motornov, V. A.; Muzalevskiy, V. M.; Tabolin, A. A.; Novikov, R. A.; Nelyubina, Y. V.; Nenajdenko, V. G.; Ioffe, S. L. *J. Org. Chem.* **2017,** *82,* 5274–5284. doi:10.1021/acs.joc.7b00578
51. Motornov, V. A.; Tabolin, A. A.; Novikov, R. A.; Nelyubina, Y. V.; Nenajdenko, V. G.; Ioffe, S. L. *Org. Chem. Front.* **2018,** *5,* 2588–2594. doi:10.1039/c8qo00623g
52. Motornov, V. A.; Tabolin, A. A.; Nelyubina, Y. V.; Nenajdenko, V. G.; Ioffe, S. L. *Org. Biomol. Chem.* **2019,** *17,* 1442–1454. doi:10.1039/c8ob03126f
53. Motornov, V. A.; Tabolin, A. A.; Nelyubina, Y. V.; Nenajdenko, V. G.; Ioffe, S. L. *Org. Biomol. Chem.* **2020,** *18,* 1436–1448. doi:10.1039/c9ob02668a
54. Aldoshin, A. S.; Tabolin, A. A.; Ioffe, S. L.; Nenajdenko, V. G. *Eur. J. Org. Chem.* **2018,** 3816–3825. doi:10.1002/ejoc.201800385
55. Motornov, V. A.; Tabolin, A. A.; Novikov, R. A.; Nelyubina, Y. V.; Ioffe, S. L.; Smolyar, I. V.; Nenajdenko, V. G. *Eur. J. Org. Chem.* **2017,** 6851–6860. doi:10.1002/ejoc.201701338
56. Aldoshin, A. S.; Tabolin, A. A.; Ioffe, S. L.; Nenajdenko, V. G. *Eur. J. Org. Chem.* **2019,** 4384–4396. doi:10.1002/ejoc.201900573
57. Larkovich, R. V.; Ponomarev, S. A.; Aldoshin, A. S.; Tabolin, A. A.; Ioffe, S. L.; Nenajdenko, V. G. *Eur. J. Org. Chem.* **2020,** 2479–2492. doi:10.1002/ejoc.202000054
58. Flid, V. R.; Gringolts, M. L.; Shamsiev, R. S.; Finkelshtein, E. S. *Russ. Chem. Rev.* **2018,** *87,* 1169–1205. doi:10.1070/rcr4834
59. Pretsch, E.; Bühlmann, P.; Badertscher, M. *Structure Determination of Organic Compounds, Tables of Spectral Data;* Springer-Verlag: Berlin, Heidelberg, 2009; p 174. doi:10.1007/978-3-540-93810-1
60. Jasiński, R.; Kwiatkowska, M.; Barański, A. *J. Phys. Org. Chem.* **2011,** *24,* 843–853. doi:10.1002/poc.1853
61. De Tollenaere, C.; Ghosez, L. *Tetrahedron* **1997,** *53,* 17127–17138. doi:10.1016/s0040-4020(97)10126-0
62. Sridhar, M.; Krishna, K. L.; Srinivas, K.; Rao, J. M. *Tetrahedron Lett.* **1998,** *39,* 6529–6532. doi:10.1016/s0040-4039(98)01357-4
63. Smart, B. E. *J. Org. Chem.* **1973,** *38,* 2027–2035. doi:10.1021/jo00951a013
64. Lee, C.; Yang, W.; Parr, R. G. *Phys. Rev. B* **1988,** *37,* 785–789. doi:10.1103/physrevb.37.785
65. Becke, A. D. *J. Chem. Phys.* **1993,** *98,* 5648–5652. doi:10.1063/1.464913
66. Vosko, S. H.; Wilk, L.; Nusair, M. *Can. J. Phys.* **1980,** *58,* 1200–1211. doi:10.1139/p80-159
67. Zhao, Y.; Truhlar, D. G. *Theor. Chem. Acc.* **2008,** *120,* 215–241. doi:10.1007/s00214-007-0310-x
68. Tomasi, J.; Mennucci, B.; Cancès, E. *J. Mol. Struct.: THEOCHEM* **1999,** *464,* 211–226. doi:10.1016/s0166-1280(98)00553-3
69. Pieniazek, S. N.; Clemente, F. R.; Houk, K. N. *Angew. Chem., Int. Ed.* **2008,** *47,* 7746–7749. doi:10.1002/anie.200801843
70. Mardirossian, N.; Head-Gordon, M. *Mol. Phys.* **2017,** *115,* 2315–2372. doi:10.1080/00268976.2017.1333644
71. Levandowski, B. J.; Houk, K. N. *J. Org. Chem.* **2015,** *80,* 3530–3537. doi:10.1021/acs.joc.5b00174
72. Opoku, E.; Tia, R.; Adei, E. *J. Phys. Org. Chem.* **2019,** *32,* e3992. doi:10.1002/poc.3992
73. McQuarrie, D. A.; Simon, J. D. *Physical chemistry: a molecular approach;* Sterling Publishing Company, Inc.: New York, NY, USA, 1997.
74. Eyring, H. *J. Chem. Phys.* **1935,** *3,* 107–115. doi:10.1063/1.1749604
75. Mardirossian, N.; Head-Gordon, M. *J. Chem. Theory Comput.* **2016,** *12,* 4303–4325. doi:10.1021/acs.jctc.6b00637
76. Fringuelli, F.; Taticchi, A. *Dienes in the Diels–Alder reaction;* John Wiley & Sons: Chichester, UK, 1990; p 179.
77. Chang, R. *Physical Chemistry for the Biosciences;* University Science Books: USA, 2005; pp 338–342.
78. Cadogan, J. I. G.; Cameron, D. K.; Gosney, I.; Millar, J. R. A.; Newlands, S. F.; Reed, D. *J. Chem. Soc., Perkin Trans. 2* **1996,** 2309–2317. doi:10.1039/p29960002309
79. Afarinkia, K.; Mahmood, F. *Tetrahedron Lett.* **2000,** *41,* 1287–1290. doi:10.1016/s0040-4039(99)02270-4
80. Lorenzo, J.; Delgado, A.; Montaña, Á. M.; Mesas, J. M.; Alegre, M.-T.; Rodríguez, M. d. C.; Avilés, F.-X. *Eur. J. Med. Chem.* **2014,** *83,* 374–388. doi:10.1016/j.ejmech.2014.06.042
81. Kiss, L.; Nonn, M.; Sillanpää, R.; Haukka, M.; Fustero, S.; Fülöp, F. *Chem. – Asian J.* **2016,** *11,* 3376–3381. doi:10.1002/asia.201601046
82. Das, M.; Du, Y.; Ribeiro, O.; Hariharan, P.; Mortensen, J. S.; Patra, D.; Skiniotis, G.; Loland, C. J.; Guan, L.; Kobilka, B. K.; Byrne, B.; Chae, P. S. *J. Am. Chem. Soc.* **2017,** *139,* 3072–3081. doi:10.1021/jacs.6b11997

License and Terms

This is an Open Access article under the terms of the Creative Commons Attribution License (https://creativecommons.org/licenses/by/4.0). Please note that the reuse, redistribution and reproduction in particular requires that the author(s) and source are credited and that individual graphics may be subject to special legal provisions.

The license is subject to the *Beilstein Journal of Organic Chemistry* terms and conditions: (https://www.beilstein-journals.org/bjoc/terms)

The definitive version of this article is the electronic one which can be found at: https://doi.org/10.3762/bjoc.17.27

BEILSTEIN JOURNAL OF ORGANIC CHEMISTRY

^{19}F NMR as a tool in chemical biology

Diana Gimenez[‡1], Aoife Phelan[‡2], Cormac D. Murphy[*2] and Steven L. Cobb[*1]

Review

Open Access

Address:
[1]Department of Chemistry, Durham University, South Road, Durham, DH13LE, UK and [2]UCD School of Biomolecular and Biomedical Science, University College Dublin, Belfield, Dublin 4, Ireland

Email:
Cormac D. Murphy[*] - cormac.d.murphy@ucd.ie;
Steven L. Cobb[*] - s.l.cobb@durham.ac.uk

* Corresponding author ‡ Equal contributors

Keywords:
biotransformation; chemical biology; fluorine; ^{19}F NMR; probes; protein structure

Beilstein J. Org. Chem. **2021,** *17,* 293–318.
https://doi.org/10.3762/bjoc.17.28

Received: 21 October 2020
Accepted: 07 January 2021
Published: 28 January 2021

This article is part of the thematic issue "Organo-fluorine chemistry V".

Guest Editor: D. O'Hagan

© 2021 Gimenez et al.; licensee Beilstein-Institut.
License and terms: see end of document.

Abstract

We previously reviewed the use of ^{19}F NMR in the broad field of chemical biology [Cobb, S. L.; Murphy, C. D. *J. Fluorine Chem.* **2009,** *130,* 132–140] and present here a summary of the literature from the last decade that has the technique as the central method of analysis. The topics covered include the synthesis of new fluorinated probes and their incorporation into macromolecules, the application of ^{19}F NMR to monitor protein–protein interactions, protein–ligand interactions, physiologically relevant ions and in the structural analysis of proteins and nucleic acids. The continued relevance of the technique to investigate biosynthesis and biodegradation of fluorinated organic compounds is also described.

Introduction

Although fluorine is abundant in the environment, it is not a nutrient nor is it a feature of biochemistry for most species [1]. This reflects its low bioavailability, as it is typically found in insoluble minerals, and its physicochemical properties, in particular its high redox potential and the poor reactivity of the fluoride ion in aqueous solution. Despite its near-absence in biology, it is a particularly important element in the broader space of chemical biology [2]. Many commercial and industrial compounds are fluorinated, including refrigerants, degreasers, drugs, pesticides and anti-stick materials, and consequently there is a high degree of interaction between fluorinated compounds and nature [3]. Furthermore, owing to the lack of naturally-occurring fluorinated compounds, fluorine is a useful probe to investigate structure and mechanism of biological molecules. Central to these studies is fluorine-19 nuclear magnetic resonance spectroscopy (^{19}F NMR), which allows the user to readily visualize changes in chemical shift and splitting pattern depending on the changes of the (biological) environment, without substantial purification or processing of samples. In 2009 we published a review describing the application of ^{19}F NMR in chemical biology [4] and here we present the advances that have been made in this field since then.

Review

Structural analysis of macromolecules using ^{19}F NMR

In order to elucidate their various functions, it is essential to have a detailed understanding of both the structure of biological molecules and the way in which they interact in their envi-

ronment and with one another. With regards to probing both the structure and the interactions between biomolecules in complex settings the analytical tool ^{19}F NMR has become invaluable. Some key highlights of how ^{19}F NMR has been employed in this area are given in the following section.

Recent advances in protein ^{19}F labelling

^{19}F NMR offers an attractive option for investigating the interactions between proteins and other biomolecules such as nucleic acids. Many of the advantages of ^{19}F NMR have already been discussed but it is worth highlighting that it is a particularly useful technique to study large proteins that cannot easily be probed by conventional NMR experiments. Given that fluorine atoms (e.g., ^{19}F labels) are not naturally present in proteins, a key element to establishing ^{19}F NMR in this area has been the development of methods that can be used to give access to ^{19}F-labelled proteins.

Methods for the introduction of unnatural amino acids into proteins have been reviewed extensively elsewhere [5-7] and here we will only discuss the most recent advances. The chemical structures of a selection of ^{19}F-labelled amino acid analogues that have been utilized in ^{19}F NMR studies in chemical biology are shown in Figure 1. In general, relatively small monofluorinated amino acids such as **1**–**4**, can be biosynthetically incorporated directly into proteins by including the fluorinated amino

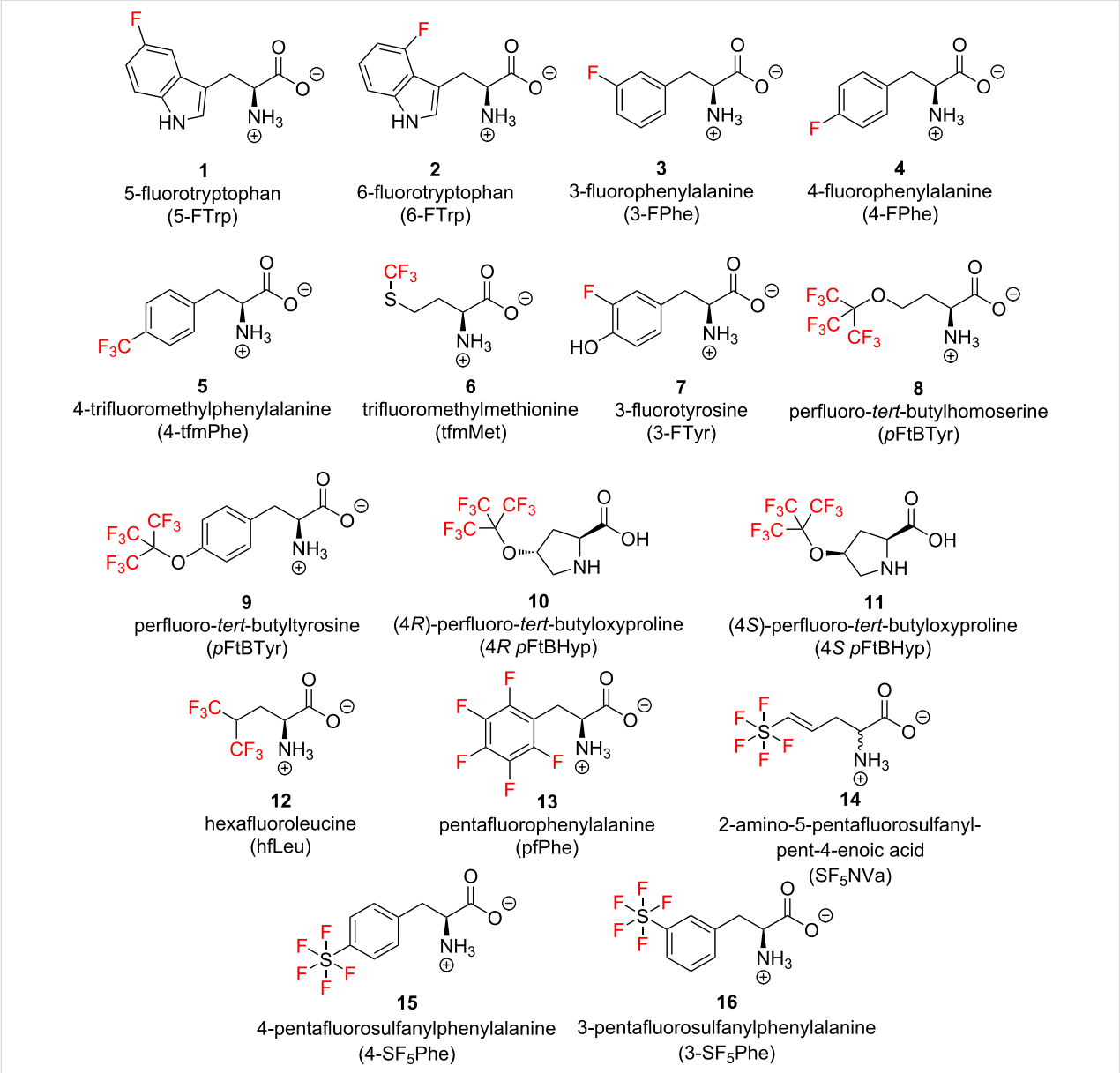

Figure 1: Selected examples of ^{19}F-labelled amino acid analogues used as probes in chemical biology.

acid in the growth medium of a suitable auxotrophic bacterium [8]. However, a challenge when producing ^{19}F-labelled proteins using this technique is that the natural amino acid translation process incorporates the specific fluorinated analogue in all the locations where the original amino acid was present, resulting in a "global" labelling of the protein. This can result in a variety of unwanted side effects, including, in some cases, structure disruption and possible ^{19}F NMR spectral overcrowding [9]. To achieve controlled site-specific amino acid incorporation the methodology pioneered by Schultz et al. [10] is often employed. Here orthogonal amber suppressor tRNA with a paired tRNA synthetase enables the introduction of a broader variety of ^{19}F-labelled acids at single site-specific positions. However, while these systems can be highly precise for certain proteins, the expression yields are strongly context dependent and can lead to poor levels of fluorinated amino acid incorporation [11,12]. To overcome this issue, Otting and co-workers have recently developed a synthetic strategy, based on a continuous exchange cell-free system (CECF), in which a key chitin-binding mutant of release factor RF1 can be removed under conditions that maintain the full activity of the S30 extract, thereby minimizing the incidence of premature translation termination and improving the expression yields by suppressing the production of truncated proteins [13]. This strategy has proven efficient for the site-specific incorporation of up to four trifluoromethylphenylalanines (**5**, Figure 1) within West Nile virus NS2B-NS3 protease (WNVpro) and for the incorporation of 5-fluorotryptophan (**1**) and 6-fluorotryptophan (**2**) in streptavidin [14].

Parallel to the development of these new strategies for recombinant fluorinated protein production, significant efforts have been made within the last decade to expand the pool of available amino acids that can be used as ^{19}F NMR reporters. Aromatic amino acids have been preferentially used as ^{19}F NMR probes both in binding and in conformational studies owing to their ready availability. However, more recently fluoro-aliphatic, and in particular perfluoro-aliphatic amino acids, have become increasingly prominent in ^{19}F NMR studies owing to their improved spectral properties. Among the first perfluorinated amino acids to be reported was perfluoro-*tert*-butylhomoserine (**8**), which was synthesized by Marsh and co-workers and incorporated into a variety of antimicrobial peptides, including MSI-78, for their NMR study on lipid bicelles (Figure 2) [15]. In contrast to more traditional amino acids, such as **1**–**4**, the perfluorinated *tert*-butyl moiety in **8** has nine equivalent fluorine atoms and no coupled hydrogens, so it gives rise to a characteristic high intensity ^{19}F NMR singlet. As shown by the authors, all peptides where **8** was introduced could be detected even at concentrations as low as 5 μM, demonstrating that *p*FtBSer is a highly sensitive tool to study binding events by way of ^{19}F NMR chemical shift and nuclear relaxation changes.

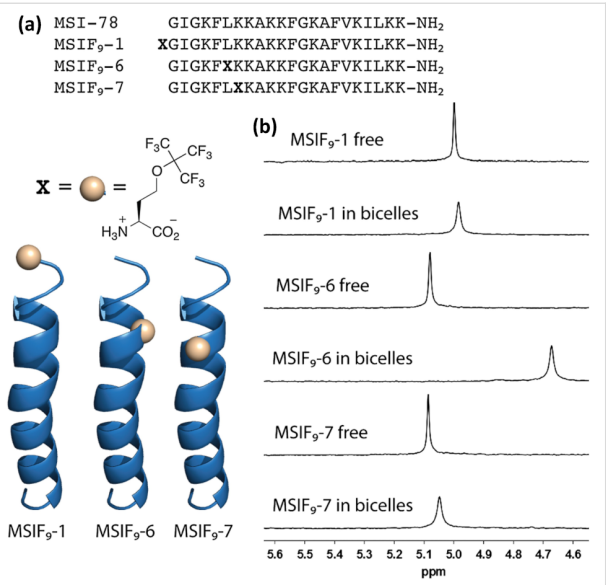

Figure 2: (a) Sequences of the antimicrobial peptide MSI-78 and *p*FtBSer-containing analogs and cartoon representations illustrating the helical location of *p*FtBSer residues. (b) ^{19}F NMR spectra showing the changes associated with MSIF9-1, MSIF9-6 and MSIF9-7 upon binding to bicelles. Figure 2 is adapted from [15]. Copyright © 2013 European Peptide Society and John Wiley & Sons, Ltd. Used with permission from Benjamin C. Buer et al., "Perfluoro-*tert*-butyl-homoserine as a sensitive ^{19}F NMR reporter for peptide–membrane interactions in solution", Journal of Peptide Science, John Wiley and Sons.

In addition to homoserine, perfluorinated analogues of both tyrosine [16] (*p*FtBTyr, **9**) and proline [17] (4*R* and 4*S*-*p*FtBHyp, **10** and **11**, Figure 1) have also been utilised as ^{19}F NMR probes, both showing promise as valuable tools for biomolecular studies. Particularly impressive is that by incorporating *p*FtBTyr (**9**) into a model peptide, Tressler and Zondlo were able to detect the presence of a sharp singlet in the ^{19}F NMR spectrum even at nanomolar peptide concentrations. It is worth noting here that, as recently reviewed in detail by Koksch [18,19], while some perfluorinated amino acids such as hexafluoroleucine (**12**, Figure 1) and pentafluorophenylalanine (**13**, Figure 1) might exhibit, in general, low α-helix propensities, others such as **8** have been found to promote significant levels of α-helix formation [15]. This specific conformational propensity seen in **8** allowed, for example, for its non-disruptive incorporation into the α-helical motif of several estrogen receptor (ER) co-activator peptides and enabled the sensitive detection of their protein–peptide interaction inhibition by the ER antagonist tamoxifen [20]. Significantly, different secondary structure conformational preferences were also found among the diastereomers of perfluoro-*tert*-butyloxyproline, with the 4*R* analogue exhibiting a higher propensity for the polypro-

line helix structure than the 4*S* [17]. This differentiated conformational bias observed highlights the potential application of these amino acids as unique probes for molecular recognition studies.

The synthesis of unnatural amino acids carrying novel fluorine-based functionalities such as -SF_5 has also recently achieved considerable interest. For instance, the work carried out within the Welch group, who reported the synthesis and NMR conformational characterization of the first heptapeptide containing a pentafluorosulfanylated aliphatic amino acid, (*E*)-2-amino-5-(pentafluorosulfanyl)pent-4-enoic acid (**14**, Figure 1), SF_5NVa [21]. Most recently, Cobb et al. [22] reported the synthesis of several pentafluorosulfanyl phenylalanine derivatives with suitable protecting groups to allow incorporation into peptides through common solid-phase peptide synthesis (SPPS) methods (**15** and **16**, Figure 1).

A second well-established methodology for the ^{19}F isotopic labelling of protein and peptides involves the post-translational chemical conjugation of an ^{19}F probe to specific amino acids present within the protein, typically cysteine and lysine residues. This approach is attractive as it can be directly applied to isotopically enrich unlabelled proteins, which may have been obtained previously from natural sources or as recombinant proteins under less demanding cell growth conditions. As shown in

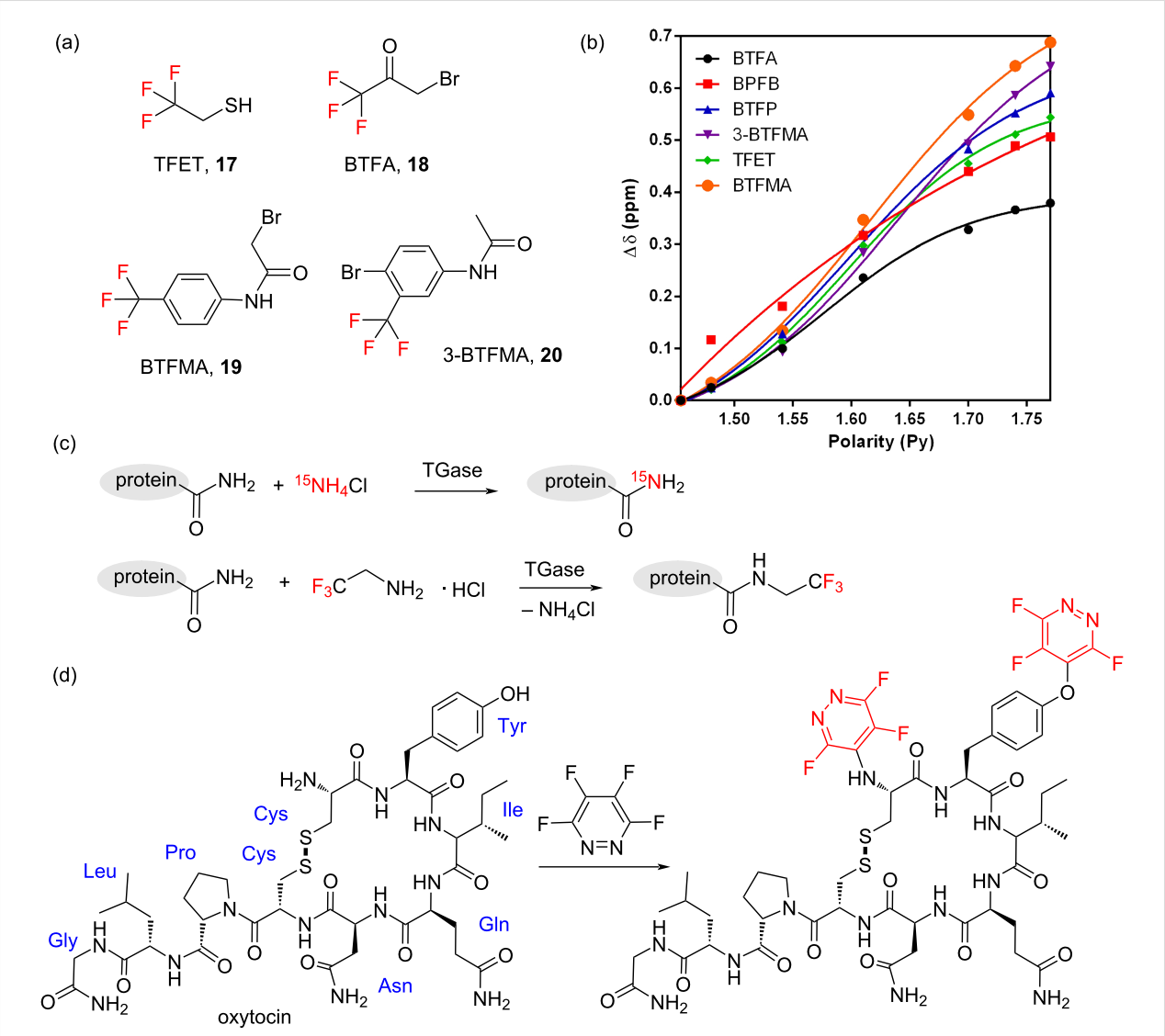

Figure 3: (a) Chemical structures of a selection of trifluoromethyl tags. (b) Comparative analysis showing the changes in ^{19}F chemical shift (Δδ) of various CF_3 tags as a function of solvent polarity. (c) Schematics showing the enzymatic isotope labelling of glutamine γ-carboxamide groups using transglutaminase (TGase) and ^{15}N-ammnonium chloride ($^{15}NH_4Cl$) or ^{19}F-2,2,2-trifluoroethylamine hydrochloride (TFEA-HCl). (d) Example of a cyclic peptide hormone, oxytocin, and its perfluoropyridazine "tagged" analogue. Figure 3b was adapted from [28]; Figure 3d was reprinted from [30].

Figure 3, these fluorine tags consist, in general, of reactive trifluoromethyl derivatives such as 2,2,2-trifluoroethanethiol (TFET, **17**) [23], 3-bromo-1,1,1-trifluoroacetone (BTFA, **18**) [24] and fluorinated haloacetamides [25] that can react with nucleophilic side chains on the protein of interest. This approach has been extensively applied to study both soluble proteins [26] and membrane proteins [27]. Fluorine tags such at TFET (**17**) or BFTA (**18**) offer a good degree of sensitive and narrow ^{19}F NMR line widths due to rapid rotation about the trifluoromethyl symmetry axis. Thus, they are very effective tools when studying small conformational changes in proteins and other real-time events, even if relatively low concentrations are employed. In addition, these fluorine tags have proven to be sensitive to very subtle changes in their environment, providing further local-site specific conformational information [28]. Recent advances in this area include the tags based on fluorinated phenylacetamides, such as the 2-bromo-*N*-(4-(trifluoromethyl)phenyl)acetamide (BTFMA, **19**) and *N*-(4-bromo-3-(trifluoromethyl)phenyl)acetamide (3-BTFMA, **20**) developed by Manglik et al. to study the structural dynamics of the cytoplasmic domain of the β2-adrenergic receptor (β2AR) [29]. In this work conjugation of the CF_3 group to an aromatic ring was shown to give rise to substantially improved ^{19}F NMR chemical shift sensitivities over the more traditional thiol-specific trifluoromethyl tags (Figure 3b) [28].

In addition to chemical modification, novel methodologies are being investigated that enable the enzymatic post-translational modification of non-nucleophilic residues, such as glutamate [31]. As recently demonstrated by Kojima and co-workers, recombinant protein transglutaminase (TGase) could be used to catalyse the chemical replacement of the γ-carboxyamide groups in Glu residues by free 2,2,2-trifluoroethylamine (TFEA-HCl) in model binding protein FKB12. This resulted in the site-specific incorporation of CF_3CH_2- motifs into these amino acids (Figure 3c). This ^{19}F-labelling strategy clearly offers new opportunities in the area as it can be easily combined with the aforementioned chemical approaches based on cysteine and lysine modification.

It is worth noting that for small proteins and peptides the chemical incorporation of the desired fluorinated amino acids using SPPS protocols still remains the method of choice, as it enables the site-specific introduction of the ^{19}F NMR probe. In addition, SPPS offers a powerful technique to access uniquely labelled peptides and proteins when combined with new strategies for peptide stapling and tagging using perfluoroaromatic reagents. Perfluorophenyl, perfluoropyridyl and perfluoropyridazinyl labelled peptides can now all be accessed, expanding even further the tool-box of ^{19}F NMR probes available for protein studies (Figure 3d) [30,32].

Protein-observed binding interactions

^{19}F NMR is a valuable analytical tool to study the binding interactions between a variety of biological substrates and ^{19}F-labelled proteins. It has also become a widely adopted method for ligand screening, enabling the evaluation of small molecule–protein interactions over a wide range of affinities. In protein-observed fluorine NMR experiments (PrOF) binding events can be readily monitored using simple 1D techniques, and the dissociation binding constant of ligands (K_d) determined from the changes in the chemical shift of the labelled nuclei within the protein. Intuitively, the largest chemical shift perturbations are expected to be seen for residues in the closest proximity to the bound ligand. An additional advantage of this method is that signal acquisition in these experiments is typically rapid, as large signal-to-noise ratios are not needed to obtain precise indication of the positive presence of binding interactions [33].

Pomerantz and co-workers analysed the difference in NMR chemical shift perturbations for the ^{1}H-(NH) and ^{19}F nuclei in native tryptophan, and 5-FTrp-labelled bromodomain protein Brd4 against a panel of ligands (Figure 4) [34]. ^{1}H NMR was found to be 6–20 times less responsive than fluorine with regards to chemical shift perturbations. Indeed, the high resolution observed in the fluorine spectra enabled the direct calculation of most of the ligand binding constants. The superior capacity of ^{19}F NMR to monitor binding events was also noted by Richards et al., when studying the interaction of human protein disulphide isomerase (hPDI) to Δ-somastatin [35]. In this work there was improved precision in the analysis of the dissociation constants due to the higher spectrum resolution and greater chemical environment sensitivity of the ^{19}F nuclei when compared to that offered by the ^{15}N.

Due to the fact that different regions of a protein give rise to unique NMR resonances, protein-observed experiments using multi-site labelled proteins can be used to provide information on changes in the chemical environment of the protein surface, which can be used to characterize binding-sites and/or conformational changes upon binding. For example, ^{19}F NMR studies on cysteine-labelled ß2-adrenergic receptor (β2AR) using either a ^{19}F-BTFA [29] or a ^{19}F-TFET [36] tag were used to explore the differential long range conformational effects induced by agonists, inverse agonists, and partial agonists on GPCR signalling. As exemplified by Liu et al. [36], in the case of multiply site-specific labelled ^{19}F-TFET-β2AR, changes in the NMR signals monitored within different helices of the protein revealed that agonist binding primarily shifted the equilibrium towards the G protein-specific active state of helix VI. In contrast, β-arrestin-biased ligands predominantly affected the conformation of specifically helix VII,

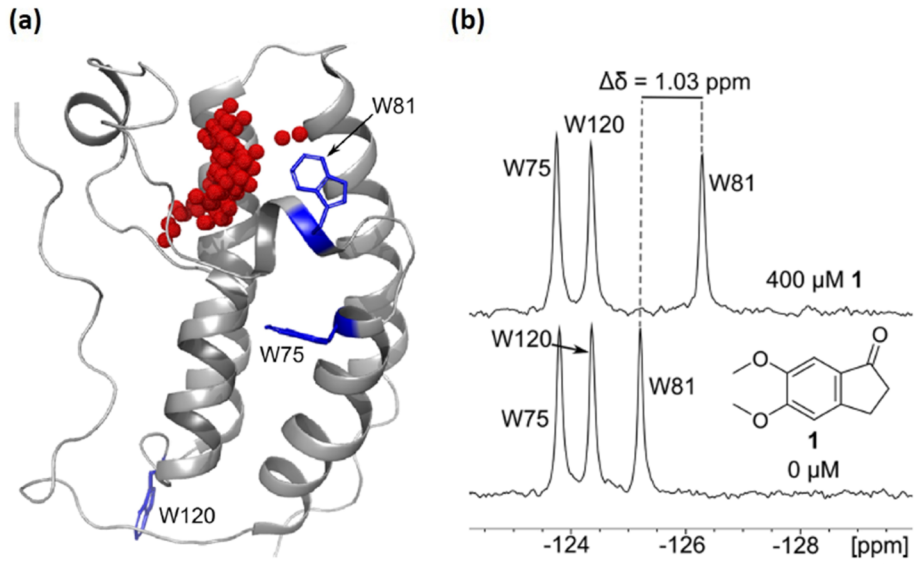

Figure 4: (a) First bromodomain of Brd4 with all three tryptophan residues displayed in blue and labelled by residue number. Red spheres indicate the acetylated lysine binding site (generated by SiteMap). PDB ID: 3UVW. (b) PrOF NMR spectrum of 5-FTrp-Brd4 and a selected ligand. In the presence of the ligand, the resonance for W81 is significantly shifted upfield consistent with binding near the acetylated lysine interaction site of Brd4. Adapted with permission from [34]. © 2016 American Chemical Society.

providing thus insights into the structural plasticity of β2AR receptor.

By taking a novel approach to the use of PrOF NMR, Stadmiller et al. have recently developed a pioneering methodology based on 1D ^{19}F NMR line shape analysis that can be utilized to simultaneously determine both thermodynamic equilibrium binding constants (K) and kinetic rates of association (k_{on}) and dissociation (k_{off}) in protein–ligand binding events [37]. In order to achieve this, they analysed the binding of four different proline-rich peptides to a 5-FTrp-labelled Src homology 3 (SH3) recognition protein domain. By comparing the results obtained using both, the newly proposed ^{19}F NMR-based analysis and the traditional 2D ^{15}N,^{1}H-HSQC experiments they could demonstrate that simple ^{19}F NMR line shape analysis achieved comparable high quantitative accuracy in the determination of all binding parameters. In addition, qualitative residue-specific information was also provided, but with a much improved and straightforward post-acquisition analysis procedure. It is clear that this more user-friendly methodology has the potential to have a significant impact in future studies of protein–ligand interactions, protein folding, and potentially small-molecule library screening, as it can broaden the accessibility of quantitative NMR spectroscopy to a wider range of laboratories.

Ligand-observed protein binding interactions

In addition to protein-observed fluorine (PrOF) NMR spectroscopy, ligand-observed fluorine NMR spectroscopy for drug screening has also evolved in the last decade to become a key tool to study the binding of drug candidates to target proteins. ^{19}F NMR-based screening, which was developed by Dalvit et al., includes fluorine chemical shift anisotropy and exchange for screening (FAXS) [38] which is a binding assay, and fluorine atoms for biochemical screening (*n*-FABS) methodology which is a functional assay [39,40]. Both of these methods have been successfully used for ligand-based screening, fragment-based functional screening and dynamic library screening, and have been recently reviewed in detail by Dalvit and Vulpetti [41,42]. The main advantages of these methods for lead compound screening is that they offer a platform not only for the rapid high-throughput screening of multiple protein small ligands, but also for the direct screening of functional inhibitors of much larger and complex biomolecules, such as enzymes.

In a recent study exemplifying this application, ^{19}F NMR has been employed to investigate the metabolism of carnitine. In animals, carnitine is biosynthesised from trimethyllysine in four enzyme-catalysed steps, which involves in the last step the action of the γ-butyrobetaine hydroxylase enzyme (hBBOX) (Figure 5a–c). As the fluorine shift of the metabolised product is distinctively different from the shift of the precursor, by producing a novel fluoromethyl analogue of the γ-butyrobetaine substrate (GBBNF) Rydzik et al. were able to monitor carnitine biosynthesis through hBBOX-catalysed GBBNF hydroxylation, both in vitro and in cell lysates [43]. Moreover, by using a competitive substrate for the enzyme, inhibition experiments

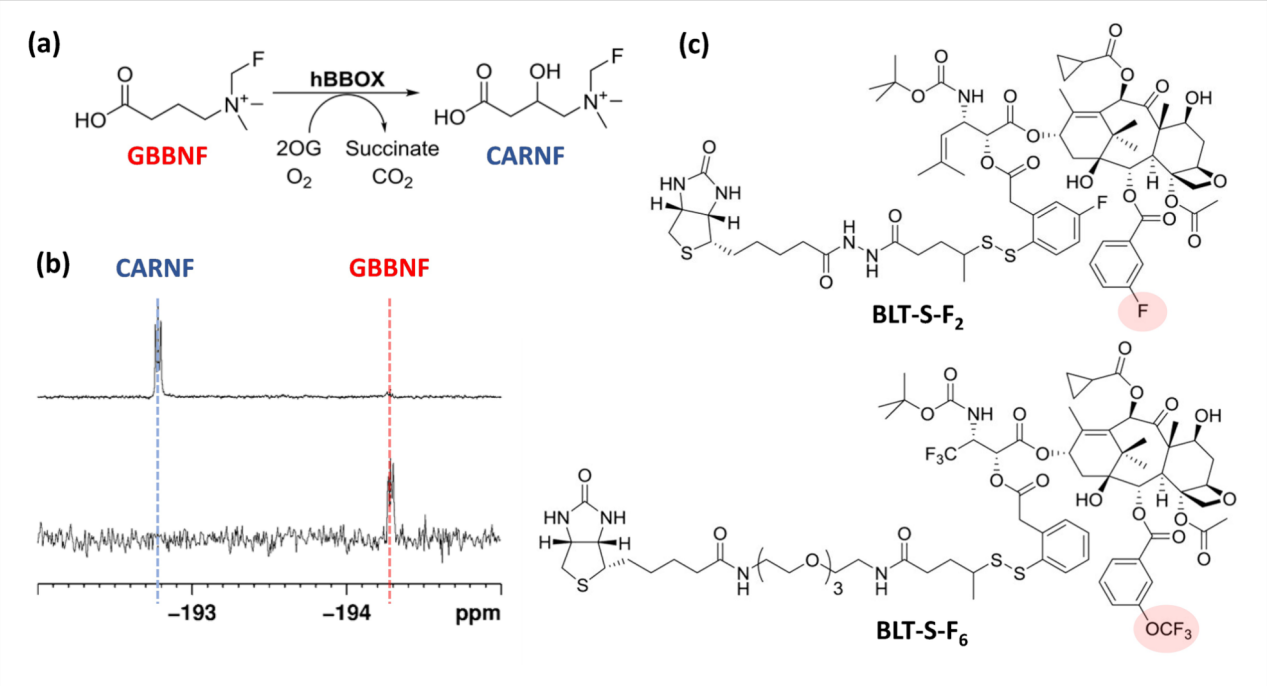

Figure 5: (a) Enzymatic hydroxylation of GBBNF in the presence of hBBOX (b) ^{19}F NMR spectra showing the conversion of GBBNF to CARNF by psBBOX. (c) Chemical structure of BLT-F2 and BLT-S-F6. Figure 5a and Figure 5b were reproduced and adapted from [43], Figure 5c was reproduced from [44].

could be directly employed to determine the IC_{50} values in the basis of fluoride release, and the extent of GBBNF turnover investigated in the presence of cell extracts.

Ojima and collaborators have also employed functional ligand-observed NMR experiments to develop a range of novel 3′-difluorovinyltaxoids, such as BLT-F2 and BLT-S-F6 (Figure 5c), that are active against drug-sensitive and multidrug-resistant (MDR) human cancer cell lines [44]. Here, the incorporation of CF_3 and CF_3O groups as NMR reporters into the tumour-targeting drug conjugates enabled the direct investigation of the mechanism of the pro-drug metabolic cleavage and the pharmacophore release by real-time ^{19}F NMR analysis. ^{19}F NMR was also employed as a convenient technique to study a range of factors that might influence the plasma and metabolic stability of the lead compounds, proving itself as a valuable alternative to more challenging conventional HPLC or ^{1}H NMR analyses.

It is also worth noting that recent investigations within the Dalvit group have further expanded the applications of *n*-FABS into the screening and direct IC_{50} measurement of bioactive substrates within intact living cells [45]. By studying mammalian cells expressing the membrane protein fatty acid amide hydrolase (FAAH), they showed that it is possible to screen and identify target inhibitors in situ using ^{19}F NMR spectroscopy (Figure 6). For this, the activity of the membrane-bound FAAH enzyme was evaluated by monitoring the hydrolysis of a fluorinated anandamide analogue ARN1203, a previously reported FAAH substrate, to arachidonic acid and 1-amino-3-fluoropropanol in the presence and absence of a broad range of known FAAH inhibitors with widely different potencies. The results clearly showed that the proposed *n*-FABS method was successful in detecting strong inhibitors of FAAH activity in cells. Also, it allowed the accurate quantification of the corresponding IC_{50} values, all of which were consistent with those obtained in previous work but measured in cell membrane extracts [46].

Structural analysis of macromolecules using ^{19}F NMR

The three-dimensional (3D) structure of biomacromolecules and their conformational dynamics are often the starting point for the development of an in-depth understanding of their function and mode of action. Owing to the large size of biomacromolecules, the high complexity of the processes in which they participate and the natural environment in which they occur, an integrated analytical approach is often required to succeed in revealing their functional architecture. Such an approach typically includes the use of a variety of high-resolution proteomic tools, cryo-electron microscopy and X-ray crystallography to achieve full molecular characterization at the atomic level. However, macromolecules such as DNA/RNA and proteins are not static entities, for which also complementary dynamic and

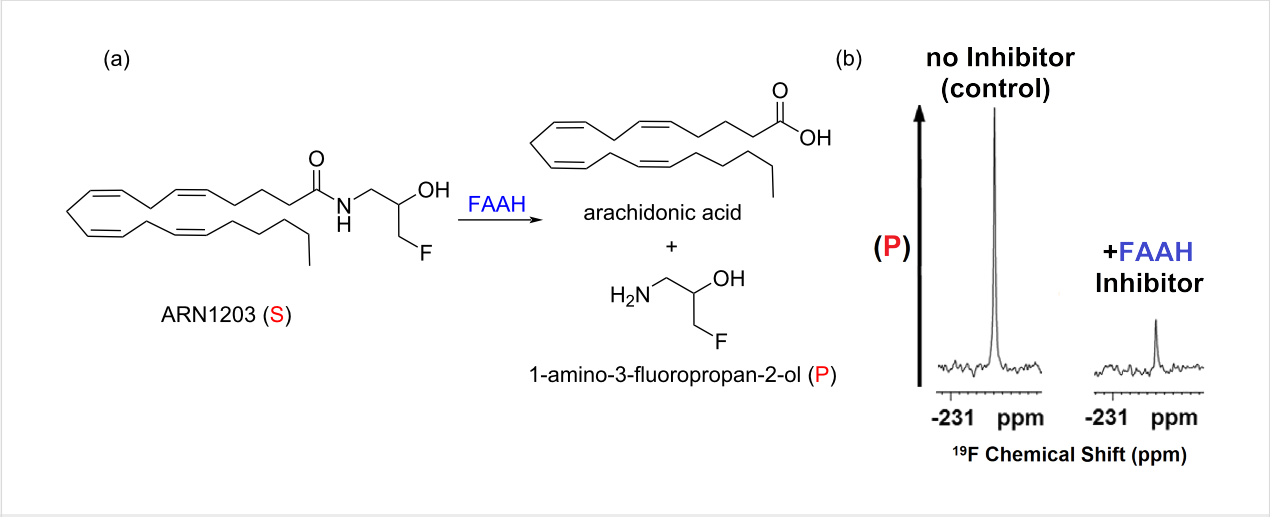

Figure 6: (a) In-cell enzymatic hydrolysis of the fluorinated anandamide analogue ARN1203 catalyzed by hFAAH. Only the fluorinated substrate and the 1-amino-3-fluoropropan-2-ol product are detected in the ^{19}F NMR spectra. (b) ^{19}F NMR spectra of ARN1203 incubated for 2.5 h in hFAAHeHEK293 intact cells in the presence and absence of an hFAAH activity inhibitor. Figure 6b was reproduced and adapted from [45].

targeted local site-specific conformational information is needed to fulfil our understanding on how these assemblies perform their biological role and function in vivo. It is in this regard that ^{19}F NMR has proven to be a valuable analytical tool, providing simultaneous access to both structural and dynamic information that would be difficult to obtain using traditional ^{13}C, ^{1}H and ^{15}N,^{1}H-HSQC NMR techniques.

Protein folding

From the late 1960s and early 1970s ^{19}F NMR has firmly established itself as a highly versatile and powerful analytical tool for studying both protein structure and conformational changes within proteins [47]. For additional information on the development of the field of ^{19}F NMR protein studies readers are encouraged to consult the excellent earlier reviews written by Gerig [48] and Danielson and Falke [49].

However, over the last 20 years the application of ^{19}F NMR in this area has shifted from the mere study of proteins and peptides as static entities, to the detailed analysis of the much more sophisticated protein transient conformational states that are produced upon substrate interaction, folding or binding. Thus, it is possible to accurately track the complete chain of events that take place within the molecule upon interaction and/or folding. Given that the intermediates involved in protein folding and binding are difficult to observe owing to the short-lived nature of the states and their marginal concentration, high sensitivity ^{19}F NMR has been employed to offer unique opportunities for their sampling and characterization in situ [50].

Prosser et al. demonstrated the utility of this approach when employing a combination of variable temperature (VT) ^{19}F NMR analysis and CD spectroscopy to study the near-native thermal folding intermediate structure of calmodulin (CAM) (Figure 7) [51]. To this end, CAM was biosynthetically enriched with 3-fluorophenylalanine (3-FPhe) and the ^{19}F NMR signals corresponding to each one of the eight 3-FPhe residues present resolved and assigned in the spectra for the native state. Changes in the ^{19}F NMR signals produced upon increasing the temperature were then used to map the evolution of the protein along the heat-induced denaturalization curve and to confirm the presence of an intermediate transient structure at 67 °C. Notably, single Lorentzian lines were observed for all 3F-Phe labelled sites regardless of the temperature employed, signifying either a single state at low temperatures or fast exchange between the native and near-native states at higher temperatures (40–70 °C). The NMR data obtained also provided evidence of the rapid ring flipping of the 3-FPhe probes, inherent to the side-chain dynamics within the protein hydrophobic interior [52-54]. ^{19}F NMR has also been used to characterize in more detail the topography of the CAM conformational changes by using molecular contrast agents. ^{19}F NMR solvent-induced isotope shift experiments, resulting from replacement of H_2O with D_2O, provide a robust measure of the relative degree that a specific labelled position is exposed to the solvent [55]. Complementary to this technique, the use of dissolved O_2 as a paramagnetic agent, having a relatively short electronic relaxation time, gives rise to paramagnetic shifts and spin–lattice relaxation rate enhancements that can be directly correlated with its accessibility to the ^{19}F-spin of interest [55,56]. This way, the combined ratio derived from both experiments was employed as a convenient measure of the solvent exposure and local hydrophobicity changes experienced at each individual fluorinated residue upon heating. Ultimately, ^{19}F NMR enables profiling of

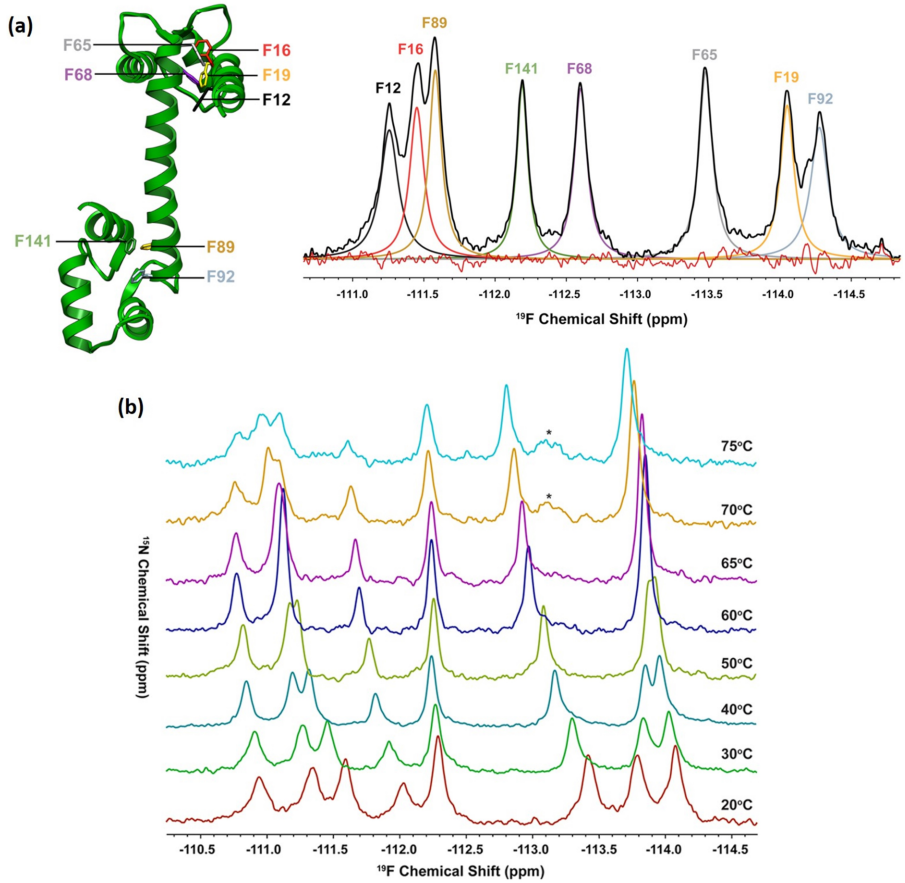

Figure 7: (a) X-ray crystal structure of CAM highlighting the location the phenylalanine residues replaced by 3-FPhe and the corresponding deconvoluted ^{19}F NMR spectrum of the fractionally labelled peptide (PDB file 3CLN). (b) ^{19}F NMR spectra of 70% 3-FPhe fractionally labelled CAM as a function of temperature. Adapted with permission from [51]. © 2013 American Chemical Society.

the specific position and nature of the conformational perturbations that the protein undergoes as it progresses from its native state along the heat-denaturation pathway [51,57].

In a much broader context, ^{19}F NMR paramagnetic relaxation enhancement experiments (PREs), have been shown to constitute a versatile tool for extracting quantitative structural distance information in selectively ^{19}F-labelled proteins. As a proof of concept, Matei et al. [58] demonstrated the applicability of this approach in studying the HIV-inactivating lectin cyanovirin-N protein as a model system (^{S52}CCV-N). Single fluorine atoms were introduced at the 4-, 5-, 6- or 7-positions of Trp49 and the 4-position of Phe4, Phe54, and Phe80 (Figure 8). Simultaneously, the paramagnetic nitroxide spin label was chemically attached to the protein by using two available Cys residues at positions 50 or 52. As the presence of an unpaired electron in the tag increases the nuclear relaxation rates of the residues that are in spatial proximity, it resulted in their spectral signal attenuation. Due to this effect being inversely correlated with the distance between the probes, the transverse ^{19}F-PRE rate (^{19}F-Γ2) was directly employed for the determination of the average distance between the ^{19}F nucleus and the paramagnetic centres, within a range of 12–24 Å. Overall, the work showed the potential applicability of ^{19}F NMR PREs as excellent alternative parameters for the quantitative analysis of site-specific intramolecular distances, with a more particular significant value in the exploration of large proteins and macromolecular complexes where substrate spectral crowding and/or background incompatibility prevents the use of other nuclei such as ^{1}H or ^{15}N PREs.

^{19}F NMR has also been applied to study the conformational heterogeneity and dynamics of a broad range of proteins and peptides upon their interaction with model lipid vesicles [59], micelles [60] and bicelles [61]. It has enabled the quantification and mechanistic characterization of intermolecular dynamic processes such as protein dimerization, oligomerization and fibrillation, even within large and especially complex systems [62,63].

In a recent study, Aramini et al. employed ^{19}F NMR to investigate the conformational dynamics within the interacting inter-

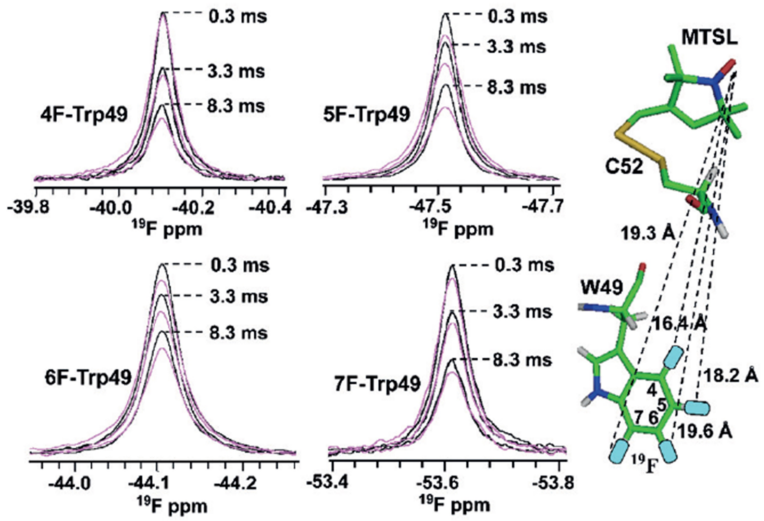

Figure 8: ^{19}F PREs of 4-F, 5-F, 6-F, 7-FTrp49 containing MTSL-modified ^{S52C}CV-N. The ^{19}F NMR resonances of oxidized (magenta) versus reduced (black) 4-F, 5-F, 6-F, and 7-FTrp49 ^{S52C}CV-N are superimposed for 0.3, 3.3, and 8.3 ms relaxation delays. PRE-derived distances are shown by dashed lines on the model. Figure 8 is reproduced from [58]. © 2016 WILEY-VCH Verlag GmbH & Co. KGaA, Weinheim. Used with permission from Elena Matei et al., "^{19}F Paramagnetic Relaxation Enhancement: A Valuable Tool for Distance Measurements in Proteins", *Angew. Chem., Int. Ed.*, John Wiley and Sons.

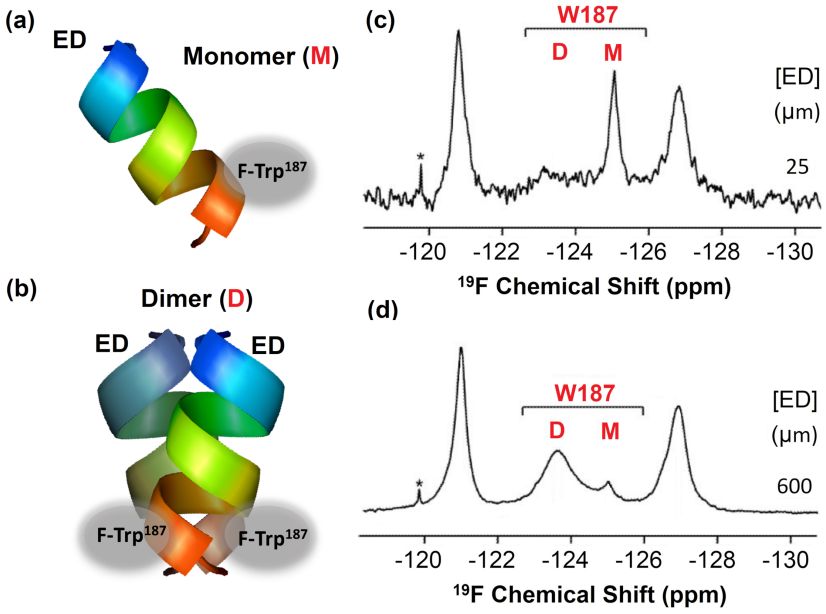

Figure 9: ^{19}F NMR as a direct probe of Ud NS1A ED homodimerization. Schematic representation showing the location of the 5-F-Trp residue in the monomer (a) and dimer (b) structure of Ud NS1A ED domain. (c, d) Concentration dependence of the ^{19}F NMR signal of 5-FTrp187 within Ud NS1A ED in low salt pH 8 buffer. Figure 9 was reproduced and adapted from [64].

face of non-structural protein 1 (NS1A) homodimer (Figure 9) [64]. Protein NS1A is a highly conserved virulence factor from influenza virus (H3N2) comprised of an N-terminal double-stranded RNA (dsRNA)-binding domain (RBD) and a multi-functional C-terminal effector domain (ED), each of which can independently form symmetric homodimers. By labelling NS1A with 5-FTrp at the different sites within the ED, Aramini et al. were able to demonstrate that a specific labelled residue, 5-FTrp187, exhibited indeed a higher degree of ^{19}F NMR line width broadening when compared to the other fluorinated amino acids incorporated upon interaction. These results demonstrated that the site-specific ^{19}F signal of 5-FTrp187

could be directly employed as a reliable reporter to monitor the monomer/dimer exchange dynamics. Moreover, it could also be employed to characterize the ED helix–helix dimer interface in more detail by means of additional 1D ^{19}F T1, T2, and CPMG relaxation dispersion experiments and solvent-induced isotope shift effects. This study also highlighted the particular advantages of employing ^{19}F NMR fluorine probes strategically labelled in the second ring of the Trp indole moiety to directly measure conformational exchange phenomena at protein-protein interfaces mediated by such residues [65].

Correct folding is essential for normal biological function of proteins [66]. The formation and accumulation of misfolded proteins has been shown to be a common pathological feature in a significant number of human disorders, including neurodegenerative Alzheimer's and Parkinson's diseases and several metabolic type II diabetes conditions. So far, the application of real-time NMR to characterize amyloid formation has been very limited [67,68], largely due to the spectral overcrowding of the 1D ^{1}H NMR spectra and the difficulties associated with performing multidimensional experiments at a fast enough rate to follow the aggregation process accurately. Despite these aforementioned challenges the Marsh laboratory has recently demonstrated the utility of ^{19}F NMR to access direct, sensitive and real-time observation of amyloid fibril formation, enabling the elucidation of the underlying mechanics of peptide fibrillation.

To study the aggregation mechanism of the model Aβ-peptide, a well-known amyloidogenic peptide related to Alzheimer's disease, Marsh and collaborators synthesized a ^{19}F-labelled Aβ1−40 peptide version in which methionine at position 35 was replaced by tfmMet (Aβ1−40-tfmMet35) [9,62]. The aggregation process was then monitored by ^{19}F NMR over a period of several weeks [62]. Upon analysis, formation of at least six spectroscopically distinguishable intermediates could be detected during fiber formation (Figure 10). Each independent intermediate was characterized on the basis of its ^{19}F NMR chemical shift and the kinetics by which each species formed or decayed were evaluated in real-time. By combining the ^{19}F NMR data with that provided by complementary analytical techniques, mass spectrometry (electrospray ionization and ion mobility), CD spectroscopy and atomic force microscopy, the authors were able to obtain detailed information about the size and secondary structure associated with some of the soluble intermediates. These included: large β-sheet oligomers formed immediately after solubilization (oligomer O1); a small oligomer that forms transiently during the early stages of the lag phase (oligomer O2) and 4 spectroscopically distinct forms of oligomers that appear during the later stages of aggregation and apparently coexist with the proto-fibrillar species (oligomers O3–O6, Figure 10).

It is worth noting that the ability to follow the formation and decay of multiple intermediate species using a single ^{19}F NMR 1D experiment provides a straightforward route for the comparative analysis of different complex aggregation behaviours. For example, another study by the Marsh group carried out using amyloidogenic tfmPhe-labelled islet amyloid polypeptide hormone (tfmF-IAPP), showed that fibril formation can indeed proceed through well differentiated and distinguishable alternative pathways [69]. In this case, the consumption of ^{19}F-labelled monomeric tfmF-IAPP was monitored in real-time by ^{19}F NMR but significantly no new ^{19}F resonances were produced during the time course of aggregation. This suggests that, unlike what is observed in the case of amyloidogenic Aβ-peptide, no soluble intermediates accumulate in the aggregation pathway of IAPP.

Conformational polymorphism is also particularly important for the infectious amyloid particles known as prions [70] and this area has been recently investigated using a range of ^{19}F NMR

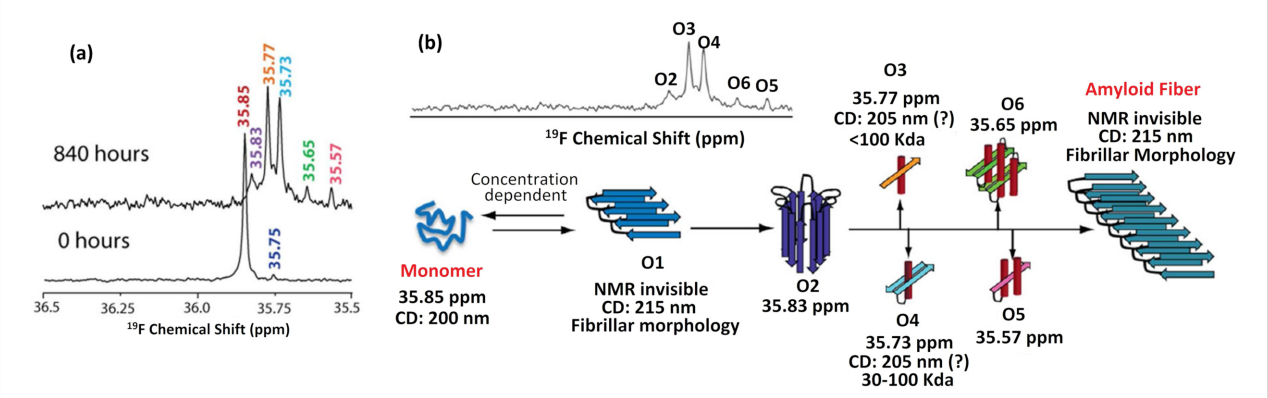

Figure 10: (a) Representative spectrum of a 182 μM sample of Aβ1-40-tfM35 at varying times indicating the major and minor peaks observed upon sample incubation. (b) Scheme describing the proposed aggregation pathway for Aβ1-40-tfM35. Adapted and reprinted with permission from [62]. © 2013 American Chemical Society.

approaches [63]. By selectively introducing 3-FPhe labels into the human prion protein segment PrP(90−231)$_\beta$ via induced auxotrophy [71], Prosser and co-workers have been able to characterize and quantify the relative populations of monomeric, octameric, and higher oligomer species that populate the pathway from the native PrP state to fibril formation. The equilibrium constants between states were also analysed as a function of both temperature and pressure, allowing to determine the enthalpic and entropic contributions to their transitions. In addition, ^{19}F NMR saturation transfer experiments allowed a convenient estimate of the kinetic rates at which the various species interconvert. This study by Prosser et al. nicely illustrates how quantitative and detailed thermodynamic and kinetic information for complex systems can be obtained by ^{19}F NMR.

Another rapidly expanding and particularly challenging area of research where ^{19}F NMR has found new applications is in the field of intrinsically disordered proteins (IDPs). IDPs play a key role in cell signalling and regulation processes and represent a distinct class of proteins that exhibit no stable 3D structure [72]. It is broadly understood that, unlike folded proteins, IDPs exist as an average combination of interconverting conformers. However, when bound to a substrate, IDPs may acquire a defined secondary structure [73]. The innate flexibility of IDPs imposes tremendous technical challenges to standard NMR analysis, as pronounced conformational averaging gives rise to narrow signal dispersion and low signal-to-noise ratios. Indeed, unless more sophisticated NMR techniques are employed, the combination of these two effects prevents the characterization of low-populated and short-lived states that might be critical for the peptide biological function [74].

The Pielak group carried out an early study on the conformational dynamics of the model IDP, α-synuclein (αSyn) using ^{19}F NMR. In this work ^{19}F NMR was employed to study several properties of a specifically 3-FTyr-labelled α-synuclein analogue, including its native conformation and the conformational changes induced by urea, spermine and sodium dodecyl sulfate (SDS) [75]. Subsequently, α-synuclein interaction with SDS micelles and model membranes have also been investigated in detail [59,76], as well as the kinetics of α-Syn oligomerization and fibril formation both in vitro [60,75] and in vivo [77,78]. In these more recent studies, incorporation of 4-tfmF residues using amber-suppressing codons at various positions was shown to be more advantageous as a ^{19}F reporting strategy, owing to the higher sensitivity and improved NMR relaxation properties of the CF_3- group. The results from these studies, summarized in Figure 11, show that while α-Syn remains disordered in solution, it acquires partial helical secondary structure in the presence of SDS and membrane-like environments. Specifically, the N-terminal region of the peptide, which includes the first 4-tfmF-labelled amino acid, was shown to be involved in the most important membrane-binding interactions and conformational changes observed, allowing the protein to adopt a metastable aggregation-prone state that is apt to stabilize further intermolecular interactions and progress to the fibril state. The C-terminus non-amyloid component region, as monitored at position 133, was in comparison found to keep largely dynamically disordered in all species formed. Moreover, results

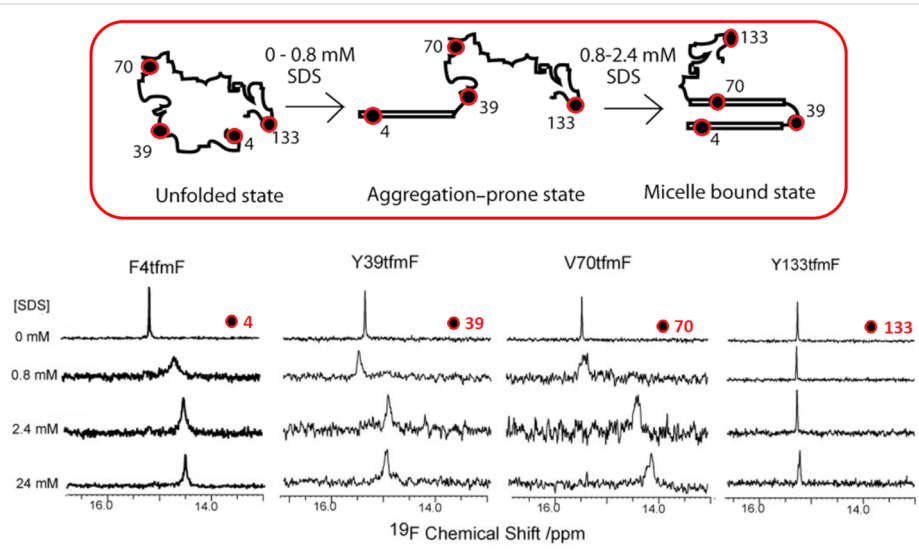

Figure 11: Illustration of the conformational switch induced by SDS in 4-tfmF-labelled α-Syn. Also shown are the ^{19}F NMR spectra of the corresponding 4-tfmF-labelled peptides at positions 4, 39, 70 and 133 in varying concentrations of SDS. Figure 11 is reproduced from [60]. Copyright © 2010 WILEY-VCH Verlag GmbH & Co. KGaA, Weinheim. Used with permission from Gui-Fang Wang et al., "Probing the Micelle-Bound Aggregation-Prone State of α-Synuclein with ^{19}F NMR Spectroscopy", ChemBioChem, John Wiley and Sons.

from these studies revealed that the fibril-forming path of α-Syn might occur without accumulation of soluble low molecular weight intermediates, as no new ^{19}F NMR signals were observed during the time-course of the aggregation process.

^{19}F NMR spectroscopy has also now been employed to analyse the conformational dynamics of IDPs upon tertiary and quaternary complex formation [79]. The Myc-Max heterodimer is a well-known oncogenic transcription factor complex able to bind to enhancer box (E-box) regions (5'-CACGTG-3') of DNA with low-nanomolar affinity, what triggers its biological function as a transcriptional regulator [80]. Previous studies have shown that in the monomeric state the two helical domains of Myc display unstable structural features, similar to those of small IDPs, existing rather as a highly flexible pair of transient α-helices [81]. Based on this, Konrat and co-workers explored a combination of ^{19}F tagging and PRE NMR spectroscopy to probe and trace the conformational changes experienced by disordered Myc upon Myc-Max heterodimerization. Going beyond, they also employed ^{19}F NMR to interrogate the changes induced in the Myc-Max heterodimer structure upon full quaternary complex formation in the presence of DNA, and another intrinsically disordered binding partner, breast cancer antigen 1 (BRCA1) (Figure 12). In this work the strategy employed involved the introduction of a perfluorinated [^{19}F]3,5-bis(trifluoromethyl)benzyl-based tag into the single cysteine residue of Myc. This modification boosted the overall spectral sensitivity even when minimal protein concentrations were employed. The structural dynamics of the Myc-Max dimer formation were then evaluated by using intermolecular PREs between ^{19}F-Myc and three differently paramagnetic spin labelled MTSL ([(1-oxyl-2,2,5,5-tetramethyl-Δ3-pyrroline-3-methyl) methanethiosulfonate]) tagged Max mutants, and novel insights revealed regarding the differential structural dynamics of Myc-Max bound to DNA and the tumour suppressor BRCA1. Given its ease of implementation, future applications of this strategy to new structural biology targets and inhibitor screening can be expected.

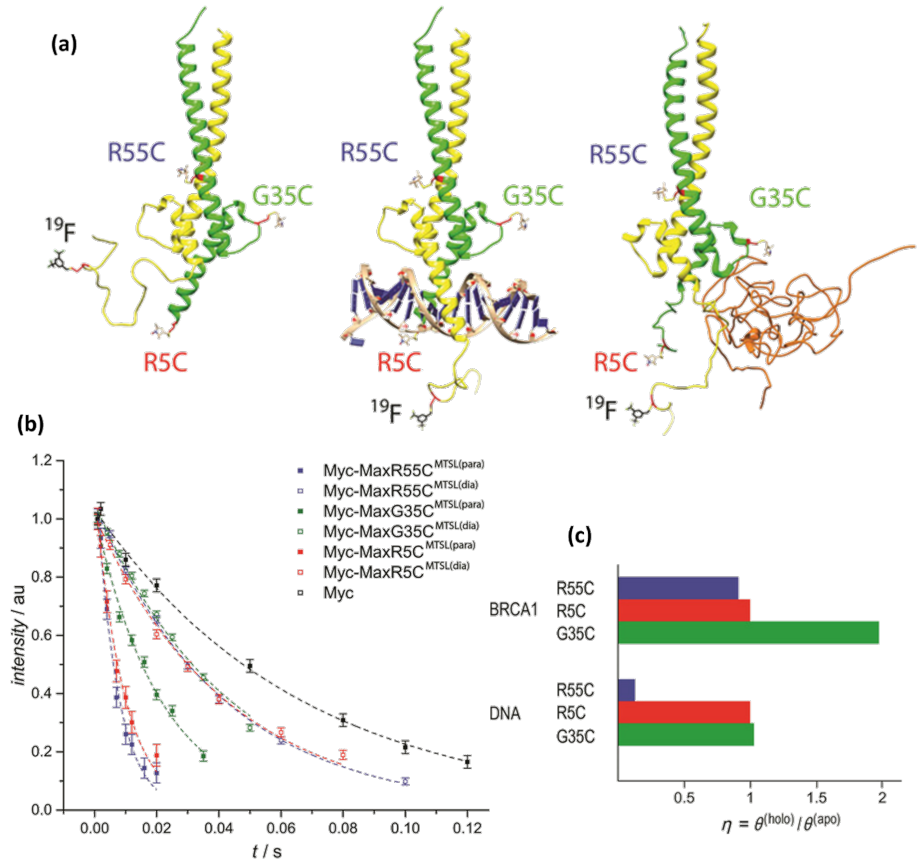

Figure 12: (a) Structural models of the Myc-Max (left), Myc-Max-DNA (middle) and Myc-Max-BRCA1 complexes (right). Myc is shown in yellow, Max in green, BRCA1 in orange. (b) ^{19}F T_2 relaxation curves of tagged ^{CF3}Myc and tagged ^{CF3}Myc in complex with three Max mutants. (c) Relative PRE rates of different ^{CF3}Myc-Max-BRCA1 and ^{CF3}Myc-Max-DNA complexes. η quantifies the relative PRE effects in the Myc complex and monomeric Myc, which was normalized to diamagnetic relaxation rates. Figure 12 is reproduced from [79]. © 2019 Wiley-VCH Verlag GmbH & Co. KGaA, Weinheim. Used with permission from Máté Somlyay et al., "^{19}F NMR Spectroscopy Tagging and Paramagnetic Relaxation Enhancement-Based Conformation Analysis of Intrinsically Disordered Protein Complexes", ChemBioChem, John Wiley and Sons.

In the field of ^{19}F NMR protein conformational studies another area that has seen increasing attention is that of membrane proteins (MPs). Despite their physiological importance, analysis of the structural biology of MPs is significantly limited due to difficulties associated with protein expression, purification, stability, solubility and structural heterogeneity [82-84]. In particular, the application of solution NMR techniques to the study of MPs has proven exceptionally challenging due to the slower tumbling rates that MPs experience within membrane mimetics environments, which results in rapidly decaying signals and generally broad linewidths [85,86]. However, technical improvements, such as cryogenically-cooled probe-heads, along with the development of new high sensitivity ^{19}F NMR probes and novel strategies to produce recombinant proteins with optimal isotope labelling have greatly opened up this field of study [87]. For example, by using highly sensitive 2,2,2-trifluoroethanethiol (TFET) ^{19}F probes, Bondarenko et al. have developed a novel TFET/MTSL ((1-oxyl-2,2,5,5-tetramethylpyrroline-3-methyl)methanethiosulfonate) orthogonal labelling scheme that enables the accurate determination of inter-subunit distances in pentameric ligand-gated ion channels (pLGICs) by means of solution ^{19}F PRE NMR experiments in micelles (Figure 13) [88]. To ensure a uniform ^{19}F PRE signal from the adjacent paramagnetic labels, the ^{19}F NMR TFET probe was tagged to a selected cysteine residue in the channel protein, L253C, and the paramagnetic probe, MTSL, was then used to label the rest of available equivalent cysteine sites in a molar ratio of 1 TFET:4 MTSL. The experimental distances, that were calculated on the basis of the corresponding ^{19}F NMR signal decay profiles, were in good agreement to those predicted for modelled MTSL-TFET pairs in adjacent subunits in the X-ray structure, showing only small discrepancies. Overall, the results of this work clearly demonstrated the value of solution ^{19}F NMR for quaternary structure determination and as an alternative approach for generating distance restraints for ion channels and other protein complexes that would be difficult to be defined by using other analytical tools.

DNA and RNA secondary and tertiary structure

^{19}F NMR spectroscopy also represents a useful analytical approach to study the structure, function and molecular dynamics of nucleic acids [89]. Following early advances by Micura and co-workers in the late 2000s that investigated the suitability of ^{19}F NMR for the conformational analysis of single and double helix RNA strands [90-93] ^{19}F NMR has found a particularly rich niche of applications in the conformational analysis of higher-ordered DNA and RNA G-quadruplex structures. G-quadruplexes are four-stranded nucleic acid secondary struc-

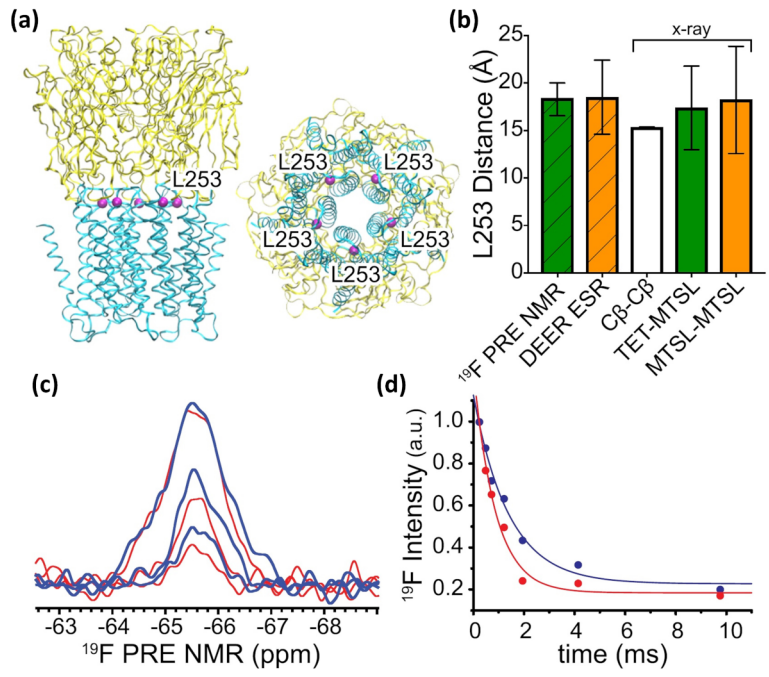

Figure 13: (a) Side (left) and bottom (right) views of the pentameric apo ELIC X-ray structure (PDB ID: 3RQU) showing the five equivalent L253 residues (purple) at the interface of the extracellular domain (yellow) and the transmembrane domain (cyan) present. (b) Distances obtained from ^{19}F PRE NMR and DEER ESR experiments are compared to distances between L253 Cβ atoms (C_β–C^β) in adjacent subunits of the ELIC structure. (c) Representative ^{19}F PRE NMR spectra of ELIC L253C-labelled with TFET and MTSL collected under paramagnetic (red) and diamagnetic (blue) conditions different with relaxation delays. (d) Single exponential decay functions, resulting in transverse relaxation rates of $R_{2,para}$ = 1153 ± 194 Hz and $R_{2,dia}$ = 714 ± 123 Hz were used to derive a distance of 18.4 ± 1.7 Å between residues 253 in the adjacent ELIC subunits. Reprinted with permission from [88]. © 2019 American Chemical Society.

tures formed in specific guanine-rich sequences showing, in general, highly polymorphic structures and various folding topologies. These structures have been suggested to play an important role in key biological processes such as gene expression and regulation [94,95], telomere length maintenance [96-98], transcription and DNA replication [99,100]. Investigation of the specific G-quadruplex structures associated with these biological events is therefore essential to understand their functions. However, because the formation of a stabilized G-quadruplex causes an overall reduction in the tumbling rates of the molecule, and thus a great decay of NMR signal sensitivity, analysis of these supramolecular structures by common NMR techniques has proved challenging.

To overcome the aforementioned issues, Virta and co-workers have explored the application of trifluoromethyl analogues of guanosine, cytidine and uridine based in 2′-*O*-[(4-trifluoromethyltriazol-1-yl)methyl] reporter groups as ^{19}F NMR probes for the detection of RNA secondary structures (Figure 14). As shown by Granqvist et al. [101], the ^{19}F NMR signals observed when employing these probes to evaluate the thermal denaturation of a range of RNA hairpins were indeed found to be sensitive enough to allow the monitoring of their secondary structural changes with relatively wide shift dispersion. It also enabled to characterize by ^{19}F NMR spectroscopic methods an RNA triple helix for the first time.

Following on from this a new range of even more sensitive ^{19}F NMR probes, based in the use of 3,5-bis(trifluoromethyl)benzene moieties have recently been reported (Figure 14a) [103]. Here, the presence of six equivalent ^{19}F atoms within the probe results key in providing a much more superior spectral enhancement, proving successful in enabling to monitor the conformational changes experienced within the DNA/RNA strains upon G-quadruplex formation both in vitro and in vivo. In addition, these novel probes have

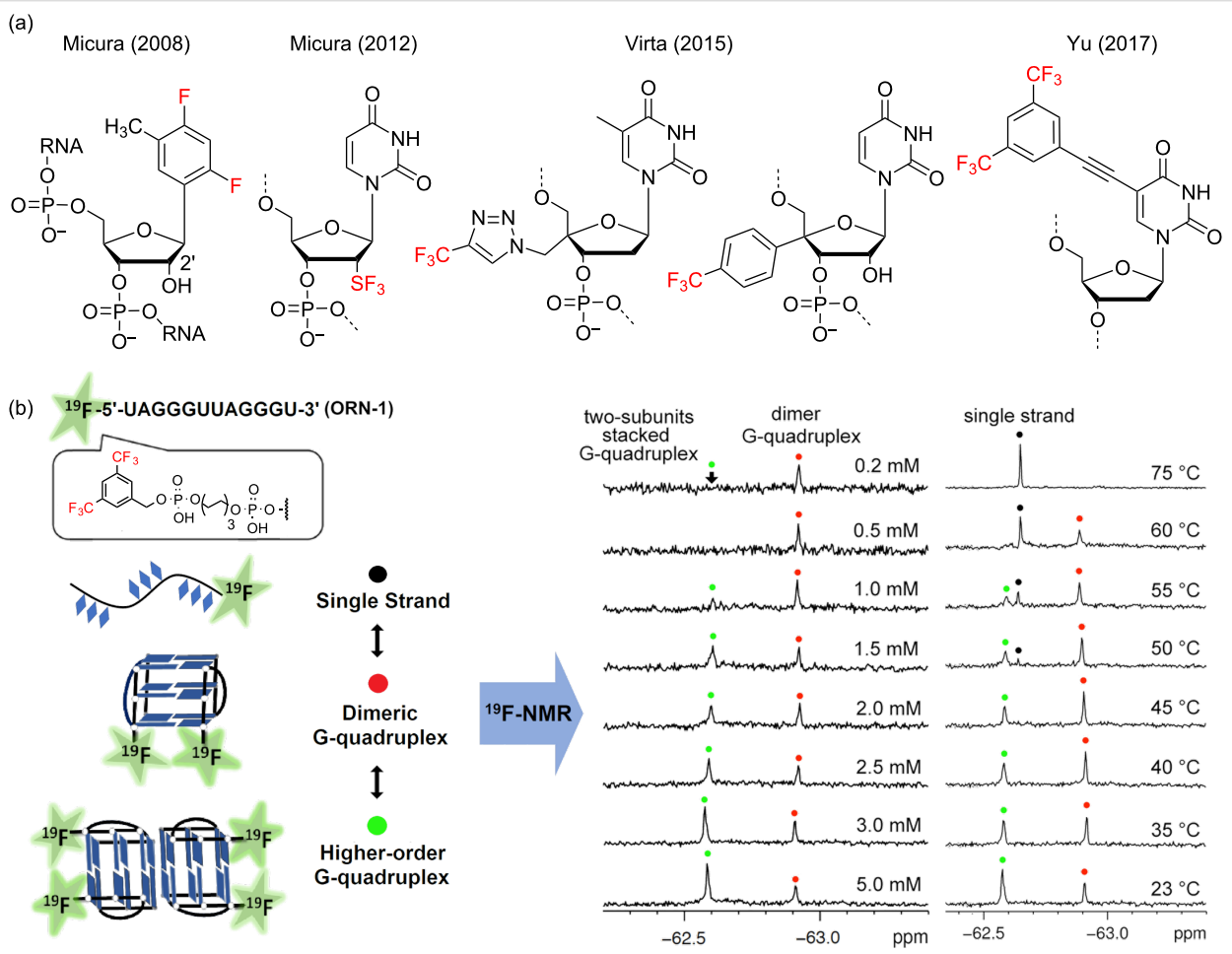

Figure 14: (a) General structure of a selection of recently developed ^{19}F-labelled nucleotides for their use as ^{19}F NMR reporters. (b) Concept for the detection different RNA structures by using ^{19}F labels and its application to the study of telomer RNA structure at different concentrations and temperatures. Red and green spots indicate formation of dimer and two-subunits stacked G-quadruplex. The peaks of single strand RNA are marked with black spots. Temperatures are indicated on the right. Figure 14 is adapted from [102].

the extra advantage that can be easily incorporated either as internally fluorinated nucleobases or as external ^{19}F-labelled terminal tags in longer oligonucleotides (Figure 14b). As a proof of concept, Bao et al. demonstrated the utility of these tags for the direct observation and quantitative thermodynamic characterization of dimeric and two-subunits stacked telomeric RNA and DNA G-quadruplexes within in living cells [99,102,104]. Moreover, by using these new reporters, ^{19}F NMR analysis has also been applied as an efficient strategy to probe and characterize the binding interactions of fluoro-labelled RNA- and DNA-based G-quadruplex complexes with different ligand molecules. This was exemplified by the Xu group who investigated the interaction of a RNA G-quadruplex and the telomeric protein TRF2 [103] and the interaction of the DNA thrombin binding aptamer (TBA) G-quadruplex with thrombin [100]. Overall, these examples demonstrate that ^{19}F NMR offers a suitable and non-perturbing approach by which to access detailed structural information of complex DNA and RNA folding topologies and sophisticated supramolecular assemblies.

Metabolism studies

Biotransformation of fluorinated xenobiotics

Fluorine is present in a large number of anthropogenic compounds, in particular pharmaceuticals, agrochemicals and anti-stain/anti-stick compounds (per- and poly-fluorinated alkyl substances, PFAS). When these compounds come into contact with microorganisms, there is a high likelihood that they will be biotransformed to some degree. In our previous review [4], we highlighted ^{19}F NMR's usefulness in following the biodegradation of compounds such as fluorophenols and fluorobenzoates. The technique has since been applied to monitor the biotransformation/biodegradation of fluorinated drugs such as flurbiprofen [105], and the pesticide cyhalothrin [106] by the fungus *Cunninghamella elegans*. In the former, ^{19}F NMR demonstrated the appearance of phase 1 (oxidative) and phase 2 (conjugative) metabolites, and in the latter, it was possible to monitor the migration of the pesticide into the biomass in the first 24 h after its introduction before being biotransformed to new trifluoromethyl-containing metabolites (Figure 15). ^{19}F NMR was also employed to determine the degree of

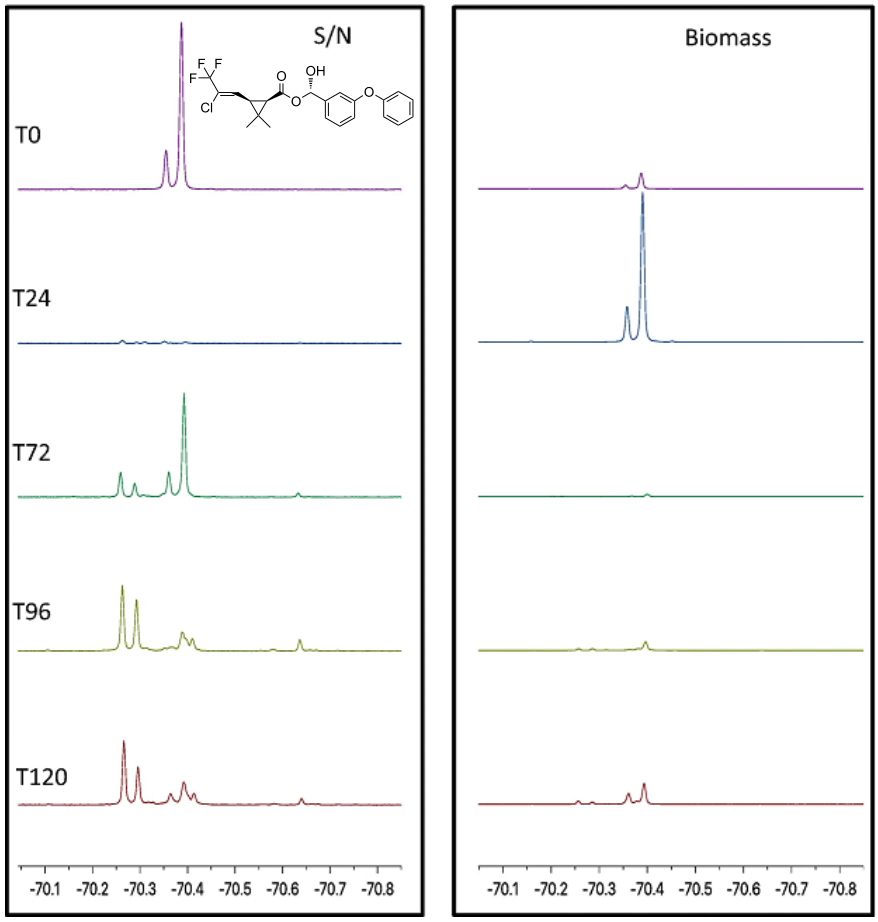

Figure 15: Monitoring biotransformation of the fluorinated pesticide cyhalothrin by the fungus *C. elegans*. The spectra are of supernatant (S/N) and biomass from cultures incubated with the pesticide at different time points. Figure 15 was reprinted from [106].

biotransformation of drug-like fluorophenylpyridine carboxylic acids in the same fungus [107]. However, aside from these few examples, the technique is not widely used by those investigating the biodegradation of fluorinated xenobiotics, with researchers more commonly relying on liquid or gas chromatography–mass spectrometry methods. Objectively, these techniques are much more sensitive than ^{19}F NMR, provide more structural information and are probably more accessible; however, it is possible that important biotransformation products may not to be detected using these techniques. For example, the fluorometabolites detected upon fungal degradation of cyhalothrin were not observed by GC–MS of culture supernatants.

When the nature of the degradation products is unknown, ^{19}F NMR is particularly useful, since even minor changes to a substrate's structure can lead to a chemical shift change. Notably, compounds with new fluorinated groups, for which there is no precedent in the literature, pose challenges for analysis of biotransformation products. For instance, the pentafluorosulfanyl (-SF_5) group is proposed as a replacement for trifluoromethyl (-CF_3) and has been incorporated into numerous biologically active compounds already [108,109]. Intuitively, investigating the biodegradation of these compounds in the absence of any reference compounds is complicated. Saccomanno et al. [110] investigated the bacterial degradation of pentafluorosulfanyl (SF_5)-substituted aminophenols and via ^{19}F NMR analysis of culture extracts was able to determine the production of new fluorinated metabolites (Figure 16). Subsequent analysis by GC–MS was required to further characterize the products, but only one could be detected (SF_5-catechol) despite the ^{19}F NMR analysis showing the presence of multiple fluorometabolites.

Detection and biosynthesis of natural organofluorine compounds

As naturally-occurring organofluorine compounds are so rare, it is possible to easily detect them in a crude, complex mixture, such as a culture medium, using ^{19}F NMR. The earliest exam-

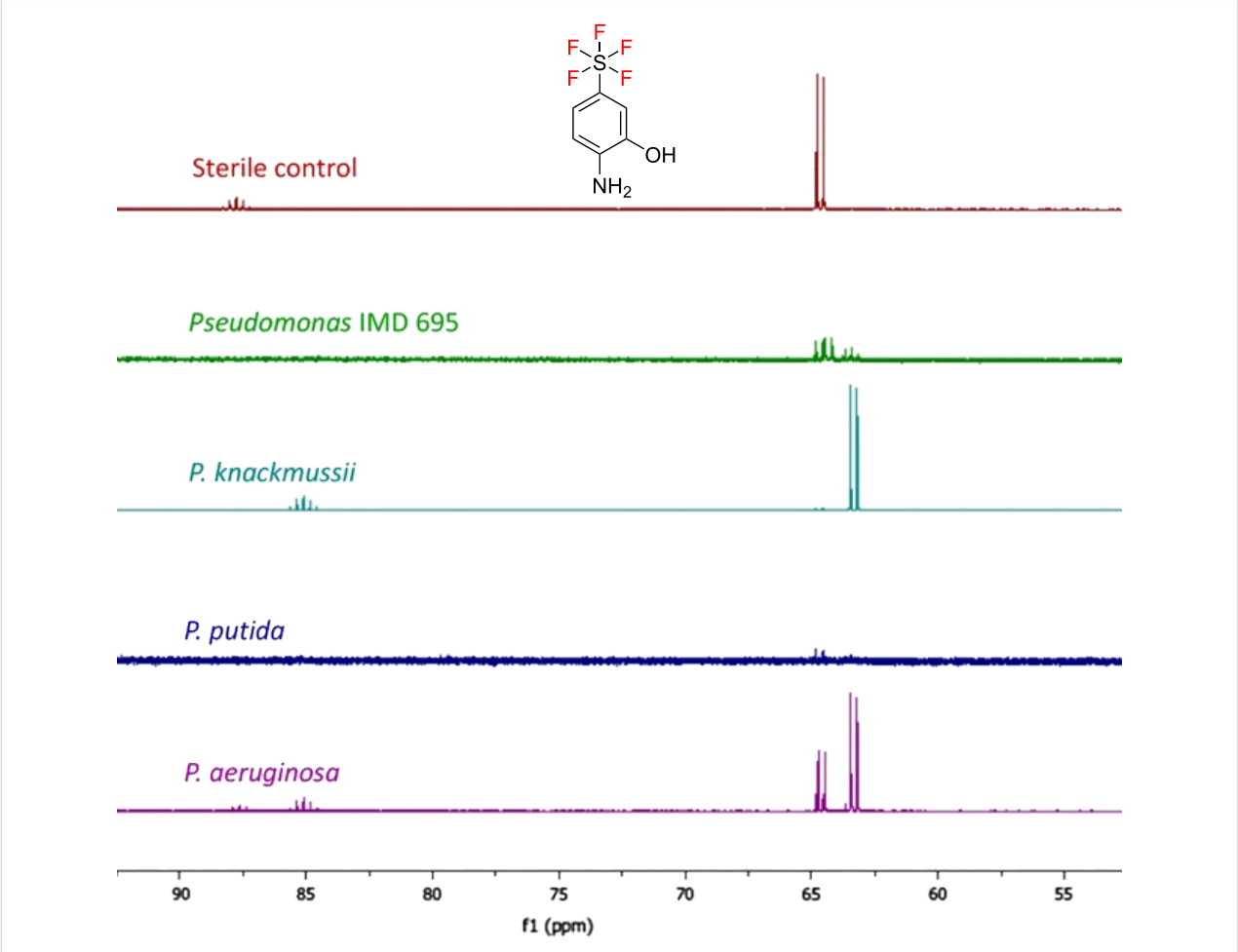

Figure 16: Following the biodegradation of emerging fluorinated pollutants by ^{19}F NMR. The spectra are from culture supernatants of different bacteria incubated with SF_5-aminophenol. Figure 16 was reprinted from [110].

ple of the technique being applied in this was in the discovery of fluoroacetate and 4-fluorothreonine in cultures of the bacterium *Streptomyces cattleya* [111]. ^{19}F NMR became a cornerstone for investigating the biosynthesis of these fluorometabolites, and was instrumental in the discovery of the very first fluorinase, which catalyses the production of 5'-fluoro-5'-deoxyadenosine (5-FDA) from fluoride ion and *S*-adenosylmethionine (SAM) [1].

While cumbersome as a tool for screening for new fluorometabolites in multiple strains, ^{19}F NMR continues to be successfully applied to the discovery of such compounds, typically after genome sequencing and scanning for genes with homology to those initially discovered in *S. cattleya*. For example, Huang et al. [112] analysed the genome sequence of the bacterium *S. xinghaiensis* NRRL-B24674, which revealed the presence of a fluorinase gene, suggesting that the microorganism could produce fluorinated compounds from fluoride ion. This was confirmed by ^{19}F NMR of culture supernatant after the bacterium was grown in medium containing 2 mM fluoride ion. Furthermore, because of the large shift changes due to minor structural differences, the observation of new fluorinated compounds in crude culture supernatants is possible. ^{19}F NMR analysis of cultures of the bacterium *Streptomyces* sp. MA37, which was isolated from a Ghanian soil sample, revealed several new resonances in addition to those known for fluoroacetate and 4-fluorothreonine (Figure 17) [113]. (2*R*,3*S*,4*S*)-5-Fluoro-2,3,4-trihydroxypentanoic acid and 5-fluoro-5-deoxy-D-ribulose were confirmed as two of the new metabolites [114]. Most recently ^{19}F NMR was the key analytical technique to assess in vivo production of 5'-FDA in an engineered *E. coli*, which, in addition to expressing the fluorinase, had its fluoride efflux protein, CrcB, deleted and a gene coding for a SAM transport protein heterologously expressed, to ensure an adequate supply of substrates [115].

Nucleocidin was famously isolated from *S. calvus* in the 1950s as it had significant anti-trypanosomal properties [116]; however, the presence of fluorine in its structure was not discovered until a decade later [117], by which time the original strains had lost their biosynthetic capability, frustrating attempts to investigate its biosynthesis. It took over 50 years to determine the reason for the loss of nucleocidin production, which was due to the presence of a point mutation in the bldA gene [118] that codes for a rare Leu-tRNA (UUA). Upon complementation with a functional gene, *S. calvus* produced nucleocidin once again, which was detected by ^{19}F NMR. Subsequent biosynthetic investigations, again relying on ^{19}F NMR, have revealed that the elaboration of this unusual fluorometabolite involves the production of glucosylated precursors [119], which are detectable in the culture supernatant (Figure 18). These are possibly inactive forms of nucleocidin, generated in the first instance so that the producing organism is protected from its deleterious effects, and can be activated outside the cell by glucosidases.

Fluorinated natural products via precursor-directed biosynthesis

The modification of known antibiotics and other natural products is an important tactic in the battle against antimicrobial resistance. In addition to fluorinated metabolites that are produced de novo from fluoride ions, it is possible to modify other secondary metabolites to incorporate fluorine by including fluorinated precursors in the culture medium. ^{19}F NMR has been applied to the detection of the new compounds in the complex supernatants of organisms producing non-ribosomal peptides and polyketides. It has been especially useful for monitoring the

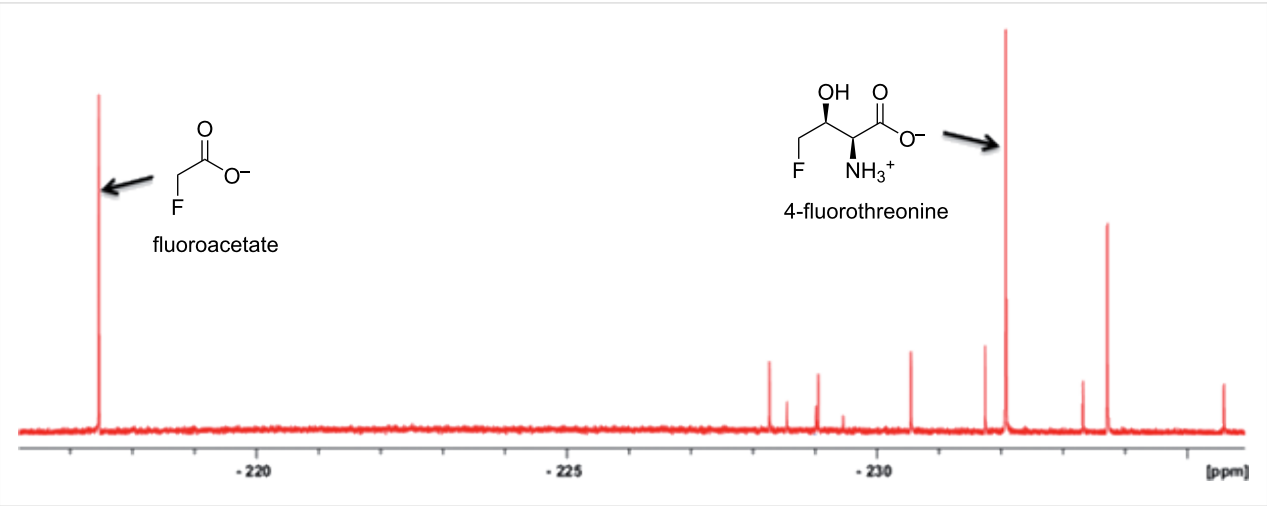

Figure 17: Discovery of new fluorinated natural products by ^{19}F NMR. The spectrum is of the culture supernatant of *Streptomyces* sp. MA37, which shows new fluorometabolites in addition to the previously identified fluoroacetate and 4-fluorothreonine. Figure 17 was reprinted from [113].

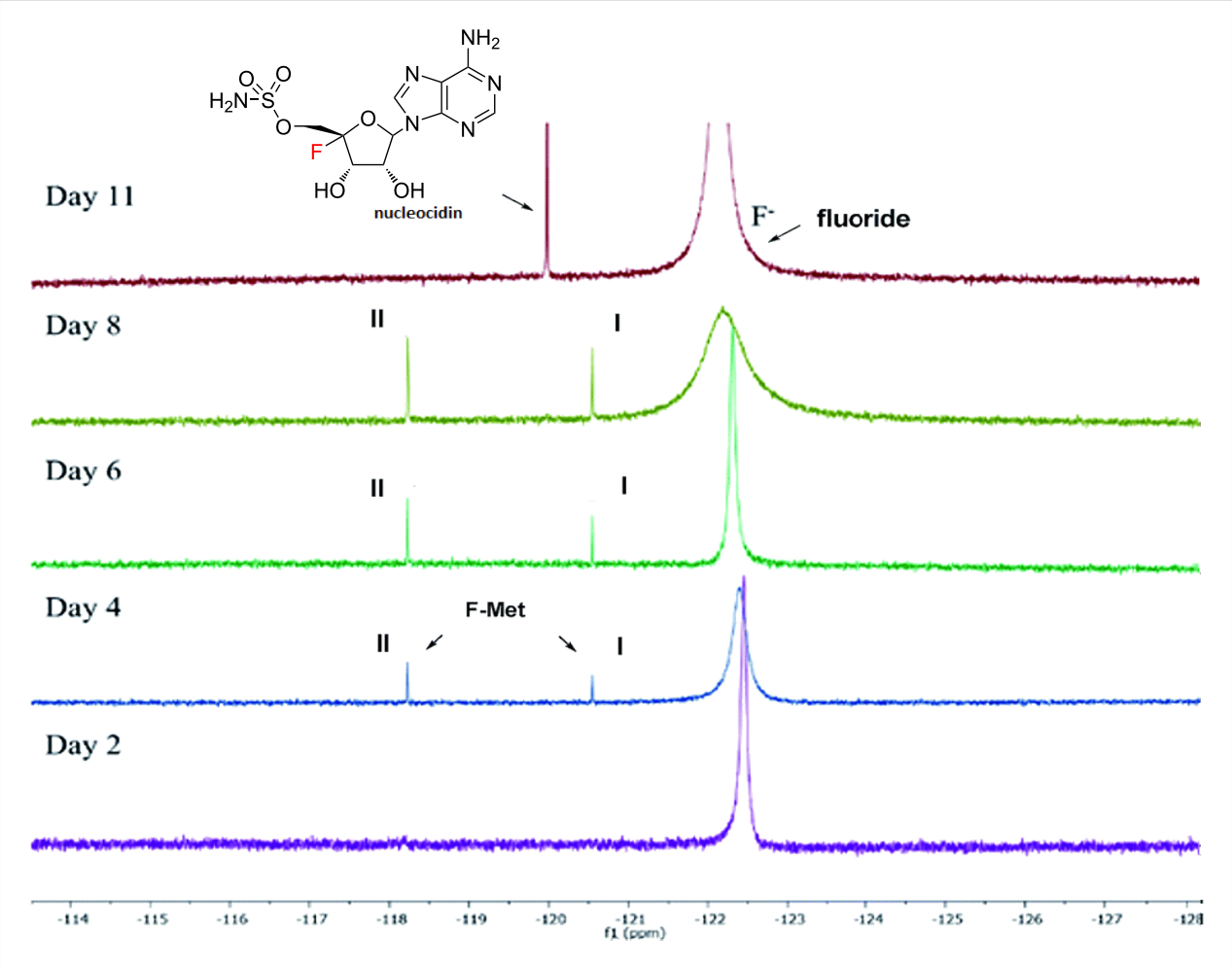

Figure 18: Application of ^{19}F NMR to investigate the biosynthesis of nucleocidin. The spectra are from culture supernatants of *S. calvus* recorded at different times during growth, showing the production of two glycosylated metabolites (I and II) that precede nucleocidin appearance in the culture. Figure 18 was reprinted from [119].

incorporation of fluorinated amino acids into lipopeptides produced by *Bacillus* sp. CS93. This bacterial strain was originally isolated from the Mayan fermented food Pozol and was found to produce the dipeptide antibiotic bacilysin and the lipopeptides iturin A, surfactin and fengycin [120]. Precursor-directed biosynthesis experiments with various fluorinated amino acids were conducted and it was observed that in iturin A and fengycin, 3-fluoro-L-tyrosine could replace tyrosine in the peptide chain [121-123]. ^{19}F NMR analysis of culture supernatants revealed that when this fluoro-amino acid was incubated with CS93, three different fluorofengycin species were biosynthesised (Figure 19), with fluorotyrosine replacing either or both tyrosine residues in the peptide ring.

Although not strictly precursor-directed biosynthesis, Piasecki and Keatinge-Clay [124] employed ^{19}F NMR to monitor biocatalytic reactions of trifluorinated surrogate substrates of different polyketide synthase activities in cell lysates of recombinant *E. coli*. Substrate and lysate were incubated in an NMR tube to enable continuous monitoring of reactions catalysed by erythromycin thioesterase (trifluoropropionyl-SNAC substrate) and various ketoreductases (3-oxo-5,5,5- and 2-methyl-3-oxo-trifluoromethylpentanoyl-SNAC substrates). ^{19}F NMR successfully resolved the diastereomers produced by the different ketoreductases assayed.

Measuring gene expression

The *lacZ* gene, which is part of the lac operon in bacteria such as *E. coli*, codes for β-galactosidase and is used extensively as a reporter of gene expression. The measurement of β-galactosidase activity is possible using a range of techniques, including ^{19}F NMR. Yu et al. [125] developed a bimodal fluorinated probe, 1-*O*-(β-D-galactopyranosyl)-3-fluorocatechol, to measure the enzyme's activity in transfected cancer cells. The principle relies on the excess Fe^{3+} ions characteristically present in tumour cells, which are scavenged by the catechol after it is re-

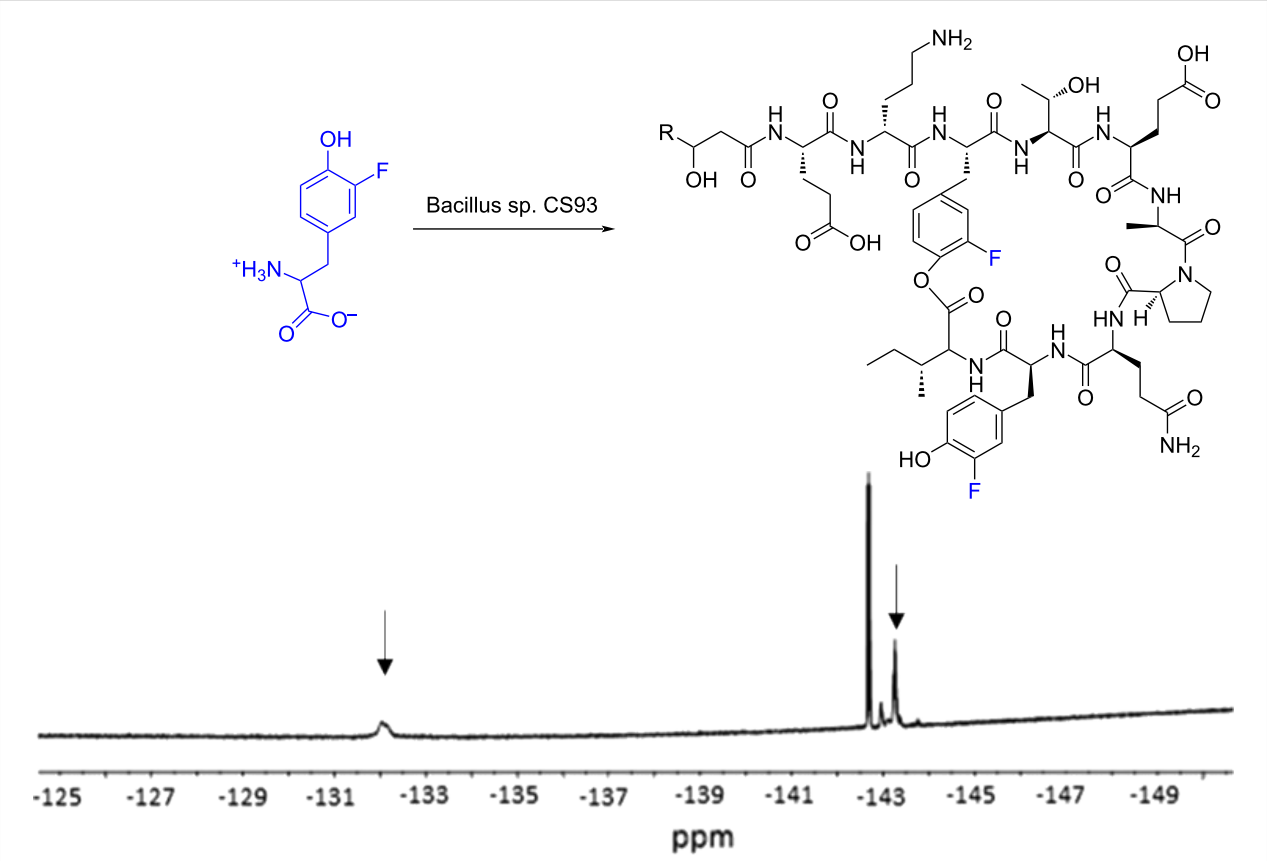

Figure 19: Detection of new fluorofengycins (indicated by arrows) in culture supernatants of *Bacillus* sp. CS93 incubated with 3-fluoro-L-tyrosine with ^{19}F NMR. Figure 19 was reprinted from [121].

leased from the sugar via the action of β-galactosidase. The resulting complex has a different chemical shift to the original compound in the ^{19}F NMR spectrum (Figure 20). The change could also be measured by ^{1}H MRI (magnetic resonance imaging) allowing improved precision and reliability of the assay.

^{19}F MRI can monitor gene expression in living cells by utilising cell-surface displayed β-lactamase (β-lac) and a specifically designed ^{19}F MRI probe [126]. The probe comprised a trifluoromethoxylated β-lactamase substrate, cephalosporin, attached to a Gd^{3+} complex, but it cannot cross the cell membrane. To avoid the need for membrane permeabilization, β-lac was fused to an extracellular region of epidermal growth factor receptor (EGFR). The non-permeable probe can bind the reporter protein on the cell surface, allowing measurement of intracellular gene expression. Hydrolysis of the probe by β-lac released the Gd^{3+} complex causing the T_2 of the ^{19}F-containing group to increase owing to a loss in the intramolecular paramagnetic relaxation enhancement (PRE). The T_2 values can affect the ^{19}F MRI signal intensity, which can be visually identified and a reduction in the thickness of peaks in

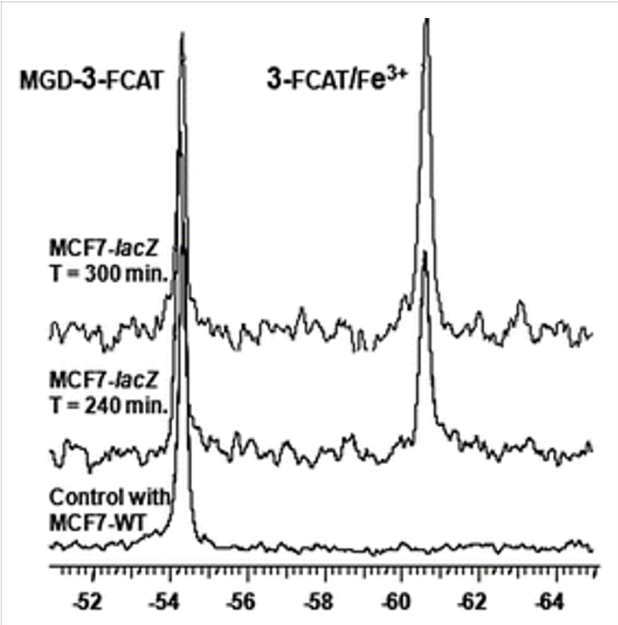

Figure 20: Measurement of β-galactosidase activity in MCF7 cancer cells expressing lacZ using ^{19}F NMR. The deglycosylated FCAT probe binds the Fe^{3+} ions present resulting in a complex that gives a new resonance in the spectrum. Figure 20 was reprinted from [125].

the ^{19}F NMR spectra can also be observed. Therefore, enzymatic degradation of the Gd-FC-lac probe would lead to the improvement of the ^{19}F MRI signal, confirming gene expression in living cells.

Physiological measurement

Detection of ions

Metal ions play an important role in biological systems and deviations in their levels can be associated with the onset of disease. The real-time detection and tracking of metal ions in vivo are of great interest, which is not possible using optical dyes. One potential way to overcome this is to employ ^{19}F-labelled chelators and sensors, whose chemical shifts are observed by ^{19}F NMR upon detection or binding to the metal ion of interest. Early work by Smith et al. [127] employed symmetrically difluorinated 1,2-bis(*o*-aminophenoxy)ethane-*N*,*N*,*N*',*N*'-tetraacetic acid (BAPTA) to determine intracellular Ca^{2+} concentration from the areas of the resonances of free and complexed forms of the chelating reagent. To improve sensitivity of the 5,5'-difluoro-BAPTA (5F-BAPTA) for ^{19}F MRI Bar-Shir et al. [128] used ion chemical exchange saturation transfer (iCEST). This approach is an extension of CEST that is used in MRI where a dynamic exchange between radiofrequency (RF) labelled protons and bulk water yields enhanced contrast. In iCEST, RF labelling at the ^{19}F frequency of Ca^{2+}-5F-BAPTA and detection of the label transfer to the frequency of free 5F-BAPTA produced a 100-fold improvement in sensitivity. A tetra-fluorine (5,5',6,6'-tetrafluoro-) BAPTA (TF-BAPTA) ion receptor was designed and successful in the detection of Zn^{2+} and Fe^{2+} due to slower exchange rates of the free and bound probe observed for both metal ions (Figure 21a) [129].

The conformational changes of biomolecules caused by metal ions has been exploited in the design of ^{19}F NMR-based ion sensors. For example, in the presence of K^+, the thrombin aptamer (5'-GGTTGGTGTGGTTGG-3') undergoes an intramolecular conformational change to promote the formation of the G quadruplex. A K^+ sensor was designed by introducing a 3,5-bis(trifluoromethyl)benzene moiety at the 5' terminal of the aptamer (^{19}F-TBA) [130]. When KCl was added, a new ^{19}F NMR signal was observed suggesting the complexation of

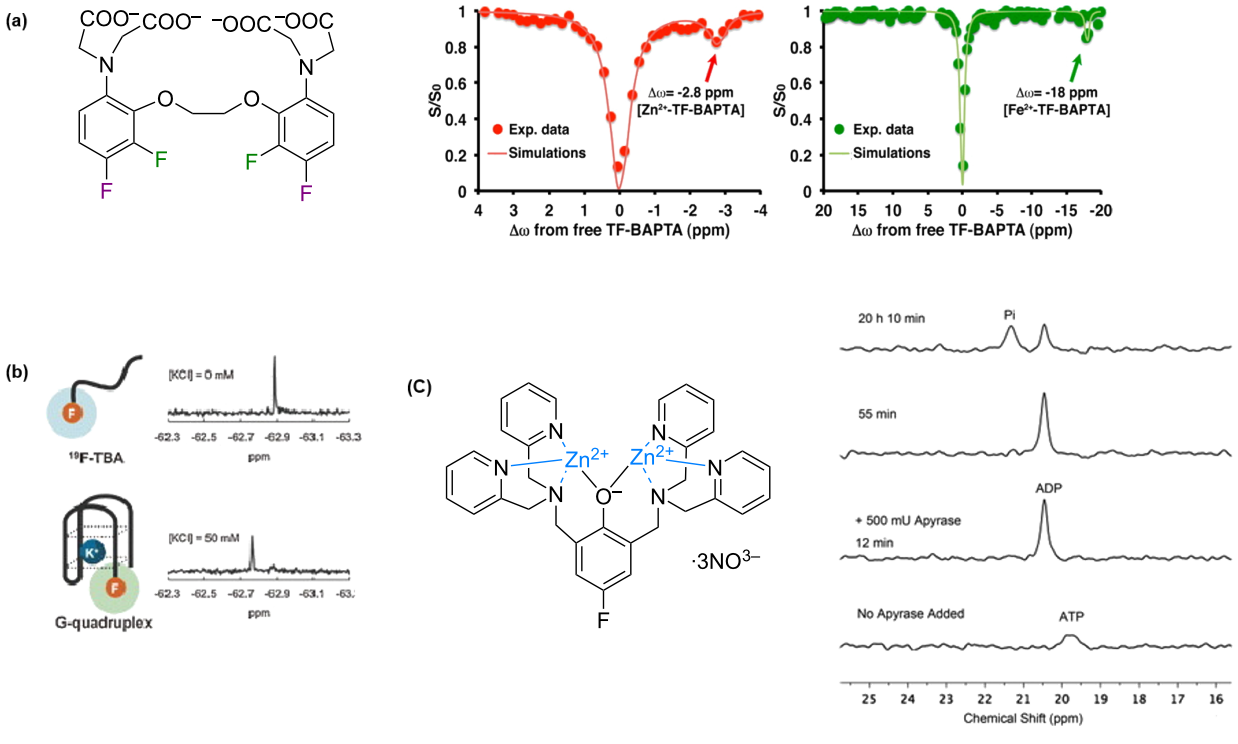

Figure 21: Detection of ions using ^{19}F NMR. (a) Structure of TF-BAPTA and its ^{19}F iCEST spectra in the presence of Zn^{2+} (red) or Fe^{2+} (green); (b) Detection of K^+ upon complexation with trifluorinated thrombin aptamer forming a G-quadruplex.; (c) Structure of fluorinated Zn^{2+}-dipicolylamine co-ordination complex and its application to the detection of phosphate released from ATP by apyrase. Figure 21a is reproduced with permission from [129], Copyright © 2014 American Chemical Society, https://pubs.acs.org/doi/10.1021/ja511313k. Further permissions related to the material excerpted should be directed to the ACS. Figure 21b is reprinted with permission from [130], © 2011 The Chemical Society of Japan. Figure 21c was reprinted from [131].

K^+ and a conformational change had occurred (Figure 21b). The sensor displayed excellent sensitivity as no new ^{19}F NMR signals and no chemical shift changes were observed upon addition of other metal ions such as Li^+, Na^+, Mg^{2+} and Ca^{2+}.

Anions, in particular phosphate, are also important physiological markers, and ^{19}F NMR can be employed for their detection. Gan et al. [131] reported the chemical shift changes upon phosphate anions binding to a Zn^{2+}-dipicolylamine co-ordination complex and used it to follow ATP hydrolysis by apyrase (Figure 21c).

Detection of biological reactive oxygen species

Reactive oxygen species (ROS), such as hydrogen peroxide (H_2O_2), superoxide (O_2^-), and hydroxyl radical (•OH), are produced as part of mitochondrial oxidative metabolism and as a response to cellular invasion by cytokines, xenobiotics, and bacteria [132]. H_2O_2 is considered to be one of the most important ROS and play a role in homeostatic regulation as well as in healthy physiological signalling pathways such as cell proliferation, differentiation and migration. Fluorescent probes are typically used to detect H_2O_2 in living organisms and although highly sensitive, the excitation and emission light are unable to penetrate deep sites in the body.

Arylboronic acids are oxidised by H_2O_2, allowing for the design of H_2O_2-responsive sensors with these substrates as reactive moieties [133]. ^{19}F-labelled phenylboronic acid was used as a substrate in the design on a ^{19}F MRI probe to detect H_2O_2 [134]. The fluorinated phenylboronic acid and the H_2O_2 interact to form a corresponding phenol, resulting in a large ^{19}F chemical shift change due to the large electron density change around the ^{19}F nucleus.

Peroxynitrite ($ONOO^-$) is a highly reactive nitrogen oxide species formed in vivo from the rapid interaction of O_2^- and nitric oxide radicals. •NO and O_2^- are endogenously formed to moderate cell signalling, whereas $ONOO^-$ production is thought to be harmful with increased levels observed in cancer and age-related pathologies. Detection $ONOO^-$ in biological samples is difficult owing to its short lifetime, strong competition from endogenous ROS scavengers and high background noises from other ROS. Two ^{19}F magnetic resonance probes, 5-fluoroisatin and 6-fluoroisatin, were developed for the detection of $ONOO^-$ based on oxidative carbonylation chemistry [135]. Both probes are highly selective for $ONOO^-$, resulting in a chemical shift change in ^{19}F NMR, which was not observed when the probes were incubated with other reactive sulphur, oxygen and nitrogen species (Figure 22).

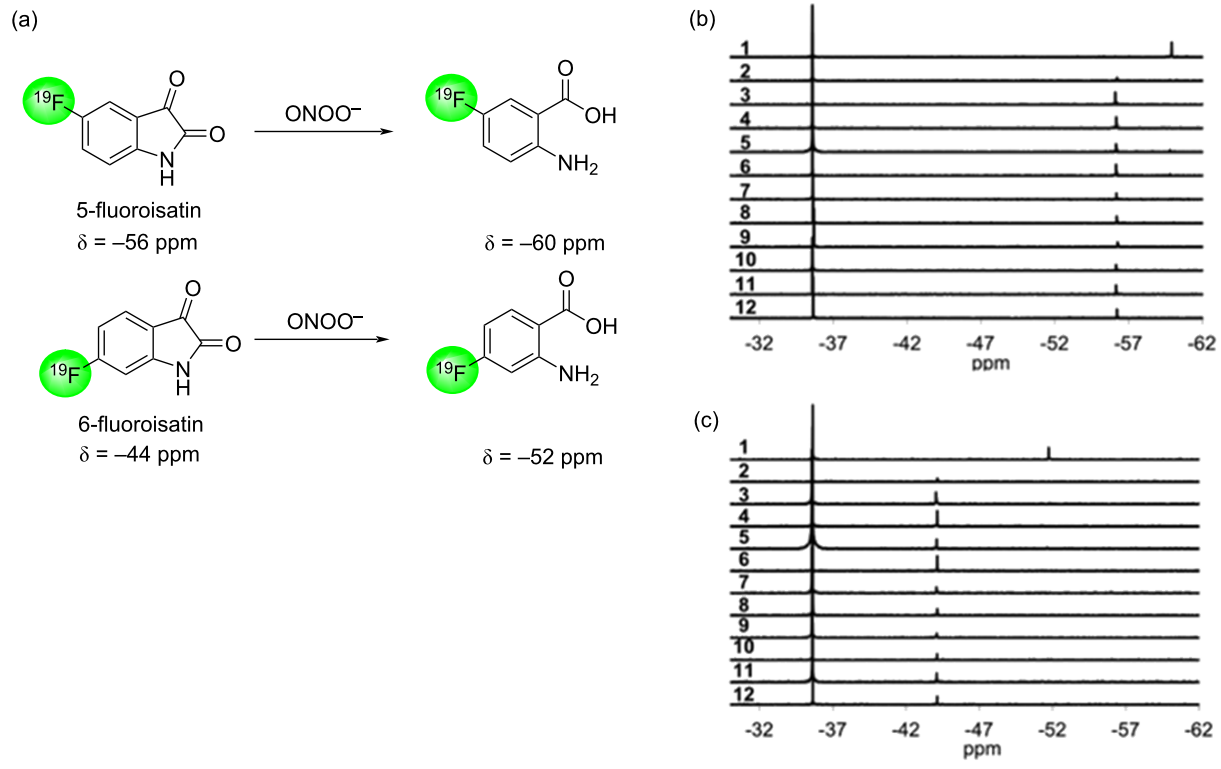

Figure 22: (a) The $ONOO^-$-mediated decarbonylation of 5-fluoroisatin and 6-fluoroisatin. The selectivity of (b) 5-fluoroisatin and (c) 6-fluoroisatin to reactive oxygen species. 1: $ONOO^-$, 2: OH, 3: GSH, 4: NO, 5: $Na_2N_2O_3$, 6: KO_2, 7: *t*-BuOOH, 8: GSNO, 9: NO_2^-, 10: ClO^-, 11: $KHSO_5$, 12: H_2O_2. Figure 22 was reprinted from [135].

Conclusion

In the decade since our previous review, ^{19}F NMR has continued to prove its versatility in several areas of chemical biology, but predominantly in the structural analysis of protein and nucleic acid, and their interactions with other biomolecules. Advances in the methods for the synthesis of fluorinated amino acids and nucleotides have been the driver for the new applications, coupled with improved sensitivity of the instrumentation. The recognition of the importance of structural biology in disease states is likely to amplify the application of ^{19}F NMR in this field. Undoubtedly, the technique will continue to be employed in all of the areas highlighted in this review, and new applications identified since fluorine's importance across a range of industries is undiminished.

Funding

The authors acknowledge funding from the Biotechnology and Biological Sciences Research council [BB/P022189/1, SLC and DG] and Science Foundation Ireland [17/BBSRC/3417, CDM and AP].

ORCID® iDs

Diana Gimenez - https://orcid.org/0000-0003-2842-6989
Aoife Phelan - https://orcid.org/0000-0002-2192-5155
Cormac D. Murphy - https://orcid.org/0000-0002-2137-3338
Steven L. Cobb - https://orcid.org/0000-0002-3790-7023

References

1. O'Hagan, D.; Deng, H. *Chem. Rev.* **2015,** *115,* 634–649. doi:10.1021/cr500209t
2. Wu, L.; Maglangit, F.; Deng, H. *Curr. Opin. Chem. Biol.* **2020,** *55,* 119–126. doi:10.1016/j.cbpa.2020.01.004
3. Murphy, C. D. *Appl. Microbiol. Biotechnol.* **2016,** *100,* 2617–2627. doi:10.1007/s00253-016-7304-3
4. Cobb, S. L.; Murphy, C. D. *J. Fluorine Chem.* **2009,** *130,* 132–143. doi:10.1016/j.jfluchem.2008.11.003
5. Wang, J.; Xie, J.; Schultz, P. G. *J. Am. Chem. Soc.* **2006,** *128,* 8738–8739. doi:10.1021/ja062666k
6. Cotton, G. J.; Muir, T. W. *Chem. Biol.* **1999,** *6,* R247–R256. doi:10.1016/s1074-5521(99)80109-4
7. Link, A. J.; Mock, M. L.; Tirrell, D. A. *Curr. Opin. Biotechnol.* **2003,** *14,* 603–609. doi:10.1016/j.copbio.2003.10.011
8. Frieden, C.; Hoeltzli, S. D.; Bann, J. G. *Methods Enzymol.* **2004,** *380,* 400–415. doi:10.1016/s0076-6879(04)80018-1
9. Marsh, E. N. G.; Suzuki, Y. *ACS Chem. Biol.* **2014,** *9,* 1242–1250. doi:10.1021/cb500111u
10. Wang, L.; Brock, A.; Herberich, B.; Schultz, P. G. *Science* **2001,** *292,* 498–500. doi:10.1126/science.1060077
11. Mills, J. H.; Lee, H. S.; Liu, C. C.; Wang, J.; Schultz, P. G. *ChemBioChem* **2009,** *10,* 2162–2164. doi:10.1002/cbic.200900254
12. Young, T. S.; Ahmad, I.; Yin, J. A.; Schultz, P. G. *J. Mol. Biol.* **2010,** *395,* 361–374. doi:10.1016/j.jmb.2009.10.030
13. Loscha, K. V.; Herlt, A. J.; Qi, R.; Huber, T.; Ozawa, K.; Otting, G. *Angew. Chem., Int. Ed.* **2012,** *51,* 2243–2246. doi:10.1002/anie.201108275
14. Singh-Blom, A.; Hughes, R. A.; Ellington, A. D. *J. Biotechnol.* **2014,** *178,* 12–22. doi:10.1016/j.jbiotec.2014.02.009
15. Buer, B. C.; Levin, B. J.; Marsh, E. N. G. *J. Pept. Sci.* **2013,** *19,* 308–314. doi:10.1002/psc.2501
16. Tressler, C. M.; Zondlo, N. J. *Org. Lett.* **2016,** *18,* 6240–6243. doi:10.1021/acs.orglett.6b02858
17. Tressler, C. M.; Zondlo, N. J. *J. Org. Chem.* **2014,** *79,* 5880–5886. doi:10.1021/jo5008674
18. Vukelić, S.; Moschner, J.; Huhmann, S.; Fernandes, R.; Berger, A. A.; Koksch, B. Synthesis of Side Chain Fluorinated Amino Acids and Their Effects on the Properties of Peptides and Proteins. In *Modern Synthesis Processes and Reactivity of Fluorinated Compounds;* Groult, H.; Leroux, F. R.; Tressaud, A., Eds.; Elsevier, 2017; pp 427–464. doi:10.1016/b978-0-12-803740-9.00015-9
19. Salwiczek, M.; Samsonov, S.; Vagt, T.; Nyakatura, E.; Fleige, E.; Numata, J.; Cölfen, H.; Pisabarro, M. T.; Koksch, B. *Chem. – Eur. J.* **2009,** *15,* 7628–7636. doi:10.1002/chem.200802136
20. Tressler, C. M.; Zondlo, N. J. *Biochemistry* **2017,** *56,* 1062–1074. doi:10.1021/acs.biochem.6b01020
21. Lim, D. S.; Lin, J.-H.; Welch, J. T. *Eur. J. Org. Chem.* **2012,** 3946–3954. doi:10.1002/ejoc.201200327
22. Grigolato, L.; Brittain, W. D. G.; Hudson, A. S.; Czyzewska, M. M.; Cobb, S. L. *J. Fluorine Chem.* **2018,** *212,* 166–170. doi:10.1016/j.jfluchem.2018.06.006
23. Loewen, M. C.; Klein-Seetharaman, J.; Getmanova, E. V.; Reeves, P. J.; Schwalbe, H.; Khorana, H. G. *Proc. Natl. Acad. Sci. U. S. A.* **2001,** *98,* 4888–4892. doi:10.1073/pnas.051633098
24. Kim, T. H.; Chung, K. Y.; Manglik, A.; Hansen, A. L.; Dror, R. O.; Mildorf, T. J.; Shaw, D. E.; Kobilka, B. K.; Prosser, R. S. *J. Am. Chem. Soc.* **2013,** *135,* 9465–9474. doi:10.1021/ja404305k
25. Kalbitzer, H. R.; Rohr, G.; Nowak, E.; Goody, R. S.; Kuhn, W.; Zimmermann, E. *NMR Biomed.* **1992,** *5,* 347–350. doi:10.1002/nbm.1940050605
26. Thomas, M. R.; Boxer, S. G. *Biochemistry* **2001,** *40,* 8588–8596. doi:10.1021/bi0101087
27. Hellmich, U. A.; Pfleger, N.; Glaubitz, C. *Photochem. Photobiol.* **2009,** *85,* 535–539. doi:10.1111/j.1751-1097.2008.00498.x
28. Ye, L.; Larda, S. T.; Frank Li, Y. F.; Manglik, A.; Prosser, R. S. *J. Biomol. NMR* **2015,** *62,* 97–103. doi:10.1007/s10858-015-9922-y
29. Manglik, A.; Kim, T. H.; Masureel, M.; Altenbach, C.; Yang, Z.; Hilger, D.; Lerch, M. T.; Kobilka, T. S.; Thian, F. S.; Hubbell, W. L.; Prosser, R. S.; Kobilka, B. K. *Cell* **2015,** *161,* 1101–1111. doi:10.1016/j.cell.2015.04.043
30. Gimenez, D.; Mooney, C. A.; Dose, A.; Sandford, G.; Coxon, C. R.; Cobb, S. L. *Org. Biomol. Chem.* **2017,** *15,* 4086–4095. doi:10.1039/c7ob00283a
31. Hattori, Y.; Heidenreich, D.; Ono, Y.; Sugiki, T.; Yokoyama, K.-i.; Suzuki, E.-i.; Fujiwara, T.; Kojima, C. *J. Biomol. NMR* **2017,** *68,* 271–279. doi:10.1007/s10858-017-0125-6
32. Spokoyny, A. M.; Zou, Y.; Ling, J. J.; Yu, H.; Lin, Y.-S.; Pentelute, B. L. *J. Am. Chem. Soc.* **2013,** *135,* 5946–5949. doi:10.1021/ja400119t
33. Dahanayake, J. N.; Kasireddy, C.; Karnes, J. P.; Verma, R.; Steinert, R. M.; Hildebrandt, D.; Hull, O. A.; Ellis, J. M.; Mitchell-Koch, K. R. Progress in Our Understanding of 19F Chemical Shifts. In *Annual Reports on NMR Spectroscopy;* Webb, G. A., Ed.; Academic Press, 2018; Vol. 93, pp 281–362. doi:10.1016/bs.arnmr.2017.08.002

34. Urick, A. K.; Calle, L. P.; Espinosa, J. F.; Hu, H.; Pomerantz, W. C. K. *ACS Chem. Biol.* **2016,** *11,* 3154–3164. doi:10.1021/acschembio.6b00730
35. Richards, K. L.; Rowe, M. L.; Hudson, P. B.; Williamson, R. A.; Howard, M. J. *Sci. Rep.* **2016,** *6,* 19518. doi:10.1038/srep19518
36. Liu, J. J.; Horst, R.; Katritch, V.; Stevens, R. C.; Wüthrich, K. *Science* **2012,** *335,* 1106–1110. doi:10.1126/science.1215802
37. Stadmiller, S. S.; Aguilar, J. S.; Waudby, C. A.; Pielak, G. J. *Biophys. J.* **2020,** *118,* 2537–2548. doi:10.1016/j.bpj.2020.03.031
38. Dalvit, C.; Fagerness, P. E.; Hadden, D. T. A.; Sarver, R. W.; Stockman, B. J. *J. Am. Chem. Soc.* **2003,** *125,* 7696–7703. doi:10.1021/ja034646d
39. Dalvit, C.; Ardini, E.; Flocco, M.; Fogliatto, G. P.; Mongelli, N.; Veronesi, M. *J. Am. Chem. Soc.* **2003,** *125,* 14620–14625. doi:10.1021/ja038128e
40. Tressler, C. M.; Zondlo, N. J. *ACS Chem. Biol.* **2020,** *15,* 1096–1103. doi:10.1021/acschembio.0c00131
41. Dalvit, C.; Vulpetti, A. *J. Med. Chem.* **2019,** *62,* 2218–2244. doi:10.1021/acs.jmedchem.8b01210
42. Dalvit, C.; Veronesi, M.; Vulpetti, A. *J. Biomol. NMR* **2020,** *74,* 613–631. doi:10.1007/s10858-020-00311-3
43. Rydzik, A. M.; Leung, I. K. H.; Thalhammer, A.; Kochan, G. T.; Claridge, T. D. W.; Schofield, C. J. *Chem. Commun.* **2014,** *50,* 1175–1177. doi:10.1039/c3cc47581f
44. Ojima, I. *J. Fluorine Chem.* **2017,** *198,* 10–23. doi:10.1016/j.jfluchem.2016.12.016
45. Veronesi, M.; Giacomina, F.; Romeo, E.; Castellani, B.; Ottonello, G.; Lambruschini, C.; Garau, G.; Scarpelli, R.; Bandiera, T.; Piomelli, D.; Dalvit, C. *Anal. Biochem.* **2016,** *495,* 52–59. doi:10.1016/j.ab.2015.11.015
46. Veronesi, M.; Romeo, E.; Lambruschini, C.; Piomelli, D.; Bandiera, T.; Scarpelli, R.; Garau, G.; Dalvit, C. *ChemMedChem* **2014,** *9,* 286–289. doi:10.1002/cmdc.201300438
47. Hong, M.; Schmidt-Rohr, K. *Acc. Chem. Res.* **2013,** *46,* 2154–2163. doi:10.1021/ar300294x
48. Gerig, J. T. *Prog. Nucl. Magn. Reson. Spectrosc.* **1994,** *26,* 293–370. doi:10.1016/0079-6565(94)80009-x
49. Danielson, M. A.; Falke, J. J. *Annu. Rev. Biophys. Biomol. Struct.* **1996,** *25,* 163–195. doi:10.1146/annurev.bb.25.060196.001115
50. Bann, J. G.; Pinkner, J.; Hultgren, S. J.; Frieden, C. *Proc. Natl. Acad. Sci. U. S. A.* **2002,** *99,* 709–714. doi:10.1073/pnas.022649599
51. Kitevski-LeBlanc, J. L.; Hoang, J.; Thach, W.; Larda, S. T.; Prosser, R. S. *Biochemistry* **2013,** *52,* 5780–5789. doi:10.1021/bi4010057
52. Skalicky, J. J.; Mills, J. L.; Sharma, S.; Szyperski, T. *J. Am. Chem. Soc.* **2001,** *123,* 388–397. doi:10.1021/ja003220l
53. Li, H.; Frieden, C. *Biochemistry* **2007,** *46,* 4337–4347. doi:10.1021/bi6026083
54. Baturin, S. J.; Okon, M.; McIntosh, L. P. *J. Biomol. NMR* **2011,** *51,* 379–394. doi:10.1007/s10858-011-9564-7
55. Evanics, F.; Bezsonova, I.; Marsh, J.; Kitevski, J. L.; Forman-Kay, J. D.; Prosser, R. S. *Biochemistry* **2006,** *45,* 14120–14128. doi:10.1021/bi061389r
56. Evanics, F.; Kitevski, J. L.; Bezsonova, I.; Forman-Kay, J.; Prosser, R. S. *Biochim. Biophys. Acta, Gen. Subj.* **2007,** *1770,* 221–230. doi:10.1016/j.bbagen.2006.10.017
57. Kitevski-LeBlanc, J. L.; Evanics, F.; Prosser, R. S. *J. Biomol. NMR* **2009,** *45,* 255–264. doi:10.1007/s10858-009-9359-2
58. Matei, E.; Gronenborn, A. M. *Angew. Chem., Int. Ed.* **2016,** *55,* 150–154. doi:10.1002/anie.201508464
59. Wang, G.-F.; Li, C.; Pielak, G. J. *Protein Sci.* **2010,** *19,* 1686–1691. doi:10.1002/pro.449
60. Wang, G.-F.; Li, C.; Pielak, G. J. *ChemBioChem* **2010,** *11,* 1993–1996. doi:10.1002/cbic.201000405
61. Buer, B. C.; Chugh, J.; Al-Hashimi, H. M.; Marsh, E. N. G. *Biochemistry* **2010,** *49,* 5760–5765. doi:10.1021/bi100605e
62. Suzuki, Y.; Brender, J. R.; Soper, M. T.; Krishnamoorthy, J.; Zhou, Y.; Ruotolo, B. T.; Kotov, N. A.; Ramamoorthy, A.; Marsh, E. N. G. *Biochemistry* **2013,** *52,* 1903–1912. doi:10.1021/bi400027y
63. Larda, S. T.; Simonetti, K.; Al-Abdul-Wahid, M. S.; Sharpe, S.; Prosser, R. S. *J. Am. Chem. Soc.* **2013,** *135,* 10533–10541. doi:10.1021/ja404584s
64. Aramini, J. M.; Hamilton, K.; Ma, L.-C.; Swapna, G. V. T.; Leonard, P. G.; Ladbury, J. E.; Krug, R. M.; Montelione, G. T. *Structure* **2014,** *22,* 515–525. doi:10.1016/j.str.2014.01.010
65. Aramini, J. M.; Ma, L.-C.; Zhou, L.; Schauder, C. M.; Hamilton, K.; Amer, B. R.; Mack, T. R.; Lee, H.-W.; Ciccosanti, C. T.; Zhao, L.; Xiao, R.; Krug, R. M.; Montelione, G. T. *J. Biol. Chem.* **2011,** *286,* 26050–26060. doi:10.1074/jbc.m111.248765
66. Dobson, C. M. *Nature* **2003,** *426,* 884–890. doi:10.1038/nature02261
67. Yan, Y.; Wang, C. *J. Mol. Biol.* **2006,** *364,* 853–862. doi:10.1016/j.jmb.2006.09.046
68. Mishra, R.; Geyer, M.; Winter, R. *ChemBioChem* **2009,** *10,* 1769–1772. doi:10.1002/cbic.200900237
69. Suzuki, Y.; Brender, J. R.; Hartman, K.; Ramamoorthy, A.; Marsh, E. N. G. *Biochemistry* **2012,** *51,* 8154–8162. doi:10.1021/bi3012548
70. Ma, B.; Nussinov, R. *J. Mol. Biol.* **2012,** *421,* 172–184. doi:10.1016/j.jmb.2011.11.023
71. Kitevski-LeBlanc, J. L.; Evanics, F.; Scott Prosser, R. *J. Biomol. NMR* **2010,** *48,* 113–121. doi:10.1007/s10858-010-9443-7
72. Uversky, V. N. *Front. Phys.* **2019,** *7,* No. 10. doi:10.3389/fphy.2019.00010
73. Sciolino, N.; Burz, D. S.; Shekhtman, A. *Proteomics* **2019,** *19,* 1800055. doi:10.1002/pmic.201800055
74. Cook, E. C.; Usher, G. A.; Showalter, S. A. The Use of 13C Direct-Detect NMR to Characterize Flexible and Disordered Proteins. In *Methods in Enzymology;* Rhoades, E., Ed.; Academic Press, 2018; Vol. 611, pp 81–100. doi:10.1016/bs.mie.2018.08.025
75. Li, C.; Lutz, E. A.; Slade, K. M.; Ruf, R. A. S.; Wang, G.-F.; Pielak, G. J. *Biochemistry* **2009,** *48,* 8578–8584. doi:10.1021/bi900872p
76. Zigoneanu, I. G.; Yang, Y. J.; Krois, A. S.; Haque, M. E.; Pielak, G. J. *Biochim. Biophys. Acta, Biomembr.* **2012,** *1818,* 512–519. doi:10.1016/j.bbamem.2011.11.024
77. Zigoneanu, I. G.; Pielak, G. J. *Mol. Pharmaceutics* **2012,** *9,* 1024–1029. doi:10.1021/mp200615m
78. Li, C.; Wang, G.-F.; Wang, Y.; Creager-Allen, R.; Lutz, E. A.; Scronce, H.; Slade, K. M.; Ruf, R. A. S.; Mehl, R. A.; Pielak, G. J. *J. Am. Chem. Soc.* **2010,** *132,* 321–327. doi:10.1021/ja907966n
79. Somlyay, M.; Ledolter, K.; Kitzler, M.; Sandford, G.; Cobb, S. L.; Konrat, R. *ChemBioChem* **2020,** *21,* 696–701. doi:10.1002/cbic.201900453
80. Coller, H. A.; Grandori, C.; Tamayo, P.; Colbert, T.; Lander, E. S.; Eisenman, R. N.; Golub, T. R. *Proc. Natl. Acad. Sci. U. S. A.* **2000,** *97,* 3260–3265. doi:10.1073/pnas.97.7.3260

81. Fieber, W.; Schneider, M. L.; Matt, T.; Kräutler, B.; Konrat, R.; Bister, K. *J. Mol. Biol.* **2001,** *307,* 1395–1410. doi:10.1006/jmbi.2001.4537
82. Sanders, C. R.; Sönnichsen, F. *Magn. Reson. Chem.* **2006,** *44* (Suppl. S1), S24–S40. doi:10.1002/mrc.1816
83. Lacapère, J.-J.; Pebay-Peyroula, E.; Neumann, J.-M.; Etchebest, C. *Trends Biochem. Sci.* **2007,** *32,* 259–270. doi:10.1016/j.tibs.2007.04.001
84. Pandey, A.; Shin, K.; Patterson, R. E.; Liu, X.-Q.; Rainey, J. K. *Biochem. Cell Biol.* **2016,** *94,* 507–527. doi:10.1139/bcb-2015-0143
85. Yu, H. *Proc. Natl. Acad. Sci. U. S. A.* **1999,** *96,* 332–334. doi:10.1073/pnas.96.2.332
86. Warschawski, D. E.; Arnold, A. A.; Beaugrand, M.; Gravel, A.; Chartrand, É.; Marcotte, I. *Biochim. Biophys. Acta, Biomembr.* **2011,** *1808,* 1957–1974. doi:10.1016/j.bbamem.2011.03.016
87. Di Pietrantonio, C.; Pandey, A.; Gould, J.; Hasabnis, A.; Prosser, R. S. *Methods Enzymol.* **2019,** *615,* 103–130. doi:10.1016/bs.mie.2018.09.029
88. Bondarenko, V.; Wells, M. M.; Chen, Q.; Singewald, K. C.; Saxena, S.; Xu, Y.; Tang, P. *ACS Chem. Biol.* **2019,** *14,* 2160–2165. doi:10.1021/acschembio.9b00692
89. Boeszoermenyi, A.; Ogórek, B.; Jain, A.; Arthanari, H.; Wagner, G. *J. Biomol. NMR* **2020,** *74,* 365–379. doi:10.1007/s10858-020-00331-z
90. Kreutz, C.; Kählig, H.; Konrat, R.; Micura, R. *J. Am. Chem. Soc.* **2005,** *127,* 11558–11559. doi:10.1021/ja052844u
91. Puffer, B.; Kreutz, C.; Rieder, U.; Ebert, M.-O.; Konrat, R.; Micura, R. *Nucleic Acids Res.* **2009,** *37,* 7728–7740. doi:10.1093/nar/gkp862
92. Graber, D.; Moroder, H.; Micura, R. *J. Am. Chem. Soc.* **2008,** *130,* 17230–17231. doi:10.1021/ja806716s
93. Fauster, K.; Kreutz, C.; Micura, R. *Angew. Chem., Int. Ed.* **2012,** *51,* 13080–13084. doi:10.1002/anie.201207128
94. Rhodes, D.; Lipps, H. J. *Nucleic Acids Res.* **2015,** *43,* 8627–8637. doi:10.1093/nar/gkv862
95. Hirashima, K.; Seimiya, H. *Nucleic Acids Res.* **2015,** *43,* 2022–2032. doi:10.1093/nar/gkv063
96. Xu, Y.; Ishizuka, T.; Yang, J.; Ito, K.; Katada, H.; Komiyama, M.; Hayashi, T. *J. Biol. Chem.* **2012,** *287,* 41787–41796. doi:10.1074/jbc.m112.342030
97. Takahama, K.; Takada, A.; Tada, S.; Shimizu, M.; Sayama, K.; Kurokawa, R.; Oyoshi, T. *Chem. Biol.* **2013,** *20,* 341–350. doi:10.1016/j.chembiol.2013.02.013
98. Wang, C.; Zhao, L.; Lu, S. *Int. J. Biol. Sci.* **2015,** *11,* 316–323. doi:10.7150/ijbs.10528
99. Bao, H.-L.; Xu, Y. *Chem. Commun.* **2020,** *56,* 6547–6550. doi:10.1039/d0cc02053b
100. Ishizuka, T.; Bao, H. L.; Xu, Y. *Methods Mol. Biol. (N. Y., NY, U. S.)* **2019,** *2035,* 407–433. doi:10.1007/978-1-4939-9666-7_26
101. Granqvist, L.; Virta, P. *J. Org. Chem.* **2015,** *80,* 7961–7970. doi:10.1021/acs.joc.5b00973
102. Bao, H.-L.; Ishizuka, T.; Sakamoto, T.; Fujimoto, K.; Uechi, T.; Kenmochi, N.; Xu, Y. *Nucleic Acids Res.* **2017,** *45,* 5501–5511. doi:10.1093/nar/gkx109
103. Bao, H.-L.; Ishizuka, T.; Iwanami, A.; Oyoshi, T.; Xu, Y. *ChemistrySelect* **2017,** *2,* 4170–4175. doi:10.1002/slct.201700711
104. Bao, H.-L.; Liu, H.-s.; Xu, Y. *Nucleic Acids Res.* **2019,** *47,* 4940–4947. doi:10.1093/nar/gkz276
105. Amadio, J.; Gordon, K.; Murphy, C. D. *Appl. Environ. Microbiol.* **2010,** *76,* 6299–6303. doi:10.1128/aem.01027-10
106. Palmer-Brown, W.; de Melo Souza, P. L.; Murphy, C. D. *Environ. Sci. Pollut. Res.* **2019,** *26,* 1414–1421. doi:10.1007/s11356-018-3689-0
107. Palmer-Brown, W.; Dunne, B.; Ortin, Y.; Fox, M. A.; Sandford, G.; Murphy, C. D. *Xenobiotica* **2017,** *47,* 763–770. doi:10.1080/00498254.2016.1227109
108. Pujol, E.; Blanco-Cabra, N.; Julián, E.; Leiva, R.; Torrents, E.; Vázquez, S. *Molecules* **2018,** *23,* 2853. doi:10.3390/molecules23112853
109. Pertusati, F.; Ferla, S.; Bassetto, M.; Brancale, A.; Khandil, S.; Westwell, A. D.; McGuigan, C. *Eur. J. Med. Chem.* **2019,** *180,* 1–14. doi:10.1016/j.ejmech.2019.07.001
110. Saccomanno, M.; Hussain, S.; O'Connor, N. K.; Beier, P.; Somlyay, M.; Konrat, R.; Murphy, C. D. *Biodegradation* **2018,** *29,* 259–270. doi:10.1007/s10532-018-9827-z
111. Sanada, M.; Miyano, T.; Iwadare, S.; Williamson, J. M.; Arison, B. H.; Smith, J. L.; Douglas, A. W.; Liesch, J. M.; Inamine, E. *J. Antibiot.* **1986,** *39,* 259–265. doi:10.7164/antibiotics.39.259
112. Huang, S.; Ma, L.; Tong, M. H.; Yu, Y.; O'Hagan, D.; Deng, H. *Org. Biomol. Chem.* **2014,** *12,* 4828–4831. doi:10.1039/c4ob00970c
113. Ma, L.; Bartholome, A.; Tong, M. H.; Qin, Z.; Yu, Y.; Shepherd, T.; Kyeremeh, K.; Deng, H.; O'Hagan, D. *Chem. Sci.* **2015,** *6,* 1414–1419. doi:10.1039/c4sc03540b
114. Wu, L.; Tong, M. H.; Kyeremeh, K.; Deng, H. *Biomolecules* **2020,** *10,* 1023. doi:10.3390/biom10071023
115. Markakis, K.; Lowe, P. T.; Davison-Gates, L.; O'Hagan, D.; Rosser, S. J.; Elfick, A. *ChemBioChem* **2020,** *21,* 1856–1860. doi:10.1002/cbic.202000051
116. Waller, C. W.; Patrick, J. B.; Fulmor, W.; Meyer, W. E. *J. Am. Chem. Soc.* **1957,** *79,* 1011–1012. doi:10.1021/ja01561a076
117. Morton, G. O.; Lancaster, J. E.; Van Lear, G. E.; Fulmor, W.; Meyer, W. E. *J. Am. Chem. Soc.* **1969,** *91,* 1535–1537. doi:10.1021/ja01034a046
118. Zhu, X. M.; Hackl, S.; Thaker, M. N.; Kalan, L.; Weber, C.; Urgast, D. S.; Krupp, E. M.; Brewer, A.; Vanner, S.; Szawiola, A.; Yim, G.; Feldmann, J.; Bechthold, A.; Wright, G. D.; Zechel, D. L. *ChemBioChem* **2015,** *16,* 2498–2506. doi:10.1002/cbic.201500402
119. Feng, X.; Bello, D.; Lowe, P. T.; Clark, J.; O'Hagan, D. *Chem. Sci.* **2019,** *10,* 9501–9505. doi:10.1039/c9sc03374b
120. Phister, T. G.; O'Sullivan, D. J.; McKay, L. L. *Appl. Environ. Microbiol.* **2004,** *70,* 631–634. doi:10.1128/aem.70.1.631-634.2004
121. O'Connor, N. K.; Hudson, A. S.; Cobb, S. L.; O'Neil, D.; Robertson, J.; Duncan, V.; Murphy, C. D. *Amino Acids* **2014,** *46,* 2745–2752. doi:10.1007/s00726-014-1830-z
122. O'Connor, N. K.; Rai, D. K.; Clark, B. R.; Murphy, C. D. *J. Fluorine Chem.* **2012,** *143,* 210–215. doi:10.1016/j.jfluchem.2012.06.033
123. Moran, S.; Rai, D. K.; Clark, B. R.; Murphy, C. D. *Org. Biomol. Chem.* **2009,** *7,* 644–646. doi:10.1039/b816345f
124. Piasecki, S. K.; Keatinge-Clay, A. T. *Synlett* **2012,** *23,* 1840–1842. doi:10.1055/s-0032-1316554
125. Yu, J.-X.; Kodibagkar, V. D.; Liu, L.; Zhang, Z.; Liu, L.; Magnusson, J.; Liu, Y. *Chem. Sci.* **2013,** *4,* 2132–2142. doi:10.1039/c3sc21099e
126. Matsushita, H.; Mizukami, S.; Mori, Y.; Sugihara, F.; Shirakawa, M.; Yoshioka, Y.; Kikuchi, K. *ChemBioChem* **2012,** *13,* 1579–1583. doi:10.1002/cbic.201200331
127. Smith, G. A.; Hesketh, R. T.; Metcalfe, J. C.; Feeney, J.; Morris, P. G. *Proc. Natl. Acad. Sci. U. S. A.* **1983,** *80,* 7178–7182. doi:10.1073/pnas.80.23.7178

128. Bar-Shir, A.; Gilad, A. A.; Chan, K. W. Y.; Liu, G.; van Zijl, P. C. M.; Bulte, J. W. M.; McMahon, M. T. *J. Am. Chem. Soc.* **2013,** *135,* 12164–12167. doi:10.1021/ja403542g
129. Bar-Shir, A.; Yadav, N. N.; Gilad, A. A.; van Zijl, P. C. M.; McMahon, M. T.; Bulte, J. W. M. *J. Am. Chem. Soc.* **2015,** *137,* 78–81. doi:10.1021/ja511313k
130. Sakamoto, T.; Hayakawa, H.; Fujimoto, K. *Chem. Lett.* **2011,** *40,* 720–721. doi:10.1246/cl.2011.720
131. Gan, H.; Oliver, A. G.; Smith, B. D. *Chem. Commun.* **2013,** *49,* 5070–5072. doi:10.1039/c3cc42169d
132. Ray, P. D.; Huang, B.-W.; Tsuji, Y. *Cell. Signalling* **2012,** *24,* 981–990. doi:10.1016/j.cellsig.2012.01.008
133. Lippert, A. R.; Van de Bittner, G. C.; Chang, C. J. *Acc. Chem. Res.* **2011,** *44,* 793–804. doi:10.1021/ar200126t
134. Nonaka, H.; An, Q.; Sugihara, F.; Doura, T.; Tsuchiya, A.; Yoshioka, Y.; Sando, S. *Anal. Sci.* **2015,** *31,* 331–335. doi:10.2116/analsci.31.331
135. Bruemmer, K. J.; Merrikhihaghi, S.; Lollar, C. T.; Morris, S. N. S.; Bauer, J. H.; Lippert, A. R. *Chem. Commun.* **2014,** *50,* 12311–12314. doi:10.1039/c4cc04292a

License and Terms

This is an Open Access article under the terms of the Creative Commons Attribution License (https://creativecommons.org/licenses/by/4.0). Please note that the reuse, redistribution and reproduction in particular requires that the author(s) and source are credited and that individual graphics may be subject to special legal provisions.

The license is subject to the *Beilstein Journal of Organic Chemistry* terms and conditions: (https://www.beilstein-journals.org/bjoc/terms)

The definitive version of this article is the electronic one which can be found at: https://doi.org/10.3762/bjoc.17.28

BEILSTEIN JOURNAL OF ORGANIC CHEMISTRY

CF_3-substituted carbocations: underexploited intermediates with great potential in modern synthetic chemistry

Anthony J. Fernandes[*1], Armen Panossian[1], Bastien Michelet[2], Agnès Martin-Mingot[2], Frédéric R. Leroux[*1] and Sébastien Thibaudeau[*2]

Review

Open Access

Address:
[1]Université de Strasbourg, Université de Haute-Alsace, CNRS, UMR 7042-LIMA, ECPM, 25 Rue Becquerel, 67087 Strasbourg, France and [2]Université de Poitiers, CNRS, IC2MP, UMR 7285, Equipe "Synthèse Organique", 4 Rue Michel Brunet, 86073 Poitiers Cedex 9, France

Email:
Anthony J. Fernandes[*] - a.fernandes.chem@gmail.com;
Frédéric R. Leroux[*] - frederic.leroux@unistra.fr;
Sébastien Thibaudeau[*] - sebastien.thibaudeau@univ-poitiers.fr

* Corresponding author

Keywords:
carbocation; organic synthesis; superelectrophile; trifluoromethyl

Beilstein J. Org. Chem. **2021,** *17,* 343–378.
https://doi.org/10.3762/bjoc.17.32

Received: 21 October 2020
Accepted: 17 December 2020
Published: 03 February 2021

This article is part of the thematic issue "Organo-fluorine chemistry V".

Guest Editor: D. O'Hagan

© 2021 Fernandes et al.; licensee Beilstein-Institut.
License and terms: see end of document.

Abstract

"The extraordinary instability of such an "ion" accounts for many of the peculiarities of organic reactions" – Franck C. Whitmore (1932). This statement from Whitmore came in a period where carbocations began to be considered as intermediates in reactions. Ninety years later, pointing at the strong knowledge acquired from the contributions of famous organic chemists, carbocations are very well known reaction intermediates. Among them, destabilized carbocations – carbocations substituted with electron-withdrawing groups – are, however, still predestined to be transient species and sometimes considered as exotic ones. Among them, the CF_3-substituted carbocations, frequently suggested to be involved in synthetic transformations but rarely considered as affordable intermediates for synthetic purposes, have long been investigated. This review highlights recent and past reports focusing on their study and potential in modern synthetic transformations.

Introduction

Carbocations are pivotal intermediates in organic chemistry, and carbocation-based synthetic chemistry continues to be a vital part of industrial and academic chemistry [1]. A countless number of carbocations have been generated and studied [2,3], and many famous organic chemists strongly participated in their development. Carbocations that are especially intriguing are the destabilized ones that have been elegantly reviewed over the past years by Gassman, Tidwell, and Creary [4-6]. The so-called electron-deficient carbocations, i.e., carbocations substituted with electron-withdrawing groups, drive original reactions, and the most important one among these cations is probably the α-(trifluoromethyl) carbocation. Many efforts are currently devoted to develop methods allowing the efficient insertion of fluorine atoms or fluorinated groups into organic

molecules [7-12]. The increasing demand for fluorinated scaffolds, due to the striking beneficial effects generally resulting from the introduction of these fluorinated motifs [13], also participated in this development. These fluorine effects are nowadays remarkably established in many domains, including medicinal, organic, and organometallic chemistry, catalysis, chemical biology, and material sciences [14-17]. In this context, deciphering the impact that can be exerted by the trifluoromethyl group on a cation and the associated consequences when facing the challenge of developing innovative synthetic methods are the subjects of this review.

Review

Quantitative parameters accounting for the electron-donating or -withdrawing ability of substituents are of major importance in synthetic organic chemistry. The Hammett constant σ for a variety of substituents [18,19] and improved values, known as σ^+, furnished by Brown et al. [20,21] – some of which are listed in Table 1 for selected substituents – were developed towards this aim. Following this classification, the CF_3 group is amongst the most electron-withdrawing substituents, with a σ_p^+ value of +0.612 for the *para*-position.

Table 1: Selection of Hammett constant σ^+ values for selected functional groups X, extracted from References [20,21].

X	σ^+	
	meta	*para*
NMe_2	n.d.	–1.7
NH_2	–0.16	–1.3
OH	+0.12[a]	–0.92
OMe	+0.047	–0.778
CH_3	–0.066	–0.311
$SiMe_3$	+0.011	+0.021
Ph	+0.109	–0.179
H	0	0
SMe	+0.158	–0.604
F	+0.352	–0.073
Cl	+0.399	+0.114
Br	+0.405	+0.150
I	+0.359	+0.135
NMe_3^+	+0.359	+0.408
CO_2Et	+0.366	+0.482
C(O)Me	+0.38[a]	+0.50[a]
CF_3	**+0.52**	**+0.612**
CN	+0.562	+0.659
NO_2	+0.674	+0.790

[a]σ values based on benzoic acid ionization.

However, as noted by Reynolds et al. [22,23], "the electronic effect of a substituent depends to a certain extent upon the electron demand in the system to which it is attached". Thus, despite the strong intrinsic electron-withdrawing character, the trifluoromethyl group was shown to modestly act as a π-electron donor when substituting a carbenium ion. Ab initio calculations were performed to account for the π-electron-donating ability of several substituents conjugated with carbocations (Table 2). It is noteworthy that amongst the several substituents studied, the CF_3 group exhibits the lowest π-electron-donation ability in each investigated carbenium series, reflecting, as one could expect, the very poor stabilizing power by π-electron donation. A trend exists in the magnitude of the parameter according to the nature of the carbenium ions, which is in line with the carbenium ion stability (alkyl < allylic < benzylic). Thus, an increased π-electron transfer is present in the least-stabilized alkylcarbenium ions, in which a higher electronic contribution from neighboring substituents is required.

Table 2: π-Electron-transfer parameters from STO-3G calculations with optimized C–X bond length (established as $\sum q_\pi$, without unit) for substituents X in alkyl, allylic, and benzylic carbenium ions. Parameters for neutral phenyl derivatives are given for comparison. Negative values indicate π-electron donation by the substituent [22,23].

X		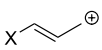	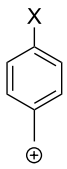	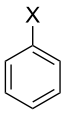
NH_2	–566	–434	–284	–115
OH	–486	–334	–202	–90
$CH{=}CH_2$	–427	–243	–148	0
F	–353	–223	–134	–70
CN	–262	–105	–33	+21
CHO	–155	–77	–20	+27
CH_3	–113	–58	–29	–8
NO_2	–76	–36	–10	+19
CF_3	**–29**	**–15**	**–4**	**+10**
H	0	0	0	0

Detailed ab initio studies have been focused on the stability of the $CF_3CH_2^+$ cation and provide pieces of thoughts on the origins of the stabilizing interactions in α-(trifluoromethyl)carbenium ions. The optimization of the geometry for $CF_3CH_2^+$ at the STO-3G level led to an energy minimum, in which one of the fluorine atoms is significantly closer to the positive carbon center (Figure 1, top, θ = 101°) [24]. However, exactly the same structural distortion was calculated for the ethyl cation. Furthermore, the very small π-electron density calculated in the 2pC orbital of $CF_3CH_2^+$ (0.04 electrons) led the authors to conclude that "there is no hyperconjugative stabilization by the CF_3 group". The presence of this attractive interaction should, how-

ever, not be discarded. Indeed, the quantitative PMO analysis at the 6-31G* level allowed, by calculating fragment orbitals (FO), the identification of the nature of this attractive interaction [25]. The latter arose from a homoconjugation interaction (−5.3 kcal·mol^{-1}) of one fluorine lone pair (πnF FO) with the empty 2pC orbital of the cationic carbon center (Figure 1, top). A second stabilizing interaction was also found and came from hyperconjugation of the CF_3 substituent, involving interactions between the empty 2pC orbital with the πCF_3 FO (−5.2 kcal·mol^{-1}). In 2018, spectroscopic evidence for the generation of the first observable fluoronium ion **1** by Letcka et al., which can be seen as a strong nF→2pC interaction (Wiberg bond order of 0.53 for each C–F bond), gave additional credit to these calculations (Figure 1, bottom) [26-28].

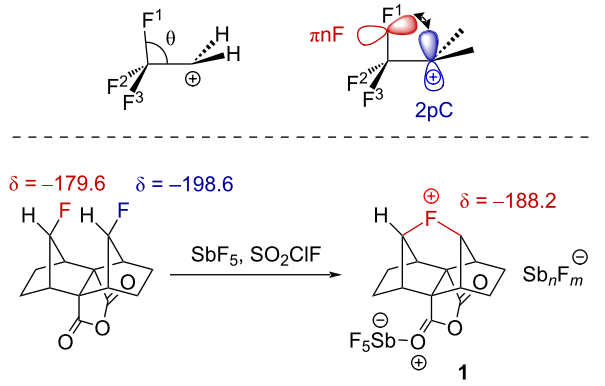

Figure 1: Stabilizing interaction in the $CF_3CH_2^+$ carbenium ion (top) and structure of the first observable fluoronium ion **1** (bottom) (δ in ppm).

The thermochemical data can also provide information on the effect of the CF_3 group on the stability of the carbenium ions. Calculations of the isodesmic reactions (1), (2), and (3) demonstrate the overall destabilizing effect of CF_3 compared to H or CH_3 when directly attached to a carbenium ion (i.e., α position, Scheme 1) [5,29]. Even an oxonium ion appears to be significantly destabilized by the presence of the CF_3 group. These data globally suggest, as one could expect, an electronic destabilizing effect of the CF_3 group when attached closely to a carbenium ion. However, any strong nF→2pC interaction might also influence the overall stability of any system.

Any perspectives toward CF_3-containing carbocation-based synthesis must take this trend into account, especially studies on the specific α-(trifluoromethyl)carbenium ions. This review aims to systematically relate the reported work in this field. For each part, a focus on a series of α-(trifluoromethyl)carbenium ions differing in its chemical environment will be scrutinized. The chapter will summarize kinetic studies and concomitant theoretical investigations on the cations formation and stability

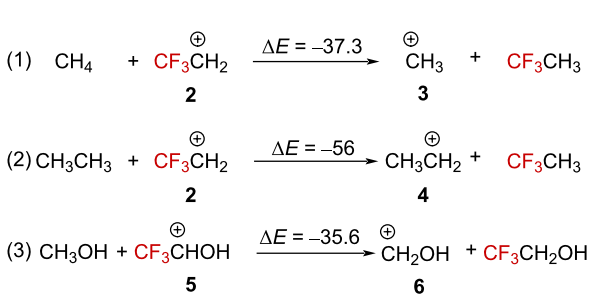

Scheme 1: Isodesmic equations accounting for the destabilizing effect of the CF_3 group. Δ*E* in kcal·mol^{-1}, calculated at the 4-31G level.

data as well as synthetic perspectives offered by the studied carbenium ions. Any discussion of the results coming from the ionization of perfluorinated substrates will not be addressed in this review [30-33].

Aryl-substituted trifluoromethylated carbenium ions

α-(Trifluoromethyl)-substituted carbenium ions: At the dawn of their outstanding studies on carbocation chemistry, Olah et al. empirically demonstrated that despite exhibiting the highest Pauling electronegativity, the fluorine atoms, when directly linked to a carbenium ion, can be engaged in significant resonance electron donation (Scheme 2) [34]. While stabilizing the positively charged carbon center via lone pair conjugation, the electron density at the fluorine atom decreases, and this phenomenon is shown by a large downfield shift in the ^{19}F NMR spectrum of **8** compared to the neutral precursor **7**.

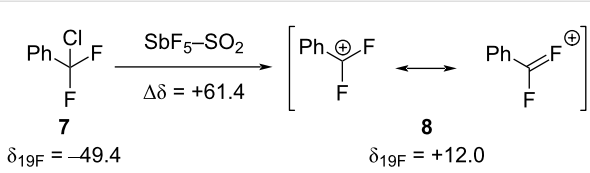

Scheme 2: Stabilizing effect of fluorine atoms by resonance electron donation in carbenium ions (δ in ppm).

Following these studies on the evaluation of fluorine atom(s) substitution on cation behavior, Olah et al. then investigated the expected destabilizing effect resulting from the presence of fluorine atoms close to a carbenium ion [35]. Thus, Olah et al. envisioned the possibility to generate α-(trifluoromethyl)carbenium ions, and this achievement led to the first direct observation of these species using low-temperature NMR experiments in situ [35]. In this study, the authors furnished spectroscopic evidence for the complete ionization of several α-(trifluoromethyl) alcohol precursors **9a–c** in a superacidic FSO_3H–SbF_5–SO_2 medium. They also brought experimental

^{19}F NMR variation values up to Δδ = +24.8 ppm (Scheme 3). This suggests a partial stabilization of the cationic center by hyperconjugation and/or fluorine lone pair interaction, resulting in a certain degree of a positive charge of one fluorine atom. Interestingly, at least one phenyl substituent was required to allow the ionization of the starting alcohols into the corresponding carbenium ions. When the aromatic substituent was absent or upon installation of an additional CF_3 group, only the corresponding protonated alcohols **10d–g** were observed.

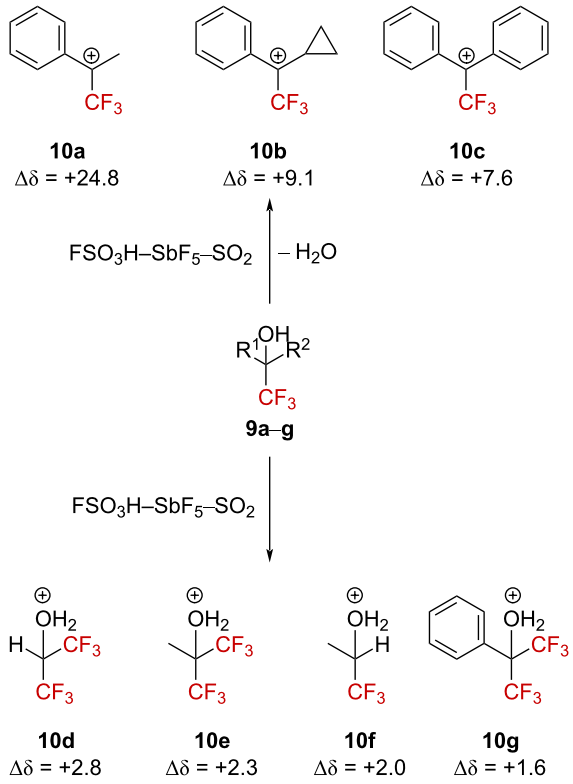

Scheme 3: Direct in situ NMR observation of α-(trifluoromethyl)carbenium ion or protonated alcohols. $\Delta\delta = \delta_{19F,product} - \delta_{19F,precursor}$ (δ in ppm).

Olah et al. also reported the ^{13}C NMR chemical shifts for carbenium ion **10c** upon ionization of the alcohol precursor **9c** in a superacid (Scheme 4) [36]. A large downfield shift was observed predominantly at the benzylic position ($\Delta\delta_{13C}$ = 110.1 ppm), with minor impacts at the *ortho*- and *para*-positions ($\Delta\delta_{13C} \approx 20$ ppm) relative to the starting alcohol **9c** [37]. These variations are fully consistent with the presence of a positive charge located at the benzylic position, with only partial stabilization of the cationic center by the phenyl groups.

Similarly, Laali et al. observed significant ^{19}F NMR downfield chemical shifts upon the formation of α-(trifluoromethyl)pyrenylcarbenium- and α-(trifluoromethyl)anthracenyl-

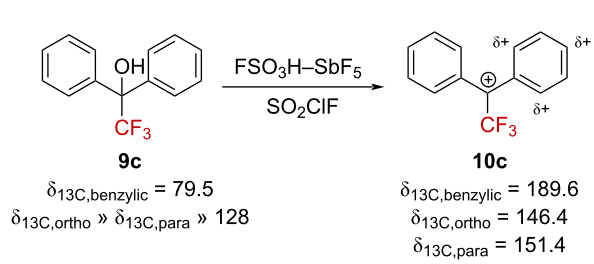

Scheme 4: Reported ^{13}C NMR chemical shifts for the α-(trifluoromethyl)carbenium ion **10c** (δ in ppm).

carbenium ions **12a–d** from the corresponding carbinols **11a–d** (Scheme 5) [38].

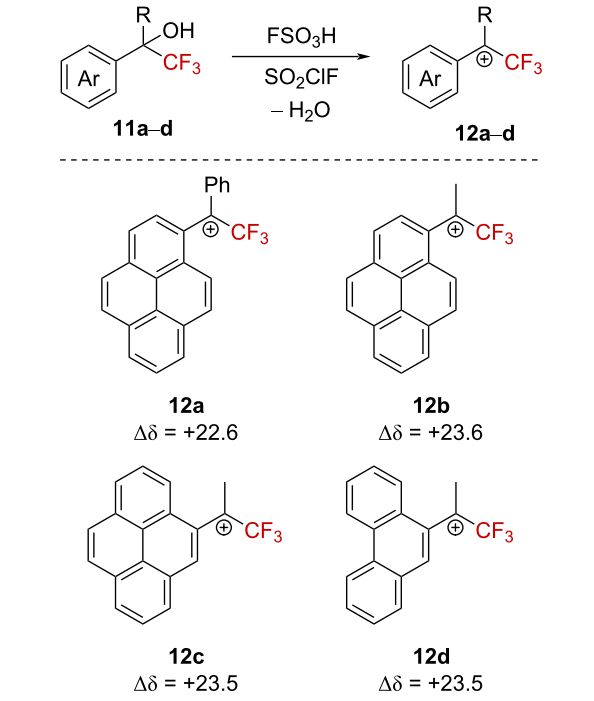

Scheme 5: Direct NMR observation of α-(trifluoromethyl)carbenium ions in situ (δ in ppm).

Tidwell et al. explored the influence of a CF_3 group on the solvolysis reaction of various benzylic sulfonate derivatives [39,40]. They found a linear free-energy relationship between the solvolysis rate of sulfonate **13f** in different solvents compared to the one of 2-adamantyl tosylate, the latter being known to undergo solvolysis via the formation of a carbenium ion. Hence, the formation of a highly destabilized α-(trifluoromethyl)carbenium ion $\mathbf{14f}_{OTs}$ was established as the rate-limiting step in the solvolysis reactions of **13f** (Scheme 6). Furthermore, the authors determined a k_{CH3}/k_{CD3} ratio of 1.54, highlighting an isotopic effect consistent with a solvolysis

mechanism involving a carbenium ion (k_{CH3}/k_{CD3} = 1.48 for 2-methyl-2-adamantyl tosylate). Also, $k_H/k_{CF3} = 2{\cdot}10^5$ was established, illustrating the retarding α-CF_3 effect in the production of a carbenium ion [41]. In the solvolysis reaction of **13f**, a mixture of the major product **15f**, resulting from solvent substitution, and the minor elimination product **16f** was observed. Further, ^{14}C labeling experiments on **13f** confirmed that the formation of the ion pair $\mathbf{14f}_{OTs}$ was a reversible process [42].

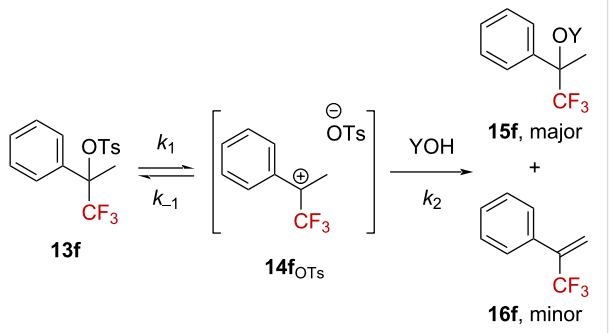

Scheme 6: Illustration of the ion pair solvolysis mechanism for sulfonate **13f**. YOH = solvent.

Later, Liu et al. explored the solvolysis of aryl derivatives **13a–i** to highlight the importance of the nature of the aromatic substituent on the solvolysis rate (Figure 2) [43]. As anticipated, a faster rate was observed for electron-donating groups, while electron-withdrawing groups slowed the process down. Plotting the Hammett–Brown correlation, established as $\log(k) = f(\sigma^+)$, gave a linear dependence of the rate with the σ^+ parameters of the aryl substituents, with a behavior in agreement with the transient formation of a carbenium ion. The slope of the straight line, $\rho^+ = -7.46$, reflects the very high electron demand induced by the CF_3 group. Remarkably, they found that CF_3 deactivates to such an extent that benzylic tosylate **13f** was approximately 10 times less reactive than benzylic tosylate **17** (Figure 2, top). Similarly to the previous study, the Grunwald–Winstein plot [44] gave a linear free-energy relationship between the solvolysis rate for derivatives **13f** or **13g** and the solvent polarity parameter Y_{OTs} [45]. The solvent participation in the solvolysis of these tertiary benzylic tosylates was thus defined as "unimportant" by the authors.

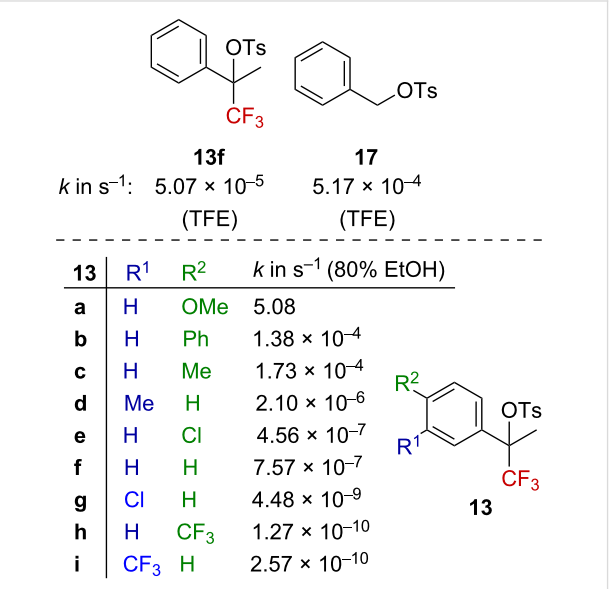

Figure 2: Solvolysis rate for **13a–i** and **17**.

Gassman and Harrington successfully measured the solvolysis kinetics of CF_3-substituted allylic triflates **18** and **19**, showing a significant solvolysis retardation with CF_3-substituted substrates (Figure 3) [46]. These results are in accordance with an earlier study that revealed that **20** was unreactive in acetone/H_2O 70:30, even over a period of 35 days at 50 °C [47].

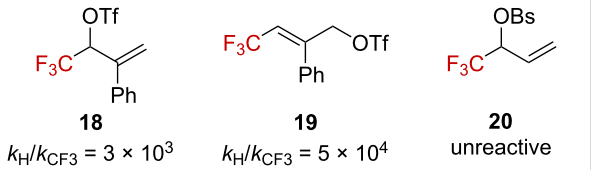

Figure 3: Structures of allyl triflates **18** and **19** and allyl brosylate **20**. Bs = *p*-$BrC_6H_4SO_2$.

Encouraged by these preliminary results, Tidwell et al. envisioned the possibility to study the solvolysis reaction of secondary benzylic sulfonates [48]. In tertiary benzylic sulfonates [39,43], a linear free-energy relationship between the solvolysis rate for the secondary benzylic tosylates **21** (Figure 4) and Y_{OTs} was obtained. Similarly, the nature of the aromatic substituent influenced the solvolysis rate, with an observed acceleration for substrates adorned with electron donor substituents and a deceleration for those carrying electron-withdrawing substituents. The Hammett–Brown correlation gave a straight line, with $\rho^+ = -10.1$ (80% EtOH, 25 °C), a significantly greater magnitude than for the tertiary derivatives (−7.46), in agreement with the transient formation of a more destabilized carbenium ion (i.e., a secondary carbenium ion). They also noticed that the greatest magnitude of ρ^+ was obtained in the most nucleophilic and less ionizing solvents, in agreement with an increased electron demand on the aromatic substituent in a poorly ionizing solvent. This also suggests that the positive charge is delocalized to a higher extent on the aromatic substituent for the secondary tosylates than for the tertiary ones. These data support the hypothesis that the transient formation of a carbenium ion is the rate-limiting step and the absence of significant solvent par-

ticipation in the latter. Richard also conducted extensive studies on the impact of the nature of the leaving group (I, Br, OSO_2R, etc.) and on the aryl substituents (NMe_2, OMe, SMe, etc.) in the derivatives **21**, substituted with a secondary CF_3 group in the benzylic position, and reported similar conclusions [49,50].

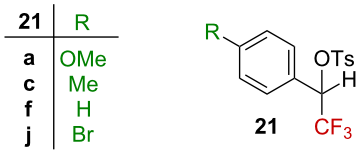

Figure 4: Structure of tosylate derivatives **21**.

A different behavior emerged from triflate derivatives **22** (Figure 5a). In addition to their enhanced reactivity (k_{Tf}/k_{Ts} = 2 × 10^4), a nonlinear free-energy relationship between the solvolysis rate and Y_{OTs} was obtained, suggesting an important solvent participation in these cases. Further investigations on **22f** showed deuterium isotope effects in agreement with the transient formation of a carbenium ion. A solvent dependence of the k_H/k_D ratio was also noticed, with the higher ratios being obtained in the most ionizing and less nucleophilic solvents (i.e., 1.34 ± 0.07 in HFIP vs 1.21 ± 0.01 in 80% EtOH). The subsequent solvolysis of enantioenriched triflate (*R*)-(−)-**22f** evidenced that in a poorly ionizing solvent, such as AcOH, solvolysis occurred with 41% inversion (and 59% racemization, i.e., product **23f** was obtained with an enantiomeric ratio of ca. 70:30 in favor of the (*S*)-enantiomer), while complete racemization was observed in more ionizing TFA or HFIP as the solvent (Figure 5b) [48]. These observations are in agreement with a process generating a carbenium ion in highly ionizing solvents (TFA, HFIP, etc.) for the tosylates derivatives, and with the concomitant formation of a contact ion pair **25f**$_{OTf}$ favoring the S_N2 process in less ionizing solvents (Figure 5c). Recent studies conducted by Moran et al. support the ionization via a S_N1 process for trifluoromethylcarbinol derivatives related to **22** under TfOH–HFIP activation [51].

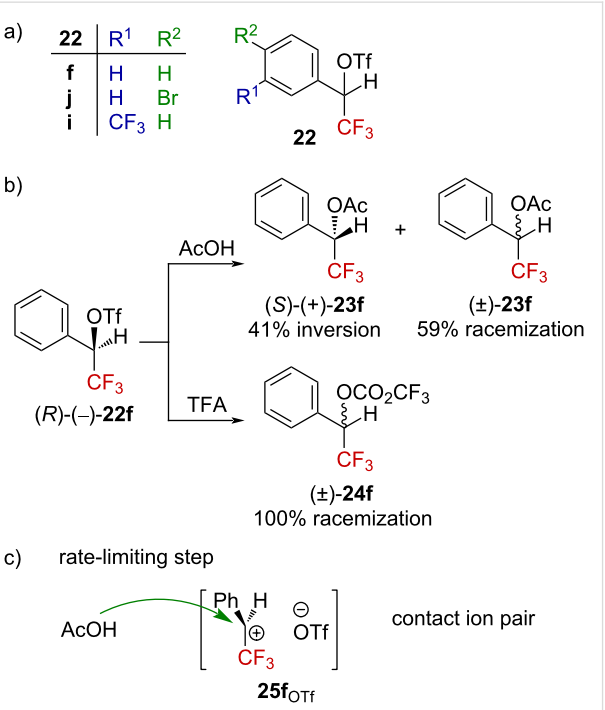

Figure 5: a) Structure of triflate derivatives **22**. b) Stereochemistry outcomes of the reaction starting from (*R*)-(–)-**22f**. c) Rate-limiting step in poorly ionizing solvents.

Tidwell et al. investigated CF_3-containing naphthyl- and anthracenylsulfonate derivatives **26** and **29** [52]. They reported that while the solvolysis of **26** afforded the expected compounds **27** and **28**, that of **29** exclusively gave the ring-substituted products **30**–**32** (Scheme 7). A Grunwald–Winstein plot gave linear dependences of the solvolysis rate against Y_{OTs} in both cases, suggesting that the formation of the carbenium ions was the rate-limiting step. Thus, the formation of products **30**–**32** is best explained by a complete charge delocalization from an α-(trifluoromethyl)carbenium ion to anthracenylcarbenium ion **33**, with subsequent trapping of **33** by the solvent.

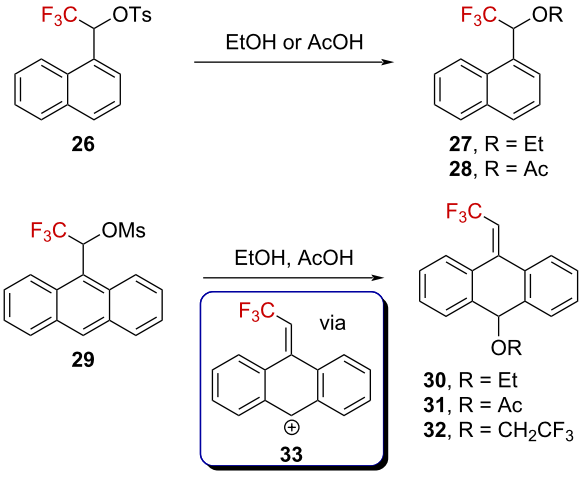

Scheme 7: Solvolysis reaction of naphthalene and anthracenyl derivatives **26** and **29**.

The solvolysis of the bisarylated α-CF_3-substituted tosylates bearing electron-withdrawing substituents was investigated by Liu and Kuo [53]. The Hammett–Brown correlation considering derivatives **34** (Figure 6) gave a linear free-energy correlation with $\rho^+ = -3.98$, which is approximately half the value of those previously reported for the benzylic α-CF_3-substituted tosylate derivatives **13** substituted by a methyl group (Figure 2)

[43,48]. The presence of the additional phenyl group, in addition to the CF_3 group, was suggested to induce a lower ρ^+ value. This could be explained in terms of a twisted electron-poor aryl ring, which was not in the plane of the carbenium ion for stereoelectronic reasons. The cation is thus stabilized by the additional phenyl ring in **35** (Figure 6).

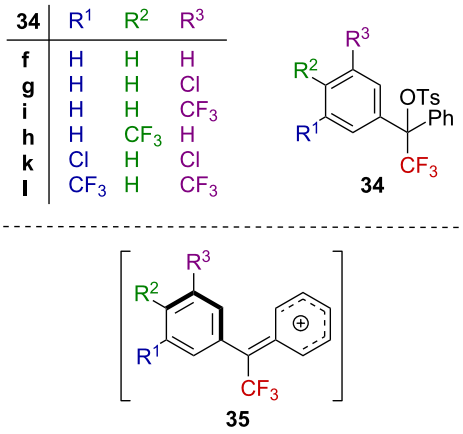

Figure 6: Structure of bisarylated derivatives **34**.

As an extension of the previous study, Liu et al. explored the solvolysis of tertiary, highly congested benzylic α-CF_3-substituted halides **36** (Figure 7) [54]. Similar to their previous results, they obtained straight lines upon plotting the Hammett–Brown or Yukawa–Tsuno correlations, with ρ^+ values from −5.9 to −7.4, depending on the solvent and on the chosen treatment. These values are close to those obtained from previous studies, suggesting a significant stabilization of the transient carbenium ion by the ring.

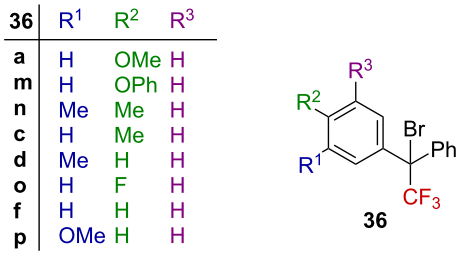

Figure 7: Structure of bisarylated derivatives **36**.

Early interest in bisarylated α-CF_3-substituted alcohols was shown by Cohen and Kaluszyner [55,56] and by Streitwieser et al. [57]. The cyclodehydration of **9c** occurs in polyphosphoric acid to afford fluorene **37** (Scheme 8) [57]. A mechanistic proposal invoking the initial generation of the α-(trifluoromethyl)carbenium ion **10c↔10c'** was mentioned by the authors [55,56]. Related studies on diphenyl derivative **9c** in a mixture of H_2SO_4 and chloroform also showed the formation of fluorene derivative **37** in 25% yield [58].

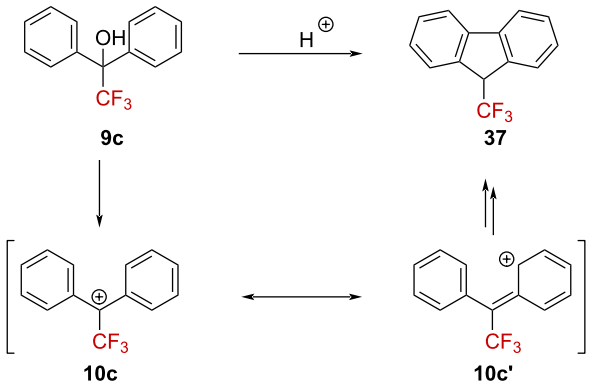

Scheme 8: Reactivity of **9c** in the presence of a Brønsted acid.

Exploiting this impact of the trifluoromethyl substituent in the cationic Nazarov electrocyclization, the synthesis of CF_3-substituted indenes **39a–c** from the α-(trifluoromethyl)allyl-substituted benzyl alcohols **38a–c** in strong acids has been reported (Scheme 9) [59]. The significant rate retardation observed upon the addition of further CF_3 groups, illustrated by the need for harsh reaction conditions, strongly supports the formation of delocalized α-(trifluoromethyl)carbenium ions **40a–c**.

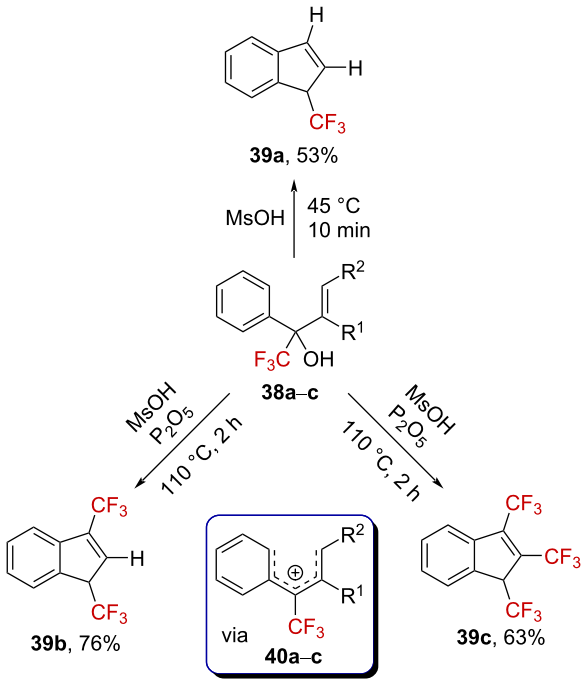

Scheme 9: Cationic electrocyclization of **38a–c** under strongly acidic conditions.

Vasilyev et al. also investigated this Nazarov electrocyclization for the synthesis of indene derivatives. Thus, a variety of indenes **42** could be readily obtained from α-(trifluoromethyl)allyl-substituted benzyl alcohols **41a** or the corresponding silyl ethers **41b** upon the reaction in a dichloromethane solution of sulfuric acid or triflic acid [60,61]. The authors also reported that indenes **42** could undergo a subsequent Friedel–Crafts alkylation when **41b** was reacted in the presence of an external aromatic partner Ar'H in pure triflic acid. Thus, a variety of α-(trifluoromethyl) silyl ethers **41b** was converted into the corresponding indanes **43** in low to high yields [62]. The *trans*-isomers were generally obtained as the major product (Scheme 10).

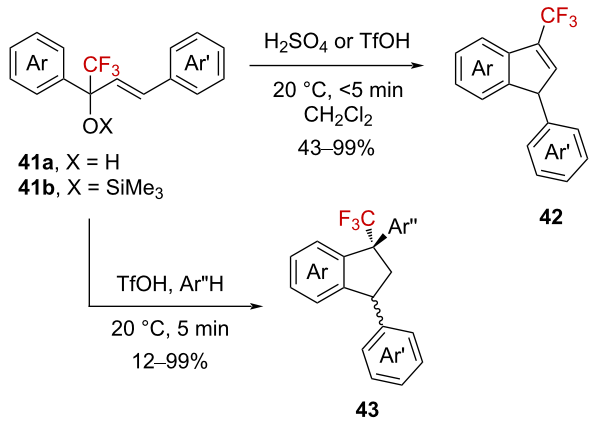

Scheme 10: Brønsted acid-catalyzed synthesis of indenes **42** and indanes **43**.

Bis[α-(trifluoromethyl)]-substituted carbenium ions: More destabilized bis(trifluoromethyl)-substituted carbenium ions have also been suggested to exist as reaction intermediates. During their investigations on the reactivity of sulfuranes under acidic conditions, Martin et al. reported that sulfurane **44** reacts with triflic acid to provide alcohol **9g** and sultine **46**, according to ^{1}H and ^{19}F NMR assignments, and triflate **45f**, which was isolated after basic workup of the reaction (59% yield) [63]. Hence, protonation of **44** led to dialkoxysulfonium triflate **47** along with the release of alcohol **9g**. The subsequent formation of the excellent sultine leaving group **46** (assumed to be as good of a leaving group as N_2) [63] is the driving force for the decomposition of **47**, generating collaterally bis(trifluoromethyl)-substituted carbenium ion intermediate **48f**$_{OTf}$. Finally, triflate **45f** is formed after ion pair recombination (Scheme 11). Similar experiments conducted with ^{18}O-labeled **44** confirmed the proposed mechanism, including the transient formation of **48f**$_{OTf}$.

The solvolysis of triflate **45f** was explored next [63]. Heating **45f** in water or methanol resulted in the expected solvolyzed

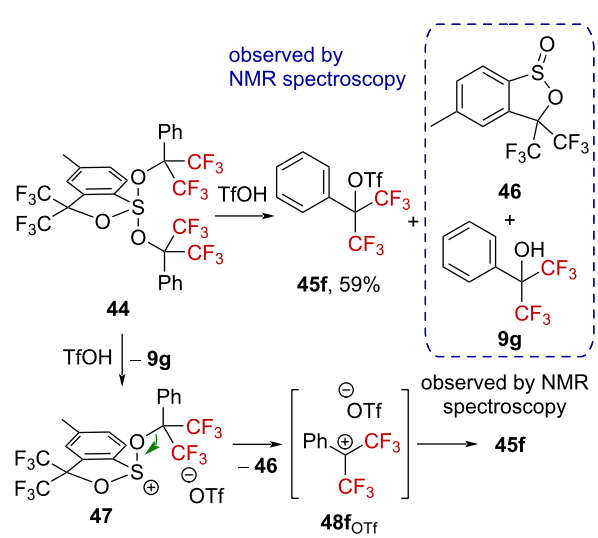

Scheme 11: Reactivity of sulfurane **44** in triflic acid.

products **9g** or **49** and the concomitant formation of **50a** or **50b** (Scheme 12a). A S_N1 mechanism was thus suggested, with formation of the benzylic cation intermediate **48f**↔**48f'**, stabilized by the phenyl group (Scheme 12b).

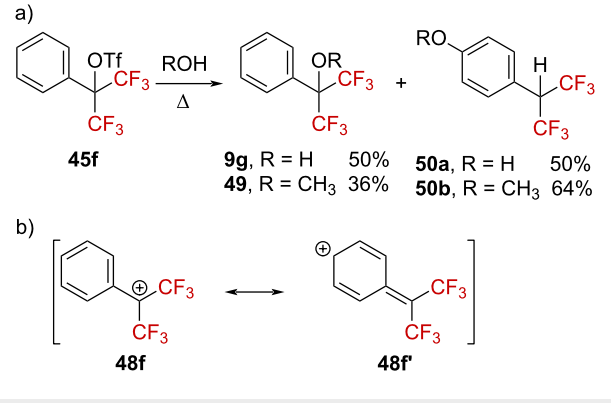

Scheme 12: Solvolysis of triflate **45f** in alcoholic solvents.

Substrate **51**, bearing a *tert*-butyl group in the *para*-position, was also submitted to solvolysis in labeled $H_2{}^{18}O$, generating the labeled benzylic alcohol ^{18}O-**52** (Scheme 13). The solvol-

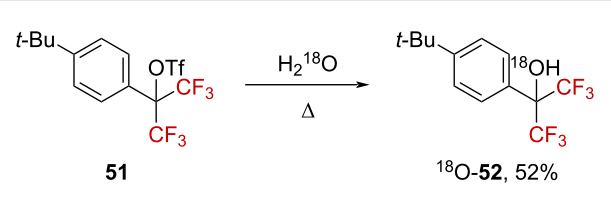

Scheme 13: Synthesis of labeled ^{18}O-**52**.

ysis of **51** was found to be much faster than that of **45f** by at least a factor of 10, encouraging the authors to suggest "a transition state resembling **48f** in the rate-limiting step".

Sulfurane **53**, bearing $OC(CF_3)_3$ groups, was also treated with triflic acid, affording dialkylsulfonium species **54** in 91% yield along with perfluoro-*tert*-butyl alcohol (Scheme 14) [63]. No further decomposition was observed in this case, suggesting that the especially challenging perfluoro-*tert*-butylcarbenium ion **55** cannot be generated.

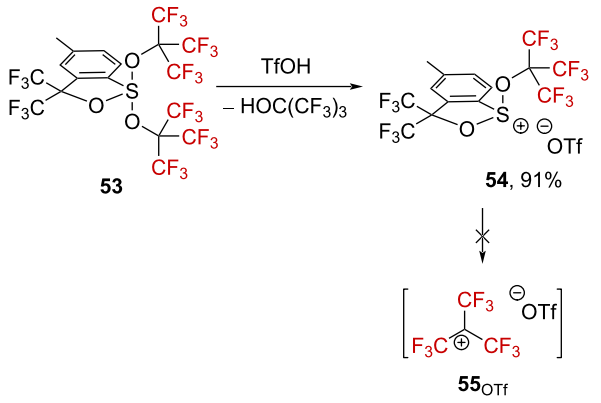

Scheme 14: Reactivity of sulfurane **53** in triflic acid.

Highly deactivated bis(trifluoromethyl)-substituted carbenium ions and their precursors were also explored in detail by Tidwell et al. [64-66] and Richard et al. [67] in solvolysis studies of di(trifluoromethyl)-substituted tosylates **56** in comparison to the monosubstituted analogue **21f** (Figure 8). A linear free-energy relationship was found upon plotting the solvolysis rate against Y_{OTs} and $\rho^+ = -10.7$ (TFA) for the Hammett–Brown correlation. The linear dependence of the rate on the solvent ionizing power, in addition to the strong effect of the substituents on the reactivity, are in agreement with the conclusions of Martin et al. [63] as they strongly support the formation of a bis(trifluoromethyl)-substituted carbenium ion **48**.

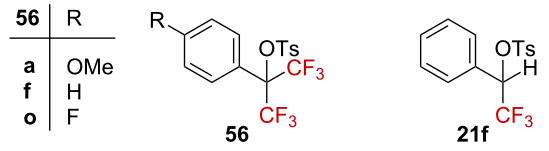

Figure 8: Structure of tosylates **56** and **21f**.

Surprisingly, a relatively low kinetic effect ($k_H/k_{CF3} = 54$, in TFA) was observed by comparing the solvolysis rate of tosylates **21f** and **56f**. For *p*-OMe derivatives **21a** and **56a**, $k_H/k_{CF3} = 2.5$ (HFIP) was obtained. These ratios are very small compared to typical k_H/k_{CF3} ratios in the 10^4–10^7 range [39-41,43,48,68]. Thus, while introducing one CF_3 group dramatically alters the reactivity, an additional CF_3 group does not seem to significantly impact the reactivity any further. The hypothesis of a ground-state strain release to explain this behavior was discarded as an analysis of the structures of **56f**, **13f**, and **21f** by X-ray diffraction crystallography revealed similar bond angle distortions [64,65]. A considerable delocalization of the positive charge in the aryl ring was therefore suggested (Scheme 15): in the dominant resonance form **25f'**, **48f'**, or **14f'**, the α-substituent (i.e., H, CH_3, or CF_3) would have a poor impact. Gas phase calculations by Tsuno et al. provided evidence for the significantly increased resonance stabilization contribution in **14f**↔**14f'** ($r = 1.4$) relative to the *t*-cumyl cation **57** (r = 1.0) [69].

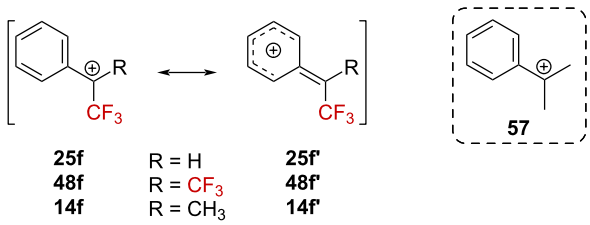

Scheme 15: Resonance forms in benzylic carbenium ions.

α-(Trifluoromethyl)heteroarylcarbenium ions

The presence of a strong electron-donating substituent could compensate the extreme deactivating power of the CF_3 group, favoring a further exploitation for synthetic purposes. In this context, Tidwell and Kwong-Chip compared the solvolysis of *N*-methylpyrrole **58** to **59** (Figure 9) [70].

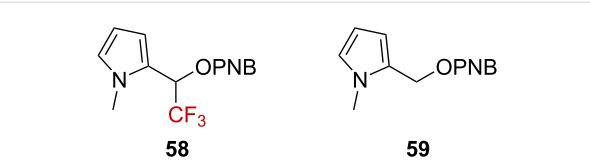

Figure 9: Structure of pyrrole derivatives **58** and **59**.

A very similar rate was determined for **58** and **59**, with $k_{CF3} = 4.40 \times 10^{-4}$ s^{-1} and $k_H = 1.84 \times 10^{-2}$ s^{-1}, respectively, providing a rate ratio of $k_H/k_{CF3} = 41.8$. Plotting the solvolysis rate of **58** against Y_{OTs} led to a linear free-energy relationship supporting the rate-limiting formation of a carbenium ion **60**. The small k_H/k_{CF3} ratio suggests here that the positive charge is highly delocalized in the pyrrole ring and should be regarded as a pyrrolium ion **60'** rather than an α-(trifluoromethyl)carbenium ion **60** (Scheme 16).

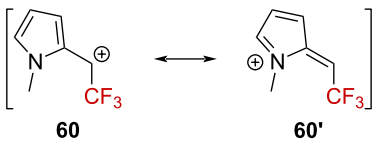

Scheme 16: Resonance structure **60**↔**60'**.

Similarly, trifluoromethyl-substituted indolium ions were invoked as intermediates in the recently reported gallium-catalyzed synthesis of unsymmetrical CF_3-substituted 3,3'- and 3,6'-bis(indolyl)methanes from trifluoromethylated 3-indolylmethanols [71]. Alcohol **61** reacts with indole **62** to provide a product **63** or **64**, depending on the temperature (Scheme 17).

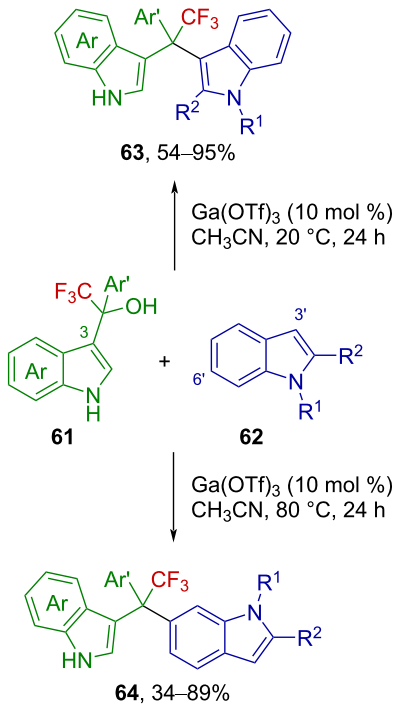

Scheme 17: $Ga(OTf)_3$-catalyzed synthesis of 3,3'- and 3,6'-bis(indolyl)methane from trifluoromethylated 3-indolylmethanols.

The authors suggested that an indolium ion **65** is produced from the activation of **61** with $Ga(OTf)_3$ and reacts with **62** in a Friedel–Crafts reaction to afford **63** (Scheme 18). Further control experiments showed that derivatives **63** were not stable at 80 °C under the reaction conditions and isomerized to furnish **64**. Based on these observations, the authors proposed that upon heating, $Ga(OTf)_3$ reacts with **63** to release an indolium ion **65** and forms an organogallium species **67** via intermediate **66**, which, after protodemetallation, releases indole **62** and regenerates the catalyst. The retro-Friedel–Crafts reaction at 80 °C at the indole C3-position thus allows the progressive conversion of the starting material into the C6-derivative **64** (Scheme 18).

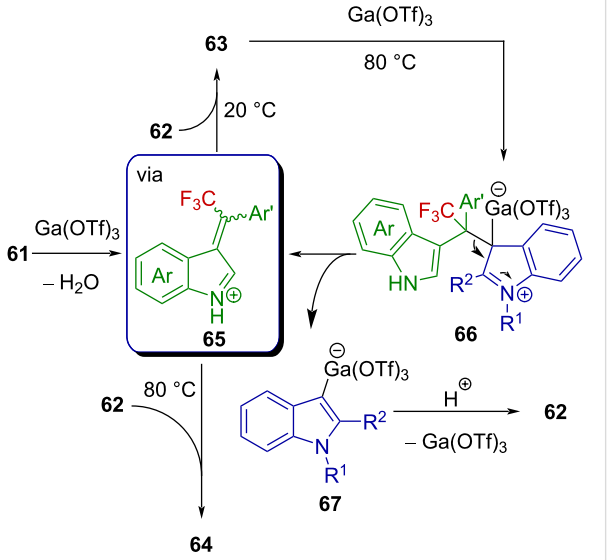

Scheme 18: Proposed reaction mechanism.

Chen et al. reported the synthesis of C2-phosphorylated indoles via 1,2-phosphorylation of 3-indolylmethanols with *H*-phosphine oxides or *H*-phosphonates under Brønsted acid activation [72]. The scope of the reaction includes one example of a CF_3-substituted 3-indolylmethanol, **68**, which is efficiently phosphorylated by **69** in the presence of a catalytic amount of camphor sulfonic acid (CSA) at 60 °C, affording **70**. The authors suggested the transient formation of an analogous indolium ion **71** (Scheme 19).

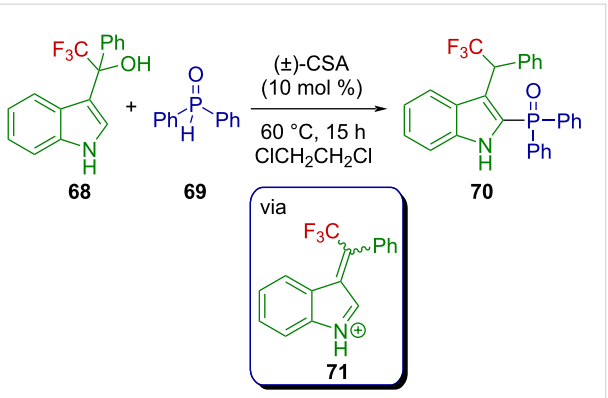

Scheme 19: Metal-free 1,2-phosphorylation of 3-indolylmethanols.

Very recently, Vasilyev and Khoroshilova investigated the superacid-promoted activation of α-(trifluoromethyl) silyl ethers

exhibiting a thiophene core [73]. At 0 °C, thiophenes **72**-Cl and **72**-Br undergo electrophilic dimerization, affording a mixture of **73**-Cl and **73**-Br (Scheme 20). When the reaction was cooled to −60 °C < *T* < −40 °C in the presence of aromatic nucleophiles, thiophenes **72**-Cl and **72**-Br could be converted into **74**-Cl and **74**-Br derivatives via a side-chain arylation reaction. When the reaction was conducted at −40 °C, the reactivity was shown to be governed by the nature of the halogen atom. For the brominated derivatives **72**-Br, the corresponding side-chain arylation reaction occurred at −60 °C, but a further hydrodehalogenation led to the bromine-free derivatives **75**. For the chlorinated derivatives **72**-Cl, a similar side-chain arylation−hydrodehalogenation sequence occurred, but an additional Friedel–Crafts arylation at the C4-position led to derivatives **76**. In this latter case, a two-step one-pot process was developed in order to access derivatives bearing two different aromatic rings.

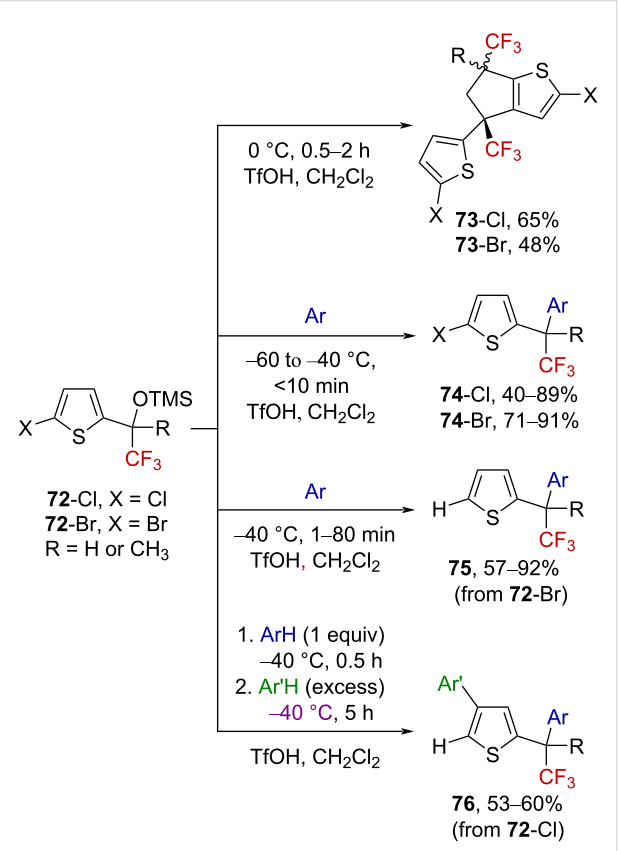

Scheme 20: Superacid-mediated arylation of thiophene derivatives.

Mechanistic investigations were then undertaken by in situ low-temperature NMR experiments, allowing the observation of thiophenium ions $\mathbf{77}_{Me}$-Cl and $\mathbf{77}_{Me}$-Br (Scheme 21). ^{19}F NMR analysis showed significant downfield shifts for the signal of the CF_3 group compared to the neutral precursors, characteristic of α-(trifluoromethyl)carbenium ions. However, and as expected, the ^{13}C NMR spectra showed considerable downfield shifts for the carbon atoms C2 and C6, suggesting a highly delocalized positive charge in the heteroaromatic ring as depicted below.

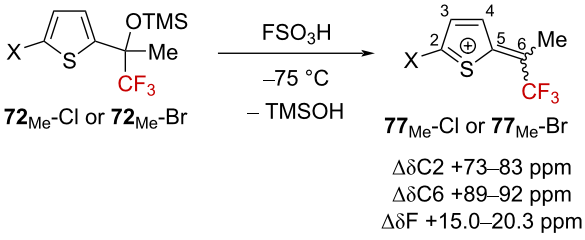

Scheme 21: In situ mechanistic NMR investigations.

α-(Trifluoromethyl)allylcarbenium ions

In 1976, Poulter et al. exploited the powerful electron-withdrawing effect of the CF_3 group to elucidate the prenyltransferase-catalyzed condensation mechanism [74,75]. The authors envisioned that substituting a methyl group in isopentenyl pyrophosphate (IPP) by a CF_3 group (Scheme 22, **79**→**78**) should greatly reduce the reaction rate in the case of an ionization–condensation–elimination mechanism, while a small acceleration should be observed in the case of a displacement–elimination mechanism.

Promising results were first obtained during investigations conducted on CF_3-substituted derivatives in S_N1- and S_N2-mechanism-based reactions (Scheme 23). A profound retardation effect for the solvolysis of **81** in acetone–H_2O (S_N1) with $k_{CH3}/k_{CF3} = 5.4 \times 10^5$ was observed, while **85** promoted the Finkelstein reaction (S_N2) about 11 times faster than **84** ($k_{CH3}/k_{CF3} = 8.9 \times 10^{-2}$, Scheme 23). This is the result of a destabilized cationic intermediate in the first case and a stabilized negatively charged transition state in the second.

When **78** was incubated in the presence of IPP and the enzyme prenyltransferase, a rate of 5.1×10^{-4} nmol·min^{-1}·mg^{-1} was measured for the condensation reaction (Scheme 24), which is to be compared to a value of 7.4×10^2 nmol·min^{-1}·mg^{-1} observed for the condensation involving IPP and geranyl pyrophosphate (GPP). **78** was 1.5×10^6 times less reactive than geranyl pyrophosphate, allowing to conclude that the condensation mechanism involving prenyltransferase as a catalyst occurs via an ionization–condensation–elimination sequence.

As suggested by the aforementioned studies, α-(trifluoromethyl)-substituted allylic carbenium ions could exist in solution. The solvolysis of CF_3-substituted allyl sulfonates was thus

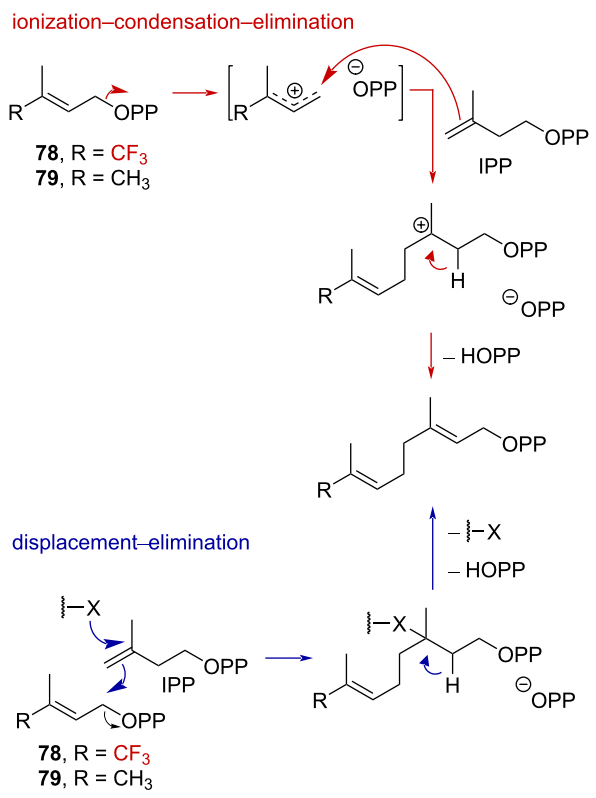

Scheme 22: Proposed mechanisms for the prenyltransferase-catalyzed condensation.

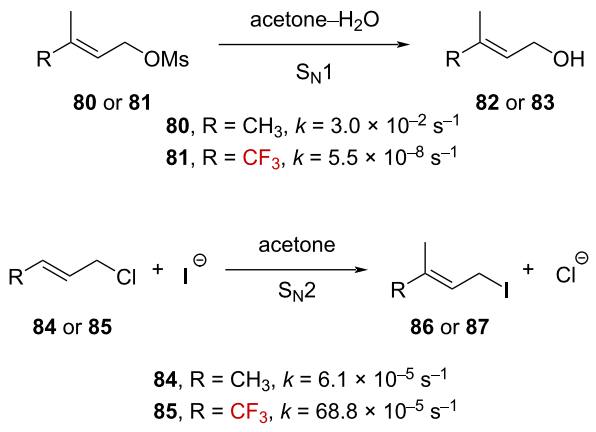

Scheme 23: Influence of a CF_3 group on the allylic S_N1- and S_N2-mechanism-based reactions.

thoroughly examined by Gassmann and Harrington [76]. The solvolysis of doubly CF_3-deactivated **90** in trifluoroethanol (TFE) required the presence of 2,6-lutidine, leading to ketone **91** and triflate **92**. This observation suggests that lutidine allows the isomerization of **90** into **93**, followed by a nucleophilic attack of the solvent at the sulfur atom (Scheme 25).

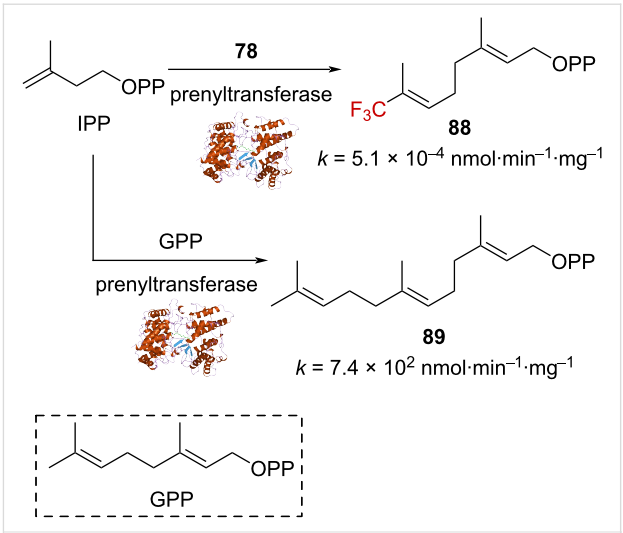

Scheme 24: Influence of the CF_3 group on the condensation reaction.

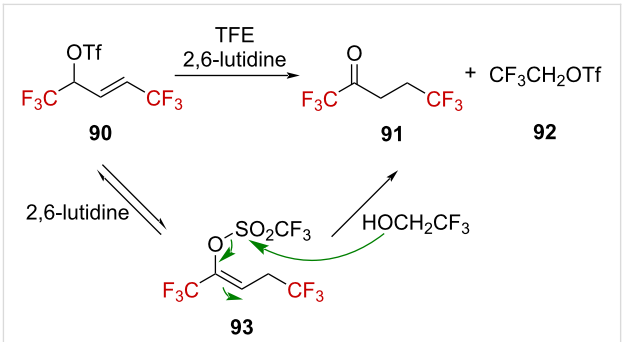

Scheme 25: Solvolysis of **90** in TFE.

The reactivity of analogous monotrifluoromethyl-substituted allyl derivatives **94**, bearing an aryl group in the vinylic position was also explored (Scheme 26). Trifluoroethanolysis of secondary triflate **94** gave a mixture of (*Z*)-**95** and (*E*)-**95** in a combined 70% yield, with an *E*/*Z* ratio of 17:83–8:92, depending on the nature of the aryl substituent (*p*-OMe or *p*-Cl, respectively). It is worth noting that the formation of S_N2 product **96** was not observed. Similar observations have been reported by Langlois et al. [77]. In order to get some insights into the mechanism, derivative **96** was synthesized and subjected to solvolysis. However, this compound was found to be stable under the reaction conditions [52]. When primary triflate **97** was subjected to solvolysis, the expected product (*Z*)-**95** was obtained, and the rate was 50–100 times faster than when starting from **94**. The Hammett–Brown correlation gave a poor dependence of the rate on the nature of the aryl substituent, and thus suggesting that the aryl group does not participate in the positive-charge stabilization. Finally, the Grunwald–Winstein plot gave a linear free-energy relationship between the rate and Y_{OTs}, supporting the formation of a carbenium ion.

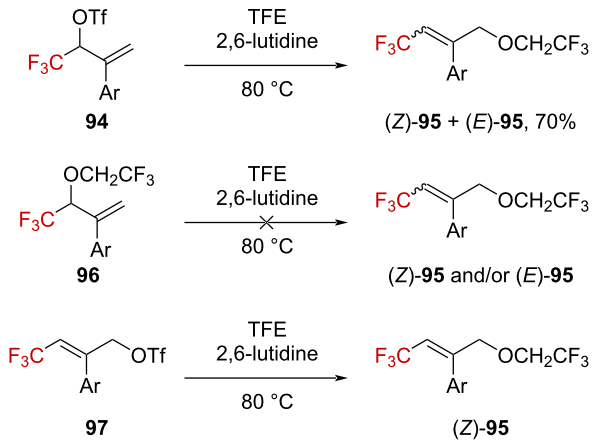

Scheme 26: Solvolysis of allyl triflates **94** and **97** and isomerization attempt of **96**.

From these observations, the authors concluded that **94** dissociates into an ion pair **98** in the rate-limiting step, in which the delocalized positive charge is highly concentrated in the γ-CF_3 position (see **98'**), which is the electronically and sterically privileged position for the solvent approach, to subsequently give **95** (Scheme 27).

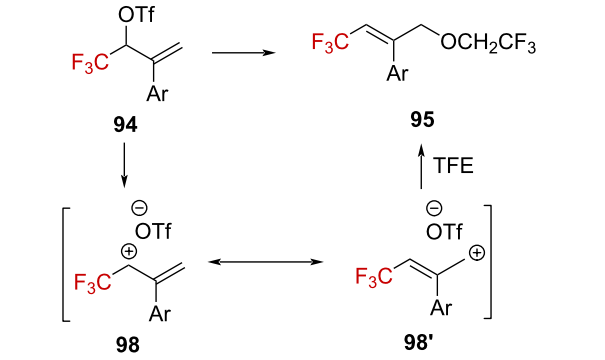

Scheme 27: Proposed mechanism for the formation of **95**.

Prakash et al. also investigated the formation of α-(trifluoromethyl)allylcarbenium ions from alcohol precursors in a superacid [78]. When allylic alcohol **99** was ionized with SbF_5 in SO_2ClF at −78 °C, the corresponding α-(trifluoromethyl)allylcarbenium ion **100** was formed. The carbons atoms C1 and C2 exhibited very different chemical shifts, δ_{C1} = 157 ppm and δ_{C2} = 290 ppm, which are to be compared to the nontrifluoromethylated analogue (δ_{C1} = 206 ppm and δ_{C2} = 251.8 ppm). The authors suggested that "the positive charge is more unevenly localized in the cation" **100**, with the resonance form **100''** contributing significantly more than **100'** (Scheme 28). This unsymmetrical delocalized structure in carbenium compound **100** was also confirmed by DFT calculations at the B3LYP/6-31G* level, with a C2–C3 bond considerably shorter than the C1–C2 bond, with d_{C2-C3} = 1.359 Å and d_{C1-C2} = 1.427 Å.

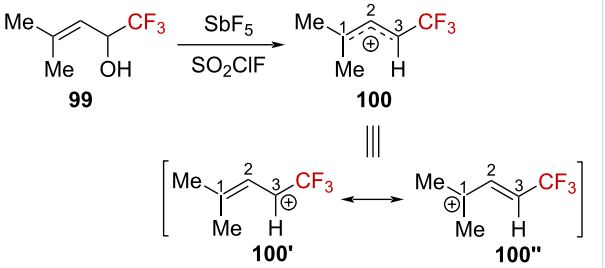

Scheme 28: Formation of α-(trifluoromethyl)allylcarbenium ion **100** in a superacid.

More recently, Vasilyev et al. reported that Lewis acid activation of α-(trifluoromethyl)allyl alcohol **101** allowed the transient formation of the corresponding α-(trifluoromethyl)allylcarbenium ion **103**↔**103'**, the resonance form **103** of which could be trapped with arenes to afford (trifluoromethyl)vinyl-substituted derivatives **102** (Scheme 29) [79,80]. It was also suggested that the resonance form **103'** has a nonnegligible contribution as this α-(trifluoromethyl)allylcarbenium ion could be trapped by some electron rich arenes (i.e., xylene, cumene, etc.). The products **104** further react to afford indanes **105** after hydroarylation. A closely related study on dibrominated allylic α-(trifluoromethyl) alcohols also invoked the transient formation of allylic carbenium ions, such as **103** [81].

α-(Trifluoromethyl)alkynylcarbenium ions

It has been reported that the complex of $Co_2(CO)_6$ and propargyl alcohols allows the facile generation of the corresponding propargylium ions (Nicholas reaction) in a relatively strong acidic medium (i.e., TFA, $BF_3{\cdot}Et_2O$, etc.). These cobalt-cluster-stabilized propargylium ions exhibit a surprisingly high thermodynamic stability, comparable to that of triarylmethylcarbenium ions and are readily observable by NMR spectroscopy or isolable as salts with relatively weakly coordinating anions (BF_4^-, PF_6^-, etc.) [82]. In this context, Gruselle et al. exploited the strong stabilization provided by Co–Co and Co–Mo bimetallic clusters to generate α-(trifluoromethyl)propargylium ions (Scheme 30). While the tertiary carbenium ion **108** was isolable as a solid [83,84], the tertiary carbenium ion **109** and the secondary derivatives **112a–c** and **113a,b** afforded oils. The secondary derivatives were much more sensitive in spite of the use of electron-rich Co–Mo clusters and could only be characterized by NMR and IR spectroscopy [85]. Upon ionization, the change in the electronic density is directly reflected by the downfield shift of the ^{19}F NMR chemical shift of the CF_3 group but also by a CO shift to a higher frequency. As a

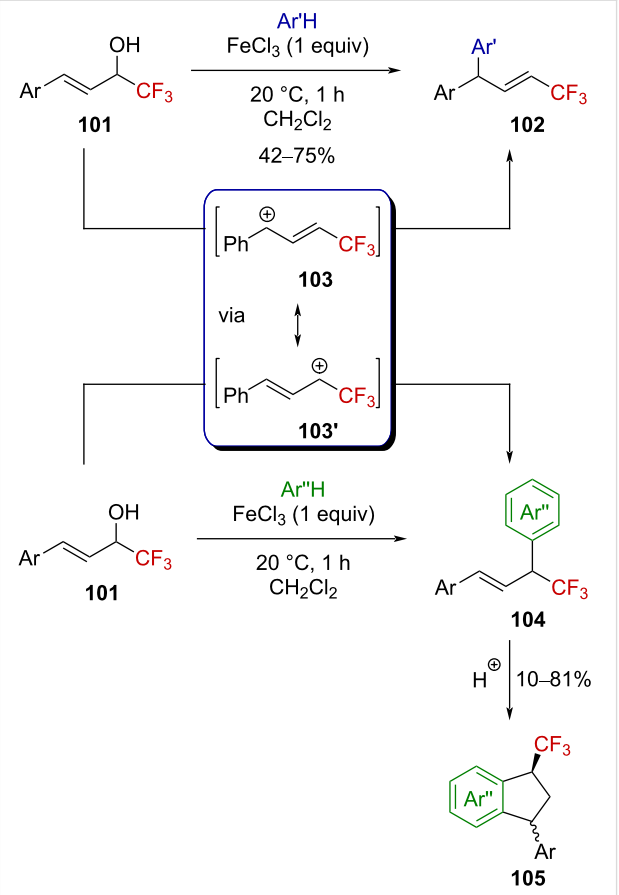

Scheme 29: Lewis acid activation of CF_3-substituted allylic alcohols.

general example, **111a** (δ_{19F} = −75.9 ppm; ν_{CO} = 2051, 2001, 1984, and 1942 cm^{-1}) affords **113a** (δ_{19F} = −59.2 ppm; ν_{CO} = 2104, 2065, 2055, 2006, and 1989 cm^{-1}), which exhibits the previously mentioned features, with $\Delta\delta_{19F}$ = +16.7 ppm and $\Delta\nu_{CO} \approx +50$ cm^{-1}.

Beyond the synthetic challenges associated with the generation of such species, the authors explored their use in organic synthesis. These metal-stabilized α-(trifluoromethyl)propargylium ions **114** could be engaged in useful transformations, such as reductions, eliminations, as well as C–O, C–N, or C–C bond formations (Scheme 31).

α-(Trifluoromethyl)propargylium has also been suggested as an intermediate in superacid-mediated Friedel–Crafts reactions [86]. When [α-(trifluoromethyl)propargyl]allyl silyl ether **120** was added to a dichloromethane solution of triflic acid in the presence of benzene, the original [3.2.2]-bridged CF_3-substituted product **121** was obtained. The authors proposed an elimination of TMSOH to generate the propargyl-substituted α-(trifluoromethyl)allylcarbenium ion **122** at first, which is a resonance form of the benzylic carbenium ion **122'**. Subsequently,

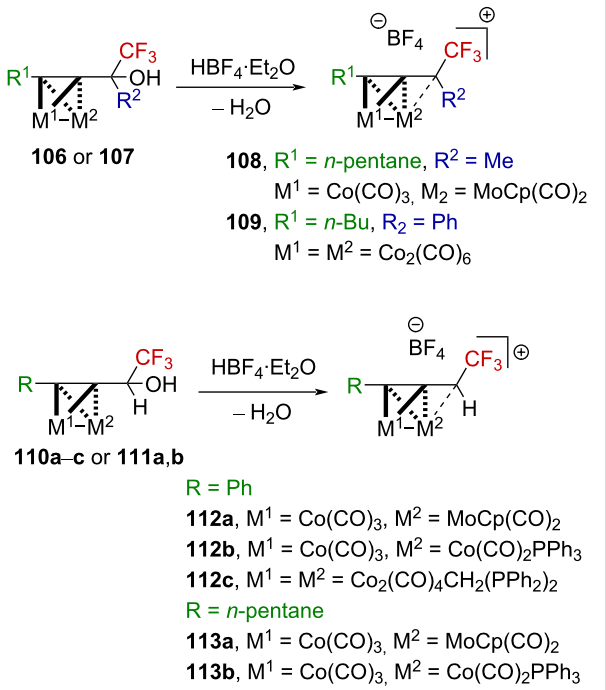

Scheme 30: Bimetallic-cluster-stabilized α-(trifluoromethyl)carbenium ions.

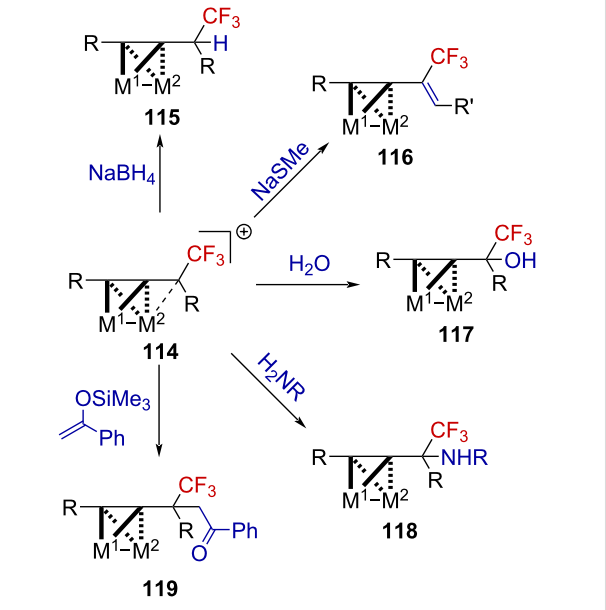

Scheme 31: Reactivity of cluster-stabilized α-(trifluoromethyl)carbenium ions.

122' reacts in a Friedel–Crafts reaction with benzene to generate **123**. After two successive hydroarylation reactions, the final product **121** is produced via the formation of vinylic and benzylic carbenium ions **124** and **125**, respectively (Scheme 32).

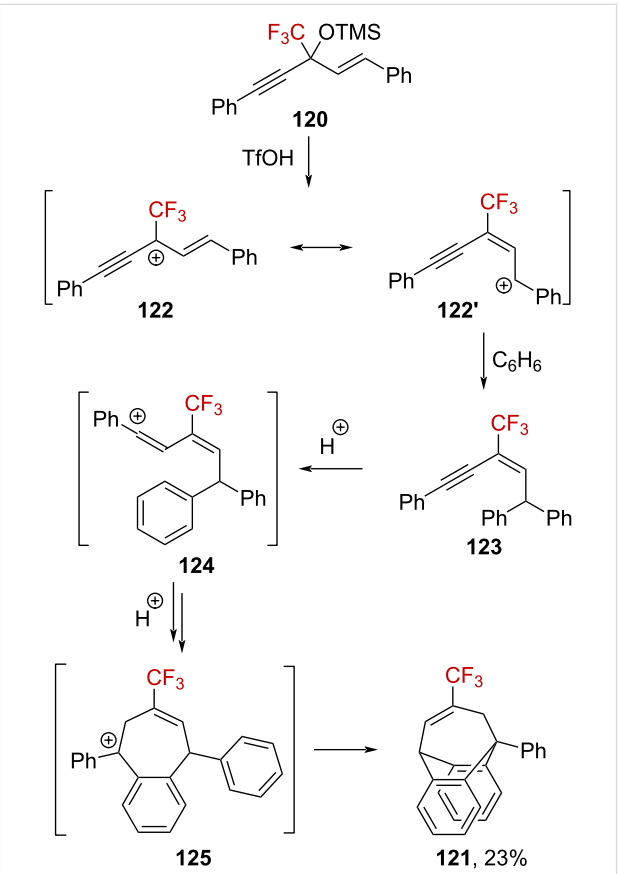

Scheme 32: α-(Trifluoromethyl)propargylium ion **122**↔**122'** generated from silyl ether **120** in a superacid.

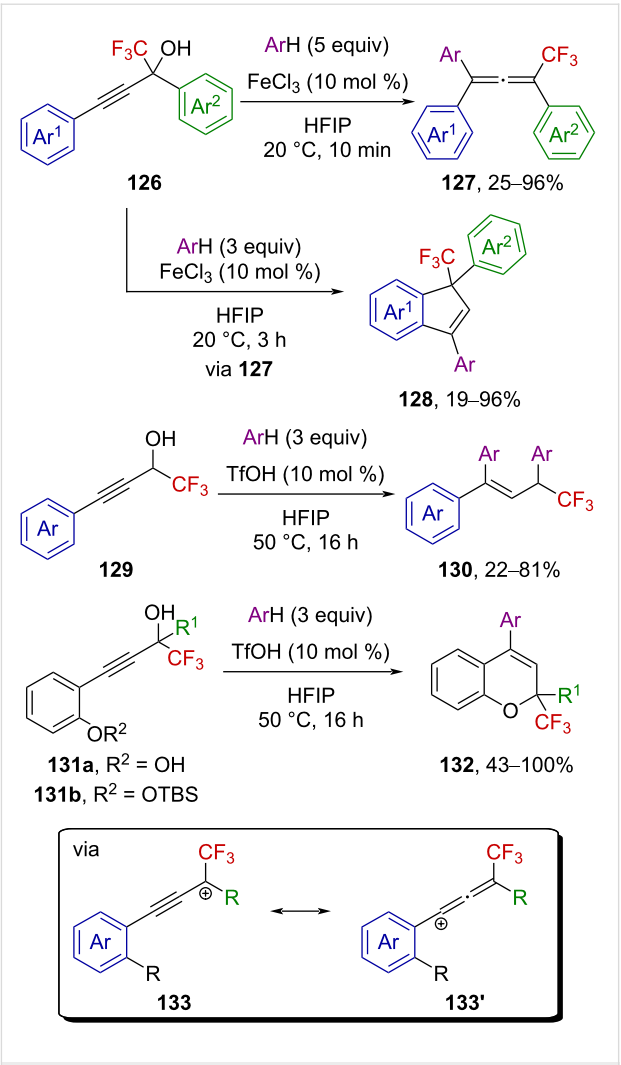

Scheme 33: Formation of α-(trifluoromethyl)propargylium ions from CF_3-substituted propargyl alcohols.

Moran et al. also investigated the reactivity of a variety of CF_3-substituted propargyl alcohols (Scheme 33) [87]. The reactivity of the benzylic (trifluoromethyl)propargyl alcohol **126** strongly depends on the reaction conditions, as allenes **127** or indenes **128** were both obtained under $FeCl_3$ activation. Indeed, with a longer reaction time, allenes **127** undergo a subsequent intramolecular hydroarylation reaction leading to indenes **128**. The authors suggested the formation of $FeCl_3$–HFIP complexes being involved in a Lewis acid-assisted Brønsted acid catalysis. The CF_3-substituted propargyl alcohol **129** was found to undergo tandem Friedel–Crafts hydroarylation reactions to give derivatives **130** under TfOH activation at 50 °C. Finally, CF_3-substituted chromene derivatives **132** were obtained under the same reaction conditions from *ortho*-hydroxy or *ortho*-silyloxy derivatives **131a** and **131b**, respectively. The common intermediate in these reactions is supposed to be α-(trifluoromethyl)propargylium ion **133**↔**133'**.

Heteroatom-substituted α-(trifluoromethyl)carbenium ions

The stabilization of carbenium ions through oxygen lone pair back-donation [35] is a common feature in organic synthesis [88-90]. In this context, Olah, Pittman, et al. investigated the protonation of a variety of trifluoromethyl ketones in a superacid [35,91]. Trifluoromethyl ketone protonation was observed by NMR spectroscopy at −60 °C in a superacidic FSO_3H–SbF_5–SO_2 solution (Scheme 34).

The ^{19}F chemical shift variation for the generated oxygen-substituted trifluoromethylated carbenium ions ranged from +7.6 to +1.4 ppm, significantly lower than for carbon-substituted α-(trifluoromethyl)carbenium ions (e.g., the carbenium ion **10a**, Δδ = +24.8 ppm), confirming the considerable contribution of the oxygen lone pair to the stabilization of the cation **142**↔**142'** (Scheme 35).

Oxygen-stabilized α-(trifluoromethyl)carbenium ions (oxocarbenium ions) have been exploited for chemical synthesis [92-94]. Ketone **143a** and ketoxime **143b** undergo Friedel–Crafts

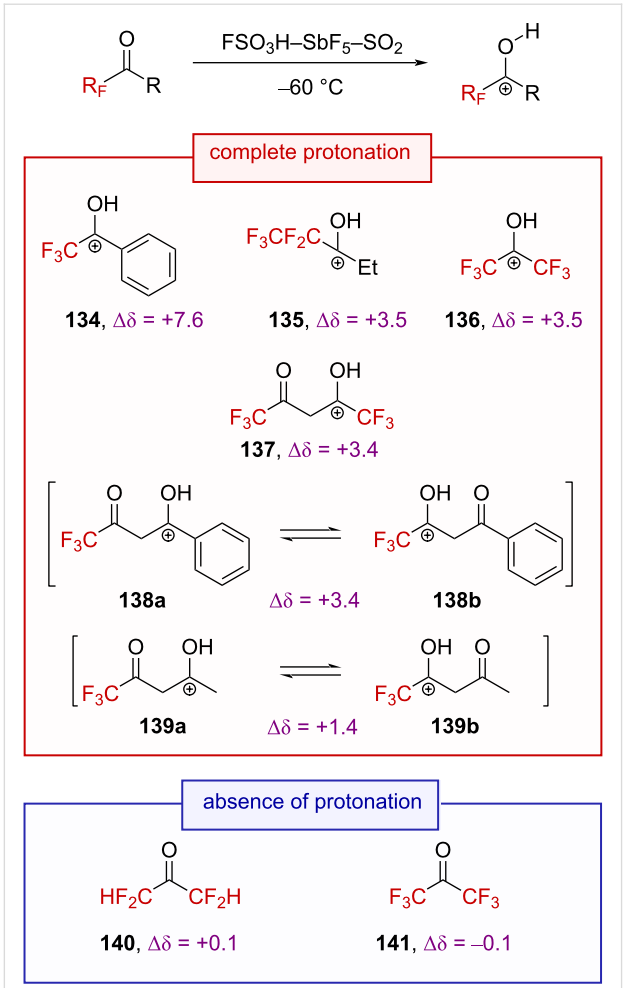

Scheme 34: Direct NMR observation of the protonation of some trifluoromethyl ketones in situ and the corresponding ^{19}F NMR chemical shifts. $\Delta\delta = \delta_{19F,product} - \delta_{19F,precursor}$ (δ in ppm).

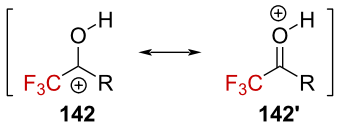

Scheme 35: Selected resonance forms in protonated fluoroketone derivatives.

reactions in the presence of Brønsted or Lewis acid to furnish the corresponding CF_3-containing tetralin derivatives **144a** and **144b**, respectively (Scheme 36). In addition, **144a** could be further converted into **146** in the presence of aromatic nucleophiles (e.g., benzene or toluene). Similarly, derivatives **147a–c** could also be converted into indanol derivatives **148a–c** in high yields (Scheme 36) [95].

Ma et al. managed the enantioselective arylation of aromatic trifluoromethyl ketones **150** with (*S*)-TRIP (Scheme 37) [96]. A

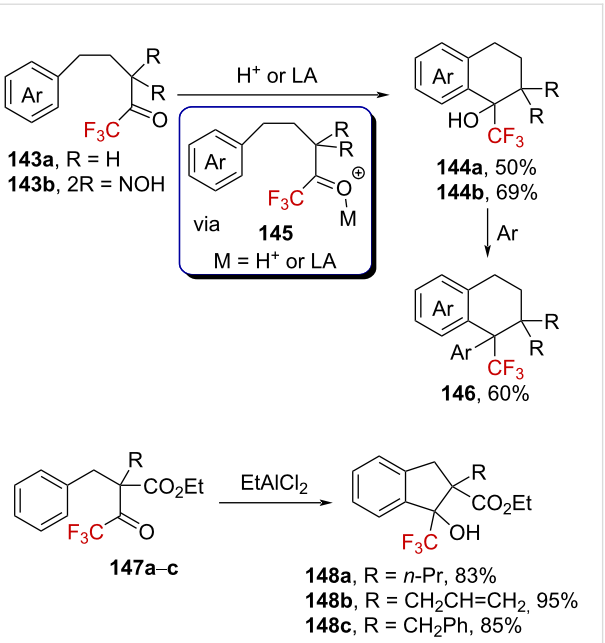

Scheme 36: Acid-catalyzed Friedel–Crafts reactions of trifluoromethyl ketones **143a**,**b** and **147a–c**.

variety of CF_3-substituted enantioenriched benzylic alcohols **61** were thus synthesized after the trapping of protonated CF_3-substituted ketones **134** (Scheme 37). Interestingly, these benzylic alcohols **61** did not undergo further arylation and were stable under the reaction conditions. In agreement with computational studies [97], this behavior was assigned to the presence of the CF_3 group, which induces a shortening of the C–O bond in the product ($d_{C–O}$ = 1.426 Å) compared to the CH_3 analogue ($d_{C–O}$ = 1.438 Å) and strongly inhibits the formation of the α-(trifluoromethyl)bisarylcarbenium ion, as illustrated by the higher activation energy needed for the dehydration (ΔE_{CF3} = 21.0 kcal·mol^{-1} vs ΔE_{CH3} = 14.8 kcal·mol^{-1} at the B3LYP/6-31+G(d,p) level). On the other hand, the first arylation reaction seems to be facilitated by the CF_3 group (ΔE_{CF3} = 16.9 kcal·mol^{-1} vs ΔE_{CH3} = 21.2 kcal·mol^{-1} at the B3LYP/6-31+G(d,p) level). Raising the temperature finally favors the dehydration and the second Friedel–Crafts reaction to afford bisarylated products **151**.

In complementary studies, Sasaki et al. reported the acid-catalyzed mono- and diarylation of CF_3-substituted α,β-ynones **152a** [98], Wu et al. reported the one-pot two-step acid-catalyzed diarylation of trifluoroacetyl coumarins **152b** [99], and Yuan et al. reported the acid-catalyzed diarylation of CF_3-substituted cyclopropyl ketone **152c** [100] (Scheme 38). In these reactions, oxygen-stabilized α-(trifluoromethyl)carbenium ions **142** are supposed to be generated by protonation or Lewis acid activation of the starting ketones.

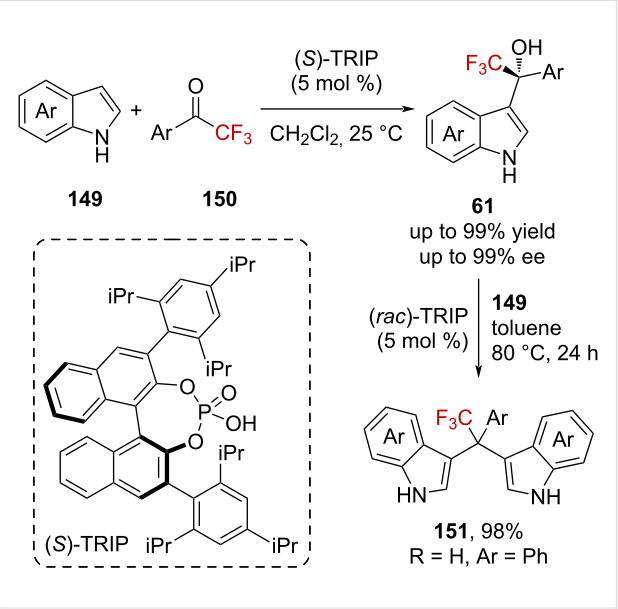

Scheme 37: Enantioselective hydroarylation of CF_3-substituted ketones.

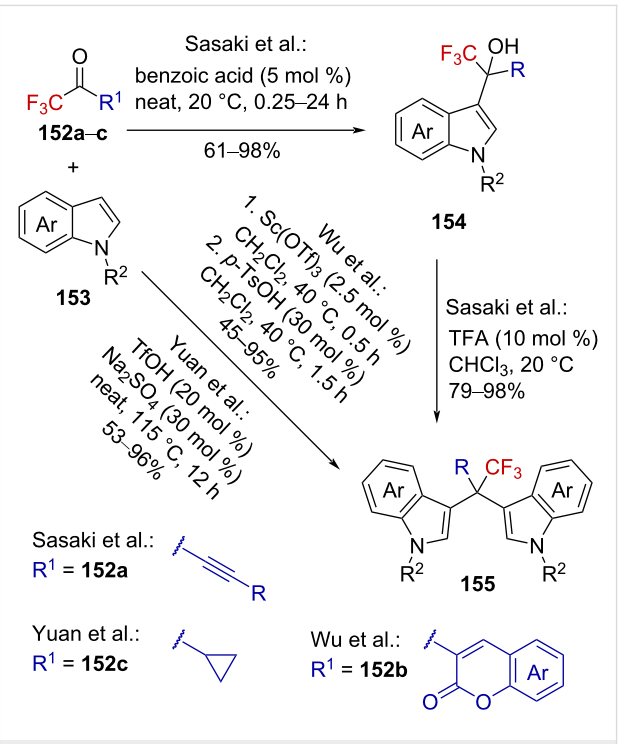

Scheme 38: Acid-catalyzed arylation of ketones **152a–c**.

Klumpp et al. explored the reactivity of CF_3-substituted superelectrophiles (defined as multiply charged cationic electrophiles [101]) generated in superacid media [102]. Hence, when trifluoroacetyl pyridine **156** was treated with benzene in triflic acid, alcohol derivative **157** was obtained. In a superacid, **156** generates a dication **158** in which the electrophilicity is enhanced through a strong charge repulsion (Scheme 39). This dication reacts with benzene to provide pyridinium–oxonium dication **159** in solution. Further arylation does not occur spontaneously, which was evident because alcohol **157** was isolated at the end of the reaction. Upon heating at 60 °C, the second arylation takes place, presumably via the formation of dicationic superelectrophile **160**. Again, due to charge repulsions as well as due to the strong electron-withdrawing effect of the CF_3 group, the positive charge adjacent to the CF_3 group is highly delocalized within the phenyl ring, and arylation occurs regioselectively at the *para*-position, affording biaryl species **161**.

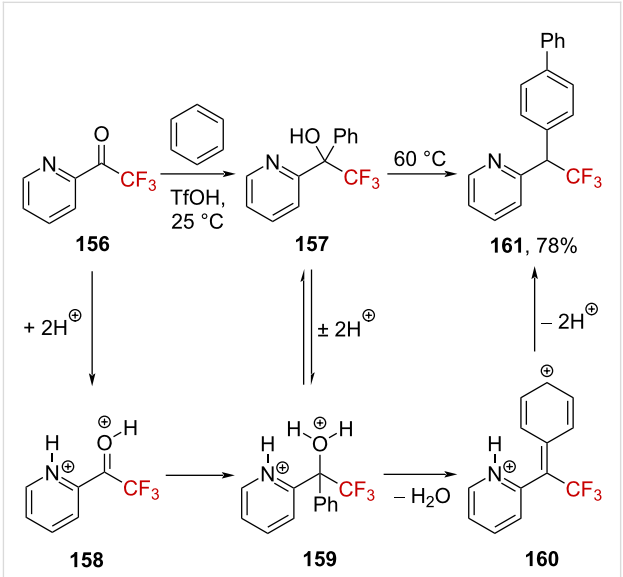

Scheme 39: Reactivity of **156** in a superacid.

Using this strategy, several trifluoromethyl ketones **162** and alcohols **163** bearing heteroaryl substituents (i.e., benzothiazole, quinoline, isoquinoline, benzimidazole, or imidazole) prone to be protonated were elegantly converted into the corresponding alcohols **163** and biphenyl compounds **161** in high yield (Scheme 40, top). The reaction of CF_3-substituted 1,3-diketones **165a–d** in TfOH was also deeply investigated by Klumpp et al. [101]. The *syn*-indanes **166a–d** could cleanly be generated after successive well-defined arylation reactions via **167** (Scheme 40, bottom). Moreover, the CF_3 group was found to be essential in this reaction as 2,4-pentanedione did not react with benzene under similar conditions.

The use of acetal derivatives in place of ketones as precursors of oxygen-stabilized α-(trifluoromethyl)carbenium ions was also investigated. For instance, the readily available hemiacetal **168** was shown to react with benzene in the presence of a Lewis acid or H_2SO_4 to form compounds **169–172** in various amounts, depending on the acid used (Scheme 41) [103]. It is assumed

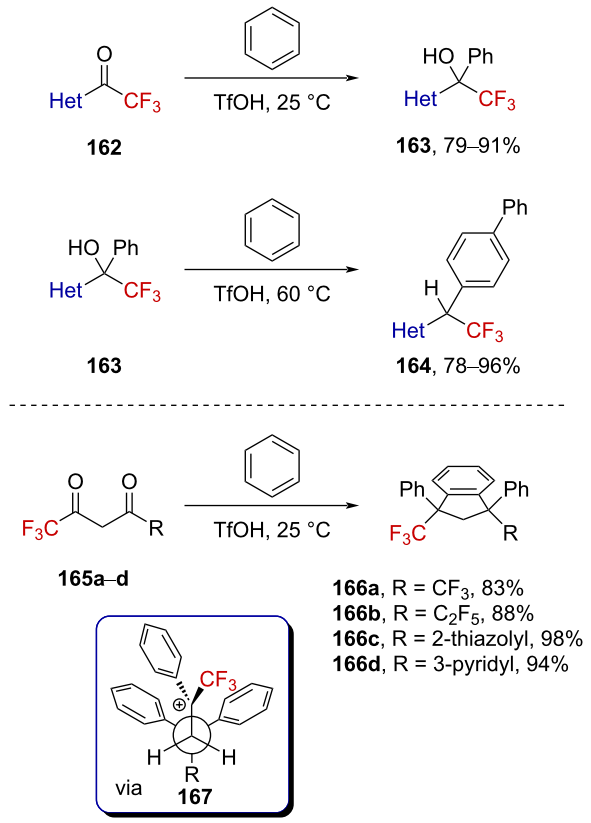

Scheme 40: Reactivity of α-CF_3-substituted heteroaromatic ketones and alcohols as well as 1,3-diketones.

that an oxygen-stabilized α-(trifluoromethyl)carbenium ion is involved. It was shown that **168** could also react with (hetero)arenes [104,105] and alkenes [106] under Lewis acid activation but also with electron-rich arenes under thermal activation [107-109].

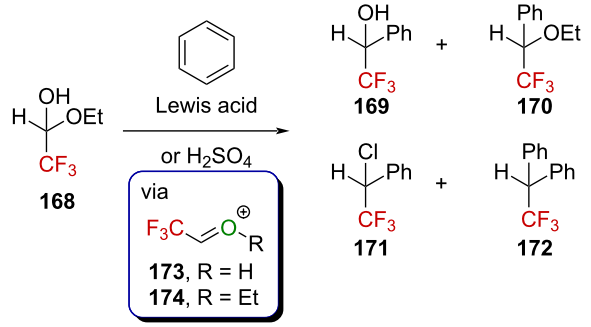

Scheme 41: Reactivity of **168** with benzene in the presence of a Lewis or Brønsted acid.

CF_3-substituted hemiacetal **168** can react with amines to furnish the corresponding hemiaminal ethers, which can be further activated by a Lewis acid to generate CF_3-substituted iminium ions able to promote Friedel–Crafts alkylations [110,111]. Ma et al. exploited this mode of activation in a Brønsted acid-catalyzed three-component asymmetric reaction [112]. Mixing hemiacetal **175**, arylaniline **176**, and indole derivatives **149** in the presence of a catalytic amount of the moderately acidic (*S*)-TRIP (pK_a = 3–4 in DMSO [113,114]) in dichloromethane afforded the chiral α-(trifluoromethyl)aminoaryl derivatives **177** in an excellent yield and enantiomeric excess (Scheme 42). The authors proposed that hemiacetal **175** and amine **176** react under the reaction conditions to give an imine in the first step, which is protonated by (*S*)-TRIP to generate the corresponding chiral CF_3-substituted iminium ion. The latter subsequently reacts via the most accessible *Re*-face with indole **149** to afford the resulting Friedel–Crafts product **177**. Worthy of note is the fact that the reaction works equally well with a CHF_2-containing hemiacetal.

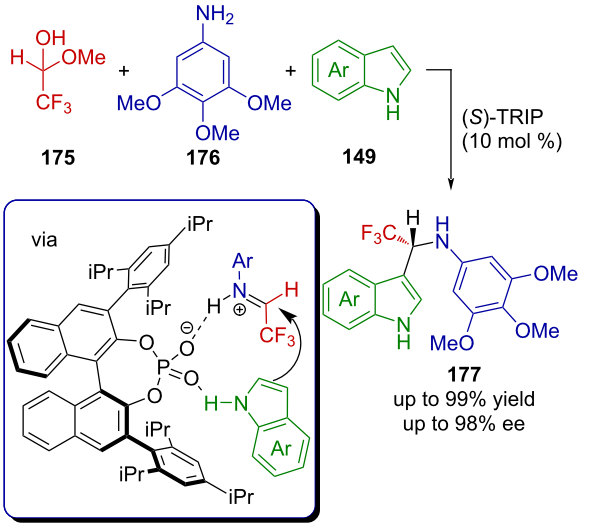

Scheme 42: Acid-catalyzed three-component asymmetric reaction.

Nitrogen-stabilized α-(trifluoromethyl)carbenium ions have also been extensively investigated. Under electrochemical conditions, trifluoromethylated iminium ions **182** were successfully generated by Fuchigami et al. [115]. Starting from tertiary amines **178a–c**, the corresponding hemiaminal ethers **179a–c** were obtained (Scheme 43). The reaction is highly regioselective as no methoxylation of **178a** and **178b** was observed on the nontrifluoromethylated alkyl substituent (Me or Et). Hence, although amines **178a–c** are more difficult to oxidize than their nonfluorinated analogues (E_{ox} ($PhNMe_2$) = +0.71 V (SCE)), the radical cation **180** is formed under the reaction conditions, and deprotonation at the methylene unit near the CF_3 group is highly favored because of the higher acidity, accounting for the observed high regioselectivity. In addition, the transient stabi-

lization of radical **181** by the captodative effect could also favor the general process.

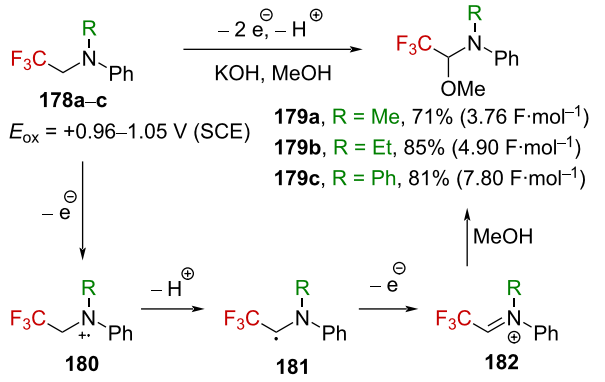

Scheme 43: Anodic oxidation of amines **178a–c** and proposed mechanism.

Lewis acid activation of trifluoromethylated hemiaminal ethers has also been studied by Fuchigami et al. [115,116]. For instance, when **179b** is treated with a slight excess of $TiCl_4$ in dichloromethane, iminium ion **182b** can be trapped by TMSCN to furnish α-(trifluoromethyl)-α-aminonitrile **183** in 40% yield. The iminium was also successfully trapped by a silyl enol ether, affording a mixture of ketone **184** and heterocycle **185** (Scheme 44).

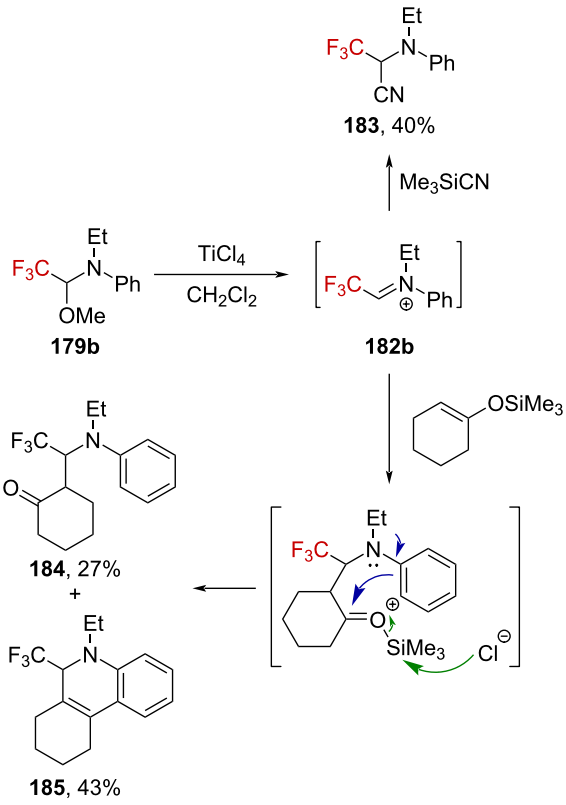

Scheme 44: Reactivity of **179b** in the presence of a strong Lewis acid.

The trifluoromethyl-substituted derivatives **186a–c** have then been exploited as a convenient source of trifluoromethylated iminium ions **187** (Scheme 45) [117-119].

Langlois, Billard, and Blond reported on the Mannich-type reaction between silylated trifluoromethylated hemiaminal derivatives **189** [120] and enolizable ketones **188** [121]. The intermediate formation of trifluoromethylated iminium ion **192** by Lewis acid activation was suggested by the authors (Scheme 46). The resulting CF_3-substituted β-amino ketones **190** could then be efficiently transformed in a one-pot procedure into the corresponding CF_3-substituted enones **191** upon Brønsted acid treatment.

Langlois and Billard then exploited the reactivity of the trifluoromethylated iminium ion **192** and extended the scope of the reaction to a larger panel of nucleophiles, including alcohols, amines, aromatic and vinyl derivatives, as well as silylated nucleophiles (Scheme 47) [122].

Brigaud and Huguenot also suggested the formation of a trifluoromethylated iminium ion **187** during the course of their studies on a Strecker-type reaction [123]. Starting from trifluoromethylated imines **193** or oxazolidines **194** and **195** bearing enantiopure chiral auxiliaries, the authors accessed the corresponding cyano derivatives **196**–**198** with different levels of diastereoselectivity (Scheme 48). Further development by Brigaud et al. allowed the synthesis of CF_3-substituted pseudoprolines structurally related to oxazolidines **194** and **195** [124].

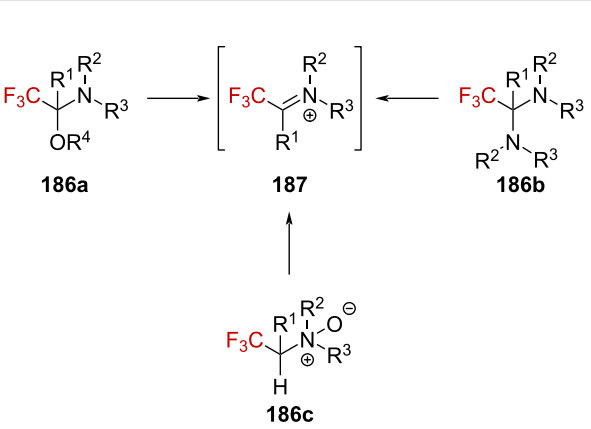

Scheme 45: Trifluoromethylated derivatives as precursors of trifluoromethylated iminium ions.

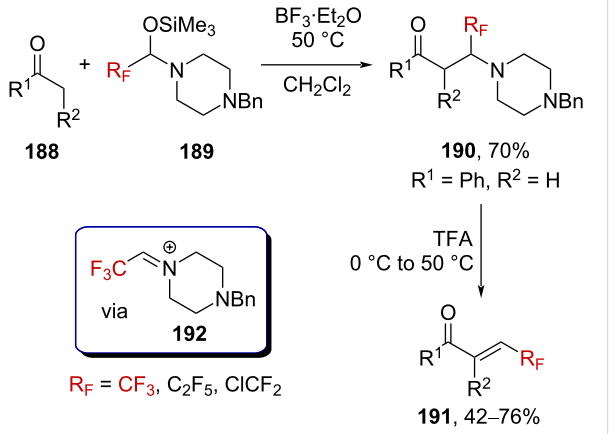

Scheme 46: Mannich reaction with trifluoromethylated hemiaminal **189**.

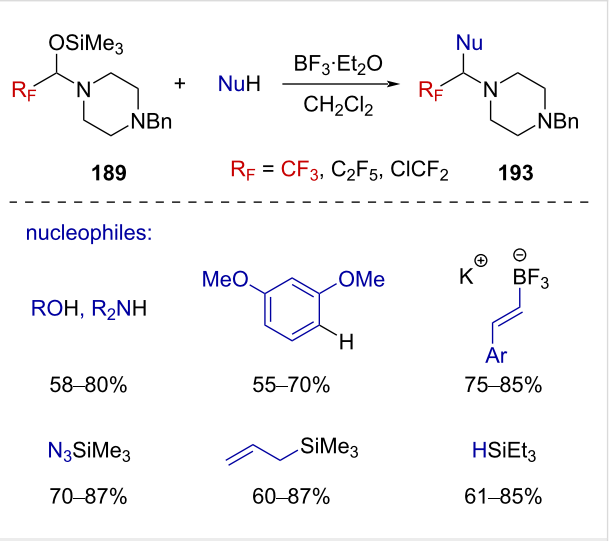

Scheme 47: Suitable nucleophiles reacting with **192** after Lewis acid activation.

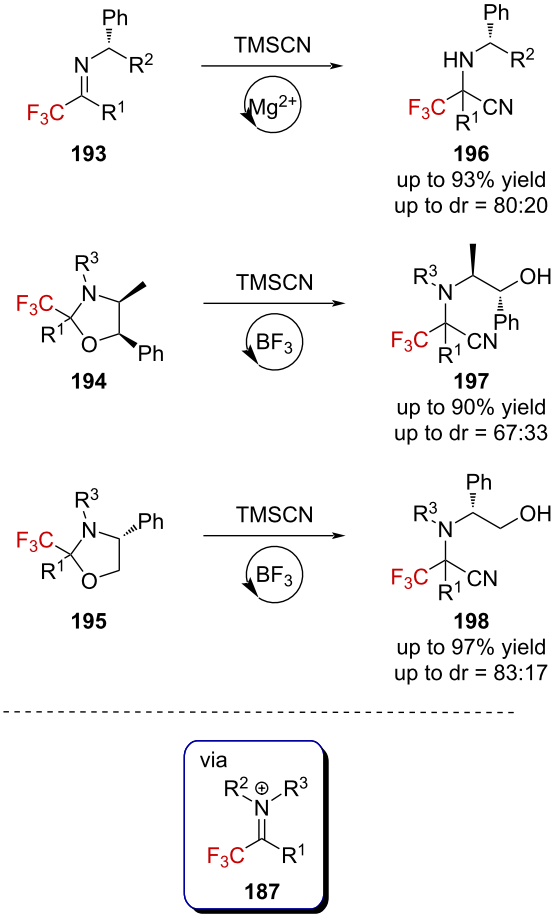

Scheme 48: Strecker reaction involving the trifluoromethylated iminium ion **187**.

Viehe et al. also contributed by developing the chloroalkylamino reagent **199**, bearing a geminal CF_3 group, which proved to be a valuable synthon for the introduction of the CF_3 group into molecules [125]. Thus, **199** exhibits a high reactivity towards many functionalities, as depicted below (Scheme 49). Interestingly, **200** and **201** are sufficiently stable to be synthesized, presumably due to electron delocalization (guanidinium ions).

Following these seminal contributions, the chemistry of CF_3-substituted iminium ions **187** was extensively exploited for synthetic purposes [126-138].

The related thioacetal **204a** was also studied and reacts with benzene upon treatment with strong Lewis acids (best with $AlCl_3$) [139]. In this case, the only product formed in the course of the reaction was **205**, isolated in 83% yield (Scheme 50). The proposed cationic intermediate in this reaction is a sulfur-stabilized α-(trifluoromethyl)carbenium ion **206** (an α-(trifluoromethyl)-substituted sulfonium cation).

Analogous to thioacetals **204a**, chloroalkylthio derivatives **207a–c**, bearing an adjacent CF_3 group, were also investigated [140]. It appeared that a sulfur-stabilized α-(trifluoromethyl)carbenium ion **208** can be generated from **207a** by chloride abstraction following Lewis acid activation (e.g., $SnCl_4$ or $ZnCl_2$), opening an avenue for this cation to react with various nucleophiles (Scheme 51). Such a cation can also be trapped intramolecularly by a phenyl moiety; however, the length of the appended alkyl chain appeared to be of the utmost importance in this transformation.

Analogous to their work on the nitrogen counterparts (vide supra), Fuchigami et al. were successful in the electrochemical production of sulfur-stabilized α-(trifluoromethyl)carbenium

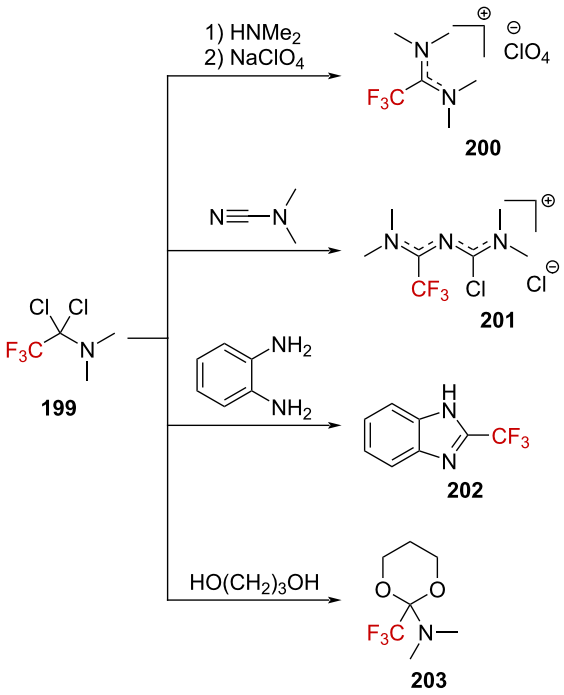

Scheme 49: Reactivity of **199** toward nucleophiles.

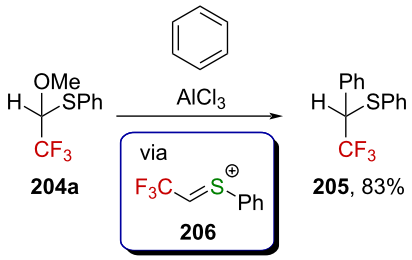

Scheme 50: Reactivity of **204a** with benzene in the presence of a Lewis acid.

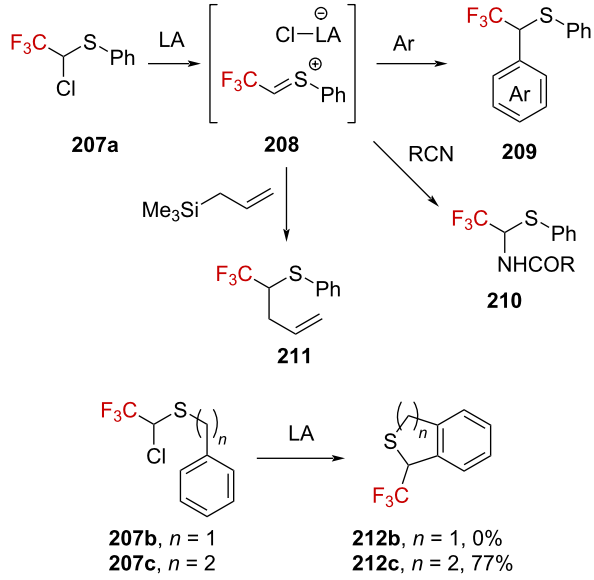

Scheme 51: Reactivity of α-(trifluoromethyl)-α-chloro sulfides in the presence of strong Lewis acids.

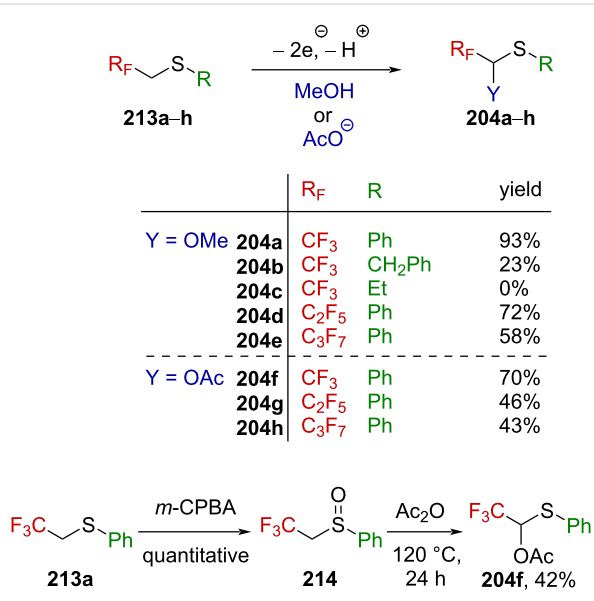

		R_F	R	yield
Y = OMe	**204a**	CF_3	Ph	93%
	204b	CF_3	CH_2Ph	23%
	204c	CF_3	Et	0%
	204d	C_2F_5	Ph	72%
	204e	C_3F_7	Ph	58%
Y = OAc	**204f**	CF_3	Ph	70%
	204g	C_2F_5	Ph	46%
	204h	C_3F_7	Ph	43%

Scheme 52: Anodic oxidation of sulfides **213a–h** and Pummerer rearrangement.

ions [139,141]. Thereby, they converted sulfides **213a–h** into thioacetals **204a–h** (Scheme 52). It is worth to note that the presence of an aromatic substituent on the sulfur atom is essential for the sulfides to react. Also, lengthening the perfluoroalkyl chain from CF_3 to C_2F_5 or C_3F_7 resulted in a significant drop in the yield. Interestingly, while the electrochemical acetoxylation of **213a** furnished **204a** in an excellent yield of 93%, the Pummerer rearrangement of sulfoxide **214** under harsh conditions turned out to be less efficient, affording **204f** in only 42% yield.

This reaction is thought to proceed stepwise via a first oxidative electron transfer, followed by deprotonation, a second oxidative electron transfer, and methoxylation or acetoxylation, respectively (Scheme 53). The driving force in this reaction is assumed to be the deprotonation of radical cation **215**, a highly destabilized species due to the presence of the strongly electron-withdrawing CF_3 substituent, which leads to radical **216**, synergistically stabilized by the electron-withdrawing CF_3 group and the electron donor sulfur atom through a captodative effect. Further oxidative electron transfer produces α-(trifluoromethyl)-substituted sulfonium ion **206**, leading to **204a**,**f** after reacting with the solvent.

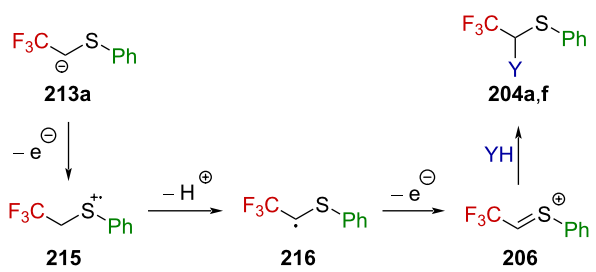

Scheme 53: Mechanism for the electrochemical oxidation of the sulfide **213a**.

α-(Trifluoromethyl)alkylcarbenium ions

Hypothetical formation of CF_3-containing alkylcarbenium ions from diazonium salts: In 1967, Mohrig et al. successfully observed the first aliphatic diazonium ion **218a** by protonation of the corresponding diazo precursor [142] **217a** in a superacid by in situ NMR spectroscopy (Scheme 54) [143]. The remarkable characteristic of this strategy was the installation of a CF_3 group in the α-position of the N_2 moiety. This strategy relies on the high electron-withdrawing effect of the CF_3 group, which greatly destabilizes nearby positive charges. As a result, the dissociation rate for the generation of molecular nitrogen was considerably reduced, allowing the observation of the diazonium ion at a low temperature. However, warming the diazonium solution up to −20 °C resulted in a vigorous evolution of N_2 gas along with the clean formation of the resulting fluorosulfonate **219**, with no direct observation of the α-(trifluoromethyl)carbenium ion.

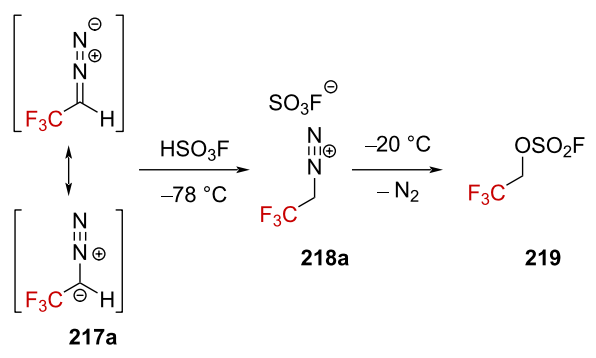

Scheme 54: Reactivity of (trifluoromethyl)diazomethane (**217a**) in HSO_3F.

Further studies were conducted by Lenoir and Dahn to shed light on the mechanism of the solvolysis of CF_3-substituted diazoalkane derivatives (Figure 10a) [144]. They measured an inverse kinetic isotope effect of k_H/k_D = 0.25 for the solvolysis of **217a** in dioxane/H_2O 60:40 in the presence of $HClO_4$ (3 ≤ pH ≤ 4) and mentioned that this low value is "typical of a preequilibrium protonation reaction" and the rate-limiting solvolysis of diazonium ion **218a** (Figure 10b, in blue). Furthermore, the addition of a strong nucleophile dramatically increased the rate. The authors thus concluded that these observations are pieces of evidence for an A2 bimolecular process, which is also in agreement with the preferred decomposition pathway of other deactivated diazoalkanes (i.e., diazoacetate, k_H/k_D = 0.34) [145,146]. Extending the investigations to diazo compound **217b** led to a different conclusion as a "normal" isotope effect of k_H/k_D = 1.67 was obtained in this case. Diderich found a comparable ratio of k_H/k_D = 2.13 for diazo compound **217c** [147]. In these latter cases, the solvolysis of diazoalkanes **217b** and **217c** is supported by an A-S_E2 mechanism including a rate-limiting proton transfer (Figure 10b, in green) as the solvolysis rate approximately corresponds to the transfer rate of a proton (or deuteron). The difference in the reactivity between **217a** and **217b**,**c** would thus be due to the easier protonation of **217b**,**c** compared to **217a**, in a similar way as to how one can expect secondary carbanions to be more basic than primaries.

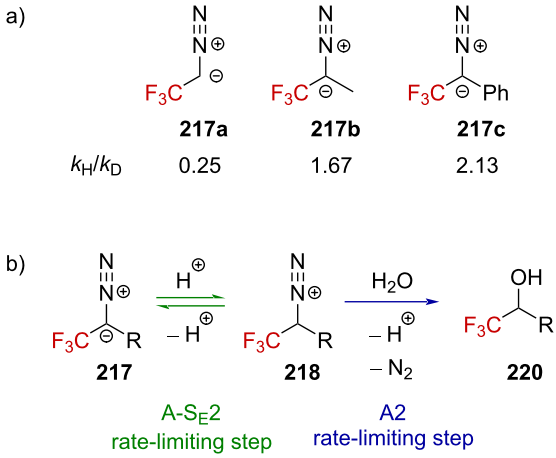

Figure 10: a) Structure of diazoalkanes **217a–c** and b) rate-limiting steps of their decomposition.

Studies on CF_3-substituted diazonium ions were next conducted by Kirmse and Gassen to determine the solvolysis mechanism [148]. They found that upon deamination of **221** using a solution of sodium nitrite in aqueous perchloric acid at pH 3.5, a 60:40 mixture of the elimination product **224** and alcohols **222** and **223** was obtained in a 95% overall yield. These alcohols result from either solvolysis (**223**, 40.3%) or rearrangement (**222**, 59.7%, reaction (1) in Scheme 55). Further investigations on the stereochemical aspects leading to product **223** showed that when enantioenriched amine (*S*)-**221** (94% ee) was subjected to deamination, product (*R*)-**223** was obtained, with an inverted configuration and an eroded enantiomeric purity of

65% ee (reaction (2) in Scheme 55). The authors thus concluded that the formation of (*R*)-**223** from (*S*)-**221** occurred by a nucleophilic substitution mechanism, with 70% inversion. Since the racemization via a diazo↔diazonium equilibrium was excluded due to negligible ^{2}D incorporation (i.e., <1%) when D_2O was used, the 30% racemization noted in the process would account for the transient formation of a trifluoromethyl-substituted carbenium ion.

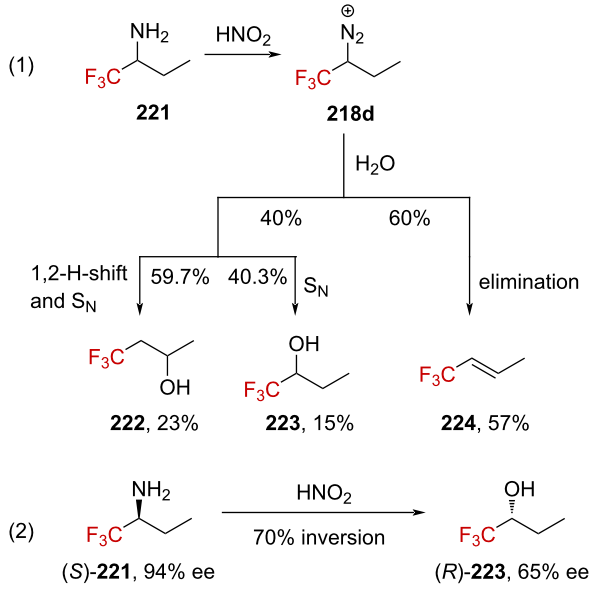

Scheme 55: Deamination reaction of racemic **221** and enantio-enriched (*S*)-**221**.

Attempts to elucidate the mechanism for the formation of **222** revealed that deuterium-labeled **221**-d_2 furnished products **223**-d_2 and **222**-d_2 upon deamination in a similar ratio and yield (Scheme 56, 41.2:58.8, 32%) as for the unlabeled **221** (Scheme 55, 40.3:59.7, 38%). This is a strong evidence for the transient formation of a carbenium ion as the isotope effect for the 1,2-H-shift is known to be very small in carbenium ions. It has been indeed previously demonstrated that a 1,2-H-shift isotope effect of k_H/k_D = 1.2–1.3 was obtained starting from 2-butyldiazonium ion **225**, which is known to decay via a carbenium ion [149,150].

In the absence of the CF_3 group, **225**-d_2 decays in a mixture of alkenes and alcohols. By taking only the alcohol mixture into account, alcohol **227**-d_2 was considered to have been obtained via a nucleophilic substitution mechanism (88%) with 25% inversion and **226**-d_2 via rearrangement (12%, Scheme 57). This contrasts with the previous results obtained for **218d**, which lead to 40.3% of the nucleophilic-substitution product **223** with 70% inversion and 59.7% of rearranged **222** when

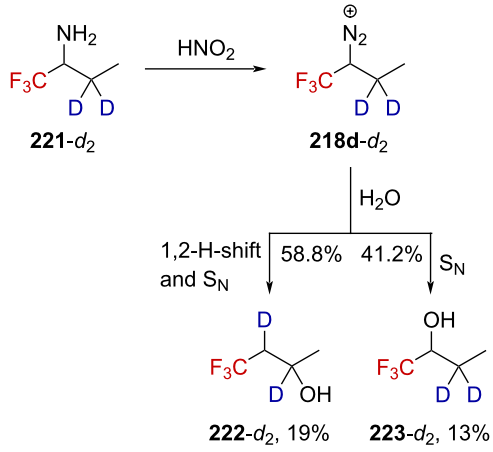

Scheme 56: Deamination reaction of labeled **221**-d_2. Elimination products were formed in this reaction, the yield of which was not determined.

only considering the mixture of alcohols (reaction (1) in Scheme 55).

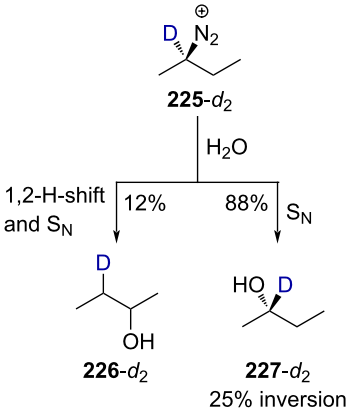

Scheme 57: Deamination reaction of **225**-d_2. Elimination products were also formed in this reaction in undetermined yield.

This would be consistent with a less labile C–N bond in **218d** and the formation of the extremely reactive α-(trifluoromethyl)carbenium ion **228** that is therefore more prone to undergo rearrangements to generate the more stabilized β-(trifluoromethyl)carbenium ion **229** (Scheme 58).

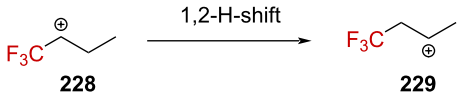

Scheme 58: Formation of **229** from **228** via 1,2-H-shift.

Further rearrangements were confirmed by the authors when alcohol **233**, resulting from a twofold 1,2-H-shift, was generated from diazonium salt **230** (Scheme 59).

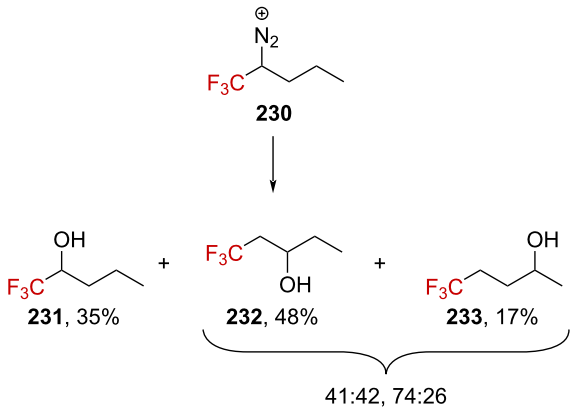

Scheme 59: Deamination reaction of **230**. Elimination products were formed in this reaction, the yield of which was not determined.

The β- and γ-CF_3 effects on the carbenium ions were also investigated by the same authors by systematically comparing the reactivity of a selected series of CF_3-containing and analogous nonfluorinated diazonium ions toward solvolysis. The diazonium ion **234** led exclusively to alcohol **222**, with the absence of any detectable rearranged products, while the CF_3-free analogous species **225** underwent 12% rearrangement (reaction (1) in Scheme 60). The diazonium ion **235** furnished alcohols **232** and **233** in a 71:29 ratio, without the detectable formation of α-(trifluoromethyl) alcohol **231**, while the analogous compound **236** provided **237** and **238** in a 84:16 ratio (reaction (2) in Scheme 60). Similarly, the terminal diazonium ion **239** decayed to produce a 97.5:2.5 ratio of alcohols **240** and **222**, a very different behavior than for **241**, which produced **242** and **226** in a 71:29 ratio (reaction (3) in Scheme 60).

Even though the direct observation of α-(trifluoromethyl)carbenium ions was not the purpose of this study, it successfully brought a better understanding on the effect of a CF_3 group close to a positive charge.

Hypothetical formation of CF_3-containing alkylcarbenium ions by activation of alcohol derivatives: The solvolysis reaction of alkyl tosylates has attracted the attention of many chemists, and successive studies revealed that hydrogen or methyl shifts were effective and most prominent in strongly acidic solvents, such as HSO_3F, with H_0 = −15.1 [151] (Scheme 61) [152-154]. This is the result of the lack of solvation of intermediate carbenium ion **245** in strong acids due to the high ionizing power and low nucleophilicity, favoring the

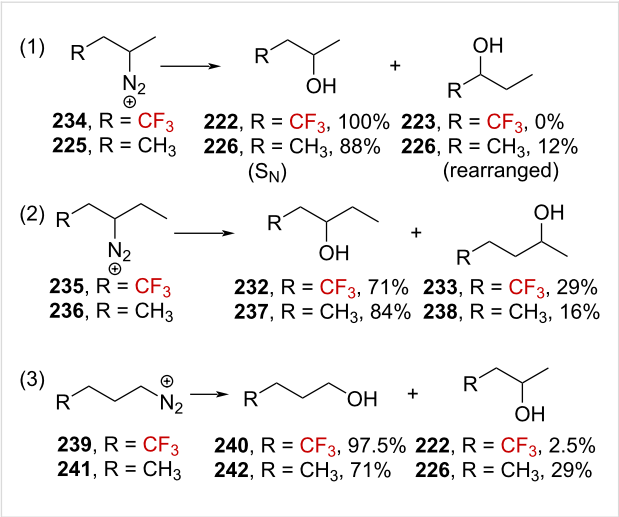

Scheme 60: Deamination of several diazonium ions. Elimination products were formed in these reactions, the yield of which was not determined.

stabilization by hyperconjugation, followed by 1,2-H-shift [155].

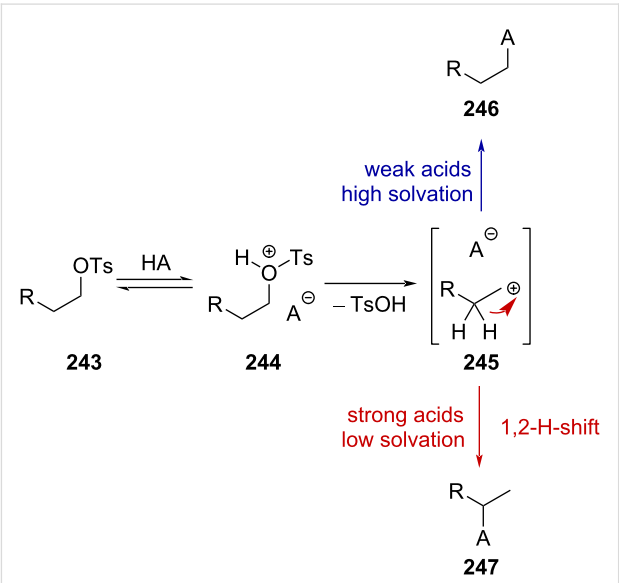

Scheme 61: Solvolysis reaction mechanism of alkyl tosylates.

In this context, Myhre and Andrews explored the reaction of α- and β-(trifluoromethyl) tosylates **248** and **249** in strongly acidic solvents (Scheme 62) [156]. Contrary to what could have been expected, no rearranged products were formed in either case, even in magic acid, HSO_3F–SbF_5 (H_0 = −23 [151]).

The solvolysis study on aliphatic trifluoromethyl tosylate derivatives in strong acids was conducted following theoretical studies [156,157]. While **248** and **252** showed a solvolysis rate

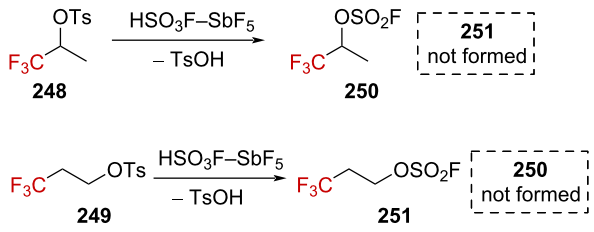

Scheme 62: Solvolysis outcome for the tosylates **248** and **249** in HSO_3FSbF_5.

comparable to that of **253** in 85–100% H_2SO_4, derivative **249** underwent solvolysis at a significantly slower rate (Figure 11). This counterintuitive behavior was not considered to be in line with the intermediary formation of a carbenium ion, as β-(trifluoromethyl)carbenium ion **254** generated from **249** is expected to be more stable than α-(trifluoromethyl)carbenium ion **2** generated from **252**.

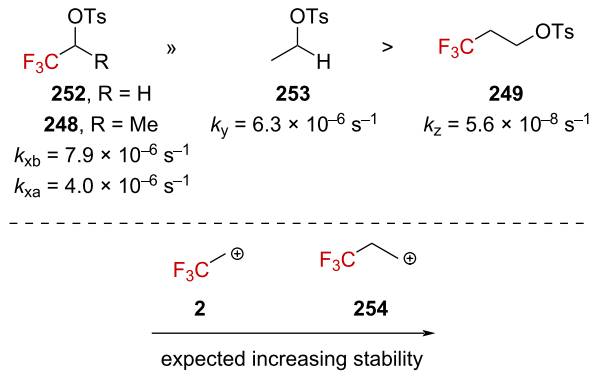

Figure 11: Solvolysis rate of **248**, **249**, **252**, and **253** in 91% H_2SO_4.

To rationalize this trend under these reaction conditions, the authors submitted the enantioenriched alcohol (+)-**255** ($[\alpha]_{365}^{25}$ +2.682, the absolute configuration was not mentioned) to two distinct reaction pathways (Scheme 63). No erosion of the specific rotation, neither through path ABDE ($[\alpha]_{365}^{25}$ +2.692), nor CDE ($[\alpha]_{365}^{25}$ +2.679) was observed, suggesting that an α-(trifluoromethyl)carbenium ion cannot be considered as a reactive intermediate.

Further labeling experiments revealed that the ^{18}O percentage in ^{18}O-**255** (24.6% ± 0.3%) remained unchanged before and after being subjected to the path A–B–D–E (24.4% ± 0.3%) or C–D–E (24.3% ± 0.3%). Hence, no C–O bond cleavage happens in any of these steps. The authors rationalized the experimental observations by invoking a dissociation mechanism involving the cleavage of the weak O–S bond, as depicted in Scheme 64. These experimental results strongly oppose those

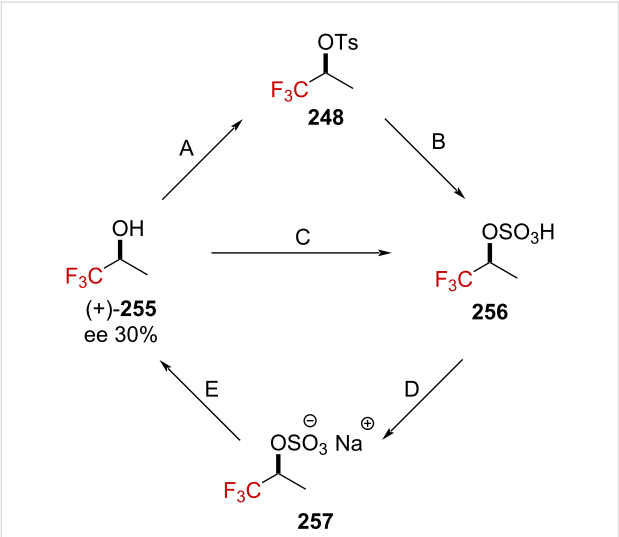

Scheme 63: Illustration of the reaction pathways. TsCl, pyridine, –5 °C (A); 98% H_2SO_4, 30 °C (B); 98% H_2SO_4, 30 °C (C); NaOH (aq), evaporation, extraction with MeOH (D); and moist Et_2O–H^+, reflux (E).

collected by Tidwell and Koshy [39] on benzylic α-(trifluoromethyl)-substituted tosylate derivatives (see section on α-(trifluoromethyl)-substituted carbenium ions), presumably due to the presence of a stabilizing phenyl moiety in the latter case.

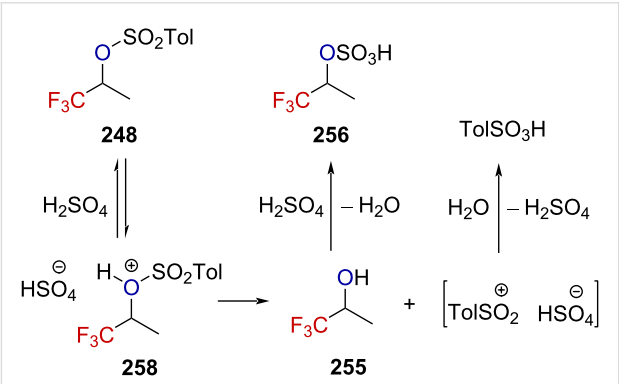

Scheme 64: Proposed solvolysis mechanism for the aliphatic tosylate **248**.

Analogous investigations on triflate derivatives were realized by Tidwell et al. [41]. Triflates are more reactive than tosylates – as illustrated by $k_{Tf}/k_{Ts} = 7 \times 10^4$ for the elimination reactions of **259** and **260** – and were thus of interest in the context of solvolysis studies. The solvolysis of **260** in various solvents led to the sole formation of the elimination product, and no nucleophilic substitution of the triflate by the solvent was observed. Similar results were also reported previously by the authors for **259** (Scheme 65) [39]. Interestingly, no dependence of the elimination rate on the ionizing power of the solvents was

observed, suggesting that the formation of an ion pair (either intimate or solvent-separated) was not the limiting step. However, the faster rate obtained in the most nucleophilic solvents implies that the solvent is involved in the rate-limiting step.

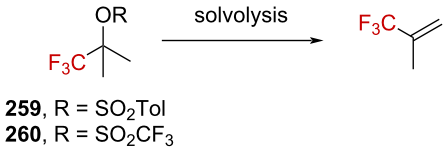

Scheme 65: Solvolysis of the derivatives **259** and **260**.

Kinetic isotope effects in the elimination reactions of **260**, **260**-d_3, and **260**-d_6 were found to be $k_{\mathbf{260}}/k_{\mathbf{260}\text{-}d3}$ = 1.78 and $k_{\mathbf{260}}/k_{\mathbf{260}\text{-}d6}$ = 3.80. The effect of the solvents and added salts on the rate proved that the medium (solvent and salt) is involved in the rate-limiting step. Furthermore, the values obtained for the secondary isotope effect agreed with the elimination as the rate-limiting step and strongly support the hypothesis that the latter occurred from an intimate ion pair.

Starting from **261**, no elimination product could be formed during the solvolysis reaction, and a 1,2-methyl shift occurred to generate **262** after solvent trapping, as reported by Roberts and Hall (Scheme 66) [158]. Kinetic studies revealed a linear free-energy relationship between the rate of the solvolysis against the Y_{OTf} values. The isolated product **262** as well as the kinetic data strongly support the formation of the β-(trifluoromethyl)carbenium ion **263** in the rate-limiting step with considerable neighboring group participation, characteristic of a k_Δ pathway.

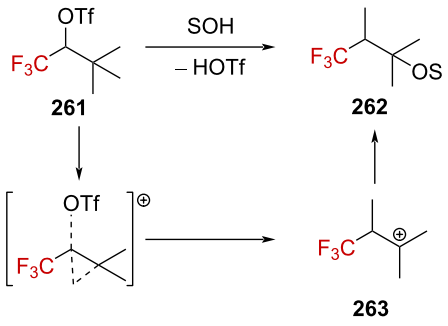

Scheme 66: Solvolysis of triflate **261**. SOH = solvent.

Bonnet-Delpon et al. successfully took advantage of the intramolecular stabilization of a cation induced by the presence of a CF_3 group to develop a method to access 1-(trifluoromethyl)tetralins [159]. For instance, upon the solvolysis of systems such as **264** in TFA/TFAA, the cyclized products **265** were obtained. Furthermore, it is known that the nontrifluoromethylated tosylate analogue undergoes the same cyclization via a k_Δ process rather than a k_c process [160]. The authors thus proposed that the aryl ring stabilizes the cation concomitantly after the elimination of the triflate anion to form the transition state **266** in the solvolysis reaction of derivatives **264**. The same cyclization reaction occurred when derivatives such as **267** were solvolyzed in TFA/H_2SO_4, affording **268** (Scheme 67). However, while the nature of the aryl substituent R^1 had a negligible effect on the rate, the latter had a convincing dependence on the nature of the substituent R^2. For benzylic systems **267**, the authors proposed a k_c pathway involving the formation of the more stable benzylic α-(trifluoromethyl)carbenium ion **269**, with a subsequent cyclization reaction.

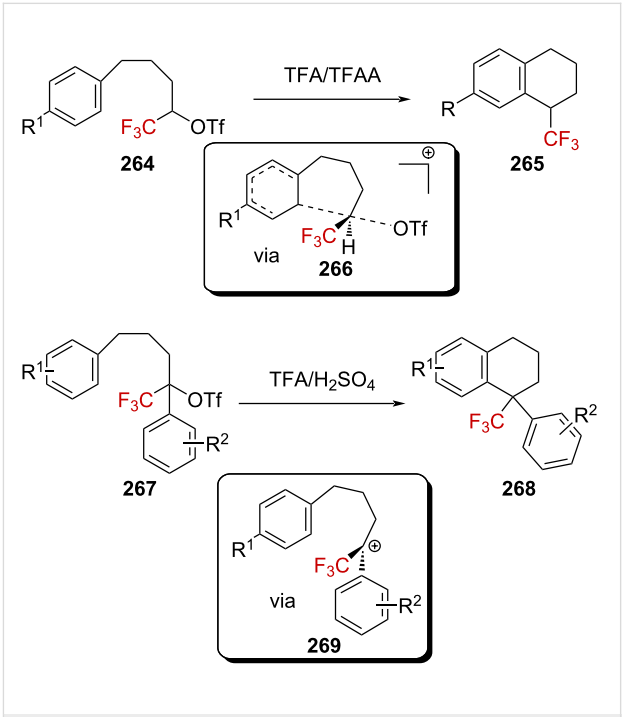

Scheme 67: Intramolecular Friedel–Crafts alkylations upon the solvolysis of triflates **264** and **267**.

Gassman and Doherty suggested that the introduction of a strongly electron-withdrawing group in the α-position of a positively charged carbon center could magnify the neighboring group participation so as to compensate for the increased electron deficiency at the incipient cationic center [4,161]. Using this strategy, Tilley et al. reported the first synthesis of strained CF_3-substituted bicyclo[1.1.0]butane **271a** via γ-silyl elimination of α-(trifluoromethyl)cyclobutyl tosylate **270a** (Scheme 68) [162]. The reaction was proposed to occur via neighboring-group participation of the silicon-based group, through homohyperconjugative stabilization of the pC orbital of the incipient α-R_F-substituted carbenium ion by a percaudal (back lobe) par-

ticipation of the σC–Si orbital (**272**, Scheme 68). Importantly, the initial W-conformation in the starting material **270a**,**b** was mandatory to allow a sufficient orbital overlap as the U-conformation (*endo*-sickle-like isomer) failed to react within the reaction time (≈12 h). In **272**, the positive charge is thus significantly delocalized at the silicon center, allowing a facile nucleophilic displacement at the silicon atom by a solvent molecule to afford **271a**,**b**. The CF_3 moiety strongly affects the stability in **271a**, which was found to be stable "indefinitely" when stored under an inert atmosphere at a low temperature and did not suffer from polymerization.

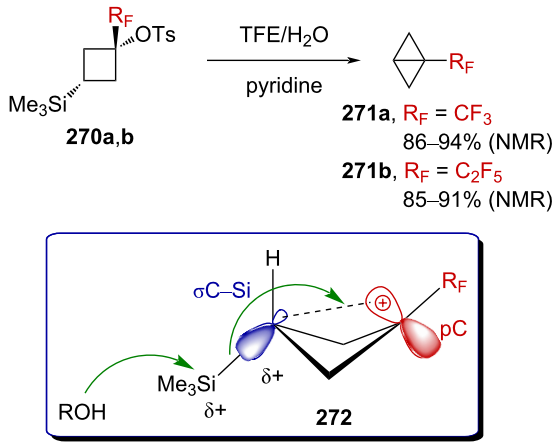

Scheme 68: α-CF_3-enhanced γ-silyl elimination of cyclobutyltosylates **270a**,**b**.

Further investigations by Tilley et al. were conducted in order to enlarge the scope of the above-mentioned 1,3-silyl elimination of α-(trifluoromethyl) tosylate, which was restricted so far to cyclobutyl derivatives, and a variety of linear or cyclic α-(trifluoromethyl)-γ-silyl sulfonates was targeted (Scheme 69) [163,164]. While the solvolysis was readily performed with tosylate-like leaving groups in the case of aromatic substituents being present, as in **273a**–**h**, or in the cyclic systems **274a**,**b**, a better leaving group, such as triflate, was generally required for alkyl derivatives **275a**–**d**.

Interestingly, CF_3-substituted cyclopropanes **281** could be obtained from linear derivative **280** but also from cyclic **279** (*cis*-**279** or *trans*-**279**) via an alternative mechanism. The proposed mechanism for the conversion of **279** into **281** invokes an alkyl shift, leading to the generation of a carbenium ion **283**, stabilized by the β-effect of silicon (via the transition state **282**), and further β-silyl elimination affords product **281** (Scheme 70). In addition, *trans*-**279** reacted approximately 12 times faster than *cis*-**279**, and thus suggesting a neighboring-group participation via the σC–Si orbital in the proposed transition state **282**.

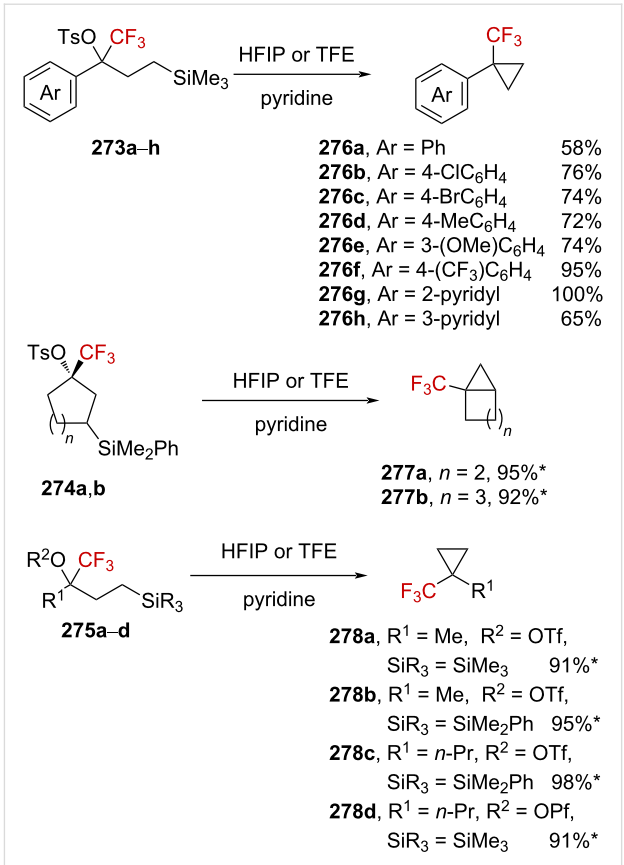

Scheme 69: γ-Silyl elimination in the synthesis of a large variety of CF_3-substituted cyclopropanes. Pf = pentafluorophenylsulfonate. For **277c** and **276g**, no pyridine was used. For **276g**, the yield refers to the protonated pyridinium tosylate. *NMR yield.

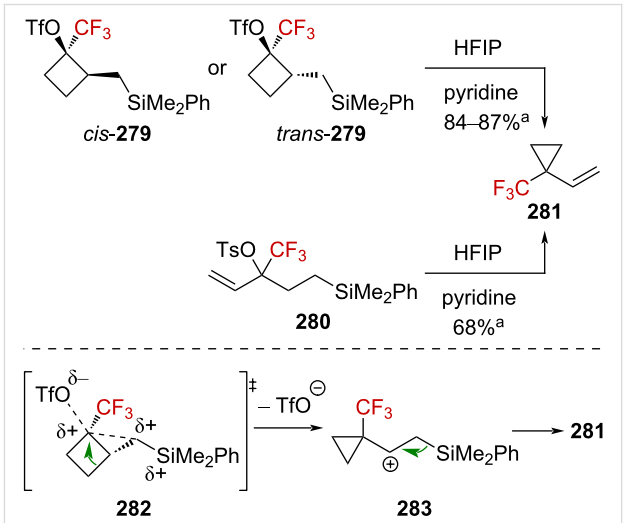

Scheme 70: Synthetic pathways to **281**. [a]NMR yields.

Very recently, Creary reported a study on the generation of CF_3-subtituted γ-silylcarbenium ions via a cyclopropylcarbinyl rearrangement [164]. When cyclopropylcarbinylcarbenium ion

284 is generated, this species is in an equilibrium with the homoallylcarbenium and cyclobutylcarbenium ions **285** and **286** (Scheme 71) [164].

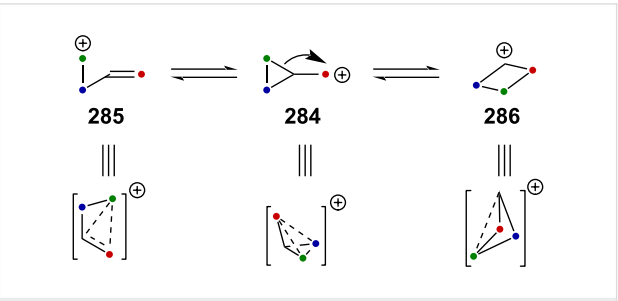

Scheme 71: The cyclopropyl-substituted homoallylcyclobutylcarbenium ion manifold.

Creary investigated the solvolysis of CF_3-substituted cyclopropylcarbinyl triflate **287a** and obtained a mixture of bicyclobutane **271a** and unrearranged solvent-substitution product **289a** in 71% and 29% yield, respectively (Scheme 72) [164]. This result was in stark contrast with those obtained with Ph- and H-substituted analogues **287b** and **287c** because the main products of the reactions in the latter cases were cyclobutanes **290b** and **290c**. As mentioned previously, this is the result of an enhanced neighboring-group participation induced by the presence of the CF_3 group in **287a**. A stronger percaudal stabilization is thus present in carbenium intermediate **272a**, which leads mainly to **271a** by solvent-assisted γ-silyl elimination.

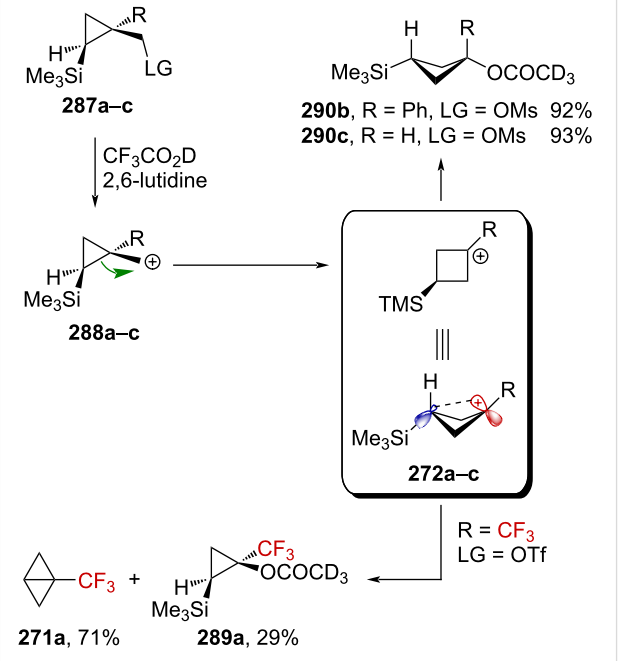

Scheme 72: Reactivity of CF_3-substituted cyclopropylcarbinyl derivatives **287a–c**. LG = leaving group.

Creary then considered the diastereomers of **287a–c**, namely **291a–c**. While **291b** led to the same product **290b**, the isomer **290a** and unsubstituted **290c** exhibited a different reactivity as they did not form the rearranged cyclobutane derivatives **290a** and **290c** (Scheme 73) [164]. It was mentioned that for isomers **291a–c**, the conformation of the corresponding cyclobutylcarbenium ions **293a–c** after the rearrangement would not allow the percaudal participation of the TMS group. Nevertheless, in the presence of a stabilizing group, such as a phenyl group, carbenium ion **293b** is sufficiently stable and can undergo ring inversion to furnish carbenium ion **272b**, stabilized by the TMS group, which finally gives **290b**. On the other hand, in the presence of a CF_3 group or a H atom, **291a** and **291c** strongly suffer from the absence of this stabilization and are mainly converted to the unrearranged products **294a** and **294c**.

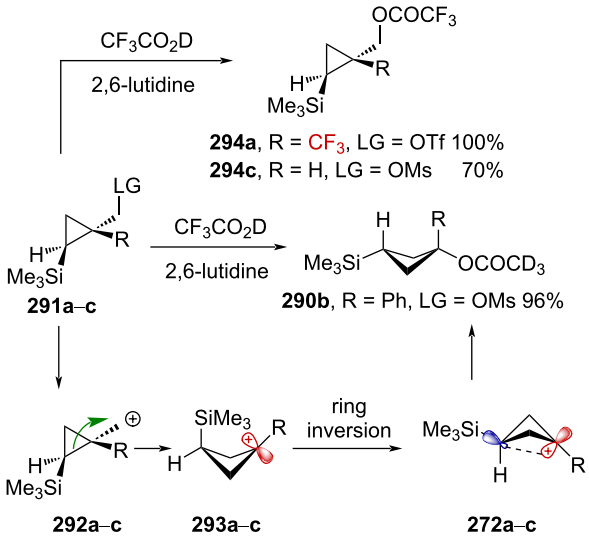

Scheme 73: Reactivity of CF_3-substituted cyclopropylcarbinyl derivatives **291a–c**.

Hypothetical formation of CF_3-containing alkylcarbenium ions by alkene activation: Because 1,1,1-trifluoropropene (TFP) undergoes an anti-Markovnikov addition in the presence of hydrogen halide, Myhre and Andrews anticipated that a similar regioselectivity may occur with HSO_3F [156]. Submitting the fluorinated olefin to HSO_3F unexpectedly led to a dimerization of TFP. The provided mechanistic explanation involves a C–F activation by the HSO_3F Brønsted superacid to generate difluorinated allylcarbenium ion **295**. It must then react with another molecule of TFP to give **296** (Scheme 74). A subsequent 1,3-hydrogen shift, driven by the formation of an allylic carbenium ion **297** from a primary carbenium ion **296**, furnished the isolated product **298** after fluorine abstraction from the anion.

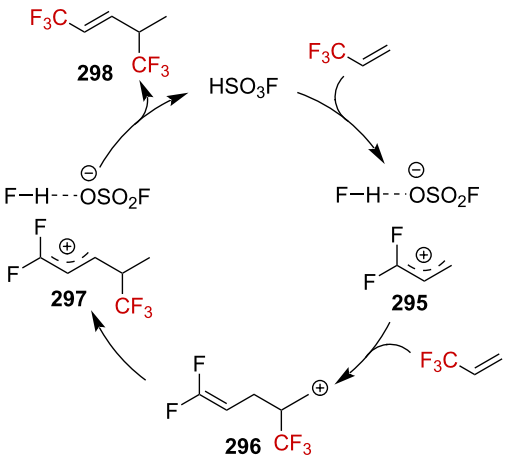

Scheme 74: Superacid-promoted dimerization or TFP.

Further evidence for the formation of the putative difluorinated allylcarbenium ion **295** was obtained by dissolving TFP in less acidic HSO_3Cl (H_0 = −13.8 [151]). In this superacidic medium, difluoroallyl sulfonate **299**, resulting from the direct trapping of **295** by the more coordinating SO_3Cl^- anion (compared to SO_3F^-), was smoothly formed (Scheme 75) [165]. Hence, this demonstrated that the C–F activation of the CF_3 moiety to generate a difluoroallylcarbenium ion **295** was favored over the formation of a secondary α-CF_3-substituted species **300** or a primary aliphatic β-(trifluoromethyl)carbenium ion **254**. Indeed, no evidence for the protonation of TFP was obtained, highlighting once more the extraordinary electron-withdrawing and deactivating potential of the CF_3 moiety. It is worthy of note that the installation of an aryl group, however, makes the protonation of α-(trifluoromethyl)styrene derivatives possible, even though a retardation of the rate of 10^4–10^7 has been measured due to the presence of the CF_3 group [68].

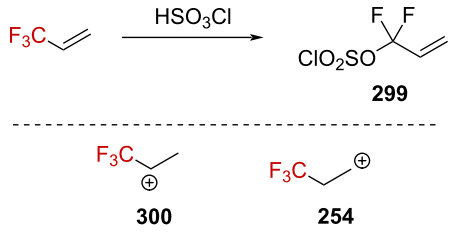

Scheme 75: Reactivity of TFP in a superacid.

To overcome the difficulty to generate trifluoromethyl-substituted alkylcarbenium ions after the activation of trifluoromethyl-substituted alkenes, the stabilization by a neighboring group could be envisaged. In the enantioselective *gem*-difluorination of styrenes catalyzed by hypervalent iodoarene species, Jacobsen et al. elegantly exploited the stabilizing effect of an aromatic ring through skeletal rearrangement via a phenonium ion intermediate [166]. Recently, Gilmour et al. synthesized highly fluorinated scaffolds using this strategy (Scheme 76) [167]. The widely accepted mechanism for this transformation involves a first fluoroiodination of an olefin **301a–c** to give **303a–c**, followed by an anchimerically assisted iodonium elimination to generate the phenonium ions **304a–c** and a subsequent regioselective fluoride addition to furnish compounds **305a–c** (Scheme 76) [168]. In this example, the phenonium species **304a–c** can be regarded as a "hidden" α-(trifluoromethyl)carbenium ion **306a–c**, in which the fluorine atom in the α position stabilizes the cation by lone pair back-donation (see **306'a–c**), favoring the whole process.

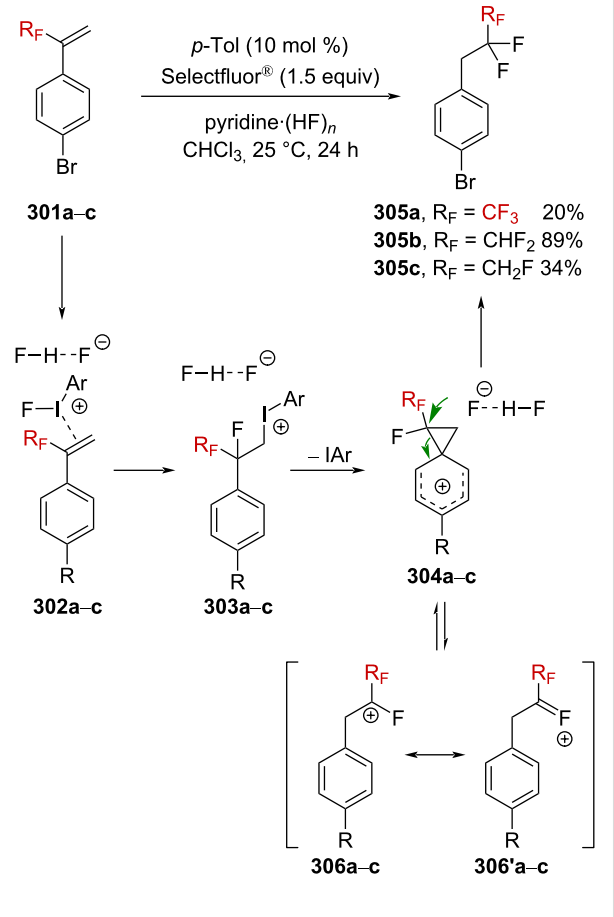

Scheme 76: *gem*-Difluorination of α-fluoroalkyl styrenes via the formation of a "hidden" α-R_F-substituted carbenium ion **306**↔**306'**.

α-(Trifluoromethyl)vinylcarbenium ions

The involvement of vinyl α-(trifluoromethyl)carbenium ions is scarcely reported in the literature. Vött et al. reported the synthesis of CF_3-containing small rings via the transient formation of vinyl cations [169]. During the course of their study, they in-

vestigated the reactivity of CF_3-substituted pentyne **307**. The solvolysis of **307** in TFA and CF_3CO_2Na led to cyclobutanone **308** and alcohol **309**. The isolation of **308** suggests the transient formation of β-(trifluoromethyl)vinyl cation **310**. However, no trace of a cyclopropyl ketone **311** was observed, indicating that this route is prohibited as it requires the generation of a more destabilized α-(trifluoromethyl)vinyl cation **312** of higher energy (Scheme 77).

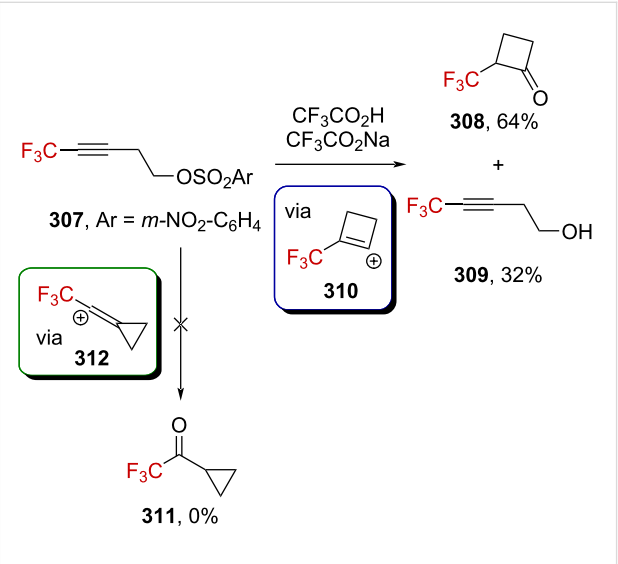

Scheme 77: Solvolysis of CF_3-substituted pentyne **307**.

The photochemical formation of α-(trifluoromethyl)vinylcarbenium ions has also been suggested by Lodder et al. (Scheme 78) [170]. UV irradiation of vinyl compound **313** led to the formation of acetylene product **315**, which is suggested to be formed via β-H-elimination from an open α-(trifluoro-methyl)vinylcarbenium ion **314**. A kinetic isotope effect study gave a k_H/k_D = 1.22 ratio, which is in perfect agreement with β-secondary isotope effect values for reactions proceeding through a carbenium ion. The observation of product **317** strongly supports this cationic mechanism, as it is not unlikely that carbenium ion **314** undergoes a 1,2-fluorine shift (although such a rearrangement has not been experimentally demonstrated so far) to generate the more stable difluorinated allyl cation **316**, which leads to **317** after internal return. Noteworthy, it has been calculated that such a vinyl cation **314** is 42.1 kcal·mol^{-1} higher in energy than the corresponding CH_3-substituted analogues.

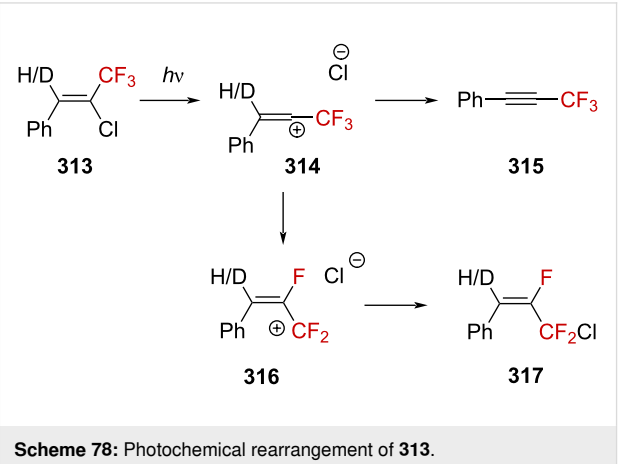

Scheme 78: Photochemical rearrangement of **313**.

Nonclassical α-(trifluoromethyl)carbenium ions

The very existence of nonclassical carbocations (3 centers, 2π-electrons) has been the subject of debate for decades. The 2-norbornyl cation became the most emblematic example, and its structure has been proposed either as two carbenium ions, **318a** and **318b**, in a rapid equilibrium or as a symmetrical cation **318c**, displaying a nonclassical pentacoordinated carbon atom (Figure 12) [171-173]. Krossing et al. eventually put an end to this debate by achieving the crystal growth and crystal structure determination of the 2-norbornyl cation, the structure of which was unequivocally assigned as **318c** [174].

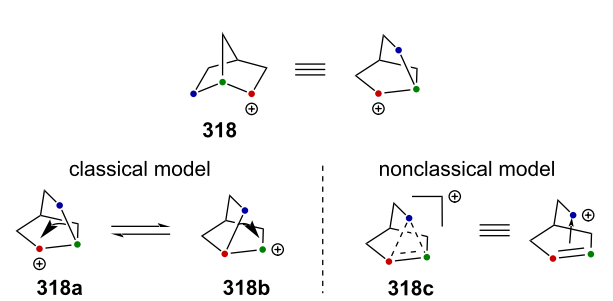

Figure 12: Structure of 2-norbornylcarbenium ion **318** and argued model for the stabilization of this cation.

In 1984, as part of their investigations on carbocation stabilization by neighboring group participation, Gassman and Hall brought evidence for the nonclassical model using a strategy involving a progressive destabilization of the resulting cation by the introduction of CF_3 groups in the norbornene derivatives **319**–**321** (Figure 13) [175]. They found a cumulative effect of the CF_3 groups on the solvolysis rate, with a 10^6-fold decelerating effect upon the introduction of each CF_3 unit. The authors concluded that "the fact that each CF_3 group decreases the rate of ionization by 10^6 provides overwhelming evidence that the interactions of the double bond […] with the incipient carbocation involve symmetrical (nonclassical) transition states **322**, rather than pairs of rapidly equilibrating (classical) cations".

2-Adamantyl tosylate is one of the main references to describe the S_N1 mechanism in which the carbenium character is maxi-

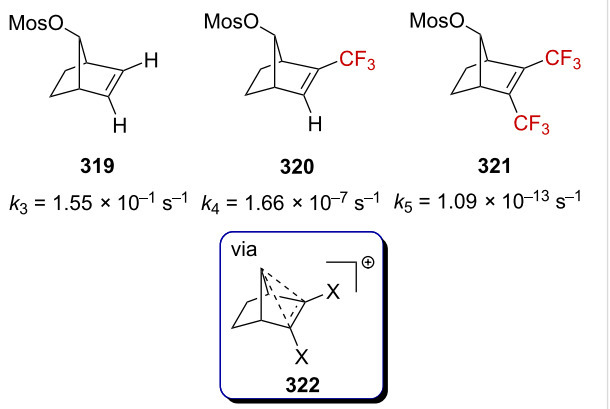

Figure 13: Structures and solvolysis rate (TFE, 25 °C) of the sulfonates **319**–**321**. Mos = *p*-$MeOC_6H_4SO_2$.

mized. For this reason, Prakash, Tidwell, et al. tried to reach the highest k_H/k_{CF3} ratio by exploring 2-adamantyl-2-trifluoromethyl tosylate (**323**), which was expected to exhibit a profound reluctance to generate a carbenium ion [176]. Ironically, the solvolysis of **323** in several solvents led to an average ratio of k_H/k_{CF3} = 2.0, the smallest ratio ever obtained to date. The explanation for this unprecedented high reactivity for an α-(trifluoromethyl)alkyl tosylate partly lies in the structure of the major solvolysis product **324** (Scheme 79). Monitoring of the reaction by NMR spectroscopy allowed the observation of intermediate **327**, which was suggested to result from a successive ion pair formation, rearrangement, and internal return. It was then observed that **327** was progressively converted into **324** at a rate 3 times slower than when it was produced from **323**. From these observations, the authors concluded that the high reactivity of **323** was attributed to the σ-donation from the C3–C4 bond, allowing the positive charge to also be shared in the β-position of the CF_3 group via intermediate **326**. Furthermore,

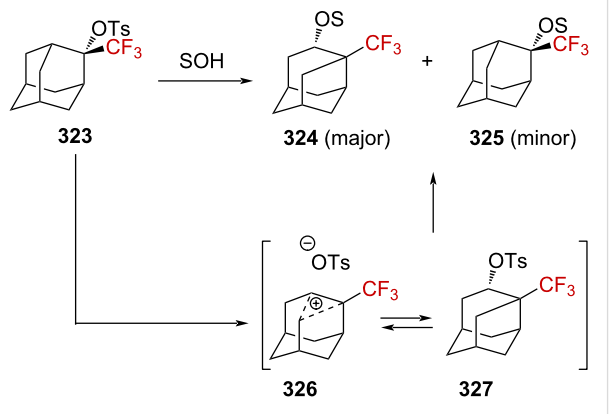

Scheme 79: Mechanism for the solvolysis of **323**. SOH = solvent.

the presence of a ground-state strain of approximately 6.5 kcal·mol^{-1} due to the presence of the CF_3 group was established in **323**, and the relief of this intrinsic strain in the transition state would act as an additional driving force and accelerate this reaction.

The solvolysis of cyclopropyl-substituted α-(trifluoromethyl) tosylate **328** was investigated by Meyer and Hanack, who reported a high tendency of **328** for rearrangements [177]. Hence, the hydrolysis of **328** led to **329** and to a mixture of the rearranged products **330**–**332** (Scheme 80).

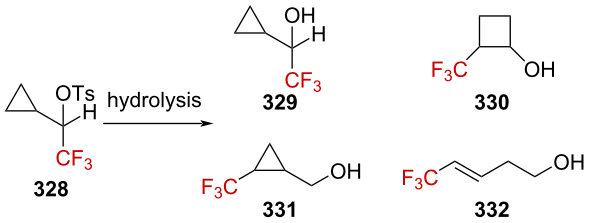

Scheme 80: Products formed by the hydrolysis of **328**.

Suspecting that **330** and **331** were obtained from the solvent trapping of the rearranged carbenium ions **336** and **337**, respectively (Scheme 81), the cyclobutyl tosylate **333** and the cyclopropyl tosylate **334** were also solvolyzed (Table 3). Interestingly, while **328** yielded 3.5% of the direct solvent-substituted product **329**, **333**, and **334** yielded 25% of **330** and 92% of **331**, respectively, as a result of the lower tendency to rearrange, due to the higher ion stability.

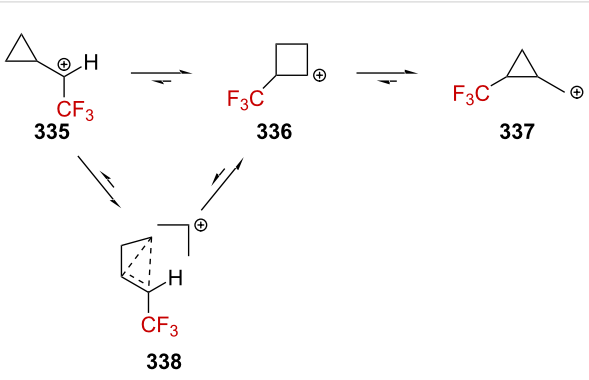

Scheme 81: Proposed carbenium ion intermediates in an equilibrium during the solvolysis of tosylates **328**, **333**, or **334**.

This suggests that **329** generates a highly reactive α-(trifluoromethyl)carbenium ion **335** upon solvolysis, which rapidly either rearranges via an alkyl shift to the β-(trifluoromethyl)carbenium ion **336** to give **330**, or to the γ-(trifluoromethyl)car-

Table 3: Solvolysis products of compounds **328**, **333**, and **334**.

	329	330	331	332
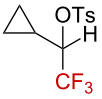 **328**	3.5%	28%	32%	34%
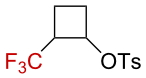 **333**	—	25%	68%	7%
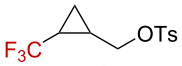 **334**	—	5%	92%	—

benium ion **338** via σ_{C-C} bond donation (i.e., a homoaromatic species), which is trapped at the primary carbon atom, similar as in norbornyl derivatives, to give **332**. Also, **336** can further rearrange by alkyl shift to give the γ-(trifluoromethyl)carbenium ion **337**, which leads to **331**. What is striking from these observations is the effect of the CF_3 group on a positive charge nearby, as it continuously moves the latter from the α- to β- or eventually from the β- to the γ-position. Kinetic studies conducted by Roberts also support the formation of carbenium ion **335** as the rate-limiting step [178].

Conclusion

Destabilized carbocations exhibit structural and electronic features that reduce their lifetimes. CF_3-substituted carbocations are probably the cations that have long been regarded as the worst possible intermediates to be generated in an organic transformation, and therefore were deeply studied as exotic species. The study of CF_3-substituted carbocations has therefore produced valuable contributions to understand their implications in synthetic transformations. Through these efforts, which are the subjects of this review, great perspectives in modern synthetic chemistry are expected as a result of the exploitation of these underestimated cationic intermediates.

Acknowledgements

The authors thank the French fluorine network (GIS-FLUOR).

Funding

We gratefully acknowledge the Frontier Research in Chemistry Foundation (FRC), the Université de Strasbourg (grant FLE-FRC-0002-0035, SuperFlOx), the Université de Poitiers, and the CNRS for financial support. The authors also acknowledge financial support from the European Union (ERDF) and the Région Nouvelle Aquitaine (SUPERDIV project-HABISAN program).

ORCID® iDs

Anthony J. Fernandes - https://orcid.org/0000-0001-8372-7982
Armen Panossian - https://orcid.org/0000-0003-2317-1200
Frédéric R. Leroux - https://orcid.org/0000-0001-8900-5753
Sébastien Thibaudeau - https://orcid.org/0000-0002-6246-5829

References

1. Naredla, R. R.; Klumpp, D. A. *Chem. Rev.* **2013,** *113,* 6905–6948. doi:10.1021/cr4001385
2. Olah, G. A.; Reddy, V. P.; Prakash, G. K. S. *Chem. Rev.* **1992,** *92,* 69–95. doi:10.1021/cr00009a003
3. Olah, G. A.; Prakash, G. K. S.; Molnár, Á.; Sommer, J. *Superacid Chemistry,* 2nd ed.; John Wiley & Sons: Hoboken, NJ, USA, 2009. doi:10.1002/9780470421604
4. Gassman, P. G.; Tidwell, T. T. *Acc. Chem. Res.* **1983,** *16,* 279–285. doi:10.1021/ar00092a003
5. Tidwell, T. T. *Angew. Chem., Int. Ed. Engl.* **1984,** *23,* 20–32. doi:10.1002/anie.198400201
6. Creary, X. *Chem. Rev.* **1991,** *91,* 1625–1678. doi:10.1021/cr00008a001
7. Liang, T.; Neumann, C. N.; Ritter, T. *Angew. Chem., Int. Ed.* **2013,** *52,* 8214–8264. doi:10.1002/anie.201206566
8. Champagne, P. A.; Desroches, J.; Hamel, J.-D.; Vandamme, M.; Paquin, J.-F. *Chem. Rev.* **2015,** *115,* 9073–9174. doi:10.1021/cr500706a
9. Neumann, C. N.; Ritter, T. *Angew. Chem., Int. Ed.* **2015,** *54,* 3216–3221. doi:10.1002/anie.201410288
10. Ma, J.-A.; Cahard, D. *Chem. Rev.* **2008,** *108,* PR1–PR43. doi:10.1021/cr800221v
11. Pupo, G.; Ibba, F.; Ascough, D. M. H.; Vicini, A. C.; Ricci, P.; Christensen, K. E.; Pfeifer, L.; Morphy, J. R.; Brown, J. M.; Paton, R. S.; Gouverneur, V. *Science* **2018,** *360,* 638–642. doi:10.1126/science.aar7941
12. Commare, B.; Schmitt, E.; Aribi, F.; Panossian, A.; Vors, J.-P.; Pazenok, S.; Leroux, F. R. *Molecules* **2017,** *22,* 977. doi:10.3390/molecules22060977
13. O'Hagan, D. *Chem. Soc. Rev.* **2008,** *37,* 308–319. doi:10.1039/b711844a
14. Meanwell, N. A. *J. Med. Chem.* **2018,** *61,* 5822–5880. doi:10.1021/acs.jmedchem.7b01788
15. Gillis, E. P.; Eastman, K. J.; Hill, M. D.; Donnelly, D. J.; Meanwell, N. A. *J. Med. Chem.* **2015,** *58,* 8315–8359. doi:10.1021/acs.jmedchem.5b00258
16. Zhou, Y.; Wang, J.; Gu, Z.; Wang, S.; Zhu, W.; Aceña, J. L.; Soloshonok, V. A.; Izawa, K.; Liu, H. *Chem. Rev.* **2016,** *116,* 422–518. doi:10.1021/acs.chemrev.5b00392
17. Ojima, I. *J. Org. Chem.* **2013,** *78,* 6358–6383. doi:10.1021/jo400301u
18. Hammett, L. P. *Chem. Rev.* **1935,** *17,* 125–136. doi:10.1021/cr60056a010
19. Hammett, L. P. *J. Am. Chem. Soc.* **1937,** *59,* 96–103. doi:10.1021/ja01280a022
20. Brown, H. C.; Okamoto, Y. *J. Am. Chem. Soc.* **1958,** *80,* 4979–4987. doi:10.1021/ja01551a055
21. McDaniel, D. H.; Brown, H. C. *J. Org. Chem.* **1958,** *23,* 420–427. doi:10.1021/jo01097a026
22. Reynolds, W. F.; Dais, P.; Taft, R. W.; Topsom, R. D. *Tetrahedron Lett.* **1981,** *22,* 1795–1797. doi:10.1016/s0040-4039(01)90441-1

23. Reynolds, W. F.; Dais, P.; MacIntyre, D. W.; Topsom, R. D.; Marriott, S.; Von Nagy-Felsobuki, E.; Taft, R. W. *J. Am. Chem. Soc.* **1983,** *105,* 378–384. doi:10.1021/ja00341a015
24. Paddon-Row, M. N.; Santiago, C.; Houk, K. N. *J. Am. Chem. Soc.* **1980,** *102,* 6561–6563. doi:10.1021/ja00541a033
25. Charpentier, M.; Fossey, J.; Tidwell, T. T.; Wolfe, S. *Can. J. Chem.* **1987,** *65,* 473–481. doi:10.1139/v87-082
26. Struble, M. D.; Scerba, M. T.; Siegler, M.; Lectka, T. *Science* **2013,** *340,* 57–60. doi:10.1126/science.1231247
27. Pitts, C. R.; Holl, M. G.; Lectka, T. *Angew. Chem., Int. Ed.* **2018,** *57,* 1924–1927. doi:10.1002/anie.201712021
28. Holl, M. G.; Pitts, C. R.; Lectka, T. *Acc. Chem. Res.* **2020,** *53,* 265–275. doi:10.1021/acs.accounts.9b00554
29. Paddon-Row, M. N.; Houk, K. N.; Tidwell, T. T. *Tetrahedron Lett.* **1982,** *23,* 383–386. doi:10.1016/s0040-4039(00)86837-9
30. Karpov, V. M.; Mezhenkova, T. V.; Platonov, V. E.; Yakobson, G. G. *J. Fluorine Chem.* **1985,** *28,* 115–120. doi:10.1016/s0022-1139(00)85197-0
31. Mezhenkova, T. V.; Sinyakov, V. R.; Karpov, V. M.; Platonov, V. E. *Russ. J. Org. Chem.* **2013,** *49,* 1454–1465. doi:10.1134/s1070428013100096
32. Zonov, Y. V.; Karpov, V. M.; Platonov, V. E. *J. Fluorine Chem.* **2014,** *162,* 71–77. doi:10.1016/j.jfluchem.2014.03.008
33. Zonov, Y. V.; Karpov, V. M.; Mezhenkova, T. V.; Rybalova, T. V.; Gatilov, Y. V.; Platonov, V. E. *J. Fluorine Chem.* **2016,** *188,* 117–125. doi:10.1016/j.jfluchem.2016.06.014
34. Olah, G. A.; Cupas, C. A.; Comisarow, M. B. *J. Am. Chem. Soc.* **1966,** *88,* 362–364. doi:10.1021/ja00954a035
35. Olah, G. A.; Pittman, C. U., Jr. *J. Am. Chem. Soc.* **1966,** *88,* 3310–3312. doi:10.1021/ja00966a024
36. Olah, G. A.; Prakash, G. K. S.; Arvanaghi, M.; Krishnamurthy, V. V.; Narang, S. C. *J. Am. Chem. Soc.* **1984,** *106,* 2378–2380. doi:10.1021/ja00320a026
37. White, J. R.; Price, G. J.; Plucinski, P. K.; Frost, C. G. *Tetrahedron Lett.* **2009,** *50,* 7365–7368. doi:10.1016/j.tetlet.2009.10.082
38. Laali, K. K.; Tanaka, M.; Hollenstein, S.; Cheng, M. *J. Org. Chem.* **1997,** *62,* 7752–7757. doi:10.1021/jo971014z
39. Koshy, K. M.; Tidwell, T. T. *J. Am. Chem. Soc.* **1980,** *102,* 1216–1218. doi:10.1021/ja00523a077
40. Allen, A. D.; Jansen, M. P.; Koshy, K. M.; Mangru, N. N.; Tidwell, T. T. *J. Am. Chem. Soc.* **1982,** *104,* 207–211. doi:10.1021/ja00365a037
41. Jansen, M. P.; Koshy, K. M.; Mangru, N. N.; Tidwell, T. T. *J. Am. Chem. Soc.* **1981,** *103,* 3863–3867. doi:10.1021/ja00403a040
42. Guo, Z.; Fry, A. *Tetrahedron Lett.* **1986,** *27,* 5059–5062. doi:10.1016/s0040-4039(00)85132-1
43. Liu, K. T.; Kuo, M. Y.; Sheu, C. F. *J. Am. Chem. Soc.* **1982,** *104,* 211–215. doi:10.1021/ja00365a038
44. Anslyn, E. V.; Dougherty, D. A. *Modern Physical Organic Chemistry;* University Science Books: Sausalito, CA, USA, 2005.
45. Schadt, F. L.; Bentley, T. W.; Schleyer, P. v. R. *J. Am. Chem. Soc.* **1976,** *98,* 7667–7675. doi:10.1021/ja00440a037
46. Harrington, C. K. Ph.D. Thesis, The Ohio State University, Columbus, OH, USA, 1976. *Diss. Abstr.* **1976,** *37,* 2248B.
47. Pegolotti, J. A.; Young, W. G. *J. Am. Chem. Soc.* **1961,** *83,* 3251–3258. doi:10.1021/ja01476a018
48. Allen, A. D.; Ambidge, I. C.; Che, C.; Micheal, H.; Muir, R. J.; Tidwell, T. *J. Am. Chem. Soc.* **1983,** *105,* 2343–2350. doi:10.1021/ja00346a039
49. Richard, J. P. *J. Am. Chem. Soc.* **1986,** *108,* 6819–6820. doi:10.1021/ja00281a068
50. Richard, J. P. *J. Am. Chem. Soc.* **1989,** *111,* 1455–1465. doi:10.1021/ja00186a047
51. Vuković, V. D.; Richmond, E.; Wolf, E.; Moran, J. *Angew. Chem., Int. Ed.* **2017,** *56,* 3085–3089. doi:10.1002/anie.201612573
52. Allen, A. D.; Girdhar, R.; Jansen, M. P.; Mayo, J. D.; Tidwell, T. T. *J. Org. Chem.* **1986,** *51,* 1324–1329. doi:10.1021/jo00358a031
53. Liu, K.-T.; Kuo, M.-Y. *Tetrahedron Lett.* **1985,** *26,* 355–358. doi:10.1016/s0040-4039(01)80816-9
54. Liu, K. T.; Chang, S. M.; Chen, H. I.; Chiu, P. F.; Wu, T. R. *J. Org. Chem.* **1991,** *56,* 1315–1317. doi:10.1021/jo00003a075
55. Cohen, S. *J. Am. Chem. Soc.* **1957,** *79,* 1499–1502. doi:10.1021/ja01563a062
56. Kaluszyner, A.; Cohen, S. *Tetrahedron* **1960,** *11,* 252–255. doi:10.1016/s0040-4020(01)93174-6
57. Streitwieser, A.; Marchand, A. P.; Pudjaatmaka, A. H. *J. Am. Chem. Soc.* **1967,** *89,* 693–694. doi:10.1021/ja00979a042
58. Dao, L. H.; Maleki, M.; Hopkinson, A. C.; Lee-Ruff, E. *J. Am. Chem. Soc.* **1986,** *108,* 5237–5242. doi:10.1021/ja00277a030
59. Gassman, P. G.; Ray, J. A.; Wenthold, P. G.; Mickelson, J. W. *J. Org. Chem.* **1991,** *56,* 5143–5146. doi:10.1021/jo00017a029
60. Martynov, M. Y.; Iakovenko, R. O.; Kazakova, A. N.; Boyarskaya, I. A.; Vasilyev, A. V. *Org. Biomol. Chem.* **2017,** *15,* 2541–2550. doi:10.1039/c7ob00406k
61. Iakovenko, R. O.; Chicca, A.; Nieri, D.; Reynoso-Moreno, I.; Gertsch, J.; Krasavin, M.; Vasilyev, A. V. *Tetrahedron* **2019,** *75,* 624–632. doi:10.1016/j.tet.2018.12.041
62. Zerov, A. V.; Bulova, A. A.; Khoroshilova, O. V.; Vasilyev, A. V. *Org. Chem. Front.* **2019,** *6,* 3264–3268. doi:10.1039/c9qo00822e
63. Astrologes, G. W.; Martin, J. C. *J. Am. Chem. Soc.* **1977,** *99,* 4400–4404. doi:10.1021/ja00455a031
64. Allen, A. D.; Kanagasabapathy, V. M.; Tidwell, T. T. *J. Am. Chem. Soc.* **1983,** *105,* 5961–5962. doi:10.1021/ja00356a065
65. Kanagasabapathy, V. M.; Sawyer, J. F.; Tidwell, T. T. *J. Org. Chem.* **1985,** *50,* 503–509. doi:10.1021/jo00204a016
66. Allen, A. D.; Kanagasabapathy, V. M.; Tidwell, T. T. *J. Am. Chem. Soc.* **1986,** *108,* 3470–3474. doi:10.1021/ja00272a050
67. Richard, J. P.; Amyes, T. L.; Bei, L.; Stubblefield, V. *J. Am. Chem. Soc.* **1990,** *112,* 9513–9519. doi:10.1021/ja00182a010
68. Koshy, K. M.; Roy, D.; Tidwell, T. T. *J. Am. Chem. Soc.* **1979,** *101,* 357–363. doi:10.1021/ja00496a014
69. Mishima, M.; Inoue, H.; Fujio, M.; Tsuno, Y. *Tetrahedron Lett.* **1989,** *30,* 2101–2104. doi:10.1016/s0040-4039(01)93723-2
70. Kwong-Chip, J.-M.; Tidwell, T. T. *Tetrahedron Lett.* **1989,** *30,* 1319–1322. doi:10.1016/s0040-4039(00)99454-1
71. Ling, Y.; An, D.; Zhou, Y.; Rao, W. *Org. Lett.* **2019,** *21,* 3396–3401. doi:10.1021/acs.orglett.9b01135
72. Zou, Y.-X.; Liu, X.-Y.; Zhang, J.; Yang, H.-L.; Yang, X.-Y.; Liu, X.-L.; Chu, Y.-W.; Chen, L. *Adv. Synth. Catal.* **2019,** *361,* 5311–5316. doi:10.1002/adsc.201900987
73. Khoroshilova, O. V.; Vasilyev, A. V. *J. Org. Chem.* **2020,** *85,* 5872–5883. doi:10.1021/acs.joc.0c00170
74. Poulter, C. D.; Satterwhite, D. M.; Rilling, H. C. *J. Am. Chem. Soc.* **1976,** *98,* 3376–3377. doi:10.1021/ja00427a056
75. Poulter, C. D.; Rilling, H. C. *Acc. Chem. Res.* **1978,** *11,* 307–313. doi:10.1021/ar50128a004
76. Gassman, P. G.; Harrington, C. K. *J. Org. Chem.* **1984,** *49,* 2258–2273. doi:10.1021/jo00186a035

77. Radix-Large, S.; Kucharski, S.; Langlois, B. R. *Synthesis* **2004,** 456–465. doi:10.1055/s-2004-815928
78. Prakash, G. K. S.; Kantamani, S.; Reddy, V. P.; Rasul, G. *Res. Chem. Intermed.* **1996,** *22,* 717–724. doi:10.1163/156856796x00278
79. Kazakova, A. N.; Iakovenko, R. O.; Muzalevskiy, V. M.; Boyarskaya, I. A.; Avdontceva, M. S.; Starova, G. L.; Vasilyev, A. V.; Nenajdenko, V. G. *Tetrahedron Lett.* **2014,** *55,* 6851–6855. doi:10.1016/j.tetlet.2014.10.083
80. Kazakova, A. N.; Iakovenko, R. O.; Boyarskaya, I. A.; Nenajdenko, V. G.; Vasilyev, A. V. *J. Org. Chem.* **2015,** *80,* 9506–9517. doi:10.1021/acs.joc.5b01398
81. Kazakova, A. N.; Iakovenko, R. O.; Boyarskaya, I. A.; Ivanov, A. Y.; Avdontceva, M. S.; Zolotarev, A. A.; Panikorovsky, T. L.; Starova, G. L.; Nenajdenko, V. G.; Vasilyev, A. V. *Org. Chem. Front.* **2017,** *4,* 255–265. doi:10.1039/c6qo00643d
82. Nicholas, K. M. *Acc. Chem. Res.* **1987,** *20,* 207–214. doi:10.1021/ar00138a001
83. Kondratenko, M. A.; Malézieux, B.; Gruselle, M.; Bonnet-Delpon, D.; Bégué, J. P. *J. Organomet. Chem.* **1995,** *487,* C15–C17. doi:10.1016/0022-328x(94)05126-v
84. Amouri, H.; Bégué, J.-P.; Chennoufi, A.; Bonnet-Delpon, D.; Gruselle, M.; Malézieux, B. *Org. Lett.* **2000,** *2,* 807–809. doi:10.1021/ol005554l
85. Gruselle, M.; Malézieux, B.; Andrés, R.; Amouri, H.; Vaissermann, J.; Melikyan, G. G. *Eur. J. Inorg. Chem.* **2000,** 359–368. doi:10.1002/(sici)1099-0682(200002)2000:2<359::aid-ejic359>3.0.co;2-v
86. Zerov, A. V.; Starova, G. L.; Suslonov, V. V.; Khoroshilova, O. V.; Vasilyev, A. V. *Org. Lett.* **2018,** *20,* 784–787. doi:10.1021/acs.orglett.7b03920
87. Noël, F.; Vuković, V. D.; Yi, J.; Richmond, E.; Kravljanac, P.; Moran, J. *J. Org. Chem.* **2019,** *84,* 15926–15947. doi:10.1021/acs.joc.9b02398
88. Beaver, M. G.; Buscagan, T. M.; Lavinda, O.; Woerpel, K. A. *Angew. Chem., Int. Ed.* **2016,** *55,* 1816–1819. doi:10.1002/anie.201507806
89. Martin, A.; Arda, A.; Désiré, J.; Martin-Mingot, A.; Probst, N.; Sinaÿ, P.; Jiménez-Barbero, J.; Thibaudeau, S.; Blériot, Y. *Nat. Chem.* **2016,** *8,* 186–191. doi:10.1038/nchem.2399
90. Adero, P. O.; Amarasekara, H.; Wen, P.; Bohé, L.; Crich, D. *Chem. Rev.* **2018,** *118,* 8242–8284. doi:10.1021/acs.chemrev.8b00083
91. Olah, G. A.; Burrichter, A.; Rasul, G.; Yudin, A. K.; Prakash, G. K. S. *J. Org. Chem.* **1996,** *61,* 1934–1939. doi:10.1021/jo9516493
92. Kray, W. D.; Rosser, R. W. *J. Org. Chem.* **1977,** *42,* 1186–1189. doi:10.1021/jo00427a018
93. Fung, S.; Abraham, N. A.; Bellini, F.; Sestanj, K. *Can. J. Chem.* **1983,** *61,* 368–371. doi:10.1139/v83-066
94. Bonnet-Delpon, D.; Charpentier-Morize, M.; Jacquot, R. *J. Org. Chem.* **1988,** *53,* 759–762. doi:10.1021/jo00239a011
95. Aubert, C.; Bégué, J.-P.; Bonnet-Delpon, D.; Mesureur, D. *J. Chem. Soc., Perkin Trans. 1* **1989,** 395–399. doi:10.1039/p19890000395
96. Nie, J.; Zhang, G.-W.; Wang, L.; Fu, A.; Zheng, Y.; Ma, J.-A. *Chem. Commun.* **2009,** 2356–2358. doi:10.1039/b900474b
97. Fu, A.; Meng, W.; Li, H.; Nie, J.; Ma, J.-A. *Org. Biomol. Chem.* **2014,** *12,* 1908–1918. doi:10.1039/c3ob42157k
98. Sasaki, S.; Ikekame, Y.; Tanayama, M.; Yamauchi, T.; Higashiyama, K. *Synlett* **2012,** *23,* 2699–2703. doi:10.1055/s-0032-1317485
99. Yuan, X.; Wu, L.; Xu, C.; Pan, Z.; Shi, L.; Yang, G.; Wang, C.; Fan, S. *Tetrahedron Lett.* **2019,** *60,* 151329. doi:10.1016/j.tetlet.2019.151329
100. Wang, Y.; Yuan, Y.; Xing, C.-H.; Lu, L. *Tetrahedron Lett.* **2014,** *55,* 1045–1048. doi:10.1016/j.tetlet.2013.12.078
101. Olah, G. A.; Klumpp, D. A. *Superelectrophiles and Their Chemistry;* John Wiley & Sons: Hoboken, NJ, USA, 2007. doi:10.1002/9780470185124
102. O'Connor, M. J.; Boblak, K. N.; Topinka, M. J.; Kindelin, P. J.; Briski, J. M.; Zheng, C.; Klumpp, D. A. *J. Am. Chem. Soc.* **2010,** *132,* 3266–3267. doi:10.1021/ja1001482
103. Guy, A.; Lobgeois, A.; Lemaire, M. *J. Fluorine Chem.* **1986,** *32,* 361–366. doi:10.1016/s0022-1139(00)81944-2
104. Gong, Y.; Kato, K.; Kimoto, H. *Bull. Chem. Soc. Jpn.* **2000,** *73,* 249–250. doi:10.1246/bcsj.73.249
105. Yuefa, G.; Katsuya, K.; Hiroshi, K. *Bull. Chem. Soc. Jpn.* **2001,** *74,* 377–383.
106. Sakumo, K.; Kuki, N.; Kuno, T.; Takagi, T.; Koyama, M.; Ando, A.; Kumadaki, I. *J. Fluorine Chem.* **1999,** *93,* 165–170. doi:10.1016/s0022-1139(98)00291-7
107. Fujii, S.; Maki, Y.; Kimoto, H.; Cohen, L. A. *J. Fluorine Chem.* **1986,** *30,* 415–428. doi:10.1016/s0022-1139(00)85096-4
108. Maki, Y.; Kimoto, H.; Fujii, S.; Senga, M.; Cohen, L. A. *J. Fluorine Chem.* **1988,** *39,* 47–59. doi:10.1016/s0022-1139(00)82736-0
109. Gong, Y.; Kato, K.; Kimoto, H. *Synlett* **1999,** 1403–1404. doi:10.1055/s-1999-2867
110. Gong, Y.; Kato, K. *J. Fluorine Chem.* **2001,** *108,* 83–86. doi:10.1016/s0022-1139(00)00407-3
111. Gong, Y.; Kato, K. *J. Fluorine Chem.* **2002,** *116,* 103–107. doi:10.1016/s0022-1139(02)00044-1
112. Zhang, G.-W.; Wang, L.; Nie, J.; Ma, J.-A. *Adv. Synth. Catal.* **2008,** *350,* 1457–1463. doi:10.1002/adsc.200800239
113. Yang, C.; Xue, X.-S.; Li, X.; Cheng, J.-P. *J. Org. Chem.* **2014,** *79,* 4340–4351. doi:10.1021/jo500158e
114. Akiyama, T.; Mori, K. *Chem. Rev.* **2015,** *115,* 9277–9306. doi:10.1021/acs.chemrev.5b00041
115. Fuchigami, T.; Nakagawa, Y.; Nonaka, T. *J. Org. Chem.* **1987,** *52,* 5489–5491. doi:10.1021/jo00233a043
116. Fuchigami, T.; Ichikawa, S.; Konno, A. *Chem. Lett.* **1989,** *18,* 1987–1988. doi:10.1246/cl.1989.1987
117. Xu, Y.; Dolbier, W. R. *J. Org. Chem.* **2000,** *65,* 2134–2137. doi:10.1021/jo991750y
118. Ates, C.; Janousek, Z.; Viehe, H. G. *Tetrahedron Lett.* **1993,** *34,* 5711–5714. doi:10.1016/s0040-4039(00)73840-8
119. Xu, Y.; Dolbier, W. R., Jr. *Tetrahedron Lett.* **1998,** *39,* 9151–9154. doi:10.1016/s0040-4039(98)02106-6
120. Billard, T.; Langlois, B. R.; Blond, G. *Tetrahedron Lett.* **2000,** *41,* 8777–8780. doi:10.1016/s0040-4039(00)01552-5
121. Blond, G.; Billard, T.; Langlois, B. R. *J. Org. Chem.* **2001,** *66,* 4826–4830. doi:10.1021/jo015587u
122. Billard, T.; Langlois, B. R. *J. Org. Chem.* **2002,** *67,* 997–1000. doi:10.1021/jo016265t
123. Huguenot, F.; Brigaud, T. *J. Org. Chem.* **2006,** *71,* 7075–7078. doi:10.1021/jo0607717
124. Chaume, G.; Barbeau, O.; Lesot, P.; Brigaud, T. *J. Org. Chem.* **2010,** *75,* 4135–4145. doi:10.1021/jo100518t
125. Rover-Kevers, M.; Vertommen, L.; Huys, F.; Merényi, R.; Janousek, Z.; Viehe, H. G. *Angew. Chem., Int. Ed. Engl.* **1981,** *20,* 1023–1024. doi:10.1002/anie.198110231

126. Bégué, J.-P.; Bonnet-Delpon, D.; Crousse, B.; Legros, J. *Chem. Soc. Rev.* **2005,** *34,* 562–572. doi:10.1039/b401707m
127. Fuchigami, T.; Ichikawa, S.; Kandeel, Z. E.; Konno, A.; Nonaka, T. *Heterocycles* **1990,** *31,* 415–417. doi:10.3987/com-89-5295
128. Okano, T.; Sakaida, T.; Eguchi, S. *Heterocycles* **1997,** *44,* 227–236. doi:10.3987/com-96-s12
129. Long, Y. O.; Higuchi, R. I.; Caferro, T. R.; Lau, T. L. S.; Wu, M.; Cummings, M. L.; Martinborough, E. A.; Marschke, K. B.; Chang, W. Y.; López, F. J.; Karanewsky, D. S.; Zhi, L. *Bioorg. Med. Chem. Lett.* **2008,** *18,* 2967–2971. doi:10.1016/j.bmcl.2008.03.062
130. Levin, V. V.; Kozlov, M. A.; Dilman, A. D.; Belyakov, P. A.; Struchkova, M. I.; Tartakovsky, V. A. *Russ. Chem. Bull.* **2009,** *58,* 484–486. doi:10.1007/s11172-010-0039-x
131. Tran, G.; Meier, R.; Harris, L.; Browne, D. L.; Ley, S. V. *J. Org. Chem.* **2012,** *77,* 11071–11078. doi:10.1021/jo302052m
132. Pandey, V. K.; Anbarasan, P. *J. Org. Chem.* **2014,** *79,* 4154–4160. doi:10.1021/jo5002998
133. Lensen, N.; Marais, J.; Brigaud, T. *Org. Lett.* **2015,** *17,* 342–345. doi:10.1021/ol503448w
134. Ben Jamaa, A.; Grellepois, F. *J. Org. Chem.* **2017,** *82,* 10360–10375. doi:10.1021/acs.joc.7b01814
135. Kudyakova, Y. S.; Bazhin, D. N.; Slepukhin, P. A.; Burgart, Y. V.; Saloutin, V. I.; Charushin, V. N. *Tetrahedron Lett.* **2017,** *58,* 744–747. doi:10.1016/j.tetlet.2017.01.026
136. Lee, A.; Zhu, J. L.; Feoktistova, T.; Brueckner, A. C.; Cheong, P. H.-Y.; Scheidt, K. A. *Angew. Chem., Int. Ed.* **2019,** *58,* 5941–5945. doi:10.1002/anie.201900600
137. Mitobe, K.; Kawasaki-Takasuka, T.; Agou, T.; Kubota, T.; Yamazaki, T. *J. Fluorine Chem.* **2019,** *218,* 36–41. doi:10.1016/j.jfluchem.2018.11.012
138. Maulide, N.; Shaaban, S.; Goncalves, C.; Tona, V.; Kaiser, D.; Hsu, C.-S. *Production of amines via a hydroaminoalkylation reaction*. WO Patent WO/2019/219942A1, Nov 21, 2019.
139. Fuchigami, T.; Yamamoto, K.; Nakagawa, Y. *J. Org. Chem.* **1991,** *56,* 137–142. doi:10.1021/jo00001a028
140. Uneyama, K.; Momota, M.; Hayashida, K.; Itoh, T. *J. Org. Chem.* **1990,** *55,* 5364–5368. doi:10.1021/jo00306a013
141. Fuchigami, T.; Nakagawa, Y.; Nonaka, T. *Tetrahedron Lett.* **1986,** *27,* 3869–3872. doi:10.1016/s0040-4039(00)83902-7
142. Mykhailiuk, P. K. *Chem. Rev.* **2020,** *120,* 12718–12755. doi:10.1021/acs.chemrev.0c00406
143. Mohrig, J. R.; Keegstra, K. *J. Am. Chem. Soc.* **1967,** *89,* 5492–5493. doi:10.1021/ja00997a056
144. Dahn, H.; Lenoir, J. H. *Helv. Chim. Acta* **1979,** *62,* 2218–2229. doi:10.1002/hlca.19790620719
145. Gross, P.; Steiner, H.; Krauss, F. *Trans. Faraday Soc.* **1936,** *32,* 877–879. doi:10.1039/tf9363200877
146. Gross, P.; Steiner, H.; Krauss, F. *Trans. Faraday Soc.* **1938,** *34,* 351–356. doi:10.1039/tf9383400351
147. Diderich, G. *Helv. Chim. Acta* **1972,** *55,* 2103–2112. doi:10.1002/hlca.19720550629
148. Gassen, K.-R.; Kirmse, W. *Chem. Ber.* **1986,** *119,* 2233–2248. doi:10.1002/cber.19861190717
149. Karabatsos, G. J.; Mount, R. A.; Rickter, D. O.; Meyerson, S. *J. Am. Chem. Soc.* **1970,** *92,* 1248–1253. doi:10.1021/ja00708a024
150. Kirmse, W.; Krause, D. *Chem. Ber.* **1975,** *108,* 1855–1863. doi:10.1002/cber.19751080609
151. Olah, G. A.; Prakash, G. K. S.; Molnár, Á.; Sommer, J. Superacid Systems. *Superacid Chemistry,* 2nd ed.; John Wiley & Sons: Hoboken, NJ, USA, 2009; pp 35–82. doi:10.1002/9780470421604.ch2
152. Reich, I. L.; Diaz, A. F.; Winstein, S. *J. Am. Chem. Soc.* **1969,** *91,* 5635–5637. doi:10.1021/ja01048a036
153. Myhre, P. C.; Brown, K. S. *J. Am. Chem. Soc.* **1969,** *91,* 5639–5641. doi:10.1021/ja01048a038
154. Myhre, P. C.; Evans, E. *J. Am. Chem. Soc.* **1969,** *91,* 5641–5644. doi:10.1021/ja01048a039
155. Diaz, A. F.; Reich, I. L.; Winstein, S. *J. Am. Chem. Soc.* **1969,** *91,* 5637–5639. doi:10.1021/ja01048a037
156. Myhre, P. C.; Andrews, G. D. *J. Am. Chem. Soc.* **1970,** *92,* 7595–7596. doi:10.1021/ja00729a020
157. Drabicky, M. J.; Myhre, P. C.; Reich, C. J.; Schmittou, E. R. *J. Org. Chem.* **1976,** *41,* 1472–1474. doi:10.1021/jo00870a043
158. Roberts, D. D.; Hall, E. W. *J. Org. Chem.* **1988,** *53,* 2573–2579. doi:10.1021/jo00246a032
159. Bonnet-Delpon, D.; Cambillau, C.; Charpentier-Morize, M.; Jacquot, R.; Mesureur, D.; Ourevitch, M. *J. Org. Chem.* **1988,** *53,* 754–759. doi:10.1021/jo00239a010
160. Takashi, A.; Junko, Y.; Yoshimasa, S. *Bull. Chem. Soc. Jpn.* **1978,** *51,* 219–224.
161. Gassman, P. G.; Doherty, M. M. *J. Am. Chem. Soc.* **1982,** *104,* 3742–3744. doi:10.1021/ja00377a043
162. Kelly, C. B.; Colthart, A. M.; Constant, B. D.; Corning, S. R.; Dubois, L. N. E.; Genovese, J. T.; Radziewicz, J. L.; Sletten, E. M.; Whitaker, K. R.; Tilley, L. J. *Org. Lett.* **2011,** *13,* 1646–1649. doi:10.1021/ol200121f
163. Mercadante, M. A.; Kelly, C. B.; Hamlin, T. A.; Delle Chiaie, K. R.; Drago, M. D.; Duffy, K. K.; Dumas, M. T.; Fager, D. C.; Glod, B. L. C.; Hansen, K. E.; Hill, C. R.; Leising, R. M.; Lynes, C. L.; MacInnis, A. E.; McGohey, M. R.; Murray, S. A.; Piquette, M. C.; Roy, S. L.; Smith, R. M.; Sullivan, K. R.; Truong, B. H.; Vailonis, K. M.; Gorbatyuk, V.; Leadbeater, N. E.; Tilley, L. J. *Chem. Sci.* **2014,** *5,* 3983–3994. doi:10.1039/c4sc01732c
164. Creary, X. *Beilstein J. Org. Chem.* **2019,** *15,* 1769–1780. doi:10.3762/bjoc.15.170
165. Myhre, P. C.; Andrews, G. D. *J. Am. Chem. Soc.* **1970,** *92,* 7596–7597. doi:10.1021/ja00729a021
166. Banik, S. M.; Medley, J. W.; Jacobsen, E. N. *Science* **2016,** *353,* 51–54. doi:10.1126/science.aaf8078
167. Scheidt, F.; Neufeld, J.; Schäfer, M.; Thiehoff, C.; Gilmour, R. *Org. Lett.* **2018,** *20,* 8073–8076. doi:10.1021/acs.orglett.8b03794
168. Carpenter, W. *J. Org. Chem.* **1966,** *31,* 2688–2689. doi:10.1021/jo01346a512
169. Hanack, M.; Bocher, S.; Herterich, I.; Hummel, K.; Vött, V. *Justus Liebigs Ann. Chem.* **1970,** *733,* 5–26. doi:10.1002/jlac.19707330103
170. van Alem, K.; Belder, G.; Lodder, G.; Zuilhof, H. *J. Org. Chem.* **2005,** *70,* 179–190. doi:10.1021/jo0487956
171. Winstein, S.; Trifan, D. S. *J. Am. Chem. Soc.* **1949,** *71,* 2953. doi:10.1021/ja01176a536
172. Winstein, S.; Shatavsky, M.; Norton, C.; Woodward, R. B. *J. Am. Chem. Soc.* **1955,** *77,* 4183–4184. doi:10.1021/ja01620a078
173. Brown, H. C.; Bell, H. M. *J. Am. Chem. Soc.* **1963,** *85,* 2324. doi:10.1021/ja00898a030
174. Scholz, F.; Himmel, D.; Heinemann, F. W.; Schleyer, P. v. R.; Meyer, K.; Krossing, I. *Science* **2013,** *341,* 62–64. doi:10.1126/science.1238849

175. Gassman, P. G.; Hall, J. B. *J. Am. Chem. Soc.* **1984,** *106,* 4267–4269. doi:10.1021/ja00327a035
176. Allen, A. D.; Krishnamurti, R.; Prakash, G. K. S.; Tidwell, T. T. *J. Am. Chem. Soc.* **1990,** *112,* 1291–1292. doi:10.1021/ja00159a085
177. Hanack, M.; Meyer, H. *Justus Liebigs Ann. Chem.* **1968,** *720,* 81–97. doi:10.1002/jlac.19687200107
178. Roberts, D. D. *J. Org. Chem.* **1991,** *56,* 5661–5665. doi:10.1021/jo00019a037

License and Terms

This is an Open Access article under the terms of the Creative Commons Attribution License (https://creativecommons.org/licenses/by/4.0). Please note that the reuse, redistribution and reproduction in particular requires that the author(s) and source are credited and that individual graphics may be subject to special legal provisions.

The license is subject to the *Beilstein Journal of Organic Chemistry* terms and conditions: (https://www.beilstein-journals.org/bjoc/terms)

The definitive version of this article is the electronic one which can be found at: https://doi.org/10.3762/bjoc.17.32

BEILSTEIN JOURNAL OF ORGANIC CHEMISTRY

Helicene synthesis by Brønsted acid-catalyzed cycloaromatization in HFIP [$(CF_3)_2CHOH$]

Takeshi Fujita*, Noriaki Shoji, Nao Yoshikawa and Junji Ichikawa*

Full Research Paper

Open Access

Address:
Division of Chemistry, Faculty of Pure and Applied Sciences, University of Tsukuba, Tsukuba, Ibaraki 305-8571, Japan

Email:
Takeshi Fujita* - fujita@chem.tsukuba.ac.jp;
Junji Ichikawa* - junji@chem.tsukuba.ac.jp

* Corresponding author

Keywords:
acid; catalyst; cyclization; fluoroalcohol; helicenes

Beilstein J. Org. Chem. **2021,** *17,* 396–403.
https://doi.org/10.3762/bjoc.17.35

Received: 28 November 2020
Accepted: 26 January 2021
Published: 09 February 2021

This article is part of the thematic issue "Organo-fluorine chemistry V".

Guest Editor: D. O'Hagan

© 2021 Fujita et al.; licensee Beilstein-Institut.
License and terms: see end of document.

Abstract

A facile synthesis of carbo- and heterohelicenes was achieved via tandem cycloaromatization of bisacetal precursors, which were readily prepared through C–C bond formation by Suzuki–Miyaura coupling. This cyclization was efficiently realized by a catalytic amount of trifluoromethanesulfonic acid (TfOH) in a cation-stabilizing solvent, 1,1,1,3,3,3-hexafluoropropan-2-ol (HFIP), which readily allowed gram-scale syntheses of higher-order helicenes, double helical helicenes, and heterohelicenes.

Introduction

Helicenes are a class of polycyclic aromatic hydrocarbons (PAH) that consist of *ortho*-fused aromatic rings arranged in a helical manner [1-6]. Since helicenes possess chirality derived from their helical structure, optically active helicenes and their derivatives exhibit characteristic properties, such as huge optical rotation [7], nonlinear optical effects [8-10], and circularly polarized light emission [11], which are rarely found in planar aromatic hydrocarbons (e.g., acenes and phenacenes). Therefore, the wide breadth of applications of helicenes as organic optical materials make them interesting synthetic targets.

Although several methods for the synthesis of helicenes have been reported, there are still specific problems in conducting these synthetic reactions for large scale production (Scheme 1). For example, the Mallory reaction [12], which is a widely used photocyclization in helicene synthesis [13,14], requires high dilution or excess amounts of oxidizing agents to suppress intermolecular side reactions (Scheme 1a). Diels–Alder (Scheme 1b) [15] and radical reactions (Scheme 1c) [16] directed toward helicene synthesis require high temperature conditions even for low to moderate yields. Olefin metathesis (Scheme 1d) [17] and alkyne trimerization (Scheme 1e) [18,19] require the use of expensive metal catalysts.

Recently, we have developed a Brønsted acid-catalyzed cycloaromatization in 1,1,1,3,3,3-hexafluoropropan-2-ol (HFIP) as solvent [20-22]. Fluoroalcohols, such as HFIP, exhibit high

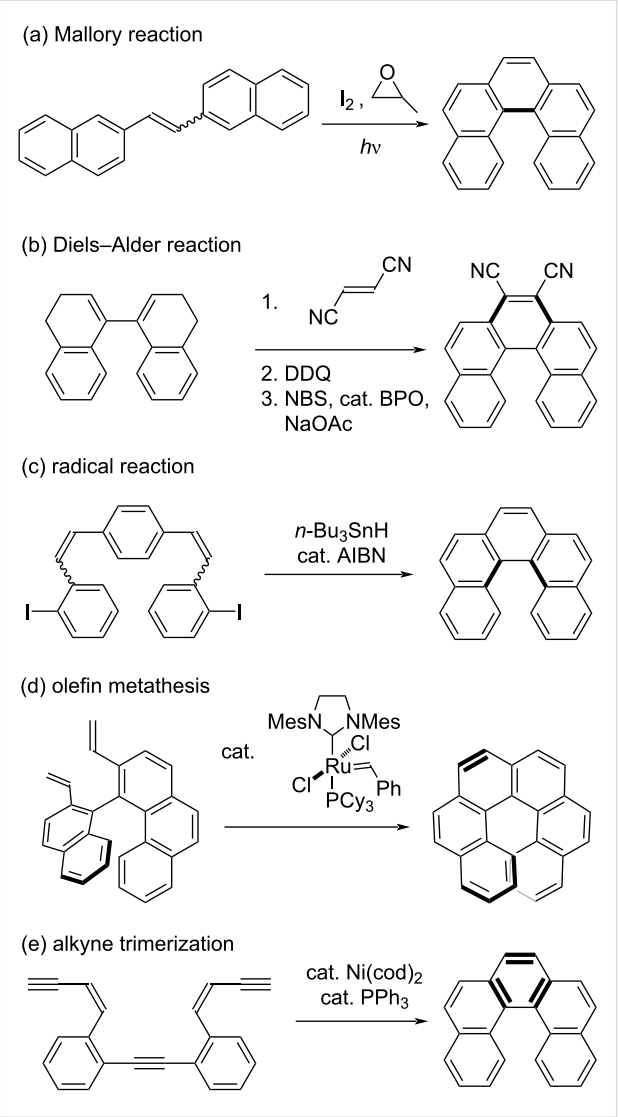

Scheme 1: Conventional methods for the synthesis of helicenes.

ionization power and low nucleophilicity, based on the electron-withdrawing inductive effect of fluorine, which helps to generate cations but does not affect cationic reactions [23-27]. Thus, HFIP greatly facilitates reactions via cationic intermediates [28]. In the presence of a catalytic amount of trifluoromethanesulfonic acid in HFIP, (biaryl-2-yl)acetoaldehydes or their acetal derivatives readily underwent intramolecular Friedel–Crafts-type C–C bond formation followed by dehydration or alcohol elimination, leading to the construction of benzene rings in the biaryl systems (Scheme 2) [20,21]. The reaction proceeded via oxocarbenium ion intermediates stabilized by HFIP. This method can be successfully applied to cyclization at multiple reaction sites. By using bisacetals bearing a naphthalene core (Ar^2) as substrates, tandem cyclization achieved the efficient synthesis of several *ortho*-fused six-hexagon benzenoids [21].

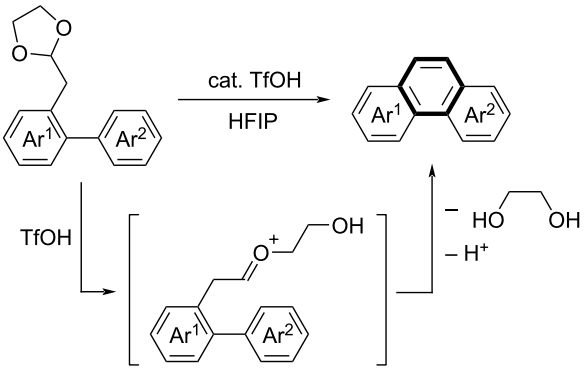

Scheme 2: Brønsted acid-catalyzed cycloaromatization of biaryls bearing an acetal moiety.

On the basis of our work mentioned above, we assumed that this powerful cycloaromatization would be applicable to helicene synthesis. Thus, the following strategies were designed to establish a versatile method for the synthesis of helicenes (Scheme 3). Tandem cycloaromatization of bisacetals bearing a teraryl core was shown to be most effective for the one-shot construction of helicene frameworks. Based on ease of preparation, symmetrical cyclization precursors would be preferable, and thus they should possess either (i) one acetal moiety on each terminal aromatic ring (Ar^2) of the teraryl core (Scheme 3, route a) or (ii) two acetal moieties on the central aromatic ring (Ar^1) (Scheme 3, route b). The teraryl structures were constructed by the formation of two C–C bonds via tandem Suzuki–Miyaura coupling of two terminal (Ar^2) and central (Ar^1) arenes. It is noted that dihalogenated arenes were adopted as components for the central aromatic ring (Ar^1) in the teraryl structure, because the diborylated arenes were less available. Either (a) the coupling of boronic acid esters bearing one acetal moiety with dihalogenated arenes or (b) the coupling of dihalogenated arenes bearing two acetal moieties with arylboronic acids were conducted for the preparation of cyclization precursors. As described above, the tandem cycloaromatization of the obtained precursors proceeded via Friedel–Crafts-type bond formation followed by elimination, which enabled a rapid and efficient synthesis of helicenes, such as higher-order helicenes, double helical helicenes, and heterohelicenes.

Results and Discussion

Carbohelicenes such as [5]helicene (**1a**) and [6]helicene (**1b**) were synthesized via Suzuki–Miyaura coupling of readily available dihalogenated arenes **2** with phenylboronic acid ester **3** bearing a (1,3-dioxolan-2-yl)methyl group [29], followed by triflic acid-catalyzed cycloaromatization (Scheme 3, route a and Scheme 4a). Treatment of 1,2-dibromobenzene (**2a**) with **3** in the presence of a palladium catalyst with SPhos afforded *o*-terphenyl derivative **4a** bearing two acetal groups in 96%

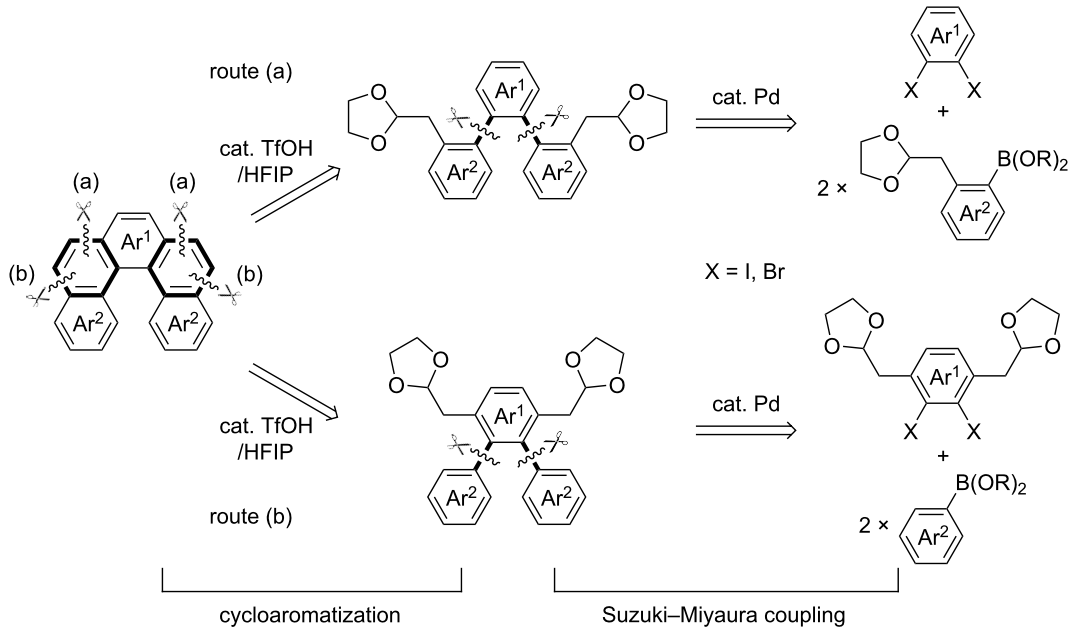

Scheme 3: Two strategies for the helicene synthesis via Suzuki–Miyaura coupling/cycloaromatization sequence.

yield (Scheme 4a). The obtained bisacetal **4a** successfully underwent cycloaromatization in the presence of 17 mol % of TfOH in HFIP to afford [5]helicene (**1a**) in 90% yield. For the synthesis of [6]helicene, 1,8-diiodonaphthalene was adopted as the substrate for Suzuki–Miyaura coupling with **3** (Scheme 3, route a and Scheme 4b). In this coupling, SPhos was also effective in providing the bisacetal precursor **4b** bearing a 1,8-diphenylnaphthalene framework in 45% yield despite high steric hindrance (Scheme 4b). Then, [6]helicene (**1b**) was obtained in 92% yield via cycloaromatization in the presence of 15 mol % of TfOH. It was noted that the gram-scale synthesis for both [5]- and [6]helicenes was possible, in which no serious decrease in yield was observed in Suzuki–Miyaura coupling and cycloaromatization (see the Experimental section) [30].

Next, double helical compounds were set as synthetic targets, because their unique optical properties have recently attracted much attention [5]. Herein, we synthesized two types of *ortho*-fused seven-hexagon benzenoids with two [4]helicene structures. According to the strategy illustrated in Scheme 3, route b, double helical helicenes **5** were synthesized using (naphthyl-1-yl)boronic acid (**7**) and dibromobenzenes **6** with two (1,3-dioxolan-2-yl)methyl groups, readily prepared from xylenes (Scheme 5). The Suzuki–Miyaura coupling of dibromobenzene **6a** with **7** effectively proceeded to afford bisacetal **8a** in 70% yield (Scheme 5a). Bisacetal **8a** successfully underwent subsequent cycloaromatization in HFIP to afford S-shaped double helical helicene **5a** in 90% yield. Similarly, C-shaped double helical helicene **5b** was obtained in high yield using *m*-dibromobenzene **6b** with two acetal moieties, prepared from *m*-xylene (Scheme 5b).

We also achieved the synthesis of heterohelicenes, which involve heteroatoms in the helicene frameworks, via a Suzuki–Miyaura coupling/cycloaromatization sequence (Scheme 3a, route a). Thus, hetero[4]-, [5]-, and [6]helicenes involving an oxygen, sulfur, or nitrogen atom were efficiently synthesized (Scheme 6). Hetero[4]helicenes **9** were synthesized via coupling of 3-bromobenzoheteroles **10**, prepared from commercially available benzoheteroles, and subsequent cycloaromatization (Scheme 6a). Again, phenylboronic acid ester **3**, used above in the synthesis of [5]- and [6]helicenes, was adopted as the coupling partner for **10**. In the presence of a palladium catalyst, treatment of 3-bromobenzofuran (**10a**), 3-bromobenzothiophene (**10b**), and 3-bromo(*N*-tosyl)indole (**10c**) with **3** afforded the corresponding acetals **11a–c** with 3-phenylbenzoheterole structures in 92%, 80%, and 93% yields, respectively. Acetals **11a–c** successfully underwent TfOH-catalyzed cycloaromatization in HFIP to afford oxa-, thia-, and aza[4]helicenes **9a–c** in 96%, 88%, and 93% yields, respectively. Thus, phenylboronic acid ester **3** bearing an acetal moiety functions as a reagent for fused naphthalene ring extension through our cross-coupling/cycloaromatization sequence [31-35].

Hetero[5]helicenes **12** were synthesized via tandem cycloaromatization using teraryl precursors, in which heterol rings were set as central aromatic rings (Ar^1) (Scheme 3, route a and Scheme 6b). As in the original strategy (Scheme 3, route a),

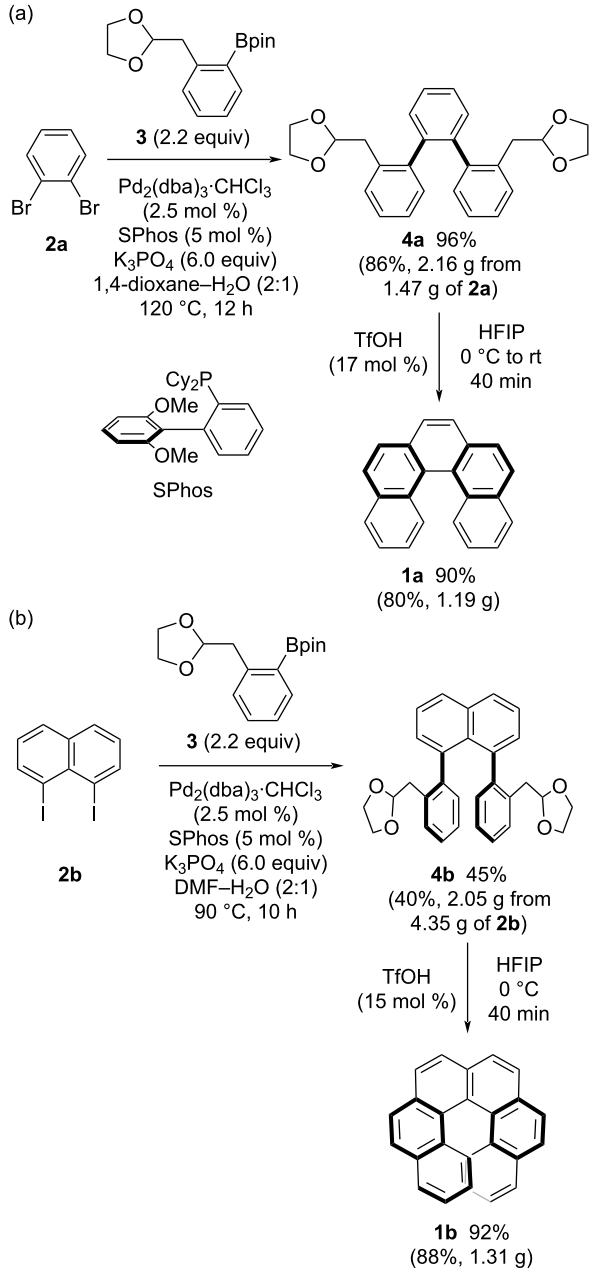

Scheme 4: Synthesis of (a) [5]helicene and (b) [6]helicene.

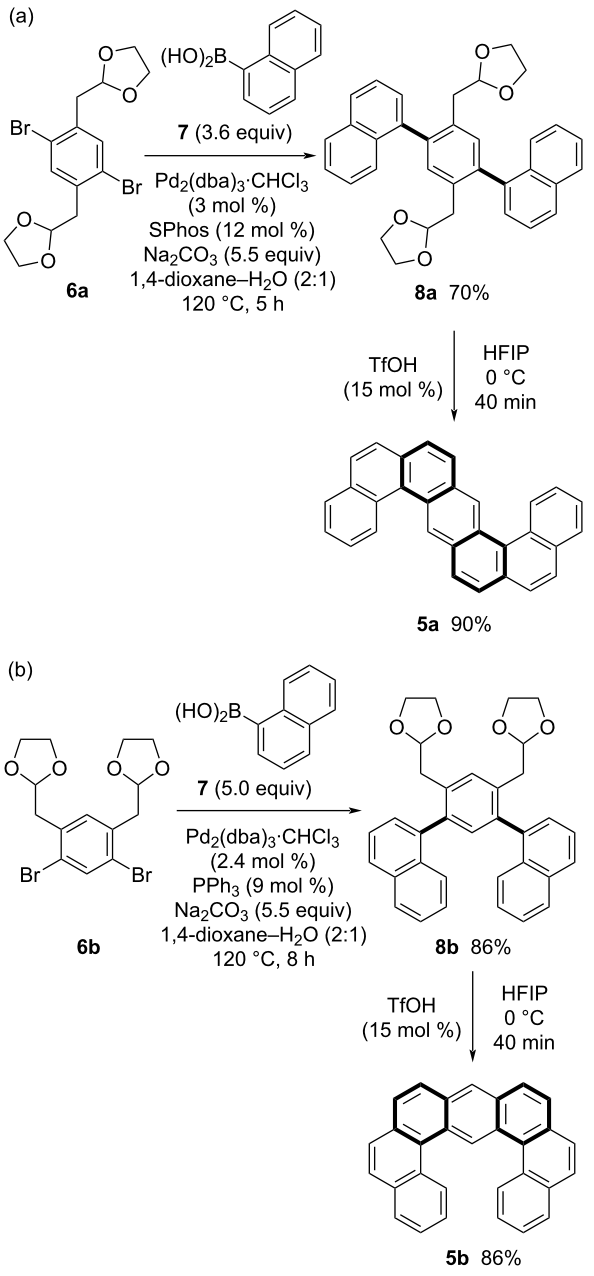

Scheme 5: Synthesis of helicenes with double helical structures.

coupling of 3,4-dibromofuran (**13a**), 3,4-dibromothiophene (**13b**), and 3,4-dibromo(*N*-tosyl)pyrrole (**13c**) with phenylboronic acid ester **3** bearing an acetal moiety proceeded to afford the corresponding bisacetals **14a**–**c** in 53%, 76%, and 78% yields, respectively. The obtained bisacetals **14a**–**c** efficiently underwent TfOH-catalyzed tandem cycloaromatization under appropriate conditions to afford oxa-, thia-, and aza[5]helicenes **12a**–**c** in 90%, 90%, and 88% yields, respectively.

Furthermore, we demonstrated the synthesis of unsymmetrical thia[6]helicene **15** as a hetero[6]helicene synthesis (Scheme 6c). 3-Bromobenzothiophene **16** bearing a (1,3-dioxolan-2-yl)methyl group at the 2-position, which was readily prepared from benzothiophene, underwent Suzuki–Miyaura coupling with boronic acid ester **17** with a biphenyl structure and an acetal moiety, to afford bisacetal **18** in 92% yield. Thus, tandem cycloaromatization of **18** effectively proceeded to afford thia[6]helicene **15** in 63% yield.

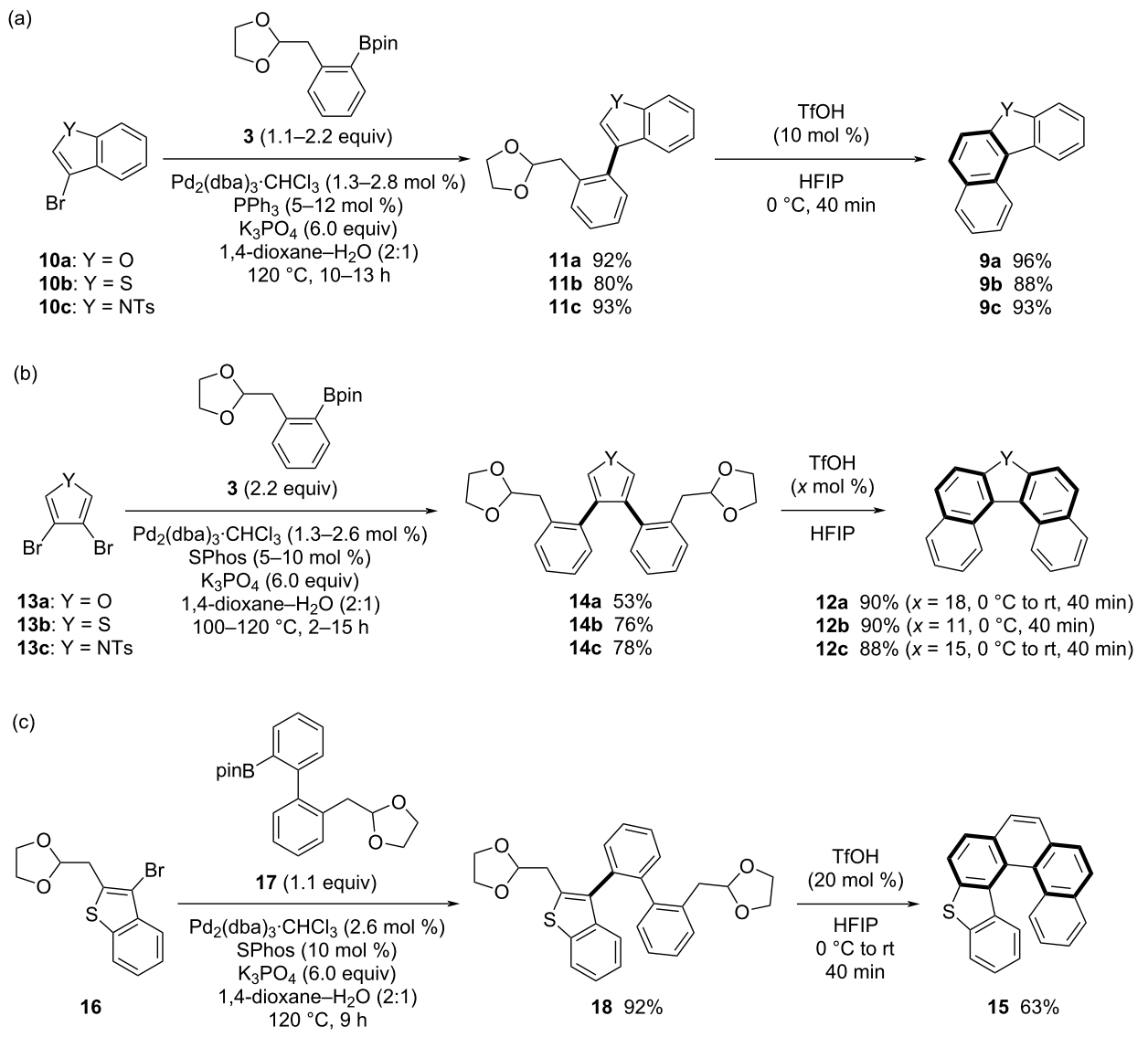

Scheme 6: Synthesis of hetero[4]-, [5]-, and [6]helicenes.

Conclusion

In summary, we developed a facile and efficient method for the synthesis of several types of helicenes using a sequence of (i) Suzuki–Miyaura coupling of acetal-containing components and (ii) catalytic cycloaromatization with the aid of a cation-stabilizing fluoroalcohol, HFIP, as solvent. Particularly, helicene synthesis using tandem cyclization of bisacetals with teraryl structures is suitable for mass production of helicenes not only because multiple aromatic rings can be constructed at the same time but also because precursors can be easily prepared from commercially available compounds. Therefore, further progress can be made in applied research on helicenes as organic electronic materials, such as circularly polarized light emitting devices and nonlinear optical materials [7-11].

Experimental

^{1}H NMR and ^{13}C NMR spectra were recorded on a Bruker Avance 500 or a JEOL ECS-400 spectrometer. Chemical shift values are given in ppm relative to internal Me_4Si (for ^{1}H NMR: δ = 0.00 ppm) and $CDCl_3$ (for ^{13}C NMR: δ = 77.0 ppm).

Column chromatography and preparative thin-layer chromatography (PTLC) were conducted on silica gel (Silica Gel 60 N, Kanto Chemical Co., Inc. for column chromatography and Wakogel B-5F, Wako Pure Chemical Inductries for PTLC). *N*,*N*-Dimethylformamide (DMF) was purified by a solvent-purification system (GlassContour) equipped with columns of activated alumina and supported-copper catalyst (Q-5) before use. 1,1,1,3,3,3-Hexafluoropropan-2-ol (HFIP) was distilled

from molecular sieves 4 Å and stored over activated molecular sieves 4 Å. 1,4-Dioxane was distilled from sodium and stored over activated molecular sieves 4 Å. 2-{2-[(1,3-Dioxolan-2-yl)methyl]phenyl}-4,4,5,5-tetramethyl-1,3,2-dioxaborolane (**3**) was prepared according to the literature procedure, and their spectral data showed good agreement with the literature data [21]. Unless otherwise noted, materials were obtained from commercial sources and used directly without further purification.

2,2''-Bis[(1,3-dioxolan-2-yl)methyl]-1,1':2',1''-terphenyl (**4a**)

A dioxane (6.6 mL) and H_2O (3.4 mL) solution of 1,2-dibromobenzene (**2a**, 471 mg, 2.00 mmol), boronate ester **3** (1.27 g, 4.39 mmol), $Pd_2(dba)_3{\cdot}CHCl_3$ (52 mg, 51 μmol), SPhos (41 mg, 0.10 mmol), and K_3PO_4 (2.53 g, 11.9 mmol) was degassed by using the freeze-pump-thaw method three times. After stirring at 120 °C for 12 h, ethyl acetate and water were added to the mixture, and organic materials were extracted with ethyl acetate three times. The combined extracts were washed with brine and dried over Na_2SO_4. After removal of the solvent under reduced pressure, the residue was purified by silica gel column chromatography (hexane/EtOAc = 3:1) to give **4a** (776 mg, 96%) as an orange oil.

^{1}H NMR (500 MHz, $CDCl_3$) δ 2.59 (dd, *J* = 14.4, 4.9 Hz, 0.8H), 2.70 (dd, *J* = 14.3, 5.3 Hz, 1.2H), 2.78–2.86 (m, 2H), 3.72–3.95 (m, 8H), 4.85–4.95 (m, 2H), 6.97–7.03 (m, 4H), 7.07–7.14 (m, 2H), 7.23–7.33 (m, 3.2H), 7.35–7.42 (m, 2.8H); ^{13}C NMR (126 MHz, $CDCl_3$) δ 37.1, 37.7, 64.6, 64.73, 64.75, 104.5, 104.6, 125.4, 125.7, 126.8, 126.87, 126.91, 126.0, 129.5, 129.6, 130.0, 130.7, 131.2, 131.6, 133.8, 134.0, 140.2, 140.9, 141.4; IR (neat) ν: 3055, 3020, 2976, 2883, 1471, 1442, 1433, 1398, 1194, 1130, 1038, 1009, 943, 872, 837, 822, 752, 706, 621, 573, 538 cm^{-1}; HRMS (EI) *m*/*z*: $[M]^+$ calcd. for $C_{26}H_{26}O_4$, 402.1826; found, 402.1815.

Gram-scale synthesis: Compound **4a** was also prepared by the method described above using 1,2-dibromobenzene (**2a**, 1.47 g, 6.24 mmol), boronate ester **3** (3.99 g, 13.8 mmol), $Pd_2(dba)_3{\cdot}CHCl_3$ (82 mg, 80 μmol), PPh_3 (84 mg, 0.32 mmol), K_3PO_4 (8.02 g, 37.8 mmol), dioxane (21 mL), and H_2O (10 mL) at 100 ºC for 6 h. Purification by silica gel column chromatography (hexane/EtOAc = 5:1) gave **4a** (2.16 g, 86%).

[5]Helicene (**1a**)

In a similar manner as described in [20], trifluoromethanesulfonic acid (7.5 mg, 50 μmol) was added to an HFIP (0.9 mL) solution of bisacetal **4a** (120 mg, 0.30 mmol) at 0 °C. After stirring at room temperature for 40 min, the reaction was quenched with phosphate buffer (pH 7). Organic materials were extracted with CH_2Cl_2 three times, and the combined extracts were washed with brine and dried over Na_2SO_4. After removal of the solvents under reduced pressure, the residue was purified by silica gel column chromatography (hexane/CH_2Cl_2 = 3:1) to give **1a** (75 mg, 90%) as a white solid.

^{1}H NMR (500 MHz, $CDCl_3$) δ 7.23 (dd, *J* = 8.4, 7.1 Hz, 2H), 7.47 (dd, *J* = 7.9, 7.1 Hz, 2H), 7.80 (s, 2H), 7.81 (d, *J* = 8.5 Hz, 2H), 7.86 (d, *J* = 8.5 Hz, 2H), 7.90 (d, *J* = 7.9 Hz, 2H), 8.49 (d, *J* = 8.4 Hz, 2H); ^{13}C NMR (126 MHz, $CDCl_3$) δ 124.3, 126.2, 126.3, 126.9, 127.2, 127.4, 127.8, 129.0, 130.7, 132.2, 132.5.

Gram-scale synthesis: Compound **1a** was also synthesized by the method described above using bisacetal **4a** (2.16 g, 5.37 mmol), trifluoromethanesulfonic acid (88 mg, 0.58 mmol), and HFIP (20 mL) at 0 °C for 40 min. Purification by silica gel column chromatography (hexane/EtOAc = 10:1) gave **1a** (1.19 g, 80%).

1,8-Bis{2-[(1,3-dioxolan-2-yl)methyl]phenyl}naphthalene (**4b**)

A DMF (6.7 mL) and H_2O (3.3 mL) solution of 1,8-diiodonaphthalene (**2b**, 759 mg, 2.00 mmol), boronate ester **3** (1.28 g, 4.40 mmol), $Pd_2(dba)_3{\cdot}CHCl_3$ (52 mg, 50 μmol), SPhos (42 mg, 0.10 mmol), and K_3PO_4 (2.54 g, 12.0 mmol) was degassed by using the freeze-pump-thaw method three times. After stirring at 90 °C for 10 h, ethyl acetate, hexane, and water were added to the mixture, and organic materials were extracted with an ethyl acetate–hexane (1:1) mixed solvent three times. The combined extracts were washed with brine and dried over Na_2SO_4. After removal of the solvent under reduced pressure, the residue was purified by silica gel column chromatography (toluene/EtOAc = 40:1) to give **4b** (409 mg, 45%) as a white solid.

^{1}H NMR (500 MHz, $CDCl_3$) δ 2.36 (dd, *J* = 14.0, 6.1 Hz, 2H), 2.52 (dd, *J* = 14.0, 4.3 Hz, 2H), 3.62–3.83 (m, 8H), 4.65 (dd, *J* = 6.1, 4.3 Hz, 2H), 6.77–6.81 (m, 2H), 6.87–6.93 (m, 4H), 7.01–7.06 (m, 2H), 7.20 (dd, *J* = 7.0, 1.3 Hz, 2H), 7.46 (dd, *J* = 8.1, 7.0 Hz, 2H), 7.91 (dd, *J* = 8.3, 1.3 Hz, 2H); ^{13}C NMR (126 MHz, $CDCl_3$) δ 38.9, 64.4, 64.7, 104.1, 124.8, 125.2, 126.8, 129.0, 129.05, 129.13, 129.9, 131.0, 133.8, 134.5, 138.8, 142.6; IR (neat) ν: 3053, 2966, 2883, 1489, 1396, 1132, 1043, 984, 831, 756 cm^{-1}; HRMS (APCI+) *m*/*z*: $[M + H]^+$ calcd. for $C_{30}H_{29}O_4$, 453.2060; found, 453.2081.

Gram-scale synthesis: Compound **4b** was also prepared by the method described above using 1,8-diiodonaphthalene (**2b**, 4.35 g, 11.4 mmol), boronate ester **3** (7.31 g, 25.2 mmol), $Pd_2(dba)_3{\cdot}CHCl_3$ (301 mg, 0.29 mmol), SPhos (239 mg, 0.58 mmol), K_3PO_4 (14.6 g, 68.7 mmol), DMF (38 mL), and

H_2O (19 mL) at 90 °C for 17 h. Purification by silica gel column chromatography (toluene/EtOAc = 40:1) gave **4b** (2.05 g, 40%).

[6]Helicene (**1b**)

In a similar manner as described in [20]. To an HFIP (0.7 mL) solution of bisacetal **4b** (91 mg, 0.20 mmol) was added trifluoromethanesulfonic acid (4.8 mg, 32 µmol) at 0 °C. After stirring at the same temperature for 40 min, the reaction was quenched with phosphate buffer (pH 7). Organic materials were extracted with ethyl acetate three times, and the combined extracts were washed with brine and dried over Na_2SO_4. After removal of the solvents under reduced pressure, the residue was purified by silica gel column chromatography (hexane/CH_2Cl_2 = 3:1) to give **1b** (60 mg, 92%) as a yellow solid.

^{1}H NMR (500 MHz, $CDCl_3$) δ 6.66 (dd, *J* = 8.5, 7.4 Hz, 2H), 7.19 (dd, *J* = 7.9, 7.4 Hz, 2H), 7.58 (d, *J* = 8.5 Hz, 2H), 7.80 (d, *J* = 7.9 Hz, 2H), 7.89 (s, 4H), 7.93 (d, *J* = 8.1 Hz, 2H), 7.96 (d, *J* = 8.1 Hz, 2H); ^{13}C NMR (126 MHz, $CDCl_3$) δ 124.0, 124.6, 125.5, 126.1, 126.8, 127.2, 127.5, 127.7, 127.8, 128.0, 129.9, 131.2, 131.7, 133.1.

Gram-scale synthesis: Compound **1b** was also synthesized by the method described above using bisacetal **4b** (2.05 g, 4.53 mmol), trifluoromethanesulfonic acid (173 mg, 1.2 mmol), and HFIP (15 mL) at 0 ºC for 3 h. Purification by silica gel column chromatography (hexane/CH_2Cl_2 = 3:1) gave **1b** (1.31 g, 88%).

Supporting Information

Supporting Information File 1

Detailed experimental procedures and spectral data.
[https://www.beilstein-journals.org/bjoc/content/supplementary/1860-5397-17-35-S1.pdf]

Acknowledgements

We acknowledge Central Glass Co., Ltd. for generous gifts of 1,1,1,3,3,3-hexafluoropropan-2-ol (HFIP) and trifluoromethanesulfonic acid (TfOH). We thank Mr. M. Hayashi for initial investigation of this work.

Funding

This work was financially supported by JSPS KAKENHI Grant Number JP19H02707 (J.I.) in Grant-in-Aid for Scientific Research (B), JSPS KAKENHI Grant Number JP18H04234 (J.I.) in Precisely Designed Catalysts with Customized Scaffolding, JSPS KAKENHI Grant Number JP20K21186 (J.I.) in Grant-in-Aid for Challenging Research (Exploratory), and JSPS KAKENHI Grant Number JP18K05116 (T.F.) in Grant-in-Aid for Scientific Research (C).

ORCID® iDs

Takeshi Fujita - https://orcid.org/0000-0001-9666-022X
Junji Ichikawa - https://orcid.org/0000-0001-6498-326X

References

1. Shen, Y.; Chen, C.-F. *Chem. Rev.* **2012,** *112,* 1463–1535. doi:10.1021/cr200087r
2. Gingras, M. *Chem. Soc. Rev.* **2013,** *42,* 968–1006. doi:10.1039/c2cs35154d
3. Gingras, M.; Félix, G.; Peresutti, R. *Chem. Soc. Rev.* **2013,** *42,* 1007–1050. doi:10.1039/c2cs35111k
4. Gingras, M. *Chem. Soc. Rev.* **2013,** *42,* 1051–1095. doi:10.1039/c2cs35134j
5. Li, C.; Yang, Y.; Miao, Q. *Chem. – Asian J.* **2018,** *13,* 884–894. doi:10.1002/asia.201800073
6. Dhbaibi, K.; Favereau, L.; Crassous, J. *Chem. Rev.* **2019,** *119,* 8846–8953. doi:10.1021/acs.chemrev.9b00033
7. Newman, M. S.; Lutz, W. B.; Lednicer, D. *J. Am. Chem. Soc.* **1955,** *77,* 3420–3421. doi:10.1021/ja01617a097
8. Verbiest, T.; Van Elshocht, S.; Kauranen, M.; Hellemans, L.; Snauwaert, J.; Nuckolls, C.; Katz, T. J.; Persoons, A. *Science* **1998,** *282,* 913–915. doi:10.1126/science.282.5390.913
9. Verbiest, T.; Van Elshocht, S.; Persoons, A.; Nuckolls, C.; Phillips, K. E.; Katz, T. J. *Langmuir* **2001,** *17,* 4685–4687. doi:10.1021/la010262u
10. Clays, K.; Wostyn, K.; Persoons, A.; Maiorana, S.; Papagni, A.; Daul, C. A.; Weber, V. *Chem. Phys. Lett.* **2003,** *372,* 438–442. doi:10.1016/s0009-2614(03)00437-8
11. Zhao, W.-L.; Li, M.; Lu, H.-Y.; Chen, C.-F. *Chem. Commun.* **2019,** *55,* 13793–13803. doi:10.1039/c9cc06861a and references cited therein.
12. Mallory, F. B.; Mallory, C. W. *Org. React.* **1984,** *30,* 1–456. doi:10.1002/0471264180.or030.01
13. Flammang-Barbieux, M.; Nasielski, J.; Martin, R. H. *Tetrahedron Lett.* **1967,** *8,* 743–744. doi:10.1016/s0040-4039(00)90586-0
14. Mori, K.; Murase, T.; Fujita, M. *Angew. Chem., Int. Ed.* **2015,** *54,* 6847–6851. doi:10.1002/anie.201502436
15. Mandal, B. K.; Sooksimuang, T. *J. Porphyrins Phthalocyanines* **2002,** *6,* 66–72. doi:10.1142/s1088424602000105
16. Harrowven, D. C.; Nunn, M. I. T.; Fenwick, D. R. *Tetrahedron Lett.* **2002,** *43,* 7345–7347. doi:10.1016/s0040-4039(02)01720-3
17. Collins, S. K.; Grandbois, A.; Vachon, M. P.; Côté, J. *Angew. Chem., Int. Ed.* **2006,** *45,* 2923–2926. doi:10.1002/anie.200504150
18. Teplý, F.; Stará, I. G.; Starý, I.; Kollárovič, A.; Šaman, D.; Rulíšek, L.; Fiedler, P. *J. Am. Chem. Soc.* **2002,** *124,* 9175–9180. doi:10.1021/ja0259584
19. Hosokawa, T.; Takahashi, Y.; Matsushima, T.; Watanabe, S.; Kikkawa, S.; Azumaya, I.; Tsurusaki, A.; Kamikawa, K. *J. Am. Chem. Soc.* **2017,** *139,* 18512–18521. doi:10.1021/jacs.7b07113
20. Fujita, T.; Takahashi, I.; Hayashi, M.; Wang, J.; Fuchibe, K.; Ichikawa, J. *Eur. J. Org. Chem.* **2017,** 262–265. doi:10.1002/ejoc.201601406

21. Takahashi, I.; Hayashi, M.; Fujita, T.; Ichikawa, J. *Chem. Lett.* **2017,** *46,* 392–394. doi:10.1246/cl.161122
22. Takahashi, I.; Fujita, T.; Shoji, N.; Ichikawa, J. *Chem. Commun.* **2019,** *55,* 9267–9270. doi:10.1039/c9cc04152d
23. Bégué, J.-P.; Bonnet-Delpon, D.; Crousse, B. *Synlett* **2004,** 18–29. doi:10.1055/s-2003-44973
24. Shuklov, I. A.; Dubrovina, N. V.; Börner, A. *Synthesis* **2007,** 2925–2943. doi:10.1055/s-2007-983902
25. Dohi, T.; Yamaoka, N.; Kita, Y. *Tetrahedron* **2010,** *66,* 5775–5785. doi:10.1016/j.tet.2010.04.116
26. Khaksar, S. *J. Fluorine Chem.* **2015,** *172,* 51–61. doi:10.1016/j.jfluchem.2015.01.008
27. Colomer, I.; Chamberlain, A. E. R.; Haughey, M. B.; Donohoe, T. J. *Nat. Rev. Chem.* **2017,** *1,* No. 88. doi:10.1038/s41570-017-0088
28. Ichikawa, J.; Miyazaki, S.; Fujiwara, M.; Minami, T. *J. Org. Chem.* **1995,** *60,* 2320–2321. doi:10.1021/jo00113a005
29. The corresoponding boronic acid was also applicable to the preparation of **4a**.
30. In the gram-scale preparation of **4a**, PPh_3 was used instead of SPhos (see the Experimental section).
31. Bowles, D. M.; Anthony, J. E. *Org. Lett.* **2000,** *2,* 85–87. doi:10.1021/ol991254w
32. Komeyama, K.; Okamoto, Y.; Takaki, K. *Angew. Chem., Int. Ed.* **2014,** *53,* 11325–11328. doi:10.1002/anie.201406807
33. Zhang, K.; Cai, L.; Jiang, X.; Garcia-Garibay, M. A.; Kwon, O. *J. Am. Chem. Soc.* **2015,** *137,* 11258–11261. doi:10.1021/jacs.5b07403
34. Fuchibe, K.; Imaoka, H.; Ichikawa, J. *Chem. – Asian J.* **2017,** *12,* 2359–2363. doi:10.1002/asia.201700870
35. Murai, M.; Ogita, T.; Takai, K. *Chem. Commun.* **2019,** *55,* 2332–2335. doi:10.1039/c9cc00270g

License and Terms

This is an Open Access article under the terms of the Creative Commons Attribution License (https://creativecommons.org/licenses/by/4.0). Please note that the reuse, redistribution and reproduction in particular requires that the author(s) and source are credited and that individual graphics may be subject to special legal provisions.

The license is subject to the *Beilstein Journal of Organic Chemistry* terms and conditions: (https://www.beilstein-journals.org/bjoc/terms)

The definitive version of this article is the electronic one which can be found at: https://doi.org/10.3762/bjoc.17.35

BEILSTEIN JOURNAL OF ORGANIC CHEMISTRY

Synthesis of trifluoromethyl ketones by nucleophilic trifluoromethylation of esters under a fluoroform/KHMDS/triglyme system

Yamato Fujihira[1], Yumeng Liang[2], Makoto Ono[1], Kazuki Hirano[2], Takumi Kagawa[3] and Norio Shibata[*1,2,4]

Letter

Open Access

Address:
[1]Department of Life Science and Applied Chemistry, Nagoya Institute of Technology, Gokiso, Showa-ku, Nagoya 466-5888, Japan, [2]Department of Nanopharmaceutical Sciences, Nagoya Institute of Technology, Gokiso, Showa-ku, Nagoya 466-5888, Japan, [3]Tosoh Finechem Corporation, 4988, Kaiseicho, Shunan, 746-0006, Japan and [4]Institute of Advanced Fluorine-Containing Materials, Zhejiang Normal University, 688 Yingbin Avenue, 321004 Jinhua, China

Email:
Norio Shibata* - nozshiba@nitech.ac.jp

* Corresponding author

Keywords:
fluoroform; greenhouse gas; HFC-23; trifluoromethyl ketones; trifluoromethylation

Beilstein J. Org. Chem. **2021,** *17,* 431–438.
https://doi.org/10.3762/bjoc.17.39

Received: 03 November 2020
Accepted: 02 February 2021
Published: 12 February 2021

This article is part of the thematic issue "Organo-fluorine chemistry V".

Guest Editor: D. O'Hagan

© 2021 Fujihira et al.; licensee Beilstein-Institut.
License and terms: see end of document.

Abstract

A straightforward method that enables the formation of biologically attractive trifluoromethyl ketones from readily available methyl esters using the potent greenhouse gas fluoroform (HCF_3, HFC-23) was developed. The combination of fluoroform and KHMDS in triglyme at −40 °C was effective for this transformation, with good yields as high as 92%. Substrate scope of the trifluoromethylation procedure was explored for aromatic, aliphatic, and conjugated methyl esters. This study presents a straightforward trifluoromethylation process of various methyl esters that convert well to the corresponding trifluoromethyl ketones. The tolerance of various pharmacophores under the reaction conditions was also explored.

Introduction

In recent decades, organofluorine molecules have received widespread attention in the field of medicinal chemistry [1-4]. The introduction of fluorine(s) into organic molecules usually leads to significant changes in the chemical and physicochemical properties of the original compounds [5,6]. Hence, the fluorination and related fluoro-functionalization of drug candidates are powerful strategies in drug design to appropriately bias their biological properties, bioavailability, and ADME [7,8]. While tremendous methodologies have been developed for the synthesis of organofluorine compounds [9,10], many of the laboratory methods are not always suitable for industrial production in terms of their synthetic complexity, handling, and

cost of target compounds [11-15]. Thus, the development of low-cost and straightforward chemical synthetic technologies, including fluorination and trifluoromethylation, are matters of considerable importance to pharmaceutical and agrochemical industries. Fluoroform (HCF_3, HFC-23) is an industrial byproduct of polytetrafluoroethylene synthesis and has become an ideal, economical feedstock for trifluoromethyl (CF_3) compounds. Rather than decomposing CF_3 compounds, it would be better to maximize the efficiency of their use [16-18]. However, taming HCF_3 as a trifluoromethylation agent is a challenge in organic chemistry [19-28], although recent rapid progress in the chemistry of HCF_3 by Grushin (for $CuCF_3$) [29-37], Prakash (for KCF_3) [38], and others [39-44], including our group [45-50], has dramatically improved the prospects. One of the problems facing the treatment of HCF_3 for nucleophilic trifluoromethylation reactions is the low stability of the directly generated CF_3 anion (CF_3^-) for decomposing to difluorocarbene ($:CF_2$) and fluoride (F^-) (Scheme 1a). Due to the formation of highly stable fluoride salts (MF), the breakdown of CF_3^- into difluorocarbene in the presence of alkali (M^+) and other metal cations is favored. In earlier studies, the solvent *N,N*-dimethylformamide (DMF), was essential for nucleophilic trifluoromethylation by HCF_3 since DMF acts as a CF_3 anion reservoir that is used as a hemiaminaloate adduct [$Me_2NCH(O)CF_3$]- (Scheme 1b) [19-28]. Although the taming CF_3 anion had been an elusive problem for decades, it has been dramatically progressed in recent years by the substantial works by Grushin [51-53] and Prakash [54]. Our group reported novel DMF-free systems for the nucleophilic trifluoromethylation reaction using HCF_3, including the phosphazene base P4-*t*-Bu (P4-*t*-Bu), in 2013 (Scheme 1c) [45] and a potassium *tert*-butoxide (*t*-BuOK) or potassium hexamethyldisilazide (KHMDS)/glyme combination in 2018 (Scheme 1d) [46]. The success of our DMF-free systems lies in the generation of sterically demanding cationic species, [P4-*t*-Bu]H^+ or glyme capsulized K^+, resulting in the stabilization of CF_3^- from HCF_3 by ion separation. The sterically demanding [P4-*t*-Bu]H^+ or encapsulation of K^+ by glymes effectively inhibits the contact of CF_3^- to K^+, preventing decomposition into CF_2 and KF. The isolated CF_3 is rather naked with a highly nucleophilic character, which is suitable for nucleophilic trifluoromethylation reactions. The K^+ and glyme combination is particularly useful for the nucleophilic trifluoromethylation of carbonyl compounds to trifluoromethyl carbinols because it does not require any expensive reagents nor very low-temperature conditions. Although the reaction has a broad substrate scope of embracing ketones, chalcones and aldehydes, the transformation of esters to trifluoromethyl ketones by this protocol was never examined [46].

Trifluoromethyl ketones (TFMKs) are valuable fluorine-containing synthetic targets of bioactive compounds [55,56] that behave as mimics of the tetrahedral transition-state intermediate of enzymatic hydrolysis of esters and amides by stabilizing their hydrates (Figure 1a) [57]. In fact, the TFMK moiety is a proven effective metal chelator in various enzyme inhibitors (Figure 1b) [58-65].

Several useful methods exist for preparing trifluoromethyl ketones [66,67], such as the direct trifluoromethylation of esters by the Ruppert–Prakash reagent (Me_3SiCF_3) [68-71], but the use of HCF_3 for this transformation reaction is still limited. In 1998, Russel and Roques examined the transformation of methyl benzoate to trifluoromethyl phenyl ketone with HCF_3 in the presence of KHMDS or KH/DMSO in DMF, but the method required DMF and only a single example was indicated (Scheme 2a) [23]. Prakash and co-workers showed the first example of the DMF-free preparation of trifluoromethyl phenyl ketone with HCF_3 in the presence of KHMDS in THF, but they did not examined the scope of the reaction (Scheme 2b) [38]. In 2018, Szymczak and co-workers showed a single example of the preparation of phenyl trifluoromethyl ketone using HCF_3-derived borazine CF_3^- in 29% yield (Scheme 2c) [43]. Very recently, Han, Lian, and co-workers reported that a protocol using diisopropylaminosodium (NaDA) was useful for the tri-

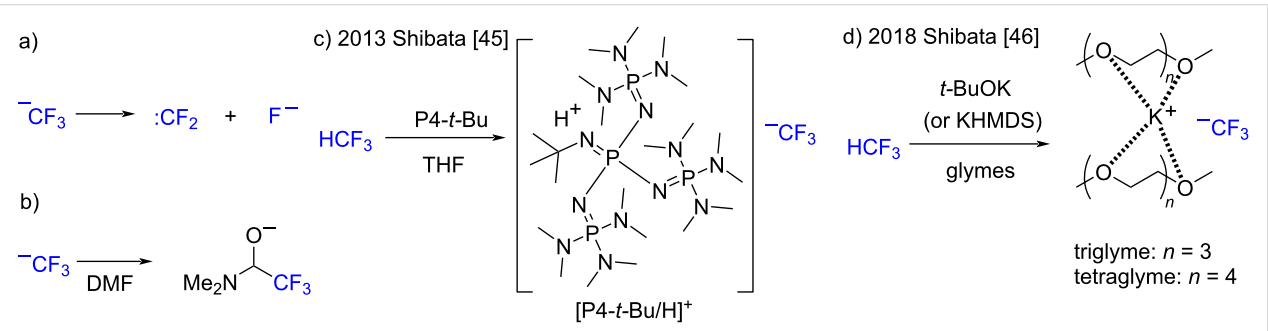

Scheme 1: Chemistry of the CF_3 anion generated from HCF_3. a) Decomposition of the trifluoromethyl anion to difluorocarbene and fluoride. b) A hemiaminaloate adduct of CF_3 anion to DMF. c) Formation of the [P4-*t*-Bu]H^+ CF_3 anion salt. d) Encapsulation of K^+ by glymes. Transformation of esters to trifluoromethyl ketones.

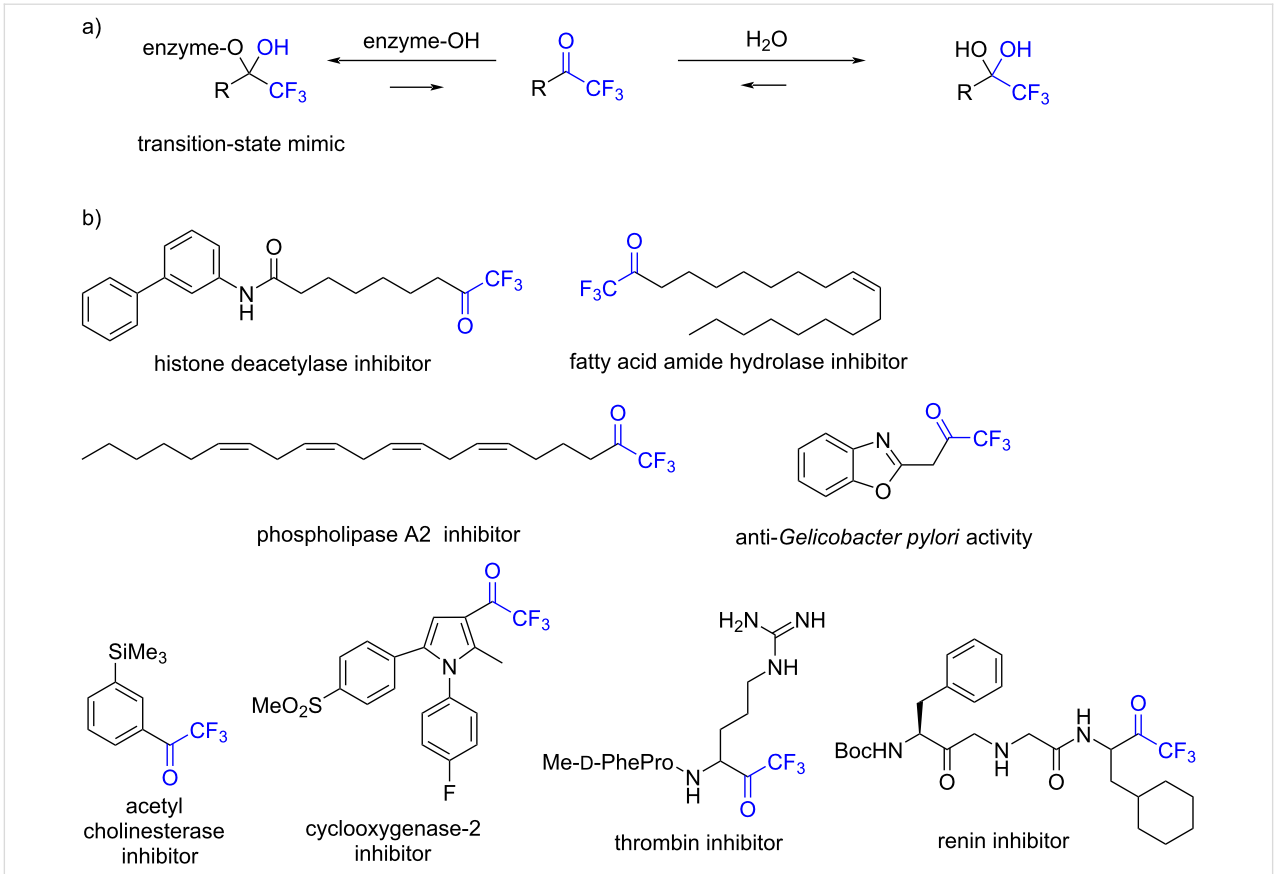

Figure 1: Trifluoromethyl ketones. a) Hydrolysis of trifluoromethyl ketones. b) Selected examples of biologically active trifluoromethyl ketones.

fluoromethylation of esters to trifluoromethyl ketones with HCF_3 at −60 °C (Scheme 2d) [44]. However, the preparation of NaDA was rather complicated and required pre-mixing of diisopropylamine, tetramethylethylenediamine (TMEDA), isoprene, and even more tedious "dispersion sodium" in *n*-heptane at 25 °C for 4 h, before the reaction of esters with HCF_3 at −60 °C. We herein extend our glyme strategy [50] shown in Scheme 1d, the HCF_3/KHMDS/triglyme system, for the synthesis of trifluoromethyl ketones from esters (Scheme 2e). The combination of HCF_3 and KHMDS in triglyme at −40 °C was found to be effective for this transformation, with good yields as high as 92%. The substrate scope of the trifluoromethylation procedure was explored for aromatic, aliphatic, and conjugated methyl esters. This study presents a straightforward trifluoromethylation process of various methyl esters that convert well to the corresponding trifluoromethyl ketones. The tolerance of various pharmacophores under the reaction conditions was also explored.

Results and Discussion

We first examined the trifluoromethylation reaction of methyl 2-naphthoate (**1a**) as a model substrate for HCF_3 to optimize the reaction conditions (Table 1). Following our glymes strategy, we initially used *t*-BuOK as the base in triglyme, and the desired trifluoromethyl ketone **2a** was obtained in 29% yield (Table 1, entry 1). We next carried out the reaction in other solvents, THF (**2a**, 5%, Table 1, entry 2) and toluene (**2a**, 0%, Table 1, entry 3), and confirmed the advantage of the triglyme that was used (Table 1, entries 1–3). Increasing the amount of *t*-BuOK to 4.0 equiv did not improve the yield (25%) of **2a** (Table 1, entry 4). When we used KHMDS to replace *t*-BuOK, the yield of **2a** improved significantly to 57% (Table 1, entry 5). As expected, tetraglyme, instead of triglyme, gave a similar good yield of 59% (Table 1, entry 6), while the transformation decreased significantly when diglyme was used (**2a**, 29%, Table 1, entry 7). Interestingly, when we stopped the reaction after 4 h, the yield increased to 76% (Table 1, entry 8). On this basis, we attempted to reduce the amount of HCF_3 to 1.1 equiv and found that the yield was not sacrificed, yielding 75% of **2a** (Table 1, entry 9). Other optimized reaction conditions did not improve the yield (see Supporting Information File 1 for an extensive list of reaction conditions, Table S1).

We explored the substrate scope of this trifluoromethylation reaction with the optimized conditions in hand (entry 9, Table 1). Various carboxylic esters were investigated in the

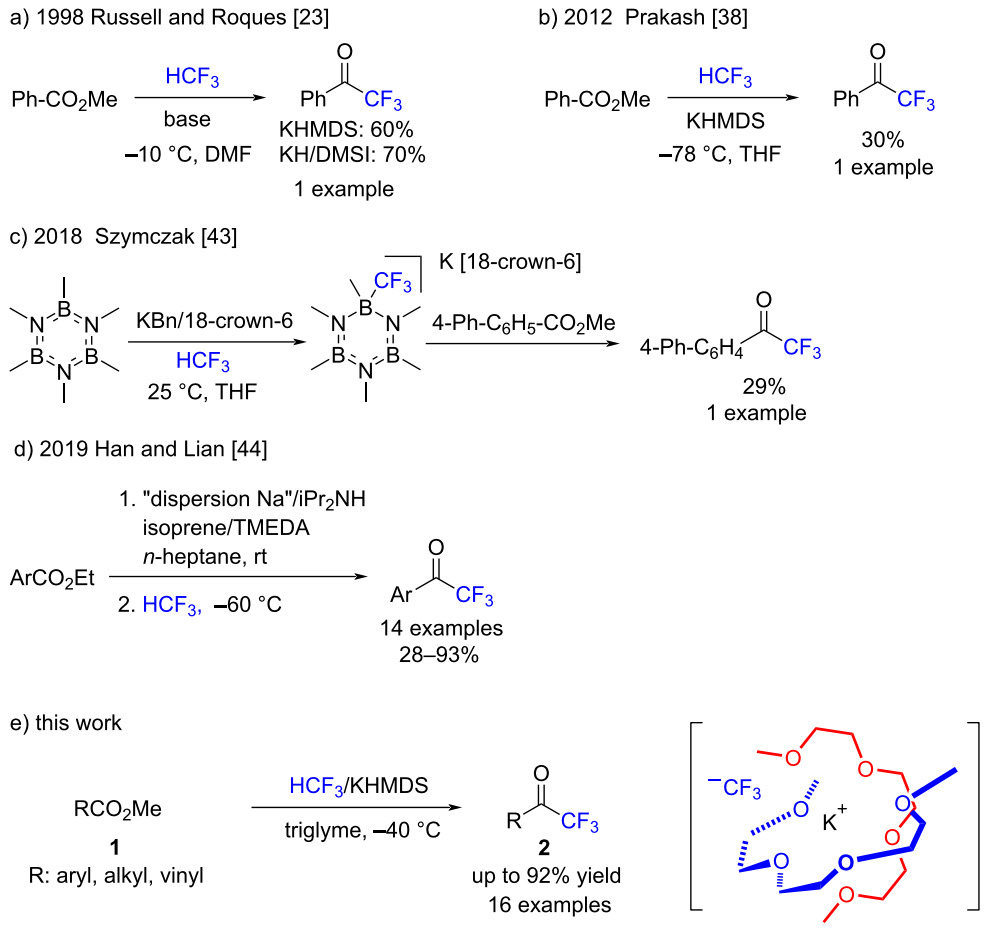

Scheme 2: Trifluoromethylation of esters by HCF_3 by a) Russell and Roques (1998), b) Prakash and co-workers (2012), c) Szymczak and co-workers (2018), d) Han, Lian and co-workers (2019), and e) our group in this work.

Table 1: Optimized reaction conditions for the conversion of **1a** to **2a**.

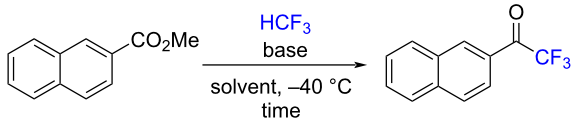

1a **2a**

Entry	Base (equiv)	Solvent	Time	Yield (%)[a]
1	*t*-BuOK (2.0)	triglyme	overnight	29
2	*t*-BuOK (2.0)	THF	overnight	5
3	*t*-BuOK (2.0)	toluene	overnight	0
4	*t*-BuOK (4.0)	triglyme	overnight	25
5	KHMDS (2.0)	triglyme	overnight	57
6	KHMDS (2.0)	tetraglyme	overnight	59
7	KHMDS (2.0)	diglyme	overnight	29
8	KHMDS (2.0)	triglyme	4 h	76
9[b]	KHMDS (2.0)	triglyme	4 h	75 (71)[c]

[a]Determined by ^{19}F NMR using a crude mixture with trifluorotoluene as the internal standard. [b]HCF_3 was 1.1 equiv. [c]Isolated yield.

presence of 1.1 equiv of HCF_3 and two equiv of KHMDS (Scheme 3). Methyl 2-naphthoate (**1a**) gave **2a** in 75% yield, but sterically demanding methyl 1-naphthoate (**1b**) gave the desired trifluoromethyl ketone **2b** in only lower yield (37%). Functionalities on the benzene ring at the *para*-position were well-tolerated in the KHMDS/glyme system. Halogen groups, such as chloro (**1c**), bromo (**1d**), and reactive iodo (**1e**) substitutions were also tolerated, resulting in the corresponding trifluoromethyl aryl ketones in moderate yields (56–63%) under basic conditions. The alkyl groups of *tert*-butyl (**1f**)- and cyclohexyl (**1g**)-substituted methyl benzoate derivatives, biphenyl benzoate (**1h**), and electron-donating 4-methoxybenzoate, were nicely transformed into aryl trifluoromethyl ketones in moderate to high yields (45–92%). Aryl substrates with a halogen attached at the *meta*- and *ortho*-positions were also accepted to furnish the desired products (**2j**–**m**) in good yields (66–82%). Moreover, di-substituted benzoate (**1n**), sterically demanding methyl adamantly carboxylate (**1o**), and conjugated methyl ester (**1p**) transformed effectively into trifluoromethyl ketones (**2o**–**p**) in moderate yields (50–62%). A gram-scale reaction was also

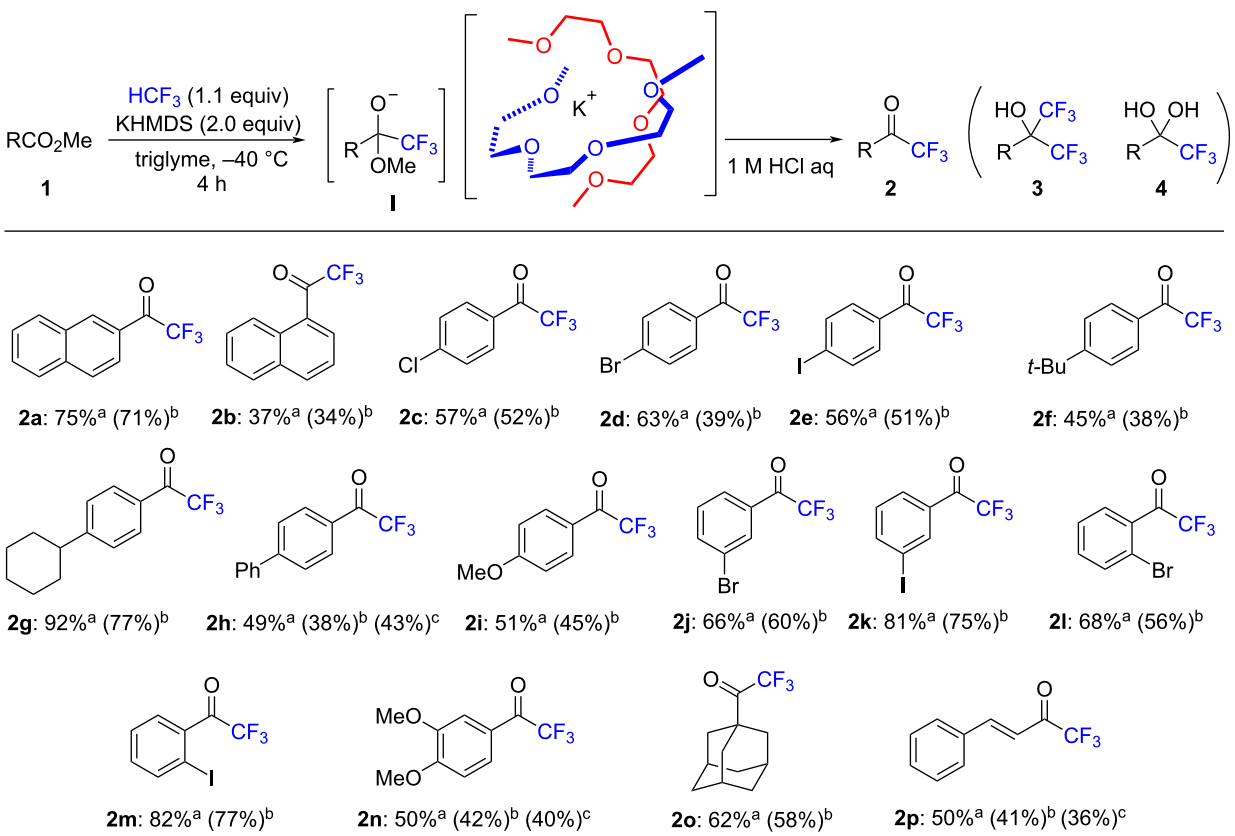

Scheme 3: Substrate scope of esters **1** for trifluoromethylation by HCF_3 under the optimized conditions. [a]Determined by ^{19}F NMR of the crude **2** with trifluorotoluene as an internal standard. [b]Isolated yield. [c]Isolated yield of gram-scale reaction by using 1 g of substrate.

carried out for **1h**, **1n**, and **1p** to furnish **2h**, **2p**, and **2n** in similar isolated yields, 43%, 40%, and 36%, respectively. The double CF_3 addition product **3** was not observed due to the preferential formation of stable tetrahedral species **I** instead of the CF_3 ketones **2** in the reaction mixture. However, all the yields were moderate to good. This fact could be explained by the appearance of hydrate products **4** in the ^{19}F NMR spectrum of the crude reaction mixture [72], while the hydrates **4** disappeared completely after purification by silica gel column chromatography [73].

Given the relevance of this trifluoromethylation reaction system for drug discovery, we conducted a robustness screening experiment to gain further information on its tolerance to various pharmacophores (Table 2). A range of common nitrogen-containing compounds such as pyridine, pyrazine, 1*H*-pyrazole, 1*H*-indole, 1-methyl-1*H*-indole, piperidine, and piperazine were subjected to screening. Pyridine and piperidine slightly hamper the reaction of **1g** (Table 2, entries 2 and 7, 80–82%). Other nitrogen-containing compounds have more effect on the yield of the reaction of **1g** (Table 2, entries 3–6, 58–72%). Next, a range of common oxygen and sulfur-containing compounds such as furan, tetrahydrofuran, 1,4-dioxane, thiophene, benzo[*b*]thiophene, dibenzo[*b*,*d*]thiophene, and diphenylsulfane were also screened. These substances also have some effect on the reaction (Table 2, entries 9–15, 63–87%). Besides, silicon-containing compound, trimethyl(phenyl)silane that is more sensitive to fluorine was screened, 79% yield were obtained in this test. To consider the frequency of these motifs in modern pharmaceutical drugs, these tests are necessary, and the resistance of the reaction was also verified from various pharmacophores to be acceptable.

Conclusion

In conclusion, the trifluoromethylation of methyl carboxylates to trifluoromethyl ketones is accomplished under basic conditions with fluoroform in triglyme at −40 °C. An equivalent amount of fluoroform was sufficient for this transformation. A wide variety of medicinally attractive aryl and alkyl trifluoromethyl ketones are obtained in good yields by a relatively simple procedure, although the protocol is not applicable to enolizable esters. Fluoroform is an economical feedstock, and

Table 2: Tolerance of various pharmacophores under the trifluoromethylation conditions.

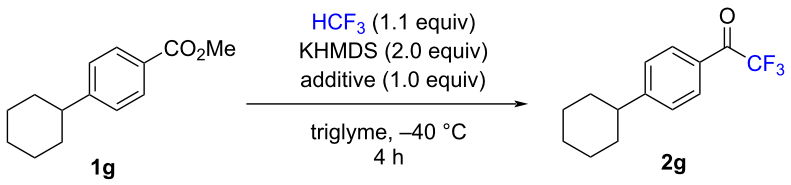

1g **2g**

Entry	Additive	Yield[a] (%)	Entry	Additive	Yield[a] (%)	Entry	Additive	Yield[a] (%)
1	–	92	7	piperidine	80	13	benzo[*b*]thiophene	78
2	pyridine	82	8	piperazine	64	14	dibenzo[*b*,*d*]thiophene	64
3	pyrazine	72	9	furan	87	15	PhSPh	75
4	pyrazole	66	10	THF	64	16	Ph-$SiMe_3$	79
5	indole	58	11	1,4-dioxane	63			
6	1-methyl-1*H*-indole	67	12	thiophene	75			

[a]Determined by ^{19}F NMR using the crude **2g** with trifluorotoluene as an internal standard.

methyl esters are readily available inexpensive precursors. Besides, glymes are versatile solvents for chemical processes in industry [74] would the protocol be useful for the industrial extension, although there are still many points to be overcome such as requirements of low temperature, two equivalents of KHMDS. Further application of this "batch protocol" for a "continuous-flow microreactor" reaction is now ongoing in our laboratory towards industrial collaboration.

Experimental

A test tube containing **1** (0.4 mmol) in triglyme (0.7 mL) was charged with HCF_3 (9.9 mL, 1.1 equiv, measured by a syringe, see the picture in Supporting Information File 1, Figure S1) by cooling in liquid nitrogen under vacuum. KHMDS (160 mg, 2.0 equiv) in triglyme (commercial grade, without drying, 0.3 mL) was added at −40 °C under nitrogen atmosphere, and the reaction mixture was stirred at the same temperature for 4 h. Thereafter, 1 M HCl aq (1.0 mL) was added, and the aqueous layer was extracted with CH_2Cl_2 (1.0 mL × 3). The combined organic layer was washed with brine, dried over Na_2SO_4, concentrated under reduced pressure, and purified by column chromatography on silica gel to give products **2**.

Supporting Information

Supporting Information File 1

Optimization of reaction conditions, general procedure and product characterization data.
[https://www.beilstein-journals.org/bjoc/content/supplementary/1860-5397-17-39-S1.pdf]

Funding

This work was supported by JSPS KAKENHI grants JP 18H02553 (KIBAN B, NS).

ORCID® iDs

Yumeng Liang - https://orcid.org/0000-0002-2846-0792
Norio Shibata - https://orcid.org/0000-0002-3742-4064

References

1. Zhu, Y.; Han, J.; Wang, J.; Shibata, N.; Sodeoka, M.; Soloshonok, V. A.; Coelho, J. A. S.; Toste, F. D. *Chem. Rev.* **2018,** *118,* 3887–3964. doi:10.1021/acs.chemrev.7b00778
2. Purser, S.; Moore, P. R.; Swallow, S.; Gouverneur, V. *Chem. Soc. Rev.* **2008,** *37,* 320–330. doi:10.1039/b610213c
3. Inoue, M.; Sumii, Y.; Shibata, N. *ACS Omega* **2020,** *5,* 10633–10640. doi:10.1021/acsomega.0c00830
4. Ogawa, Y.; Tokunaga, E.; Kobayashi, O.; Hirai, K.; Shibata, N. *iScience* **2020,** *23,* 101467. doi:10.1016/j.isci.2020.101467
5. Gillis, E. P.; Eastman, K. J.; Hill, M. D.; Donnelly, D. J.; Meanwell, N. A. *J. Med. Chem.* **2015,** *58,* 8315–8359. doi:10.1021/acs.jmedchem.5b00258
6. Park, B. K.; Kitteringham, N. R.; O'Neill, P. M. *Annu. Rev. Pharmacol. Toxicol.* **2001,** *41,* 443–470. doi:10.1146/annurev.pharmtox.41.1.443
7. Isanbor, C.; O'Hagan, D. *J. Fluorine Chem.* **2006,** *127,* 303–319. doi:10.1016/j.jfluchem.2006.01.011
8. Wang, J.; Sánchez-Roselló, M.; Aceña, J. L.; del Pozo, C.; Sorochinsky, A. E.; Fustero, S.; Soloshonok, V. A.; Liu, H. *Chem. Rev.* **2014,** *114,* 2432–2506. doi:10.1021/cr4002879
9. Kirsch, P. *Modern Fluoroorganic Chemistry Synthesis, Reactivity, Applications;* Wiley-VCH: Weinheim, Germany, 2004. doi:10.1002/352760393x
10. Liang, T.; Neumann, C. N.; Ritter, T. *Angew. Chem., Int. Ed.* **2013,** *52,* 8214–8264. doi:10.1002/anie.201206566

11. Mazloomi, Z.; Bansode, A.; Benavente, P.; Lishchynskyi, A.; Urakawa, A.; Grushin, V. V. *Org. Process Res. Dev.* **2014,** *18,* 1020–1026. doi:10.1021/op500109v
12. Musio, B.; Gala, E.; Ley, S. V. *ACS Sustainable Chem. Eng.* **2018,** *6,* 1489–1495. doi:10.1021/acssuschemeng.7b04012
13. Harsanyi, A.; Sandford, G. *Org. Process Res. Dev.* **2014,** *18,* 981–992. doi:10.1021/op500141c
14. Caron, S. *Org. Process Res. Dev.* **2020,** *24,* 470–480. doi:10.1021/acs.oprd.0c00030
15. Glenadel, Q.; Alazet, S.; Baert, F.; Billard, T. *Org. Process Res. Dev.* **2016,** *20,* 960–964. doi:10.1021/acs.oprd.6b00062
16. McCulloch, A.; Lindley, A. A. *Atmos. Environ.* **2007,** *41,* 1560–1566. doi:10.1016/j.atmosenv.2006.02.021
17. Han, W.; Li, Y.; Tang, H.; Liu, H. *J. Fluorine Chem.* **2012,** *140,* 7–16. doi:10.1016/j.jfluchem.2012.04.012
18. Grushin, V. V. *Chim. Oggi* **2014,** *32* (3), 81–90.
19. Shono, T.; Ishifune, M.; Okada, T.; Kashimura, S. *J. Org. Chem.* **1991,** *56,* 2–4. doi:10.1021/jo00001a002
20. Symons, E. A.; Clermont, M. J. *J. Am. Chem. Soc.* **1981,** *103,* 3127–3130. doi:10.1021/ja00401a034
21. Barhdadi, R.; Troupel, M.; Périchon, J. *Chem. Commun.* **1998,** 1251–1252. doi:10.1039/a801406j
22. Folléas, B.; Marek, I.; Normant, J.-F.; Jalmes, L. S. *Tetrahedron Lett.* **1998,** *39,* 2973–2976. doi:10.1016/s0040-4039(98)00391-8
23. Russell, J.; Roques, N. *Tetrahedron* **1998,** *54,* 13771–13782. doi:10.1016/s0040-4020(98)00846-1
24. Mispelaere, C.; Roques, N. *Tetrahedron Lett.* **1999,** *40,* 6411–6414. doi:10.1016/s0040-4039(99)01369-6
25. Folléas, B.; Marek, I.; Normant, J.-F.; Saint-Jalmes, L. *Tetrahedron* **2000,** *56,* 275–283. doi:10.1016/s0040-4020(99)00951-5
26. Large, S.; Roques, N.; Langlois, B. R. *J. Org. Chem.* **2000,** *65,* 8848–8856. doi:10.1021/jo000150s
27. Billard, T.; Bruns, S.; Langlois, B. R. *Org. Lett.* **2000,** *2,* 2101–2103. doi:10.1021/ol005987o
28. van der Born, D.; Herscheid, J. D. M.; Orru, R. V. A.; Vugts, D. J. *Chem. Commun.* **2013,** *49,* 4018–4020. doi:10.1039/c3cc37833k
29. Tomashenko, O. A.; Escudero-Adán, E. C.; Martínez Belmonte, M.; Grushin, V. V. *Angew. Chem., Int. Ed.* **2011,** *50,* 7655–7659. doi:10.1002/anie.201101577
30. Zanardi, A.; Novikov, M. A.; Martin, E.; Benet-Buchholz, J.; Grushin, V. V. *J. Am. Chem. Soc.* **2011,** *133,* 20901–20913. doi:10.1021/ja2081026
31. Lishchynskyi, A.; Novikov, M. A.; Martin, E.; Escudero-Adán, E. C.; Novák, P.; Grushin, V. V. *J. Org. Chem.* **2013,** *78,* 11126–11146. doi:10.1021/jo401423h
32. Lishchynskyi, A.; Berthon, G.; Grushin, V. V. *Chem. Commun.* **2014,** *50,* 10237–10240. doi:10.1039/c4cc04930f
33. Novák, P.; Lishchynskyi, A.; Grushin, V. V. *J. Am. Chem. Soc.* **2012,** *134,* 16167–16170. doi:10.1021/ja307783w
34. Novák, P.; Lishchynskyi, A.; Grushin, V. V. *Angew. Chem., Int. Ed.* **2012,** *51,* 7767–7770. doi:10.1002/anie.201201613
35. Konovalov, A. I.; Benet-Buchholz, J.; Martin, E.; Grushin, V. V. *Angew. Chem., Int. Ed.* **2013,** *52,* 11637–11641. doi:10.1002/anie.201306272
36. Konovalov, A. I.; Lishchynskyi, A.; Grushin, V. V. *J. Am. Chem. Soc.* **2014,** *136,* 13410–13425. doi:10.1021/ja507564p
37. Romine, A. M.; Nebra, N.; Konovalov, A. I.; Martin, E.; Benet-Buchholz, J.; Grushin, V. V. *Angew. Chem., Int. Ed.* **2015,** *54,* 2745–2749. doi:10.1002/anie.201411348
38. Prakash, G. K. S.; Jog, P. V.; Batamack, P. T. D.; Olah, G. A. *Science* **2012,** *338,* 1324–1327. doi:10.1126/science.1227859
39. He, L.; Tsui, G. C. *Org. Lett.* **2016,** *18,* 2800–2803. doi:10.1021/acs.orglett.6b00999
40. Xiang, J.-X.; Ouyang, Y.; Xu, X.-H.; Qing, F.-L. *Angew. Chem., Int. Ed.* **2019,** *58,* 10320–10324. doi:10.1002/anie.201905782
41. Geri, J. B.; Szymczak, N. K. *J. Am. Chem. Soc.* **2017,** *139,* 9811–9814. doi:10.1021/jacs.7b05408
42. Biggadike, K.; Boudjelal, M.; Clackers, M.; Coe, D. M.; Demaine, D. A.; Hardy, G. W.; Humphreys, D.; Inglis, G. G. A.; Johnston, M. J.; Jones, H. T.; House, D.; Loiseau, R.; Needham, D.; Skone, P. A.; Uings, I.; Veitch, G.; Weingarten, G. G.; McLay, I. M.; Macdonald, S. J. F. *J. Med. Chem.* **2007,** *50,* 6519–6534. doi:10.1021/jm070778w
43. Geri, J. B.; Wade Wolfe, M. M.; Szymczak, N. K. *Angew. Chem., Int. Ed.* **2018,** *57,* 1381–1385. doi:10.1002/anie.201711316
44. Han, Z.; Chen, S.; Tu, Y.; Lian, X.; Li, G. *Eur. J. Org. Chem.* **2019,** 4658–4661. doi:10.1002/ejoc.201900250
45. Kawai, H.; Yuan, Z.; Tokunaga, E.; Shibata, N. *Org. Biomol. Chem.* **2013,** *11,* 1446–1450. doi:10.1039/c3ob27368g
46. Saito, T.; Wang, J.; Tokunaga, E.; Tsuzuki, S.; Shibata, N. *Sci. Rep.* **2018,** *8,* 11501. doi:10.1038/s41598-018-29748-1
47. Okusu, S.; Tokunaga, E.; Shibata, N. *Org. Lett.* **2015,** *17,* 3802–3805. doi:10.1021/acs.orglett.5b01778
48. Okusu, S.; Hirano, K.; Tokunaga, E.; Shibata, N. *ChemistryOpen* **2015,** *4,* 581–585. doi:10.1002/open.201500160
49. Punna, N.; Saito, T.; Kosobokov, M.; Tokunaga, E.; Sumii, Y.; Shibata, N. *Chem. Commun.* **2018,** *54,* 4294–4297. doi:10.1039/c8cc01526k
50. Hirano, K.; Saito, T.; Fujihira, Y.; Sedgwick, D. M.; Fustero, S.; Shibata, N. *J. Org. Chem.* **2020,** *85,* 7976–7985. doi:10.1021/acs.joc.0c00796
51. Lishchynskyi, A.; Miloserdov, F. M.; Martin, E.; Benet-Buchholz, J.; Escudero-Adán, E. C.; Konovalov, A. I.; Grushin, V. V. *Angew. Chem., Int. Ed.* **2015,** *54,* 15289–15293. doi:10.1002/anie.201507356
52. Miloserdov, F. M.; Konovalov, A. I.; Martin, E.; Benet-Buchholz, J.; Escudero-Adán, E. C.; Lishchynskyi, A.; Grushin, V. V. *Helv. Chim. Acta* **2017,** *100,* e1700032. doi:10.1002/hlca.201700032
53. Harlow, R. L.; Benet-Buchholz, J.; Miloserdov, F. M.; Konovalov, A. I.; Marshall, W. J.; Escudero-Adán, E. C.; Martin, E.; Lishchynskyi, A.; Grushin, V. V. *Helv. Chim. Acta* **2018,** *101,* e1800015. doi:10.1002/hlca.201800015
54. Prakash, G. K. S.; Wang, F.; Zhang, Z.; Haiges, R.; Rahm, M.; Christe, K. O.; Mathew, T.; Olah, G. A. *Angew. Chem., Int. Ed.* **2014,** *53,* 11575–11578. doi:10.1002/anie.201406505
55. Bégué, J.-P.; Bonnet-Delpon, D. *Tetrahedron* **1991,** *47,* 3207–3258. doi:10.1016/s0040-4020(01)86391-2
56. Kawase, M. *J. Synth. Org. Chem., Jpn.* **2001,** *59,* 755–765. doi:10.5059/yukigoseikyokaishi.59.755
57. Gelb, M. H.; Svaren, J. P.; Abeles, R. H. *Biochemistry* **1985,** *24,* 1813–1817. doi:10.1021/bi00329a001
58. Frey, R. R.; Wada, C. K.; Garland, R. B.; Curtin, M. L.; Michaelides, M. R.; Li, J.; Pease, L. J.; Glaser, K. B.; Marcotte, P. A.; Bouska, J. J.; Murphy, S. S.; Davidsen, S. K. *Bioorg. Med. Chem. Lett.* **2002,** *12,* 3443–3447. doi:10.1016/s0960-894x(02)00754-0
59. Patricelli, M. P.; Patterson, J. E.; Boger, D. L.; Cravatt, B. F. *Bioorg. Med. Chem. Lett.* **1998,** *8,* 613–618. doi:10.1016/s0960-894x(98)00073-0

60. Lehn, M.; Griessbach, K. *Pharm. Pharmacol. Commun.* **1999,** *5,* 389–393. doi:10.1111/j.1469-0691.1999.tb00846.x
61. Hornsperger, J.-M.; Collard, J.-N.; Heydt, J.-G.; Giacobini, E.; Funes, S.; Dow, J.; Schirlin, D. *Biochem. Soc. Trans.* **1994,** *22,* 758–763. doi:10.1042/bst0220758
62. Parrilla, A.; Villuendas, I.; Guerrero, A. *Bioorg. Med. Chem.* **1994,** *2,* 243–252. doi:10.1016/s0968-0896(00)82167-7
63. Neises, B.; Broersma, R. J.; Tarnus, C.; Piriou, F.; Remy, J. M.; Lintz, C.; Heminger, E. F.; Kutcher, L. W. *Bioorg. Med. Chem.* **1995,** *3,* 1049–1061. doi:10.1016/0968-0896(95)00097-z
64. Patel, D. V.; Rielly-Gauvin, K.; Ryono, D. E.; Free, C. A.; Smith, S. A.; Petrillo, E. W., Jr. *J. Med. Chem.* **1993,** *36,* 2431–2447. doi:10.1021/jm00069a001
65. Kawase, M.; Harada, H.; Saito, S.; Cui, J.; Tani, S. *Bioorg. Med. Chem. Lett.* **1999,** *9,* 193–194. doi:10.1016/s0960-894x(98)00726-4
66. Wu, W.; Weng, Z. *Synthesis* **2018,** *50,* 1958–1964. doi:10.1055/s-0036-1591971
67. Kelly, C. B.; Mercadante, M. A.; Leadbeater, N. E. *Chem. Commun.* **2013,** *49,* 11133–11148. doi:10.1039/c3cc46266h
68. Wiedemann, J.; Heiner, T.; Mloston, G.; Prakash, G. K. S.; Olah, G. A. *Angew. Chem., Int. Ed.* **1998,** *37,* 820–821. doi:10.1002/(sici)1521-3773(19980403)37:6<820::aid-anie820>3.0.co;2-m
69. Singh, R. P.; Cao, G.; Kirchmeier, R. L.; Shreeve, J. M. *J. Org. Chem.* **1999,** *64,* 2873–2876. doi:10.1021/jo982494c
70. Kawano, Y.; Kaneko, N.; Mukaiyama, T. *Bull. Chem. Soc. Jpn.* **2006,** *79,* 1133–1145. doi:10.1246/bcsj.79.1133
71. Cui, B.; Sun, H.; Xu, Y.; Duan, L.; Li, Y.-M. *Tetrahedron* **2017,** *73,* 6754–6762. doi:10.1016/j.tet.2017.10.021
72. Kadoh, Y.; Tashiro, M.; Oisaki, K.; Kanai, M. *Adv. Synth. Catal.* **2015,** *357,* 2193–2198. doi:10.1002/adsc.201500131
73. Jiang, X.-D.; Matsukawa, S.; Kakuda, K.-i.; Fukuzaki, Y.; Zhao, W.-L.; Li, L.-S.; Shen, H.-B.; Kojima, S.; Yamamoto, Y. *Dalton Trans.* **2010,** *39,* 9823–9829. doi:10.1039/c0dt00539h
74. Tang, S.; Zhao, H. *RSC Adv.* **2014,** *4,* 11251–11287. doi:10.1039/c3ra47191h

License and Terms

This is an Open Access article under the terms of the Creative Commons Attribution License (https://creativecommons.org/licenses/by/4.0). Please note that the reuse, redistribution and reproduction in particular requires that the author(s) and source are credited and that individual graphics may be subject to special legal provisions.

The license is subject to the *Beilstein Journal of Organic Chemistry* terms and conditions: (https://www.beilstein-journals.org/bjoc/terms)

The definitive version of this article is the electronic one which can be found at: https://doi.org/10.3762/bjoc.17.39

BEILSTEIN JOURNAL OF ORGANIC CHEMISTRY

Biochemistry of fluoroprolines: the prospect of making fluorine a bioelement

Vladimir Kubyshkin[*1], Rebecca Davis[1] and Nediljko Budisa[*1,2]

Review

Open Access

Address:
[1]Department of Chemistry, University of Manitoba, 144 Dysart Rd., Winnipeg, R3T 2N2, Canada and [2]Institute of Chemistry, Technical University of Berlin, Müller-Breslau-Str. 10, 10623 Berlin, Germany

Email:
Vladimir Kubyshkin[*] - vladimir.kubyshkin@umanitoba.ca;
Nediljko Budisa[*] - nediljko.budisa@umanitoba.ca

* Corresponding author

Keywords:
amino acids; evolution; fluorine; proline; proteins

Beilstein J. Org. Chem. **2021,** *17,* 439–460.
https://doi.org/10.3762/bjoc.17.40

Received: 05 November 2020
Accepted: 22 January 2021
Published: 15 February 2021

This article is part of the thematic issue "Organo-fluorine chemistry V".

Guest Editor: D. O'Hagan

© 2021 Kubyshkin et al.; licensee Beilstein-Institut.
License and terms: see end of document.

Abstract

Due to the heterocyclic structure and distinct conformational profile, proline is unique in the repertoire of the 20 amino acids coded into proteins. Here, we summarize the biochemical work on the replacement of proline with (4*R*)- and (4*S*)-fluoroproline as well as 4,4-difluoroproline in proteins done mainly in the last two decades. We first recapitulate the complex position and biochemical fate of proline in the biochemistry of a cell, discuss the physicochemical properties of fluoroprolines, and overview the attempts to use these amino acids as proline replacements in studies of protein production and folding. Fluorinated proline replacements are able to elevate the protein expression speed and yields and improve the thermodynamic and kinetic folding profiles of individual proteins. In this context, fluoroprolines can be viewed as useful tools in the biotechnological toolbox. As a prospect, we envision that proteome-wide proline-to-fluoroproline substitutions could be possible. We suggest a hypothetical scenario for the use of laboratory evolutionary methods with fluoroprolines as a suitable vehicle to introduce fluorine into living cells. This approach may enable creation of synthetic cells endowed with artificial biodiversity, containing fluorine as a bioelement.

Introduction

Nature employs a rather small set of chemical elements for constructing the core biochemical makeup. Most elements of the periodic table are excluded from the biochemical world. Not surprisingly, researches have been intrigued by an idea to introduce certain elements into biochemical schemes artificially. Of the many possible elements to introduce, fluorine is arguably the most suited for being used as an artificial bioelement [1]. Organofluorine chemistry is very diverse, and many organofluorine compounds are compatible with biochemical settings [2,3]. In addition, a number of organofluorine compounds occur in the metabolism of some niche organisms [4-7].

Proteins are key molecular entities acting in cellular processes, and they serve for numerous biochemical functions, such as structural, catalytic, energetic, and transport. The introduction of organofluorine components into proteins is typically

expected to alter their structure, stability and/or specific features associated with their functional roles [8-11]. The replacement of natural amino acid residues with the ones containing fluorine have been particularly well characterized for their use as spectroscopic probes, mainly in ^{19}F NMR applications [12-15]. It is typical that the incorporation of fluorine into certain molecular fragments changes the local polarity as well as the electronic and conformational properties. These factors may translate into an altered structure and stability of a protein containing a fluorinated fragment. What consequences fluorination would have regarding the fitness and survival of the organism relying on fluorine-containing proteins remains an open question.

In this context, the substitution of the proline residue with fluorinated analogues (fluoroprolines, Figure 1) creates an option for making fluorine a component of a living organism. Fluoroprolines were found to be generally compatible with the cellular machinery, in particular the one that transports them inside the cells and incorporates them into proteins [16]. The effects of fluoroprolines have been examined in a number of protein structures. These studies demonstrated an altered stability and altered folding kinetics that occurred upon the proline-to-fluoroproline replacement, as reviewed in [17]. Nonetheless, no whole-cell adaptation to fluoroprolines has been accomplished to date. This critical review aims to assess the potential of fluoroprolines to affect the biochemical composition of microbial organisms, with the focus on *Escherichia coli* (*E. coli*). In our analysis, we will recapitulate the canonical functions of proline in cellular biochemistry and the potential of fluoroprolines to fulfill them. Here, by fluoroprolines, we will only refer to 4-monofluoroprolines and 4,4-difluoroproline, which are the best biochemically characterized proline analogues (Figure 1). Many other fluorinated proline analogues exist, as summarized elsewhere [18,19]. They are not included in this review due to a scarcity of biochemical studies.

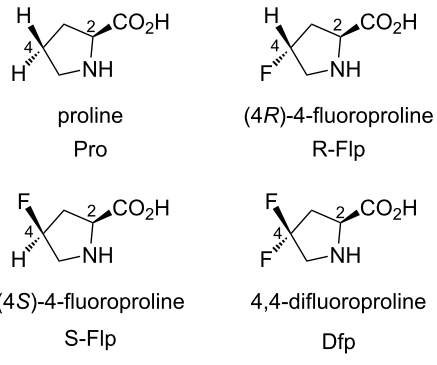

Figure 1: The structures of the fluoroprolines discussed herein.

Review

1 The special role of proline in proteins

In accord with contemporary evolution theories, a primitive proteome of protocells is thought to have developed from a small set of amino acids, with proline generally being among the first structures in this list [20]. It is possible that the initial role of proline was metabolic or based on its organocatalytic features that were essential for the development of primitive molecular life [21]. Furthermore, such an evolution model suggests that the first protein-biosynthesis-generated structures are based on variable backbone elements; proline (cyclic and chiral), glycine (acyclic and achiral) or alanine (acyclic and chiral). Subsequent acquisition of the functional side-chains for this repertoire led to the recruitment of amino acids that are essentially derived from alanine, leading to the α-helix-dominated protein world as we know it [22]. For this reason, most amino acids in proteins can be exchanged for alanine by point mutations while leaving the secondary structure intact. In molecular biology, the alanine scanning method takes advantage of the fact that alanine mimics the secondary structure preferences of most proteinogenic amino acids, allowing the relative importance of each side chain for the biological function to be determined [23]. Classical X-ray crystallography also employs the polyalanine model for backbone chain tracing to elucidate three-dimensional structures of proteins.

However, the substitution of proline by one of the remaining 19 coded amino acids can be harmful to protein folding and the functional properties. This is usually explained by the absence of the amide hydrogen atom and the cyclic nature of the proline ring, which exhibits a distinct conformational profile [24]. These are the general reasons why proline is poorly compatible with regular α-helical and β-sheet structure architectures, which are typical for the polyalanine backbone. Consequently, proline often identifies secondary structure breaks in protein sequences (Figure 2A and Figure 2B). This way of reasoning makes proline (as well as glycine) a kind of foreign structural element in the predominantly alanine-based protein architectures, or in other words, it is an alien in the “alanine world”.

How could proline be replaced in protein structures of living organisms? In protein evolution, mutations obey a simple "similar replaces similar" rule since the disruption of the resulting protein structure is minimized by the modest changes in the amino acid backbone. Hence, when global substitution of proline is aimed at, it should possibly be ascribed to its analogous structures. Most typical among proline analogues would be hydroxy-, fluoro-, alkyl-, dehydroprolines, analogues having ring size variations, and *N*-alkylamino acids (Figure 2C). To clearly discriminate the alanine and proline-based architectures, we recently proposed to call this set of structures the “proline

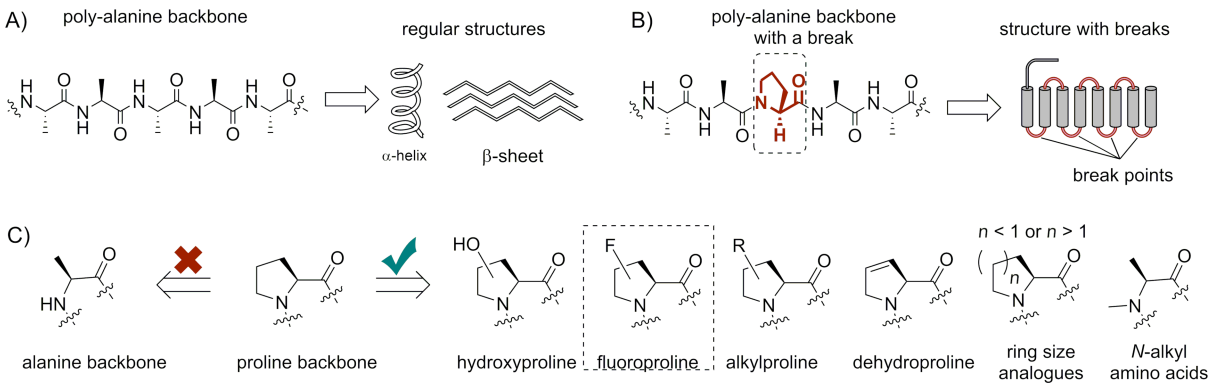

Figure 2: The distinction between "the alanine and the proline worlds". While the polyalanine backbone leads to the formation of regular secondary structures (A), proline residues create breaks in it (B). C) The set of amino acids that are typically considered as proline analogues.

world" [25]. Pioneering experiments on the substitution of proline by fluorinated proline analogues in proteins date back to the 1960s [26-28]. These experiments were predominantly conducted to address the role of proline residue hydroxylation in collagen.

The conformational rigidity featured in proline residues as well as the high conformational stability of the *trans*- and *cis*-amide conformers assign proline another important structural role: the structure freezer. The incorporation of proline residues in connecting loops has been described as a general strategy towards the thermodynamic stabilization of proteins [29-31]. The regulation of the proline content in proteins is an evolutionary strategy for environmental adaptation in extremophilic organisms. Proline is of a higher abundance in the proteomes of thermophilic organisms (organisms living at a high temperature) and of a lower abundance in the proteomes of psychrophilic organisms (organisms living at a cold temperature) [32,33]. In this way, the proline residue content is utilized to balance out the environmental temperature conditions.

Due to the lack of the side-chain functional groups, posttranslational modifications of proline residues are sparse. The most common among them is hydroxylation at position 4 by molecular oxygen, which is mediated by prolyl-4-hydroxylase [34]. This process has a remarkable relevance in the stabilization of collagen in higher organisms [35]. The experimental expression of the hydroxylating enzyme in *E. coli* has been previously achieved [36,37]. Bacterial prolyl hydroxylases have been characterized, and they are able to oxidize proline and analogous structures in recombinantly expressed proteins [38]. Nonetheless, we are still missing evidences of natural posttranslational modifications of proline residues occurring in native *E. coli*.

2 Physicochemical properties of fluoroprolines

Organofluorine compounds have become very common in various medicinal chemistry applications due to a number of special features [39,40]. Perhaps, the most notable trait among them is their stability. The carbon–fluorine bond is one of the strongest covalent bonds, and this is the strongest single bond that carbon can make. This is why molecular fragments that contain isolated C–F bonds appear inert under biochemically relevant conditions (Notwithstanding exceptions [41]). Fluoroprolines can be easily handled both as free amino acids and as residues in peptides and proteins. Nonetheless, when compared to the parent proline structure, fluoroprolines possess a number of altered properties. Some properties of the amino acids in common model compounds are summarized in Table 1 and will be discussed below.

2.1 Molecular size

Replacing hydrogen with fluorine increases the molecular size of congeneric molecules. The molecular volume increases gradually in the row: Pro < Flp < Dfp. However, compared to other amino acid size differences, this increase appears to be quite unspectacular (Figure 3). For example, the volume difference between Pro and Dfp is smaller than the difference between Val and Ile. It is therefore not surprising that Flp and Dfp can in principle be recognized as proline by natural enzyme binding pockets. The successful experimental incorporation of fluoroprolines into proteins based on the recognition of fluoroprolines by the native enzyme aminoacyl-tRNA synthetase (vide infra) proves this assumption.

2.2 Local polarity

Another important feature of fluoroprolines is their local electrostatic potential (local polarity). In proline, position 4 contains

Table 1: Summarized molecular features of the methyl esters of *N*-acetylamino acids as model compounds.[a]

entry	compound	COSMO volume (in water), Å^3	surface electrostatic potential at C^4	log*P*	preferred C^4-pucker	amide bond		
						$K_{trans/cis}$ (in water, 25 °C)	$k_{cis\text{-}to\text{-}trans}$ (in water, 37 °C), s^{-1}	$k_{trans\text{-}to\text{-}cis}$ (in water, 37 °C), s^{-1}
Pro	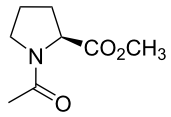	214	positive	−0.44 ± 0.05	*endo*/*exo* mix	4.95 ± 0.05	0.033 ± 0.002	0.0070 ± 0.0005
R-Flp	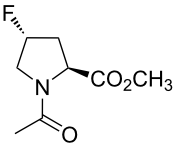	222	positive and negative	−0.66 ± 0.03	*exo*	7.16 ± 0.31	0.087 ± 0.009	0.012 ± 0.002
S-Flp	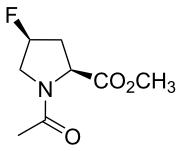	221	negative and positive	−0.84 ± 0.05	*endo*	2.62 ± 0.07	0.041 ± 0.004	0.016 ± 0.002
Dfp	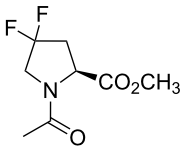	230	negative	−0.29 ± 0.04	*endo*/*exo* mix	3.49 ± 0.11	0.163 ± 0.016	0.049 ± 0.003

[a]See references [16,19,51,52,55] for details.

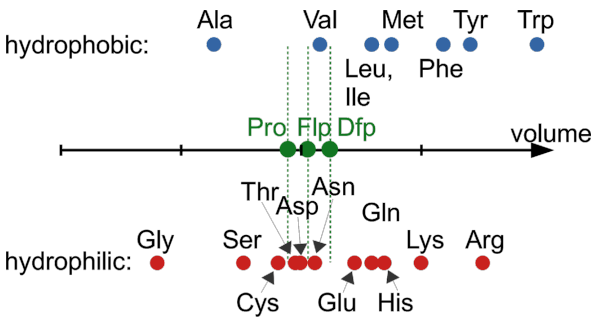

Figure 3: Molecular volume for 20 coded amino acids and fluoroprolines. The COSMO volume was calculated for aqueous solutions of free amino acids. The amino acids are classified as hydrophobic or hydrophilic according to their side chains. The scale is 50–250 Å^3, with the tick step of 50 Å^3.

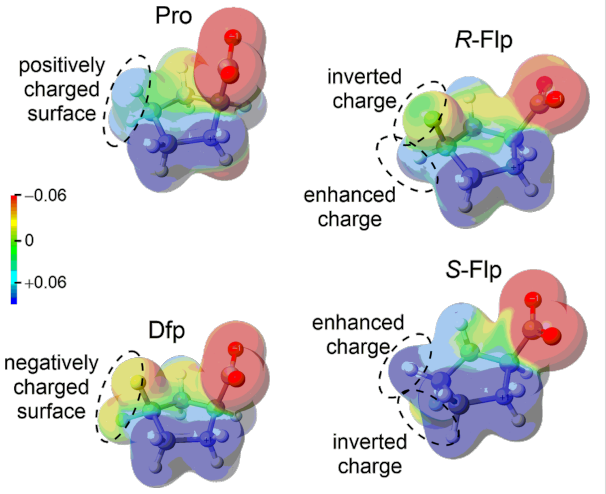

Figure 4: Comparative analysis of the electrostatic potential for proline and fluoroprolines (electrostatic potential on the van der Waals surface).

a positive surface potential due to the hydrogen atoms at the exterior (Figure 4). This local charge plays an important role in the interaction of proline with the environment in a protein. For example, when a side chain of an aromatic residue docks onto the proline residue, they engage in a donor–acceptor interaction, while the aliphatic C–H bonds of the proline ring serve as electron acceptors. This phenomenon is known as the aromatic-proline motif [42,43]. The substitution of a hydrogen atom at position 4 by fluorine inverts the sign of the potential. The fluorine atom creates a surface that is negatively charged, while the remaining C–H bond in Flp acquires an enhanced positive

charge due to the electron-withdrawing effect of fluorine. Based on these considerations, a fluoroproline–aromatic-system interaction has been previously utilized in the engineering of a few peptide therapeutics [44,45].

2.3 Lipophilicity

The impact of fluorine substitution on the global polarity of the molecule is another parameter that should be considered. The global polarity can be typically analyzed by measurements of the molecular partitioning, e.g., the lipophilicity index log*P*. For aliphatic organofluorine compounds, this parameter takes into account the polarity of the carbon–fluorine bond, the combination of dipoles within the molecule, and the molecular volume [46,47]. The experimental log*P* values demonstrate that the monofluoroprolines *R*-Flp and *S*-Flp are slightly less lipophilic, while Dfp is slightly more lipophilic compared to proline (Figure 5) [19]. Although, the difference is small, it may have an impact on the overall features of the peptides and proteins that rely on polarity.

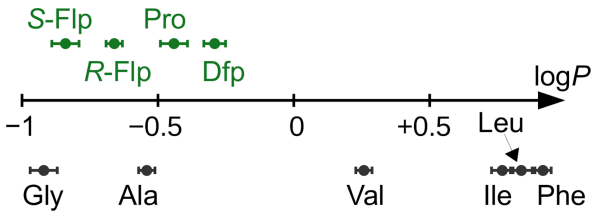

Figure 5: Experimental log*P* data for methyl esters of *N*-acetylamino acids.

2.4 Proline puckering

In addition to the general impact of fluorination, there are some properties specifically attributed to the proline residue that appear altered in fluoroprolines. The first one to mention is the conformation of the pyrrolidine ring, which exhibits a dynamic transition between several distinct states in a relatively fast kinetic mode (roughly on a GHz scale) [48,49]. For simplicity, two conformations are considered most commonly, usually called C^4-puckers. In the *endo*-pucker, the carbon atom C^4 is displaced from the ring plane towards the carboxylate group, while in the *exo*-pucker, it is displaced in the opposite direction (Figure 6). Although, this may look like a mere side-chain conformation transition, this has a remarkable relevance. In principle, the whole pyrrolidine ring is conjunct with the backbone, and thus there is no conformational transition that would occur separately in the backbone and in the side chain; both should occur at the same time. In this way, the pucker influences the backbone folding, thereby stabilizing or destabilizing particular secondary structure folds.

Fluorination creates a pucker bias due to orbital interactions of the carbon–fluorine bond within the molecule, known as the *gauche*-effect [50]. The parent proline structure has a negligible energetic difference between the conformations. However, *R*-Flp stabilizes the C^4-*exo*-pucker, while *S*-Flp stabilizes the C^4-*endo* system [51]. It is believed that Dfp has no conformational preference akin to proline [52]. The stabilization of the puckers is one of the most prominent features of fluoroprolines that justifies their use in protein engineering. The "freezing" of certain proline pucker conformations due to stereospecific fluorination has an effect on the packing within a protein structure as well as the backbone folding parameters (vide infra).

2.5 Thermodynamics of the amide rotation

Another special feature of proline is the comparatively similar intrinsic stability of the amide rotamers in the peptidyl-prolyl fragments. Usually, a peptide bond exhibits a high preference

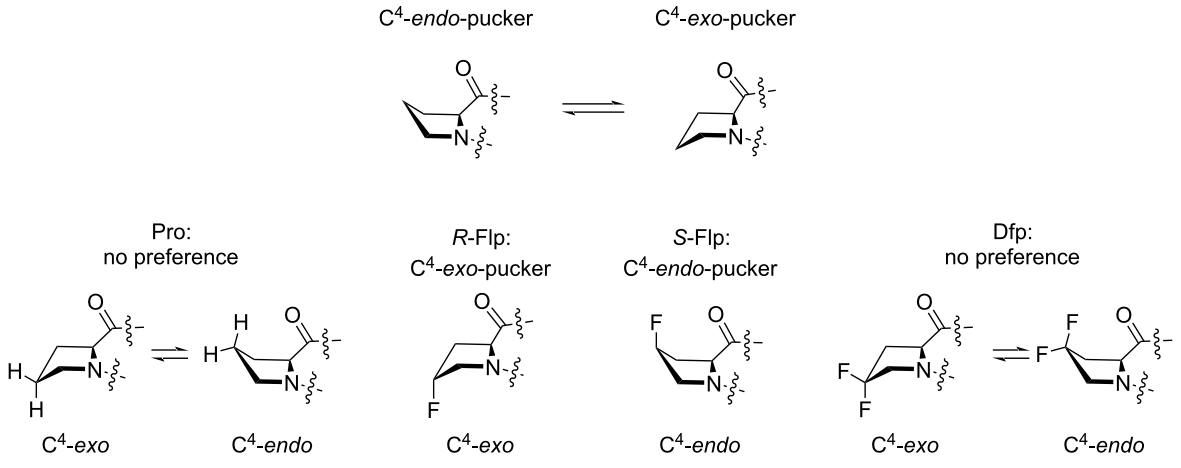

Figure 6: The conformational dependence of the proline ring on the fluorination at position 4.

towards the *trans*-amide, represented by a dihedral angle ω of 180°. In peptidyl-prolyl, however, *trans*- and *cis*-conformations (ω = 180° and 0°, respectively) are of comparatively similar stability, while the *trans*-amide is more stable (Figure 7) [53]. In a folded protein, the overall conformation dictates the amide rotation state. Nonetheless, when the protein is unfolded, the *trans*/*cis* isomerism can create numerous subpopulations, and the resulting heterogeneity can markedly complicate folding. In addition, the stability of the amide bonds translates into the thermodynamic stability of the protein structures by altering the free energy of folding.

Fluoroprolines alter the relative thermodynamic stability of the amide conformers. Compared to proline, *R*-Flp provides a higher stability to the *trans*-conformer, while the *S*-Flp increases the stability of the *cis*-amide. The relative stabilization is usually about 1–2 kJ·mol^{-1} when measured for the typical model compounds. Dfp exhibits a relatively weak destabilization of the *trans*-amide [16,52]. These energetic preferences should be considered when judging the stability of the folded structures containing fluoroprolines.

2.6 Kinetics of the amide rotation

The kinetic stability of the amide conformers generates another important aspect of protein folding. Generally, the amide rotation is considered very slow in biochemical settings [54]. The process becomes slightly faster when proline is replaced by fluorinated analogues. The acceleration occurs due to the electron-withdrawing effect of the fluorine atoms. According to the data for the model compounds in water [16,19], the *cis*-to-*trans* rotation velocity increases in the order Pro < *S*-Flp < *R*-Flp < Dfp. For the opposite process, the *trans*-to-*cis* rotation, the order is slightly different; Pro < *R*-Flp < *S*-Flp < Dfp (Figure 7). The process typically occurs in a mHz kinetic mode, as measured with the model compounds [16,19,55]. Environmental factors can change the velocity as well. For example, in the nonpolar environment of a protein interior or a hydrophobic pocket of a chaperone, the process may occur much faster [53]. Some protein sequences require the action of peptidyl-prolyl *cis*/*trans* isomerases, natural enzymes meant to facilitate the amide rotation around peptidyl-prolyl [56]. Some other common factors, such as the pH value or the ionic strength, are believed to have a very minor, if any, influence [53]. The enhancement of the amide rotation rate by fluoroprolines can have an effect on the overall protein folding velocity. An impairment of the folding kinetic pathways can also lead to aggregation and misfolding issues, affecting the protein production.

2.7 Other properties

The acid–base transitions also appear altered in fluoroprolines primarily due to the electron-withdrawing effect of the fluorine atoms (Table 2) [16,19,55,57,58]. This effect may potentially influence the properties of proteins carrying terminal proline residues [59].

3 Proline uptake and metabolism

As the simplest and most basic set of structures, amino acids are involved in numerous biochemical processes in cells (Figure 8). The amino acid uptake and metabolism systems establish the concentration of the amino acid in the cells. The intracellular concentration enables the involvement of the amino acid in various cellular processes, and it reflects the cellular life cycle as well as the environmental perturbations, including starvation, oxygenation, osmolarity changes and other types of stress. For example, in exponentially growing *E. coli*, the intracellular concentration of proline was determined as 3.9×10^{-4} mol·L^{-1}. This data ranks proline as the 41st in the list of metabolites and as the 9th among the amino acids coded into proteins [60].

The two main pathways for proline biosynthesis involve the synthesis from either glutamate or ornithine [61]. Both sources of amino acids are derived from the core metabolic processes. The connection to the central metabolism makes it difficult to make interventions in the production of proline in the cells. For example, in order to create an organism that fully lacks the ability to synthesize proline (which is called a proline auxotrophic strain), one should delete or inactivate genes involved in the metabolism of ornithine and glutamate. As the result, this may lead to an unnecessary accumulation of other amino acids and their metabolic derivatives, which may impact

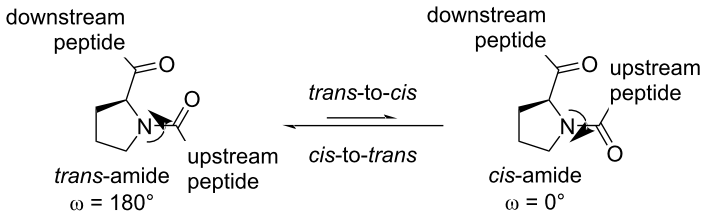

Figure 7: Rotation around the peptidyl-prolyl fragments in polypeptide structures is important for correct overall folding.

Table 2: Acid–base transitions in fluoroprolines.[a]

	ammonium moiety		carboxylic acid moiety			
			cis-amide conformation		*trans*-amide conformation	
entry	structure	pK_a	structure	pK_a	structure	pK_a
Pro	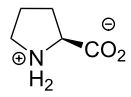	10.68	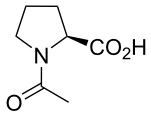	2.85	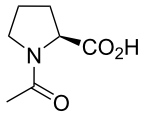	3.55
R-Flp	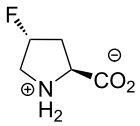	9.10	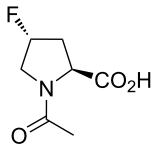	2.37	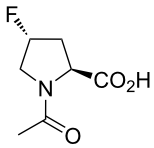	3.19
S-Flp	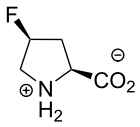	9.10	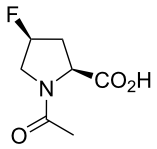	2.87	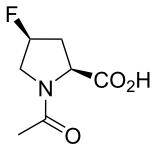	3.39
Dfp	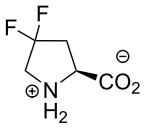	7.15	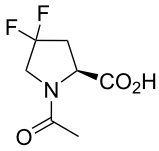	2.34	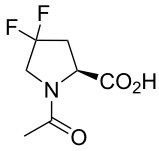	2.93

[a]Determined in aqueous solution at 298 K. The error for the pK_a value is ±0.10 for the ammonium group and ±0.05 for the carboxylic acid group. For details see references [16,19,57,58].

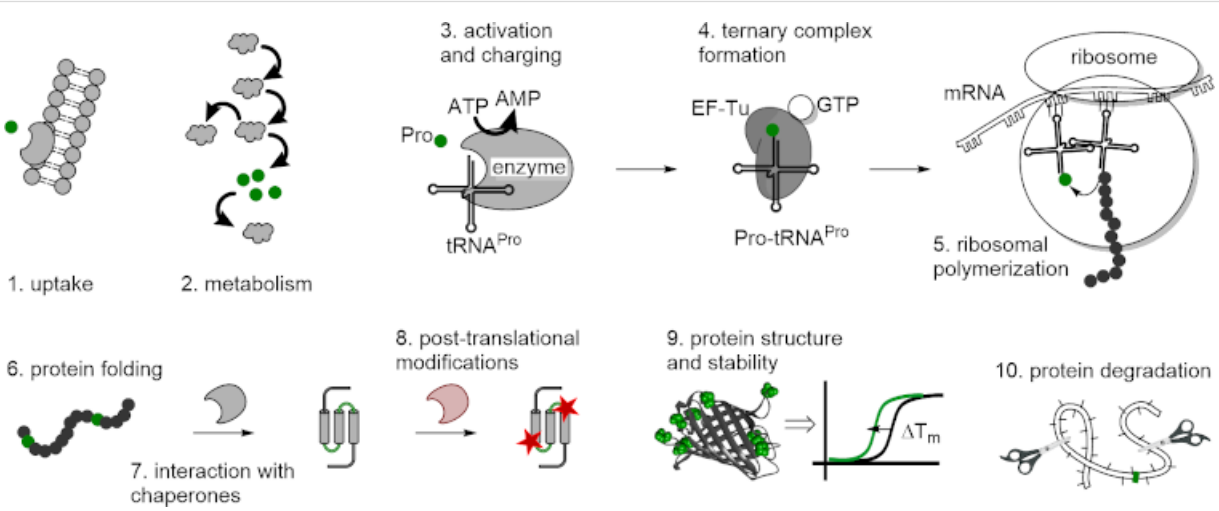

Figure 8: The complex fate of a protein-encoded amino acid in the cell (EF-Tu – elongation factor thermo unstable).

cellular homeostasis. In addition, proline metabolism is related to stress response and scavenging of reactive oxygen species in many organisms [62].

In *E. coli*, the main path for proline synthesis starts from glutamate, which is phosphorylated by the action of glutamate 5-kinase (enzyme proB, Figure 9A). The resulting intermediate undergoes reduction into glutamate semialdehyde via the action of the γ-glutamyl phosphate reductase proA. The semialdehyde then undergoes spontaneous cyclization to form 1-pyrroline-5-carboxylate. In the final step, 1-pyrroline-5-carboxylate is reduced via the action of the pyrroline-5-carboxylate reductase

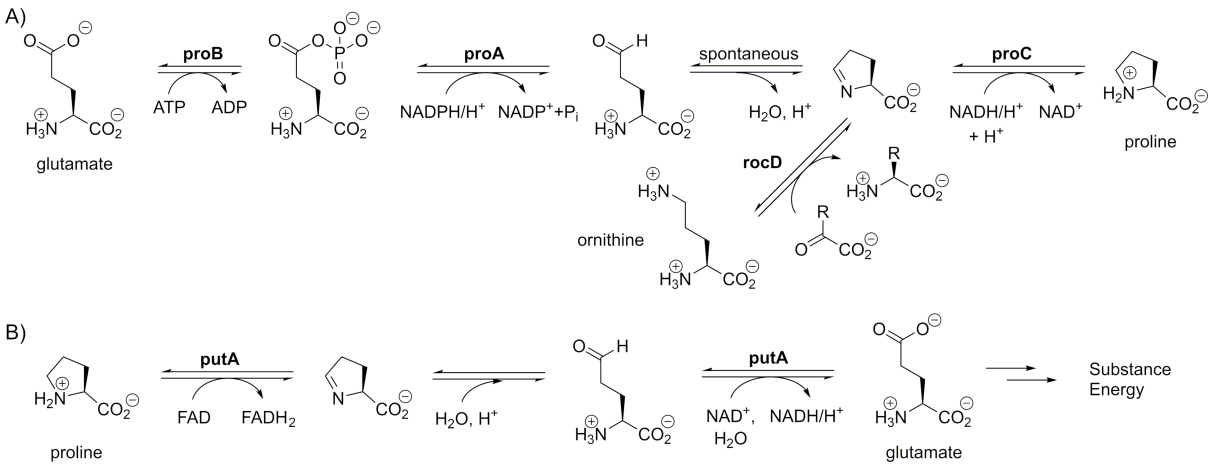

Figure 9: Metabolic routes for proline in *E. coli*. A) Synthesis of proline and B) degradation of proline.

proC, generating proline. Alternatively, glutamate semialdehyde can be created from ornithine via the action of a pyridoxal phosphate-dependent enzyme, the ornithine-oxo-acid aminotransferase rocD. Very recently, some fluorinated proline analogues were prepared via a chemoenzymatic transformation using the leucine hydroxylase griE [63,64].

In addition to the biosynthetic schemes, proline can be supplied to cells exogenously and taken up by specific permeases. Proline uptake serves two general functions: 1) the utilization of proline as a nutrient and 2) the uptake of proline in response to osmotic stress. The proline/sodium symporter putP is a transporter system that pumps proline into the cells, together with sodium ions. It is present in various organisms (including *E. coli*) and mainly supplies proline as an external nutrient [65]. Another important transport system is the ATP-binding proline/betaine transporter. In *E. coli*, this permease activates in the course of osmotic shock response, represented by the transporter gene *proP* and the *proU* operon. The genes *proV* (encoding an ATP-binding protein) and *proW* (encoding a permease) as well as *proX* (encoding a periplasmic protein) are located on the *proU* operon. The proline/betaine transporters accumulate proline and various other substrates inside the cells under high external salinity. They are tolerant to the transport of proline analogues, such as pipecolic acid [66].

In *E. coli*, the catabolism of proline occurs via the action of the bifunctional enzyme putA (Figure 9B) [67]. It sequentially degrades proline to glutamate, which can be later deaminated to an essential metabolite, α-ketoglutarate, with many metabolic options, such as an entry into the citric acid cycle. The dehydrogenation of proline is involved in numerous biochemical processes. For example, the dehydrogenation of proline linked to an acyl carrier protein makes a first step in the biosynthesis of some neurotoxins from cyanobacteria (*ana* gene cluster) [68]. The catabolic degradation of proline plays an important role in the development of cancer cells, making the inhibition of the proline dehydrogenase a promising method in cancer therapy [69,70]. There is no information on a possible intracellular degradation of fluoroprolines, although, they are included in some therapeutic dehydrogenase inhibition schemes [71]. Conversely, there is strong evidence that other proline analogues, dehydroproline and thiaproline, are oxidatively degraded in *E. coli* by the action of the bifunctional enzyme putA and the reductase proC [72]. Future research should examine whether fluoroprolines are metabolically inert substrates capable of accumulating at a high level in the cells without causing significant disturbances in the physiology of the host microbial organism.

The transport and metabolism of proline are important factors that should be considered in engineering bacterial strains capable of incorporating proline analogues into proteins. In order to express protein-containing fluoroprolines, one should take a strain that is unable to produce the original substrate–proline. Proline auxotrophic strains are typically produced by the deletion of the genes responsible for proline biosynthesis (Figure 9A). However, some strains, such as *E. coli* JM83, are known to be readily proline auxotrophic [73], and thus can be subjected for the expression of proteins with exogenously supplied fluoroprolines [74]. Experiments demonstrated that the intracellular accumulation of fluoroprolines from the medium can occur without additional manipulations. For some analogues, an osmotic shock triggers the uptake and accumulation of proline substitutes into the cells. Gruskin and co-workers successfully demonstrated the incorporation of hydroxyproline into recombinant proteins in proline auxotrophic *E. coli* in media with hyperosmotic sodium chloride concentrations [75]. To obtain high in vivo concentrations of the proline analogue,

they took advantage of the phenomenon that proline and similar solutes actively accumulate in cells in response to the hyperosmotic shock in bacteria [76]. This enabled *E. coli* to accumulate proline substitutes in hyperosmotic media (e.g., with 0.6 M sodium chloride) and provided a sufficient intracellular concentration of the analogue loaded onto $tRNA^{Pro}$ to support protein synthesis. The relevance of this scheme towards the intracellular accumulation of fluoroprolines still remains questionable.

4 Fluoroprolines in protein biosynthesis

In the genetic code, proline is assigned to four codons within the CC codon block: CCU, CCA, CCG and CCC. The entire genome of *E. coli* (strain MG1655) contains 59905 proline codons, whereby the CCC is rarely used (7401 occurrences), in contrast to most abundant CCG codons (31603 occurrences) [77].

The incorporation of proline into proteins is accomplished by the natural biosynthetic machinery via a complex stepwise process (see steps 3–5 in Figure 8). The initial recognition of any amino acid that participates in protein biosynthesis occurs in an enzyme called aminoacyl-tRNA synthetase (AARS). An AARS usually performs several sequential steps (Figure 10A). First, an amino acid that fits into the binding pocket reacts with

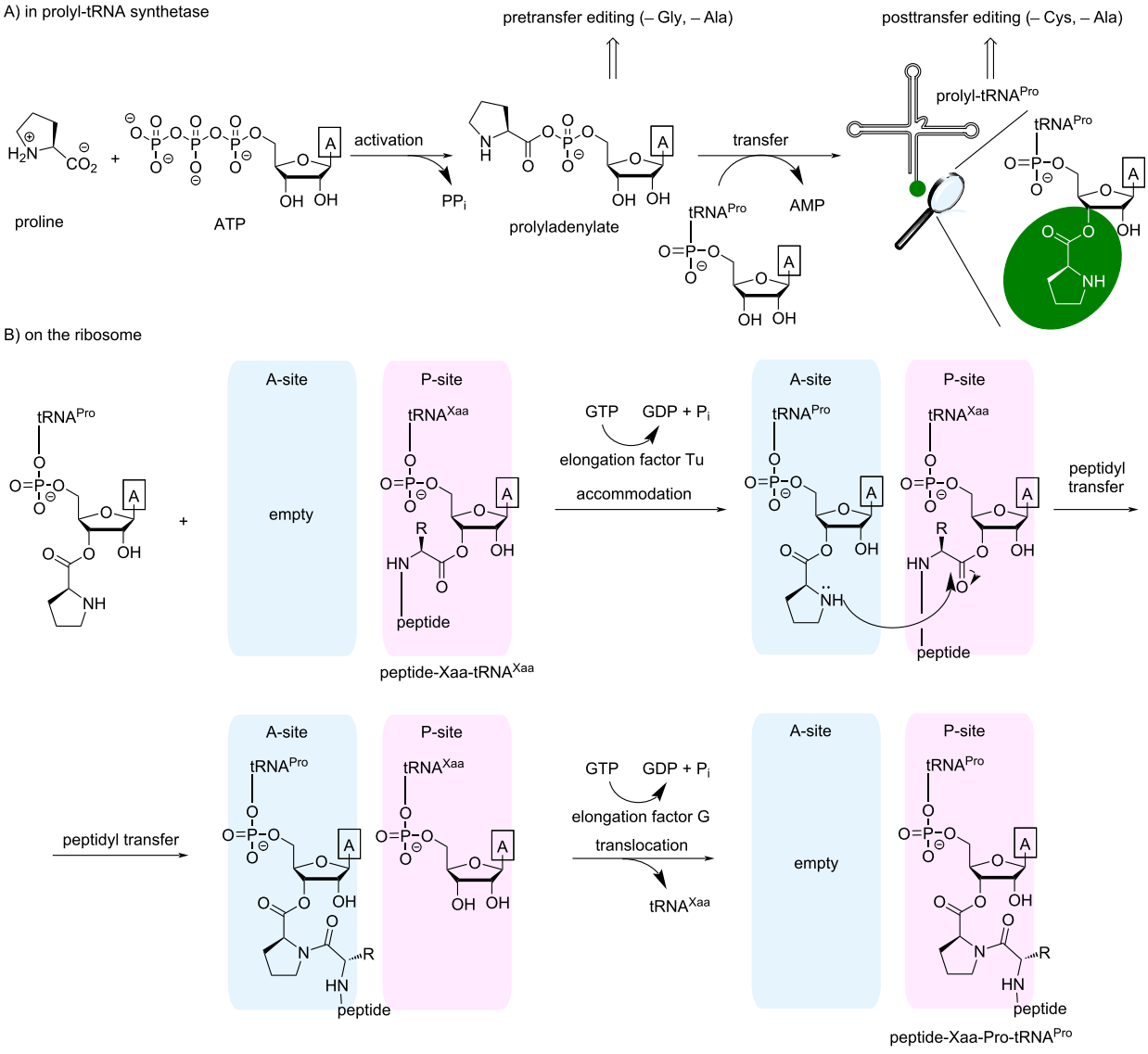

Figure 10: A complete flowchart for the proline incorporation into proteins during ribosomal biosynthesis. A) Activation and loading (charging) of an amino acid onto the $tRNA^{Pro}$. B) The ribosomal cycle. A framed "A" identifies an adenine moiety. The A- and P-sites are the aminoacyl- and peptidyl-tRNA ribosome binding sites, respectively. The exit site (E-site) is not mentioned.

a molecule of ATP creating an aminoacyl adenylate. This step is called activation. An aminoacyl adenylate is a mixed anhydride, and therefore it is a highly reactive species, which quickly undergoes further transformation. In the subsequent step, the aminoacyl adenylate reacts with the CCA 3'-end element of bound tRNA, thereby creating an ester bond with the cognate tRNA. The *E. coli* genome contains three $tRNA^{Pro}$ entities, having the anticodons CGG (recognizes CCG codon), GGG (recognizes CCC and CCU codons) and UGG (recognizes CCA, CCU and CCG codons). This set of $tRNA^{Pro}$ exhibits an average level of charging compared to other tRNAs from *E. coli* [78].

Prolyl-tRNA synthetase (ProRS) belongs to a class IIa AARSs. In addition to the main activation and charging steps described above, the bacterial ProRS (gene *proS*) performs a few additional proofreading steps. Alanine and glycine are amino acids smaller than proline but with a similar polarity, and they can be activated by ProRS. If this happens, aminoacyl adenylate is released from the enzyme to be hydrolyzed by water. This process is called pretransfer editing. Cysteine is an amino acid that has a similar molecular volume to proline, and therefore cysteine can undergo activation and transfer by ProRS. To correct for this error, the transfer step is followed by the swinging of the charged tRNA to another pocket that is meant for the recognition of Cys-$tRNA^{Pro}$ (the yeaK editing domain). If the amino acid is correct, the charged tRNA is released from the enzyme, and if cysteine is loaded on it, it is hydrolyzed. This process is called posttransfer editing step. There is also alanine posttransfer editing [79,80]. In *E. coli*, both pre- and posttransfer editing occur in ProRS. They only discriminate against substrates that are smaller than proline, whereas fluoroprolines are slightly larger than proline by volume (Figure 3). The ability of fluoroprolines to fit into the proline activation pocket and to avoid editing enables the use of natural ProRS for the incorporation of these substrates into proteins in place of proline. The enzyme accepts the substrate that is available; preferably proline, if it is present in the cells, and fluoroprolines once proline is depleted.

In general, amino acid analogues are less suitable for natural AARSs than their canonical substrates. Therefore, the intracellular concentration of an analogue should be high enough to promote the misacylation of cognate $tRNA^{Pro}$. Another strategy towards the accumulation of the charged tRNA is to increase the genomic background activity of the ProRS by plasmid-directed coexpression of the native or mutant enzyme by a strong promoter during the incorporation experiment. Early experiments demonstrated sufficient activation of fluoroprolines by ProRS [81]. Conticello et al. reported that the native genomic background activity of ProRS was sufficient to load fluoroprolines to $tRNA^{Pro}$ with a similar efficiency as proline [82]. A docking study showed that the binding of fluoroprolines to the ProRS from *E. coli* occurs in a similar fashion and with similar binding energy to that of the native substrate, proline [83].

After being released from ProRS, the charged Pro-$tRNA^{Pro}$ binds to the elongation factor Tu, which also binds a molecule of guanosine triphosphate (GTP). The resulting complex (known as the ternary complex) docks to an empty A-site of a translating ribosome (Figure 10B). If the mRNA codon matches the anticodon of the $tRNA^{Pro}$, GTP undergoes hydrolysis, allowing the elongation factor Tu to leave the complex. This event is followed by the peptidyl transfer reaction, which forms a new peptide bond. Subsequently, the ribosome binds the elongation factor G carrying a molecule of GTP, the hydrolysis of which leads to a translocation event in which the empty tRNA leaves and peptidyl-tRNA moves to the P-site. The A-site remains empty, allowing the next ternary complexes to bind in response to the next codon in the mRNA sequence [84].

The translational incorporation of proline into proteins is a slow process when compared to other canonical substrates [85]. It has been shown that fluoroprolines, when used as proline substitutes, can substantially alter the velocity of translation. In a survey of proline analogues, it was found that *R*-Flp restores the reactivity of proline at the P-site to a level comparable to that of other coded amino acids (Figure 11) [57]. The enhance-

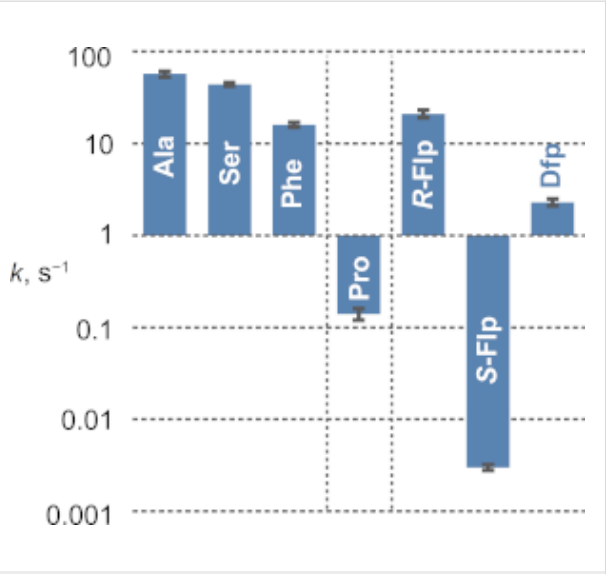

Figure 11: Amide bond formation capacities of fluoroprolines compared to some coded amino acids measured on ribosomes in an in vitro experimental setup. The rates of reaction between formyl-methionyl-aminoacyl-tRNA at the P-site and puromycin at the A-site of a translating ribosome (at 37 °C) were determined [57].

ment of the translation velocity was also observed for Dfp. For *S*-Flp, however, the reaction was substantially slowed down even compared to the native substrate proline. The origin of this effect is not fully clear. It might be linked to the electrophilicity of the carboxylic acid moiety that experiences an electron-withdrawing effects from the fluorine atom (see the comparison of the acidity in Table 2) [58].

In another study, $tRNA^{Pro}$ was preloaded with proline analogues, and a test sequence (formyl-Met-Lys-Lys-Lys-Xaa-Asp-Tyr-Lys-Asp-Asp-Asp-Asp-Lys-OH, Xaa = proline analogue) was expressed in an in vitro system. It was found that the yield of the target peptide increases in the order Pro ≈ *R*-Flp < *S*-Flp ≈ Dfp [86]. The origin of the effect is unclear. Nonetheless, these results show that *S*-Flp can actually produce better peptide yields compared to *R*-Flp, in spite of the poor translation velocity found in other experiments. Evidently, fluoroprolines are capable of producing spectacular changes in protein translation. Their elucidation might reveal unknown features of ribosomal translation that might be correlated to the physiochemical properties of fluoroprolines.

Where there are three or more consecutive prolines in the sequence, the ribosome stalls. The alleviation of the stalled ribosome occurs due to the action of elongation factor P, as was recently discovered independently by two groups [87,88]. Elongation factor P binds the exit site of the stalled ribosomes and recognizes specific identity elements of the $tRNA^{Pro}$ at the P-site [89]. The overall effect of elongation factor P binding is that it restricts the set of conformations available in the peptidyl transfer center, and this suppresses the entropic costs of the reaction [57,90]. It has been suggested that ribosome stalling has a regulatory function in protein production as about one third of the *E. coli* genome contains stalling-inducing oligoproline stretches [91]. In general, the translation of oligoproline- and proline-rich sequences has to cope with the inefficient accommodation of prolyl-tRNA, a slowed rate of peptide bond formation at proline residues [85], and collisions between the nascent polyproline chain and the exit tunnel, in particular the residue G2061 [90].

We and others investigated whether ribosome stalling can be mitigated by proline analogues. For example, in the case of three consecutive *R*-Flp or Dfp residues, stalling was nearly absent in an in vitro experiment, while *S*-Flp exhibited stronger stalling compared to the natural substrate proline [57]. The strong stalling induced by *S*-Flp may preclude the production of proteins with this substrate as the in vivo expression of enzymes with oligoproline stretches might be completely suppressed with this analogue (vide infra). Chin and co-workers reported the directed evolution on ribosomes that yielded a variant (dubbed as O-d2d8) with mutations in the peptidyl transferase center and exit tunnel, able to efficiently polymerize proline-rich sequences in the absence of elongation factor P [92]. It is possible to presume that such ribosome variants could reduce *S*-Flp-induced ribosome stalling, although experimental demonstration is lacking. From the reported data, it follows that *S*-Flp may enhance ribosomal synthesis when it is a single residue in a sequence, while in the case of consecutive proline residues, *R*-Flp is a substitute that is expected for best production.

The folding of the peptide chain to secondary structure elements starts immediately after the synthesis, inside the ribosome tunnel. The tunnel accommodates between 30 and 40 amino acid residues [93,94]. The trigger factor (gene *tig*) is a generic chaperone that facilitates the folding of the N-terminal protein section emerging from the ribosome [95]. The proline residue is associated with a dedicated set of chaperones called peptidyl-prolyl *cis*/*trans* isomerases (PPIases), which correct the *cis*–*trans* rotameric state of proline in the protein sequence [53,96]. *E. coli* carries a diverse set of the chaperones of this class (e.g., the genes *ppiA*, *ppiB*, *fkpA*, *fklB* and more), including periplasmic chaperones (e.g., gene *surA*). A previous study showed that the presence of *S*-Flp, *R*-Flp and Dfp in a protein sequence may alter the chaperone-mediated folding efficiency by orders of magnitude [97]. The putative reason for this is the difference in the polarity of fluoroproline-containing sites, which alters the accommodation of the protein in the chaperone pockets. Furthermore, the proline-to-fluoroproline replacement may generate disturbances in the protein structure and stability, as discussed in the next sections.

5 The structural contexts of fluoroprolines in proteins

As discussed in chapter 1, proline is generally poorly compatible with the common secondary structure context of alanine-based residues. Nonetheless, there are specific structural motifs that are more common for proline residues, i.e., representing the "proline world": the collagen helix, polyproline helix, turns, loops, and fragments lacking a persistent structure.

5.1 Collagen triple helix

Many studies reported the role of proline-to-fluoroproline replacement in the collagen helix. The collagen triple helix is a super-secondary structure featured by collagen, the protein that constitutes the extracellular matrix in higher animals. When introduced at a certain position in the structure, *R*-Flp and *S*-Flp exhibit prominent effects on the thermal stability of the protein. The effect originates from the stabilization of the pyrrolidine ring puckers, which has an effect on the packing of the triple helix [98]. The reader is referred to dedicated reviews on

collagen model studies that discuss the impact of fluoroprolines in more detail [35,99].

5.2 Polyproline-II helix

The polyproline-II (P_{II}) helix is a secondary structure that precedes the collagen helix in the folding hierarchy. It is a left-handed extended helix that attained its name from the original discovery in polymeric proline. The P_{II} helix occurs in various proteins, and it is particularly common in proline-rich sequence fragments [100]. Studies of oligomeric peptides showed that the replacement of proline with *R*-Flp exerts a stabilizing effect on the P_{II} helix formation, while *S*-Flp has an opposite, destabilizing effect [101,102].

Proline-rich sequences are common in SH3 binding domains of proteins. A study identified a minimal binding motif (peptide Pro-Pro-Pro-Leu-Pro-Pro-Lys-Pro-Lys-Phe) and demonstrated that the recognition occurs when the peptide is structured in the form of a P_{II} helix [103]. In spite of this fact, the replacement of proline with the P_{II}-stabilizing analogue *R*-Flp failed to improve the binding to SH3 [104,105]. These observations indicated that the polyproline binding is not only sensitive to the secondary structure adopted by the substrate, but an altered polarity and steric features of fluoroprolines should play a role.

Our recent study included the incorporation of fluoroprolines into the bacteriophage T4 fibritin C-terminal domain (foldon). The results showed that *S*-Flp and *R*-Flp exhibited opposite stability effects when incorporated at the positions Pro-4 and Pro-7, despite the fact that both residues are located in the N-terminal P_{II} helix. This result was interpreted by differences in the local polar interactions created by the carbon–fluorine bond within the interior of the foldon domain [106].

5.3 Turns and loops

Another structural context common for proline residues is turns. A peptidyl-prolyl in the *cis*-amide conformation is essential for the formation of type-VI β-turns [107]. Other types of β-turns also favor the presence of proline. A study of a model peptide (acetyl-Xaa-Gly-$NHCH_3$, Xaa = proline analogue) showed that type-I β-turns tolerate favored pucker conformations of both *R*-Flp and *S*-Flp. In contrast, type-II β-turns prefer the formation of the C^4-*exo*-pucker in both *R*-Flp and *S*-Flp residues, and thereby type-II β-turns experience stability changes from the intrinsic pucker biases exerted by fluoroprolines [108]. As a result, fluoroprolines could significantly impact the transition temperature in elastin-like sequences [108,109]. In ligand-gated ion channels, proline residues are involved in numerous loop positions as well as in the transmembrane helices, and the incorporation of fluoroprolines has shown distinct effects on their activity [110-113].

5.4 Intrinsically disordered proteins

Proline residues are overrepresented in proteins that are lacking persistent structures, known as intrinsically disordered proteins [114]. Here, proline acts with a dual role: 1) as a breaker, proline precludes the formation of regular secondary-structure motifs and 2) as a conformationally constrained residue, proline nucleates the formation of structures needed for binding with other proteins [115,116]. The potential role of fluoroprolines on the structural and functional features of intrinsically disordered proteins remains unclear.

6 Fluoroprolines in crystal structures of proteins

Several high-resolution crystal structures have been reported for proteins containing fluoroprolines. In a study of enhanced green fluorescent protein from *Aquorea victoria*, fluoroprolines were incorporated at ten proline positions [117]. The incorporation of *R*-Flp resulted in an insoluble protein, indicating associated folding issues. In contrast, the protein containing *S*-Flp produced a well-structured fluorescent protein, exhibiting faster folding kinetics and producing crystals suitable for diffraction. The structure (Figure 12A) displayed ten *S*-Flp residues: nine with a *trans*-amide and one with a *cis*-amide (position 89). With the exception of one residue (position 56), all pyrrolidine rings were found in a C^4-*endo*-pucker conformation. This result is consistent with the intrinsic *endo*-pucker bias of *S*-Flp (Figure 6), which appears reproduced in the complex protein structure.

A study of collagen mimetics demonstrated an elevated thermal stability for the collagen helix formed by repeating *R*-Flp-Gly-*S*-Mep units (where *S*-Mep is (4*S*)-methylproline) [118]. The collagen triple helix was found in the crystal structure of the protein (all residues were in the *trans*-amide conformation). The structure showed the *R*-Flp and *S*-Mep residues adopting *exo*- and *endo*-pucker conformations, respectively. This arrangement created a tight packing between the *R*-Flp and *S*-Mep side-chains, as shown in Figure 12B. The packing effect has an implication on the thermostability of the triple helix [35,98,99].

In another study, fluoroprolines were incorporated in KlenTag DNA polymerase from a thermophilic organism, *Thermus aquaticus* [119]. The expression of the target protein was only observed with *R*-Flp, but not with *S*-Flp. The protein containing *R*-Flp exhibited a slightly lowered stability compared to the parent enzyme. The crystal structure depicts *R*-Flp at 32 different positions (Figure 12C), including two proline residues forming *cis*-amide bonds (positions 300 and 579) and two oligoproline stretches (positions 300–302 and 368–369). A defined pucker could be observed clearly in 28 out of 32 residues; 26 residues out of this set were in the *exo*-pucker con-

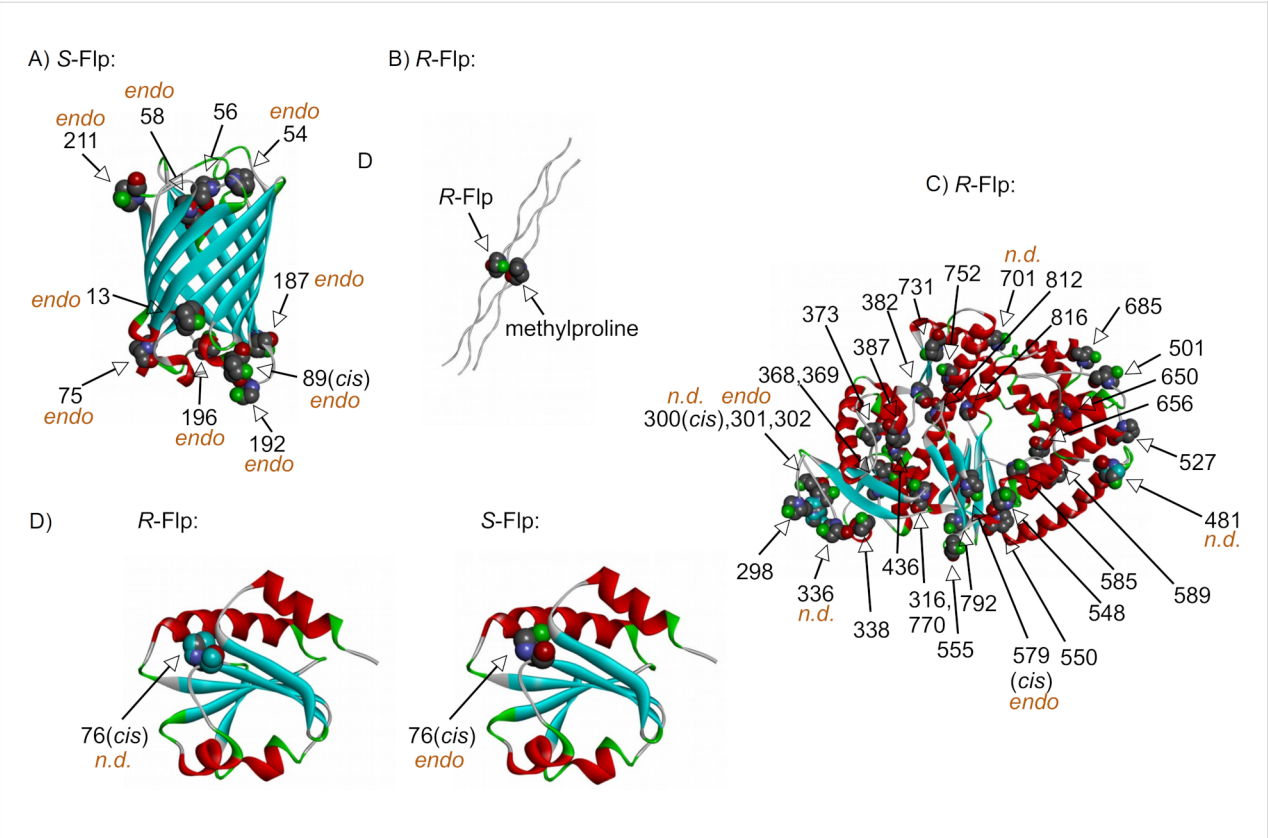

Figure 12: Ribbon representation of the X-ray crystal structures of proteins containing fluoroprolines. A) Enhanced green fluorescent protein (pdb: 2q6p), B) collagen mimicking model (pdb: 3ipn), only one fluoroproline residue is shown, C) KlenTag DNA polymerase (pdb: 4dle) and D) thioredoxin A (pdb: 4hua and 4hu9). All C^4-*endo*- and undefined puckers are labeled accordingly, assuming that the rest of the residues adopt the *exo*-pucker conformation. All *cis*-amide positions are labeled as well, assuming the default arrangement being *trans*.

formation. In contrast, the crystal structure of the wild-type protein showed 18 residues adopting single pucker conformations, and only 7 from this set were in the *exo*-pucker conformation. This observation showed that the preference of the *R*-Flp to adopt a C^4-*exo*-pucker conformation is retained in the protein structure. A defined side-chain conformation of the *R*-Flp-containing protein was proposed to be the reason for the ease of the protein crystallization. Finally, the study revealed a few polar interactions of the fluoropyrrolidine ring within the protein microenvironment.

In a study on thioredoxin, four out of five proline residues were mutated to alanine, and the only remaining proline residue was the one adopting a *cis*-amide-bond conformation (position 76) [120]. Both *S*-Flp and *R*-Flp were incorporated into the mutant. The resulting protein variant showed an elevated stability in the reduced, and a lowered stability in the oxidized form of the protein. Crystal structures of the proteins containing Pro, *S*-Flp and *R*-Flp at position 76 demonstrated their high similarity (Figure 12D). The variants containing Pro and *R*-Flp did not show a clearly defined pucker, whereas the variant with *S*-Flp was found in a single C^4-*endo*-pucker conformation.

Overall, the crystal structures illustrate that the pucker preference observed in small molecules (Figure 6) reoccurs in the protein structures, given that a statistically significant number of residues is analyzed. Nonetheless, in some individual cases, the native preference of a fluoroproline residue can be overridden due to the residue microenvironment and the overall packing of the protein structure.

7 The stability of proteins containing fluoroprolines

In the context of biochemical science, it is common to assume that structural changes and stability differences correlate with each other. For a protein, an overall sum of the secondary structures can be easily evaluated by chiroptic methods, such as circular dichroism, which assesses the backbone folding [121,122]. Changes in the denaturing conditions can be tracked by circular dichroism or fluorescence-based assays very easily. Alterations in the regular fold would usually be associated with alterations in the energy of the folding. These observations created a common conception that structure and stability experience the same trends. The less the structure is preserved, the less stable the folding of the protein is, and vice versa.

However, in proteins with fluorinated amino acids, structure and stability do not necessarily correlate, as demonstrated by studies on aromatic amino acids [123]. In fact, the survey of the crystal structures presented in chapter 6 demonstrates that the native backbone fold of the protein can remain unaltered, while associated biochemical assays may show notable differences in the thermodynamic stability of the fluoroproline-containing proteins. How could it happen that the stability is affected but the structure is not? First of all, in contract to classical mutations (e.g., the replacement of proline with serine), a substitution of an amino acid by a fluorinated analogue generates very little disturbance to the structure itself ("atomic mutations"). At the same time, it alters the conformational and polar features of the residues. For example, for fluoroprolines, there is an adaptive dynamic of the pucker in the pyrrolidine ring. One could expect, for instance, that a replacement amino acid would have to adopt an unfavorable conformation in order to fit to the overall structure (e.g., an *exo*-pucker conformation for *S*-Flp). Under these circumstances, the entire protein structure may be formed as expected; however, the replacement amino acid would strain the whole structure. Such a scenario would result in a lowering of the melting point and an elevated susceptibility of the structure towards denaturing agents. Thus, the stability will be impacted, while structure remains intact. For that reason, these two properties should be assessed separately when discussing fluoroprolines as well as other fluorinated amino acid substitutions [124-126].

As a matter of fact, most of the literature dealing with hydrogen-to-fluorine atomic mutations in proteins reports changes in the stability and not in the structure. Stability changes have been reported for barstar [16,127], tryptophan cage miniprotein [128], the villin headpiece subdomain [129], *T. thermohydrosulfuricus* lipase [130-132], human ubiquitin [133], single-chain Fv format protein [134], KlenTag DNA polymerase [135], thioredoxin A [120], β2-microglobulin [136], red fluorescent protein [137,138], Pin1 WW domain [139], bacteriophage T4 fibritin C-terminal domain [106] and ribonuclease A [140] (Table 3). These results have been explained by considering the conformational bias of the residues (pucker, *trans*/*cis* equilibrium), an altered hydrophobicity and polarity and the local environment at the substitution sites. An elevated folding velocity, presumable due to faster amide rotation kinetics, has been reported for fluoroproline containing cysteine-rich minicollagen domains [141], green fluorescent protein [117,142], ubiquitin [133], β2-microglobulin [136], thioredoxin A [119,143] and red fluorescent protein [137]. In addition, the effects of the fluoroproline incorporation on the enzymatic performance were characterized for a few enzymes [59,130-132,135] and the activity of ion channels [110-113]. These studies generally showed the preservation of the fold of the parent enzymes inferred from the preservation of their native activities.

From these data, it could be deduced that fluoroprolines generally cause minimal perturbations in protein structures. This

Table 3: Stability changes in proteins and protein domains produced upon proline-to-fluoroproline replacements.[a]

protein		number of replaced proline residues	change in the thermodynamic stability			references
			R-Flp	*S*-Flp	Dfp	
barstar		1	↓	↑	≈	[16,127]
tryptophan cage miniprotein		1	↑	↓	not examined	[128]
enhanced green fluorescent protein		10	insoluble	folded, no data	not examined	[117,142]
villin headpiece subdomain		1	↓	≈	not examined	[129]
T. thermohydrosulfuricus lipase		6	↓	↓	not examined	[130-132]
human ubiquitin		3	↑	no production	not examined	[133]
single chain Fv format protein		8	↑	insoluble	not examined	[134]
KlenTag DNA polymerase		32	↓	no production	not examined	[119,135]
thioredoxin A single proline	reduced	1	↑	↑	not examined	[120,143]
	oxidized	1	↓	↓		
β2-microglobulin		1	↓	↑	↓	[136]
bacteriophage T4 fibritin C-terminal domain	2	position 4 position 7	↓ ↑	↑ ↓	not examined	[106]
red fluorescent protein (mRFP1)		12 (11)	↑	insoluble	not examined	[137,138]
Pin1 WW domain		1	↓	↑	not examined	[139]
ribonuclease A		1	not examined	↑	not examined	[140]

[a]As summarized from the thermal stability and other reported data that reflect the stability.

hypothesis is indeed supported by the wealth of available protein studies. However, such a conclusion would be premature. We would like to recapitulate at this point that a study of a protein relies on its production, which is mainly achieved via living cells. If fluoroprolines alter the protein folding, a misfolded sample would usually be prone to aggregation and/or degradation by the cellular machinery. This may be seen as a lack of protein production or as the protein being insoluble. Only proteins that maintain the overall folding will be properly produced, isolated and characterized in a biochemistry laboratory. This requirement creates a natural bias in the biochemical literature, which largely ignores so-called "negative results". A misfolded protein is a typical negative result, which is usually neglected for further investigations. Structural disturbances are also not welcome in spectroscopic studies of fluorine-labeled proteins by ^{19}F NMR spectroscopy. Effectively, it is much better and easier to study a protein that is properly folded, rather than a protein that is misfolded. This is why the structural changes cannot be ruled out, despite the fact that no such instance has been documented in the literature. They may be "hiding" among the proteins that demonstrate a lack of expression or proteins that showed incoherent laboratory results and were therefore never recorded in the scientific correspondence.

The failure to express a certain protein carrying the proline-to-fluoroproline substitution is not uncommon in laboratory practice. It can be caused by various factors: 1) an improper fermentation setup, 2) a lack of translation (e.g., due to the ribosome stalling with *S*-Flp), 3) a lack of interaction with chaperones, 4) misfolding that leads to aggregation, 5) an inhibitory effect of the target protein on the cellular machinery and 6) misfolding that leads to rapid degradation of the protein, to name a few. A misfolding can occur for reasons such as an altered structure, incorrect velocity of the folding steps, and lowering the stability of the protein below handling temperature (Figure 13). In contrast, a folded protein can be produced, isolated and characterized.

Figure 14 illustrates the expression of two proteins with fluoroprolines. The expression of *Geobacillus thermoleovorans* lipase (GTL) yielded a properly folded sample with *R*-Flp and an insoluble protein with *S*-Flp (Figure 14A). The lack of solubility in the latter case indicates critical folding issues induced by the presence of *S*-Flp in the sequence. With α-amylase from *Pyrococcus woesei* (PWA), the expression experiment in the presence of *S*-Flp failed to produce the full-length protein (Figure 14B). The interpretation for this fact is the lack of protein expression due to the ribosome stalling induced by the

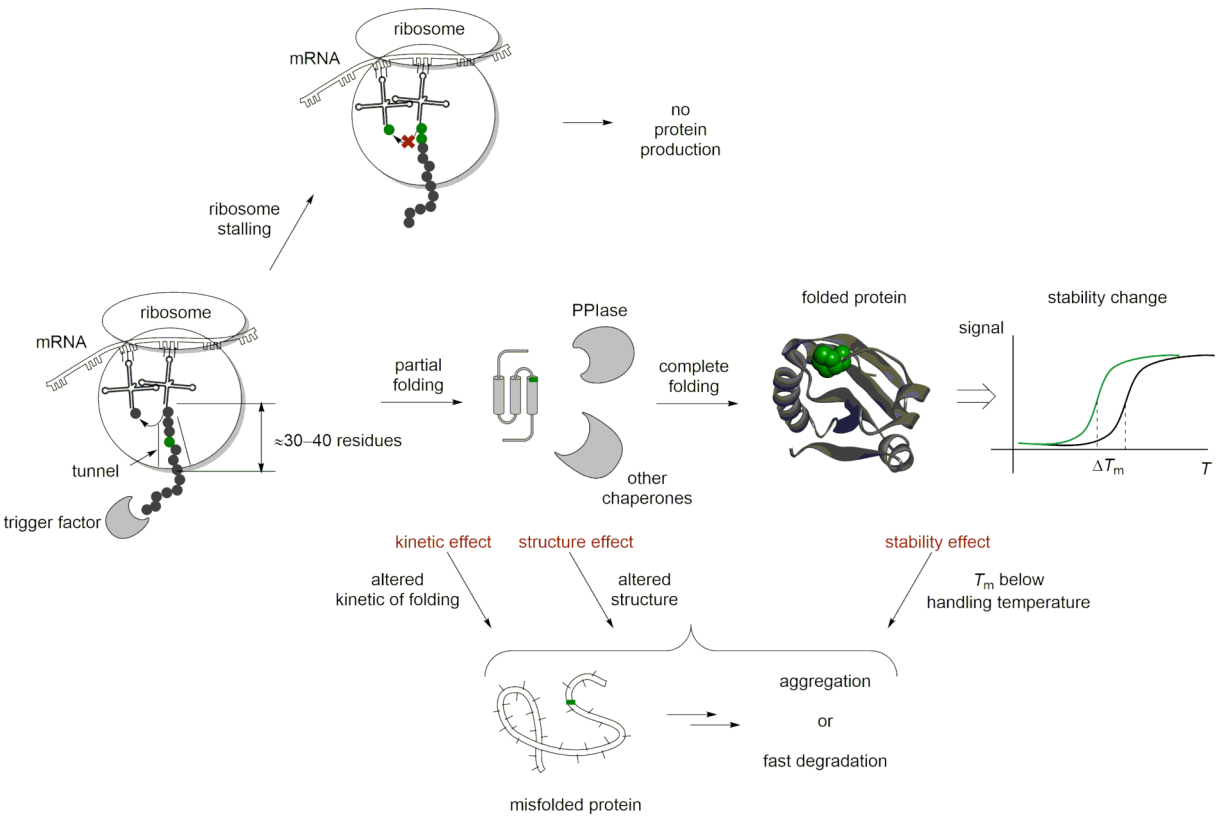

Figure 13: Problems and phenomena associated with the production of a protein-containing proline-to-fluoroproline substitution.

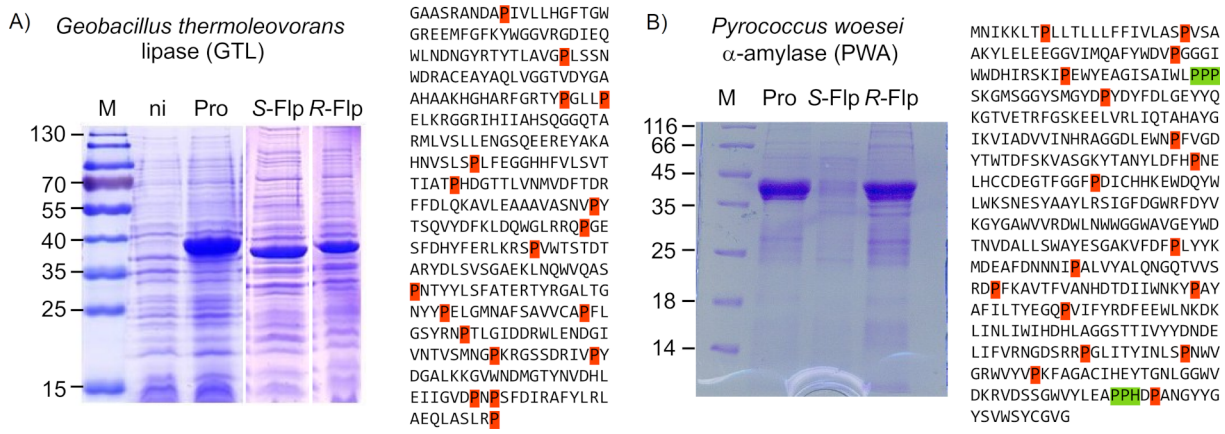

Figure 14: Effects of fluoroprolines on recombinant protein expression using the auxotrophic expression host *Escherichia coli* JM83. Left: sodium dodecyl sulfate–polyacrylamide gel electrophoresis expression profiles. Right: sequence compositions of corresponding proteins with marked single proline residues (orange) and oligoproline stretches (green). ni – non-induced (control) cell fraction, M – molecular weight (kDa) marker.
A) *Geobacillus thermoleovorans* lipase (GTL) with 18 individual proline residues distributed throughout the protein sequence is expressed in the insoluble (inclusion bodies) form in the presence of *S*-Flp (Federica Agostini, unpublished results). B) In the presence of *S*-Flp in the growth medium, no expression of α-amylase from *Pyrococcus woesei* (PWA) could be detected (Michael Hoesl, unpublished results). Note, that in addition to 17 individual proline residues in the sequence, PWA also contains two additional oligoproline stretches. However, expressions in the presence of *R*-Flp yielded soluble and active variants for both enzymes.

oligoproline stretches in the sequence of the target protein. These two examples illustrate a diversity of complications that could hinder protein studies with fluoroprolines.

On the other hand, in the presence of *R*-Flp, the folded and fully active PWA enzyme was isolated, clearly demonstrating the ability of this analog to abolish the ribosome stalling issues in vivo. This is in full agreement with the in vitro results, showing attenuation of the stalling in oligoproline stretches with three consecutive *R*-Flp residues in the absence of elongation factor P [57]. Therefore, the use of fluoroprolines could be considered as an interesting biotechnological strategy and opportunity to optimize the expression of proteins and enzymes of interest by circumventing translational issues.

The final aspect of the protein chemistry is protein degradation. Aliphatic fluorinated amino acids have been utilized towards an enhanced proteolytic stability of peptides [144]. The information regarding the impact of fluoroprolines in peptide and protein degradation is lacking though.

8 The potency of computational modeling in the design of proteins containing fluoroprolines

The conformational consequences of the fluorination of the 4-position of proline have been well studied using computational methods. The latter provided extensive documentation of the electrostatic interactions within the molecules and the observed conformational biases [145,146]. These studies have been further extended to examine the influence of neighbouring amino acids and short peptide chains [108]. However, there has been little done to explore the energetic significance of the conformational preferences and interactions of fluoroprolines in folded proteins [147]. Early work using molecular dynamics has explored differences in the ring pucker conformation and the interactions of fluoroprolines with water molecules in collagenous structures. Yet, there is still much left unexplored in this area, including models examining the enhanced stability of proteins containing fluoroprolines. This is particularly important since the systematic incorporation of fluoroprolines and other proline-based derivatives will facilitate the encoded cellular synthesis of biopolymers with a nonnatural backbone chemistry.

The lack of computational models is likely due to limited structural and stability data on fluoroproline-containing peptides. As the field continues to grow and in-depth characterization of these newly designed fluoroprolines becomes available, so too can the accuracy of computational models used to evaluate the effects of fluoroprolines on protein stability. Several factors that influence the conformational preferences of fluoroprolines in a folded protein have already been identified, indicating that intermolecular forces may override the inherent preferences for ring pucker (see chapter 6). To better understand the roles of stereoelectronic factors and intermolecular forces in dictating the ring conformation and protein stability, future research must include detailed systematic studies involving site-selective mutations of fluoroproline. From these studies, the impact of individual fluoroproline residues in a protein can be assessed,

and factors involved in an increased stability can be assessed using molecular dynamics and quantum mechanics/molecular mechanics studies. The results of this future work would help to identify key features that need to be considered when designing a fluoroproline-containing protein: which sequence positions are most critical to enhance the protein stability, and which diastereomer of fluoroproline to introduce into the protein sequence to obtain a desired effect.

9 Towards living cells relying on the supplement of fluoroprolines

The success of the incorporation of fluoroprolines into proteins by "hijacking" the native *E. coli* machinery suggests a potential of proteome-wide substitution with these proline analogues. Indeed, if fluoroprolines can substitute proline in a single protein, why not substitute proline in a whole cell? Instrumentally, the production of a protein containing a fluoroproline can be done in a relatively easy manner (Figure 15A). First, a proline auxotrophic strain should be enaculated in a medium under a limited proline concentration, which does not allow the culture to grow fully to the stationary phase point. After the proline in the medium is used up, the fluoroprolines should be added, and the the target protein gene is induced, leading to a production of the protein of interest. In this way, the cell machinery is forced to accept fluoroproline for the protein polymerization due to the lack of proline in the medium. Such machination is often referred to as selective pressure, thus the method is called selective pressure incorporation. It leads to production of a protein, where all proline residues are subjected for replacement with the substitute, thus the incorporation is global. Although efficient in production of single proteins, this method makes use of the native microbial culture, which remains unaltered in this approach.

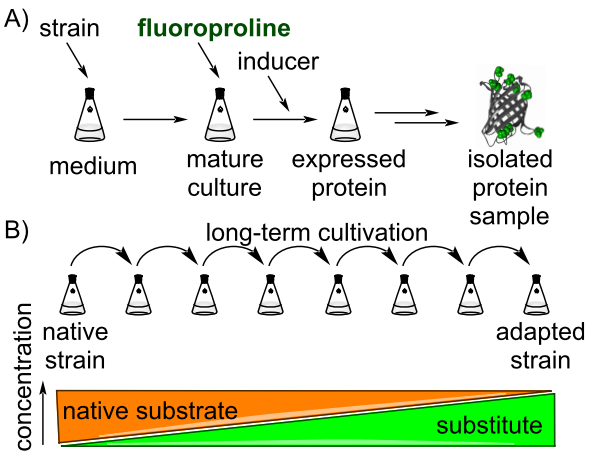

Figure 15: A) Experimental setup for the incorporation of fluoroprolines into proteins. B) Adaptive laboratory evolution (ALE) experiment for the replacement of a canonical substrate with an artificial substitute.

Conversely, the introduction of fluoroprolines into the proteome of a living organism implies alteration of the entire proteome of the cell. Potentially, such an intrusion could be addressed by following the general strategies known as bottom-up and top-down [148]. The bottom-up approach implies the recreation of a living cell from the first principles, while in the top-down approach, an already existing complex living organism should be redesigned [149,150]. The bottom-up approach could be exemplified as the synthetic recreation of compartments that bear functions of organelles or living cells.

Efforts have been directed towards a bacterial adaptation to tryptophan-to-fluorotryptophan replacement via the engineering of the corresponding AARS [151,152]. In another approach, an adaptation of *E. coli* to fluorotryptophan was successfully performed using adaptive laboratory evolution (ALE) [153,154]. In ALE, the driving force for the adaptation was created by the gradual replacement of indole (tryptophan) by its fluorinated analogue, while the bacterial strain was not able to produce its own tryptophan via the native cellular machinery. The cells first had to allow the diffusion or uptake of fluoroindole, followed by a simple metabolic conversion to fluorotryptophan, which serves as a replacement for all tryptophan residues in the proteome. Since the cells are dependent on the presence of tryptophan in the growth medium, fluorotryptophan was used in this experimental setup as a nutrient essential for growth. The selective pressure to adapt cells to the fluorinated tryptophans was thus achieved by combining metabolically modified cells (auxotrophs) with the externally created artificial conditions, i.e., a defined growth medium with a controlled chemical composition. (Figure 15B).

The replacement of proline by fluoroprolines could be attempted instrumentally in a similar fashion. Nonetheless, in contrast to tryptophan, this replacement may be facilitated by the beneficial molecular effects of fluoroprolines in protein chemistry. For example, high-resolution X-ray structures showed that the enhanced green fluorescent protein (Figure 12A) with its β-barrel structures contains proline residues with pyrrolidine rings exhibiting predominantly C^4-*endo*-puckers. It is reasonable to expect that the incorporation of *S*-Flp, which favors *endo*-puckers, will further increase the refolding capacity of these proteins, while *R*-Flp-containing protein will be irreversibly unfolded after expression (including purification and refolding attempts). On the other hand, some proteins, such as the KlenTag DNA polymerase (Figure 12C), perform better when containing *R*-Flp as the proline substitute. Although the biochemistry of fluoroproline incorporation still did not provide a critical mass of experimental evidence for

generalizations, it is not difficult to imagine the scenario in which the adaptation of, e.g., auxotrophic *E. coli* strains to grow in the exclusive presence of fluoroproline might only work with a certain mixture of both diastereomers, instead of the analogues being added to the culture substrate individually. The hypothetical adaptation of the bacterium or other cells to one of the fluoroproline residues would certainly be an enormous breakthrough, as it would not only require the reconfiguration of numerous metabolic and regulatory networks but also an accompanying co- and posttranslational folding of the resulting polypeptides.

By performing experiments to achieve the proteome-wide insertion of fluoroprolines into microbial cells, we should be able to answer the question to what extent naturally evolved protein scaffolds and related cellular machineries and systems are suitable for the accommodation and integration of these isosteric building blocks. The adaptation of bacteria to fluorinated tryptophans discussed above is rather the exception, since tryptophan is a rare amino acid (only 20688 codons in the *E. coli* genome [77]), and hydrogen-to-fluorine replacement on the indole side-chains represent "atomic mutations", which are known to be well tolerated even in investigated isolated proteins [123,124,155] and proteomes [153,154]. Thus, it should be taken into account that the natural structural scaffolds with hydrocarbon cores have been formed and optimized through billions of years of evolution and may not be suitable to accommodate a large number of fluorine atoms [1,8]. We have shown this in our previous experiments on the global substitution of methionine (37698 codons) and leucine residues (144466 codons) in cellular proteins by related trifluoromethylated analogues [156]. These experimental attempts lead to the conclusion that the inclusion of such a fluorine-containing building block would require a novel repackaging of the protein core [132].

While trifluoromethylated analogues of coded amino acids (such as Val, Leu, Ile, Met or some aromatic side-chains) are simply too bulky, steric bulk should not be the main barrier to the accommodation of fluoroprolines in proteins and proteomes (see chapter 2.1). Nevertheless, the incorporation of fluoroprolines into the proteome changes the backbone features of each individual protein and subsequently could lead to a large number of misfolded proteins promoting the expression or down- and upregulation of genes encoding chaperones and proteases. Next, it may induce the stress response that normally redirects energy resources and regulatory networks otherwise dedicated to growth. To overcome such an unpleasant scenario, cells will only survive if they are able to evolve appropriate "coping" mechanisms, allowing them to grow continuously in the presence of fluoroprolines.

This scenario should create the selective pressure as the fundamental basis of adaptation experiments of cells and may lead to the accumulation of random mutations in their genomes. Cellular phenotypes with a suitable set of mutations that favor the use of fluoroproline, which should also provide them with a fitness gain over the generations in a given environment (medium). In other words, these cells with suitable mutations, accompanied by reconfigured metabolic, lipid composition, signaling and transcription networks, should proliferate and assert themselves in the culture medium faster than the others. This could be a possible evolutionary scenario to convert fluoroprolines from stressors to proteinogenic amino acids that support cell growth, i.e., essential nutrients.

Once this goal has been achieved, one could further evolve the fluoroproline-dependent organism towards a state where proline is no longer accepted as the protein constituent. Nonetheless, at the present state of enzyme engineering, it is not possible to envision how a fluoroproline-accepting-proline-rejecting enzymatic mechanism could be developed as the molecular volume and polarity are very similar for these amino acids. Perhaps, the simultaneous engineering of the activation pocket of ProRS towards fluoroprolines as slightly larger substrates, and editing the pockets towards proline as a slightly smaller substrate could lead to the creation of a dedicated fluoroprolyl-tRNA synthetase. However, it is still unclear how to achieve such a sophisticated engineering or how to introduce this manipulation into a living organism without immediate lethal effects for the host organism.

Finally, in order to achieve a true "fluorine life" with a top-down approach, the metabolism itself must be reengineered or created de novo to ensure a continuous supply of the fluorine-containing metabolic blocks. Furthermore, structural and kinetic readjustment of otherwise highly conserved translation factors and the achievements of the novel quality control of fluoroproline-based protein translation should reshape the mechanism behind the flow of genetic information, especially if xeno nucleic acids are included in this process [157,158]. We are only at the beginning of a long journey. For the time being, it remains to be seen whether fluoroprolines could be a suitable vehicle to take us beyond the horizons of the “alanine world” towards the novel “proline world” [25].

Conclusion

Despite the seemingly simple structure, proline is a peculiar amino acid involved in numerous cellular processes. The unique features created by proline residues in proteins justify the essential role of proline in biochemistry. Moreover, our recent theory suggests that proline was one of the first amino acids recruited for protein translation [22]. This suggests that the proteome

originally evolved around proline as its universal constituent, which makes the proteome-wide replacement of proline a challenging task.

Fluoroprolines might be excellent candidates to address this challenge. These proline analogues create minimal perturbations in the volume and polarity of the parent proline residue. At the same time, their conformational effects alter protein production and folding. The enhancement of the protein stability, facilitated interaction with chaperones, elevated folding velocities, the mitigation of ribosome stalling – each of these effects known for fluoroprolines can create an advantage for cell fitness and survival, thereby forming a driving force for the adaptation for proline-to-fluoroproline replacement. At present, it is still unclear to what extent fluoroprolines could fulfill all functional tasks of proline residues. While favoring one of the C^4-puckers and *cis*- or *trans*-amide bonds, fluoroprolines disfavor the others. The negative surface potential created by the fluorine atom and the dipole of the carbon–fluorine bond can cause additional problems for the packing inside the protein interior, which originally evolved to accommodate proline residues. At the same time, many details on the interaction of fluoroprolines with the cellular machinery are still missing, and they should be addressed by future research.

Seminal experiments on the adaptation of the whole cell to fluoroprolines are expected in the nearest future. They should provide novel information on the basic chemical makeup of life and create a path towards artificial biodiversity that involves fluorine as a bioelement.

Acknowledgements

We thank Michael Hoesl and Federica Agostini for the expression gels of the proteins depicted in Figure 14.

Funding

The work of N. B. and V. K. was funded by the Canada Research Chairs Program (grant no. 950-231971). R. D. would like to thank the NSERC-DG program for funding.

ORCID® iDs

Vladimir Kubyshkin - https://orcid.org/0000-0002-4467-4205
Nediljko Budisa - https://orcid.org/0000-0001-8437-7304

References

1. Budisa, N.; Kubyshkin, V.; Schulze-Makuch, D. *Life* **2014,** *4,* 374–385. doi:10.3390/life4030374
2. Johnson, B. M.; Shu, Y.-Z.; Zhuo, X.; Meanwell, N. A. *J. Med. Chem.* **2020,** *63,* 6315–6386. doi:10.1021/acs.jmedchem.9b01877
3. Wu, L.; Maglangit, F.; Deng, H. *Curr. Opin. Chem. Biol.* **2020,** *55,* 119–126. doi:10.1016/j.cbpa.2020.01.004
4. O'Hagan, D.; Harper, D. B. *J. Fluorine Chem.* **1999,** *100,* 127–133. doi:10.1016/s0022-1139(99)00201-8
5. Chan, K. K. J.; O'Hagan, D. *Methods Enzymol.* **2012,** *516,* 219–235. doi:10.1016/b978-0-12-394291-3.00003-4
6. Leong, L. E. X.; Khan, S.; Davis, C. K.; Denman, S. E.; McSweeney, C. S. *J. Anim. Sci. Biotechnol.* **2017,** *8,* No. 55. doi:10.1186/s40104-017-0180-6
7. Wu, L.; Deng, H. *Org. Biomol. Chem.* **2020,** *18,* 6236–6240. doi:10.1039/d0ob01358g
8. Merkel, L.; Budisa, N. *Org. Biomol. Chem.* **2012,** *10,* 7241–7261. doi:10.1039/c2ob06922a
9. Salwiczek, M.; Nyakatura, E. K.; Gerling, U. I. M.; Ye, S.; Koksch, B. *Chem. Soc. Rev.* **2012,** *41,* 2135–2171. doi:10.1039/c1cs15241f
10. Marsh, E. N. G. *Acc. Chem. Res.* **2014,** *47,* 2878–2886. doi:10.1021/ar500125m
11. Berger, A. A.; Völler, J.-S.; Budisa, N.; Koksch, B. *Acc. Chem. Res.* **2017,** *50,* 2093–2103. doi:10.1021/acs.accounts.7b00226
12. Cobb, S. L.; Murphy, C. D. *J. Fluorine Chem.* **2009,** *130,* 132–143. doi:10.1016/j.jfluchem.2008.11.003
13. Kitevski-LeBlanc, J. L.; Prosser, R. S. *Prog. Nucl. Magn. Reson. Spectrosc.* **2012,** *62,* 1–33. doi:10.1016/j.pnmrs.2011.06.003
14. Marsh, E. N. G.; Suzuki, Y. *ACS Chem. Biol.* **2014,** *9,* 1242–1250. doi:10.1021/cb500111u
15. Arntson, K. E.; Pomerantz, W. C. K. *J. Med. Chem.* **2016,** *59,* 5158–5171. doi:10.1021/acs.jmedchem.5b01447
16. Renner, C.; Alefelder, S.; Bae, J. H.; Budisa, N.; Huber, R.; Moroder, L. *Angew. Chem., Int. Ed.* **2001,** *40,* 923–925.
17. Newberry, R. W.; Raines, R. T. 4-Fluoroprolines: Conformational Analysis and Effects on the Stability and Folding of Peptides and Proteins. In *Peptidomimetics I;* Lubell, W. D., Ed.; Topics in Heterocyclic Chemistry, Vol. 48; Springer: Cham, Switzerland, 2016; pp 1–25. doi:10.1007/7081_2015_196
18. Verhoork, S. J. M.; Killoran, P. M.; Coxon, C. R. *Biochemistry* **2018,** *57,* 6132–6143. doi:10.1021/acs.biochem.8b00787
19. Kubyshkin, V. *Beilstein J. Org. Chem.* **2020,** *16,* 1837–1852. doi:10.3762/bjoc.16.151
20. Trifonov, E. N. *Gene* **2000,** *261,* 139–151. doi:10.1016/s0378-1119(00)00476-5
21. Hein, J. E.; Blackmond, D. G. *Acc. Chem. Res.* **2012,** *45,* 2045–2054. doi:10.1021/ar200316n
22. Kubyshkin, V.; Budisa, N. *Int. J. Mol. Sci.* **2019,** *20,* 5507. doi:10.3390/ijms20215507
23. Morrison, K. L.; Weiss, G. A. *Curr. Opin. Chem. Biol.* **2001,** *5,* 302–307. doi:10.1016/s1367-5931(00)00206-4
24. MacArthur, M. W.; Thornton, J. M. *J. Mol. Biol.* **1991,** *218,* 397–412. doi:10.1016/0022-2836(91)90721-h
25. Kubyshkin, V.; Budisa, N. *Curr. Opin. Biotechnol.* **2019,** *60,* 242–249. doi:10.1016/j.copbio.2019.05.006
26. Gottlieb, A. A.; Fujita, Y.; Udenfriend, S.; Witkop, B. *Biochemistry* **1965,** *4,* 2507–2513. doi:10.1021/bi00887a034
27. Bakerman, S.; Martin, R. L.; Burgstahler, A. W.; Hayden, J. W. *Nature* **1966,** *212,* 849–850. doi:10.1038/212849a0
28. Takeuchi, T.; Rosenbloom, J.; Prockop, D. J. *Biochim. Biophys. Acta, Protein Struct.* **1969,** *175,* 156–164. doi:10.1016/0005-2795(69)90154-8
29. Fu, H.; Grimsley, G. R.; Razvi, A.; Scholtz, J. M.; Pace, C. N. *Proteins: Struct., Funct., Bioinf.* **2009,** *77,* 491–498. doi:10.1002/prot.22509

30. Ge, M.; Pan, X.-M. *Extremophiles* **2009,** *13,* 481–489. doi:10.1007/s00792-009-0233-7
31. Huang, J.; Jones, B. J.; Kazlauskas, R. J. *Biochemistry* **2015,** *54,* 4330–4341. doi:10.1021/acs.biochem.5b00333
32. De Maayer, P.; Anderson, D.; Cary, C.; Cowan, D. A. *EMBO Rep.* **2014,** *15,* 508–517. doi:10.1002/embr.201338170
33. Brininger, C.; Spradlin, S.; Cobani, L.; Evilia, C. *Semin. Cell Dev. Biol.* **2018,** *84,* 158–169. doi:10.1016/j.semcdb.2017.12.016
34. Gorres, K. L.; Raines, R. T. *Crit. Rev. Biochem. Mol. Biol.* **2010,** *45,* 106–124. doi:10.3109/10409231003627991
35. Shoulders, M. D.; Raines, R. T. *Annu. Rev. Biochem.* **2009,** *78,* 929–958. doi:10.1146/annurev.biochem.77.032207.120833
36. Kersteen, E. A.; Higgin, J. J.; Raines, R. T. *Protein Expression Purif.* **2004,** *38,* 279–291. doi:10.1016/j.pep.2004.09.008
37. Neubauer, A.; Neubauer, P.; Myllyharju, J. *Matrix Biol.* **2005,** *24,* 59–68. doi:10.1016/j.matbio.2004.11.004
38. Smart, T. J.; Hamed, R. B.; Claridge, T. D. W.; Schofield, C. J. *Bioorg. Chem.* **2020,** *94,* 103386. doi:10.1016/j.bioorg.2019.103386
39. O'Hagan, D. *Chem. Soc. Rev.* **2008,** *37,* 308–319. doi:10.1039/b711844a
40. Purser, S.; Moore, P. R.; Swallow, S.; Gouverneur, V. *Chem. Soc. Rev.* **2008,** *37,* 320–330. doi:10.1039/b610213c
41. Pan, Y. *ACS Med. Chem. Lett.* **2019,** *10,* 1016–1019. doi:10.1021/acsmedchemlett.9b00235
42. Thomas, K. M.; Naduthambi, D.; Zondlo, N. J. *J. Am. Chem. Soc.* **2006,** *128,* 2216–2217. doi:10.1021/ja057901y
43. Zondlo, N. J. *Acc. Chem. Res.* **2013,** *46,* 1039–1049. doi:10.1021/ar300087y
44. Huang, K.-Y.; Horng, J.-C. *Biochemistry* **2015,** *54,* 6186–6194. doi:10.1021/acs.biochem.5b00880
45. Somovilla, V. J.; Bermejo, I. A.; Albuquerque, I. S.; Martínez-Sáez, N.; Castro-López, J.; García-Martín, F.; Compañón, I.; Hinou, H.; Nishimura, S.-I.; Jiménez-Barbero, J.; Asensio, J. L.; Avenoza, A.; Busto, J. H.; Hurtado-Guerrero, R.; Peregrina, J. M.; Bernardes, G. J. L.; Corzana, F. *J. Am. Chem. Soc.* **2017,** *139,* 18255–18261. doi:10.1021/jacs.7b09447
46. Müller, K. *Chimia* **2014,** *68,* 356–362. doi:10.2533/chimia.2014.356
47. Jeffries, B.; Wang, Z.; Felstead, H. R.; Le Questel, J.-Y.; Scott, J. S.; Chiarparin, E.; Graton, J.; Linclau, B. *J. Med. Chem.* **2020,** *63,* 1002–1031. doi:10.1021/acs.jmedchem.9b01172
48. Kang, Y. K.; Young Choi, H. *Biophys. Chem.* **2004,** *111,* 135–142. doi:10.1016/j.bpc.2004.05.006
49. Kang, Y. K. *J. Phys. Chem. B* **2007,** *111,* 10550–10556. doi:10.1021/jp073411b
50. Hunter, L. *Beilstein J. Org. Chem.* **2010,** *6,* No. 38. doi:10.3762/bjoc.6.38
51. Gerig, J. T.; McLeod, R. S. *J. Am. Chem. Soc.* **1973,** *95,* 5725–5729. doi:10.1021/ja00798a046
52. Shoulders, M. D.; Kamer, K. J.; Raines, R. T. *Bioorg. Med. Chem. Lett.* **2009,** *19,* 3859–3862. doi:10.1016/j.bmcl.2009.03.168
53. Fischer, G. *Chem. Soc. Rev.* **2000,** *29,* 119–127. doi:10.1039/a803742f
54. Wedemeyer, W. J.; Welker, E.; Scheraga, H. A. *Biochemistry* **2002,** *41,* 14637–14644. doi:10.1021/bi020574b
55. Eberhardt, E. S.; Panasik, N.; Raines, R. T. *J. Am. Chem. Soc.* **1996,** *118,* 12261–12266. doi:10.1021/ja9623119
56. Lu, K. P.; Finn, G.; Lee, T. H.; Nicholson, L. K. *Nat. Chem. Biol.* **2007,** *3,* 619–629. doi:10.1038/nchembio.2007.35
57. Doerfel, L. K.; Wohlgemuth, I.; Kubyshkin, V.; Starosta, A. L.; Wilson, D. N.; Budisa, N.; Rodnina, M. V. *J. Am. Chem. Soc.* **2015,** *137,* 12997–13006. doi:10.1021/jacs.5b07427
58. Kubyshkin, V.; Durkin, P.; Budisa, N. *New J. Chem.* **2016,** *40,* 5209–5220. doi:10.1039/c5nj03611a
59. Lukesch, M. S.; Pavkov-Keller, T.; Gruber, K.; Zangger, K.; Wiltschi, B. *Sci. Rep.* **2019,** *9,* 2697. doi:10.1038/s41598-019-39484-9
60. Bennett, B. D.; Kimball, E. H.; Gao, M.; Osterhout, R.; Van Dien, S. J.; Rabinowitz, J. D. *Nat. Chem. Biol.* **2009,** *5,* 593–599. doi:10.1038/nchembio.186
61. Fichman, Y.; Gerdes, S. Y.; Kovács, H.; Szabados, L.; Zilberstein, A.; Csonka, L. N. *Biol. Rev. Cambridge Philos. Soc.* **2015,** *90,* 1065–1099. doi:10.1111/brv.12146
62. Liang, X.; Zhang, L.; Natarajan, S. K.; Becker, D. F. *Antioxid. Redox Signaling* **2013,** *19,* 998–1011. doi:10.1089/ars.2012.5074
63. Zwick, C. R., III; Renata, H. *J. Am. Chem. Soc.* **2018,** *140,* 1165–1169. doi:10.1021/jacs.7b12918
64. Zwick, C. R., III; Renata, H. *J. Org. Chem.* **2018,** *83,* 7407–7415. doi:10.1021/acs.joc.8b00248
65. Jung, H.; Hilger, D.; Raba, M. *Front. Biosci.* **2012,** *17,* 745–759. doi:10.2741/3955
66. Gouesbet, G.; Jebbar, M.; Talibart, R.; Bernard, T.; Blanco, C. *Microbiology (London, U. K.)* **1994,** *140,* 2415–2422. doi:10.1099/13500872-140-9-2415
67. Liu, L.-K.; Becker, D. F.; Tanner, J. J. *Arch. Biochem. Biophys.* **2017,** *632,* 142–157. doi:10.1016/j.abb.2017.07.005
68. Mann, S.; Lombard, B.; Loew, D.; Mejean, A.; Ploux, O. *Biochemistry* **2011,** *50,* 7184–7197. doi:10.1021/bi200892a
69. Tanner, J. J.; Fendt, S.-M.; Becker, D. F. *Biochemistry* **2018,** *57,* 3433–3444. doi:10.1021/acs.biochem.8b00215
70. Scott, G. K.; Yau, C.; Becker, B. C.; Khateeb, S.; Mahoney, S.; Jensen, M. B.; Hann, B.; Cowen, B. J.; Pegan, S. D.; Benz, C. C. *Mol. Cancer Ther.* **2019,** *18,* 1374–1385. doi:10.1158/1535-7163.mct-18-1323
71. Scott, G. K.; Benz, C. C. Inhibition of proline catabolism for the treatment of cancer and other therapeutic applications. W.O. Patent WO/2016/077632/A2, Nov 13, 2014.
72. Deutch, C. E.; Klarstrom, J. L.; Link, C. L.; Ricciardi, D. L. *Curr. Microbiol.* **2001,** *42,* 442–446. doi:10.1007/s002840010245
73. Yanisch-Perron, C.; Vieira, J.; Messing, J. *Gene* **1985,** *33,* 103–119. doi:10.1016/0378-1119(85)90120-9
74. Larregola, M.; Moore, S.; Budisa, N. *Biochem. Biophys. Res. Commun.* **2012,** *421,* 646–650. doi:10.1016/j.bbrc.2012.04.031
75. Buechter, D. D.; Paolella, D. N.; Leslie, B. S.; Brown, M. S.; Mehos, K. A.; Gruskin, E. A. *J. Biol. Chem.* **2003,** *278,* 645–650. doi:10.1074/jbc.m209364200
76. Glaasker, E.; Konings, W. N.; Poolman, B. *J. Bacteriol.* **1996,** *178,* 575–582. doi:10.1128/jb.178.3.575-582.1996
77. Lajoie, M. J.; Kosuri, S.; Mosberg, J. A.; Gregg, C. J.; Zhang, D.; Church, G. M. *Science* **2013,** *342,* 361–363. doi:10.1126/science.1241460
78. Avcilar-Kucukgoze, I.; Bartholomäus, A.; Cordero Varela, J. A.; Kaml, R. F.-X.; Neubauer, P.; Budisa, N.; Ignatova, Z. *Nucleic Acids Res.* **2016,** *44,* 8324–8334. doi:10.1093/nar/gkw697
79. Wong, F.-C.; Beuning, P. J.; Nagan, M.; Shiba, K.; Musier-Forsyth, K. *Biochemistry* **2002,** *41,* 7108–7115. doi:10.1021/bi012178j
80. Kumar, S.; Das, M.; Hadad, C. M.; Musier-Forsyth, K. *J. Biol. Chem.* **2012,** *287,* 3175–3184. doi:10.1074/jbc.m111.313619

81. Shirota, F. N.; Nagasawa, H. T.; Elberling, J. A. *J. Med. Chem.* **1977,** *20,* 1176–1181. doi:10.1021/jm00219a013
82. Kim, W.; George, A.; Evans, M.; Conticello, V. P. *ChemBioChem* **2004,** *5,* 928–936. doi:10.1002/cbic.200400052
83. Saravanan Prabhu, N.; Ayyadurai, N.; Deepankumar, K.; Chung, T.; Lim, D. J.; Yun, H. *J. Mol. Catal. B: Enzym.* **2012,** *78,* 57–64. doi:10.1016/j.molcatb.2012.02.004
84. Rodnina, M. V. *Cold Spring Harbor Perspect. Biol.* **2018,** *10,* a032664. doi:10.1101/cshperspect.a032664
85. Wohlgemuth, I.; Brenner, S.; Beringer, M.; Rodnina, M. V. *J. Biol. Chem.* **2008,** *283,* 32229–32235. doi:10.1074/jbc.m805316200
86. Kawakami, T.; Ishizawa, T.; Murakami, H. *J. Am. Chem. Soc.* **2013,** *135,* 12297–12304. doi:10.1021/ja405044k
87. Ude, S.; Lassak, J.; Starosta, A. L.; Kraxenberger, T.; Wilson, D. N.; Jung, K. *Science* **2013,** *339,* 82–85. doi:10.1126/science.1228985
88. Doerfel, L. K.; Wohlgemuth, I.; Kothe, C.; Peske, F.; Urlaub, H.; Rodnina, M. V. *Science* **2013,** *339,* 85–88. doi:10.1126/science.1229017
89. Katoh, T.; Wohlgemuth, I.; Nagano, M.; Rodnina, M. V.; Suga, H. *Nat. Commun.* **2016,** *7,* No. 11657. doi:10.1038/ncomms11657
90. Huter, P.; Arenz, S.; Bock, L. V.; Graf, M.; Frister, J. O.; Heuer, A.; Peil, L.; Starosta, A. L.; Wohlgemuth, I.; Peske, F.; Nováček, J.; Berninghausen, O.; Grubmüller, H.; Tenson, T.; Beckmann, R.; Rodnina, M. V.; Vaiana, A. C.; Wilson, D. N. *Mol. Cell* **2017,** *68,* 515–527. doi:10.1016/j.molcel.2017.10.014
91. Qi, F.; Motz, M.; Jung, K.; Lassak, J.; Frishman, D. *PLoS Comput. Biol.* **2018,** *14,* e1005987. doi:10.1371/journal.pcbi.1005987
92. Schmied, W. H.; Tnimov, Z.; Uttamapinant, C.; Rae, C. D.; Fried, S. D.; Chin, J. W. *Nature* **2018,** *564,* 444–448. doi:10.1038/s41586-018-0773-z
93. Marino, J.; von Heijne, G.; Beckmann, R. *FEBS Lett.* **2016,** *590,* 655–660. doi:10.1002/1873-3468.12098
94. Mercier, E.; Rodnina, M. V. *Biochemistry* **2018,** *57,* 3460–3464. doi:10.1021/acs.biochem.8b00293
95. Kramer, G.; Boehringer, D.; Ban, N.; Bukau, B. *Nat. Struct. Mol. Biol.* **2009,** *16,* 589–597. doi:10.1038/nsmb.1614
96. Galat, A. *Biomolecules* **2019,** *9,* 74. doi:10.3390/biom9020074
97. Golbik, R.; Yu, C.; Weyher-Stingl, E.; Huber, R.; Moroder, L.; Budisa, N.; Schiene-Fischer, C. *Biochemistry* **2005,** *44,* 16026–16034. doi:10.1021/bi051442w
98. DeRider, M. L.; Wilkens, S. J.; Waddell, M. J.; Bretscher, L. E.; Weinhold, F.; Raines, R. T.; Markley, J. L. *J. Am. Chem. Soc.* **2002,** *124,* 2497–2505. doi:10.1021/ja0166904
99. Fallas, J. A.; O'Leary, L. E. R.; Hartgerink, J. D. *Chem. Soc. Rev.* **2010,** *39,* 3510–3527. doi:10.1039/b919455j
100. Adzhubei, A. A.; Sternberg, M. J. E.; Makarov, A. A. *J. Mol. Biol.* **2013,** *425,* 2100–2132. doi:10.1016/j.jmb.2013.03.018
101. Horng, J.-C.; Raines, R. T. *Protein Sci.* **2006,** *15,* 74–83. doi:10.1110/ps.051779806
102. Lin, Y.-J.; Horng, J.-C. *Amino Acids* **2014,** *46,* 2317–2324. doi:10.1007/s00726-014-1783-2
103. Yu, H.; Chen, J. K.; Feng, S.; Dalgarno, D. C.; Brauer, A. W.; Schrelber, S. L. *Cell* **1994,** *76,* 933–945. doi:10.1016/0092-8674(94)90367-0
104. Ruzza, P.; Siligardi, G.; Donella-Deana, A.; Calderan, A.; Hussain, R.; Rubini, C.; Cesaro, L.; Osler, A.; Guiotto, A.; Pinna, L. A.; Borin, G. *J. Pept. Sci.* **2006,** *12,* 462–471. doi:10.1002/psc.750
105. Borgogno, A.; Ruzza, P. *Amino Acids* **2013,** *44,* 607–614. doi:10.1007/s00726-012-1383-y
106. Dietz, D.; Kubyshkin, V.; Budisa, N. *ChemBioChem* **2015,** *16,* 403–406. doi:10.1002/cbic.201402654
107. Ball, J. B.; Hughes, R. A.; Alewood, P. F.; Andrews, P. R. *Tetrahedron* **1993,** *49,* 3467–3478. doi:10.1016/s0040-4020(01)90207-8
108. Kim, W.; McMillan, R. A.; Snyder, J. P.; Conticello, V. P. *J. Am. Chem. Soc.* **2005,** *127,* 18121–18132. doi:10.1021/ja054105j
109. Catherine, C.; Oh, S. J.; Lee, K.-H.; Min, S.-E.; Won, J.-I.; Yun, H.; Kim, D.-M. *Biotechnol. Bioprocess Eng.* **2015,** *20,* 417–422. doi:10.1007/s12257-015-0190-1
110. Limapichat, W.; Lester, H. A.; Dougherty, D. A. *J. Biol. Chem.* **2010,** *285,* 8976–8984. doi:10.1074/jbc.m109.060939
111. Rienzo, M.; Rocchi, A. R.; Threatt, S. D.; Dougherty, D. A.; Lummis, S. C. R. *J. Biol. Chem.* **2016,** *291,* 6272–6280. doi:10.1074/jbc.m115.694372
112. Mosesso, R.; Dougherty, D. A.; Lummis, S. C. R. *Biochemistry* **2018,** *57,* 4036–4043. doi:10.1021/acs.biochem.8b00379
113. Mosesso, R.; Dougherty, D. A.; Lummis, S. C. R. *ACS Chem. Neurosci.* **2019,** *10,* 3327–3333. doi:10.1021/acschemneuro.9b00315
114. Theillet, F.-X.; Kalmar, L.; Tompa, P.; Han, K.-H.; Selenko, P.; Dunker, A. K.; Daughdrill, G. W.; Uversky, V. N. *Intrinsically Disord. Proteins* **2013,** *1,* e24360. doi:10.4161/idp.24360
115. Lee, C.; Kalmar, L.; Xue, B.; Tompa, P.; Daughdrill, G. W.; Uversky, V. N.; Han, K.-H. *Biochim. Biophys. Acta, Gen. Subj.* **2014,** *1840,* 993–1003. doi:10.1016/j.bbagen.2013.10.042
116. Mateos, B.; Conrad-Billroth, C.; Schiavina, M.; Beier, A.; Kontaxis, G.; Konrat, R.; Felli, I. C.; Pierattelli, R. *J. Mol. Biol.* **2020,** *432,* 3093–3111. doi:10.1016/j.jmb.2019.11.015
117. Steiner, T.; Hess, P.; Bae, J. H.; Wiltschi, B.; Moroder, L.; Budisa, N. *PLoS One* **2008,** *3,* e1680. doi:10.1371/journal.pone.0001680
118. Shoulders, M. D.; Satyshur, K. A.; Forest, K. T.; Raines, R. T. *Proc. Natl. Acad. Sci. U. S. A.* **2010,** *107,* 559–564. doi:10.1073/pnas.0909592107
119. Holzberger, B.; Obeid, S.; Welte, W.; Diederichs, K.; Marx, A. *Chem. Sci.* **2012,** *3,* 2924–2931. doi:10.1039/c2sc20545a
120. Rubini, M.; Schärer, M. A.; Capitani, G.; Glockshuber, R. *ChemBioChem* **2013,** *14,* 1053–1057. doi:10.1002/cbic.201300178
121. Kelly, S. M.; Jess, T. J.; Price, N. C. *Biochim. Biophys. Acta, Proteins Proteomics* **2005,** *1751,* 119–139. doi:10.1016/j.bbapap.2005.06.005
122. Miles, A. J.; Wallace, B. A. *Chem. Soc. Rev.* **2006,** *35,* 39–51. doi:10.1039/b316168b
123. Welte, H.; Zhou, T.; Mihajlenko, X.; Mayans, O.; Kovermann, M. *Sci. Rep.* **2020,** *10,* 2640. doi:10.1038/s41598-020-59446-w
124. Budisa, N.; Huber, R.; Golbik, R.; Minks, C.; Weyher, E.; Moroder, L. *Eur. J. Biochem.* **1998,** *253,* 1–9. doi:10.1046/j.1432-1327.1998.2530001.x
125. Biava, H.; Budisa, N. *Eng. Life Sci.* **2014,** *14,* 340–351. doi:10.1002/elsc.201300049
126. Odar, C.; Winkler, M.; Wiltschi, B. *Biotechnol. J.* **2015,** *10,* 427–446. doi:10.1002/biot.201400587
127. Budisa, N. *Engineering the genetic code;* Wiley-VCH: Weinheim, Germany, 2006; p 239.
128. Naduthambi, D.; Zondlo, N. J. *J. Am. Chem. Soc.* **2006,** *128,* 12430–12431. doi:10.1021/ja0648458
129. Zheng, T.-Y.; Lin, Y.-J.; Horng, J.-C. *Biochemistry* **2010,** *49,* 4255–4263. doi:10.1021/bi100323v
130. Hoesl, M. G.; Acevedo-Rocha, C. G.; Nehring, S.; Royter, M.; Wolschner, C.; Wiltschi, B.; Budisa, N.; Antranikian, G. *ChemCatChem* **2011,** *3,* 213–221. doi:10.1002/cctc.201000253

131. Acevedo-Rocha, C. G.; Hoesl, M. G.; Nehring, S.; Royter, M.; Wolschner, C.; Wiltschi, B.; Antranikian, G.; Budisa, N. *Catal. Sci. Technol.* **2013,** *3,* 1198–1201. doi:10.1039/c3cy20712a
132. Merkel, L.; Schauer, M.; Antranikian, G.; Budisa, N. *ChemBioChem* **2010,** *11,* 1505–1507. doi:10.1002/cbic.201000295
133. Crespo, M. D.; Rubini, M. *PLoS One* **2011,** *6,* e19425. doi:10.1371/journal.pone.0019425
134. Edwardraja, S.; Sriram, S.; Govindan, R.; Budisa, N.; Lee, S.-G. *Mol. BioSyst.* **2011,** *7,* 258–265. doi:10.1039/c0mb00154f
135. Holzberger, B.; Marx, A. *J. Am. Chem. Soc.* **2010,** *132,* 15708–15713. doi:10.1021/ja106525y
136. Torbeev, V. Y.; Hilvert, D. *Proc. Natl. Acad. Sci. U. S. A.* **2013,** *110,* 20051–20056. doi:10.1073/pnas.1310414110
137. Deepankumar, K.; Nadarajan, S. P.; Ayyadurai, N.; Yun, H. *Biochem. Biophys. Res. Commun.* **2013,** *440,* 509–514. doi:10.1016/j.bbrc.2013.09.062
138. Deepankumar, K.; Nadarajan, S. P.; Bae, D.-H.; Baek, K.-H.; Choi, K.-Y.; Yun, H. *Biotechnol. Bioprocess Eng.* **2015,** *20,* 67–72. doi:10.1007/s12257-014-0456-z
139. Tang, H.-C.; Lin, Y.-J.; Horng, J.-C. *Proteins: Struct., Funct., Bioinf.* **2014,** *82,* 67–76. doi:10.1002/prot.24359
140. Arnold, U.; Raines, R. T. *Org. Biomol. Chem.* **2016,** *14,* 6780–6785. doi:10.1039/c6ob00980h
141. Boulègue, C.; Milbradt, A. G.; Renner, C.; Moroder, L. *J. Mol. Biol.* **2006,** *358,* 846–856. doi:10.1016/j.jmb.2006.02.031
142. Nadarajan, S. P.; Deepankumar, K.; Seo, J.-H.; Yun, H. *Biotechnol. Bioprocess Eng.* **2017,** *22,* 504–511. doi:10.1007/s12257-017-0257-2
143. Roderer, D.; Glockshuber, R.; Rubini, M. *ChemBioChem* **2015,** *16,* 2162–2166. doi:10.1002/cbic.201500342
144. Huhmann, S.; Koksch, B. *Eur. J. Org. Chem.* **2018,** 3667–3679. doi:10.1002/ejoc.201800803
145. Song, I. K.; Kang, Y. K. *J. Phys. Chem. B* **2005,** *109,* 16982–16987. doi:10.1021/jp044337p
146. Song, I. K.; Kang, Y. K. *J. Phys. Chem. B* **2006,** *110,* 1915–1927. doi:10.1021/jp054351h
147. Mooney, S. D.; Kollman, P. A.; Klein, T. E. *Biopolymers* **2002,** *64,* 63–71. doi:10.1002/bip.10123
148. Ausländer, S.; Ausländer, D.; Fussenegger, M. *Angew. Chem., Int. Ed.* **2017,** *56,* 6396–6419. doi:10.1002/anie.201609229
149. Fredens, J.; Wang, K.; de la Torre, D.; Funke, L. F. H.; Robertson, W. E.; Christova, Y.; Chia, T.; Schmied, W. H.; Dunkelmann, D. L.; Beránek, V.; Uttamapinant, C.; Llamazares, A. G.; Elliott, T. S.; Chin, J. W. *Nature* **2019,** *569,* 514–518. doi:10.1038/s41586-019-1192-5
150. Reinkemeier, C. D.; Girona, G. E.; Lemke, E. A. *Science* **2019,** *363,* eaaw2644. doi:10.1126/science.aaw2644
151. Mat, W.-K.; Xue, H.; Wong, J. T.-F. *PLoS One* **2010,** *5,* e12206. doi:10.1371/journal.pone.0012206
152. Yu, A. C.-S.; Yim, A. K.-Y.; Mat, W.-K.; Tong, A. H.-Y.; Lok, S.; Xue, H.; Tsui, S. K.-W.; Wong, J. T.-F.; Chan, T.-F. *Genome Biol. Evol.* **2014,** *6,* 629–641. doi:10.1093/gbe/evu044
153. Bacher, J. M.; Ellington, A. D. *J. Bacteriol.* **2001,** *183,* 5414–5425. doi:10.1128/jb.183.18.5414-5425.2001
154. Agostini, F.; Sinn, L.; Petras, D.; Schipp, C. J.; Kubyshkin, V.; Berger, A. A.; Dorrestein, P. C.; Rappsilber, J.; Budisa, N.; Koksch, B. *ACS Cent. Sci.* **2021,** *7,* 81–92. doi:10.1021/acscentsci.0c00679
155. Minks, C.; Huber, R.; Moroder, L.; Budisa, N. *Biochemistry* **1999,** *38,* 10649–10659. doi:10.1021/bi990580g
156. Budisa, N.; Pipitone, O.; Siwanowicz, I.; Rubini, M.; Pal, P. P.; Holak, T. A.; Gelmi, M. L. *Chem. Biodiversity* **2004,** *1,* 1465–1475. doi:10.1002/cbdv.200490107
157. Whitford, C. M.; Dymek, S.; Kerkhoff, D.; März, C.; Schmidt, O.; Edich, M.; Droste, J.; Pucker, B.; Rückert, C.; Kalinowski, J. *J. Biol. Eng.* **2018,** *12,* 13. doi:10.1186/s13036-018-0105-8
158. Duffy, K.; Arangundy-Franklin, S.; Holliger, P. *BMC Biol.* **2020,** *18,* 112. doi:10.1186/s12915-020-00803-6

License and Terms

This is an Open Access article under the terms of the Creative Commons Attribution License (https://creativecommons.org/licenses/by/4.0). Please note that the reuse, redistribution and reproduction in particular requires that the author(s) and source are credited and that individual graphics may be subject to special legal provisions.

The license is subject to the *Beilstein Journal of Organic Chemistry* terms and conditions: (https://www.beilstein-journals.org/bjoc/terms)

The definitive version of this article is the electronic one which can be found at: https://doi.org/10.3762/bjoc.17.40

BEILSTEIN JOURNAL OF ORGANIC CHEMISTRY

Synthesis and physicochemical evaluation of fluorinated lipopeptide precursors of ligands for microbubble targeting

Masayori Hagimori*[1,2,3,§], Estefanía E. Mendoza-Ortega[1] and Marie Pierre Krafft*[1]

Full Research Paper

Open Access

Address:
[1]Institut Charles Sadron (CNRS), University of Strasbourg, 23 rue du Loess, 67034 Strasbourg CEDEX 2, France, [2]Faculty of Pharmaceutical Sciences, Mukogawa Women's University, 11-68 Koshien Kyubancho, Nishinomiya 663-8179, Japan and [3]Graduate School of Biomedical Sciences, Nagasaki University, 1-7-1 Sakamoto, Nagasaki 852-8501, Japan

Email:
Masayori Hagimori* - hagimori@mukogawa-u.ac.jp;
Marie Pierre Krafft* - krafft@unistra.fr

* Corresponding author
§ This work was achieved during his stay at the Institut Charles Sadron, Strasbourg.

Keywords:
adsorption at fluid interfaces; drug delivery; microbubble targeting; molecular imaging; monolayer; perfluoroalkylated lipopeptide; solid-phase peptide synthesis

Beilstein J. Org. Chem. **2021,** *17,* 511–518.
https://doi.org/10.3762/bjoc.17.45

Received: 26 November 2020
Accepted: 18 January 2021
Published: 19 February 2021

This article is part of the thematic issue "Organo-fluorine chemistry V".

Guest Editor: D. O'Hagan

© 2021 Hagimori et al.; licensee Beilstein-Institut.
License and terms: see end of document.

Abstract

Ligand-targeted microbubbles are focusing interest for molecular imaging and delivery of chemotherapeutics. Lipid–peptide conjugates (lipopeptides) that feature alternating serine–glycine $(SG)_n$ segments rather than classical poly(oxyethylene) linkers between the lipid polar head and a targeting ligand were proposed for the liposome-mediated, selective delivery of anticancer drugs. Here, we report the synthesis of perfluoroalkylated lipopeptides (*F*-lipopeptides) bearing two hydrophobic chains (C_nF_{2n+1}, n = 6, 7, 8, **1**–**3**) grafted through a lysine moiety on a hydrophilic chain composed of a lysine–serine–serine (KSS) sequence followed by 5 SG sequences. These *F*-lipopeptides are precursors of targeting lipopeptide conjugates. A hydrocarbon counterpart with a $C_{10}H_{21}$ chain (**4**) was synthesized for comparison. The capacity for the *F*-lipopeptides to spontaneously adsorb at the air/water interface and form monolayers when combined with dipalmitoylphosphatidylcholine (DPPC) was investigated. The *F*-lipopeptides **1**–**3** demonstrated a markedly enhanced tendency to form monolayers at the air/water interface, with equilibrium surface pressures reaching ≈7–10 mN m^{-1} versus less than 1 mN m^{-1} only for their hydrocarbon analog **4**. The *F*-lipopeptides penetrate in the DPPC monolayers in both liquid expanded (LE) and liquid condensed (LC) phases without interfacial film destabilization. By contrast, **4** provokes delipidation of the interfacial film. The incorporation of the *F*-lipopeptides **1**–**3** in microbubbles with a shell of DPPC and dipalmitoylphosphatidylethanolamine-PEG2000 decreased their mean diameter and increased their stability, the best results being obtained for the C_8F_{17}-bearing lipopeptide **3**. By contrast, the hydrocarbon lipopeptide led to microbubbles with a larger mean diameter and a significantly lower stability.

Introduction

Various nano- and microsystems, including micelles, liposomes, and microbubbles, have been developed as imaging agents and to selectively deliver chemotherapeutics to tumor cells [1-6]. An increased specificity for tumor cells can be gained through ligand-mediated active targeting, which involves the use of targeting ligands, such as monoclonal antibodies, antibody fragments, proteins, peptides, and other small molecules, including vitamins and carbohydrates [7,8]. The targeting ligands are coupled to the surface of the carrier to selectively target tumor cells that overexpress a particular cell surface receptor [7,9-14]. To this aim, ligand–lipid conjugates have been developed in research and preclinical development for liposome targeting for decades. In particular, peptide ligands offer significant advantages, including efficient synthesis routes, versatility, and safety [15-17]. Various effective receptor-binding peptides have been identified by the phage display technology [18]. The peptides can be readily prepared through solid-phase peptide synthesis (SPPS), a highly reproducible method with minimal side reactions. Many peptide–lipid conjugates (lipopeptides) have been used as the amphiphilic components of drug delivery systems with anticancer properties, such as the tripeptide Arg–Gly–Asp (RGD) that binds to integrin $\alpha_v\beta_3$, which is expressed on endothelial cells of various malignant tumors [15,19-22]. Other lipopeptides display cell penetrating properties, such as the transactivator of the transcription (TAT) peptide. Moreover, peptides being smaller than the antibodies generally induce a lower immunogenicity [15-17]. Micro- and nanocarriers are often covered by poly(ethylene glycol) (PEG) stealth coatings that significantly enhance blood circulation times by allowing them to evade immune detection. PEGs often play a key role in the design of the ligands as a spacer between the nanocarrier surface and the lipid. PEGs have, however, some shortcomings, such as a broad molecular weight distribution, large steric hindrance, and the occurrence of side reactions due to reactive groups introduced during PEG to lipids (or peptides) connecting reactions [23-25]. In particular, the PEG layer grafted on the surface of certain nanocarriers restricts the exposure of functional peptides [26,27].

Novel ligand-grafted lipids have been proposed for the preparation of functional drug carriers for clinical applications [25,28,29]. In order to alleviate the steric hindrance effect of PEG chains, a novel spacer consisting of alternating serine–glycine sequences $(SG)_n$ was introduced between the ligand and lipid within the molecular structure [30]. These lipopeptides have a discrete molecular weight and are produced by Fmoc (fluorenylmethoxycarbonyl protecting group) SPPS, a procedure in which the peptide chain is assembled stepwise while attached to an insoluble resin support, which allows the easy removal of the byproducts at each step by washing. The human epidermal growth factor receptor-2 (HER2)-targeting KCCYSL peptide–$(SG)_n$–lipids in which the $(SG)_n$ (n = 3, 5, 7) sequence was used as a spacer allowed the reduction of the steric hindrance when compared to the conventional PEG2000 spacer [28]. Liposomes containing these peptide ligands dramatically increased cellular association in HER2-positive cells. Other lipids grafted to the RGD peptide and SG spacer were integrated in PEGylated liposomes and were efficiently associated with integrin $\alpha_v\beta_3$-expressing Colon-26 cells [25].

One of our general objectives is to synthesize lipopeptides specifically designed for the incorporation in the phospholipid shell of medical microbubbles (MBs) (Scheme 1a). DPPC is widely used in the formulation of MBs, often in combination with a PEGylated dipalmitoylphosphatidylethanolamine (DPPE-PEG2000) that further enhances MB stability [31-33]. It is noteworthy that most of the phospholipid-stabilized MBs investigated in research and preclinical development are stabilized by a fluorocarbon (FC) gas [11,31,34]. FCs are known to contribute to MB stabilization through an osmotic effect [31]. In addition, FCs were also found to act as co-surfactants to the phospholipid molecules of the MB shell and strongly reduce its interfacial tension [35,36]. Recent studies have reported that the fluorine–fluorine interactions that develop between the FC and the MB shell component (e.g., fluorinated biomarkers [37] and fluorinated nanoparticles, including dendronized iron oxide nanoparticles [38] and nanodiamonds [39]) efficiently reinforce the interfacial film cohesion, thus enhancing the stability of the MBs. Various types of perfluoroalkylated amphiphiles have been reported that were designed for biomedical applications and display highly effective nanoemulsion and MB stabilizing characteristics [40-42].

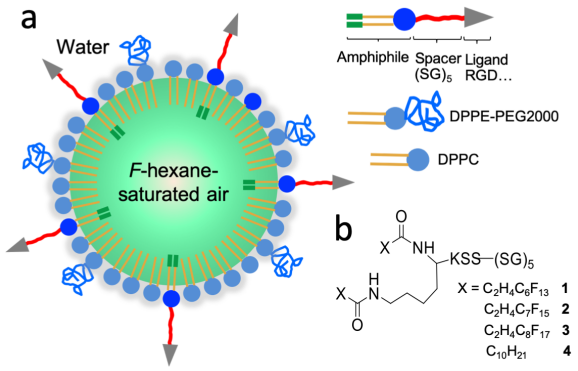

Scheme 1: a) Schematic representation of a perfluorohexane-stabilized microbubble with a fluorinated lipopeptide anchored in its phospholipid shell and b) structures of the perfluoroalkylated lipopeptides **1–3** and of the hydrocarbon analog **4**.

In this work, we report the synthesis of a series of *F*-lipopeptides that are precursors of targeting lipopeptide conjugates and are specifically designed to be incorporated in the shell of phospholipid microbubbles. In a first step, the $(SG)_5$KSS peptide chain is assembled stepwise using a Fmoc solid-phase peptide synthesis procedure. In a second step, the two perfluoroalkylated chains are grafted to the peptide chain through a lysine moiety. Next, the surface activity of the synthesized lipopeptides is investigated by assessing their ability to self-assemble into spontaneously adsorbed monolayers at the air/water interface and also to adsorb on a DPPC monolayer spread at the air/water interface. Finally, the size and stability characteristics of perfluorohexane (*F*-hexane)-stabilized microbubbles with DPPC/DPPE-PEG2000 shells and incorporating the new *F*-lipopeptides were determined and compared to those of reference MBs of similar phospholipid composition.

Results and Discussion

Synthesis and characterization of the lipid–peptide conjugates

Since the degree of fluorination of the hydrophobic chains of the lipid conditions the extent of fluorous interactions developed with the FC gas, we have selected various perfluoroalkyl chain lengths (C_6F_{13}, C_7F_{15}, and C_8F_{17}). The length of the $(SG)_n$ sequence was set to $n = 5$, which was found optimal in a previous report [28]. We synthetized three perfluoroalkylated double-chain peptide–lipid conjugates, $(SG)_5$-KSS-K(C_2H_4-C_nF_{2n+1})$_2$ with $n = 6$ (**1**), 7 (**2**) and 8 (**3**) (Scheme 1b). The hydrocarbon analog fitted with two $C_{10}H_{21}$ chains (**4**) was also prepared.

The *F*-lipopeptide conjugates **1**–**3** and hydrocarbon analog **4** were obtained by a Fmoc solid-phase peptide synthesis method, in which the peptide sequence was stepwisely elongated, and eventually conjugated with the (perfluoroalkyl)ethyl acids (Scheme 2). After the cleavage from the resin, the Fmoc groups of the amino acids were removed, and the *F*-lipopeptides were purified using a dialysis membrane. According to mass spectrometry, FTIR, and HPLC analysis, the products **1**–**4** had high purity (>99%) (Supporting Information File 1, Figures S1–S12).

Behavior of lipid-peptide conjugates at the air/water interface

Spontaneous adsorption of lipid–peptide conjugates at the air/water interface. In order to investigate the capacity for *F*-lipopeptides **1**–**3** to spontaneously self-assemble into ordered monolayers at the air/water interface, we injected a solution of each peptide–lipid conjugate in DMSO into the aqueous subphase of an adsorption trough. The variation of the surface pressure π was measured over time at 25 °C (Figure 1). In all cases, π increased, reflecting a progressive adsorption at the interface, then reached a plateau, and stabilized at the equilibrium surface

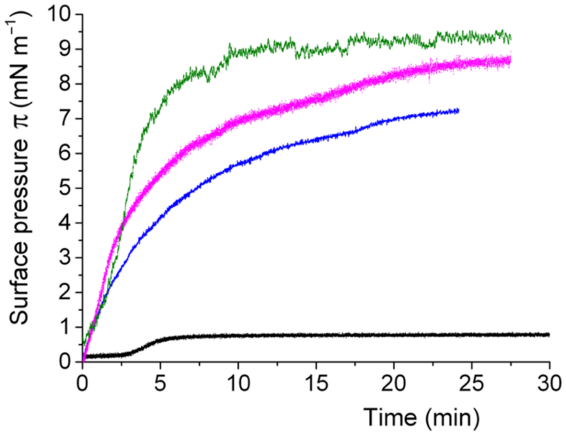

Figure 1: Adsorption kinetics of perfluoroalkylated lipopeptides **1**–**3** and the hydrocarbon analog **4** at the air/water interface (25 °C). Variation of surface pressure π as a function of time for **1** (blue), **2** (magenta), **3** (green), and **4** (black).

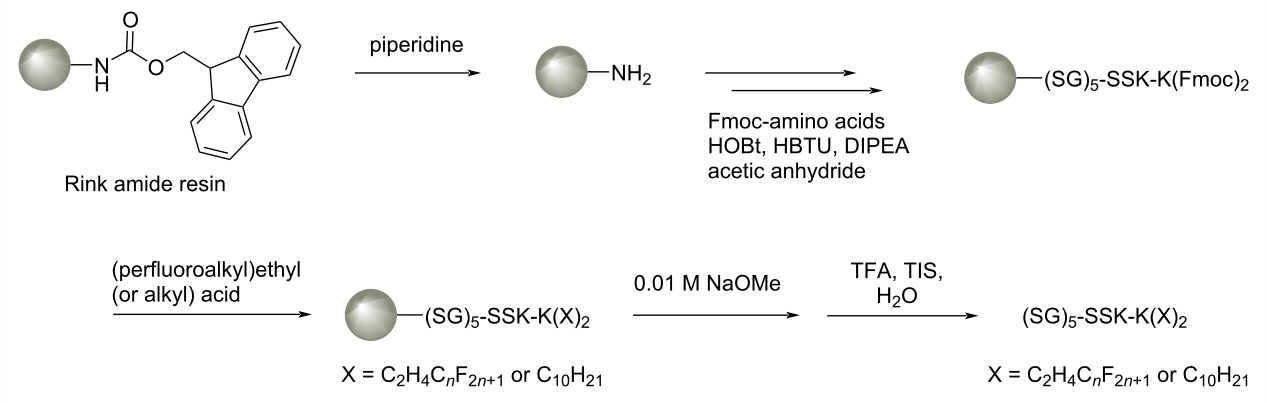

Scheme 2: Solid-phase synthesis of *F*-lipopeptides **1**–**3** and hydrocarbon counterpart **4**.

pressure (π_{eq}). The adsorption kinetics demonstrate that the *F*-lipopeptides formed stable monolayers at the interface. The π_{eq} values increased with the degree of fluorination of the *F*-lipopeptides (≈7.2 mN m^{-1} for **1**, 8.6 mN m^{-1} for **2**, and 9.4 mN m^{-1} for **3**; ±0.5 mN m^{-1}), reflecting their increasingly hydrophobic character. By contrast, the hydrocarbon analog **4** adsorbed considerably less, reaching a π_{eq} value of only 0.7 mN m^{-1}. The adsorption of the *F*-lipopeptides is also much faster than that of the hydrocarbon compound (characteristic time of adsorption $\tau \approx 0.5$ min for **1**–**3** versus ≈2.5 min for **4**).

Adsorption of lipid–peptide conjugates on a phospholipid monolayer spread at the air/water interface. DPPC is widely used in the formulation of liposomes and microbubbles [31,33]. In order to investigate the ability of the *F*-lipopeptides to form mixed monolayers with DPPC at the air/water interface, the *F*-lipopeptides were injected in the aqueous sub-phase of a Langmuir monolayer of DPPC. Depending on the volume of the DPPC solution deposited, the monolayer is either in the liquid expanded (LE, 5 mN m^{-1}) or in the liquid condensed (LC, 19 mN m^{-1}) phase (Figure 2a,b). In the LE phase, the π values of the *F*-lipopeptides were significantly higher than that of the DPPC monolayer (Figure 2a) and remained stable over time, which means that the lipopeptides are inserted in the DPPC monolayer. On the other hand, the injection of the hydrocarbon analog **4** was not followed by an increase of π, which suggests that **4** is not adsorbed in the DPPC monolayer. In the LC phase, π_{eq} is ≈19 mN m^{-1} for DPPC alone. We observed that π_{eq} increased significantly after the injection of the *F*-lipopeptides, reflecting the insertion in the DPPC monolayer. The higher the degree of fluorination, the higher the amount inserted, with a maximal efficiency observed for lipopeptide **3** (C_8F_{17}). However, the behavior of the *F*-lipopeptide **2** with an odd number of carbon atoms (C_7F_{15}) is closer to that of **1** (C_6F_{13}) than to that of **3**, and not intermediate, as it could have been expected. It may possibly be that this comportment can be ascribed to odd/even effects, which are known to impact on the adsorption process of surfactants [43]. For example, surfactants with an odd number of carbon atoms in their alkyl chain were less effective for emulsifying liquid crystals than those with an even number of carbons [44]. The behavior of the hydrocarbon lipopeptide **4** was markedly different, with a decrease of the surface pressure over time, and a much lower π_{eq}. This not only means that the hydrocarbon analog is not recruited at the interface, but also that there is a significant loss of molecules, and that contact of the hydrocarbon lipid with the DPPC monolayer causes a delipidation of the interface.

Generation of microbubbles from combinations of DPPC and lipid–peptide conjugates

Next, we have investigated whether microbubbles incorporating the lipopeptides in the shell could be produced and what their effect on the size characteristics and stability of the resulting MBs would be. We therefore selected DPPC and DPPE-PEG2000 as the main MB shell components. The PEGylated phospholipid is often used in MB formulations to increase MB half-lives. The microbubbles were prepared by mechanical agitation using a Vialmix shaker and were characterized by optical microscopy immediately after the preparation and over time. The results show that the incorporation of *F*-lipopeptides **1**–**3** led to MBs that are somewhat smaller than those made from DPPC alone (e.g., 1.9 ± 0.6 µm with *F*-lipopeptide **3** versus 2.5 ± 0.8 µm without, Figure 3a,b). Microbubbles with similar mean diameters were obtained with the two other

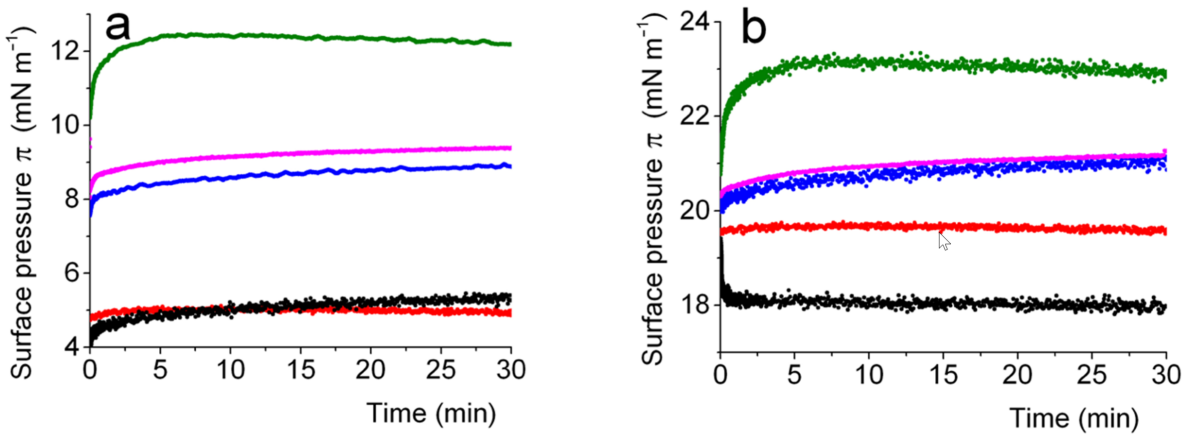

Figure 2: Adsorption of perfluoroalkylated lipopeptides **1**–**3** and hydrocarbon analog **4** on DPPC monolayers spread at the air/water interface a) in the liquid expanded (LE) and b) in the liquid condensed (LC) phases (25 °C). Variation of the surface pressure π as a function of time for a DPPC monolayer (red), and after injection of the lipopeptides in the aqueous sub-phase of a DPPC monolayer for *F*-lipopeptides: **1** (blue), **2** (magenta), **3** (green), and hydrocarbon analog **4** (black).

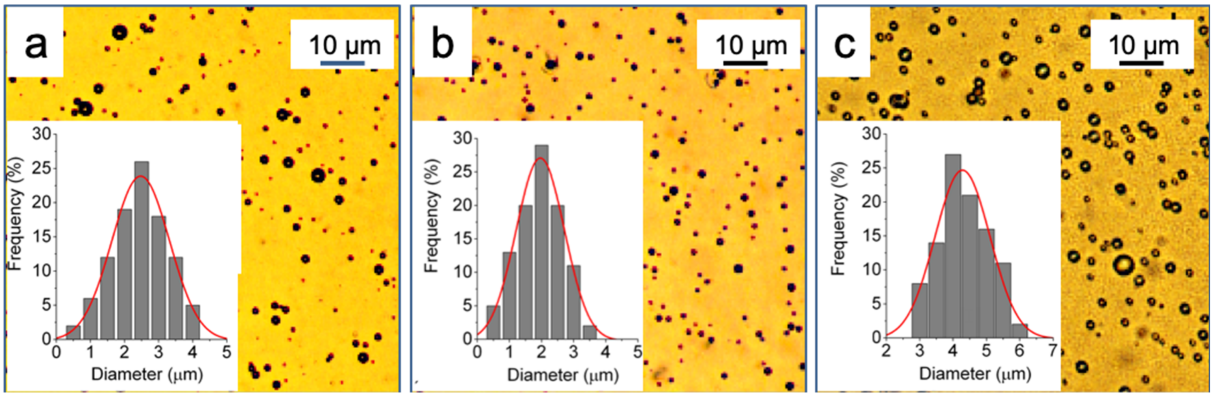

Figure 3: Optical micrographs and corresponding size distribution of the perfluorohexane-stabilized microbubbles with a shell of a) DPPC, b) DPPC/*F*-lipopeptide **3**, and c) DPPC/hydrocarbon analog **4**.

F-lipopeptides. By contrast, the incorporation of the hydrocarbon analog **4** led to a marked increase in the mean MB diameter (4.3 ± 0.9 µm, Figure 3c).

Finally, we have investigated the stability of the microbubbles over time at room temperature. The MBs containing the *F*-lipopeptides were found to be more stable than the reference DPPC/DPPE-PEG2000 MBs (Figure 4). The most stable MBs were those containing the *F*-lipopeptide **3** with a half-life of 1.1 ± 0.2 h, as compared to 0.6 ± 0.2 for DPPC MBs. MBs incorporating the *F*-lipopeptides **1** and **2** displayed intermediate half-lives.

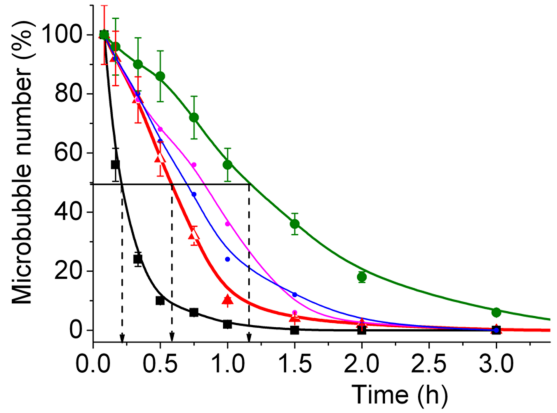

Figure 4: Half-lives of microbubbles (25 °C) containing *F*-lipopeptides **1**–**3** and hydrocarbon analog **4**.

The reduction in size of the MBs incorporating the *F*-lipopeptides compared to those incorporating the hydrocarbon compound **4** can be explained by the faster diffusion of the former lipopeptides to the interface and by their larger value of π_{eq}, hence a lower surface tension at the bubble surface. The enhanced MB stability over time and the fact that the half-life increases with fluorocarbon chain length support the view that stabilizing interactions develop between the *F*-lipopeptide and perfluorohexane in the bubble's interfacial film.

Conclusion

A series of lipopeptides carrying C_nF_{2n+1} chains (n = 6, 7, 8, **1**–**3**) or $C_{10}H_{21}$ chains (**4**) grafted through a lysine moiety on a peptide chain composed of a KSS sequence followed by 5 SG sequences were synthesized by Fmoc solid-phase peptide synthesis. The investigation of the physicochemical properties of these lipopeptides at the air/water interface demonstrates that the fluorination substantially improves the surface-active properties. In our experimental conditions, the fluorination enables a significantly larger and faster adsorption, both at the surface of water and on the DPPC monolayers in both the LE and LC states. By contrast, the adsorption of the hydrocarbon analog is only possible when the phospholipid monolayer is in the LE state, whilst its adsorption in the LC state is not only prohibited, but even provokes a delipidation of the interface. The incorporation of the perfluoroalkylated lipopeptides in the phospholipid shells of perfluorohexane-stabilized microbubbles significantly reduces their mean size and increases their stability. By contrast, larger bubbles with shorter half-lives are obtained with the hydrocarbon analog. Our results establish that a fluorination of the precursors of targeting ligand–peptide conjugates can considerably facilitate microbubble generation due to faster diffusion to the air/water interface, and augment their stability through interfacial fluorine–fluorine interactions.

Experimental

Materials. We purchased Fmoc-protected amino acids, *N*,*N*-dimethylformamide (DMF), dichloromethane (DCM), methanol, 1-hydroxybenzotriazole (HOBT), 2-(1*H*-benzotriazole-1-yl)-1,1,3,3-tetramethyluronium hexafluorophosphate (HBTU), *N*,*N*-diisopropylethylamine (DIPEA), piperidine, acetic an-

hydride, trifluoroacetic acid (TFA), triisopropylsilane (TIS), Rink Amide AM resin (4-(2',4'-dimethoxyphenyl-Fmoc-aminomethyl)phenoxyacetamido-aminomethyl resin, 100–200 mesh), and Tube-O-DIALYZER™ mini dialysis system (MWCO 1K) from Merck (Darmstadt, Germany). 1,2-Dipalmitoylphosphatidylcholine (DPPC, >99%) and 1,2-dipalmitoyl-*sn*-glycero-3-phosphoethanolamine-*N*-[methoxy(polyethylene glycol)-2000] (DPPE-PEG2000, >99%) were purchased from Avanti Polar Lipids (Alabaster, AL, USA) and used without further purification. Perfluorohexane came from Fluorochem (>98%). A HEPES (*N*-2-(hydroxyethyl)piperazine-*N*′-(2-ethanesulfonic acid), powder, 99.5%, Corning, NY) buffer solution (20 mM) in 150 mM NaCl was prepared and adjusted to pH 7.4 using 0.1 N NaOH. Chloroform (99.4%) was purchased from VWR (Avantor, Fontenay-sous-Bois). Ultrapure water was obtained from a Milli-Q (Millipore Corp.) system (surface tension: 72.1 mN m^{-1} at 20 °C, resistivity: 18.2 MΩ cm). Mass spectra (MS) and HRMS were performed using a JMS-700 spectrometer (JEOL, Japan). RP-HPLC chromatograms were recorded on a Prominence system (Shimadzu, Japan). FTIR spectra were recorded on IRAffinity-1 (Shimadzu, Japan) spectrometer.

General procedure for the synthesis of perfluoroalkylated lipopeptides. All *F*-lipopeptides $(SG)_5$-KSS-K$(C_2H_4$-$C_nF_{2n+1})_2$ with n = 6 (**1**), 7 (**2**), 8 (**3**) and hydrocarbon analog $(SG)_5$-KSS-K$(C_{10}H_{21})_2$ were synthesized using an Fmoc solid-phase peptide synthesis (SPPS) method. Rink Amide AM resin (0.1 mmol) in a 10 mL column was suspended in 5 mL of DMF and swollen overnight. After washing with DMF (3 × 2 mL), the Fmoc groups of the Rink amide AM resin were activated with 20% of piperidine in DMF (2 mL) for 20 min. After washing with DMF (3 × 2 mL), Fmoc-Ser(*t*-Bu)-OH (3 equiv) as the first Fmoc-amino acid and the mixture of HBTU, HOBT, and DIPEA (3 equiv/3 equiv/6 equiv) in DMF were added to the resin and shaken for 30 min. The reaction was monitored using a Kaiser test based on the reaction of ninhydrin. After washing with DMF (3 × 2 mL) and DCM (3 × 2 mL), 25% of acetic anhydride in DCM (2 mL) was added for capping the unreacted amino acids and the mixture was shaken for 5 min. In a similar manner, each of the peptide chains was elongated by coupling Fmoc-Ser(*t*-Bu)-OH (3 equiv), Fmoc-Gly-OH (3 equiv) and Fmoc-Lys(Boc)-OH (3 equiv) to the Rink Amide AM resin. After introducing Fmoc-Lys(Fmoc)-OH as the terminal amino acid, the Fmoc groups of Fmoc-Lys(Fmoc)-OH were activated with 2 × 20% of piperidine in DMF (2 mL) for 20 min, and the coupling reaction with perfluoroalkylated acids (3 equiv) or alkyl acid (3 equiv) was performed 3 times with HBTU/HOBT/DIPEA (6 equiv/6 equiv/12 equiv) for 3 h. After capping the reaction with 25% of acetic anhydride in DCM (2 mL), the column was washed with DCM (3 × 2 mL), DMF (3 × 2 mL), and methanol (3 × 2 mL), and dried overnight. A solution of 2.5 mL of TFA/TIS/H_2O 94:2.5:2.5 (v/v/v) was added to the column for cleaving the compound from the resin, and the reaction was performed for 3 h. The TFA/TIS/H_2O solution including the crude product was collected in a 50 mL Erlenmeyer flask. The column was washed 3 times with TFA (1.5 mL), and the washing solutions were combined. After drying the solution with argon gas, the residue was washed with 20 mL of diethyl ether. The product was collected by filtration and purified by dialysis using a Tube-O-DIALYZER™ mini dialysis system. The purity of the final products was analyzed by a high-performance liquid chromatography (HPLC) system using a reversed-phase column (COSMOSIL 5C18-AR-II 4.6 × 250 mm) with water and acetonitrile 20:80 (v/v) at a flow rate of 0.5 mL/min.

$(SG)_5$-KSS-K$(C_2H_4$-$C_6F_{13})_2$ (**1**) was synthesized according to the general procedure using 4,4,5,5,6,6,7,7,8,8,9,9,9-tridecafluorononanoic acid. Yield: 121 mg (6.3%); FABMS (*m*/*z*): 1916 $[M + H]^+$; HRMS (*m*/*z*): $[M + H]^+$ calcd for $C_{61}H_{84}F_{26}N_{17}O_{23}$, 1916.5511; found: 1916.5509; purity (retention time): >99% (13.8 min).

$(SG)_5$-KSS-K$(C_2H_4$-$C_7F_{15})_2$ (**2**) was synthesized according to the general procedure using 4,4,5,5,6,6,7,7,8,8,9,9,10,10,10-pentadecafluorodecanoic acid. Yield: 95 mg (4.7%); FABMS (*m*/*z*): 2016 $[M + H]^+$; HRMS (*m*/*z*): $[M + H]^+$ calcd for $C_{63}H_{84}F_{30}N_{17}O_{23}$, 2016.5447; found, 2016.5448; purity (retention time): >99% (14.8 min).

$(SG)_5$-KSS-K$(C_2H_4$-$C_8F_{17})_2$ (**3**) was synthesized according to the general procedure using 4,4,5,5,6,6,7,7,8,8,9,9,10,10,11,11,11-heptadecafluoroundecanoic acid. Yield: 111 mg (5.2%); FABMS (*m*/*z*): 2116 $[M + H]^+$; HRMS (*m*/*z*): $[M + H]^+$ calcd for $C_{65}H_{84}F_{34}N_{17}O_{23}$, 2116.5383; found, 2116.5381; purity (retention time): >99% (13.8 min).

$(SG)_5$-KSS-K$(C_{10}H_{21})_2$ (**4**) was synthesized according to the general procedure using undecanoic acid. Yield: 70 mg (4.7%); FABMS (*m*/*z*): 1504 $[M + H]^+$; HRMS (*m*/*z*): $[M + H]^+$ calcd for $C_{65}H_{118}N_{17}O_{23}$,1504.8586; found, 1504.8585; purity (retention time): >99% (13.9 min).

Adsorption kinetics of lipopeptides at the air/water interface. The experiments were conducted in a home-made Teflon adsorption trough (11.9 × 5.0 × 0.3 cm^3) filled with HEPES buffer (pH 7.4). The surface pressure π was measured using the Wilhelmy plate method. The temperature was maintained at 25 ± 0.5 °C. For the spontaneous formation of monolayers (Gibbs films) at the air/water interface, 50 µL of the solutions of the lipopeptides **1**–**4** in DMSO (1 mmol L^{-1}) were injected into the aqueous phase. For the experiment concerning the adsorp-

tion of lipopeptides on a DPPC Langmuir monolayer, a solution of DPPC in chloroform (1 mmol L^{-1}) was deposited on the surface of the aqueous phase. Depending on the volume deposited (9 µL or 18 µL), DPPC monolayers were obtained in the liquid expended or in the liquid condensed phase. Ten minutes were allowed to evaporate chloroform. Then, 50 µL of the solutions (1 mmol L^{-1}) of the lipopeptides in DMSO were injected in the aqueous sub-phase and the surface pressure was monitored over time. Three separate experiments were conducted for each lipopeptide. The error in the surface pressure measurements was ±0.5 mN m^{-1}.

Preparation and characterization of lipopeptide-containing microbubbles. DPPC (50 mmol L^{-1}) and DPPE-PEG2000 (DPPC/DPPE-PEG2000 molar ratio 9:1) were dispersed in a HEPES buffer solution (0.9 mL) by magnetic stirring for 3–6 h at 50 °C. Fifty µL of the lipopeptide solution in DMSO were injected into the phospholipid dispersion and subjected to agitation/amalgamation using a Vialmix® device (2 cycles of 45 s, Lantheus Medical Imaging N. Billerica, MA) at room temperature and under *F*-hexane-saturated N_2 at room temperature (for details, see [39]). The resulting foam was immediately diluted with 5 mL of HEPES buffer. Size fractionation of the microbubbles was achieved by flotation for 60 min. Reference microbubbles shelled with DPPC/DPPE-PEG2000 were prepared using the same protocol. Two to three droplets of the bubble dispersion were placed into a concave glass slide, covered with a glass slide and observed with a Nikon Eclipse 90i microscope (transmission mode, Nikon Instruments Europe, Amsterdam, The Netherlands). A rapid image acquisition was achieved using a Lumenera Infinity 2 charge-coupled device (CCD) camera (Lumenera, Ottawa, Canada). The bubble mean diameter and distribution width after preparation and upon time were determined on 5–10 slides using Fiji (an open-source image processing package [45]) and the standard deviations were calculated using Origin9 (OriginLab Corp. Northampton, MA, USA).

Supporting Information

Supporting Information File 1

Mass spectrometry and FTIR data as well as RP-HPLC chromatograms of lipopeptides **1**–**4**.
[https://www.beilstein-journals.org/bjoc/content/supplementary/1860-5397-17-45-S1.pdf]

Funding

The work was supported by JSPS KAKENHI Grant Number JP18KK0439 and JP20K08139. We also acknowledge CONACYT (Mexico) for a Ph.D. fellowship (E.E.M.O., grant #459199).

ORCID® iDs

Estefanía E. Mendoza-Ortega - https://orcid.org/0000-0002-2388-7834
Marie Pierre Krafft - https://orcid.org/0000-0002-3379-2783

Preprint

A non-peer-reviewed version of this article has been previously published as a preprint: https://doi.org/10.3762/bxiv.2020.133.v1

References

1. Ferrara, K. W.; Borden, M. A.; Zhang, H. *Acc. Chem. Res.* **2009,** *42,* 881–892. doi:10.1021/ar8002442
2. Sercombe, L.; Veerati, T.; Moheimani, F.; Wu, S. Y.; Sood, A. K.; Hua, S. *Front. Pharmacol.* **2015,** *6,* 286. doi:10.3389/fphar.2015.00286
3. Su, S.; Kang, P. M. *Pharmaceutics* **2020,** *12,* 837. doi:10.3390/pharmaceutics12090837
4. Siemer, S.; Wünsch, D.; Khamis, A.; Lu, Q.; Scherberich, A.; Filippi, M.; Krafft, M. P.; Hagemann, J.; Weiss, C.; Ding, G.-B.; Stauber, R. H.; Gribko, A. *Nanomaterials* **2020,** *10,* 383. doi:10.3390/nano10020383
5. Chowdhury, S. M.; Abou-Elkacem, L.; Lee, T.; Dahl, J.; Lutz, A. M. *J. Controlled Release* **2020,** *326,* 75–90. doi:10.1016/j.jconrel.2020.06.008
6. Osei, E.; Al-Asady, A. *J. Radiother. Pract.* **2020,** *19,* 291–298. doi:10.1017/s1460396919000633
7. Noble, G. T.; Stefanick, J. F.; Ashley, J. D.; Kiziltepe, T.; Bilgicer, B. *Trends Biotechnol.* **2014,** *32,* 32–45. doi:10.1016/j.tibtech.2013.09.007
8. Li, J.; Tan, T.; Zhao, L.; Liu, M.; You, Y.; Zeng, Y.; Chen, D.; Xie, T.; Zhang, L.; Fu, C.; Zeng, Z. *ACS Appl. Bio Mater.* **2020,** *3,* 5500–5528. doi:10.1021/acsabm.0c00705
9. Bae, K. H.; Chung, H. J.; Park, T. G. *Mol. Cells* **2011,** *31,* 295–302. doi:10.1007/s10059-011-0051-5
10. Tang, K.; Zhang, Y.; Zhang, H.; Xu, P.; Liu, J.; Ma, J.; Lv, M.; Li, D.; Katirai, F.; Shen, G.-X.; Zhang, G.; Feng, Z.-H.; Ye, D.; Huang, B. *Nat. Commun.* **2012,** *3,* 1282. doi:10.1038/ncomms2282
11. Wang, S.; Hossack, J. A.; Klibanov, A. L. *J. Drug Targeting* **2018,** *26,* 420–434. doi:10.1080/1061186x.2017.1419362
12. Li, H.; Zhao, J.; Wang, A.; Li, Q.; Cui, W. *Colloids Surf., A* **2020,** *590,* 124486. doi:10.1016/j.colsurfa.2020.124486
13. Saito, A.; Yamamoto, S.; Ochi, R.; Inoue, K.; Hadano, S.; Watanabe, S.; Nakayama, T.; Niko, Y. *Bull. Chem. Soc. Jpn.* **2020,** *93,* 568–575. doi:10.1246/bcsj.20200014
14. Wang, H.; Wu, L.; Sun, X. *Chest* **2020,** *157,* 1579–1590. doi:10.1016/j.chest.2019.11.036
15. Hagimori, M.; Fuchigami, Y.; Kawakami, S. *Chem. Pharm. Bull.* **2017,** *65,* 618–624. doi:10.1248/cpb.c17-00098
16. Wang, J.; Fang, T.; Li, M.; Zhang, W.; Zhang, Z.-P.; Zhang, X.-E.; Li, F. *J. Mater. Chem. B* **2018,** *6,* 3716–3726. doi:10.1039/c8tb00186c
17. Isidro-Llobet, A.; Kenworthy, M. N.; Mukherjee, S.; Kopach, M. E.; Wegner, K.; Gallou, F.; Smith, A. G.; Roschangar, F. *J. Org. Chem.* **2019,** *84,* 4615–4628. doi:10.1021/acs.joc.8b03001
18. Molek, P.; Strukelj, B.; Bratkovic, T. *Molecules* **2011,** *16,* 857–887. doi:10.3390/molecules16010857
19. Wang, Q.; Ma, X.; Jia, J.; Fei, H. *J. Mater. Chem. B* **2016,** *4,* 1535–1543. doi:10.1039/c5tb02783g

20. Wang, C.; Su, L.; Wu, C.; Wu, J.; Zhu, C.; Yuan, G. *Drug Dev. Ind. Pharm.* **2016,** *42,* 1938–1944. doi:10.1080/03639045.2016.1185435
21. Silva, S.; Almeida, A. J.; Vale, N. *Biomolecules* **2019,** *9,* 22. doi:10.3390/biom9010022
22. Reithmeier, H.; Herrmann, J.; Göpferich, A. *J. Controlled Release* **2001,** *73,* 339–350. doi:10.1016/s0168-3659(01)00354-6
23. Lehtinen, J.; Magarkar, A.; Stepniewski, M.; Hakola, S.; Bergman, M.; Róg, T.; Yliperttula, M.; Urtti, A.; Bunker, A. *Eur. J. Pharm. Sci.* **2012,** *46,* 121–130. doi:10.1016/j.ejps.2012.02.009
24. Koniev, O.; Wagner, A. *Chem. Soc. Rev.* **2015,** *44,* 5495–5551. doi:10.1039/c5cs00048c
25. Suga, T.; Kato, N.; Hagimori, M.; Fuchigami, Y.; Kuroda, N.; Kodama, Y.; Sasaki, H.; Kawakami, S. *Mol. Pharmaceutics* **2018,** *15,* 4481–4490. doi:10.1021/acs.molpharmaceut.8b00476
26. Allen, T. M.; Hansen, C.; Martin, F.; Redemann, C.; Yau-Young, A. *Biochim. Biophys. Acta, Biomembr.* **1991,** *1066,* 29–36. doi:10.1016/0005-2736(91)90246-5
27. Klibanov, A. L.; Maruyama, K.; Beckerleg, A. M.; Torchilin, V. P.; Huang, L. *Biochim. Biophys. Acta, Biomembr.* **1991,** *1062,* 142–148. doi:10.1016/0005-2736(91)90385-l
28. Suga, T.; Fuchigami, Y.; Hagimori, M.; Kawakami, S. *Int. J. Pharm.* **2017,** *521,* 361–364. doi:10.1016/j.ijpharm.2017.02.041
29. Suga, T.; Watanabe, M.; Sugimoto, Y.; Masuda, T.; Kuroda, N.; Hagimori, M.; Kawakami, S. *J. Drug Delivery Sci. Technol.* **2019,** *49,* 668–673. doi:10.1016/j.jddst.2018.12.037
30. Craig, J. A.; Rexeisen, E. L.; Mardilovich, A.; Shroff, K.; Kokkoli, E. *Langmuir* **2008,** *24,* 10282–10292. doi:10.1021/la702434p
31. Schutt, E. G.; Klein, D. H.; Mattrey, R. M.; Riess, J. G. *Angew. Chem., Int. Ed.* **2003,** *42,* 3218–3235. doi:10.1002/anie.200200550
32. Hernot, S.; Klibanov, A. L. *Adv. Drug Delivery Rev.* **2008,** *60,* 1153–1166. doi:10.1016/j.addr.2008.03.005
33. Sirsi, S. R.; Borden, M. A. *Adv. Drug Delivery Rev.* **2014,** *72,* 3–14. doi:10.1016/j.addr.2013.12.010
34. Chong, W. K.; Papadopoulou, V.; Dayton, P. A. *Abdom. Radiol.* **2018,** *43,* 762–772. doi:10.1007/s00261-018-1516-1
35. Rossi, S.; Waton, G.; Krafft, M. P. *Langmuir* **2010,** *26,* 1649–1655. doi:10.1021/la9025987
36. Szíjjártó, C.; Rossi, S.; Waton, G.; Krafft, M. P. *Langmuir* **2012,** *28,* 1182–1189. doi:10.1021/la2043944
37. Yang, G.; O'Duill, M.; Gouverneur, V.; Krafft, M. P. *Angew. Chem., Int. Ed.* **2015,** *54,* 8402–8406. doi:10.1002/anie.201502677
38. Shi, D.; Wallyn, J.; Nguyen, D.-V.; Perton, F.; Felder-Flesch, D.; Bégin-Colin, S.; Maaloum, M.; Krafft, M. P. *Beilstein J. Nanotechnol.* **2019,** *10,* 2103–2115. doi:10.3762/bjnano.10.205
39. Mendoza-Ortega, E. E.; Dubois, M.; Krafft, M. P. *ACS Appl. Nano Mater.* **2020,** *3,* 8897–8905. doi:10.1021/acsanm.0c01651
40. Nakahara, H.; Lee, S.; Krafft, M. P.; Shibata, O. *Langmuir* **2010,** *26,* 18256–18265. doi:10.1021/la103118d
41. Nguyen, P. N.; Trinh Dang, T. T.; Waton, G.; Vandamme, T.; Krafft, M. P. *ChemPhysChem* **2011,** *12,* 2646–2652. doi:10.1002/cphc.201100425
42. Sadtler, V. M.; Jeanneaux, F.; Krafft, M. P.; Rábai, J.; Riess, J. G. *New J. Chem.* **1998,** *22,* 609–613. doi:10.1039/a708757h
43. Lunkenheimer, K.; Barzyk, W.; Hirte, R.; Rudert, R. *Langmuir* **2003,** *19,* 6140–6150. doi:10.1021/la034379p
44. Varghese, N.; Shetye, G. S.; Yang, S.; Wilkens, S.; Smith, R. P.; Luk, Y.-Y. *J. Colloid Interface Sci.* **2013,** *412,* 95–99. doi:10.1016/j.jcis.2013.08.044
45. Nguyen, P. N.; Veschgini, M.; Tanaka, M.; Waton, G.; Vandamme, T.; Krafft, M. P. *Chem. Commun.* **2014,** *50,* 11576–11579. doi:10.1039/c3cc47840h

License and Terms

This is an Open Access article under the terms of the Creative Commons Attribution License (https://creativecommons.org/licenses/by/4.0). Please note that the reuse, redistribution and reproduction in particular requires that the author(s) and source are credited and that individual graphics may be subject to special legal provisions.

The license is subject to the *Beilstein Journal of Organic Chemistry* terms and conditions: (https://www.beilstein-journals.org/bjoc/terms)

The definitive version of this article is the electronic one which can be found at: https://doi.org/10.3762/bjoc.17.45

BEILSTEIN JOURNAL OF ORGANIC CHEMISTRY

Metal-free visible-light-enabled vicinal trifluoromethyl dithiolation of unactivated alkenes

Xiaojuan Li[1], Qiang Zhang[1], Weigang Zhang[*1], Jinzhu Ma[*2], Yi Wang[*1] and Yi Pan[1]

Full Research Paper

Open Access

Address:
[1]State Key Laboratory of Coordination Chemistry, Jiangsu Key Laboratory of Advanced Organic Materials, and Collaborative Innovation Center of Advanced Microstructures, School of Chemistry and Chemical Engineering, Nanjing University, Nanjing 210023, China and [2]School of pharmacy, Wannan Medical College, Wuhu, 241002, China

Email:
Weigang Zhang[*] - wgzhang@nju.edu.cn; Jinzhu Ma[*] - mane2011@126.com; Yi Wang[*] - yiwang@nju.edu.cn

* Corresponding author

Keywords:
alkenes; difunctionalization; metal-free; photoredox; trifluoromethylthiolation

Beilstein J. Org. Chem. **2021,** *17,* 551–557.
https://doi.org/10.3762/bjoc.17.49

Received: 13 January 2021
Accepted: 12 February 2021
Published: 24 February 2021

This article is part of the thematic issue "Organo-fluorine chemistry V".

Guest Editor: D. O'Hagan

© 2021 Li et al.; licensee Beilstein-Institut.
License and terms: see end of document.

Abstract

The difunctionalization of alkenes involving a trifluoromethylthio group (SCF_3) for the conversion of versatile and readily available olefins into structurally more complex molecules has been successfully studied. However, the disproportionate dithiolation of alkenes is unknown. Herein, a transition-metal-free protocol is presented for the vicinal trifluoromethylthio–thiolation of unactivated alkenes via a radical process under mild conditions with a broad substrate scope and excellent tolerance.

Introduction

The incorporation of fluorine atoms into drug molecules will significantly enhance the physical, chemical, and biological properties of the pharmaceuticals [1-6]. Modifying drug candidates by introducing fluorine-containing (such as $-CF_3$, $-CF_2H$, $-C_2F_5$, $-SCF_3$, $-OCF_3$) moieties has become a substantial strategy for medicinal research [2,7,8]. Among the fluorinated functionalities, the trifluoromethylthio group (SCF_3) has strong electron-withdrawing properties and a higher lipophilicity (π_R = 1.44), compared with CF_3 (π_R = 0.88) and SCH_3 (π_R = 0.61), which could improve the pharmaceuticals' ability to cross lipid membranes [9,10]. Along these lines, the introduction of the SCF_3 group into small molecules has attracted great attention in organofluorine methodology [11-17].

The vicinal difunctionalization of olefins to introduce two functional groups across a double bond has appeared as a powerful transformation to rapidly increase molecular complexity in synthetic chemistry with improved efficiency [18-22]. Various transition-metal-mediated approaches for the trifluoromethylthio (SCF_3) difunctionalization of alkenes, such as cyanation [23], etherification [24-27], amination [28-30], chlorination [31,32], hydrogenation [33], trifluoromethylation [34], phos-

phonization [35], arylation [36-38], trifluoromethylthiolation [39], fluorination [40], and selenylation [41] have been reported (Scheme 1a). However, the visible-light-induced trifluoromethylthio difunctionalization of alkenes remained underdeveloped. For instance, Magnier and co-workers have documented a practical intramolecular carbotrifluoromethylthiolation of acrylamides under irradiation of visible light [38]. In 2017, the photoredox-catalyzed intermolecular trifluoromethylthio–trifluoromethylation and thiosulfonylation reaction of unactivated alkenes have been respectively developed by Liu [34] and Xu [42]. Recently, Qing [43] and co-workers reported an efficient *anti*-Markovnikov hydrotrifluoromethylthiolation of alkenes utilizing trifluoromethanesulfonic anhydride (Tf_2O) as a radical trifluoromethylthiolating reagent through a deoxygenative reduction and a photoredox radical pathway (Scheme 1b). The C–S bond [44,45] is an important structural motif that is widely present in natural products, drug molecules, biologically active molecules, and functional materials. However, the highly selective incorporation of two different sulfur-bearing moieties across double bonds remains challenging [42]. Herein, we describe a visible-light-enabled cascade radical difunctionalization of unactivated alkenes for the construction of partially trifluoromethylated dithioethers with a broad substrate scope and a good chemical tolerance (Scheme 1c).

Results and Discussion

We evaluated the reaction conditions for this trifluoromethylthio–thiolation and found out that under irradiation of blue LEDs, allyl boronate **1a** (0.1 mmol), disulfide **2a** (1.0 equiv) and *N*-(trifluoromethylthio)phthalimide (Phth-SCF_3, **3**, 1.5 equiv), the desired trifluoromethylthiolated product **4a** was obtained in 71% yield with 1,2,3,5-tetrakis(carbazol-9-yl)-4,6-dicyanobenzene (4CzIPN, 2 mol %) as the photocatalyst and KH_2PO_4 (10 mol %) as the base (Table 1, entry 1). The yield of **4a** was not increased when 2 equiv of K_2HPO_4 were used (Table 1, entry 2) and no difunctionalized product was observed with DMA as the solvent (Table 1, entry 4). The employment of KH_2PO_4 as base and $[Ir(dF(CF_3)ppy)_2(dtbby)]PF_6$ as the photocatalyst furnished the product in very low yields (Table 1, entries 3 and 5). The control experiments indicated that 4CzIPN, K_2HPO_4 or visible-light were indispensable for the reaction to proceed (Table 1, entries 6–8).

With the optimized reaction conditions determined, we next examined the substrate scope of the disulfides (Scheme 2). Using borate-substituted olefins, the intermolecular trifluoromethylthio–thiolation induced by the sequential radical difunctionalization proceeded smoothly in a chemoselective fashion. Both, with electron-withdrawing and electron-donating groups substituted aryldisulfides were tolerated to access products **4a**–**g**. The homoallylic borate (**1b**) was also converted into the corresponding product **4h** in a moderate yield.

In order to further examine the generality of the reaction, we have extended this protocol to a range of unactivated alkenes.

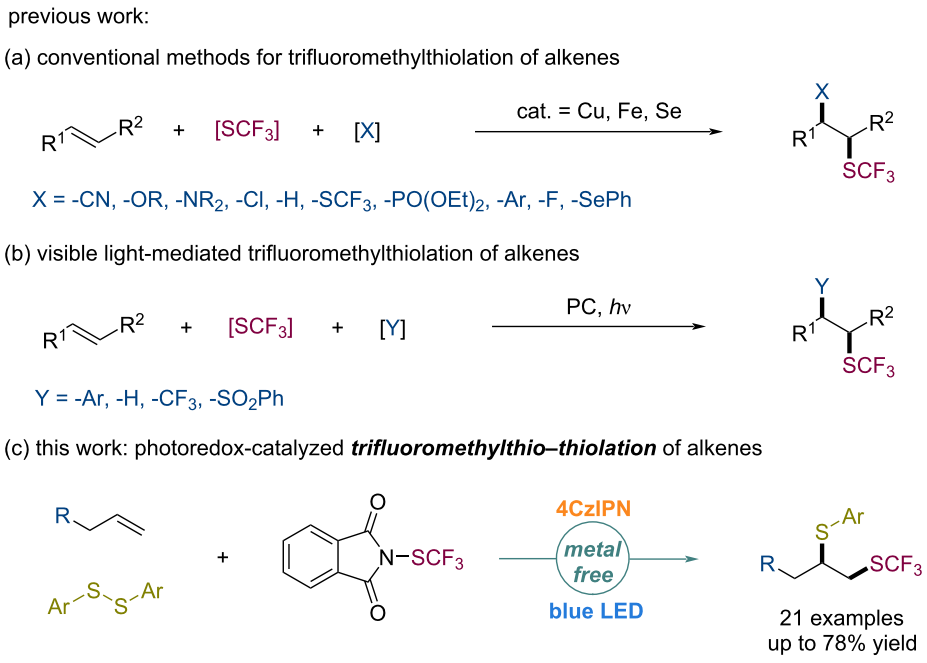

Scheme 1: Origin of the reaction design.

Table 1: Optimization of the reaction conditions.[a]

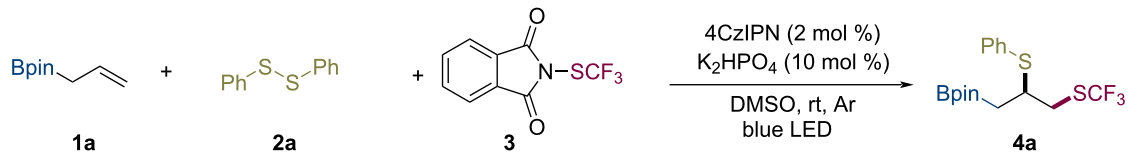

1a 2a 3 4a

entry	deviation from the reaction conditions	yield[b] (%)
1	none	71
2	2.0 equiv K_2HPO_4	70
3	KH_2PO_4 instead of K_2HPO_4	34
4	DMA instead of DMSO	trace
5	$[Ir(dF(CF_3)ppy)_2(dtbby)]PF_6$ instead of 4CzIPN	43
6	no K_2HPO_4	0
7	without 4CzIPN	0
8	in darkness	0

[a]Reaction conditions: **1a** (0.1 mmol), **2a** (1.0 equiv), **3** (1.5 equiv), 4CzIPN (2 mol %), K_2HPO_4 (10 mol %), rt, Ar, 24 h. [b]Crude yields were determined by ^{19}F NMR using trifluoromethoxybenzene as an internal standard.

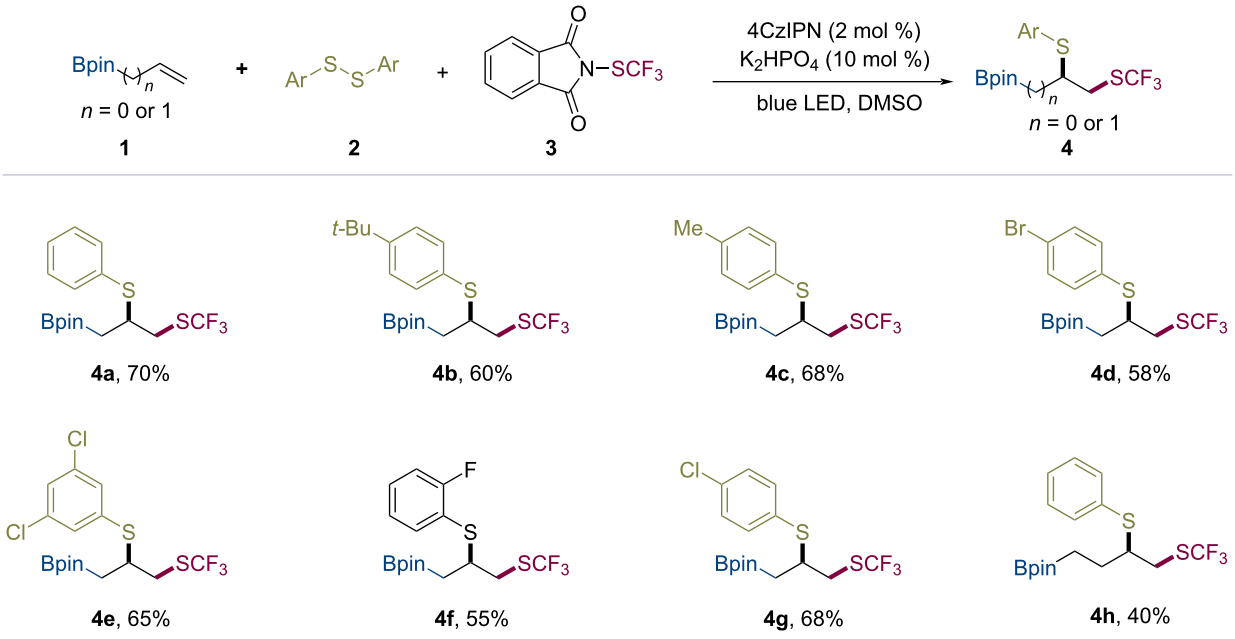

Scheme 2: Substrate scope of disulfides.

Terminal alkenes containing ester (**5a**–**d**) and oxygenated alkyl (**5e**–**g**) functionalities were tolerated under this framework (Scheme 3). The tested 1-phenyl-3-butene substrates transformed into the desired products **5h** and **5i** in good yields. Also olefins containing amido (**5j**) and sulfonate (**5k**) functionalities furnished the corresponding SCF_3 adducts. In addition, boldenone- and D-glucose-derived terminal alkenes were compatible with the conditions affording the corresponding products **5l** and **5m** in moderate to good yields.

To gain insight into the reaction mechanism, control experiments were conducted under the standard conditions (Scheme 4). The radical-trapping agent 2,2,6,6-tetramethylpiperidin-1-oxyl (TEMPO, 3.0 equiv) completely prevented the

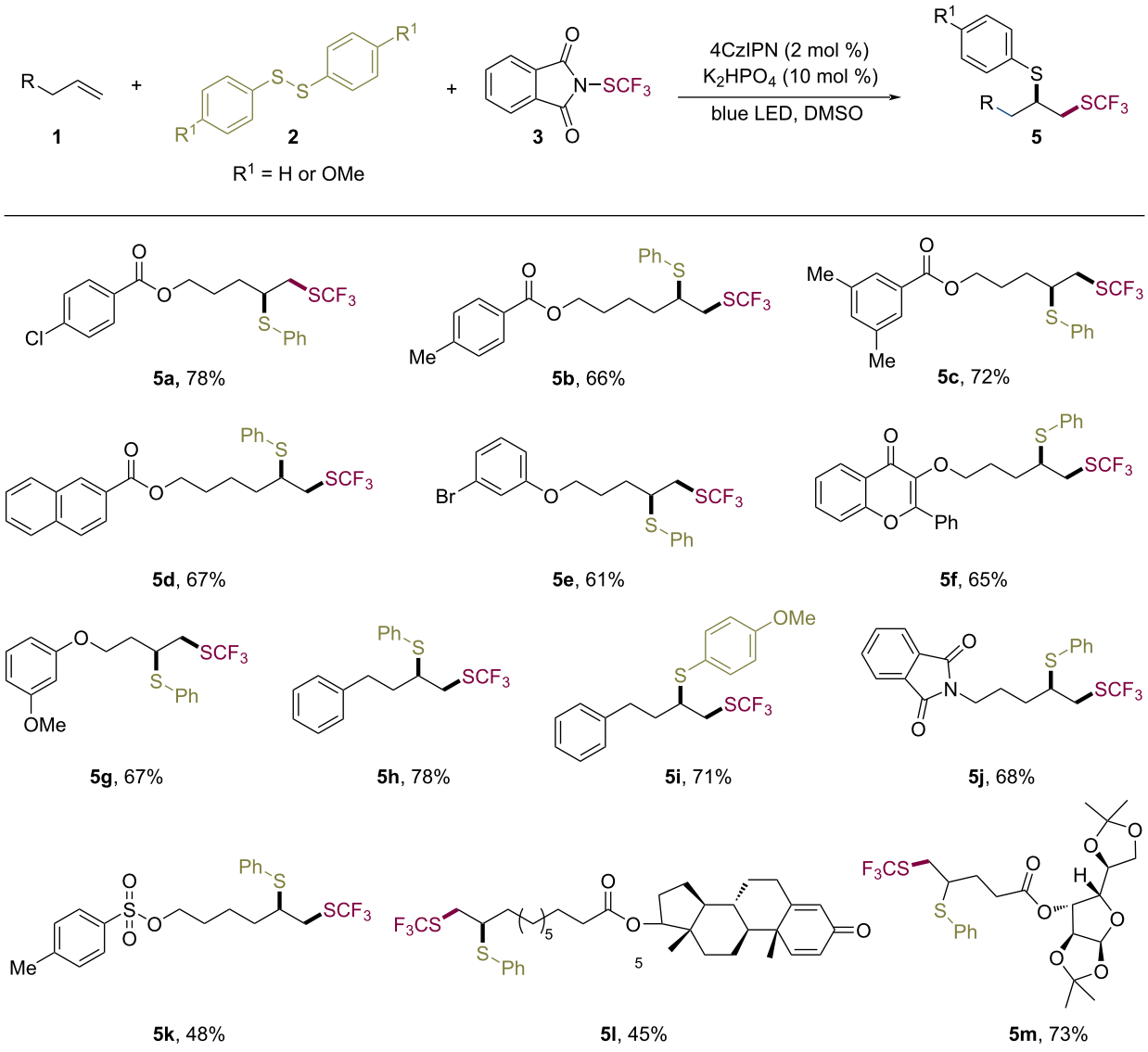

Scheme 3: Substrate scope of unactivated alkenes.

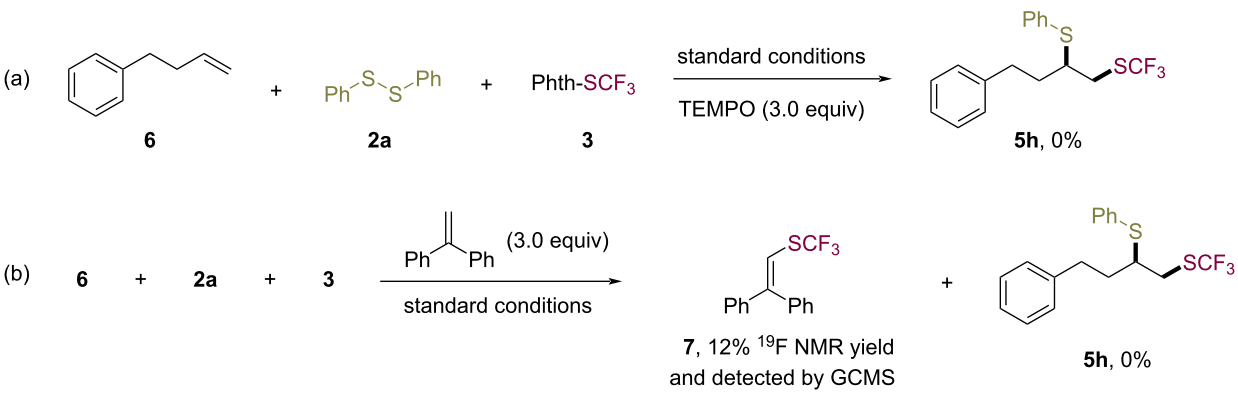

Scheme 4: Control experiments.

reaction. When diphenylethylene (3.0 equiv) was added to the reaction mixture, the desired product **5h** was not obtained, and the vinyltrifluoromethylsulfide **7** was afforded in 12% yield [46,47].

Based on the above results and previous literature reports [33,38,48], a plausible mechanism for the trifluoromethylthio–thiolation is proposed (Scheme 5). In solution, two resonance structures can be formulated for Phth-SCF_3, **3** ($E_{1/2}^{red}$ = −0.45 V vs SCE) [49] and the intermediate **I** [50]. The complexation of the intermediate **I** with K_2HPO_4 provides the intermediate **II**. Then, 4CzIPN* (4CzIPN$^+$/4CzIPN*: $E_{1/2}^{red}$ = −1.04 V vs SCE) [51] reduces the intermediate **II** to generate a phthalimide anion (Phth$^-$ [50]) and a trifluoromethylthio radical under irradiation. The SCF_3 radical readily reacts with the unactivated alkenes to give the intermediate **B**. The subsequent addition of **B** to disulfide **2** affords the difunctionalized products **4** or **5** and the thiophenyl radical **C** [52]. Finally, the oxidation of radical **C** by 4CzIPN$^+$ closes the catalytic cycle [53].

Conclusion

In summary, we described a visible-light-induced cascade radical difunctionalization of unactivated alkenes to provide partially trifluoromethylated dithioethers. The approach features practical conditions, good functional group tolerance, and a broad substrate scope allowing the incorporation of two distinctive sulfur-containing motifs into terminal olefins.

Supporting Information

Supporting Information File 1

Full experimental details, compound characterization, and copies of NMR spectra.
[https://www.beilstein-journals.org/bjoc/content/supplementary/1860-5397-17-49-S1.pdf]

Funding

We gratefully acknowledge the financial support from the National Natural Science Foundation of China (Nos. 21772085, 21971107, 22071101) and the Fundamental Research Funds for the Central Universities (Nos. 020514380220, 020514380131, 020514913412, 020514913214). We also thank the Collaborative Innovation Center of Advanced Microstructures and the Jiangsu Provincial Key Laboratory of Photonic and Electronic Materials at Nanjing University for support.

ORCID® iDs

Jinzhu Ma - https://orcid.org/0000-0002-0581-3137
Yi Wang - https://orcid.org/0000-0002-8700-7621

Preprint

A non-peer-reviewed version of this article has been previously published as a preprint: https://doi.org/10.3762/bxiv.2021.1.v1

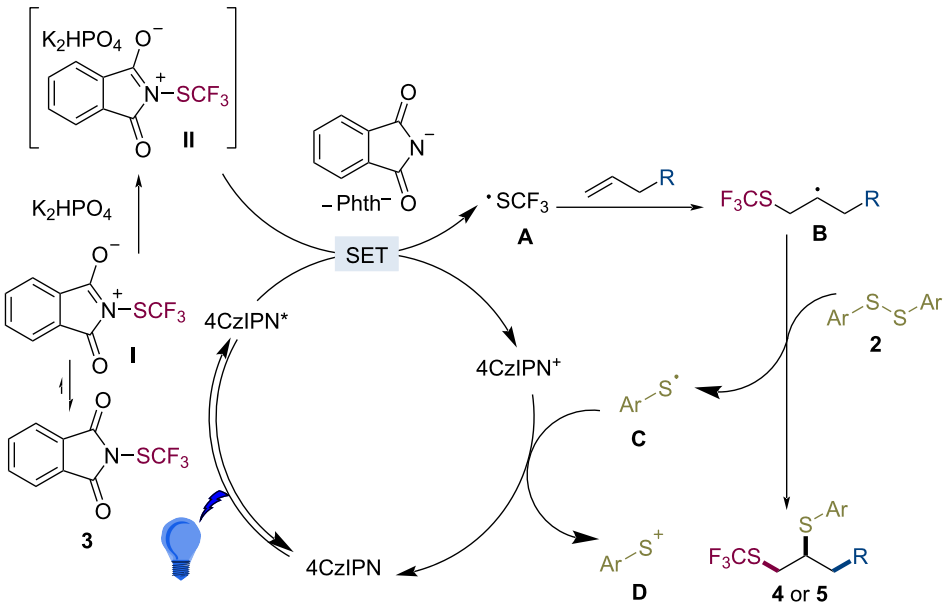

Scheme 5: Proposed mechanism.

References

1. Yang, X.; Wu, T.; Phipps, R. J.; Toste, F. D. *Chem. Rev.* **2015,** *115,* 826–870. doi:10.1021/cr500277b
2. Wang, J.; Sánchez-Roselló, M.; Aceña, J. L.; del Pozo, C.; Sorochinsky, A. E.; Fustero, S.; Soloshonok, V. A.; Liu, H. *Chem. Rev.* **2014,** *114,* 2432–2506. doi:10.1021/cr4002879
3. O'Hagan, D. *Chem. Soc. Rev.* **2008,** *37,* 308–319. doi:10.1039/b711844a
4. Müller, K.; Faeh, C.; Diederich, F. *Science* **2007,** *317,* 1881–1886. doi:10.1126/science.1131943
5. Liang, T.; Neumann, C. N.; Ritter, T. *Angew. Chem., Int. Ed.* **2013,** *52,* 8214–8264. doi:10.1002/anie.201206566
6. Manteau, B.; Pazenok, S.; Vors, J.-P.; Leroux, F. R. *J. Fluorine Chem.* **2010,** *131,* 140–158. doi:10.1016/j.jfluchem.2009.09.009
7. Guo, S.; Cong, F.; Guo, R.; Wang, L.; Tang, P. *Nat. Chem.* **2017,** *9,* 546–551. doi:10.1038/nchem.2711
8. Shao, X.; Hong, X.; Lu, L.; Shen, Q. *Tetrahedron* **2019,** *75,* 4156–4166. doi:10.1016/j.tet.2019.05.061
9. Hansch, C.; Leo, A.; Taft, R. W. *Chem. Rev.* **1991,** *91,* 165–195. doi:10.1021/cr00002a004
10. Hansch, C.; Leo, A.; Unger, S. H.; Kim, K. H.; Nikaitani, D.; Lien, E. J. *J. Med. Chem.* **1973,** *16,* 1207–1216. doi:10.1021/jm00269a003
11. Xu, C.; Ma, B.; Shen, Q. *Angew. Chem., Int. Ed.* **2014,** *53,* 9316–9320. doi:10.1002/anie.201403983
12. Glenadel, Q.; Alazet, S.; Billard, T. *J. Fluorine Chem.* **2015,** *179,* 89–95. doi:10.1016/j.jfluchem.2015.06.007
13. Ferry, A.; Billard, T.; Langlois, B. R.; Bacqué, E. *Angew. Chem., Int. Ed.* **2009,** *48,* 8551–8555. doi:10.1002/anie.200903387
14. Mukherjee, S.; Maji, B.; Tlahuext-Aca, A.; Glorius, F. *J. Am. Chem. Soc.* **2016,** *138,* 16200–16203. doi:10.1021/jacs.6b09970
15. Boiko, V. N. *Beilstein J. Org. Chem.* **2010,** *6,* 880–921. doi:10.3762/bjoc.6.88
16. Xu, X.-H.; Matsuzaki, K.; Shibata, N. *Chem. Rev.* **2015,** *115,* 731–764. doi:10.1021/cr500193b
17. Wu, H.; Xiao, Z.; Wu, J.; Guo, Y.; Xiao, J.-C.; Liu, C.; Chen, Q.-Y. *Angew. Chem., Int. Ed.* **2015,** *54,* 4070–4074. doi:10.1002/anie.201411953
18. Chen, Y.; Li, L.; Ma, Y.; Li, Z. *J. Org. Chem.* **2019,** *84,* 5328–5338. doi:10.1021/acs.joc.9b00339
19. Yin, G.; Mu, X.; Liu, G. *Acc. Chem. Res.* **2016,** *49,* 2413–2423. doi:10.1021/acs.accounts.6b00328
20. Wang, X.-X.; Lu, X.; He, S.-J.; Fu, Y. *Chem. Sci.* **2020,** *11,* 7950–7956. doi:10.1039/d0sc02054k
21. Tu, H.-Y.; Zhu, S.; Qing, F.-L.; Chu, L. *Synthesis* **2020,** *52,* 1346–1356. doi:10.1055/s-0039-1690842
22. Dhungana, R. K.; KC, S.; Basnet, P.; Giri, R. *Chem. Rec.* **2018,** *18,* 1314–1340. doi:10.1002/tcr.201700098
23. Ji, M.; Wu, Z.; Yu, J.; Wan, X.; Zhu, C. *Adv. Synth. Catal.* **2017,** *359,* 1959–1962. doi:10.1002/adsc.201700218
24. Xiang, H.; Yang, C. *Org. Lett.* **2014,** *16,* 5686–5689. doi:10.1021/ol502751k
25. Zhu, L.; Wang, G.; Guo, Q.; Xu, Z.; Zhang, D.; Wang, R. *Org. Lett.* **2014,** *16,* 5390–5393. doi:10.1021/ol502624z
26. Xu, C.; Shen, Q. *Org. Lett.* **2015,** *17,* 4561–4563. doi:10.1021/acs.orglett.5b02315
27. Zhu, Z.; Luo, J.; Zhao, X. *Org. Lett.* **2017,** *19,* 4940–4943. doi:10.1021/acs.orglett.7b02406
28. Luo, J.; Liu, Y.; Zhao, X. *Org. Lett.* **2017,** *19,* 3434–3437. doi:10.1021/acs.orglett.7b01392
29. Xiao, Q.; He, Q.; Li, J.; Wang, J. *Org. Lett.* **2015,** *17,* 6090–6093. doi:10.1021/acs.orglett.5b03116
30. Luo, J.; Zhu, Z.; Liu, Y.; Zhao, X. *Org. Lett.* **2015,** *17,* 3620–3623. doi:10.1021/acs.orglett.5b01727
31. Jia, Y.; Qin, H.; Wang, N.; Jiang, Z.-X.; Yang, Z. *J. Org. Chem.* **2018,** *83,* 2808–2817. doi:10.1021/acs.joc.7b03261
32. Jiang, L.; Ding, T.; Yi, W.-b.; Zeng, X.; Zhang, W. *Org. Lett.* **2018,** *20,* 2236–2240. doi:10.1021/acs.orglett.8b00581
33. Yang, T.; Lu, L.; Shen, Q. *Chem. Commun.* **2015,** *51,* 5479–5481. doi:10.1039/c4cc08655d
34. Fang, J.; Wang, Z.-K.; Wu, S.-W.; Shen, W.-G.; Ao, G.-Z.; Liu, F. *Chem. Commun.* **2017,** *53,* 7638–7641. doi:10.1039/c7cc01903c
35. Xiao, Z.; Liu, Y.; Zheng, L.; Zhou, X.; Xie, Y.; Liu, C.; Guo, Y.; Chen, Q.-Y. *Tetrahedron* **2018,** *74,* 6213–6219. doi:10.1016/j.tet.2018.09.019
36. Xiao, Z.; Liu, Y.; Zheng, L.; Liu, C.; Guo, Y.; Chen, Q.-Y. *J. Org. Chem.* **2018,** *83,* 5836–5843. doi:10.1021/acs.joc.8b00650
37. Yin, F.; Wang, X.-S. *Org. Lett.* **2014,** *16,* 1128–1131. doi:10.1021/ol403739w
38. Dagousset, G.; Simon, C.; Anselmi, E.; Tuccio, B.; Billard, T.; Magnier, E. *Chem. – Eur. J.* **2017,** *23,* 4282–4286. doi:10.1002/chem.201700734
39. Liu, Y.-L.; Qing, F.-L.; Xu, X.-H. *Eur. J. Org. Chem.* **2020,** 1015–1018. doi:10.1002/ejoc.201901836
40. Liu, X.; Liang, Y.; Ji, J.; Luo, J.; Zhao, X. *J. Am. Chem. Soc.* **2018,** *140,* 4782–4786. doi:10.1021/jacs.8b01513
41. Saravanan, P.; Anbarasan, P. *Chem. Commun.* **2019,** *55,* 4639–4642. doi:10.1039/c9cc00815b
42. Li, H.; Shan, C.; Tung, C.-H.; Xu, Z. *Chem. Sci.* **2017,** *8,* 2610–2615. doi:10.1039/c6sc05093j
43. Ouyang, Y.; Xu, X.-H.; Qing, F.-L. *Angew. Chem., Int. Ed.* **2019,** *58,* 18508–18512. doi:10.1002/anie.201911323
44. Beletskaya, I. P.; Ananikov, V. P. *Chem. Rev.* **2011,** *111,* 1596–1636. doi:10.1021/cr100347k
45. Otsuka, S.; Nogi, K.; Yorimitsu, H. *Top. Curr. Chem.* **2018,** *376,* 13. doi:10.1007/s41061-018-0190-7
46. Li, H.; Liu, S.; Huang, Y.; Xu, X.-H.; Qing, F.-L. *Chem. Commun.* **2017,** *53,* 10136–10139. doi:10.1039/c7cc06232j
47. Honeker, R.; Garza-Sanchez, R. A.; Hopkinson, M. N.; Glorius, F. *Chem. – Eur. J.* **2016,** *22,* 4395–4399. doi:10.1002/chem.201600190
48. Xu, W.; Ma, J.; Yuan, X.-A.; Dai, J.; Xie, J.; Zhu, C. *Angew. Chem., Int. Ed.* **2018,** *57,* 10357–10361. doi:10.1002/anie.201805927
49. Pluta, R.; Nikolaienko, P.; Rueping, M. *Angew. Chem., Int. Ed.* **2014,** *53,* 1650–1653. doi:10.1002/anie.201307484
50. Rahman, M.; Buchspies, J.; Szostak, M. *Catalysts* **2019,** *9,* 129. doi:10.3390/catal9020129
51. Luo, J.; Zhang, J. *ACS Catal.* **2016,** *6,* 873–877. doi:10.1021/acscatal.5b02204
52. Jin, Y.; Yang, H.; Fu, H. *Chem. Commun.* **2016,** *52,* 12909–12912. doi:10.1039/c6cc06994k
53. Straathof, N. J. W.; Cramer, S. E.; Hessel, V.; Noël, T. *Angew. Chem., Int. Ed.* **2016,** *55,* 15549–15553. doi:10.1002/anie.201608297

License and Terms

This is an Open Access article under the terms of the Creative Commons Attribution License (https://creativecommons.org/licenses/by/4.0). Please note that the reuse, redistribution and reproduction in particular requires that the author(s) and source are credited and that individual graphics may be subject to special legal provisions.

The license is subject to the *Beilstein Journal of Organic Chemistry* terms and conditions: (https://www.beilstein-journals.org/bjoc/terms)

The definitive version of this article is the electronic one which can be found at: https://doi.org/10.3762/bjoc.17.49

BEILSTEIN JOURNAL OF ORGANIC CHEMISTRY

Development of *N*-F fluorinating agents and their fluorinations: Historical perspective

Teruo Umemoto*, Yuhao Yang and Gerald B. Hammond*

Review

Open Access

Address:
Department Chemistry, University of Louisville, Lousiville, Kentucky 40292, USA

Email:
Teruo Umemoto* - teruo.umemoto@louisville.edu;
Gerald B. Hammond* - gb.hammond@louisville.edu

* Corresponding author

Keywords:
N-F fluorinating agent; fluorination; fluorodiazoniabicyclo[2.2.2]octane salt; fluoropyridinium salt; fluorosulfonimide

Beilstein J. Org. Chem. **2021,** *17,* 1752–1813.
https://doi.org/10.3762/bjoc.17.123

Received: 24 March 2021
Accepted: 06 July 2021
Published: 27 July 2021

This article is part of the thematic issue "Organo-fluorine chemistry V".

Guest Editor: D. O'Hagan

© 2021 Umemoto et al.; licensee Beilstein-Institut.
License and terms: see end of document.

Abstract

This review deals with the historical development of all *N*-F fluorinating agents developed so far. The unique properties of fluorine make fluorinated organic compounds attractive in many research areas and therefore fluorinating agents are important. *N*-F agents have proven useful by virtue of their easy handling. This reagent class includes many types of *N*-F compounds: perfluoro-*N*-fluoropiperidine, *N*-fluoro-2-pyridone, *N*-fluoro-*N*-alkylarenesulfonamides, *N*-fluoropyridinium salts and derivatives, *N*-fluoroquinuclidium salts, *N*-fluoro-trifluoromethanesulfonimide, *N*-fluoro-sultams, *N*-fluoro-benzothiazole dioxides, *N*-fluoro-lactams, *N*-fluoro-*o*-benzenedisulfonimide, *N*-fluoro-benzenesulfonimide, 1-alkyl-4-fluoro-1,4-diazoniabicyclo[2.2.2]octane salts, *N*-fluoropyridinium-2-sulfonate derivatives, 1-fluoro-4-hydroxy-1,4-diazoniabicyclo[2.2.2]octane salts, *N*-fluorodinitroimidazole, *N*-fluoro-trichloro-1,3,5-triazinium salt, *N*-F ethano-Tröger's base derivatives, *N*-fluoro-methanesulfonimide, *N*-fluoro-*N*-arylarenesulfonamides, bis*N*-F salts such as *N*,*N*'-difluorobipyridinium salts and *N*,*N*'-difluoro-1,4-diazoniabicyclo[2.2.2]octane salts, and their many derivatives and analogs, including chiral *N*-F reagents such as optically active *N*-fluoro-sultam derivatives, *N*-fluoro-alkaloid derivatives, DABCO-based *N*-F derivatives, and *N*-F binaphthyldisulfonimides. The synthesis and reactions of these reagents are described chronologically and the review also discusses the relative fluorination power of each reagent and their mechanisms chronicling developments from a historical perspective.

Introduction

Fluorinated organic compounds occupy an important position in pharmaceuticals [1], agrochemicals [2], and materials [3]. Especially, in the first two areas, the presence of fluorine has attracted attention during the last decades. Nowadays, a considerable number of medicines [4,5] and agrochemicals [6] contain at least one fluorine atom in their structures. The fluorine atom has unique properties such as the highest electronegativity, extremely low polarization, strong C–F bonds, and the smallest size after a hydrogen atom [7]. Thus, introduction of fluorine into selective positions of a bioactive compound can produce

remarkable changes in efficacy. Fluorine-scan/fluorine editing of a lead molecule is now a routine step in drug discovery [8]. Organofluorine compounds are very rare in nature [9] and therefore without natural compounds, chemical processes are required to generate building blocks. Molecular fluorine (F_2) is a useful fluorinating reagent, however, unlike Cl_2 and Br_2, F_2 is extremely reactive, toxic, and corrosive and its handling requires specialist skills and equipment. Therefore, easy-to-handle and selective fluorinating agents are essential for the wide-spread advancement of organofluorine chemistry to non-specialist chemists. Alternatives to F_2, such as perchloryl fluoride ($FClO_3$) [10] and the *O*-F reagents such as CF_3OF [11], $CF_2(OF)_2$ [11], $CsOSO_2OF$ [12], CF_3COOF [13], and CH_3COOF [14] have been used as fluorinating agents for many years. However, these reagents have significant risks for safe handling. Although XeF_2 [15] was considered as a safer alternative, it is expensive because of the scarcity of Xe in nature. The appearance of the safe and easy-to-handle *N*-F fluorinating agents described in this review have brought about a breakthrough in synthetic fluorine chemistry enabling an increasing number of researchers to engage in organofluorine chemistry. Their development has significantly contributed towards the current 'golden age' of fluorine chemistry. The *N*-F fluorinating agents now stand out as particularly useful electrophilic or radical fluorinating agents by virtue of their easy handling, efficiency, and selectivity. These non-hygroscopic nature and stability make them easier to handle than nucleophilic fluoride reagents. Potassium fluoride (KF) and naked fluoride anion salts are extremely sensitive to moisture, while HF seriously attacks human skin. The *N*-F fluorinating agents can be classified into two categories: these are neutral and cationic. This review covers the chronological advancement of these reagents regardless of their classification, as they advanced side by side.

Review

1. Historical progress of *N*-F fluorinating agents

1-1. Perfluoro-*N*-fluoropiperidine

The history of the *N*-F compounds acting as fluorine atom-transfer reagents can be traced back to 1964 when Banks and co-worker [16] first reported that perfluoro-*N*-fluoropiperidine (**1-1**) could fluorinate the sodium salt of 2-nitropropane to form 2-fluoro-2-nitropropane in a 40% yield (Scheme 1). The reaction with sodium diethyl malonate was also reported to produce the difluoromalonate, but in a very low yield of ca. 5%.

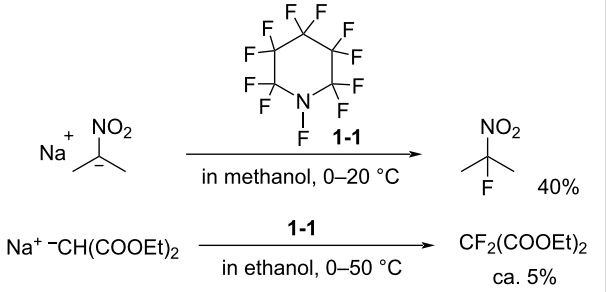

Scheme 1: Fluorination with *N*-F amine **1-1**.

N-F amine **1-1** is very volatile (bp 49.5 °C), and could only be prepared in 7.5% or 13% yield by electrochemical fluorination of pyridine or 2-fluoropyridine in anhydrous hydrogen fluoride [17,18] (Scheme 2). Not surprisingly, **1-1** did not become a popular reagent.

In 1967, Banks et al. reported reactions of **1-1** with piperidine and triphenylphosphine, -arsine, and -stibine (Scheme 3, entries 1 and 2) [19]. The former reaction gave adduct **1-3** as a major product and the latter showed good fluorine-transfer to the hetero atoms. In 1972, German et al. reported the reaction with sodium phenoxide, which gave a small amount (5%) of fluorophenols **1-6** and a larger amount of adduct **1-7** (Scheme 3, entry 3) [20]. These data showed that the fluorinations with **1-1** were suppressed by the formation of perfluoro-3,4,5,6-tetrahydropyridine (**1-5**), which was reactive to the nucleophilic substrates existing in the reaction mixture.

In 1986, Banks and co-worker reported the preparation of polymeric analogues of perfluoro-*N*-fluoropiperidine (**1-1**) [21] and then in 1991, Banks et al. reported the improved yields of the reactions of **1-1** with sodium salts of 2-nitropropane, malonate esters, and a keto ester, and phenylmagnesium bromide [22].

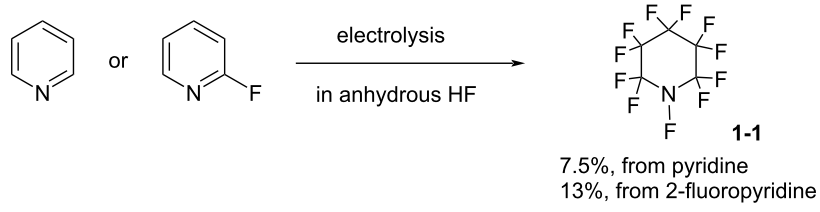

Scheme 2: Preparation of *N*-F amine **1-1**.

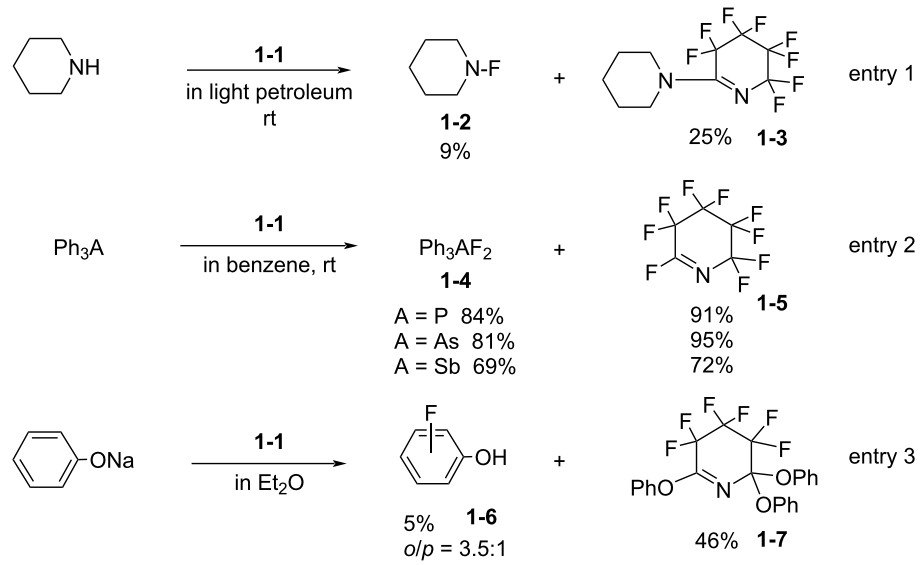

Scheme 3: Reactions of *N*-F amine **1-1**.

However, the fluorinated products were still accompanied by considerable amounts of byproducts resulting from the reaction of the substrates with **1-5**.

1-2. *N*-Fluoroperfluorosuccinimide and *N*-fluoroperfluoroglutarimide

In 1981, Yagupols'kii and co-worker reported the synthesis of *N*-fluoroperfluorosuccinimide (**2-1**) and *N*-fluoroperfluoroglutarimide (**2-2**) by reaction of precursor imides with XeF_2 (Scheme 4) [23]. However, there were no reports on the fluorination capability of these *N*-F compounds. The purpose of this research was to establish if the presence of perfluoroacyl groups was sufficient to stabilize the Xe–N bond. Their experiment revealed that the intermediate F–Xe-N compounds were not detected, but *N*-fluoroimides **2-1** and **2-2** were formed. The stability of these *N*-F compounds was low, since they decomposed to $H_2NCO(CF_2)_nCOOH$ upon standing with air.

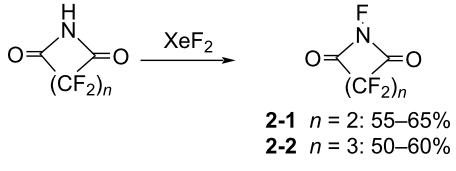

Scheme 4: Synthesis of *N*-F perfluoroimides **2-1** and **2-2**.

1-3. 1-Fluoro-2-pyridone

In 1983, Purrington and co-worker synthesized 1-fluoro-2-pyridone (**3-1**) as a fluorination agent [24]. When 2-(trimethylsiloxy)pyridine was allowed to react with 5% F_2 diluted with N_2 in a freon solvent at −78 °C, 1-fluoro-2-pyridone was obtained in 63% yield (Scheme 5).

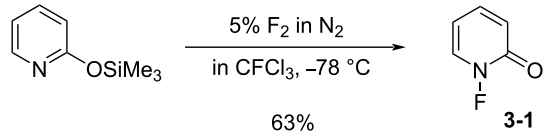

Scheme 5: Synthesis of 1-fluoro-2-pyridone (**3-1**).

The fluorination efficiency of **3-1** was higher than perfluoro-*N*-fluoropiperidine (**1-1**) and the yields of reaction with sodium diethyl malonates improved to between 9–39%; a difluorinated byproduct was obtained when the substituent R was H (Scheme 6). Further applications were investigated by the same authors in 1984 [25]. Grignard reagents and enamines could be fluorinated, but in very low yields and unfortunately, this reagent was not so stable.

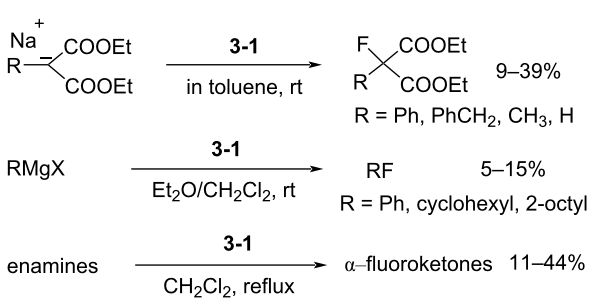

Scheme 6: Fluorination with 1-fluoro-2-pyridone (**3-1**).

Notably, attempts to prepare *N*-fluorosuccinimide from succinimide, or one of its salts by reaction with fluorine (F_2), trifluoromethyl hypofluorite, or perchloryl fluoride in a variety of solvents, and at temperatures ranging from −78 °C to room temperature, all but failed, as reported in the margin of the paper cited in [24].

1-4. *N*-Fluoro-*N*-alkylarenesulfonamides

In 1984, a series of stable *N*-fluoro-*N*-alkylsulfonamides **4-1a–g** was reported by Barnette [26]. The treatment of *N*-alkylsulfonamides with very dilute F_2 (1% or 5%) in N_2 at −78 °C afforded the fluorinated products **4-1a–g**. As detailed in Figure 1, various kinds of *N*-fluoro-*N*-alkylsulfonamides were synthesized by this method. However, the yields were low except for the case of compound **4-1d**. In the cases of secondary and tertiary alkyl groups on the amine side, low yields were obtained and these were attributed to concomitant N–S-bond cleavage reactions with F_2. This method, using the dilute F_2, was inefficient for their production due to long reaction times.

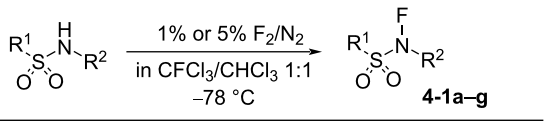

compound	R^1	R^2	F_2 in N_2	yield(%)
4-1a	4-$CH_3C_6H_4$-	CH_3-	1%	59%
4-1b	4-$CH_3C_6H_4$-	$(CH_3)_3C$-	5%	14%
4-1c	4-$CH_3C_6H_4$-	exo-2-norbornyl	1%	47%
4-1d	4-$CH_3C_6H_4$-	endo-2-norbornyl	1%	71%
4-1e	4-$CH_3C_6H_4$-	cyclohexyl	5%	11%
4-1f	4-$CH_3C_6H_4$-	$(CH_3)_3CCH_2$-	5%	57%
4-1g	$CH_3CH_2CH_2CH_2$-	$(CH_3)_3CCH_2$-	1%	50%

Figure 1: Synthesis of *N*-F sulfonamides **4-1a–g**.

N-Fluoro-*N*-alkyl-*p*-toluenesulfonamides **4-1b**,**c**,**f** proved to be efficient fluorinating agents in the fluorination of carbanions (Scheme 7). The yields of reactions with sodium malonates and Grignard reagents were largely improved to up to 81% and 50%, respectively. The carbanions of aromatics, ketones, nitroalkanes, amides, etc. could also be reasonably well fluorinated and this study showed great progress. However, although these fluorinating agents were stable and easy-to-handle, their fluorinating power was low. They could fluorinate only reactive carbanions, but not aromatics, olefins, vinyl acetates, trimethylsilyl or alkyl enol ethers, and so on.

Soon after (1986), Schwartz and co-worker reported the stereospecific synthesis of alkenyl fluorides with *N*-fluoro-*N*-*tert*-butylbenzenesulfonamide (**4-1h**), a compound which is soluble at low temperature [27]. Alkenyllithium reagents, generated in situ, reacted at −120 °C with **4-1h** in THF/Et_2O/pentane to give the desired alkenyl fluorides **4-2** in good yields (Scheme 8). However, reactions that were run above −120 °C, or in pure ether or THF gave higher yields of the protonated products **4-3**.

1-5. *N*-Fluoropyridinium salts and their derivatives

In 1986, Umemoto et al. reported *N*-fluoropyridinium triflate and its derivatives **5-4** as new stable cationic fluorinating agents. These possessed either electron-donating or -withdrawing substituents on the pyridinium nuclei, and were the first reactive, easy-to-handle fluorinating agents with wide application [28,29]. The work continued with additional disclosures until 1991 [30-34]. Before that, reactive fluorinating reagents were difficult to handle because of toxicity, a tendency to explode, instability, and/or hygroscopicity, while easy-to-handle reagents had limited application because of their low reactivity.

Umemoto et al. found that the hygroscopic pyridine·F_2 complex **5-2a** decomposing vigorously at temperatures above −2 °C [35], which was formed by the fluorination of pyridine (10% F_2/N_2) at low temperature in a freon solvent, could undergo straightforward counteranion replacement with a non-nucleophilic anion. Therefore, exchange with salts such as sodium triflate in acetonitrile generated non-hygroscopic *N*-fluoropyridinium triflate salts as highly thermally stable reagents as illustrated in Scheme 9 [28]. Moreover, they found that the fluorination power (reactivity) of these *N*-fluoropyridinium salts could be tuned by the substituents on the pyridinium nuclei.

The transformation of the unstable pyridine·F_2 complex to stable *N*-fluoropyridinium salts could be conducted by direct fluorination (10% F_2/N_2) of the pyridine in acetonitrile and in the presence of a suitable salt at low temperature (method B in Scheme 10). This one-step process was successfully applied to many other pyridine derivatives (method B in Figure 2).

It was finally shown that the stable *N*-fluoropyridinium salts **5-4** could be synthesized in four different ways using 10% F_2/N_2 [28,31,33] (Scheme 10): method A (stepwise method) involved the fluorination of a pyridine derivative with F_2/N_2, to form a pyridine·F_2 complex **5-2**, followed by treatment with a non-nucleophilic anion salt, acid, or silyl derivative. Method B (one-step method) involved the fluorination of a pyridine derivative with F_2/N_2 in the presence of a non-nucleophilic anion salt. Method C involved mixing a pyridine derivative with an acid or its silyl derivative, forming a salt **5-5**, before fluorination. Method D involved mixing a pyridine derivative with a Lewis acid, forming complex **5-6**, and then the fluorination with F_2/N_2 was carried out.

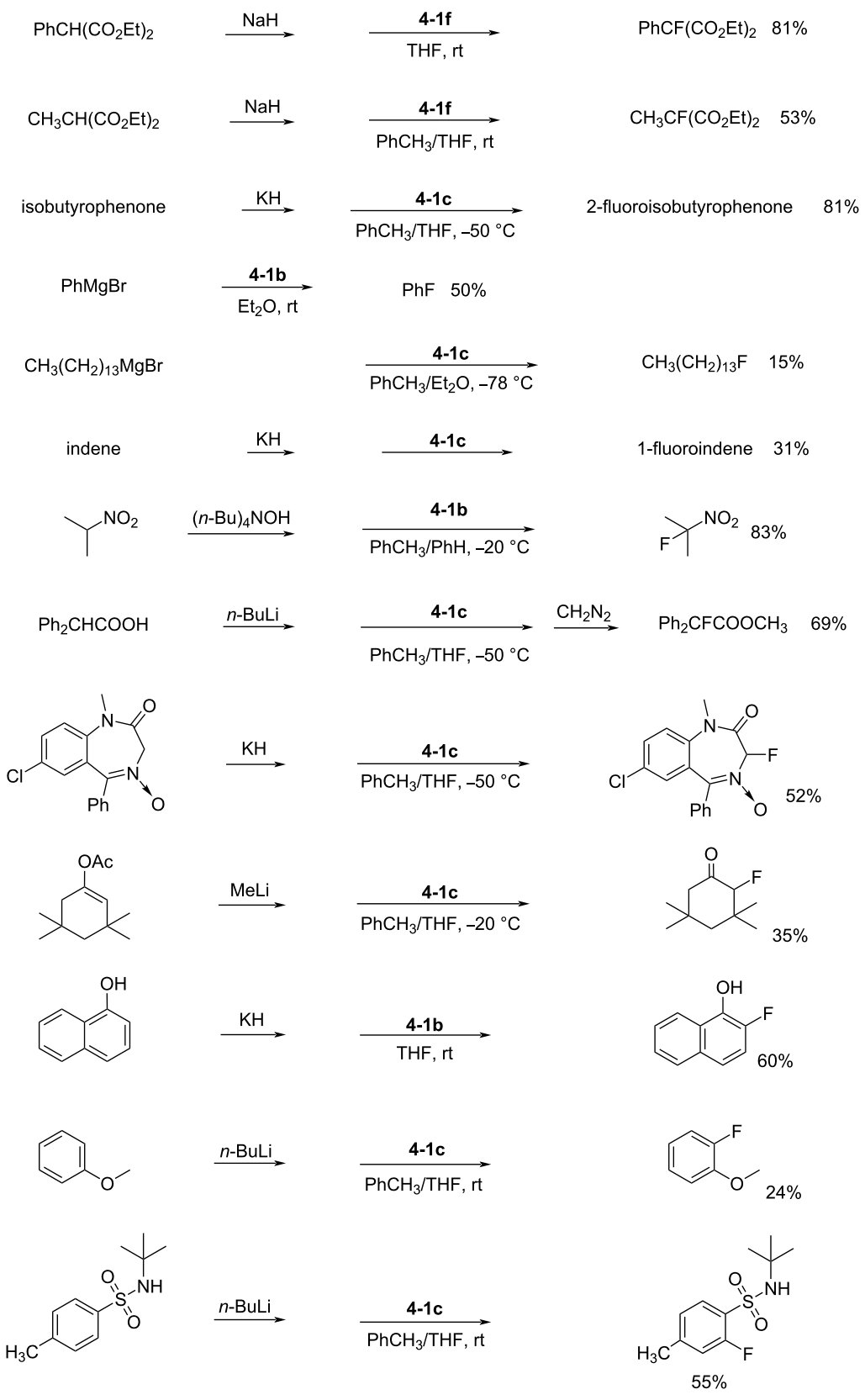

Scheme 7: Fluorination with *N*-F reagent **4-1b**,**c**,**f**.

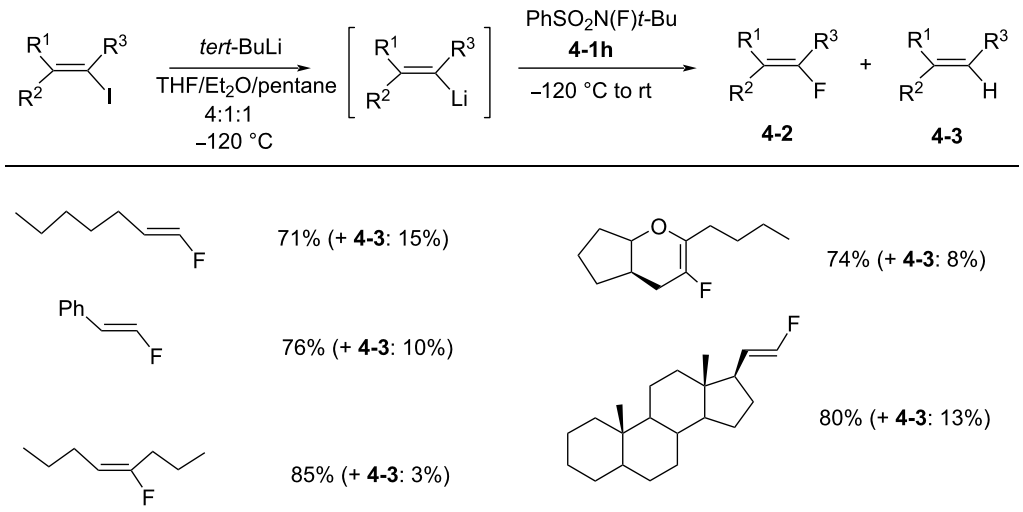

Scheme 8: Fluorination of alkenyllithiums with *N*-F **4-1h**.

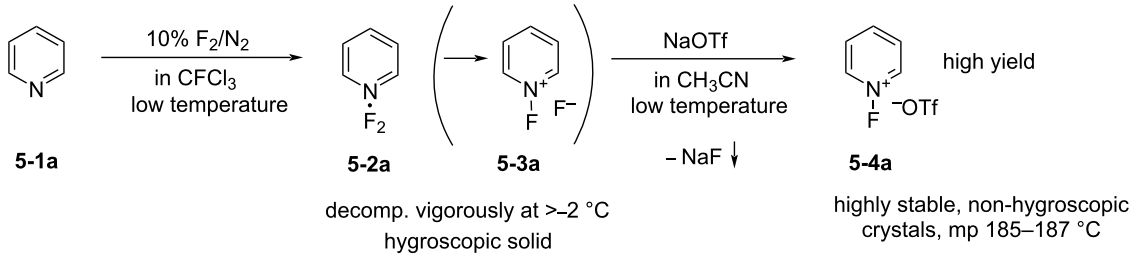

Scheme 9: Synthesis of *N*-fluoropyridinium triflate (**5-4a**).

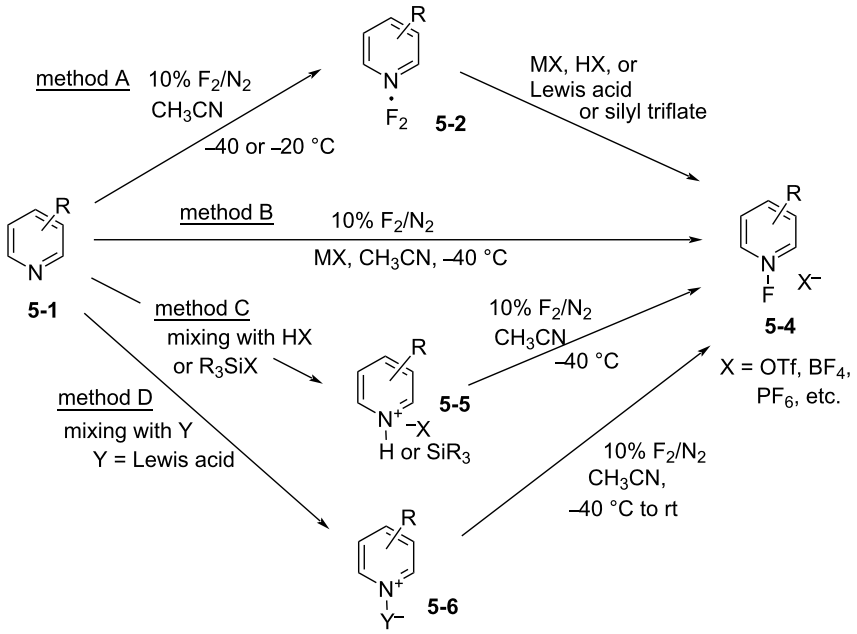

Scheme 10: Synthetic methods for *N*-F-pyridinium salts.

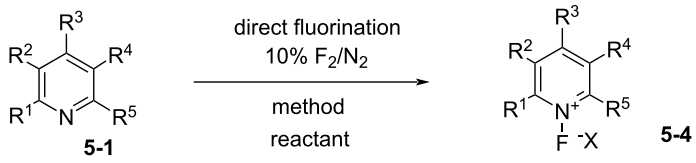

compound	X	R^1	R^2	R^3	R^4	R^5	method	reactant	yield (%)
5-4a	OTf	H	H	H	H	H	B	NaOTf	75%
4a	OTf	H	H	H	H	H	C	TfOH	96%[a]
4b	BF_4	H	H	H	H	H	B	$NaBF_4$	78%
4c	PF_6	H	H	H	H	H	B	$NaPF_6$	83%
4d	AsF_6	H	H	H	H	H	B	$NaAsF_6$	66%
4e	SbF_6	H	H	H	H	H	B	$LiSbF_6$	93%
4f	ONf	H	H	H	H	H	B	NaONf	87%
4g	OMs	H	H	H	H	H	C	MsOH	79%
4h	OTf	H	H	Me	H	H	B	NaOTf	90%
4i	OTf	H	Me	H	Me	H	B	NaOTf	60%
4j	OTf	Me	H	Me	H	Me	B	KOTf	81%
4k	BF_4	Me	H	Me	H	Me	B	$NaBF_4$	70%
4l	OTf	CH_2OMe	H	H	H	CH_2COMe	B	NaOTf	85%
4m	OTf	CH_2OMe	H	CH_2OMe	H	CH_2COMe	B	NaOTf	73%
4n	OTf	CH_2OAc	H	H	H	CH_2OAc	B	NaOTf	74%
4o	OTf	OMe	H	H	H	H	B	NaOTf	73%
4p	OTf	F	H	H	H	H	B	LiOTf	23%
4q	OTf	Cl	H	H	H	H	B	NaOTf	71%
4r	OTf	Cl	H	H	H	Cl	C	TfOH	62%
4s	BF_4	Cl	H	H	H	Cl	D	$BF_3/HF/H_2O$[b]	76%
4t	OTf	H	Cl	H	Cl	H	B	LiOTf	77%
4u	BF_4	H	Cl	H	Cl	H	D	BF_3OEt_2	87%
4v	OTf	Cl	Cl	Cl	Cl	Cl	C	TfOH	85%
4w	BF_4	Cl	Cl	Cl	Cl	Cl	D	BF_3	87%
4x	OTf	H	CF_3	H	CF_3	H	C	$TfOSiMe_3$	68%
4y	OTf	COOMe	H	H	H	COOMe	B	NaOTf	72%
4z	OTf	COOMe	H	COOMe	H	COOMe	B	LiOTf	15%
4za	OTf	COMe	H	H	H	H	B	NaOTf	72%
4zb	BF_4	CN	H	H	H	H	B	$LiBF_4$	78%
4zc	OTf	H	H	CN	H	H	B	LiOTf	84%
4zd	OTf	CN	H	H	H	CN	B	LiOTf	50%
4ze	OTf	H	H	NO_2	H	H	B	LiOTf	86%

Figure 2: Synthesis of various *N*-fluoropyridinium salts. Note: [a]this yield was the one by the improved method reported in [37]; [b]this improved method was reported in [38].

In total, sixty-two stable *N*-fluoropyridinium salts possessing different non-nucleophilic counteranions and electron-withdrawing or -donating groups were efficiently synthesized [33]. Figure 2 shows 31 examples and their methods of preparation. Umemoto and co-worker also reported the synthesis of a polymer version, poly(vinyl-*N*-fluoropyridinium salts) of these reagents [36].

The reactivities of many *N*-fluoropyridinium salts were examined [32] and mainly five kinds of *N*-fluoropyridinium salts, shown in Scheme 11, emerged as useful fluorinating agents due to their availability. The fluorination power greatly changed depending on the electron density at the nitrogen, an aspect controlled by the electronic nature of the substituents. The fluorinating power increased in the order of 2,4,6-triMe **5-4j** < unsubstituted **4a** < 3,5-diCl **4t** < 2,6-diCl **4r** < pentachloro **4v**, in good agreement with the decreasing order of the pK_a values of the pyridines. For example, in order to fluorinate phenol, triMe **5-4j** needed heating at 100 °C in a haloalkane solvent for 24 h, whereas pentachloro **5-4v** required only room temperature within 0.1 h for a successful reaction. The salt **5-4v** was so powerful that it fluorinated an equimolar amount of benzene in dichloromethane in 2 h at 40 °C. In general, triflate salts were more effective than BF_4 salts because of the higher solubility of the triflate salts in a haloalkane solvent.

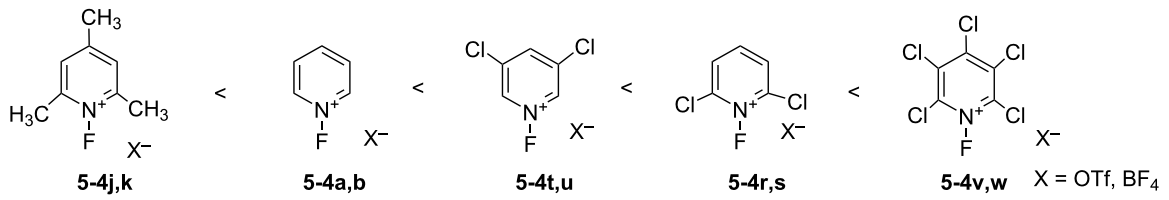

Scheme 11: Fluorination power order of *N*-fluoropyridinium salts.

As outlined in Scheme 12, fluorinations of many kinds of substrates with these *N*-fluoropyridinium salts were performed. It was shown that less reactive substrates can be fluorinated well with the more powerful reagents, and reactive substrates can be fluorinated with less powerful reagents, a match process which minimizes side reactions. Thus, these *N*-fluoropyridinium salts made possible the fluorination of a diversity of nucleophilic organic compounds with different reactivities ranging across aromatics, carbanions (Grignard reagents, enolate anions), active methylene compounds, olefins, silyl enol ethers, vinyl acetates, sulfides and so on, under mild conditions with high selectivity and yields [29-32]. All these reactions could be carried out routinely using standard glassware in normal laboratory environments and without any specialist training.

Some interesting observations are noted: *N*-Fluoro-2,6-bis(methoxymethyl)pyridinium triflate (**5-4l**) fluorinated the trimethylsilyl ether of γ-butyrolactone and 1-cyclohexenyl acetate in much higher yields than the *N*-fluoro-2,4,6-trimethyl salt **5-4j** [32]. Thus, as seen in Scheme 13, **5-4l** converted the Corey lactone **5-7** via its silyl ether **5-8** to the fluorinated lactone **5-9** in a very satisfactory overall yield [32]. *N*-Fluoro-2,6-bis(CH_2OAc)pyridinium triflate **5-4n** [32], *N*-fluoro-2,6-bis(COOMe)pyridinium triflate **5-4y** [30,32], and *N*-fluoro-2-cyano- and -2,6-dicyanopyridinium tetrafluoroborates [39] were useful reagents, too. These non-chlorinated reagents avoid chlorinated byproducts, an occurrence that was observed when other powerful fluorinating agents such as *N*-fluoro-2,3,4,5,6-pentachloropyridinium salts were used [40].

In 1991, *N*-fluoropyridinium pyridine heptafluorodiborate (NFPy), $C_5H_5NF(C_5H_5N)B_2F_7$, was introduced as a fluorinating agent [41]. NFPy was prepared by the reaction of fluorine with pyridine·BF_3 complex and its fluorination ability is shown in Scheme 14. However, it was subsequently reported that the correct structure was *N*-fluoropyridinium pyridinium tetrafluoroborate trifluorohydroxyborate, $C_5H_5NF(C_5H_5NH)BF_4(BF_3OH)$, which was a 1:1 mixture of the *N*-fluoropyridinium salt and *N*-hydropyridinium salt (anion parts; BF_4 and BF_3OH), based on an X-ray diffraction study of a commercial sample [42].

1-6. *N*-Fluoroquinuclidinium fluoride

In 1986 as the *N*-F pyridinium reagents were emerging, Banks et al. disclosed the quaternary ammonium *N*-F reagent, *N*-fluoroquinuclidinium fluoride (**6-1**) [43]. They subsequently followed with more detailed results in 1988 [44]. Quinuclidine was fluorinated by neat fluorine in trichlorofluoromethane at −72 °C, affording the product **6-1** in 86% yield (Scheme 15). Fluorination examples with **6-1** are shown in Scheme 16.

This reagent proved to be very hygroscopic and deteriorated in air. In terms of fluorination yields, *N*-fluoroquinuclidinium fluoride (**6-1**) was however superior to Purrington's 1-fluoro-2-pyridone (**3-1**) [24,25], but inferior to Barnette's *N*-fluoro-*N*-alkylarenesulfonamides **4-1** [26] and Umemoto's *N*-fluoropyridinium salts **5-4** [29,32].

1-7. *N*-Fluoroperfluoroalkanesulfonimides

In 1987, DesMarteau et al. reported the synthesis of a series of *N*-fluoroperfluoroalkanesulfonimides **7-1**. These were prepared by reacting *N,N*-bis(perfluoroalkanesulfonyl)amides with 100% F_2 at −196 °C to 22 °C [45] (Scheme 17). All of these *N*-fluoroperfluoroalkanesulfonimides were stable over time at 22 °C, if stored in a fluoropolymer container. However, **7-1d** decomposed at the melting point of 60 °C.

It was shown that *N*-fluorotrifluoromethanesulfonimide **7-1a** (mp −69.8 °C) had a much higher reactivity than the sulfonamide reagents such as Barnette's *N*-fluoro-*N*-alkylarenesulfonamides, since the electronic density on the nitrogen was greatly decreased by two strong electron-withdrawing CF_3SO_2 groups. Reagent **7-1a** reacted slowly with benzene and toluene under neat conditions, whereas activated aromatics such as phenol, cresol, and naphthalene were fluorinated in chloroform at 22 °C (Scheme 18). The *N*-F imide reagent **7-1a** fluorinated the sodium salt of diethyl 1-methylmalonate at −10 °C to give the corresponding fluoro product in high yield (96%).

Later (1991 and 1992), the same laboratory reported fluorination reactions of functionalized carbonyl compounds, 1,3-dicarbonyl derivatives, olefins, and steroids with **7-1a** [46-49] (Scheme 19).

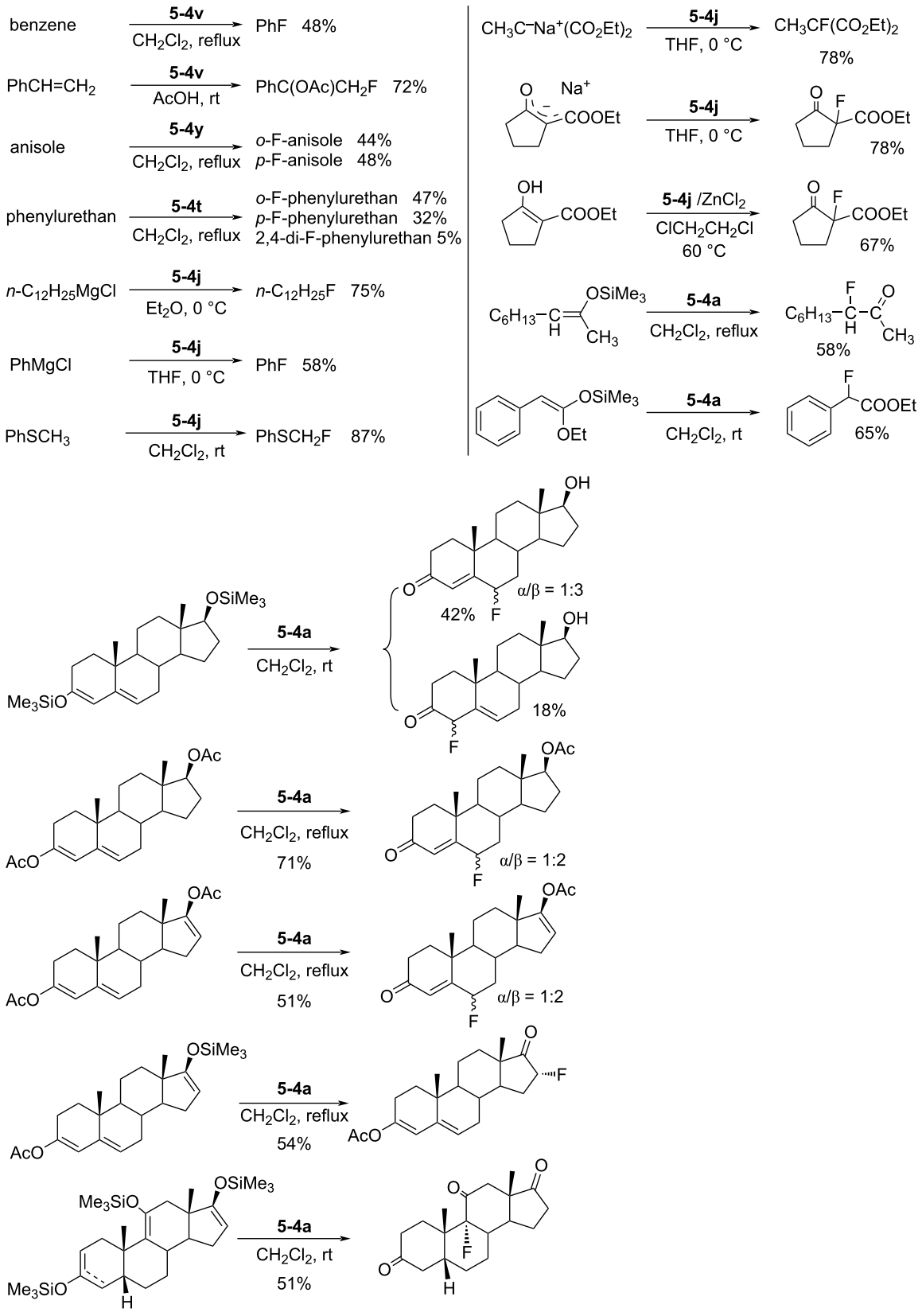

Scheme 12: Fluorinations with *N*-F salts **5-4**.

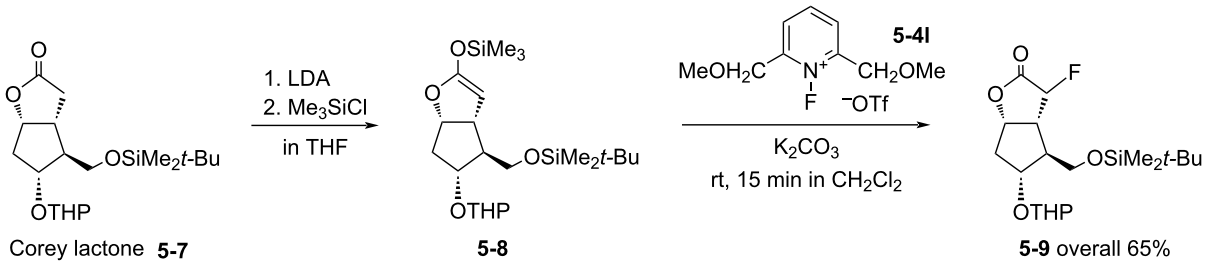

Scheme 13: Fluorination of Corey lactone **5-7** with *N*-F-bis(methoxymethyl) salt **5-4l**.

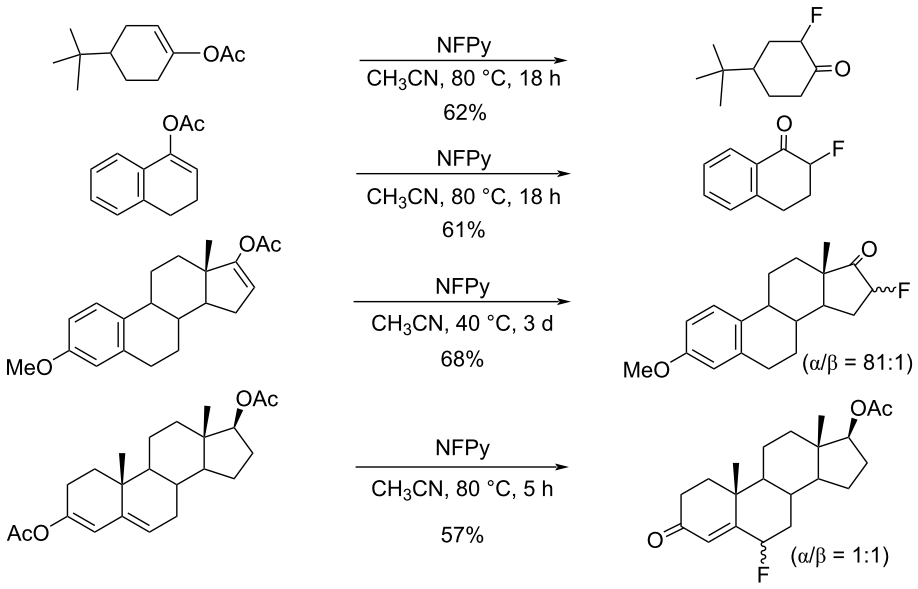

Scheme 14: Fluorination with NFPy.

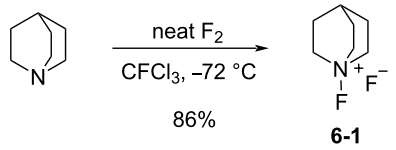

Scheme 15: Synthesis of the *N*-F reagent, *N*-fluoroquinuclidinium fluoride (**6-1**).

1-8. *N*-Fluoroquinuclidinium triflate

In 1988, Banks and co-worker developed the stable and nonhygroscopic *N*-fluoroquinuclidinium triflate (**8-1**) [50], which was an alternative to *N*-fluoroquinuclidinium fluoride (**6-1**) (Scheme 20). The triflate **8-1** was prepared in high yield by the counteranion replacement reaction developed by Umemoto and co-worker [28]. The fluorinating power of triflate **8-1** was the same as that of the fluoride **6-1**, but its nonhygroscopic nature made it a useful fluorinating agent in terms of handling and storage. Details on the synthesis and reactivities of triflate **8-1**

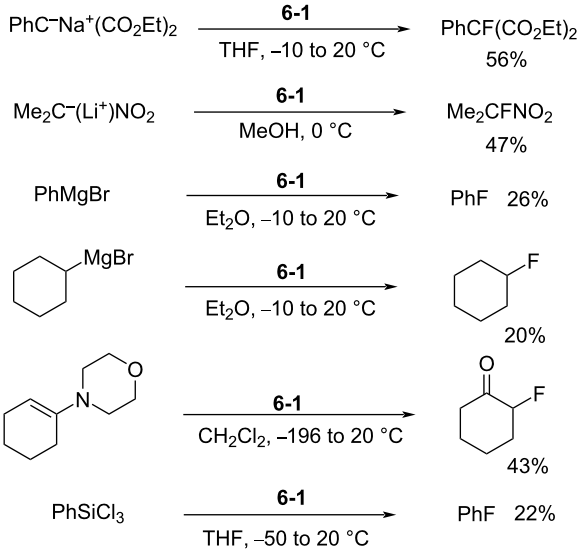

Scheme 16: Fluorinations achieved with *N*-F fluoride **6-1**.

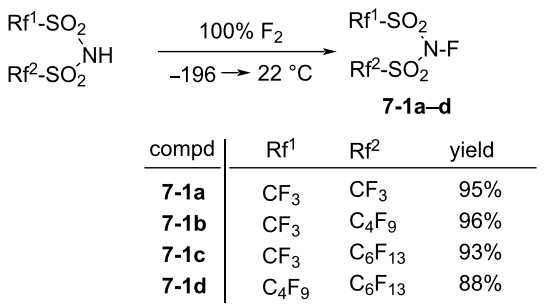

compd	Rf^1	Rf^2	yield
7-1a	CF_3	CF_3	95%
7-1b	CF_3	C_4F_9	96%
7-1c	CF_3	C_6F_{13}	93%
7-1d	C_4F_9	C_6F_{13}	88%

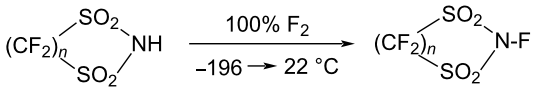

7-1e *n* = 2: 77%
7-1f *n* = 3; 61%
7-1g *n* = 4: 86%

Scheme 17: Synthesis of *N*-F imides **7-1a–g**.

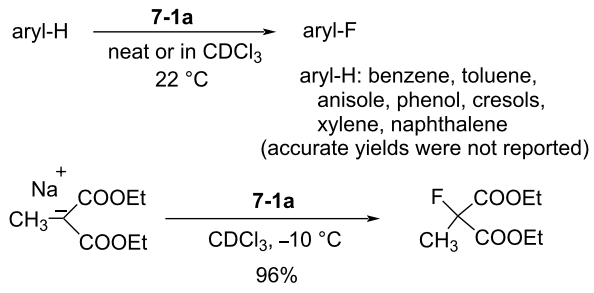

Scheme 18: Fluorination with $(CF_3SO_2)_2NF$, **7-1a**.

and other salts having CF_3COO^-, $C_3F_7COO^-$, and BF_4^- counterions were reported in 1991 [51].

1-9. Optically active *N*-fluorosultams

In 1988, the first optically active *N*-F fluorinating agents, chiral *N*-fluorosultams, were synthesized by Lang and co-worker [52]. A camphor-derived imine was reduced or methylated, followed by direct fluorination (10% F_2/N_2) to give optically active *N*-F reagents **9-1** and **9-2** in 75% and 80% yield, respectively (Scheme 21). These *N*-fluorosultams were stable below 100 °C.

The enantioselectivities of products were examined after the fluorination of different metal enolates. In the best case a 63% yield and 70% enantiomeric excess (ee) was obtained. Even though other products gave less satisfactory outcomes, the potential of the *N*-F fluorinating agents for an enantioselective fluorination was demonstrated (Scheme 22).

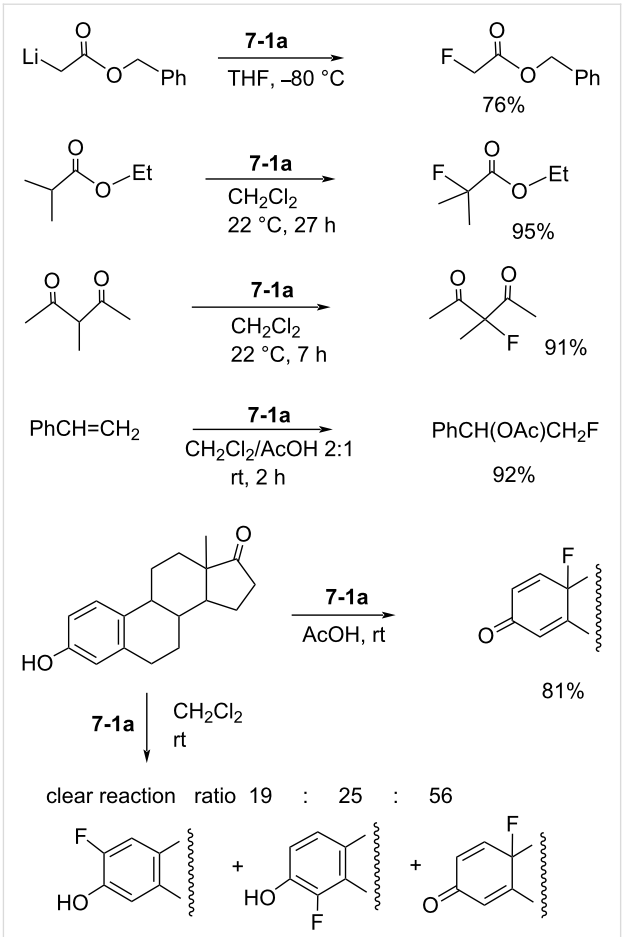

Scheme 19: Fluorination reactions of various substrates with **7-1a**.

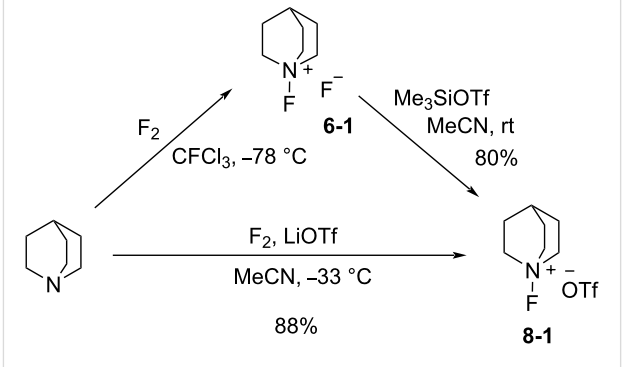

Scheme 20: Synthesis of *N*-F triflate **8-1**.

1-10. *N*-Fluoro-3,3-dimethylbenzothiazole dioxide

In 1989, Lang and co-worker developed the saccharin-derived *N*-fluorosultam *N*-fluoro-3,3-dimethyl-2,3-dihydro-1,2-benzothiazole-1,1-dioxide (**10-2**) from the known precursor **10-1** (Scheme 23) [53]. A direct fluorination using 10% F_2/N_2 at −40 °C gave *N*-F reagent **10-2** in 74% yield. Another method, via the *N*-trimethylsilylation, was also reported but in low effi-

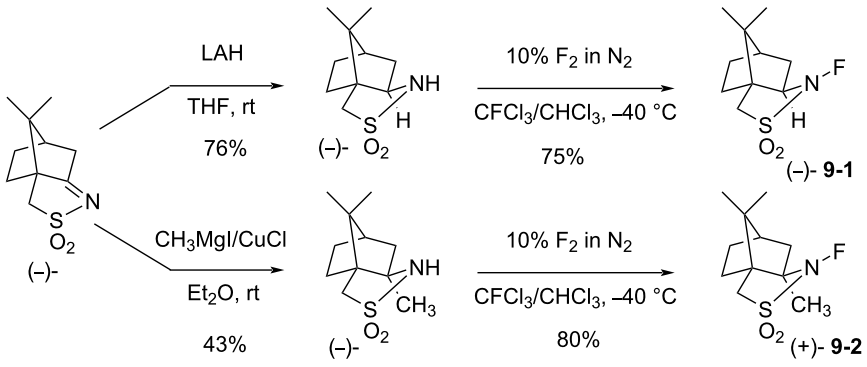

Scheme 21: Synthesis of chiral *N*-fluoro sultams **9-1** and **9-2**.

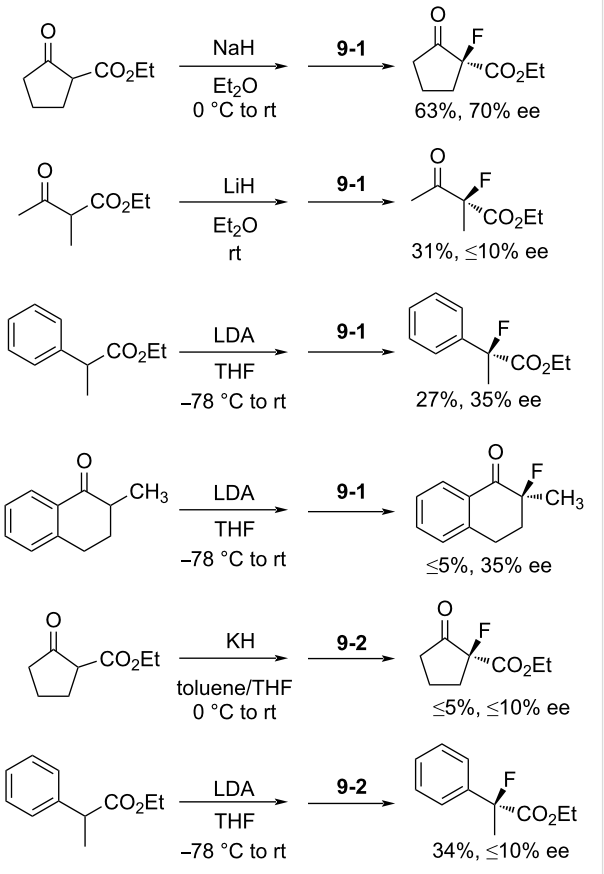

Scheme 22: Fluorination with chiral *N*-fluoro sultams **9-1** and **9-2**.

ciency. This *N*-F reagent is a colorless, thermally stable (<200 °C) solid with a mp of 114–116 °C.

The reagent **10-2** having no α-proton to the *N*-F site proved to be a good choice for fluorinating enolate anions (Scheme 24). The side reaction, involving HF elimination, and which was a problem in reactions with the Barnette's reagents **4-1** having the α-proton(s) except for **4-1b** [26], was avoided here. The HF elimination is a decomposition process that is observed with *N*-F reagents that have an α-proton and occurs under strong base conditions.

1-11. Perfluoro[*N*-fluoro-*N*-(4-pyridyl)methanesulfonamide]

In 1990, Banks and co-worker reported perfluoro[*N*-fluoro-*N*-(4-pyridyl)methanesulfonamide] (**11-2**) [54]. Starting from pentafluoropyridine, the precursor **11-1** was prepared as illustrated in Scheme 25. Treatment of **11-1** with neat F_2 in acetonitrile at −10 °C under reduced pressure gave *N*-fluoro-sulfonamide **11-2** in 89% yield. This product was however a 9:1 mixture of the *N*-F reagent **11-2** and the protonated compound of **11-1**.

The fluorination of benzene and anisole under excess substrate conditions gave fluorobenzene and fluoroanisoles in 88% and 98% yield, respectively. The reaction with sodium diethyl phenylmalonate gave the fluorinated product in 93% yield (Scheme 26).

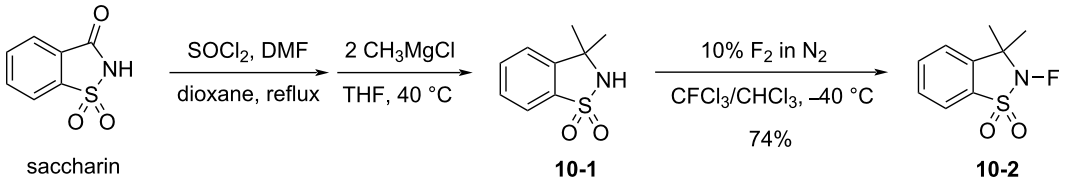

Scheme 23: Synthesis of saccharin-derived *N*-fluorosultam **10-2**.

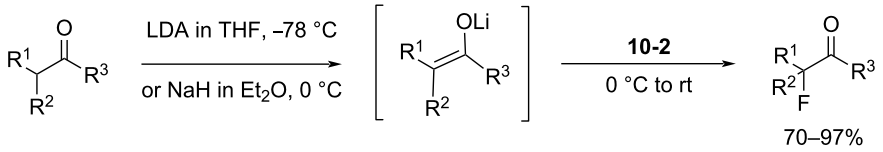

Scheme 24: Fluorination with *N*-fluorosultam **10-2**.

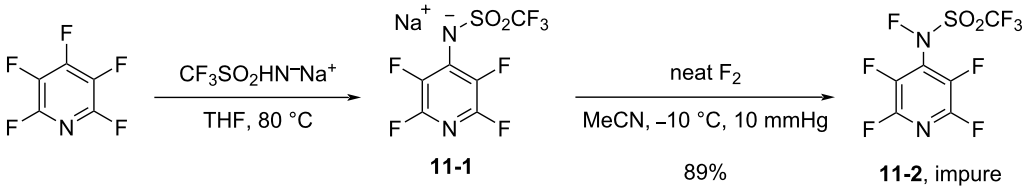

Scheme 25: Synthesis of *N*-F reagent **11-2**.

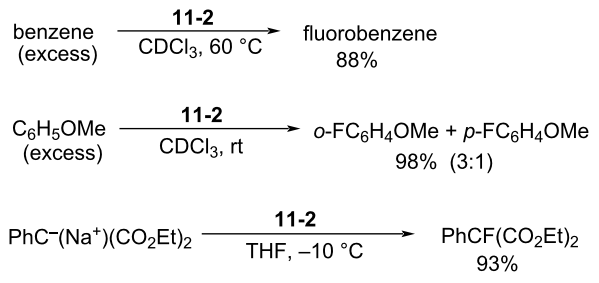

Scheme 26: Fluorination with *N*-F reagent **11-2**.

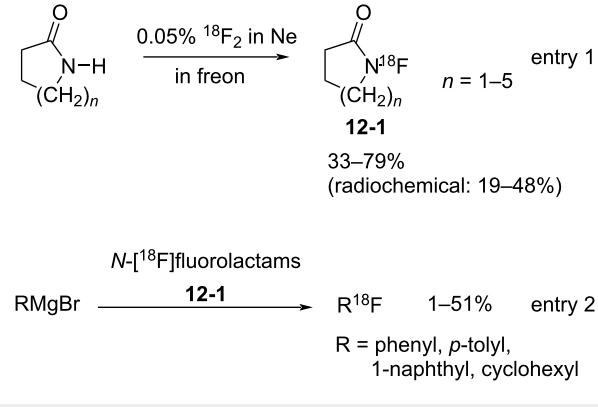

Scheme 27: Synthesis and reaction of *N*-fluorolactams **12-1**.

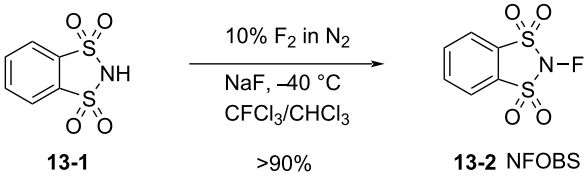

Scheme 28: Synthesis of NFOBS **13-2**.

1-12. *N*-Fluorolactams

A new class of *N*-F fluorinating agents, *N*-fluorolactams **12-1**, was synthesized by Sathyamurthy et al. in 1990 [55]. These compounds had already been prepared by Grakauskas and co-worker in 1970 [56], but in low yields and the *N*-fluorolactams were not recognized as fluorinating agents at that time. For positron emission tomography (PET), Sathyamurthy et al. allowed these lactams to react with 0.05% $^{18}F_2$/Ne in a freon and obtained the *N*-[^{18}F]fluorolactams **12-1** in good yields (Scheme 27, entry 1). The ^{18}F-transfer ability was demonstrated by fluorination reactions with various Grignard reagents in up to 51% yield (Scheme 27, entry 2). In the event the β-elimination of HF proved to be an obstacle for the fluorination of strong bases such as phenyllithium.

1-13. *N*-Fluoro-*o*-benzenedisulfonimide

In 1991, Davis and co-worker reported *N*-fluoro-*o*-benzenedisulfonimide (NFOBS, **13-2**) as a fluorination reagent. NFOBS was prepared by the direct fluorination of its corresponding sulfonimide **13-1** with 10% F_2/N_2 in the presence of NaF and in high yield (Scheme 28) [57].

NFOBS is a stable and crystalline solid of mp 139–140 °C (dec) with good fluorinating power. Its usefulness was demonstrated through fluorination reactions with different types of carbanions (Scheme 29). For example, reactions with enolates gave α-fluorinated products in 65–100% yields. Azaenolates could be fluorinated in moderate yields. A fluorination reaction with phenylmagnesium bromide provided fluorobenzene in 80% yield, an outcome which was better than that of *N*-fluoropyridinium triflate **5-4j** (Umemoto's reagent, 58%) and *N*-fluorosul-

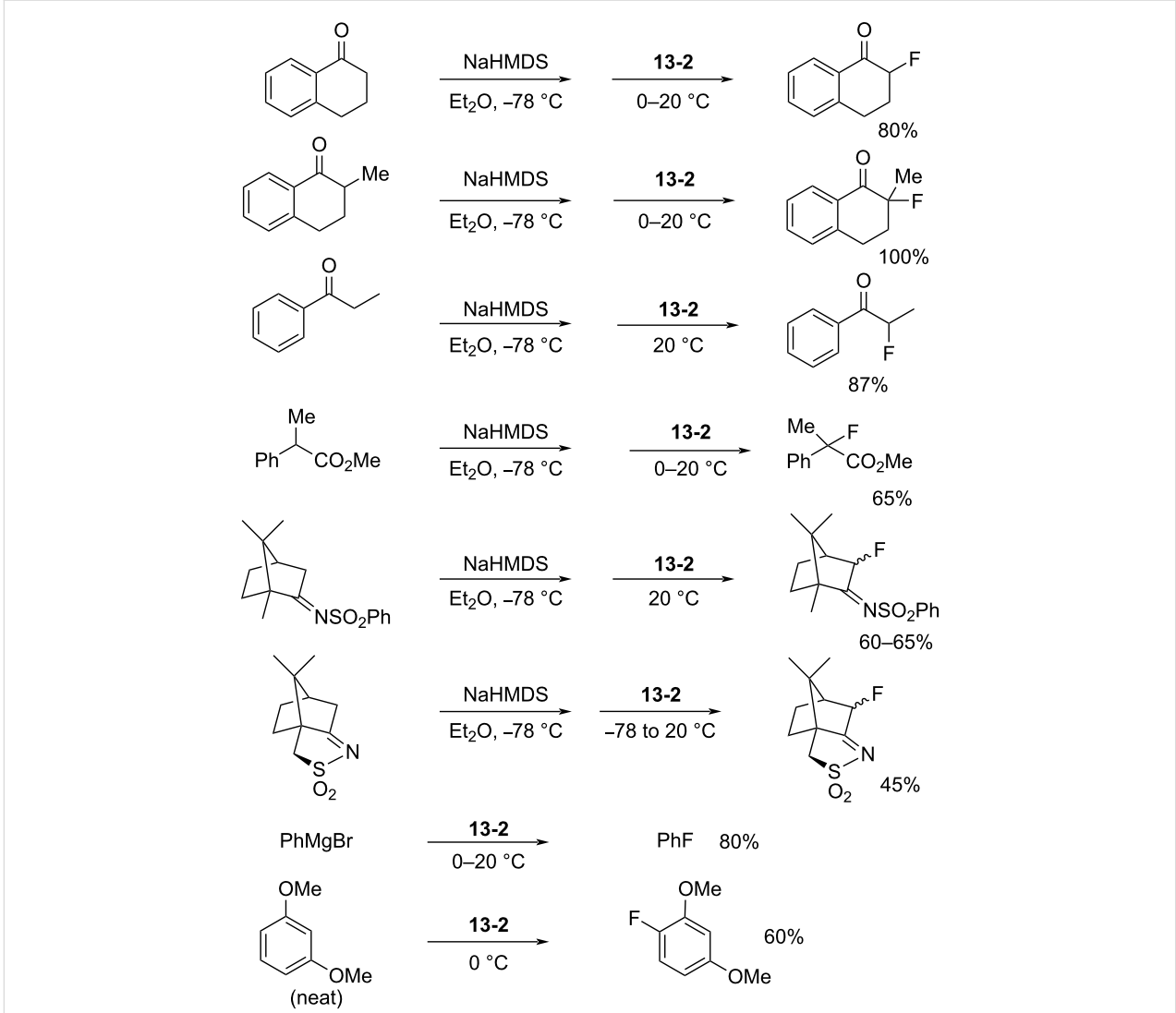

Scheme 29: Fluorination with NFOBS **13-2**.

fonamide **4-1b** (Barnette's reagent, 50%). NFOBS was able to fluorinate 1,3-dimethoxybenzene under neat conditions, while attempts to fluorinate toluene and acetophenone failed. The details of these reactions and applications were described in a full paper later published in 1995 [58].

1-14. *N*-Fluorobenzenesulfonimide (NFSI)

In 1991, *N*-fluorobenzenesulfonimide (NFSI, **14-2**) was synthesized by Differding and co-worker [59]. It was prepared from benzenesulfonimide **14-1** in good yield by its reaction with 10% F_2/N_2 in acetonitrile at −40 °C (Scheme 30). NFSI is a stable and non-hygroscopic crystalline solid with a mp of 114–116 °C.

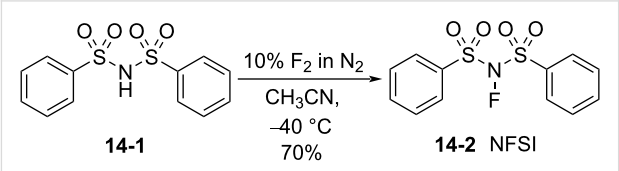

Scheme 30: Synthesis of NFSI (**14-2**).

NFSI was shown to fluorinate a variety of nucleophiles. As seen in Scheme 31, trimethylsilyl enol ethers, enolate anions of ketones and esters, and aryl- and vinyllithiums were fluorinated with NFSI in moderate to high yields. Although aromatics such as anisole, toluene, and acetanilide could also be fluorinated by NFSI, these reactions required neat conditions and high temperatures, indicating that NFSI was not so powerful.

1-15. *N*-Fluorosaccharin and *N*-fluorophthalimide

In 1991, Gakh et al. reported the synthesis of *N*-fluorosaccharin (**15-1**) and *N*-fluorophthalimide (**15-2**) in their studies on the re-

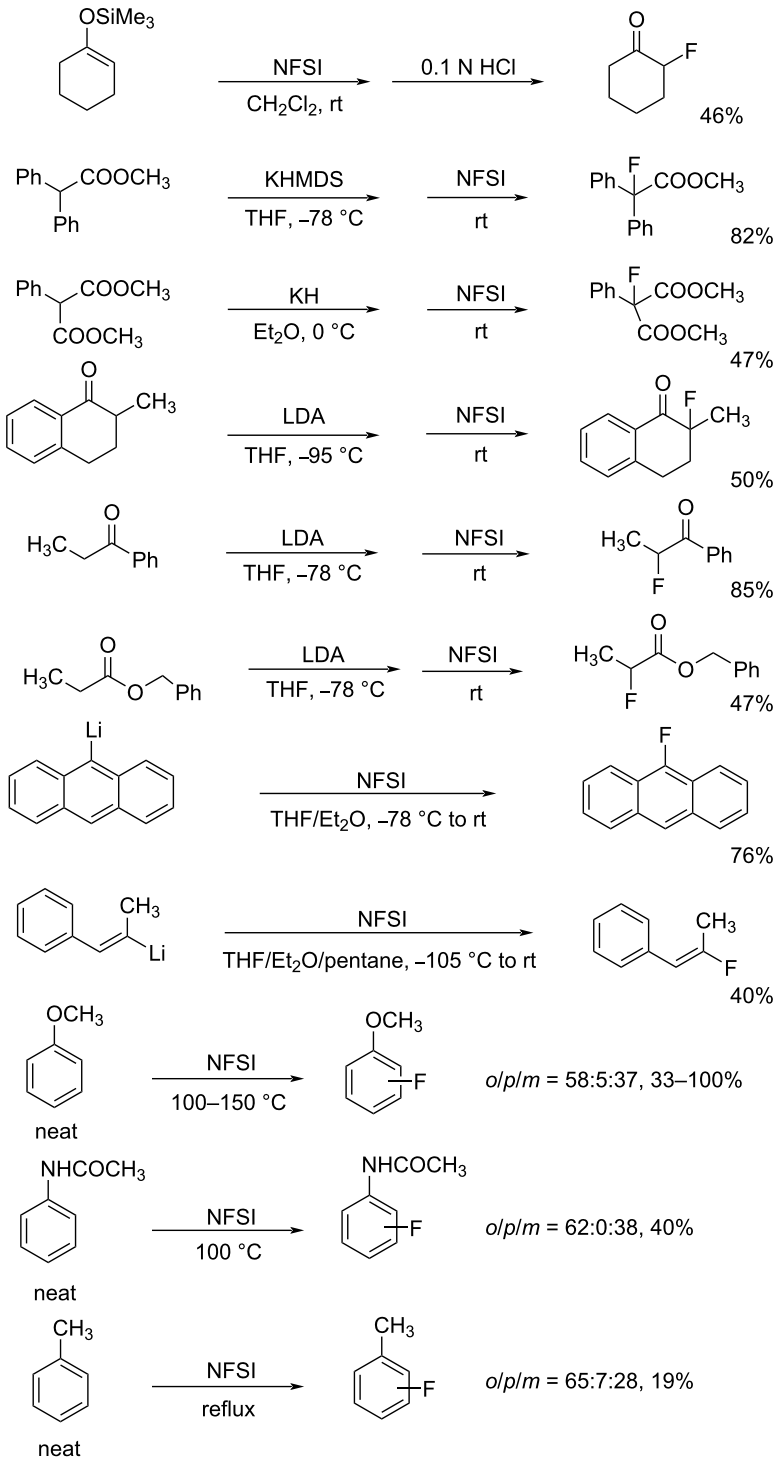

Scheme 31: Fluorination with NFSI **14-2**.

activity of cesium fluoroxysulfate ($Cs^{+-}OSO_2OF$) [60]. Sodium salts of saccharin and phthalimide reacted with cesium fluoroxysulfate in acetonitrile at 0–5 °C to give **15-1** and **15-2** in 69% and 48% yields, respectively (Scheme 32). However, they did not report any fluorination reactions with **15-1** and **15-2**. A transfer reaction failed to generate *N*-fluorosuccinimide from the reaction of the sodium salt of succinimide with cesium fluoroxysulfate.

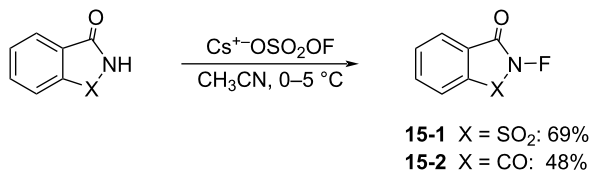

Scheme 32: Synthesis of *N*-fluorosaccharin (**15-1**) and *N*-fluorophthalimide (**15-2**).

1-16. 1-Alkyl-4-fluoro-1,4-diazoniabicyclo[2.2.2]octane salts

In 1992, Banks et al. reported a new series of *N*-fluoro diquaternary ammonium salts, 1-alkyl-4-fluoro-1,4-diazoniabicylco[2.2.2]octane salts **16-3a–d** (Scheme 33) [42]. The salts **16-3** were synthesized in high yields after alkylation of 1,4-diazabicyclo[2.2.2]octane (**16-1**), followed by the Umemoto's fluorination/counteranion replacement reaction of the resulting monoquaternary ammonium salts **16-2** with 10% F_2/N_2 in acetonitrile at −40 to −20 °C. The resultant salts **16-3** proved to be stable, non-hygroscopic, crystalline solids with high fluorinating power. The salt **16-3a** was chosen as the commercial reagent, Selectfluor™, from a cost-effectiveness viewpoint.

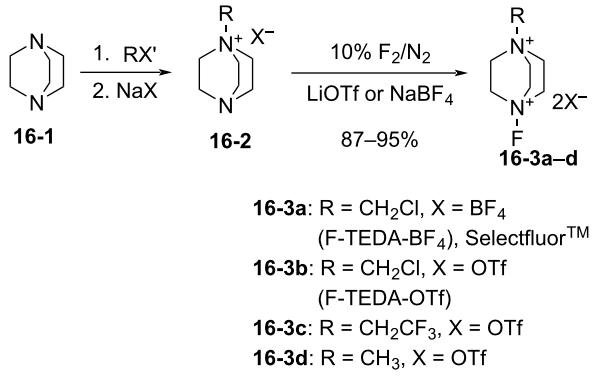

Scheme 33: Synthesis of *N*-F salts **16-3**.

The fluorinating power of reagents **16-3** strengthened as the electronegativity of the R group increased in the order of CH_3 < CH_2Cl < CH_2CF_3. The reagents **16-3** were able to fluorinate enol and conjugated enol acetates of steroids, sodium malonates, enamines, Grignard reagents, and aromatic compounds under mild conditions. In each case Selectfluor gave the corresponding fluorinated products in good to high yields (Scheme 34).

As can be seen in Figure 3 and Figure 4, two years later (1994), Banks et al. reported mono- and difluorinations of various 1,3-dicarbonyl compounds using Selectfluor (**16-3a**) [61].

In 1995, the same group reported that Selectfluor reacted with quinuclidine to form *N*-fluoroquinuclidinium tetrafluoroborate in quantitative yield [62] (Scheme 35). They described this as a "transfer fluorination" since there was an intermolecular transfer of the fluorine atom of Selectfluor to the nitrogen of quinuclidine. In 1996, full details were published on the reactivities of all **16-3** reagents and the syntheses of **16-3** and intermediates **16-2** including additionally C_2H_5 and C_8H_{17} as R group and PF_6^- and FSO_3^- as anion X^- [63,64].

The generous provision of free samples of Selectfluor after its commercialization resulted in many publications concerning its applications from a diversity of research groups and in a short time period (1992–1995): These included fluorinations of alkylbenzenes (entry 1, Scheme 36) [65], Grignard reagents (entry 2) [65], electron-rich alkenes (entry 3) [65,66], alkyl sulfides (entry 4) [65,67], 1,3-dicarbonyl compounds [65,68], phosphonate esters (entry 5) [65], steroidal silyl enol ethers and enol acetates (entry 6) [65], pyrimidine bases and nucleosides (entry 7) [67,69], phenylalkynes (entry 8) [70], anthraquinones (entry 9) [71], vinylstannanes (entry 10) [72], trialkylstannylindoles [73], and cyclopentadienylthallium (entry 11, Scheme 36) [74].

1-17. Optically active *N*-fluoro-2,10-(3,3-dichlorocamphorsultam)

In 1993, Davis et al. reported the synthesis of the second optically active *N*-fluoro-2,10-(3,3-dichlorocamphorsultam) **17-2** [75] (Scheme 37).

The maximum enantioselectivity of enolates of β-ketoesters with (−)-**9-1** or **(+)-9-2**, first prepared by Lang in 1988 (see section 1-9), was 70% ee. The asymmetric fluorination with (+)- or (−)-**17-2** afforded up to 75% ee as indicated in Scheme 38. The dichloro reagent **17-2** gave higher yields than the non-chloro reagent **9-1** because of the greater reactivity of **17-2**.

1-18. Zwitterionic *N*-fluoropyridinium salts

In 1995, Umemoto and co-worker disclosed a zwitterionic *N*-fluoropyridinium salt system **18-2** which had a broad fluorinating power and high selectivity [76]. A series of *N*-fluoropyridinium-2-sulfonates with electron-withdrawing or -donating substituents were synthesized in high yields by fluorination of the corresponding pyridinium-2-sulfonates **18-1** with 10% F_2/N_2 in acetonitrile or a mixture of acetonitrile/water at −40 to −10 °C (Figure 5). In a few cases, a catalytic amount of triethylamine was used to improve the yields. The starting pyridinium-2-sulfonates possessing an electron-withdrawing group(s) were prepared in high yields from the reaction of the corresponding 2-chloropyridines with sodium sulfite. All of these *N*-F reagents are easy-to-handle and stable crystalline solids.

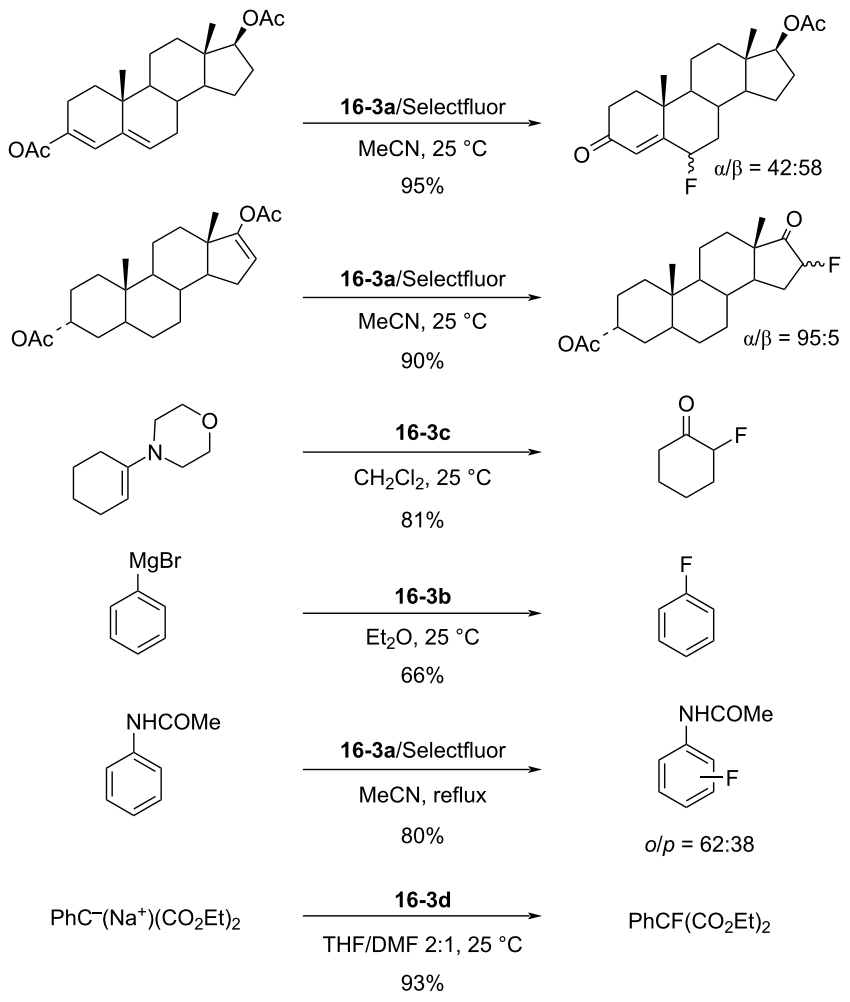

Scheme 34: Fluorination with *N*-F salts **16-3**.

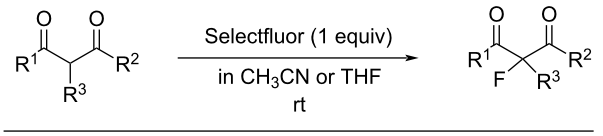

entry	R^1	R^2	base	R^3	time	yield %
1	- $(CH_2)_3$ -		non	Me	19 h	84
2	Ph	Ph	non	H	5 h	84
3	Ph	OEt	non	H	54 h	22
4	Me	OEt	non	H	120 h	(57 crude)
5	OEt	OEt	NaH	Ph	20 h	93
6	Ph	NMe_2	non	H	3 h	87
7	Ph	N(Me)CH(Ph)Me	non	H	67 h	80

Figure 3: Monofluorination with Selectfluor (**16-3a**).

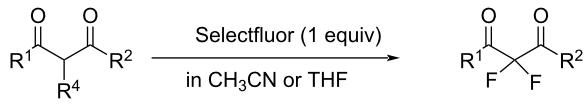

entry	R^1	R^2	R^4	mol ratio*	base	temp	time	yield %
1	Ph	Ph	H	2.1	non	rt	192 h	78
2	Ph	NMe_2	H	3.2	non	40 °C	647 h	91
3	Ph	OEt	F	1.1	NaH	rt	24 h	95
4	Ph	NMe_2	F	1.2	NaH	rt	27 h	73

*mol ratio = Selectfluor:substrate

Figure 4: Difluorination with Selectfluor (**16-3a**).

The nature of the lipophilic alkyl or trifluoromethyl substituents had a significant effect on the reactivity. Previously, *N*-fluoropyridinium-2-sulfonate and its 6-chloro derivative had been synthesized and shown to have excellent selectivity in fluorination reactions, but these reagents exhibited a low reactivity due to their low solubility in organic solvents [32].

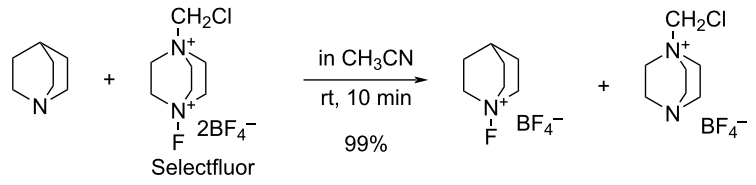

Scheme 35: Transfer fluorination of Selectfluor (**16-3a**).

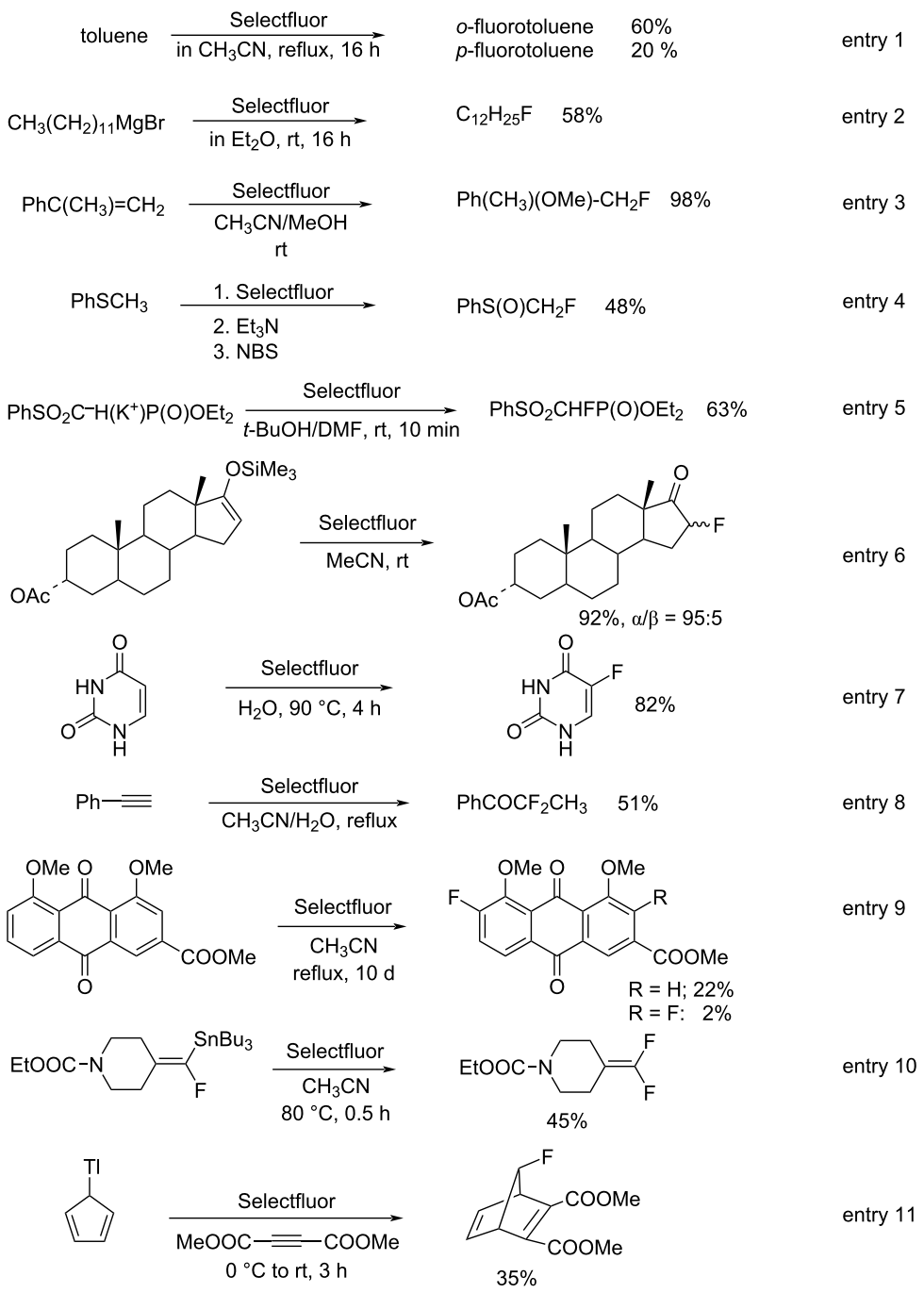

Scheme 36: Fluorination of substrates with Selectfluor (**16-3a**).

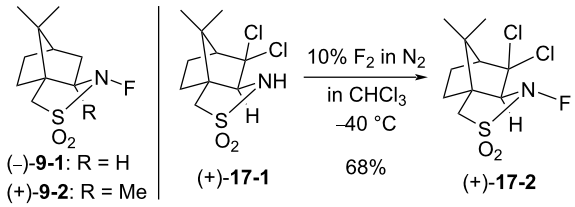

Scheme 37: Synthesis of chiral *N*-fluoro-sultam **17-2**.

Their fluorinating power increased in the order of **18-2a** < **2b** ≈ **2c** ≈ **2d** ≈ **2e** < **2f** < **2g** < **2h**, consistent with the order of the pK_a values of the pyridines (Scheme 39). The least powerful **18-2a** was suitable for the fluorination of reactive carbanions and easily oxidizable sulfides, whereas the most powerful **18-2h** was suitable for less-reactive substrates such as olefins, aromatics, and neutral active methylene compounds. *N*-Fluoro-6-(trifluoromethyl)pyridinium-2-sulfonate (**18-2f'**) was prepared later [77].

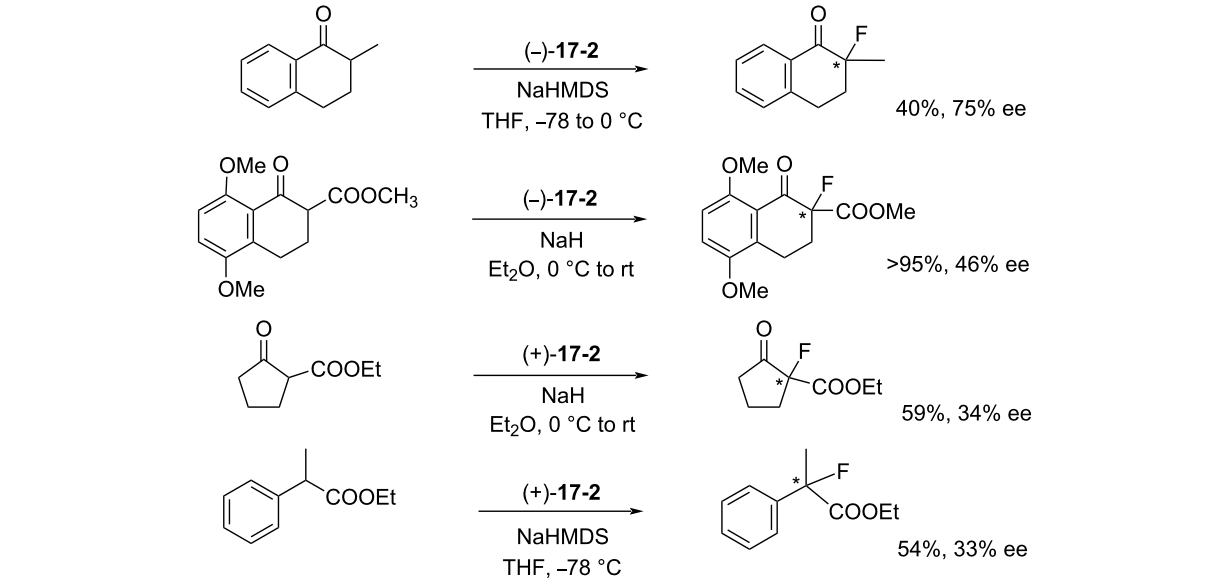

Scheme 38: Asymmetric fluorination with chiral **17-2**.

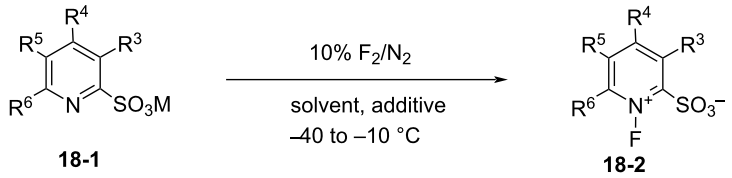

entry	**18-1**	substituent R				additive	solvent	temp. (°C)	product **18-2**	yield of **18-2** (%)
		R^3	R^4	R^5	R^6					
1	**18-1a** (M = Na)	H	CH_3	H	CH_3	–	CH_3CN/H_2O 10:1	–20	**18-2a**	88
2	**18-1b** (M = H)	H	CH_3	H	H	Et_3N	CH_3CN	–20	**18-2b**	91
3	**18-1c** (M = H)	H	C_2H_5	H	H	–	CH_3CN	–20	**18-2c**	79
4	**18-1d** (M = H)	H	*t*-Bu	H	H	–	CH_3CN/H_2O 20:1	–20	**18-2d**	84
5	**18-1e** (M = H)	H	H	H	CH_3	–	CH_3CN/H_2O 10:1	–20	**18-2e**	65
6	**18-1f** (M = H)	H	H	CF_3	H	Et_3N	CH_3CN	–20	**18-2f**	95
7	**18-1g** (M = H)	Cl	H	CF_3	H	–	CH_3CN	–10	**18-2g**	84
8	**18-1h** (M = H)	H	CF_3	H	CF_3	–	CH_3CN	–40	**18-2h**	95

Figure 5: Synthesis of Zwitterionic *N*-fluoropyridinium salts **18-2a–h**.

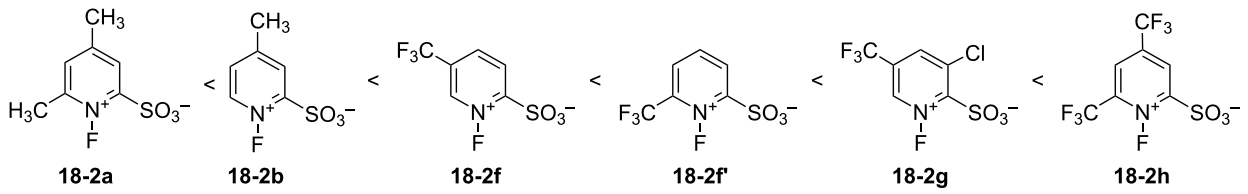

Scheme 39: Fluorinating power order of zwitterionic *N*-fluoropyridinium salts.

As shown in Scheme 40, the **18-2** pyridinium series proved to be effective fluorinating agents for a wide range of substrates. Moreover, an extremely high *ortho*-selectivity was observed in the fluorination of phenol. This could be attributed to a hydrogen-bonding interaction between the sulfonate anion and the phenol hydroxy group in the transition state. This assumption

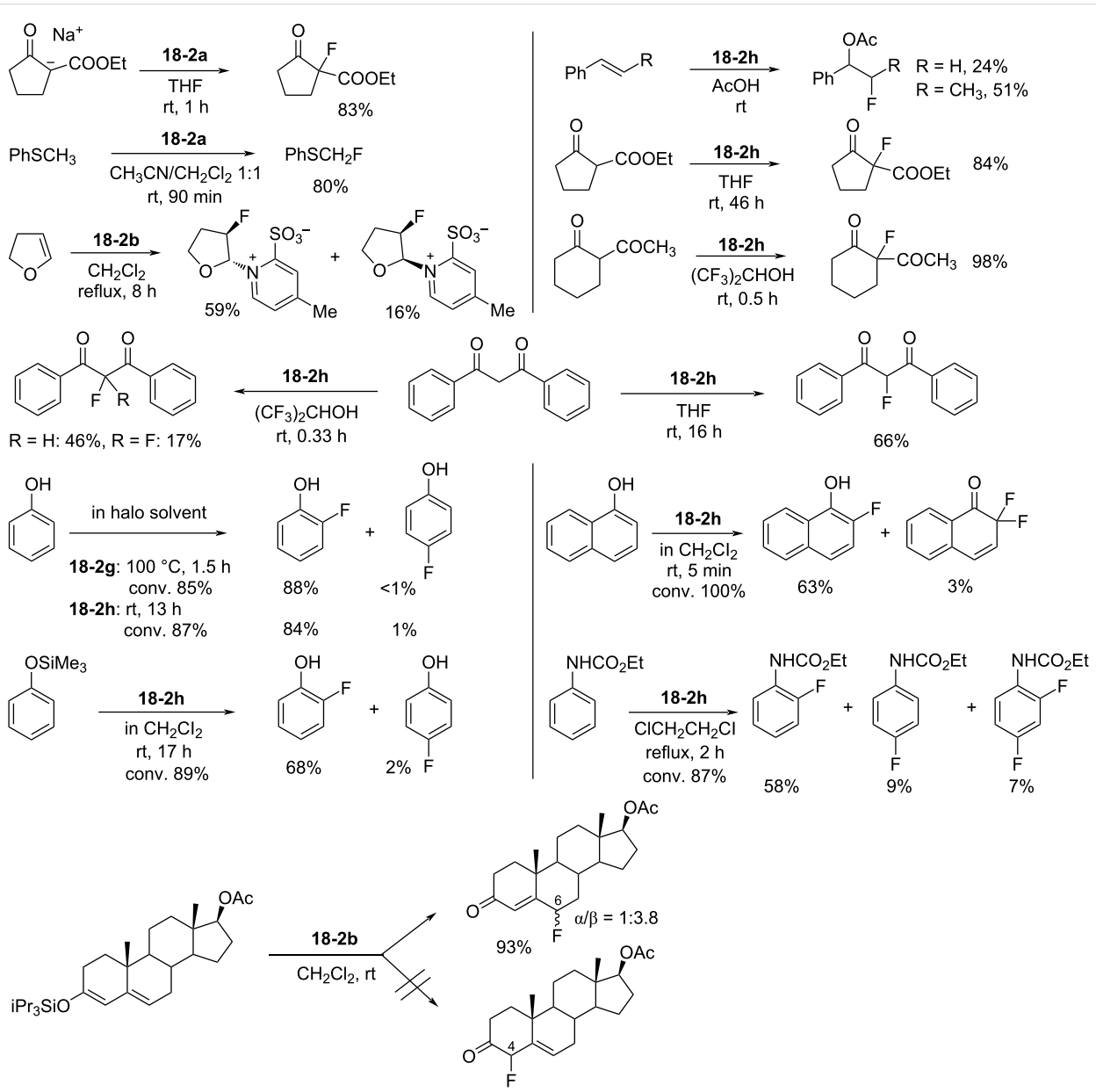

Scheme 40: Fluorination with zwitterionic **18-2**.

could also explain the high *o*-selectivity obtained in the fluorinations of naphthol, phenylurethane, and trimethylsilyl ether of phenol, and the exclusive 6-selectivity observed in the fluorination of conjugated enol triisopropylsilyl ethers of steroids. An additional advantage of the **18-2** reagents is that, after the fluorinations, the resulting pyridine-sulfonic acids are easily removed in an aqueous work-up.

As illustrated in Scheme 41, triflic acid was shown to promote the fluorination of anisole with **18-2h**. While the reaction time was ≈30 h without the additive (entry 1, Scheme 41), 1 equiv of TfOH shortened this to less than 1 h (entry 2). Therefore, it would appear that this additive acted as a catalyst. With 0.1 equiv of TfOH, the reaction time was 5.5 h (entry 3) which can be attributed to the strong electron-withdrawing effect of the 2-SO_3H substituent formed by the protonation of the sulfonate anion in **18-2h**.

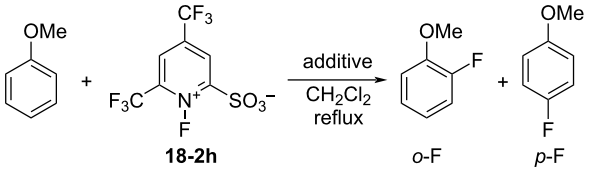

entry	additive	time h	conv.%	yield %	
				o-F	*p*-F
1	non	29.5	80	30	46
2	TfOH (1 equiv)	0.3	85	26	54
3	TfOH (0.1 equiv)	5.5	81	30	53

Scheme 41: Activation of salt **18-2h** with TfOH.

1-19. 1-Fluoro-4-hydroxy-1,4-diazoniabicyclo[2.2.2]octane salts (NFTh)

In 1995, Poss and Shia disclosed the synthesis and fluorination reactivity of 1-fluoro-4-hydroxy-1,4-diazoniabicyclo[2.2.2]octane bis(tetrafluoroborate) (**19-2**, NFTh/Accufluor^{TM}) in a patent [78]. According to the patent, NFTh was prepared by fluorination of 1,4-diazabicyclo[2.2.2]octane *N*-oxide (**19-1**) in acetonitrile or water with 10% F_2/N_2 in the presence of HBF_4, $NaBF_4$, BF_3 etherate, and/or BF_3 at −35 °C or 8–9 °C. Scheme 42 shows the preparation of NFTh, a white solid that decomposes at 125 °C.

The fluorination scope of NFTh is shown in Scheme 43 [79,80]. NFTh reacted with aromatics, enols, ketones, activated olefins, and substrates with active methylene groups to produce the corresponding fluorinated products in good to high yields. NFTh is a powerful fluorinating agent comparable to Selectfluor. Since NFTh has an acidic proton, its effectiveness is curtailed in the case of anionic substrates.

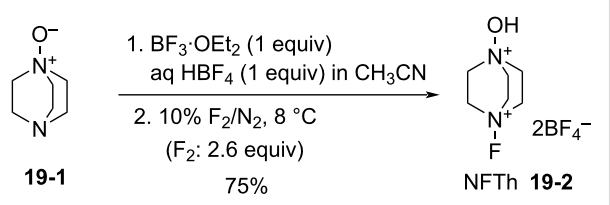

Scheme 42: Synthesis of NFTh, **19-2**.

1-20. *N*-Fluorobenzo-oxathiazone dioxide

In 1995, Cabrera and co-worker claimed 3-fluorobenzo-1,2,3-oxathiazin-4-one 2,2-dioxide (**20-2**) to be a useful fluorinating agent; **20-2** is a stable crystalline compound that was prepared in 83% yield by fluorination of its precursor **20-1** with 5% F_2/N_2 in acetonitrile and in the presence of NaF at −40 °C [81] (Scheme 44). They also tried to prepare *N*-fluorosaccharin (**20-3**) from saccharin with the F_2/N_2 system, but failed. Reagent **20-3** was synthesized using cesium fluoroxysulfate in 1991 (see section 1-15).

Reagent **20-2** proved useful for the fluorination of both neutral and anionic nucleophiles under mild conditions. Scheme 45 illustrates some pertinent examples. Phenyl Grignard reagent, active methylene compounds, and a conjugated enol acetate of a steroid were all fluorinated in moderate to high yields. The fluorination of anisole required high temperature and neat conditions suggesting that the fluorination power of **20-2** is not so high.

1-21. Perfluoro[*N*-fluoro-*N*-(4-pyridyl)acetamide]

In 1996, the Banks group reported perfluoro[*N*-fluoro-*N*-(4-pyridyl)acetamide] (**21-3**) as a carboxamide analogue of perfluoro[*N*-fluoro-*N*-(4-pyridyl)methanesulfonamide] (**11-2**, see section 1-11) [82]. Its precursor, **21-2**, was prepared from pentafluoropyridine by either one of two methods (Scheme 46). Precursor **21-2** was treated with neat F_2 at 10–20 mmHg pressure in acetonitrile at −35 °C to produce the *N*-F carboxamide **21-3** in 75% yield but the resulting product was a 79:18 mixture of the desired *N*-F product **21-3** and the protonated compound **21-1**.

As a reagent *N*-F carboxamide **21-2** fluorinated electron-rich substrates such as sodium diethyl (phenyl)malonate, 1-morpholinocyclohexene, phenol, and anisole (Scheme 47). The fluorination power of the carboxamide **21-2** was less than that of its *N*-F sulfonamide analog **11-2**.

1-22. *N,N'*-Difluoro-1,4-diazoniabicyclo[2.2.2]octane salts

In 1996, Umemoto and co-worker reported the successful synthesis of various *N,N'*-difluoro-1,4-diazoniabicyclo[2.2.2]oc-

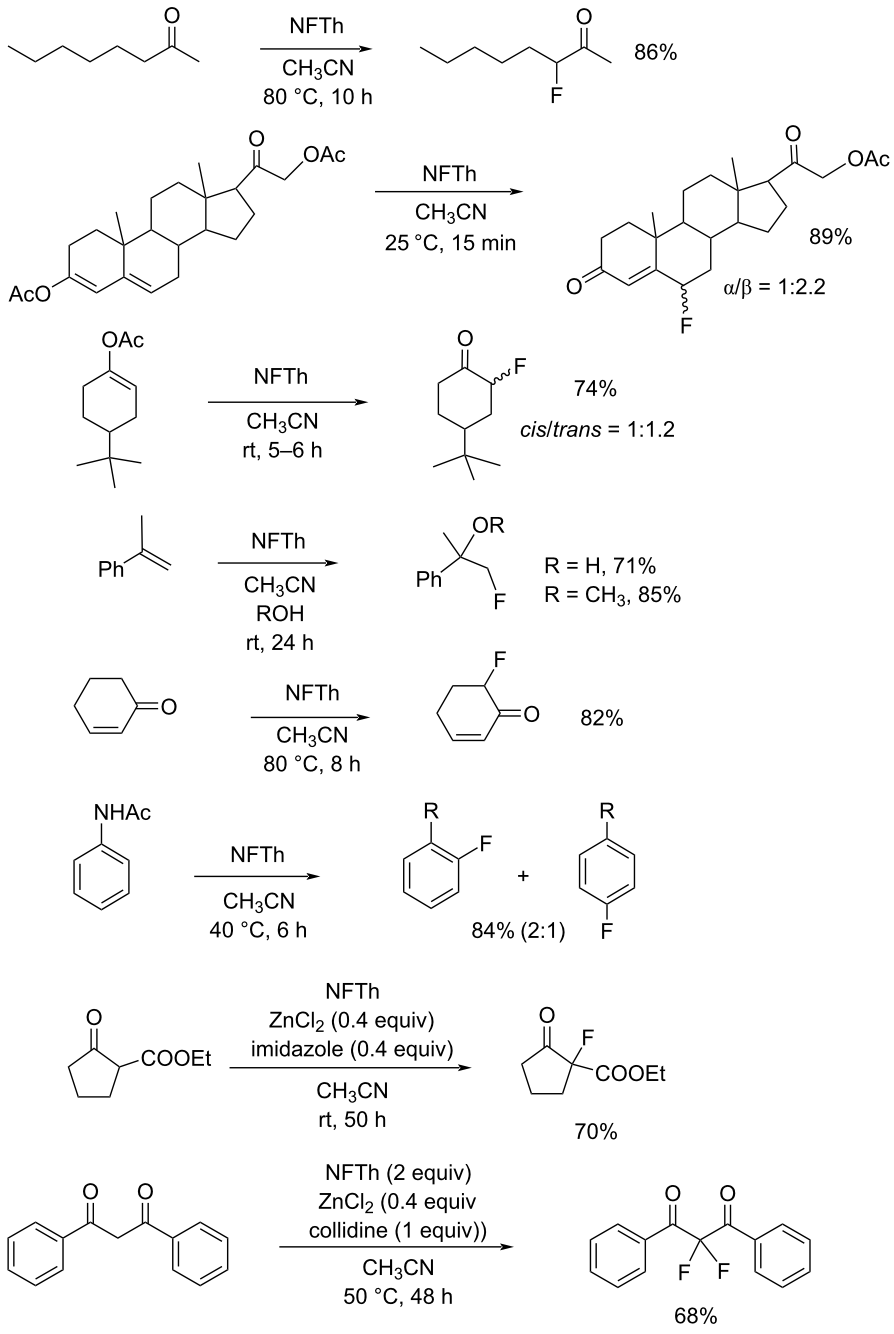

Scheme 43: Fluorination with NFTh, **19-2**.

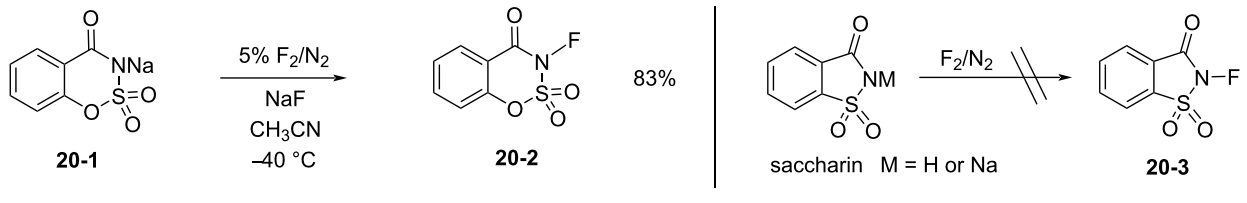

Scheme 44: Synthesis of 3-fluorobenzo-1,2,3-oxathiazin-4-one 2,2-dioxide (**20-2**).

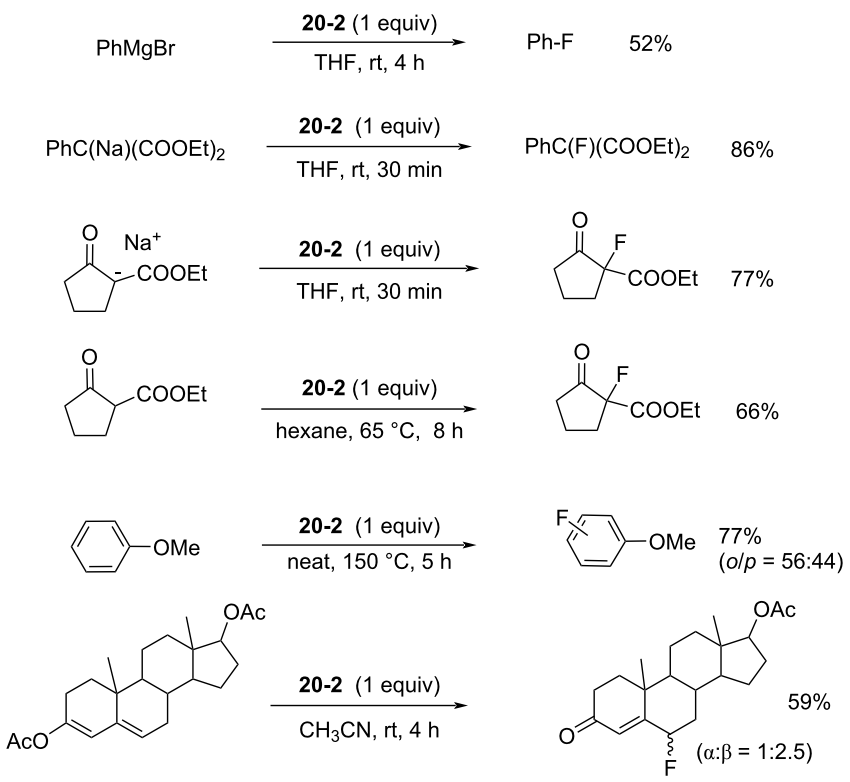

Scheme 45: Fluorination with **20-2**.

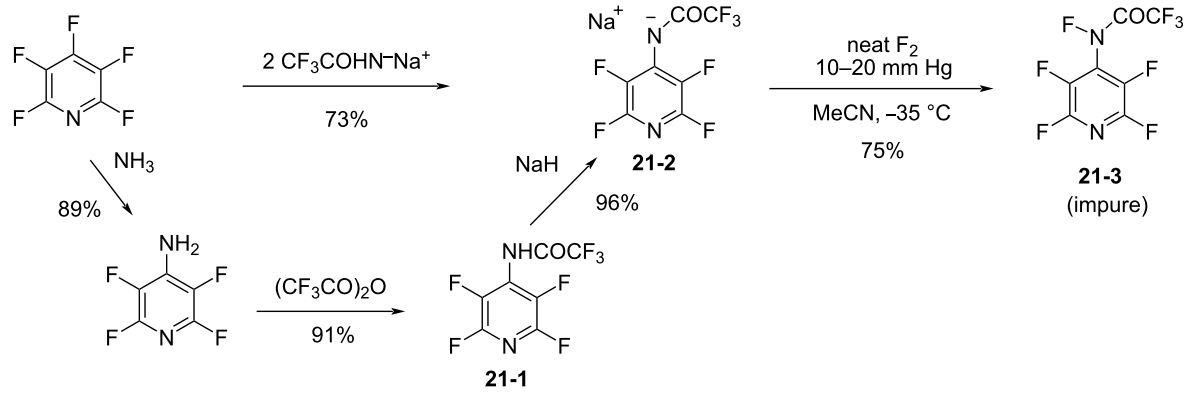

Scheme 46: Synthesis of *N*-F amide **21-3**.

tane salts **22-1a**–**f** in a pure form and in good to excellent yields (Scheme 48) [83]. All the salts were fully identified by elemental analysis and spectral analysis. Previously, in 1992, Banks and co-workers described how attempts to synthesize **22-1** proved to be unsatisfactory [42] and in 1995, they reported their synthesis characterized only by ^{19}F NMR and described that the salts were moisture-sensitive [84].

The synthesis is sensitive to solvents and the amount of Brønsted acids (HX). *N,N'*-Difluoro-1,4-diazoniabicyclo[2.2.2]octane bistriflate (**22-1a**), bis(hydrogensulfate) **22-1b**, hydrogensulfate bishydrogenfluoride fluoride **22-1c**, bishexafluoroantimonate **22-1e**, and bishexafluorophosphate **22-1f** were prepared in a pure form by fluorination of 1,4-diazabicyclo[2.2.2]octane (DABCO) with 10% F_2/N_2 in hexafluoroisopropanol in the presence of two molar equivalents or fewer of HX (one-step method, Scheme 48). The bisSbF_6 salt **22-1e** and bisPF_6 **22-1f** could also be prepared in a pure form by using acetonitrile as the solvent. However, bisBF_4 salt **22-1d** could not be satisfactorily synthesized by this one-step protocol

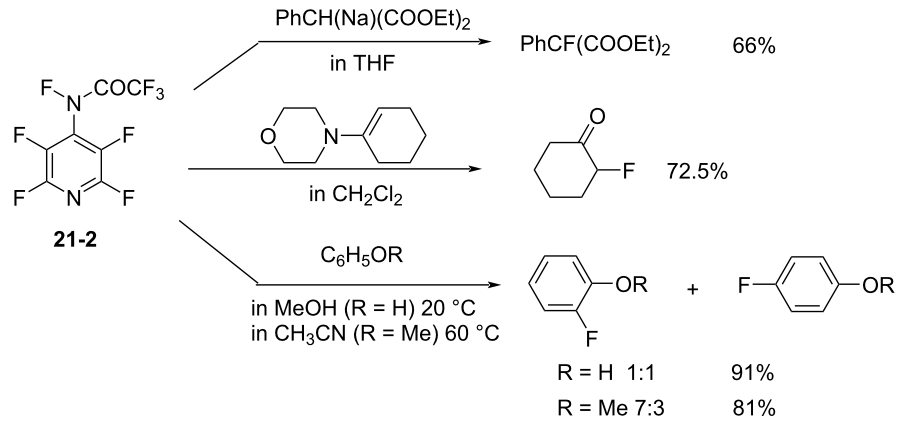

Scheme 47: Fluorination with *N*-F amide **21-2**.

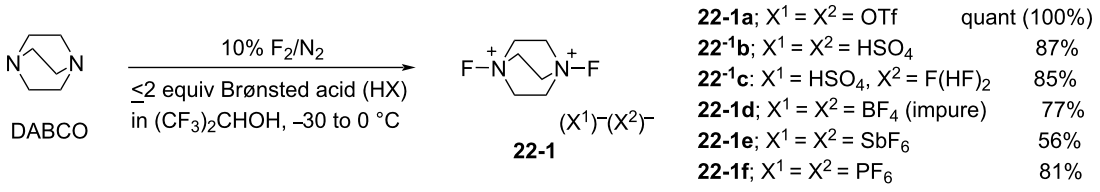

Scheme 48: Synthesis of *N,N'*-difluorodiazoniabicyclo[2.2.2]octane salts **22-1**.

because an inseparable mixture of **22-1d** and the DABCO·2HBF$_4$ salt formed.

BisBF$_4$ **22-1d** was considered to be commercially valuable because of its low preparative cost. Umemoto and co-worker found a clean counteranion replacement reaction of the intermediate $(F^-)_x(HF)_y(HSO_4^-)_z$ salts (x + z = 2) by using BF_3 etherate and thus solved the problem with a simple two-step one-pot method; (step 1) fluorination of a mixture of DABCO and 1.5 molar equivalents of H_2SO_4 with 10% F_2/N_2 in acetonitrile at −20 °C, and (step 2) treatment of the resulting reaction mixture with 2.1 molar equivalents of BF_3 etherate at −20 °C to room temperature, gave pure **22-1d** as a white precipitate (Scheme 49). By applying this telescoped method, pure **22-1d** was easily obtained in 88% yield only after simple filtration of the reaction mixture and no further purification was needed. Pure **22-1d** is non-hygroscopic and forms a stable crystalline solid with a high decomposition point of ca. 170 °C.

The bisOTf salt **22-1a**, bisBF$_4$ **22-1d**, bisSbF$_6$ **22-1e**, and bisPF$_6$ **22-1f** are easy-to-handle because they are non-hygroscopic and stable crystals. As shown in Figure 6, **22-1a**,**d**,**e** mediated a quantitative conversion of anisole to isomers of fluoroanisole at room temperature after 15 min, whereas Select-

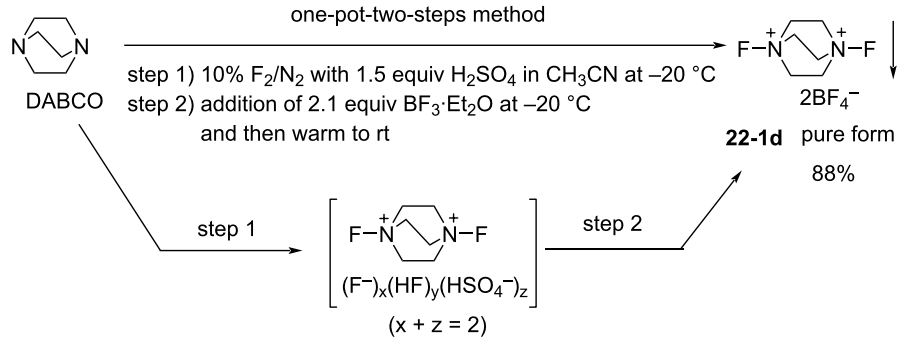

Scheme 49: One-pot synthesis of *N,N'*-difluoro-1,4-diazoniabicyclo[2.2.2]octane bistetrafluoroborate salt (**22-1d**).

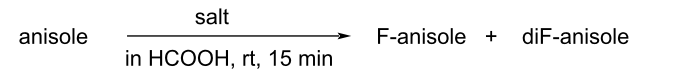

entry	salt	conversion (%)	yield (%)		
			o-F-anisole	*p*-F-anisole	2,4-diF-anisole
1	**22-1a**	100	21	24	4
2	**22-1d**	100	30	29	5
3	**22-1e**	100	22	23	5
4	Selectfluor	19	3	2	0

Figure 6: Fluorination of anisole with **22-1a**, **d**, **e**.

fluor (**16-3a**) only produced fluoroanisole with a 19% conversion. This demonstrated that **22-1** is a much more powerful reagent than Selectfluor, a power that is attributed to the high electronegativity of the fluorine atom compared to the $ClCH_2$ group.

By using the bistetrafluoroborate salt **22-1d**, many substrates such as aromatics, active methylene compounds and their salts, olefins, and enol acetates were efficiently fluorinated (Scheme 50). It was shown also that only one of the two N–F groups of **22-1** is used for *C*-fluorination, while the other N–F plays an activating role.

1-23. Bis-*N*-fluoro reagents derived from precursors containing two heterocycles

In 1997, the Banks group reported bis-*N*-fluoro reagents **23-1**–**3** and related salts **23-4**,**5** by the fluorination of precursors containing two heterocycles (Scheme 51) [85]. Reagents **23-1–3** and **-5** were obtained in good yields and **23-4** was also obtained, but as an impure product. The reagents **23**-**1** and **23**-**2** are bis-Selectfluor-type reagents and **23**-**3** is a bis-*N*-fluoropyridinium reagent. The fluorinating ability of reagents **23-2**, -**4**, and -**5** were examined as shown in Scheme 52.

1-24. *N,N'*-Difluorobipyridinium salts

In 1998, the Umemoto group reported a new series of *N,N'*-difluorobipyridinium salts **24-2**, *N,N'*-difluoro-2,2'-, -2,4'-, -3,3'-, and -4,4'-bipyridinium salts. These were synthesized by the direct fluorination of bipyridines **24-1** with 10–20% F_2/N_2 in the presence of a Lewis acid, a Brønsted acid, or its metal salt in acetonitrile or as a 50:1 mixture of acetonitrile/formic acid at −40 to 0 °C. The yields were good to excellent [86] (Figure 7). The trimer **24-3** and polymer homologues **24-4** were also prepared. The *N,N'*-difluorobipyridinium salts are stable and generally furnished non-hygroscopic free flowing materials, however, this was less the case for those derivatives with electron-withdrawing substituents.

Controlled fluorination reactions with these reagents (Figure 8) clearly showed a power order of 2,2'- (**24-2a**) >> 2,4'- (**24-2c**) > 3,3'- (**24-2f**) ≈ 4,4'- (**24-2g**) >> *N*-fluoropyridinium triflate (Scheme 53), which is again in good agreement with the pK_a values of the bipyridines. The 2,2'-isomers had the highest power (reactivity) among the dipyridinium isomers, and they were much more reactive than the monomeric *N*-fluoropyridinium triflate (**5-4a**).

In contrast to the *N,N'*-difluoro-1,4-diazoniabicyclo[2.2.2]octane salts **22-1**, both of the *N*-F moieties in **24-2** were effective in fluorinations and they reacted sequentially. *N,N'*-Difluoro-2,2'-bipyridinium bis(tetrafluoroborate) (**24-2b**, X = BF_4, SynFluor™, MEC-31) was chosen as a representative of this class to assess fluorination capability because of its low production cost and high fluorine content per molecule. As a result, SynFluor™ (**24-2b**) proved to be a practical reagent for the fluorination of many substrates affording the products in good to high yields (Scheme 54 and Scheme 55). SynFluor can be considered a powerful fluorinating agent with a high fluorine content, F: 103 g/1 kg (comparison; 54 g/1 kg for Selectfluor).

1-25. *N*-Fluoro-2,4-dinitroimidazole

In 1998, Laali et al. reported the fluorination of polycyclic aromatic hydrocarbons (PAHs) with *N*-fluoro-2,4-dinitroimidazole (**25-1**) [87] (Scheme 56). This reagent is a white solid that was prepared by Forohar et al. through fluorination of 2,4-dinitroimidazole (5% F_2 in N_2 at −40 °C) [88]. Although additional information on **25-1** was not available, it was noticed [87] that the polynitro compound **25-1** is potentially dangerous towards detonation.

Laali et al. attempted to fluorinate some polycyclic aromatics with Selectfluor, but intractable mixtures were obtained. Thus, they examined the utility of **25-1** in the fluorination of polycyclic aromatics. Although a detailed optimization was con-

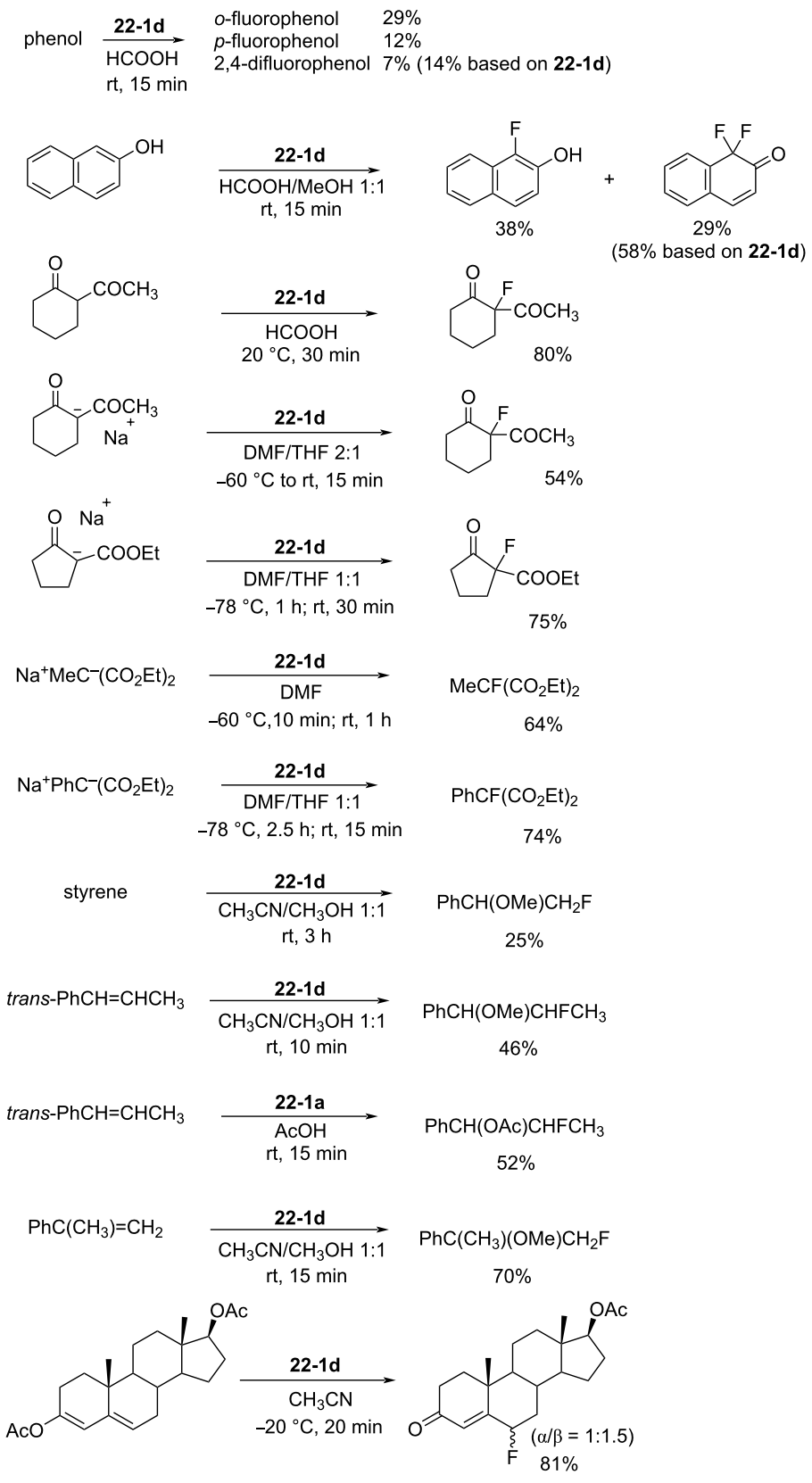

Scheme 50: Fluorination with *N,N'*-diF bisBF$_4$ **22-1d**.

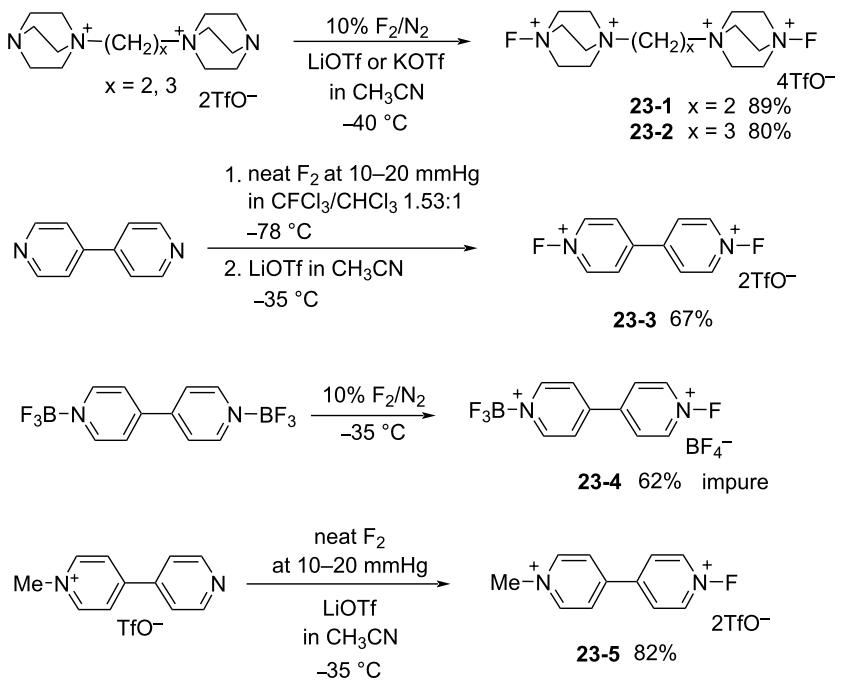

Scheme 51: Synthesis of bis-N-F reagents **23-1**–**5**.

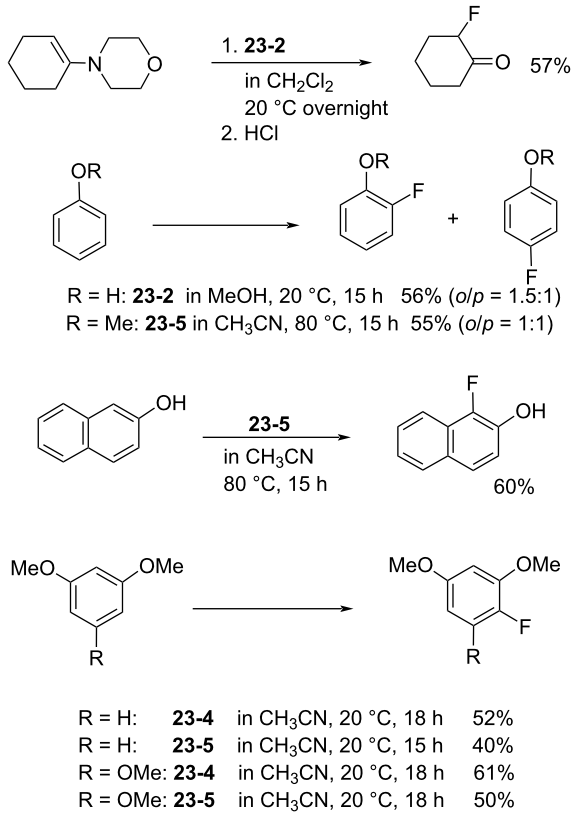

Scheme 52: Fluorination with **23-2**, **4**, **5**.

ducted, the fluorination of over 20 polycyclic aromatics was poor giving products in very low yields, varying from 27% to 3% depending on the substrate. The fluorinations were accompanied by tar formation and dimerization. Scheme 57 illustrates some representative examples.

1-26. Perfluoro-(*N*-fluoro-2,2,6,6-tetramethylpiperidine) and its 2,6-dimethyl analogue

In 1999, the Banks group reported the syntheses of perfluoro-(*N*-fluoro-2,2,6,6-tetramethylpiperidine) (**26-1**) and its 2,6-dimethyl analogue **26-2**, reagents which do not have α-fluorine atoms adjacent to the *N*-F site [89] (Scheme 58). These reagents overcame the drawback of perfluoro-*N*-fluoropiperidine (**1-1**) which does contain α-fluorine atoms (see section 1-1).

The fluorinating ability of reagents **26-1** and -**2** was tested in fluorinations of the sodium salt of a keto ester (Scheme 59). Reagents **26-1** and -**2** were superior to **1-1** and **26-3** where the α-fluorine atoms can be eliminated after fluorine-transfer from the *N*-F site.

1-27. *N*-Fluoro-3-ethyl-3-methyldioxobenzothiazinone and (*R*)- and (*S*)-*N*-fluoro-3-cyclohexyl-3-methylbenzoisothiazole dioxide

In 1999, Takeuchi et al. reported *N*-fluoro-3-ethyl-3-methyl-1,1-dioxo-2,3-dihydro-1*H*-1λ^6-benzo[*e*]1,2-thiazin-4-one (**27-2**) as an efficient reagent for the fluorination of carbanions [90].

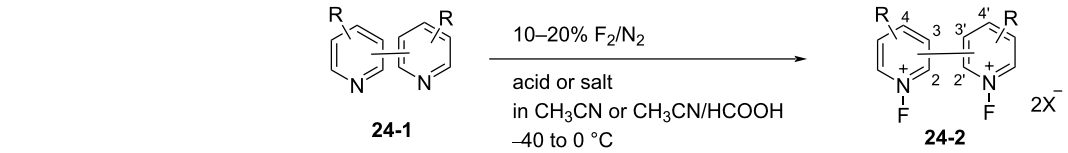

24-1 24-2

entry	bipyridyl	acid or salt	solvent	temp	product	R + bonding	X	yield (%)
1	2,2'-	TfOH	CH_3CN	–20	**24-2a**	2,2'-	OTf	86
2	2,2'-	BF_3	CH_3CN/HCOOH 50:1	0	**-2b**	2,2'-	BF_4	89
3	2,4'-	TfOH	CH_3CN	–20	**-2c**	2,4'-	OTf	92
4	2,4'-	BF_3	CH_3CN	–20	**-2d**	2,4'-	BF_4	86
5	2,4'-	HPF_6	CH_3CN	–20	**-2e**	2,4'-	PF_6	64
6	3,3'-	TfOLi	CH_3CN	–40	**-2f**	3,3'-	OTf	75
7	4,4'-	TfOH	CH_3CN	–20	**-2g**	4,4'-	OTf	91
8	4,4'-	BF_3	CH_3CN/HCOOH 49:1	0	**-2h**	4,4'-	BF_4	95
9	4,4'-	SbF_5	CH_3CN	–20	**-2i**	4,4'-	SbF_6	91
10	4,4'-diMe-2,2'-	BF_3	CH_3CN	–20	**-2j**	4,4'-diMe-2,2'-	BF_4	73
11	4,4'-diCl-2,2'-	BF_3	CH_3CN	–20	**-2k**	4,4'-diCl-2,2'-	BF_4	79
12	4,4'-diPh-2,2'-	BF_3	CH_3CN	–20	**-2l**	4,4'-diPh-2,2'-	BF_4	64
13	4,4'-di(COOMe)-2,2'-	SbF_5	CH_3CN	–20	**-2m**	4,4'-di(COOMe)-2,2'-	BF_4	97
14	5,5'-diCF_3-2,2'-	TfOH	CH_3CN	–20	**-2n**	4,4'-diCF_3-2,2'-	OTf	72

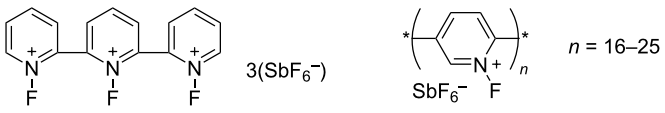

24-3 24-4

Figure 7: Synthesis of *N,N'*-difluorobipyridinium salts **24-2**.

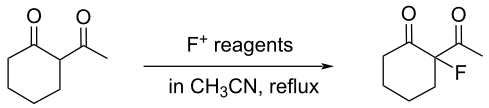

entry	F^+ reagent	reaction time	yield (%)
1	2,2'- (**24-2a**)	< 5 min	85
2	2,4'- (**24-2c**)	2 h	78
3	3,3'- (**24-2f**)	5 h	70
4	4,4'- (**24-2g**)	5 h	87
5	*N*-fluoropyridinium triflate (**5-4a**)	19 h	79

Figure 8: Controlled fluorination of *N,N'*-diF **24-2**.

The precursor **27-1**, which was prepared in a three step protocol from saccharin, was fluorinated with $FClO_3$ to give **27-2** in good yield (Scheme 60). Direct fluorination of **27-1** with 10% F_2/N_2 had failed because of decomposition. Various ketone enolates were successfully fluorinated with reagent **27-2** in good to high yields [90].

In addition, Takeuchi et al. reported that optically active *N*-fluorosultams, (*R*)- and (*S*)-*N*-fluoro-3-cyclohexyl-3-methyl-2,3-dihydrobenzo[1,2-*d*]isothiazole 1,1-dioxides **27-6** (Scheme 61) were efficient reagents for the asymmetric fluorination of enolates [91].

To showcase his methodology, they first synthesized acyclic optically active *N*-fluoro sulfonamides **27-7**–**9** (Scheme 62) and attempted the enantioselective fluorination of some enolates in 1997 [92]. However, the best result was an enantiomeric excess of 48% with a chemical yield of 53% after the enolate anion of 2-benzyl-α-tetralone was treated with **27-8**.

As summarized in Scheme 61, Takeuchi et al. prepared the enantiomers of cyclic *N*-F sulfonamide **27-6** by the approach used

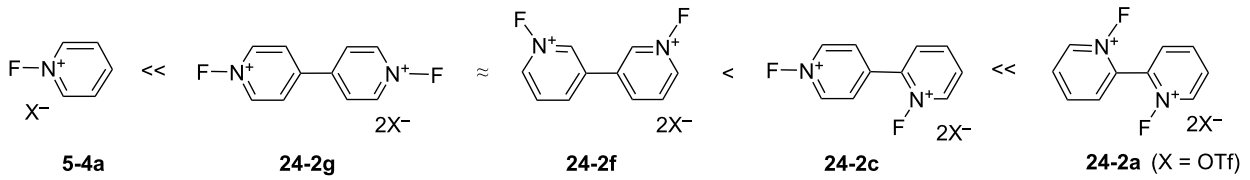

Scheme 53: Fluorinating power of *N,N'*-diF salts **24-2** and *N*-F salt **5-4a**.

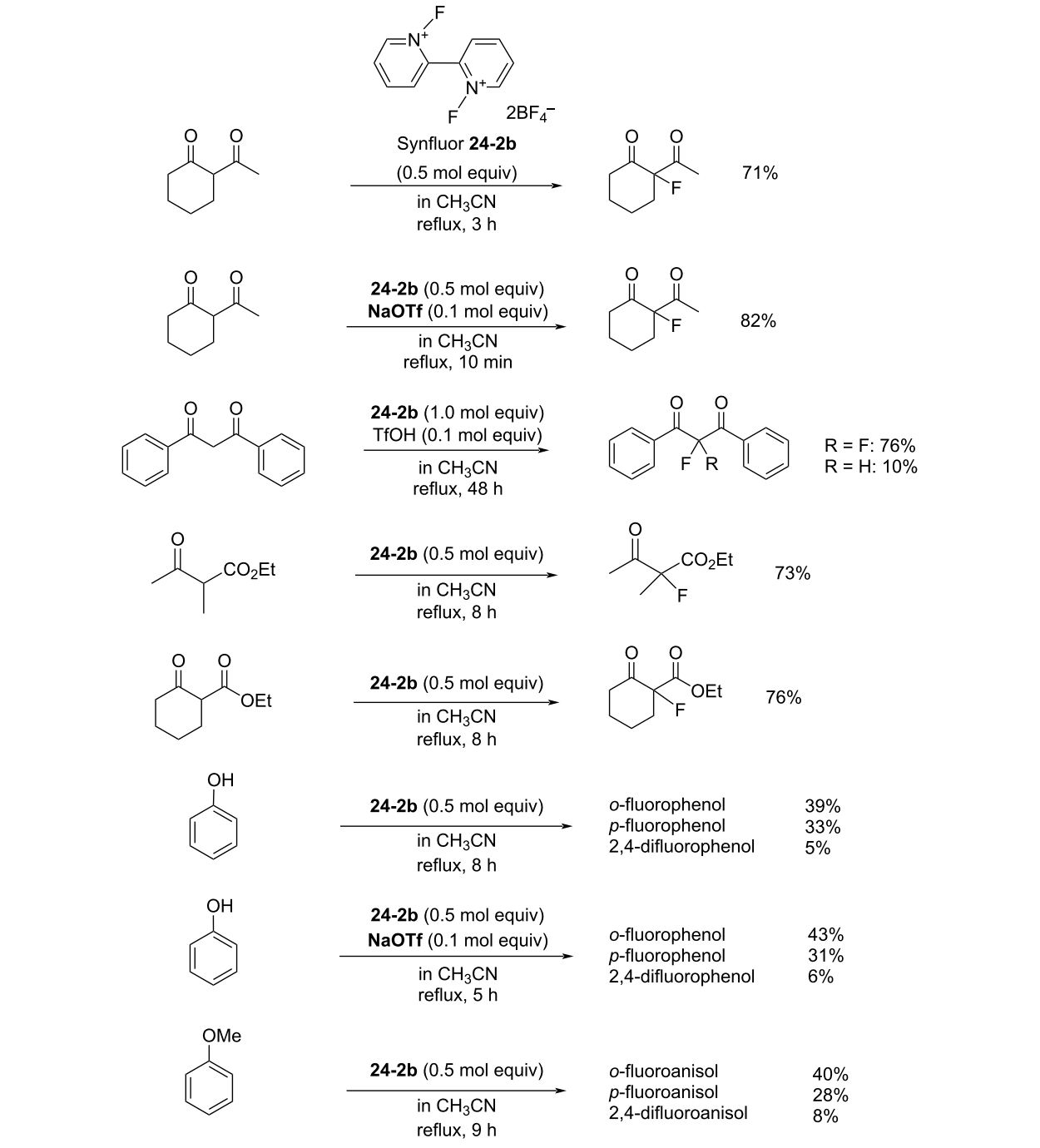

Scheme 54: Fluorination reactions with Synfluor™ (**24-2b**).

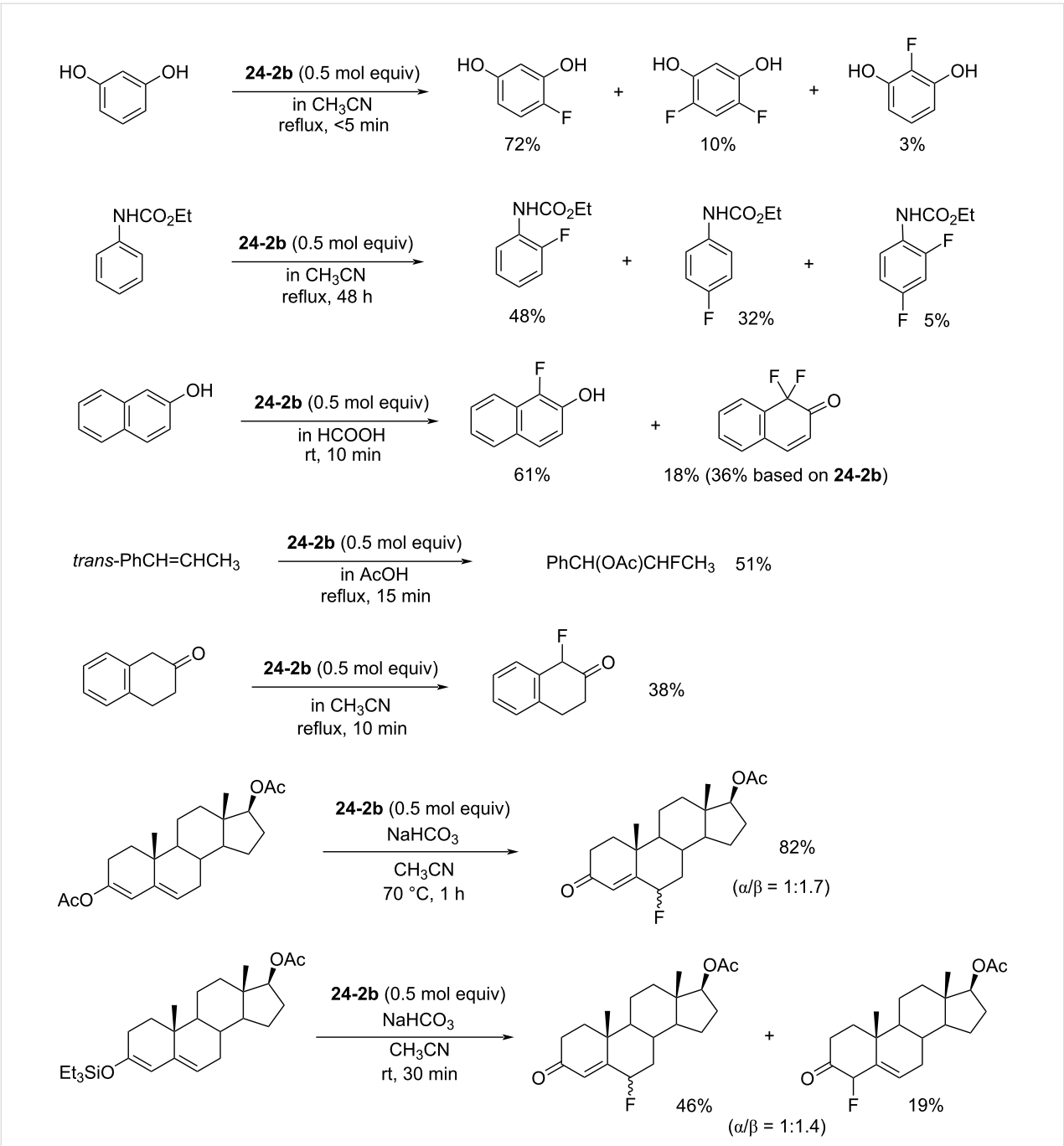

Scheme 55: Additional fluorination reactions with Synfluor™ (**24-2b**).

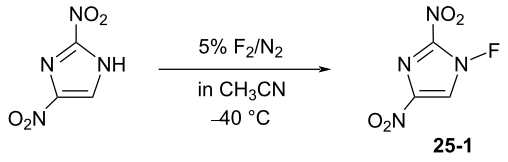

Scheme 56: Synthesis of *N*-F **25-1**.

by Lang for *N*-fluorosultams [53]. A cyclohexyl ring was introduced nucleophilically into imine **27-3** and the resulting **27-4** was treated with (−)-menthoxyacetyl chloride, followed by separation of the diastereomers. The chiral auxiliary was then removed with LiOH and the resulting sultams **27-5** as single enantiomers were fluorinated with 15% F_2/He in the presence of KF to produce optically pure *N*-fluorosultam reagents (*R*)- and (*S*)-**27-6**.

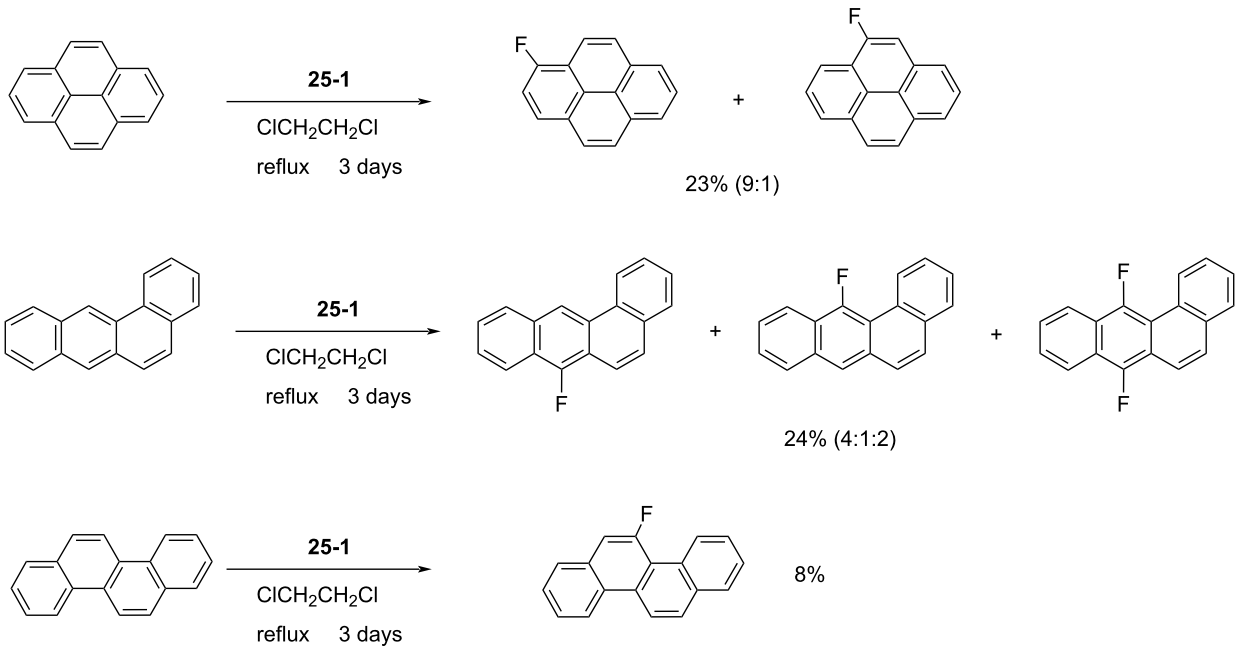

Scheme 57: Fluorination of polycyclic aromatics with **25-1**.

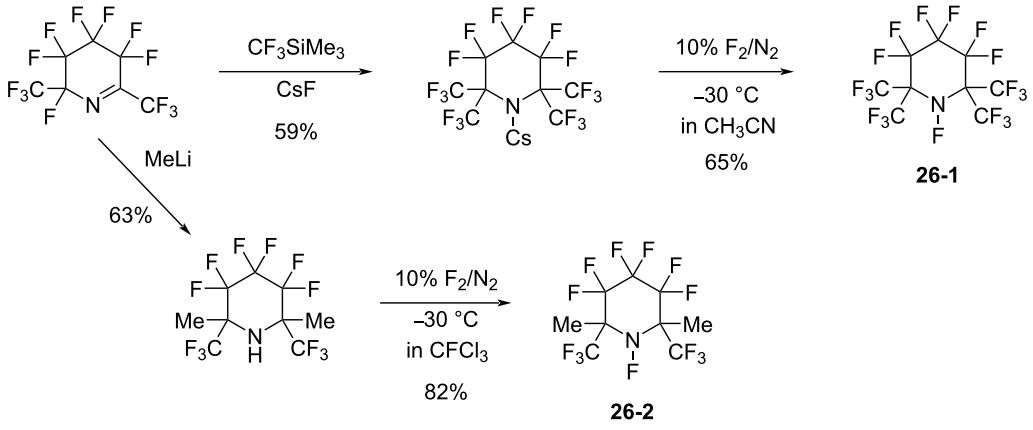

Scheme 58: Synthesis of **26-1** and dimethyl analog **26-2**.

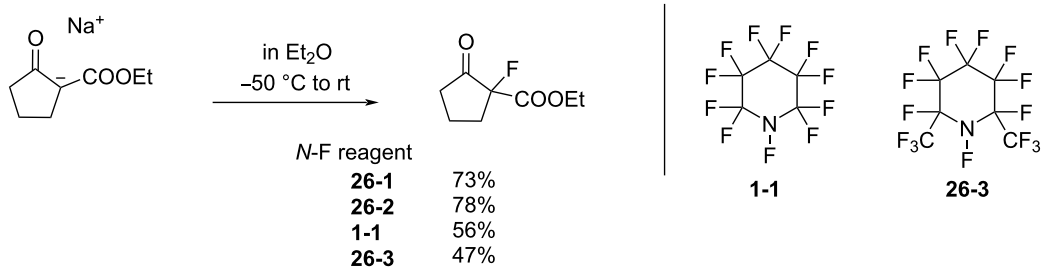

Scheme 59: Fluorination with reagents **26-1**, **26-2**, **1-1**, and **26-3**.

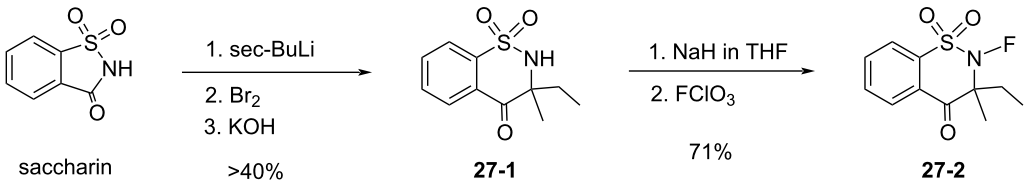

Scheme 60: Synthesis of *N*-F reagent **27-2**.

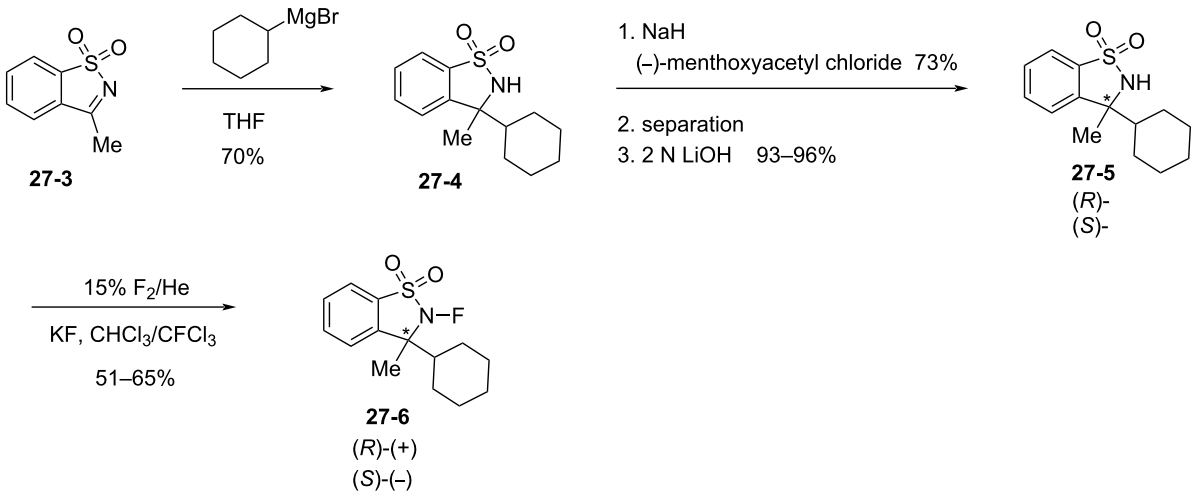

Scheme 61: Synthesis of chiral *N*-F reagents **27-6**.

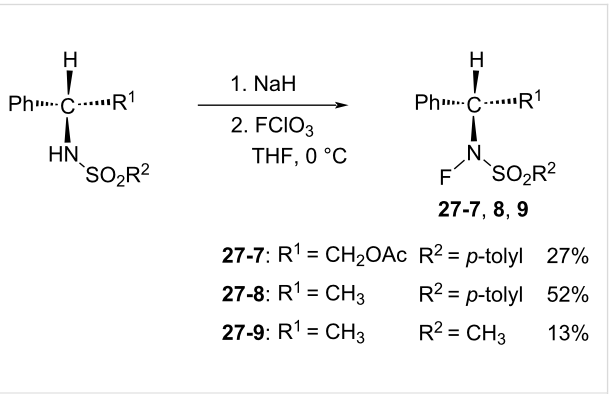

Scheme 62: Synthesis of chiral *N*-F **27-7–9**.

Enantioselective fluorinations of typical enolates were then performed (Scheme 63). The (*R*)-**27-6** reagent gave up to 79% yield and 88% enantiomeric excess in the case of 2-benzyl-α-tetralone.

1-28. (*R*)- and (*S*)-*N*-fluoro-3-*tert*-butyl-7-nitro-benzothiazine 1,1-dioxides and spiro-type analogues

In 2000, the Takeuchi group reported their second series of chiral *N*-fluorosultam reagents, (*R*)- and (*S*)-*N*-fluoro-3-*tert*-

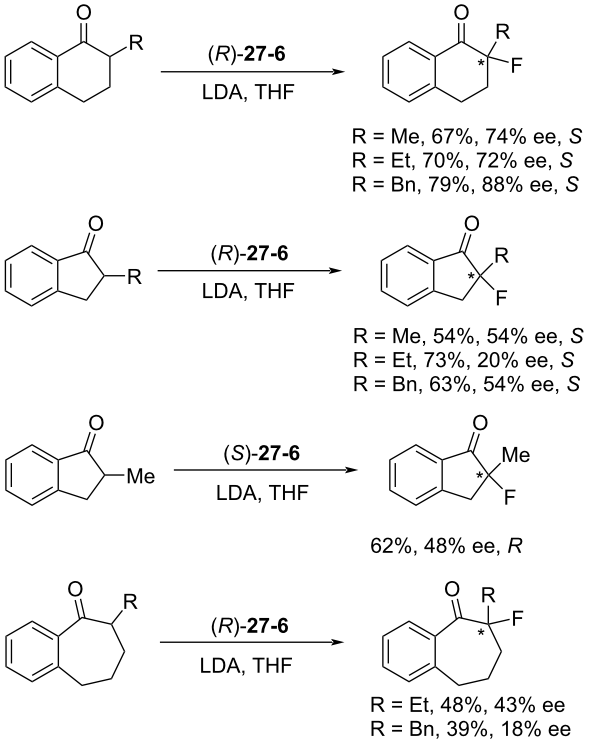

Scheme 63: Asymmetric fluorination with **27-6**.

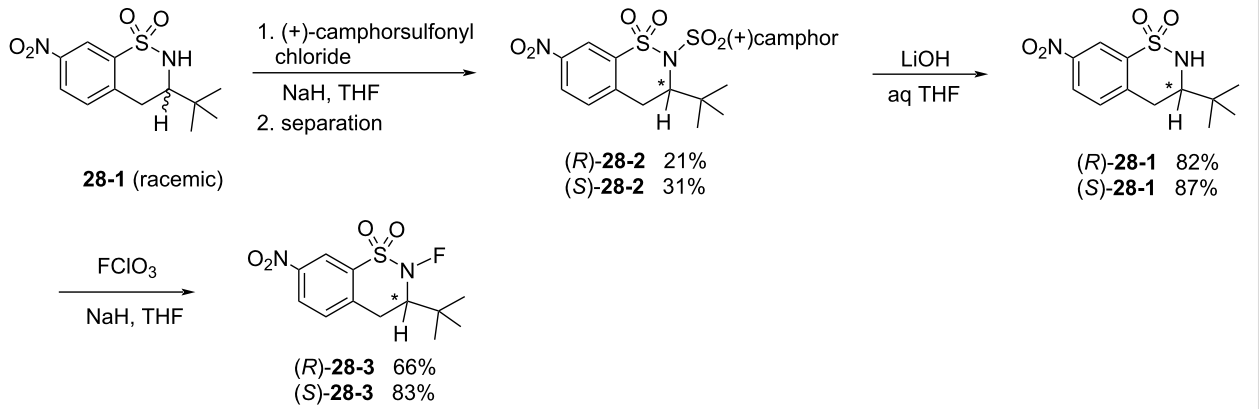

Scheme 64: Synthesis of chiral *N*-F reagents **28-3**.

butyl-7-nitro-3,4-dihydro-2*H*-benzo[*e*][1,2]thiazine 1,1-dioxides **28-3** [93] (Scheme 64). Racemic **28-1** reacted with (+)-10-camphorsulfonyl chloride to give a mixture of the diastereomers of **28-2**, which was accompanied by 45% of unreacted **28-1**. Interestingly, pure (*R*)-isomer **28-1** was obtained in 20% yield from the unreacted **28-1**. The diastereomer separation of **28-2** was achieved by column chromatography to separate the (*R*)- and (*S*)-isomers of **28-2** in 21 and 31% yields, respectively. Deprotection followed by fluorination with $FClO_3$ gave (*R*)- and (*S*)-**28-3** in good yields. X-ray crystallography was used to determine the structure and confirm the absolute stereochemistry of (*S*)-**28-3**.

The optically active reagents (*R*)- and (*S*)-**28-3** were effective in the enantioselective fluorination of cyclic ketones, as is illustrated with representative in Scheme 65.

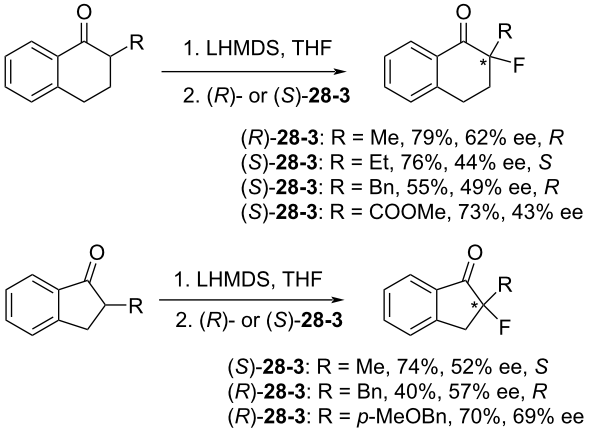

Scheme 65: Asymmetric fluorination with **28-3**.

In addition, the Takeuchi group reported a spiro-type analogue, (2'*S*,3*R*,5'*R*)-2-fluoro-2'-methylethyl-5'-methyl-2*H*,4*H*-spiro[benzo[*e*][1,2]thiazine-3,1'-cyclohexane]-1,1-dione (**28-7a**) [94], as their third chiral reagent in this sultam series. As can be seen in Scheme 66, **28-4** was treated with BuLi followed by

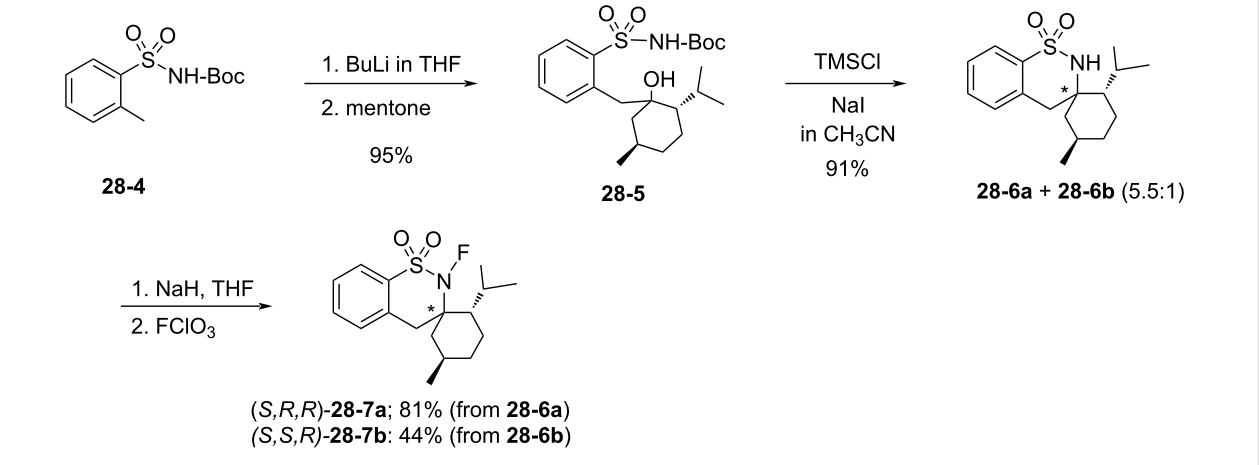

Scheme 66: Synthesis of chiral *N*-F reagents **28-7**.

reaction with optically active menthone to give **28-5**, which was converted to enantiomers of spiro sultams **28-6a** and **28-6b** in high yield. The spiro sultams **28-6a** and **-6b** were separated and each was fluorinated with $FClO_3$ to give (2'*S*,3*R*,5'*R*)-isomer **28-7a** and (2'*S*,3*S*,5'*R*)-isomer **28-7b** in 81% and 44% yield, respectively.

Figure 9 summarizes the outcomes of asymmetric fluorination reactions of enolates of aryl ketones using **28-7a** and **-7b**. In the event isomer **28-7a** yielded much better ees than **28-7b**. Although **28-7a** gave a maximum 70% ee (entry 6, Figure 9), it was less than that obtained (74% ee) by *N*-fluorosultam (*R*)-**27-6** with the same substrate (see the previous section 1-27).

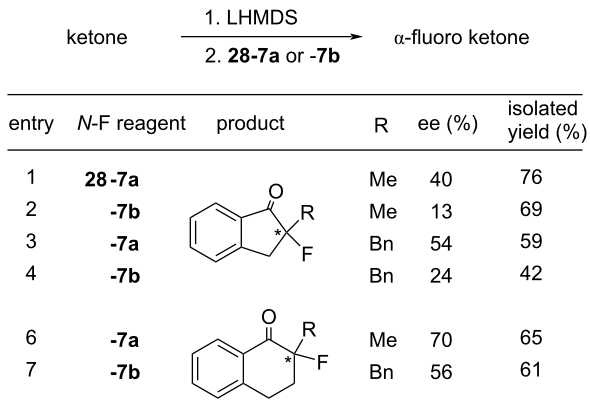

Figure 9: Asymmetric fluorination with **28-7**.

1-29. *N*-Fluorinated cinchona alkaloid derivatives by combination with Selectfluor

In 2000, Shibata and Takeuchi reported a far more practical enantioselective fluorination method. They discovered that the fluorination of carbanions with Selectfluor occurred in a highly enantioselective manner when carried out in the presence of cinchona alkaloid derivatives [95]. This method consisted of two simple steps. Firstly, the cinchona alkaloid is reacted with Selectfluor in acetonitrile at room temperature for 1 h, and then this is followed by addition of the substrate. The resulting mixture is stirred at a suitable temperature. They proposed that Selectfluor transfers fluorine to the alkaloid to give a chiral *N*-F alkaloid species, in a manner that followed the fluorine transfer reported by Banks when quinuclidine was *N*-fluorinated with Selectfluor [62] (Scheme 67). Subsequently, in 2001, Shibata et al. presented full details of their studies including the definitive identification of *N*-fluorinated cinchona alkaloids by X-ray crystallography analysis and further applications [96]. This method proved to be far more practical than the enantiomeric sulfonamide-type *N*-F reagents developed until then.

Many cinchona alkaloid derivatives were tested for their ability to fluorinate substrates such as cyclic and acyclic ketones and esters. Scheme 67 shows two typical examples of *N*-F cinchona alkaloid species, **29-2** and **29-4**, formed from dihydroquinine 4-chlorobenzoate (DHQB, **29-1**) and dihydroquinidine acetate (DHQDA, **29-3**) with Selectfluor. As a result, high chemical yields and high enantiomeric excesses were obtained for many substrates as summarized in Scheme 68. The DHQB/Select-

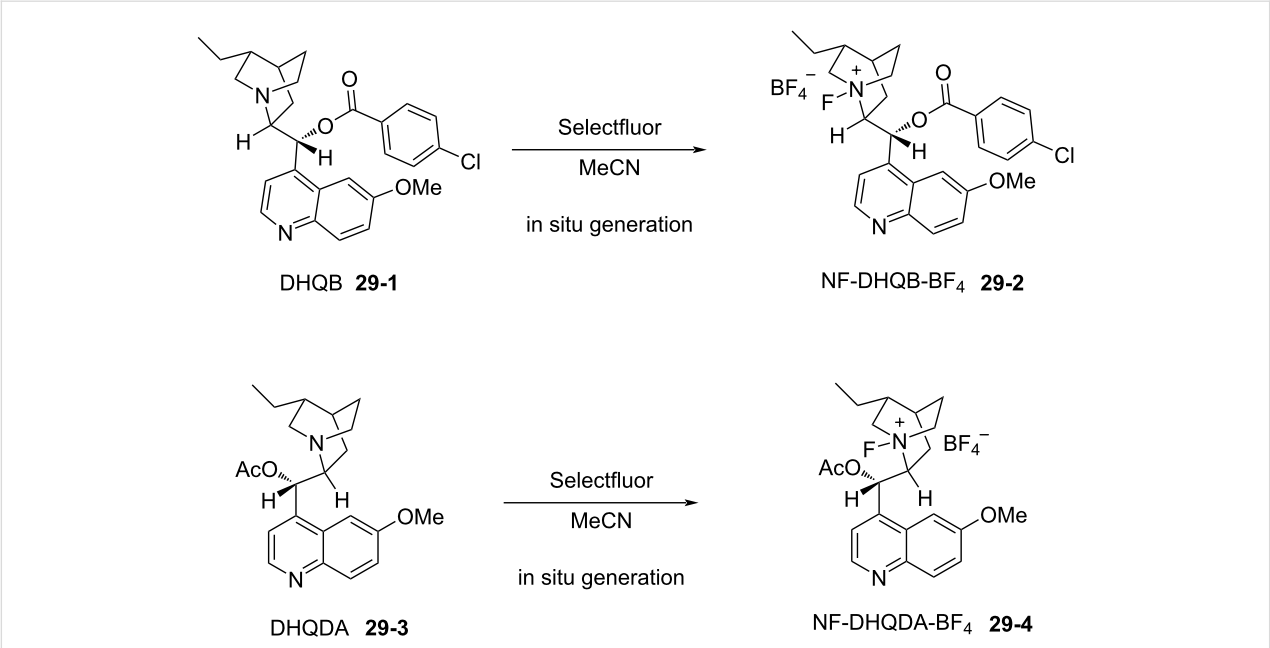

Scheme 67: In situ formation of *N*-fluorinated cinchona alkaloids with Selectfluor™.

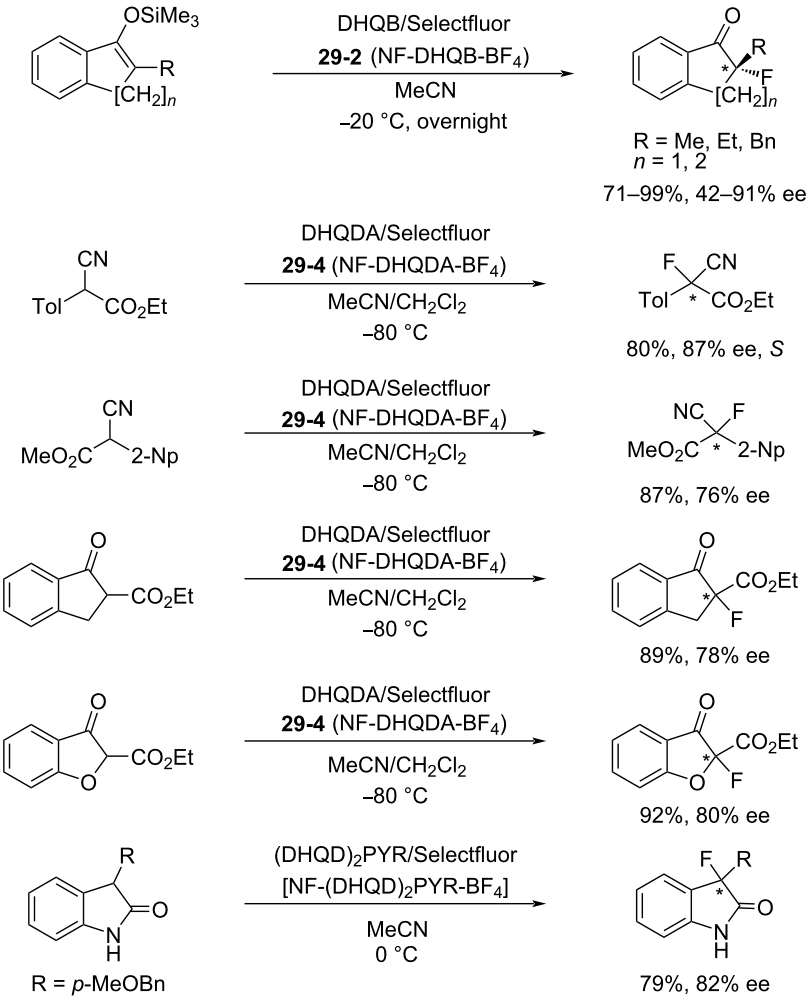

Scheme 68: Asymmetric fluorination with *N*-F alkaloids formed in situ.

fluor combination was effective for the fluorination of silyl enol ethers of indanones and tetralones, forming the fluorinated products in up to 91% ee. The DHQDA/Selectfluor combination was effective also for acyclic esters, with outcomes up to 87% ee, and for cyclic keto esters, up to 80% ee. For oxindoles, the $(DHQD)_2PYR$/Selectfluor combination was effective too, generating the products with up to 82% ee.

1-30. Enantiopure *N*-fluorocinchona alkaloid salts

Only six days after the report by Shibata and Takeuchi appeared (Oct. 2000), Cahard et al. reported the synthesis and application of similar enantiopure *N*-fluoro salts of cinchona alkaloids through the reaction of the alkaloids with Selectfluor [97]. Following the precedent from Banks's fluorine-transfer reaction from Selectfluor to the *N*-site of quinuclidine [62], Cahard et al. isolated four *N*-fluorocinchona alkaloid salts, F-CD-BF_4 **30-1**, F-CN-BF_4 **30-2**, F-QN-BF_4 **30-3**, and F-QD-BF_4 **30-4** in good yields (Scheme 69). Soon after in 2001, they reported the X-ray structural analysis of F-CD-BF_4 **30-1** [98].

The enantioselective fluorination of the sodium enolate of 2-methyl-1-tetralone was examined using these *N*-F alkaloid salts (Scheme 70). F-CD-BF_4 **30-1** gave the highest result with a 56% ee. F-CD-BF_4 **30-1** is a nonhygroscopic, free-flowing solid with a high decomposition point (189 °C, dec).

Enantioselective fluorinations of the sodium enolates of other ketones and β-keto esters with F-CD-BF_4 **30-1** were also investigated. The trimethylsilyl enol ether of 2-methyl-1-tetralone was examined, too (up to 61%ee, 93% yield). These experiments gave the fluorinated products in excellent chemical yields but with lower enantiomeric excesses than the Shibata and Takeuchi's protocol.

1-31. *N*-Fluoro-*p*-chlorobenzoylquinine salt: another *N*-F reagent of cinchona alkaloid

In 2003, Cahard et al. reported the transfer fluorination of a cinchona alkaloid, *p*-chlorobenzoylquinine (pClBzQN, **31-1**) using not only Selectfluor^{TM} (F-TEDA-BF_4) but also other

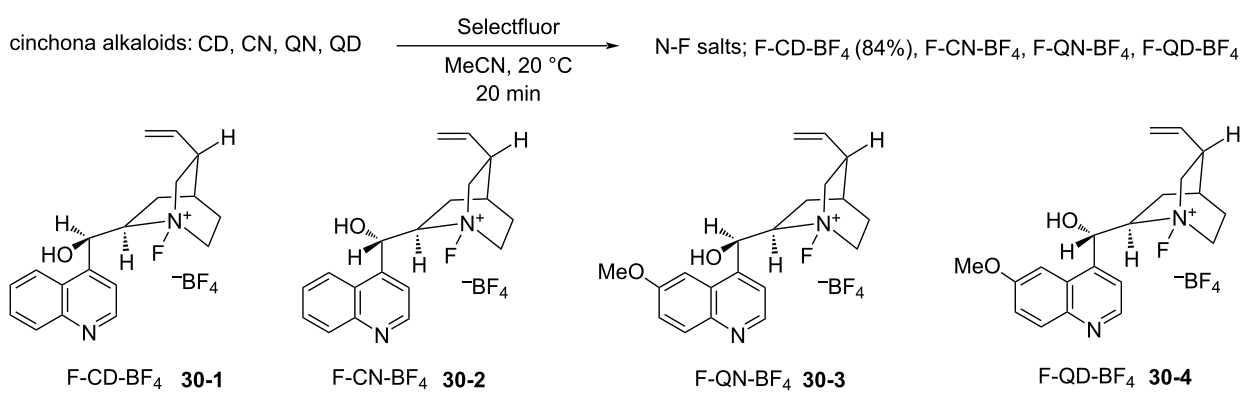

Scheme 69: Synthesis of *N*-fluorocinchona alkaloids with Selectfluor.

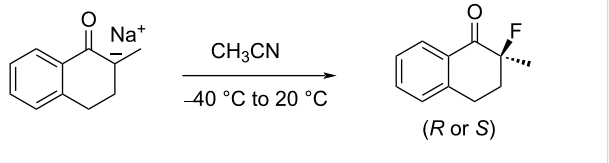

F-CD-BF$_4$ **30-1**	98%, 50% ee
F-CD-BF$_4$ **30-1** (–60 °C)	80%, 56% ee
F-CN-BF$_4$ **30-2**	70%, 40% ee
F-QN-BF$_4$ **30-3**	98%, 20% ee
F-QD-BF$_4$ **30-4**	87%, 27% ee

Scheme 70: Asymmetric fluorination with **30-1**–**4**.

powerful *N*-F fluorinating agents such as 1-fluoro-4-hydroxy-1,4-diazoniabicyclo[2.2.2]octane bistetrafluoroborate (NFTh, **19-2**), *N*-fluorobenzenesulfonimide (NFSI), and *N*-fluoro-2,6-dichloropyridinium tetrafluoroborate (**5-4s**) (Scheme 71) [99].

These reactions produced F-pClBzQN-X **31-2** quantitatively at 20 °C within 30 min in acetonitrile or in an ionic liquid such as 1-hexyl-3-methylimidazolinium hexafluorophosphate [hmim][PF$_6$]. However, the less powerful reagents, *N*-fluoroquinuclidinium tetrafluoroborate, *N*-fluoro-*N*-methyl-*p*-toluenesulfonamide (**4-1a**), *N*-fluoropyridinium triflate (**5-4a**), *N*-fluoro-2,4,6-trimethylpyridinium tetrafluoroborate (**5-4k**), and *N,N'*-difluoro-2,2'-bipyridinium bistetrafluoroborate (**24-2b**) failed. Among the five effective fluorine-transfer reagents, the 2,6-dichloropyridinium salt **5-4s** was more cost effective because it has a higher fluorine content (**5-4s**, 3.94 mmol/g) than the others (Selectfluor, 2.82 mmol/g; F-TEDA-OTf, 2.09 mmol/g; NFTh, 3.11 mmol/g; NFSI, 3.17 mmol/g).

The enantioselective fluorination of F-pClBzQN-X **31-2** was examined on trimethylsilyl enol ethers of methyl- and benzylindanones **31-3** and -**4** (Figure 10). High chemical yields and ees

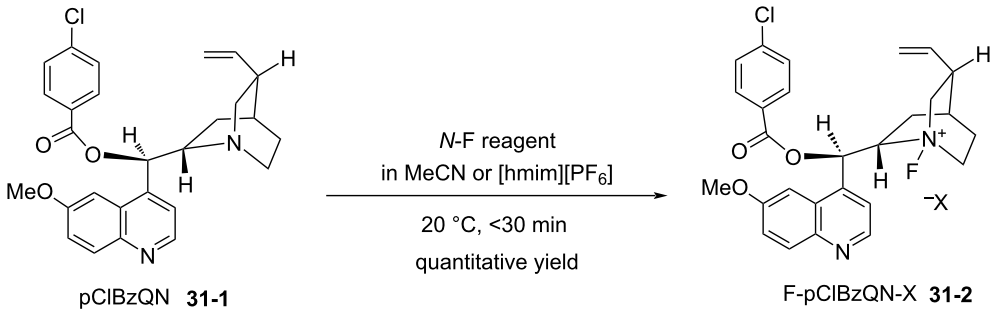

N-F reagent	F-pClBzQN-X
Selectfluor (F-TEDA-BF$_4$)	X = BF$_4$
F-TEDA-OTf	X = OTf
NFTh	X = BF$_4$
NFSI	X = N(SO$_2$Ph)$_2$
N-F-2,6-diCl-pyridinium BF$_4$	X = BF$_4$

Scheme 71: Transfer fluorination from various *N*-F reagents.

(88–97% and 81–85% ee) were obtained in the reactions of benzyl derivative **31-4** with F-pClBzQN-X [X = BF_4 or $N(SO_2Ph)_2$] prepared in situ from the *N*-F reagents and pClBzQN (entries 4–8 in Figure 10).

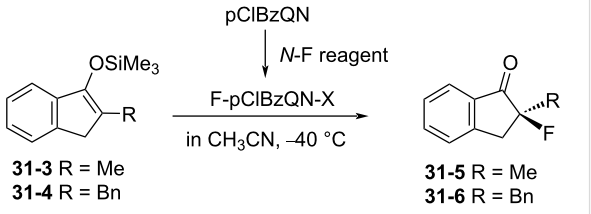

31-3 R = Me
31-4 R = Bn

31-5 R = Me
31-6 R = Bn

entry	*N*-F reagent	substrate	product	yield (%)	ee (%)
1	Selectfluor	**31-3**	**31-5**	90	64
2	NFSI	**31-3**	**31-5**	91	62
3	*N*-F-2,6-diCl-pyridinium BF_4	**31-3**	**31-5**	97	67
4	Selectfluor	**31-4**	**31-6**	98	84
5	F-TEDA-OTf	**31-4**	**31-6**	88	81
6	NFTh	**31-4**	**31-6**	92	82
7	NFSI	**31-4**	**31-6**	94	85
8	*N*-F-2,6-diCl-pyridinium BF_4	**31-4**	**31-6**	97	81

Figure 10: Asymmetric fluorination of silyl enol ethers.

1-32. *N*-Fluoro-2,4,6-trichloro-1,3,5-triazinium tetrafluoroborate

In 2003, Banks et al. reported the synthesis of *N*-fluoro-2,4,6-trichloro-1,3,5-triazinium tetrafluoroborate (**32-2**) and its fluorination of aromatic compounds [100]. Although the syntheses of *N*-fluoro-2,4,6-trifluoro-1,3,5-triazinium hexafluoroarsenate and *N*-fluoro-2,4,6-trichloro-1,3,5-triazinium hexafluoroarsenate had been reported a decade earlier (1993) [101], their fluorination ability had not been disclosed.

Salt **32-2** was prepared in high yield in a small-scale batch reactor (Scheme 72). Accordingly, 100% F_2 (1 equiv) and BF_3 (1 equiv) gas were condensed into a stainless steel autoclave cooled at −196 °C, which contained cyanuric chloride (**32-1**, 1 equiv) in $CFCl_3$. This was followed by gradual warming to room temperature and the reaction mixture was stored for 5 days. The resultant salt **32-2** is a moisture-sensitive white solid that decomposes at 153–155 °C.

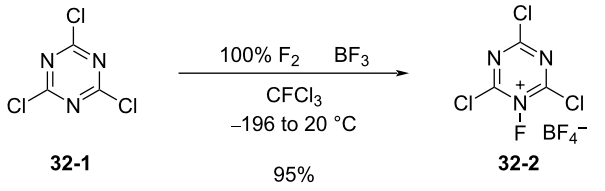

32-1 **32-2**

Scheme 72: Synthesis of *N*-fluoro salt **32-2**.

Reagent **32-2** reacted with deactivated benzenes such as chlorobenzene and nitrobenzene at ambient temperature (Scheme 73). This outcome indicated that **32-2** was a more powerful fluorinating reagent than the *N*-fluoropentachloropyridinium salts **5-4v**,**w**. However, reagent **32-2** is not easy-to-handle because of its moisture-sensitivity.

1-33. Bulky *N*-fluorobenzenesulfonimides (NFBSI)

In 2011, Shibata et al. reported a bulky NFSI analog, *N*-fluoro-(3,5-di-*tert*-butyl-4-methoxy)benzenesulfonimide (NFBSI, **33-3**) [102]. This stable and crystalline reagent was synthesized in 57% yield by fluorination of bis(3,5-di-*tert*-butyl-4-methoxybenzenesulfonyl)amide (**33-2**) with 10% F_2/N_2 in the presence of NaF in acetonitrile at −40 °C (Scheme 74). X-ray crystal structure analysis revealed that the fluorine atom of NFBSI was surrounded by four bulky *tert*-butyl substituents.

This feature improved the enantioselectivity in cinchona alkaloid-catalyzed enantioselective fluorinations. The enantiomeric excesses of the products obtained with NFBSI **33-3** increased by 18% compared to that of $(PhSO_2)_2NF$ (NFSI, **14-2**), while the chemical yields decreased (Scheme 75). Since the active fluorination agent in these reactions is considered to be the in situ generated *N*-fluorocinchona alkaloid salt, after fluorine transfer from NFBSI or NFSI to generate a counter anion, the bulky in situ generated counter anion may help enhance the % ee of the products.

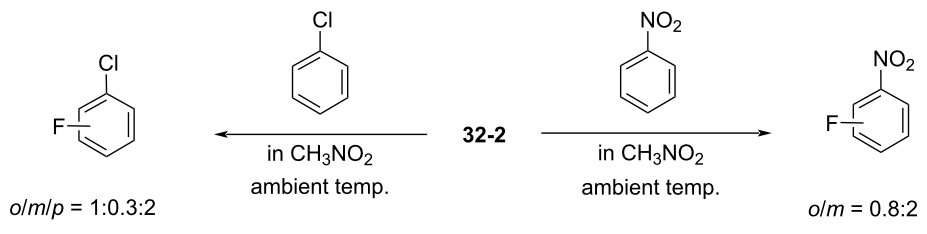

Scheme 73: Reactivity of *N*-fluorotriazinium salt **32-2**.

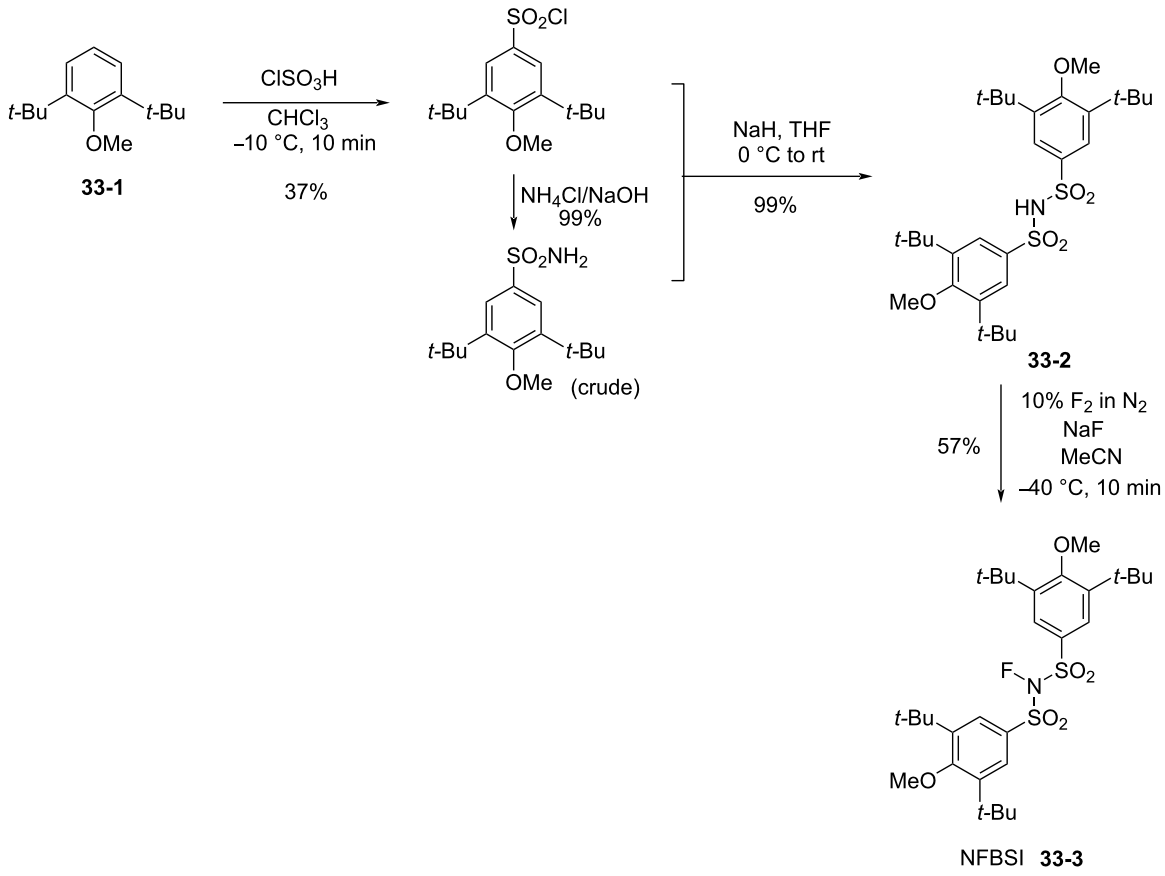

Scheme 74: Synthesis of bulky *N*-fluorobenzenesulfonimide NFBSI **33-3**.

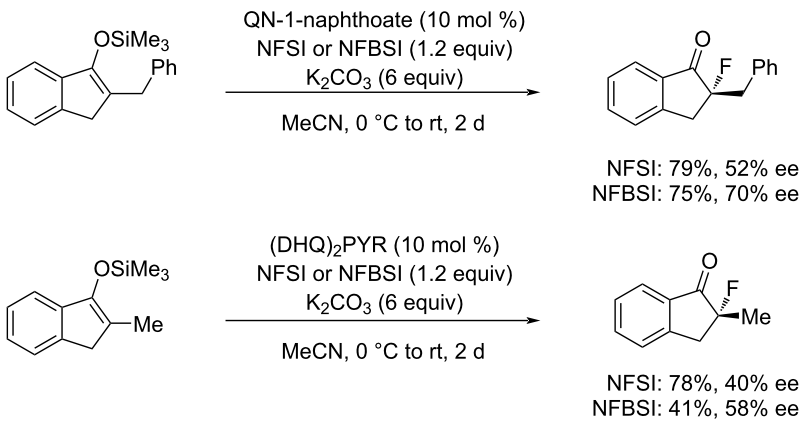

Scheme 75: Comparison of NFSI and NFBSI.

1-34. *p*-Substituted *N*-fluorobenzenesulfonimides

In 2012, Yang et al. reported an efficient process for the preparation of *p*-substituted *N*-fluorobenzenesulfonimides **34-3** [103]. The traditional process involved the direct fluorination of benzensulfonimides in acetonitrile in the presence of a large excess of NaF. They prepared the sodium salts **34-2** (precipitates) with 2% aq NaOH solution and treated the air-dried precipitates with 10% F_2/N_2 in acetonitrile (Scheme 76). This process considerably improved the yields of the *N*-fluorobenzenesulfonimides **34-3**.

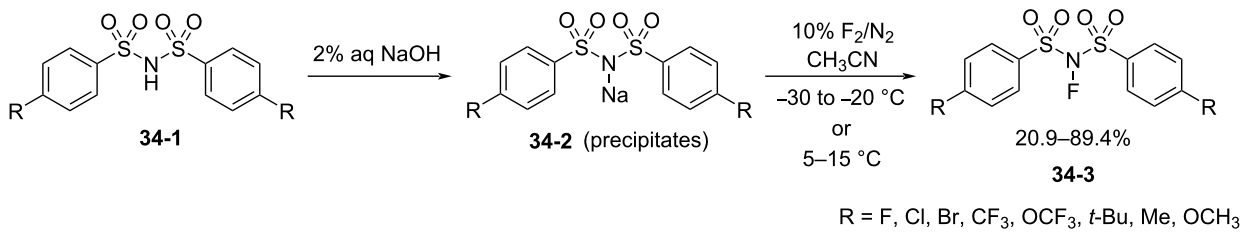

Scheme 76: Synthesis of *p*-substituted *N*-fluorobenzenesulfonimides **34-3**.

In 2013, the same group reported the enantioselective fluorination of oxindoles **34-5** with **34-3** in the presence of a catalytic amount of bis-cinchona alkaloid $(DHQD)_2PHAL$ **34-4** (Figure 11) [104]. In these reactions, the actual enantioselective fluorinating agents should be the *N*-F cinchona alkaloid salts formed in situ after the transfer from **34-3**. Electron-donating groups (R) afforded higher enantioselectivities compared to R = H (NFSI, **14-2**), while chemical yields were decreased. For example, while NFSI afforded 56% ee and 66% chemical yield (entry 1, Figure 11), R = OMe (**34-3a**) and *tert*-butyl (**34-3b**) gave 94% ee and 96% ee (entries 2 and 3 in Figure 11), but with only 49% and 17% chemical yields, respectively. Electron-withdrawing groups, R = CF_3 **34-3c** and OCF_3 **34-3d**, failed to furnish the fluorinated product under the same conditions (entries 8 and 9, Figure 11).

A year later (2014), the Yang group published the synthesis of other substituted NFSI derivatives and examined the enantioselective fluorination of 2-oxindoles catalyzed by chiral palladium complexes [105].

1-35. Two Selectfluor analogues, 1-fluoro-4-[3',4'-bis(trifluoromethyl)phenylmethyl]- and -(pentafluorophenyl)methyl-1,4-diazoniabicyclo[2.2.2]octane salts

In March 2013, Toste et al. reported the enantioselective 1,4-fluoroamination of conjugated dienes using Selectfluor in an anionic, phase-transfer catalysis in a nonpolar solvent [106]. Diene **35-1** was treated with Selectfluor and (*R*)-TCYP **35-3** as a catalyst to give **35-2** in 91% chemical yield and 96% ee (Scheme 77). In this case, the actual fluorinating species was considered to be the salt containing 1-chloromethy-4-fluoro-

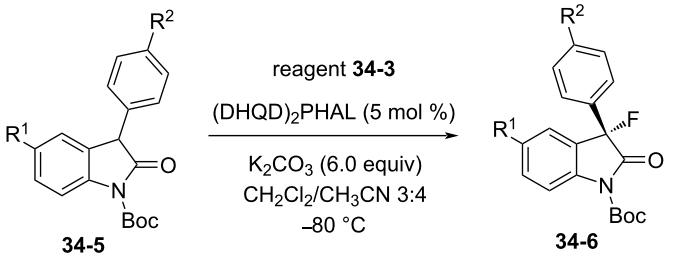

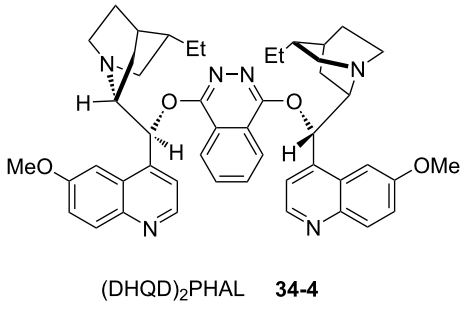

entry	substrate	reagent NFSI, **34-3a–d**		time	yield	ee
1	$R^1 = R^2 = H$	NFSI	R = H	48 h	66%	56%
2	$R^1 = R^2 = H$	**34-3a**	OMe	96 h	49%	94%
3	$R^1 = R^2 = H$	**34-3b**	*t*-Bu	96 h	17%	96%
4	$R^1 = R^2 = Me$	NFSI	H (NFSI)	36 h	99%	70%
5	$R^1 = R^2 = Me$	**34-3c**	F	36 h	98%	75%
6	$R^1 = R^2 = Me$	**34-3a**	OMe	96 h	57%	70%
7	$R^1 = R^2 = Me$	**34-3b**	*t*-Bu	96 h	40%	88%
8	$R^1 = R^2 = Me$	**34-3c**	CF_3	84 h	0%	–
9	$R^1 = R^2 = Me$	**34-3d**	OCF_3	72 h	0%	–

Figure 11: Asymmetric fluorination with **34-3** and a chiral catalyst **34-4**.

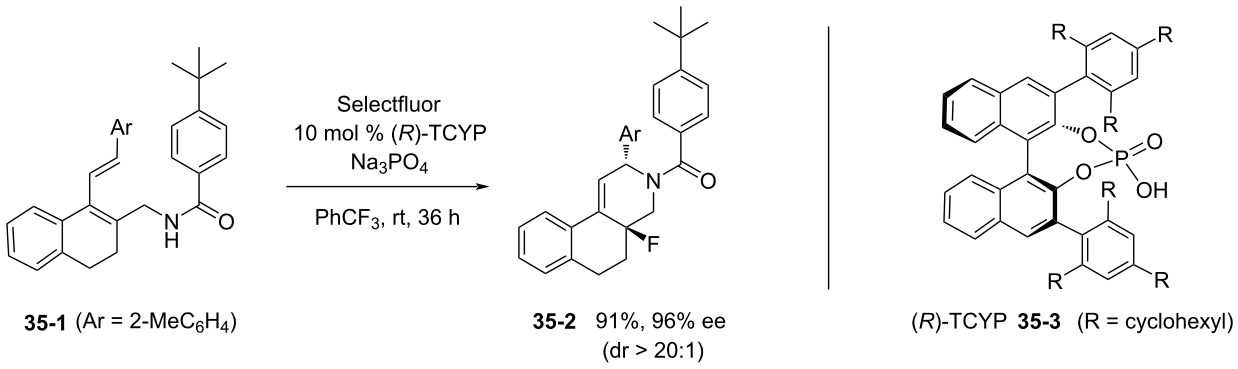

35-1 (Ar = 2-MeC$_6$H$_4$) **35-2** 91%, 96% ee (dr > 20:1) (*R*)-TCYP **35-3** (R = cyclohexyl)

Scheme 77: 1,4-Fluoroamination with Selecfluor and a chiral catalyst.

1,4-diazoniabicyclo[2.2.2]octane as the cation and (*R*)-TCYP as the anion, which could be formed in the non-polar organic layer.

However, since the reaction with the less reactive diene **35-6a** occurred in very low yield (<10%) (Figure 12, entry 1), they synthesized two new Selectfluor analogues, 1-fluoro-4-[3',4'-bis(trifluoromethyl)phenylmethyl]- and -(pentafluorophenyl)methyl-1,4-diazoniabicyclo[2.2.2]octane bistetrafluoroborates **35-5a** and **35-5b**, by treating the precursor **35-4** with XeF_2 in the presence of sodium tetrafluoroborate [106] (Scheme 78).

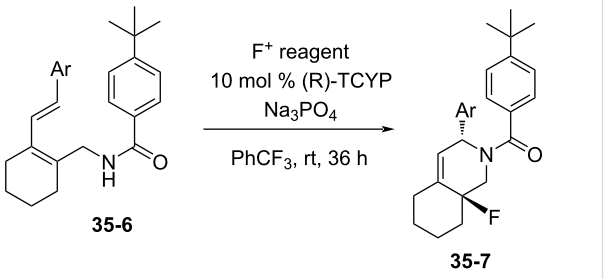

35-6 **35-7**

entry	F^+ reagent	product	Ar	yield (%)	ee (%)	dr
1	Selectfluor	**35-7a**	phenyl	<10	0	–
2	**35-5a**	**35-7a**	phenyl	70	76	14:1
3	**35-5b**	**35-7a**	phenyl	15	5	–
4	**35-5a**	**35-7b**	2-Me-phenyl	65	73	8.3:1
5	**35-5a**	**35-7c**	4-Me-phenyl	75	89	>20:1

Figure 12: Asymmetric fluoroamination with **35-5a**, **b**.

Reagent **35-5a** showed much improved chemical yields (65–75%) and enantioselectivities (73–89% ee) in fluorocyclization reactions with diene **35-6** (Figure 12, entries 2, 4, and 5) than reagent **35-5b**. Although there may be an electron-deficiency effect, this could also be attributed to the strong lipophilic effect of the bis(CF_3)phenyl group in **35-5a** to the organic layer ($PhCF_3$).

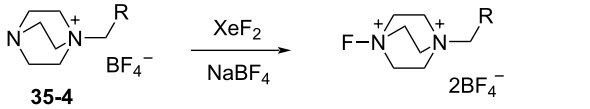

35-4

35-5a: R = 3,5-(CF$_3$)$_2$C$_6$H$_3$, 51%
35-5b: R = C$_6$F$_5$, 29%

Scheme 78: Synthesis of Selectfluor analogs **35-5a**, **b**.

1-36. Chiral dicationic DABCO-based *N*-F reagents

In June 2013, Gouverneur et al. reported the synthesis of chiral dicationic DABCO-based *N*-F reagents **36-5** that made possible the asymmetric electrophilic fluorocyclization of monoolefins with carbon nucleophiles [107]. This can be contrasted with Toste's method, described in section 1-35 above, for asymmetric fluorocyclization of dienes with nitrogen nucleophiles using Selectfluor and an optically active phase-transfer catalyst, a reaction which did not work for monoolefins with carbon nucleophiles.

As shown in Scheme 79, the chiral DABCO core **36-3** was prepared from an enantiopure vicinal diamine **36-1** using the reported method. The precursor **36-4** was fluorinated with either 10% F_2/N_2 or *N*-fluoropentachloropyridinium triflate (**5-1v**) to produce optically active products **36-5a**, **-5b**, and **-5c** in high yields. This fluorination which uses the shelf-stable, easy-to-handle *N*-fluoropentachloropyridinium triflate (**5-1v**) was advantageous as it allowed the in situ formation of the chiral reagents **36-5**.

The solubility, reactivity, and enantioselectivity of these types of reagents could be tuned by varying the substituents on the

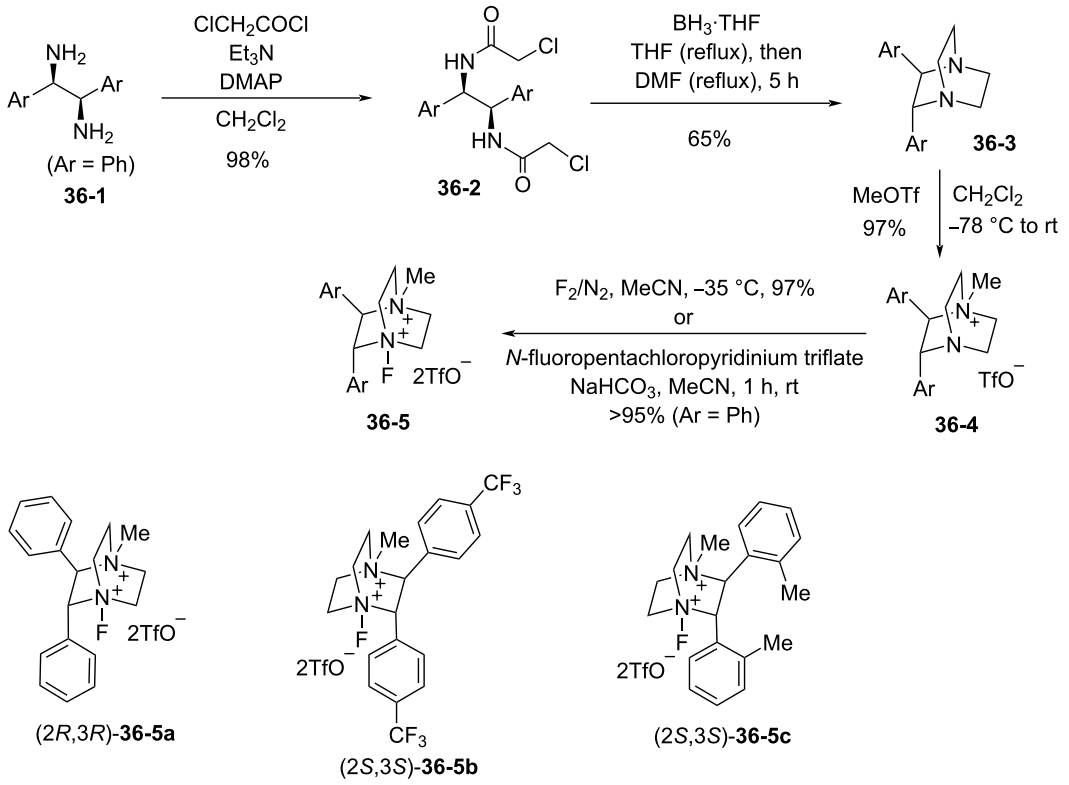

Scheme 79: Synthesis of chiral dicationic DABCO-based *N*-F reagents **36-5**.

aryl rings and the *p*-trifluoromethyl-derivative **36-5b** proved to be the most efficient for this type of reaction (Scheme 80). Up to 99% chemical yield and an average of 71% ee were obtained for a series of indene derivatives. However, the enantioselectivity was low (19% ee) for the case of a dihydronaphthalene derivative (the bottom in Scheme 80). Racemates of these fluoro products were prepared in high yields with *N*-fluoro-2,6-dichloropyridinium triflate (**5-1r**).

1-37. Chiral *N*-fluorobinaphthyldisulfonimides

In June 2013, the same month as the report described above from Gouverneur's lab, Shibata, Ma, and Cahard disclosed a chiral *N*-fluorobinaphthyldisulfonimide **37-2a** and its bis[3,5-bis(trifluoromethyl)phenyl] derivative **37-2b** as enantioselective fluorination agents, compounds which were prepared in 67% and 27% yields, respectively, by fluorination of the NH precursors **37-1** with 0.2% F_2/N_2 (Scheme 81) [108]. In both cases, side-products were formed but not characterized. The precursors **37-1** had been synthesized by List [109] and Giernoth [110] and previously used as organocatalysts.

The fluorination ability of **37-2a** and **-2b** was evaluated with β-keto ester derivatives (Scheme 82). Moderate yields and good enantioselectivities of the fluorinated products were obtained. Reagent **37-2b** clearly gave a better selectivity than the unsubstituted **37-2a** (86% ee vs 17% ee).

For an enantioselective synthesis of the potent Maxi-K potassium channel opener MaxPost **37-4** (R = H), the *N*-Boc-protected substrate **37-3** was fluorinated with **37-2b**, giving the precursor **37-4** (R = Boc) in 51% yield and with 57% ee (Scheme 83).

The oxidative aminofluorination of indene (**37-5**) with **37-2a** and **-2b** gave four diastereomers **37-6a** and **-6b** in 77 and 76% yield, respectively; however, no asymmetric induction was observed (Scheme 84).

1-38. *N*-Fluoromethanesulfonimide (Me-NFSI)

In 2016, Shibata et al. reported the synthesis and reactivity of *N*-fluoromethanesulfonimide (Me-NFSI, **38-2**) [111]. Me-NFSI was first reported in a patent in 1994 [112], however, the reported fluorinations were vague. Prior to Shibata's report, Me-NFSI had not appeared in the literature in over 20 years. Although Me-NFSI is vulnerable with acidic protons on the methyl groups, Shibata realized the high atom economy of Me-NFSI and claimed that Me-NFSI was more effective for the fluorination of active methines than $(PhSO_2)_2NF$ (NFSI, **14-2**)

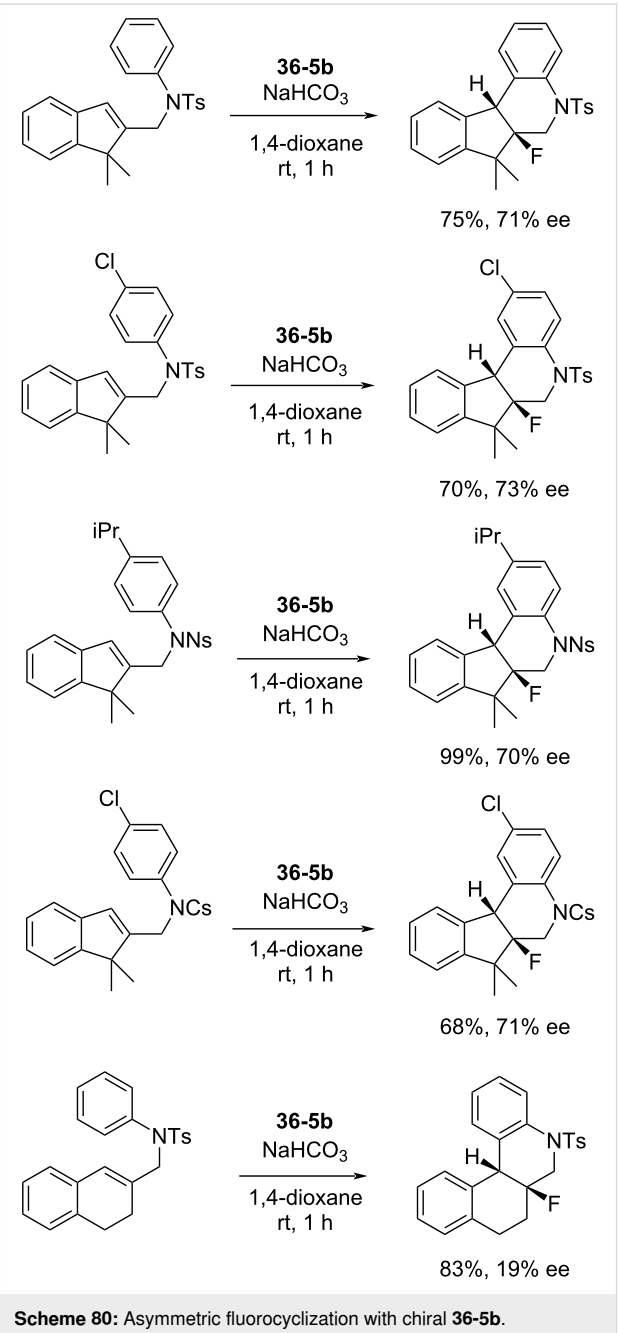

Scheme 80: Asymmetric fluorocyclization with chiral **36-5b**.

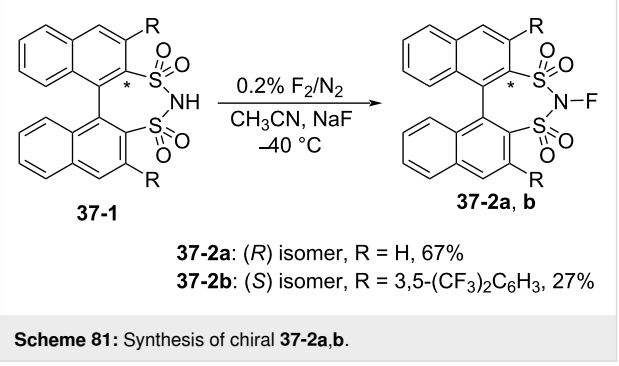

Scheme 81: Synthesis of chiral **37-2a**,**b**.

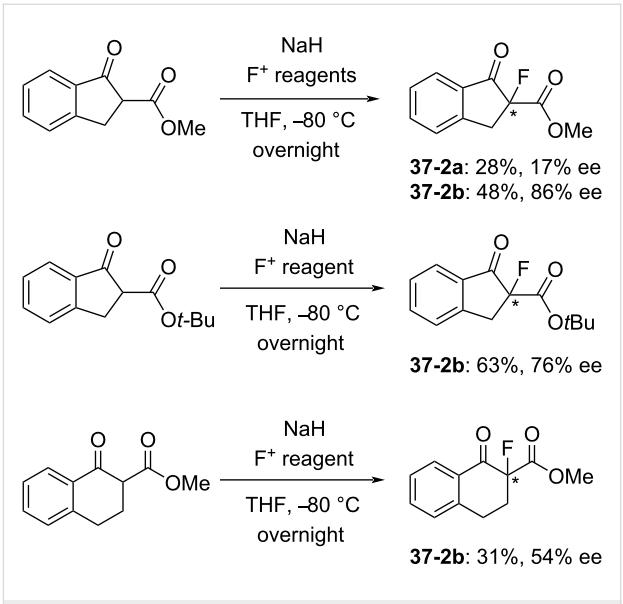

Scheme 82: Asymmetric fluorination with chiral **37-2a**,**b**.

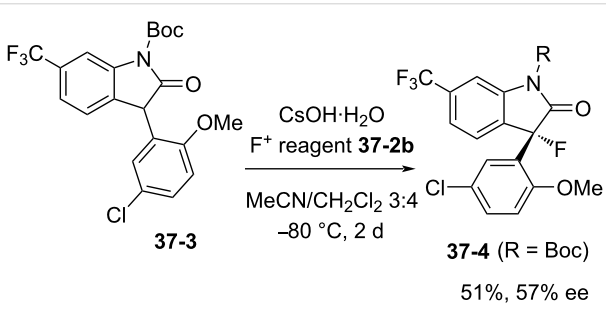

Scheme 83: Asymmetric fluorination with chiral **37-2b**.

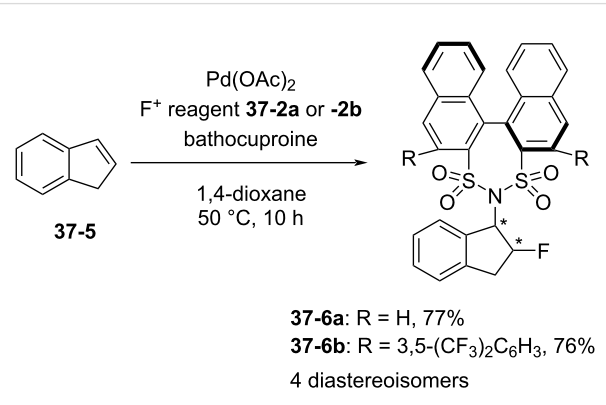

Scheme 84: Reaction of indene with chiral **37-2a**,**b**.

under Lewis acid-catalysis and non-catalysis. Me-NFSI was prepared in good yield by the fluorination of methanesulfonimide **38-1** with 10% F_2/N_2 in acetonitrile at −40 °C in the presence of NaF (Scheme 85).

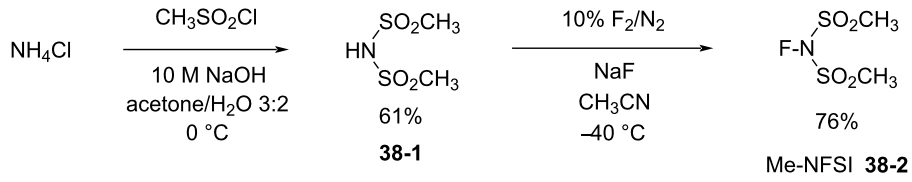

Scheme 85: Synthesis of Me-NFSI, **38-2**.

Many active methine compounds were fluorinated in high yields using Me-NFSI in the presence of 10 mol % $Ti(OiPr)_4$ in methylene chloride as a solvent at room temperature (Scheme 86). The reactions with Me-NFSI were faster than those with NFSI. In particular, the fluorination of sterically demanding *tert*-butyl keto ester **38-3b** with Me-NFSI gave the product **38-4b** in 90% yield within only 5 min (92% in 3 h), while NFSI gave the product in 20% yield after 10 min and the yield gradually increased to 80% over 24 h. The faster reaction of Me-NFSI was explained by the activation of its *N*-F moiety via the stronger complexation with the Lewis acid $Ti(OiPr)_4$ than NFSI.

For the fluorination of malonates, different conditions were needed. Treatment with 2 equiv of Me-NFSI in the presence of 20 mol % $Ti(OiPr)_4$ in toluene at reflux temperature gave the fluorinated malonates in satisfactory yields (Scheme 87).

Keto esters were fluorinated in high yields with Me-NFSI employing methanol or water as solvent under catalysis-free conditions (entries 1–3, Scheme 88).

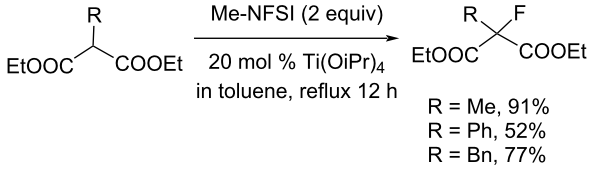

Scheme 87: Fluorination of malonates with Me-NFSI.

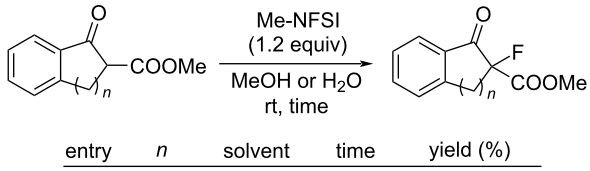

entry	*n*	solvent	time	yield (%)
1	1	MeOH	1 h	96
2	1	H_2O	4 h	96 (by GC)
3	2	MeOH	24 h	91
4	3	MeOH	24 h	35

Scheme 88: Fluorination of keto esters with Me-NFSI.

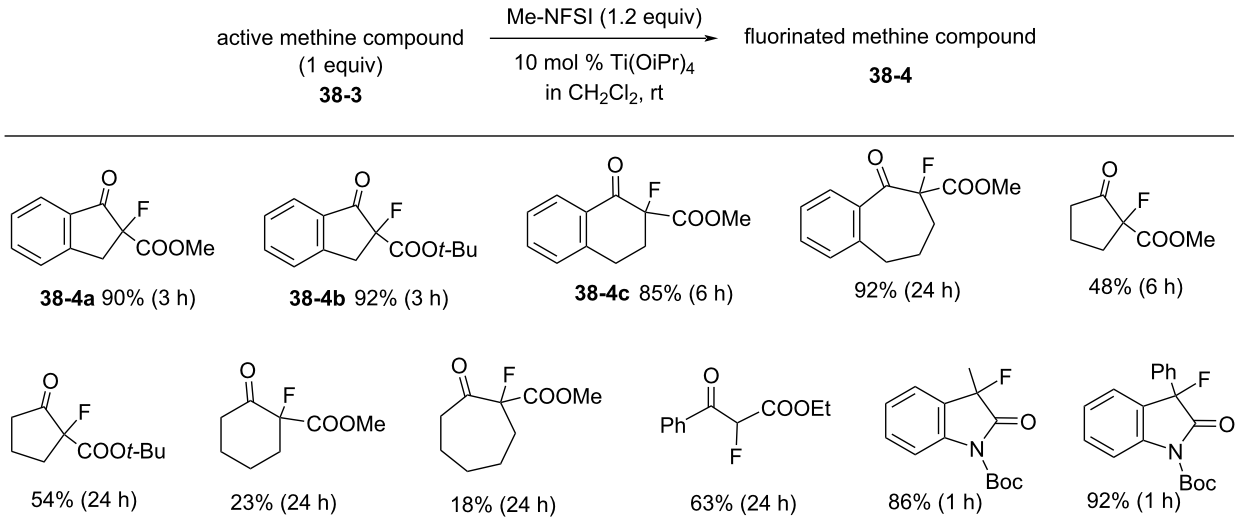

Scheme 86: Fluorination of active methine compounds with Me-NFSI.

1-39. An *N*–F reagent derived from the ethano-Tröger's base

In 2016, Gouverneur and Cvengroš reported the synthesis of a novel *N*-F reagent **39-3** derived from the ethylene-bridged Tröger's base **39-1** [113]. The fluorination of the precursor **39-2,** obtained from **39-1,** was achieved only after reaction with *N*-fluoropentachloropyridinium triflate (**5-1v**) in acetonitrile at −35 °C, giving the *N*-F reagent **39-3** in higher than 95% conversion (Scheme 89). All other attempts to fluorinate, either with F_2, XeF_2, Selectfluor, or *N*-fluoro-2,6-dichloropyridinium triflate (**5-1r**) failed. This suggested that reagent **39-3** was more reactive than the other known reagents such as Selectfluor, but less active than the *N*-fluoropentachloropyridinium salts. The salt **39-3** is not stable and decomposition occurred when a solution of **39-3** in acetonitrile was left standing at room temperature for 8 hours or more. Therefore, **39-3** was best prepared with **5-1v** immediately before use. The characterization of **39-3** was made by high-resolution mass spectrometry and NMR spectroscopic analyses containing 2D ^{19}F-^{15}N heteronuclear correlation experiments.

Reagent **39-3** had the ability to formally transfer F^+ onto the Selectfluor precursor **39-4** to form a Selectfluor analog **39-5** (Scheme 90). The fluorine transfer of **39-3** to the precursor **39-4** was completed after 5 min at room temperature in acetonitrile.

The ability of **39-3** to fluorinate *C*-substrates was investigated. The fluorination of benzene, anisole, and fluorobenzene with **39-3** occurred faster than with Selectfluor (Scheme 91). The fluorination of styrenes **39-10** provided the expected addition products **39-11**–**14** in good yields. However, **39-3** did not react with less-activated alkenes, such as cyclohexene.

1-40. 1-Cyanomethyl-4-fluoro-1,4-diazoniabicyclo[2.2.2]octane bistriflate

In early 2018, Lan and Liu reported the synthesis of 1-cyanomethyl-4-fluoro-1,4-diazoniabicyclo[2.2.2]octane bistriflate (Selectfluor^{CN}) employing the same method as for Selectfluor (Scheme 92) [114].

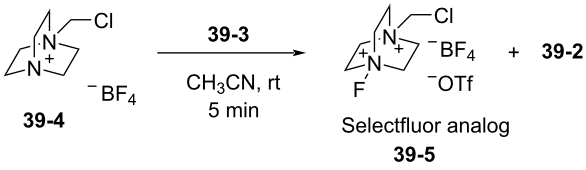

Scheme 90: Fluorine transfer from *N*-F **39-3**.

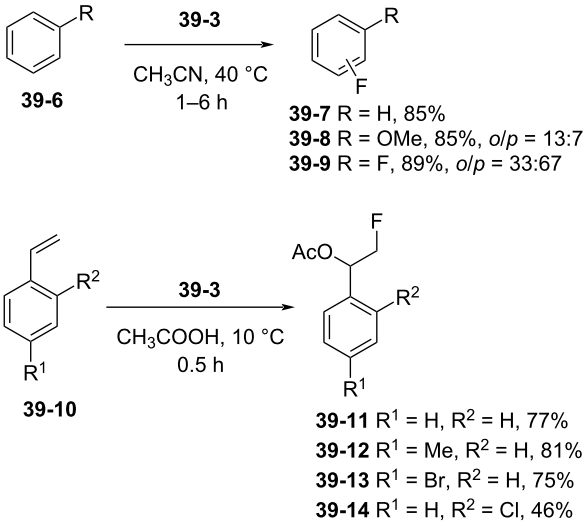

Scheme 91: Fluorination with *N*-F **39-3**.

As shown in Scheme 93, Selectfluor^{CN} was used as an oxidant to improve the Pd-catalyzed bistrifluoromethoxylation of alkenes with $AgOCF_3$. It was shown that the yield of the bis(CF_3O) product **40-4** increased as the fluorinating power of the *N*-F reagent increased in the order of NFSI < **16-3** (R = Me) < Selectfluor (R = CH_2Cl) < Selectfluor^{CN} (R = CH_2CN). A considerable number of olefin derivatives were bistrifluoromethoxylated using this method with Selectfluor^{CN} [114].

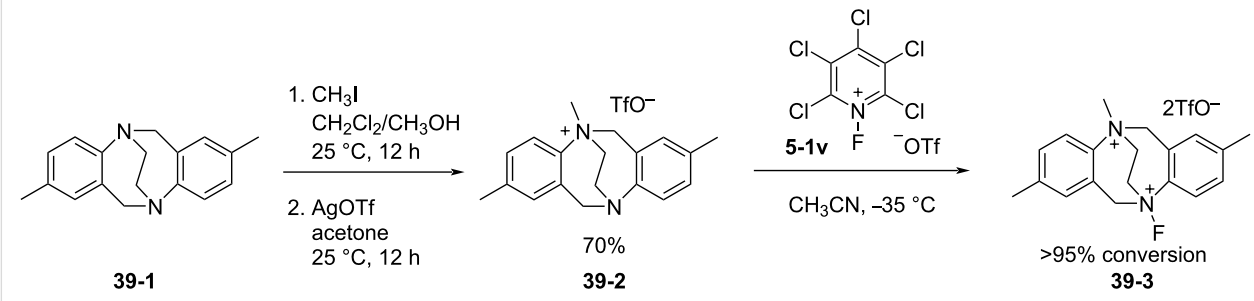

Scheme 89: Synthesis of *N*-F **39-3** derived from the ethylene-bridged Tröger's base.

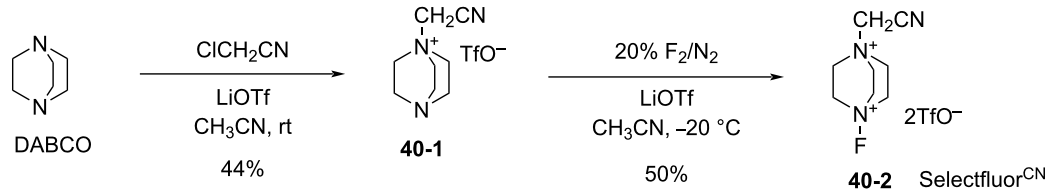

Scheme 92: Synthesis of Selectfluor^{CN}.

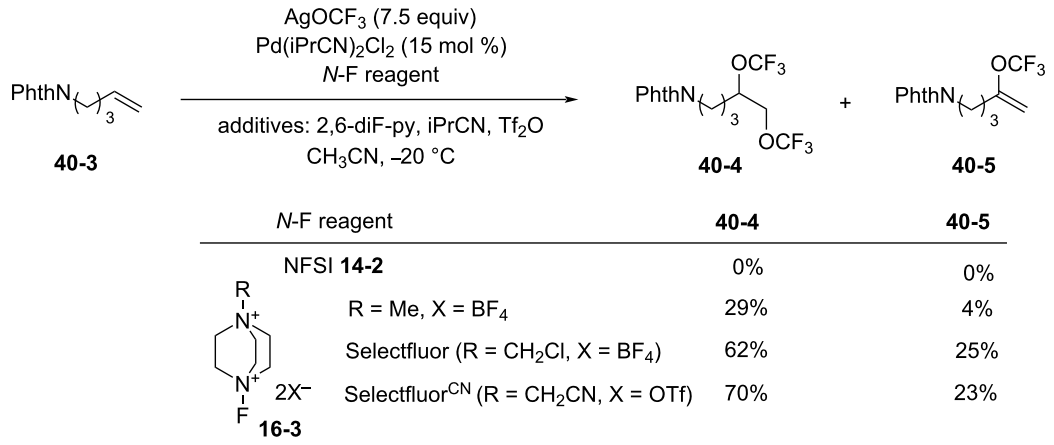

Scheme 93: Bistrifluoromethoxylation of alkenes using Selectfluor^{CN}.

1-41. *N*-Fluoro-*N*-aryl-arenesulfonamides (NFAS)

In 2018, Zipse and Renaud reported the synthesis of a series of *N*-fluoro-*N*-aryl-arenesulfonamides (NFAS) **41-2** suitable for radical fluorination, by reacting **41-1** with NFSI in the presence of cesium carbonate in methylene chloride and in moderate to good yields (Figure 13) [115]. They suggested that NFAS belongs to a third generation of radical fluorinating agents.

These authors designed NFAS **41-2a–i** as having a low *N*-F homolytic bond-dissociation energy (BDE). They demonstrated experimentally that NFAS **41-2** were more useful for radical fluorinations than *N*-fluoro-*N*-alkyl-arenesulfonamides **4-1**, *N*-fluoro-*N*-alkyl-arylamides, NFSI **14-2**, and Selectfluor, all of which have higher N–F homolytic BDEs than NFAS **41-2** (Scheme 94).

The hydrofluorinated products were obtained in moderate yields along with good stereoselectivities in some cases (Scheme 95).

As for the less nucleophilic terminal alkenes, remote fluorinated products were favored via the 1,5 H-atom abstraction process (Scheme 96).

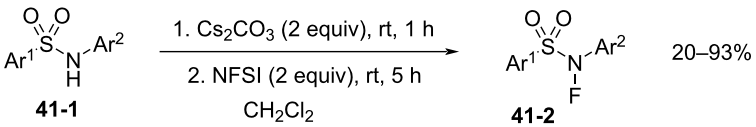

	Ar^1	Ar^2	yield (%)		Ar^1	Ar^2	yield (%)
41-2a	phenyl	4-CF_3-phenyl	80	**41-2f**	2,4,6-triMe-phenyl	4-CF_3-phenyl	89
-2b	phenyl	3,5-diCF_3-phenyl	93	**-2g**	2,4,6-tri-iPr-phenyl	4-CF_3-phenyl	72
-2c	phenyl	3,5-diF-phenyl	20	**-2h**	4-MeO-2,6-diMe-phenyl	4-CF_3-phenyl	53
-2d	4-Cl-phenyl	4-CF_3-phenyl	42	**-2i**	2,4,6-triMe-phenyl	3-CF_3-phenyl	40
-2e	4-MeO-phenyl	4-CF_3-phenyl	87				

Figure 13: Synthesis of NFAS **41-2**.

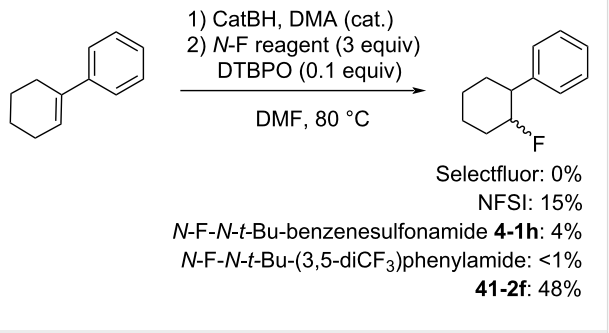

Scheme 94: Radical fluorination with different *N*-F reagents.

Decarboxylative fluorination of *tert*-butyl peresters also proved that these NFAS (**41-2a** and **-2f**) were better choices than NFSI and Selectfluor (Scheme 97).

2. Evaluation of fluorinating power of *N*-F fluorinating agents

It emerges from the overview above that many *N*-F fluorination reagent variants have been developed, each with a different fluorination power (reactivity). Therefore, the power ordering of *N*-F reagents has become a matter of interest. Early on, Umemoto et al. revealed that the fluorinating power of *N*-fluoropyridinium salt systems could be tuned by the electron density at the nitrogen site, a property which is controlled by the electronic nature of the substituents. In order to quantitatively explain the variability of the *N*-F reagents, many attempts have been made: Theoretical calculations were performed by Hachisuka and Umemoto in 1991 [116,117], Woolf in 1994 [118], and Fainzil'berg in 1994 and 2001 [119,120]; N-F 19-fluorine NMR chemical shift analysis was accessed by Umemoto in 1991 [34]; measurements of peak reduction potentials were carried out by Gilicinski in 1992 [121], Differding in 1992 [122], Evans in 1999 [123], Zhang in 2013 [104], and reported by Umemoto in 2016 [124]; relative fluorination rates (kinetic data) were conducted by Togni in 2004 [125], and electromotive forces with Li, Mg, and Zn metals were reported by Umemoto in 2016 [124].

In a significant advancement in this regard, in 2016 Xue and Cheng published a comprehensive energetic scale for the quantitative estimation of the fluorinating power of *N*-F reagents [126,127]. They applied the Fluorine Plus Detachment (FPD) energy parameter, introduced by Christe and Dixon in 1992 [128], to electrophilic *N*-F reagents and calculated the FPD energies of 130 *N*-F reagents (Scheme 98).

As seen in Figure 14, a large number of *N*-F reagents were clearly arranged in their power order; the smaller the FPD value

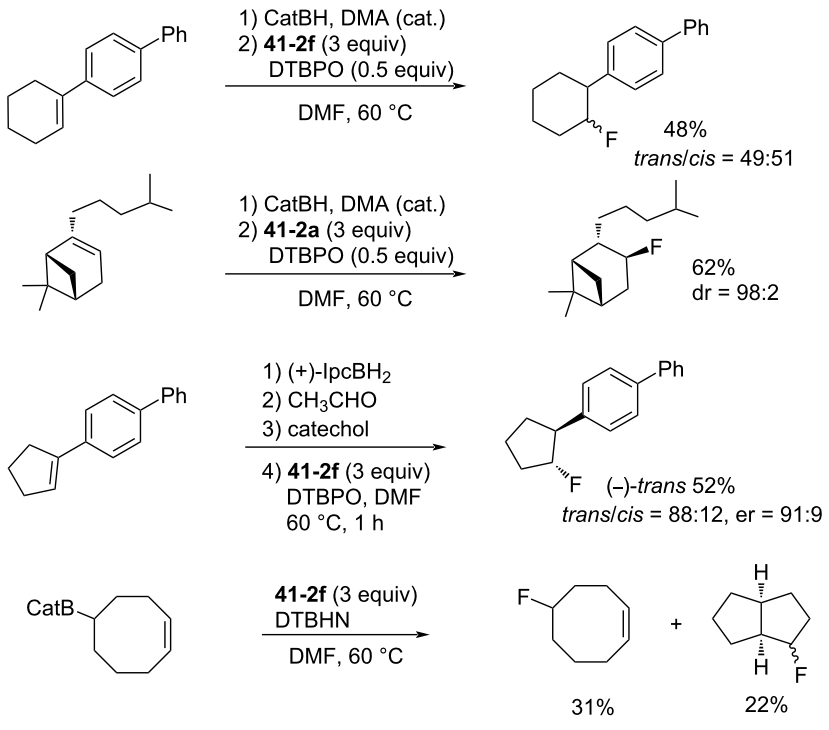

Scheme 95: Radical fluorination of alkenes with NFAS **41-2**.

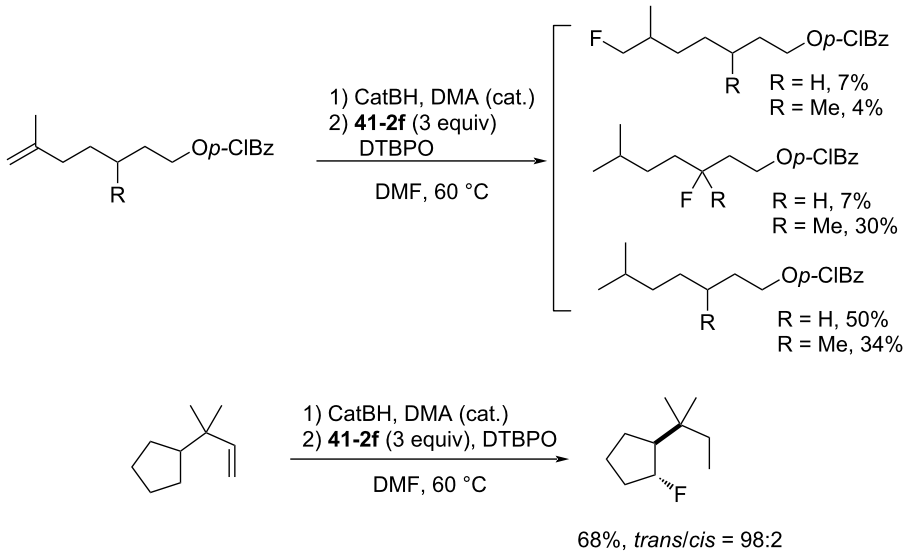

Scheme 96: Radical fluorination of alkenes with NFAS **41-2f**.

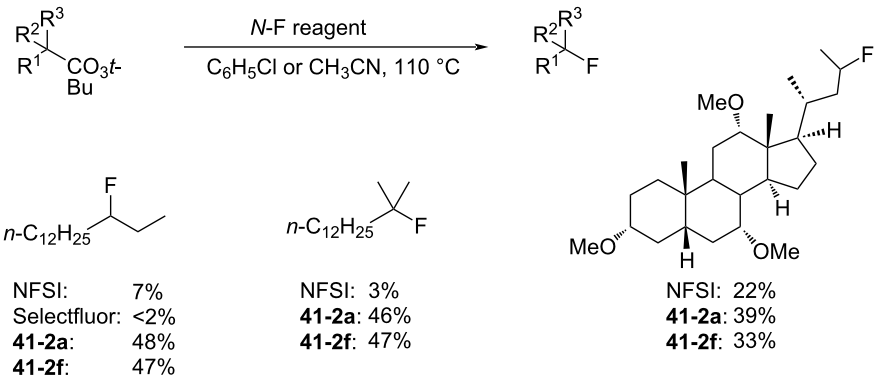

Scheme 97: Decarboxylative fluorination with NFAS **41-2a**,**f**.

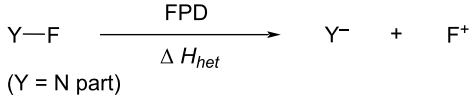

Scheme 98: Fluorine plus detachment (FPD).

the stronger the fluorinating power. This energetic scale is useful for an evaluation of the electrophilic fluorinating power of the *N*-F reagents.

In addition, since some *N*-F reagents have been proven to be useful radical fluorinating agents [129-135], Xue and Cheng introduced the *N*-F homolytic bond-dissociation energy (BDE) parameter for radical fluorination abilities of *N*-F reagents in 2017 (Scheme 99) [127,136]. They calculated the BDE strength of 88 *N*-F reagents and clearly arranged them in terms of their radical fluorination power; the smaller the BDE value the stronger the radical fluorinating power (Figure 15). The BDE is useful for identifying and designing new atomic fluorine sources.

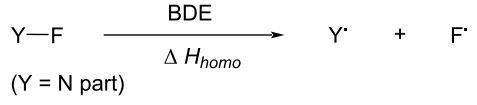

Scheme 99: *N*-F homolytic bond dissociation energy (BDE).

In 2018, another significant advancement was reported. Since FPD and BDE are thermodynamic parameters, they cannot be

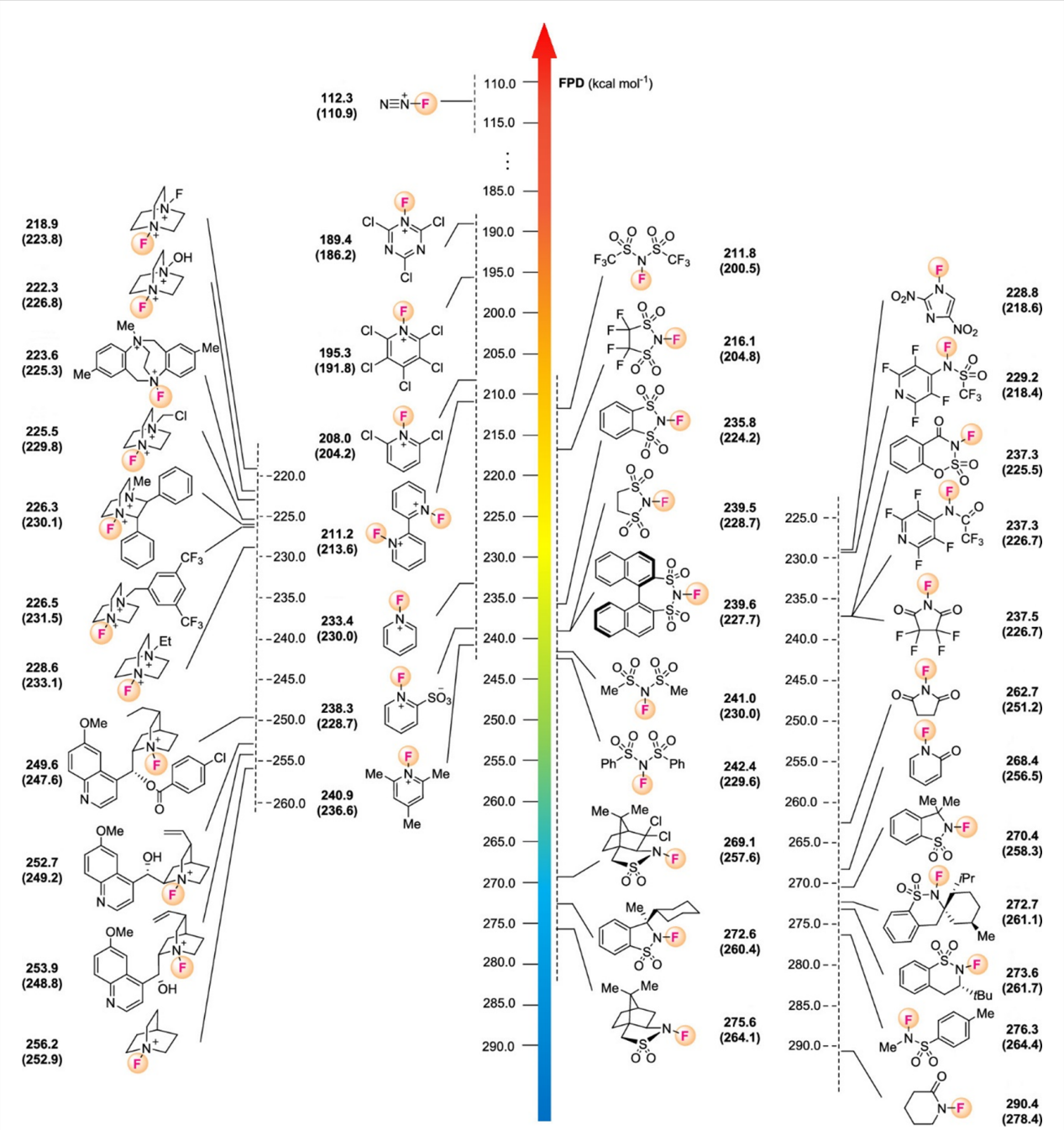

Figure 14: FPD values of representative *N*-F reagents in CH_2Cl_2 and CH_3CN (in parentheses). Adapted with permission from ref. [127]. Copyright 2020 American Chemical Society.

directly used for predicting reaction rates. Mayr et al. [137] and Hodgson et al. [138] independently reported the quantitative reactivity scales for electrophilic fluorinations of popular *N*-F reagents. They provided detailed kinetic fluorination studies of a series of popular *N*-F fluorinating agents such as *N*-fluoropyridinium salt derivatives, NFSI, and Selectfluor™ with enamines, carbanions, or 1,3-diketones. Figure 16 shows the relative reactivity scale of the popular *N*-F reagents, which covers eight orders of magnitude. These reactivity scales can be used for predicting the actual fluorination rates of *N*-F fluorinating agents. Hodgson et al. further advanced their kinetic studies with *N*-F fluorinating agents in 2019 [139] and 2020 [140].

In 2019, Zhang et al. reported detailed theoretical calculations of the fluorination of benzene with 16 different disubstituted *N*-fluoropyridinium salts in acetonitrile solution and as a result,

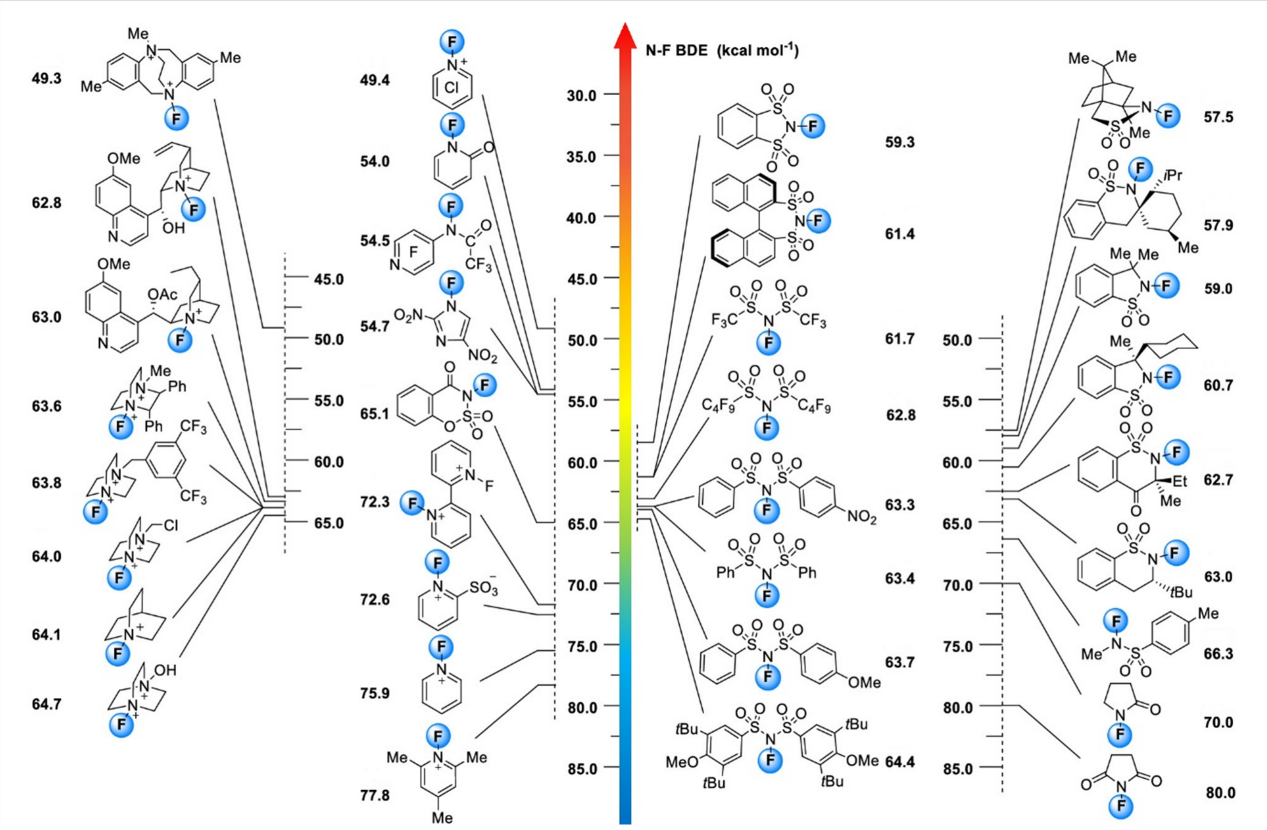

Figure 15: BDE values of representative *N*-F reagents in CH_3CN. Adapted with permission from ref. [127]. Copyright 2020 American Chemical Society.

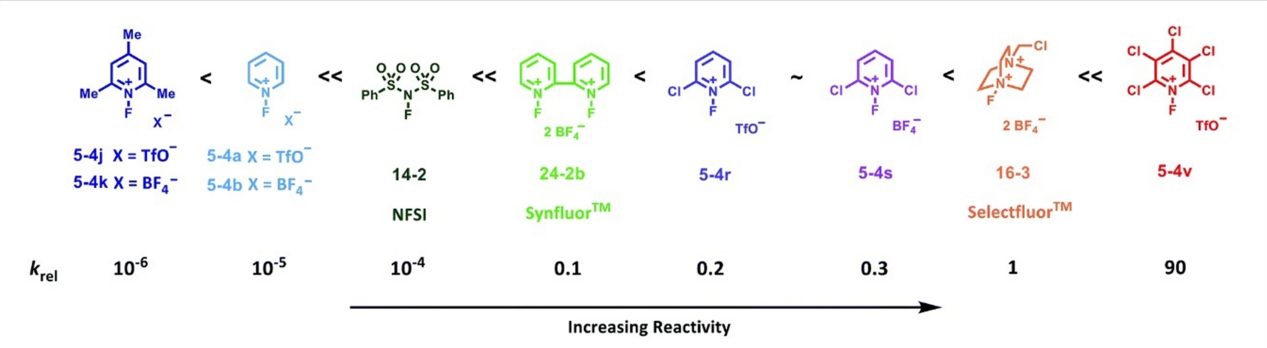

Figure 16: Quantitative reactivity scale for popular *N*-F reagents. Adapted with permission from ref. [138], published by the Royal Society of Chemistry.

suggested a 2,6-dinitro-substituted *N*-fluoropyridinium salt as the most promising fluorinating reagent [141].

3. Reaction mechanisms of *N*-F fluorinating agents

Another noteworthy issue is the reaction mechanism for the fluorination with *N*-F reagents. There have been long standing arguments regarding which mechanism is operating in these fluorinations: a single-electron transfer (SET) or a nucleophilic substitution (S_N2) mechanism (Scheme 100) [22,142]. In the SET process, a single-electron transfer from a substrate (Nu^-) to a *N*-F reagent [N-F] occurs to form a radical anion $[N\text{-}F]^{\bullet-}$ and a $Nu^{\bullet}$ radical, and the former undertakes the homolytic N–F bond cleavage to give a $F^{\bullet}$ radical and a $N:^-$ anion, and then the $F^{\bullet}$ radical and the $Nu^{\bullet}$ radical combine to generate the final product Nu–F. In the S_N2 mechanism, a nucleophile directly attacks the F atom of the *N*-F reagent to give the fluorinated product via the heterolytic cleavage of the N–F bond. The key point is

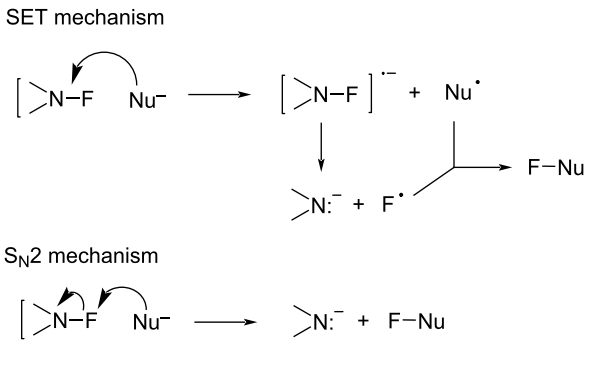

Scheme 100: SET and S_N2 mechanisms.

whether the N–F bond cleaves homolytically or heterolytically. The prime cause of this argument is based on the fact that the formation of F^+ requires extremely high energy (ionization potential of F, 1681.0 kJ/mol) and contrasts significantly with that of other halogenations (Cl, 1251.2 kJ/mol; Br, 1139.9 kJ/mol).

In 1991, Umemoto et al. explained the observed fluorination reactions of *N*-fluoropyridinium salts with anionic and neutral substrates by SET processes involving a F• radical species [32]. Soon after, in 1992, Kochi et al. reported fluorination reactions of aromatic compounds with *N*-fluoropyridinium salts via electron donor–acceptor complexes, with outcomes which also supported the SET mechanism [143,144]. In 1992, DesMarteau et al. proposed a similar SET process for the fluorination with *N*-fluoroperfluoroalkanesulfonimide [48]. On the other hand, in 1991, Differding and co-worker investigated radical clock experiments to monitor the reaction for the presence of intermediate radicals [145] (Scheme 101).

As illustrated in Scheme 102, the reactions of potassium enolate **I** of citronellic ester with the *N*-F reagents **10-1**, **14-2** (NFSI), or

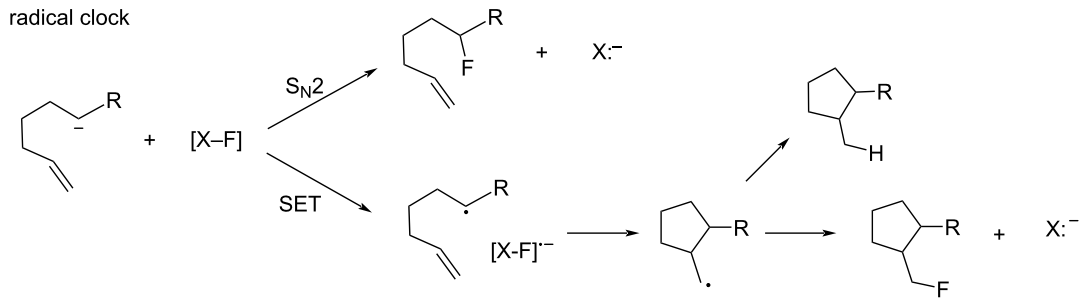

Scheme 101: Radical clock reactions.

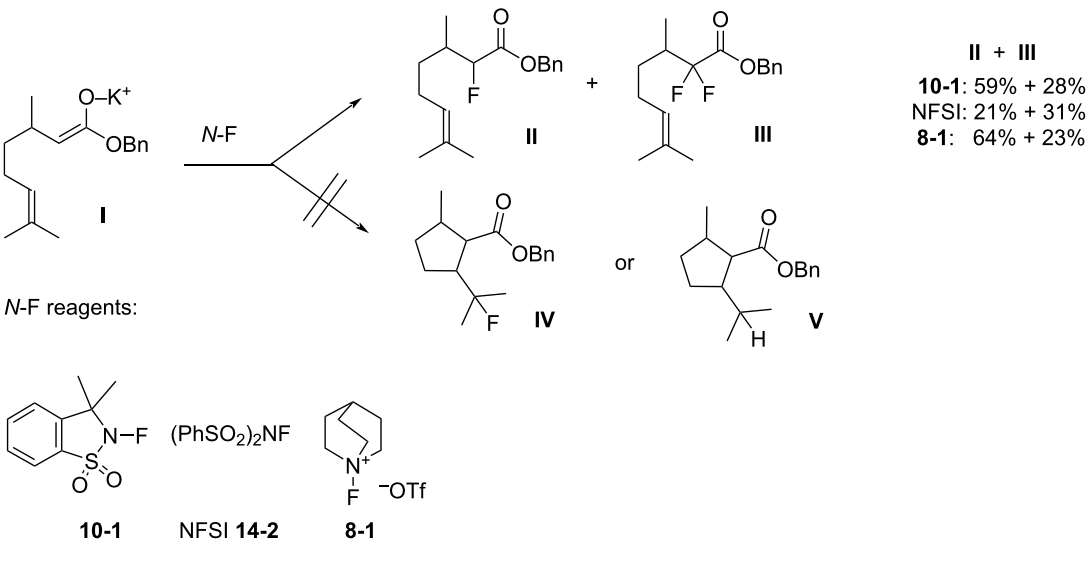

Scheme 102: Reaction of potassium enolate of citronellic ester with *N*-F reagents, **10-1**, NFSI, and **8-1**.

8-1 produced only the non-cyclized products **II** and **III**. They also showed that the observed reaction rates were much faster than the calculated electron-transfer rates and therefore they concluded that a S_N2 mechanism occurred to give the fluorinated products [146].

In 1995, based on the study on the fluorination reactions of the *N*-F reagent NFOBS **13-2**, Davis et al. described that all of their available data supported the S_N2 reaction process, but the SET mechanism could not be rigorously excluded [58]. In 1998, Zupan et al. studied the reactions of norbornene with Selectfluor, NFTh **19-2**, and *N*-fluoro-2,6-dichloropyridinium triflate [147]. Although their results ended toward S_N2, they too could not completely exclude the SET. Soon after, in 1999, Wong et al. reported their studies using compound **VI** having a phenylcyclopropyl moiety which was the hypersensitive radical probe (rate: 10^{11} s^{-1}) (Scheme 103) [148].

They found that Selectfluor (OTf salt) produced product **VII** in 45% yield with no rearrangement products despite the complete consumption of **VI** (entry 1, Scheme 103). This result is aligned with the S_N2 mechanism, however, the reaction of **VI** with Selecfluor was completely blocked by the radical scavenger, 2,2,6,6-tetramethylpiperidinoxyl (TEMPO), which suggested a SET mechanism. The reaction of **VI** with NFSI gave **VII** (40%) and a product **IX** (5%) derived from the rearrangement fluoro product **VIII** (entry 2 in Scheme 103). This result is consistent with the SET mechanism. In their review published in 2005 [149], Wong discussed these results in more detail. Since the reactivity of the radical ($F^{\cdot}$) is extremely fast and diffusion-controlled, the combination of $F^{\cdot}$ with any alkyl radical $R^{\cdot}$ should proceed at an equal or greater rate than the cyclization of the alkyl radical as observed in the case of Differding [145] and the ring-opening of the cyclopropyl radical in the case of Wong [148]. Despite extensive research, the mechanism remains unclear as a result of the difficulty of assessing reaction rates. The key may be the lifetime of the intermediate N-F radical or radical anion, $[N\text{-}F]^{\cdot}$ or $[N\text{-}F]^{\cdot-}$, which releases the radical $F^{\cdot}$. Finally, Wong mentioned that, if these radicals react faster than the rates of diffusion, anything beyond that would probably remain unproven [149].

In the meantime, in 2002, Togni and Rothlisberger provided evidence which strongly supported the SET mechanism from their studies on the fluorination mechanism of β-ketoesters with Selectfluor and a chiral $TiCl_2$(TADDOLato) catalyst [150]. Their computational study suggested a one-electron transfer followed by simultaneous N–F bond cleavage and the accompanying experimental outcomes demonstrated that a chlorination side reaction was quenched by a radical scavenger, while the fluorination reaction was unaffected. Since Selectfluor is inert towards chloride, they proposed that any $[N\text{-}F]^{\bullet}$ radical formed by the SET process would react with chloride ions (Cl^-) present in the reaction solution to form the relatively stable $Cl^{\bullet}$ radical, which caused the side chlorination.

On the other hand, in 2002, Laali and co-worker reported that competitive fluorination studies of mesitylene and durene with

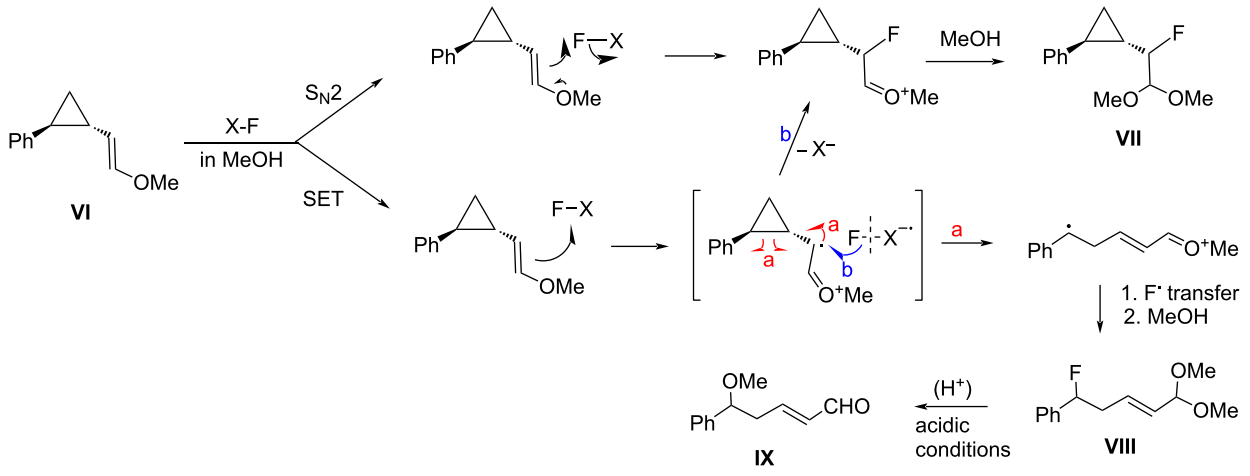

entry	X–F	nucleophile	product	mechanism type
1	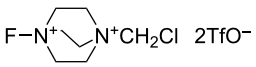	MeOH	**VII** (45%)	S_N2/SET
2	$(PhSO_2)_2N$-F (NFSI)	MeOH	**VII** (40%) + **IX** (5%)	SET

Scheme 103: Reaction of compound **IV** with Selectfluor (OTf) and NFSI.

Selecfluor in CH_3CN and an ionic liquid supported the conventional polar mechanism (S_N2) [151]. However, in 2006, Stavber et al. made similar competition studies and proposed a SET process as the dominant mechanism that explained the higher reactivity of durene viz-à-viz mesitylene towards Selectfluor in aq CH_3CN [152]. In 2009, Shubin et al. performed competitive studies of mesitylene and durene with NFSI under solvent-free reaction conditions and reported that the reaction rate ratio (k_{Mes}/k_{Dur}) followed a polar mechanism [153].

Since 2015, many papers supporting either SET or S_N2 mechanisms have appeared, including those reported by C. Liu et al. (SET) in 2015 [154], Chen et al. (S_N2) in 2016 [155], Tang et al. (SET) in 2016 [156], F. Liu et al. (SET) in 2016 [157] and 2017 [158], Mayr et al. (S_N2) in 2018 [137], Hodgson et al. (S_N2) in 2018 [138], Li et al. (SET) in 2018 [159], Shi et al. (SET) in 2018 [160], Li et al. (SET) in 2019 [161], Mernyak et al. (SET) in 2019 [162], and Nelson et al. (S_N2) in 2019 [163].

TEMPO has been often used as a radical scavenger to explore the reaction mechanisms of *N*-F fluorinating agents but, in Nelson's paper [163] in 2019, it was revealed that Selectfluor reacted with TEMPO (**X**) to form the oxoammonium salt **XI** (Scheme 104). This author concluded that the use of TEMPO as a radical trap in the reactions with Selectfluor was unreliable. This conclusion was subsequently confirmed by Borodkin et al. [164]. The latest review [165] by Hodgson and co-worker in 2021 discussed the reactivities and reaction mechanisms of electrophilic *N*-F fluorinating agents in detail.

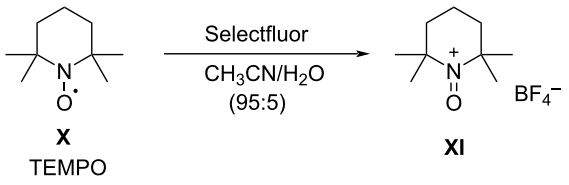

Scheme 104: Reaction of TEMPO with Selecfluor.

Conclusion

A historical timeline on the progress of *N*-F fluorinating reagents and their fluorinations has been described in this review. Table 1 shows a historical list of all the *N*-F reagents. The fluorination power and reaction mechanism of the *N*-F fluorinating agents have also been summarized briefly and from a historical perspective. The fluorination reactions described here for each *N*-F fluorinating agent are those reported at the time. The synthetic applications of each *N*-F reagent since then are too numerous to be covered in this review. As many reviews on the reactions and applications of the *N*-F fluorinating agents have been published [39,133,142,165-181], readers are recommended to consult these reviews.

The seminal work of perfluoro-*N*-fluoropiperidine by Banks was reported in 1964 [16]. However, this compound could not be contemplated for two decades because of the very low yields in its production and fluorination reactions. At that time, $FClO_3$ [10] and *O*-F reagents such as CF_3OF and $CF_2(OF)_2$ [11] were used as electrophilic fluorinating agents despite their inherent safety issues. The real attention on *N*-F compounds started in the 1980's when the first report on a *N*-F fluorinating agent, *N*-fluoro-2-pyridone, was published by Purrington in 1983 [24]. The next year, Barnette reported *N*-fluoro-*N*-alkylarenesulfonamides that were easy-to-handle, stable crystalline compounds useful for the fluorination of carbanions [26]. Soon after (1986), Umemoto reported a series of *N*-fluoropyridinium triflates as easy-to-handle, reactive, and widely applicable reagents [28,29].

Since then, many *N*-F fluorinating agents have been reported, one after another, as follows: powerful *N*-fluorotrifluoromethanesulfonimide by DesMarteau in 1987 [45], mild *N*-fluorosultams including first chiral *N*-fluorosultams by Lang in 1988 [52] and 1989 [53], less reactive *N*-fluorolactams by Sathyamurthy in 1990 [55], moderate *N*-fluoro-*o*-benzenedisulfonimide (NFOBS) [57] and *N*-fluorobenzenesulfonimide (NFSI) [59] by Davis and Differding, respectively, in 1991, and powerful 1-chloromethyl-4-fluoro-1,4-diazoniabicyclo[2.2.2]octane bistetrafluoroborate (Selectfluor™) by Banks in 1992 [42]. Currently popular *N*-F fluorinating agents such as *N*-fluoropyridinium salts, NFSI, and Selectfluor were developed within a decade from the first Purrington's report (1983).

After this first rush, other notable *N*-F reagents were developed such as a series of zwitterionic *N*-fluoropyridinium salts by Umemoto in 1995 [76], another Selectfluor-type reagent, 1-fluoro-4-hydroxy-1,4-diazoniabicyclo[2.2.2]octane bistetrafluoroborate (NFTh/Accufluor™) by Poss and Shia in 1995 [78], a more powerful reagent, 1,4-difluoro-1,4-diazoniabicyclo[2.2.2]octane bistetrafluoroborate by Umemoto in 1996 [83], and a powerful and high fluorine-content reagent, *N*,*N*'-difluoro-2,2'-bipyridinium bistetrafluoroborate (Synfluor™) by Umemoto in 1998 [86].

In 2000, practical chiral reagents, *N*-fluorinated chiral cinchona alkaloids were reported by Shibata and Takeuchi [95] and by Cahard [97]. In 2003, Cahard demonstrated that the chiral *N*-fluorocinchona alkaloids could be prepared quantitatively with not only Selectfluor but also with other powerful *N*-F fluorinating agents such as NFTh, NFSI, and *N*-fluoro-2,6-

Table 1: Chronological list of the development of *N*-F fluorinating agents.

year	structure	"F" source	yield	references
1964	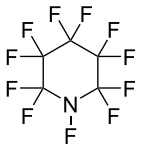	HF	7.5–13%	[16-22]
1981	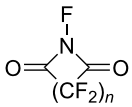 n = 2, 3	XeF_2	50–65%	[23]
1983	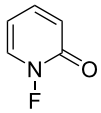	5% F_2/N_2	63%	[24,25]
1984	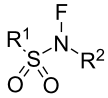 R^1 = *p*-tolyl, *n*-butyl; R^2 = methyl, *tert*-butyl, exo/endo-2-norbornyl, cyclohexyl, neopentyl	1–5% F_2/N_2	11–71%	[26,27]
1986–1991	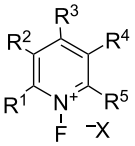 X = OTf, BF_4, PF_6, AsF_6, SbF_6, ONf, OMs, etc. R^1, R^2, R^3, R^4, R^5 = H, Me, Cl, F, COOMe, OMe, CH_2OMe, CH_2OAc, CF_3, CN, NO_2, OMenth, etc.; (total 62 examples)	10% F_2/N_2	15–96%	[28-34,36-41]
1986	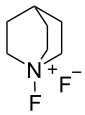 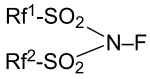	100% F_2	86%	[43,44]
1987	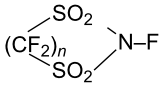 n = 2, 3, 4 $Rf^{1,2}$ = CF_3, C_4F_9, C_6F_{13}	100% F_2	61–96%	[45-49]
1988	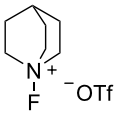	100% F_2	80–88%	[50,51]
1988	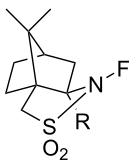 R = H, CH_3	10% F_2/N_2	75–80%	[52]

Table 1: Chronological list of the development of *N*-F fluorinating agents. (continued)

1989	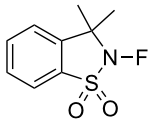	10% F_2/N_2	74%	[53]
1990	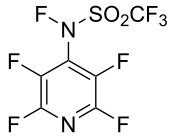	100% F_2	89%	[54]
1990	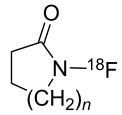 *n* = 1–5	0.05% $^{18}F_2$/Ne	33–79%	[55,56]
1991	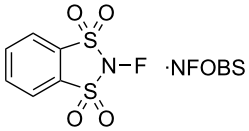 ·NFOBS	10% F_2/N_2	>90%	[57,58]
1991	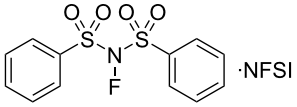 ·NFSI	10% F_2/N_2	70%	[59]
1991	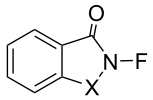 X = SO_2, CO	$Cs^{+-}OSO_2OF$	48–69%	[60]
1992	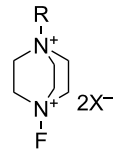 X = OTf, BF_4 R = CH_3, CH_2Cl, CH_2CF_3 Selectfluor™ (R = CH_2Cl, X = BF_4)	10% F_2/N_2	87–95%	[42,61-74]
1993	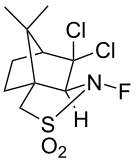	10% F_2/N_2	68%	[75]
1995	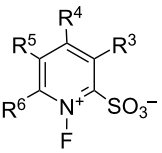 R^3, R^4, R^5, R^6 = H, CH_3, CF_3, Cl, C_2H_5, *tert*-butyl	10% F_2/N_2	65–95%	[76]
1995	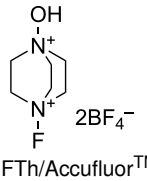 NFTh/Accufluor™	10% F_2/N_2	75%	[78-80]

Table 1: Chronological list of the development of *N*-F fluorinating agents. (continued)

1995	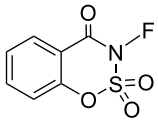	5% F_2/N_2	83%	[81]
1996	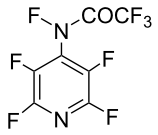	100% F_2	75%	[82]
1996	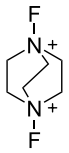 $(X^1)^-(X^2)^-$ X^1, X^2 = OTf, BF_4, HSO_4, SbF_6, PF_6, etc.	10% F_2/N_2	56–87%	[83]
1997	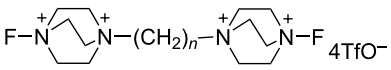 *n* = 2, 3	10% F_2/N_2	62–82%	[85]
	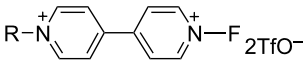 R = BF_3, F, CH_3			
1997	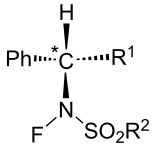 R^1 = CH_3, CH_2OCOCH_3 R^2 = CH_3, *p*-tolyl	$FClO_3$	13–52%	[92]
1998	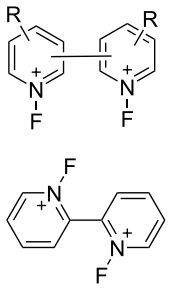 $2BF_4^-$ Synfluor™ X = OTf, BF_4, PF_6, SbF_6 bipyridyl = 2,2', 2,4', 3,3', 4,4'; R = H, CH_3, Cl, CF_3, Ph, $COOCH_3$	10-20% F_2/N_2	64–97%	[86]
1998	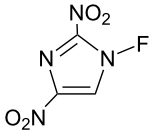	5% F_2/N_2	–	[87,88]
1999	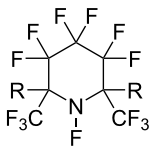 R = CH_3, CF_3	10% F_2/N_2	65–82%	[89]

Table 1: Chronological list of the development of *N*-F fluorinating agents. (continued)

1999	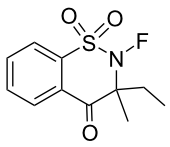	$FClO_3$	71%	[90]
1999	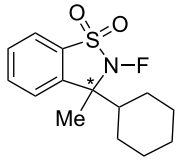 (*R*)-(+) (*S*)-(–)	15% F_2/He	51–65%	[91]
2000	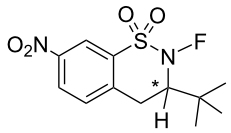 (*R*), (*S*)	$FClO_3$	66–83%	[93]
2000	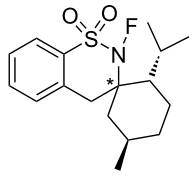 (*S*,*R*,*R*), (*S*,*S*,*R*)	$FClO_3$	44–81%	[94]
2000	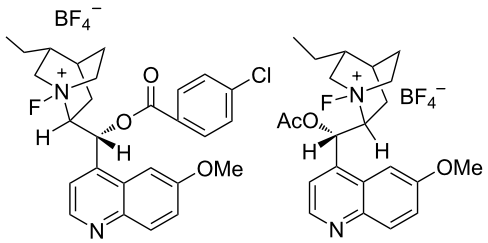	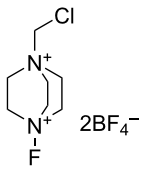 Selectfluor™	prepared in situ	[95,96]
2000	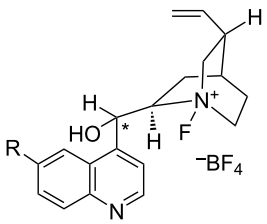 R = H, OCH_3	Selectfluor™	84%	[97,98]
2003	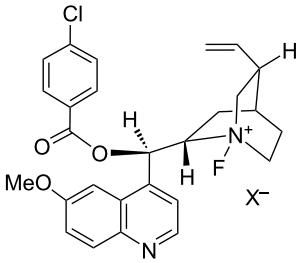 X = BF_4, OTf, $N(SO_2Ph)_2$	Selectfluor (F-TEDA-BF_4) F-TEDA-OTf NFTh NFSI *N*-F-diCl-pyridinium BF_4	100%	[99]

Table 1: Chronological list of the development of *N*-F fluorinating agents. (continued)

2003	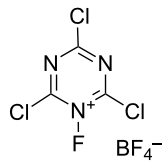	100% F_2	95%	[100]
2011	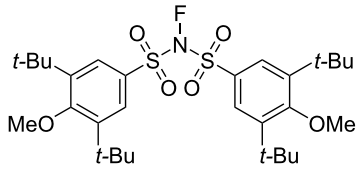 NFBSI	10% F_2/N_2	57%	[102]
2012	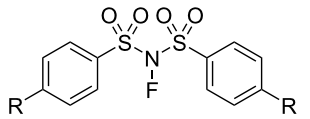 R = F, Cl, Br, CF_3, OCF_3, *t*-Bu, Me, OCH_3	10% F_2/N_2	20.9–89.4%	[103-105]
2013	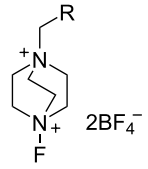 R = 3,5-$(CF_3)_2C_6H_3$, C_6F_5	XeF_2	29–51%	[106]
2013	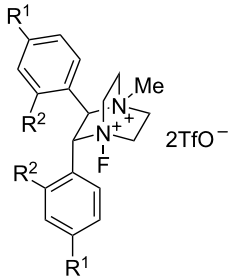 R^1 = H, CF_3; R^2 = H, CH_3	10% F_2/N_2 or 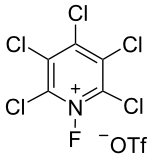	>95%	[107]
2013	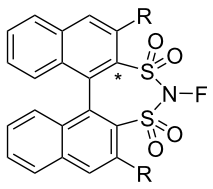 (*R*), R = H; (*S*), R = 3,5-$(CF_3)_2C_6H_3$	0.2% F_2/N_2	27–67%	[108]
2016	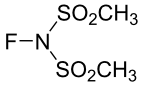 Me-NFSI	10% F_2/N_2	76%	[111]
2016	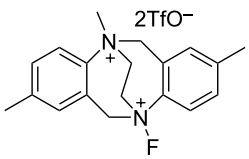	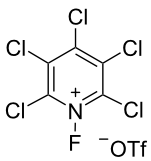	>95% conversion	[113]

Table 1: Chronological list of the development of *N*-F fluorinating agents. (continued)

2018	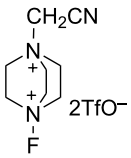	20% F_2/N_2	50%	[114]
2018	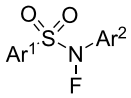 Ar^1 = C_6H_5, 4-Cl-C_6H_4, 2,4,6-triMe-C_6H_2, etc.; Ar^2 = 4-CF_3-C_6H_4, 3-CF_3-C_6H_4, 3,5-di$CF_3C_6H_3$	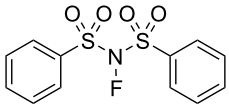 NFSI	20–93%	[115]

dichloropyridinium tetrafluoroborate [99]. After a break of a decade, in 2013, chiral dicationic DABCO-based *N*-F reagents **36-5** and chiral *N*-fluorobinaphthyldisulfonimides **37-2** were reported by Gouverneur [107] and by Shibata, Ma, and Cahard [108], respectively. In 2016, Shibata reported *N*-fluoromethanesulfonimide (Me-NFSI) as a high atom-economy reagent [111] and Gouverneur and Cvingroš reported a novel *N*-F reagent **39-3** derived from the ethylene-bridged Tröger base [113]. More recently, Zipse and Renaud in 2018, disclosed *N*-fluoro-*N*-aryl-arenesulfonamides (NFAS) as radical fluorinating agents [115].

A very large number of *N*-F fluorinating agents have been developed so far and a considerable number of easy-to-handle *N*-F reagents have been commercialized. In particular, Selectfluor, NFSI, and *N*-fluoropyridinium salt derivatives are produced in factories on a large scale. This has greatly contributed to the remarkable advancement of organofluorine chemistry. Before the appearance of *N*-F reagents, electrophilic fluorinating agents were thought dangerous and difficult to handle and special techniques were required. Chemists avoided them. Now, practicing chemists use them without any problem. The *N*-F reagents have brought such a dramatic change that many chemists nowadays may not realize the magnitude of this change and the contributions of the pioneers.

For practitioners in the field, high thermal stability and non-hygroscopicity of reagents are key factors for easy handling and a long shelf life. Many *N*-F reagents satisfy this requirement, however, there are limitations as the fluorinating power increases. *N*-Fluoropentachloropyridinium triflate (**5-4v**) and tetrafluoroborate (**5-4w**) rank as the most powerful of the non-hygroscopic and thermally stable *N*-F agents. However, the more powerful *N*-fluoro-2,4,6-trichloro-1,3,5-triazinium tetrafluoroborate (**31-2**) is moisture-sensitive and not easy-to-handle. *N,N'*-Difluoro-1,4-diazoniabicyclo[2.2.2]octane bistetrafluoroborate (**22-1d)** ranks top in the easy-to-handle 1,4-diazoniabicyclo[2.2.]octane salt series. Salt **22-1d** is more powerful than Selectfluor. Unfortunately, synthetic chemists have had little chance to use it because it has not been commercialized due to patent issues despite its simple one-pot process using cheap materials. However, since all the patents have now expired, it is expected that **22-1d** may soon be commercialized.

It is now rare for researchers and laboratories to use molecular fluorine (F_2) in universities and institutes, because of strict safety regulations, although 20% or 10% F_2 diluted with N_2 can be handled without significant problems. As a result, currently reported fluorination reactions have been limited to the use of a few commercially available and inexpensive *N*-F reagents such as Selectfluor and NFSI. As mentioned in this review, there are many other useful *N*-F fluorinating agents and the plentiful supply will satisfy the strong demand for fluorinations. That said, there is still room for improvement or refinement. The authors think that further research and development on *N*-F fluorinating reagents is needed for the advancement of synthetic fluorine chemistry but, for this to happen, it would be highly desirable to develop a safe and convenient F_2 generator.

Funding

We are grateful to the National Institutes of Health (R01GM121660) for financial support.

ORCID® iDs

Teruo Umemoto - https://orcid.org/0000-0002-8718-8127
Gerald B. Hammond - https://orcid.org/0000-0002-9814-5536

References

1. Ojima, I., Ed. *Fluorine in Medicinal Chemistry and Chemical Biology;* John Wiley & Sons, Ltd: Chichester, United Kingdom, 2009. doi:10.1002/9781444312096
See for a selected book.
2. Jeschke, P. *ChemBioChem* **2004,** *5,* 570–589. doi:10.1002/cbic.200300833

3. Berger, R.; Resnati, G.; Metrangolo, P.; Weber, E.; Hulliger, J. *Chem. Soc. Rev.* **2011,** *40,* 3496–3508. doi:10.1039/c0cs00221f
4. Inoue, M.; Sumii, Y.; Shibata, N. *ACS Omega* **2020,** *5,* 10633–10640. doi:10.1021/acsomega.0c00830
5. Mei, H.; Remete, A. M.; Zou, Y.; Moriwaki, H.; Fustero, S.; Kiss, L.; Soloshonok, V. A.; Han, J. *Chin. Chem. Lett.* **2020,** *31,* 2401–2413. doi:10.1016/j.cclet.2020.03.050
6. Ogawa, Y.; Tokunaga, E.; Kobayashi, O.; Hirai, K.; Shibata, N. *iScience* **2020,** *23,* 101467. doi:10.1016/j.isci.2020.101467
7. Uneyama, K., Ed. *Organofluorine Chemistry;* Blackwell Publishing: Oxford, United Kingdom, 2006. doi:10.1002/9780470988589
8. Ramachandran, P. V. *Future Med. Chem.* **2009,** *1,* 771–772. doi:10.4155/fmc.09.67
9. Harper, D. B.; O'Hagan, D. *Nat. Prod. Rep.* **1994,** *11,* 123–133. doi:10.1039/np9941100123
10. Schlosser, M.; Heinz, G. *Chem. Ber.* **1969,** *102,* 1944–1953. doi:10.1002/cber.19691020620
11. Barton, D. H. R. *Pure Appl. Chem.* **1977,** *49,* 1241–1249. doi:10.1351/pac197749091241
12. Appelman, E. H.; Basile, L. J.; Thompson, R. C. *J. Am. Chem. Soc.* **1979,** *101,* 3384–3385. doi:10.1021/ja00506a046
13. Rozen, S.; Lerman, O. *J. Am. Chem. Soc.* **1979,** *101,* 2782–2784. doi:10.1021/ja00504a073
14. Rozen, S.; Lerman, O.; Kol, M.; Hebel, D. *J. Org. Chem.* **1985,** *50,* 4753–4758. doi:10.1021/jo00224a019
15. Filler, R. *Isr. J. Chem.* **1978,** *17,* 71–79. doi:10.1002/ijch.197800010
16. Banks, R. E.; Williamson, G. E. *Chem. Ind. (London)* **1964,** 1864–1865.
17. Banks, R. E.; Cheng, W. M.; Haszeldine, R. N. *J. Chem. Soc.* **1962,** 3407–3416. doi:10.1039/jr9620003407
18. Banks, R. E.; Ginsberg, A. E.; Haszeldine, R. N. *J. Chem. Soc.* **1961,** 1740–1743. doi:10.1039/jr9610001740
19. Banks, R. E.; Haszeldine, R. N.; Hatton, R. *Tetrahedron Lett.* **1967,** *8,* 3993–3996. doi:10.1016/s0040-4039(01)89722-7
20. Polishchuk, V. R.; German, L. S. *Tetrahedron Lett.* **1972,** *13,* 5169–5172. doi:10.1016/s0040-4039(01)85198-4
21. Banks, R. E.; Tsiliopoulos, E. *J. Fluorine Chem.* **1986,** *34,* 281–285. doi:10.1016/s0022-1139(00)85081-2
22. Banks, R. E.; Murtagh, V.; Tsiliopoulos, E. *J. Fluorine Chem.* **1991,** *52,* 389–401. doi:10.1016/s0022-1139(00)80353-x
23. Yagupols'kii, Y. L.; Savina, T. I. *J. Org. Chem. USSR* **1981,** *17,* 1180–1181.
24. Purrington, S. T.; Jones, W. A. *J. Org. Chem.* **1983,** *48,* 761–762. doi:10.1021/jo00153a037
25. Purrington, S. T.; Jones, W. A. *J. Fluorine Chem.* **1984,** *26,* 43–46. doi:10.1016/s0022-1139(00)85117-9
26. Barnette, W. E. *J. Am. Chem. Soc.* **1984,** *106,* 452–454. doi:10.1021/ja00314a050
27. Lee, S. H.; Schwartz, J. *J. Am. Chem. Soc.* **1986,** *108,* 2445–2447. doi:10.1021/ja00269a052
28. Umemoto, T.; Tomita, K. *Tetrahedron Lett.* **1986,** *27,* 3271–3274. doi:10.1016/s0040-4039(00)84772-3
29. Umemoto, T.; Kawada, K.; Tomita, K. *Tetrahedron Lett.* **1986,** *27,* 4465–4468. doi:10.1016/s0040-4039(00)84980-1
30. Umemoto, T.; Tomizawa, G. *Bull. Chem. Soc. Jpn.* **1986,** *59,* 3625–3629. doi:10.1246/bcsj.59.3625
31. Umemoto, T.; Tomita, K.; Kawada, K. *Org. Synth.* **1990,** *69,* 129–140. doi:10.15227/orgsyn.069.0129
32. Umemoto, T.; Fukami, S.; Tomizawa, G.; Harasawa, K.; Kawada, K.; Tomita, K. *J. Am. Chem. Soc.* **1990,** *112,* 8563–8575. doi:10.1021/ja00179a047
33. Umemoto, T.; Harasawa, K.; Tomizawa, G.; Kawada, K.; Tomita, K. *Bull. Chem. Soc. Jpn.* **1991,** *64,* 1081–1092. doi:10.1246/bcsj.64.1081
34. Umemoto, T.; Harasawa, K.; Tomizawa, G.; Kawada, K.; Tomita, K. *J. Fluorine Chem.* **1991,** *53,* 369–377. doi:10.1016/s0022-1139(00)80960-4
35. Meinert, H. *Z. Chem.* **1965,** *5,* 64. doi:10.1002/zfch.19650050208
36. Umemoto, T.; Tomita, K. *N*-Fluoropyridinium salt-containing polymer. *Jpn. Kokai Tokkyo Koho* S63-295610, Dec 2, 1988.
37. Nukui, K.; Kamiya, K. Production method of *N*-fluoropyridinium salts. Jpn. Patent 3038065, May 8, 2000.
38. Fukami, S.; Nukui, K.; Kawada, K. Production method of *N*-fluoropyridinium tetrafluoroborate. *Jpn. Kokai Tokkyo Koho* H09-255657, Sept 30, 1997.
39. Kawada, K. *N-Fluoropyridinium Salt Fluorination for Preparing Aryl Fluorides*. In *Fluorination;* Hu, J.; Umemoto, T., Eds.; Springer: Singapore, 2020. doi:10.1007/978-981-10-1855-8_40-2
40. Naruta, Y.; Tani, F.; Maruyama, K. *Tetrahedron Lett.* **1992,** *33,* 1069–1072. doi:10.1016/s0040-4039(00)91863-x
41. Poss, A. J.; Van der Puy, M.; Nalewajek, D.; Shia, G. A.; Wagner, W. J.; Frenette, R. L. *J. Org. Chem.* **1991,** *56,* 5962–5964. doi:10.1021/jo00020a051
42. Banks, R. E.; Mohialdin-Khaffaf, S. N.; Lal, G. S.; Sharif, I.; Syvret, R. G. *J. Chem. Soc., Chem. Commun.* **1992,** 595–596. doi:10.1039/c39920000595
43. Banks, R. E.; Du Boisson, R. A.; Tsiliopoulos, E. *J. Fluorine Chem.* **1986,** *32,* 461–466. doi:10.1016/s0022-1139(00)81953-3
44. Banks, R. E.; Du Boisson, R. A.; Morton, W. D.; Tsiliopoulos, E. *J. Chem. Soc., Perkin Trans. 1* **1988,** 2805–2811. doi:10.1039/p19880002805
45. Singh, S.; DesMarteau, D. D.; Zuberi, S. S.; Witz, M.; Huang, H.-N. *J. Am. Chem. Soc.* **1987,** *109,* 7194–7196. doi:10.1021/ja00257a051
46. Resnati, G.; DesMarteau, D. D. *J. Org. Chem.* **1991,** *56,* 4925–4929. doi:10.1021/jo00016a022
47. Xu, Z.-Q.; DesMarteau, D. D.; Gotoh, Y. *J. Chem. Soc., Chem. Commun.* **1991,** 179–181. doi:10.1039/c39910000179
48. DesMarteau, D. D.; Xu, Z.-Q.; Witz, M. *J. Org. Chem.* **1992,** *57,* 629–635. doi:10.1021/jo00028a042
49. Pennington, W. T.; Resnati, G.; DesMarteau, D. D. *J. Org. Chem.* **1992,** *57,* 1536–1539. doi:10.1021/jo00031a038
50. Banks, R. E.; Sharif, I. *J. Fluorine Chem.* **1988,** *41,* 297–300. doi:10.1016/s0022-1139(00)81553-5
51. Banks, R. E.; Sharif, I. *J. Fluorine Chem.* **1991,** *55,* 207–214. doi:10.1016/s0022-1139(00)80123-2
52. Differding, E.; Lang, R. W. *Tetrahedron Lett.* **1988,** *29,* 6087–6090. doi:10.1016/s0040-4039(00)82271-6
53. Differding, E.; Lang, R. W. *Helv. Chim. Acta* **1989,** *72,* 1248–1252. doi:10.1002/hlca.19890720609
54. Banks, R. E.; Khazaei, A. *J. Fluorine Chem.* **1990,** *46,* 297–305. doi:10.1016/s0022-1139(00)80997-5
55. Satyamurthy, N.; Bida, G. T.; Phelps, M. E.; Barrio, J. R. *J. Org. Chem.* **1990,** *55,* 3373–3374. doi:10.1021/jo00297a071
56. Grakauskas, V.; Baum, K. *J. Org. Chem.* **1970,** *35,* 1545–1549. doi:10.1021/jo00830a061
57. Davis, F. A.; Han, W. *Tetrahedron Lett.* **1991,** *32,* 1631–1634. doi:10.1016/s0040-4039(00)74290-0

58. Davis, F. A.; Han, W.; Murphy, C. K. *J. Org. Chem.* **1995,** *60,* 4730–4737. doi:10.1021/jo00120a014
59. Differding, E.; Ofner, H. *Synlett* **1991,** 187–189. doi:10.1055/s-1991-20673
60. Gakh, A. A.; Romaniko, S. V.; Ugrak, B. I.; Fainzilberg, A. A. *Tetrahedron* **1991,** *47,* 7447–7458. doi:10.1016/s0040-4020(01)89746-5
61. Banks, R. E.; Lawrence, N. J.; Popplewell, A. L. *J. Chem. Soc., Chem. Commun.* **1994,** 343–344. doi:10.1039/c39940000343
62. Abdul-Ghani, M.; Banks, E. R.; Besheesh, M. K.; Sharif, I.; Syvret, R. G. *J. Fluorine Chem.* **1995,** *73,* 255–257. doi:10.1016/0022-1139(94)03225-o
63. Banks, R. E.; Besheesh, M. K.; Mohialdin-Khaffaf, S. N.; Sharif, I. *J. Chem. Soc., Perkin Trans. 1* **1996,** 2069–2076. doi:10.1039/p19960002069
64. Banks, R. E.; Besheesh, M. K.; Mohialdin-Khaffaf, S. N.; Sharif, I. *J. Fluorine Chem.* **1996,** *78,* 43–50. doi:10.1016/0022-1139(96)03395-7
65. Lal, G. S. *J. Org. Chem.* **1993,** *58,* 2791–2796. doi:10.1021/jo00062a023
66. Stavber, S.; Sotler, T.; Zupan, M. *Tetrahedron Lett.* **1994,** *35,* 1105–1108. doi:10.1016/s0040-4039(00)79977-1
67. Lal, G. S. *Synth. Commun.* **1995,** *25,* 725–737. doi:10.1080/00397919508011410
68. Brown, D. S.; Marples, B. A.; Smith, P.; Walton, L. *Tetrahedron* **1995,** *51,* 3587–3606. doi:10.1016/0040-4020(95)00075-j
69. Lal, G. S.; Pastore, W.; Pesaresi, R. *J. Org. Chem.* **1995,** *60,* 7340–7342. doi:10.1021/jo00127a046
70. Zupan, M.; Iskra, J.; Stavber, S. *J. Org. Chem.* **1995,** *60,* 259–260. doi:10.1021/jo00106a045
71. Brunavs, M.; Dell, C. P.; Owton, W. M. *J. Fluorine Chem.* **1994,** *68,* 201–203. doi:10.1016/0022-1139(93)03042-k
72. Matthews, D. P.; Miller, S. C.; Jarvi, E. T.; Sabol, J. S.; McCarthy, J. R. *Tetrahedron Lett.* **1993,** *34,* 3057–3060. doi:10.1016/s0040-4039(00)93378-1
73. Hodson, H. F.; Madge, D. J.; Slawin, A. N. Z.; Widdowson, D. A.; Williams, D. J. *Tetrahedron* **1994,** *50,* 1899–1906. doi:10.1016/s0040-4020(01)80862-0
74. McClinton, M. A.; Sik, V. *J. Chem. Soc., Perkin Trans. 1* **1992,** 1891–1895. doi:10.1039/p19920001891
75. Davis, F. A.; Zhou, P.; Murphy, C. K. *Tetrahedron Lett.* **1993,** *34,* 3971–3974. doi:10.1016/s0040-4039(00)60592-0
76. Umemoto, T.; Tomizawa, G. *J. Org. Chem.* **1995,** *60,* 6563–6570. doi:10.1021/jo00125a049
77. MEC Reagents: Fluorinating agents and Perfluoroalkylating agents; Daikin Chemical Sales company Brochure, 1997.
78. Poss, A. J.; Shia, G. 1-Substituted-4-fluoro-1,4-diazoniabicyclo[2.2.2]octane salts and their application as fluorinating agents. U.S. Patent US5,459,267, Oct 17, 1995.
79. Stavber, S.; Zupan, M. *Tetrahedron Lett.* **1996,** *37,* 3591–3594. doi:10.1016/0040-4039(96)00630-2
80. Poss, A. J.; Shia, G. A. *Tetrahedron Lett.* **1999,** *40,* 2673–2676. doi:10.1016/s0040-4039(99)00303-2
81. Cabrera, I.; Appel, W. K. *Tetrahedron* **1995,** *51,* 10205–10208. doi:10.1016/0040-4020(95)00597-2
82. Banks, R. E.; Besheesh, M. K.; Tsiliopoulos, E. *J. Fluorine Chem.* **1996,** *78,* 39–42. doi:10.1016/0022-1139(95)03380-7
83. Umemoto, T.; Nagayoshi, M. *Bull. Chem. Soc. Jpn.* **1996,** *69,* 2287–2295. doi:10.1246/bcsj.69.2287
84. Banks, R. E.; Besheesh, M. K. *J. Fluorine Chem.* **1995,** *74,* 165–166. doi:10.1016/0022-1139(95)03295-o
85. Banks, R. E.; Besheesh, M. K.; Mohialdin-Khaffaf, S. N.; Sharif, I. *J. Fluorine Chem.* **1997,** *81,* 157–161. doi:10.1016/s0022-1139(96)03521-x
86. Umemoto, T.; Nagayoshi, M.; Adachi, K.; Tomizawa, G. *J. Org. Chem.* **1998,** *63,* 3379–3385. doi:10.1021/jo972338q
87. Laali, K. K.; Tanaka, M.; Forohar, F.; Cheng, M.; Fetzer, J. C. *J. Fluorine Chem.* **1998,** *91,* 185–190. doi:10.1016/s0022-1139(98)00224-3
88. Forohar, F.; Damavarapu, R.; Jayasuriya, K.; Kwok, T. J. 13th Winter Fluorine Conference; St. Petersburg, Florida, USA, 1997; p 39.
89. Banks, R. E.; Besheesh, M. K.; Lawrence, N. J.; Tovell, D. J. *J. Fluorine Chem.* **1999,** *97,* 79–84. doi:10.1016/s0022-1139(99)00032-9
90. Takeuchi, Y.; Liu, Z.; Suzuki, E.; Shibata, N.; Kirk, K. L. *J. Fluorine Chem.* **1999,** *97,* 65–67. doi:10.1016/s0022-1139(99)00028-7
91. Takeuchi, Y.; Suzuki, T.; Satoh, A.; Shiragami, T.; Shibata, N. *J. Org. Chem.* **1999,** *64,* 5708–5711. doi:10.1021/jo9904011
92. Takeuchi, Y.; Satoh, A.; Suzuki, T.; Kameda, A.; Dohrin, M.; Satoh, T.; Koizumi, T.; Kirk, K. L. *Chem. Pharm. Bull.* **1997,** *45,* 1085–1088. doi:10.1248/cpb.45.1085
93. Shibata, N.; Liu, Z.; Takeuchi, Y. *Chem. Pharm. Bull.* **2000,** *48,* 1954–1958. doi:10.1248/cpb.48.1954
94. Liu, Z.; Shibata, N.; Takeuchi, Y. *J. Org. Chem.* **2000,** *65,* 7583–7587. doi:10.1021/jo0055584
95. Shibata, N.; Suzuki, E.; Takeuchi, Y. *J. Am. Chem. Soc.* **2000,** *122,* 10728–10729. doi:10.1021/ja002732x
96. Shibata, N.; Suzuki, E.; Asahi, T.; Shiro, M. *J. Am. Chem. Soc.* **2001,** *123,* 7001–7009. doi:10.1021/ja010789t
97. Cahard, D.; Audouard, C.; Plaquevent, J.-C.; Roques, N. *Org. Lett.* **2000,** *2,* 3699–3701. doi:10.1021/ol006610l
98. Cahard, D.; Audouard, C.; Plaquevent, J.-C.; Toupet, L.; Roques, N. *Tetrahedron Lett.* **2001,** *42,* 1867–1869. doi:10.1016/s0040-4039(01)00017-x
99. Baudequin, C.; Loubassou, J.-F.; Plaquevent, J.-C.; Cahard, D. *J. Fluorine Chem.* **2003,** *122,* 189–193. doi:10.1016/s0022-1139(03)00085-x
100. Banks, R. E.; Besheesh, M. K.; Fraenk, W.; Klapötke, T. M. *J. Fluorine Chem.* **2003,** *124,* 229–232. doi:10.1016/j.jfluchem.2003.08.010
101. Schleyer, P. v. R.; Buzek, P.; Klapötke, T. M.; Tornieporth-Oetting, I. C.; Broschag, M.; Pickardt, J. *Inorg. Chem.* **1993,** *32,* 1523–1524. doi:10.1021/ic00060a033
102. Yasui, H.; Yamamoto, T.; Ishimaru, T.; Fukuzumi, T.; Tokunaga, E.; Akikazu, K.; Shiro, M.; Shibata, N. *J. Fluorine Chem.* **2011,** *132,* 222–225. doi:10.1016/j.jfluchem.2011.01.005
103. Chen, G.; Chen, F.; Zhang, Y.; Yang, X.; Yuan, X.; Wu, F.; Yang, X. *J. Fluorine Chem.* **2012,** *133,* 155–159. doi:10.1016/j.jfluchem.2011.10.012
104. Zhang, Y.; Yang, X.-J.; Xie, T.; Chen, G.-L.; Zhu, W.-H.; Zhang, X.-Q.; Yang, X.-Y.; Wu, X.-Y.; He, X.-P.; He, H.-M. *Tetrahedron* **2013,** *69,* 4933–4937. doi:10.1016/j.tet.2013.04.037
105. Wang, F.; Li, J.; Hu, Q.; Yang, X.; Wu, X.-Y.; He, H. *Eur. J. Org. Chem.* **2014,** 3607–3613. doi:10.1002/ejoc.201402072

106. Shunatona, H. P.; Früh, N.; Wang, Y.-M.; Rauniyar, V.; Toste, F. D. *Angew. Chem., Int. Ed.* **2013,** *52,* 7724–7727. doi:10.1002/anie.201302002
107. Wolstenhulme, J. R.; Rosenqvist, J.; Lozano, O.; Ilupeju, J.; Wurz, N.; Engle, K. M.; Pidgeon, G. W.; Moore, P. R.; Sandford, G.; Gouverneur, V. *Angew. Chem., Int. Ed.* **2013,** *52,* 9796–9800. doi:10.1002/anie.201304845
108. Zhu, C.-L.; Maeno, M.; Zhang, F.-G.; Shigehiro, T.; Kagawa, T.; Kawada, K.; Shibata, N.; Ma, J.-A.; Cahard, D. *Eur. J. Org. Chem.* **2013,** 6501–6505. doi:10.1002/ejoc.201300956
109. Ratjen, L.; García-García, P.; Lay, F.; Beck, M. E.; List, B. *Angew. Chem., Int. Ed.* **2011,** *50,* 754–758. doi:10.1002/anie.201005954
110. Treskow, M.; Neudörfl, J.; Giernoth, R. *Eur. J. Org. Chem.* **2009,** 3693–3697. doi:10.1002/ejoc.200900548
111. Fukushi, K.; Suzuki, S.; Kamo, T.; Tokunaga, E.; Sumii, Y.; Kagawa, T.; Kawada, K.; Shibata, N. *Green Chem.* **2016,** *18,* 1864–1868. doi:10.1039/c5gc02612a
112. Bohlmann, R. N-Fluorosulfonimides, process for their production, as well as their use as fluorinating agents. WO Patent WO94/24098, Oct 27, 1994.
113. Pereira, R.; Wolstenhulme, J.; Sandford, G.; Claridge, T. D. W.; Gouverneur, V.; Cvengroš, J. *Chem. Commun.* **2016,** *52,* 1606–1609. doi:10.1039/c5cc08375c
114. Chen, C.; Luo, Y.; Fu, L.; Chen, P.; Lan, Y.; Liu, G. *J. Am. Chem. Soc.* **2018,** *140,* 1207–1210. doi:10.1021/jacs.7b11470
115. Meyer, D.; Jangra, H.; Walther, F.; Zipse, H.; Renaud, P. *Nat. Commun.* **2018,** *9,* 4888. doi:10.1038/s41467-018-07196-9
116. Hachisuka, H.; Kitano, M. *J. Fluorine Chem.* **1991,** *54,* 205. doi:10.1016/s0022-1139(00)83715-x
117. Kitano, M.; Hachisuka, H.; Umemoto, T. 16th National Meeting on Fluorine Chemistry, Oct 21, 1991; Nagoya, Japan; pp 101–102.
118. Sudlow, K.; Woolf, A. A. *J. Fluorine Chem.* **1994,** *66,* 9–11. doi:10.1016/0022-1139(93)02929-9
119. Solkan, V. N.; Fainzil'berg, A. A. *Russ. J. Org. Chem.* **1994,** *30,* 1200.
120. Fainzil'berg, A. A.; Faustov, V. I. *Russ. J. Org. Chem.* **2001,** *37,* 755–756. doi:10.1023/a:1012436925944
121. Gilicinski, A. G.; Pez, G. P.; Syvret, R. G.; Lal, G. S. *J. Fluorine Chem.* **1992,** *59,* 157–162. doi:10.1016/s0022-1139(00)80214-6
122. Differding, E.; Bersier, P. M. *Tetrahedron* **1992,** *48,* 1595–1604. doi:10.1016/s0040-4020(01)88718-4
123. Oliver, E. W.; Evans, D. H. *J. Electroanal. Chem.* **1999,** *474,* 1–8. doi:10.1016/s0022-0728(99)00296-x
124. Adachi, K.; Takahashi, I.; Harada, M.; Umemoto, T. *J. Fluorine Chem.* **2016,** *183,* 100–111. doi:10.1016/j.jfluchem.2015.09.013
125. Toullec, P. Y.; Devillers, I.; Frantz, R.; Togni, A. *Helv. Chim. Acta* **2004,** *87,* 2706–2711. doi:10.1002/hlca.200490240
126. Xue, X.-S.; Wang, Y.; Li, M.; Cheng, J.-P. *J. Org. Chem.* **2016,** *81,* 4280–4289. doi:10.1021/acs.joc.6b00683
127. Li, M.; Xue, X.-S.; Cheng, J.-P. *Acc. Chem. Res.* **2020,** *53,* 182–197. doi:10.1021/acs.accounts.9b00393
128. Christe, K. O.; Dixon, D. A. *J. Am. Chem. Soc.* **1992,** *114,* 2978–2985. doi:10.1021/ja00034a033
129. Rueda-Becerril, M.; Chatalova Sazepin, C.; Leung, J. C. T.; Okbinoglu, T.; Kennepohl, P.; Paquin, J.-F.; Sammis, G. M. *J. Am. Chem. Soc.* **2012,** *134,* 4026–4029. doi:10.1021/ja211679v
130. Sibi, M. P.; Landais, Y. *Angew. Chem., Int. Ed.* **2013,** *52,* 3570–3572. doi:10.1002/anie.201209583
131. Shigehisa, H.; Aoki, T.; Yamaguchi, S.; Shimizu, N.; Hiroya, K. *J. Am. Chem. Soc.* **2013,** *135,* 10306–10309. doi:10.1021/ja405219f
132. Shigehisa, H.; Nishi, E.; Fujisawa, M.; Hiroya, K. *Org. Lett.* **2013,** *15,* 5158–5161. doi:10.1021/ol402696h
133. Chatalova-Sazepin, C.; Hemelaere, R.; Paquin, J.-F.; Sammis, G. M. *Synthesis* **2015,** *47,* 2554–2569. doi:10.1055/s-0034-1378824
134. Champagne, P. A.; Desroches, J.; Hamel, J.-D.; Vandamme, M.; Paquin, J.-F. *Chem. Rev.* **2015,** *115,* 9073–9174. doi:10.1021/cr500706a
135. Szpera, R.; Moseley, D. F. J.; Smith, L. B.; Sterling, A. J.; Gouverneur, V. *Angew. Chem., Int. Ed.* **2019,** *58,* 14824–14848. doi:10.1002/anie.201814457
136. Yang, J.-D.; Wang, Y.; Xue, X.-S.; Cheng, J.-P. *J. Org. Chem.* **2017,** *82,* 4129–4135. doi:10.1021/acs.joc.7b00036
137. Timofeeva, D. S.; Ofial, A. R.; Mayr, H. *J. Am. Chem. Soc.* **2018,** *140,* 11474–11486. doi:10.1021/jacs.8b07147
138. Rozatian, N.; Ashworth, I. W.; Sandford, G.; Hodgson, D. R. W. *Chem. Sci.* **2018,** *9,* 8692–8702. doi:10.1039/c8sc03596b
139. Rozatian, N.; Beeby, A.; Ashworth, I. W.; Sandford, G.; Hodgson, D. R. W. *Chem. Sci.* **2019,** *10,* 10318–10330. doi:10.1039/c9sc04185k
140. Rozatian, N.; Harsanyi, A.; Murray, B. J.; Hampton, A. S.; Chin, E. J.; Cook, A. S.; Hodgson, D. R. W.; Sandford, G. *Chem. – Eur. J.* **2020,** *26,* 12027–12035. doi:10.1002/chem.202001120
141. Du, X.; Zhang, H.; Yao, Y.; Lu, Y.; Wang, A.; Wang, Y.; Li, Z. *Theor. Chem. Acc.* **2019,** *138,* No. 28. doi:10.1007/s00214-019-2417-2
142. Lal, G. S.; Pez, G. P.; Syvret, R. G. *Chem. Rev.* **1996,** *96,* 1737–1756. doi:10.1021/cr941145p
143. Lee, K. Y.; Kochi, J. K. *J. Chem. Soc., Perkin Trans. 2* **1992,** 1011–1017. doi:10.1039/p29920001011
144. Bockman, T. M.; Lee, K. Y.; Kochi, J. K. *J. Chem. Soc., Perkin Trans. 2* **1992,** 1581–1594. doi:10.1039/p29920001581
145. Differding, E.; Rüegg, G. M. *Tetrahedron Lett.* **1991,** *32,* 3815–3818. doi:10.1016/s0040-4039(00)79383-x
146. Differring, E.; Wehrli, M. *Tetrahedron Lett.* **1991,** *32,* 3819–3822. doi:10.1016/s0040-4039(00)79384-1
147. Zupan, M.; Škulj, P.; Stavber, S. *Chem. Lett.* **1998,** *27,* 641–642. doi:10.1246/cl.1998.641
148. Vincent, S. P.; Burkart, M. D.; Tsai, C.-Y.; Zhang, Z.; Wong, C.-H. *J. Org. Chem.* **1999,** *64,* 5264–5279. doi:10.1021/jo990686h
149. Nyffeler, P. T.; Durón, S. G.; Burkart, M. D.; Vincent, S. P.; Wong, C.-H. *Angew. Chem., Int. Ed.* **2005,** *44,* 192–212. doi:10.1002/anie.200400648
150. Piana, S.; Devillers, I.; Togni, A.; Rothlisberger, U. *Angew. Chem., Int. Ed.* **2002,** *41,* 979–982. doi:10.1002/1521-3773(20020315)41:6<979::aid-anie979>3.0.co;2-e
151. Laali, K. K.; Borodkin, G. I. *J. Chem. Soc., Perkin Trans. 2* **2002,** 953–957. doi:10.1039/b111725d
152. Kralj, P.; Zupan, M.; Stavber, S. *J. Org. Chem.* **2006,** *71,* 3880–3888. doi:10.1021/jo060213s
153. Andreev, R. V.; Borodkin, G. I.; Shubin, V. G. *Russ. J. Org. Chem.* **2009,** *45,* 1468–1473. doi:10.1134/s107042800910008x
154. Geng, C.; Du, L.; Liu, F.; Zhu, R.; Liu, C. *RSC Adv.* **2015,** *5,* 33385–33391. doi:10.1039/c4ra15202f
155. Chen, Q.; Zeng, J.; Yan, X.; Huang, Y.; Wen, C.; Liu, X.; Zhang, K. *J. Org. Chem.* **2016,** *81,* 10043–10048. doi:10.1021/acs.joc.6b01932
156. Li, C.-T.; Yuan, X.; Tang, Z.-Y. *Tetrahedron Lett.* **2016,** *57,* 5624–5627. doi:10.1016/j.tetlet.2016.11.003
157. Wu, S.-W.; Liu, F. *Org. Lett.* **2016,** *18,* 3642–3645. doi:10.1021/acs.orglett.6b01691

158. Wu, S.-W.; Liu, J.-L.; Liu, F. *Chem. Commun.* **2017,** *53,* 12321–12324. doi:10.1039/c7cc07165e
159. Zhang, Y.; Wen, C.; Li, J. *Org. Biomol. Chem.* **2018,** *16,* 1912–1920. doi:10.1039/c7ob03059b
160. Fan, X.; Wang, Q.; Wei, Y.; Shi, M. *Chem. Commun.* **2018,** *54,* 10503–10506. doi:10.1039/c8cc05634j
161. Zhou, J.; Fang, Y.; Wang, F.; Li, J. *Org. Biomol. Chem.* **2019,** *17,* 4470–4474. doi:10.1039/c9ob00467j
162. Jójárt, R.; Traj, P.; Kovács, É.; Horváth, Á.; Schneider, G.; Szécsi, M.; Pál, A.; Paragi, G.; Mernyák, E. *Molecules* **2019,** *24,* 1783. doi:10.3390/molecules24091783
163. Wood, S. H.; Etridge, S.; Kennedy, A. R.; Percy, J. M.; Nelson, D. J. *Chem. – Eur. J.* **2019,** *25,* 5574–5585. doi:10.1002/chem.201900029
164. Borodkin, G. I.; Elanov, I. R.; Gatilov, Y. V.; Shubin, V. G. *J. Fluorine Chem.* **2019,** *228,* 109412. doi:10.1016/j.jfluchem.2019.109412
165. Rozatian, N.; Hodgson, D. R. W. *Chem. Commun.* **2021,** *57,* 683–712. doi:10.1039/d0cc06339h
166. Furin, G. G. In *Methods of Organic Chemistry (Houben-Weyl), Organo-fluorine Compounds Vol E10a;* Baasner, B.; Hagemann, H.; Tatlow, J. C., Eds.; Thieme: Stuttgart, New York, 1999; pp 432–499.
167. Banks, R. E. *J. Fluorine Chem.* **1998,** *87,* 1–17. doi:10.1016/s0022-1139(97)00127-9
168. Singh, R. P.; Shreeve, J. M. *Acc. Chem. Res.* **2004,** *37,* 31–44. doi:10.1021/ar030043v
169. Kiselyov, A. S. *Chem. Soc. Rev.* **2005,** *34,* 1031–1037. doi:10.1039/b509217p
170. Umemoto, T. N-Fluoropyridinium Salts, Synthesis and Fluorination Chemistry. In *Advances in Organic Synthesis;* Laali, K. K., Ed.; Bentham Science Publishers Ltd.: Netherlands, 2006; Vol. 2, pp 159–181. doi:10.2174/978160805198410602010159
171. Umemoto, T. Preparation, Reactivity, and Applications of N-Fluoropyridinium Salts. In *Fluorinated Heterocycles;* Gakh, A. A.; Kirk, K. L., Eds.; ACS Symposium Series, Vol. 1003; American Chemical Society: Washington, DC, USA, 2009; pp 37–58. doi:10.1021/bk-2009-1003.ch003
172. Baudoux, J.; Cahard, D. Electrophilic Fluorination with N–F Reagents. In *Organic Reactions;* Denmark, S. E., Ed.; John Wiley & Sons, 2008; pp 347–672. doi:10.1002/0471264180.or069.02
173. de Azambuja, F.; Altman, R. A. NFSI and Its Analogs Fluorination for Preparing Alkenyl Fluorides. In *Fluorination;* Hu, J.; Umemoto, T., Eds.; Springer: Singapore, 2018. doi:10.1007/978-981-10-1855-8_20-1
174. Yan, H.; Zhu, C. NFSI Radical Fluorination for Preparing Alkyl Fluorides. In *Fluorination;* Hu, J.; Umemoto, T., Eds.; Springer: Singapore, 2018. doi:10.1007/978-981-10-1855-8_1-1
175. Guyon, H.; Cahard, D. Selectfluor and Its Analogs Electrophilic Fluorination for Preparing Alkyl Fluorides. In *Fluorination;* Hu, J.; Umemoto, T., Eds.; Springer: Singapore, 2018. doi:10.1007/978-981-10-1855-8_8-1
176. de Azambuja, F.; Altman, R. A. SelectFluor and Its Analogs Fluorination for Preparing Alkenyl Fluorides. In *Fluorination;* Hu, J.; Umemoto, T., Eds.; Springer: Singapore, 2018. doi:10.1007/978-981-10-1855-8_19-1
177. Yan, H.; Zhu, C. SelectFluor Radical Fluorination for Preparing Alkyl Fluorides. In *Fluorination;* Hu, J.; Umemoto, T., Eds.; Springer: Singapore, 2018. doi:10.1007/978-981-10-1855-8_2-1
178. Chen, C.; Chen, P.; Liu, G. *N,N'*-Difluoro-1,4-Diazoniabicyclo[2.2.2]octane Salt Electrophilic Fluorination. In *Fluorination;* Hu, J.; Umemoto, T., Eds.; Springer: Singapore, 2018. doi:10.1007/978-981-10-1855-8_47-1
179. Kawada, K. *N*-Fluoropyridinium Salt Electrophilic Fluorination for Preparing Alkyl Fluorides. In *Fluorination;* Hu, J.; Umemoto, T., Eds.; Springer: Singapore, 2018. doi:10.1007/978-981-10-1855-8_21-2
180. Kawada, K. *N*-Fluoropyridinium Salt Radical Fluorination for Preparing Alkyl Fluorides. In *Fluorination;* Hu, J.; Umemoto, T., Eds.; Springer: Singapore, 2018. doi:10.1007/978-981-10-1855-8_41-1
181. Wang, G.; Ma, J.-A. NFSI and Its Analogs Electrophilic Fluorination for Preparing Alkyl Fluorides. In *Fluorination;* Hu, J.; Umemoto, T., Eds.; Springer: Singapore, 2018. doi:10.1007/978-981-10-1855-8_6-1

License and Terms

This is an Open Access article under the terms of the Creative Commons Attribution License (https://creativecommons.org/licenses/by/4.0). Please note that the reuse, redistribution and reproduction in particular requires that the author(s) and source are credited and that individual graphics may be subject to special legal provisions.

The license is subject to the *Beilstein Journal of Organic Chemistry* terms and conditions: (https://www.beilstein-journals.org/bjoc/terms)

The definitive version of this article is the electronic one which can be found at: https://doi.org/10.3762/bjoc.17.123